

# A Computational and Experimental Investigation of a Three-Dimensional Hypersonic Scramjet Inlet Flow Field

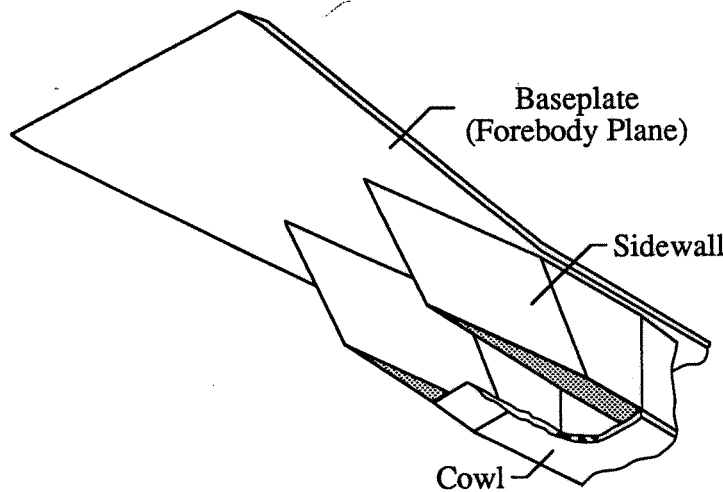
by

Scott Douglas Holland

GRANT  
IN-02-CR

COVERPAGE

39595  
P- 676



A dissertation submitted to the Graduate Faculty of  
North Carolina State University  
in partial fulfillment of the  
requirements for the Degree of  
Doctor of Philosophy

Aerospace Engineering  
Hypersonic Aerodynamics

Raleigh, North Carolina  
1991

ACCESSIONING, REPRODUCTION AND DISTRIBUTION  
BY OR FOR NASA PERMITTED

(NASA-CR-188788) A COMPUTATIONAL AND  
EXPERIMENTAL INVESTIGATION OF A  
THREE-DIMENSIONAL HYPersonic SCRAMJET INLET  
FLOW FIELD Ph.D. Thesis (North Carolina  
State Univ.) 676 p  
N91-31083  
Unclas  
CSCL 01A G3/02 0039595

## **Abstract**

**HOLLAND, SCOTT DOUGLAS. A Computational and Experimental Investigation of a Three-Dimensional Hypersonic Scramjet Inlet Flow Field (Under the direction of Dr. John N. Perkins.)**

Since careful design of primary engine components such as the inlet is necessary to exploit effectively the potential of propulsion-airframe integration, a combined computational and experimental parametric study of the internal aerodynamics of a generic three-dimensional sidewall compression scramjet inlet configuration has been performed. The study was designed to demonstrate the utility of computational fluid dynamics as a design tool in hypersonic inlet flow fields, to provide a detailed account of the nature and structure of the internal flow interactions, and to provide a comprehensive surface property and flow field database to determine the effects of contraction ratio, cowl position, and Reynolds number on the performance of a hypersonic scramjet inlet configuration. The work proceeded in several phases: the initial inviscid assessment of the internal shock structure, the preliminary computational parametric study, the coupling of the optimized configuration with the physical limitations of the facility, the wind tunnel blockage assessment, and the computational and experimental parametric study of the final configuration. A total of 256 channels of pressure data, including static pressure orifices, pitot pressures, and entrance and exit flow rakes, along with oil flow and infrared thermography provided a detailed experimental description of the flow. Generally good agreement is obtained between the computation and experiment. For the higher contraction ratios, a large forward separation of the inflow boundary layer is observed. The dominant effect of forward cowl placement is an increase in mass capture, while the principle effect of decreased Reynolds number is an increase in internal shock strength due to increased sidewall displacement thicknesses.

Copyright ©1991 by Scott Douglas Holland. All Rights Reserved.

ACCESSIONING, REPRODUCTION AND DISTRIBUTION  
BY OR FOR NASA PERMITTED

# **A Computational and Experimental Investigation of a Three-Dimensional Hypersonic Scramjet Inlet Flow Field**

by  
**Scott D. Holland**


A dissertation submitted to the Graduate Faculty of  
North Carolina State University  
in partial fulfillment of the  
requirements for the Degree of  
Doctor of Philosophy

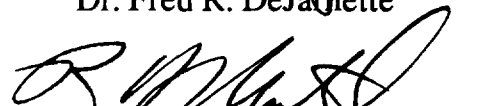
**Aerospace Engineering  
Hypersonic Aerodynamics**

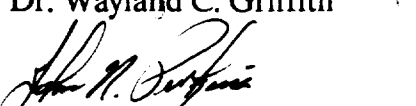
Raleigh, North Carolina  
1991

Approved by:

  
\_\_\_\_\_  
Dr. Fred R. DeJarnette

  
\_\_\_\_\_  
Dr. Wayland C. Griffith

  
\_\_\_\_\_  
Dr. Robert H. Martin

  
\_\_\_\_\_  
Dr. John N. Perkins, Chairman



*To my wife Cathy,  
whose love and devotion  
through these past 4 years  
truly serve to redefine the words*

*And to our daughter Rachel.*

## **Biography**

The author was born on [REDACTED] in [REDACTED]. He graduated from Menchville High School in 1982; in the fall of the same year, he joined the Aerospace and Ocean Engineering Department at Virginia Polytechnic Institute and State University. Following his graduation in June 1986, he remained with the department to pursue a Master of Science degree. In July of 1987, he completed his thesis, "Experimental Investigation of Turbulent Flow in the Near Wake of a Propeller," under Dr. Joseph A. Schetz. The author then joined the Aerospace Engineering Department at North Carolina State University to pursue the Degree of Doctor of Philosophy in Hypersonic Aerodynamics.

## **Acknowledgements**

I would like to take this opportunity to express my appreciation to the many people who have helped make this work possible. I am indebted to the members of my committee for the guidance offered over the course of this project. In particular, I want to thank my advisor, Dr. John N. Perkins. When we first arrived at Langley, you introduced me as your young protege. I have worked hard to be worthy of that title. You have taught me much, and I am proud to think of you as my friend.

I would also like to thank Joyce Pollard. When I first arrived on campus in the summer of 1987, you took me under your wing and helped me fight my way through that initial maze of paperwork; since that time, you have always been instrumental in solving any of the numerous difficulties I have encountered while away from campus. You were my first friend at NC State.

My parents, Ruth and Alvin Holland, also deserve many thanks. You taught me through both word and example how to live life. You taught me independence, ambition, and that "you can do anything you set my mind to," perhaps the qualities which set me on a course leading to a PhD. But more than all that, you taught me love and compassion. While no parent can provide his child success, I am well aware of the many sacrifices the two of you made through the years to provide me opportunity. There is nothing I can say and nothing I can do to ever repay you for all you have done for me, except to do my best to provide the same opportunity to our children. Thanks again, Mom and Dad.

I cannot begin to adequately express my gratitude to my wife Cathy for her vigilant support through these many years. You made me laugh at times when I thought I had forgotten how. You have been my greatest source of encouragement; you always believed in me. And during the times when the flames appeared to be springing up around me faster than I could stamp them out, in your own subtle way you always reminded me to look for the Fourth Man in the fire (Daniel 3:24-25). These pages represent a significant sacrifice on your part, too. Without your support and encouragement, this certainly would not have been possible. For all that you do for me, I want to say thank you, and I love you.

There are a number of people at NASA Langley deserving of thanks. I would like to thank Carl Trexler and Wayne Guy of the Hypersonic Propulsion Branch for their help in defining the problem and for their continuing interest, Lona Howser for her help in all manner of computer problems, Kamran Daryabeigi for his work on the infrared thermography, Jeff Hodge (the facility engineer for the 31 Inch Mach 10 Tunnel) for his work in all aspects of the testing, data acquisition, and reduction, the staff of the 31 Inch Mach 10 Tunnel for their dedication through sometimes long hours, the Experimental Hypersonics Branch of the Space Systems Division for their support and for the use of their facilities for the experimental work, and my officemates Bert Senter and Anne Edwards for their constant encouragement.

I would also like to acknowledge the NAS program at NASA Ames for use of their computational facilities as well as the North Carolina Supercomputing Center. This work was supported in part through the NCSU Hypersonic Center of Excellence Program under NASA/ONR/AFOSR Grant NAGW-1072.

# Table of Contents

LIST OF TABLES	ix
LIST OF FIGURES	x
LIST OF SYMBOLS	lxxi
1. INTRODUCTION	1
2. LITERATURE REVIEW	7
2.1 3-D Shock Wave-Laminar Boundary Layer Interactions	8
2.2 3-D Shock Wave-Turbulent Boundary Layer Interactions	10
2.3 Hypersonic Inlet Shock Wave-Boundary Layer Interactions	13
2.3.1 Scope of Recent 2-D Inlet Research	13
2.3.2 Review of 3-D Shock-Boundary Layer Inlet Work	15
2.3.3 Three-Dimensional Inlet Component Work	18
3. INLET DESIGN CONSIDERATIONS	22
3.1 Flight Considerations	22
3.2 Ground Based Test Considerations	24
3.2.1 Description of Wind Tunnel Facilities	24
3.2.2 Aerodynamic Simulation	26
3.2.3 Size and Weight Constraints	28
3.2.4 Aerothermodynamic Loading	30
3.2.5 Instrumentation Response Time	32
3.3 Fundamental Internal Flow Phenomena	33
4. COMPUTATIONAL PARAMETRICS	38
4.1 Configuration Description	39
4.2 Inlet Code	40
4.3 Averaged Exit Plane Properties	41
4.3.1 Mass Capture	43
4.3.2 Throat Mach Number	43
4.3.3 Total Pressure Recovery	44
4.3.4 Area Weighted P/P1	45
4.4 Conclusions	46

5. EXPERIMENTAL CONFIGURATION	47
5.1 Component Sizing	49
5.2 Test Techniques	53
5.2.1 Pressure Measurements	53
5.2.1.1 Calibration of Pressure Sensors	53
5.2.1.2 Data Reduction and Uncertainty	54
5.2.2 Surface Temperature Measurements	56
5.2.3 Flow Visualization	57
5.3 Wind Tunnel Blockage Assessment	57
5.3.1 Results	58
5.3.1.1 Model Cross-Sectional Area Distribution	58
5.3.1.2 Pressure Data	59
5.3.2 Conclusion	62
5.4 Test Matrix	62
6. COMPUTATIONAL RESULTS	64
6.1 Contraction Ratio Effects	66
6.1.1 Contraction Ratio = 3, $Re = 2.15$ million/ft, 0% Cowl	73
6.1.2 Contraction Ratio = 5, $Re = 2.15$ million/ft, 0% Cowl	81
6.1.3 Contraction Ratio = 9, $Re = 2.15$ million/ft, 0% Cowl	88
6.2 Cowl Placement Effects	95
6.2.1 Summary of Cowl Position Effects	97
6.2.2 Shock Structure for the 50% Cowl, $CR = 3$ , $Re = 2.15$ million/ft Configuration	97
6.3 Reynolds Number Effects	101
6.3.1 Summary of Reynolds Number Effects	103
6.3.2 Shock Structure for the $Re = 0.55$ million/ft, $CR = 3$ , 0% Cowl Configuration	104
7. EXPERIMENTAL RESULTS	107
7.1 Contour Plots	107
7.1.1 Contraction Ratio and Cowl Location Effects	110
7.1.2 Reynolds Number Effects	115
7.2 Line Plots	118
7.2.1 Contraction Ratio Effects	119
7.2.2 Cowl Position Effects	127
7.2.3 Reynolds Number Effects	130
7.3 Oil Flow Results	132
7.4 Surface Temperature Measurements	133

8. EXPLICIT COMPARISON OF COMPUTATION AND EXPERIMENT	135
8.1 Contour Plot Comparison	136
8.2 Exit Plane Rake Data	138
8.3 Entrance Plane Rake Data	139
9. CONCLUSIONS	140
10. REFERENCES	146
11. APPENDIX A: Code Overview	154
A.1 The Governing Equations	154
A.2 Transforming the Governing Equations	157
A.2.1 A General Coordinate Transformation	158
A.2.2 The Transformed Governing Equations	160
A.3 Boundary Conditions	162
A.4 MacCormack's Method	162
12. FIGURES	165

## **List of Tables**

Table 3.2.2.1: Mach Number/Reynolds Number Matching for 31 Inch Mach 10 Tunnel	28
Table 3.2.4.1: Properties of Aluminum, Copper, and Steel	31
Table 4.3.1: Performance Parameters for Computational Parametric Study	42
Table 5.4.1: Test Matrix (runs) for $Re = 0.55$ million/ft	63
Table 5.4.2: Test Matrix (runs) for $Re = 1.14$ million/ft	63
Table 5.4.3: Test Matrix (runs) for $Re = 2.15$ million/ft	63
Table 6.1.1: Summary of Computed Inlet Performance Performance	72
Table 7.1.1.1: Inviscid Shock Impingement Locations	110



# List of Figures

Figure 1.1:	Propulsion-Airframe Integration	166
Figure 1.2:	Inlet Model Shown in Flight Orientation	167
Figure 2.1:	Internal Reflected Shock Structure	168
Figure 2.2:	Flow Spillage Due to Swept Shock Sheet Emanating from Sidewall Leading Edge	168
Figure 3.2.1.1:	Model Injection Sequence, Showing Model Retracted Prior to Injection, Model Injected into the Tunnel, and Model Injected into Technician Work Area	169
Figure 3.2.3.1:	Dimensioned Wind Tunnel Injection Plate	170
Figure 3.2.3.2:	Injection Carriage/Chamber Detail	170
Figure 3.3.1:	Shock after Shoulder, Shock on Shoulder, and Shock before Shoulder	171
Figure 3.3.2:	Mach Number Components for Modified 2-D Oblique Shock Theory	172
Figure 3.3.3:	Region of Flow Spillage for Shock Angles Corresponding to Low and High Mach Number Inflow	173
Figure 3.3.4:	Centered Expansion Model of Baseplate Interaction Region	173
Figure 4.3.1.1:	Leading Edge Sweep and Cowl Position Effects on Inlet Mass Capture	174
Figure 4.3.2.1:	Leading Edge Sweep and Cowl Position Effects on Inlet Throat Mach Number	174
Figure 4.3.3.1:	Leading Edge Sweep and Cowl Position Effects on Inlet Total Pressure Recovery	174
Figure 4.3.4.1:	Leading Edge Sweep and Cowl Position Effects on Inlet Area Weighted P/P1	174
Figure 5.1:	Inlet on Injection Plate Viewed From Underneath Tunnel	175
Figure 5.2:	Sidewall Orifice Locations and Identification of Coordinate System	176
Figure 5.3:	Baseplate Orifice Locations and Coordinate System Identification	177
Figure 5.1.1:	Inlet Injected into Inviscid Core	178
Figure 5.1.2:	Photograph of Inlet Model on Injection Plate	179
Figure 5.1.3:	Photograph of Inlet Model Injected into Tunnel Test Section	180
Figure 5.2.2.1:	Sketch of Scanning Infrared Thermography System	181
Figure 5.3.1.1.1:	Inlet Frontal and Profile Views at Angle of Attack, Ranging from 0 to 15°	182
Figure 5.3.1.1.2:	Cross-sectional Area Distribution for Inlet Model	183
Figure 5.3.1.2.1:	Injection Plate Pressures, Tunnel Empty	184

Figure 5.3.1.2.2: Cowl Effects, $Re=2.15$ million/ft, $CR=3$ , Centerline Pressures	185
Figure 5.3.1.2.3: Cowl Effects, $Re=2.15$ million/ft, $CR=3$ , Injection Plate Pressures	185
Figure 5.3.1.2.4: Cowl Effects, $Re=2.15$ million/ft, $CR=3$ , Pitot Pressures	185
Figure 5.3.1.2.5: Cowl Effects, $Re=2.15$ million/ft, $CR=5$ , Centerline Pressures	186
Figure 5.3.1.2.6: Cowl Effects, $Re=2.15$ million/ft, $CR=5$ , Injection Plate Pressures	186
Figure 5.3.1.2.7: Cowl Effects, $Re=2.15$ million/ft, $CR=5$ , Pitot Pressures	186
Figure 5.3.1.2.8: Cowl Effects, $Re=2.15$ million/ft, $CR=9$ , Centerline Pressures	187
Figure 5.3.1.2.9: Cowl Effects, $Re=2.15$ million/ft, $CR=9$ , Injection Plate Pressures	187
Figure 5.3.1.2.10: Cowl Effects, $Re=2.15$ million/ft, $CR=9$ , Pitot Pressures	187
Figure 5.3.1.2.11: Contraction Ratio Effects, $Re=2.15$ million/ft, 0% Cowl, Centerline Pressures	188
Figure 5.3.1.2.12: Contraction Ratio Effects, $Re=2.15$ million/ft, 0% Cowl, Injection Plate Pressures	188
Figure 5.3.1.2.13: Contraction Ratio Effects, $Re=2.15$ million/ft, 0% Cowl, Pitot Pressures	188
Figure 5.3.1.2.14: Reynolds Number Effects, $CR=5$ , 0% Cowl, Centerline Pressures	189
Figure 5.3.1.2.15: Reynolds Number Effects, $CR=5$ , 0% Cowl, Injection Plate Pressures	189
Figure 5.3.1.2.16: Reynolds Number Effects, $CR=5$ , 0% Cowl, Pitot Pressures	189
Figure 5.3.1.2.17: Angle of Attack= $15^\circ$ , $CR=9$ , 50% Cowl, Injection Plate Pressures	190
Figure 6.1: Computational Grid of Inlet Sidewall and Baseplate	191
Figure 6.1.1(a): Pressure Contours at $Z/H=0.25$ for $CR=3$ , $Re=2.15$ million/ft, 0% Cowl	192
Figure 6.1.1(b): Pressure Contours at $Z/H=0.50$ for $CR=3$ , $Re=2.15$ million/ft, 0% Cowl	192
Figure 6.1.1(c): Pressure Contours at $Z/H=0.75$ for $CR=3$ , $Re=2.15$ million/ft, 0% Cowl	192
Figure 6.1.2: Sidewall and Baseplate Pressure Contours for $CR=3$ , $Re=2.15$ million/ft, 0% Cowl	193
Figure 6.1.3: Centerline Pressure Contours for $CR=3$ , $Re=2.15$ million/ft, 0% Cowl	194
Figure 6.1.4: Streamwise Separation ( $U<0$ ) for $CR=3$ , $Re=2.15$ million/ft, 0% Cowl	195
Figure 6.1.5: Simulated Oil Flow for $CR=3$ , $Re=2.15$ million /ft, 0% Cowl	196
Figure 6.1.6: Exit Plane Pressure Contours for $CR=3$ , $Re=2.15$ million/ft, 0% Cowl	197
Figure 6.1.7: Exit Plane Mach Number Contours for $CR=3$ , $Re=2.15$ million/ft, 0% Cowl	198
Figure 6.1.8(a): Pressure Contours at $Z/H=0.25$ for $CR=5$ , $Re=2.15$ million/ft, 0% Cowl	199
Figure 6.1.8(b): Pressure Contours at $Z/H=0.50$ for $CR=5$ , $Re=2.15$ million/ft, 0% Cowl	199
Figure 6.1.8(c): Pressure Contours at $Z/H=0.75$ for $CR=5$ , $Re=2.15$ million/ft, 0% Cowl	199

Figure 6.1.9:	Sidewall and Baseplate Pressure Contours for CR=5, Re=2.15 million/ft, 0% Cowl	200
Figure 6.1.10:	Centerline Pressure Contours for CR=5, Re=2.15 million/ft, 0% Cowl	201
Figure 6.1.11:	Streamwise Separation ( $U < 0$ ) for CR=5, Re=2.15 million/ft, 0% Cowl	202
Figure 6.1.12:	Simulated Oil Flow for CR=5, Re=2.15 million /ft, 0% Cowl	203
Figure 6.1.13:	Exit Plane Pressure Contours for CR=5, Re=2.15 million/ft, 0% Cowl	204
Figure 6.1.14:	Exit Plane Mach Number Contours for CR=5, Re=2.15 million/ft, 0% Cowl	205
Figure 6.1.15(a):	Pressure Contours at $Z/H=0.25$ for CR=9, Re=2.15 million/ft, 0% Cowl	206
Figure 6.1.15(b):	Pressure Contours at $Z/H=0.50$ for CR=9, Re=2.15 million/ft, 0% Cowl	206
Figure 6.1.15(c):	Pressure Contours at $Z/H=0.75$ for CR=9, Re=2.15 million/ft, 0% Cowl	206
Figure 6.1.16:	Sidewall and Baseplate Pressure Contours for CR=9, Re=2.15 million/ft, 0% Cowl	207
Figure 6.1.17:	Centerline Pressure Contours for CR=9, Re=2.15 million/ft, 0% Cowl	208
Figure 6.1.18:	Streamwise Separation ( $U < 0$ ) for CR=9, Re=2.15 million/ft, 0% Cowl	209
Figure 6.1.19:	Simulated Oil Flow for CR=9, Re=2.15 million /ft, 0% Cowl	210
Figure 6.1.20:	Exit Plane Pressure Contours for CR=9, Re=2.15 million/ft, 0% Cowl	211
Figure 6.1.21:	Exit Plane Mach Number Contours for CR=9, Re=2.15 million/ft, 0% Cowl	212
Figure 6.1.1.1:	Pressure Contours at $I=31$ , $x'/Tx'=0.04$ for CR=3, 0% Cowl, Re=2.15 million/ft	213
Figure 6.1.1.2:	Crossflow Velocity Vectors at $I=31$ , $x'/Tx'=0.04$ for CR=3, 0% Cowl, Re=2.15 million/ft	214
Figure 6.1.1.3:	Pressure Contours at $I=35$ , $x'/Tx'=0.20$ for CR=3, 0% Cowl, Re=2.15 million/ft	215
Figure 6.1.1.4:	Crossflow Velocity Vectors at $I=35$ , $x'/Tx'=0.20$ for CR=3, 0% Cowl, Re=2.15 million/ft	216
Figure 6.1.1.5:	Pressure Contours at $I=40$ , $x'/Tx'=0.40$ for CR=3, 0% Cowl, Re=2.15 million/ft	217
Figure 6.1.1.6:	Crossflow Velocity Vectors at $I=40$ , $x'/Tx'=0.40$ for CR=3, 0% Cowl, Re=2.15 million/ft	218
Figure 6.1.1.7:	Pressure Contours at $I=45$ , $x'/Tx'=0.60$ for CR=3, 0% Cowl, Re=2.15 million/ft	219
Figure 6.1.1.8:	Crossflow Velocity Vectors at $I=45$ , $x'/Tx'=0.60$ for CR=3, 0% Cowl, Re=2.15 million/ft	220
Figure 6.1.1.9:	Particle Traces at $I=45$ , $x'/Tx'=0.60$ for CR=3, 0% Cowl, Re=2.15 million/ft	221
Figure 6.1.1.10:	Pressure Contours at $I=50$ , $x'/Tx'=0.79$ for CR=3, 0% Cowl, Re=2.15 million/ft	222
Figure 6.1.1.11:	Crossflow Velocity Vectors at $I=50$ , $x'/Tx'=0.79$ for CR=3, 0% Cowl, Re=2.15 million/ft	223
Figure 6.1.1.12:	Particle Traces at $I=50$ , $x'/Tx'=0.79$ for CR=3, 0% Cowl, Re=2.15 million/ft	224
Figure 6.1.1.13:	Pressure Contours at $I=52$ , $x'/Tx'=0.87$ for CR=3, 0% Cowl, Re=2.15 million/ft	225

Figure 6.1.1.14:	Crossflow Velocity Vectors at $I=52$ , $x'/Tx'=0.87$ for $CR=3$ , 0% Cowl, $Re=2.15$ million/ft	226
Figure 6.1.1.15:	Particle Traces at $I=52$ , $x'/Tx'=0.87$ for $CR=3$ , 0% Cowl, $Re=2.15$ million/ft	227
Figure 6.1.1.16:	Pressure Contours at $I=54$ , $x'/Tx'=0.96$ for $CR=3$ , 0% Cowl, $Re=2.15$ million/ft	228
Figure 6.1.1.17:	Crossflow Velocity Vectors at $I=54$ , $x'/Tx'=0.96$ for $CR=3$ , 0% Cowl, $Re=2.15$ million/ft	229
Figure 6.1.1.18:	Particle Traces at $I=54$ , $x'/Tx'=0.96$ for $CR=3$ , 0% Cowl, $Re=2.15$ million/ft	230
Figure 6.1.1.19:	Pressure Contours at $I=55$ , $x'/Tx'=1.00$ for $CR=3$ , 0% Cowl, $Re=2.15$ million/ft	231
Figure 6.1.1.20:	Crossflow Velocity Vectors at $I=55$ , $x'/Tx'=1.00$ for $CR=3$ , 0% Cowl, $Re=2.15$ million/ft	232
Figure 6.1.1.21:	Particle Traces at $I=55$ , $x'/Tx'=1.00$ for $CR=3$ , 0% Cowl, $Re=2.15$ million/ft	233
Figure 6.1.1.22:	Pressure Contours at $I=56$ , $xs'/Te'=0.06$ for $CR=3$ , 0% Cowl, $Re=2.15$ million/ft	234
Figure 6.1.1.23:	Crossflow Velocity Vectors at $I=56$ , $xs'/Te'=0.06$ for $CR=3$ , 0% Cowl, $Re=2.15$ million/ft	235
Figure 6.1.1.24:	Particle Traces at $I=56$ , $xs'/Te'=0.06$ for $CR=3$ , 0% Cowl, $Re=2.15$ million/ft	236
Figure 6.1.1.25:	Pressure Contours at $I=60$ , $xs'/Te'=0.29$ for $CR=3$ , 0% Cowl, $Re=2.15$ million/ft	237
Figure 6.1.1.26:	Crossflow Velocity Vectors at $I=60$ , $xs'/Te'=0.29$ for $CR=3$ , 0% Cowl, $Re=2.15$ million/ft	238
Figure 6.1.1.27:	Particle Traces at $I=60$ , $xs'/Te'=0.29$ for $CR=3$ , 0% Cowl, $Re=2.15$ million/ft	239
Figure 6.1.1.28:	Pressure Contours at $I=65$ , $xs'/Te'=0.58$ for $CR=3$ , 0% Cowl, $Re=2.15$ million/ft	240
Figure 6.1.1.29:	Crossflow Velocity Vectors at $I=65$ , $xs'/Te'=0.58$ for $CR=3$ , 0% Cowl, $Re=2.15$ million/ft	241
Figure 6.1.1.30:	Particle Traces at $I=65$ , $xs'/Te'=0.58$ for $CR=3$ , 0% Cowl, $Re=2.15$ million/ft	242
Figure 6.1.1.31:	Pressure Contours at $I=72$ , $xs'/Te'=1.00$ (Exit Plane) for $CR=3$ , 0% Cowl, $Re=2.15$ million/ft	243
Figure 6.1.1.32:	Crossflow Velocity Vectors at $I=72$ , $xs'/Te'=1.00$ (Exit Plane) for $CR=3$ , 0% Cowl, $Re=2.15$ million/ft	244
Figure 6.1.1.33:	Particle Traces at $I=72$ , $xs'/Te'=1.00$ (Exit Plane) for $CR=3$ , 0% Cowl, $Re=2.15$ million/ft	245
Figure 6.1.2.1:	Pressure Contours at $I=31$ , $x'/Tx'=0.04$ for $CR=5$ , 0% Cowl, $Re=2.15$ million/ft	246
Figure 6.1.2.2:	Crossflow Velocity Vectors at $I=31$ , $x'/Tx'=0.04$ for $CR=5$ , 0% Cowl, $Re=2.15$ million/ft	247
Figure 6.1.2.3:	Pressure Contours at $I=35$ , $x'/Tx'=0.20$ for $CR=5$ , 0% Cowl, $Re=2.15$ million/ft	248
Figure 6.1.2.4:	Crossflow Velocity Vectors at $I=35$ , $x'/Tx'=0.20$ for $CR=5$ , 0% Cowl, $Re=2.15$ million/ft	249
Figure 6.1.2.5:	Pressure Contours at $I=40$ , $x'/Tx'=0.40$ for $CR=5$ , 0% Cowl, $Re=2.15$ million/ft	250

Figure 6.1.2.6:	Crossflow Velocity Vectors at $I=40$ , $x'/Tx'=0.40$ for $CR=5$ , 0% Cowl, $Re=2.15$ million/ft	251
Figure 6.1.2.7:	Particle Traces at $I=40$ , $x'/Tx'=0.40$ for $CR=5$ , 0% Cowl, $Re=2.15$ million/ft	252
Figure 6.1.2.8:	Pressure Contours at $I=45$ , $x'/Tx'=0.60$ for $CR=5$ , 0% Cowl, $Re=2.15$ million/ft	253
Figure 6.1.2.9:	Crossflow Velocity Vectors at $I=45$ , $x'/Tx'=0.60$ for $CR=5$ , 0% Cowl, $Re=2.15$ million/ft	254
Figure 6.1.2.10:	Particle Traces at $I=45$ , $x'/Tx'=0.60$ for $CR=5$ , 0% Cowl, $Re=2.15$ million/ft	255
Figure 6.1.2.11:	Pressure Contours at $I=50$ , $x'/Tx'=0.79$ for $CR=5$ , 0% Cowl, $Re=2.15$ million/ft	256
Figure 6.1.2.12:	Crossflow Velocity Vectors at $I=50$ , $x'/Tx'=0.79$ for $CR=5$ , 0% Cowl, $Re=2.15$ million/ft	257
Figure 6.1.2.13:	Particle Traces at $I=50$ , $x'/Tx'=0.79$ for $CR=5$ , 0% Cowl, $Re=2.15$ million/ft	258
Figure 6.1.2.14:	Pressure Contours at $I=52$ , $x'/Tx'=0.87$ for $CR=5$ , 0% Cowl, $Re=2.15$ million/ft	259
Figure 6.1.2.15:	Crossflow Velocity Vectors at $I=52$ , $x'/Tx'=0.87$ for $CR=5$ , 0% Cowl, $Re=2.15$ million/ft	260
Figure 6.1.2.16:	Particle Traces at $I=52$ , $x'/Tx'=0.87$ for $CR=5$ , 0% Cowl, $Re=2.15$ million/ft	261
Figure 6.1.2.17:	Pressure Contours at $I=54$ , $x'/Tx'=0.96$ for $CR=5$ , 0% Cowl, $Re=2.15$ million/ft	262
Figure 6.1.2.18:	Crossflow Velocity Vectors at $I=54$ , $x'/Tx'=0.96$ for $CR=5$ , 0% Cowl, $Re=2.15$ million/ft	263
Figure 6.1.2.19:	Particle Traces at $I=54$ , $x'/Tx'=0.96$ for $CR=5$ , 0% Cowl, $Re=2.15$ million/ft	264
Figure 6.1.2.20:	Pressure Contours at $I=55$ , $x'/Tx'=1.00$ for $CR=5$ , 0% Cowl, $Re=2.15$ million/ft	265
Figure 6.1.2.21:	Crossflow Velocity Vectors at $I=55$ , $x'/Tx'=1.00$ for $CR=5$ , 0% Cowl, $Re=2.15$ million/ft	266
Figure 6.1.2.22:	Particle Traces at $I=55$ , $x'/Tx'=1.00$ for $CR=5$ , 0% Cowl, $Re=2.15$ million/ft	267
Figure 6.1.2.23:	Pressure Contours at $I=56$ , $xs'/Te'=0.06$ for $CR=5$ , 0% Cowl, $Re=2.15$ million/ft	268
Figure 6.1.2.24:	Crossflow Velocity Vectors at $I=56$ , $xs'/Te'=0.06$ for $CR=5$ , 0% Cowl, $Re=2.15$ million/ft	269
Figure 6.1.2.25:	Particle Traces at $I=56$ , $xs'/Te'=0.06$ for $CR=5$ , 0% Cowl, $Re=2.15$ million/ft	270
Figure 6.1.2.26:	Pressure Contours at $I=60$ , $xs'/Te'=0.29$ for $CR=5$ , 0% Cowl, $Re=2.15$ million/ft	271
Figure 6.1.2.27:	Crossflow Velocity Vectors at $I=60$ , $xs'/Te'=0.29$ for $CR=5$ , 0% Cowl, $Re=2.15$ million/ft	272
Figure 6.1.2.28:	Particle Traces at $I=60$ , $xs'/Te'=0.29$ for $CR=5$ , 0% Cowl, $Re=2.15$ million/ft	273
Figure 6.1.2.29:	Pressure Contours at $I=65$ , $xs'/Te'=0.58$ for $CR=5$ , 0% Cowl, $Re=2.15$ million/ft	274
Figure 6.1.2.30:	Crossflow Velocity Vectors at $I=65$ , $xs'/Te'=0.58$ for $CR=5$ , 0% Cowl, $Re=2.15$ million/ft	275
Figure 6.1.2.31:	Particle Traces at $I=65$ , $xs'/Te'=0.58$ for $CR=5$ , 0% Cowl, $Re=2.15$ million/ft	276

Figure 6.1.2.32:	Pressure Contours at $I=72$ , $x_s'/T_e'=1.00$ (Exit Plane) for $CR=5$ , 0% Cowl, $Re=2.15$ million/ft	277
Figure 6.1.2.33:	Crossflow Velocity Vectors at $I=72$ , $x_s'/T_e'=1.00$ (Exit Plane) for $CR=5$ , 0% Cowl, $Re=2.15$ million/ft	278
Figure 6.1.2.34:	Particle Traces at $I=72$ , $x_s'/T_e'=1.00$ (Exit Plane) for $CR=5$ , 0% Cowl, $Re=2.15$ million/ft	279
Figure 6.1.3.1:	Pressure Contours at $I=31$ , $x'/Tx'=0.04$ for $CR=9$ , 0% Cowl, $Re=2.15$ million/ft	280
Figure 6.1.3.2:	Crossflow Velocity Vectors at $I=31$ , $x'/Tx'=0.04$ for $CR=9$ , 0% Cowl, $Re=2.15$ million/ft	281
Figure 6.1.3.3:	Pressure Contours at $I=35$ , $x'/Tx'=0.20$ for $CR=9$ , 0% Cowl, $Re=2.15$ million/ft	282
Figure 6.1.3.4:	Crossflow Velocity Vectors at $I=35$ , $x'/Tx'=0.20$ for $CR=9$ , 0% Cowl, $Re=2.15$ million/ft	283
Figure 6.1.3.5:	Pressure Contours at $I=40$ , $x'/Tx'=0.40$ for $CR=9$ , 0% Cowl, $Re=2.15$ million/ft	284
Figure 6.1.3.6:	Crossflow Velocity Vectors at $I=40$ , $x'/Tx'=0.40$ for $CR=9$ , 0% Cowl, $Re=2.15$ million/ft	285
Figure 6.1.3.7:	Particle Traces at $I=40$ , $x'/Tx'=0.40$ for $CR=9$ , 0% Cowl, $Re=2.15$ million/ft	286
Figure 6.1.3.8:	Pressure Contours at $I=45$ , $x'/Tx'=0.60$ for $CR=9$ , 0% Cowl, $Re=2.15$ million/ft	287
Figure 6.1.3.9:	Crossflow Velocity Vectors at $I=45$ , $x'/Tx'=0.60$ for $CR=9$ , 0% Cowl, $Re=2.15$ million/ft	288
Figure 6.1.3.10:	Particle Traces at $I=45$ , $x'/Tx'=0.60$ for $CR=9$ , 0% Cowl, $Re=2.15$ million/ft	289
Figure 6.1.3.11:	Pressure Contours at $I=50$ , $x'/Tx'=0.79$ for $CR=9$ , 0% Cowl, $Re=2.15$ million/ft	290
Figure 6.1.3.12:	Crossflow Velocity Vectors at $I=50$ , $x'/Tx'=0.79$ for $CR=9$ , 0% Cowl, $Re=2.15$ million/ft	291
Figure 6.1.3.13:	Particle Traces at $I=50$ , $x'/Tx'=0.79$ for $CR=9$ , 0% Cowl, $Re=2.15$ million/ft	292
Figure 6.1.3.14:	Pressure Contours at $I=52$ , $x'/Tx'=0.87$ for $CR=9$ , 0% Cowl, $Re=2.15$ million/ft	293
Figure 6.1.3.15:	Crossflow Velocity Vectors at $I=52$ , $x'/Tx'=0.87$ for $CR=9$ , 0% Cowl, $Re=2.15$ million/ft	294
Figure 6.1.3.16:	Particle Traces at $I=52$ , $x'/Tx'=0.87$ for $CR=9$ , 0% Cowl, $Re=2.15$ million/ft	295
Figure 6.1.3.17:	Pressure Contours at $I=54$ , $x'/Tx'=0.96$ for $CR=9$ , 0% Cowl, $Re=2.15$ million/ft	296
Figure 6.1.3.18:	Crossflow Velocity Vectors at $I=54$ , $x'/Tx'=0.96$ for $CR=9$ , 0% Cowl, $Re=2.15$ million/ft	297
Figure 6.1.3.19:	Particle Traces at $I=54$ , $x'/Tx'=0.96$ for $CR=9$ , 0% Cowl, $Re=2.15$ million/ft	298
Figure 6.1.3.20:	Pressure Contours at $I=55$ , $x'/Tx'=1.00$ for $CR=9$ , 0% Cowl, $Re=2.15$ million/ft	299
Figure 6.1.3.21:	Crossflow Velocity Vectors at $I=55$ , $x'/Tx'=1.00$ for $CR=9$ , 0% Cowl, $Re=2.15$ million/ft	300
Figure 6.1.3.22:	Particle Traces at $I=55$ , $x'/Tx'=1.00$ for $CR=9$ , 0% Cowl, $Re=2.15$ million/ft	301

Figure 6.1.3.23:	Pressure Contours at $I=56$ , $x_s'/Te'=0.06$ for $CR=9$ , 0% Cowl, $Re=2.15$ million/ft	302
Figure 6.1.3.24:	Crossflow Velocity Vectors at $I=56$ , $x_s'/Te'=0.06$ for $CR=9$ , 0% Cowl, $Re=2.15$ million/ft	303
Figure 6.1.3.25:	Crossflow Velocity Vectors Near Cowl at $I=56$ , $x_s'/Te'=0.06$ for $CR=9$ , 0% Cowl, $Re=2.15$ million/ft	304
Figure 6.1.3.26:	Crossflow Velocity Vectors Near Baseplate for $I=56$ , $x_s'/Te'=0.06$ for $CR=9$ , 0% Cowl, $Re=2.15$ million/ft	305
Figure 6.1.3.27:	Particle Traces at $I=56$ , $x_s'/Te'=0.06$ for $CR=9$ , 0% Cowl, $Re=2.15$ million/ft	306
Figure 6.1.3.28:	Pressure Contours at $I=60$ , $x_s'/Te'=0.29$ for $CR=9$ , 0% Cowl, $Re=2.15$ million/ft	307
Figure 6.1.3.29:	Crossflow Velocity Vectors at $I=60$ , $x_s'/Te'=0.29$ for $CR=9$ , 0% Cowl, $Re=2.15$ million/ft	308
Figure 6.1.3.30:	Crossflow Velocity Vectors Near Cowl at $I=60$ , $x_s'/Te'=0.29$ for $CR=9$ , 0% Cowl, $Re=2.15$ million/ft	309
Figure 6.1.3.31:	Crossflow Velocity Vectors Near Baseplate at $I=60$ , $x_s'/Te'=0.29$ for $CR=9$ , 0% Cowl, $Re=2.15$ million/ft	310
Figure 6.1.3.32:	Particle Traces at $I=60$ , $x_s'/Te'=0.29$ for $CR=9$ , 0% Cowl, $Re=2.15$ million/ft	311
Figure 6.1.3.33:	Pressure Contours at $I=65$ , $x_s'/Te'=0.58$ for $CR=9$ , 0% Cowl, $Re=2.15$ million/ft	312
Figure 6.1.3.34:	Crossflow Velocity Vectors at $I=65$ , $x_s'/Te'=0.58$ for $CR=9$ , 0% Cowl, $Re=2.15$ million/ft	313
Figure 6.1.3.35:	Particle Traces at $I=65$ , $x_s'/Te'=0.58$ for $CR=9$ , 0% Cowl, $Re=2.15$ million/ft	314
Figure 6.1.3.36:	Pressure Contours at $I=72$ , $x_s'/Te'=1.00$ (Exit Plane) for $CR=9$ , 0% Cowl, $Re=2.15$ million/ft	315
Figure 6.1.3.37:	Crossflow Velocity Vectors at $I=72$ , $x_s'/Te'=1.00$ (Exit Plane) for $CR=9$ , 0% Cowl, $Re=2.15$ million/ft	316
Figure 6.1.3.38:	Particle Traces at $I=72$ , $x_s'/Te'=1.00$ (Exit Plane) for $CR=9$ , 0% Cowl, $Re=2.15$ million/ft	317
Figure 6.2.1(a):	Pressure Contours at $Z/H=0.25$ for $CR=3$ , $Re=2.15$ million/ft, 50% Cowl	318
Figure 6.2.1(b):	Pressure Contours at $Z/H=0.50$ for $CR=3$ , $Re=2.15$ million/ft, 50% Cowl	318
Figure 6.2.1(c):	Pressure Contours at $Z/H=0.75$ for $CR=3$ , $Re=2.15$ million/ft, 50% Cowl	318
Figure 6.2.2:	Sidewall and Baseplate Pressure Contours for $CR=3$ , $Re=2.15$ million/ft, 50% Cowl	319
Figure 6.2.3:	Centerline Pressure Contours for $CR=3$ , $Re=2.15$ million/ft, 50% Cowl	320
Figure 6.2.4:	Streamwise Separation ( $U<0$ ) for $CR=3$ , $Re=2.15$ million/ft, 50% Cowl	321
Figure 6.2.5:	Simulated Oil Flow for $CR=3$ , $Re=2.15$ million /ft, 50% Cowl	322
Figure 6.2.6:	Exit Plane Pressure Contours for $CR=3$ , $Re=2.15$ million/ft, 50% Cowl	323
Figure 6.2.7:	Exit Plane Mach Number Contours for $CR=3$ , $Re=2.15$ million/ft, 50% Cowl	324
Figure 6.2.2.1:	Pressure Contours at $I=43$ , $x'/Tx'=0.50$ for $CR=3$ , 50% Cowl, $Re=2.15$ million/ft	325

Figure 6.2.2.2:	Crossflow Velocity Vectors at $I=43$ , $x'/Tx'=0.50$ for $CR=3$ , 50% Cowl, $Re=2.15$ million/ft	326
Figure 6.2.2.3:	Pressure Contours at $I=45$ , $x'/Tx'=0.60$ for $CR=3$ , 50% Cowl, $Re=2.15$ million/ft	327
Figure 6.2.2.4:	Crossflow Velocity Vectors at $I=45$ , $x'/Tx'=0.60$ for $CR=3$ , 50% Cowl, $Re=2.15$ million/ft	328
Figure 6.2.2.5:	Pressure Contours at $I=50$ , $x'/Tx'=0.79$ for $CR=3$ , 50% Cowl, $Re=2.15$ million/ft	329
Figure 6.2.2.6:	Crossflow Velocity Vectors at $I=50$ , $x'/Tx'=0.79$ for $CR=3$ , 50% Cowl, $Re=2.15$ million/ft	330
Figure 6.2.2.7:	Pressure Contours at $I=52$ , $x'/Tx'=0.87$ for $CR=3$ , 50% Cowl, $Re=2.15$ million/ft	331
Figure 6.2.2.8:	Crossflow Velocity Vectors at $I=52$ , $x'/Tx'=0.87$ for $CR=3$ , 50% Cowl, $Re=2.15$ million/ft	332
Figure 6.2.2.9:	Pressure Contours at $I=55$ , $x'/Tx'=1.00$ for $CR=3$ , 50% Cowl, $Re=2.15$ million/ft	333
Figure 6.2.2.10:	Crossflow Velocity Vectors at $I=55$ , $x'/Tx'=1.00$ for $CR=3$ , 50% Cowl, $Re=2.15$ million/ft	334
Figure 6.2.2.11:	Pressure Contours at $I=60$ , $xs'/Te'=0.29$ for $CR=3$ , 50% Cowl, $Re=2.15$ million/ft	335
Figure 6.2.2.12:	Crossflow Velocity Vectors at $I=60$ , $xs'/Te'=0.29$ for $CR=3$ , 50% Cowl, $Re=2.15$ million/ft	336
Figure 6.2.2.13:	Pressure Contours at $I=72$ , $xs'/Te'=1.00$ (Exit Plane) for $CR=3$ , 50% Cowl, $Re=2.15$ million/ft	337
Figure 6.2.2.14:	Crossflow Velocity Vectors at $I=72$ , $xs'/Te'=1.00$ (Exit Plane) for $CR=3$ , 50% Cowl, $Re=2.15$ million/ft	338
Figure 6.3.1(a):	Pressure Contours at $Z/H=0.25$ for $CR=3$ , $Re=0.55$ million/ft, 0% Cowl	339
Figure 6.3.1(b):	Pressure Contours at $Z/H=0.50$ for $CR=3$ , $Re=0.55$ million/ft, 0% Cowl	339
Figure 6.3.1(c):	Pressure Contours at $Z/H=0.75$ for $CR=3$ , $Re=0.55$ million/ft, 0% Cowl	339
Figure 6.3.2:	Sidewall and Baseplate Pressure Contours for $CR=3$ , $Re=0.55$ million/ft, 0% Cowl	340
Figure 6.3.3:	Centerline Pressure Contours for $CR=3$ , $Re=0.55$ million/ft, 0% Cowl	341
Figure 6.3.4:	Streamwise Separation ( $U<0$ ) for $CR=3$ , $Re=0.55$ million/ft, 0% Cowl	342
Figure 6.3.5:	Simulated Oil Flow for $CR=3$ , $Re=0.55$ million /ft, 0% Cowl	343
Figure 6.3.6:	Exit Plane Pressure Contours for $CR=3$ , $Re=0.55$ million/ft, 0% Cowl	344
Figure 6.3.7:	Exit Plane Mach Number Contours for $CR=3$ , $Re=0.55$ million/ft, 0% Cowl	345
Figure 6.3.2.1:	Pressure Contours at $I=31$ , $x'/Tx'=0.04$ for $CR=3$ , 0% Cowl, $Re=0.55$ million/ft	346



Figure 6.3.2.2:	Crossflow Velocity Vectors at $I=31$ , $x'/Tx'=0.04$ for $CR=3$ , 0% Cowl, $Re=0.55$ million/ft	347
Figure 6.3.2.3:	Pressure Contours at $I=40$ , $x'/Tx'=0.40$ for $CR=3$ , 0% Cowl, $Re=0.55$ million/ft	348
Figure 6.3.2.4:	Crossflow Velocity Vectors at $I=40$ , $x'/Tx'=0.40$ for $CR=3$ , 0% Cowl, $Re=0.55$ million/ft	349
Figure 6.3.2.5:	Pressure Contours at $I=50$ , $x'/Tx'=0.79$ for $CR=3$ , 0% Cowl, $Re=0.55$ million/ft	350
Figure 6.3.2.6:	Crossflow Velocity Vectors at $I=50$ , $x'/Tx'=0.79$ for $CR=3$ , 0% Cowl, $Re=0.55$ million/ft	351
Figure 6.3.2.7:	Particle Traces at $I=50$ , $x'/Tx'=0.79$ for $CR=3$ , 0% Cowl, $Re=0.55$ million/ft	352
Figure 6.3.2.8:	Pressure Contours at $I=54$ , $x'/Tx'=0.96$ for $CR=3$ , 0% Cowl, $Re=0.55$ million/ft	353
Figure 6.3.2.9:	Crossflow Velocity Vectors at $I=54$ , $x'/Tx'=0.96$ for $CR=3$ , 0% Cowl, $Re=0.55$ million/ft	354
Figure 6.3.2.10:	Pressure Contours at $I=55$ , $x'/Tx'=1.00$ for $CR=3$ , 0% Cowl, $Re=0.55$ million/ft	355
Figure 6.3.2.11:	Crossflow Velocity Vectors at $I=55$ , $x'/Tx'=1.00$ for $CR=3$ , 0% Cowl, $Re=0.55$ million/ft	356
Figure 6.3.2.12:	Particle Traces at $I=55$ , $x'/Tx'=1.00$ for $CR=3$ , 0% Cowl, $Re=0.55$ million/ft	357
Figure 6.3.2.13:	Pressure Contours at $I=72$ , $xs'/Te'=1.00$ (Exit Plane) for $CR=3$ , 0% Cowl, $Re=0.55$ million/ft	358
Figure 6.3.2.14:	Crossflow Velocity Vectors at $I=72$ , $xs'/Te'=1.00$ (Exit Plane) for $CR=3$ , 0% Cowl, $Re=0.55$ million/ft	359
Figure 6.3.2.15:	Particle Traces at $I=72$ , $xs'/Te'=1.00$ (Exit Plane) for $CR=3$ , 0% Cowl, $Re=0.55$ million/ft	360
Figure 7.1.1.1(a):	$P/P_{inf}$ Baseplate Contours, $CR=3$ , $Re=0.55$ million/ft, 0% Cowl, (run64)	361
Figure 7.1.1.1(b):	$P/P_{inf}$ Sidewall Contours, $CR=3$ , $Re=0.55$ million/ft, 0% Cowl, (run64)	361
Figure 7.1.1.2(a):	$P/P_{inf}$ Baseplate Contours, $CR=5$ , $Re=0.55$ million/ft, 0% Cowl, (run44)	362
Figure 7.1.1.2(b):	$P/P_{inf}$ Sidewall Contours, $CR=5$ , $Re=0.55$ million/ft, 0% Cowl, (run44)	362
Figure 7.1.1.3(a):	$P/P_{inf}$ Baseplate Contours, $CR=9$ , $Re=0.55$ million/ft, 0% Cowl, (run47)	363
Figure 7.1.1.3(b):	$P/P_{inf}$ Sidewall Contours, $CR=9$ , $Re=0.55$ million/ft, 0% Cowl, (run47)	363
Figure 7.1.1.4(a):	$P/P_{inf}$ Baseplate Contours, $CR=3$ , $Re=0.55$ million/ft, 25% Cowl, (run61)	364
Figure 7.1.1.4(b):	$P/P_{inf}$ Sidewall Contours, $CR=3$ , $Re=0.55$ million/ft, 25% Cowl, (run61)	364
Figure 7.1.1.5(a):	$P/P_{inf}$ Baseplate Contours, $CR=5$ , $Re=0.55$ million/ft, 25% Cowl, (run41)	365
Figure 7.1.1.5(b):	$P/P_{inf}$ Sidewall Contours, $CR=5$ , $Re=0.55$ million/ft, 25% Cowl, (run41)	365
Figure 7.1.1.6(a):	$P/P_{inf}$ Baseplate Contours, $CR=9$ , $Re=0.55$ million/ft, 25% Cowl, (run50)	366
Figure 7.1.1.6(b):	$P/P_{inf}$ Sidewall Contours, $CR=9$ , $Re=0.55$ million/ft, 25% Cowl, (run50)	366
Figure 7.1.1.7(a):	$P/P_{inf}$ Baseplate Contours, $CR=3$ , $Re=0.55$ million/ft, 50% Cowl, (run58)	367

Figure 7.1.1.7(b): P/Pinf Sidewall Contours, CR=3, Re=0.55 million/ft, 50% Cowl, (run58)	367
Figure 7.1.1.8(a): P/Pinf Baseplate Contours, CR=5, Re=0.55 million/ft, 50% Cowl, (run37)	368
Figure 7.1.1.8(b): P/Pinf Sidewall Contours, CR=5, Re=0.55 million/ft, 50% Cowl, (run37)	368
Figure 7.1.1.9(a): P/Pinf Baseplate Contours, CR=5, Re=0.55 million/ft, 50% Cowl, (run38)	369
Figure 7.1.1.9(b): P/Pinf Sidewall Contours, CR=5, Re=0.55 million/ft, 50% Cowl, (run38)	369
Figure 7.1.1.10(a): P/Pinf Baseplate Contours, CR=9, Re=0.55 million/ft, 50% Cowl, (run55)	370
Figure 7.1.2.10(b): P/Pinf Sidewall Contours, CR=9, Re=0.55 million/ft, 50% Cowl, (run55)	370
Figure 7.1.2.1(a): P/Pinf Baseplate Contours, CR=3, Re=1.14 million/ft, 0% Cowl, (run65)	371
Figure 7.1.2.1(b): P/Pinf Sidewall Contours, CR=3, Re=1.14 million/ft, 0% Cowl, (run65)	371
Figure 7.1.2.2(a): P/Pinf Baseplate Contours, CR=3, Re=1.14 million/ft, 0% Cowl, (run67)	372
Figure 7.1.2.2(b): P/Pinf Sidewall Contours, CR=3, Re=1.14 million/ft, 0% Cowl, (run67)	372
Figure 7.1.2.3(a): P/Pinf Baseplate Contours, CR=5, Re=1.14 million/ft, 0% Cowl, (run45)	373
Figure 7.1.2.3(b): P/Pinf Sidewall Contours, CR=5, Re=1.14 million/ft, 0% Cowl, (run45)	373
Figure 7.1.2.4(a): P/Pinf Baseplate Contours, CR=9, Re=1.14 million/ft, 0% Cowl, (run48)	374
Figure 7.1.2.4(b): P/Pinf Sidewall Contours, CR=9, Re=1.14 million/ft, 0% Cowl, (run48)	374
Figure 7.1.2.5(a): P/Pinf Baseplate Contours, CR=3, Re=1.14 million/ft, 25% Cowl, (run63)	375
Figure 7.1.2.5(b): P/Pinf Sidewall Contours, CR=3, Re=1.14 million/ft, 25% Cowl, (run63)	375
Figure 7.1.2.6(a): P/Pinf Baseplate Contours, CR=5, Re=1.14 million/ft, 25% Cowl, (run42)	376
Figure 7.1.2.6(b): P/Pinf Sidewall Contours, CR=5, Re=1.14 million/ft, 25% Cowl, (run42)	376
Figure 7.1.2.7(a): P/Pinf Baseplate Contours, CR=9, Re=1.14 million/ft, 25% Cowl, (run52)	377
Figure 7.1.2.7(b): P/Pinf Sidewall Contours, CR=9, Re=1.14 million/ft, 25% Cowl, (run52)	377
Figure 7.1.2.8(a): P/Pinf Baseplate Contours, CR=3, Re=1.14 million/ft, 50% Cowl, (run59)	378
Figure 7.1.2.8(b): P/Pinf Sidewall Contours, CR=3, Re=1.14 million/ft, 50% Cowl, (run59)	378
Figure 7.1.2.9(a): P/Pinf Baseplate Contours, CR=5, Re=1.14 million/ft, 50% Cowl, (run39)	379
Figure 7.1.2.9(b): P/Pinf Sidewall Contours, CR=5, Re=1.14 million/ft, 50% Cowl, (run39)	379
Figure 7.1.2.10(a): P/Pinf Baseplate Contours, CR=9, Re=1.14 million/ft, 50% Cowl, (run56)	380
Figure 7.1.2.10(b): P/Pinf Sidewall Contours, CR=9, Re=1.14 million/ft, 50% Cowl, (run56)	380
Figure 7.1.2.11(a): P/Pinf Baseplate Contours, CR=3, Re=2.15 million/ft, 0% Cowl, (run66)	381
Figure 7.1.2.11(b): P/Pinf Sidewall Contours, CR=3, Re=2.15 million/ft, 0% Cowl, (run66)	381
Figure 7.1.2.12(a): P/Pinf Baseplate Contours, CR=5, Re=2.15 million/ft, 0% Cowl, (run46)	382

Figure 7.1.2.12(b): P/Pinf Sidewall Contours, CR=5, Re=2.15 million/ft, 0% Cowl, (run46)	382
Figure 7.1.2.13(a): P/Pinf Baseplate Contours, CR=9, Re=2.15 million/ft, 0% Cowl, (run49)	383
Figure 7.1.2.13(b): P/Pinf Sidewall Contours, CR=9, Re=2.15 million/ft, 0% Cowl, (run49)	383
Figure 7.1.2.14(a): P/Pinf Baseplate Contours, CR=3, Re=2.15 million/ft, 25% Cowl, (run62)	384
Figure 7.1.2.14(b): P/Pinf Sidewall Contours, CR=3, Re=2.15 million/ft, 25% Cowl, (run62)	384
Figure 7.1.2.15(a): P/Pinf Baseplate Contours, CR=5, Re=2.15 million/ft, 25% Cowl, (run43)	385
Figure 7.1.2.15(b): P/Pinf Sidewall Contours, CR=5, Re=2.15 million/ft, 25% Cowl, (run43)	385
Figure 7.1.2.16(a): P/Pinf Baseplate Contours, CR=9, Re=2.15 million/ft, 25% Cowl, (run53)	386
Figure 7.1.2.16(b): P/Pinf Sidewall Contours, CR=9, Re=2.15 million/ft, 25% Cowl, (run53)	386
Figure 7.1.2.17(a): P/Pinf Baseplate Contours, CR=9, Re=2.15 million/ft, 25% Cowl, (run54)	387
Figure 7.1.2.17(b): P/Pinf Sidewall Contours, CR=9, Re=2.15 million/ft, 25% Cowl, (run54)	387
Figure 7.1.2.18(a): P/Pinf Baseplate Contours, CR=3, Re=2.15 million/ft, 50% Cowl, (run60)	388
Figure 7.1.2.18(b): P/Pinf Sidewall Contours, CR=3, Re=2.15 million/ft, 50% Cowl, (run60)	388
Figure 7.1.2.19(a): P/Pinf Baseplate Contours, CR=5, Re=2.15 million/ft, 50% Cowl, (run40)	389
Figure 7.1.2.19(b): P/Pinf Sidewall Contours, CR=5, Re=2.15 million/ft, 50% Cowl, (run40)	389
Figure 7.1.2.20(a): P/Pinf Baseplate Contours, CR=9, Re=2.15 million/ft, 50% Cowl, (run57)	390
Figure 7.1.2.20(b): P/Pinf Sidewall Contours, CR=9, Re=2.15 million/ft, 50% Cowl, (run57)	390
Figure 7.2.1.1: CR Effects, Re=2.15million/ft, 0% Cowl, Centerline Pressures	391
Figure 7.2.1.2: CR Effects, Re=2.15million/ft, 0% Cowl, CR=3 Centerline Pressures	391
Figure 7.2.1.3: CR Effects, Re=2.15million/ft, 0% Cowl, CR=5 Centerline Pressures	391
Figure 7.2.1.4: CR Effects, Re=2.15million/ft, 0% Cowl, CR=9 Centerline Pressures	391
Figure 7.2.1.5: CR Effects, Re=2.15million/ft, 0% Cowl, Baseplate Pressures	391
Figure 7.2.1.6: CR Effects, Re=2.15million/ft, 0% Cowl, Baseplate Pressures	391
Figure 7.2.1.7: CR Effects, Re=2.15million/ft, 0% Cowl, Baseplate Pressures	391
Figure 7.2.1.8: CR Effects, Re=2.15million/ft, 0% Cowl, Baseplate Pressures	391
Figure 7.2.1.9: CR Effects, Re=2.15million/ft, 0% Cowl, Baseplate Pressures	391
Figure 7.2.1.10: CR Effects, Re=2.15million/ft, 0% Cowl, Baseplate Pressures	392
Figure 7.2.1.11: CR Effects, Re=2.15million/ft, 0% Cowl, Baseplate Pressures	392
Figure 7.2.1.12: CR Effects, Re=2.15million/ft, 0% Cowl, Baseplate Pressures	392
Figure 7.2.1.13: CR Effects, Re=2.15million/ft, 0% Cowl, Baseplate Pressures	392
Figure 7.2.1.14: CR Effects, Re=2.15million/ft, 0% Cowl, Baseplate Pressures	393

Figure 7.2.1.15:	CR Effects, Re=2.15million/ft, 0% Cowl, Baseplate Pressures	392
Figure 7.2.1.16:	CR Effects, Re=2.15million/ft, 0% Cowl, Baseplate Pressures	392
Figure 7.2.1.17:	CR Effects, Re=2.15million/ft, 0% Cowl, Baseplate Pressures	392
Figure 7.2.1.18:	CR Effects, Re=2.15million/ft, 0% Cowl, Baseplate Pressures	392
Figure 7.2.1.19:	CR Effects, Re=2.15million/ft, 0% Cowl, Baseplate Pressures	393
Figure 7.2.1.20:	CR Effects, Re=2.15million/ft, 0% Cowl, Baseplate Pressures	393
Figure 7.2.1.21:	CR Effects, Re=2.15million/ft, 0% Cowl, Baseplate Pressures	393
Figure 7.2.1.22:	CR Effects, Re=2.15million/ft, 0% Cowl, Baseplate Pressures	393
Figure 7.2.1.23:	CR Effects, Re=2.15million/ft, 0% Cowl, Baseplate Pressures	393
Figure 7.2.1.24:	CR Effects, Re=2.15million/ft, 0% Cowl, Baseplate Pressures	393
Figure 7.2.1.25:	CR Effects, Re=2.15million/ft, 0% Cowl, Baseplate Pressures	393
Figure 7.2.1.26:	CR Effects, Re=2.15million/ft, 0% Cowl, Baseplate Pressures	393
Figure 7.2.1.27:	CR Effects, Re=2.15million/ft, 0% Cowl, Cowl Pressures	393
Figure 7.2.1.28:	CR Effects, Re=2.15million/ft, 0% Cowl, Sidewall Centerline Pressures	394
Figure 7.2.1.29:	CR Effects, Re=2.15million/ft, 0% Cowl, Sidewall Centerline Pressures	394
Figure 7.2.1.30:	CR Effects, Re=2.15million/ft, 0% Cowl, Sidewall Pressures	394
Figure 7.2.1.31:	CR Effects, Re=2.15million/ft, 0% Cowl, Sidewall Pressures	394
Figure 7.2.1.32:	CR Effects, Re=2.15million/ft, 0% Cowl, Sidewall Pressures	394
Figure 7.2.1.33:	CR Effects, Re=2.15million/ft, 0% Cowl, Sidewall Pressures	394
Figure 7.2.1.34:	CR Effects, Re=2.15million/ft, 0% Cowl, Sidewall Pressures	394
Figure 7.2.1.35:	CR Effects, Re=2.15million/ft, 0% Cowl, Sidewall Pressures	394
Figure 7.2.1.36:	CR Effects, Re=2.15million/ft, 0% Cowl, Sidewall Pressures	394
Figure 7.2.1.37:	CR Effects, Re=2.15million/ft, 0% Cowl, Sidewall Pressures	395
Figure 7.2.1.38:	CR Effects, Re=2.15million/ft, 0% Cowl, Sidewall Pressures	395
Figure 7.2.1.39:	CR Effects, Re=2.15million/ft, 0% Cowl, Sidewall Pressures	395
Figure 7.2.1.40:	CR Effects, Re=2.15million/ft, 0% Cowl, Sidewall Pressures	395
Figure 7.2.1.41:	CR Effects, Re=2.15million/ft, 0% Cowl, Sidewall Pressures	395
Figure 7.2.1.42:	CR Effects, Re=2.15million/ft, 0% Cowl, Sidewall Pressures	395
Figure 7.2.1.43:	CR Effects, Re=2.15million/ft, 0% Cowl, Sidewall Pressures	395
Figure 7.2.1.44:	CR Effects, Re=2.15million/ft, 0% Cowl, Sidewall Pressures	395
Figure 7.2.1.45:	CR Effects, Re=2.15million/ft, 0% Cowl, Sidewall Pressures	395

Figure 7.2.1.46:	CR Effects, Re=2.15million/ft, 0% Cowl, Sidewall Pressures	396
Figure 7.2.1.47:	CR Effects, Re=2.15million/ft, 0% Cowl, Sidewall Pressures	396
Figure 7.2.1.48:	CR Effects, Re=2.15million/ft, 0% Cowl, Sidewall Pressures	396
Figure 7.2.1.49:	CR Effects, Re=2.15million/ft, 0% Cowl, Sidewall Pressures	396
Figure 7.2.1.50:	CR Effects, Re=2.15million/ft, 0% Cowl, Sidewall Pressures	396
Figure 7.2.1.51:	CR Effects, Re=2.15million/ft, 0% Cowl, Sidewall Pressures	396
Figure 7.2.1.52:	CR Effects, Re=2.15million/ft, 0% Cowl, Sidewall Pressures	396
Figure 7.2.1.53:	CR Effects, Re=2.15million/ft, 0% Cowl, Sidewall Pressures	396
Figure 7.2.1.54:	CR Effects, Re=2.15million/ft, 0% Cowl, Sidewall Pressures	396
Figure 7.2.1.55:	CR Effects, Re=1.14million/ft, 0% Cowl, Centerline Pressures	397
Figure 7.2.1.56:	CR Effects, Re=1.14million/ft, 0% Cowl, CR=3 Centerline Pressures	397
Figure 7.2.1.57:	CR Effects, Re=1.14million/ft, 0% Cowl, CR=5 Centerline Pressures	397
Figure 7.2.1.58:	CR Effects, Re=1.14million/ft, 0% Cowl, CR=9 Centerline Pressures	397
Figure 7.2.1.59:	CR Effects, Re=1.14million/ft, 0% Cowl, Baseplate Pressures	397
Figure 7.2.1.60:	CR Effects, Re=1.14million/ft, 0% Cowl, Baseplate Pressures	397
Figure 7.2.1.61:	CR Effects, Re=1.14million/ft, 0% Cowl, Baseplate Pressures	397
Figure 7.2.1.62:	CR Effects, Re=1.14million/ft, 0% Cowl, Baseplate Pressures	397
Figure 7.2.1.63:	CR Effects, Re=1.14million/ft, 0% Cowl, Baseplate Pressures	397
Figure 7.2.1.64:	CR Effects, Re=1.14million/ft, 0% Cowl, Baseplate Pressures	398
Figure 7.2.1.65:	CR Effects, Re=1.14million/ft, 0% Cowl, Baseplate Pressures	398
Figure 7.2.1.66:	CR Effects, Re=1.14million/ft, 0% Cowl, Baseplate Pressures	398
Figure 7.2.1.67:	CR Effects, Re=1.14million/ft, 0% Cowl, Baseplate Pressures	398
Figure 7.2.1.68:	CR Effects, Re=1.14million/ft, 0% Cowl, Baseplate Pressures	398
Figure 7.2.1.69:	CR Effects, Re=1.14million/ft, 0% Cowl, Baseplate Pressures	398
Figure 7.2.1.70:	CR Effects, Re=1.14million/ft, 0% Cowl, Baseplate Pressures	398
Figure 7.2.1.71:	CR Effects, Re=1.14million/ft, 0% Cowl, Baseplate Pressures	398
Figure 7.2.1.72:	CR Effects, Re=1.14million/ft, 0% Cowl, Baseplate Pressures	398
Figure 7.2.1.73:	CR Effects, Re=1.14million/ft, 0% Cowl, Baseplate Pressures	399
Figure 7.2.1.74:	CR Effects, Re=1.14million/ft, 0% Cowl, Baseplate Pressures	399
Figure 7.2.1.75:	CR Effects, Re=1.14million/ft, 0% Cowl, Baseplate Pressures	399
Figure 7.2.1.76:	CR Effects, Re=1.14million/ft, 0% Cowl, Baseplate Pressures	399

Figure 7.2.1.77:	CR Effects, Re=1.14million/ft, 0% Cowl, Baseplate Pressures	399
Figure 7.2.1.78:	CR Effects, Re=1.14million/ft, 0% Cowl, Baseplate Pressures	399
Figure 7.2.1.79:	CR Effects, Re=1.14million/ft, 0% Cowl, Baseplate Pressures	399
Figure 7.2.1.80:	CR Effects, Re=1.14million/ft, 0% Cowl, Baseplate Pressures	399
Figure 7.2.1.81:	CR Effects, Re=1.14million/ft, 0% Cowl, Cowl Pressures	399
Figure 7.2.1.82:	CR Effects, Re=1.14million/ft, 0% Cowl, Sidewall Centerline Pressures	400
Figure 7.2.1.83:	CR Effects, Re=1.14million/ft, 0% Cowl, Sidewall Centerline Pressures	400
Figure 7.2.1.84:	CR Effects, Re=1.14million/ft, 0% Cowl, Sidewall Pressures	400
Figure 7.2.1.85:	CR Effects, Re=1.14million/ft, 0% Cowl, Sidewall Pressures	400
Figure 7.2.1.86:	CR Effects, Re=1.14million/ft, 0% Cowl, Sidewall Pressures	400
Figure 7.2.1.87:	CR Effects, Re=1.14million/ft, 0% Cowl, Sidewall Pressures	400
Figure 7.2.1.88:	CR Effects, Re=1.14million/ft, 0% Cowl, Sidewall Pressures	400
Figure 7.2.1.89:	CR Effects, Re=1.14million/ft, 0% Cowl, Sidewall Pressures	400
Figure 7.2.1.90:	CR Effects, Re=1.14million/ft, 0% Cowl, Sidewall Pressures	400
Figure 7.2.1.91:	CR Effects, Re=1.14million/ft, 0% Cowl, Sidewall Pressures	401
Figure 7.2.1.92:	CR Effects, Re=1.14million/ft, 0% Cowl, Sidewall Pressures	401
Figure 7.2.1.93:	CR Effects, Re=1.14million/ft, 0% Cowl, Sidewall Pressures	401
Figure 7.2.1.94:	CR Effects, Re=1.14million/ft, 0% Cowl, Sidewall Pressures	401
Figure 7.2.1.95:	CR Effects, Re=1.14million/ft, 0% Cowl, Sidewall Pressures	401
Figure 7.2.1.96:	CR Effects, Re=1.14million/ft, 0% Cowl, Sidewall Pressures	401
Figure 7.2.1.97:	CR Effects, Re=1.14million/ft, 0% Cowl, Sidewall Pressures	401
Figure 7.2.1.98:	CR Effects, Re=1.14million/ft, 0% Cowl, Sidewall Pressures	401
Figure 7.2.1.99:	CR Effects, Re=1.14million/ft, 0% Cowl, Sidewall Pressures	401
Figure 7.2.1.100:	CR Effects, Re=1.14million/ft, 0% Cowl, Sidewall Pressures	402
Figure 7.2.1.101:	CR Effects, Re=1.14million/ft, 0% Cowl, Sidewall Pressures	402
Figure 7.2.1.102:	CR Effects, Re=1.14million/ft, 0% Cowl, Sidewall Pressures	402
Figure 7.2.1.103:	CR Effects, Re=1.14million/ft, 0% Cowl, Sidewall Pressures	402
Figure 7.2.1.104:	CR Effects, Re=1.14million/ft, 0% Cowl, Sidewall Pressures	402
Figure 7.2.1.105:	CR Effects, Re=1.14million/ft, 0% Cowl, Sidewall Pressures	402
Figure 7.2.1.106:	CR Effects, Re=1.14million/ft, 0% Cowl, Sidewall Pressures	402

Figure 7.2.1.107: CR Effects, Re=1.14million/ft, 0% Cowl, Sidewall Pressures	402
Figure 7.2.1.108: CR Effects, Re=1.14million/ft, 0% Cowl, Sidewall Pressures	402
Figure 7.2.1.109: CR Effects, Re=0.55million/ft, 0% Cowl, Centerline Pressures	403
Figure 7.2.1.110: CR Effects, Re=0.55million/ft, 0% Cowl, CR=3 Centerline Pressures	403
Figure 7.2.1.111: CR Effects, Re=0.55million/ft, 0% Cowl, CR=5 Centerline Pressures	403
Figure 7.2.1.112: CR Effects, Re=0.55million/ft, 0% Cowl, CR=9 Centerline Pressures	403
Figure 7.2.1.113: CR Effects, Re=0.55million/ft, 0% Cowl, Baseplate Pressures	403
Figure 7.2.1.114: CR Effects, Re=0.55million/ft, 0% Cowl, Baseplate Pressures	403
Figure 7.2.1.115: CR Effects, Re=0.55million/ft, 0% Cowl, Baseplate Pressures	403
Figure 7.2.1.116: CR Effects, Re=0.55million/ft, 0% Cowl, Baseplate Pressures	403
Figure 7.2.1.117: CR Effects, Re=0.55million/ft, 0% Cowl, Baseplate Pressures	403
Figure 7.2.1.118: CR Effects, Re=0.55million/ft, 0% Cowl, Baseplate Pressures	404
Figure 7.2.1.119: CR Effects, Re=0.55million/ft, 0% Cowl, Baseplate Pressures	404
Figure 7.2.1.120: CR Effects, Re=0.55million/ft, 0% Cowl, Baseplate Pressures	404
Figure 7.2.1.121: CR Effects, Re=0.55million/ft, 0% Cowl, Baseplate Pressures	404
Figure 7.2.1.122: CR Effects, Re=0.55million/ft, 0% Cowl, Baseplate Pressures	404
Figure 7.2.1.123: CR Effects, Re=0.55million/ft, 0% Cowl, Baseplate Pressures	404
Figure 7.2.1.124: CR Effects, Re=0.55million/ft, 0% Cowl, Baseplate Pressures	404
Figure 7.2.1.125: CR Effects, Re=0.55million/ft, 0% Cowl, Baseplate Pressures	404
Figure 7.2.1.126: CR Effects, Re=0.55million/ft, 0% Cowl, Baseplate Pressures	404
Figure 7.2.1.127: CR Effects, Re=0.55million/ft, 0% Cowl, Baseplate Pressures	405
Figure 7.2.1.128: CR Effects, Re=0.55million/ft, 0% Cowl, Baseplate Pressures	405
Figure 7.2.1.129: CR Effects, Re=0.55million/ft, 0% Cowl, Baseplate Pressures	405
Figure 7.2.1.130: CR Effects, Re=0.55million/ft, 0% Cowl, Baseplate Pressures	405
Figure 7.2.1.131: CR Effects, Re=0.55million/ft, 0% Cowl, Baseplate Pressures	405
Figure 7.2.1.132: CR Effects, Re=0.55million/ft, 0% Cowl, Baseplate Pressures	405
Figure 7.2.1.133: CR Effects, Re=0.55million/ft, 0% Cowl, Baseplate Pressures	405
Figure 7.2.1.134: CR Effects, Re=0.55million/ft, 0% Cowl, Baseplate Pressures	405
Figure 7.2.1.135: CR Effects, Re=0.55million/ft, 0% Cowl, Cowl Pressures	405
Figure 7.2.1.136: CR Effects, Re=0.55million/ft, 0% Cowl, Sidewall Centerline Pressures	406
Figure 7.2.1.137: CR Effects, Re=0.55million/ft, 0% Cowl, Sidewall Centerline Pressures	406

Figure 7.2.1.138: CR Effects, Re=0.55million/ft, 0% Cowl, Sidewall Pressures	406
Figure 7.2.1.139: CR Effects, Re=0.55million/ft, 0% Cowl, Sidewall Pressures	406
Figure 7.2.1.140: CR Effects, Re=0.55million/ft, 0% Cowl, Sidewall Pressures	406
Figure 7.2.1.141: CR Effects, Re=0.55million/ft, 0% Cowl, Sidewall Pressures	406
Figure 7.2.1.142: CR Effects, Re=0.55million/ft, 0% Cowl, Sidewall Pressures	406
Figure 7.2.1.143: CR Effects, Re=0.55million/ft, 0% Cowl, Sidewall Pressures	406
Figure 7.2.1.144: CR Effects, Re=0.55million/ft, 0% Cowl, Sidewall Pressures	406
Figure 7.2.1.145: CR Effects, Re=0.55million/ft, 0% Cowl, Sidewall Pressures	407
Figure 7.2.1.146: CR Effects, Re=0.55million/ft, 0% Cowl, Sidewall Pressures	407
Figure 7.2.1.147: CR Effects, Re=0.55million/ft, 0% Cowl, Sidewall Pressures	407
Figure 7.2.1.148: CR Effects, Re=0.55million/ft, 0% Cowl, Sidewall Pressures	407
Figure 7.2.1.149: CR Effects, Re=0.55million/ft, 0% Cowl, Sidewall Pressures	407
Figure 7.2.1.150: CR Effects, Re=0.55million/ft, 0% Cowl, Sidewall Pressures	407
Figure 7.2.1.151: CR Effects, Re=0.55million/ft, 0% Cowl, Sidewall Pressures	407
Figure 7.2.1.152: CR Effects, Re=0.55million/ft, 0% Cowl, Sidewall Pressures	407
Figure 7.2.1.153: CR Effects, Re=0.55million/ft, 0% Cowl, Sidewall Pressures	407
Figure 7.2.1.154: CR Effects, Re=0.55million/ft, 0% Cowl, Sidewall Pressures	408
Figure 7.2.1.155: CR Effects, Re=0.55million/ft, 0% Cowl, Sidewall Pressures	408
Figure 7.2.1.156: CR Effects, Re=0.55million/ft, 0% Cowl, Sidewall Pressures	408
Figure 7.2.1.157: CR Effects, Re=0.55million/ft, 0% Cowl, Sidewall Pressures	408
Figure 7.2.1.158: CR Effects, Re=0.55million/ft, 0% Cowl, Sidewall Pressures	408
Figure 7.2.1.159: CR Effects, Re=0.55million/ft, 0% Cowl, Sidewall Pressures	408
Figure 7.2.1.160: CR Effects, Re=0.55million/ft, 0% Cowl, Sidewall Pressures	408
Figure 7.2.1.161: CR Effects, Re=0.55million/ft, 0% Cowl, Sidewall Pressures	408
Figure 7.2.1.162: CR Effects, Re=0.55million/ft, 0% Cowl, Sidewall Pressures	408
Figure 7.2.1.163: CR Effects, Re=2.15million/ft, 25% Cowl, Centerline Pressures	409
Figure 7.2.1.164: CR Effects, Re=2.15million/ft, 25% Cowl, CR=3 Centerline Pressures	409
Figure 7.2.1.165: CR Effects, Re=2.15million/ft, 25% Cowl, CR=5 Centerline Pressures	409
Figure 7.2.1.166: CR Effects, Re=2.15million/ft, 25% Cowl, CR=9 Centerline Pressures	409
Figure 7.2.1.167: CR Effects, Re=2.15million/ft, 25% Cowl, Baseplate Pressures	409
Figure 7.2.1.168: CR Effects, Re=2.15million/ft, 25% Cowl, Baseplate Pressures	409



Figure 7.2.1.169: CR Effects, Re=2.15million/ft, 25% Cowl, Baseplate Pressures	409
Figure 7.2.1.170: CR Effects, Re=2.15million/ft, 25% Cowl, Baseplate Pressures	409
Figure 7.2.1.171: CR Effects, Re=2.15million/ft, 25% Cowl, Baseplate Pressures	409
Figure 7.2.1.172: CR Effects, Re=2.15million/ft, 25% Cowl, Baseplate Pressures	410
Figure 7.2.1.173: CR Effects, Re=2.15million/ft, 25% Cowl, Baseplate Pressures	410
Figure 7.2.1.174: CR Effects, Re=2.15million/ft, 25% Cowl, Baseplate Pressures	410
Figure 7.2.1.175: CR Effects, Re=2.15million/ft, 25% Cowl, Baseplate Pressures	410
Figure 7.2.1.176: CR Effects, Re=2.15million/ft, 25% Cowl, Baseplate Pressures	410
Figure 7.2.1.177: CR Effects, Re=2.15million/ft, 25% Cowl, Baseplate Pressures	410
Figure 7.2.1.178: CR Effects, Re=2.15million/ft, 25% Cowl, Baseplate Pressures	410
Figure 7.2.1.179: CR Effects, Re=2.15million/ft, 25% Cowl, Baseplate Pressures	410
Figure 7.2.1.180: CR Effects, Re=2.15million/ft, 25% Cowl, Baseplate Pressures	410
Figure 7.2.1.181: CR Effects, Re=2.15million/ft, 25% Cowl, Baseplate Pressures	411
Figure 7.2.1.182: CR Effects, Re=2.15million/ft, 25% Cowl, Baseplate Pressures	411
Figure 7.2.1.183: CR Effects, Re=2.15million/ft, 25% Cowl, Baseplate Pressures	411
Figure 7.2.1.184: CR Effects, Re=2.15million/ft, 25% Cowl, Baseplate Pressures	411
Figure 7.2.1.185: CR Effects, Re=2.15million/ft, 25% Cowl, Baseplate Pressures	411
Figure 7.2.1.186: CR Effects, Re=2.15million/ft, 25% Cowl, Baseplate Pressures	411
Figure 7.2.1.187: CR Effects, Re=2.15million/ft, 25% Cowl, Baseplate Pressures	411
Figure 7.2.1.188: CR Effects, Re=2.15million/ft, 25% Cowl, Baseplate Pressures	411
Figure 7.2.1.189: CR Effects, Re=2.15million/ft, 25% Cowl, Cowl Pressures	411
Figure 7.2.1.190: CR Effects, Re=2.15million/ft, 25% Cowl, Sidewall Centerline Pressures	412
Figure 7.2.1.191: CR Effects, Re=2.15million/ft, 25% Cowl, Sidewall Centerline Pressures	412
Figure 7.2.1.192: CR Effects, Re=2.15million/ft, 25% Cowl, Sidewall Pressures	412
Figure 7.2.1.193: CR Effects, Re=2.15million/ft, 25% Cowl, Sidewall Pressures	412
Figure 7.2.1.194: CR Effects, Re=2.15million/ft, 25% Cowl, Sidewall Pressures	412
Figure 7.2.1.195: CR Effects, Re=2.15million/ft, 25% Cowl, Sidewall Pressures	412
Figure 7.2.1.196: CR Effects, Re=2.15million/ft, 25% Cowl, Sidewall Pressures	412
Figure 7.2.1.197: CR Effects, Re=2.15million/ft, 25% Cowl, Sidewall Pressures	412
Figure 7.2.1.198: CR Effects, Re=2.15million/ft, 25% Cowl, Sidewall Pressures	412
Figure 7.2.1.199: CR Effects, Re=2.15million/ft, 25% Cowl, Sidewall Pressures	413

Figure 7.2.1.200: CR Effects, Re=2.15million/ft, 25% Cowl, Sidewall Pressures	413
Figure 7.2.1.201: CR Effects, Re=2.15million/ft, 25% Cowl, Sidewall Pressures	413
Figure 7.2.1.202: CR Effects, Re=2.15million/ft, 25% Cowl, Sidewall Pressures	413
Figure 7.2.1.203: CR Effects, Re=2.15million/ft, 25% Cowl, Sidewall Pressures	413
Figure 7.2.1.204: CR Effects, Re=2.15million/ft, 25% Cowl, Sidewall Pressures	413
Figure 7.2.1.205: CR Effects, Re=2.15million/ft, 25% Cowl, Sidewall Pressures	413
Figure 7.2.1.206: CR Effects, Re=2.15million/ft, 25% Cowl, Sidewall Pressures	413
Figure 7.2.1.207: CR Effects, Re=2.15million/ft, 25% Cowl, Sidewall Pressures	413
Figure 7.2.1.208: CR Effects, Re=2.15million/ft, 25% Cowl, Sidewall Pressures	414
Figure 7.2.1.209: CR Effects, Re=2.15million/ft, 25% Cowl, Sidewall Pressures	414
Figure 7.2.1.210: CR Effects, Re=2.15million/ft, 25% Cowl, Sidewall Pressures	414
Figure 7.2.1.211: CR Effects, Re=2.15million/ft, 25% Cowl, Sidewall Pressures	414
Figure 7.2.1.212: CR Effects, Re=2.15million/ft, 25% Cowl, Sidewall Pressures	414
Figure 7.2.1.213: CR Effects, Re=2.15million/ft, 25% Cowl, Sidewall Pressures	414
Figure 7.2.1.214: CR Effects, Re=2.15million/ft, 25% Cowl, Sidewall Pressures	414
Figure 7.2.1.215: CR Effects, Re=2.15million/ft, 25% Cowl, Sidewall Pressures	414
Figure 7.2.1.216: CR Effects, Re=2.15million/ft, 25% Cowl, Sidewall Pressures	414
Figure 7.2.1.217: CR Effects, Re=1.14million/ft, 25% Cowl, Centerline Pressures	415
Figure 7.2.1.218: CR Effects, Re=1.14million/ft, 25% Cowl, CR=3 Centerline Pressures	415
Figure 7.2.1.219: CR Effects, Re=1.14million/ft, 25% Cowl, CR=5 Centerline Pressures	415
Figure 7.2.1.220: CR Effects, Re=1.14million/ft, 25% Cowl, CR=9 Centerline Pressures	415
Figure 7.2.1.221: CR Effects, Re=1.14million/ft, 25% Cowl, Baseplate Pressures	415
Figure 7.2.1.222: CR Effects, Re=1.14million/ft, 25% Cowl, Baseplate Pressures	415
Figure 7.2.1.223: CR Effects, Re=1.14million/ft, 25% Cowl, Baseplate Pressures	415
Figure 7.2.1.224: CR Effects, Re=1.14million/ft, 25% Cowl, Baseplate Pressures	415
Figure 7.2.1.225: CR Effects, Re=1.14million/ft, 25% Cowl, Baseplate Pressures	415
Figure 7.2.1.226: CR Effects, Re=1.14million/ft, 25% Cowl, Baseplate Pressures	416
Figure 7.2.1.227: CR Effects, Re=1.14million/ft, 25% Cowl, Baseplate Pressures	416
Figure 7.2.1.228: CR Effects, Re=1.14million/ft, 25% Cowl, Baseplate Pressures	416
Figure 7.2.1.229: CR Effects, Re=1.14million/ft, 25% Cowl, Baseplate Pressures	416

Figure 7.2.1.230: CR Effects, Re=1.14million/ft, 25% Cowl, Baseplate Pressures	416
Figure 7.2.1.231: CR Effects, Re=1.14million/ft, 25% Cowl, Baseplate Pressures	416
Figure 7.2.1.232: CR Effects, Re=1.14million/ft, 25% Cowl, Baseplate Pressures	416
Figure 7.2.1.233: CR Effects, Re=1.14million/ft, 25% Cowl, Baseplate Pressures	416
Figure 7.2.1.234: CR Effects, Re=1.14million/ft, 25% Cowl, Baseplate Pressures	416
Figure 7.2.1.235: CR Effects, Re=1.14million/ft, 25% Cowl, Baseplate Pressures	417
Figure 7.2.1.236: CR Effects, Re=1.14million/ft, 25% Cowl, Baseplate Pressures	417
Figure 7.2.1.237: CR Effects, Re=1.14million/ft, 25% Cowl, Baseplate Pressures	417
Figure 7.2.1.238: CR Effects, Re=1.14million/ft, 25% Cowl, Baseplate Pressures	417
Figure 7.2.1.239: CR Effects, Re=1.14million/ft, 25% Cowl, Baseplate Pressures	417
Figure 7.2.1.240: CR Effects, Re=1.14million/ft, 25% Cowl, Baseplate Pressures	417
Figure 7.2.1.241: CR Effects, Re=1.14million/ft, 25% Cowl, Baseplate Pressures	417
Figure 7.2.1.242: CR Effects, Re=1.14million/ft, 25% Cowl, Baseplate Pressures	417
Figure 7.2.1.243: CR Effects, Re=1.14million/ft, 25% Cowl, Cowl Pressures	417
Figure 7.2.1.244: CR Effects, Re=1.14million/ft, 25% Cowl, Sidewall Centerline Pressures	418
Figure 7.2.1.245: CR Effects, Re=1.14million/ft, 25% Cowl, Sidewall Centerline Pressures	418
Figure 7.2.1.246: CR Effects, Re=1.14million/ft, 25% Cowl, Sidewall Pressures	418
Figure 7.2.1.247: CR Effects, Re=1.14million/ft, 25% Cowl, Sidewall Pressures	418
Figure 7.2.1.248: CR Effects, Re=1.14million/ft, 25% Cowl, Sidewall Pressures	418
Figure 7.2.1.249: CR Effects, Re=1.14million/ft, 25% Cowl, Sidewall Pressures	418
Figure 7.2.1.250: CR Effects, Re=1.14million/ft, 25% Cowl, Sidewall Pressures	418
Figure 7.2.1.251: CR Effects, Re=1.14million/ft, 25% Cowl, Sidewall Pressures	418
Figure 7.2.1.252: CR Effects, Re=1.14million/ft, 25% Cowl, Sidewall Pressures	418
Figure 7.2.1.253: CR Effects, Re=1.14million/ft, 25% Cowl, Sidewall Pressures	419
Figure 7.2.1.254: CR Effects, Re=1.14million/ft, 25% Cowl, Sidewall Pressures	419
Figure 7.2.1.255: CR Effects, Re=1.14million/ft, 25% Cowl, Sidewall Pressures	419
Figure 7.2.1.256: CR Effects, Re=1.14million/ft, 25% Cowl, Sidewall Pressures	419
Figure 7.2.1.257: CR Effects, Re=1.14million/ft, 25% Cowl, Sidewall Pressures	419
Figure 7.2.1.258: CR Effects, Re=1.14million/ft, 25% Cowl, Sidewall Pressures	419
Figure 7.2.1.259: CR Effects, Re=1.14million/ft, 25% Cowl, Sidewall Pressures	419
Figure 7.2.1.260: CR Effects, Re=1.14million/ft, 25% Cowl, Sidewall Pressures	419

Figure 7.2.1.261: CR Effects, Re=1.14million/ft, 25% Cowl, Sidewall Pressures	419
Figure 7.2.1.262: CR Effects, Re=1.14million/ft, 25% Cowl, Sidewall Pressures	420
Figure 7.2.1.263: CR Effects, Re=1.14million/ft, 25% Cowl, Sidewall Pressures	420
Figure 7.2.1.264: CR Effects, Re=1.14million/ft, 25% Cowl, Sidewall Pressures	420
Figure 7.2.1.265: CR Effects, Re=1.14million/ft, 25% Cowl, Sidewall Pressures	420
Figure 7.2.1.266: CR Effects, Re=1.14million/ft, 25% Cowl, Sidewall Pressures	420
Figure 7.2.1.267: CR Effects, Re=1.14million/ft, 25% Cowl, Sidewall Pressures	420
Figure 7.2.1.268: CR Effects, Re=1.14million/ft, 25% Cowl, Sidewall Pressures	420
Figure 7.2.1.269: CR Effects, Re=1.14million/ft, 25% Cowl, Sidewall Pressures	420
Figure 7.2.1.270: CR Effects, Re=1.14million/ft, 25% Cowl, Sidewall Pressures	420
Figure 7.2.1.271: CR Effects, Re=0.55million/ft, 25% Cowl, Centerline Pressures	421
Figure 7.2.1.272: CR Effects, Re=0.55million/ft, 25% Cowl, CR=3 Centerline Pressures	421
Figure 7.2.1.273: CR Effects, Re=0.55million/ft, 25% Cowl, CR=5 Centerline Pressures	421
Figure 7.2.1.274: CR Effects, Re=0.55million/ft, 25% Cowl, CR=9 Centerline Pressures	421
Figure 7.2.1.275: CR Effects, Re=0.55million/ft, 25% Cowl, Baseplate Pressures	421
Figure 7.2.1.276: CR Effects, Re=0.55million/ft, 25% Cowl, Baseplate Pressures	421
Figure 7.2.1.277: CR Effects, Re=0.55million/ft, 25% Cowl, Baseplate Pressures	421
Figure 7.2.1.278: CR Effects, Re=0.55million/ft, 25% Cowl, Baseplate Pressures	421
Figure 7.2.1.279: CR Effects, Re=0.55million/ft, 25% Cowl, Baseplate Pressures	421
Figure 7.2.1.280: CR Effects, Re=0.55million/ft, 25% Cowl, Baseplate Pressures	422
Figure 7.2.1.281: CR Effects, Re=0.55million/ft, 25% Cowl, Baseplate Pressures	422
Figure 7.2.1.282: CR Effects, Re=0.55million/ft, 25% Cowl, Baseplate Pressures	422
Figure 7.2.1.283: CR Effects, Re=0.55million/ft, 25% Cowl, Baseplate Pressures	422
Figure 7.2.1.284: CR Effects, Re=0.55million/ft, 25% Cowl, Baseplate Pressures	422
Figure 7.2.1.285: CR Effects, Re=0.55million/ft, 25% Cowl, Baseplate Pressures	422
Figure 7.2.1.286: CR Effects, Re=0.55million/ft, 25% Cowl, Baseplate Pressures	422
Figure 7.2.1.287: CR Effects, Re=0.55million/ft, 25% Cowl, Baseplate Pressures	422
Figure 7.2.1.288: CR Effects, Re=0.55million/ft, 25% Cowl, Baseplate Pressures	422
Figure 7.2.1.289: CR Effects, Re=0.55million/ft, 25% Cowl, Baseplate Pressures	423
Figure 7.2.1.290: CR Effects, Re=0.55million/ft, 25% Cowl, Baseplate Pressures	423
Figure 7.2.1.291: CR Effects, Re=0.55million/ft, 25% Cowl, Baseplate Pressures	423

Figure 7.2.1.292: CR Effects, $Re=0.55$ million/ft, 25% Cowl, Baseplate Pressures	423
Figure 7.2.1.293: CR Effects, $Re=0.55$ million/ft, 25% Cowl, Baseplate Pressures	423
Figure 7.2.1.294: CR Effects, $Re=0.55$ million/ft, 25% Cowl, Baseplate Pressures	423
Figure 7.2.1.295: CR Effects, $Re=0.55$ million/ft, 25% Cowl, Baseplate Pressures	423
Figure 7.2.1.296: CR Effects, $Re=0.55$ million/ft, 25% Cowl, Baseplate Pressures	423
Figure 7.2.1.297: CR Effects, $Re=0.55$ million/ft, 25% Cowl, Cowl Pressures	423
Figure 7.2.1.298: CR Effects, $Re=0.55$ million/ft, 25% Cowl, Sidewall Centerline Pressures	424
Figure 7.2.1.299: CR Effects, $Re=0.55$ million/ft, 25% Cowl, Sidewall Centerline Pressures	424
Figure 7.2.1.300: CR Effects, $Re=0.55$ million/ft, 25% Cowl, Sidewall Pressures	424
Figure 7.2.1.301: CR Effects, $Re=0.55$ million/ft, 25% Cowl, Sidewall Pressures	424
Figure 7.2.1.302: CR Effects, $Re=0.55$ million/ft, 25% Cowl, Sidewall Pressures	424
Figure 7.2.1.303: CR Effects, $Re=0.55$ million/ft, 25% Cowl, Sidewall Pressures	424
Figure 7.2.1.304: CR Effects, $Re=0.55$ million/ft, 25% Cowl, Sidewall Pressures	424
Figure 7.2.1.305: CR Effects, $Re=0.55$ million/ft, 25% Cowl, Sidewall Pressures	424
Figure 7.2.1.306: CR Effects, $Re=0.55$ million/ft, 25% Cowl, Sidewall Pressures	424
Figure 7.2.1.307: CR Effects, $Re=0.55$ million/ft, 25% Cowl, Sidewall Pressures	425
Figure 7.2.1.308: CR Effects, $Re=0.55$ million/ft, 25% Cowl, Sidewall Pressures	425
Figure 7.2.1.309: CR Effects, $Re=0.55$ million/ft, 25% Cowl, Sidewall Pressures	425
Figure 7.2.1.310: CR Effects, $Re=0.55$ million/ft, 25% Cowl, Sidewall Pressures	425
Figure 7.2.1.311: CR Effects, $Re=0.55$ million/ft, 25% Cowl, Sidewall Pressures	425
Figure 7.2.1.312: CR Effects, $Re=0.55$ million/ft, 25% Cowl, Sidewall Pressures	425
Figure 7.2.1.313: CR Effects, $Re=0.55$ million/ft, 25% Cowl, Sidewall Pressures	425
Figure 7.2.1.314: CR Effects, $Re=0.55$ million/ft, 25% Cowl, Sidewall Pressures	425
Figure 7.2.1.315: CR Effects, $Re=0.55$ million/ft, 25% Cowl, Sidewall Pressures	425
Figure 7.2.1.316: CR Effects, $Re=0.55$ million/ft, 25% Cowl, Sidewall Pressures	426
Figure 7.2.1.317: CR Effects, $Re=0.55$ million/ft, 25% Cowl, Sidewall Pressures	426
Figure 7.2.1.318: CR Effects, $Re=0.55$ million/ft, 25% Cowl, Sidewall Pressures	426
Figure 7.2.1.319: CR Effects, $Re=0.55$ million/ft, 25% Cowl, Sidewall Pressures	426
Figure 7.2.1.320: CR Effects, $Re=0.55$ million/ft, 25% Cowl, Sidewall Pressures	426
Figure 7.2.1.321: CR Effects, $Re=0.55$ million/ft, 25% Cowl, Sidewall Pressures	426
Figure 7.2.1.322: CR Effects, $Re=0.55$ million/ft, 25% Cowl, Sidewall Pressures	426

Figure 7.2.1.323: CR Effects, Re=0.55million/ft, 25% Cowl, Sidewall Pressures	426
Figure 7.2.1.324: CR Effects, Re=0.55million/ft, 25% Cowl, Sidewall Pressures	426
Figure 7.2.1.325: CR Effects, Re=2.15million/ft, 50% Cowl, Centerline Pressures	427
Figure 7.2.1.326: CR Effects, Re=2.15million/ft, 50% Cowl, CR=3 Centerline Pressures	427
Figure 7.2.1.327: CR Effects, Re=2.15million/ft, 50% Cowl, CR=5 Centerline Pressures	427
Figure 7.2.1.328: CR Effects, Re=2.15million/ft, 50% Cowl, CR=9 Centerline Pressures	427
Figure 7.2.1.329: CR Effects, Re=2.15million/ft, 50% Cowl, Baseplate Pressures	427
Figure 7.2.1.330: CR Effects, Re=2.15million/ft, 50% Cowl, Baseplate Pressures	427
Figure 7.2.1.331: CR Effects, Re=2.15million/ft, 50% Cowl, Baseplate Pressures	427
Figure 7.2.1.332: CR Effects, Re=2.15million/ft, 50% Cowl, Baseplate Pressures	427
Figure 7.2.1.333: CR Effects, Re=2.15million/ft, 50% Cowl, Baseplate Pressures	427
Figure 7.2.1.334: CR Effects, Re=2.15million/ft, 50% Cowl, Baseplate Pressures	428
Figure 7.2.1.335: CR Effects, Re=2.15million/ft, 50% Cowl, Baseplate Pressures	428
Figure 7.2.1.336: CR Effects, Re=2.15million/ft, 50% Cowl, Baseplate Pressures	428
Figure 7.2.1.337: CR Effects, Re=2.15million/ft, 50% Cowl, Baseplate Pressures	428
Figure 7.2.1.338: CR Effects, Re=2.15million/ft, 50% Cowl, Baseplate Pressures	428
Figure 7.2.1.339: CR Effects, Re=2.15million/ft, 50% Cowl, Baseplate Pressures	428
Figure 7.2.1.340: CR Effects, Re=2.15million/ft, 50% Cowl, Baseplate Pressures	428
Figure 7.2.1.341: CR Effects, Re=2.15million/ft, 50% Cowl, Baseplate Pressures	428
Figure 7.2.1.342: CR Effects, Re=2.15million/ft, 50% Cowl, Baseplate Pressures	428
Figure 7.2.1.343: CR Effects, Re=2.15million/ft, 50% Cowl, Baseplate Pressures	429
Figure 7.2.1.344: CR Effects, Re=2.15million/ft, 50% Cowl, Baseplate Pressures	429
Figure 7.2.1.345: CR Effects, Re=2.15million/ft, 50% Cowl, Baseplate Pressures	429
Figure 7.2.1.346: CR Effects, Re=2.15million/ft, 50% Cowl, Baseplate Pressures	429
Figure 7.2.1.347: CR Effects, Re=2.15million/ft, 50% Cowl, Baseplate Pressures	429
Figure 7.2.1.348: CR Effects, Re=2.15million/ft, 50% Cowl, Baseplate Pressures	429
Figure 7.2.1.349: CR Effects, Re=2.15million/ft, 50% Cowl, Baseplate Pressures	429
Figure 7.2.1.350: CR Effects, Re=2.15million/ft, 50% Cowl, Baseplate Pressures	429
Figure 7.2.1.351: CR Effects, Re=2.15million/ft, 50% Cowl, Cowl Pressures	429
Figure 7.2.1.352: CR Effects, Re=2.15million/ft, 50% Cowl, Sidewall Centerline Pressures	430

Figure 7.2.1.353: CR Effects, $Re=2.15$ million/ft, 50% Cowl, Sidewall Centerline Pressures	430
Figure 7.2.1.354: CR Effects, $Re=2.15$ million/ft, 50% Cowl, Sidewall Pressures	430
Figure 7.2.1.355: CR Effects, $Re=2.15$ million/ft, 50% Cowl, Sidewall Pressures	430
Figure 7.2.1.356: CR Effects, $Re=2.15$ million/ft, 50% Cowl, Sidewall Pressures	430
Figure 7.2.1.357: CR Effects, $Re=2.15$ million/ft, 50% Cowl, Sidewall Pressures	430
Figure 7.2.1.358: CR Effects, $Re=2.15$ million/ft, 50% Cowl, Sidewall Pressures	430
Figure 7.2.1.359: CR Effects, $Re=2.15$ million/ft, 50% Cowl, Sidewall Pressures	430
Figure 7.2.1.360: CR Effects, $Re=2.15$ million/ft, 50% Cowl, Sidewall Pressures	430
Figure 7.2.1.361: CR Effects, $Re=2.15$ million/ft, 50% Cowl, Sidewall Pressures	431
Figure 7.2.1.362: CR Effects, $Re=2.15$ million/ft, 50% Cowl, Sidewall Pressures	431
Figure 7.2.1.363: CR Effects, $Re=2.15$ million/ft, 50% Cowl, Sidewall Pressures	431
Figure 7.2.1.364: CR Effects, $Re=2.15$ million/ft, 50% Cowl, Sidewall Pressures	431
Figure 7.2.1.365: CR Effects, $Re=2.15$ million/ft, 50% Cowl, Sidewall Pressures	431
Figure 7.2.1.366: CR Effects, $Re=2.15$ million/ft, 50% Cowl, Sidewall Pressures	431
Figure 7.2.1.367: CR Effects, $Re=2.15$ million/ft, 50% Cowl, Sidewall Pressures	431
Figure 7.2.1.368: CR Effects, $Re=2.15$ million/ft, 50% Cowl, Sidewall Pressures	431
Figure 7.2.1.369: CR Effects, $Re=2.15$ million/ft, 50% Cowl, Sidewall Pressures	431
Figure 7.2.1.370: CR Effects, $Re=2.15$ million/ft, 50% Cowl, Sidewall Pressures	432
Figure 7.2.1.371: CR Effects, $Re=2.15$ million/ft, 50% Cowl, Sidewall Pressures	432
Figure 7.2.1.372: CR Effects, $Re=2.15$ million/ft, 50% Cowl, Sidewall Pressures	432
Figure 7.2.1.373: CR Effects, $Re=2.15$ million/ft, 50% Cowl, Sidewall Pressures	432
Figure 7.2.1.374: CR Effects, $Re=2.15$ million/ft, 50% Cowl, Sidewall Pressures	432
Figure 7.2.1.375: CR Effects, $Re=2.15$ million/ft, 50% Cowl, Sidewall Pressures	432
Figure 7.2.1.376: CR Effects, $Re=2.15$ million/ft, 50% Cowl, Sidewall Pressures	432
Figure 7.2.1.377: CR Effects, $Re=2.15$ million/ft, 50% Cowl, Sidewall Pressures	432
Figure 7.2.1.378: CR Effects, $Re=2.15$ million/ft, 50% Cowl, Sidewall Pressures	432
Figure 7.2.1.379: CR Effects, $Re=1.14$ million/ft, 50% Cowl, Centerline Pressures	433
Figure 7.2.1.380: CR Effects, $Re=1.14$ million/ft, 50% Cowl, CR=3 Centerline Pressures	433
Figure 7.2.1.381: CR Effects, $Re=1.14$ million/ft, 50% Cowl, CR=5 Centerline Pressures	433
Figure 7.2.1.382: CR Effects, $Re=1.14$ million/ft, 50% Cowl, CR=9 Centerline Pressures	433
Figure 7.2.1.383: CR Effects, $Re=1.14$ million/ft, 50% Cowl, Baseplate Pressures	433

Figure 7.2.1.384: CR Effects, Re=1.14million/ft, 50% Cowl, Baseplate Pressures	433
Figure 7.2.1.385: CR Effects, Re=1.14million/ft, 50% Cowl, Baseplate Pressures	433
Figure 7.2.1.386: CR Effects, Re=1.14million/ft, 50% Cowl, Baseplate Pressures	433
Figure 7.2.1.387: CR Effects, Re=1.14million/ft, 50% Cowl, Baseplate Pressures	433
Figure 7.2.1.388: CR Effects, Re=1.14million/ft, 50% Cowl, Baseplate Pressures	434
Figure 7.2.1.389: CR Effects, Re=1.14million/ft, 50% Cowl, Baseplate Pressures	434
Figure 7.2.1.390: CR Effects, Re=1.14million/ft, 50% Cowl, Baseplate Pressures	434
Figure 7.2.1.391: CR Effects, Re=1.14million/ft, 50% Cowl, Baseplate Pressures	434
Figure 7.2.1.392: CR Effects, Re=1.14million/ft, 50% Cowl, Baseplate Pressures	434
Figure 7.2.1.393: CR Effects, Re=1.14million/ft, 50% Cowl, Baseplate Pressures	434
Figure 7.2.1.394: CR Effects, Re=1.14million/ft, 50% Cowl, Baseplate Pressures	434
Figure 7.2.1.395: CR Effects, Re=1.14million/ft, 50% Cowl, Baseplate Pressures	434
Figure 7.2.1.396: CR Effects, Re=1.14million/ft, 50% Cowl, Baseplate Pressures	434
Figure 7.2.1.397: CR Effects, Re=1.14million/ft, 50% Cowl, Baseplate Pressures	435
Figure 7.2.1.398: CR Effects, Re=1.14million/ft, 50% Cowl, Baseplate Pressures	435
Figure 7.2.1.399: CR Effects, Re=1.14million/ft, 50% Cowl, Baseplate Pressures	435
Figure 7.2.1.400: CR Effects, Re=1.14million/ft, 50% Cowl, Baseplate Pressures	435
Figure 7.2.1.401: CR Effects, Re=1.14million/ft, 50% Cowl, Baseplate Pressures	435
Figure 7.2.1.402: CR Effects, Re=1.14million/ft, 50% Cowl, Baseplate Pressures	435
Figure 7.2.1.403: CR Effects, Re=1.14million/ft, 50% Cowl, Baseplate Pressures	435
Figure 7.2.1.404: CR Effects, Re=1.14million/ft, 50% Cowl, Baseplate Pressures	435
Figure 7.2.1.405: CR Effects, Re=1.14million/ft, 50% Cowl, Cowl Pressures	435
Figure 7.2.1.406: CR Effects, Re=1.14million/ft, 50% Cowl, Sidewall Centerline Pressures	436
Figure 7.2.1.407: CR Effects, Re=1.14million/ft, 50% Cowl, Sidewall Centerline Pressures	436
Figure 7.2.1.408: CR Effects, Re=1.14million/ft, 50% Cowl, Sidewall Pressures	436
Figure 7.2.1.409: CR Effects, Re=1.14million/ft, 50% Cowl, Sidewall Pressures	436
Figure 7.2.1.410: CR Effects, Re=1.14million/ft, 50% Cowl, Sidewall Pressures	436
Figure 7.2.1.411: CR Effects, Re=1.14million/ft, 50% Cowl, Sidewall Pressures	436
Figure 7.2.1.412: CR Effects, Re=1.14million/ft, 50% Cowl, Sidewall Pressures	436
Figure 7.2.1.413: CR Effects, Re=1.14million/ft, 50% Cowl, Sidewall Pressures	436
Figure 7.2.1.414: CR Effects, Re=1.14million/ft, 50% Cowl, Sidewall Pressures	436



Figure 7.2.1.415: CR Effects, $Re=1.14$ million/ft, 50% Cowl, Sidewall Pressures	437
Figure 7.2.1.416: CR Effects, $Re=1.14$ million/ft, 50% Cowl, Sidewall Pressures	437
Figure 7.2.1.417: CR Effects, $Re=1.14$ million/ft, 50% Cowl, Sidewall Pressures	437
Figure 7.2.1.418: CR Effects, $Re=1.14$ million/ft, 50% Cowl, Sidewall Pressures	437
Figure 7.2.1.419: CR Effects, $Re=1.14$ million/ft, 50% Cowl, Sidewall Pressures	437
Figure 7.2.1.420: CR Effects, $Re=1.14$ million/ft, 50% Cowl, Sidewall Pressures	437
Figure 7.2.1.421: CR Effects, $Re=1.14$ million/ft, 50% Cowl, Sidewall Pressures	437
Figure 7.2.1.422: CR Effects, $Re=1.14$ million/ft, 50% Cowl, Sidewall Pressures	437
Figure 7.2.1.423: CR Effects, $Re=1.14$ million/ft, 50% Cowl, Sidewall Pressures	437
Figure 7.2.1.424: CR Effects, $Re=1.14$ million/ft, 50% Cowl, Sidewall Pressures	438
Figure 7.2.1.425: CR Effects, $Re=1.14$ million/ft, 50% Cowl, Sidewall Pressures	438
Figure 7.2.1.426: CR Effects, $Re=1.14$ million/ft, 50% Cowl, Sidewall Pressures	438
Figure 7.2.1.427: CR Effects, $Re=1.14$ million/ft, 50% Cowl, Sidewall Pressures	438
Figure 7.2.1.428: CR Effects, $Re=1.14$ million/ft, 50% Cowl, Sidewall Pressures	438
Figure 7.2.1.429: CR Effects, $Re=1.14$ million/ft, 50% Cowl, Sidewall Pressures	438
Figure 7.2.1.430: CR Effects, $Re=1.14$ million/ft, 50% Cowl, Sidewall Pressures	438
Figure 7.2.1.431: CR Effects, $Re=1.14$ million/ft, 50% Cowl, Sidewall Pressures	438
Figure 7.2.1.432: CR Effects, $Re=1.14$ million/ft, 50% Cowl, Sidewall Pressures	438
Figure 7.2.1.433: CR Effects, $Re=0.55$ million/ft, 50% Cowl, Centerline Pressures	439
Figure 7.2.1.434: CR Effects, $Re=0.55$ million/ft, 50% Cowl, CR=3 Centerline Pressures	439
Figure 7.2.1.435: CR Effects, $Re=0.55$ million/ft, 50% Cowl, CR=5 Centerline Pressures	439
Figure 7.2.1.436: CR Effects, $Re=0.55$ million/ft, 50% Cowl, CR=9 Centerline Pressures	439
Figure 7.2.1.437: CR Effects, $Re=0.55$ million/ft, 50% Cowl, Baseplate Pressures	439
Figure 7.2.1.438: CR Effects, $Re=0.55$ million/ft, 50% Cowl, Baseplate Pressures	439
Figure 7.2.1.439: CR Effects, $Re=0.55$ million/ft, 50% Cowl, Baseplate Pressures	439
Figure 7.2.1.440: CR Effects, $Re=0.55$ million/ft, 50% Cowl, Baseplate Pressures	439
Figure 7.2.1.441: CR Effects, $Re=0.55$ million/ft, 50% Cowl, Baseplate Pressures	439
Figure 7.2.1.442: CR Effects, $Re=0.55$ million/ft, 50% Cowl, Baseplate Pressures	440
Figure 7.2.1.443: CR Effects, $Re=0.55$ million/ft, 50% Cowl, Baseplate Pressures	440
Figure 7.2.1.444: CR Effects, $Re=0.55$ million/ft, 50% Cowl, Baseplate Pressures	440
Figure 7.2.1.445: CR Effects, $Re=0.55$ million/ft, 50% Cowl, Baseplate Pressures	440

Figure 7.2.1.446: CR Effects, Re=0.55million/ft, 50% Cowl, Baseplate Pressures	440
Figure 7.2.1.447: CR Effects, Re=0.55million/ft, 50% Cowl, Baseplate Pressures	440
Figure 7.2.1.448: CR Effects, Re=0.55million/ft, 50% Cowl, Baseplate Pressures	440
Figure 7.2.1.449: CR Effects, Re=0.55million/ft, 50% Cowl, Baseplate Pressures	440
Figure 7.2.1.450: CR Effects, Re=0.55million/ft, 50% Cowl, Baseplate Pressures	440
Figure 7.2.1.451: CR Effects, Re=0.55million/ft, 50% Cowl, Baseplate Pressures	441
Figure 7.2.1.452: CR Effects, Re=0.55million/ft, 50% Cowl, Baseplate Pressures	441
Figure 7.2.1.453: CR Effects, Re=0.55million/ft, 50% Cowl, Baseplate Pressures	441
Figure 7.2.1.454: CR Effects, Re=0.55million/ft, 50% Cowl, Baseplate Pressures	441
Figure 7.2.1.455: CR Effects, Re=0.55million/ft, 50% Cowl, Baseplate Pressures	441
Figure 7.2.1.456: CR Effects, Re=0.55million/ft, 50% Cowl, Baseplate Pressures	441
Figure 7.2.1.457: CR Effects, Re=0.55million/ft, 50% Cowl, Baseplate Pressures	441
Figure 7.2.1.458: CR Effects, Re=0.55million/ft, 50% Cowl, Baseplate Pressures	441
Figure 7.2.1.459: CR Effects, Re=0.55million/ft, 50% Cowl, Cowl Pressures	441
Figure 7.2.1.460: CR Effects, Re=0.55million/ft, 50% Cowl, Sidewall Centerline Pressures	442
Figure 7.2.1.461: CR Effects, Re=0.55million/ft, 50% Cowl, Sidewall Centerline Pressures	442
Figure 7.2.1.462: CR Effects, Re=0.55million/ft, 50% Cowl, Sidewall Pressures	442
Figure 7.2.1.463: CR Effects, Re=0.55million/ft, 50% Cowl, Sidewall Pressures	442
Figure 7.2.1.464: CR Effects, Re=0.55million/ft, 50% Cowl, Sidewall Pressures	442
Figure 7.2.1.465: CR Effects, Re=0.55million/ft, 50% Cowl, Sidewall Pressures	442
Figure 7.2.1.466: CR Effects, Re=0.55million/ft, 50% Cowl, Sidewall Pressures	442
Figure 7.2.1.467: CR Effects, Re=0.55million/ft, 50% Cowl, Sidewall Pressures	442
Figure 7.2.1.468: CR Effects, Re=0.55million/ft, 50% Cowl, Sidewall Pressures	442
Figure 7.2.1.469: CR Effects, Re=0.55million/ft, 50% Cowl, Sidewall Pressures	443
Figure 7.2.1.470: CR Effects, Re=0.55million/ft, 50% Cowl, Sidewall Pressures	443
Figure 7.2.1.471: CR Effects, Re=0.55million/ft, 50% Cowl, Sidewall Pressures	443
Figure 7.2.1.472: CR Effects, Re=0.55million/ft, 50% Cowl, Sidewall Pressures	443
Figure 7.2.1.473: CR Effects, Re=0.55million/ft, 50% Cowl, Sidewall Pressures	443
Figure 7.2.1.474: CR Effects, Re=0.55million/ft, 50% Cowl, Sidewall Pressures	443
Figure 7.2.1.475: CR Effects, Re=0.55million/ft, 50% Cowl, Sidewall Pressures	443

Figure 7.2.1.476: CR Effects, Re=0.55million/ft, 50% Cowl, Sidewall Pressures	443
Figure 7.2.1.477: CR Effects, Re=0.55million/ft, 50% Cowl, Sidewall Pressures	443
Figure 7.2.1.478: CR Effects, Re=0.55million/ft, 50% Cowl, Sidewall Pressures	444
Figure 7.2.1.479: CR Effects, Re=0.55million/ft, 50% Cowl, Sidewall Pressures	444
Figure 7.2.1.480: CR Effects, Re=0.55million/ft, 50% Cowl, Sidewall Pressures	444
Figure 7.2.1.481: CR Effects, Re=0.55million/ft, 50% Cowl, Sidewall Pressures	444
Figure 7.2.1.482: CR Effects, Re=0.55million/ft, 50% Cowl, Sidewall Pressures	444
Figure 7.2.1.483: CR Effects, Re=0.55million/ft, 50% Cowl, Sidewall Pressures	444
Figure 7.2.1.484: CR Effects, Re=0.55million/ft, 50% Cowl, Sidewall Pressures	444
Figure 7.2.1.485: CR Effects, Re=0.55million/ft, 50% Cowl, Sidewall Pressures	444
Figure 7.2.1.486: CR Effects, Re=0.55million/ft, 50% Cowl, Sidewall Pressures	444
Figure 7.2.2.1: Cowl Effects, CR=3, Re=2.15million/ft, CR=3 Centerline Pressures	445
Figure 7.2.2.2: Cowl Effects, CR=3, Re=2.15million/ft, CR=5 Centerline Pressures	445
Figure 7.2.2.3: Cowl Effects, CR=3, Re=2.15million/ft, CR=9 Centerline Pressures	445
Figure 7.2.2.4: Cowl Effects, CR=3, Re=2.15million/ft, Baseplate Pressures	445
Figure 7.2.2.5: Cowl Effects, CR=3, Re=2.15million/ft, Baseplate Pressures	445
Figure 7.2.2.6: Cowl Effects, CR=3, Re=2.15million/ft, Baseplate Pressures	445
Figure 7.2.2.7: Cowl Effects, CR=3, Re=2.15million/ft, Baseplate Pressures	445
Figure 7.2.2.8: Cowl Effects, CR=3, Re=2.15million/ft, Baseplate Pressures	445
Figure 7.2.2.9: Cowl Effects, CR=3, Re=2.15million/ft, Baseplate Pressures	445
Figure 7.2.2.10: Cowl Effects, CR=3, Re=2.15million/ft, Baseplate Pressures	446
Figure 7.2.2.11: Cowl Effects, CR=3, Re=2.15million/ft, Baseplate Pressures	446
Figure 7.2.2.12: Cowl Effects, CR=3, Re=2.15million/ft, Baseplate Pressures	446
Figure 7.2.2.13: Cowl Effects, CR=3, Re=2.15million/ft, Baseplate Pressures	446
Figure 7.2.2.14: Cowl Effects, CR=3, Re=2.15million/ft, Baseplate Pressures	446
Figure 7.2.2.15: Cowl Effects, CR=3, Re=2.15million/ft, Baseplate Pressures	446
Figure 7.2.2.16: Cowl Effects, CR=3, Re=2.15million/ft, Baseplate Pressures	446
Figure 7.2.2.17: Cowl Effects, CR=3, Re=2.15million/ft, Baseplate Pressures	446
Figure 7.2.2.18: Cowl Effects, CR=3, Re=2.15million/ft, Baseplate Pressures	446
Figure 7.2.2.19: Cowl Effects, CR=3, Re=2.15million/ft, Baseplate Pressures	447
Figure 7.2.2.20: Cowl Effects, CR=3, Re=2.15million/ft, Baseplate Pressures	447

Figure 7.2.2.21:	Cowl Effects, CR=3, Re=2.15million/ft, Baseplate Pressures	447
Figure 7.2.2.22:	Cowl Effects, CR=3, Re=2.15million/ft, Baseplate Pressures	447
Figure 7.2.2.23:	Cowl Effects, CR=3, Re=2.15million/ft, Baseplate Pressures	447
Figure 7.2.2.24:	Cowl Effects, CR=3, Re=2.15million/ft, Baseplate Pressures	447
Figure 7.2.2.25:	Cowl Effects, CR=3, Re=2.15million/ft, Baseplate Pressures	447
Figure 7.2.2.26:	Cowl Effects, CR=3, Re=2.15million/ft, Cowl Pressures	447
Figure 7.2.2.27:	Cowl Effects, CR=3, Re=2.15million/ft, Sidewall Centerline Pressures	447
Figure 7.2.2.28:	Cowl Effects, CR=3, Re=2.15million/ft, Sidewall Centerline Pressures	448
Figure 7.2.2.29:	Cowl Effects, CR=3, Re=2.15million/ft, Sidewall Pressures	448
Figure 7.2.2.30:	Cowl Effects, CR=3, Re=2.15million/ft, Sidewall Pressures	448
Figure 7.2.2.31:	Cowl Effects, CR=3, Re=2.15million/ft, Sidewall Pressures	448
Figure 7.2.2.32:	Cowl Effects, CR=3, Re=2.15million/ft, Sidewall Pressures	448
Figure 7.2.2.33:	Cowl Effects, CR=3, Re=2.15million/ft, Sidewall Pressures	448
Figure 7.2.2.34:	Cowl Effects, CR=3, Re=2.15million/ft, Sidewall Pressures	448
Figure 7.2.2.35:	Cowl Effects, CR=3, Re=2.15million/ft, Sidewall Pressures	448
Figure 7.2.2.36:	Cowl Effects, CR=3, Re=2.15million/ft, Sidewall Pressures	448
Figure 7.2.2.37:	Cowl Effects, CR=3, Re=2.15million/ft, Sidewall Pressures	449
Figure 7.2.2.38:	Cowl Effects, CR=3, Re=2.15million/ft, Sidewall Pressures	449
Figure 7.2.2.39:	Cowl Effects, CR=3, Re=2.15million/ft, Sidewall Pressures	449
Figure 7.2.2.40:	Cowl Effects, CR=3, Re=2.15million/ft, Sidewall Pressures	449
Figure 7.2.2.41:	Cowl Effects, CR=3, Re=2.15million/ft, Sidewall Pressures	449
Figure 7.2.2.42:	Cowl Effects, CR=3, Re=2.15million/ft, Sidewall Pressures	449
Figure 7.2.2.43:	Cowl Effects, CR=3, Re=2.15million/ft, Sidewall Pressures	449
Figure 7.2.2.44:	Cowl Effects, CR=3, Re=2.15million/ft, Sidewall Pressures	449
Figure 7.2.2.45:	Cowl Effects, CR=3, Re=2.15million/ft, Sidewall Pressures	449
Figure 7.2.2.46:	Cowl Effects, CR=3, Re=2.15million/ft, Sidewall Pressures	450
Figure 7.2.2.47:	Cowl Effects, CR=3, Re=2.15million/ft, Sidewall Pressures	450
Figure 7.2.2.48:	Cowl Effects, CR=3, Re=2.15million/ft, Sidewall Pressures	450
Figure 7.2.2.49:	Cowl Effects, CR=3, Re=2.15million/ft, Sidewall Pressures	450
Figure 7.2.2.50:	Cowl Effects, CR=3, Re=2.15million/ft, Sidewall Pressures	450
Figure 7.2.2.51:	Cowl Effects, CR=3, Re=2.15million/ft, Sidewall Pressures	450

Figure 7.2.2.52:	Cowl Effects, CR=3, Re=2.15million/ft, Sidewall Pressures	450
Figure 7.2.2.53:	Cowl Effects, CR=3, Re=2.15million/ft, Sidewall Pressures	450
Figure 7.2.2.54:	Cowl Effects, CR=3, Re=1.14million/ft, CR=3 Centerline Pressures	451
Figure 7.2.2.55:	Cowl Effects, CR=3, Re=1.14million/ft, CR=5 Centerline Pressures	451
Figure 7.2.2.56:	Cowl Effects, CR=3, Re=1.14million/ft, CR=9 Centerline Pressures	451
Figure 7.2.2.57:	Cowl Effects, CR=3, Re=1.14million/ft, Baseplate Pressures	451
Figure 7.2.2.58:	Cowl Effects, CR=3, Re=1.14million/ft, Baseplate Pressures	451
Figure 7.2.2.59:	Cowl Effects, CR=3, Re=1.14million/ft, Baseplate Pressures	451
Figure 7.2.2.60:	Cowl Effects, CR=3, Re=1.14million/ft, Baseplate Pressures	451
Figure 7.2.2.61:	Cowl Effects, CR=3, Re=1.14million/ft, Baseplate Pressures	451
Figure 7.2.2.62:	Cowl Effects, CR=3, Re=1.14million/ft, Baseplate Pressures	451
Figure 7.2.2.63:	Cowl Effects, CR=3, Re=1.14million/ft, Baseplate Pressures	452
Figure 7.2.2.64:	Cowl Effects, CR=3, Re=1.14million/ft, Baseplate Pressures	452
Figure 7.2.2.65:	Cowl Effects, CR=3, Re=1.14million/ft, Baseplate Pressures	452
Figure 7.2.2.66:	Cowl Effects, CR=3, Re=1.14million/ft, Baseplate Pressures	452
Figure 7.2.2.67:	Cowl Effects, CR=3, Re=1.14million/ft, Baseplate Pressures	452
Figure 7.2.2.68:	Cowl Effects, CR=3, Re=1.14million/ft, Baseplate Pressures	452
Figure 7.2.2.69:	Cowl Effects, CR=3, Re=1.14million/ft, Baseplate Pressures	452
Figure 7.2.2.70:	Cowl Effects, CR=3, Re=1.14million/ft, Baseplate Pressures	452
Figure 7.2.2.71:	Cowl Effects, CR=3, Re=1.14million/ft, Baseplate Pressures	452
Figure 7.2.2.72:	Cowl Effects, CR=3, Re=1.14million/ft, Baseplate Pressures	453
Figure 7.2.2.73:	Cowl Effects, CR=3, Re=1.14million/ft, Baseplate Pressures	453
Figure 7.2.2.74:	Cowl Effects, CR=3, Re=1.14million/ft, Baseplate Pressures	453
Figure 7.2.2.75:	Cowl Effects, CR=3, Re=1.14million/ft, Baseplate Pressures	453
Figure 7.2.2.76:	Cowl Effects, CR=3, Re=1.14million/ft, Baseplate Pressures	453
Figure 7.2.2.77:	Cowl Effects, CR=3, Re=1.14million/ft, Baseplate Pressures	453
Figure 7.2.2.78:	Cowl Effects, CR=3, Re=1.14million/ft, Baseplate Pressures	453
Figure 7.2.2.79:	Cowl Effects, CR=3, Re=1.14million/ft, Cowl Pressures	453
Figure 7.2.2.80:	Cowl Effects, CR=3, Re=1.14million/ft, Sidewall Centerline Pressures	453
Figure 7.2.2.81:	Cowl Effects, CR=3, Re=1.14million/ft, Sidewall Centerline Pressures	454
Figure 7.2.2.82:	Cowl Effects, CR=3, Re=1.14million/ft, Sidewall Pressures	454

Figure 7.2.2.83:	Cowl Effects, CR=3, Re=1.14million/ft, Sidewall Pressures	454
Figure 7.2.2.84:	Cowl Effects, CR=3, Re=1.14million/ft, Sidewall Pressures	454
Figure 7.2.2.85:	Cowl Effects, CR=3, Re=1.14million/ft, Sidewall Pressures	454
Figure 7.2.2.86:	Cowl Effects, CR=3, Re=1.14million/ft, Sidewall Pressures	454
Figure 7.2.2.87:	Cowl Effects, CR=3, Re=1.14million/ft, Sidewall Pressures	454
Figure 7.2.2.88:	Cowl Effects, CR=3, Re=1.14million/ft, Sidewall Pressures	454
Figure 7.2.2.89:	Cowl Effects, CR=3, Re=1.14million/ft, Sidewall Pressures	454
Figure 7.2.2.90:	Cowl Effects, CR=3, Re=1.14million/ft, Sidewall Pressures	455
Figure 7.2.2.91:	Cowl Effects, CR=3, Re=1.14million/ft, Sidewall Pressures	455
Figure 7.2.2.92:	Cowl Effects, CR=3, Re=1.14million/ft, Sidewall Pressures	455
Figure 7.2.2.93:	Cowl Effects, CR=3, Re=1.14million/ft, Sidewall Pressures	455
Figure 7.2.2.94:	Cowl Effects, CR=3, Re=1.14million/ft, Sidewall Pressures	455
Figure 7.2.2.95:	Cowl Effects, CR=3, Re=1.14million/ft, Sidewall Pressures	455
Figure 7.2.2.96:	Cowl Effects, CR=3, Re=1.14million/ft, Sidewall Pressures	455
Figure 7.2.2.97:	Cowl Effects, CR=3, Re=1.14million/ft, Sidewall Pressures	455
Figure 7.2.2.98:	Cowl Effects, CR=3, Re=1.14million/ft, Sidewall Pressures	455
Figure 7.2.2.99:	Cowl Effects, CR=3, Re=1.14million/ft, Sidewall Pressures	456
Figure 7.2.2.100:	Cowl Effects, CR=3, Re=1.14million/ft, Sidewall Pressures	456
Figure 7.2.2.101:	Cowl Effects, CR=3, Re=1.14million/ft, Sidewall Pressures	456
Figure 7.2.2.102:	Cowl Effects, CR=3, Re=1.14million/ft, Sidewall Pressures	456
Figure 7.2.2.103:	Cowl Effects, CR=3, Re=1.14million/ft, Sidewall Pressures	456
Figure 7.2.2.104:	Cowl Effects, CR=3, Re=1.14million/ft, Sidewall Pressures	456
Figure 7.2.2.105:	Cowl Effects, CR=3, Re=1.14million/ft, Sidewall Pressures	456
Figure 7.2.2.106:	Cowl Effects, CR=3, Re=1.14million/ft, Sidewall Pressures	456
Figure 7.2.2.107:	Cowl Effects, CR=3, Re=0.55million/ft, CR=3 Centerline Pressures	457
Figure 7.2.2.108:	Cowl Effects, CR=3, Re=0.55million/ft, CR=5 Centerline Pressures	457
Figure 7.2.2.109:	Cowl Effects, CR=3, Re=0.55million/ft, CR=9 Centerline Pressures	457
Figure 7.2.2.110:	Cowl Effects, CR=3, Re=0.55million/ft, Baseplate Pressures	457
Figure 7.2.2.111:	Cowl Effects, CR=3, Re=0.55million/ft, Baseplate Pressures	457
Figure 7.2.2.112:	Cowl Effects, CR=3, Re=0.55million/ft, Baseplate Pressures	457

Figure 7.2.2.113: Cowl Effects, CR=3, Re=0.55million/ft, Baseplate Pressures	457
Figure 7.2.2.114: Cowl Effects, CR=3, Re=0.55million/ft, Baseplate Pressures	457
Figure 7.2.2.115: Cowl Effects, CR=3, Re=0.55million/ft, Baseplate Pressures	457
Figure 7.2.2.116: Cowl Effects, CR=3, Re=0.55million/ft, Baseplate Pressures	458
Figure 7.2.2.117: Cowl Effects, CR=3, Re=0.55million/ft, Baseplate Pressures	458
Figure 7.2.2.118: Cowl Effects, CR=3, Re=0.55million/ft, Baseplate Pressures	458
Figure 7.2.2.119: Cowl Effects, CR=3, Re=0.55million/ft, Baseplate Pressures	458
Figure 7.2.2.120: Cowl Effects, CR=3, Re=0.55million/ft, Baseplate Pressures	458
Figure 7.2.2.121: Cowl Effects, CR=3, Re=0.55million/ft, Baseplate Pressures	458
Figure 7.2.2.122: Cowl Effects, CR=3, Re=0.55million/ft, Baseplate Pressures	458
Figure 7.2.2.123: Cowl Effects, CR=3, Re=0.55million/ft, Baseplate Pressures	458
Figure 7.2.2.124: Cowl Effects, CR=3, Re=0.55million/ft, Baseplate Pressures	458
Figure 7.2.2.125: Cowl Effects, CR=3, Re=0.55million/ft, Baseplate Pressures	459
Figure 7.2.2.126: Cowl Effects, CR=3, Re=0.55million/ft, Baseplate Pressures	459
Figure 7.2.2.127: Cowl Effects, CR=3, Re=0.55million/ft, Baseplate Pressures	459
Figure 7.2.2.128: Cowl Effects, CR=3, Re=0.55million/ft, Baseplate Pressures	459
Figure 7.2.2.129: Cowl Effects, CR=3, Re=0.55million/ft, Baseplate Pressures	459
Figure 7.2.2.130: Cowl Effects, CR=3, Re=0.55million/ft, Baseplate Pressures	459
Figure 7.2.2.131: Cowl Effects, CR=3, Re=0.55million/ft, Baseplate Pressures	459
Figure 7.2.2.132: Cowl Effects, CR=3, Re=0.55million/ft, Cowl Pressures	459
Figure 7.2.2.133: Cowl Effects, CR=3, Re=0.55million/ft, Sidewall Centerline Pressures	459
Figure 7.2.2.134: Cowl Effects, CR=3, Re=0.55million/ft, Sidewall Centerline Pressures	460
Figure 7.2.2.135: Cowl Effects, CR=3, Re=0.55million/ft, Sidewall Pressures	460
Figure 7.2.2.136: Cowl Effects, CR=3, Re=0.55million/ft, Sidewall Pressures	460
Figure 7.2.2.137: Cowl Effects, CR=3, Re=0.55million/ft, Sidewall Pressures	460
Figure 7.2.2.138: Cowl Effects, CR=3, Re=0.55million/ft, Sidewall Pressures	460
Figure 7.2.2.139: Cowl Effects, CR=3, Re=0.55million/ft, Sidewall Pressures	460
Figure 7.2.2.140: Cowl Effects, CR=3, Re=0.55million/ft, Sidewall Pressures	460
Figure 7.2.2.141: Cowl Effects, CR=3, Re=0.55million/ft, Sidewall Pressures	460
Figure 7.2.2.142: Cowl Effects, CR=3, Re=0.55million/ft, Sidewall Pressures	460
Figure 7.2.2.143: Cowl Effects, CR=3, Re=0.55million/ft, Sidewall Pressures	461

Figure 7.2.2.144: Cowl Effects, CR=3, Re=0.55million/ft, Sidewall Pressures	461
Figure 7.2.2.145: Cowl Effects, CR=3, Re=0.55million/ft, Sidewall Pressures	461
Figure 7.2.2.146: Cowl Effects, CR=3, Re=0.55million/ft, Sidewall Pressures	461
Figure 7.2.2.147: Cowl Effects, CR=3, Re=0.55million/ft, Sidewall Pressures	461
Figure 7.2.2.148: Cowl Effects, CR=3, Re=0.55million/ft, Sidewall Pressures	461
Figure 7.2.2.149: Cowl Effects, CR=3, Re=0.55million/ft, Sidewall Pressures	461
Figure 7.2.2.150: Cowl Effects, CR=3, Re=0.55million/ft, Sidewall Pressures	461
Figure 7.2.2.151: Cowl Effects, CR=3, Re=0.55million/ft, Sidewall Pressures	461
Figure 7.2.2.152: Cowl Effects, CR=3, Re=0.55million/ft, Sidewall Pressures	462
Figure 7.2.2.153: Cowl Effects, CR=3, Re=0.55million/ft, Sidewall Pressures	462
Figure 7.2.2.154: Cowl Effects, CR=3, Re=0.55million/ft, Sidewall Pressures	462
Figure 7.2.2.155: Cowl Effects, CR=3, Re=0.55million/ft, Sidewall Pressures	462
Figure 7.2.2.156: Cowl Effects, CR=3, Re=0.55million/ft, Sidewall Pressures	462
Figure 7.2.2.157: Cowl Effects, CR=3, Re=0.55million/ft, Sidewall Pressures	462
Figure 7.2.2.158: Cowl Effects, CR=3, Re=0.55million/ft, Sidewall Pressures	462
Figure 7.2.2.159: Cowl Effects, CR=3, Re=0.55million/ft, Sidewall Pressures	462
Figure 7.2.2.160: Cowl Effects, CR=5, Re=2.15million/ft, CR=3 Centerline Pressures	463
Figure 7.2.2.161: Cowl Effects, CR=5, Re=2.15million/ft, CR=5 Centerline Pressures	463
Figure 7.2.2.162: Cowl Effects, CR=5, Re=2.15million/ft, CR=9 Centerline Pressures	463
Figure 7.2.2.163: Cowl Effects, CR=5, Re=2.15million/ft, Baseplate Pressures	463
Figure 7.2.2.164: Cowl Effects, CR=5, Re=2.15million/ft, Baseplate Pressures	463
Figure 7.2.2.165: Cowl Effects, CR=5, Re=2.15million/ft, Baseplate Pressures	463
Figure 7.2.2.166: Cowl Effects, CR=5, Re=2.15million/ft, Baseplate Pressures	463
Figure 7.2.2.167: Cowl Effects, CR=5, Re=2.15million/ft, Baseplate Pressures	463
Figure 7.2.2.168: Cowl Effects, CR=5, Re=2.15million/ft, Baseplate Pressures	463
Figure 7.2.2.169: Cowl Effects, CR=5, Re=2.15million/ft, Baseplate Pressures	464
Figure 7.2.2.170: Cowl Effects, CR=5, Re=2.15million/ft, Baseplate Pressures	464
Figure 7.2.2.171: Cowl Effects, CR=5, Re=2.15million/ft, Baseplate Pressures	464
Figure 7.2.2.172: Cowl Effects, CR=5, Re=2.15million/ft, Baseplate Pressures	464
Figure 7.2.2.173: Cowl Effects, CR=5, Re=2.15million/ft, Baseplate Pressures	464
Figure 7.2.2.174: Cowl Effects, CR=5, Re=2.15million/ft, Baseplate Pressures	464



Figure 7.2.2.175: Cowl Effects, CR=5, Re=2.15million/ft, Baseplate Pressures	464
Figure 7.2.2.176: Cowl Effects, CR=5, Re=2.15million/ft, Baseplate Pressures	464
Figure 7.2.2.177: Cowl Effects, CR=5, Re=2.15million/ft, Baseplate Pressures	464
Figure 7.2.2.178: Cowl Effects, CR=5, Re=2.15million/ft, Baseplate Pressures	465
Figure 7.2.2.179: Cowl Effects, CR=5, Re=2.15million/ft, Baseplate Pressures	465
Figure 7.2.2.180: Cowl Effects, CR=5, Re=2.15million/ft, Baseplate Pressures	465
Figure 7.2.2.181: Cowl Effects, CR=5, Re=2.15million/ft, Baseplate Pressures	465
Figure 7.2.2.182: Cowl Effects, CR=5, Re=2.15million/ft, Baseplate Pressures	465
Figure 7.2.2.183: Cowl Effects, CR=5, Re=2.15million/ft, Baseplate Pressures	465
Figure 7.2.2.184: Cowl Effects, CR=5, Re=2.15million/ft, Baseplate Pressures	465
Figure 7.2.2.185: Cowl Effects, CR=5, Re=2.15million/ft, Cowl Pressures	465
Figure 7.2.2.186: Cowl Effects, CR=5, Re=2.15million/ft, Sidewall Centerline Pressures	465
Figure 7.2.2.187: Cowl Effects, CR=5, Re=2.15million/ft, Sidewall Centerline Pressures	466
Figure 7.2.2.188: Cowl Effects, CR=5, Re=2.15million/ft, Sidewall Pressures	466
Figure 7.2.2.189: Cowl Effects, CR=5, Re=2.15million/ft, Sidewall Pressures	466
Figure 7.2.2.190: Cowl Effects, CR=5, Re=2.15million/ft, Sidewall Pressures	466
Figure 7.2.2.191: Cowl Effects, CR=5, Re=2.15million/ft, Sidewall Pressures	466
Figure 7.2.2.192: Cowl Effects, CR=5, Re=2.15million/ft, Sidewall Pressures	466
Figure 7.2.2.193: Cowl Effects, CR=5, Re=2.15million/ft, Sidewall Pressures	466
Figure 7.2.2.194: Cowl Effects, CR=5, Re=2.15million/ft, Sidewall Pressures	466
Figure 7.2.2.195: Cowl Effects, CR=5, Re=2.15million/ft, Sidewall Pressures	466
Figure 7.2.2.196: Cowl Effects, CR=5, Re=2.15million/ft, Sidewall Pressures	467
Figure 7.2.2.197: Cowl Effects, CR=5, Re=2.15million/ft, Sidewall Pressures	467
Figure 7.2.2.198: Cowl Effects, CR=5, Re=2.15million/ft, Sidewall Pressures	467
Figure 7.2.2.199: Cowl Effects, CR=5, Re=2.15million/ft, Sidewall Pressures	467
Figure 7.2.2.200: Cowl Effects, CR=5, Re=2.15million/ft, Sidewall Pressures	467
Figure 7.2.2.201: Cowl Effects, CR=5, Re=2.15million/ft, Sidewall Pressures	467
Figure 7.2.2.202: Cowl Effects, CR=5, Re=2.15million/ft, Sidewall Pressures	467
Figure 7.2.2.203: Cowl Effects, CR=5, Re=2.15million/ft, Sidewall Pressures	467
Figure 7.2.2.204: Cowl Effects, CR=5, Re=2.15million/ft, Sidewall Pressures	467
Figure 7.2.2.205: Cowl Effects, CR=5, Re=2.15million/ft, Sidewall Pressures	468

Figure 7.2.2.206: Cowl Effects, CR=5, Re=2.15million/ft, Sidewall Pressures	468
Figure 7.2.2.207: Cowl Effects, CR=5, Re=2.15million/ft, Sidewall Pressures	468
Figure 7.2.2.208: Cowl Effects, CR=5, Re=2.15million/ft, Sidewall Pressures	468
Figure 7.2.2.209: Cowl Effects, CR=5, Re=2.15million/ft, Sidewall Pressures	468
Figure 7.2.2.210: Cowl Effects, CR=5, Re=2.15million/ft, Sidewall Pressures	468
Figure 7.2.2.211: Cowl Effects, CR=5, Re=2.15million/ft, Sidewall Pressures	468
Figure 7.2.2.212: Cowl Effects, CR=5, Re=2.15million/ft, Sidewall Pressures	468
Figure 7.2.2.213: Cowl Effects, CR=5, Re=1.14million/ft, CR=3 Centerline Pressures	469
Figure 7.2.2.214: Cowl Effects, CR=5, Re=1.14million/ft, CR=5 Centerline Pressures	469
Figure 7.2.2.215: Cowl Effects, CR=5, Re=1.14million/ft, CR=9 Centerline Pressures	469
Figure 7.2.2.216: Cowl Effects, CR=5, Re=1.14million/ft, Baseplate Pressures	469
Figure 7.2.2.217: Cowl Effects, CR=5, Re=1.14million/ft, Baseplate Pressures	469
Figure 7.2.2.218: Cowl Effects, CR=5, Re=1.14million/ft, Baseplate Pressures	469
Figure 7.2.2.219: Cowl Effects, CR=5, Re=1.14million/ft, Baseplate Pressures	469
Figure 7.2.2.220: Cowl Effects, CR=5, Re=1.14million/ft, Baseplate Pressures	469
Figure 7.2.2.221: Cowl Effects, CR=5, Re=1.14million/ft, Baseplate Pressures	469
Figure 7.2.2.222: Cowl Effects, CR=5, Re=1.14million/ft, Baseplate Pressures	470
Figure 7.2.2.223: Cowl Effects, CR=5, Re=1.14million/ft, Baseplate Pressures	470
Figure 7.2.2.224: Cowl Effects, CR=5, Re=1.14million/ft, Baseplate Pressures	470
Figure 7.2.2.225: Cowl Effects, CR=5, Re=1.14million/ft, Baseplate Pressures	470
Figure 7.2.2.226: Cowl Effects, CR=5, Re=1.14million/ft, Baseplate Pressures	470
Figure 7.2.2.227: Cowl Effects, CR=5, Re=1.14million/ft, Baseplate Pressures	470
Figure 7.2.2.228: Cowl Effects, CR=5, Re=1.14million/ft, Baseplate Pressures	470
Figure 7.2.2.229: Cowl Effects, CR=5, Re=1.14million/ft, Baseplate Pressures	470
Figure 7.2.2.230: Cowl Effects, CR=5, Re=1.14million/ft, Baseplate Pressures	470
Figure 7.2.2.231: Cowl Effects, CR=5, Re=1.14million/ft, Baseplate Pressures	471
Figure 7.2.2.232: Cowl Effects, CR=5, Re=1.14million/ft, Baseplate Pressures	471
Figure 7.2.2.233: Cowl Effects, CR=5, Re=1.14million/ft, Baseplate Pressures	471
Figure 7.2.2.234: Cowl Effects, CR=5, Re=1.14million/ft, Baseplate Pressures	471
Figure 7.2.2.235: Cowl Effects, CR=5, Re=1.14million/ft, Baseplate Pressures	471

Figure 7.2.2.236: Cowl Effects, CR=5, Re=1.14million/ft, Baseplate Pressures	471
Figure 7.2.2.237: Cowl Effects, CR=5, Re=1.14million/ft, Baseplate Pressures	471
Figure 7.2.2.238: Cowl Effects, CR=5, Re=1.14million/ft, Cowl Pressures	471
Figure 7.2.2.239: Cowl Effects, CR=5, Re=1.14million/ft, Sidewall Centerline Pressures	471
Figure 7.2.2.240: Cowl Effects, CR=5, Re=1.14million/ft, Sidewall Centerline Pressures	472
Figure 7.2.2.241: Cowl Effects, CR=5, Re=1.14million/ft, Sidewall Pressures	472
Figure 7.2.2.242: Cowl Effects, CR=5, Re=1.14million/ft, Sidewall Pressures	472
Figure 7.2.2.243: Cowl Effects, CR=5, Re=1.14million/ft, Sidewall Pressures	472
Figure 7.2.2.244: Cowl Effects, CR=5, Re=1.14million/ft, Sidewall Pressures	472
Figure 7.2.2.245: Cowl Effects, CR=5, Re=1.14million/ft, Sidewall Pressures	472
Figure 7.2.2.246: Cowl Effects, CR=5, Re=1.14million/ft, Sidewall Pressures	472
Figure 7.2.2.247: Cowl Effects, CR=5, Re=1.14million/ft, Sidewall Pressures	472
Figure 7.2.2.248: Cowl Effects, CR=5, Re=1.14million/ft, Sidewall Pressures	472
Figure 7.2.2.249: Cowl Effects, CR=5, Re=1.14million/ft, Sidewall Pressures	473
Figure 7.2.2.250: Cowl Effects, CR=5, Re=1.14million/ft, Sidewall Pressures	473
Figure 7.2.2.251: Cowl Effects, CR=5, Re=1.14million/ft, Sidewall Pressures	473
Figure 7.2.2.252: Cowl Effects, CR=5, Re=1.14million/ft, Sidewall Pressures	473
Figure 7.2.2.253: Cowl Effects, CR=5, Re=1.14million/ft, Sidewall Pressures	473
Figure 7.2.2.254: Cowl Effects, CR=5, Re=1.14million/ft, Sidewall Pressures	473
Figure 7.2.2.255: Cowl Effects, CR=5, Re=1.14million/ft, Sidewall Pressures	473
Figure 7.2.2.256: Cowl Effects, CR=5, Re=1.14million/ft, Sidewall Pressures	473
Figure 7.2.2.257: Cowl Effects, CR=5, Re=1.14million/ft, Sidewall Pressures	473
Figure 7.2.2.258: Cowl Effects, CR=5, Re=1.14million/ft, Sidewall Pressures	474
Figure 7.2.2.259: Cowl Effects, CR=5, Re=1.14million/ft, Sidewall Pressures	474
Figure 7.2.2.260: Cowl Effects, CR=5, Re=1.14million/ft, Sidewall Pressures	474
Figure 7.2.2.261: Cowl Effects, CR=5, Re=1.14million/ft, Sidewall Pressures	474
Figure 7.2.2.262: Cowl Effects, CR=5, Re=1.14million/ft, Sidewall Pressures	474
Figure 7.2.2.263: Cowl Effects, CR=5, Re=1.14million/ft, Sidewall Pressures	474
Figure 7.2.2.264: Cowl Effects, CR=5, Re=1.14million/ft, Sidewall Pressures	474
Figure 7.2.2.265: Cowl Effects, CR=5, Re=1.14million/ft, Sidewall Pressures	474
Figure 7.2.2.266: Cowl Effects, CR=5, Re=0.55million/ft, CR=3 Centerline Pressures	475

Figure 7.2.2.267: Cowl Effects, CR=5, Re=0.55million/ft, CR=5 Centerline Pressures	475
Figure 7.2.2.268: Cowl Effects, CR=5, Re=0.55million/ft, CR=9 Centerline Pressures	475
Figure 7.2.2.269: Cowl Effects, CR=5, Re=0.55million/ft, Baseplate Pressures	475
Figure 7.2.2.270: Cowl Effects, CR=5, Re=0.55million/ft, Baseplate Pressures	475
Figure 7.2.2.271: Cowl Effects, CR=5, Re=0.55million/ft, Baseplate Pressures	475
Figure 7.2.2.272: Cowl Effects, CR=5, Re=0.55million/ft, Baseplate Pressures	475
Figure 7.2.2.273: Cowl Effects, CR=5, Re=0.55million/ft, Baseplate Pressures	475
Figure 7.2.2.274: Cowl Effects, CR=5, Re=0.55million/ft, Baseplate Pressures	475
Figure 7.2.2.275: Cowl Effects, CR=5, Re=0.55million/ft, Baseplate Pressures	476
Figure 7.2.2.276: Cowl Effects, CR=5, Re=0.55million/ft, Baseplate Pressures	476
Figure 7.2.2.277: Cowl Effects, CR=5, Re=0.55million/ft, Baseplate Pressures	476
Figure 7.2.2.278: Cowl Effects, CR=5, Re=0.55million/ft, Baseplate Pressures	476
Figure 7.2.2.279: Cowl Effects, CR=5, Re=0.55million/ft, Baseplate Pressures	476
Figure 7.2.2.280: Cowl Effects, CR=5, Re=0.55million/ft, Baseplate Pressures	476
Figure 7.2.2.281: Cowl Effects, CR=5, Re=0.55million/ft, Baseplate Pressures	476
Figure 7.2.2.282: Cowl Effects, CR=5, Re=0.55million/ft, Baseplate Pressures	476
Figure 7.2.2.283: Cowl Effects, CR=5, Re=0.55million/ft, Baseplate Pressures	476
Figure 7.2.2.284: Cowl Effects, CR=5, Re=0.55million/ft, Baseplate Pressures	477
Figure 7.2.2.285: Cowl Effects, CR=5, Re=0.55million/ft, Baseplate Pressures	477
Figure 7.2.2.286: Cowl Effects, CR=5, Re=0.55million/ft, Baseplate Pressures	477
Figure 7.2.2.287: Cowl Effects, CR=5, Re=0.55million/ft, Baseplate Pressures	477
Figure 7.2.2.288: Cowl Effects, CR=5, Re=0.55million/ft, Baseplate Pressures	477
Figure 7.2.2.289: Cowl Effects, CR=5, Re=0.55million/ft, Baseplate Pressures	477
Figure 7.2.2.290: Cowl Effects, CR=5, Re=0.55million/ft, Baseplate Pressures	477
Figure 7.2.2.291: Cowl Effects, CR=5, Re=0.55million/ft, Cowl Pressures	477
Figure 7.2.2.292: Cowl Effects, CR=5, Re=0.55million/ft, Sidewall Centerline Pressures	477
Figure 7.2.2.293: Cowl Effects, CR=5, Re=0.55million/ft, Sidewall Centerline Pressures	478
Figure 7.2.2.294: Cowl Effects, CR=5, Re=0.55million/ft, Sidewall Pressures	478
Figure 7.2.2.295: Cowl Effects, CR=5, Re=0.55million/ft, Sidewall Pressures	478
Figure 7.2.2.296: Cowl Effects, CR=5, Re=0.55million/ft, Sidewall Pressures	478
Figure 7.2.2.297: Cowl Effects, CR=5, Re=0.55million/ft, Sidewall Pressures	478

Figure 7.2.2.298: Cowl Effects, CR=5, Re=0.55million/ft, Sidewall Pressures	478
Figure 7.2.2.299: Cowl Effects, CR=5, Re=0.55million/ft, Sidewall Pressures	478
Figure 7.2.2.300: Cowl Effects, CR=5, Re=0.55million/ft, Sidewall Pressures	478
Figure 7.2.2.301: Cowl Effects, CR=5, Re=0.55million/ft, Sidewall Pressures	478
Figure 7.2.2.302: Cowl Effects, CR=5, Re=0.55million/ft, Sidewall Pressures	479
Figure 7.2.2.303: Cowl Effects, CR=5, Re=0.55million/ft, Sidewall Pressures	479
Figure 7.2.2.304: Cowl Effects, CR=5, Re=0.55million/ft, Sidewall Pressures	479
Figure 7.2.2.305: Cowl Effects, CR=5, Re=0.55million/ft, Sidewall Pressures	479
Figure 7.2.2.306: Cowl Effects, CR=5, Re=0.55million/ft, Sidewall Pressures	479
Figure 7.2.2.307: Cowl Effects, CR=5, Re=0.55million/ft, Sidewall Pressures	479
Figure 7.2.2.308: Cowl Effects, CR=5, Re=0.55million/ft, Sidewall Pressures	479
Figure 7.2.2.309: Cowl Effects, CR=5, Re=0.55million/ft, Sidewall Pressures	479
Figure 7.2.2.310: Cowl Effects, CR=5, Re=0.55million/ft, Sidewall Pressures	479
Figure 7.2.2.311: Cowl Effects, CR=5, Re=0.55million/ft, Sidewall Pressures	480
Figure 7.2.2.312: Cowl Effects, CR=5, Re=0.55million/ft, Sidewall Pressures	480
Figure 7.2.2.313: Cowl Effects, CR=5, Re=0.55million/ft, Sidewall Pressures	480
Figure 7.2.2.314: Cowl Effects, CR=5, Re=0.55million/ft, Sidewall Pressures	480
Figure 7.2.2.315: Cowl Effects, CR=5, Re=0.55million/ft, Sidewall Pressures	480
Figure 7.2.2.316: Cowl Effects, CR=5, Re=0.55million/ft, Sidewall Pressures	480
Figure 7.2.2.317: Cowl Effects, CR=5, Re=0.55million/ft, Sidewall Pressures	480
Figure 7.2.2.318: Cowl Effects, CR=5, Re=0.55million/ft, Sidewall Pressures	480
Figure 7.2.2.319: Cowl Effects, CR=9, Re=2.15million/ft, CR=3 Centerline Pressures	481
Figure 7.2.2.320: Cowl Effects, CR=9, Re=2.15million/ft, CR=5 Centerline Pressures	481
Figure 7.2.2.321: Cowl Effects, CR=9, Re=2.15million/ft, CR=9 Centerline Pressures	481
Figure 7.2.2.322: Cowl Effects, CR=9, Re=2.15million/ft, Baseplate Pressures	481
Figure 7.2.2.323: Cowl Effects, CR=9, Re=2.15million/ft, Baseplate Pressures	481
Figure 7.2.2.324: Cowl Effects, CR=9, Re=2.15million/ft, Baseplate Pressures	481
Figure 7.2.2.325: Cowl Effects, CR=9, Re=2.15million/ft, Baseplate Pressures	481
Figure 7.2.2.326: Cowl Effects, CR=9, Re=2.15million/ft, Baseplate Pressures	481
Figure 7.2.2.327: Cowl Effects, CR=9, Re=2.15million/ft, Baseplate Pressures	481
Figure 7.2.2.328: Cowl Effects, CR=9, Re=2.15million/ft, Baseplate Pressures	482

Figure 7.2.2.329: Cowl Effects, CR=9, Re=2.15million/ft, Baseplate Pressures	482
Figure 7.2.2.330: Cowl Effects, CR=9, Re=2.15million/ft, Baseplate Pressures	482
Figure 7.2.2.331: Cowl Effects, CR=9, Re=2.15million/ft, Baseplate Pressures	482
Figure 7.2.2.332: Cowl Effects, CR=9, Re=2.15million/ft, Baseplate Pressures	482
Figure 7.2.2.333: Cowl Effects, CR=9, Re=2.15million/ft, Baseplate Pressures	482
Figure 7.2.2.334: Cowl Effects, CR=9, Re=2.15million/ft, Baseplate Pressures	482
Figure 7.2.2.335: Cowl Effects, CR=9, Re=2.15million/ft, Baseplate Pressures	482
Figure 7.2.2.336: Cowl Effects, CR=9, Re=2.15million/ft, Baseplate Pressures	482
Figure 7.2.2.337: Cowl Effects, CR=9, Re=2.15million/ft, Baseplate Pressures	483
Figure 7.2.2.338: Cowl Effects, CR=9, Re=2.15million/ft, Baseplate Pressures	483
Figure 7.2.2.339: Cowl Effects, CR=9, Re=2.15million/ft, Baseplate Pressures	483
Figure 7.2.2.340: Cowl Effects, CR=9, Re=2.15million/ft, Baseplate Pressures	483
Figure 7.2.2.341: Cowl Effects, CR=9, Re=2.15million/ft, Baseplate Pressures	483
Figure 7.2.2.342: Cowl Effects, CR=9, Re=2.15million/ft, Baseplate Pressures	483
Figure 7.2.2.343: Cowl Effects, CR=9, Re=2.15million/ft, Baseplate Pressures	483
Figure 7.2.2.344: Cowl Effects, CR=9, Re=2.15million/ft, Cowl Pressures	483
Figure 7.2.2.345: Cowl Effects, CR=9, Re=2.15million/ft, Sidewall Centerline Pressures	483
Figure 7.2.2.346: Cowl Effects, CR=9, Re=2.15million/ft, Sidewall Centerline Pressures	484
Figure 7.2.2.347: Cowl Effects, CR=9, Re=2.15million/ft, Sidewall Pressures	484
Figure 7.2.2.348: Cowl Effects, CR=9, Re=2.15million/ft, Sidewall Pressures	484
Figure 7.2.2.349: Cowl Effects, CR=9, Re=2.15million/ft, Sidewall Pressures	484
Figure 7.2.2.350: Cowl Effects, CR=9, Re=2.15million/ft, Sidewall Pressures	484
Figure 7.2.2.351: Cowl Effects, CR=9, Re=2.15million/ft, Sidewall Pressures	484
Figure 7.2.2.352: Cowl Effects, CR=9, Re=2.15million/ft, Sidewall Pressures	484
Figure 7.2.2.353: Cowl Effects, CR=9, Re=2.15million/ft, Sidewall Pressures	484
Figure 7.2.2.354: Cowl Effects, CR=9, Re=2.15million/ft, Sidewall Pressures	484
Figure 7.2.2.355: Cowl Effects, CR=9, Re=2.15million/ft, Sidewall Pressures	485
Figure 7.2.2.356: Cowl Effects, CR=9, Re=2.15million/ft, Sidewall Pressures	485
Figure 7.2.2.357: Cowl Effects, CR=9, Re=2.15million/ft, Sidewall Pressures	485
Figure 7.2.2.358: Cowl Effects, CR=9, Re=2.15million/ft, Sidewall Pressures	485

Figure 7.2.2.359: Cowl Effects, CR=9, Re=2.15million/ft, Sidewall Pressures	485
Figure 7.2.2.360: Cowl Effects, CR=9, Re=2.15million/ft, Sidewall Pressures	485
Figure 7.2.2.361: Cowl Effects, CR=9, Re=2.15million/ft, Sidewall Pressures	485
Figure 7.2.2.362: Cowl Effects, CR=9, Re=2.15million/ft, Sidewall Pressures	485
Figure 7.2.2.363: Cowl Effects, CR=9, Re=2.15million/ft, Sidewall Pressures	485
Figure 7.2.2.364: Cowl Effects, CR=9, Re=2.15million/ft, Sidewall Pressures	486
Figure 7.2.2.365: Cowl Effects, CR=9, Re=2.15million/ft, Sidewall Pressures	486
Figure 7.2.2.366: Cowl Effects, CR=9, Re=2.15million/ft, Sidewall Pressures	486
Figure 7.2.2.367: Cowl Effects, CR=9, Re=2.15million/ft, Sidewall Pressures	486
Figure 7.2.2.368: Cowl Effects, CR=9, Re=2.15million/ft, Sidewall Pressures	486
Figure 7.2.2.369: Cowl Effects, CR=9, Re=2.15million/ft, Sidewall Pressures	486
Figure 7.2.2.370: Cowl Effects, CR=9, Re=2.15million/ft, Sidewall Pressures	486
Figure 7.2.2.371: Cowl Effects, CR=9, Re=2.15million/ft, Sidewall Pressures	486
Figure 7.2.2.372: Cowl Effects, CR=9, Re=1.14million/ft, CR=3 Centerline Pressures	487
Figure 7.2.2.373: Cowl Effects, CR=9, Re=1.14million/ft, CR=5 Centerline Pressures	487
Figure 7.2.2.374: Cowl Effects, CR=9, Re=1.14million/ft, CR=9 Centerline Pressures	487
Figure 7.2.2.375: Cowl Effects, CR=9, Re=1.14million/ft, Baseplate Pressures	487
Figure 7.2.2.376: Cowl Effects, CR=9, Re=1.14million/ft, Baseplate Pressures	487
Figure 7.2.2.377: Cowl Effects, CR=9, Re=1.14million/ft, Baseplate Pressures	487
Figure 7.2.2.378: Cowl Effects, CR=9, Re=1.14million/ft, Baseplate Pressures	487
Figure 7.2.2.379: Cowl Effects, CR=9, Re=1.14million/ft, Baseplate Pressures	487
Figure 7.2.2.380: Cowl Effects, CR=9, Re=1.14million/ft, Baseplate Pressures	487
Figure 7.2.2.381: Cowl Effects, CR=9, Re=1.14million/ft, Baseplate Pressures	488
Figure 7.2.2.382: Cowl Effects, CR=9, Re=1.14million/ft, Baseplate Pressures	488
Figure 7.2.2.383: Cowl Effects, CR=9, Re=1.14million/ft, Baseplate Pressures	488
Figure 7.2.2.384: Cowl Effects, CR=9, Re=1.14million/ft, Baseplate Pressures	488
Figure 7.2.2.385: Cowl Effects, CR=9, Re=1.14million/ft, Baseplate Pressures	488
Figure 7.2.2.386: Cowl Effects, CR=9, Re=1.14million/ft, Baseplate Pressures	488
Figure 7.2.2.387: Cowl Effects, CR=9, Re=1.14million/ft, Baseplate Pressures	488
Figure 7.2.2.388: Cowl Effects, CR=9, Re=1.14million/ft, Baseplate Pressures	488
Figure 7.2.2.389: Cowl Effects, CR=9, Re=1.14million/ft, Baseplate Pressures	488

Figure 7.2.2.390: Cowl Effects, CR=9, Re=1.14million/ft, Baseplate Pressures	489
Figure 7.2.2.391: Cowl Effects, CR=9, Re=1.14million/ft, Baseplate Pressures	489
Figure 7.2.2.392: Cowl Effects, CR=9, Re=1.14million/ft, Baseplate Pressures	489
Figure 7.2.2.393: Cowl Effects, CR=9, Re=1.14million/ft, Baseplate Pressures	489
Figure 7.2.2.394: Cowl Effects, CR=9, Re=1.14million/ft, Baseplate Pressures	489
Figure 7.2.2.395: Cowl Effects, CR=9, Re=1.14million/ft, Baseplate Pressures	489
Figure 7.2.2.396: Cowl Effects, CR=9, Re=1.14million/ft, Baseplate Pressures	489
Figure 7.2.2.397: Cowl Effects, CR=9, Re=1.14million/ft, Cowl Pressures	489
Figure 7.2.2.398: Cowl Effects, CR=9, Re=1.14million/ft, Sidewall Centerline Pressures	489
Figure 7.2.2.399: Cowl Effects, CR=9, Re=1.14million/ft, Sidewall Centerline Pressures	490
Figure 7.2.2.400: Cowl Effects, CR=9, Re=1.14million/ft, Sidewall Pressures	490
Figure 7.2.2.401: Cowl Effects, CR=9, Re=1.14million/ft, Sidewall Pressures	490
Figure 7.2.2.402: Cowl Effects, CR=9, Re=1.14million/ft, Sidewall Pressures	490
Figure 7.2.2.403: Cowl Effects, CR=9, Re=1.14million/ft, Sidewall Pressures	490
Figure 7.2.2.404: Cowl Effects, CR=9, Re=1.14million/ft, Sidewall Pressures	490
Figure 7.2.2.405: Cowl Effects, CR=9, Re=1.14million/ft, Sidewall Pressures	490
Figure 7.2.2.406: Cowl Effects, CR=9, Re=1.14million/ft, Sidewall Pressures	490
Figure 7.2.2.407: Cowl Effects, CR=9, Re=1.14million/ft, Sidewall Pressures	490
Figure 7.2.2.408: Cowl Effects, CR=9, Re=1.14million/ft, Sidewall Pressures	491
Figure 7.2.2.409: Cowl Effects, CR=9, Re=1.14million/ft, Sidewall Pressures	491
Figure 7.2.2.410: Cowl Effects, CR=9, Re=1.14million/ft, Sidewall Pressures	491
Figure 7.2.2.411: Cowl Effects, CR=9, Re=1.14million/ft, Sidewall Pressures	491
Figure 7.2.2.412: Cowl Effects, CR=9, Re=1.14million/ft, Sidewall Pressures	491
Figure 7.2.2.413: Cowl Effects, CR=9, Re=1.14million/ft, Sidewall Pressures	491
Figure 7.2.2.414: Cowl Effects, CR=9, Re=1.14million/ft, Sidewall Pressures	491
Figure 7.2.2.415: Cowl Effects, CR=9, Re=1.14million/ft, Sidewall Pressures	491
Figure 7.2.2.416: Cowl Effects, CR=9, Re=1.14million/ft, Sidewall Pressures	491
Figure 7.2.2.417: Cowl Effects, CR=9, Re=1.14million/ft, Sidewall Pressures	492
Figure 7.2.2.418: Cowl Effects, CR=9, Re=1.14million/ft, Sidewall Pressures	492
Figure 7.2.2.419: Cowl Effects, CR=9, Re=1.14million/ft, Sidewall Pressures	492
Figure 7.2.2.420: Cowl Effects, CR=9, Re=1.14million/ft, Sidewall Pressures	492



Figure 7.2.2.421: Cowl Effects, CR=9, Re=1.14million/ft, Sidewall Pressures	492
Figure 7.2.2.422: Cowl Effects, CR=9, Re=1.14million/ft, Sidewall Pressures	492
Figure 7.2.2.423: Cowl Effects, CR=9, Re=1.14million/ft, Sidewall Pressures	492
Figure 7.2.2.424: Cowl Effects, CR=9, Re=1.14million/ft, Sidewall Pressures	492
Figure 7.2.2.425: Cowl Effects, CR=9, Re=0.55million/ft, CR=3 Centerline Pressures	493
Figure 7.2.2.426: Cowl Effects, CR=9, Re=0.55million/ft, CR=5 Centerline Pressures	493
Figure 7.2.2.427: Cowl Effects, CR=9, Re=0.55million/ft, CR=9 Centerline Pressures	493
Figure 7.2.2.428: Cowl Effects, CR=9, Re=0.55million/ft, Baseplate Pressures	493
Figure 7.2.2.429: Cowl Effects, CR=9, Re=0.55million/ft, Baseplate Pressures	493
Figure 7.2.2.430: Cowl Effects, CR=9, Re=0.55million/ft, Baseplate Pressures	493
Figure 7.2.2.431: Cowl Effects, CR=9, Re=0.55million/ft, Baseplate Pressures	493
Figure 7.2.2.432: Cowl Effects, CR=9, Re=0.55million/ft, Baseplate Pressures	493
Figure 7.2.2.433: Cowl Effects, CR=9, Re=0.55million/ft, Baseplate Pressures	493
Figure 7.2.2.434: Cowl Effects, CR=9, Re=0.55million/ft, Baseplate Pressures	494
Figure 7.2.2.435: Cowl Effects, CR=9, Re=0.55million/ft, Baseplate Pressures	494
Figure 7.2.2.436: Cowl Effects, CR=9, Re=0.55million/ft, Baseplate Pressures	494
Figure 7.2.2.437: Cowl Effects, CR=9, Re=0.55million/ft, Baseplate Pressures	494
Figure 7.2.2.438: Cowl Effects, CR=9, Re=0.55million/ft, Baseplate Pressures	494
Figure 7.2.2.439: Cowl Effects, CR=9, Re=0.55million/ft, Baseplate Pressures	494
Figure 7.2.2.440: Cowl Effects, CR=9, Re=0.55million/ft, Baseplate Pressures	494
Figure 7.2.2.441: Cowl Effects, CR=9, Re=0.55million/ft, Baseplate Pressures	494
Figure 7.2.2.442: Cowl Effects, CR=9, Re=0.55million/ft, Baseplate Pressures	494
Figure 7.2.2.443: Cowl Effects, CR=9, Re=0.55million/ft, Baseplate Pressures	495
Figure 7.2.2.444: Cowl Effects, CR=9, Re=0.55million/ft, Baseplate Pressures	495
Figure 7.2.2.445: Cowl Effects, CR=9, Re=0.55million/ft, Baseplate Pressures	495
Figure 7.2.2.446: Cowl Effects, CR=9, Re=0.55million/ft, Baseplate Pressures	495
Figure 7.2.2.447: Cowl Effects, CR=9, Re=0.55million/ft, Baseplate Pressures	495
Figure 7.2.2.448: Cowl Effects, CR=9, Re=0.55million/ft, Baseplate Pressures	495
Figure 7.2.2.449: Cowl Effects, CR=9, Re=0.55million/ft, Baseplate Pressures	495
Figure 7.2.2.450: Cowl Effects, CR=9, Re=0.55million/ft, Cowl Pressures	495
Figure 7.2.2.451: Cowl Effects, CR=9, Re=0.55million/ft, Sidewall Centerline Pressures	495

Figure 7.2.2.452: Cowl Effects, CR=9, Re=0.55million/ft, Sidewall Centerline Pressures	496
Figure 7.2.2.453: Cowl Effects, CR=9, Re=0.55million/ft, Sidewall Pressures	496
Figure 7.2.2.454: Cowl Effects, CR=9, Re=0.55million/ft, Sidewall Pressures	496
Figure 7.2.2.455: Cowl Effects, CR=9, Re=0.55million/ft, Sidewall Pressures	496
Figure 7.2.2.456: Cowl Effects, CR=9, Re=0.55million/ft, Sidewall Pressures	496
Figure 7.2.2.457: Cowl Effects, CR=9, Re=0.55million/ft, Sidewall Pressures	496
Figure 7.2.2.458: Cowl Effects, CR=9, Re=0.55million/ft, Sidewall Pressures	496
Figure 7.2.2.459: Cowl Effects, CR=9, Re=0.55million/ft, Sidewall Pressures	496
Figure 7.2.2.460: Cowl Effects, CR=9, Re=0.55million/ft, Sidewall Pressures	496
Figure 7.2.2.461: Cowl Effects, CR=9, Re=0.55million/ft, Sidewall Pressures	497
Figure 7.2.2.462: Cowl Effects, CR=9, Re=0.55million/ft, Sidewall Pressures	497
Figure 7.2.2.463: Cowl Effects, CR=9, Re=0.55million/ft, Sidewall Pressures	497
Figure 7.2.2.464: Cowl Effects, CR=9, Re=0.55million/ft, Sidewall Pressures	497
Figure 7.2.2.465: Cowl Effects, CR=9, Re=0.55million/ft, Sidewall Pressures	497
Figure 7.2.2.466: Cowl Effects, CR=9, Re=0.55million/ft, Sidewall Pressures	497
Figure 7.2.2.467: Cowl Effects, CR=9, Re=0.55million/ft, Sidewall Pressures	497
Figure 7.2.2.468: Cowl Effects, CR=9, Re=0.55million/ft, Sidewall Pressures	497
Figure 7.2.2.469: Cowl Effects, CR=9, Re=0.55million/ft, Sidewall Pressures	497
Figure 7.2.2.470: Cowl Effects, CR=9, Re=0.55million/ft, Sidewall Pressures	498
Figure 7.2.2.471: Cowl Effects, CR=9, Re=0.55million/ft, Sidewall Pressures	498
Figure 7.2.2.472: Cowl Effects, CR=9, Re=0.55million/ft, Sidewall Pressures	498
Figure 7.2.2.473: Cowl Effects, CR=9, Re=0.55million/ft, Sidewall Pressures	498
Figure 7.2.2.474: Cowl Effects, CR=9, Re=0.55million/ft, Sidewall Pressures	498
Figure 7.2.2.475: Cowl Effects, CR=9, Re=0.55million/ft, Sidewall Pressures	498
Figure 7.2.2.476: Cowl Effects, CR=9, Re=0.55million/ft, Sidewall Pressures	498
Figure 7.2.2.477: Cowl Effects, CR=9, Re=0.55million/ft, Sidewall Pressures	498
Figure 7.2.3.1: Re Effects, CR=3, 0% Cowl, CR=3 Centerline Pressures	499
Figure 7.2.3.2: Re Effects, CR=3, 0% Cowl, CR=5 Centerline Pressures	499
Figure 7.2.3.3: Re Effects, CR=3, 0% Cowl, CR=9 Centerline Pressures	499
Figure 7.2.3.4: Re Effects, CR=3, 0% Cowl, Baseplate Pressures	499

Figure 7.2.3.5:	Re Effects, CR=3, 0% Cowl, Baseplate Pressures	499
Figure 7.2.3.6:	Re Effects, CR=3, 0% Cowl, Baseplate Pressures	499
Figure 7.2.3.7:	Re Effects, CR=3, 0% Cowl, Baseplate Pressures	499
Figure 7.2.3.8:	Re Effects, CR=3, 0% Cowl, Baseplate Pressures	499
Figure 7.2.3.9:	Re Effects, CR=3, 0% Cowl, Baseplate Pressures	499
Figure 7.2.3.10:	Re Effects, CR=3, 0% Cowl, Baseplate Pressures	500
Figure 7.2.3.11:	Re Effects, CR=3, 0% Cowl, Baseplate Pressures	500
Figure 7.2.3.12:	Re Effects, CR=3, 0% Cowl, Baseplate Pressures	500
Figure 7.2.3.13:	Re Effects, CR=3, 0% Cowl, Baseplate Pressures	500
Figure 7.2.3.14:	Re Effects, CR=3, 0% Cowl, Baseplate Pressures	500
Figure 7.2.3.15:	Re Effects, CR=3, 0% Cowl, Baseplate Pressures	500
Figure 7.2.3.16:	Re Effects, CR=3, 0% Cowl, Baseplate Pressures	500
Figure 7.2.3.17:	Re Effects, CR=3, 0% Cowl, Baseplate Pressures	500
Figure 7.2.3.18:	Re Effects, CR=3, 0% Cowl, Baseplate Pressures	500
Figure 7.2.3.19:	Re Effects, CR=3, 0% Cowl, Baseplate Pressures	501
Figure 7.2.3.20:	Re Effects, CR=3, 0% Cowl, Baseplate Pressures	501
Figure 7.2.3.21:	Re Effects, CR=3, 0% Cowl, Baseplate Pressures	501
Figure 7.2.3.22:	Re Effects, CR=3, 0% Cowl, Baseplate Pressures	501
Figure 7.2.3.23:	Re Effects, CR=3, 0% Cowl, Baseplate Pressures	501
Figure 7.2.3.24:	Re Effects, CR=3, 0% Cowl, Baseplate Pressures	501
Figure 7.2.3.25:	Re Effects, CR=3, 0% Cowl, Baseplate Pressures	501
Figure 7.2.3.26:	Re Effects, CR=3, 0% Cowl, Cowl Pressures	501
Figure 7.2.3.27:	Re Effects, CR=3, 0% Cowl, Sidewall Centerline Pressures	501
Figure 7.2.3.28:	Re Effects, CR=3, 0% Cowl, Sidewall Centerline Pressures	502
Figure 7.2.3.29:	Re Effects, CR=3, 0% Cowl, Sidewall Pressures	502
Figure 7.2.3.30:	Re Effects, CR=3, 0% Cowl, Sidewall Pressures	502
Figure 7.2.3.31:	Re Effects, CR=3, 0% Cowl, Sidewall Pressures	502
Figure 7.2.3.32:	Re Effects, CR=3, 0% Cowl, Sidewall Pressures	502
Figure 7.2.3.33:	Re Effects, CR=3, 0% Cowl, Sidewall Pressures	502
Figure 7.2.3.34:	Re Effects, CR=3, 0% Cowl, Sidewall Pressures	502
Figure 7.2.3.35:	Re Effects, CR=3, 0% Cowl, Sidewall Pressures	502

Figure 7.2.3.36:	Re Effects, CR=3, 0% Cowl, Sidewall Pressures	502
Figure 7.2.3.37:	Re Effects, CR=3, 0% Cowl, Sidewall Pressures	503
Figure 7.2.3.38:	Re Effects, CR=3, 0% Cowl, Sidewall Pressures	503
Figure 7.2.3.39:	Re Effects, CR=3, 0% Cowl, Sidewall Pressures	503
Figure 7.2.3.40:	Re Effects, CR=3, 0% Cowl, Sidewall Pressures	503
Figure 7.2.3.41:	Re Effects, CR=3, 0% Cowl, Sidewall Pressures	503
Figure 7.2.3.42:	Re Effects, CR=3, 0% Cowl, Sidewall Pressures	503
Figure 7.2.3.43:	Re Effects, CR=3, 0% Cowl, Sidewall Pressures	503
Figure 7.2.3.44:	Re Effects, CR=3, 0% Cowl, Sidewall Pressures	503
Figure 7.2.3.45:	Re Effects, CR=3, 0% Cowl, Sidewall Pressures	503
Figure 7.2.3.46:	Re Effects, CR=3, 0% Cowl, Sidewall Pressures	504
Figure 7.2.3.47:	Re Effects, CR=3, 0% Cowl, Sidewall Pressures	504
Figure 7.2.3.48:	Re Effects, CR=3, 0% Cowl, Sidewall Pressures	504
Figure 7.2.3.49:	Re Effects, CR=3, 0% Cowl, Sidewall Pressures	504
Figure 7.2.3.50:	Re Effects, CR=3, 0% Cowl, Sidewall Pressures	504
Figure 7.2.3.51:	Re Effects, CR=3, 0% Cowl, Sidewall Pressures	504
Figure 7.2.3.52:	Re Effects, CR=3, 0% Cowl, Sidewall Pressures	504
Figure 7.2.3.53:	Re Effects, CR=3, 0% Cowl, Sidewall Pressures	504
Figure 7.2.3.54:	Re Effects, CR=3, 25% Cowl, CR=3 Centerline Pressures	505
Figure 7.2.3.55:	Re Effects, CR=3, 25% Cowl, CR=5 Centerline Pressures	505
Figure 7.2.3.56:	Re Effects, CR=3, 25% Cowl, CR=9 Centerline Pressures	505
Figure 7.2.3.57:	Re Effects, CR=3, 25% Cowl, Baseplate Pressures	505
Figure 7.2.3.58:	Re Effects, CR=3, 25% Cowl, Baseplate Pressures	505
Figure 7.2.3.59:	Re Effects, CR=3, 25% Cowl, Baseplate Pressures	505
Figure 7.2.3.60:	Re Effects, CR=3, 25% Cowl, Baseplate Pressures	505
Figure 7.2.3.61:	Re Effects, CR=3, 25% Cowl, Baseplate Pressures	505
Figure 7.2.3.62:	Re Effects, CR=3, 25% Cowl, Baseplate Pressures	505
Figure 7.2.3.63:	Re Effects, CR=3, 25% Cowl, Baseplate Pressures	506
Figure 7.2.3.64:	Re Effects, CR=3, 25% Cowl, Baseplate Pressures	506
Figure 7.2.3.65:	Re Effects, CR=3, 25% Cowl, Baseplate Pressures	506
Figure 7.2.3.66:	Re Effects, CR=3, 25% Cowl, Baseplate Pressures	506

Figure 7.2.3.67:	Re Effects, CR=3, 25% Cowl, Baseplate Pressures	506
Figure 7.2.3.68:	Re Effects, CR=3, 25% Cowl, Baseplate Pressures	506
Figure 7.2.3.69:	Re Effects, CR=3, 25% Cowl, Baseplate Pressures	506
Figure 7.2.3.70:	Re Effects, CR=3, 25% Cowl, Baseplate Pressures	506
Figure 7.2.3.71:	Re Effects, CR=3, 25% Cowl, Baseplate Pressures	506
Figure 7.2.3.72:	Re Effects, CR=3, 25% Cowl, Baseplate Pressures	507
Figure 7.2.3.73:	Re Effects, CR=3, 25% Cowl, Baseplate Pressures	507
Figure 7.2.3.74:	Re Effects, CR=3, 25% Cowl, Baseplate Pressures	507
Figure 7.2.3.75:	Re Effects, CR=3, 25% Cowl, Baseplate Pressures	507
Figure 7.2.3.76:	Re Effects, CR=3, 25% Cowl, Baseplate Pressures	507
Figure 7.2.3.77:	Re Effects, CR=3, 25% Cowl, Baseplate Pressures	507
Figure 7.2.3.78:	Re Effects, CR=3, 25% Cowl, Baseplate Pressures	507
Figure 7.2.3.79:	Re Effects, CR=3, 25% Cowl, Cowl Pressures	507
Figure 7.2.3.80:	Re Effects, CR=3, 25% Cowl, Sidewall Centerline Pressures	507
Figure 7.2.3.81:	Re Effects, CR=3, 25% Cowl, Sidewall Centerline Pressures	508
Figure 7.2.3.82:	Re Effects, CR=3, 25% Cowl, Sidewall Pressures	508
Figure 7.2.3.83:	Re Effects, CR=3, 25% Cowl, Sidewall Pressures	508
Figure 7.2.3.84:	Re Effects, CR=3, 25% Cowl, Sidewall Pressures	508
Figure 7.2.3.85:	Re Effects, CR=3, 25% Cowl, Sidewall Pressures	508
Figure 7.2.3.86:	Re Effects, CR=3, 25% Cowl, Sidewall Pressures	508
Figure 7.2.3.87:	Re Effects, CR=3, 25% Cowl, Sidewall Pressures	508
Figure 7.2.3.88:	Re Effects, CR=3, 25% Cowl, Sidewall Pressures	508
Figure 7.2.3.89:	Re Effects, CR=3, 25% Cowl, Sidewall Pressures	508
Figure 7.2.3.90:	Re Effects, CR=3, 25% Cowl, Sidewall Pressures	509
Figure 7.2.3.91:	Re Effects, CR=3, 25% Cowl, Sidewall Pressures	509
Figure 7.2.3.92:	Re Effects, CR=3, 25% Cowl, Sidewall Pressures	509
Figure 7.2.3.93:	Re Effects, CR=3, 25% Cowl, Sidewall Pressures	509
Figure 7.2.3.94:	Re Effects, CR=3, 25% Cowl, Sidewall Pressures	509
Figure 7.2.3.95:	Re Effects, CR=3, 25% Cowl, Sidewall Pressures	509
Figure 7.2.3.96:	Re Effects, CR=3, 25% Cowl, Sidewall Pressures	509
Figure 7.2.3.97:	Re Effects, CR=3, 25% Cowl, Sidewall Pressures	509

Figure 7.2.3.98: Re Effects, CR=3, 25% Cowl, Sidewall Pressures	509
Figure 7.2.3.99: Re Effects, CR=3, 25% Cowl, Sidewall Pressures	510
Figure 7.2.3.100: Re Effects, CR=3, 25% Cowl, Sidewall Pressures	510
Figure 7.2.3.101: Re Effects, CR=3, 25% Cowl, Sidewall Pressures	510
Figure 7.2.3.102: Re Effects, CR=3, 25% Cowl, Sidewall Pressures	510
Figure 7.2.3.103: Re Effects, CR=3, 25% Cowl, Sidewall Pressures	510
Figure 7.2.3.104: Re Effects, CR=3, 25% Cowl, Sidewall Pressures	510
Figure 7.2.3.105: Re Effects, CR=3, 25% Cowl, Sidewall Pressures	510
Figure 7.2.3.106: Re Effects, CR=3, 25% Cowl, Sidewall Pressures	510
Figure 7.2.3.107: Re Effects, CR=3, 50% Cowl, CR=3 Centerline Pressures	511
Figure 7.2.3.108: Re Effects, CR=3, 50% Cowl, CR=5 Centerline Pressures	511
Figure 7.2.3.109: Re Effects, CR=3, 50% Cowl, CR=9 Centerline Pressures	511
Figure 7.2.3.110: Re Effects, CR=3, 50% Cowl, Baseplate Pressures	511
Figure 7.2.3.111: Re Effects, CR=3, 50% Cowl, Baseplate Pressures	511
Figure 7.2.3.112: Re Effects, CR=3, 50% Cowl, Baseplate Pressures	511
Figure 7.2.3.113: Re Effects, CR=3, 50% Cowl, Baseplate Pressures	511
Figure 7.2.3.114: Re Effects, CR=3, 50% Cowl, Baseplate Pressures	511
Figure 7.2.3.115: Re Effects, CR=3, 50% Cowl, Baseplate Pressures	511
Figure 7.2.3.116: Re Effects, CR=3, 50% Cowl, Baseplate Pressures	512
Figure 7.2.3.117: Re Effects, CR=3, 50% Cowl, Baseplate Pressures	512
Figure 7.2.3.118: Re Effects, CR=3, 50% Cowl, Baseplate Pressures	512
Figure 7.2.3.119: Re Effects, CR=3, 50% Cowl, Baseplate Pressures	512
Figure 7.2.3.120: Re Effects, CR=3, 50% Cowl, Baseplate Pressures	512
Figure 7.2.3.121: Re Effects, CR=3, 50% Cowl, Baseplate Pressures	512
Figure 7.2.3.122: Re Effects, CR=3, 50% Cowl, Baseplate Pressures	512
Figure 7.2.3.123: Re Effects, CR=3, 50% Cowl, Baseplate Pressures	512
Figure 7.2.3.124: Re Effects, CR=3, 50% Cowl, Baseplate Pressures	512
Figure 7.2.3.125: Re Effects, CR=3, 50% Cowl, Baseplate Pressures	513
Figure 7.2.3.126: Re Effects, CR=3, 50% Cowl, Baseplate Pressures	513
Figure 7.2.3.127: Re Effects, CR=3, 50% Cowl, Baseplate Pressures	513

Figure 7.2.3.128: Re Effects, CR=3, 50% Cowl, Baseplate Pressures	513
Figure 7.2.3.129: Re Effects, CR=3, 50% Cowl, Baseplate Pressures	513
Figure 7.2.3.130: Re Effects, CR=3, 50% Cowl, Baseplate Pressures	513
Figure 7.2.3.131: Re Effects, CR=3, 50% Cowl, Baseplate Pressures	513
Figure 7.2.3.132: Re Effects, CR=3, 50% Cowl, Cowl Pressures	513
Figure 7.2.3.133: Re Effects, CR=3, 50% Cowl, Sidewall Centerline Pressures	513
Figure 7.2.3.134: Re Effects, CR=3, 50% Cowl, Sidewall Centerline Pressures	514
Figure 7.2.3.135: Re Effects, CR=3, 50% Cowl, Sidewall Pressures	514
Figure 7.2.3.136: Re Effects, CR=3, 50% Cowl, Sidewall Pressures	514
Figure 7.2.3.137: Re Effects, CR=3, 50% Cowl, Sidewall Pressures	514
Figure 7.2.3.138: Re Effects, CR=3, 50% Cowl, Sidewall Pressures	514
Figure 7.2.3.139: Re Effects, CR=3, 50% Cowl, Sidewall Pressures	514
Figure 7.2.3.140: Re Effects, CR=3, 50% Cowl, Sidewall Pressures	514
Figure 7.2.3.141: Re Effects, CR=3, 50% Cowl, Sidewall Pressures	514
Figure 7.2.3.142: Re Effects, CR=3, 50% Cowl, Sidewall Pressures	514
Figure 7.2.3.143: Re Effects, CR=3, 50% Cowl, Sidewall Pressures	515
Figure 7.2.3.144: Re Effects, CR=3, 50% Cowl, Sidewall Pressures	515
Figure 7.2.3.145: Re Effects, CR=3, 50% Cowl, Sidewall Pressures	515
Figure 7.2.3.146: Re Effects, CR=3, 50% Cowl, Sidewall Pressures	515
Figure 7.2.3.147: Re Effects, CR=3, 50% Cowl, Sidewall Pressures	515
Figure 7.2.3.148: Re Effects, CR=3, 50% Cowl, Sidewall Pressures	515
Figure 7.2.3.149: Re Effects, CR=3, 50% Cowl, Sidewall Pressures	515
Figure 7.2.3.150: Re Effects, CR=3, 50% Cowl, Sidewall Pressures	515
Figure 7.2.3.151: Re Effects, CR=3, 50% Cowl, Sidewall Pressures	515
Figure 7.2.3.152: Re Effects, CR=3, 50% Cowl, Sidewall Pressures	516
Figure 7.2.3.153: Re Effects, CR=3, 50% Cowl, Sidewall Pressures	516
Figure 7.2.3.154: Re Effects, CR=3, 50% Cowl, Sidewall Pressures	516
Figure 7.2.3.155: Re Effects, CR=3, 50% Cowl, Sidewall Pressures	516
Figure 7.2.3.156: Re Effects, CR=3, 50% Cowl, Sidewall Pressures	516
Figure 7.2.3.157: Re Effects, CR=3, 50% Cowl, Sidewall Pressures	516
Figure 7.2.3.158: Re Effects, CR=3, 50% Cowl, Sidewall Pressures	516

Figure 7.2.3.159: Re Effects, CR=3, 50% Cowl, Sidewall Pressures	516
Figure 7.2.3.160: Re Effects, CR=5, 0% Cowl, CR=3 Centerline Pressures	517
Figure 7.2.3.161: Re Effects, CR=5, 0% Cowl, CR=5 Centerline Pressures	517
Figure 7.2.3.162: Re Effects, CR=5, 0% Cowl, CR=9 Centerline Pressures	517
Figure 7.2.3.163: Re Effects, CR=5, 0% Cowl, Baseplate Pressures	517
Figure 7.2.3.164: Re Effects, CR=5, 0% Cowl, Baseplate Pressures	517
Figure 7.2.3.165: Re Effects, CR=5, 0% Cowl, Baseplate Pressures	517
Figure 7.2.3.166: Re Effects, CR=5, 0% Cowl, Baseplate Pressures	517
Figure 7.2.3.167: Re Effects, CR=5, 0% Cowl, Baseplate Pressures	517
Figure 7.2.3.168: Re Effects, CR=5, 0% Cowl, Baseplate Pressures	517
Figure 7.2.3.169: Re Effects, CR=5, 0% Cowl, Baseplate Pressures	518
Figure 7.2.3.170: Re Effects, CR=5, 0% Cowl, Baseplate Pressures	518
Figure 7.2.3.171: Re Effects, CR=5, 0% Cowl, Baseplate Pressures	518
Figure 7.2.3.172: Re Effects, CR=5, 0% Cowl, Baseplate Pressures	518
Figure 7.2.3.173: Re Effects, CR=5, 0% Cowl, Baseplate Pressures	518
Figure 7.2.3.174: Re Effects, CR=5, 0% Cowl, Baseplate Pressures	518
Figure 7.2.3.175: Re Effects, CR=5, 0% Cowl, Baseplate Pressures	518
Figure 7.2.3.176: Re Effects, CR=5, 0% Cowl, Baseplate Pressures	518
Figure 7.2.3.177: Re Effects, CR=5, 0% Cowl, Baseplate Pressures	518
Figure 7.2.3.178: Re Effects, CR=5, 0% Cowl, Baseplate Pressures	519
Figure 7.2.3.179: Re Effects, CR=5, 0% Cowl, Baseplate Pressures	519
Figure 7.2.3.180: Re Effects, CR=5, 0% Cowl, Baseplate Pressures	519
Figure 7.2.3.181: Re Effects, CR=5, 0% Cowl, Baseplate Pressures	519
Figure 7.2.3.182: Re Effects, CR=5, 0% Cowl, Baseplate Pressures	519
Figure 7.2.3.183: Re Effects, CR=5, 0% Cowl, Baseplate Pressures	519
Figure 7.2.3.184: Re Effects, CR=5, 0% Cowl, Baseplate Pressures	519
Figure 7.2.3.185: Re Effects, CR=5, 0% Cowl, Cowl Pressures	519
Figure 7.2.3.186: Re Effects, CR=5, 0% Cowl, Sidewall Centerline Pressures	519
Figure 7.2.3.187: Re Effects, CR=5, 0% Cowl, Sidewall Centerline Pressures	520
Figure 7.2.3.188: Re Effects, CR=5, 0% Cowl, Sidewall Pressures	520
Figure 7.2.3.189: Re Effects, CR=5, 0% Cowl, Sidewall Pressures	520



Figure 7.2.3.190: Re Effects, CR=5, 0% Cowl, Sidewall Pressures	520
Figure 7.2.3.191: Re Effects, CR=5, 0% Cowl, Sidewall Pressures	520
Figure 7.2.3.192: Re Effects, CR=5, 0% Cowl, Sidewall Pressures	520
Figure 7.2.3.193: Re Effects, CR=5, 0% Cowl, Sidewall Pressures	520
Figure 7.2.3.194: Re Effects, CR=5, 0% Cowl, Sidewall Pressures	520
Figure 7.2.3.195: Re Effects, CR=5, 0% Cowl, Sidewall Pressures	520
Figure 7.2.3.196: Re Effects, CR=5, 0% Cowl, Sidewall Pressures	521
Figure 7.2.3.197: Re Effects, CR=5, 0% Cowl, Sidewall Pressures	521
Figure 7.2.3.198: Re Effects, CR=5, 0% Cowl, Sidewall Pressures	521
Figure 7.2.3.199: Re Effects, CR=5, 0% Cowl, Sidewall Pressures	521
Figure 7.2.3.200: Re Effects, CR=5, 0% Cowl, Sidewall Pressures	521
Figure 7.2.3.201: Re Effects, CR=5, 0% Cowl, Sidewall Pressures	521
Figure 7.2.3.202: Re Effects, CR=5, 0% Cowl, Sidewall Pressures	521
Figure 7.2.3.203: Re Effects, CR=5, 0% Cowl, Sidewall Pressures	521
Figure 7.2.3.204: Re Effects, CR=5, 0% Cowl, Sidewall Pressures	521
Figure 7.2.3.205: Re Effects, CR=5, 0% Cowl, Sidewall Pressures	522
Figure 7.2.3.206: Re Effects, CR=5, 0% Cowl, Sidewall Pressures	522
Figure 7.2.3.207: Re Effects, CR=5, 0% Cowl, Sidewall Pressures	522
Figure 7.2.3.208: Re Effects, CR=5, 0% Cowl, Sidewall Pressures	522
Figure 7.2.3.209: Re Effects, CR=5, 0% Cowl, Sidewall Pressures	522
Figure 7.2.3.210: Re Effects, CR=5, 0% Cowl, Sidewall Pressures	522
Figure 7.2.3.211: Re Effects, CR=5, 0% Cowl, Sidewall Pressures	522
Figure 7.2.3.212: Re Effects, CR=5, 0% Cowl, Sidewall Pressures	522
Figure 7.2.3.213: Re Effects, CR=5, 25% Cowl, CR=3 Centerline Pressures	523
Figure 7.2.3.214: Re Effects, CR=5, 25% Cowl, CR=5 Centerline Pressures	523
Figure 7.2.3.215: Re Effects, CR=5, 25% Cowl, CR=9 Centerline Pressures	523
Figure 7.2.3.216: Re Effects, CR=5, 25% Cowl, Baseplate Pressures	523
Figure 7.2.3.217: Re Effects, CR=5, 25% Cowl, Baseplate Pressures	523
Figure 7.2.3.218: Re Effects, CR=5, 25% Cowl, Baseplate Pressures	523
Figure 7.2.3.219: Re Effects, CR=5, 25% Cowl, Baseplate Pressures	523
Figure 7.2.3.220: Re Effects, CR=5, 25% Cowl, Baseplate Pressures	523

Figure 7.2.3.221: Re Effects, CR=5, 25% Cowl, Baseplate Pressures	523
Figure 7.2.3.222: Re Effects, CR=5, 25% Cowl, Baseplate Pressures	524
Figure 7.2.3.223: Re Effects, CR=5, 25% Cowl, Baseplate Pressures	524
Figure 7.2.3.224: Re Effects, CR=5, 25% Cowl, Baseplate Pressures	524
Figure 7.2.3.225: Re Effects, CR=5, 25% Cowl, Baseplate Pressures	524
Figure 7.2.3.226: Re Effects, CR=5, 25% Cowl, Baseplate Pressures	524
Figure 7.2.3.227: Re Effects, CR=5, 25% Cowl, Baseplate Pressures	524
Figure 7.2.3.228: Re Effects, CR=5, 25% Cowl, Baseplate Pressures	524
Figure 7.2.3.229: Re Effects, CR=5, 25% Cowl, Baseplate Pressures	524
Figure 7.2.3.230: Re Effects, CR=5, 25% Cowl, Baseplate Pressures	524
Figure 7.2.3.231: Re Effects, CR=5, 25% Cowl, Baseplate Pressures	525
Figure 7.2.3.232: Re Effects, CR=5, 25% Cowl, Baseplate Pressures	525
Figure 7.2.3.233: Re Effects, CR=5, 25% Cowl, Baseplate Pressures	525
Figure 7.2.3.234: Re Effects, CR=5, 25% Cowl, Baseplate Pressures	525
Figure 7.2.3.235: Re Effects, CR=5, 25% Cowl, Baseplate Pressures	525
Figure 7.2.3.236: Re Effects, CR=5, 25% Cowl, Baseplate Pressures	525
Figure 7.2.3.237: Re Effects, CR=5, 25% Cowl, Baseplate Pressures	525
Figure 7.2.3.238: Re Effects, CR=5, 25% Cowl, Cowl Pressures	525
Figure 7.2.3.239: Re Effects, CR=5, 25% Cowl, Sidewall Centerline Pressures	525
Figure 7.2.3.240: Re Effects, CR=5, 25% Cowl, Sidewall Centerline Pressures	526
Figure 7.2.3.241: Re Effects, CR=5, 25% Cowl, Sidewall Pressures	526
Figure 7.2.3.242: Re Effects, CR=5, 25% Cowl, Sidewall Pressures	526
Figure 7.2.3.243: Re Effects, CR=5, 25% Cowl, Sidewall Pressures	526
Figure 7.2.3.244: Re Effects, CR=5, 25% Cowl, Sidewall Pressures	526
Figure 7.2.3.245: Re Effects, CR=5, 25% Cowl, Sidewall Pressures	526
Figure 7.2.3.246: Re Effects, CR=5, 25% Cowl, Sidewall Pressures	526
Figure 7.2.3.247: Re Effects, CR=5, 25% Cowl, Sidewall Pressures	526
Figure 7.2.3.248: Re Effects, CR=5, 25% Cowl, Sidewall Pressures	526
Figure 7.2.3.249: Re Effects, CR=5, 25% Cowl, Sidewall Pressures	527
Figure 7.2.3.250: Re Effects, CR=5, 25% Cowl, Sidewall Pressures	527

Figure 7.2.3.251: Re Effects, CR=5, 25% Cowl, Sidewall Pressures	527
Figure 7.2.3.252: Re Effects, CR=5, 25% Cowl, Sidewall Pressures	527
Figure 7.2.3.253: Re Effects, CR=5, 25% Cowl, Sidewall Pressures	527
Figure 7.2.3.254: Re Effects, CR=5, 25% Cowl, Sidewall Pressures	527
Figure 7.2.3.255: Re Effects, CR=5, 25% Cowl, Sidewall Pressures	527
Figure 7.2.3.256: Re Effects, CR=5, 25% Cowl, Sidewall Pressures	527
Figure 7.2.3.257: Re Effects, CR=5, 25% Cowl, Sidewall Pressures	527
Figure 7.2.3.258: Re Effects, CR=5, 25% Cowl, Sidewall Pressures	528
Figure 7.2.3.259: Re Effects, CR=5, 25% Cowl, Sidewall Pressures	528
Figure 7.2.3.260: Re Effects, CR=5, 25% Cowl, Sidewall Pressures	528
Figure 7.2.3.261: Re Effects, CR=5, 25% Cowl, Sidewall Pressures	528
Figure 7.2.3.262: Re Effects, CR=5, 25% Cowl, Sidewall Pressures	528
Figure 7.2.3.263: Re Effects, CR=5, 25% Cowl, Sidewall Pressures	528
Figure 7.2.3.264: Re Effects, CR=5, 25% Cowl, Sidewall Pressures	528
Figure 7.2.3.265: Re Effects, CR=5, 25% Cowl, Sidewall Pressures	528
Figure 7.2.3.266: Re Effects, CR=5, 50% Cowl, CR=3 Centerline Pressures	529
Figure 7.2.3.267: Re Effects, CR=5, 50% Cowl, CR=5 Centerline Pressures	529
Figure 7.2.3.268: Re Effects, CR=5, 50% Cowl, CR=9 Centerline Pressures	529
Figure 7.2.3.269: Re Effects, CR=5, 50% Cowl, Baseplate Pressures	529
Figure 7.2.3.270: Re Effects, CR=5, 50% Cowl, Baseplate Pressures	529
Figure 7.2.3.271: Re Effects, CR=5, 50% Cowl, Baseplate Pressures	529
Figure 7.2.3.272: Re Effects, CR=5, 50% Cowl, Baseplate Pressures	529
Figure 7.2.3.273: Re Effects, CR=5, 50% Cowl, Baseplate Pressures	529
Figure 7.2.3.274: Re Effects, CR=5, 50% Cowl, Baseplate Pressures	529
Figure 7.2.3.275: Re Effects, CR=5, 50% Cowl, Baseplate Pressures	530
Figure 7.2.3.276: Re Effects, CR=5, 50% Cowl, Baseplate Pressures	530
Figure 7.2.3.277: Re Effects, CR=5, 50% Cowl, Baseplate Pressures	530
Figure 7.2.3.278: Re Effects, CR=5, 50% Cowl, Baseplate Pressures	530
Figure 7.2.3.279: Re Effects, CR=5, 50% Cowl, Baseplate Pressures	530
Figure 7.2.3.280: Re Effects, CR=5, 50% Cowl, Baseplate Pressures	530
Figure 7.2.3.281: Re Effects, CR=5, 50% Cowl, Baseplate Pressures	530

Figure 7.2.3.282: Re Effects, CR=5, 50% Cowl, Baseplate Pressures	530
Figure 7.2.3.283: Re Effects, CR=5, 50% Cowl, Baseplate Pressures	530
Figure 7.2.3.284: Re Effects, CR=5, 50% Cowl, Baseplate Pressures	531
Figure 7.2.3.285: Re Effects, CR=5, 50% Cowl, Baseplate Pressures	531
Figure 7.2.3.286: Re Effects, CR=5, 50% Cowl, Baseplate Pressures	531
Figure 7.2.3.287: Re Effects, CR=5, 50% Cowl, Baseplate Pressures	531
Figure 7.2.3.288: Re Effects, CR=5, 50% Cowl, Baseplate Pressures	531
Figure 7.2.3.289: Re Effects, CR=5, 50% Cowl, Baseplate Pressures	531
Figure 7.2.3.290: Re Effects, CR=5, 50% Cowl, Baseplate Pressures	531
Figure 7.2.3.291: Re Effects, CR=5, 50% Cowl, Cowl Pressures	531
Figure 7.2.3.292: Re Effects, CR=5, 50% Cowl, Sidewall Centerline Pressures	531
Figure 7.2.3.293: Re Effects, CR=5, 50% Cowl, Sidewall Centerline Pressures	532
Figure 7.2.3.294: Re Effects, CR=5, 50% Cowl, Sidewall Pressures	532
Figure 7.2.3.295: Re Effects, CR=5, 50% Cowl, Sidewall Pressures	532
Figure 7.2.3.296: Re Effects, CR=5, 50% Cowl, Sidewall Pressures	532
Figure 7.2.3.297: Re Effects, CR=5, 50% Cowl, Sidewall Pressures	532
Figure 7.2.3.298: Re Effects, CR=5, 50% Cowl, Sidewall Pressures	532
Figure 7.2.3.299: Re Effects, CR=5, 50% Cowl, Sidewall Pressures	532
Figure 7.2.3.300: Re Effects, CR=5, 50% Cowl, Sidewall Pressures	532
Figure 7.2.3.301: Re Effects, CR=5, 50% Cowl, Sidewall Pressures	532
Figure 7.2.3.302: Re Effects, CR=5, 50% Cowl, Sidewall Pressures	533
Figure 7.2.3.303: Re Effects, CR=5, 50% Cowl, Sidewall Pressures	533
Figure 7.2.3.304: Re Effects, CR=5, 50% Cowl, Sidewall Pressures	533
Figure 7.2.3.305: Re Effects, CR=5, 50% Cowl, Sidewall Pressures	533
Figure 7.2.3.306: Re Effects, CR=5, 50% Cowl, Sidewall Pressures	533
Figure 7.2.3.307: Re Effects, CR=5, 50% Cowl, Sidewall Pressures	533
Figure 7.2.3.308: Re Effects, CR=5, 50% Cowl, Sidewall Pressures	533
Figure 7.2.3.309: Re Effects, CR=5, 50% Cowl, Sidewall Pressures	533
Figure 7.2.3.310: Re Effects, CR=5, 50% Cowl, Sidewall Pressures	533
Figure 7.2.3.311: Re Effects, CR=5, 50% Cowl, Sidewall Pressures	534
Figure 7.2.3.312: Re Effects, CR=5, 50% Cowl, Sidewall Pressures	534

Figure 7.2.3.313: Re Effects, CR=5, 50% Cowl, Sidewall Pressures	534
Figure 7.2.3.314: Re Effects, CR=5, 50% Cowl, Sidewall Pressures	534
Figure 7.2.3.315: Re Effects, CR=5, 50% Cowl, Sidewall Pressures	534
Figure 7.2.3.316: Re Effects, CR=5, 50% Cowl, Sidewall Pressures	534
Figure 7.2.3.317: Re Effects, CR=5, 50% Cowl, Sidewall Pressures	534
Figure 7.2.3.318: Re Effects, CR=5, 50% Cowl, Sidewall Pressures	534
Figure 7.2.3.319: Re Effects, CR=9, 0% Cowl, CR=3 Centerline Pressures	535
Figure 7.2.3.320: Re Effects, CR=9, 0% Cowl, CR=5 Centerline Pressures	535
Figure 7.2.3.321: Re Effects, CR=9, 0% Cowl, CR=9 Centerline Pressures	535
Figure 7.2.3.322: Re Effects, CR=9, 0% Cowl, Baseplate Pressures	535
Figure 7.2.3.323: Re Effects, CR=9, 0% Cowl, Baseplate Pressures	535
Figure 7.2.3.324: Re Effects, CR=9, 0% Cowl, Baseplate Pressures	535
Figure 7.2.3.325: Re Effects, CR=9, 0% Cowl, Baseplate Pressures	535
Figure 7.2.3.326: Re Effects, CR=9, 0% Cowl, Baseplate Pressures	535
Figure 7.2.3.327: Re Effects, CR=9, 0% Cowl, Baseplate Pressures	535
Figure 7.2.3.328: Re Effects, CR=9, 0% Cowl, Baseplate Pressures	536
Figure 7.2.3.329: Re Effects, CR=9, 0% Cowl, Baseplate Pressures	536
Figure 7.2.3.330: Re Effects, CR=9, 0% Cowl, Baseplate Pressures	536
Figure 7.2.3.331: Re Effects, CR=9, 0% Cowl, Baseplate Pressures	536
Figure 7.2.3.332: Re Effects, CR=9, 0% Cowl, Baseplate Pressures	536
Figure 7.2.3.333: Re Effects, CR=9, 0% Cowl, Baseplate Pressures	536
Figure 7.2.3.334: Re Effects, CR=9, 0% Cowl, Baseplate Pressures	536
Figure 7.2.3.335: Re Effects, CR=9, 0% Cowl, Baseplate Pressures	536
Figure 7.2.3.336: Re Effects, CR=9, 0% Cowl, Baseplate Pressures	536
Figure 7.2.3.337: Re Effects, CR=9, 0% Cowl, Baseplate Pressures	537
Figure 7.2.3.338: Re Effects, CR=9, 0% Cowl, Baseplate Pressures	537
Figure 7.2.3.339: Re Effects, CR=9, 0% Cowl, Baseplate Pressures	537
Figure 7.2.3.340: Re Effects, CR=9, 0% Cowl, Baseplate Pressures	537
Figure 7.2.3.341: Re Effects, CR=9, 0% Cowl, Baseplate Pressures	537
Figure 7.2.3.342: Re Effects, CR=9, 0% Cowl, Baseplate Pressures	537
Figure 7.2.3.343: Re Effects, CR=9, 0% Cowl, Baseplate Pressures	537

Figure 7.2.3.344: Re Effects, CR=9, 0% Cowl, Cowl Pressures	537
Figure 7.2.3.345: Re Effects, CR=9, 0% Cowl, Sidewall Centerline Pressures	537
Figure 7.2.3.346: Re Effects, CR=9, 0% Cowl, Sidewall Centerline Pressures	538
Figure 7.2.3.347: Re Effects, CR=9, 0% Cowl, Sidewall Pressures	538
Figure 7.2.3.348: Re Effects, CR=9, 0% Cowl, Sidewall Pressures	538
Figure 7.2.3.349: Re Effects, CR=9, 0% Cowl, Sidewall Pressures	538
Figure 7.2.3.350: Re Effects, CR=9, 0% Cowl, Sidewall Pressures	538
Figure 7.2.3.351: Re Effects, CR=9, 0% Cowl, Sidewall Pressures	538
Figure 7.2.3.352: Re Effects, CR=9, 0% Cowl, Sidewall Pressures	538
Figure 7.2.3.353: Re Effects, CR=9, 0% Cowl, Sidewall Pressures	538
Figure 7.2.3.354: Re Effects, CR=9, 0% Cowl, Sidewall Pressures	538
Figure 7.2.3.355: Re Effects, CR=9, 0% Cowl, Sidewall Pressures	539
Figure 7.2.3.356: Re Effects, CR=9, 0% Cowl, Sidewall Pressures	539
Figure 7.2.3.357: Re Effects, CR=9, 0% Cowl, Sidewall Pressures	539
Figure 7.2.3.358: Re Effects, CR=9, 0% Cowl, Sidewall Pressures	539
Figure 7.2.3.359: Re Effects, CR=9, 0% Cowl, Sidewall Pressures	539
Figure 7.2.3.360: Re Effects, CR=9, 0% Cowl, Sidewall Pressures	539
Figure 7.2.3.361: Re Effects, CR=9, 0% Cowl, Sidewall Pressures	539
Figure 7.2.3.362: Re Effects, CR=9, 0% Cowl, Sidewall Pressures	539
Figure 7.2.3.363: Re Effects, CR=9, 0% Cowl, Sidewall Pressures	539
Figure 7.2.3.364: Re Effects, CR=9, 0% Cowl, Sidewall Pressures	540
Figure 7.2.3.365: Re Effects, CR=9, 0% Cowl, Sidewall Pressures	540
Figure 7.2.3.366: Re Effects, CR=9, 0% Cowl, Sidewall Pressures	540
Figure 7.2.3.367: Re Effects, CR=9, 0% Cowl, Sidewall Pressures	540
Figure 7.2.3.368: Re Effects, CR=9, 0% Cowl, Sidewall Pressures	540
Figure 7.2.3.369: Re Effects, CR=9, 0% Cowl, Sidewall Pressures	540
Figure 7.2.3.370: Re Effects, CR=9, 0% Cowl, Sidewall Pressures	540
Figure 7.2.3.371: Re Effects, CR=9, 0% Cowl, Sidewall Pressures	540
Figure 7.2.3.372: Re Effects, CR=9, 25% Cowl, CR=3 Centerline Pressures	541
Figure 7.2.3.373: Re Effects, CR=9, 25% Cowl, CR=5 Centerline Pressures	541

Figure 7.2.3.374: Re Effects, CR=9, 25% Cowl, CR=9 Centerline Pressures	541
Figure 7.2.3.375: Re Effects, CR=9, 25% Cowl, Baseplate Pressures	541
Figure 7.2.3.376: Re Effects, CR=9, 25% Cowl, Baseplate Pressures	541
Figure 7.2.3.377: Re Effects, CR=9, 25% Cowl, Baseplate Pressures	541
Figure 7.2.3.378: Re Effects, CR=9, 25% Cowl, Baseplate Pressures	541
Figure 7.2.3.379: Re Effects, CR=9, 25% Cowl, Baseplate Pressures	541
Figure 7.2.3.380: Re Effects, CR=9, 25% Cowl, Baseplate Pressures	541
Figure 7.2.3.381: Re Effects, CR=9, 25% Cowl, Baseplate Pressures	542
Figure 7.2.3.382: Re Effects, CR=9, 25% Cowl, Baseplate Pressures	542
Figure 7.2.3.383: Re Effects, CR=9, 25% Cowl, Baseplate Pressures	542
Figure 7.2.3.384: Re Effects, CR=9, 25% Cowl, Baseplate Pressures	542
Figure 7.2.3.385: Re Effects, CR=9, 25% Cowl, Baseplate Pressures	542
Figure 7.2.3.386: Re Effects, CR=9, 25% Cowl, Baseplate Pressures	542
Figure 7.2.3.387: Re Effects, CR=9, 25% Cowl, Baseplate Pressures	542
Figure 7.2.3.388: Re Effects, CR=9, 25% Cowl, Baseplate Pressures	542
Figure 7.2.3.389: Re Effects, CR=9, 25% Cowl, Baseplate Pressures	542
Figure 7.2.3.390: Re Effects, CR=9, 25% Cowl, Baseplate Pressures	543
Figure 7.2.3.391: Re Effects, CR=9, 25% Cowl, Baseplate Pressures	543
Figure 7.2.3.392: Re Effects, CR=9, 25% Cowl, Baseplate Pressures	543
Figure 7.2.3.393: Re Effects, CR=9, 25% Cowl, Baseplate Pressures	543
Figure 7.2.3.394: Re Effects, CR=9, 25% Cowl, Baseplate Pressures	543
Figure 7.2.3.395: Re Effects, CR=9, 25% Cowl, Baseplate Pressures	543
Figure 7.2.3.396: Re Effects, CR=9, 25% Cowl, Baseplate Pressures	543
Figure 7.2.3.397: Re Effects, CR=9, 25% Cowl, Cowl Pressures	543
Figure 7.2.3.398: Re Effects, CR=9, 25% Cowl, Sidewall Centerline Pressures	543
Figure 7.2.3.399: Re Effects, CR=9, 25% Cowl, Sidewall Centerline Pressures	544
Figure 7.2.3.400: Re Effects, CR=9, 25% Cowl, Sidewall Pressures	544
Figure 7.2.3.401: Re Effects, CR=9, 25% Cowl, Sidewall Pressures	544
Figure 7.2.3.402: Re Effects, CR=9, 25% Cowl, Sidewall Pressures	544
Figure 7.2.3.403: Re Effects, CR=9, 25% Cowl, Sidewall Pressures	544
Figure 7.2.3.404: Re Effects, CR=9, 25% Cowl, Sidewall Pressures	544

Figure 7.2.3.405: Re Effects, CR=9, 25% Cowl, Sidewall Pressures	544
Figure 7.2.3.406: Re Effects, CR=9, 25% Cowl, Sidewall Pressures	544
Figure 7.2.3.407: Re Effects, CR=9, 25% Cowl, Sidewall Pressures	544
Figure 7.2.3.408: Re Effects, CR=9, 25% Cowl, Sidewall Pressures	545
Figure 7.2.3.409: Re Effects, CR=9, 25% Cowl, Sidewall Pressures	545
Figure 7.2.3.410: Re Effects, CR=9, 25% Cowl, Sidewall Pressures	545
Figure 7.2.3.411: Re Effects, CR=9, 25% Cowl, Sidewall Pressures	545
Figure 7.2.3.412: Re Effects, CR=9, 25% Cowl, Sidewall Pressures	545
Figure 7.2.3.413: Re Effects, CR=9, 25% Cowl, Sidewall Pressures	545
Figure 7.2.3.414: Re Effects, CR=9, 25% Cowl, Sidewall Pressures	545
Figure 7.2.3.415: Re Effects, CR=9, 25% Cowl, Sidewall Pressures	545
Figure 7.2.3.416: Re Effects, CR=9, 25% Cowl, Sidewall Pressures	545
Figure 7.2.3.417: Re Effects, CR=9, 25% Cowl, Sidewall Pressures	546
Figure 7.2.3.418: Re Effects, CR=9, 25% Cowl, Sidewall Pressures	546
Figure 7.2.3.419: Re Effects, CR=9, 25% Cowl, Sidewall Pressures	546
Figure 7.2.3.420: Re Effects, CR=9, 25% Cowl, Sidewall Pressures	546
Figure 7.2.3.421: Re Effects, CR=9, 25% Cowl, Sidewall Pressures	546
Figure 7.2.3.422: Re Effects, CR=9, 25% Cowl, Sidewall Pressures	546
Figure 7.2.3.423: Re Effects, CR=9, 25% Cowl, Sidewall Pressures	546
Figure 7.2.3.424: Re Effects, CR=9, 25% Cowl, Sidewall Pressures	546
Figure 7.2.3.425: Re Effects, CR=9, 50% Cowl, CR=3 Centerline Pressures	547
Figure 7.2.3.426: Re Effects, CR=9, 50% Cowl, CR=5 Centerline Pressures	547
Figure 7.2.3.427: Re Effects, CR=9, 50% Cowl, CR=9 Centerline Pressures	547
Figure 7.2.3.428: Re Effects, CR=9, 50% Cowl, Baseplate Pressures	547
Figure 7.2.3.429: Re Effects, CR=9, 50% Cowl, Baseplate Pressures	547
Figure 7.2.3.430: Re Effects, CR=9, 50% Cowl, Baseplate Pressures	547
Figure 7.2.3.431: Re Effects, CR=9, 50% Cowl, Baseplate Pressures	547
Figure 7.2.3.432: Re Effects, CR=9, 50% Cowl, Baseplate Pressures	547
Figure 7.2.3.433: Re Effects, CR=9, 50% Cowl, Baseplate Pressures	547
Figure 7.2.3.434: Re Effects, CR=9, 50% Cowl, Baseplate Pressures	548
Figure 7.2.3.435: Re Effects, CR=9, 50% Cowl, Baseplate Pressures	548



Figure 7.2.3.436: Re Effects, CR=9, 50% Cowl, Baseplate Pressures	548
Figure 7.2.3.437: Re Effects, CR=9, 50% Cowl, Baseplate Pressures	548
Figure 7.2.3.438: Re Effects, CR=9, 50% Cowl, Baseplate Pressures	548
Figure 7.2.3.439: Re Effects, CR=9, 50% Cowl, Baseplate Pressures	548
Figure 7.2.3.440: Re Effects, CR=9, 50% Cowl, Baseplate Pressures	548
Figure 7.2.3.441: Re Effects, CR=9, 50% Cowl, Baseplate Pressures	548
Figure 7.2.3.442: Re Effects, CR=9, 50% Cowl, Baseplate Pressures	548
Figure 7.2.3.443: Re Effects, CR=9, 50% Cowl, Baseplate Pressures	549
Figure 7.2.3.444: Re Effects, CR=9, 50% Cowl, Baseplate Pressures	549
Figure 7.2.3.445: Re Effects, CR=9, 50% Cowl, Baseplate Pressures	549
Figure 7.2.3.446: Re Effects, CR=9, 50% Cowl, Baseplate Pressures	549
Figure 7.2.3.447: Re Effects, CR=9, 50% Cowl, Baseplate Pressures	549
Figure 7.2.3.448: Re Effects, CR=9, 50% Cowl, Baseplate Pressures	549
Figure 7.2.3.449: Re Effects, CR=9, 50% Cowl, Baseplate Pressures	549
Figure 7.2.3.450: Re Effects, CR=9, 50% Cowl, Cowl Pressures	549
Figure 7.2.3.451: Re Effects, CR=9, 50% Cowl, Sidewall Centerline Pressures	549
Figure 7.2.3.452: Re Effects, CR=9, 50% Cowl, Sidewall Centerline Pressures	550
Figure 7.2.3.453: Re Effects, CR=9, 50% Cowl, Sidewall Pressures	550
Figure 7.2.3.454: Re Effects, CR=9, 50% Cowl, Sidewall Pressures	550
Figure 7.2.3.455: Re Effects, CR=9, 50% Cowl, Sidewall Pressures	550
Figure 7.2.3.456: Re Effects, CR=9, 50% Cowl, Sidewall Pressures	550
Figure 7.2.3.457: Re Effects, CR=9, 50% Cowl, Sidewall Pressures	550
Figure 7.2.3.458: Re Effects, CR=9, 50% Cowl, Sidewall Pressures	550
Figure 7.2.3.459: Re Effects, CR=9, 50% Cowl, Sidewall Pressures	550
Figure 7.2.3.460: Re Effects, CR=9, 50% Cowl, Sidewall Pressures	550
Figure 7.2.3.461: Re Effects, CR=9, 50% Cowl, Sidewall Pressures	551
Figure 7.2.3.462: Re Effects, CR=9, 50% Cowl, Sidewall Pressures	551
Figure 7.2.3.463: Re Effects, CR=9, 50% Cowl, Sidewall Pressures	551
Figure 7.2.3.464: Re Effects, CR=9, 50% Cowl, Sidewall Pressures	551
Figure 7.2.3.465: Re Effects, CR=9, 50% Cowl, Sidewall Pressures	551
Figure 7.2.3.466: Re Effects, CR=9, 50% Cowl, Sidewall Pressures	551

Figure 7.2.3.467: Re Effects, CR=9, 50% Cowl, Sidewall Pressures	551
Figure 7.2.3.468: Re Effects, CR=9, 50% Cowl, Sidewall Pressures	551
Figure 7.2.3.469: Re Effects, CR=9, 50% Cowl, Sidewall Pressures	551
Figure 7.2.3.470: Re Effects, CR=9, 50% Cowl, Sidewall Pressures	552
Figure 7.2.3.471: Re Effects, CR=9, 50% Cowl, Sidewall Pressures	552
Figure 7.2.3.472: Re Effects, CR=9, 50% Cowl, Sidewall Pressures	552
Figure 7.2.3.473: Re Effects, CR=9, 50% Cowl, Sidewall Pressures	552
Figure 7.2.3.474: Re Effects, CR=9, 50% Cowl, Sidewall Pressures	552
Figure 7.2.3.475: Re Effects, CR=9, 50% Cowl, Sidewall Pressures	552
Figure 7.2.3.476: Re Effects, CR=9, 50% Cowl, Sidewall Pressures	552
Figure 7.2.3.477: Re Effects, CR=9, 50% Cowl, Sidewall Pressures	552
Figure 7.3.1: Oil Flow on Inlet Sidewall for CR=3, Re=2.15 million/ft, 0% Cowl	553
Figure 7.3.2: Oil Flow on Inlet Sidewall for CR=5, Re=2.15 million/ft, 0% Cowl	554
Figure 7.3.3: Oil Flow on Baseplate for CR=9, Re=2.15 million/ft, 0% Cowl Showing Forward Extent of Separation	555
Figure 7.3.4: Oil Flow on Baseplate for CR=9, Re=2.15 million/ft, 0% Cowl Showing Oil Streaks Exiting Front of Inlet and Spilling around Sidewalls	556
Figure 7.3.5: Close up of Oil Flow on Baseplate and Sidewall for CR=9, Re=2.15 million/ft, 0% Cowl	557
Figure 7.3.6: Close up of Oil Flow on Baseplate for CR=9, Re=2.15 million/ft, 0% Cowl Showing Oil Streaks Exiting Front of Inlet and Spilling around Sidewalls	558
Figure 7.4.1: Baseplate Axial Centerline Surface Temperature Distribution from Prerun to 10 seconds for CR=3, Re=2.15 million/ft, 0% Cowl Configuration	559
Figure 7.4.2: Baseplate Axial Centerline Surface Temperature Distribution from Prerun to 10 seconds for CR=3, Re=0.55 million/ft, 0% Cowl Configuration	559
Figure 8.1a: Comparison of Baseplate Centerline Pressure Distribution from CFD and Experiment, CR=3, Re=2.15 million/ft, 0% Cowl	560
Figure 8.1b: Comparison of Sidewall Centerline Pressure Distribution from CFD and Experiment, CR=3, Re=2.15 million/ft, 0% Cowl	560
Figure 8.2a: Comparison of Baseplate Centerline Pressure Distribution from CFD and Experiment, CR=5, Re=2.15 million/ft, 0% Cowl	560
Figure 8.2b: Comparison of Sidewall Centerline Pressure Distribution from CFD and Experiment, CR=5, Re=2.15 million/ft, 0% Cowl	560
Figure 8.3a: Comparison of Baseplate Centerline Pressure Distribution from CFD and Experiment, CR=9, Re=2.15 million/ft, 0% Cowl	561

Figure 8.3b:	Comparison of Sidewall Centerline Pressure Distribution from CFD and Experiment, CR=9, Re=2.15 million/ft, 0% Cowl	561
Figure 8.4a:	Comparison of Baseplate Centerline Pressure Distribution from CFD and Experiment, CR=3, Re=2.15 million/ft, 50% Cowl	561
Figure 8.4b:	Comparison of Sidewall Centerline Pressure Distribution from CFD and Experiment, CR=3, Re=2.15 million/ft, 50% Cowl	561
Figure 8.5a:	Comparison of Baseplate Centerline Pressure Distribution from CFD and Experiment, CR=3, Re=0.55 million/ft, 0% Cowl	562
Figure 8.5b:	Comparison of Sidewall Centerline Pressure Distribution from CFD and Experiment, CR=3, Re=0.55 million/ft, 0% Cowl	562
Figure 8.1.1a:	P/Pinf Measured Baseplate Contours, CR=3, Re=2.15 million/ft, 0% Cowl, (run66)	563
Figure 8.1.1b:	P/Pinf Computed Baseplate Contours, CR=3, Re=2.15 million/ft, 0% Cowl	563
Figure 8.1.2a:	P/Pinf Measured Sidewall Contours, CR=3, Re=2.15 million/ft, 0% Cowl, (run66)	564
Figure 8.1.2b:	P/Pinf Computed Sidewall Contours, CR=3, Re=2.15 million/ft, 0% Cowl	564
Figure 8.1.3a:	P/Pinf Measured Baseplate Contours, CR=5, Re=2.15 million/ft, 0% Cowl, (run46)	565
Figure 8.1.3b:	P/Pinf Computed Baseplate Contours, CR=5, Re=2.15 million/ft, 0% Cowl	565
Figure 8.1.4a:	P/Pinf Measured Sidewall Contours, CR=5, Re=2.15 million/ft, 0% Cowl, (run46)	566
Figure 8.1.4b:	P/Pinf Computed Sidewall Contours, CR=5, Re=2.15 million/ft, 0% Cowl	566
Figure 8.1.5a:	P/Pinf Measured Baseplate Contours, CR=9, Re=2.15 million/ft, 0% Cowl, (run49)	567
Figure 8.1.5b:	P/Pinf Computed Baseplate Contours, CR=9, Re=2.15 million/ft, 0% Cowl	567
Figure 8.1.6a:	P/Pinf Measured Sidewall Contours, CR=9, Re=2.15 million/ft, 0% Cowl, (run49)	568
Figure 8.1.6b:	P/Pinf Computed Sidewall Contours, CR=9, Re=2.15 million/ft, 0% Cowl	568
Figure 8.1.7a:	P/Pinf Measured Baseplate Contours, CR=3, Re=2.15 million/ft, 50% Cowl, (run60)	569
Figure 8.1.7b:	P/Pinf Computed Baseplate Contours, CR=3, Re=2.15 million/ft, 50% Cowl	569
Figure 8.1.8a:	P/Pinf Measured Sidewall Contours, CR=3, Re=2.15 million/ft, 50% Cowl, (run60)	570

Figure 8.1.8b:	P/Pinf Computed Sidewall Contours, CR=3, Re=2.15 million/ft, 50% Cowl	570
Figure 8.1.9a:	P/Pinf Measured Baseplate Contours, CR=3, Re=0.55 million/ft, 0% Cowl, (run64)	571
Figure 8.1.9b:	P/Pinf Computed Baseplate Contours, CR=3, Re=0.55 million/ft, 0% Cowl	571
Figure 8.1.10a:	P/Pinf Measured Sidewall Contours, CR=3, Re=0.55 million/ft, 0% Cowl, (run64)	572
Figure 8.1.10b:	P/Pinf Computed Sidewall Contours, CR=3, Re=0.55 million/ft, 0% Cowl	572
Figure 8.2.1:	Comparison of Measured and Computed Pitot/Pinf Exit Plane Contours, CR=3, Re=2.15 million/ft, 0% Cowl, (run73)	573
Figure 8.2.2:	Comparison of Measured and Computed Pitot/Pinf Exit Plane Contours, CR=5, Re=2.15 million/ft, 0% Cowl, (run91)	574
Figure 8.2.3:	Comparison of Measured and Computed Pitot/Pinf Exit Plane Contours, CR=9, Re=2.15 million/ft, 0% Cowl, (run94)	575
Figure 8.2.4:	Comparison of Measured and Computed Pitot/Pinf Exit Plane Contours, CR=3, Re=2.15 million/ft, 50% Cowl, (run81)	576
Figure 8.2.5:	Comparison of Measured and Computed Pitot/Pinf Exit Plane Contours, CR=3, Re=0.55 million/ft, 0% Cowl, (run71)	577
Figure 8.2.6:	Pitot/Pinf Exit Plane Contours, CR=3, Re=0.55 million/ft, 0% Cowl, (run71)	578
Figure 8.2.7:	Pitot/Pinf Exit Plane Contours, CR=5, Re=0.55 million/ft, 0% Cowl, (run89)	579
Figure 8.2.8:	Pitot/Pinf Exit Plane Contours, CR=9, Re=0.55 million/ft, 0% Cowl, (run92)	580
Figure 8.2.9:	Pitot/Pinf Exit Plane Contours, CR=3, Re=0.55 million/ft, 25% Cowl, (run76)	581
Figure 8.2.10:	Pitot/Pinf Exit Plane Contours, CR=5, Re=0.55 million/ft, 25% Cowl, (run86)	582
Figure 8.2.11:	Pitot/Pinf Exit Plane Contours, CR=9, Re=0.55 million/ft, 25% Cowl, (run95)	583
Figure 8.2.12:	Pitot/Pinf Exit Plane Contours, CR=3, Re=0.55 million/ft, 50% Cowl, (run78)	584
Figure 8.2.13:	Pitot/Pinf Exit Plane Contours, CR=5, Re=0.55 million/ft, 50% Cowl, (run83)	585
Figure 8.2.14:	Pitot/Pinf Exit Plane Contours, CR=9, Re=0.55 million/ft, 50% Cowl, (run97)	586
Figure 8.2.15:	Pitot/Pinf Exit Plane Contours, CR=3, Re=1.14 million/ft, 0% Cowl, (run72)	587
Figure 8.2.16:	Pitot/Pinf Exit Plane Contours, CR=5, Re=1.14 million/ft, 0% Cowl, (run90)	588
Figure 8.2.17:	Pitot/Pinf Exit Plane Contours, CR=9, Re=1.14 million/ft, 0% Cowl, (run93)	589
Figure 8.2.18:	Pitot/Pinf Exit Plane Contours, CR=3, Re=1.14 million/ft, 25% Cowl, (run77)	590
Figure 8.2.19:	Pitot/Pinf Exit Plane Contours, CR=5, Re=1.14 million/ft, 25% Cowl, (run87)	591
Figure 8.2.20:	Pitot/Pinf Exit Plane Contours, CR=9, Re=1.14 million/ft, 25% Cowl, (run96)	592
Figure 8.2.21:	Pitot/Pinf Exit Plane Contours, CR=3, Re=1.14 million/ft, 50% Cowl, (run79)	593

Figure 8.2.22:	Pitot/Pinf Exit Plane Contours, CR=5, Re=1.14 million/ft, 50% Cowl, (run84)	594
Figure 8.2.23:	Pitot/Pinf Exit Plane Contours, CR=9, Re=1.14 million/ft, 50% Cowl, (run98)	595
Figure 8.2.24:	Pitot/Pinf Exit Plane Contours, CR=3, Re=2.15 million/ft, 0% Cowl, (run73)	596
Figure 8.2.25:	Pitot/Pinf Exit Plane Contours, CR=5, Re=2.15 million/ft, 0% Cowl, (run91)	597
Figure 8.2.26:	Pitot/Pinf Exit Plane Contours, CR=9, Re=2.15 million/ft, 0% Cowl, (run94)	598
Figure 8.2.27:	Pitot/Pinf Exit Plane Contours, CR=3, Re=2.15 million/ft, 25% Cowl, (run75)	599
Figure 8.2.28:	Pitot/Pinf Exit Plane Contours, CR=5, Re=2.15 million/ft, 25% Cowl, (run88)	600
Figure 8.2.29:	Pitot/Pinf Exit Plane Contours, CR=3, Re=2.15 million/ft, 50% Cowl, (run81)	601
Figure 8.2.30:	Pitot/Pinf Exit Plane Contours, CR=5, Re=2.15 million/ft, 50% Cowl, (run85)	602
Figure 8.3.1:	Entrance Boundary Layer Pitot Profile, CR=3, Re=2.15 million/ft, 0% Cowl	603
Figure 8.3.2:	Entrance Boundary Layer Mach Number Profile, CR=3, Re=2.15 million/ft, 0% Cowl	603
Figure 8.3.3:	Entrance Boundary Layer Velocity Profile, CR=3, Re=2.15 million/ft, 0% Cowl	603
Figure 8.3.4:	Entrance Boundary Layer Temperature Profile, CR=3, Re=2.15 million/ft, 0% Cowl	603
Figure 8.3.5:	Entrance Boundary Layer Pitot Profile, CR=3, Re=0.55 million/ft, 0% Cowl	604
Figure 8.3.6:	Entrance Boundary Layer Mach Number Profile, CR=3, Re=0.55 million/ft, 0% Cowl	604
Figure 8.3.7:	Entrance Boundary Layer Velocity Profile, CR=3, Re=0.55 million/ft, 0% Cowl	604
Figure 8.3.8:	Entrance Boundary Layer Temperature Profile, CR=3, Re=0.55 million/ft, 0% Cowl	604

## List of Symbols

$c_p$	specific head at constant pressure
CR	contraction ratio, W/g
$c_v$	specific heat at constant volume
Cx'	distance from cowl leading edge to inlet throat, inch
CW	clockwise
CCW	counter clockwise
d	distance model can protrude off injection plate and clear side of tunnel during injection process, see Eqn. 3.2.3.2 and Figure 3.2.3.2.
$d_1$	distance between center of injection carriage circle and the center of injection plate when fully retracted, see Figure 3.2.3.2.
e	internal energy
$E_t$	total internal energy per unit volume
g	throat gap, inch
H	height of inlet, 4.0 inches
ID	inside diameter, inch
j	Jacobian matrix
k	thermal conductivity
l.e.	leading edge
$L_{bp}$	length of baseplate, see Eqn. 3.2.3.1.
M, $M_1$	freestream Mach number
$M_{1N}$	component of freestream Mach number normal to leading edge
$M_{1CF}$	component of freestream Mach number parallel to leading edge (crossflow)
$M_2$	resultant post-shock Mach vector
$M_{2N}$	post-shock component of Mach vector normal to l.e. in plane of wedge

$M_{2CF}$	post-shock component of Mach vector parallel to l.e. in plane of wedge (crossflow)
OD	outside diameter, inch
$p$	local static pressure, psia
$p_{\infty}, p_{inf}$	static pressure of freestream, psia
$p_{t,1}$	tunnel stagnation pressure, psia
$Pr$	Prandtl number, $\mu c_p/k$
$q$	dynamic pressure, heat flux
$R$	gas constant
$R_c$	radius of circle turned by injection carriage, see Figure 3.2.3.2.
$R_{inj}$	radius of semi-circle on injection plate, see Figure 3.2.3.1.
$Re$	Reynolds number
$Re_{\theta}$	Reynolds number based on momentum thickness
$T$	static temperature, K
$T_1$	static temperature upstream of shock, K
$T_2$	static temperature downstream of shock, K
$T_{t,1}$	tunnel stagnation temperature, K
$T_{wall}$	wall temperature, K
$Tx'$	distance from sidewall leading edge to throat, inch
$Te'$	distance from throat shoulder to exit at a given height, inch
$W$	inlet width at the sidewall leading edge, inch
$W_{bp}$	width of baseplate, see Eqn. 3.2.3.1.
$x$	axial distance measured from baseplate leading edge, inch
$x'$	axial distance measured from sidewall leading edge, inch
$xs'$	distance measured from shoulder at the throat at a given height, inch
$y$	lateral distance from inlet plane of symmetry, inch

$y_{\text{wall}}$	local half-width of the inlet, inch
$z$	coordinate completing right-hand set
$Z$	vertical distance down sidewall measured from baseplate, inch
$U, F, G, H$	vectors in Navier-Stokes equations, see Eqn. A.1.1.
$U', F', G', H'$	vectors in transformed Navier-Stokes equations, see Eqn. A.2.2.1

### Greek

$\beta$	angle measured in plane of wedge, deg, see Eqn. 3.3.5.
$\Gamma$	angle measured in plane of wedge, deg, see Eqn. 3.3.4.
$\gamma$	ratio of specific heats
$\delta$	sidewall compression angle, deg; also boundary layer thickness
$\delta_{\text{eff}}$	effective sidewall compression angle, measured normal to sidewall leading edge, deg
$\delta^*$	boundary layer displacement thickness, inch
$\zeta$	spillage angle, deg, see Eqn. 3.3.6.
$\eta_{\text{ke}}$	kinetic energy efficiency
$\theta$	boundary layer momentum thickness, inch
$\theta_{\text{eff}}$	effective oblique shock angle, measured normal to sidewall leading edge, deg
$\Lambda$	leading edge sweep angle, deg
$\mu$	viscosity
$\rho$	density
$\tau$	shear stress
$\xi, \eta, \zeta$	transformed coordinate set, see Section A.2.1.



# **Introduction**

The present work describes the results of a combined computational and experimental parametric investigation of the internal aerodynamics of a generic three-dimensional sidewall compression scramjet inlet at Mach 10. Though geometrically simple, inlets of this genre generate a very complicated flow field, in which corner flow, shock induced separation, and shock-shock/shock-boundary layer interactions are among the flow characteristics. Each of these issues have been addressed separately by other researchers, but the desired result of the interactions generated by the inlet is the creation of a nearly uniform, supersonic, compressed flow at the combustor face. The prediction of such complicated flow fields is of particular interest to vehicle designers and analysts for whom high local pressure gradients and high heating influence the total aerodynamic and structural design of the flight vehicle. The goals of the combined numerical and experimental investigation are three-fold: to demonstrate the utility of computational fluid dynamics as a design tool in hypersonic inlet flow fields, to provide a detailed account of the nature and structure of the internal flow interactions, and to provide a comprehensive surface property and flow field database to determine the effects of contraction ratio, cowl position, and Reynolds number on the performance of a hypersonic scramjet inlet configuration. Computational fluid dynamics is used to drive the design of the experimental configuration; the experimental work is in turn used to provide a validation for the computational parametrics.

The termination of the X-15 project in 1968 significantly affected the state of hypersonic research in this country; in particular, hypersonic propulsion suffered. As early as the late 1950's, the concept of a supersonic combustion ramjet (scramjet) was analytically demonstrated to be both feasible and attractive for high Mach number flight. By the mid-1960's, NASA, the Air Force, and the Navy embarked on a program to develop the scramjet engine concept into a complete flight experiment, but the termination of the X-15 halted the flight phase of NASA's hypersonic research engine (HRE), since the X-15 was to have been the test bed for the full-scale flight experiment. In the same year, the Air Force ended both its low-speed, fixed geometry scramjet project and the Marquardt dual-mode scramjet development program. Henry and McLellan (1971) report that although these projects were prevented from actual flight tests, several ground based, research-sized engines were successfully tested, showing the feasibility of providing sufficient specific impulse at Mach numbers up to 8, with no adverse effects expected at still higher Mach numbers.

Recent programs have again focused attention on the attractive potential of hypersonic flight. Dutton and Carroll(1988) and Carlson (1983) report that the U.S. Navy is considering an airbreathing missile system capable of high Mach number, long range flight, employing scramjets as the primary propulsion system. The National Aero-Space Plane (X-30) is also reported to use supersonic combustion ramjets for high Mach number propulsion (e.g., Williams(1986) and Kandebo(1988)). Ramjets, like other propulsion systems, are designed to convert the energy released by combustion of a fuel into thrust. Dugger (1960) examined subsonic and supersonic combustion in hypersonic ramjet engines. It was noted that decelerating the hypersonic flow through compressive turning to a lower but still supersonic velocity had the advantage of a lower static temperature entering

the combustor as compared to shocking the flow down to subsonic velocities. A lower static temperature means that the energy added by burning the fuel would be stored by means of an increased static temperature; this energy could then be recovered in the form of thrust as the hot exhaust expands out the nozzle. A higher static temperature (as in the case of subsonic combustor entrance flow) means that additional energy will tend to dissociate the flow. The energy stored in this manner would be unrecoverable as the dissociated gas molecules exit the engine. Thus it is clear that a supersonic combustion ramjet (scramjet) greatly enhances the capability for high Mach number flight.

Maintaining the flight of a vehicle at hypersonic speeds will require a propulsion system which is highly efficient, adding minimum weight and drag. Weight and component complexity may be minimized by considering a fixed geometry inlet, while the requirement for increased efficiency may be met by integrating the propulsion system with the underside of the airframe (see Figure 1.1). This concept makes use of the forebody bow shock, which precompresses the flow in the vertical direction prior to the inlet entrance. It has been shown that not only does the use of this precompression reduce the total turning required to obtain the desired compression, but it also reduces by a factor of three the size of the inlet needed to provide the thrust necessary to maintain a vehicle at Mach 10 (Henry and Anderson(1973)). It was further shown that when the engine is properly integrated with the airframe, the forebody and aftbody can influence up to 70 percent of the total thrust. Since an inlet would be limited by the dimensions of the shock layer, and since the inlet should process a maximum amount of the oncoming stream, this concept necessarily requires ingestion of the forebody boundary layer. It is anticipated that the boundary layer on a full scale flight vehicle would be large at the inlet entrance. As a result, further turning in the

vertical direction, as in two-dimensional inlets, would greatly increase the risk of large scale separation regions at the entrance of the inlet due to the shock-boundary layer interaction. A possible solution to the problem involves the use of a three-dimensional inlet (Figure 1.2), wherein further compression is accomplished in the horizontal direction by wedge shaped sidewalls, reducing the total in-plane turning the flow must encounter to obtain the desired compression. The leading edges of these sidewalls are swept both to reduce the aerothermal loads on the leading edge and to provide a window for spillage at the lower Mach numbers to aid in starting the inlet. The sweep has the effect of turning the flow away from the forebody plane, spilling out ahead of the cowl. As the Mach number is increased, the sidewall shock angles become smaller, effectively partially closing that spillage window and increasing the mass capture, thereby making the inlet more efficient at higher Mach numbers. A secondary effect is to relieve the crossflow pressure gradients induced by the horizontal compression, thereby reducing the likelihood of separation. These characteristics make it possible to consider a fixed geometry inlet for use over a wide Mach number range.

In the past, scramjet inlet research has been limited primarily to experimental work. The past two decades have brought tremendous advances in numerical methods and in computer hardware development which have created an enhanced capability for calculating increasingly more complicated flow fields. These advances have allowed computational fluid dynamics (CFD) to mature to the point where it may now be used in certain applications as an engineering design tool. The greatest advantage of computational fluid dynamics is that it provides flow field data, where experimental data is typically limited to surface measurements or global flow field measurements. White, Drummond, and Kumar (1987) point out the utility of CFD as providing parametric studies in a timely and cost effective

manner, and once wind tunnel data is obtained, to aid in the explanation of unusual or unexpected phenomena by giving detailed flow field data. Additionally, the code's ability to match the surface measurements obtained experimentally gives the designer greater confidence in the computed flow field data and in the possibility of using the code to extrapolate outside the range of test conditions available experimentally. The present work uses CFD in this design and analysis capacity. Since instrumented wind tunnel models are quite expensive, CFD has been utilized to minimize the costs of fabrication by eliminating from consideration designs which promise poor performance. Following the parametric study, an optimization of the chosen configuration was performed. A wind tunnel model was then designed, fabricated, and tested in the 31 Inch Mach 10 Tunnel at the NASA Langley Research Center to provide a comparison with experiment.

The three-dimensional Navier-Stokes code (SCRAMIN) of Kumar (1986) has been chosen for this study since it uses a well-known and well-proven numerical scheme and has shown favorable comparison with experiment at lower Mach numbers (2 to 6, which, as a result of this study, is extended to 10). In its original form, SCRAMIN was written for the CYBER-203 vector processor in the SL/1 programming language, which permitted the use of 32-bit arithmetic, thereby allowing the primary memory to be increased to two million words. This code is well-suited for running on the Cray Y-MP, which has sufficient memory to allow computation on larger, more refined computational domains. The code solves the three-dimensional Navier-Stokes equations in full conservation form by MacCormack's method, an explicit, unsplit, time-dependent, predictor-corrector method. Fourth-order damping is imposed to damp oscillations near shocks. As may be inferred by the fact that the code was originally run on the vector processor, it yields to a high degree of vectorization.

The combined numerical and experimental investigation of the internal aerodynamics of a three-dimensional sidewall compression inlet in hypersonic flow is documented in the following manner. Chapter 2 presents an overview of research pertinent to inlet work and to the broader category of shock-boundary layer interactions. Chapter 3 presents both flight and ground based testing considerations relative to inlet testing, including a discussion of the fundamental internal inlet interactions. Chapter 4 paints in broad strokes the relationship of various geometric and aerodynamic parameters to inlet performance. Emphasis here is placed on the global effects rather than the fine detail of the internal aerodynamics to provide a viable inlet configuration based on overall performance. Chapter 5 presents the details of the final configuration as affected by the results of the computational parametric study and the physical constraints of the wind tunnel. A great deal of attention is paid to testing techniques and their associated uncertainties. Additionally, an assessment of wind tunnel blockage effects due to the size and orientation of the large scale model is given. A detailed discussion of the computational results is presented in Chapter 6, with attention given to the internal flow phenomena. Chapter 7 presents the voluminous experimental data. Contour plots of the inlet sidewall and baseplate emphasize the global effects of contraction ratio, cowl location, and Reynolds number; line plots present a more quantitative comparison of these effects. In Chapter 8, direct comparisons between measured and computed surface and flow field quantities are presented. A summary of the conclusions are presented in Chapter 9. Finally, a detailed discussion of the CFD code is provided in the appendix.

## **Literature Review**

An inlet configuration represents a particularly complex flow field. A uniform inlet inflow condition would certainly be desirable, but the necessity of ingesting the forebody boundary layer introduced by the airframe-propulsion integration concept precludes this. Increasing the complexity of the flow field are two three-dimensional skewed shock waves which emanate from the swept leading edges of the wedge-shaped sidewalls, reflect off the centerline, and return as incident shock waves on the sidewalls (see Figure 2.1). The interaction between these shock waves and the forebody boundary layer enhances the possibility of separation. The spillage, or downturning, of the flow due to the sweep (see Figure 2.2) causes the flow to impinge on the cowl, creating a cowl shock inside the inlet, which also may tend to separate the sidewall boundary layer in the vicinity of the throat. In order to understand such a complex flow field, one must examine the individual flow phenomena, such as corner flow and shock induced separation. Much work has been done in past years in the area of corner flow, but in order to narrow this broad field, only those dealing with wedge-induced shocks interacting with flat plate boundary layers will be considered. Additionally, a review of pertinent skewed shock-boundary layer interactions, incident shock-boundary layer interactions, and ramjet/scramjet inlet work is herein presented.

## **2.1 Three-Dimensional Shock Wave-Laminar Boundary Layer Interactions**

Much of the work in three-dimensional shock-boundary layer interactions has been performed on 90 degree interior corners aligned with the freestream. Stainback (1960) performed an experimental investigation at Mach 4.95 over a range of Reynolds numbers sufficient to span transition. An increase of 10 to 12 percent in static pressure was noted in the interaction region compared to the undisturbed flat plate pressures. The laminar flow heat transfer rate was also higher than theoretical values for the flat plate at the same conditions, decreasing with distance from the corner and increasing unit Reynolds number. The corner had only a negligible effect on the turbulent flow heat transfer rate and transition Reynolds number. Stainback (1964) identified a region immediately adjacent to the corner juncture which he termed the near-corner viscous interaction region, in which most of the theoretical work had been done, and a far-corner region, the region of the interaction of the inviscid flow field with the boundary layer, in which most of the experimental work had been presented. Heat transfer and flow visualization data taken at Mach 8 in both interaction regions were presented. Evidence of what might be a vortex system produced by the leading edge of the corner was found, supporting the concept postulated by Bogdonoff and Vas (1957). Stainback and Weinstein (1967) identified three flow phenomena which influenced the skin friction and heat transfer near a corner: the mutual interaction of the boundary layers, a vortex system produced by the leading edge of the corner, and the reattachment following the shock-induced separation. The former tended to decrease the local skin friction and heat transfer in the near-corner region, while the latter two both resulted in an increased heat transfer rate outboard of the



mutual boundary layer interaction region. This study was conducted at Mach 8 over a range of Reynolds numbers sufficient to span transition. Partially successful correlations for laminar peak heating and the location of laminar peak heating were obtained for some of the geometries tested. The turbulent flow results indicated that the increase in peak heating was not as substantial for a turbulent boundary layer as for a laminar boundary layer. Charwat and Redekeopp (1967) identified the basic laminar flow interaction structure for supersonic flow (Mach 2.5 to Mach 4.0), which appear to agree with the hypersonic experimental data of Watson and Weinstein (1971) at Mach 20, though distorted by vortices and thick boundary layers. Mach 20 oil flow and electron beam data documented the location of the vortex to coincide with the first peak in heat transfer rate. They further found this increase in heat transfer rate and peak pressure to increase with Mach number, compared to the undisturbed local wedge pressures and heating rates. Cooper and Hankey (1973) investigated a highly asymmetric axial corner flow for fully laminar Mach 12.5 flow. An extensive flow field survey (over 1500 impact pressures), oil flows, and surface pressures, revealed two large vortices within the boundary layer which contribute to the high heating rates. Further, the shock emanating from the 15 degree wedge separated the boundary layer on the adjacent flat plate, yielding regions of high heating at the reattachment points.

Degrez and Ginoux (1983) performed a parametric study of a three-dimensional skewed shock wave laminar boundary layer interaction at Mach 2.25. Oblique shock waves were generated from a series of wedges at 4, 6, and 8 degrees incidence to interact with an established flat plate boundary layer. Static pressures and surface flow visualization revealed extensive separation caused by self-induced viscous/inviscid interactions which, over the range of test conditions, were found to vary little with wedge angle (shock strength). The evolution of the

flow structure was studied, and it was hypothesized that the flow evolved gradually from  $\alpha = 0^\circ$  to extensively separated cases, rendering all debate over the definition of incipient separation moot. They concluded that, assuming the flow to be symmetrical (i.e., the same compression angle on either side of the fin), the existence of a 3D focus on the plane of symmetry indicates the existence of a vortex for all angles  $\alpha$ , and likewise the existence of a line of separation for all angles. They argued that at small angles, the line of separation and vortex are located close to the wall, and with increasing angles, move outward toward and finally past the shock location, gaining size and significance.

## **2.2 Three-Dimensional Shock Wave-Turbulent Boundary Layer Interactions**

Much attention has been focused on the interaction of a swept shock on turbulent boundary layers. In addition to some of the works previously mentioned (which included both laminar and turbulent flows), McCabe (1966) offered a simple approximate theory to predict incipient separation based on the convection of vorticity in the boundary layer going through the shock wave. Korkegi (1971) provided an extensive review of viscous interactions associated with high Mach number flight. An additional simple correlation of incipient turbulent boundary layer separation due to skewed shock interactions was presented by Korkegi (1973). For small Mach numbers,

$$M_1 * \theta_i = 0.30 \quad [2.2.1]$$

correlated the experimental data, but for  $2 < M < 3.4$ ,  $\theta_i$  was found to be independent of Mach number. The correlation has not been verified above this range. This study also found that a skewed shock appears to be prone to separating a boundary layer for a lower shock pressure ratio than in the case of a normal shock. Korkegi (1975) provided a direct comparison of the separation phenomena on a two-dimensional ramp with a sidewall configuration. The ramp shock interacted three-dimensionally with the sidewall boundary layer and two-dimensionally with the boundary layer approaching the ramp; thus, both two- and three-dimensional incipient separation could be studied. The incipient separation angle was plotted as a function of Mach number for both two- and three-dimensional interactions. For the flat plate (2-D) interaction, data from Law (1974), Sterret and Emery (1962), Gary and Rhudy (1970), Batham (1972), Elfstrom (1972), and others were included. Two empirical correlations for the pressure rise for incipient separation, both of which neglected the effects of Reynolds number and wall temperature as second order, were presented. For the skewed shock-sidewall (3-D) boundary layer interaction, Equation 2.2.1 was plotted with data from one unpublished report from Law and data from Neumann and Token (1974), for Mach numbers up to 6. Goldberg's (1973) data at Mach 5.9, which did not agree with this correlation, were not included in the plot since Korkegi found that the incipient separation angle was not determined with sufficient accuracy.

The very definition of incipient separation is an issue which has created some difficulty. McCabe (1966) defined it by the convergence of the surface streamlines, while others (e.g., Holden (1978)) have identified it by seeking an inflection point in the surface pressure data. In recent years, a number of researchers have produced an extensive study of shock boundary layer interactions at Mach 3, aimed

primarily at obtaining similarity laws, scaling laws, and parametric effects for the cases of no separation, incipient separation, and full separation. Among these are Dolling (1984), Dolling and Bogdonoff (1983), Settles and Bogdonoff (1982), Bogdonoff (1985), and Lu and Settles (1983). A summary of the recent swept shock/boundary layer interactions with emphasis on the last 5 years' work was presented in the review article of Settles and Dolling (1990). While these efforts have met with a great measure of success, they have not been extended into the Mach number range of interest for the present study.

Crossing shock interactions for inlet type configurations have also been under investigation in recent years. Mee, Stalker, and Stollery (1986) and Mee and Stalker (1987) investigated a Mach 1.85 interaction between two fins at symmetric and asymmetric incidence to the flow in the presence of a turbulent boundary layer. They found that intersecting shock interactions can produce an overall pressure rise equivalent to a single shock interaction with a reduced likelihood of separation. Crossing shock interactions were also examined experimentally at a Mach number of 2.95 in Batcho, et al. (1989) and numerically in Narayanswami, et al. (1991). While much work has been done in the area of crossing shock/boundary layer interactions, the work has not been extended into the Mach number range of interest for the present study.

## **2.3 Hypersonic Inlet Shock Wave–Boundary Layer Interactions**

Hypersonic inlets and inlet-type configurations have been studied by a number of different experimenters. A brief indication of the scope of recent research is given. Then, in-depth coverage is given to three-dimensional inlet configurations which are more directly applicable to the current work.

### **2.3.1 Scope of Recent 2-D Research**

Waltrup (1986) indicated that past research in hypersonic inlet flows had been primarily concerned with the determination of the more global engineering parameters of mass capture, pressure recovery, and exit conditions including pressure, temperature, and velocity profiles. Hunt, et al. (1982) documented capture area and inlet pressure recovery for several hypersonic airbreathing missile concepts under consideration at the NASA Langley Research Center. A number of researchers have concerned themselves with characterizing the inflow boundary. Dillion, et al. (1981) conducted flow field surveys at the engine inlet face of four hypersonic airbreathing missile concepts to determine the forebody boundary layer and inviscid shock layer, since they strongly effect the optimum location and performance of the engine; in each instance, these characteristics were found to be strong functions of the nose shape. Hunt, Johnston, and Riebe (1983) made flow field surveys on a representative missile forebody model designed according to the constraints of the U.S. Navy vertical box launcher. The mass flow and total pressure improved with increased effectiveness of the forebody compression.

Johnston and Hunt (1984) presented Mach 6 flow field and boundary layer data from the forebody of an airbreathing missile configuration. When the flight Mach number and Reynolds number at altitude were matched, it was found that transition occurred aft of the inlet face. Other factors were mentioned which could cause the location of transition to move both fore and aft; it was finally conceded that the inlet might possibly have to contend with the much more easily separated laminar boundary layer. The location of transition was then identified as a factor of critical importance and deserving of further study. Other research efforts have included the internal shock wave-boundary layer interactions induced by uniform inflow into circular (e.g., Om and Childs (1983)) and square (Gessner, Ferguson, and Lo (1987)) ducts. Instabilities, unsteadiness, and low frequency oscillations in inlet/combustor flow fields have been examined by Sajben, Bogar, and Kroutil (1984). In this effort, a simulated inlet was created using a supersonic diffuser device. Yanta, et al. (1988) indicated that the experimental database on internal ramjet/scramjet inlet flow in which the flow has undergone some precompression is relatively sparse. The velocity profiles inside a two-dimensional Mach 4 inlet were measured using a two-dimensional Laser Doppler Velocimeter (LDV). Mach number surveys, skin friction measurements, wall pressures, and internal density profiles were also obtained using a laser holographic interferometer and shadowgraphs. Their work determined that their boundary layer bleed device was effective in increasing the inlet efficiency.

### 2.3.2 Review of Three-Dimensional Shock-Boundary Layer Inlet Work

The bulk of the three-dimensional inlet work has been performed through the Air Force Flight Dynamics Laboratory and the NASA Langley Research Center. Keith, et al. (1965) performed shock tunnel tests on five compression models at freestream Mach numbers between 2 and 15. The boundary layer characteristics were documented and favorable comparisons between theoretical and measured heat transfer rates in the interaction region were shown for both laminar and turbulent flow. Correlations of laminar boundary layer separation pressure plateaus were extended to higher Mach numbers. Of the five models tested, only model B bears direct applicability to the current work. Model B, designed to study oblique, skewed shock wave-boundary layer interactions, consisted of two wedge shaped sidewalls mounted normal to a flat plate ramp. These sidewalls were pivoted to provide variable sidewall compression angles ranging from 0 to 5 degrees measured with respect to the freestream. A second set of sidewalls was constructed which had a leading edge sweep of 70 degrees. Data taken included pressure, wall heat transfer, and schlieren photographs. A series of 14 runs was made with Model B, seven with unswept sidewalls, two with heat flux gauges installed, and the remaining five with the swept sidewall configuration. In each of the runs, the effect of the small favorable tunnel pressure gradient was noticeable. Thus, the measured pressures were referenced to the ramp-only pressure distribution. Since the sidewalls obstructed the view of the interior flow field, the location of the sidewall shock intersection could not be directly obtained. An analytical estimate was based on the average Mach number at the sidewall leading edge, as provided by the GE/Bertram shock shape program. The observed pressure rise occurred upstream of the calculated intersection. The shocks were

found contribute crossflow pressure gradients which fed into the center and tended to increase the axial pressure gradient. This pressure rise occurred smoothly, indicating that no significant separation of the boundary layer occurred for the shock pressure ratios tested. The heat transfer data indicated a laminar flow over the upstream regions, but the measured values diverged from laminar theory in the adverse pressure gradient region; it was suggested that the adverse pressure gradient had induced transition. Based on axial pressure and heat transfer curves for this model, it was concluded that the flow did not separate. Further, since the centerline pressures were higher than the off centerline measurements, significant crossflow was found to occur. (Effects of the downturning of the flow induced by the swept compression surfaces were neglected.)

Kutschenreuter, et al. (1965) presented a continuation of the previous work using continuous flow tests rather than shock tube tests. This work extended that of the previous paper, especially in the area of swept sidewall compression configurations. A combined experimental and analytical program for both laminar and turbulent boundary layer-shock wave interactions was presented for a nominal Mach number of 10. Data included boundary layer profiles upstream and downstream of and wall pressure distributions through the interaction region. As before, only one of the models tested bears significant relevance to the present work, namely Model D. This model consisted of the fixed 3 degree ramp of model C on which two 60 degree swept sidewall compression surfaces were mounted. These vanes could be pivoted to provide 6 to 8 degrees of horizontal turning, thereby varying the shock strength and associated pressure rise. The ramp was instrumented with 69 static pressure orifices and 11 thermocouples. The right-hand sidewall had 17 static pressure taps on the compression surface and 2 on the top. The left-hand sidewall had 5 taps located to mirror the right-hand sidewall



(to assure symmetry of the flow structure between the sidewalls) and 5 surface-embedded thermocouples also located in the same locations as 5 of the pressure ports on the opposite sidewall. The purpose of the thermocouples, however, was to monitor the surface temperature in the interest of maintaining the structural integrity of the aluminum model rather than for providing heat transfer data. The model was tested in the NASA-Ames 3.5 Foot Hypersonic Wind Tunnel, which is capable of obtaining Mach 5, 7, and 10 flow, operating at a Reynolds number per foot of between 0.2 and 3.5 million at Mach 7 and between 0.5 and 2.2 million at Mach 10. The stagnation pressure could be varied between 50 and 600 psia for Mach 7 and between 400 and 1800 psia for Mach 10.

It is evident from the discussion of the Model D data that the main purpose of this particular experimental configuration was to formulate a flow model which yielded to simplified analysis which would be in agreement with experimental data. The downturning of the flow due to the wedge sweep was initially neglected as small (though usually on the order of a few degrees), so that strip theory might be used. It was subsequently found that the GE/Bertram method could be used directly for the case of sharp leading edges and with only slight modification for blunted leading edges. For the case of a finite span, however, another refinement to the flow model was made. The sweep of the vanes led to a slight downturning of the flow; however, in the corner region, the flow vector must lie parallel to the ramp as well as reflect the downturning. This was modelled as an expansion fan behind the shock which would accommodate both the downturning and the flow tangency boundary condition on the flat ramp. This model was called the "shock-expansion" flow model. The measured sidewall pressure distributions in the interaction region tended to support this flow model. In fact, better agreement was obtained for the shock-expansion model than for either swept wedge or strip theory

for 6 degree vanes with and without boundary layer trips and the 8 degree vanes with boundary layer trips.

The centerline pressure distributions indicated that neither the 6 degree nor the 8 degree turbulent tests produced separation. The 6 degree laminar flow did, however, separate, and the pressure plateau was found to be well predicted by Erdos-Pallone (1962) theory. The authors indicated that the static pressure profile data was only of limited value, so that only first order corrections could be made for normal pressure gradients in reducing the pitot data to Mach number profiles. Nonetheless, increases in the boundary layer thickness and mass flow were observed compared to the ramp-only data, the reverse of the trends seen for two-dimensional interactions.

### 2.3.3 Three-Dimensional Inlet Component Work

The concept of propulsion-airframe integration is not unique to this decade. Gregory, Wilcox, and Williams (1967) and Johnston, Cabbage, and Weidner (1971) have considered this concept in the global sense of its effects on the total aircraft throughout the entire flight trajectory in terms of vehicle performance, stability, and control. A similar study for hypersonic missiles was presented by Hunt, Lawing, Marcum, and Cabbage (1978). Parametric studies on certain components have also been performed. Details of a forebody design technique were given by Edwards (1976). The engine nozzle-airframe design is the subject of Small, Weidner, and Johnston (1976). Anderson (1974) provided an examination of the injector/combustor design as pertaining to the performance of the scramjet unit. Finally, the inlet has been given much attention as an individual component. A review of some of the pertinent inlet data is given in this section.

Trexler (1974) presented a brief summary of Mach 6 survey data in the inlet region of the Langley Integrated Scramjet Module. A more complete data set was later presented over a Mach number range of 2.3 to 6.0 for the same integrated scramjet module (Trexler (1975)). Boundary layer trips on the foreplate provided the inlet with a thick turbulent boundary layer, simulating the vehicle forebody boundary layer. The low pressure gradient on this surface (i.e. no ramp compression on this surface) was found to permit ingestion of this boundary layer without separation. The sweep of the sidewall compression surfaces provided a window for spillage to allow the inlet to start at low Mach numbers. The added drag due to this spillage was not determined, but it was noted that the spillage would augment the lift since it turns the flow in a downward direction. Fuel was introduced by three struts located in the inlet throat region; the struts aided in the compression process. Trexler and Souders (1975) presented wall static pressure distributions, oil flow data, wall surface temperature measurements, pitot surveys, and gross performance parameters for a detailed evaluation of a baseline inlet configuration. The presence of the strut showed that this was more an inlet/combustor combination rather than strictly an inlet component study, and thus the direct applicability of this to the present work is diminished. However, it was demonstrated that at a Mach number of 6, the inlet (with an average contraction ratio of 7) would start and that starting was enhanced by the downturning due to the sidewall sweep, that the inlet capture and kinetic energy efficiency were acceptable (94 and 97.7 percent, respectively), and that the forebody boundary layer could be ingested with no adverse effects.

Holland and Perkins (1990) reported on Mach 6 testing of three-dimensional sidewall compression scramjet inlets with leading edge sweep angles of 30 and 70 degrees in tetrafluoromethane. By testing in both tetrafluoromethane ( $\gamma = 1.2$ )

and air ( $\gamma = 1.4$ ), the explicit effects of the ratio of specific heats (and hence the normal shock density ratio) could be obtained. The tetrafluoromethane results (the first phase) were reported with respect to the effects of leading edge sweep, contraction ratio, cowl position, and Reynolds number. In addition to pressure data, schlieren movies were made of each run to detail the flow spillage. It was found that increased leading edge sweep increased the flow spillage and decreased the compression of the inlet. Forward placement of the cowl led to increased mass capture of the inlet. Although the Reynolds number range available spanned less than an order of magnitude, an overall increase in inlet compression was noted with decreasing Reynolds number. The results made a first step toward the explicit determination of low  $\gamma$  effects and added to a sparse database of inlet tests in complex gases (first known inlet test in tetrafluoromethane), thereby providing a point of comparison for CFD codes for viral gas computations.

There also appears to have been recent foreign interest in three-dimensional inlet configurations similar to the Langley Integrated Scramjet Module. Vinogradov, et al. (1989) reported on numerical and experimental work in the USSR for inlets with and without struts at Mach numbers between 2 and 6. They found that their fixed geometry inlet with swept compression surfaces started in the Mach 1.8 to 2.1 range and exhibited performance characteristics better than those obtained for fixed geometry two-dimensional inlets. They also showed good agreement between computation and experiment for the greater part of the inlet flow field. Kanda, et al. (1989) reported on work done in Japan at Mach 4 on six inlet configurations based on the Langley inlet. Schlieren photographs of the flow beneath the model indicated the presence of a shear layer formed due to the flow downturning. This shear layer was observed to discontinuously change its direction between the leading edge and the cowl, even when the cowl was removed. [The

reason for this discontinuous change in direction of the shear layer, as the present work demonstrates, is that even based solely on inviscid considerations (appropriately modified to account for the three-dimensional effects of leading edge sweep), each of the internal reflected shocks incrementally increases the flow downturning.] They compared total pressure recovery and mass capture at Mach 4 for leading edge sweeps of 30, 45, and 60°; their results indicated a slight increase in total pressure recovery and mass capture between 30 and 45° and a significant decrease in both parameters at 60°. They therefore report an optimum sweep angle of 45° for Mach 4 operation. In addition to the experimental work, they made approximate calculations of the pressure field using the two-dimensional oblique shock relations. They also made use of a two-dimensional Navier-Stokes code, which they concluded was useful, but due to the strong three-dimensional nature of the flow field, a full three-dimensional code was required. Their tests also included the effects of contraction ratio, but they accomplished the increase in contraction ratio by increasing the wedge angle of the sidewalls. Thus in the notation of the present study, their effects of contraction ratio and sidewall compression angle are coupled and therefore not directly applicable to the present work.

## **Inlet Design Considerations**

### **3.1 Flight Considerations**

Many problems arise when attempting to maintain the flight of a vehicle at hypersonic speeds. Increasing the maximum design flight Mach number from 2 to 12 requires a ten-fold increase in the size, and subsequently weight, of the engine (Johnston, Cubbage, and Weidner (1971)). In order to maintain these high Mach numbers, the entire vehicle must be considered part of the propulsion system. Henry and Anderson (1973) have shown that the vehicle forebody and afterbody can influence up to 70 percent of the total thrust when the engine is properly integrated with the airframe. They further showed that the precompression accomplished by the bow shock could not only reduce the total turning required to obtain the desired compression, but could also reduce by a factor of three the size of the inlet needed to provide the thrust required to maintain the vehicle at Mach 10. Edwards (1976) developed a means of designing a forebody which provided a uniformly precompressed inflow at the inlet entrance. When the airframe is designed to take advantage of the vehicle bow shock precompression, the inlet height is limited to the area between the underside of the vehicle and the bow shock (see Figure 1.1). Since this area is much wider than it is tall, this suggests breaking the engine into several identical rectangular modules. Making the modules identical has two major advantages: the component complexity and weight are minimized since the problem of complex fuel scheduling for dissimilar engines is avoided, and the modules lend themselves to ground based testing.

Henry and Anderson (1973) also performed a trade-off study to determine whether a fixed or variable geometry inlet would be better suited for a hypersonic aircraft. In order to keep the velocities in the combustor low, a scramjet engine should have a large inlet contraction ratio at high flight Mach numbers, thereby minimizing the momentum losses and maximizing the thrust. A fixed geometry inlet is contraction ratio limited by the constraint that it must start at lower Mach numbers, that is, establish supersonic flow throughout the inlet. They assumed a  $q = 1000$  psf flight trajectory and 8 degrees of turning due to the bow shock and compared the specific impulse as a function of Mach number for a fixed geometry inlet with contraction ratios in the range of 6 to 10 with a variable geometry inlet capable of a contraction ratio of 25 in the Mach 8 to 10 range. Their results indicated that the variable geometry would perform only 16 percent better than the fixed geometry, at a penalty of increased component complexity and joint, seal, and cooling problems. Each of these would in turn increase the weight of the engine, tending to cancel out the increase in specific impulse. Thus, they determined that sufficient justification to employ a variable geometry scramjet was lacking. In either case, the propulsive forces necessary to maintain hypersonic flight are large compared with the aerodynamic forces. It has been found that favorable interference effects can be obtained when the afterbody is properly designed to avoid the large trim penalties of is properly designed to avoid the large trim penalties of poorly integrated engines (Small, Weidner, and Johnston (1976)).

## **3.2 Ground Based Test Considerations**

Design of the present model evolved through trade-offs of many parameters, including issues such as the desired aerodynamic simulation, size and weight constraints, heat transfer, and model structural integrity. Each of these issues will be addressed with emphasis placed on how they each influenced the design of the present model.

### **3.2.1 Description of Wind Tunnel Facilities**

The facility used for the present work was the 31-Inch Mach 10 Tunnel, located at the NASA Langley Research Center. A brief outline of the tunnel performance characteristics can be found in Penaranda and Freda(1985); a lengthier discussion, in Miller(1990), of which the following is a summary. Formerly known as the Continuous Flow Hypersonic Tunnel, this facility was originally designed to run in a blowdown start, continuous flow mode. Due to energy conservation measures, the facility has operated in a blowdown mode only since the mid-1970's. The test gas, dry air, is supplied from the air storage system, having a volume of 875 cubic feet and rated for a maximum pressure of 4400 psia. A 12.5-MW electrical resistance heater located in a vertical pressure vessel heats the gas to a nominal temperature of 1850° R to prevent air liquefaction in the 31-by 31-inch square test section. The maximum reservoir pressure is approximately 1500 psia. Screens are placed at the upstream end of the 12-inch diameter settling chamber, which is in turn faired into the upstream end of the 1.07-inch square throat. The settling chamber, nozzle, throat, test section, adjustable second minimum, and subsonic diffuser are all water cooled. The 31-Inch Mach 10 Tunnel



is the only hypersonic facility in the USA to have a three-dimensional contoured nozzle(Beckwith and Miller 1990). The inviscid contours for the four walls were designed by the method of Beckwith, Ridyard, and Cromer (1952). Beckwith and Miller (1990) point out that, due to its three-dimensional contoured design, the Mach 10 nozzle is free of the centerline disturbance characteristically observed in axisymmetric contoured nozzles. Primarily due to this highly uniform core flow, Miller (1984) identified this facility as particularly attractive for CFD computer code calibration studies.

The model is supported on a hydraulically operated, sidewall mounted injection system capable of injecting the model to centerline in less than 0.6 second. Prior to injection, the model is stored in a housing which is isolated from the test section by a sliding door. This enclosure rotates about a vertical axis to provide access to the model. Though somewhat inconvenient in that it blocks the optical path for the schlieren, this sidewall mounted rotating arrangement allows access to the model without opening the test section to atmosphere; hence, model changes could be made easily without having to shut down the tunnel when it was operated in continuous mode (see Figure 3.2.1.1).

Typically the pitot pressure of the tunnel is not obtained during the run due to the orientation of the injection system and location of the model in the facility. The computation of freestream conditions therefore relies on measured values of reservoir pressure  $p_{t1}$ , temperature  $T_{t1}$ , the results of an unpublished calibration, and corrections factors accounting for imperfect-gas effects in the reservoir. The present model did, however, have pitot probes to measure the freestream pitot pressure, but since the measured pressures agreed with the facility calibration within the accuracy of the measurement, the procedure to calculate freestream conditions remained unmodified.

### 3.2.2 Aerodynamic Simulation

It is important to know which points in a flight trajectory are simulated by the facility. The 31 Inch Mach 10 Tunnel operates at a fixed nominal Mach number and a variable Reynolds number. In order to match the Mach number/Reynolds number for a given trajectory, the following procedure was used. First, it is recognized that the ratio of Mach number to unit Reynolds number can be given as:

$$\frac{M}{Re_{unit}} = \frac{\mu}{\rho (\gamma RT)^{\frac{1}{2}}} \quad [3.2.2.1]$$

Pressure, density, temperature (and hence viscosity), etc. are given as functions of altitude in the U.S. Standard Atmosphere (1976). Thus at a given altitude, the ratio of Mach number and unit Reynolds number is fixed. It then remains only to find the associated trajectory. The dynamic pressure  $q$  can be written as:

$$q = \frac{1}{2} \gamma p M^2 \quad [3.2.2.2]$$

With the Mach number given and the pressure specified via the altitude, the dynamic pressure of the trajectory which simulates the Mach number and Reynolds number is determined. This would be sufficient if the inlet (during flight) were to be in the freestream, but since forebody compression is an integral part of the overall propulsion system, the post-oblique shock values must be used for density, temperature, etc. instead of the freestream values. Since the forebody compression is configuration specific, it was deemed simpler to specify an altitude (and hence pressure, temperature, etc.) and a set of presumed forebody deflection angles (e.g.

0, 6, 12, and 18 degrees) and compute the Mach number and unit Reynolds number for constant  $q$  trajectories between  $q = 1000$  psf and 2000 psf. Tables for a given altitude generated in this fashion identify numerous points which are simulated by the tunnel test conditions. For example, at an altitude of 110,000 ft, a 1050 psf trajectory yields Mach 10 flow for  $Re = 0.65$  million/ft. When a  $6^\circ$  forebody deflection is assumed, a higher Reynolds number matching is obtained for a  $q = 2000$  psf trajectory (see Table 3.2.2.1). Additional points can be obtained using the above method.

Table 3.2.2.1: Mach Number/Reynolds Number Matching for  
31 Inch Mach 10 Tunnel

Z(ft)= 110000 P(psi)= 0.1030 T(K)= 232.4358			
Assumed Forebody Deflection Angle DELTA(deg)= 0			
Theta (deg)	Q (psf)	Mach Number	Re(/ft) (millions)
0.0000	1000.	9.813	0.6458
0.0000	1100.	10.291	0.6773
0.0000	1200.	10.749	0.7075
0.0000	1300.	11.188	0.7364
0.0000	1400.	11.610	0.7641
0.0000	1500.	12.018	0.7910
0.0000	1600.	12.412	0.8169
0.0000	1700.	12.794	0.8421
0.0000	1800.	13.165	0.8665
0.0000	1900.	13.526	0.8902
0.0000	2000.	13.877	0.9133

Assumed Forebody Deflection Angle DELTA(deg)= 6			
Theta (deg)	Q (psf)	Mach Number	Re(/ft) (millions)
10.5288	1000.	7.835	1.0754
10.2943	1100.	8.120	1.1441
10.0846	1200.	8.411	1.2122
9.9122	1300.	8.657	1.2751
9.7578	1400.	8.895	1.3365
9.6170	1500.	9.131	1.3971
9.4966	1600.	9.336	1.4538
9.3861	1700.	9.538	1.5094
9.2895	1800.	9.717	1.5618
9.1950	1900.	9.910	1.6155
9.1137	2000.	10.076	1.6652

### 3.2.3 Size and Weight Constraints

Since the model must be injected into the tunnel, the maximum injectable size must be addressed. The injection plate is 34 inches long by 26 inches wide, formed by two 13 inch semi-circles joined by an 8 inch long straight segment (Figure 3.2.3.1). The length to width relationship of the maximum sized rectangular plate

(oriented parallel to the injection plate) that will fit through such an opening is given by

$$W_{bp} = 2 [R_{inj}^2 - ((L_{bp} - 8) / 2)^2]^{1/2}, \quad 8 \leq L_{bp} \leq 34 \text{ in}, \quad [3.2.3.1]$$

where  $R_{inj}$  is the radius of the semi-circle on the injection plate (13 inches), and  $W_{bp}$  and  $L_{bp}$  are the width and length of the rectangular plate, respectively. In the event that the plate is to be injected perpendicular to the injection plate, the length is the only consideration pertinent to the injection orifice, i.e. the length cannot exceed 34 inches. This is not however the only consideration. When the model is retracted from the wind tunnel, the entire injection carriage is rotated 90 degrees about a vertical axis to allow the model to be injected into a room where technicians can easily access it, as shown in Figure 3.2.1.1. The distance a model can protrude off the retracted injection plate and still be able to clear the side of the tunnel as the carriage is rotated is a function of the location on the injection plate. This relationship is given by

$$d(x) = [R_c^2 - x^2]^{1/2} - d_1, \quad [3.2.3.2]$$

where  $R_c$  is the radius of the circle turned by the injection carriage (40-1/8 inches),  $x$  is the axial location on the plate measured from the center of the plate, and  $d_1$  is the distance between the center of the circle turned by the injection carriage and the center of the plate when the plate is fully retracted (15-7/16 inches) (see Figure 3.2.3.2). Thus it is evident that at the upstream-most position of the injection plate, the model may protrude no more than 20.9 inches (5.4 inches past tunnel centerline) and at the middle of the plate, no more than 24.7 inches (9.2 inches past tunnel centerline).

Weight concerns are also significant. It was found that the injection system had been rated to withstand a 200lb load on the injection plate for a previous test. Thus, if the model could be kept under that requirement, no further structural analysis or modification of the injection mechanism would be necessary.

#### 3.2.4 Aerothermodynamic Loading

As with a full scale flight vehicle, aerodynamic heating plays an important role in the design process. Since the total temperature of the flow in the 31 Inch Mach 10 tunnel was maintained at 1850 deg R, thermal loads on the sharp leading edges of a model were anticipated to be severe. It was therefore desirable to construct the model out of a material which had high strength, light weight, a low coefficient of thermal expansion, a high thermal conductivity, and was easily machinable. A low coefficient of thermal expansion was necessary to prevent warping of the sharp (thin) leading edges as they heated up. High conductivity was of utmost importance in that heat which builds up at the sharp leading edges must be rapidly conducted away rather than building up to the point where the surface temperature approaches the melting point, allowing the material to warp. A comparison of aluminum, copper, and stainless steel is given in Table 3.2.4.1 (taken from Materials Selector (1974)).

**Table 3.2.4.1: Properties of Aluminum, Copper, and Steel**

Property	Al (2024)	Cu 102 (OHFC)	Stainless Steel (304)
Density(lb/cu.in.)	0.100	0.323	0.29
Melting Temp Range(°F)	935-1180	1981	2550-2650
Thermal conductivity (Btu/hr/sq.ft./°F/ft)	109.2 77°F	226 68°F	9.4 212°F
Coef. of Ther. Exp. (per °F, 68-572 °F)	13.7x10 <sup>-6</sup>	9.8x10 <sup>-6</sup> (32-212)	9.6x10 <sup>-6</sup>
Max. Yld Str, 1000psi	(0.2%)	(0.5%)	
Annealed	11	10-11	42, 35, 35
Heat Treated	50(T3)		
Machinability	A	B	C

From the information in the table, it is evident that while aluminum would be considered desirable due to its strength to weight ratio and ease of machining, it is a poor choice for the present study due to its melting point, coefficient of thermal expansion, and thermal conductivity. Heat conduction away from the sharp leading edge is only modest, leading to higher temperatures which may easily exceed the melting point (recall that  $T_{t1}$  is on the order of 1370 deg F). Even if the leading edge does not melt, the higher coefficient of thermal expansion indicates that the leading edge is more likely to deflect during the run. Stainless steel has a higher strength to weight ratio than copper, but it is difficult (and hence more costly) to machine and has an extremely low thermal conductivity. Even though the stainless steel could withstand the increased leading edge temperatures brought about by the poorer heat conduction without melting, stainless has approximately the same coefficient of thermal expansion as copper. Hence the increase in leading edge

temperature would increase the risk of surface deflections due to local expansion of the material. Thus copper was selected by means of trade-off. During the relatively short run times of the present work, the high thermal conductivity permits rapid heat conduction, allowing the model surface temperature distribution to remain relatively uniform, rising slowly during the run. This is of benefit to CFD comparisons in that for short runs, copper will more closely mimic the constant wall temperature boundary conditions.

### 3.2.5 Instrumentation Response Time

The 31 Inch Mach 10 Tunnel is capable of test times of up to 60 seconds. In the interest of minimizing heating exposure of the model, it is desirable to keep the test duration as short as possible without adversely affecting the quality of the measurements. When low pressure measurements are involved, it is especially important to minimize the tubing length between the orifice and the measurement device to reduce the lag (or settling) time. For the present model, this was accomplished by placing the measurement devices (ESP-32 modules) inside an enclosure on the baseplate. Pressures were observed to settle in less than 1 second, allowing for a test duration of 10 seconds or less, even for runs where the exit plane rake was introduced to obtain pitot pressures at multiple lateral locations within the inlet exit plane. During the run, cooling air was introduced to avoid heating the ESP bay; thermocouples placed in the bay and attached to each ESP module revealed that the temperatures in that region increased by no more than 1 deg F during the test. Thus, quickened response time due to the proximity of the ESP modules to the orifices allowed for reduced run times and hence reduced thermal loads on the model structure and associated instrumentation. The quality of the



data was maintained since the walls remained at relatively constant temperature since they did not have sufficient time to develop large thermal gradients.

### **3.3 Fundamental Internal Flow Phenomena**

A necessary first step in any research effort is an initial assessment of the flow physics. When the flow encounters the wedge-shaped sidewalls, a complex shock structure develops. Consider first the inviscid flow past a pair of infinitely tall unswept (2-D) wedges located opposite one another, i.e. an unswept inlet of infinite height. A pair of shock sheets extend from the leading edge of the wedges to the centerline, where they intersect and reflect back as incident shocks on the sidewalls. The reflected shocks cancel if they are incident at the shoulder in the throat; otherwise they continue to reflect if they strike ahead of the shoulder. Figure 3.3.1 illustrates the three possibilities: shock on shoulder, shock ahead of shoulder, and shock after shoulder. This reflected shock pattern has been demonstrated computationally for a sidewall compression inlet of similar design in Mach 5 air (perfect gas) for a leading edge sweep of  $45^\circ$  (Kumar(1982)). Though the flow conditions were different, the prominent features of the flow are similar to the present configuration. The addition of leading edge sweep to the sidewalls causes the shock sheets generated by the leading edge, the line along which the shocks intersect on the centerline, and the line along which the reflected shocks impinge on the sidewalls to be swept at the leading edge sweep angle. Shock interactions of this nature occur along lines of constant leading edge sweep angle.

This trend was also demonstrated computationally; see for example Figures 5 and 6 of Kumar(1982).

The shock pattern is largely dictated by the sidewall compression angle,  $\delta$ , the inflow Mach number,  $M_1$ , and the contraction ratio,  $CR(= W/g$ , see Figure 1.2). The sidewall compression angle and the inflow Mach number determine the inviscid shock angle through oblique shock theory. The addition of leading edge sweep requires that another component of the inflow Mach number (the component parallel to the leading edge) be calculated through the shock and hence alters the application of the theory as given below. For a fixed sidewall compression angle and Mach number (and hence fixed shock angles), the location of the shock impingement point is determined by the distance between the sidewalls, or in other words, the contraction ratio. Thus, increasing the contraction ratio (bringing the sidewalls closer together) increases the compression of the inlet by causing the internal flow to encounter a greater number of reflected oblique shocks.

Sweeping the leading edges back has an additional effect of turning the flow away from the bottom surface toward the cowl as the flow passes through the swept shocks. This turning is shown qualitatively by considering the inviscid flow between two infinitely long swept wedges (i.e. neglecting end effects) using oblique shock theory, modified for the inclusion of leading sweep. Figure 3.3.2 shows the oncoming freestream Mach vector broken into components parallel and normal to the swept leading edge. Two-dimensional oblique shock theory may be applied directly to the normal component ( $M_{1N}$ ) to determine its post-shock components, noting that the effective wedge angle ( $\delta_{eff}$ ), the wedge angle measured normal to the leading edge, is given by

$$\delta_{\text{eff}} = \tan^{-1} ( \tan \delta / \cos \Lambda ) \quad [3.3.1]$$

and is greater than  $\delta$ . The equations to find the resultant Mach vector behind the oblique shock for the 2-D theory may be found in several texts (see for example Anderson (1982)) where three equations may be combined to give (in the notation of this study)  $M_{2N}$  in terms of  $M_{1N}$ , the ratio of specific heats, and the effective wedge and shock angles as:

$$M_{2N} = \frac{\left\{ \frac{M_{1N}^2 \sin^2 \theta_{\text{eff}} + [2/(\gamma-1)]}{[2\gamma/(\gamma-1)] M_{1N}^2 \sin^2 \theta_{\text{eff}} - 1} \right\}^{\frac{1}{2}}}{\sin(\theta_{\text{eff}} - \delta_{\text{eff}})} \quad [3.3.2]$$

The parallel (or crossflow) component ( $M_{1CF}$ ) must be treated separately. It should be noted that while the component of velocity parallel to the shock remains unchanged through the shock, the Mach number associated with that velocity vector decreases due to the increase in static temperature and hence the speed of sound across the shock, as

$$M_{2CF} = M_{1CF} (T_1/T_2)^{\frac{1}{2}} = M_1 \sin \Lambda (T_1/T_2)^{\frac{1}{2}}. \quad [3.3.3]$$

With the components behind the shock known, the resultant magnitude and direction of the Mach vector can be determined. The spillage angle  $\zeta$  can be determined as the difference between two angles,  $\Gamma$  and  $\beta$ , in the plane of the wedge, as shown in Figure 3.3.2. The angle the leading edge makes with the x-y plane measured in the plane of the wedge  $\Gamma$  is given by:

$$\Gamma = \sin^{-1} \left[ \frac{\sin \delta}{\sin \delta_{\text{eff}}} \right] \quad [3.3.4]$$

The angle which the resultant makes with the leading edge in the plane of the wedge  $\beta$  is given by:

$$\beta = \tan^{-1} \left[ \frac{M_{2N}}{M_{2CF}} \right] = \tan^{-1} \left[ \frac{M_{2N}}{(T_1/T_2)^{\frac{1}{2}} M_1 \sin \Lambda} \right]. \quad [3.3.5]$$

Clearly the difference between these two angles is the spillage angle  $\zeta$ ,

$$\zeta = \Gamma - \beta = \sin^{-1} \left[ \frac{\sin \delta}{\sin \delta_{\text{eff}}} \right] - \tan^{-1} \left[ \frac{M_{2N}}{(T_1/T_2)^{\frac{1}{2}} M_1 \sin \Lambda} \right]. \quad [3.3.6]$$

This spillage angle,  $\zeta$ , is on the order of a few degrees and is increased incrementally by each reflected shock (i.e.,  $\zeta$  for shock bay 3 of Figure 3.3.1 is greater than  $\zeta$  for shock bay 2). When the cowl is fully retracted, this downturned flow spills out of the inlet. This spillage is important in helping the inlet start at lower Mach numbers. As the Mach number is increased, the area (in the plane of the cowl) behind the shock sheets is decreased since the shocks lie closer to the sidewalls (Figure 3.3.3). This effectively reduces that spillage window and increases the mass capture of the inlet, making the inlet more efficient at high Mach numbers. It is these characteristics which make it possible to consider a fixed geometry inlet for use over a wide Mach number range. Compared to an aft placement, the cowl forward configuration captures more of the mass that would have otherwise spilled out. It is expected that a shock would develop on the cowl

lip inside the inlet as the downturned flow impinges on the cowl and is turned back parallel to the cowl surface, further increasing the compression and decreasing the total pressure recovery of the inlet.

For inlets of finite height, end effects can play a large role in determining the inviscid internal flow characteristics of the inlet. Particularly when the inlet height is small, modified oblique shock theory does not adequately account for the behavior of the flow. Spillage effects tend to cause a pressure relief near the bottom of the inlet, yielding lower pressures than would be expected by the modified oblique shock theory. Additionally, in order to insure that the flow vector downstream of the shock sheet lies not only in the plane of the downturned flow but also in the plane of the baseplate, Kutschenreuter, et al.(1965) hypothesized the existence of a centered expansion originating from the shock sheet/baseplate interface (Figure 3.3.4). This permits the flow vector to be positioned in both planes and predicts pressures near the bottom surface to be lower than in the center of the inlet where end effects are of lesser importance.

## **Computational Parametrics**

Since careful design of primary engine components such as the inlet is necessary to exploit effectively the potential of propulsion-airframe integration, a computational parametric study of three-dimensional sidewall compression scramjet inlets was performed to identify the effects of various geometric parameters on inlet performance. The parameters considered for the study included the leading edge sweep angle, varied between 30 and 60 degrees, and the cowl position, located at the throat and at two forward positions. A laminar boundary layer and cold wall ( $T_{\text{wall}}=300\text{K}$ ) boundary conditions were imposed. The parametric study was performed for a Mach number of 10 and a unit freestream Reynolds number of  $2.15 \times 10^6/\text{ft}$  at a geometric contraction ratio of 5. The performance of the various configurations was assessed in terms of the gross parameters of mass capture, throat Mach number, total pressure recovery, and area weighted internal pressure ratios. One  $0^\circ$  sweep computation was included to determine if significant changes in the gross flow field parameters occurred by introducing leading edge sweep of up to  $30^\circ$ .

The purpose of the computational parametrics was to identify inlet characteristics pertinent to the optimization of the configuration; this was therefore, in a sense, a trade off study of leading edge sweep and cowl position. Since the final product of the computational parametric study was a wind tunnel model to be used for comparison with prediction, the boundary conditions considered enveloped the anticipated test environment (i.e., the laminar boundary layer and constant 300K wall temperature boundary conditions). Since instrumented wind tunnel models are quite expensive, CFD was utilized to

minimize the costs of fabrication by eliminating from consideration designs which promise poor performance.

## **4.1 Configuration Description**

Much of the experimental work on the three-dimensional sidewall compression inlet concept has been performed by Trexler(1975,1988a,1988b; and Sounders, 1975); additionally, some low Mach number supersonic computational work on this type of configuration has been performed by Kumar(1986). Favorable comparisons between experiment and computation have been presented by Kumar and Trexler (1988) on a generic scramjet engine configuration at a nominal Mach number of 4 using the CFD code of Kumar (1986). This code (or versions thereof) has recently been used with good results in computation of a variety of inlet flow fields. Srinivasan, McClinton, and Kamath (1989) presented results using a version of the code to compute the three-dimensional turbulent, reacting flow through the entire Langley Parametric Scramjet Engine at an inflow Mach number of 6.25. Sekar, Thomas, and Srinivasan (1990) have used the code to compute flow in one of Langley's Arc-Heated Scramjet Test Facility's Mach 6 nozzles and subsequently through the Parametric Scramjet Inlet. Kumar, Singh, and Trexler (1990) have performed a numerical study of the effects of reverse sweep on a scramjet inlet performance at Mach 4.5.

Since both a computational and experimental database exist at lower supersonic Mach numbers, this geometry was adopted for the present Mach 10 parametric study. The inlet sidewalls were 7.2 inches in height with a total length of 31 inches. The baseplate extended only one inch ahead of the sidewall leading

edge. Hence there was no entrance boundary layer, and the configuration was said to model an uninstalled inlet. The distance from the sidewall leading edge to the constant area throat was 22.8 inches. Leading edge sweeps between 30 and 60 degrees were selected for the present parametric study to represent a range of moderate to highly swept cases. A  $0^\circ$  sweep case was also included to determine the effect of introducing sweep. The sidewall compression angle was fixed at 6 degrees, and the contraction ratio, defined by the ratio of the inlet entrance width to the throat gap ( $W/g$ ), was fixed at 5. The cowl position was defined by the forward extent of the cowl ahead of the throat as a percentage of the distance between the constant area throat and the sidewall leading edge. Thus, when the cowl was moved forward halfway between the beginning of the throat and the sidewall leading edge, it was termed 50% Cowl. Likewise, when the cowl was forward of the throat by one quarter of the distance between the throat and sidewall leading edge, it was termed 25% Cowl. Finally, when the cowl was located at the throat, it was termed 0% Cowl.

## 4.2 Inlet Code

The three-dimensional Reynolds-averaged Navier-Stokes code of Kumar (1986) was adapted to perform the present parametric study. (A detailed discussion of the governing equations, transformation of the governing equations to a generalized coordinate system, and the solution procedure is presented in the appendix.) The code solves the governing equations in full conservation form using MacCormack's time-asymptotic, explicit, predictor-corrector method (MacCormack(1969)). This method is second order accurate in time and space and



yields to a high degree of vectorization. The present work made use of an algebraic grid generation technique with linear connecting functions, described in Smith (1981), to obtain the Jacobian and metric data. In order to cluster the grid points near the boundaries in the physical domain, the grid refinement function of Roberts (1970) was included in the transformation for the y and z coordinates.

Since shock-boundary layer interactions depend on the size and character of the incoming boundary layer, the present configuration removed this dependency by modelling an uninstalled inlet, i.e. no incoming boundary layer was imposed at the inflow boundary. The inflow boundary was maintained at freestream conditions, while an extrapolation boundary condition was applied at the exit plane. On solid surfaces, all velocity components as well as the normal pressure gradient were required to vanish. A constant temperature distribution ( $T_{\text{wall}} = 300\text{K}$ ) provided the thermal boundary condition. Open boundaries are calculated assuming vanishing normal gradients in velocity, temperature, and pressure. Since the flow field was symmetric, only half of the field was computed and symmetry boundary conditions were imposed. The initial conditions were given by assigning freestream conditions to each grid point, except at the boundaries where appropriate boundary conditions were applied.

### **4.3 Averaged Exit Plane Properties**

For each of the gross flow field parameters of mass capture, throat Mach number, total pressure recovery, and area weighted internal pressure ratios, a discussion of the general trends is presented. Since these parameters may vary considerably across the inlet exit plane, the determination of a single representative

(average) number tends to obscure the true complexity of the flow field. Nevertheless, averaged values are presented for purposes of gross, generalized comparisons. In addition to the range of leading edge sweep considered, a single 0° sweep configuration was computed to explicitly identify the effect of introducing sweep. A tabular summary of the performance parameters is given in Table 4.3.1.

Table 4.3.1: Performance Parameters for Computational Parametric Study

L.E. Sweep (degrees)	Percent Mass Capture	Throat Mach Number	Total Pressure Recovery	P/P <sub>inf</sub>
<u>0% Cowl</u>				
0	96.73	5.202	0.430	19.91
30	96.05	5.345	0.443	18.78
35	95.70	5.369	0.445	18.65
40	94.99	5.410	0.452	18.31
45	94.05	5.449	0.461	18.00
50	92.92	5.483	0.472	17.50
55	91.42	5.545	0.483	16.74
60	88.51	5.623	0.499	15.66
<u>25% Cowl</u>				
30	98.28	5.227	0.439	20.45
45	96.90	5.303	0.455	19.95
60	94.03	5.516	0.514	18.75
<u>50% Cowl</u>				
30	99.41	5.176	0.431	21.12
45	98.26	5.256	0.452	20.74
60	96.65	5.507	0.522	18.91

#### 4.3.1 Mass Capture

Figure 4.3.1.1 presents the effects of leading edge sweep and cowl position on mass capture. In general, the mass capture decreases with increasing leading edge sweep. It was previously noted that the leading edge sweep promotes the turning of the flow toward the cowl plane. This increase in spillage is observed as a decrease in mass capture. It is also noted that the effect of a forward cowl position is the capture of the downturned flow which would have otherwise spilled out ahead of the cowl. A significant effort was expended for the 0% Cowl configuration to better identify the shape of the curve. The mass capture is observed to decrease monotonically in an almost parabolic fashion. It is important to note that sweeping the leading edge from 0 to 30° has an almost negligible effect on mass capture, which was seen to degrade by only 0.68%, taking on ever increasing significance above 30° sweep.

#### 4.3.2 Throat Mach Number

Figure 4.3.2.1 presents the momentum averaged throat Mach number variation with leading edge sweep and cowl position. It is observed that the throat Mach number increases with leading edge sweep and decreases with forward cowl position. As the leading edge sweep angle is increased, the strength of the leading edge shocks is decreased, yielding a higher post-shock Mach number. A forward cowl position, however, tends to lower the throat Mach number due to the lip shock formed on the cowl. When the cowl is in a more forward position, the cowl lip shock extends higher in the throat exit plane than for an aft cowl placement. Since

more of the  $\text{exit}$  plane is affected by this lip shock, the average throat Mach number decreases. Comparison of the  $30^\circ$  sweep throat Mach number with the  $0^\circ$  sweep configuration indicates that below  $30^\circ$ , there is no sudden change in the rate at which the throat Mach number decreased, since the per degree change in average Mach number between 0 and  $30^\circ$  is nearly that of the 30 to  $35^\circ$  range.

#### 4.3.3 Total Pressure Recovery

Figure 4.3.3.1 indicates that the total pressure recovery increases with leading edge sweep. It was previously noted that the shock sheets generated from the swept sidewall leading edges become weaker as the sweep is increased. This yields a higher total pressure recovery in the post-shock region. It is likewise expected that the forward placement of the cowl would tend to lower the average total pressure recovery due to the cowl shock formed on the lip, in the same sense that the average throat Mach number is decreased by the forward placement of the cowl. It is noted that this is in fact the case for a leading edge sweep of  $30^\circ$ . As the leading edge sweep is increased, however, the effect of the cowl placement is observed to reverse. The averaged total pressure recovery for a  $60^\circ$  leading edge sweep increases with forward cowl placement. This is indicative of a truly complex interaction, which is partially obscured by the averaging process. With the increase in leading edge sweep comes a significant increase in spillage. The flow which spills is the high pressure, high velocity flow near the cowl. The low momentum boundary layer flow is captured for each sweep angle. Since the capture area is smaller for increased sweep angles, the boundary layer flow occupies an increasingly larger proportion of the flow captured by the inlet, which, when

averaged, yields an effective decrease in total pressure recovery of the inlet. When the cowl is brought forward, more of the high momentum, compressed core flow is captured. It appears that on average, despite the strengthened cowl lip shock, the increased capture yields a net increase in total pressure recovery. It is also significant to note that the effect of leading edge sweep on the total pressure recovery below  $30^\circ$  is negligible.

#### 4.3.4 Area Weighted $P/P_1$

Figure 4.3.4.1 indicates that for all the configurations under consideration, the inlet compression ranged between 15 and 22. The compression is observed to decrease with increasing leading edge sweep angle due to the weakened swept internal shocks and the spillage of an increasing amount of the high pressure flow near the cowl plane. For the cowl forward positions, the loss of some of the high pressure fluid is compensated for by the compression due to the cowl lip shock. While this is insufficient to cause an increase in the average compression, it does decrease the rate of degradation of average compression with respect to the leading edge sweep angle. Since the spillage is minimized as the leading edge sweep tends toward zero, the loss of the high pressure fluid is minimized and a reduction in leading edge sweep from  $30$  to  $0^\circ$  yields less of a change in compression than the change from  $60$  to  $30^\circ$ .

## 4.4 Conclusions

Among the most important inlet parameters are mass capture, total pressure recovery, and internal compression. It was found that, compared to the unswept configuration, the inlet sidewalls could be swept by up to  $30^\circ$  without adversely affecting the inlet performance while enhancing the low Mach number starting performance (via swept shock induced spillage) and decreasing the aerothermal loading on the inlet leading edges. The mass capture was found to decrease with increasing sidewall leading edge sweep, since the sweep promoted downturning of the flow. Forward placement of the cowl increased the mass capture by preventing the flow from spilling out. While the forward cowl position tended to increase the average compression of the inlet exit plane due to the cowl lip shock, it did so at the cost of additional flow nonuniformity and decreased total pressure recovery. The 60 degree configuration showed a significantly lower mass capture and internal compression than the 45 degree configuration but had a much higher total pressure recovery. An increase in leading edge sweep, however, necessarily requires an increase in length (and hence weight) to obtain the same geometric contraction, an undesirable quality for an engine component. The 45 degree configuration had nearly the same mass capture and internal compression as the 30 degree configuration with a 5-7 percent improvement in total pressure recovery. From consideration of the mass capture, total pressure recovery, and internal compression, the 45 degree leading edge sweep appears to be the optimum sweep angle.

## Experimental Configuration

The leading edge sweep for the experimental configuration ( $\Lambda$ ) was fixed at 45 degrees as a result of the computational parametrics. This has been further supported by the experimental work of Kanda, et al.(1989) (see Section 2.3.3). As with the computational parametrics, the sidewall compression angle was fixed at 6 degrees as a result of a trade off (Trexler(1975)) between larger compression angles leading to stronger internal shocks and increased risk of boundary layer separation and smaller compression angles leading to weaker internal shocks but requiring the inlet to be longer to obtain the same contraction ratio, imposing a size and weight penalty on the inlet. The models were injected into the tunnel in flight orientation, with the cowl on bottom. The forebody plane was represented by a flat plate, also called the baseplate. A sketch of the inlet model was given in Figure 1.2.

The contraction ratio, the ratio of the inlet entrance width to the throat gap,  $W/g$  (see Figure 1.2), could be varied between the runs by laterally moving one of the sidewalls. The model was designed with only one movable sidewall to prevent covering the orifices in the heavily instrumented near corner region with the sidewall when the contraction ratio was increased. This also simplified the sidewall alignment procedure. Hence there were three effective centerlines; each must be instrumented to obtain the centerline pressure distributions. The requirement for a fixed sidewall and the three effective centerlines led to an awkward coordinate system. The logical choice for the x-direction was axially down the inlet centerline. The y-direction was chosen positive toward the fixed sidewall. This led to a convenient nondimensionalization:  $y/y_{wall}$ , the percentage of the distance between the centerline and the sidewall at a given downstream station. Due to the mounting

requirements of the model on the injection plate, the fixed sidewall was necessarily located nearer the injection plate, as shown in Figure 5.1, which shows the model on the injection plate viewed from under the tunnel. The completion of the right-handed set places  $z$  such that  $z < 0$  on the inlet sidewalls. Thus distances down the inlet sidewalls measured from the baseplate are reported in terms of  $Z$  (which is the absolute value of  $z$ ) to allow for positive distances.

A total of 256 channels of pressure data was available for the experimental work. Figures 5.2 and 5.3 show the distribution of the orifices: 89 static pressure orifices were distributed on the fixed sidewall, concentrated in regions of strong interactions, 5 static pressure orifices located on the movable sidewall to assure zero yaw, 131 static pressure orifices were distributed in 25 lateral arrays on the baseplate, 14 static pressure orifices on the cowl centerline, 3 pitot probes at the baseplate leading edge plane, and the remaining 14 channels are reserved for various pitot rakes for the entrance and exit planes. Axial nondimensionalization was based on the distance from the sidewall leading edge to the throat,  $Tx'$  (Figure 5.2). Since shock interactions on the sidewall occur along lines of constant sweep, the orifices were arranged in arrays along lines of constant sweep ( $x'/Tx' = \text{constant}$ ) as well as horizontal arrays.

The cowl position was defined by the distance between the cowl leading edge and the constant area throat as a percentage of the distance between the sidewall leading edge and the throat,  $Cx'/Tx'$  in Figure 5.2. Thus, when the cowl was moved forward halfway between the beginning of the throat and the sidewall leading edge, it was termed 50% Cowl ( $Cx'/Tx' = 0.50$ ). Likewise, when the cowl was forward of the throat by one quarter of the distance between the throat and sidewall leading edge, it was termed 25% Cowl. Finally, when the cowl was located at the throat, it was termed 0% Cowl.



The results of the computational parametrics indicated that the 45 degree leading edge sweep offers promise as an efficient design and hence has been chosen for further computational and experimental study. This design must be coupled with the capabilities and limitations of the test facility, as outlined in Chapter 3. This chapter will present the design specifications for the wind tunnel model fabrication.

## 5.1 Component Sizing

As outlined in Sec. 3.2.3, there were physical limits to the maximum size of the model which were imposed by the tunnel. Since it was desired to have the capability of placing the model at angle of attack, the model was oriented with the baseplate normal to the injection plate; angle of attack could be achieved by rotating the circular injection plate insert on which the model legs were mounted. Thus the length of the plate was limited only by the maximum length of the injection plate, namely 34 inches. A length of 30 inches was chosen since it gave sufficient clearance at each end and allowed the model to be injected at 15° angle of attack with a leading edge clearance of slightly over 0.5 inch.

With the length of the baseplate established, the next logical concern was the width. Assuming disturbances move inboard along Mach lines, the plate must be wide enough such that the Mach cones originating on the corners do not enter the inlet for the largest entrance width. For Mach 10, the Mach angle  $\mu$  is 5.739 deg. For a 30 inch long plate, the Mach cones originating at the leading edge would encompass only 6 inches of the total width (3 inches on each side). Thus if the entrance of the inlet were at the end of the plate, this would dictate a plate 6 inches

wider than the maximum entrance width. The second consideration was related to clearance when the injection carriage was rotated to allow access for model changes. Based on the measurements and equations of Sec. 3.2.3, for a 30 inch long baseplate centered axially on the injection plate, the leading edge could extend no farther than 21.8 inches from the injection plate (6.2 inches beyond the tunnel centerline). In the interest of staying within the weight requirements, the plate should be as narrow as possible. A leading edge width of 10 inches was found to meet or exceed all the above criteria. It was further noted that significant weight savings could be obtained by reducing the baseplate width downstream of the leading edge. Since the model was sized to fit in the 20 Inch Mach 6 tunnel also, the narrowing occurred at the Mach angle for Mach 6 ( $9.6^\circ$ ), a more stringent condition than the Mach 10 Mach angle.

The inlet height was dependent on the core size and on the placement of the inlet in the test core. Since the need to minimize the lag time in the pressure measurement requires the placement of the pressure sensors inside the model, a 3.5-inch bay was necessarily located on the baseplate to accommodate the sensors. In order for the entire model to be immersed in the inviscid core, the baseplate should be placed on the tunnel centerline (Figure 5.1.1). Thus the inlet sidewalls were limited to a maximum height of half the core size. In order to allow space for the interaction between the inviscid stream and the flow spilling from the inlet near the cowl, the inlet height was fixed at 4 inches, approximately 60% of the core half-height. This size also made it a 1/9 scale height, based on a 3-foot inlet height for a NASP-like vehicle reported in Clausen and King(1990).

With the maximum height and length of the domain established, the next consideration was the length of the compression portion of the inlet, i.e. the distance from the leading edge to the constant area throat. Among the parameters

to be varied was the geometric contraction ratio. Since the height at the entrance is equivalent to the height at the throat, the contraction ratio reduces to  $(WH)/(gH) = W/g$ , the ratio of the entrance width to the throat gap. In order to obtain multiple interaction types, it was desirable that the inlet be designed for the shock to reflect and impinge aft of the shoulder at the throat for at least one contraction ratio, subject to the need for sufficient inlet compression. When the distance from the leading edge to the throat was 9.51 inches, this requirement was met for a contraction ratio of 3; this also had the advantage of having nominal throat gaps for various contraction ratios: 1 inch throat gap for  $CR = 3$ , 0.5 inch throat gap for  $CR = 5$ , and 0.25 inch throat gap for  $CR = 9$ . The large throat gap was desirable to maximize the instrumentation density for a highly instrumented model.

Since it was desired to reduce the blockage (and wake) of the model and allow for the placement of a pitot rake in the exit plane, the last 5 inches of the inlet were internally flared at  $5^\circ 43'$  to provide a 0.5 inch expansion for each sidewall. Thus the exit area at the end of the model was increased by a factor of 2 over the inlet throat area for a contraction ratio of 3. For a contraction ratio of 5, the ratio of exit area to throat area was 3, and for a contraction ratio of 9, it was 5. (By also narrowing the outboard sides of inlet sidewalls, a total of approximately 6.5 pounds of copper was removed from the model.)

Entrance and exit plane rakes were used to obtain pitot profiles. The entrance rake had 11 probes constructed from stainless steel tubing with a 0.020 inch ID and 0.040 inch OD. The tubes were internally beveled and vertically compressed to an internal vertical gap of 0.010 inch. The 11 tubes spanned 1.5 inches and were placed on 0.15 inch centers. The exit plane rake also had 11 tubes which were placed on 0.285 inch centers. These tubes were constructed of 0.040 inch ID, 0.060

inch OD stainless tubing and were also beveled. Since this rake was used to measure the core flow and not the baseplate or cowl boundary layer, the probe was not flattened.

As outlined in Sec. 3.2.4, the material for the model was chosen to be copper primarily due to its high thermal conductivity. In order to maintain structural integrity (prevent warping) of the leading edges, it was necessary to protect these thin edges. This was accomplished by choosing a material with a high thermal conductivity to rapidly remove the heating. The thin leading edges were also protected on the outboard side of the leading edges by a coating of zirconia oxide, an insulating material. Leading edge radii were based on previous experience with copper models in high temperature test environments and were fabricated by truncating the leading edge, for the case of the baseplate, 0.07 inch aft of the theoretical sharp leading edge and rounding to a 0.01 inch radius. The wedge angle of the baseplate leading edge was determined by a trade off of leading edge thinness and aerodynamic heating. It was desired that the leading edge be thin but rapidly increase (larger wedge angle) to establish a thermal mass into which the leading edge heating could be conducted. By increasing the wedge angle however, the shock strength and hence heating was increased. By decreasing the leading edge wedge angle from  $20^\circ$  to  $15^\circ$ , the shock strength decreased by a factor of nearly 2. Further reduction yielded less dramatic changes in shock strength with a significant reduction of mass near the leading edge. Thus the leading edge wedge and pressure sensor bay enclosure angles were fixed at  $15^\circ$ . Photographs of the model on the injection plate and injected in the tunnel are presented in Figures 5.1.2 and 5.1.3, respectively.

## **5.2 Test Techniques**

### **5.2.1 Pressure Measurements**

The pitot pressures and surface static pressures were measured by an electronically scanned pressure (ESP) silicon sensor (ESP-32 model 780B, manufactured by Pressure Systems, Inc. (PSI)). The ESP modules each contain 32 sensors and were located inside the model to minimize tubing length and hence settling (lag) time. In order to maintain the ESP modules at constant temperature, atmospheric air was bled into the ESP bay. Thermocouples placed in the bay on each module indicated that the temperature increased by no more than 1 degree F during the run. In addition to the 32 sensors, each module contained internal multiplexing and amplification to provide a scanner for a high data rate. A pneumatically controlled slide allowed the transducers to be calibrated on-line prior to each run. In anticipation of widely differing pressure ranges on the model, the pressure orifices were connected to modules rated for either 0.36 psi, 2.5 psi, or 5.0 psi full-scale.

#### **5.2.1.1 Calibration of Pressure Sensors**

The calibration of the ESP system was accomplished by sequentially applying three known pressures (vacuum levels) to the ESP module and measuring the voltage output. From these three pressure-voltage points, a second order curve fit defined the pressure-voltage relationship (which was essentially linear) over the range of the module. A hard vacuum reference was provided for the differential sensors by a turbomolecular vacuum pump. Vacuum levels for the calibration were provided by a vacuum pump. Direct connection to the pump yielded the low end

calibration point. Bleeding the vacuum slightly provided a midrange (i.e. 1.25 psi for a 2.5 psi module) calibration point. The third calibration point was obtained by increasing the bleed until the pressure was approximately the maximum rated pressure for the module. These three pressures could be pre-set for each range module used during the test. Each of the calibration pressures was measured by a digiquartz calibration standard (a high accuracy vibrating quartz pressure standard manufactured by Paroscientific, Inc.). For the 2.5 psi and 5.0 psi modules, a digiquartz rated for 30 psia which was calibrated in the 0-5 psia range was used. (The digiquartz calibration employed 4 points, hence giving a third order curve fit of pressure vs. voltage. The calibration coefficients for the digiquartz were preprogrammed into the pressure calibration unit (PCU) and the data reduction software.) For the 0.36 psi module, an MKS calibration standard (a precision vacuum/pressure sensor incorporating a capacitive diaphragm gauge manufactured by MKS, Inc.) rated at a maximum of 100 mm Hg ( $\sim 2$  psi) was employed.

#### 5.2.1.2 Data Reduction and Uncertainty

The calibration coefficients for each pressure port were stored in the data acquisition computer (HP9000 series 300) so that the output voltage could be converted to measured pressure. In order to improve the accuracy of the calibration, a 100 mm Hg MKS head was installed just behind the injection plate to measure the calibration pressures for the lowest range (0.36 psi) module. Additionally, prior to testing, the calibration pressures were measured at the ESP modules with a 100 mm Hg MKS head to determine the pressure differential between the modules and the MKS head. At the lowest calibration pressure, a small differential was measured and added to the calibration pressure to correct it to the calibration pressure at the module. At the higher calibration pressures, the

differential was negligible. This effectively removed the uncertainties associated with line loss in the calibration. (This also highlights the need to keep tubing length between the orifice and the ESP module to a minimum when measuring very low pressures.) With the calibration thus corrected, the pressure data reduction was accomplished via the curve fit. Calibration pressures obtained in this manner are believed to be accurate to 0.5%.

Manufacturer specifications indicate that the overall system uncertainty was 0.07% full scale. Thus the largest error was obtained when measuring the lowest pressures. For example, 0.07% full scale for a 0.36 psi module corresponds to an uncertainty of 0.00025 psi. When measuring pressures in the vicinity of freestream static (0.03psi for  $Re = 2.15 \times 10^6/ft$ ), this amounts to a relative uncertainty of 0.84%. At the lowest Reynolds number ( $0.55 \times 10^6/ft$ ), the freestream static pressure is approximately 0.009 psi, so that at that level, the relative uncertainty would be 2.8%. For the 2.5 psi module, a 0.07% full scale uncertainty corresponds to 0.00175 psi. Ideally this range would be used to measure pressures no lower than the maximum of the next lowest range pressure model (0.36 psi). In this case, the relative uncertainty is 0.5%. In order to prevent the 0.36 psi modules from being overscaled, orifices where the maximum anticipated pressure for any given configuration in the test matrix exceeded 0.3 psi were connected to the 2.5 psi module. This led to a few instances where for some configurations, the 2.5 psi module was used to measure pressures below 0.36 psi. For the  $Re = 2.15 \times 10^6/ft$  runs, the lowest measured pressure for this range module was 0.13 psi, and the corresponding relative uncertainty was 1.3%. For the  $Re = 0.55 \times 10^6/ft$  runs, the minimum pressure fell to approximately 0.07 psi, representing a relative uncertainty of 2.5%. The 5.0 psi modules were used strictly for pitot measurements, for which the worst case relative uncertainty was 0.35%. Thus for

the high Reynolds number runs, the worst case relative uncertainty in the pressure measurements was 1.3%, and for the low Reynolds number runs, 2.8%.

### 5.2.2 Surface Temperature Measurements

The technique for obtaining surface temperature distributions using infrared thermography has been well described in Gauffre (1988) and Daryabeigi, et al. (1991); the latter is briefly summarized here. Infrared radiation is the thermal radiation emitted from an object solely due to its temperature and falls within the 0.7 to 30  $\mu\text{m}$  range of the electromagnetic spectrum. Infrared imaging systems are used to detect that radiation and convert it to a two dimensional monochrome image of the infrared radiation intensity variations across the target. For the present test, a commercially available Agema 880 infrared imaging system was used. This system was sensitive to the 8 to 12  $\mu\text{m}$  range of the electromagnetic spectrum and is shown schematically in Figure 5.2.2.1. The device contains a single mercury-cadmium-telluride detector cooled by liquid nitrogen. A television-type raster scanning of the target area was obtained by a pair of synchronized mirrors (also shown in the figure). A zinc selenide window optimized for 98% transmission of infrared radiation in the 8-12 $\mu\text{m}$  range was installed at the bottom wall of the 31 Inch Mach 10 Tunnel test section. A spatial resolution of 0.08 inch was obtained with the present scanning system. The thermal resolution was 0.1° C (for the 20 to 100° C range of calibration). The data were digitized with an 8 bit resolution and displayed and stored as 140 lines of data with 140 samples across each line.

The system was calibrated by placing a blackbody radiator in the tunnel at the location which would be occupied by the model during the run. The infrared imager then scanned the blackbody and the results were compared to



thermocouple data placed on the blackbody. The results revealed a temperature measurement uncertainty of  $1.67^{\circ}\text{C}$  over the  $20\text{-}100^{\circ}\text{C}$  calibration range. Prior to the IR runs, the model was painted flat black to decrease surface reflectivity.

### 5.2.3 Flow Visualization

Surface flow visualization by means of surface oil flow has been common practice in many wind tunnel investigations for a number of years to study the flow in the boundary layer under a variety of interactions (see for example Meyer(1966) or Zheng(1988)). The method consists of applying a base coat of a low viscosity vacuum oil to the surface of interest. For the present test, a nontoxic, nonirritating silicone fluid (available in a wide range of viscosities) was used. Discrete dots of a mixture of a higher viscosity oil with white artist's paint were placed on the surface prior to the run. Surface flow directions were obtained from post-run photographs of the oil streaks.

## **5.3 Wind Tunnel Blockage Assessment**

In order to increase the instrumentation density in interaction regions for a highly instrumented model, it was desirable to make the model as large as possible. When the cross-sectional area of a model becomes large relative to the inviscid core size of the tunnel, the effects of blockage must be considered. In order to assess these effects, a blockage model (an inexpensive, much less densely instrumented version of the configuration) was designed based on the results of the computational parametric study and fabricated for preliminary testing in the

31 Inch Mach 10 Tunnel at the NASA Langley Research Center. Since it was desired to determine both the effect of the model on the performance of the wind tunnel and also to determine if the inlet would start, the model possessed a total of 32 static pressure orifices distributed on the forebody plane and sidewalls; seventeen static pressure orifices on the tunnel wall and 3 pitot probes on the model monitored the tunnel performance. This section presents the blockage aspects of the effects of contraction ratio, cowl location, Reynolds number, and angle of attack. These results are also available in Holland, et al. (1991).

### 5.3.1 Results

The generic three-dimensional sidewall scramjet inlet model had a leading edge sweep of 45 degrees and possessed 32 static pressure orifices distributed on the baseplate and sidewalls. The effects of cowl position, contraction ratio, and Reynolds number on the internal static pressure distributions were documented in a total of 25 runs. A global description of the inviscid and viscous interactions for the sidewall compression inlet has been provided in Section 3.3.

#### 5.3.1.1 Model Cross-Sectional Area Distribution

Figure 5.3.1.1.1 shows the profile and front views of the configuration as the angle of attack is increased. Due to the size of the ESP bay, the model cross-sectional area changes little as the angle of attack is increased. A cross-sectional area distribution for the model at zero angle of attack is given in Figure 5.3.1.1.2. The maximum cross-sectional area of 52 sq. in. represents 5.4% of the total area of the test section and 30.7% of the inviscid core.

#### 5.3.1.2 Pressure Data

Figure 5.3.1.2.1 is a plot of the pressures on the injection plate when no model was present. For the 3 Reynolds numbers, it is evident that the tunnel sidewall static pressure was slightly greater than the calculated freestream static. Fischer, et al. (1970) presented a compilation of sidewall to freestream static pressure measurements in several supersonic and hypersonic facilities. A curve fit of the data indicates that the sidewall pressure may exceed the freestream static pressure by 6% at Mach 10, though there was considerable variation among facilities. A smaller deviation was observed in the present work, which increased with decreasing unit Reynolds number (0.2% at 2.15 million/ft, 1.5% at 1.14 million/ft, and 3.2% at 0.55 million/ft). A nonconstant pressure distribution was noted for the lowest Reynolds number run. This was most likely due to a poor seal between the injection plate and the tunnel sidewall, causing a slight mass transfer as the pressure in the injection chamber equilibrated with the freestream static pressure. This was more pronounced at the low Reynolds number, for which the freestream static pressure was lowest. An additional disturbance was noted past 13 inches due to the proximity to the mounting holes for the model assembly, and the data beyond this point were disregarded for comparison purposes. These three runs are used as a baseline against which the data for the model-injected runs are compared to evaluate the effects of blockage.

Figure 5.3.1.2.2 shows the pressure distributions along the baseplate of the inlet for a contraction ratio of 3 at a freestream unit Reynolds number of 2.15 million per foot for 0%, 25%, 50%, and no cowl (denoted NOC in the figure) configurations. The figure indicates that the cowl location (or even the presence or absence of a cowl) for a contraction ratio of 3 has a negligible effect on the baseplate pressures. The pressures on the baseplate near the leading edge are low,

rising to a plateau at the entrance to the inlet, possibly indicating a small separation region. The pressure is seen to rise sharply as the shocks generated from the sidewall leading edges reach the centerline. A slight pressure relief is then observed as the flow expands around the corner into the constant area throat region before the shock reflections increase the pressure again. The pressure then rapidly decreases toward freestream static as the flow expands out the back of the inlet. Static pressures on the sidewall of the tunnel (Figure 5.3.1.2.3) are low and uniform, indicating that for this configuration, the position, presence, or absence of the cowl has no effect on the tunnel flow conditions; hence, no blockage is noted. (Pressure orifices past  $X = 15$  inches are influenced by their proximity to the support struts which hold the model and thus are disregarded.) Figure 5.3.1.2.4 also shows no effect on the ratio of measured to calculated freestream pitot pressure.

Likewise, for a contraction ratio of 5, Figure 5.3.1.2.5 demonstrates no cowl effects. Tunnel sidewall pressures (Figure 5.3.1.2.6) and freestream pitot pressures (Figure 5.3.1.2.7) are again observed to be uniform. Since the  $CR = 9$  (Figure 5.3.1.2.8) shows the same lack of dependence on the cowl, it appears that the baseplate is out of the domain of influence of the cowl, but as will be demonstrated in Section 7.2.2, a closer examination of the more detailed data indicate that this is not the case. Tunnel sidewall pressures (Figure 5.3.1.2.9) and pitot pressures (Figure 5.3.1.2.10) remain unaffected by the cowl position at  $CR = 9$ .

Since little influence of the cowl on the baseplate is noted in this data, it is sufficient to compare the contraction ratio effects for one cowl position. Figure 5.3.1.2.11 presents the contraction ratio effects for a 0% Cowl (cowl at the throat), unit Reynolds number of 2.15 million per foot configuration. The effect of moving the sidewalls closer together (increasing the contraction ratio) is to increase the

overall compression of the inlet. Moving from a CR = 3 to 5 tends to increase the plateau pressure at the inlet entrance, possibly indicating a slightly larger separation region. The maximum pressure in the inlet is also observed to increase. The shock reflection pattern denoted by the peak-dip-peak pattern of the CR = 3 is not as pronounced. The contraction ratio of 9 likewise demonstrates a sharper pressure rise to a higher maximum pressure in the inlet. Despite the high internal pressure, it is believed that the inlet is started, since the pressures were steady with time and well below that of the post-normal shock value (static pressure increases by a factor of 116.5 for a normal shock at Mach 10). Figures 5.3.1.2.12 and 5.3.1.2.13 again indicate that no blockage effects are evident in the tunnel sidewall static and freestream pitot pressures, respectively.

Reynolds number effects are presented in Figures 5.3.1.2.14 - 5.3.1.2.16 for a contraction ratio of 5, 0% Cowl configuration. It is observed that the interactions are the same but at a higher compression for the lower Reynolds number, due to the increased boundary layer displacement thickness causing stronger shock interactions. It is also noteworthy that the disturbance caused by the support strut on the tunnel sidewall pressures extends farther forward for the lower Reynolds number. As previously noted, the pressure measurements at the front of the injection plate are perturbed by the slight gap at the interface between the injection plate and the tunnel sidewall. At 4 inches aft, however, the pressures have relaxed to the same value, indicating no evidence of tunnel blockage.

The model was also injected at 15° angle of attack at a contraction ratio of 9 and 50% Cowl to determine the effect on tunnel performance. Figure 5.3.1.2.17 demonstrates that although the disturbance due to the support struts (also at angle of attack) is increased, the static pressure on the tunnel sidewall remains unaffected by the presence and orientation of the model.

### **5.3.2 Conclusions**

A model of a generic, sidewall compression scramjet inlet with a leading edge sweep of 45 degrees was tested in the 31 Inch Mach 10 facility at the NASA Langley Research Center. Since the model dimensions were large with respect to the tunnel core, the present model was constructed prior to fabrication of a highly instrumented model to determine first if the tunnel could remain started following injection of the model and secondly to determine if the inlet itself would start. For each of the configurations tested, the tunnel remained started for the duration of the run, based on the pitot and tunnel sidewall pressure distributions. These measurements indicated no evidence of tunnel blockage due to the presence or orientation of the model. Furthermore, the inlet appeared to start and remain started, based on the 32 static pressure orifices distributed on the baseplate and sidewalls.

## **5.4 Test Matrix**

Now that the effects (or lack thereof) of the model size on the performance of the facility has been established, it is necessary to define the test sequence for the highly instrumented model. As previously indicated, there are three principle parametric variables: contraction ratio, cowl position, and Reynolds number. Each of these variables has 3 nominal values, yielding a total of 27 configurations to be tested. The test matrix can be thought of as a 3x3x3 cube. On the front face of the cube is the variation of contraction ratio and cowl position for a nominal freestream unit Reynolds number of 0.55 million/ft. Run numbers are provided in Table 5.4.1. A similar arrangement for Reynolds numbers of 1.14 million/ft and

2.15 million/ft is given in Tables 5.4.2 and 5.4.3, respectively. (Configurations having more than one run number were used as a check on repeatability.)

Table 5.4.1: Test Matrix (runs) for Re=0.55 million/ft

	0% Cowl	25% Cowl	50% Cowl
CR=3	64	61	58
CR=5	44	41	37,38
CR=9	47	50	55

Table 5.4.2: Test Matrix (runs) for Re=1.14 million/ft

	0% Cowl	25% Cowl	50% Cowl
CR=3	65,67	63	59
CR=5	45	42	39
CR=9	48	52	56

Table 5.4.3: Test Matrix (runs) for Re=2.15 million/ft

	0% Cowl	25% Cowl	50% Cowl
CR=3	66	62	60
CR=5	46	43	40
CR=9	49	53,54	57

## Computational Results

In Chapter 4, computational fluid dynamics was used to provide a parametric study designed to provide an inlet with characteristics suitable to a candidate configuration for a hypersonic vehicle. The discussion of the inlet characteristics emphasized the gross inlet performance parameters. Now that the results of that study, coupled with wind tunnel constraints, have yielded a candidate wind tunnel model, it is necessary to provide a detailed examination of the internal flow characteristics. This chapter will present an in-depth discussion of the flow interactions. Since CFD provides internal flow characteristics, full use will be made of the flow field data to identify shock locations, separation regions, and flow streamlines. Simulated oil flows of the surface streamlines and crossflow streamlines are generated by restricting the particle traces to a two-dimensional plane.

The computational grid for the configuration is presented in Figure 6.1. It should be noted that for the contraction ratio of 3 plots, the lateral scale has been exaggerated by a factor of 2, and for the contraction ratios of 5 and 9, by a factor of 3 in order to more clearly view the interactions. The mesh has 86 grid points in the axial direction, 31 laterally, and 61 vertically (46 inside the inlet and 15 underneath --not shown-- for the flow spillage). The grid is swept at the leading edge sweep angle to better resolve interactions which occur in planes of constant leading edge sweep. It should be noted that the plots of rectangular crossflow planes appear narrower at the cowl plane than at the baseplate since, due to the sweep of the grid, the cowl plane is farther away than the baseplate. The sidewall leading edge is located at  $I=30$  and mounts to the forebody plane (baseplate) 9 inches aft of the



baseplate leading edge. For each of the 3 contraction ratios presented, the inflow boundary layer was allowed to develop naturally on the baseplate. At the inlet entrance station, the laminar boundary layer thickness (based on  $u = 0.995U_e$ ) was found to be  $\delta = 0.35$  inch. The displacement thickness was computed to be  $\delta^* = 0.20$  inch, and the inlet inflow momentum thickness was  $\theta = 0.0076$  inch. The Reynolds number based on momentum thickness was  $Re_\theta = 1361.6$ . Tauber (1990) presented empirical correlations of transition measurements. The equation

$$Re_\theta/M_e = \text{constant} \quad [6.1]$$

was found to be an approximate correlation for supersonic or hypersonic boundary layer edge velocities, where the constant varies between 150 and 350 depending upon the ratio of roughness height to momentum thickness among other parameters. For the Mach 10 inflow,  $Re_\theta/M_e = 136$ , which is less than the value for transition. The throat begins at  $I = 55$ ; the shoulder is also swept at the leading edge sweep angle. The inlet exit (combustor entrance) is a vertical plane located at  $I = 72$ , 25 inches aft of the baseplate leading edge. As indicated in the figure, the inlet throat is longer near the baseplate than at the cowl plane due to the difference in sweep of the throat entrance and exit. In order to accommodate the swept throat entrance and vertical exit, the grid is linearly transitioned from swept to vertical in this region. The aft expansion added to the wind tunnel model to minimize tunnel blockage and to accommodate the rake mechanism was also modeled in the  $I = 72$  to 86 region. The entire model was 30 inches long. For convenience, plots of crossflow planes are overlaid with reference lines dividing the inlet height and local width into 10 evenly spaced segments. In each of the crossflow planes presented, the inlet centerline is the left boundary and the inlet sidewall is the right boundary.

Thus,  $y/y_{\text{wall}}$  increases from 0 to 1 from right to left on the page. Additionally, the baseplate is at the top and the cowl at the bottom, so that  $Z/H$  goes from 0 to 1 from the top of the page to the bottom.

Since each computation requires a significant expenditure of CPU time, the entire experimental test matrix is not duplicated. Due to the large number of plots required to fully document the flow fields, a summary of the global contraction ratio effects is presented to provide a quick understanding of the flow features prior to the detailed discussion. Shock interactions and internal vortices in particular are highlighted by the crossflow plane-by-plane discussion. Contraction ratios of 3, 5, and 9 for a  $Re = 2.15$  million/ft and 0% Cowl configuration are presented. A  $CR = 3$ ,  $Re = 2.15$  million/ft, 50% Cowl configuration is also presented to establish the effects of cowl placement. A  $CR = 3$ ,  $Re = 0.55$  million/ft, 0% Cowl configuration is added to the set to provide the Reynolds number effects. A comparison of the full test matrix is reserved for the discussion of the experimental data.

## 6.1 Contraction Ratio Effects

The pressure contours presented in Figures 6.1.1a, b, and c show the internal shock structure at three horizontal stations,  $Z/H = 0.25$ ,  $0.50$ , and  $0.75$ , respectively, for a contraction ratio of 3. The shock generated from the sidewall leading edge is observed to strike the centerline at approximately 69% of the distance between the leading edge and the throat entrance ( $x'/Tx' = 0.69$ ), reflecting back to impinge on

the sidewall just aft of the shoulder (throat entrance). In the horizontal center plane (Figure 6.1.1b), the shock is observed to again reflect, reaching approximately the centerline at the exit plane. It is important to note that since the length of the throat varies with vertical position in the inlet, the position of the shock at the exit plane varies as a function of  $Z/H$ . For example, at  $Z/H = 0.25$  (Figure 6.1.1a), the shock appears to have reflected from the centerline just ahead of the exit plane, the shock is located very near the centerline of the inlet for the mid-height (Figure 6.1.1b), and the shock has not quite reached the centerline nearer to the cowl (Figure 6.1.1c). Figure 6.1.2 shows sidewall and baseplate pressure contours. Among the noteworthy interactions demonstrated in the figure are the strong pressure rise and relaxation near the sidewall leading edge (the so-called  $\chi$ -bar interaction), the shock impingement aft of the shoulder, the expansion of the flow around the shoulder (particularly evident on the baseplate aft of the shoulder), and the cowl shock near the bottom of the figure. These features will be discussed in detail in the next sections, however it is instructive to note that in conjunction with Figure 6.1.3, the centerline pressure contours, the swept oblique shock train can be reconstructed. The first centerline shock impingement is observed to have a slightly irregular shape at approximately  $Z/H = 0.5$  due to the effects of the weak compression formed due to the displacement effects of the boundary layer growth at the baseplate leading edge. Regions of flow separation are indicated in Figure 6.1.4, which shows contours of negative axial velocity. A small separation is observed just aft of the shoulder at the sidewall impingement location. Additionally, the glancing shock is observed to separate the baseplate boundary layer both upstream and downstream of the centerline reflection. Interactions on the inlet sidewall are also presented by way of sidewall and baseplate particle traces (Figure 6.1.5). By restricting the particles to their

respective planes, a simulated oil flow is created. The shock impingement in particular is clearly evident. It is also observed that in the uppermost 25% of the inlet, the sidewall flow patterns indicate an upward movement until the flow separates (denoted by the accumulation line) in the immediate vicinity of the corner. Diverging streamlines on the baseplate indicate a flow reattachment. This pattern is typical of what Kubota and Stollery (1982) referred to as an induced layer. There exists a downward component over much of the sidewall, which is expected based on inviscid considerations. Near the  $Z/H=1.0$ , the sidewall streamlines are observed to turn downward more sharply as the compressed flow expands downward into the freestream. This turning is more severe in the low momentum boundary layer, leading to a highly skewed, helical velocity distribution in the boundary layer. The cowl shock is observed to influence much of the throat. The extent of that influence is identified in the static pressure distribution in the exit plane (Figure 6.1.6). Since individual crossflow planes will be discussed in detail in the coming sections, it will suffice for now to note that the exit plane is non-uniform both vertically and horizontally. That notwithstanding, Figure 6.1.7 shows the Mach number distribution to be significantly more uniform.

Pressure contours for 3 horizontal planes for a contraction ratio of 5 configuration are presented in Figures 6.1.8a,b,c for  $Z/H=0.25$ ,  $0.50$ , and  $0.75$ , respectively. These plots reveal a multiply reflecting shock pattern, most clearly seen in the horizontal centerplane (Figure 6.1.8b). The shock appears to strike the centerline at approximately  $x'/Tx'=0.58$ , reflect and impinge on the sidewall at  $x'/Tx'=0.94$ , and reflect back to strike the centerline at approximately  $x'/Tx'=1.0$ . At this point, the shock pattern begins to be interfered with by an expansion from the throat shoulder as the flow turns the corner from wedge to freestream aligned.

The effects of the expansion are observed both locally in the immediate vicinity of the sidewall corner as the pressure in shock bay 4 (see Figure 3.3.1) relaxes and globally as the expansion causes a downstream relaxation of pressure even in shock bay 5 on the centerline. A total of 8 shock bays are observed before the exit is reached. Upon each reflection, the shock becomes less and less distinct. Interestingly enough, the highest pressure region is located in shock bay 5 on the centerline. At the exit (or combustor entrance), the maximum has relaxed significantly. The shock impingement pattern can also be observed by comparing the sidewall and centerline pressure distributions, Figures 6.1.9 and 6.1.10, respectively. In addition to the sidewall leading edge shock system, the cowl shock is more distinct for the contraction ratio of 5 both at the sidewall and on the centerline. This is likely due to the increase in downturning the flow has undergone from an increased number of swept shocks. As this more strongly downturned flow impinges on the cowl, a stronger shock forms. As with the contraction ratio of 3, streamwise separation is observed only in small, isolated regions which correspond to the sidewall shock impingements(Figure 6.1.11). The fact that the separation regions are swept indicates that the sweep of the shock structure has been preserved throughout the multiple shock reflection process. Additional regions of reversed flow are observed on the baseplate in the vicinity of the centerline shock reflection and also in the corner region at the approximate location of shock impingement.

Particle traces on the sidewall and baseplate (Figure 6.1.12) indicate the surface flow patterns. The separation at the first shock impingement on the sidewall is evident. It also appears that the sidewall shock impingement affects the corner region, as a reverse flow region develops in the vicinity of the impingement and appears to feed forward of the impingement. Strong flow downturning is observed

on the sidewall at the impingement. The flow appears to reattach near the throat and then separate again just downstream of the shoulder due to the second sidewall shock impingement. The effects of the cowl are evident both in terms of turning the flow and in terms of the corner flow. A line of separation lies close to the cowl, and slightly above that is a reattachment, noted by the diverging surface streamlines. The cowl shock is observed to influence the sidewall streamlines in the bottom 25% of the inlet at the exit plane.

As with the contraction ratio of 3 (Figure 6.1.6), the contraction ratio of 5 exit plane pressure contours (Figure 6.1.13) demonstrate horizontal and vertical nonuniformity, with strong pressure gradients located near the cowl. Mach number contours (Figure 6.1.14) indicate low Mach number regions in the cowl corner and in the baseplate corner, extending to the centerline. It will be demonstrated in the coming sections that the low Mach number region near the baseplate is dominated by multiple vortices whose origins can be traced to the crossflow induced by the sidewall/baseplate corner interaction.

The shock structure for the contraction ratio of 9 configuration is given in Figures 6.1.15 a,b, and c for  $Z/H = 0.25, 0.50$ , and  $0.75$ , respectively. The shock is observed to strike the centerline at  $x'/Tx' = 0.52$  and reflect and impinge on the sidewall at  $x'/Tx' = 0.775$ . The shock continues to reflect, striking the centerline again at  $x'/Tx' = 0.90$  and then impinging on the sidewall at approximately the shoulder ( $x'/Tx' = 1.00$ ). Sidewall and baseplate pressures (Figure 6.1.16) indicate swept impingements leading up to the throat. The cowl shock is observed in the throat region in both the sidewall pressure plots and the centerline pressure plots (Figure 6.1.17). The cowl shock is observed to be much stronger than for either the contraction ratio of 3 or 5, interacting with approximately 50% of the inlet exit

plane. The increase in shock strength on the cowl is due to the increased downturning caused by the flow passing through 4 swept reflected shocks, each of which incrementally increase the flow downturning.

Streamwise separation is observed by the contours of negative axial velocity in Figure 6.1.18. Separation is observed only in the region of the first sidewall interaction, extending into the sidewall/baseplate corner. Small centerline separations on the baseplate are also observed both fore and aft of the centerline shock impingement. These separations may be linked directly to the strong crossflows induced by the glancing shock and corner interactions. Figure 6.1.19 shows the simulated oil flow on the baseplate and sidewall. Regions of separation and strong downturning are observed at each of the sidewall impingements. (Past the shoulder, there is no evidence of significant shock interactions.) Particle traces on the baseplate show significant upstream influence ahead of the inviscid location of the shock emanating from the swept sidewall leading edge. When this strong crossflow reaches the centerline, small separation regions are noted. Additionally, the sidewall/baseplate corner is again observed to have characteristics of the aforementioned induced layer, where the flow lifts off the sidewall as it moves toward the baseplate and reattaches on the baseplate, leaving a very small corner recirculation region. The contraction ratio of 9 exit plane pressure contours (Figure 6.1.20) indicate that the flow is highly compressed and highly asymmetric, especially vertically. The flow is characterized by high post cowl shock pressures in the lower half of the inlet and lower pressures in the vortically dominated baseplate region. Mach number contours (Figure 6.1.21) again show a nominally uniform exit for a large portion of the inlet exit plane.

A summary of the contraction ratio effects on mass capture, throat Mach number, total pressure recovery,  $P_{t2}/P_{inf}$ , and inlet compression is given in Table 6.1.1. (Performance parameters for the 50% Cowl configuration and a low Reynolds number computation are also included in the table for later reference.) Inviscidly it was demonstrated that each of the reflected shocks incrementally increased the downturning of the flow. Thus when more of the reflected shocks occur forward of the cowl, an increase in flow spillage is expected. The table shows that as the contraction ratio is increased from 3 to 9, the mass capture decreases from 93.4% to 87.9%. The increased number of internal shocks degrades the average throat Mach number from 6.30 at a contraction ratio of 3 to 4.29 for a contraction ratio of 9. The total pressure recovery also decreases from 0.61 at a contraction ratio of 3 to 0.34 for a contraction ratio of 9. Kinetic energy efficiency ( $\eta_{ke}$ ) for all the configurations is high but decreasing from 99.2% to 98.19% for contraction ratios of 3 and 9, respectively. The increased contraction ratio yielded a greatly increased compression ratio in the inlet, from 9.2 at a contraction ratio of 3 to 43.7 at a contraction ratio of 9. High internal compression is desirable to obtain pressures in the combustor sufficient to maintain combustion.

Table 6.1.1: Summary of Computed Inlet Performance Parameters

Configuration CR/ Re /Cowl ( $\times 10^6$ ) (%)	$\eta_{ke}$ %	% Mass Capture	Mach Number	Total Pressure Recovery	$P_{t2}/$ $P_{inf}$	$P/$ $P_{inf}$
3/2.15/ 0	99.24	93.4	6.30	0.6090	361.56	9.203
5/2.15/ 0	98.50	91.0	5.17	0.3994	519.89	18.695
9/2.15/ 0	98.19	87.9	4.29	0.3395	832.07	43.692
3/2.15/50	98.82	98.0	5.99	0.4758	352.99	9.732
3/0.55/ 0	98.71	90.4	5.72	0.4480	309.02	9.698



It is therefore observed that the principle influence on inlet performance due to contraction ratio is an increase in the number of internal reflected shocks the flow encounters, each of which increase the flow downturning (and hence spillage) and compression while degrading the total pressure recovery, kinetic energy efficiency, and throat Mach number. The detailed plane-by-plane discussion which follows indicate that there are two principle influences on exit plane nonuniformity: the increased downturning yields a stronger cowl shock which is observed to affect more of the exit plane, and the crossflow induced by the cornerflow/glancing shock interaction is observed to significantly affect the exit plane in the vicinity of the baseplate.

#### 6.1.1 Contraction Ratio = 3, $Re = 2.15$ million/ft, 0% Cowl

At  $I = 31$  ( $x'/Tx' = 0.04$ ), the glancing shock is just forming. Based on the pressure contours (Figure 6.1.1.1), the shock is located at  $y/y_{wall} = 0.92$ . A single horizontal contour band marks the location of the weak compression formed due to the boundary layer growth on the baseplate. A slight expansion is observed in the immediate vicinity in the sidewall/baseplate corner. Velocity vectors (Figure 6.1.1.2) indicate both an inward and downward turning induced by the wedge. Beyond the lateral bounds of the glancing shock, virtually no turning is observed. Above  $Z/H = 0.07$ , there is an upward movement of the flow toward the baseplate within the shock layer (below that, there is a slight downward movement, as expected due to inviscid considerations). Above  $Z/H = 0.05$ , the glancing shock appears to bend toward the corner and dissipate (i.e. the pressure rise becomes insignificant). At about that point, a strong crossflow on the baseplate is induced.

The flow in the immediate vicinity of the corner moves upward to the corner and then across the baseplate; Kubota and Stollery (1982) have observed this interaction and refer to it as an induced layer.

At  $I = 35$  ( $x'/Tx' = 0.20$ ), the shock has moved to approximately  $y/y_{wall} = 0.80$ , based on the pressure contours (Figure 6.1.1.3) and velocity vectors (Figure 6.1.1.4). An expansion around the sidewall/baseplate corner is noted in the pressure contours, leaving an isolated constant pressure zone in the immediate corner. Velocity vectors indicate the beginnings of a small recirculation region occupying the corner-most 2% of the span and height. The velocity vectors also indicate that the influence of the induced layer reaches as low as  $Z/H = 0.32$  within the sidewall boundary layer. Below that point, the sidewall boundary layer turning is nominally that of the rest of the post-shock flow. The crossflow induced on the baseplate is observed to influence the baseplate boundary layer strongly as far over as  $y/y_{wall} = 0.55$ , and weakly to  $y/y_{wall} = 0.15$ . The thickness of this induced layer is approximately 4% of the inlet height. Both the velocity vectors and the pressure contours demonstrate another expansion process at the bottom of the inlet, as the flow compressed by the glancing shock expands downward into the lower pressure freestream.

At  $I = 40$  ( $x'/Tx' = 0.40$ ), the shock has moved to  $y/y_{wall} = 0.55$ . Pressure contours (Figure 6.1.1.5) show that the corner expansion has become still more pronounced, occupying the top 10% of the inlet height. The corner recirculation now occupies a larger percentage of the span, preventing the induced layer from reattaching on the baseplate until  $y/y_{wall} = 0.90$ . The induced layer entrains fluid from the sidewall boundary layer down as far as  $Z/H = 0.38$  (Figure 6.1.1.6). At this axial station, the flow induced across the baseplate reaches the centerline, forming a recirculation region on the baseplate, causing a crossflow separation at

$y/y_{\text{wall}} = 0.25$ . The maximum height of this recirculation is  $Z/H = 0.04$ . A strong expansion and turning at the bottom of the inlet, particularly in the sidewall boundary layer is noted. This is a convenient point to note the significant upstream influence of the glancing shock structure on the baseplate boundary layer. At this axial station ( $x'/Tx' = 0.40$ ), the shock has reached  $y/y_{\text{wall}} = 0.55$ , but at  $x'/Tx' = 0.20$ , there was significant crossflow at  $y/y_{\text{wall}} = 0.55$ .

At  $I = 45$  ( $x'/Tx' = 0.60$ ), the shock location appears to have progressed to approximately  $y/y_{\text{wall}} = 0.20$  (Figure 6.1.1.7). Velocity vectors (Figure 6.1.1.8) show that the flow between the shock and the centerline is disturbed only slightly. The region where the glancing shock intersects the baseplate boundary layer is beginning to take on the appearance of a clockwise rotating (CW) vortex, fed primarily by the induced layer crossflow. The center of this vortical region is approximately  $y/y_{\text{wall}} = 0.40$ ,  $Z/H = 0.08$ . The flow toward the centerline is much stronger and the counter-clockwise (CCW) recirculation at the centerline is more evident. This reverse flow region has also taken on a vortical appearance, centered at approximately  $y/y_{\text{wall}} = 0.10$ ,  $Z/H = 0.03$ , causing the crossflow to lift off the baseplate at  $y/y_{\text{wall}} = 0.40$ . The small recirculation in the immediate corner is greatly diminished. Particle traces restricted to the crossflow plane (Figure 6.1.1.9) enhance the vortical features and shock locations. It should be noted that since the axial component of velocity has been removed to restrict the particle traces to the crossflow plane, the features are somewhat exaggerated. What might appear to be a tightly wound vortex might not even make one complete revolution in the length of the domain if the axial velocity were large.

Based on the very high centerline pressures (Figure 6.1.1.10), at an axial station of  $I = 50$  ( $x'/Tx' = 0.79$ ), the shock has already reflected from the centerline and is located at  $y/y_{\text{wall}} = 0.10$ . The center of the CW vortex (Figure 6.1.1.11) is located

at approximately  $y/y_{\text{wall}}=0.31$ ,  $Z/H=0.09$ . The CCW rotating centerline vortex appears to be centered at  $y/y_{\text{wall}}=0.07$ ,  $Z/H=0.04$  and causes the crossflow separation on the baseplate at  $y/y_{\text{wall}}=0.20$ . Much more of the main crossflow appears to be turned downward by the increasing size of this centerline vortex, inducing a more strongly downturned flow at the centerline. Particle traces (Figure 6.1.1.12) restricted to the crossflow plane enhance the visualization of the vortical flows, demonstrating the size and location of the vortices. The clockwise rotating vortex has grown in size while the centerline (CCW) vortex is being pushed toward the centerline into more a triangular shape by the strong crossflow. Toward the horizontal centerline of the inlet, the post reflection-shock flow exhibits a strong downward component. The modification to inviscid oblique shock theory (Section 3.3) indicated that the spillage angle increased behind each reflected shock. Though the reflected shock turns the inviscid flow back to the axial direction, it also accentuates the downturning.

At  $I = 52$  ( $x'/Tx' = 0.87$ ), the pressure contours (Figure 6.1.1.13) indicate that the glancing shock has moved inward to  $y/y_{\text{wall}} = 0.30$  and is irregularly shaped. As was previously noted for Figure 6.1.3 (the axial centerline pressure distribution), the irregular shape of the shock at  $Z/H = 0.5$  is due to the effects of the weak compression formed on the leading edge of the baseplate due to the displacement effects of the boundary layer. Velocity vectors (Figure 6.1.1.14) show the center of the CCW centerline vortex to be at approximately  $y/y_{\text{wall}} = 0.08$ ,  $Z/H = 0.02$ , yielding a crossflow separation on the baseplate at approximately  $y/y_{\text{wall}} = 0.20$ . The clockwise rotating corner recirculation (which is fed by the induced crossflow) causes the sidewall boundary layer to lift off at  $Z/H = 0.05$ , reattaching on the baseplate at  $y/y_{\text{wall}} = 0.80$ . The interface between the reflected shock and the CW vortex occurs at approximately  $Z/H = 0.2$ , i.e. the high post-reflected shock

pressures abruptly give way the much lower vortex pressures at about this point. This vortex appears to be centered at  $y/y_{\text{wall}} = 0.25$ ,  $Z/H = 0.10$ . In the post-reflected shock region, the turning toward the centerline is no longer noted; however, the downturning appears to be enhanced. The expansion of the flow into the freestream (particularly in the sidewall boundary layer) is again noted at the  $Z/H = 1.0$  station. Particle traces restricted to the crossflow plane (Figure 6.1.1.15) demonstrate the above named features. (By being restricted to the crossflow plane, the particle traces exaggerate the in-plane turning, thereby aiding in the visualization of the phenomena.)

At  $I = 54$  ( $x'/Tx' = 0.96$ ), the reflected shock has moved to approximately  $y/y_{\text{wall}} = 0.50$  and has retained its somewhat irregular shape (Figure 6.1.1.16). The shock has reached a station at nearly the left-most extent of the main vortex, yet it is still unable to influence the region above  $Z/H = 0.25$ , a region which is vortically dominated. The center of the CW vortex appears to be in the vicinity of  $y/y_{\text{wall}} = 0.28$ ,  $Z/H = 0.10$  (Figure 6.1.1.17). The CCW vortex at the centerline is taking on a more flattened appearance, centered at approximately  $y/y_{\text{wall}} = 0.15$ ,  $Z/H = 0.02$ , causing the crossflow to lift off the baseplate at  $y/y_{\text{wall}} = 0.42$ .  $Z/H = 0.16$  appears to be the horizontal dividing line between upward deflected and downward deflected flow in the pre-reflected shock region. Flow above this point is induced across the baseplate and is influenced by the CW vortex. A region of more strongly downturned sidewall boundary layer flow exists just below this point. Below that, the boundary layer shows little downward deflection again until the flow begins to expand into the freestream. The particle traces in this crossflow plane (Figure 6.1.1.18) show that the vorticity in the immediate corner is less distinct. The corner flow causes the flow reattachment on the baseplate to occur at approximately  $y/y_{\text{wall}} = 0.81$ . The particle traces in this plane also reveal the

irregular shape of the reflected shock as well as the strong downturning in the post-reflected shock region.

At  $I = 55$  ( $x'/Tx' = 1.00$ ), the throat plane, the (irregularly shaped) reflected shock has progressed to  $y/y_{\text{wall}} = 0.62$ . Pressure contours (Figure 6.1.1.19) indicate that the influence of the vortical region near the baseplate has increased to  $Z/H = 0.23$  and also demonstrate the beginnings of a shock of the leading edge of the cowl ( $Z/H = 1.0$ ). The downturned flow which formerly expanded into the freestream now impinges on the cowl. Based on the velocity vectors (Figure 6.1.1.20), the vortical structure in the sidewall/baseplate corner is somewhat more distinct and wider in this plane. Centered at approximately  $y/y_{\text{wall}} = 0.80$ ,  $Z/H = 0.02$ , the vortex prevents crossflow reattachment, partly due to the strong reverse flow caused by the strengthened centerline vortex, which is centered at approximately  $y/y_{\text{wall}} = 0.11$ ,  $Z/H = 0.03$ .  $Z/H = 0.17$  is approximately the horizontal dividing line between upward and downward deflected flow near the sidewall. The location of this line appears to be coupled in part to the location of the main vortex, i.e. whether the flow is being scavenged upward into the vortex or repelled downward by the reverse flow on the bottom of the vortex. Particle traces (Figure 6.1.1.21) again reveal the effects of the three vortices as well as present the irregular shape of the flow downturning. A broadened region is noted near the cowl/sidewall juncture where there appears to exist the beginnings of a recirculation region similar to that observed in the sidewall/baseplate corner closer to the front of the inlet.

Due to the gradually changing sweep of the grid in the throat region to return the grid to a vertical orientation at the exit plane, in the strictest sense, it no longer logical to refer to the " $I = \text{constant}$ " planes with regard to the  $x'/Tx'$  notation, since  $x'/Tx'$  varies with  $Z/H$  in the throat region. Rather, these planes will be referred to

according to the percentage of the distance between the swept shoulder and the vertical exit plane. The notation for this will be  $x_s'/Te'$ , where  $x_s'$  is the distance from the swept shoulder to the grid plane measured at constant  $Z/H$  and  $Te'$  is the distance from the swept shoulder to the exit of the throat. This notation is analogous to  $x/c$  for a swept and/or tapered wing. The grid in fact resembles a short swept wing if only the grid in the inlet throat (Figure 6.1) were plotted.

At  $I=56$  ( $x_s'/Te'=0.06$ ), the reflected shock appears to be almost to the sidewall, and it is certainly interacting with it (Figure 6.1.1.22). Velocity vectors (Figure 6.1.1.23) indicate the center of the CW vortex to be approximately  $y/y_{wall}=0.28$ ,  $Z/H=0.12$ . Flow along the bottom half of the clockwise rotating vortex is induced toward the wall; this influence is severely limited, as the majority of the flow in the vicinity of the vortex has retained its toward-the-centerline component, even though the shock appears to have passed.  $Z/H=0.17$  is again observed to be a horizontal dividing streamline, with flow above moving upward and flow below moving downward. The corner vortex appears to be centered at  $y/y_{wall}=0.78$ ,  $Z/H=0.02$  and is clearly forced off the wall by a strong toward-the-wall flow persisting in the top 1% of the inlet. The centerline vortex appears to be centered at  $y/y_{wall}=0.09$ ,  $Z/H=0.02$  and induces a strong crossflow toward the sidewall across the baseplate. The downward flow along the sidewall appears to be deflected toward the centerline in the region between  $Z/H=0.38$  and  $Z/H=0.65$  as if the flow were moving around a pocket of separation. The particle traces (Figure 6.1.1.24) indicate the same patterns and accentuate the unexpected turning toward the wall in the vicinity of  $Z/H=0.40$ .

At  $I=60$  ( $x_s'/Te'=0.29$ ), the pressure contours (Figure 6.1.1.25) indicate that the newest significant features of the flow are the cowl shock and the corner interaction at the cowl. Figure 6.1.1.26 indicates that a recirculation region exists in

the cowl/sidewall corner and also shows the cowl shock location to be at approximately  $Z/H = 0.96$  by the abrupt change in velocity vector direction. Significant changes are also indicated in the baseplate region. The CCW corner vortex ( $y/y_{\text{wall}} = 0.79$ ,  $Z/H = 0.05$ ) has appeared to grow as it is fed by the toward-the-wall crossflow on the baseplate plane. This strong crossflow, upon impinging on the sidewall forms a small clockwise recirculation at  $y/y_{\text{wall}} = 0.95$ ,  $Z/H = 0.01$ . The CCW corner vortex has grown to nearly the size of the CW vortex, which is now centered at  $y/y_{\text{wall}} = 0.21$ ,  $Z/H = 0.10$  and continues to feed the centerline vortex ( $y/y_{\text{wall}} = 0.09$ ,  $Z/H = 0.01$ ). The shock appears to have reflected from the sidewall, but it is becoming less distinct, partly due to the fact that the planes in the throat gradually transition from swept at the leading edge sweep angle to vertical at the exit plane, meaning that the swept shock is being cut more and more vertically. The flow downturning (especially in the sidewall boundary layer) and the resultant cowl shock are evident. Also evident is the low pressure corner flow at the juncture of the sidewall and cowl, which induces a toward-the-wall crossflow on the cowl. The particle traces (Figure 6.1.1.27) accentuate the same trends.

At  $I = 65$  ( $x_s'/Te' = 0.58$ ), the flow pattern near the baseplate has changed little (Figure 6.1.1.28). Near the cowl, however, a flow pattern similar to that of the baseplate region has developed, namely, two corner vortices have formed (Figure 6.1.1.29). The CW vortex is fed primarily by the downturned sidewall boundary layer flow, which lifts off the sidewall at  $Z/H = 0.86$ . The CCW vortex is fed by the strong crossflow which impinges on the sidewall and curls back along the cowl. The cowl shock appears to be located at  $Z/H = 0.91$ . The particle traces (Figure 6.1.1.30) clearly indicate this newly formed vortical flow in the cowl corner. The location of the sidewall shock is also evident due to the enhanced turning after its



passing. It is again emphasized that the shock is distorted in this view due to the sweep of the grid relative to the sweep of the shock.

At the exit plane,  $I = 72$ , Figure 6.1.1.31 shows that, due to the sweep of the grid relative to the sweep of the shock, the shock now appears as a "V", slanting diagonally down to the centerline and reflecting back toward the sidewall. The shock is diminished to a weak compression spread over half the domain. The cowl shock has risen to  $Z/H = 0.90$  and is distorted toward the wall due to the corner interaction. Velocity vectors (Figure 6.1.1.32) show the combined influence of the CCW corner vortex and the CW vortex has eliminated the crossflow on the baseplate and diminished the centerline vortex. The particle traces (Figure 6.1.1.33) indicate more clearly the diagonal shape of the shock in this view.

#### 6.1.2 Contraction Ratio = 5, $Re = 2.15$ million/ft, 0% Cowl

At  $I = 31$  ( $x'/Tx' = 0.04$ ), the sidewall shock is just forming. Figure 6.1.2.1 presents the pressure contours and Figure 6.1.2.2, the velocity vectors. Pressure contours locate the shock at approximately  $y/y_{wall} = 0.96$  and indicate the expansion of the sidewall flow around the corner across the baseplate. A single horizontal constant pressure band located at  $Z/H = 0.32$  marks the limit of the weak compression caused by the displacement effects of the boundary layer growth from the baseplate leading edge. Based on velocity vectors, the shock is observed to induce a strong inboard flow as well as a slight downward flow. This downward flow is enhanced near the cowl plane, driven by the pressure differential between the flow behind the shock and the undisturbed freestream beneath the cowl plane. The inward flow along the baseplate is noted as far inward as  $y/y_{wall} = 0.42$ . In the

corner region, the shock is observed to curve inward toward the corner. The beginnings of a corner vortex are evident in the region where the shock appears to curve. Above  $Z/H = 0.08$ , the flow is induced upward across the corner and begins to move across the baseplate.

At  $I = 35$  ( $x'/Tx' = 0.20$ ), the sidewall shock has moved to approximately  $y/y_{wall} = 0.76$ . Figures 6.1.2.3 and 6.1.2.4 show the pressure contours and velocity vectors, respectively. The induced layer in the corner and on the baseplate has increased both in size and in momentum. The lateral flow in the baseplate boundary layer can be observed well beyond  $y/y_{wall} = 0.25$ . The thickness of this layer is approximately 4% of the inlet height. The influence down the sidewall extends to  $Z/H = 0.35$ . Beyond that, the boundary layer turns downward with the core flow. The beginnings of a small recirculation region in the immediate corner is evident. At the cowl plane, the flow downturning is larger for the boundary layer than for the core flow. In light of the orders of magnitude difference between the boundary layer and the inviscid flow in axial velocity (or momentum), the reason for this is clear: a low momentum particle passing through a region of lateral pressure gradient will turn farther as a result of the increased residence time of the particle (relative to a high momentum particle) within the influence of the pressure gradient.

At  $I = 40$  ( $x'/Tx' = 0.40$ ), Figure 6.1.2.5 presents the pressure contours. The shock is located at  $y/y_{wall} = 0.40$ . The corner expansion is noted in the upper 15% of the inlet. Based on the velocity vectors (Figure 6.1.2.6), the beginnings of a centerline vortex are evident as the induced layer reaches the centerline and recirculates back along the baseplate. This causes the baseplate boundary layer to lift off the surface at  $y/y_{wall} = 0.38$ . The glancing shock formed from the sidewall leading edge is still highly curved as the shock enters the baseplate boundary layer.

In the immediate vicinity of the corner a small recirculation region is visible. Throughout the inlet the dividing streamline on the sidewall (the line about which the boundary layer is angled either up or down) appears to be coupled with the location of maximum pressure in the shock layer, which is the downward most extent of the forebody compression. Particle traces (Figure 6.1.2.7) indicate the small recirculation region in the corner and the centerline recirculation, but the CW vortex observed for the  $CR = 3$  case is not yet evident. There exists some flow turning in the region where the shock is curved, but a vortex is not indicated.

At  $I = 45$  ( $x'/Tx' = 0.60$ ), the glancing shock is located at the centerline based on pressure contours (Figure 6.1.2.8) and velocity vectors (Figure 6.1.2.9). Only at this point does the CW vortex appear, perhaps enhanced by the turning generated by the increased crossflow. At this plane, the flow throughout the inlet is toward the centerline, with a slight downward component. There is a strong induced layer across the baseplate toward the centerline, which strengthens the centerline vortex. This vortex causes the lateral flow on the baseplate to lift off at  $y/y_{wall} = 0.45$ . The increased size of the vortex causes the induced layer to be angled downward more strongly, which imparts more rotation to the reversed flow which is now appearing as a vortex. The particle traces (Figure 6.1.2.10) indicate the existence of 3 vortices: the corner vortex, the CCW centerline vortex, and the CW vortex. The traces also show the flow to be uniformly turned inward, all the way to the centerline, indicating the shock location to be the centerline. The expansion at the cowl plane is again noted.

At  $I = 50$  ( $x'/Tx' = 0.79$ ), the glancing shock has reflected from the centerline and has reached  $y/y_{wall} = 0.38$ . In the region toward the centerline (the post-reflected shock region), the flow has undergone still more compression and still more downturning. The shock shape (Figure 6.1.2.11) is slightly distorted at  $Z/H = 0.50$

due to the effects of the forebody compression. In the region toward the wall, the flow is still turned toward the centerline (it is still shock bay 2 of Figure 3.3.1). The CW vortex has increased in size and remains a low pressure region despite the fact that it is located above the post-reflected shock region. As the shock nears the sidewall, its presence is felt in the boundary layer (Figure 6.1.2.12). The flow is more strongly turned downward in the boundary layer beginning in the vicinity of  $Z/H=0.50$ . Particle traces (Figure 6.1.2.13) also indicate the shock to be at approximately  $y/y_{wall}=0.38$ , as evidenced by the strong downturning in the post-reflected shock region. It is also evident that the influence of the shock is halted above  $Z/H=0.19$ , perhaps by the presence of the CW vortex. Stronger downturning within the sidewall boundary layer is also noted.

At  $I=52$  ( $x'/Tx'=0.87$ ), the shock has progressed to  $y/y_{wall}=0.75$ , based on the pressure contours, velocity vectors, and in-plane particle traces (Figures 6.1.2.14-16, respectively), and the flow structure is much like that for  $x'/Tx'=0.79$ . The expansion of the flow into the freestream is clearly observed to influence more than just the sidewall boundary layer in this plane. There is strong downturning in this region, which is enhanced by the proximity of the shock impingement on the sidewall and its associated line of separation, along which the flow in the boundary layer sharply turns. For the first time, it is observed that the centerline vortex induces a toward-the-wall component sufficient to lift the corner vortex off the baseplate, centering it at  $y/y_{wall}=0.75$ ,  $Z/H=0.02$ . Particle traces in this plane indicate that the upward extent of the influence of the shock is  $Z/H=0.25$ . The CW vortex is still evident, as are the centerline and corner vortices.

At  $I=54$  ( $x'/Tx'=0.96$ ), the shock has reflected from the sidewall and is moving toward the centerline. Pressure contours (Figure 6.1.2.17) place the location of the shock to be at approximately  $y/y_{wall}=0.45$ . A comparison of downward

component of velocity (Figure 6.1.2.18) on either side of that point indicates that the reflected shock has again increased the downturning. As before, the strongest downturning is in the boundary layer. The three vortices in the baseplate region are still evident. Particle traces of this plane (Figure 6.1.2.19) again indicate that the shape of the shock is distorted due to the influence of the forebody compression.

$I = 55$  ( $x'/Tx' = 1.00$ ) is the throat plane. At this point, the shock has reached the centerline (Figure 6.1.2.20). This is evidenced by the relatively uniform compression and flow angularity (Figure 6.1.2.21) across the span of the inlet. Features of interest in this plane are the CW vortex, which has been displaced downward by the increased size of the corner vortex, the strong toward-the-wall crossflow on the baseplate which has spawned a new recirculation region in the sidewall/baseplate corner, and effects of the downturned flow as it begins to strike a solid surface, namely, the cowl. At this location, a sharp rise in pressure is noted as a shock forms on the cowl. Due to the fairly uniform inboard flow, the particle traces (Figure 6.1.2.22) yield little information. However, the new corner recirculation is apparent.

In the throat region, the grid sweep gradually changes from the shoulder at the throat to a vertical exit plane. Thus the  $x'/Tx'$  designation is replaced with  $xs'/Te'$ , a parameter indicating locations in the throat as a percentage of the distance between the swept shoulder and the vertical exit. Figures 6.1.2.23-6.1.2.25 show the pressure contours, velocity vectors, and particle traces respectively at  $I = 56$  ( $xs'/Te' = 0.06$ ). The only new feature is that, now that the shock has begun to reflect from the centerline, a strong crossflow across the baseplate toward the wall is induced. It is also interesting to note that another induced layer/corner recirculation is established at the cowl. The cowl shock appears to have risen to  $Z/H = 0.96$ . The particle traces indicate the corner recirculation at the cowl and

also show that the corner vortex causes the sidewall boundary layer to separate at  $Z/H = 0.94$ .

At  $I = 60$  ( $x'/Tx' = 0.29$ ), the shock appears to be significantly distorted (Figure 6.1.2.26), since the  $I = 60$  plane is now more steeply inclined than the shock (since the grid is more widely spaced near the baseplate to return the planes to vertical at the exit plane). Therefore, the shock appears to make contact with the wall near the cowl ( $Z/H = 0.85$ ), slanting away from toward the centerline both above and below this point. The velocity vectors and particle traces (Figures 6.1.2.27-28, respectively) indicate more clearly the shape of the shock in this plane. The flow is observed to be fairly uniformly turned throughout the inlet toward the wall and downward. On the cowl, there is a strong flow toward the wall driven by the pressure difference between the post-cowl shock flow and the low pressure corner region. The location of the glancing shock (which in the cowl plane appears to be the mid-span) appears to be a factor in creating the pressure differential which induces the crossflow. The sidewall boundary layer separation as a result of this corner flow is observed to move upward to  $Z/H = 0.85$ . As the CW vortex has been pushed downward, a flow in the sidewall/baseplate corner has developed which is like that observed farther upstream at the centerline. A strong crossflow impinges on the sidewall forming a recirculation region which causes the crossflow to lift off the baseplate at  $y/y_{wall} = 0.90$ . The CW vortex, now centered at approximately  $y/y_{wall} = 0.25$ ,  $Z/H = 0.14$ , is observed to exert an influence down as low as  $Z/H = 0.20$ . The particle traces (Figure 6.1.2.28) demonstrate the extent of the vortices near the baseplate. Two additional separation regions are noted on the sidewall, located at  $Z/H = 0.10$  and  $Z/H = 0.21$ . The region near the cowl also demonstrates the corner vortices and the location of the cowl shock ( $Z/H = 0.95$ ).

At  $I = 65$  ( $x_s'/Te' = 0.58$ ), the pressure contours (Figure 6.1.2.29) indicate that the shocks have become much less distinct. Velocity vectors (Figure 6.1.2.30) show that the CW vortex has almost vanished. It is very small, both in size and in rotational velocity. The CCW vortex has moved downward slightly and is now centered at  $y/y_{wall} = 0.60$ ,  $Z/H = 0.07$ . The newly formed corner vortex system at the cowl has increased its strength and size. The primary trend throughout the entire inlet is downturning. The lateral movement varies dependent upon the location relative to the glancing shock. The cowl corner flow has developed into a strongly upturned flow which has caused the sidewall boundary layer to separate at approximately  $Z/H = 0.83$ . Also interesting to note is that the above  $Z/H = 0.50$ , the sidewall boundary layer is deflected upward. Again, interpretation of this pattern in this view is complicated by the fact that the sweep of the plane is dramatically different than the sweep of the shock interactions. Particle traces (Figure 6.1.2.31) in this view are useful to demonstrate the difference in rotation and size of numerous vortices.

$I = 72$  is the exit plane ( $x_s'/Te' = 1.00$ ). The grid is vertical; the shock structure is swept at 45 degrees. Therefore, the shocks appear to cut the exit plane on diagonals from either the sidewall to the centerline or the centerline to the sidewall. It is interesting to note that the shock structure has dissipated to the point where there is little variation in pressure (Figure 6.1.2.32), and little variation in turning (Figures 6.1.2.33 and 6.1.2.34). As a reminder, in order to plot the velocity vectors and particle traces in the crossflow plane, the axial ( $u$ ) component of velocity has been removed, so that what is seen is an exaggerated view of the flow, i.e. if the axial component is large enough, even what appears to be a tightly wound vortex might make only one complete revolution in the length of the inlet, though the appearance of these cross sections might lead one to think otherwise. The cowl

shock is observed to have moved up to approximately  $Z/H = 0.87$ . As one might expect, the highest pressure in the exit plane is under this cowl shock. In the vicinity of the cowl shock, there is strong upturning in the sidewall boundary layer. Particle traces (Figure 6.1.2.34) show that most of the vorticity has dissipated at the exit plane. The CW vortex has left only a remnant of downturned flow at the centerline. Interestingly enough, while what was previously called the corner vortex has dissipated, a new weak vortical pattern has appeared at the centerline. The vortically influenced region of the flow engulfs the top 25% of the inlet height. While the pressures are relatively high, the vortices have prevented the higher pressure core flow from reaching the baseplate region. Thus a measure of the baseplate pressure does not yield a good quantitative indication of the compression of the core flow of the inlet. Only flow field data can provide this information, hence the need for rake data in the experimental portion of this work. Particle traces emphasize the decrease in vorticity and also yield a better look at the diagonally shaped shock location based on the location of flow turning. The cowl shock appears to be located at  $Z/H = 0.87$  based on flow turning and hence affects 13% of the exit plane.

### 6.1.3 Contraction Ratio = 9, $Re = 2.15$ million/ft, 0% Cowl Configuration

Figure 6.1.3.1 presents the static pressure contours across the span of the inlet at  $x'/Tx' = 0.04$ . At this station, the swept oblique shock is just forming on the leading edge and is located at  $y/y_{wall} = 0.88$ . In the immediate corner between the sidewall and baseplate, it appears that the flow compressed by the sidewall shock expands around the corner across the baseplate toward the centerline. This is no different



than either the  $CR = 3$  or  $5$  configurations discussed previously. The velocity vectors in this crossflow plane (Figure 6.1.3.2) also demonstrate the expansion toward the centerline.

Figure 6.1.3.3 demonstrates the inward movement of the swept shock. At this plane, located at  $x'/Tx' = 0.20$ , the shock has progressed to approximately  $y/y_{wall} = 0.65$ . A horizontal expansion between the shock and the sidewall is noted as the compressed flow expands out into the lower pressure freestream. Additional features noted in the figure are the expansion in the baseplate/sidewall corner and the horizontal weak compression from the baseplate leading edge at approximately  $Z/H = 0.35$ . At this station, the inboard flow induced by the corner flow is greatly enhanced, as indicated in Figure 6.1.3.4, where the velocity vectors indicate that the crossflow is observed as far as  $y/y_{wall} = 0.30$ , though the shock has progressed only about half that distance. Velocity vectors also indicate the expansion of the post-oblique shock flow into the freestream.

At the  $x'/Tx' = 0.40$  station (Figure 6.1.3.5), the shock has progressed to approximately  $y/y_{wall} = 0.25$ . The vertical extent of the shock appears to have diminished, i.e. the corner expansion and associated crossflow dominate the top 15% of the inlet height. This increased displacement of the shock is observed to be due to the crossflow, as seen in Figure 6.1.3.6. The crossflow induced by the corner expansion has reached the centerline by this downstream station. In impinging on the centerline, the flow divides, turning both upward and downward. The upturned flow curls back on itself, causing the flow toward the centerline to lift off the surface at approximately  $y/y_{wall} = 0.38$ , forming a crossflow separation. The added displacement of this crossflow separation (10% of the height) is observed to yield a region of compressed downturned flow in the  $Z/H = 0.10-0.20$  region, possibly indicating that a (horizontal) separation shock has formed between the glancing

shock and the centerline. Also noted in the figure is a small region of recirculation in the baseplate/sidewall corner. This region is limited to approximately 2% of the height and 10% of the span. In the center of the inlet, another region of recirculation is observed to be forming, also due to the crossflow. This recirculation is centered spanwise in the inlet at about  $Z/H = 0.06$ . The figure also demonstrates that the flow is uniformly turned inward and downward by the swept glancing shock emanating from the sidewall leading edge. The particle traces (Figure 6.1.3.7) demonstrate the shape of the shock (namely, the bend toward the corner at  $Z/H = 0.15$ ), the shock location of approximately  $y/y_{\text{wall}} = 0.25$ , and the vorticity in the corner, center, and at the centerline.

At  $x'/Tx' = 0.60$  (Figure 6.1.3.8), the shock has reflected from the centerline. This is evidenced by both the much higher pressures in the centermost 15% of the inlet, and by the increased downturning in that region (Figure 6.1.3.9), indicative of flow which has passed through an additional swept shock. The aforementioned vortical patterns are much more visible. The CW vortex is centered at approximately  $y/y_{\text{wall}} = 0.32$ ,  $Z/H = 0.08$ . The centerline vortex is centered at approximately  $y/y_{\text{wall}} = 0.10$  and  $Z/H = 0.04$ . This recirculation causes the toward-the-centerline crossflow to lift off the baseplate at approximately  $y/y_{\text{wall}} = 0.30$ . Additionally, the vorticity in the sidewall/baseplate region has grown slightly, taking up approximately 15% of the span and 4% of the height. Careful examination of the cowl plane reveals that there is a downward component of the flow (spillage) spanning the majority of the inlet which is enhanced near the sidewall by the expansion of the flow into the freestream. The lower momentum flow in the sidewall boundary layer is more strongly affected by this expansion than the higher momentum core flow. Particle traces in this plane (Figure 6.1.3.10) indicate the 3 vortical regions. Additionally, the particle traces indicate the

location of the shock ( $y/y_{\text{wall}} = 0.10$ ) as the change from toward the centerline flow to a more downward flow.

At  $x'/Tx' = 0.79$  (Figure 6.1.3.11), the pressure contours reveal the shock to have moved to  $y/y_{\text{wall}} = 0.70$ , and already an influence is imposed on the sidewall. This is likely due to a separation region just upstream of the sidewall impingement point. The velocity vectors (Figure 6.1.3.12) indicate strong downturning in the sidewall boundary layer. Also indicated by the velocity vectors is that the toward-the-wall component of velocity along the baseplate has reached the sidewall, lifting the corner vortex off the wall. Particle traces (Figure 6.1.3.13) provide a clearer view of the shock location and vorticity.

At  $x'/Tx' = 0.87$  (Figure 6.1.3.14), the shock impingement region has been reached. The shock appears to have moved back to the mid-span, leaving a region of very high pressure at the sidewall. Though the pressure near the baseplate has risen substantially compared to upstream stations, the baseplate remains somewhat isolated from this high compression region by the crossflow-induced vortices. Figure 6.1.3.15 presents the velocity vectors for this plane, which indicate the post-reflected shock flow has an incremented downward component, especially in the sidewall boundary layer. Strong flow spillage is noted from the boundary layer flow at the cowl plane. The corner vortex has gained significantly in size and rotation and is now centered at approximately  $y/y_{\text{wall}} = 0.70$ ,  $Z/H = 0.02$ . The toward the wall crossflow has reached the wall and curled back, yielding a CCW rotation. Particle traces (Figure 6.1.3.16) indicate the flow throughout the flow field is nominally uniformly directed.

At  $x'/Tx' = 0.96$  (Figure 6.1.3.17), the clear definition of a shock structure is lost. There appears to be something of a compression at the mid-span. Since higher pressures are noted at the centerline, this compression has reflected from the

centerline. The last interaction with the sidewall boundary layer (and the associated separation) has yielded a compression fan which has not coalesced into a well defined shock prior to reaching the centerline. The resultant reflection from the centerline is observed to span much of the inlet width. The vortically dominated region ( $Z/H < 0.15$ ) is again observed to be isolated from the glancing shock interactions occurring at greater  $Z/H$ . Velocity vectors (Figure 6.1.3.18) indicate the strong downturning in the sidewall boundary layer and associated flow spillage at the cowl plane. The toward-the-wall crossflow on the baseplate has increased in magnitude and, upon impinging on the sidewall, divides, creating another region of recirculation. The CW vortex has lost much of its vorticity by this station, leaving only a region of downturned flow on the centerline. Particle traces are given in Figure 6.1.3.19.

At the throat ( $x'/Tx' = 1.00$ ) (Figure 6.1.3.20), the pressure contours are nominally unchanged, with the exception of the cowl region. The compression due to the cowl shock is evident in the  $Z/H=0.98$  region. Velocity vectors (Figure 6.1.3.21) indicate that a substantial downward flow in the sidewall boundary layer to impinge with the cowl. The remaining core flow likewise still possesses a downward component, though not as large as the boundary layer. The region in the sidewall/baseplate corner is still dominated by vortical flow, however the remnants of the CW vortex yield a region of low pressure downturned flow near the centerline. A closer examination of the cowl region indicates that the sidewall boundary layer impingement on the cowl divides and forms a recirculation which causes the sidewall boundary layer to lift off the surface at approximately  $Z/H=0.95$ . Particle traces (Figure 6.1.3.22) show the corner flow in the sidewall/baseplate juncture and the region of downturning left from the CW vortex.

Due to the gradually changing sweep of the grid in the throat region to return the grid to a vertical orientation at the exit plane, the  $x'/Tx'$  notation is replaced with  $xs'/Te'$ , where  $xs'$  is the distance from the swept shoulder to the grid plane measured at constant  $Z/H$  and  $Te'$  is the distance from the swept shoulder to the exit of the throat. At a station slightly beyond the shoulder ( $xs'/Te' = 0.06$ ), Figure 6.1.3.23 indicates that the cowl shock produces pressures on the order of twice that found elsewhere in the plane. The velocity vectors (Figure 6.1.3.24) indicate that the flow has significant downturning throughout with the strongest turning in the sidewall boundary layer. A corner vortex (Figure 6.1.3.25) is seen to develop at the cowl, occupying 30% of the span and 5% of the inlet height. The sidewall boundary layer is observed to lift off the sidewall at approximately  $Z/H = 0.93$ . Toward the baseplate, the remnants of the CW vortex are still evident (Figure 6.1.3.26). The downturning at the centerline is resultant from the proximity of the vortex to its mirror image across the centerline, which is opposite in rotation and hence increases the centerline turning. Particle traces (Figure 6.1.3.27) highlight the regions of vorticity.

At  $xs'/Te' = 0.29$  (Figure 6.1.3.28), the pressure contours reveal a large pressure rise near the cowl at the centerline resulting from the displacement effects of the corner vortex. Figures 6.1.3.29-30 reveal that the vortex occupies the bottom 10% of the inlet height and approximately 40% of the span. The sidewall boundary layer is observed to separate at approximately  $Z/H = 0.87$ . The pressure is observed to rise significantly as this inward turned flow strikes the centerline. Figure 6.1.3.31 indicates that the flow in the throat near the baseplate is highly vortically dominated. This vortical flow limits the shock induced pressure rise in the upper 20% of the inlet. The particle traces shown in Figure 6.1.3.32 indicate that beyond  $Z/H = 0.25$ , the flow in the core uniformly turns downward. The CCW

vortex on the baseplate is centered at  $Z/H = 0.05$ ,  $y/y_{\text{wall}} = 0.65$ . At the cowl, the particle traces reveal the upward extent of the sidewall boundary layer separation to be  $Z/H = 0.86$ .

At  $xs'/Te' = 0.58$  (Figure 6.1.3.33), the pressure contours indicate that the cowl shock has increased in size and that a secondary high pressure region has developed at the centerline due to the sidewall boundary layer separation. This too is observed to have increased in size, now causing the sidewall boundary layer to separate at  $Z/H = 0.75$  (Figure 6.1.3.34). Near the baseplate, the CCW vortex is observed to have moved farther downward and toward the centerline, centered at approximately  $Z/H = 0.07$ ,  $y/y_{\text{wall}} = 0.58$ . Particle traces (Figure 6.1.3.35) indicate that only the middle 50% of the inlet flow is nominally uniform.

At the exit plane (Figure 6.1.3.36), with the exception of the bottom 25% of the inlet which is dominated by the cowl flow, nominally uniform pressures are observed. Likewise, the velocity vectors at the exit plane (Figure 6.1.3.37) reveal a slightly downturned but otherwise uniform core flow. A low pressure region near the baseplate persists, however the previously observed vorticity is significantly diminished. The high pressure cowl flow is seen to induce a strong upward flow in the sidewall boundary layer which influences the boundary layer throughout the lower 60% of the inlet height. This upturned boundary layer flow is limited to only 10% of the span. Particle traces (Figure 6.1.3.38) also indicate the relative uniformity of the flow.

## 6.2 Cowl Placement Effects

Now that the dominant flow characteristics have been firmly established with the detailed discussion of the contraction ratio effects, the cowl placement effects will be presented only by way of differences noted between the 50% Cowl and the previously discussed 0% Cowl location for a  $CR=3$ ,  $Re=2.15$  million/ft configuration. Since a set of "summary plots" were included in the discussion of the contraction ratio effects to first identify the global interactions, this discussion will begin with a similar set of plots before progressing on to the plane-by-plane discussion. Figures 6.2.1a,b,c present the pressure contours and hence internal shock structure for horizontal planes of constant height at  $Z/H=0.25$ ,  $0.50$ , and  $0.75$  respectively. A comparison of these plots with Figures 6.1.1 indicate that in these 3 planes, the shock structure is unchanged by the forward movement of the cowl. Only a small increment in pressure (a single contour line spanning from the sidewall to the glancing shock) is noted near the sidewall at approximately  $x'/Tx'=0.75$ . This is borne out by comparison of the sidewall pressure contours in Figure 6.2.2 with the 0% Cowl in Figure 6.1.2. The shock emanating from the cowl lip (shown by the  $P/P_{inf} \approx 5$  contour line) appears to reach the  $Z/H=0.75$  station at approximately the location indicated. Compression of up to 9 is observed in the cowl/sidewall corner. Beyond the sidewall shock impingement, there appear to be only slight changes in the throat region. The region beneath  $Z/H=0.75$  is dominated by pressure ratios of approximately 20, compared with 15 for the 0% Cowl. This accounts for the slight increase in average exit plane compression of 5% (Table 6.1.1) from 9.203 for 0% Cowl to 9.698 for 50% Cowl. Centerline pressures (Figure 6.2.3) likewise indicate that the domain of influence of the cowl is quite limited. While the cowl shock appears to remain intact through the first

glancing shock centerline reflection, the second reflection appears to dominate, and much of its explicit effects vanish ahead of the exit plane. It is interesting to note that while the cowl shock in the cowl forward position has the potential to influence more of the exit plane, the aft cowl produces higher pressures (due in part to the fact that the shock is stronger and turns the flow at a stronger angle) over a slightly smaller area, tending to cancel out much of the expected increase in average compression at the exit plane.

Regions of streamwise separation are shown by plotting contours of negative axial velocity (Figure 6.2.4). A comparison with the 0% Cowl configuration (Figure 6.1.4) indicates that the separation along the sidewall impingement line is enhanced by the presence of the cowl shock in the lower 25% of the inlet. While the forward extent is increased on the sidewall, the separation in the cowl/sidewall corner at the throat entrance ( $x'/Tx' = 1.00$ ) is greatly diminished. Sidewall and baseplate particle traces are presented in Figure 6.2.5. The location of the cowl is observed to have no effect on the upper half of the inlet. Forward of the cowl at  $Z/H = 1.00$ , the strong flow downturning caused by the high pressure post oblique shock flow expanding into the freestream for the 0% Cowl configuration (Figure 6.1.5) is interrupted by the presence of the cowl, which prevents the flow spillage and further compresses the flow. A corner flow is observed to develop in the sidewall/cowl corner much like that of the baseplate/sidewall corner, with lines of separation, reattachment, and upstream influence evident. (In this case, the cowl plate is viewed as the fin interacting with the boundary layer established on the sidewall.) Exit plane pressure contours (Figure 6.2.6) indicate that the forward placement of the cowl has little effect on the nonuniformity of the exit plane compared with the 0% Cowl (Figure 6.1.6). In fact, the magnitudes of the pressures show only a nominal increase in the lower 25% of the inlet. Likewise, a



comparison of the exit plane Mach number plots (Figure 6.2.7 for the 50% Cowl, and Figure 6.1.7 for the 0% Cowl configuration) show little deviation.

#### 6.2.1 Summary of Cowl Position Effects

A global comparison of cowl position effects indicates that the primary changes in the flow structure are localized and do not have a strong effect on the exit plane. Table 6.1.1 also includes the performance parameters for this configuration and indicates that the primary effect of moving the cowl forward is to capture the downturned flow which would have otherwise spilled out ahead of the cowl. The mass capture is observed to increase from 93.4% to 98.0%. The average exit Mach number decreases slightly from 6.3 to 6.0 due to the fact that the cowl shock affects a larger percentage of the exit area than for a 0% Cowl configuration. The effects of the cowl shock also cause a decrease in the total pressure recovery from 0.61 to 0.48 and in kinetic energy efficiency from 99.24% to 98.82%. Likewise the pitot pressure ratio ( $P_{t2}/P_{inf}$ ) decreases slightly from 361.6 to 353.0. A slight increase in average inlet compression is also observed, from 9.20 to 9.73. The most dramatic effect is a nearly 5% increase in inlet capture, at a cost of decreased total pressure recovery.

#### 6.2.2 Shock Structure for the 50% Cowl, CR = 3, Re = 2.15million/ft Configuration

Since it has been previously demonstrated that the effects of the cowl are highly localized, the planes ahead of the cowl leading edge are not presented, and regions away from the cowl in planes aft of the leading edge which are unchanged from the

0% Cowl configuration are not discussed. At  $I=43$  ( $x'/Tx'=0.50$ ), the pressure contours (Figure 6.2.2.1) indicate that the glancing shock is located at approximately  $y/y_{wall}=0.40$ . The velocity vectors (Figure 6.2.2.2) show that the flow near the cowl is turned uniformly toward the centerline in the post reflected shock region, but at approximately  $Z/H=0.97$ , the downward component has been removed. It is therefore evident that the shock forming on the leading edge is located here. There appears to be a small recirculation region in the vicinity of the corner, over which the downturned sidewall flow is turning. There is a significant resemblance to the induced layer observed in the sidewall/baseplate corner.

At  $I=45$  ( $x'/Tx'=0.60$ ), the glancing shock (Figure 6.2.2.3) is observed to be located at  $y/y_{wall}=0.20$ . The cowl shock has reached  $Z/H=0.95$ , and there is a clearer view of the interaction between the two shocks. The flow nearer the sidewall has a higher total compression, since the flow has been compressed first by the glancing shock, then by the cowl shock. The intersection of the two shocks produces what almost appears as an expansion under the cowl shock, since the centerline cowl flow has only undergone the cowl shock compression. The velocity vectors (Figure 6.2.2.4) indicate a uniformly inward turned flow across the cowl which accelerates near the shock intersection point. Upon reaching the lower pressure region toward the centerline, the flow is observed to turn upward slightly as it meets its mirror reflection at the centerline. The corner flow is observed to cause the downturned sidewall flow to reverse at approximately  $Z/H=0.88$ .

At  $I=50$  ( $x'/Tx'=0.79$ ), the pressure contours (Figure 6.2.2.5) indicate that the glancing shock has reflected from the centerline and is located at  $Z/H=0.20$ . The velocity vectors (Figure 6.2.2.6) show significant upstream influence of the cowl shock on the sidewall boundary layer, causing a crossflow separation at  $Z/H=0.75$ . The flow across the cowl toward the centerline has begun to curl back toward the

sidewall and is observed to influence the cowl boundary layer as far inboard as  $y/y_{\text{wall}} = 0.42$ .

At  $I = 52$  ( $x'/Tx' = 0.87$ ), the shock is observed to be located at  $y/y_{\text{wall}} = 0.30$ , and the cowl shock, at  $Z/H = 0.86$  (Figure 6.2.2.7). Velocity vectors (Figure 6.2.2.8) reveal a centerline recirculation pattern which is almost a mirror image of the pattern observed in the pattern noted on the baseplate at the centerline. The flow toward the centerline has formed a CCW recirculation above and a CW recirculation below the point where the flow impinges on the centerline. The latter influences the cowl flow to nearly the corner. Again the sidewall boundary layer is observed to be influenced well above the cowl shock location.

At the throat entrance plane  $I = 55$ , the pressure contours (Figure 6.2.2.9) indicate that the shock has reached  $y/y_{\text{wall}} = 0.62$ . The cowl shock appears to have broadened significantly in the region near the centerline (it has passed through the shock reflecting from the centerline) and is located at approximately  $Z/H = 0.84$ . A vortical structure is now observed in the velocity vectors (Figure 6.2.2.10) under the cowl shock near the sidewall centered at approximately  $y/y_{\text{wall}} = 0.62$ ,  $Z/H = 0.97$ . The flow across the cowl toward the wall has now impinged on the wall and divided, yielding another recirculation on the cowl. The upstream influence of the sidewall shock impingement is evident in the sidewall boundary layer flow in that the upturned flow on the sidewall has been lifted off the sidewall by the separation due to the shock impingement located slightly downstream of this plane. (Recall that Figure 6.2.4, the streamwise separation plot, showed that the streamwise separation at the sidewall shock impingement fed forward to the throat plane.)

At  $I = 60$ , located 29% of the distance between the sweep throat shoulder and the vertical exit plane ( $xs'/Te' = 0.29$ ), pressure contours indicate complex flow pattern (Figure 6.2.2.11) which is complicated further by the sweep of the grid

relative to the sweep of the interaction. At this station, the shock has reflected from the sidewall and is moving back toward the centerline. The cowl shock appears fragmented and diffused by the multiple passing of the glancing shock. The compression at the centerline is observed to reach as high as approximately  $Z/H=0.78$ . The velocity vectors (Figure 6.2.2.12) again indicate the corner vortices in the cowl/sidewall corner.

At the exit plane,  $I=72$ , the pressure contours (Figure 6.2.2.13) indicate a significant distortion of the shock structure due to the sweep of the shock structure with respect to the vertical exit plane. It is nevertheless noted that the cowl shock is difficult to identify. It appears that the multiple interactions with the glancing shock have significantly obscured its effects. Velocity vectors (Figure 6.2.2.14) again indicate that the corner vortices have survived the crossing shock.

By way of summary, it appears that the crossing shocks have a detrimental effect on the cowl shock, tending to obscure and disperse its compression. While the 50% Cowl configuration has the greatest potential to influence the exit plane (simply due to the fact that the inviscid cowl shock would be expected to reach farther into the exit plane), it must encounter more glancing shock interactions which tend to cancel out this effect. On the other hand, the 0% Cowl is observed to generate a stronger shock due to a stronger local downturning at the cowl leading edge, and, though it does not reach as far up into the inlet at the exit plane, the cowl shock encounters fewer reflected shocks. The combination of these effects leads to the observation that the forward cowl has a smaller impact on the average exit parameters than might be expected. As previously noted, the principle benefit of the cowl forward configuration is the increased mass capture.

### 6.3 Reynolds Number Effects

As with the cowl placement effects, with the  $Re = 2.15$  million/ft configuration described in such detail, the effects of decreasing the Reynolds number to 0.55 million/ft will be discussed only to the extent that the results differ from the higher Reynolds number computation for the  $CR = 3$ , 0% Cowl configuration. A change in the Reynolds number by definition yields a change in the boundary layer thickness. At the low Reynolds number, viscous forces take on greater significance relative to the inertia. The laminar boundary layer thickness at the inlet entrance (based on  $u = 0.995U_e$ ) was found to be  $\delta = 0.60$  inch. The displacement thickness computed to be  $\delta^* = 0.32$  inch, and the inlet inflow momentum thickness was  $\theta = 0.0130$  inch. The Reynolds number based on momentum thickness  $Re_\theta = 595.83$ , yielding  $Re_\theta/M_e = 59.6$ , which is much less than the empirical transition values of 150 to 350 presented in Tauber (1990).

Figures 6.3.1a,b,c present the pressure contours in horizontal planes located at  $Z/H = 0.25$ ,  $0.50$ , and  $0.75$ , respectively. Due to the increased boundary layer displacement thickness, the shock angle on the sidewall leading edge is larger than for the higher Reynolds number calculation, leading to a centerline impingement at a more forward location. The shock is observed to strike the centerline at approximately  $x'/Tx' = 0.65$ , reflecting back and impinging on the sidewall slightly ahead of the shoulder. The shock continues to reflect but is somewhat weakened by the expansion at the shoulder. Thus while the explicit effect of decreased Reynolds number is an increase in shock strength via increased boundary layer displacement, the fortuitous placement of the shock just ahead of the shoulder expansion yields only a limited increase in compression. Figure 6.3.2 shows the baseplate and sidewall pressure distribution. The impingement of the shock on the

sidewall just ahead of the shoulder is evident. The aft deflection of the contours near the shoulder on the baseplate and on the sidewalls indicate the effects of the expansion. A comparison of the sidewall and baseplate compression for the high (Figure 6.1.2) and low Reynolds number configuration indicates little difference beyond the shock impingement. At the centerline (Figure 6.3.3), the first shock impingement is clearly observed; however, due to the interaction between the shock reflecting from the sidewall and the expansion emanating from just downstream, the second shock impingement on the centerline is more diffused. Streamwise separation (Figure 6.3.4) on the sidewall is virtually eliminated. This is believed to be due primarily to the proximity of the impingement to the shoulder. Separation on the baseplate is enhanced, however, likely due to the thicker baseplate boundary layer which interacts with the glancing shock. A comparison of the surface particle traces for the 2.15 million/ft configuration (Figure 6.1.5) and for the 0.55million/ft configuration (Figure 6.3.5) indicates that the majority of the flow field is unchanged by the Reynolds number. Again, the shock impingement point is observed to have moved slightly ahead of the shoulder, as noted by the downward deflection of streamlines. Exit plane pressure contours (Figure 6.3.6) again indicate, compared with the  $Re = 2.15$  million/ft configuration (Figure 6.1.6), that there is little difference except near the cowl. The cowl shock region differs due to the relative location of the glancing shock. Figures 6.3.1 showed the glancing shock to be more diffuse and hence less destructive to the cowl shock. A comparison of the Mach number contours indicates that the forward movement of the shock impingements (slightly stronger shocks) has yielded a decrease in the overall exit Mach number while retaining the same primary trends.

### 6.3.1 Summary of Reynolds Number Effects

The primary effect of decreasing the freestream Reynolds number is observed to be an increase in internal shock strengths. For this particular configuration, these increases in pressure are somewhat offset by the fortuitous placement of the shock almost on the shoulder at the throat. The interaction of the shoulder expansion with the shock tends to temper this increase. Table 6.1.1 provides the global inlet performance parameters for the  $Re = 0.55$  million/ft case in addition to the other configurations. A comparison of this configuration with the 2.15million/ft case indicates that the primary effect is a strengthened shock structure, as demonstrated by the decrease in average throat Mach number from 6.3 to 5.7, a decrease in total pressure recovery from 0.61 to 0.45, and in nondimensionalized pitot pressure from 361.6 to 309.0. There is an accompanying increase in average compression from 9.2 to 9.7. Since the kinetic energy efficiency is a strong function of total pressure recovery, a decrease from 99.24% to 98.71% is noted. A 3% decrease in mass capture was also noted. While a portion of this is due to the strengthened shocks, an additional spillage increment is observed due to the forward position of the shock impingement. Ahead of the impingement, strong downturning is noted in the boundary layer. When this impingement occurred aft of the cowl leading edge, the flow turned downward by the shock impingement was still captured by the inlet. When the shock impingement occurred ahead of the cowl leading edge, the flow turned downward by the shock impingement spilled out ahead of the cowl and was not captured.

### 6.3.2 Shock Structure for the $Re = 0.55$ million/ft, $CR = 3$ , 0% Cowl Configuration

Since it has been previously demonstrated that the effects of Reynolds number are relatively subtle (as compared to the contraction ratio), it will suffice to compare only a few planes to demonstrate the differences between the low and high Reynolds number internal structures.

Figure 6.3.2.1 presents the pressure contours at  $I = 31$  ( $x'/Tx' = 0.04$ ). Comparison with Figure 6.1.1.1 ( $Re = 2.15$ million/ft) indicates that the shock location is nominally the same. Velocity vectors however (Figure 6.3.2.2) indicate that the induced flow across the baseplate is thicker (8% of the inlet height compared to 5% for  $Re = 2.15$ million/ft, Figure 6.1.1.2). In addition to the thickness, a weak crossflow is observed to exist as far across the baseplate as  $y/y_{wall} = 0.60$ , compared to a negligible crossflow for the high Reynolds number.

At  $I = 40$  ( $x'/Tx' = 0.40$ ), Figure 6.3.2.3 indicates the shock to be located at approximately  $y/y_{wall} = 0.50$ , compared to  $y/y_{wall} = 0.55$  for the high Reynolds number (Figure 6.1.1.5) (i.e., the shock is 5% of the span closer to the sidewall for the high Reynolds number). A comparison of velocity vectors (Figures 6.3.2.4 and 6.1.1.6 for the 0.55 and 2.15 million/ft, respectively) indicates that, while the induced layer is thicker for the low Reynolds number, the upstream influence is greater for the high Reynolds number, since the crossflow has already reached the centerline and begun to recirculate. The upstream influence is especially greater when it is considered that the shock has not progressed as far across the inlet as for the low Reynolds number.

At  $I = 50$  ( $x'/Tx' = 0.79$ ), the pressure contours indicate the shock to have reflected from the centerline and is located at  $y/y_{wall} = 0.19$  (Figure 6.3.2.5),



compared to  $y/y_{\text{wall}} = 0.10$  for the high Reynolds number. A comparison of velocity vectors at this plane (Figure 6.3.2.6 for the low and Figure 6.1.1.11 for the high Reynolds number) shows that the high Reynolds number (previously noted for having higher crossflow) demonstrates a more pronounced centerline vortex, but the CW vortex in the low Reynolds number configuration is located farther down into the inlet ( $Z/H = 0.12$ , compared to  $Z/H = 0.09$ ), thereby displacing the effects of the glancing shock farther away from the baseplate. The vortical region occupies the top 20% of the inlet height for the low Reynolds number compared to 17%. This amounts to nominally an 18% increase in the size of the vortically dominated region. It is also noted that there is a stronger downflow in the sidewall boundary layer at the bottom of the inlet for the low Reynolds number configuration. The size of the vortical region is well demonstrated in Figure 6.3.2.7, particle traces restricted to the crossflow plane.

At  $I = 54$  ( $x'/Tx' = 0.96$ ), the pressure contours (Figure 6.3.2.8) indicate that the shock is located close to the sidewall boundary layer (at approximately  $y/y_{\text{wall}} = 0.58$ ), compared with 0.50 for the high Reynolds number, though pressure contours in horizontal planes (i.e., Figures 6.3.1a,b,c) and sidewall particle traces (Figure 6.3.5) clearly demonstrated a strong sidewall interaction. Of particular interest in this plane is the spillage, demonstrated by the velocity vectors in Figure 6.3.2.9. When compared to Figure 6.1.1.17 (the high Reynolds number), the difference in the flow downturning in the sidewall boundary layer is striking. As previously mentioned, ahead of the sidewall shock reflection, the sidewall boundary layer is observed to turn sharply downward. Since this interaction occurs ahead of the cowl lip, this downturned flow is observed to spill out. For the high Reynolds number case, while some downward flow is observed, the flow turning due to the sidewall shock interaction is aft of the shoulder at the throat and hence

aft of the cowl lip. That flow is therefore captured by the inlet for the high Reynolds number case.

Figures 6.3.2.10-6.3.2.12 present the pressure contours, velocity vectors, and particle traces at the throat plane ( $I=55$ ,  $x'/Tx'=1.00$ ), respectively. The beginnings of the cowl shock is noted in the pressure contours. The velocity vectors and particle traces indicate that the cowl/sidewall corner has already developed a recirculation. Figure 6.1.1.20 shows that the high Reynolds number flow yields a slight upward flow in the corner but is not as responsive to generating a recirculation as the low Reynolds number flow.

At the exit plane ( $I=65$ ,  $xs'/Te'=1.00$ ), Figures 6.3.2.13-15 present the pressure contours, velocity vectors, and particle traces. While the overall flow structure is similar, it is noted that the vortices near the baseplate occupy a the top 24% of the inlet height, compared to approximately 20% at the high Reynolds number (Figure 6.1.1.33).

By way of summary, it appears that the principle effect of a decrease in Reynolds number is a forward movement of the shock impingement points. The increased shock strength yields a decrement in total pressure recovery and related parameters. A modest increase in average compression is noted. The forward placement of the first shock impingement location to a position slightly ahead of the throat produces a decrease in mass capture for the 0% Cowl due to the increased downturning ahead of the impingement spilling ahead of the cowl lip.

## **Experimental Results**

During the course of the extensive test program, voluminous quantities of data were obtained. A total of 8 ESP-32 (Electronically Scanned Pressure) sensors provided 256 channels of data. For the wall static pressure measurements, the sampling rate was hardware limited to 4 frames per second and a total of 40 frames (10 seconds) of data. Each "frame" consisted of an average of 8 samples. A total of 89 pressure orifices were located on the sidewall with 131 on the baseplate. In the interest of being concise, contour plots of the pressures on these surfaces are presented for comparison of the salient features among the configurations. Individual line plots of the various lateral and axial arrays of static pressure orifices are also presented to provide a comparison of the relative magnitudes. In order to minimize the total number of plots, these data are presented by way of comparison plots, comparing the effects of contraction ratio, cowl position, or Reynolds number. A general discussion of data trends and their relation to the internal flow physics is included with the contraction ratio comparisons and is not repeated for the additional sets of comparison plots.

### **7.1 Contour Plots**

Since the orifices were concentrated in the expected interaction regions, it was necessary to interpolate to obtain additional points to regularize the locations for the contour plotter, i.e. to create an  $N \times M$  grid of pressure data. The pressure orifice locations are identified with a circle; the artificially generated (or phantom)

points are indicated by the small cross-hairs. Since the baseplate pressure orifices were arranged in lateral arrays, these data posed no difficulty to the contour plotter. For the sake of convenience, the outline of the cowl is drawn on the bottom of the sidewall contour figures to visually mark the cowl position. The contraction ratio is varied by positioning one sidewall progressively closer to the other. In the baseplate contour plots, the outline of the fixed sidewall is drawn. When the movable sidewall is positioned for a contraction ratio of 9, a portion of that sidewall is visible in the plot and it is also sketched. Since at a contraction ratio of 9, the movable sidewall covers 9 pressure orifices (located on what was the centerline for the contraction ratio of 3), the resolution in the throat for that configuration is slightly diminished. In order to more easily view the contours in the throat, the y-scale is expanded by a factor of 3. Comparisons among sets of contour plots can often be misleading when the scales of the contours differ greatly among the plots, i.e. the meaning of the density of contour lines is lost. In order to avoid this pitfall, the contour plots are plotted using the same sets of contour levels. On the baseplate, lines of constant compression ( $P/P_{inf}$ ) between 1.0 and 10.0 in increments of 0.5, between 11.0 and 19.0 in increments of 1.0, between 20.0 and 38.0 in increments of 2.0, and between 40.0 and 140.0 in increments of 10.0 are plotted for all the plots. All of the sidewall plots present lines of constant compression ( $P/P_{inf}$ ) between 1.0 and 35.0 in increments of 2.0, between 40.0 and 120.0 in increments of 5.0, and between 130.0 and 480.0 in increments of 10.0 are plotted for all the plots.

There are four fundamental interactions which are observable in the contour plots: the glancing shocks passing over the baseplate, the glancing shock impingements on the sidewalls, the corner flow, and the cowl effects. The planar shock sheets generated by the swept leading edges glance across the baseplate,

strike the centerline, and reflect back onto the sidewalls as incident shocks. If these interactions are purely inviscid, the sweep is preserved.

With a total of 30 sets of contour plots representing a total of 27 configurations, there exists no convenient way to present the plots which offers a sequential comparison of figures. The plots are therefore arranged in groups. Some comparisons can be made by examining sequential figures, however it will be necessary to examine plots from different groups (non-sequentially ordered) to complete the comparisons. The plots are arranged in major groups based on Reynolds number. Within each major grouping are groups based on cowl location. The plots within groups of cowl location are arranged in order of increasing contraction ratio. Additionally, plots of both the baseplate and sidewall for a given configuration are placed on the same page. Contraction ratio effects for a given cowl position and Reynolds number are evident by comparison of sequential pages. Thus the  $Re = 0.55$  million/ft major grouping is presented first, within which are 3 subgroupings: 0, 25, and 50% cowl. So the three contraction ratios for the  $Re = 0.55$  million/ft, 0% cowl are followed by the three contraction ratios for the  $Re = 0.55$  million/ft, 25% cowl, which is followed by the three contraction ratios for the  $Re = 0.55$  million/ft, 50% cowl configuration. The pattern is the same for the  $Re = 1.14$  and  $2.15$  million/ft. Since the effect of Reynolds number is subtle, a typical Reynolds number (0.55 million/ft) is used to present the details of the contraction ratio and cowl position effects. Following this discussion, the effects of Reynolds number will be addressed by way of comparison of differences in the remaining groups of plots.

### 7.1.1 Contraction Ratio and Cowl Location Effects

The effects of contraction ratio may be demonstrated by first considering inviscid effects. The modification to two dimensional oblique shock theory presented in Section 3.3 makes it possible to compute the inviscid internal shock structure. A  $6^\circ$  wedge angle swept at  $45^\circ$  generates a shock sheet which impinges on the sidewall 10.08 inches aft of the leading edge ( $x'/Tx' = 1.06$ ). Table 7.1.1.1 provides the location of the inviscid glancing shock intersection at the centerline and the reflected shock sidewall impingements both in inches and as a percent of the distance from the leading edge to the throat ( $x'/Tx'$ ) for contraction ratios of 3, 5, and 9. The table clearly demonstrates the forward progression of the shock interactions with increasing contraction ratio.

Table 7.1.1.1: Inviscid Shock Impingement Locations

	Centerline		Sidewall Impingement	
	$x'$ (in)	$x'/Tx'$	$x'$ (in)	$x'/Tx'$
CR=3	8.0193	0.84	10.0752	1.06
CR=5	6.6827	0.70	8.3960	0.88
CR=9	6.0145	0.63	7.5564	0.79

Figures 7.1.1.1 demonstrate the pressure contours on the inlet baseplate and sidewall for a contraction ratio of 3,  $Re = 0.55$  million/ft, 0% Cowl configuration. The four primary interactions are evident in varying degrees. The baseplate pressure contours indicate some upstream influence ahead of the inviscid shock location near the front of the inlet, but the influence of the glancing shocks appears

to dissipate about half way between the leading edge and the throat. From this point back to the throat, the pressures are observed to be nearly uniform across the span of the inlet. The axial baseplate pressure rise is interrupted near the sidewall at the throat by what appears as a local expansion. This is likewise evident on the sidewall plot (Figure 7.1.1.1b), as the axial pressure rise due to the shock impingement observed at the sidewall centerline does not extend to the baseplate. A region of lower pressure persists in the near corner region on the sidewall. As the computational results indicated, this region is highly vortically dominated, yielding lower pressures down the length of the corner. The sidewall shock impingement is observed very near the shoulder. Though no further shock impingement points are noted on the sidewall, it cannot be said that the shock has cancelled on the shoulder. CFD results indicate that the impingement occurs slightly downstream of the shoulder and the shock continues to reflect, but would reach the sidewall downstream of the exit plane and hence is not observed in the plot. Each segment of the reflecting swept shock system imparts a downward component to the flow, as demonstrated in Section 3.3. As a result of the downturning, a shock forms on the cowl; this cowl shock is observed to influence only a small percentage of the exit plane.

Figures 7.1.1.1, 7.1.1.2, and 7.1.1.3 present the baseplate and sidewall pressure contours for contraction ratios of 3, 5, and 9, respectively. In the baseplate region, there are only two notable effects of contraction ratio: the expansion at the throat observed for the contraction ratio of 3 is not seen for the higher contraction ratios (in part due to the overall higher pressures dominating the region due to the more forward shock impingements), and a quantitative increase in the overall static pressure with increasing contraction ratio is noted. The increase in static pressure is believed to be the result of a small separation region which forms ahead of the

glancing shock. Computationally it was demonstrated that there is turning in the boundary layer significantly ahead of the inviscid shock location. When the entrance width is sufficiently large, the disturbance from the corner appears to be damped before reaching the centerline (far upstream of the inviscid shock location). This appears to allow the boundary layer to remain attached up to the region where the shocks intersect at the centerline. For the contraction ratio of 5 case, however, there is still significant crossflow at the centerline, which leads to a separation ahead of the glancing shock centerline intersection. This separation region is observed to increase in magnitude with increasing contraction ratio. This is due to the fact that the crossflow velocities in a given crossflow plane attenuate with distance away from the sidewall. Therefore, the closer the centerline is to the sidewall, the stronger the crossflows which collide at the centerline. The resultant separation therefore increases in size with increasing contraction ratio with an attendant increase in baseplate pressure.

By far the most dramatic contraction ratio effects are observed on the inlet sidewall. The shock is observed to impinge at approximately the shoulder for a contraction ratio of 3, but for a contraction ratio of 5 the impingement has moved to approximately  $x'/Tx' = 0.78$  (somewhat ahead of the inviscid impingement point of 0.88). For the contraction ratio of 9, the impingement occurs at  $x'/Tx' = 0.68$  (compared with the inviscid location of 0.79). The impingement ahead of the inviscid location should be of no surprise, since the displacement of the sidewall boundary layer has the effect of increasing the wedge angle and hence the shock strength, causing the shock to strike both the centerline and the sidewall at more forward positions. For the contraction ratio of 5, the pressure is observed to rise following the shock impingement until the shoulder is reached. A localized expansion is noted on the sidewall in the centerline region prior to the



recompression of the second impingement at approximately  $x'/Tx' = 1.2$ . The shocks and expansion are observed to be attenuated toward the baseplate as a result of the corner flow, the disturbance appearing to emanate from the juncture of the leading edge of the sidewall and the baseplate. Additionally, the cowl shock appears to become more prominent for increasing contraction ratio. Since the shock impingements occur farther forward for increasing contraction ratio, the flow in the throat region has passed through more shocks, each of which has enhanced the downturning of the flow, as the contraction ratio is increased. Hence the cowl shock becomes stronger since the flow incidence angle is greater for increased contraction ratio. The contraction ratio of 5 plot shows a cowl shock which is stronger and extends farther up into the exit plane. Even though the cowl has not been moved, the post-cowl shock region becomes a larger percentage of the exit plane, enhancing any vertical asymmetry in the exit plane.

Similar features become even more strongly accentuated for the contraction ratio of 9. At the throat, the sidewall static pressures down to  $Z/H = 0.5$  have been perturbed by the corner flow. Additionally, the cowl has also increased its domain of influence on the sidewall as previously discussed. The first sidewall impingement is located at  $x'/Tx' = 0.68$ , with a second impingement at approximately 1.03. Significantly higher pressures in the cowl region are noted, since the flow near the cowl has passed through 3 shocks, each of which have incrementally increased the downturning. The post-cowl shock region is seen to affect approximately 25% of the exit plane.

Figures 7.1.1.4, 7.1.1.5, and 7.1.1.6 present the contraction ratio effects for the same configuration with the cowl moved forward of the throat by 25% of the distance between the leading edge and the cowl. The salient features of the flow remain unchanged with the exception of the cowl region. The contraction ratio of

3 configuration (Figure 7.1.1.4) shows the sidewall shock impingement slightly aft of the shoulder, but the impingement of the downturned flow on the cowl causes the pressure contours which formerly were swept with the shock impingement to be turned toward the cowl leading edge. The influence of the cowl shock is weak in this region since the flow striking it has been through only one shock. Past the sidewall impingement point, the pressures near the cowl are observed to rise by a factor of 2 as compared to the 0% Cowl case. The post-reflected shock flow, having again passed through the glancing shock, becomes more inclined with respect to the cowl and impinges on it, forming a region of higher pressure just aft of the sidewall impingement point. For the same reasons, the contraction ratio of 5 configuration (Figure 7.1.1.5) yields forward deflected contours near the cowl leading edge (which is located just forward of the first sidewall impingement point) and higher pressures in the post-reflected shock region near the cowl. While both sidewall impingements are visible, the second impingement is obscured near the cowl as a result of the cowl shock and the corner flow. At a contraction ratio of 9, the first impingement is not affected by the forward placement of the cowl since the impingement occurs forward of the leading edge. As the flow passes through the series of reflected swept oblique shocks, its downturning is enhanced, such that when throat is reached, a larger disturbance in the cowl region is noted than for the 0% Cowl configuration. The combination of the pressure increase due to the second sidewall impingement and the impingement of the downturned flow on the cowl produce pressures over 3.5 times that of the 0% Cowl configuration.

The 50% Cowl configuration for the three contraction ratios at  $Re = 0.55$  million/ft is presented in Figures 7.1.1.7, 7.1.1.8, 7.1.1.9, and 7.1.1.10. For the contraction ratio of 3 (Fig. 7.1.1.7), the (inviscid) glancing shock hits the centerline at  $x'/Tx' = 0.84$ , returning to the sidewall at  $x'/Tx' = 1.06$ . Thus, over half of the

region between the glancing shock from the sidewall leading edge and its centerline reflection is enclosed by the cowl. In this instance, much of the flow which would have spilled out for the 0% Cowl configuration has been captured by the cowl. Since this flow has been turned downward by only the initial glancing shock, the cowl shock is weak and deflects some of the pressure contours from the impingement region forward. A region of significantly higher pressure develops at the impingement of the shock on the sidewall. As this shock reflects back toward the centerline, the flow downturning is increased, yielding a region of flow impinging on the cowl and accompanying higher pressures. Likewise for the contraction ratio of 5 configuration, the only significant change occurs in that more of the flow is captured by the cowl which in turn increases the compression as this captured flow is turned by the cowl. At each impingement point, the pressure rise is observed in the cowl region to be greater than for the cowl aft positions. Figure 7.1.1.9 is included at this point to indicate the excellent repeatability observed throughout the test sequence. At the contraction ratio of 9 (Figure 7.1.1.10), the swept shock impingement appears to have been turned vertical by the shock. It is however more likely that, since a small separation region is known to exist just forward of the shock impingement line, the interaction between the cowl shock and the shock impingement point has yielded a large sidewall separation.

### 7.1.2 Reynolds Number Effects

A similar set of plots is presented in Figures 7.1.2.1-7.1.2.10 for a freestream unit Reynolds number of 1.14 million per foot. Likewise, Figures 7.1.2.11-7.1.2.20 present the contraction ratio and cowl location effects for a Reynolds number of 2.15 million/ft. (Figures 7.1.2.2 and 7.1.2.17 duplicate the configurations of their

respective preceding figures to demonstrate the repeatability of the data.) Decreasing the Reynolds number indicates by definition that the viscous forces take on greater significance with respect to the momentum forces. Hence, boundary layer thicknesses are expected to increase and, more importantly to the inviscid flow field, the displacement thicknesses increase, causing all surfaces to possess effectively larger wedge angles. This in turn causes the sidewalls to generate stronger shocks and increases the internal compression of the inlet. Beyond the displacement effects, an increased boundary layer thickness influences the shock impingements and reflections and may increase the likelihood of flow separation. Since the range of Reynolds numbers obtainable in the present facility span less than an order of magnitude, large changes, such as the presence or absence of separations, are not anticipated, but rather the trends related to the extent and strength of such interactions.

For each of the Reynolds numbers tested, the baseplate pressure contours demonstrate the nominal interactions previously discussed. Pressure levels in general tend to decrease with increasing Reynolds number. For example, a comparison of the location of the  $P/P_{\text{inf}}=4.0$  contour in Figures 7.1.1.1, 7.1.2.1, and 7.1.2.11 (CR = 3, 0% Cowl) indicates that the pressure rises to this level by  $x'/Tx' = 0.85$  for  $Re = 2.15$  million/ft,  $x'/Tx' = 0.58$  for  $Re = 1.14$  million/ft, and  $x'/Tx' = 0.55$  for  $Re = 0.55$  million/ft. The forward movement of the pressure rise is indicative of an increasing glancing shock strength due to increased sidewall boundary layer thickness with decreasing Reynolds number as well as the increased viscous interaction of the shock with the baseplate boundary layer and the enhanced viscous corner flow. This is observed for all the contraction ratios and cowl positions.

The sidewall plots likewise reveal a more distinct interaction for the lower Reynolds numbers. This is in part due to the fact that the larger interactions associated with the lower Reynolds number runs (interactions which span several static pressure orifices) are more easily resolved. Though a total of 89 static pressure orifices are located on the sidewall, there still exists significant spacing between the orifices. The average instrumentation density on the sidewall is given by  $89 \text{ orifices} / 56 \text{ sq.in.} = 1.6 \text{ orifices per square inch}$ , though the orifices were clustered to improve the density in interaction regions. Interpolating among data points to locate lines of constant pressure adds an additional smearing effect. Thus, larger scale (those which influence multiple orifices) are better displayed in the contour plots. Particularly for the contraction ratio of 3, the lower Reynolds number contours appear to be better defined.

The contraction ratio of 9, 50% Cowl configuration (Figures 7.1.1.10, 7.1.2.10, and 7.1.2.20) serves to demonstrate the relationship between the size of the interaction and the Reynolds number. For the  $Re = 2.15 \text{ million/ft}$  configuration (Figure 7.1.2.20), the multiple shock impingements and slight expansion at the throat are visible. The effect of the cowl shock is small, causing a nominal pressure rise near the cowl ahead of the sidewall impingement. When the Reynolds number is reduced to  $0.55 \text{ million/ft}$  (Figure 7.1.1.10), a much stronger forward deflection of the pressure contours is evident, resulting from the combined effects of stronger glancing shock-induced downturned flow impinging on the cowl and a thicker sidewall boundary layer to interact with the shock impingement and cowl shock. It is therefore evident that the primary effect of decreased Reynolds number is by way of displacement effects and enhanced shock-boundary layer interactions (larger separation zones). A more quantitative discussion of Reynolds number effects is given in the discussion of the line plots.

## 7.2 Line Plots

The test matrix was presented in Tables 5.4.1-5.4.3. If the three tables were stacked one behind the other, a three-dimensional matrix (cube) would be formed. On the front face of this cube are 9 blocks representing the various cowl positions (horizontally arrayed) and the contraction ratios (vertically arrayed) for a given Reynolds number. Two additional 3x3 stacks of blocks also representing the cowl positions and contraction ratios are located behind the first stack, each representing a different Reynolds number. It is therefore evident that a complete study of contraction ratio effects requires making 9 comparisons: the three cowl positions for each of the three Reynolds numbers. This would be the equivalent of examining vertically stacked blocks in the cube. Cowl position effects likewise require 9 comparisons: three contraction ratios for each of the three Reynolds numbers. This would be equivalent to examining horizontally arranged blocks in the cube. Finally, the effects of Reynolds number requires 9 additional comparisons: the three contraction ratios for each of the 3 cowl positions. This equivalent to examining the rows spanning the three tables, or in other words, rows of blocks running front to back in the cube. When all of these are considered, it is noted that a total of 27 sets of comparisons are required for completeness.

Each of the sets of comparisons contains approximately 53 plots. First, the ratio of local to freestream static pressure ( $P/P_{inf}$ ) is presented along the three effective centerlines (if the particular set of plots is a contraction ratio effect set, then an additional plot comparing the respective centerline distributions is also included). Then the pressure distributions along each of the 25 lateral arrays on the baseplate (from the leading edge through the inlet exit plane) are presented. Following that, the pressure distribution on the centerline of the cowl is presented.

Since there were 5 orifices placed on the movable sidewall to mirror the positions of orifices on the fixed sidewall, each of the centerline pressure distributions for both sidewalls are presented to demonstrate the symmetry (i.e., the sidewalls were well aligned with zero yaw). Following these plots, pressure distributions along 9 axial arrays on the sidewall at increasing values of  $Z/H$  are presented. Finally, the sidewall pressures are replotted to give the pressure distribution from the baseplate to the cowl along 16 lines of constant sweep, i.e.  $x'/Tx' = \text{constant}$ .

Due to the overwhelming numbers of plots required to present these for each of the 27 comparisons, each of the 27 sets is not discussed. Rather, a typical case from each of the 9 contraction ratio effects, 9 cowl placement effects, and 9 Reynolds number effects is discussed in detail, and only differing, anomalous, or otherwise noteworthy plots from each of the other 8 sets will be discussed.

### 7.2.1 Contraction Ratio Effects

Figures 7.2.1.1-7.2.1.54 present the contraction ratio effects for the  $Re = 2.15$  million/ft, 0% Cowl configuration. In order to optimize the instrumentation density, orifices were concentrated in the sidewall/baseplate corner region. In order to prevent covering numerous orifices when increasing the contraction ratio by moving the sidewalls closer together, it was deemed more efficient to fix one sidewall and heavily instrument that corner. An increase in contraction ratio was accomplished by moving the other sidewall. While this has the disadvantage of having three effective centerlines, it minimizes the number of orifices covered (and hence rendered useless) when the contraction ratio was increased. Figure 7.2.1.1. presents the pressure distributions for contraction ratios of 3, 5, and 9 along their

respective centerlines. The so-called  $\chi$ -bar interaction is evident in that the pressure is observed to be higher near the leading edge ( $P/P_{inf} \sim 2.3$  at 1 inch aft of the leading edge,  $x'/Tx' = -0.841$ ), relaxing back to  $P/P_{inf} \sim 1.7$  near the inlet entrance. For the contraction ratio of 3, the pressure is observed to rise slightly near the inlet entrance ( $x'/Tx' = 0.11$ ) to a plateau of approximately  $P/P_{inf} = 2.3$ . The pressure remains relatively constant at that level until it gradually ramps up to  $P/P_{inf} = 8.5$  at the inlet throat, beginning at  $x'/Tx' = 0.6$ . The effects of the corner expansion are observed, as the pressure relaxes slightly over the next three orifices to  $P/P_{inf} = 8.0$ . A secondary rise to  $P/P_{inf} = 8.2$  is noted at  $x'/Tx' = 1.3$ . At this point, the compression then drops to approximately 7.5 and begins a gradual rise toward the exit. This sawtooth pattern is the result of a multiply reflecting internal shock. The computational results indicated that the pressures observed on the baseplate did not well indicate the compression of the core flow of the inlet due to the vortical interactions resulting from the induced crossflow on the baseplate, but it is noted here that the effects of the shock pattern, though perhaps tempered by the vortical flow, nevertheless influence the baseplate static pressures. The inviscid shock calculations indicated that the leading edge shock should reach the centerline at  $x'/Tx' = 0.84$  (Table 7.1.1.1). The location of the initial pressure rise in the data indicates significant upstream influence of the crossing shock pattern. It is interesting to note that for the contraction ratios of 5 and 9, a higher pressure is noted ahead of the inlet entrance plane than for the contraction ratio of 3. At  $x'/Tx' = -0.1$ , a compression of 2.5 is noted, compared to approximately 1.7 for the contraction ratio of 3. (Examination of Figure 7.2.1.2 shows that the first indication of a pressure rise on the baseplate for the higher contraction ratios occurs at  $x'/Tx' = -0.38$ .) This may be indicative of a separation caused by the crossing shocks which has fed forward of the inlet entrance. For each of the contraction ratios of 5



and 9, the pressure is observed to gradually increase toward the throat, in contrast to the plateau region noted for the contraction ratio of 3. For a contraction ratio of 5, the pressure rise becomes more significant at  $x'/Tx' = 0.63$ , reaching a peak compression of  $P/P_{inf} = 11.0$  at the throat. The location of the sudden increase in compression is noted to be near the inviscid shock centerline intersection point of  $x'/Tx' = 0.70$ , again indicating significant upstream influence, not only in that the pressure rise is noted to begin ahead of the inviscid shock centerline reflection point, but also in that the pressure increase is observed to cause a gradual increase in pressure from as far forward as the inlet entrance, rather than from a plateau as with the contraction ratio of 3. Aft of the shoulder, the pressure expands to a compression of 10.5, before rapidly rising to 11.5 at  $x'/Tx' = 1.24$ . A gradual decrease in compression is again noted until a local minimum of 11.0 is reached at  $x'/Tx' = 1.41$ . An increase in compression is then noted to a maximum of 13 at the inlet exit. Again the sawtooth pattern, which in this instance rises and falls with greater frequency than the  $CR = 3$  configuration due to the forward movement of impingement points (and hence more impingements within the same length) with increased contraction ratio, indicates that the viscous, vortical baseplate flow has not entirely isolated the baseplate pressures from the effects of the glancing shock. The pressure rise for the contraction ratio of 9 is observed to be much greater than either the contraction ratios of 3 or 5. Beginning at  $x'/Tx' = 0.60$ , the pressure is observed to rise rapidly to the throat entrance. While this location appears to correspond well with the inviscid prediction of the shock intersection at the centerline ( $x'/Tx' = 0.63$ ), the upstream influence of the crossing shocks is noted via the gradual increase in compression from the entrance plane of the inlet. The pressure rise in the inlet is observed to be rapid, interrupted by the expansion at the shoulder of the throat. The expansion does not cause the pressure to relax, but

rather tempers the strong pressure rise, keeping the compression at approximately 23.5 between  $x'/Tx' = 1.0$  and 1.07. A peak compression of 37 is noted at  $x'/Tx' = 1.58$  ( $x'/Tx' = 1.68$  shows a significant drop in pressure as the flow begins to expand out the aft end of the inlet). The previously noted sawtooth pattern is no longer noted. The effects of the discrete glancing shocks are more effectively isolated from the baseplate region by the viscous, vortical flow in the vicinity of the baseplate; the overall increase in compression is, however, imposed on the baseplate.

Figures 7.2.1.2-7.2.1.4 show the pressure distribution down the same array of pressure orifices, the arrays designated as the centerline for the contraction ratios of 3, 5, and 9, respectively. It should be noted that this provides a lateral comparison of pressures, since the array designated the CR = 3 centerline is on the inlet centerline for the contraction ratio of 3 but is significantly off centerline for the contraction ratios of 5 and 9. It is noted that the flow appears nominally laterally uniform, as the salient features are preserved regardless of lateral position. Also Figure 7.2.1.2 indicates that for each of the three contraction ratios, the pressures leading up to the inlet entrance plane demonstrated good repeatability, and also indicates that the pressure rise due to the apparent separation feeding forward of the inlet extends forward no farther than  $x'/Tx' = -0.65$ .

Figures 7.2.1.5-7.2.1.26 present the lateral pressure distribution across the baseplate at 22 axial stations beginning one inch from the baseplate leading edge and proceeding downstream through the inlet to the exit plane. It should be noted that the same pressure orifices were used for each contraction ratio, but since the effective centerline moves as a result of achieving increased contraction ratio by moving only one sidewall, the orifices have different lateral positions relative to the

centerline for different contraction ratios. At one inch aft of the baseplate leading edge ( $x'/Tx' = -0.8412$ ), the pressures are observed to be uniform for each of the contraction ratios at  $P/P_{inf} = 2.2$  (Figure 7.2.1.5). At  $x'/Tx' = -0.5258$  (Figure 7.2.1.6) however, it is noted that there has begun to be a deviation between the contraction ratio of 3 data and the higher contraction ratios. The apparent separation region which influenced the axial data is here observed to have a significant upstream extent. The overall pressure level has decreased, however, from the upstream station. The highest compression for any of the contraction ratios was 1.7. At  $x'/Tx' = -0.1052$  (Figure 7.2.1.7), the increased pressures for the higher contraction ratios are clearly noted, as the compression for the contraction ratios of 5 and 9 is approximately 2.4, compared to 1.35 for the contraction ratio of 3. Also of interest is the uniformity of the contraction ratio of 3 pressures, in contrast to the dome shaped pressure distribution for the higher contraction ratios. A pressure relief is noted outboard of the location of the two inlet sidewalls. At the inlet entrance station ( $x'/Tx' = 0.000$ ), Figure 7.2.1.8 shows that the contraction ratio of 3 distribution indicates a slight increase in pressure near the inlet sidewall leading edge. The contraction ratios of 5 and 9 show that the compression is nearly twice that of the CR = 3 data and that a pressure relief is noted near the sidewall leading edge as some of the high pressure, separated flow spills around the side of the inlet. (It is noted that this situation would be different for a full scale flight vehicle since the engine modules would be placed side by side. Therefore, there would not exist a lower pressure region to the located outboard of the inlet sidewall toward which the flow could turn.) Once inside the inlet, however, ( $x'/Tx' = 0.1052$ , Figure 7.2.1.9) the flow is trapped laterally by the sidewalls and a laterally uniform distribution is noted. The pressure levels are still notably higher for the higher contraction ratios. This is the first downstream station where a significant

difference is noted in the pressures between the contraction ratios of 5 and 9. The nominal compression levels for the  $CR=3$ , 5, and 9 are 1.9, 2.6, and 2.9, respectively. It is interesting to note that from the inlet entrance to the throat plane (Figures 7.2.1.10-7.2.1.18), there remains a relatively linear relationship between the contraction ratios, that is, the differential between  $CR=3$  and 5 is nominally that between 5 and 9. The scales on the plots vary as the magnitudes increase, but the relative spacing between the curves remains proportionate. Particularly for the contraction ratio of 3, the lateral pressure distributions near the front of the inlet indicate a higher pressure in the immediate corner of the sidewall and baseplate. Previous research in fin interactions (e.g., Neumann and Token (1974)) has indicated that away from the corner, a plot of the lateral pressure distribution demonstrates a trough at approximately the shock location before it rises to its plateau value away from the wall. The present data do not indicate the trough, though it could have occurred between the orifices. Both at the higher contraction ratio and farther into the inlet, this influence is diminished. From the throat to the exit plane (Figures 7.2.1.18-7.2.1.26), the pressures for the contraction ratio of 9 tend to show much more significant increases in pressure, as previously indicated by the axial pressure distributions (Figure 7.2.1.1). Laterally, the compression is relatively uniform (as was typical of the baseplate contour plots).

Figure 7.2.1.27 shows the pressure distribution on the cowl for the various contraction ratios. As has been previously indicated, the flow downturning is increased incrementally by each reflected shock through which the flow passes. Thus, the higher contraction ratio cases are expected to have higher cowl pressures, since the cowl shock is anticipated to be stronger for higher contraction ratios. This trend is reflected in the data. The  $CR=3$  cowl pressure distribution shows little effect of the crossing shock pattern. (It should be noted that the exit plane on

the cowl surface is  $x'/Tx' = 1.26$ , such that data beyond that point are subject to the expansion of the sidewalls aft of the exit plane.) The sawtooth pattern is more evident for the contraction ratio of 5. In the interest of comparison with the  $CR = 3$  data, an average compression over the first half of the cowl length for the  $CR = 5$  data is 55, nearly twice the value for the  $CR = 3$  data. In addition to the increased downturning, the increased number of reflected shocks has also increased the static pressure, which combined with a stronger cowl shock, yields a large increase in compression on the cowl. The same is also true (and to an even greater extent) for the  $CR = 9$  data. An average value for the  $CR = 9$  cowl surface compression is approximately 170, in excess of 3 times the compression for the  $CR = 5$  data.

Pressure distributions down the sidewall centerlines for the fixed and movable sidewalls are found in Figures 7.2.1.28 and 7.2.1.29, respectively. The forward progression of the shock impingement is well indicated. The pressure rise for the  $CR = 3$  data does not occur until  $x'/Tx' = 1.07$ , whereas for the  $CR = 5$  data, the first pressure peak occurs at approximately  $x'/Tx' = 0.90$ . The expansion aft of the impingement brings the pressure to a minimum compression of 11 at  $x'/Tx' = 1.07$ . The second sidewall shock impingement is observed to increase the compression to another local maximum of 24. Following the peak is another trough of approximately 11 at  $x'/Tx' = 1.32$ . At the exit plane, the pressure is again rising. The sawtooth pattern clearly indicates multiple shock impingements, and their locations correspond well with the predicted values. The contraction ratio of 9 data indicate a peak compression of approximately 30 at  $x'/Tx' = 0.84$ . There is a slight relaxation of pressure prior to the throat, but no local expansion at the throat is observed. The next compression peak ( $P/P_{inf} \sim 64$ ) occurs aft of the shoulder at  $x'/Tx' = 1.15$ . The CFD results indicated the second sidewall impingement to occur slightly ahead of this location, coinciding with the shoulder. Comparison with

Figure 7.2.1.29 indicates that the sidewalls were well aligned both with each other and with the freestream.

Figures 7.2.1.30-7.2.1.38 show the axial pressure distribution on the sidewall along lines of constant height, beginning near the baseplate/sidewall corner and progressing toward the cowl. The main features observed at the centerline ( $Z/H=0.5$ ) are present in varying degrees over the entire sidewall. The principle notation regarding these figures is that in all cases, there is increased compression with increasing contraction ratio. The interpretation of these figures is best made by way of contour plots, which were presented in Section 7.1; the line plots are presented for completeness.

Figures 7.2.1.39-7.2.1.54 show the pressure distribution on the sidewall along lines of constant  $x'/Tx'$ , i.e. lines which run parallel to the leading edge. Highlighted in these plots are the end effects. As has been previously mentioned, the end effects play an important role in the overall inlet performance. Pressures near the bottom of the inlet demonstrate a pressure relief due in part to the spillage of the core flow but more due to the localized expansion of the compressed post oblique shock flow near the wall expanding into a lower pressure freestream below the inlet. Additionally, in order to resolve the problem of the flow vector being simultaneously in the plane of the baseplate and turned downward by the shock, Kutschenreuter, et al. (1965) hypothesized the existence of a centered expansion originating from the shock sheet/baseplate interface, as was shown in Figure 3.3.4. While there is no immediate evidence of such an expansion, it proves a useful mnemonic. At  $x'/Tx' = 0.1042$  (Figure 7.2.1.39), the pressures are observed to be lowest in the sidewall/baseplate corner due to the corner (induced) flow. At the bottom of the inlet ( $Z/H = 1.0$ ), the anticipated pressure relief is noted. Aft of the cowl leading edge, however, this relief is not noted, due to the compression of

the cowl shock and the cessation of spillage.

Sets of figures demonstrating the contraction ratio effects for the remaining eight combinations of cowl location and Reynolds number are included at this point for reference. Comparisons among the sets of plots to infer cowl position and Reynolds number effects will not be made, since plots making explicit comparisons of these effects are presented in the following sections.

### 7.2.2 Cowl Position Effects

Cowl position effects for the 9 combinations of contraction ratio and Reynolds number are presented in Figures 7.2.2.1-7.2.2.477. Since the salient features of the flow have already been identified in the discussion of the contraction ratio, this discussion will concentrate solely on the effects of the cowl on the static pressure measurements (internal compression).

Examination of the centerline pressure distributions for the contraction ratio of 3,  $Re = 2.15$  million/ft configuration (Figures 7.2.2.1-7.2.2.3) indicates that there exists a slight increase in centerline pressure distribution as a result of the forward placement of the cowl. This is better observed in the pressure distributions along lateral arrays beginning near the baseplate leading edge (Figures 7.2.2.4-7.2.2.25). It is noted that from very near the leading edge ( $x'/Tx' = -0.52$ ), the forward cowl position causes an increase in the magnitude of the (nominally uniform) lateral pressure distribution. The effect appears to be diminished with increasing distance inside the inlet from the leading edge. Since the effect is small, the overall increase in magnitude of the axial baseplate pressure distribution diminishes the relative

significance of the effect, as a  $\Delta(P/P_{inf}) = 0.1$  represents a 10% increase in  $P/P_{inf}$  at 1.0 but only a 2% increase at  $P/P_{inf} = 5$ .

The cowl pressures are shown in Figure 7.2.2.26. It is apparent that the pressures for the three cowl positions appear to overlap each other, indicating that the pressure distribution on the cowl is driven primarily by the internal shock locations as well as the location of the orifice relative to the throat entrance. It was demonstrated computationally that a major constituent of the sidewall/baseplate corner flow was induced crossflow, and that, when the sidewalls were sufficiently far apart, the crossflow was damped before interacting at the centerline. A similar induced crossflow is initiated at the cowl, and due to the proximity of the sidewalls at the throat, the crossflow rapidly reaches the centerline, forming recirculation regions which dominate the span. This crossflow is enhanced by the downturning imparted to both the core flow and the sidewall flow by the glancing shocks.

The axial pressure distribution on the sidewall along lines of constant height (Figures 7.2.2.27-7.2.2.37) indicates that except near the cowl (located at  $Z/H = 1.0$ ), the effects of the cowl are very small relative to the magnitude of the pressure. This is better illustrated in the distribution along lines of constant sweep (Figures 7.2.2.38 - 7.2.2.53). In the vicinity of the cowl plane, the pressure distribution is observed to increase sharply, and this increase is noted farther forward for the forward cowl positions, as would be expected.

Although it was stated earlier that comparisons among sets of plots would not be made (since that would constitute a contraction ratio or Reynolds number comparison, and those comparisons are presented and discussed explicitly in other sections), it is necessary to make such comparisons in order to adequately discuss the small increase in pressure noted over much of the domain with forward cowl placement. The set of figures just discussed (Figures 7.2.2.1-7.2.2.53) represent a



CR = 3, Re = 2.15 million/ft configuration. Figures 7.2.2.54-7.2.2.106 represent the CR = 3, Re = 1.14 million/ft configuration, and Figures 7.2.2.107-7.2.2.159 represent a CR = 3, Re = 0.55 million/ft configuration. Comparison among these three sets indicates that the baseplate pressure differential among the three cowl positions is increased with decreased Reynolds number. At a Reynolds number of 0.55 million/ft, the differential is noted much farther into the inlet than for the high Reynolds number. For example, the lateral pressure distributions on the baseplate for the three cowl positions collapse to approximately the same pressure at  $x'/Tx' = 0.42$  at Re = 2.15 million/ft, at  $x'/Tx' = 1.0$  for Re = 1.14 million/ft, and the pressures never seem to come to the same level for the Re = 0.55 million/ft. Since the boundary layer thickness increases with decreased Reynolds number, the disturbance from the cowl is best able to transmit through the thicker boundary layer associated with the lowest Reynolds number. A comparison of the CR = 3 plots with the same sets for CR = 5 (Figures 7.2.2.160-7.2.2.318) indicates that this forward effect of the cowl is not generally noted at the higher Reynolds numbers. Only at a Reynolds number of 0.55 million/ft do the CR = 5 baseplate data ahead of the throat indicate any influence of the cowl position. This influence does not feed forward of the inlet entrance and is observed in the entrance plane only near the sidewall. At the contraction ratio of 9 (Figures 7.2.2.319-7.2.2.477), the influence of the cowl on the baseplate ahead of the throat is again not indicated for the high Reynolds number. It was previously noted that the higher contraction ratios created a separation on the baseplate which fed significantly forward of the inlet entrance. Since the slight increase in pressure due to the cowl position is not noted, it is clear that this increase is second order compared to the pressure increase due to the separation. It should be noted that in the regions near the cowl, the cowl position is still observed to have the effect of increased local compression

for the cowl forward positions, but these regions are typically limited to the sidewall for  $Z/H > 0.5$ .

### 7.2.3 Reynolds Number Effects

The Reynolds number effects for the  $CR = 3$ , 0% Cowl configuration are demonstrated in Figures 7.2.3.1-7.2.3.53. It is clear even from the first figure that the Reynolds number has a significant impact on the flow structure (and hence pressure distribution). The  $\chi$ -bar interaction is observed at the leading edge of the baseplate; additionally, the compression on the baseplate is observed to increase due to the increased boundary layer growth with decreased Reynolds number. The pressure rise on the baseplate due to the glancing shock interaction is observed to move forward with decreasing Reynolds number, located at  $x'/Tx' = 0.1$  for  $Re = 2.15$  million/ft and approximately -0.2 for the lower Reynolds numbers. It was previously noted computationally that the glancing shock impinges on the sidewall aft of the shoulder at  $Re = 2.15$  million/ft and approximately on the shoulder for  $Re = 0.55$  million/ft. The throat pressure distribution becomes much more uniform when the shock impingement coincides with the shoulder; the sharp increase in pressure due to the shock is tempered by the throat expansion. (For an inviscid reflection, the shock would be said to cancel at the shoulder.) The increased flat plate compression is also observed in the lateral pressure distributions (Figures 7.2.3.4-7.2.3.25). The flow separation ahead of the inlet is observed in Figure 7.2.3.6 at  $x'/Tx' = -0.1052$ . At the high Reynolds number, the pressure distribution is uniform; however, at  $Re = 1.14$  and  $0.55$  million/ft, the pressure is not only higher than at  $x'/Tx' = -0.52$  (the next upstream station), but it demonstrates a significant

pressure relief as the flow spills around the outside of the inlet sidewalls. The higher pressure region toward the inlet centerline is observed even into the inlet as far as  $x'/Tx' = 0.52$ , where the lateral pressure distribution becomes nominally uniform. The cowl pressures (Figure 7.2.3.26) also appear particularly sensitive to Reynolds number.

The sidewall axial pressure distributions are given in Figures 7.2.3.27 - 7.2.3.37. Again, an overall increase in compression is noted, primarily by way of increased compressive turning due to the increased displacement thickness with decreased Reynolds number. The forward progression of the sidewall shock impingement is particularly evident in the sidewall centerline plot (Figure 7.2.3.32). At  $Re = 2.15$  million/ft, the pressures climb to a plateau at  $x'/Tx' = 1.2$ . The peak moves forward to approximately  $x'/Tx' = 1.06$  for  $Re = 1.14$  million/ft. At  $Re = 0.55$  million/ft, the peak pressure is noted at approximately  $x'/Tx' = 0.96$ . Figures 7.2.3.38-7.2.3.39 replot the sidewall data along lines of constant  $x'/Tx'$ . They again demonstrate the overall increase in compression with decreasing Reynolds number.

The Reynolds number effects for the other eight combinations of contraction ratio and cowl position are presented in Figures 7.2.3.54-7.2.3.477. Since the effect of Reynolds number is adequately described in a typical case, the plots for the other configurations are included for reference without further discussion.

## 7.3 Oil Flow Results

Surface streamlines were obtained using oil flow. Prior to the run, a base coat of a low viscosity silicone fluid was applied to the model surface. Discrete dots of a mixture of a higher viscosity oil and white artist's paint were placed on the surface. Figures 7.3.1-7.3.6 are post-run photographs of the oil streaks for three configurations. Figure 7.3.1 shows the interior wall of the inlet (one sidewall and the cowl were removed following the run for the photographs) for a  $CR = 3$ ,  $Re = 2.15$  million/ft, 0% Cowl configuration. Several features are evident. The compression from the boundary layer growth on the leading edge of the baseplate is evident in the lower half of the inlet. A weak feathered pattern is noted just below a line of convergence on the sidewall near the corner, possibly indicating the presence of a vortex. The line of convergence and the stagnant region in the immediate corner are consistent with the induced layer previously discussed. Additionally, since the sidewall shock impinges very near the shoulder, no large scale separation regions are noted in the vicinity of the impingement. A single line of convergence is noted arcing from the baseplate just upstream of the shoulder and may be the only indication of a separation. Multiple lines of convergence (possibly the result of vortices shed from the shock impingement) are noted in the throat downstream of the impingement.

Figure 7.3.2 demonstrates the forward progression of the shock impingement (for  $CR = 5$ ) and the strong downturning/separation associated with the impingement. This photograph more clearly shows the vortex located just below the line of convergence on the sidewall. Additionally, the effects of the baseplate leading edge compression are also evident at about the half-height of the inlet sidewall. Near the cowl plane, the oil streaks indicate strong downturning at the

first impingement point. A second swept line of convergence is noted in the throat at the second sidewall impingement point.

At a contraction ratio of 9, Figures 7.3.3-7.3.6 indicate that the dominant flow feature is the large scale separation on the baseplate. Near the baseplate leading edge, the oil streaks are observed to flow uniformly downstream until approximately  $x'/Tx' = -0.4$ . (This corresponds well with the observed pressure rise on the baseplate at  $x'/Tx' = -0.38$ , Figure 7.2.1.2.) In the immediate vicinity of the sidewall leading edge, the surface streamlines indicate that the flow on the surface is moving upstream and is spilling around the outside of the inlet, as was suggested by the dome shaped CR = 9 pressure distribution at  $x'/Tx' = -0.1$ , Figure 7.2.1.7. As was previously noted, this flow pattern would not be duplicated exactly on a full scale flight vehicle since there would be no lateral pressure relief due to the presence of other identical engine modules on either side of a given module. Due to this lack of a lateral pressure relief this separation would likely be more severe on a flight vehicle.

## **7.4 Surface Temperature Measurements**

The primary objective of the IR measurements is the verification of wall thermal boundary conditions for the computational work. Theoretically, qualitative heat transfer trends may be inferred when a model is injected into a freestream at significant temperature difference. In this case, thermal equilibrium is not achieved, and the surface temperature variation with time within the first seconds following model injection is related to the heat transfer (using the semi-infinite slab theory), as the heat transfer by convection becomes large relative

to the heat transfer by conduction. Gauffre (1988) points out, however, that a great deal of work remains in the calibration of such experiments, particularly for metal models. For the present model, the semi-infinite slab assumption is violated within the first 0.8 second for the 0.75 inch thick baseplate. At the leading edge, where the thickness tends toward zero, the assumptions are violated even sooner. Since the IR system used for the test was hardware limited to capturing 6.25 frames per second, with the capability of storing only one image per second, heat transfer data were not obtained. A surface temperature mapping was obtained, however. The increased heat transfer associated with laminar to turbulent transition may result in a sudden change in axial surface temperature distribution, depending upon the thermophysical properties of the material. If transition were to occur however, it is unlikely that the associated increase in heat transfer rate would be sufficient to overcome the ability of copper to conduct the heat away, thereby diffusing any surface temperature increase. Thus, for the present work, the utility of IR is limited to its principle objective of verification of the wall thermal boundary conditions.

Figures 7.4.1 and 7.4.2 show the temperature time history for the axial centerline of the baseplate from the leading edge of the flat plate to approximately  $x'/Tx' = 0.40$  for a nominal freestream unit Reynolds number of 2.15 and 0.55 million/ft, respectively. It is observed that in each case, the leading edge temperature rises rapidly, but the remaining portion of the plate maintains its nominal pre-injection temperature. While the leading edge heating was not modelled in the CFD, it is observed that for the majority of the baseplate, the assumption of a constant wall temperature distribution was acceptable.

## Explicit Comparison of Computation and Experiment

Chapters 6 and 7 presented the results of the computation and experiment, respectively. In order to assess how well the results from both phases complimented each other, it is necessary to explicitly compare the results. Figures 8.1-8.5 show the comparison between computed and measured compression down the baseplate and sidewall centerlines. The salient features of the flow are captured in the computation, and the quantitative agreement is generally good. For a contraction ratio of 3, Figures 8.1a,b show excellent agreement. The pressure peak at the throat on the baseplate is overpredicted by about 10%, but the sidewall pressure distribution shows an extremely close fit. At the contraction ratio of 5, however, the baseplate pressure (Figure 8.2a) in the throat is overpredicted by as much as 50%, while the pressure rise upstream of the inlet entrance due to the flow separation is not captured. The sidewall centerline pressure distribution (Figure 8.2b) indicates that the rapid pressure rises and declines are predicted in the correct locations, but that the first peak is underpredicted by 25% and the second by 8%, though the local minimums are well predicted in both location and magnitude. At  $CR = 9$  (Figure 8.3a), the computation predicts a more uniformly compressed throat region and misses the peak compression by approximately 13%. Again, the upstream pressure rise due to the baseplate separation is not captured. The sidewall pressures (Figure 8.3b) indicate a qualitative agreement in that the features are predicted in the correct locations, but again the magnitudes are significantly underpredicted. Figures 8.4a and 8.4b correspond to the  $CR = 3$ ,

$Re = 2.15$  million/ft, 50% Cowl configuration. It is noted that good agreement (both qualitatively and quantitatively) is achieved on both the baseplate and sidewall centerlines. For the  $CR = 3$ ,  $Re = 0.55$  million/ft, 0% Cowl configuration (Figures 8.5a,b), however, significantly poorer results are obtained. Not only is the upstream separation significantly underpredicted, the throat pressure distribution is overpredicted. Similarly on the sidewall, the pressure peak at the shoulder due to the forward movement of the shock impingement is missed. Instead, the throat pressure peak is distributed somewhat more uniformly over the entire throat region.

It appears that in weakly interacting regions, the code performs well, predicting both the locations and magnitudes of the interactions. When the interactions become stronger by increasing the contraction ratio or boundary layer thickness (by decreasing the Reynolds number), the code demonstrates poorer agreement in magnitudes. Part of the poorer agreement may lie in the modeling of the flow field. The code computes the entire domain assuming laminar interactions. If in fact the shock boundary layer interactions inside the inlet have caused the interactions to become transitional or turbulent, then differences between measured and predicted pressures would be expected since the assumptions of the model have been violated.

## 8.1 Contour Plot Comparison

In addition to line plots, contour plots are presented for comparison between the computation and experiment. Figures 8.1.1a,b and 8.1.2a,b present the baseplate and sidewall pressure distributions obtained from both computation and



experiment for the  $CR=3$ ,  $Re=2.15$  million/ft, 0% Cowl configuration. The agreement on both the baseplate and sidewalls is quite good. It should be noted that some differences between the computed and measured contours should be expected due to the effect of finite sampling. The computational grid on the sidewall surface provided pressures at 2021 points, compared to 89 static pressure orifices. At the contraction ratio of 5 (Figures 8.1.3a,b and 8.1.4a,b), it is evident that the computed pressure contours show a sharper picture of the location of the shock on the baseplate, primarily due to the grid density. Good qualitative agreement is noted even at the contraction ratio of 9 (Figures 8.1.5a,b and 8.1.6a,b). Both sidewall shock impingements are in good agreement. In fact, the sidewall contour plot indicates a much better agreement throughout the inlet than the single centerline plot showed (i.e., the measured contours show that the measured centerline pressure distribution is in this case not a good indicator of the overall shock reflections). It is again observed for the  $CR=3$ ,  $Re=2.15$  million/ft, 50% Cowl configuration (Figures 8.1.7a,b and 8.1.8a,b) and for the  $CR=3$ ,  $Re=0.55$  million/ft, 0% Cowl configuration (Figures 8.1.9a,b and 8.1.10a,b) that the overall agreement between computed and measured pressure distributions is significantly better than the single centerline pressure distributions indicate. It seems therefore evident conclusions pertaining to how well the flow structure has been captured are better drawn when the comparison is made over the whole flow structure and not over a single array. In this way, the effects of a spurious data are dispersed. Such comparisons of contour plots, however, can lead to incorrect conclusions when the instrumentation density is particularly unfavorable for contour plotting (i.e., when interpolation must be performed over large regions with limited instrumentation).

## 8.2 Exit Plane Rake Data

Figures 8.2.1-8.2.5 present pitot rake data taken in the exit plane of the inlet compared to the computed values. The data principally show the exit plane shock structure; the agreement with the experimental data also provides a validation for the computational data, thereby lending credibility to the other computed flow field variables. Figures 8.2.1 and 8.2.2 are for the  $Re = 2.15$  million/ft, 0% Cowl,  $CR = 3$  and 5 configurations, respectively. Good qualitative as well as quantitative agreement is achieved for these configurations. Near the sidewall, the shape of the experimental contours indicates some interference effects from the sidewall. This is an expected result, since pitot measurements are highly intrusive. Despite the fact that almost half the distance from the sidewall to the centerline is affected by interference effects, the center portion of the  $CR = 9$  data show good agreement with experiment (Figure 8.2.3). For the 50% Cowl configuration (Figure 8.2.4), it is evident that the cowl shock is significantly more pronounced in the experimental data than in the computed. For the low Reynolds number configuration (Figure 8.2.5), the agreement is somewhat better.

Overall, the comparisons of the flow field measured and computed pitot pressures are quite good. This lends credence to the remainder of the computed exit plane properties. Figures 8.2.6-8.2.30 present the rake data for the configurations for which no computed data were available. Since the data are significantly similar to those just discussed, the plots are included here for reference without further discussion.

### 8.3 Entrance Plane Rake Data

An 11 probe pitot rake was installed at the inlet entrance station on the outboard side of the sidewalls. The rake was made from stainless steel tubing with a 0.020 inch ID and 0.040 inch OD. The tubes were internally beveled and vertically compressed to an internal vertical gap of 0.010 inch. The 11 tubes spanned 1.5 inches and were on 0.15 inch centers. Figure 8.3.1 shows the comparison between CFD and experiment for a  $CR = 3$ ,  $Re = 2.15$  million/ft, 0% Cowl configuration. The CFD appears to underpredict the boundary layer thickness, since the experimental total pressure distribution is significantly lower, especially near the wall. The CFD also shows a more significant influence of the weak leading edge compression in the  $Z/\delta \sim 2$  region. This irregularity is likewise reflected in the Mach number profiles, Figure 8.3.2. Figure 8.3.3 shows a well developed velocity boundary layer. Figure 8.3.4 shows a typical cold wall thermal boundary layer, with a temperature bulge due to viscous dissipation increasing the maximum temperature in the boundary layer by 30% over the wall temperature. Figures 8.3.5 - 8.3.8 present the same plots for the  $CR = 3$ ,  $Re = 0.55$  million/ft, 0% Cowl configuration, and similar results are noted.

## **Conclusions**

Since careful design of primary engine components such as the inlet is necessary to exploit effectively the potential of propulsion-airframe integration, a combined computational and experimental parametric study of the internal aerodynamics of a generic three-dimensional sidewall compression scramjet inlet configuration has been performed. The study was designed to demonstrate the utility of computational fluid dynamics as a design tool in hypersonic inlet flow fields, to provide a detailed account of the nature and structure of the internal flow interactions, and to provide a comprehensive surface property and flow field database to determine the effects of contraction ratio, cowl position, and Reynolds number on the performance of a hypersonic scramjet inlet configuration. The work proceeded in several phases: the initial inviscid assessment of the internal shock structure, the preliminary computational parametric study, the coupling of the optimized configuration with the physical limitations of the facility, the wind tunnel blockage assessment, and the computational and experimental parametric study of the final configuration.

A modification to two-dimensional oblique shock theory was derived to accommodate the three-dimensional effects of leading edge sweep. It was found that the effect of sweep was to impart a downward component to the flow. This component was increased as the flow passed through each of the reflected shocks. When the cowl was located in an aft position, this downturned flow spilled from the inlet. This spillage is important in helping the inlet start at lower Mach numbers. Further, the shock induced spillage also provides a variable geometry quality to the

fixed geometry inlet in that, as the Mach number is increased, the area (in the plane of the cowl) behind the shock sheets is decreased, since the shocks lie closer to the sidewalls. This reduces the spillage (and increases the mass capture) by partially closing the spillage window, making the inlet more efficient at high Mach numbers. It is these characteristics which make it possible to consider a fixed geometry inlet for use over a wide Mach number range.

A computational parametric study was then performed to identify inlet characteristics pertinent to the optimization of the configuration; this was therefore, in a sense, a trade off study of leading edge sweep and cowl position. Since instrumented wind tunnel models are quite expensive, CFD was utilized to minimize the costs of fabrication by eliminating from consideration designs which promise poor performance. The primary interest was in the variation of the performance parameters of mass capture, throat Mach number, total pressure recovery, and internal compression with leading edge sweep (varied between  $0^\circ$  and  $60^\circ$ ) and cowl position (located at the throat and at two forward positions). It was found that, compared to the unswept configuration, the inlet sidewalls may be swept by up to  $30^\circ$  without adversely affecting the inlet performance. The introduction of sweep also had the added benefits of enhancing the low Mach number starting performance (via swept shock induced spillage) and decreasing the aerothermal loading on the inlet leading edges. The mass capture was found to decrease with increasing sidewall leading edge sweep due to the increase in flow downturning. Forward placement of the cowl was observed to increase the mass capture by preventing the flow from spilling out. While the forward cowl position tended to increase the average compression of the inlet exit plane due to the cowl lip shock, it did so at the cost of additional flow nonuniformity and decreased total pressure recovery. The 60 degree configuration showed a significantly lower mass

capture and internal compression than the 45 degree configuration but had a much higher total pressure recovery. To maintain the same geometric contraction ratio, an increase in leading edge sweep necessarily requires an increase in length (and hence weight), an undesirable quality for an engine component. The 45 degree configuration had nearly the same mass capture and internal compression as the 30 degree configuration with a 5-7 percent improvement in total pressure recovery. From consideration of the trade off of mass capture, total pressure recovery, and internal compression, the optimum leading edge sweep angle was determined to be 45°.

Once the configuration was established, it was necessary to couple the model design requirements with the physical constraints of the facility. In order to increase the instrumentation density on the model, it was desirable to make the model as large as possible. When the cross-sectional area of the model becomes large relative to the inviscid core size of the facility, the effects of wind tunnel blockage must be assessed. A blockage model (an inexpensive, much less densely instrumented version of the configuration) was designed and tested. The results of the study indicated that, based on pitot pressure measurements and tunnel wall static pressures, the tunnel remained started for the duration of each run; additionally, these data indicated no evidence of tunnel blockage due to the presence and orientation of the inlet model. Static pressure distributions inside the inlet also indicated that the inlet started for each of the test configurations.

With the configuration (and its sizing relative to the facility) established, CFD was again employed to provide a detailed examination of the internal flow characteristics. It was found that, while the salient features of the internal shock reflections were predicted by the inviscid calculations, the interaction of the internal shocks with the baseplate and sidewall boundary layers affected a

significant segment of the flow. The principle effect of the swept shock glancing across the baseplate boundary layer was observed to be an induced crossflow. When the sidewalls were located sufficiently far apart, the crossflow velocity was damped significantly before reaching the centerline, and the flow was observed to remain attached up to the glancing shock/centerline intersection. When the sidewalls were brought closer together (increased contraction ratio), the crossflow velocity near the centerline well upstream of the glancing shock location was observed to be nonzero. The crossflow which collided at the centerline formed recirculation regions which were strengthened by the continued reflections of the internal shocks. The vortical regions were observed to occupy a significant percentage of the exit plane (up to 25%) and were typically lower in static pressure, pitot pressure, and Mach number than the core flow. Large regions of crossflow separations were observed on the baseplate, but axial separation was observed only in the vicinity of the shock/centerline intersection. These crossflow interactions appeared to serve as a buffer between the baseplate and the glancing shocks in the core. For this reason, it can be concluded that for high speed three-dimensional inlet interactions, the surface property measurements on the baseplate would not be expected to well represent the flow field interactions. Simulated oil flows generated for the baseplate and sidewalls did, however, indicate the induced layer corner interaction and the location of the sidewall impingements. A small region of streamwise separation was found to accompany the sidewall impingement lines, which were also swept at the leading edge sweep angle, indicating that the sweep was preserved through the repeated shock reflections. In the vicinity of the cowl plane ( $Z/H = 1.0$ ), the downturning of the flow was observed to be more severe as the compressed post-glancing shock flow expanded out the bottom of the inlet into the lower pressure freestream.

The cowl shock was observed to be obscured and dispersed by the crossing shocks. While the 50% Cowl configuration had the greatest potential to influence the exit plane (simply due to the fact that the inviscid cowl shock would be expected to reach farther into the exit plane), it encountered more glancing shock interactions which tended to cancel out this effect. On the other hand, the 0% Cowl was observed to generate a stronger shock due to a stronger local downturning at the cowl leading edge, and, though it did not reach as far up into the inlet at the exit plane, the cowl shock encountered fewer reflected shocks. The combination of these effects led to the conclusion that the forward cowl has a smaller impact on the exit plane than expected. The principle benefit of the cowl forward configuration was the increased mass capture.

The principle effect of a decrease in Reynolds number was a forward movement of the shock impingement lines due to the increased displacement of the sidewall boundary layers. The increased shock strength yielded a decrement in total pressure recovery and related parameters. A modest increase in average compression was noted. The decrease in Reynolds number from 2.15 million/ft to 0.55 million/ft caused the first shock impingement location move from slightly aft of the throat shoulder to slightly ahead of the throat. This produced a decrease in mass capture for the 0% Cowl since the downturning at the shock impingement line occurred ahead of the cowl and hence spilled from the inlet.

Comparisons of the voluminous experimental data with the computed flow field indicated generally good agreement for each of the five computed configurations, particularly for configurations which exhibited no significant axial separation. It was found that comparison of the contour plots provided a clearer indication of the phenomena captured by the calculation. A significant separation on the baseplate was observed to feed forward of the inlet entrance for contraction



ratios of 5 and 9. Surface streamlines (oil flows) near the entrance of the inlet indicated significant reverse flow as the flow spilled around the inlet sidewalls. Measured pressures in front of the inlet entrance showed a dome shaped pressure distribution for the higher contraction ratios, indicating the lateral pressure relief as the flow spilled around the sidewalls.

It appears that in weakly interacting regions, the code performs well, predicting both the locations and magnitudes of the interactions. When the interactions become stronger by increasing the contraction ratio or boundary layer thickness (by decreasing the Reynolds number), the code demonstrates poorer agreement in magnitudes. Thus, for the contraction ratio of 3, where such separation does not exist, the code provides good quantitative as well as qualitative agreement. Good agreement is also obtained between the computed and measured pitot distribution in the exit plane. The code's ability to provide good qualitative (and for most cases quantitative) agreement between the computed and experimental data lends credence to the computed internal interactions. The salient features of this complicated flow field are observed to be well predicted.

The three-dimensional sidewall compression inlet affords a relatively simple, generic geometry, while producing a highly complex flow field dominated by shock/shock and shock/boundary layer viscous interactions. Though studies of individual interactions such as corner flow or shock/boundary layer interactions are quite useful to a fundamental understanding of the flow physics, the results of the present work indicate that, due to the strong effects of the induced crossflows and their interactions at the centerline, the inlet flow field cannot adequately be addressed as a superposition of its individual interactions.

# References

- Anderson, G. Y.(1974): An Examination of Injector/Combustor Design Effects on Scramjet Performance. Presented at the 2nd International Symposium on Air Breathing Engines, Sheffield, England, March 25-29, 1974.
- Anderson, J. D., Jr.(1982): Modern Compressible Flow. McGraw-Hill Book Co., 1982.
- Batcho, P. F., Ketchum, A. C., Bogdonoff, S. M., and Fernando, E. M.(1989): Preliminary Study of the Interactions Caused by Crossing Shock Waves and a Turbulent Boundary Layer. 27th Aerospace Sciences Meeting, Reno, NV, January 9-12, 1989, AIAA-89-0359.
- Batham, J. P.(1972): An Experimental Study of Turbulent Separating and Reattaching Flows at a High Mach Number. J. Fluid Mechanics, Vol. 52, Pt. 3, April 1972, pp. 425-435.
- Bogdonoff, Seymour M.(1985): Three-Dimensional Shock Wave and Turbulent Boundary Layer Interactions. MAE Report 1723(Princ. Univ.), Sept. 1985, AFOSR-TR-85-1242. (N86-31010).
- Carlson, Charles H.(1983): Preliminary Scramjet Design for Hypersonic Airbreathing Missile Application. NASA CR-3742, Nov. 1983.
- Charwat, A. F., and Redekeopp, L. G.(1967): Supersonic Interference Flow along the Corner of Intersecting Wedges. AIAA Journal, Vol. 5, No. 3, March 1967.
- Clausen, R. D., and King, P. I.(1990): A Computational Model for Thickening Boundary Layers with Mass Addition for Hypersonic Engine Inlet Testing. AIAA/SAE/ASME/ASEE 26th Joint Propulsion Conference, July 16-18, 1990, Orlando, FL, AIAA-90-2219.
- Committee on Extension to the Standard Atmosphere(1976): U.S. Standard Atmosphere, 1976. Government Printing Office, Washington, D.C.
- Cooper, James R. and Hankey, Wilbur L., Jr.(1973): Flow Field Measurements in an Asymmetric Axial Corner at  $M=12.5$ . AIAA 6th Fluid and Plasma Dynamics Conference, Palm Springs, CA, July 16-18, 1973, AIAA-73-676.
- Daryabeigi, Kamran, Alderfer, David, and Borg, Stephen (1991): Wind Tunnel and Flight Flow Visualization Using Infrared Imaging. Presented at the 37th ISA International Instrumentation Symposium, May 5-9, 1991, San Diego, CA.

- Degrez, G., and Ginoux, J. J.(1983): Three-Dimensional Skewed Shock Wave Laminar Boundary Layer Interaction at Mach 2.25. AIAA 16th Fluid and Plasma Dynamics Conference, Danvers, MA, July 12-14, 1983. AIAA-83-1755.
- Dillon, James L., Marcum, Don C., Jr., Johnston, Patrick J., and Hunt, James L.(1981): Aerodynamic and Inlet Flow Characteristics of Several Hypersonic Airbreathing Missile Concepts. J. Aircraft, Vol. 18, No. 4, April 1981, pp. 231-237.
- Dolling, D. S.(1984): Effects of Mach Number on Upstream Influence in Sharp Fin Induced Shock Wave Turbulent Boundary Layer Interaction, AIAA 22nd Aerospace Sciences Meeting, January 9-12, 1984, Reno, NV, AIAA-84-0095.
- Dolling, D. S., and Bogdonoff, S. M.(1983): Upstream Influence in Sharp Fin-Induced Shock Wave Turbulent Boundary Layer Interaction. AIAA Journal, Vol. 21, No. 1, Jan. 1983, pp. 143-145.
- Dugger, G. L.(1960): "Comparison of Hypersonic Ramjets with Subsonic and Supersonic Combustion," Fourth AGARD Colloquium, Milan, Italy; also Combustion and Propulsion-High Mach Number Air Breathing Engines, Edited by Jaumotte, Rothrock, and Le Febvre, Pergamon Press, NY, 1960.
- Dutton, J. C., and Carroll, B. F.(1988): Numerical and Experimental Investigation of Multiple Shock Wave/Turbulent Boundary Layer Interactions in a Rectangular Duct. Department of Mechanical and Industrial Engineering, University of Illinois at Urbana-Champaign, UILU ENG-88-4401, January, 1988. N88-22320.
- Edwards, C. L. W.(1976): A Forebody Design Technique for Highly Integrated Bottom-Mounted Scramjets with Application to a Hypersonic Research Airplane. NASA TN-D-8369, Dec. 1976. (Also NASA TM X-71971, Nov. 1974.)
- Erdoes, J., and Pallone, A.(1962): Shock Boundary Layer Interaction and Flow Separation. From Proceedings of the 1962 Heat Transfer and Fluid Mechanics Institute, pp. 239-254, printed by Stanford University Press, Stanford, CA, 1962.
- Elfstrom, G. M.(1972): Turbulent Hypersonic Flow at a Wedge-Compression Corner. J. Fluid Mechanics, Vol.53, Pt.1, May 1972, pp. 113-127.
- Fletcher, C. A. J. (1988): Computational Techniques for Fluid Dynamics 2, Specific Techniques for Different Flow Categories. Springer Series in Computational Physics, Springer-Verlag Berlin.
- Gary, J. D., and Rhudy, R. W.(1970): Investigation of Flat-Plate Aspect Ratio Effects on Ramp-Induced, Adiabatic, Boundary Layer Separation at Supersonic and Hypersonic Speeds. AEDC-TR-70(235), March 1971, Arnold Engineering Development Center, Tullahoma, TN. 71N-24744.

- Gauffre, G.(1988): Detection of Laminar-Turbulent Transition by Infrared Thermography. Rech. Aérosp. No. 1988-2, pp.12-22.
- Gessner, F. B., Ferguson, S. D., and Lo, C. H.(1987): Experiments on Supersonic Turbulent Flow Development in a Square Duct. AIAA Journal, Vol. 25, No. 5, May 1987, pp.690-697.
- Goldberg, Theodore J.(1973): Three-Dimensional Separation for Interaction of Shock Waves with Turbulent Boundary Layers. AIAA Journal, Vol. 11, No. 11, Nov. 1973, pp. 1573-1575.
- Gregory, T. J., Wilcox, D. E., and Williams, L. J.(1967): The Effects of Propulsion System-Airframe Interactions on the Performance of Hypersonic Aircraft. AIAA-67-493, 1967.
- Henry, John R., and Anderson, Griffin Y.(1973): Design Considerations for the Airframe-Integrated Scramjet. NASA TM X-2895, Dec. 1973.
- Henry, J. R., and McLellan, C. H.(1971): Air-Breathing Launch Vehicle for Earth-Orbit Shuttle--New Technology and Development Approach. J. Aircraft, Vol. 8, No. 5, May 1971, pp. 381-387.
- Holden, M. S.(1978): A Study of Flow Separation in Regions of Shock Wave-Boundary Layer Interaction in Hypersonic Flow. AIAA 11th Fluid and Plasma Dynamics Conference, Seattle, WA, July 10-12, 1978, AIAA-78-1169.
- Holland, S. D., and Perkins, J. N.(1990): Mach 6 Testing of Two Generic Three-Dimensional Sidewall Compression Scramjet Inlets in Tetrafluoromethane. AIAA 28th Aerospace Sciences Meeting, January 8-11, 1990, Reno, NV, AIAA-90-0530.
- Holland, S. D., Hodge, J. S., and Perkins, J. N.(1991): Wind Tunnel Blockage Study of a Generic Three-Dimensional Sidewall Compression Scramjet Inlet at Mach 10. AIAA 29th Aerospace Sciences Meeting, Reno, NV, January 7-10, 1991, AIAA-91-0294.
- Hunt, J. L., Johnston, P. J., Cabbage, J. M., Dillon, J.L., Richie, C. B., Marcum, D. C., Jr., and Carlson, C. H.(1982): Hypersonic Airbreathing Missile Concepts Under Study at Langley. AIAA 20th Aerospace Sciences Meeting, Jan. 11-14, 1982, Orlando, FL, AIAA-82-0316.
- Hunt, J. L., Johnston, P. J., and Riebe, G. D.(1983): Flow Fields and Aerodynamic Characteristics for Hypersonic Missiles with Mid-Fuselage Inlets. AIAA 21st Aerospace Sciences Meeting, Jan. 10-13, 1983, Reno, NV, AIAA-83-0542.
- Hunt, J. L., Lawing, D. C. Marcum, and Cabbage, J. M.(1978): Conceptual Study of Hypersonic Airbreathing Missiles. AIAA 16th Aerospace Sciences Meeting, Huntsville, AL, Jan. 16-18, 1978. AIAA 78-6.

- Johnston, P. J., Cubbage, J. M., and Weidner, J. P.(1971): Studies of Engine-Airframe Integration on Hypersonic Aircraft. *J. Aircraft*, Vol. 8, No. 7, July 1971, pp.495-501.(Also AIAA Paper 70-542.)
- Johnston, P. J., and Hunt, J. L.(1984): Mach 6 Flow-Field and Boundary Layer Surveys Beneath the Forebody of an Airbreathing Missile. *AIAA 22nd Aerospace Sciences Meeting*, Jan. 9-12, 1984, Reno, NV, AIAA-84-0233.
- Kanda, T., Komuro, T., Masuya, G., Kudo, K., Murakami, A., Tani, K., Wakamatsu, Y., and Chinzei, N.(1989): Mach 4 Testing of Scramjet Inlet Model. *AIAA/ASME/SAE/ASEE 25th Joint Propulsion Conference*, Monterey, CA, July 10-12, 1989, AIAA-89-2680.
- Kandebo, Stanley W.(1988): "Researchers Pursue X-30 Spaceplane Technologies for 1990 Evaluation." *Aviation Week and Space Technology*, August 8, 1988, pp.49-53.
- Keith, J. S., Kutschenreuter, P. H., Jr., and Nettleton, P. H.(1965): Investigation of Hypersonic Inlet Shock-Wave Boundary Layer Interaction. *AFFDL-TR-65-36*. (N65-26443).
- Korkegi, Robert H.(1971): Survey of Viscous Interactions Associated with High Mach Number Flight. *AIAA Journal*, Vol. 9, No. 5, May 1971, pp. 771-784.
- Korkegi, R. H.(1973): A Simple Correlation for Incipient Turbulent Boundary-Layer Separation due to a Skewed Shock Wave. *AIAA Journal*, Vol. 11, No. 11, Nov. 1973, pp.1578-1579.
- Korkegi, R. H.(1975): Comparison of Shock-Induced Two- and Three Dimensional Incipient Turbulent Separation. *AIAA Journal*, Vol. 13, No. 4, April 1975.
- Kubota, H., and Stollery, J. L.(1982): An Experimental Study of the Interaction Between a Glancing Shock Wave and a Turbulent Boundary Layer. *Journal of Fluid Mechanics*, Vol. 116, pp. 431-458, March 1982.
- Kumar, A.(1982): Three-Dimensional Inviscid Analysis of the Scramjet Inlet Flow Field. *AIAA 20th Aerospace Sciences Meeting*, Orlando, FL, Jan. 11-14, 1982. AIAA-82-0060.
- Kumar, A.(1985): Numerical Simulation of Flow Through Scramjet Inlets Using a Three-Dimensional Navier-Stokes Code. *AIAA 18th Fluid Dynamics and Plasmadynamics and Lasers Conference*, July 16-18, 1985. AIAA-85-1664.
- Kumar, Ajay(1986): Numerical Simulation of Scramjet Inlet Flow Fields. *NASA TP-2517*, May 1986.
- Kumar, Ajay, and Trexler, Carl A.(1988): Analysis and Performance of Scramjet Inlets Utilizing a Three-Dimensional Navier-Stokes Code. 88N14936, In *Langley Symposium on Aerodynamics*, Vol. 1, pp.187-208, avail. 88N14926.

- Kumar, Ajay, Singh, D. J., and Trexler, C. A.(1990): A Numerical Study of the Effects of Reverse Sweep on a Scramjet Inlet Performance. Presented at the AIAA/SAE/ASME/ASEE 26th Joint Propulsion Conference, Orlando, FL, July 16-18, 1990, AIAA-90-2218.
- Kutschenreuter, Paul, H., Jr., Brown, David L., and Hoelmer, Werner(1965): Investigation of Hypersonic Inlet Shock-Wave Boundary Layer Interaction. Part II. Continuous Flow Test Analyses. AFFDL-TR-65-36, Contract AF33(657)-11747, General Electric Co., Evendale, Ohio.
- Law, C. Herbert(1974): Supersonic, Turbulent Boundary-Layer Separation. AIAA Journal, Vol. 12, No. 6, June 1974, pp. 794-797.
- Lu, F., and Settles, G. S.(1983): Conical Similarity of Shock Boundary Layer Interactions Generated by Swept Fins. AIAA-83-1756, July 1983.
- MacCormack, Robert W.(1969): The Effect of Viscosity in Hypervelocity Impact Cratering. AIAA Hypervelocity Impact Conference, April 30 - May 2, 1969, AIAA-69-354.
- Materials Selector(1974), Materials Engineering, Mid-September 1973, Vol. 78, No. 4, Reinhold Publishing Company, Inc.
- McCabe, A.(1966): The Three-Dimensional Interaction of a Shock Wave with a Turbulent Boundary Layer. The Aeronautical Quarterly, Vol. 17, Pt. 3, August 1966, pp. 231-252.
- Mee, D. J, Stalker, R. J., and Stollery, J. L.(1986): Glancing Interactions Between Single and Intersecting Oblique Shock Waves and a Turbulent Boundary Layer. Journal of Fluid Mechanics, Vol. 170, pp. 411-433, 1986.
- Mee, D. J., and Stalker, R. J.(1987): Investigation of Weak Shock-Shock and Shock-Expansion Intersection in the Presence fo a Turbulent Boundary Layer. AIAA 25th Aerospace Sciences Meeting, Reno, NV, Jan. 12-15, 1987, AIAA-87-0549.
- Meyer, R. F.(1966): A Note on a Technique of Surface Flow Visualisation. National Research Council of Canada Aeronautical Report LR-457.
- Miller, C. G.(1990): Langley Hypersonic Aerodynamic/Aerothermodynamic Testing Capabilities - Present and Future. AIAA 16th Aerodynamic Ground Testing Conference, June 18-20, 1990, Seattle, WA, AIAA-90-1376.
- Miller, C. G.(1984): Experimental and Predicted Heating Distributions for Biconics at Incidence in Air at Mach 10. NASA-TP-2334, 1984.
- Narayanswami, N., Knight, D., Bogdonoff, S. M., and Horstman, C. C.(1991): Crossing Shock Wave-Turbulent Boundary Interactions. 29th Aerospace Sciences Meeting, Reno, NV, January 7-10, 1991, AIAA-91-0649.

- Neumann, R. D., and Token, K. H.(1975): Prediction of Surface Phenomena Induced by Three-Dimensional Interactions on Planar Turbulent Boundary Layers. Paper 74-058, International Astronautical Federation XXV Congress, Amsterdam, The Netherlands, Oct. 1974. Avail. A75-13703.
- Om, D., and Childs, M. E.(1983): An Experimental Investigation of Multiple Shock Wave/Turbulent Boundary Layer Interactions in a Circular Duct. AIAA 16th Fluid and Plasma Dynamics Conference, Danvers, MA, July 12-14, 1983, AIAA-83-1744.
- Peyret, Roger, and Taylor, Thomas (1983): Computational Methods for Fluid Flow, Springer Series in Computational Physics, Springer-Verlag New York.
- Roberts, Glyn O.(1970): Computational Meshes for Boundary Layer Problems. Proceedings of the Second International Conference on Numerical Methods in Fluid Dynamics. Lecture Notes in Physics, Volume 8, Maurice Holt, ed., Sept. 15-19, 1970, pp.171-177.
- Sajben, M., Bogar, T. J., and Kroutil, J. C.(1984): Forced Oscillation Experiments in Supercritical Diffuser Flows. AIAA Journal, Vol. 22, No. 4, April 1984, pp.465-474.
- Sekar, B., Thomas, S., and Srinivasan, S.(1990): A Numerical Parametric Study of a Scramjet Inlet in a Mach 6 Arc Heated Test Facility. 28th Aerospace Sciences Meeting, Reno, NV, Jan. 8-11, 1990, AIAA-90-0531.
- Settles, Gary S., and Bogdonoff, Seymour M.(1982): Scaling of Two- and Three-Dimensional Shock/Turbulent Boundary-Layer Interactions at Compression Corners. AIAA Journal, Vol. 20, No.6, pp.782-789, June 1982, Article No. 81-0334R.
- Settles, G. S., and Dolling, D. S.(1990): Swept Shock/Boundary Layer Interactions - tutorial and Update. 28th Aerospace Sciences Meeting, Jan. 8-11, 1990, Reno, NV, AIAA-90-0375.
- Small, William J., Weidner, John P., and Johnston, P. J.(1976): Scramjet Nozzle Design and Analysis as Applied to a Highly Integrated Hypersonic Research Airplane. NASA TN D-8334, Nov. 1976 (also previously NASA-TM-X-71972, Nov. 1974).
- Smith, R. E.(1981): Two-boundary Grid Generation for the Solution fo the Three-Dimensional Compressible Navier-Stokes Equations. Ph.D. Dissertation, Old Dominion University, 1981. Also NASA TM-83123, May 1981.
- Srinivasan, S., McClinton, C. R., and Kamath, P. S.(1989): Numerical Simulation of Flow Through the Langley Parametric Scramjet Engine. SAE Aerospace Technology Conference and Exposition, Anaheim, CA, September 25-28, 1989, SAE-892314.

- Stainback, P. Calvin(1960): An Experimental Investigation at a Mach Number of 4.95 of Flow in the Vicinity of a 90 deg Interior Corner Alined with the Free-Stream Velocity. NASA TN D-184, Feb. 1960.
- Stainback, P. Calvin(1964): Heat-Transfer Measurements at a Mach Number of 8 in the Vicinity of a 90 deg Interior Corner Alined with the Free-Stream Velocity. NASA TN D-2417, August 1964.
- Stainback, P. Calvin, and Weinstein, Leonard M.(1967): Aerodynamic Heating in the Vicinity of Corners at Hypersonic Speeds. Dec. 1967, NASA TN D-1014, 1967.
- Sterret, J. R., and Emery, J. C.(1962): Experimental Separation Studies for Two-Dimensional Wedges and Curved Surfaces at  $M=4.8$  to 6.2. NASA TN-D-1014, 1962.
- Tauber, M. E.(1990): A Brief Review of Some Mechanisms Causing Boundary Layer Transition at High Speeds. June 1990, NASA-TM-102834.
- Taylor, Angus E., and Mann, W. Robert(1983): *Advanced Calculus*. Third edition, John Wiley and Sons, Inc., New York.
- Trexler, Carl A.(1974): Performance of an Inlet for an Integrated Scramjet Concept. J. Aircraft, Vol. 11, No. 9, September 1974.
- Trexler, Carl A.(1975): Inlet Performance of the Integrated Langley Scramjet Module (Mach 2.3 to 7.6), AIAA/SAE 11th Propulsion Conference, Sept. 29-Oct.1, 1975, Anaheim, CA, AIAA-75-1212.
- Trexler, Carl A.(1988a): Tests of Two Sidewall-Compression Scramjet Inlets at Mach 18.1 to 21.6 in Helium. National Aero-Space Plane Technology Report, February, 1988.
- Trexler, Carl A., and Souders, Sue W.(1975): Design and Performance at a Local Mach Number of 6 of an Inlet for an Integrated Scramjet Concept. NASA TN D-7944, August 1975.
- Trexler, Carl A.(1988b): Inlet Starting Predictions for Sidewall-Compression Scramjet Inlets. AIAA/SAE/ASME/ASEE 24th Joint Propulsion Conference, July 11-13, 1988, Boston, MA. AIAA-88-3257.
- Vinogradov, V., Stepanov, V., and Alexadrovich, E.(1989): Numerical and Experimental Investigation of Airframe-Integrated Inlet for High Velocities. AIAA/ASME/SAE/ASEE 25th Joint Propulsion Conference, Monterey, CA, July 10-12, 1989, AIAA-89-2679.
- Waltrup, Paul J.(1986): Liquid Fueled Supersonic Combustion Ramjets: A Research Perspective of the Past, Present, and Future. AIAA 24th Aerospace Sciences Meeting, Jan. 6-9, 1986, Reno, NV, AIAA-86-0158.



- Watson, Ralph D., and Weinstein, Leonard M.(1971): A Study of Hypersonic Corner Flow Interactions. AIAA Journal, Vol. 9, No. 7, July 1971.
- White, M. E., Drummond, J. P., and Kumar, A.(1987): Evolution and Application of CFD Techniques for Scramjet Applications. AIAA Journal of Propulsion and Power, Vol. 3, No. 5, Sept.-Oct., 1987, pp. 423-439. (Also AIAA-86-0160).
- Williams, R. M.(1986): National Aero-Space Plane: Technology for America's Future. Aerospace America, November 1986, p. 18.
- Yanta, William J., Collier, Arnold S., Spring, W. Charles, III, Boyd, Christopher F., McArthur, J. Craig(1988): Experimental Measurements of the Flow in a Scramjet Inlet at Mach 4. AIAA 26th Aerospace Sciences Meeting, Jan. 11-14, 1988, Reno, NV, AIAA-88-0271.
- Zheng, Chingfa (1988): Study of Experimental Technique of Oil Flow with Emphasis on Quantitative Determination of the Flow Position Parameters on the Surface. NASA-TT-20341 (Translation of document originally published in Acta Aerodynamica Sinica, Vol. 5, Dec. 1987, pp.383-389).

## Appendix A: Code Overview

The demand for a more detailed and more accurate knowledge of fluid flow fields has driven both experimental and computational fluid dynamicists to increasingly more innovative approaches. The past two decades have brought tremendous advances in numerical methods and in computer hardware development which have created an enhanced capability for calculating increasingly more complicated flow fields. The three dimensional Reynolds-averaged Navier-Stokes code of Kumar (1985) is adapted to perform a parametric study to identify a promising design, thereby minimizing the cost of fabricating and testing models which yield inferior performance.

### A.1 The Governing Equations

The governing equations for a viscous, compressible, heat conducting fluid are the Navier-Stokes equations. This set of equations includes the continuity equation, the x, y, and z momentum equations, and the energy equation, though historically only the momentum equations were identified as the Navier-Stokes equations, derived independently by the Frenchman Claude Louis M. H. Navier in 1827 and the Englishman George Stokes in 1845. These five equations can be written concisely in vector notation as

$$\frac{\delta U}{\delta t} + \frac{\delta F}{\delta x} + \frac{\delta G}{\delta y} + \frac{\delta H}{\delta z} = 0 \quad [A.1.1]$$

where

$$U = \begin{Bmatrix} \rho \\ \rho u \\ \rho v \\ \rho w \\ E_t \end{Bmatrix}$$

$$F = \begin{Bmatrix} \rho u \\ \rho u^2 + p - \tau_{xx} \\ \rho uv - \tau_{xy} \\ \rho uw - \tau_{xz} \\ (E_t + p)u - u\tau_{xx} - v\tau_{xy} - w\tau_{xz} + q_x \end{Bmatrix}$$

$$G = \begin{Bmatrix} \rho v \\ \rho uv - \tau_{xy} \\ \rho v^2 + p - \tau_{yy} \\ \rho vw - \tau_{yz} \\ (E_t + p)v - u\tau_{xy} - v\tau_{yy} - w\tau_{yz} + q_y \end{Bmatrix}$$

$$H = \begin{Bmatrix} \rho w \\ \rho uw - \tau_{xz} \\ \rho vw - \tau_{yz} \\ \rho w^2 + p - \tau_{zz} \\ (E_t + p)w - u\tau_{xz} - v\tau_{yz} - w\tau_{zz} + q_z \end{Bmatrix} .$$

Here,  $E_t$  is the total internal energy per unit volume and is given by:

$$E_t = \rho \{ c_v T + (u^2 + v^2 + w^2)/2 \} . \quad [A.1.2]$$

Additionally, the heat flux and stress terms in the above are given by the following:

$$\begin{aligned} \tau_{xx} &= 2\mu \left[ \frac{\delta u}{\delta x} - \frac{\Delta}{3} \right] \\ \tau_{yy} &= 2\mu \left[ \frac{\delta v}{\delta y} - \frac{\Delta}{3} \right] \\ \tau_{zz} &= 2\mu \left[ \frac{\delta w}{\delta z} - \frac{\Delta}{3} \right] \end{aligned} \quad [A.1.3]$$

$$\tau_{xy} = \tau_{yx} = \mu \left[ \frac{\delta u}{\delta y} + \frac{\delta v}{\delta x} \right]$$

$$\tau_{xz} = \tau_{zx} = \mu \left[ \frac{\delta u}{\delta z} + \frac{\delta w}{\delta x} \right]$$

$$\tau_{yz} = \tau_{zy} = \mu \left[ \frac{\delta w}{\delta y} + \frac{\delta v}{\delta z} \right]$$

$$q_x = -k \frac{\delta T}{\delta x}$$

$$q_y = -k \frac{\delta T}{\delta y}$$

$$q_z = -k \frac{\delta T}{\delta z}$$

where

$$\Delta = \frac{\delta u}{\delta x} + \frac{\delta v}{\delta y} + \frac{\delta w}{\delta z}$$

$$\mu = \mu_\ell$$

$$k = c_p \left[ \frac{\mu_\ell}{Pr_\ell} \right] .$$

The laminar viscosity coefficient  $\mu_\ell$  is given as a function of temperature by Sutherland's law:

$$\mu_\ell = 1.458 \times 10^{-6} * T^{1.5} / (110. + T) . \quad [A.1.4]$$

Thus, there are five coupled partial differential equations to solve for seven unknowns:  $\rho$ ,  $u$ ,  $v$ ,  $w$ ,  $e$ ,  $T$ ,  $p$ . The two remaining required equations may be obtained from the state relations among thermodynamic variables. For a fluid with

non-changing composition (i.e. no diffusion or finite-rate chemistry), the thermodynamic state is fixed by any two independent thermodynamic variables, so that the two needed equations may be of the form:

$$p = p(e, \rho) \quad \text{and} \quad T = T(e, \rho) . \quad [\text{A.1.4}]$$

The equation of state for a perfect gas is

$$p = \rho RT , \quad [\text{A.1.5}]$$

where  $R$  is the gas constant. Additionally, for a calorically perfect gas,

$$e = c_v T , \quad [\text{A.1.6}]$$

where  $c_v$  is the specific heat at constant volume. The equations as given above form a complete set which is solvable in conjunction with a compatible set of boundary conditions.

## A.2 Transforming the Governing Equations

The governing equations have been presented in Cartesian coordinates. It is often desirable, however, to cluster the grid points in the physical domain. Reducing the grid spacing in regions of strong gradients, such as in the boundary layer where viscous forces are large, allows the code to accurately resolve the rapidly changing flow field. Computing on an irregularly spaced Cartesian grid often introduces numerical difficulties. For example, the maximum allowable time step for stability is limited for the entire grid by the minimum mesh spacing. Additionally, application of the boundary conditions for an irregularly spaced

boundary on a Cartesian mesh is inexact due to the interpolation errors which occur when the boundary falls between mesh points. To avoid these difficulties, the governing equations are transformed from the physical domain  $(x,y,z)$  with non-uniform spacing to a uniformly spaced computational domain  $(\xi,\eta,\zeta)$  by a body-fitted coordinate transformation. A general transformation of the governing equations is presented, and the transformed equations are then returned to conservation-law form.

### A.2.1 A General Coordinate Transformation

The physical domain and the computational domain are related through a unique, single-valued transformation (or mapping) which has continuous derivatives such that if  $(x,y,z)$  represents the physical domain and  $(\xi,\eta,\zeta)$  represents the computational domain:

$$\begin{aligned}\xi &= \xi(x,y,z) \\ \eta &= \eta(x,y,z) \\ \zeta &= \zeta(x,y,z) \\ \tau &= t\end{aligned}\tag{A.2.1.1}$$

and conversely,

$$\begin{aligned}x &= x(\xi,\eta,\zeta) \\ y &= y(\xi,\eta,\zeta) \\ z &= z(\xi,\eta,\zeta) \\ t &= \tau\end{aligned}\tag{A.2.1.2}$$

We say that the transformation maps the physical domain into the computational domain. In order for the transformation to be one-to-one, that is, nonsingular, we

require that the Jacobian of the transformation be nonvanishing. The Jacobian matrix specifies the rates of change of the computational coordinates with respect to the physical coordinates and is given by:

$$j = \frac{\delta(\xi, \eta, \zeta)}{\delta(x, y, z)} = \begin{bmatrix} \frac{\delta \xi}{\delta x} & \frac{\delta \xi}{\delta y} & \frac{\delta \xi}{\delta z} \\ \frac{\delta \eta}{\delta x} & \frac{\delta \eta}{\delta y} & \frac{\delta \eta}{\delta z} \\ \frac{\delta \zeta}{\delta x} & \frac{\delta \zeta}{\delta y} & \frac{\delta \zeta}{\delta z} \end{bmatrix}, \quad [\text{A.2.1.3}]$$

following the notation of Taylor and Mann (1983). The derivatives of the dependent variables with respect to the new coordinate system are obtained through repeated application of the chain rule. For example, since  $u(x, y, z)$  is mapped into  $u(\xi(x, y, z), \eta(x, y, z), \zeta(x, y, z))$

$$\frac{\delta u}{\delta x} = \frac{\delta u}{\delta \xi} \frac{\delta \xi}{\delta x} + \frac{\delta u}{\delta \eta} \frac{\delta \eta}{\delta x} + \frac{\delta u}{\delta \zeta} \frac{\delta \zeta}{\delta x} + \frac{\delta u}{\delta \tau} \frac{\delta \tau}{\delta x} \quad [\text{A.2.1.4}]$$

The last term is included for completeness, though for the transformation given,  $\tau \neq \tau(x)$  and thus the last term is identically zero.

### A.2.2 The Transformed Governing Equations

In strong conservation form, the transformed governing equations can be written as follows:

$$\frac{\delta U'}{\delta t} + \frac{\delta F'}{\delta \xi} + \frac{\delta G'}{\delta \eta} + \frac{\delta H'}{\delta \zeta} = 0 \quad [\text{A.2.2.1}]$$

where

$$\begin{aligned} U' &= JU \\ F' &= J\xi_x F + J\xi_y G + J\xi_z H \\ G' &= J\eta_x F + J\eta_y G + J\eta_z H \\ H' &= J\zeta_x F + J\zeta_y G + J\zeta_z H \end{aligned} \quad [\text{A.2.2.2}]$$

$$J = \det \begin{bmatrix} x_\xi & x_\eta & x_\zeta \\ y_\xi & y_\eta & y_\zeta \\ z_\xi & z_\eta & z_\zeta \end{bmatrix} .$$

The coefficients of F, G, and H are termed the metrics of the transformation and describe the rate of change of the computational coordinates with respect to the physical coordinates. Unless the transformation is analytically specified, these derivatives are not in general directly available. Since the transformation is required to be non-singular, the inverses of the metrics exist. The relationship between the metrics and the inverse metrics follows from a cofactor expansion of the Jacobian matrix along an appropriate row. For example, the coefficients of F involve derivatives with respect to x and may be determined by evaluating the determinate of the Jacobian by a cofactor expansion along the first row as

$$J = x_\xi \begin{vmatrix} y_\eta & y_\zeta \\ z_\eta & z_\zeta \end{vmatrix} - x_\eta \begin{vmatrix} y_\xi & y_\zeta \\ z_\xi & z_\zeta \end{vmatrix} + x_\zeta \begin{vmatrix} y_\xi & y_\eta \\ z_\xi & z_\eta \end{vmatrix} \quad [\text{A.2.2.3}]$$



Then

$$\begin{aligned}
 J\xi_x &= \begin{vmatrix} Y_\eta & Y_\zeta \\ z_\eta & z_\zeta \end{vmatrix} = Y_\eta z_\zeta - Y_\zeta z_\eta \\
 J\eta_x &= - \begin{vmatrix} Y_\xi & Y_\zeta \\ z_\xi & z_\zeta \end{vmatrix} = Y_\zeta z_\xi - Y_\xi z_\zeta \\
 J\zeta_x &= \begin{vmatrix} Y_\xi & Y_\eta \\ z_\xi & z_\eta \end{vmatrix} = Y_\xi z_\eta - Y_\eta z_\xi
 \end{aligned} \tag{A.2.2.4}$$

Likewise, expansion of the determinate of the Jacobian matrix by a cofactor expansion along the second row provides

$$\begin{aligned}
 J\xi_y &= x_\zeta z_\eta - x_\eta z_\zeta \\
 J\eta_y &= x_\xi z_\zeta - x_\zeta z_\xi \\
 J\zeta_y &= x_\eta z_\xi - x_\xi z_\eta
 \end{aligned} \tag{A.2.2.5}$$

and finally, expansion along the third row yields

$$\begin{aligned}
 J\xi_z &= x_\eta Y_\zeta - x_\zeta Y_\eta \\
 J\eta_z &= x_\zeta Y_\xi - x_\xi Y_\zeta \\
 J\zeta_z &= x_\xi Y_\eta - x_\eta Y_\xi
 \end{aligned} \tag{A.2.2.6}$$

The metrics are now stated as explicit functions of the inverse metrics, which may be obtained numerically using finite differences, even when the transformation is not analytically specified. The present work makes use of an algebraic grid generation technique with linear connecting functions, described in Smith (1981), to obtain the Jacobian and metric data. In order to cluster the grid points near the boundaries in the physical domain, the grid refinement function of Roberts (1970) is included in the transformation for the y and z coordinates.

### A.3 Boundary and Initial Conditions

Since shock-boundary layer interactions depend on the size and character of the incoming boundary layer, the inflow boundary layer was allowed to develop naturally over the length of the baseplate ahead of the inlet entrance. The inflow boundary was maintained at freestream conditions, while an extrapolation boundary condition was applied at the exit plane. On solid surfaces, all velocity components as well as the normal pressure gradient are required to vanish. A constant temperature distribution ( $T_{\text{wall}} = 300\text{K}$ ) provides the thermal boundary condition. Open boundaries are calculated assuming vanishing normal gradients in velocity, temperature, and pressure. Since the flow field is symmetric, only half of the field is computed and symmetry boundary conditions are imposed. The initial conditions are given by assigning freestream conditions to each grid point except at the boundaries, where appropriate boundary conditions are applied.

### A.4 MacCormack's Method

The transformed governing equations are solved in full conservation form by MacCormack's time-asymptotic, explicit, predictor-corrector method. This scheme is a variation of the two step Lax-Wendroff method in which  $U^{n+1}(i,j,k)$  is approximated by a Taylor series about  $U^n(i,j,k)$ , where the spacial derivatives of the governing equations have been substituted for the time derivative. The two step method applies one-sided differences taken in the opposite direction for each step. At the next time step, the direction of differencing is alternated. Though each stage is only first-order accurate, the combination of the stages yields a

second-order accurate scheme in both time and space. As applied to the governing equations, the method is given as follows.

Predictor:

$$\begin{aligned}
 \overline{U^{n+1}}(i, j, k) = & U^n(i, j, k) - \frac{\Delta t}{\Delta \xi} (F^n(i+1, j, k) - F^n(i, j, k)) \\
 & - \frac{\Delta t}{\Delta \eta} (G^n(i, j+1, k) - G^n(i, j, k)) \\
 & - \frac{\Delta t}{\Delta \zeta} (H^n(i, j, k+1) - H^n(i, j, k))
 \end{aligned}
 \tag{A.4.1}$$

Corrector:

$$\begin{aligned}
 U^{n+1}(i, j, k) = & \frac{1}{2} \left[ U^n(i, j, k) + \overline{U^{n+1}}(i, j, k) \right. \\
 & - \frac{\Delta t}{\Delta \xi} (\overline{F^{n+1}}(i, j, k) - \overline{F^{n+1}}(i-1, j, k)) \\
 & - \frac{\Delta t}{\Delta \eta} (\overline{G^{n+1}}(i, j, k) - \overline{G^{n+1}}(i, j-1, k)) \\
 & \left. - \frac{\Delta t}{\Delta \zeta} (\overline{H^{n+1}}(i, j, k) - \overline{H^{n+1}}(i, j, k-1)) \right]
 \end{aligned}
 \tag{A.4.2}$$

Fletcher (1988) indicates that this method is the most widely used explicit method for solution of the Navier-Stokes equations. As indicated in Section 4.1, the code chosen for the present work has been used to solve numerous types of internal high speed flow interaction (inlet) configurations and has shown favorable comparisons with experimental data.

# Figures

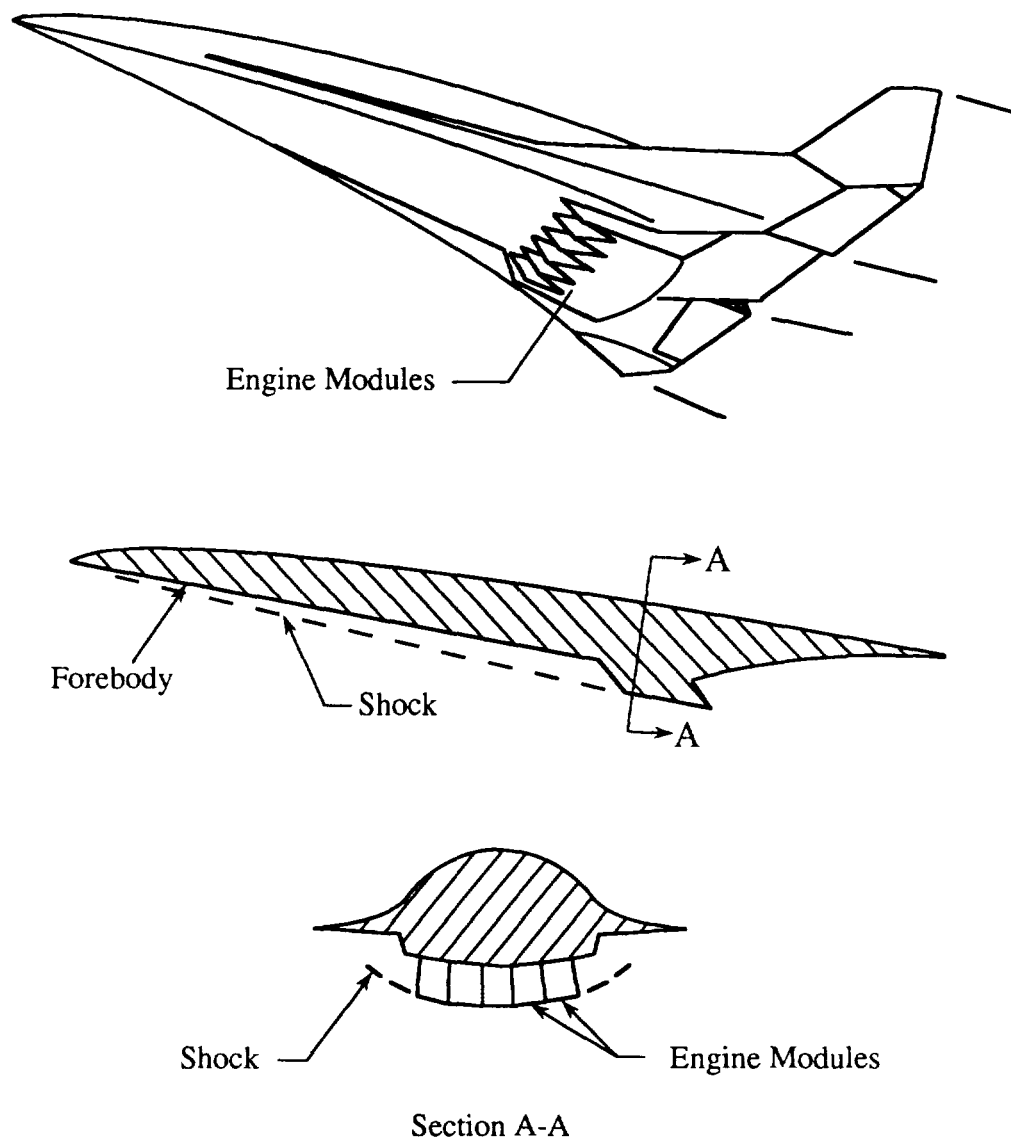


Figure 1.1: Propulsion-Airframe Integration

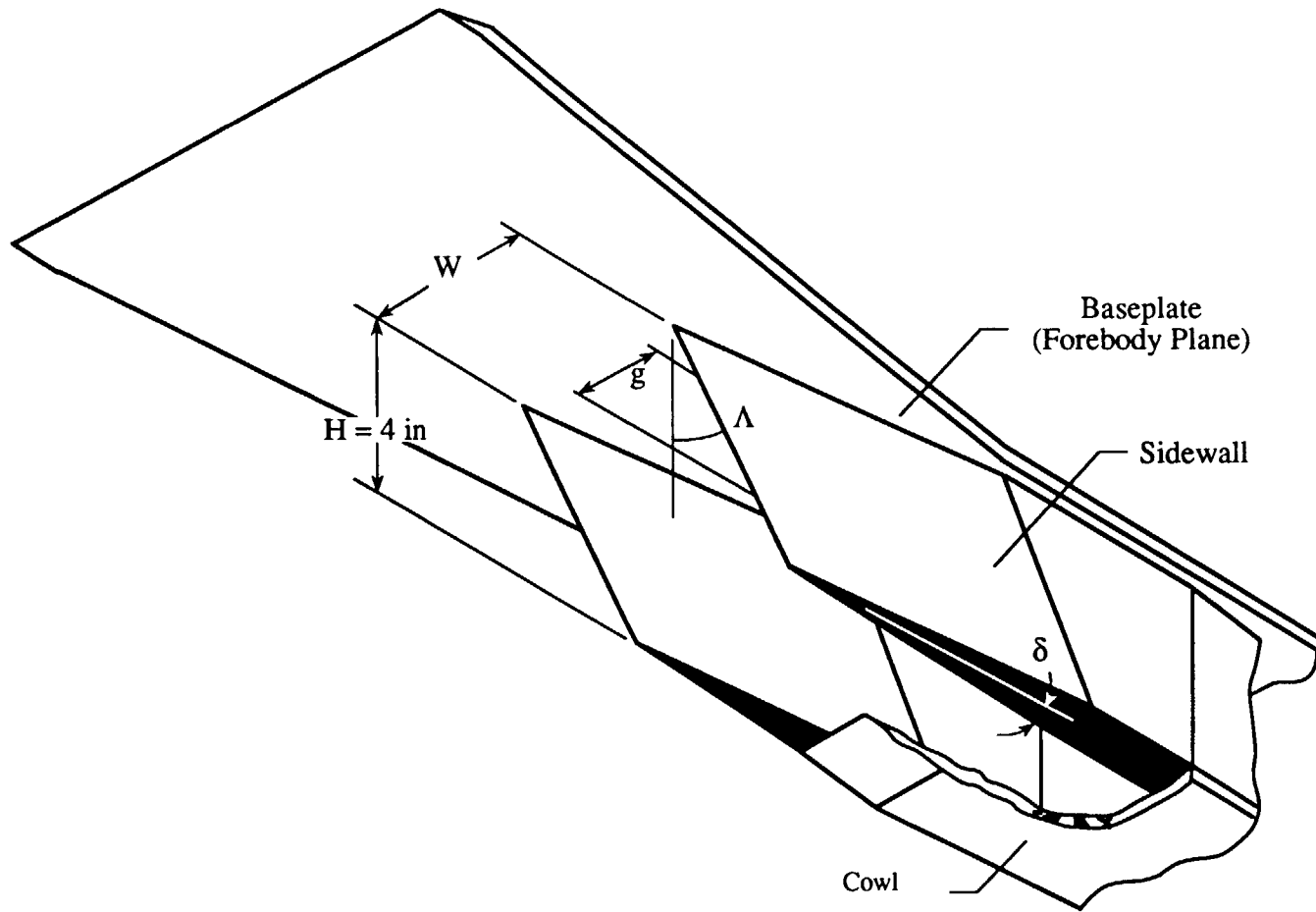


Figure 1.2: Inlet Model Shown in Flight Orientation

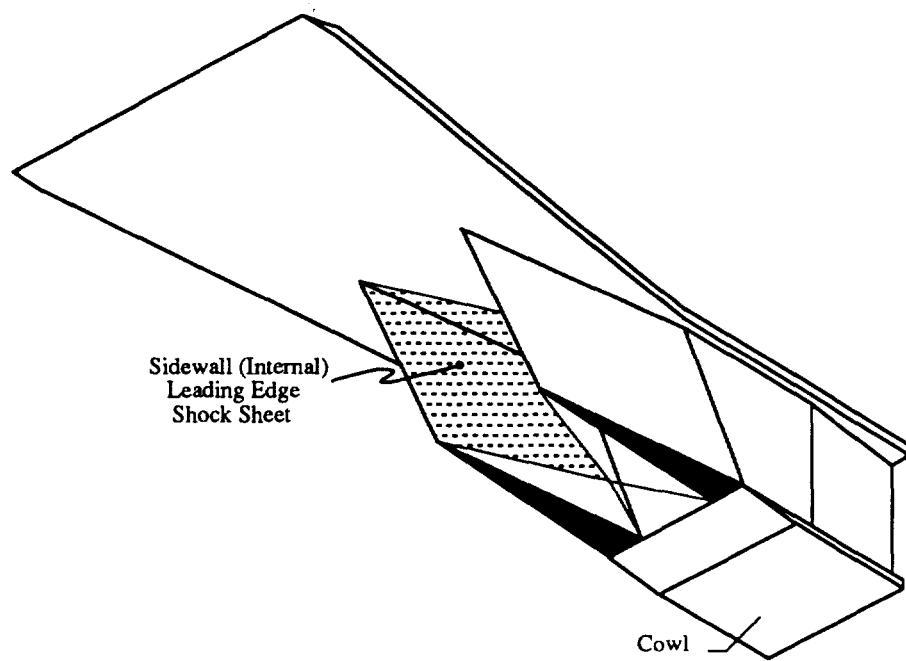


Figure 2.1: Internal Reflected Shock Structure

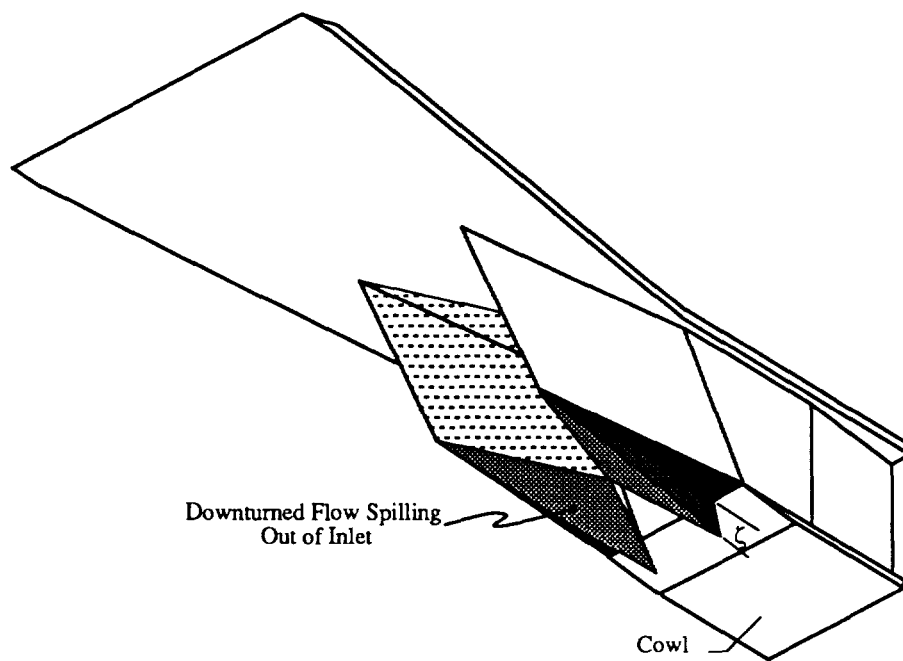


Figure 2.2: Flow Spillage Due to Swept Shock Sheet  
Emanating from Sidewall Leading Edge  
(Spillage Angle  $\xi$  is exaggerated.)



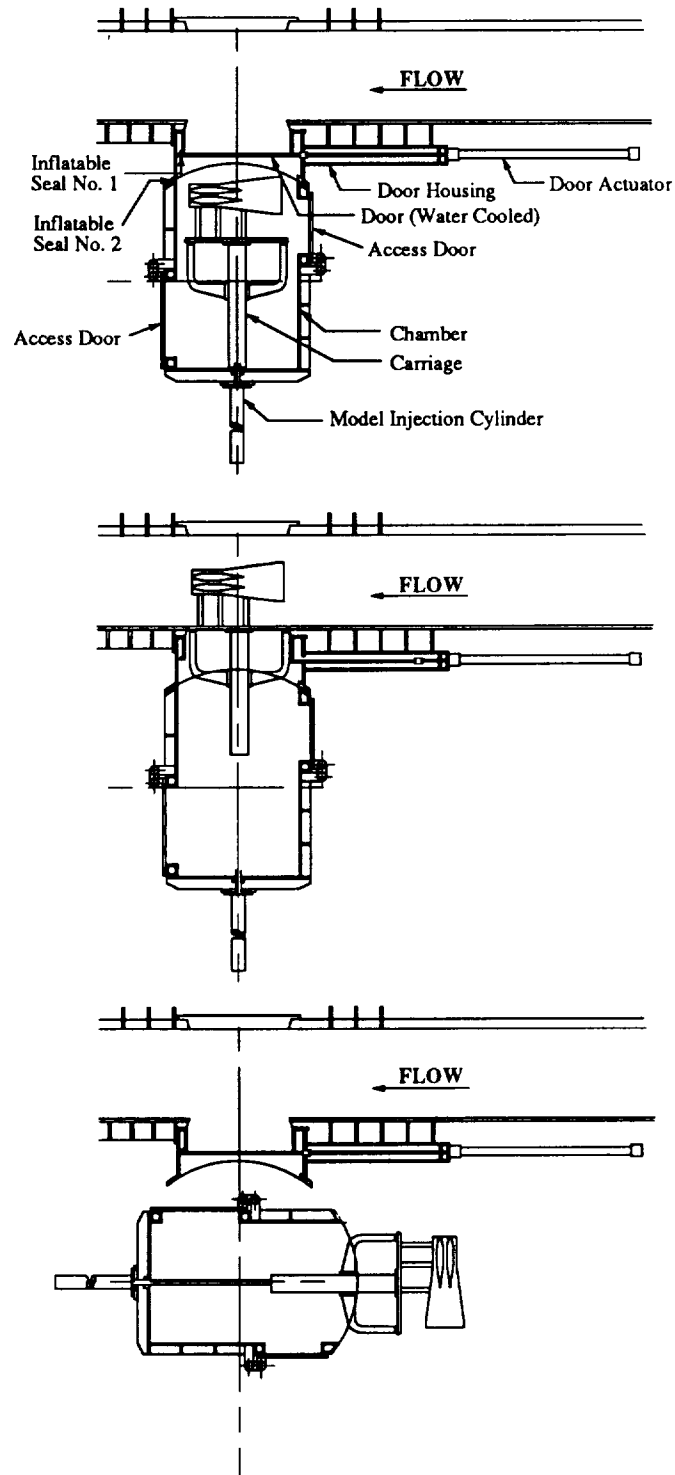


Figure 3.2.1.1: Model Injection Sequence, Showing Model Retracted Prior to Injection, Model Injected into the Tunnel, and Model Injected into Technician Work Area

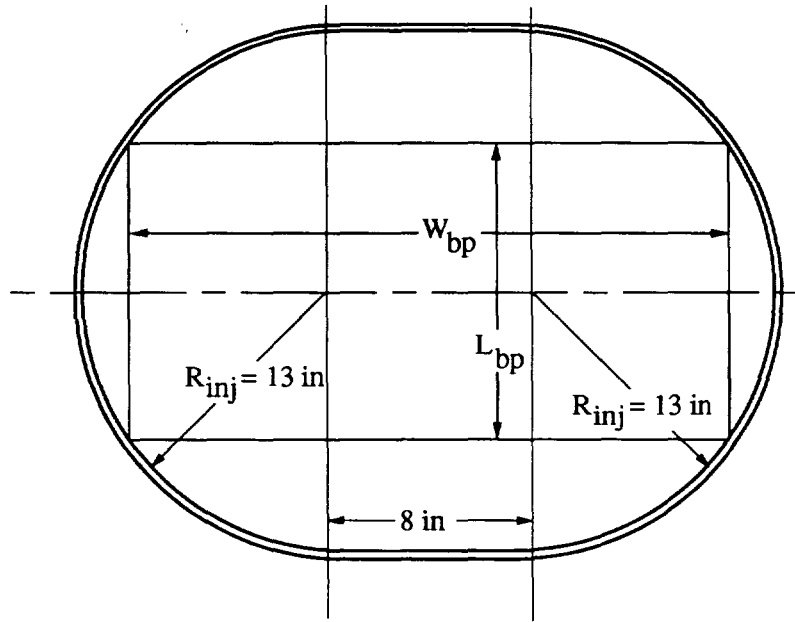


Figure 3.2.3.1: Dimensioned Wind Tunnel Injection Plate

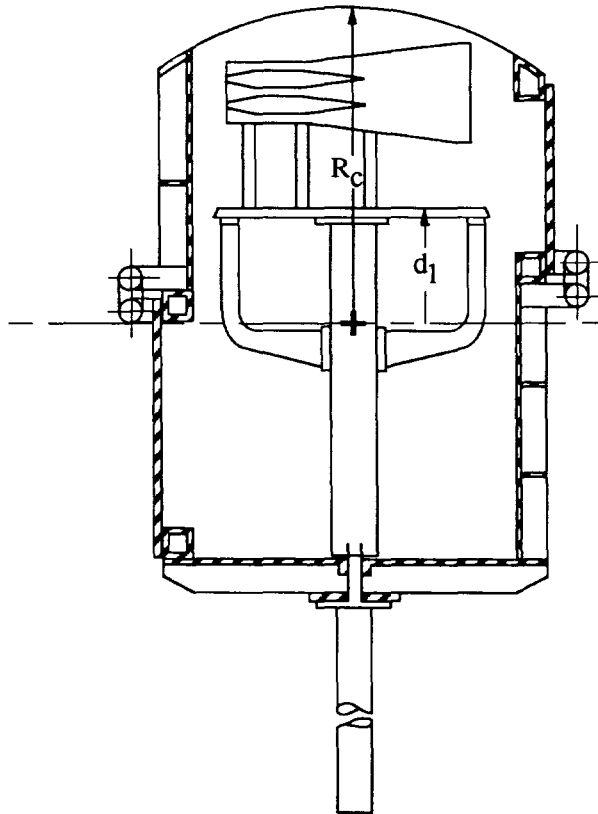


Figure 3.2.3.2: Injection Carriage/Chamber Detail

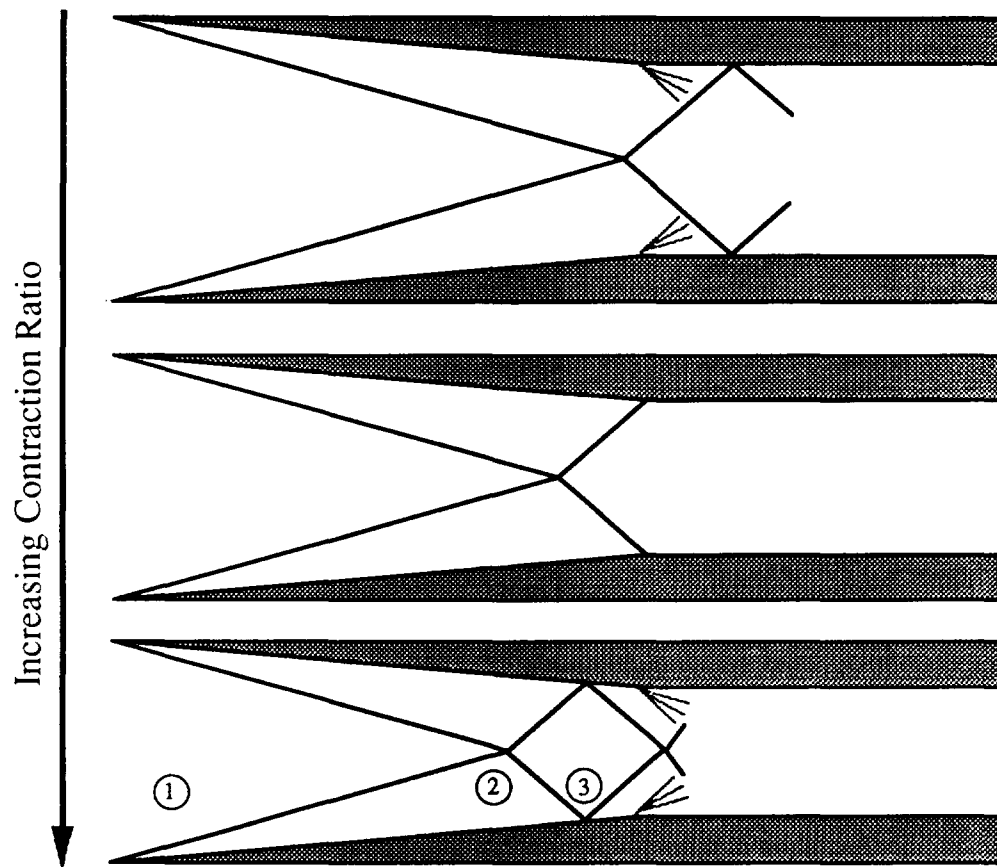


Figure 3.3.1: Inviscid Internal Shock Interactions:  
Shock after shoulder,  
Shock on shoulder,  
Shock before shoulder.

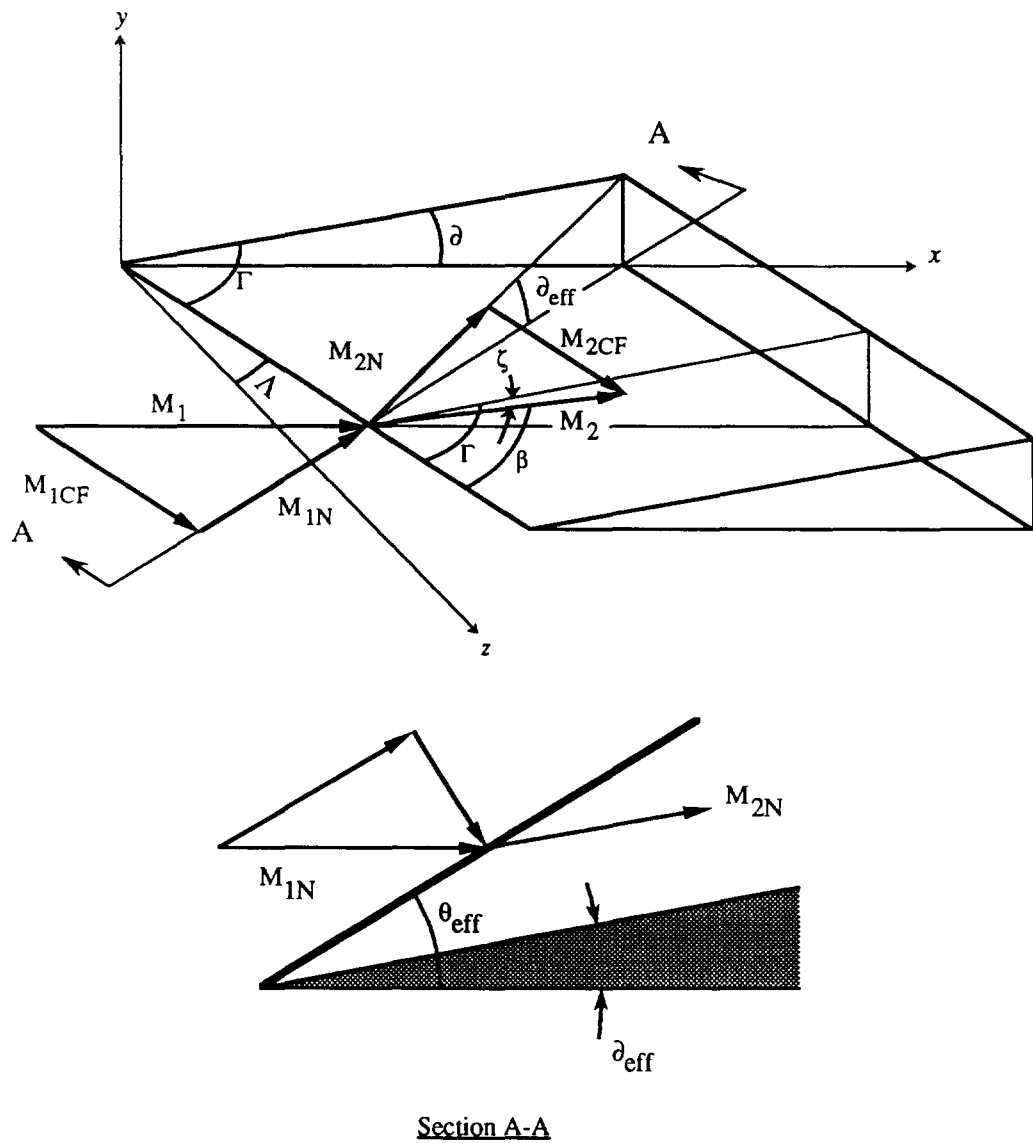


Figure 3.3.2: Mach Number Components for Modified 2-D Oblique Shock Theory

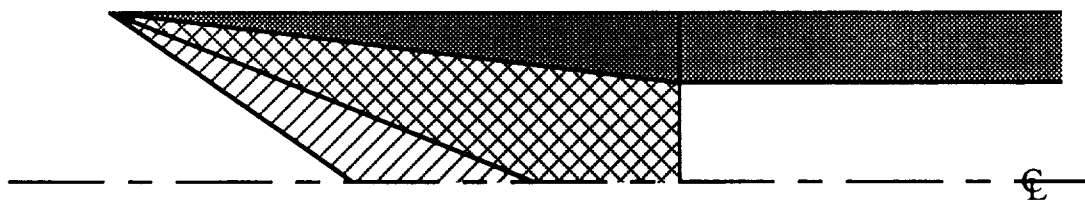




Figure 3.3.3: Region of Flow Downturning for Shock Angles Corresponding to Low  and High  Mach Number Inflow

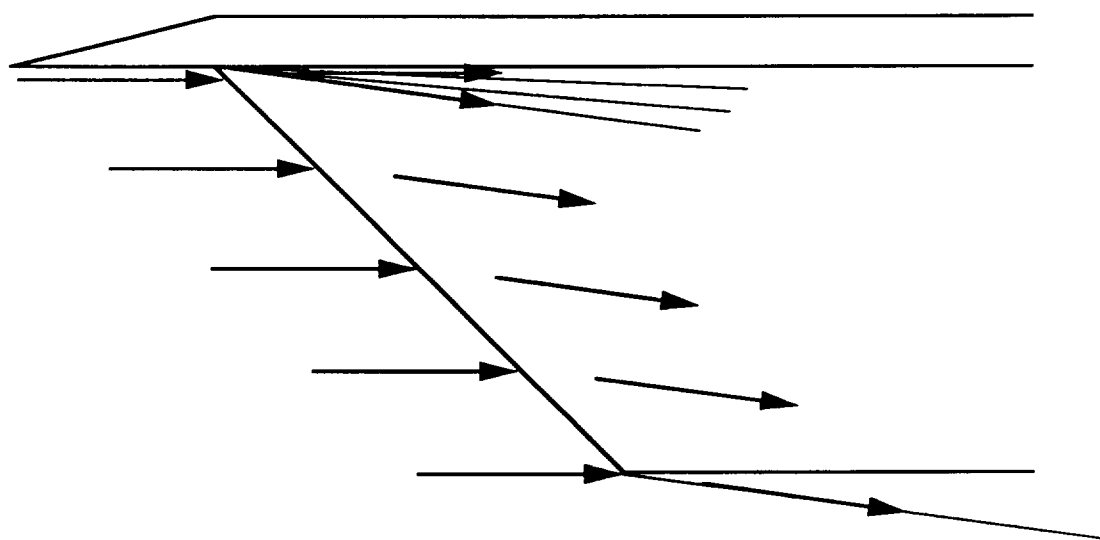


Figure 3.3.4: Centered Expansion Model of Baseplate Interaction Region

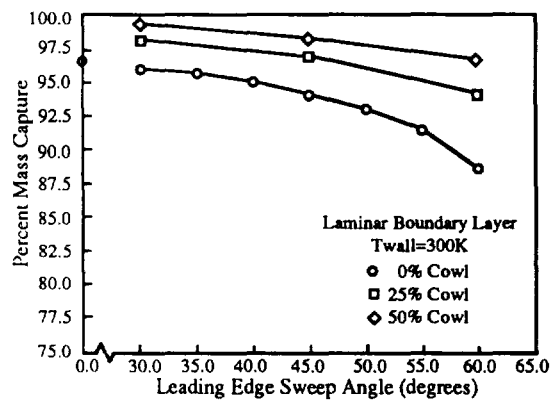


Figure 4.3.1.1: Leading Edge Sweep and Cowl Position Effects on Inlet Mass Capture

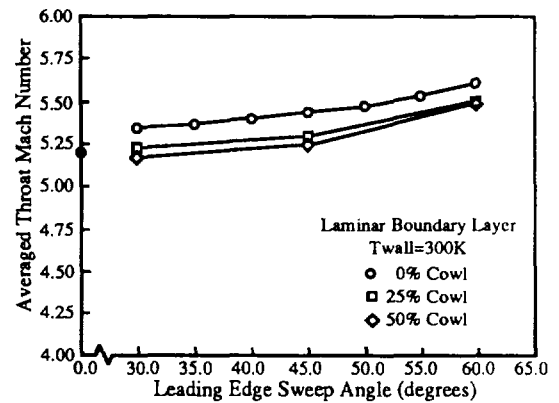


Figure 4.3.2.1: Leading Edge Sweep and Cowl Position Effects on Inlet Throat Mach Number

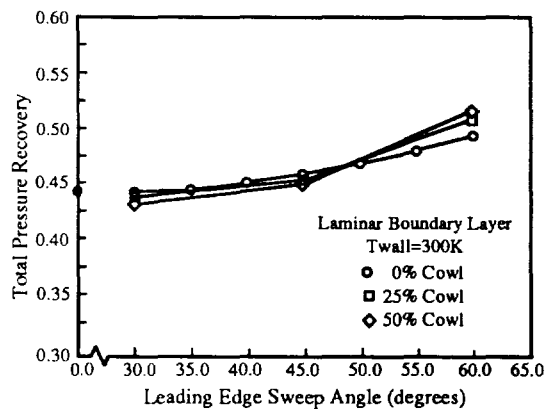


Figure 4.3.3.1: Leading Edge Sweep and Cowl Position Effects on Inlet Total Pressure Recovery

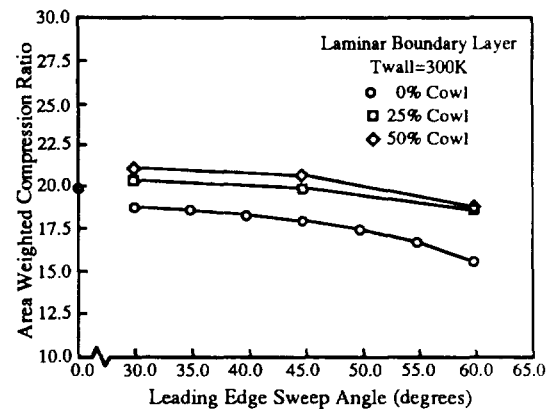


Figure 4.3.4.1: Leading Edge Sweep and Cowl Position Effects on Inlet Area Weighted Compression

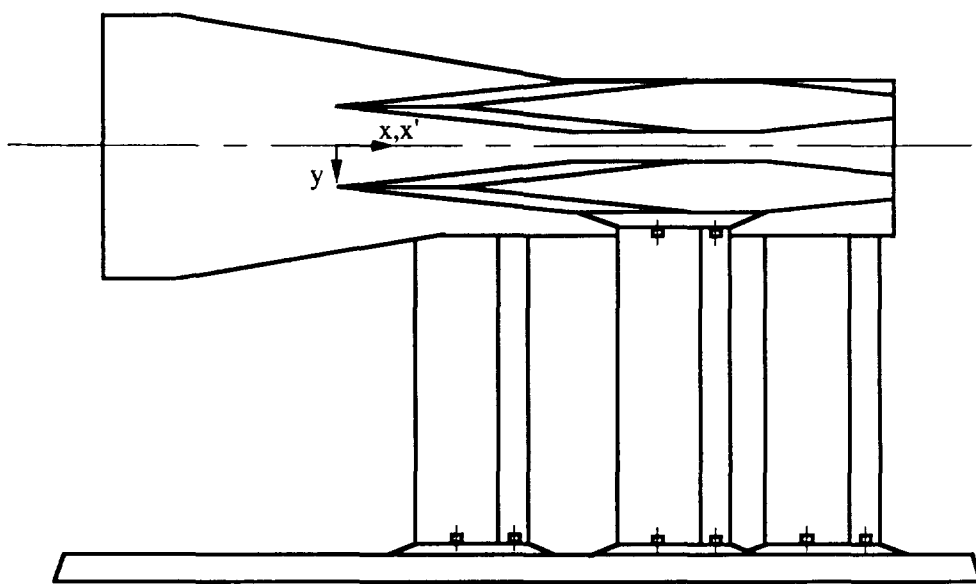


Figure 5.1: Inlet on Injection Plate Viewed From Underneath Tunnel

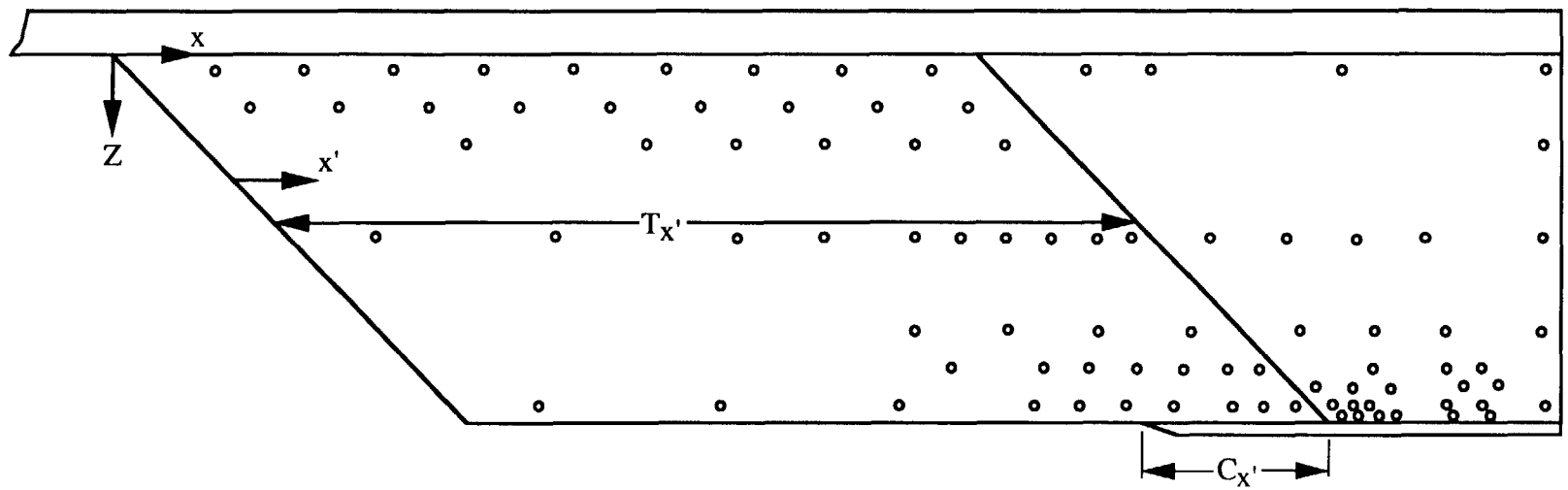


Figure 5.2: Sidewall Orifice Locations and Identification of Coordinate System



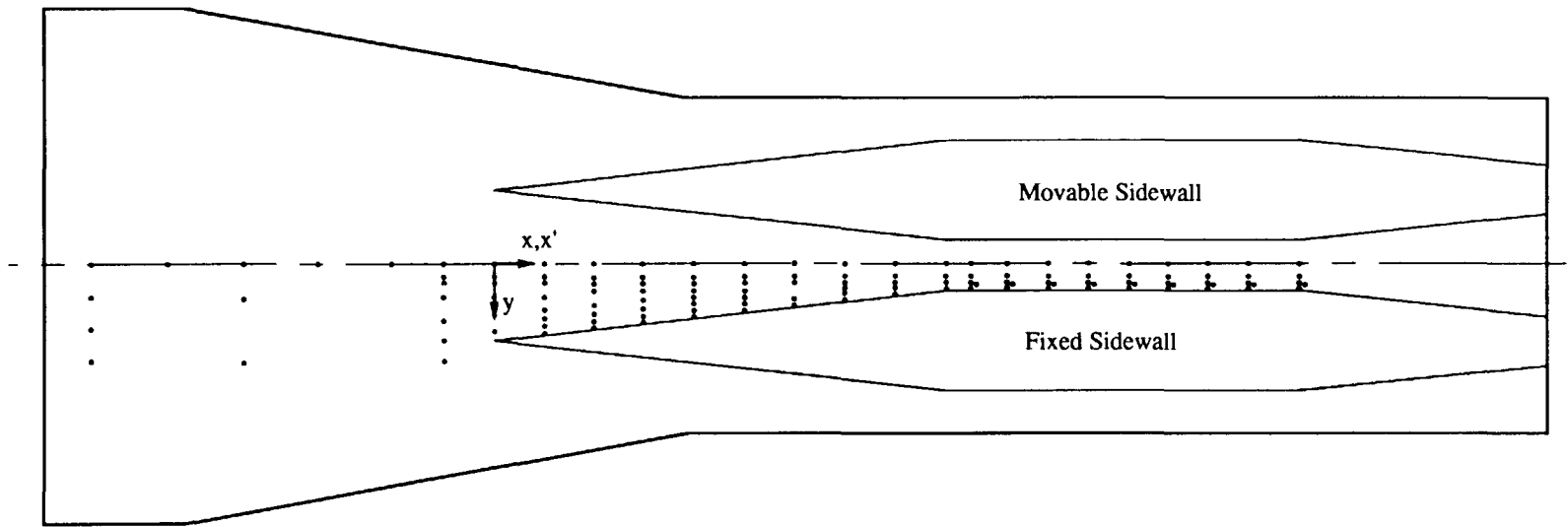


Figure 5.3: Baseplate Orifice Locations and Coordinate System Identification  
(Centerline Shown for CR=3 Configuration)

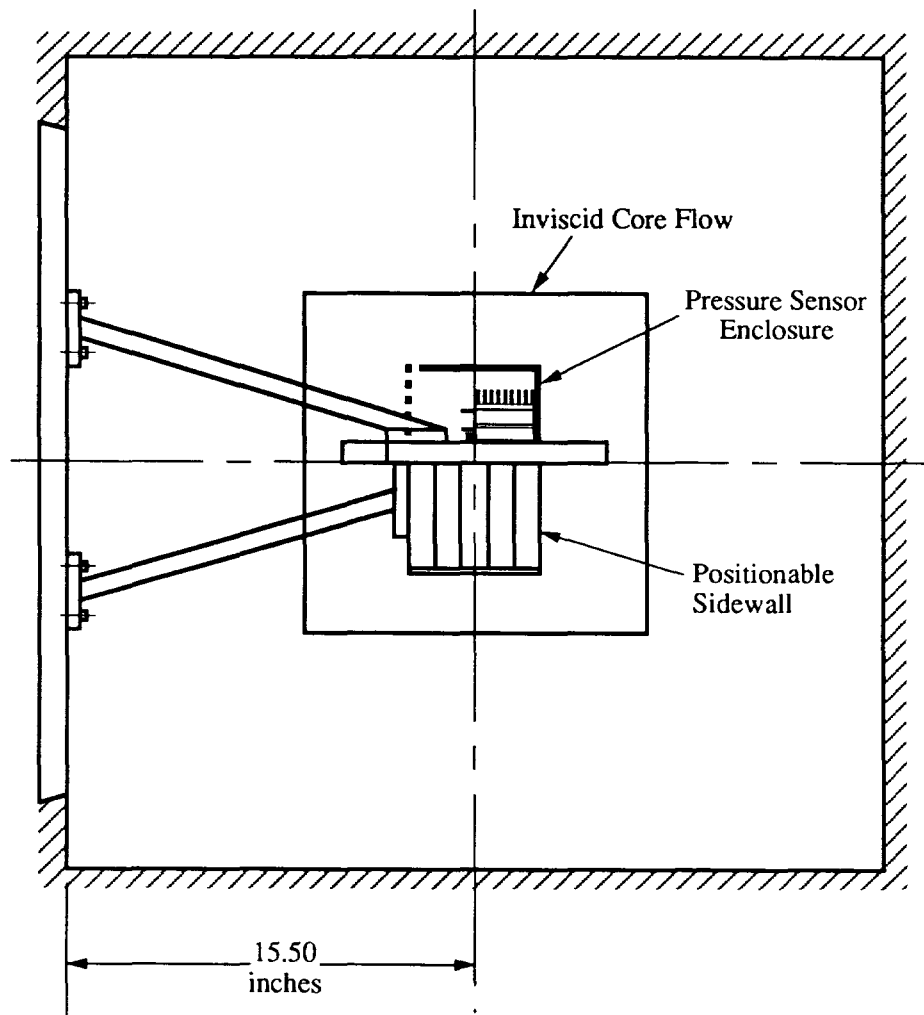


Figure 5.1.1: Inlet Injected into Inviscid Core Flow

ORIGINAL PAGE  
BLACK AND WHITE PHOTOGRAPH

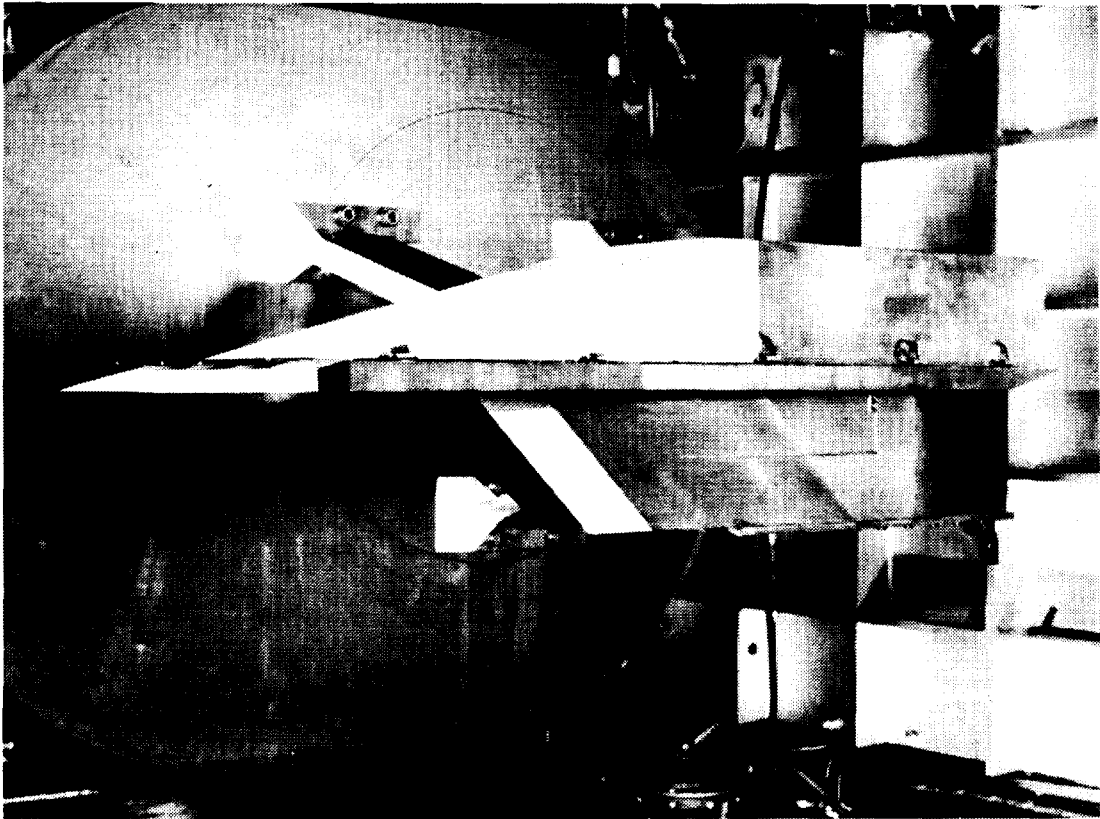


Figure 5.1.2: Photograph of Inlet Model on Injection Plate

ORIGINAL PAGE  
BLACK AND WHITE PHOTOGRAPH

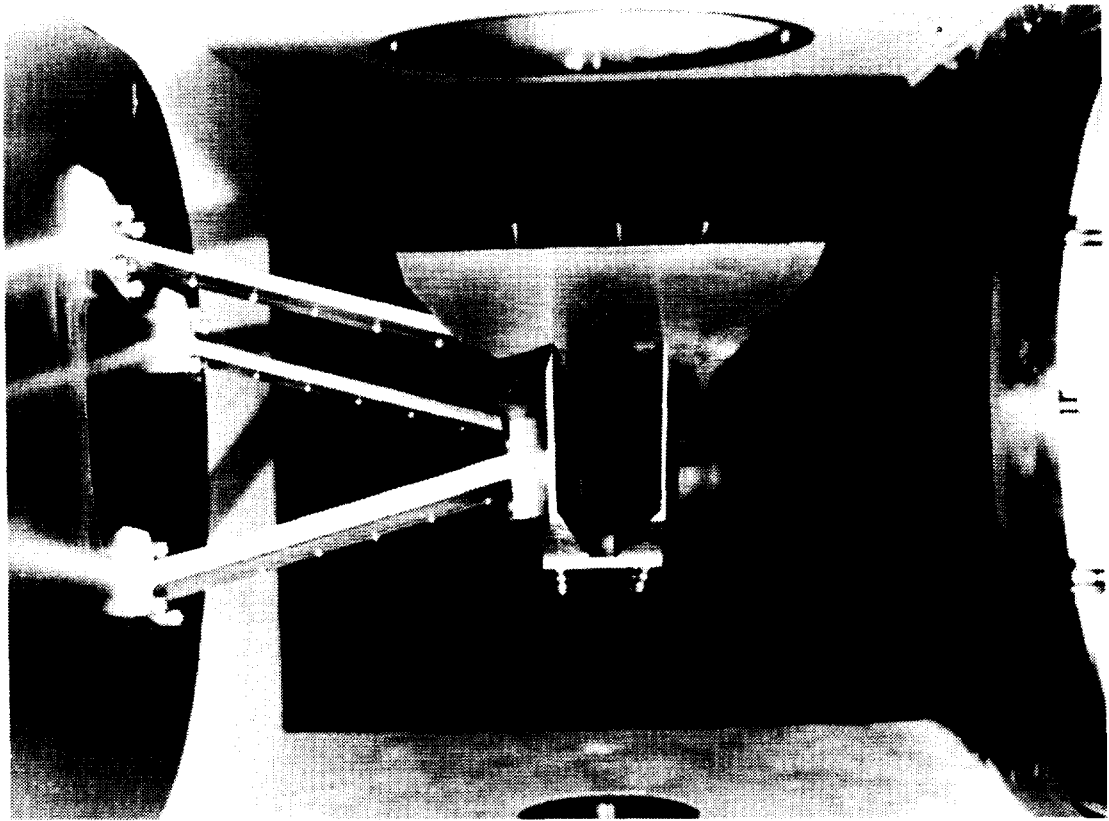


Figure 5.1.3: Photograph of Inlet Model Injected into Tunnel Test Section

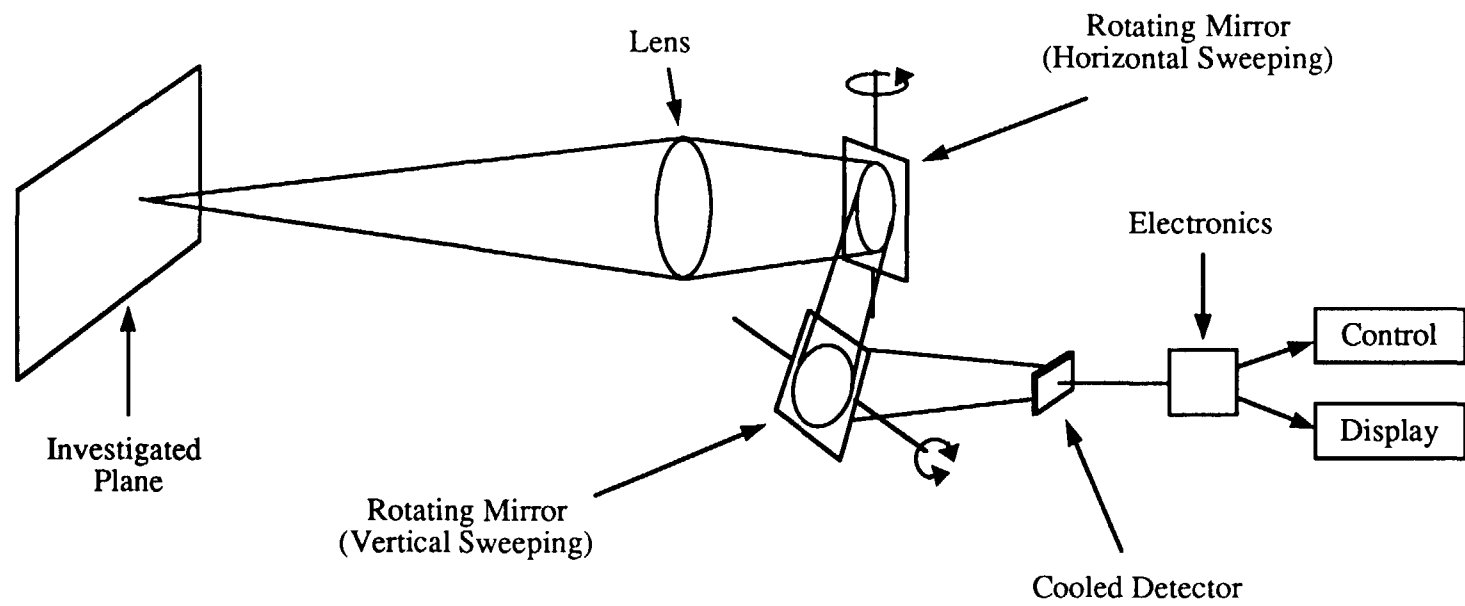
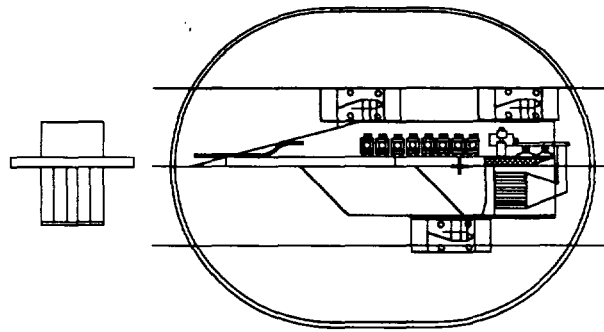
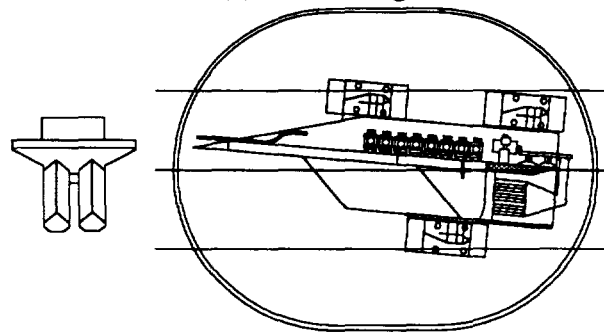


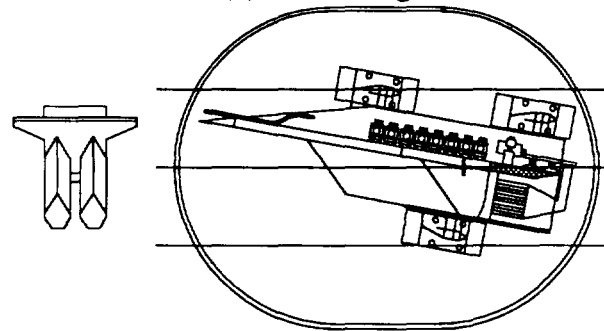
Figure 5.2.2.1: Schematic of Infrared Thermography System



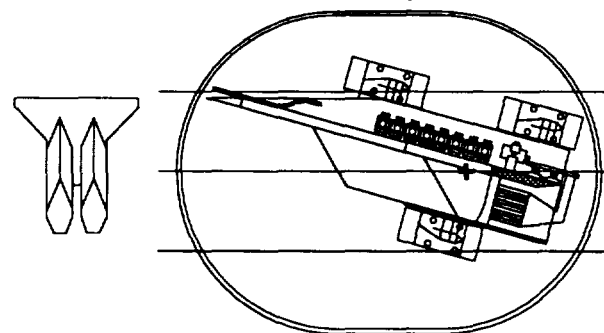
(a)  $\alpha = 0$  degrees



(b)  $\alpha = 5$  degrees



(c)  $\alpha = 10$  degrees



(d)  $\alpha = 15$  degrees

Figure 5.3.1.1.1: Inlet Frontal and Profile Views at Angles of Attack Between 0 and 15 degrees

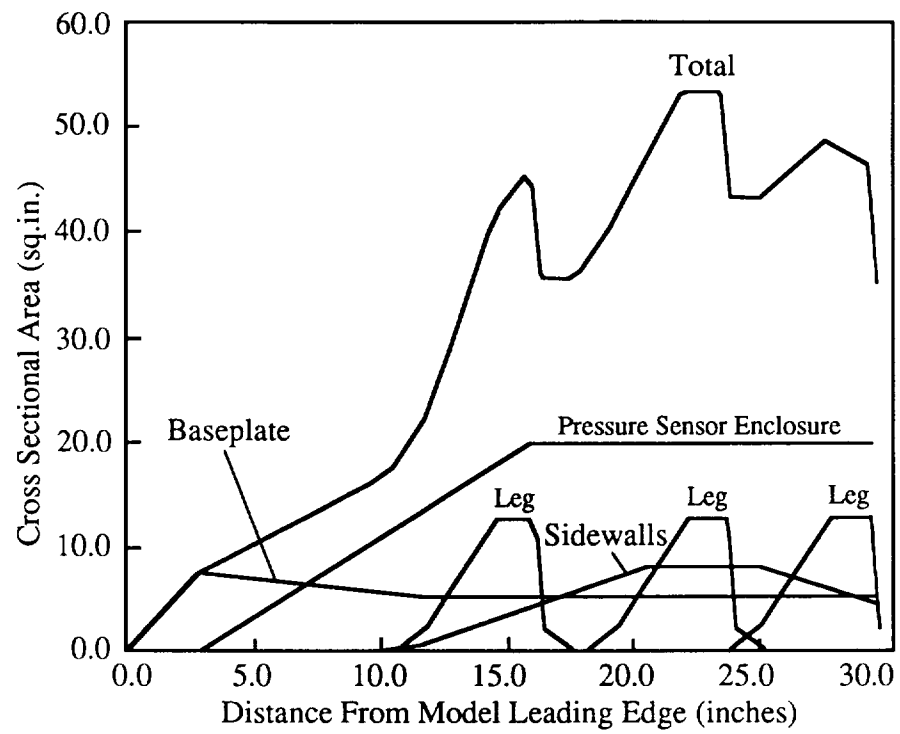


Figure 5.3.1.2: Cross Sectional Area Distribution for Inlet Model

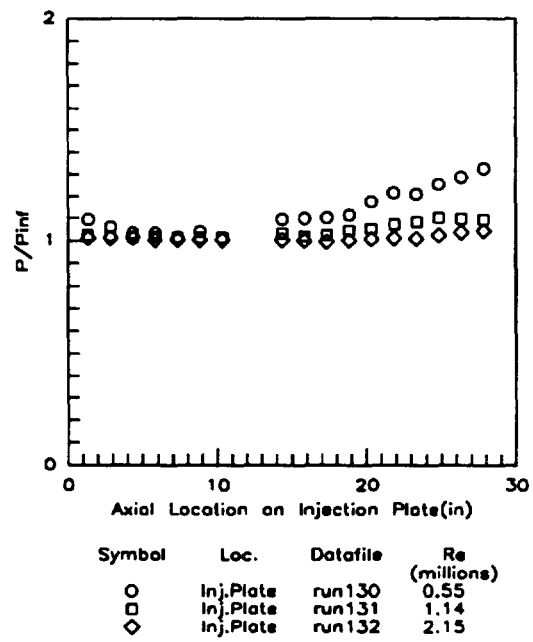


Figure 5.3.1.2.1: Injection Plate Pressures  
(Tunnel Empty)



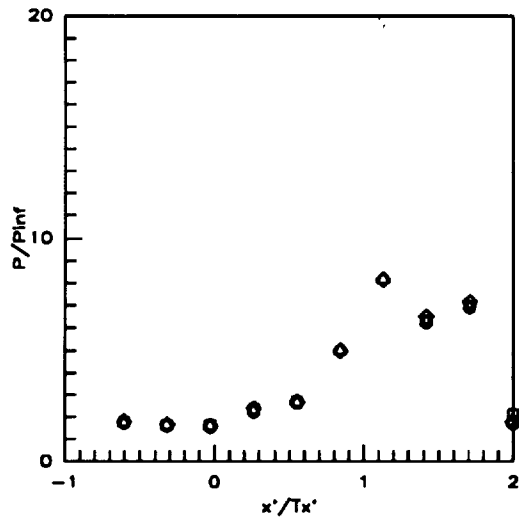


Figure 5.3.1.2.2: Cowl Effects  
(Re=2.15 million/ft, CR=3)  
Centerline Pressures

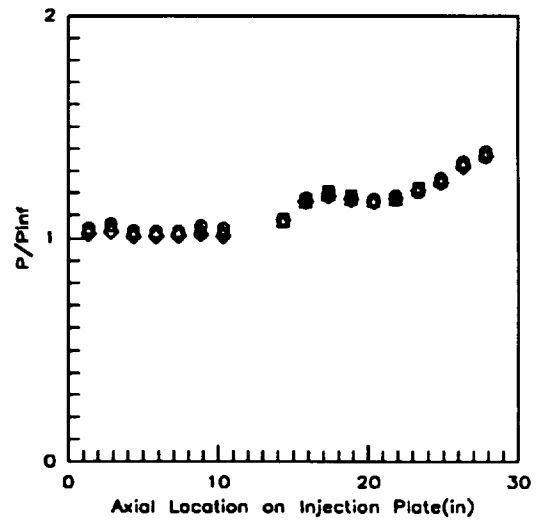


Figure 5.3.1.2.3: Cowl Effects  
(Re=2.15 million/ft, CR=3)  
Injection Plate Pressures

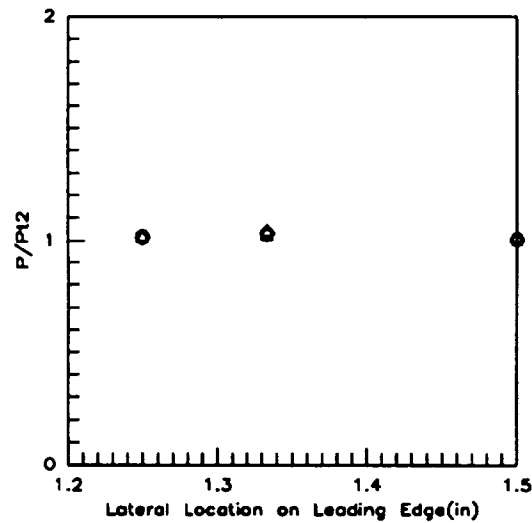


Figure 5.3.1.2.4: Cowl Effects  
(Re=2.15 million/ft, CR=3)  
Pitot Pressures

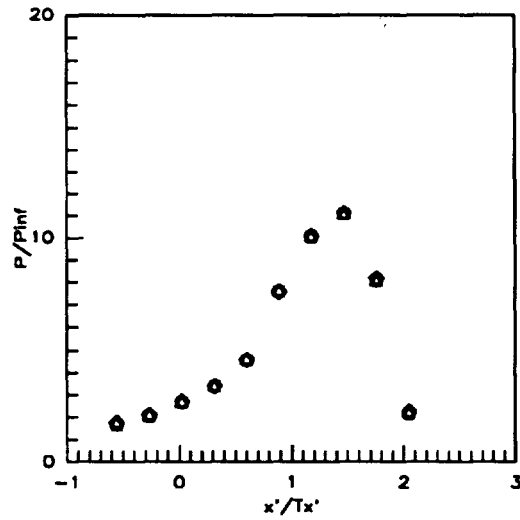


Figure 5.3.1.2.5: Cowl Effects  
(Re=2.15 million/ft, CR=5)  
Centerline Pressures

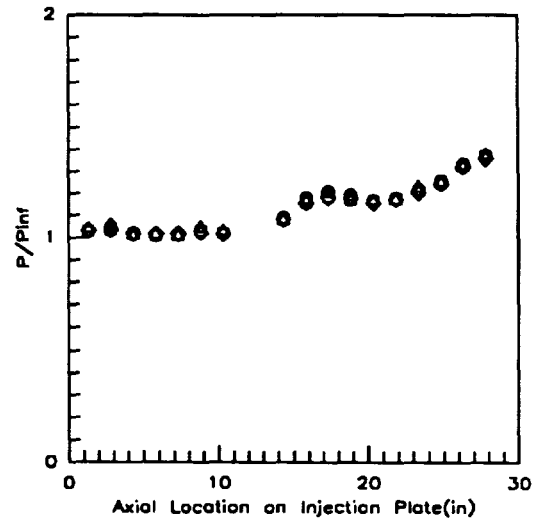


Figure 5.3.1.2.6: Cowl Effects  
(Re=2.15 million/ft, CR=5)  
Injection Plate Pressures

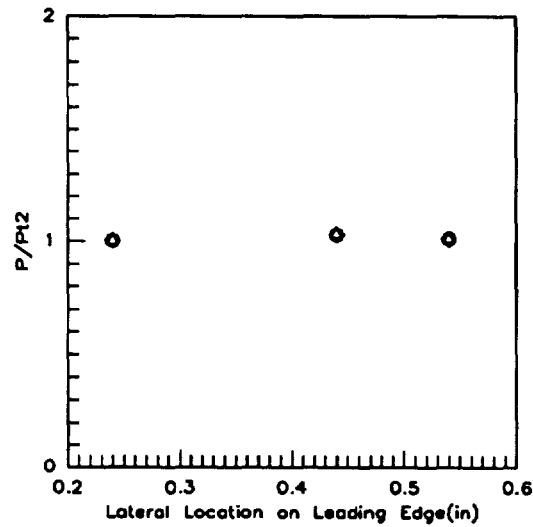


Figure 5.3.1.2.7: Cowl Effects  
(Re=2.15 million/ft, CR=5)  
Pitot Pressures

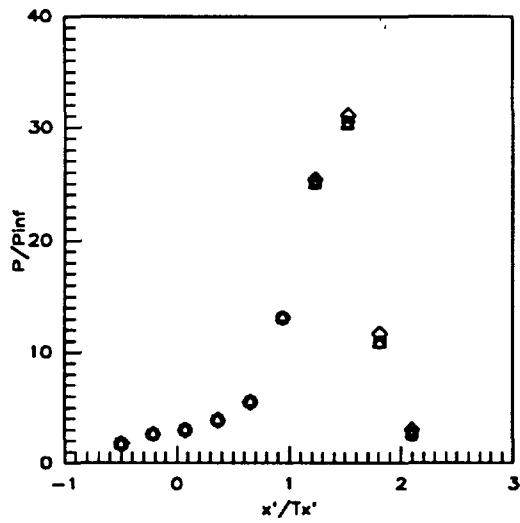


Figure 5.3.1.2.8: Cowl Effects  
(Re=2.15 million/ft, CR=9)  
Centerline Pressures

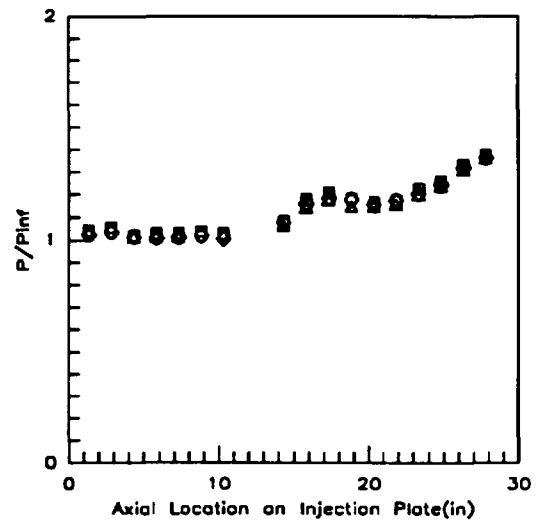


Figure 5.3.1.2.9: Cowl Effects  
(Re=2.15 million/ft, CR=9)  
Injection Plate Pressures

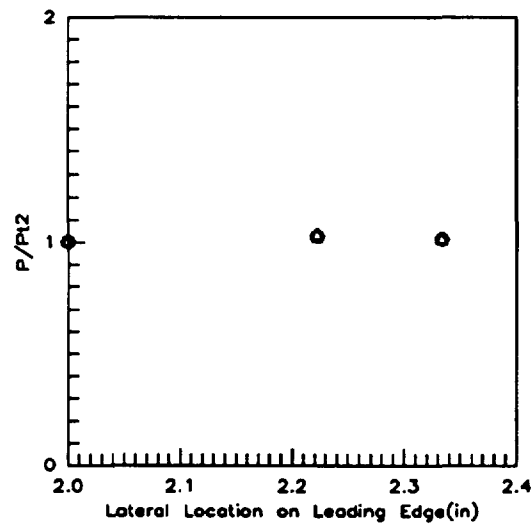


Figure 5.3.1.2.10: Cowl Effects  
(Re=2.15 million/ft, CR=9)  
Pitot Pressures

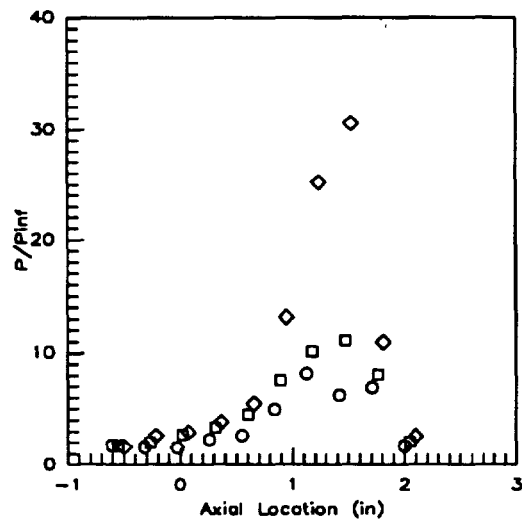


Figure 5.3.1.2.11: Contraction Ratio Effects  
( $Re=2.15$  million/ft, 0% Cowl)  
Centerline Pressures

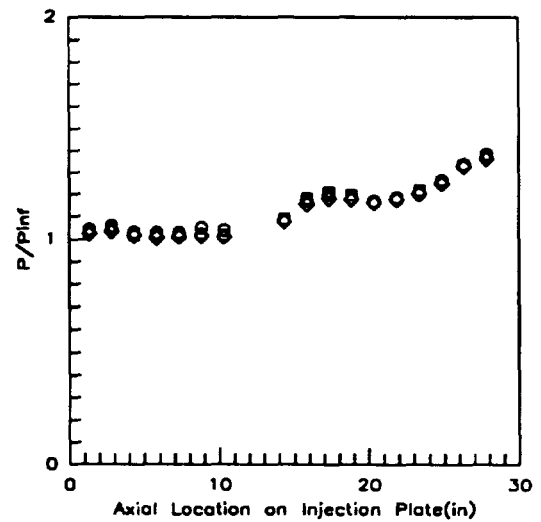


Figure 5.3.1.2.12: Contraction Ratio Effects  
( $Re=2.15$  million/ft, 0% Cowl)  
Injection Plate Pressures

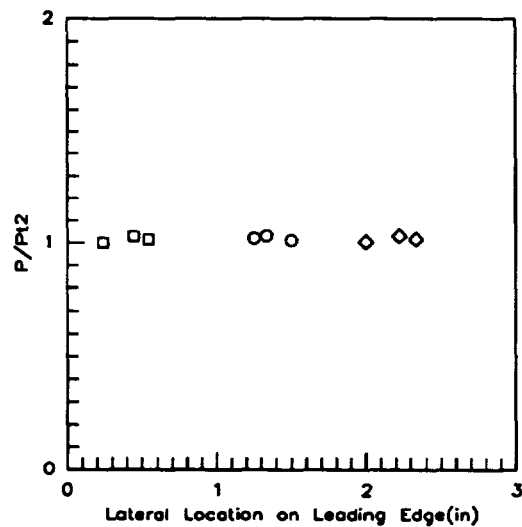


Figure 5.3.1.2.13: Contraction Ratio Effects  
( $Re=2.15$  million/ft, 0% Cowl)  
Pitot Pressures

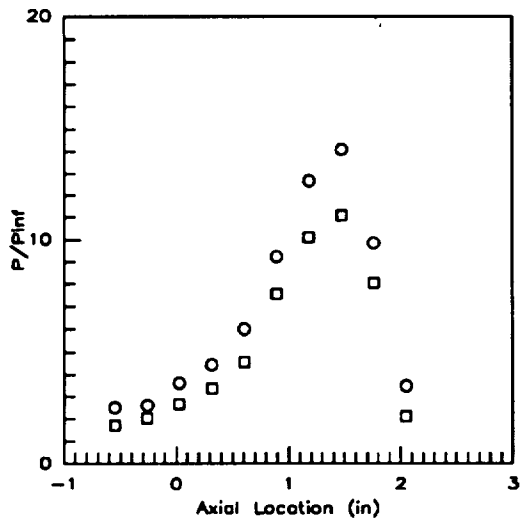


Figure 5.3.1.2.14: Reynolds Number Effects  
(CR=5, 0% Cowl)  
Centerline Pressures

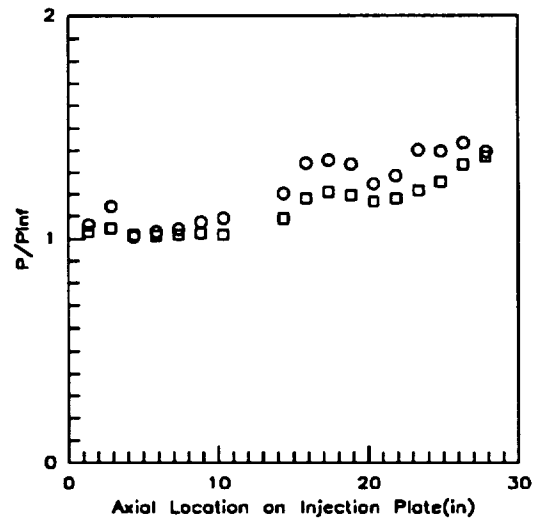


Figure 5.3.1.2.15: Reynolds Number Effects  
(CR=5, 0% Cowl)  
Injection Plate Pressures

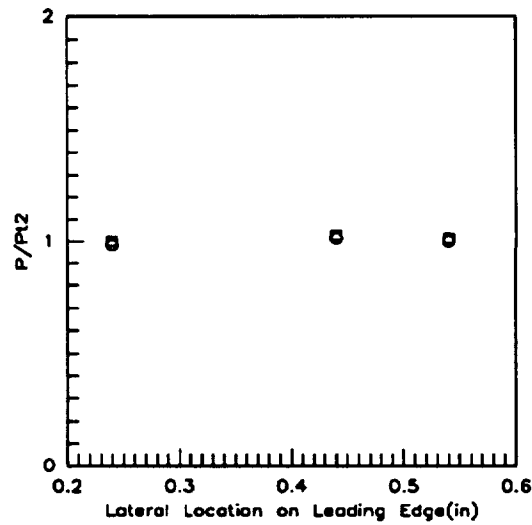


Figure 5.3.1.2.16: Reynolds Number Effects  
(CR=5, 0% Cowl)  
Pitot Pressures

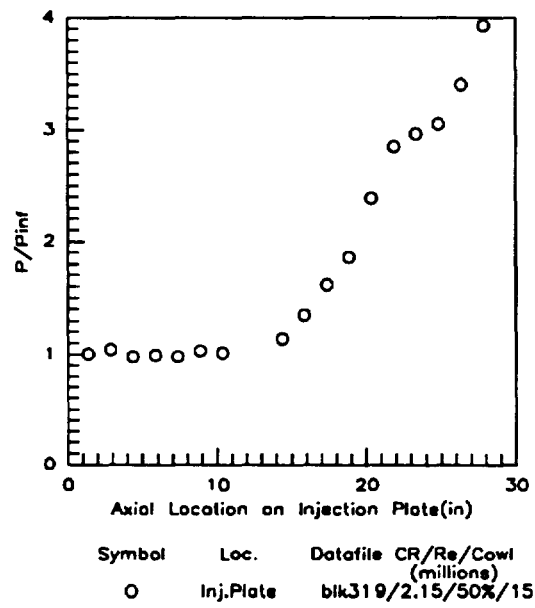


Figure 5.3.1.2.17: AoA = 15 deg.  
 (CR=9, 50% Cowl)  
 Injection Plate Pressures

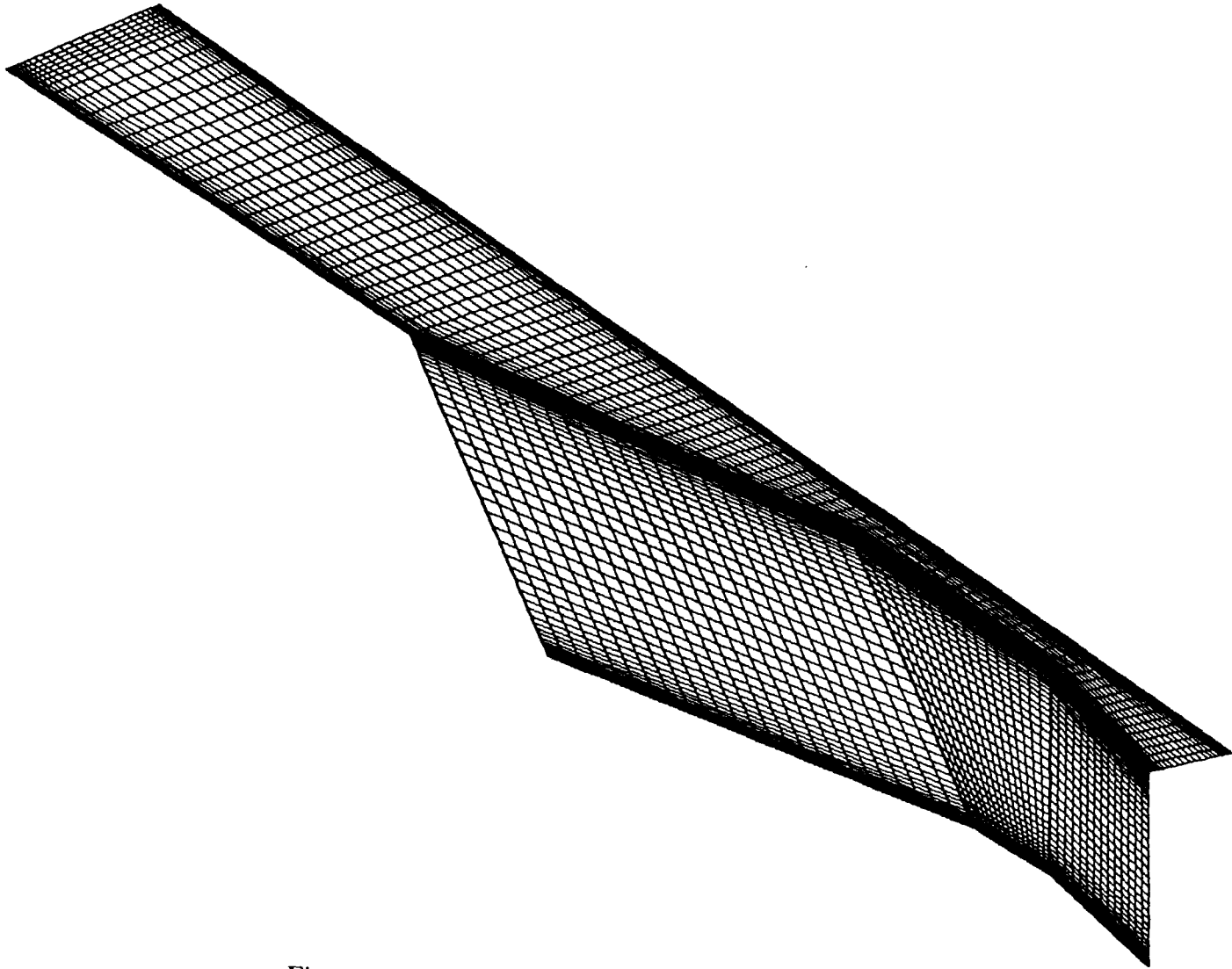


Figure 6.1: Computational Grid of Inlet Sidewall and Baseplate



Figure 6.1.1(a): Pressure Contours at  $Z/H = 0.25$  for  $CR = 3$ ,  
 $Re = 2.15$  million/ft, 0% Cowl



Figure 6.1.1(b): Pressure Contours at  $Z/H = 0.50$  for  $CR = 3$ ,  
 $Re = 2.15$  million/ft, 0% Cowl



Figure 6.1.1(c): Pressure Contours at  $Z/H = 0.75$  for  $CR = 3$ ,  
 $Re = 2.15$  million/ft, 0% Cowl



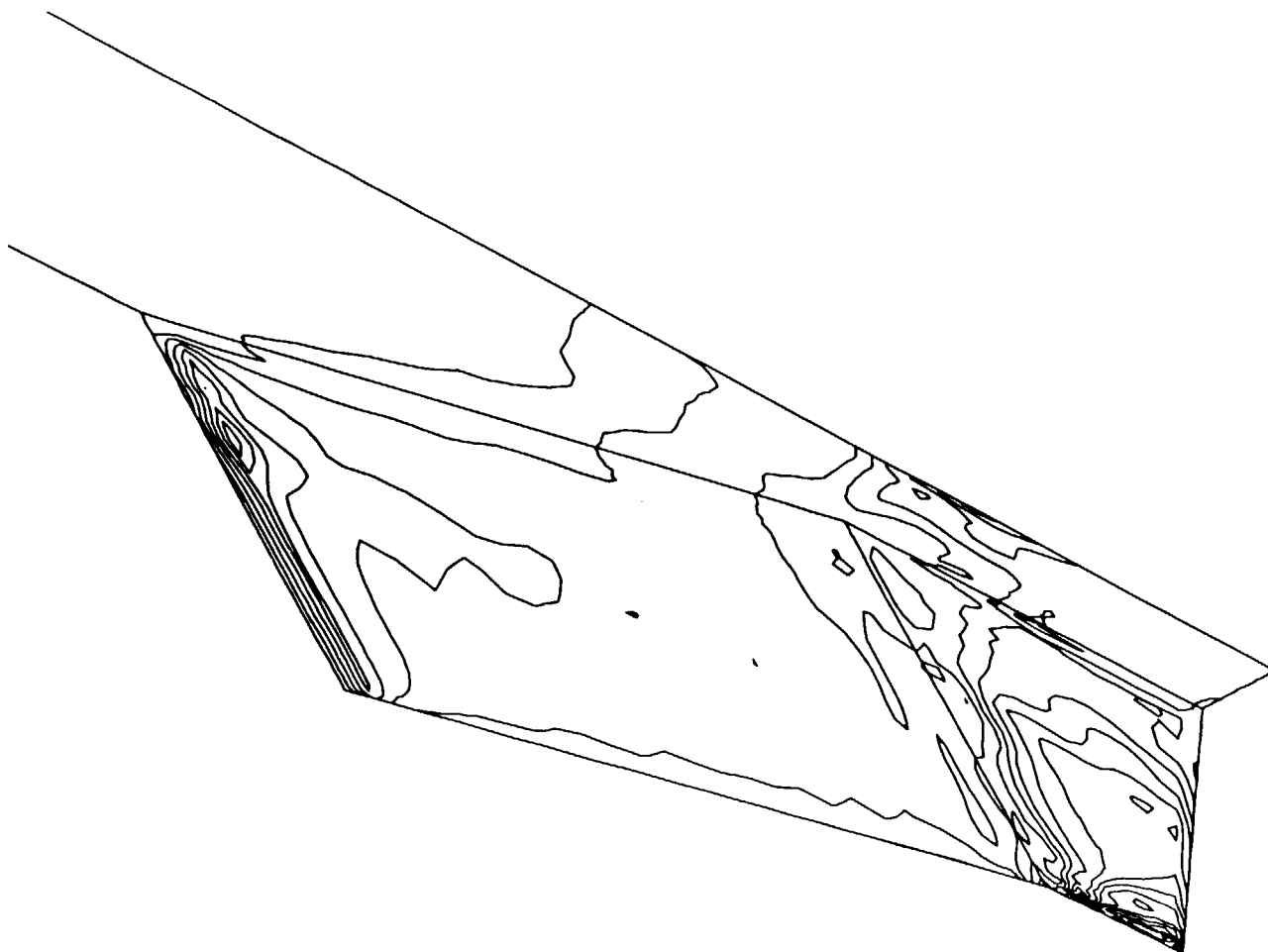


Figure 6.1.2: Sidewall and Baseplate Pressure Contours for  $CR = 3$ ,  
 $Re = 2.15$  million/ft, 0% Cowl

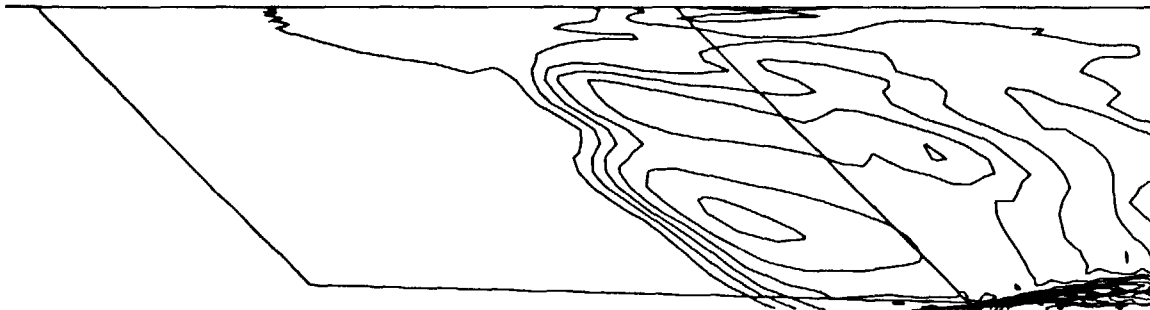


Figure 6.1.3: Centerline Pressure Contours for  $CR = 3$ ,  
 $Re = 2.15$  million/ft, 0% Cowl

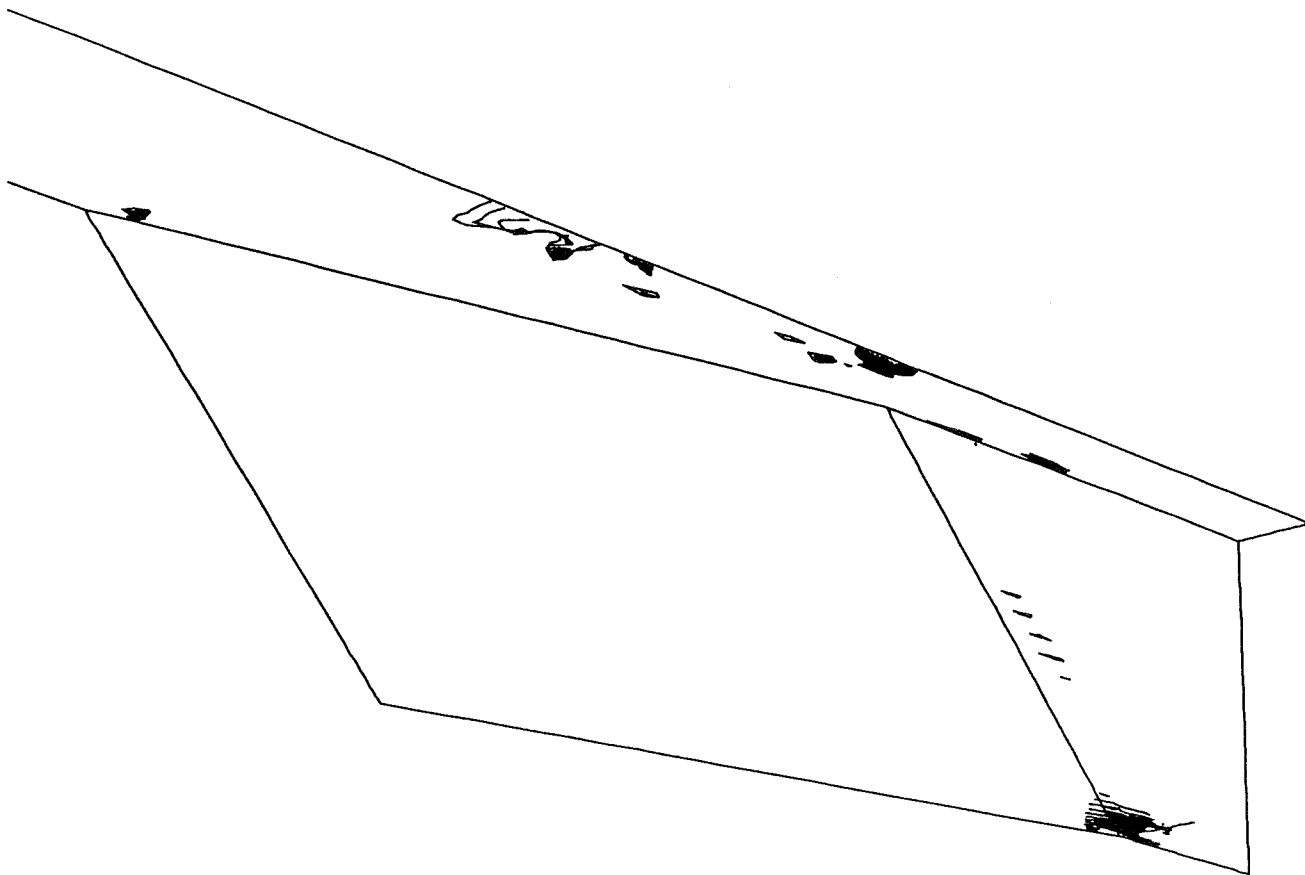


Figure 6.1.4: Streamwise Separation ( $U < 0$ ) for  $CR = 3$ ,  
 $Re = 2.15$  million/ft, 0% Cowl

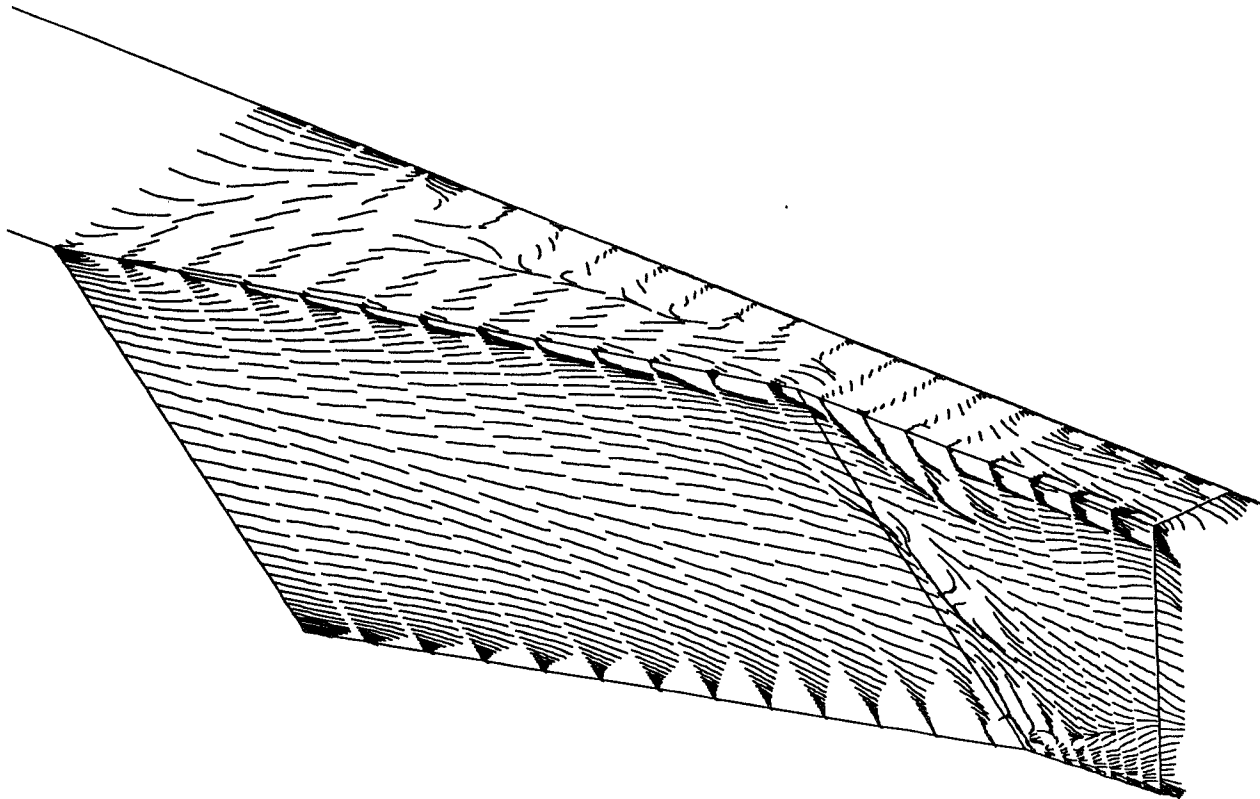


Figure 6.1.5: Simulated Oil Flow for  $CR = 3$ ,  $Re = 2.15$  million /ft, 0% Cowl

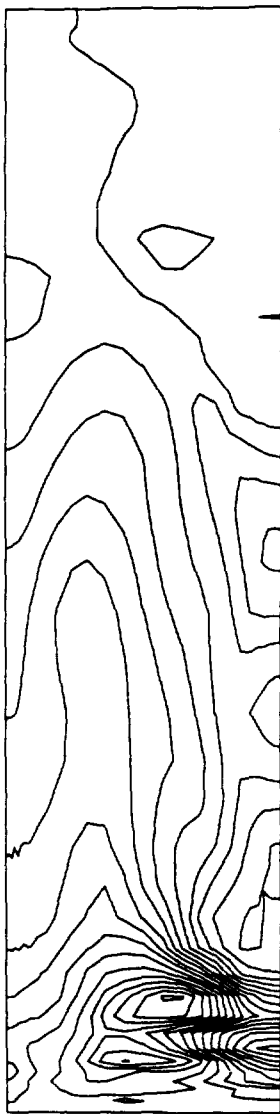


Figure 6.1.6: Exit Plane Pressure Contours for  $CR = 3$ ,  
 $Re = 2.15$  million/ft, 0% Cowl

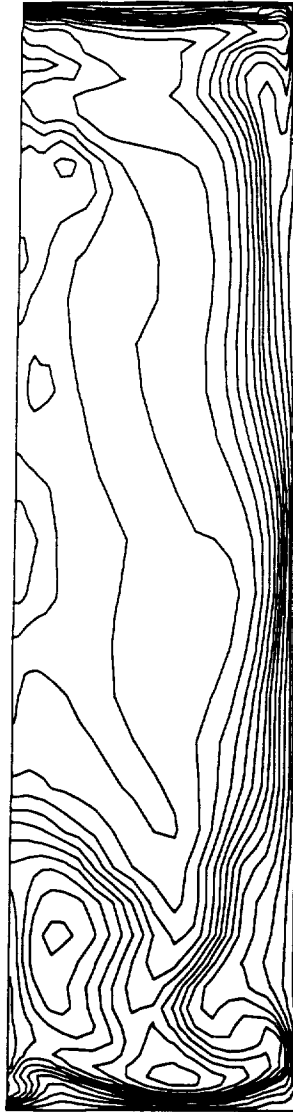


Figure 6.1.7: Exit Plane Mach Number Contours for  $CR = 3$ ,  
 $Re = 2.15$  million/ft, 0% Cowl

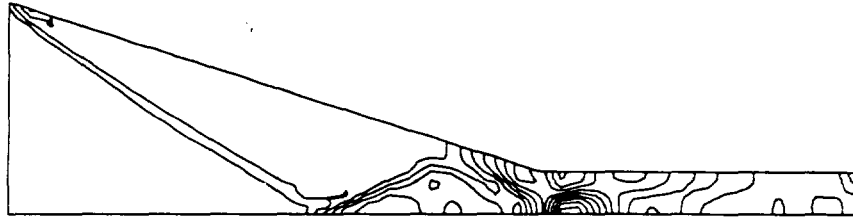


Figure 6.1.8(a): Pressure Contours at  $Z/H = 0.25$  for  $CR = 5$ ,  
 $Re = 2.15$  million/ft, 0% Cowl

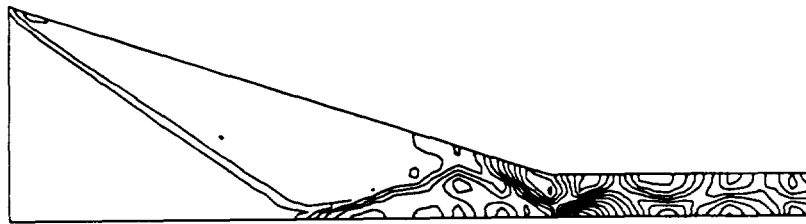


Figure 6.1.8(b): Pressure Contours at  $Z/H = 0.50$  for  $CR = 5$ ,  
 $Re = 2.15$  million/ft, 0% Cowl

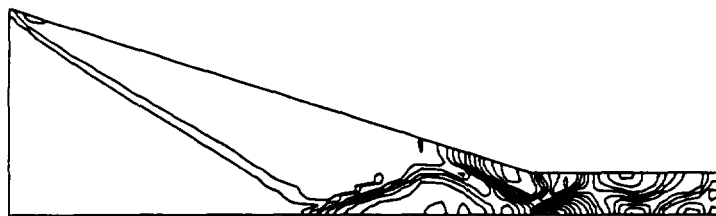


Figure 6.1.8(c): Pressure Contours at  $Z/H = 0.75$  for  $CR = 5$ ,  
 $Re = 2.15$  million/ft, 0% Cowl

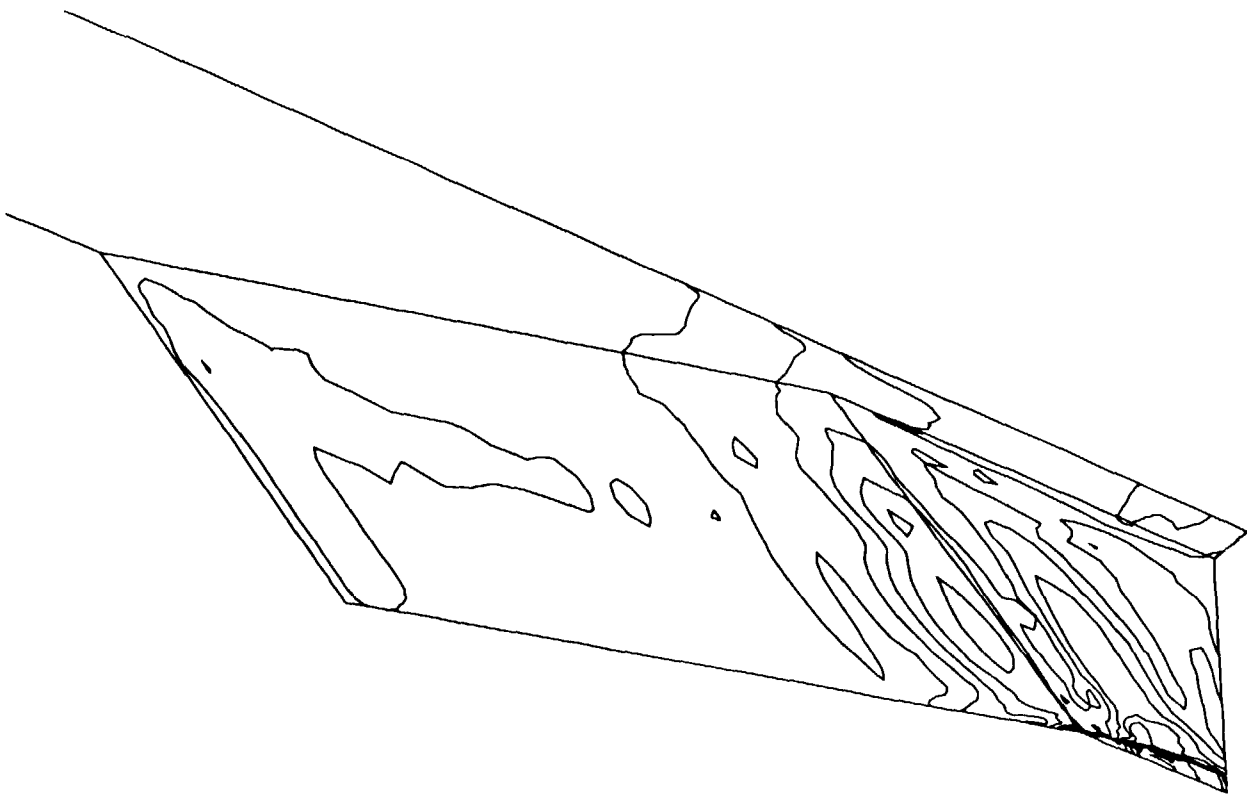


Figure 6.1.9: Sidewall and Baseplate Pressure Contours for  $CR = 5$ ,  
 $Re = 2.15$  million/ft, 0% Cowl





Figure 6.1.10: Centerline Pressure Contours for  $CR = 5$ ,  
 $Re = 2.15$  million/ft, 0% Cowl

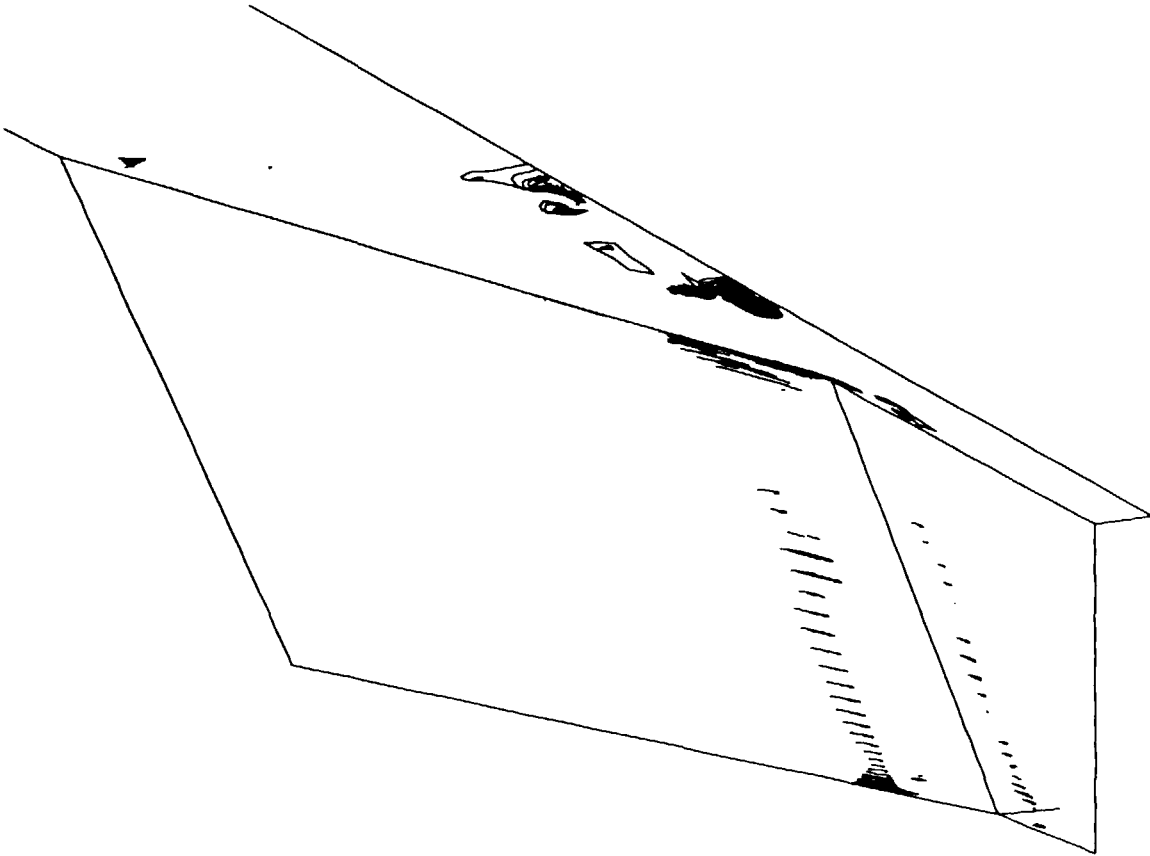


Figure 6.1.11: Streamwise Separation ( $U < 0$ ) for  $CR = 5$ ,  
 $Re = 2.15$  million/ft, 0% Cowl

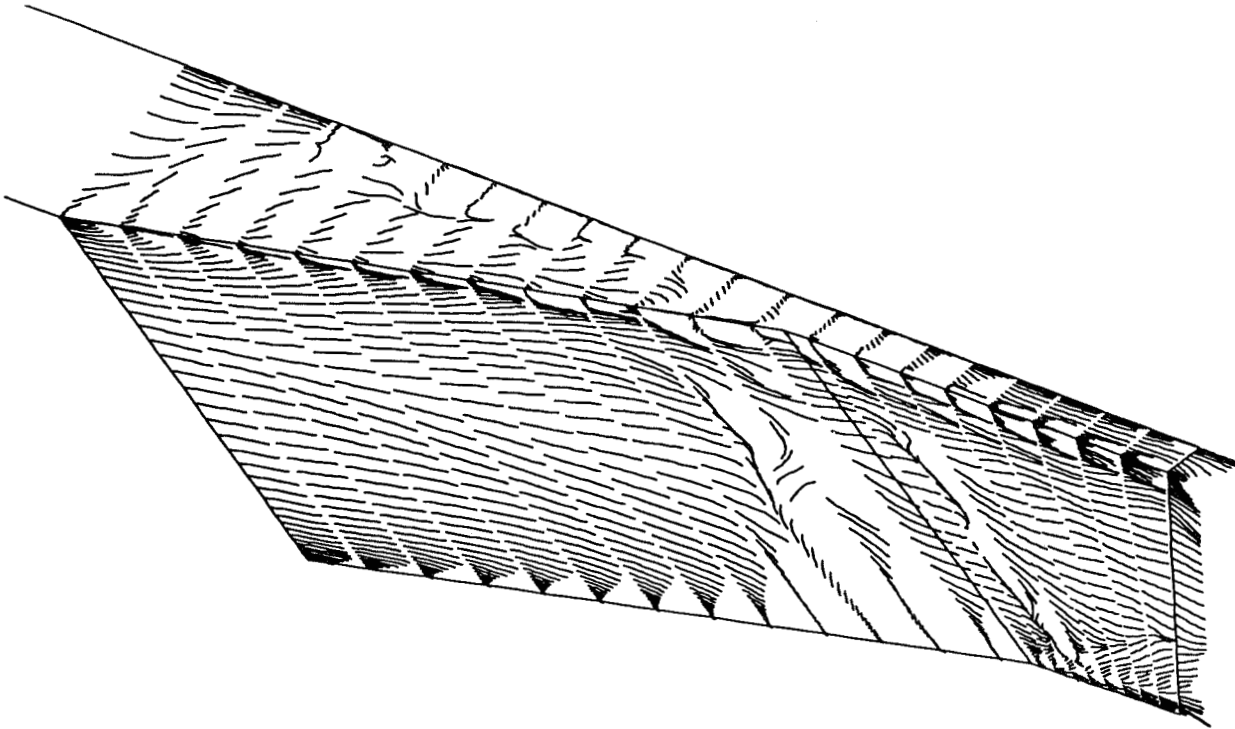


Figure 6.1.12: Simulated Oil Flow for  $CR = 5$ ,  $Re = 2.15$  million /ft, 0% Cowl

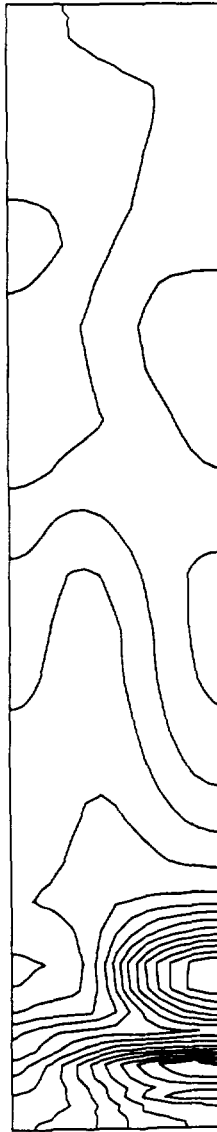


Figure 6.1.13: Exit Plane Pressure Contours for CR = 5,  
Re = 2.15 million/ft, 0% Cowl

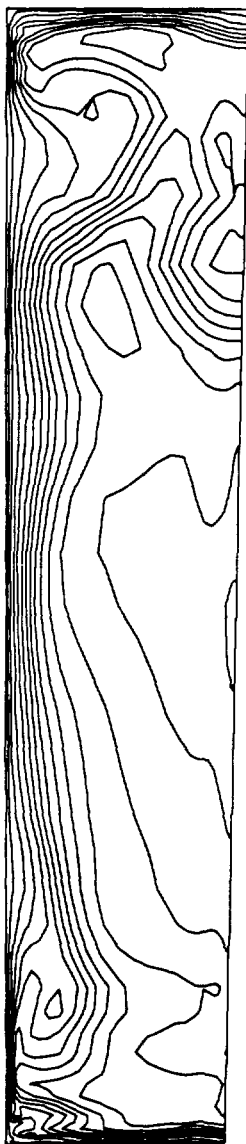


Figure 6.1.14: Exit Plane Mach Number Contours for  $CR = 5$ ,  
 $Re = 2.15$  million/ft, 0% Cowl

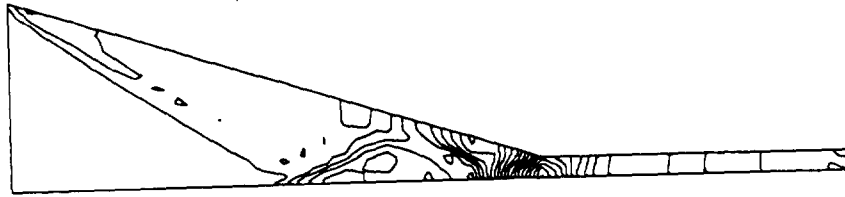


Figure 6.1.15(a): Pressure Contours at  $Z/H = 0.25$  for  $CR = 9$ ,  
 $Re = 2.15$  million/ft, 0% Cowl



Figure 6.1.15(b): Pressure Contours at  $Z/H = 0.50$  for  $CR = 9$ ,  
 $Re = 2.15$  million/ft, 0% Cowl

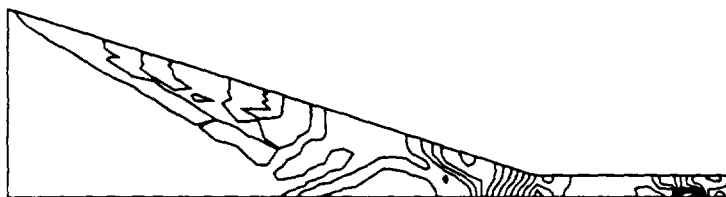


Figure 6.1.15(c): Pressure Contours at  $Z/H = 0.75$  for  $CR = 9$ ,  
 $Re = 2.15$  million/ft, 0% Cowl

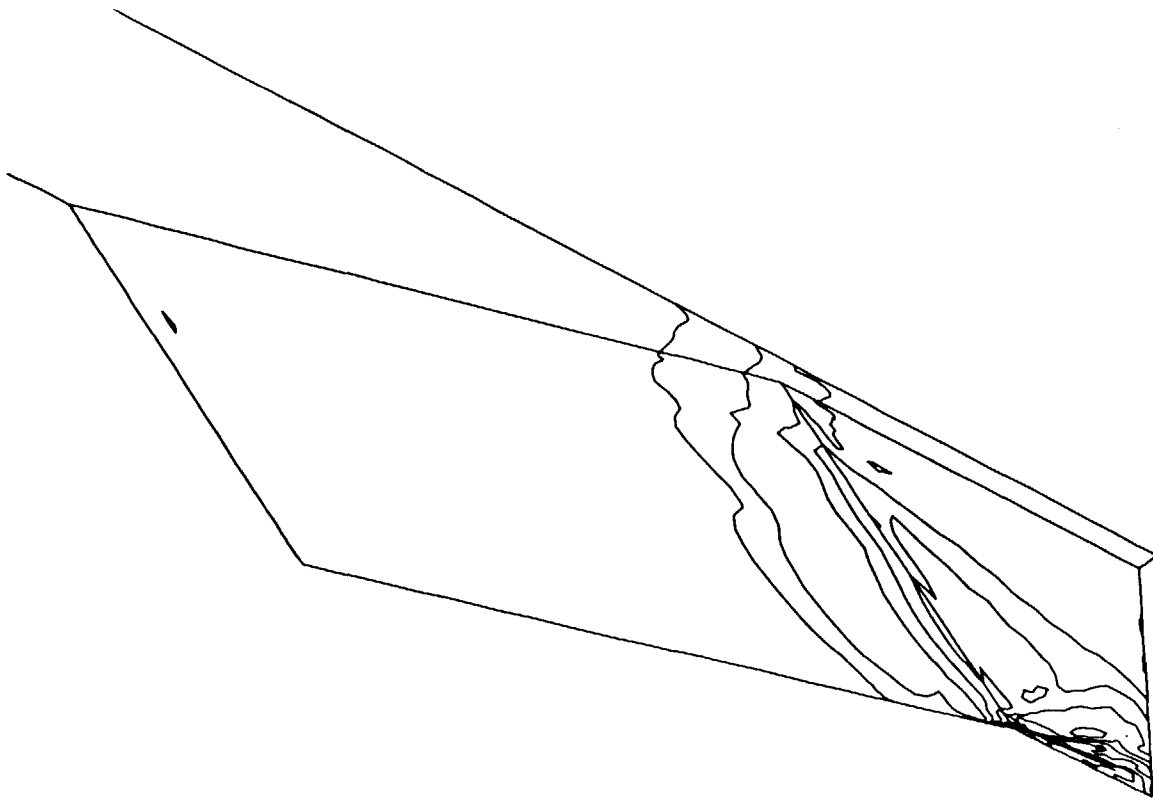


Figure 6.1.16: Sidewall and Baseplate Pressure Contours for  $CR = 9$ ,  
 $Re = 2.15$  million/ft, 0% Cowl

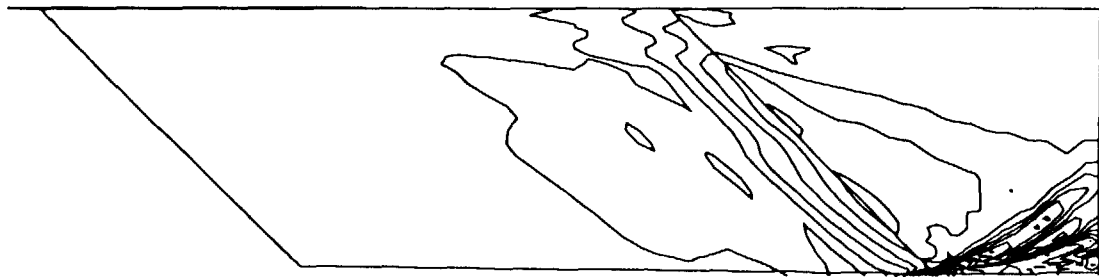
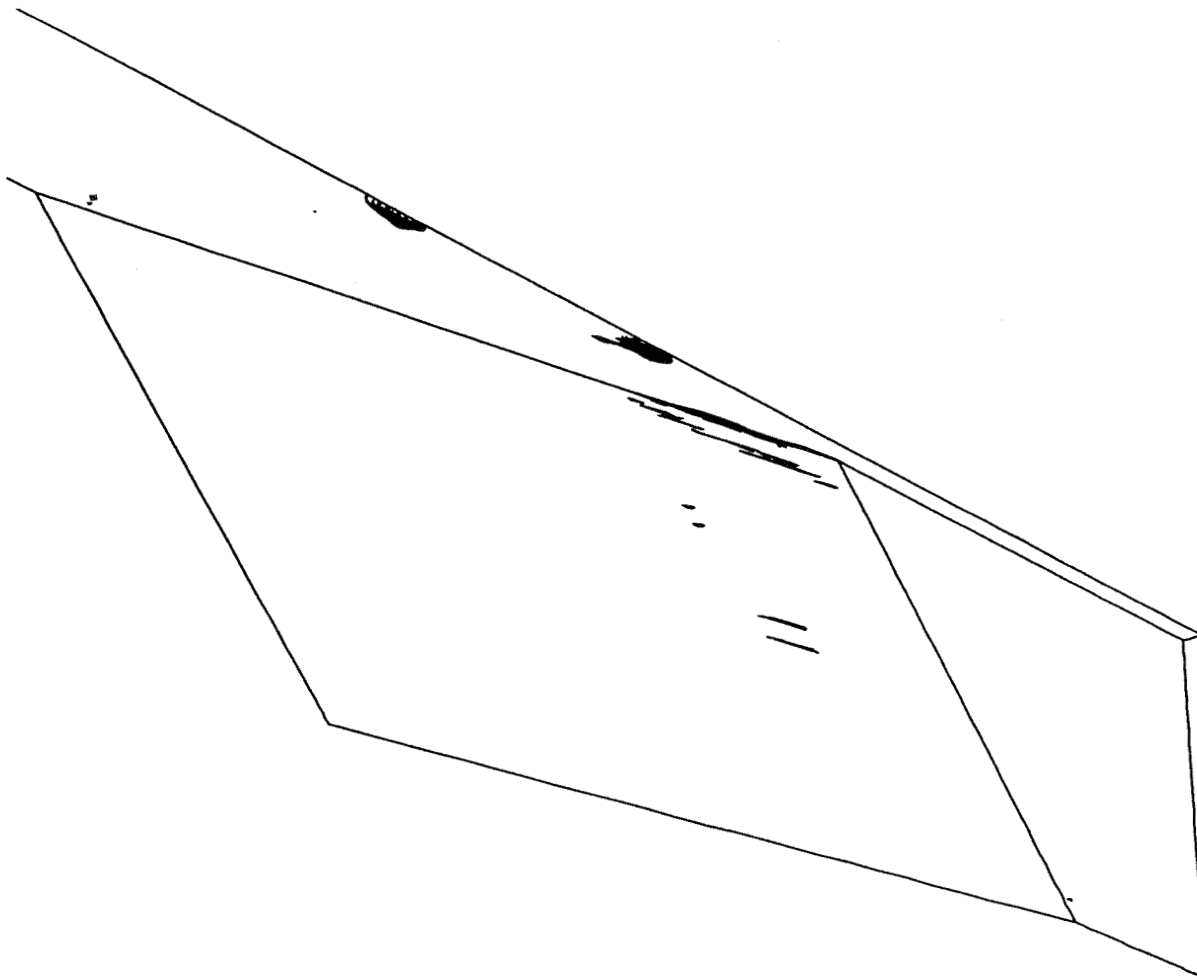


Figure 6.1.17: Centerline Pressure Contours for  $CR = 9$ ,  
 $Re = 2.15$  million/ft, 0% Cowl





**Figure 6.1.18: Streamwise Separation ( $U < 0$ ) for CR = 9, Re = 2.15 million/ft, 0% Cowl**

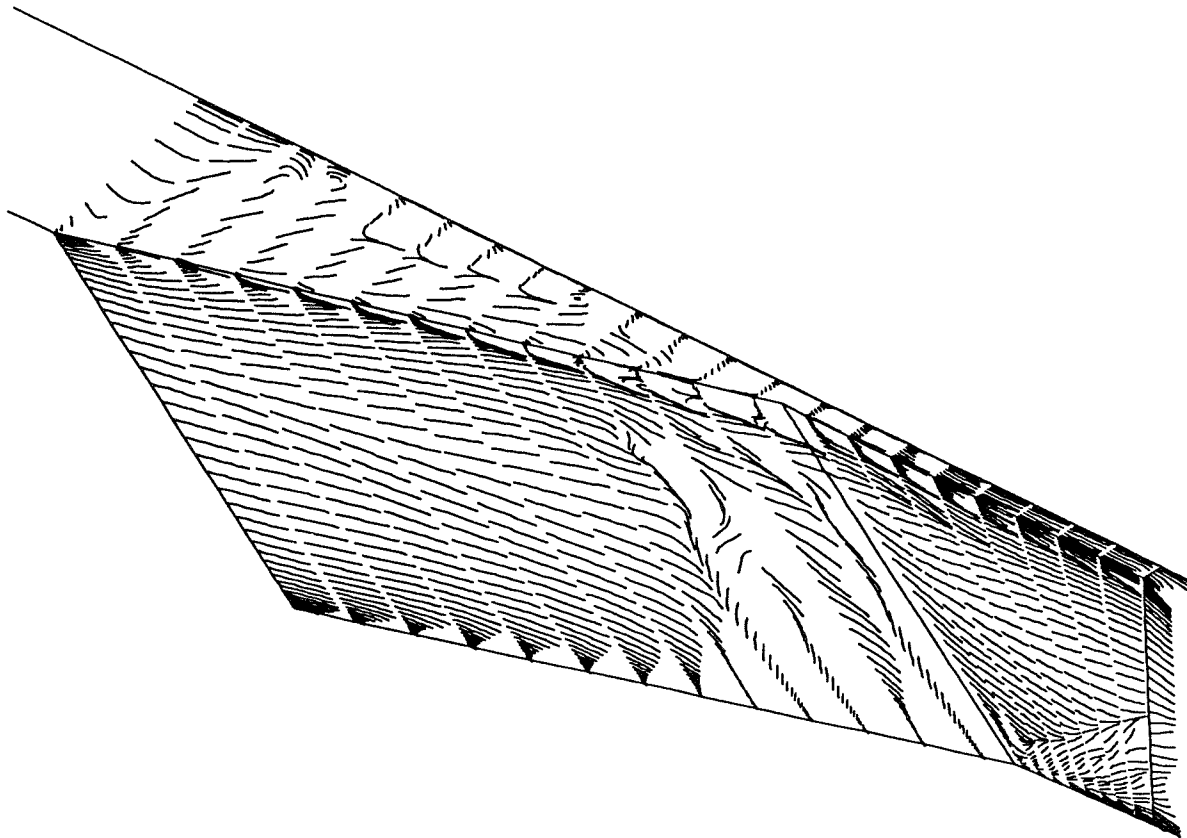


Figure 6.1.19: Simulated Oil Flow for  $CR = 9$ ,  $Re = 2.15$  million /ft, 0% Cowl



Figure 6.1.20: Exit Plane Pressure Contours for  $CR = 9$ ,  $Re = 2.15$  million/ft, 0% Cowl



Figure 6.1.21: Exit Plane Mach Number Contours for  $CR = 9$ ,  
 $Re = 2.15$  million/ft, 0% Cowl

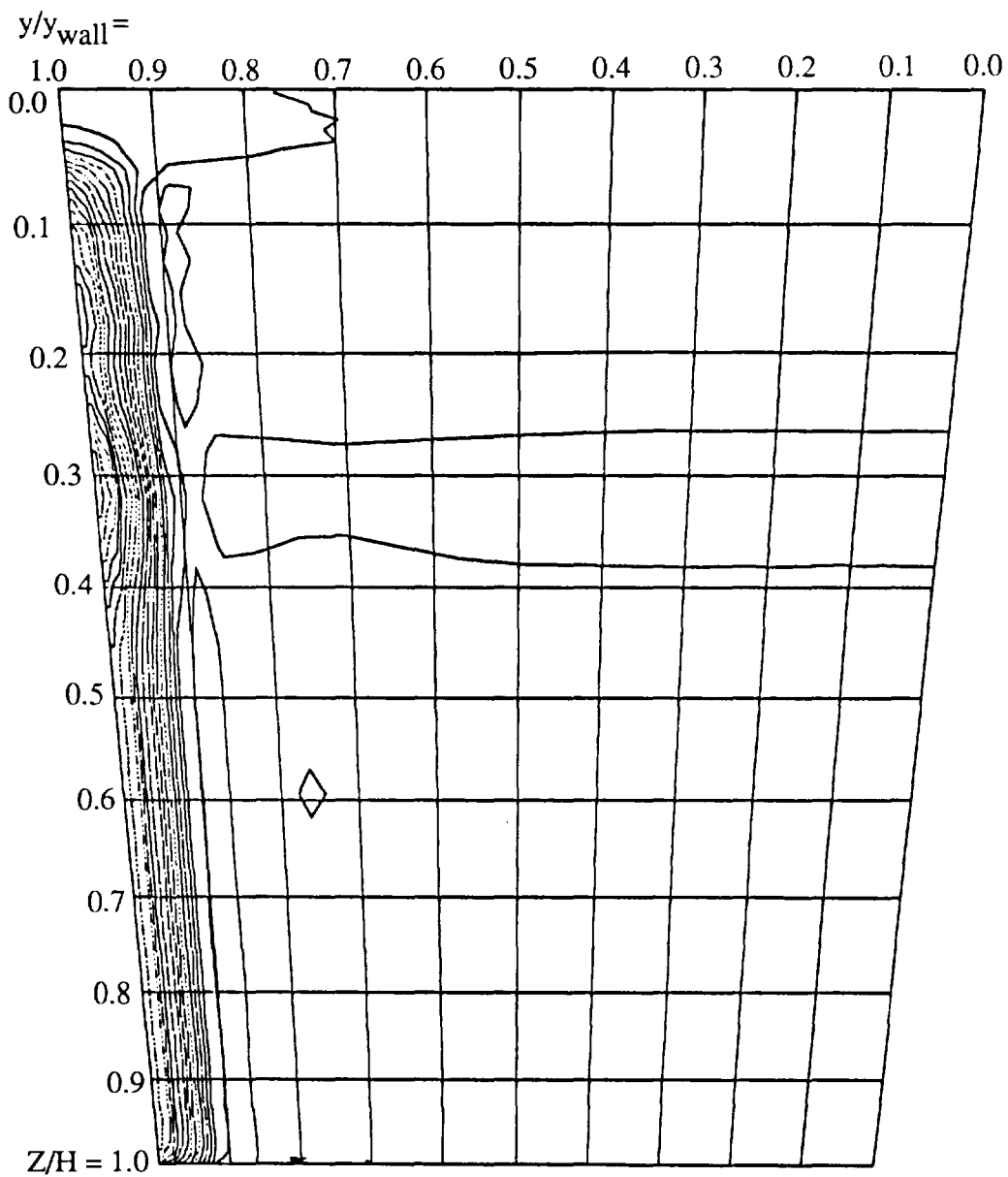


Figure 6.1.1.1: Pressure Contours at  $I=31$ ,  $x'/Tx'=0.04$  for  $CR=3$ ,  
0% Cowl,  $Re=2.15$  million/ft

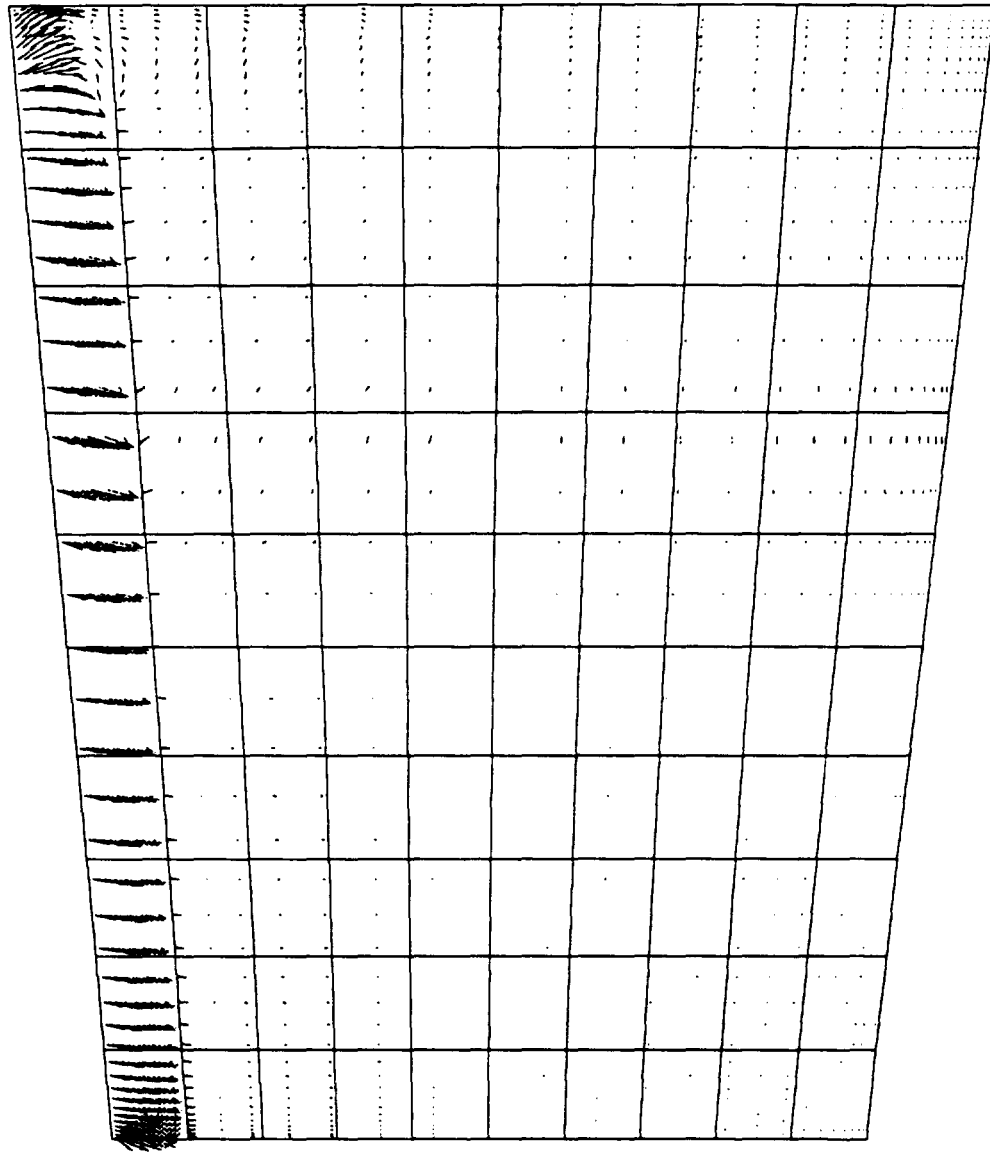


Figure 6.1.1.2: Crossflow Velocity Vectors at  $I = 31$ ,  $x'/Tx' = 0.04$  for  $CR = 3$ ,  
0% Cowl,  $Re = 2.15$  million/ft

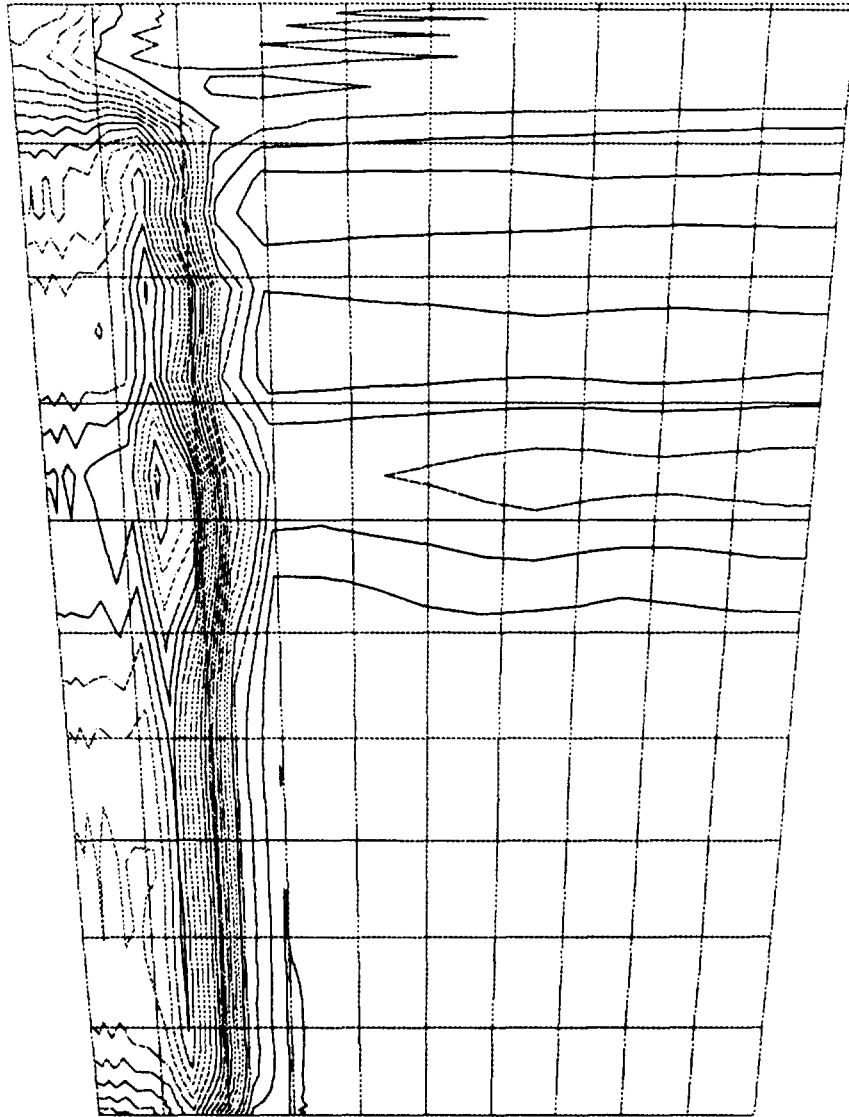


Figure 6.1.1.3: Pressure Contours at  $I = 35$ ,  $x'/Tx' = 0.20$  for  $CR = 3$ ,  
0% Cowl,  $Re = 2.15$  million/ft

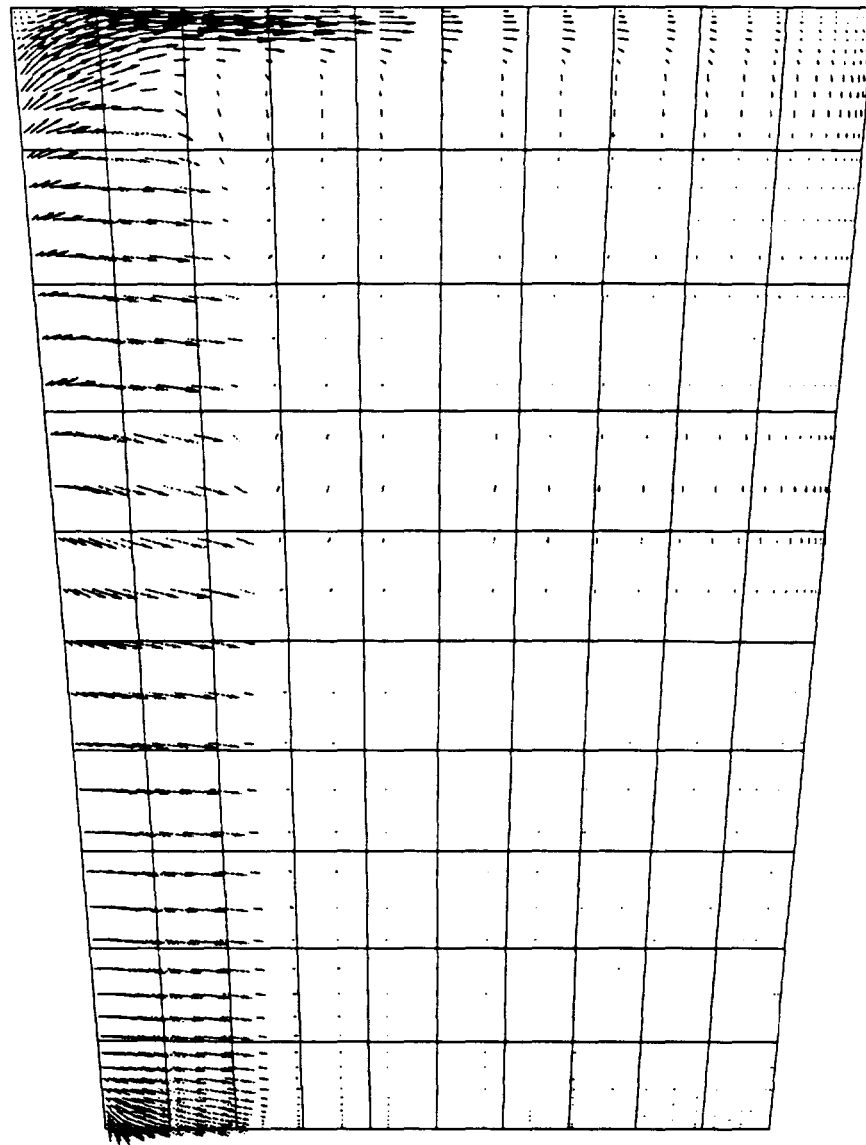


Figure 6.1.1.4: Crossflow Velocity Vectors at  $I = 35$ ,  $x'/Tx' = 0.20$  for  $CR = 3$ ,  
0% Cowl,  $Re = 2.15$  million/ft



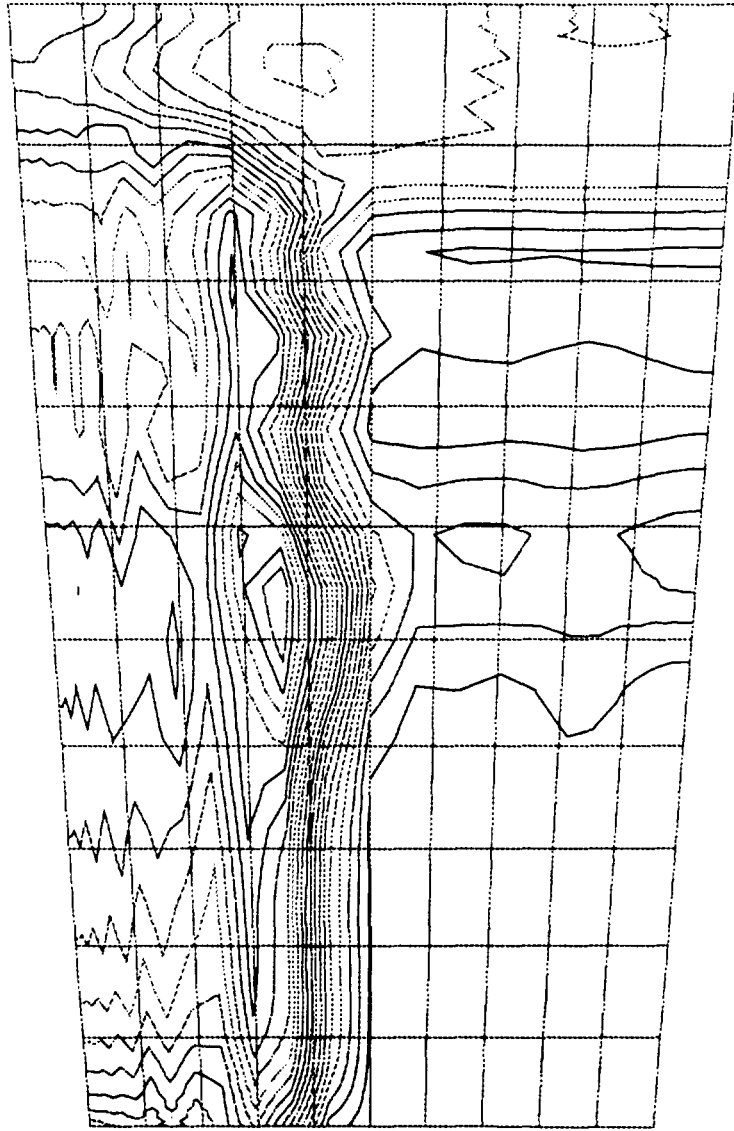


Figure 6.1.1.5: Pressure Contours at  $I = 40$ ,  $x'/Tx' = 0.40$  for  $CR = 3$ ,  
0% Cowl,  $Re = 2.15$  million/ft

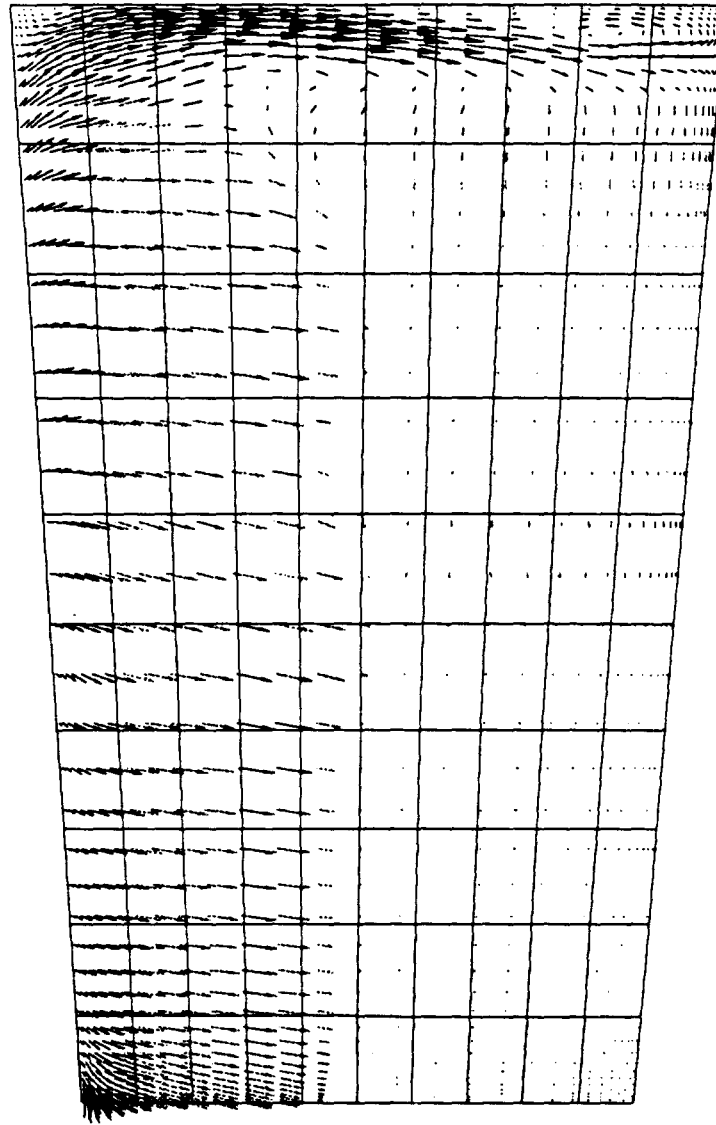


Figure 6.1.1.6: Crossflow Velocity Vectors at  $I = 40$ ,  $x'/T_x' = 0.40$  for  $CR = 3$ ,  
0% Cowl,  $Re = 2.15$  million/ft

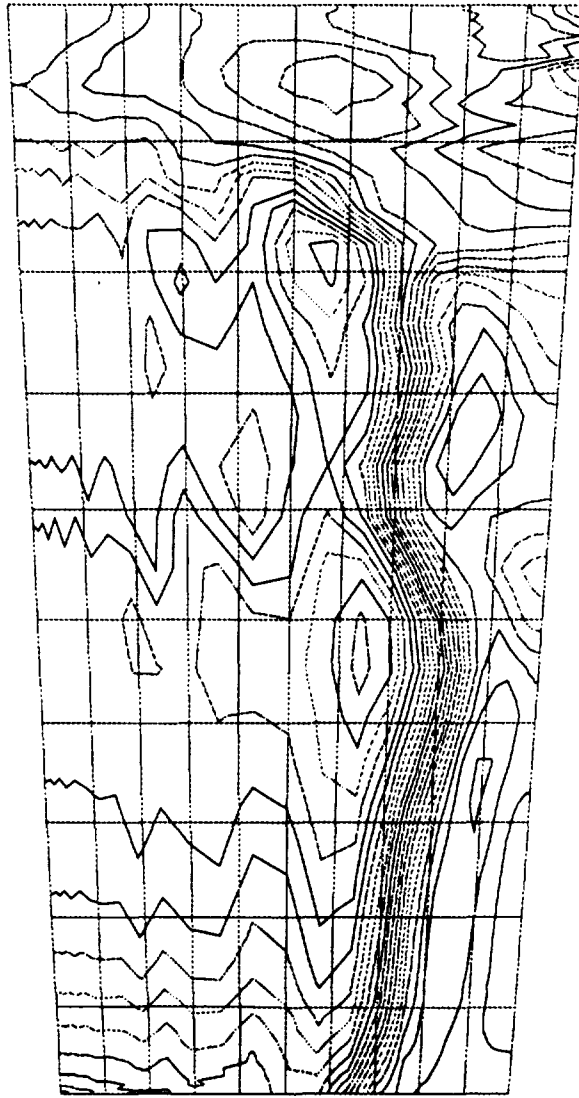


Figure 6.1.1.7: Pressure Contours at  $I=45$ ,  $x'/Tx' = 0.60$  for  $CR = 3$ ,  
0% Cowl,  $Re = 2.15$  million/ft

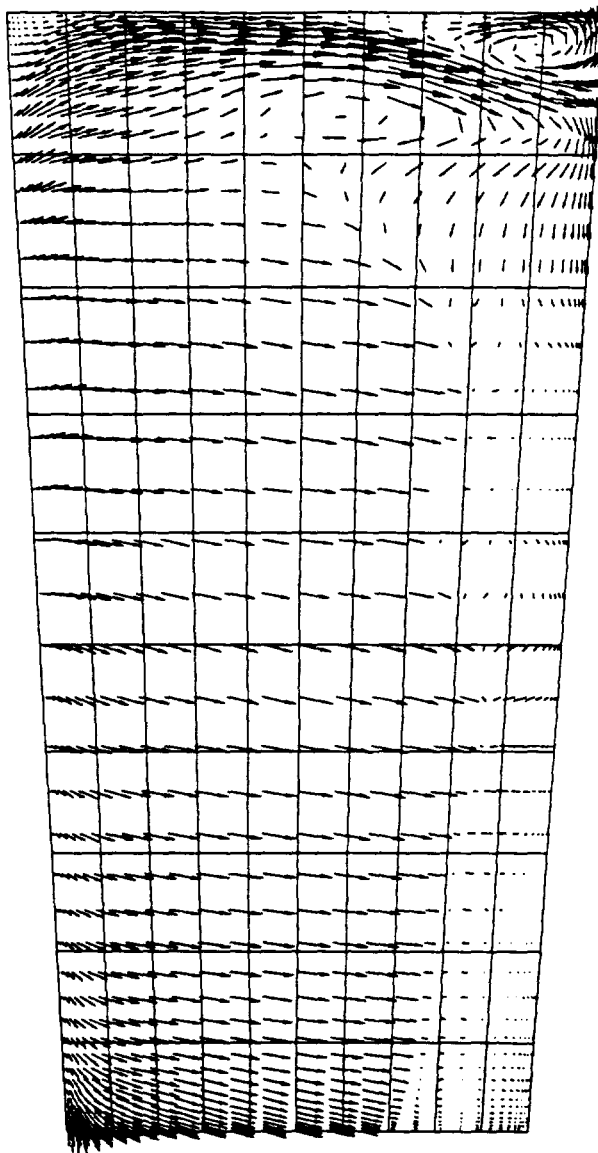


Figure 6.1.1.8: Crossflow Velocity Vectors at  $I = 45$ ,  $x'/Tx' = 0.60$  for  $CR = 3$ ,  
0% Cowl,  $Re = 2.15$  million/ft

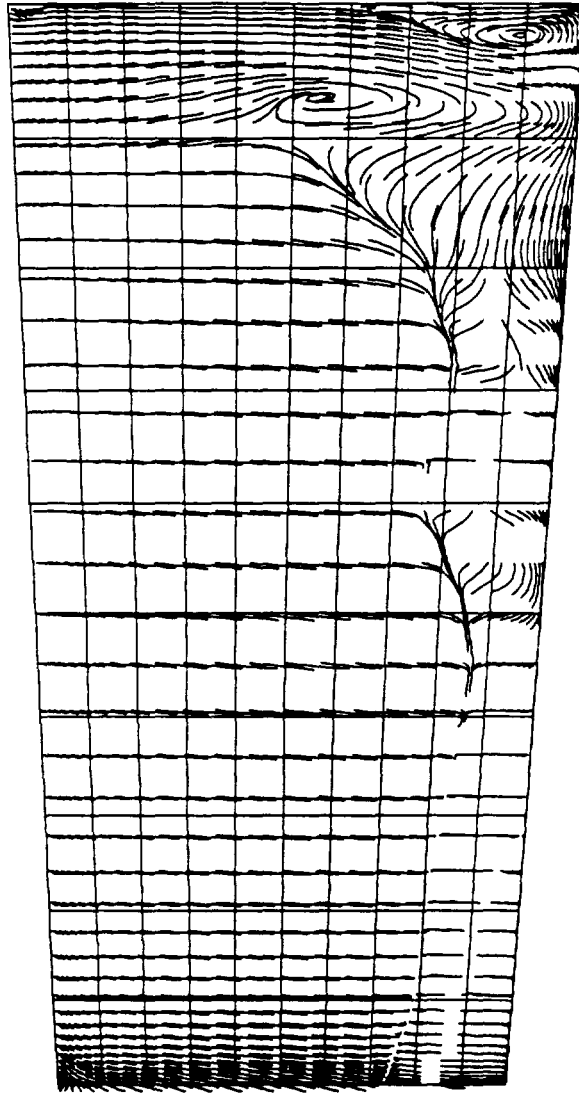


Figure 6.1.1.9: Particle Traces at  $I = 45$ ,  $x'/Tx' = 0.60$  for  $CR = 3$ ,  
0% Cowl,  $Re = 2.15$  million/ft

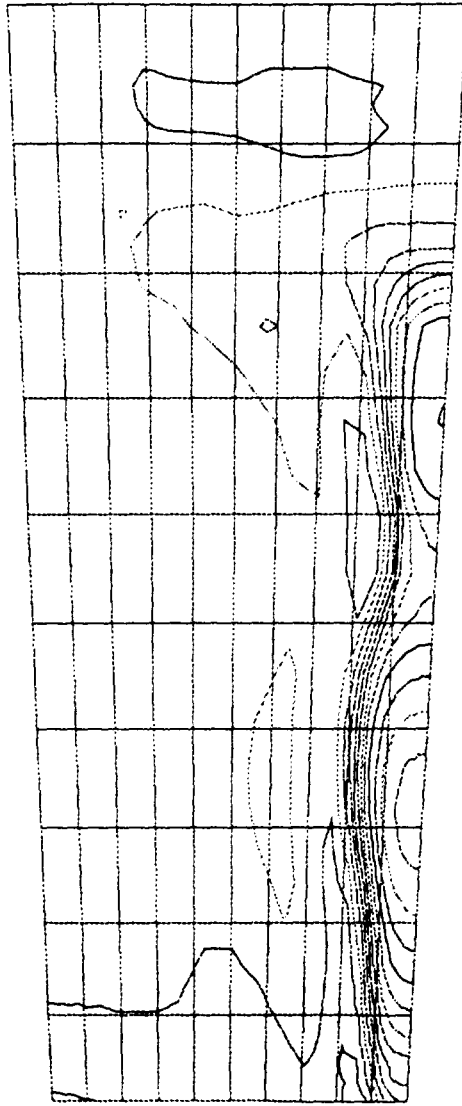


Figure 6.1.1.10: Pressure Contours at  $I = 50$ ,  $x'/Tx' = 0.79$  for  $CR = 3$ ,  
0% Cowl,  $Re = 2.15$  million/ft

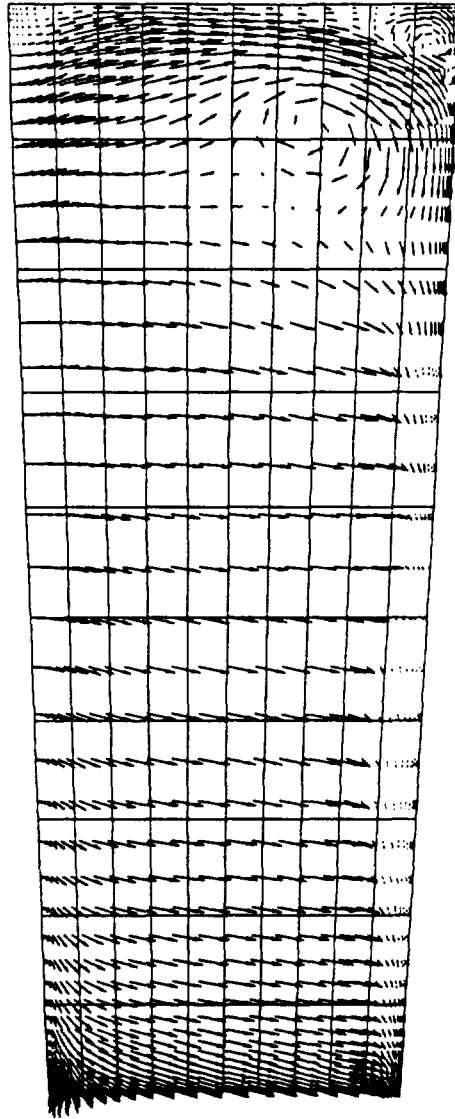


Figure 6.1.1.11: Crossflow Velocity Vectors at  $I = 50$ ,  $x'/Tx' = 0.79$  for  $CR = 3$ ,  
0% Cowl,  $Re = 2.15$  million/ft

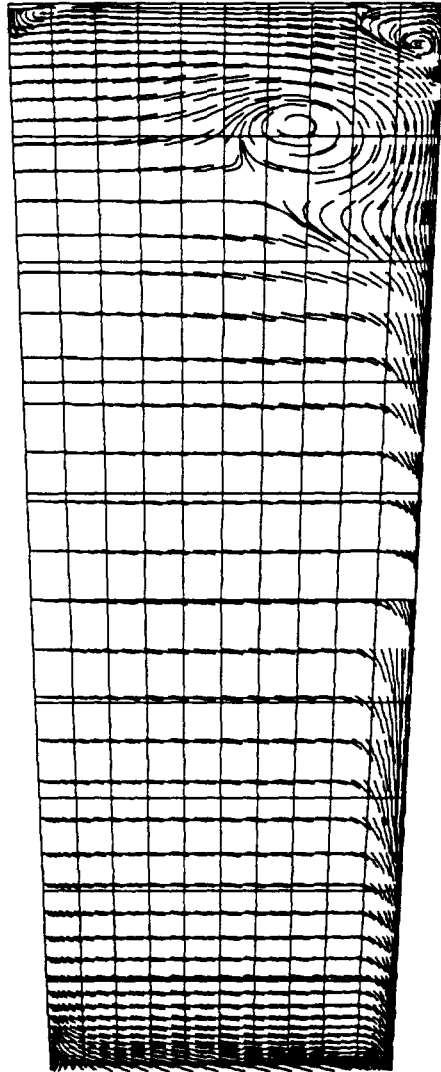


Figure 6.1.1.12: Particle Traces at  $I = 50$ ,  $x'/Tx' = 0.79$  for  $CR = 3$ ,  
0% Cowl,  $Re = 2.15$  million/ft



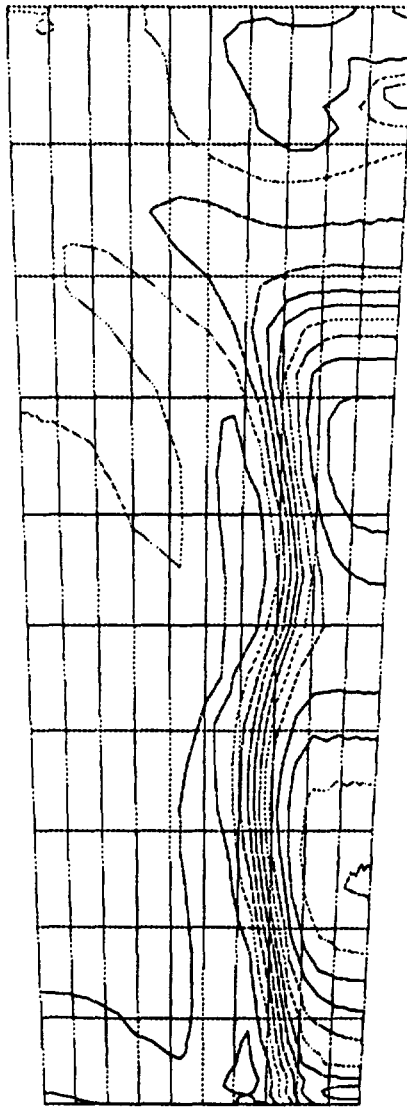


Figure 6.1.1.13: Pressure Contours at  $I = 52$ ,  $x'/Tx' = 0.87$  for  $CR = 3$ ,  
0% Cowl,  $Re = 2.15$  million/ft

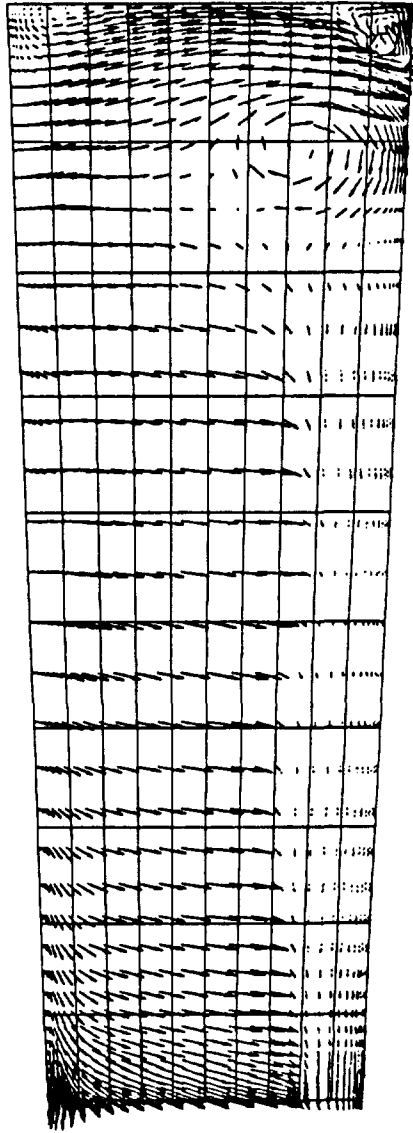


Figure 6.1.1.14: Crossflow Velocity Vectors at  $I = 52$ ,  $x'/Tx' = 0.87$  for  $CR = 3$ ,  
0% Cowl,  $Re = 2.15$  million/ft

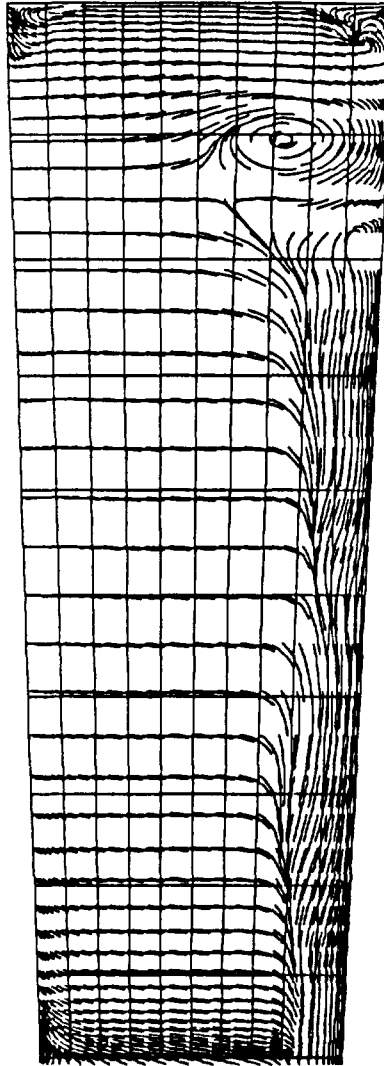


Figure 6.1.1.15: Particle Traces at  $I = 52$ ,  $x'/Tx' = 0.87$  for  $CR = 3$ ,  
0% Cowl,  $Re = 2.15$  million/ft

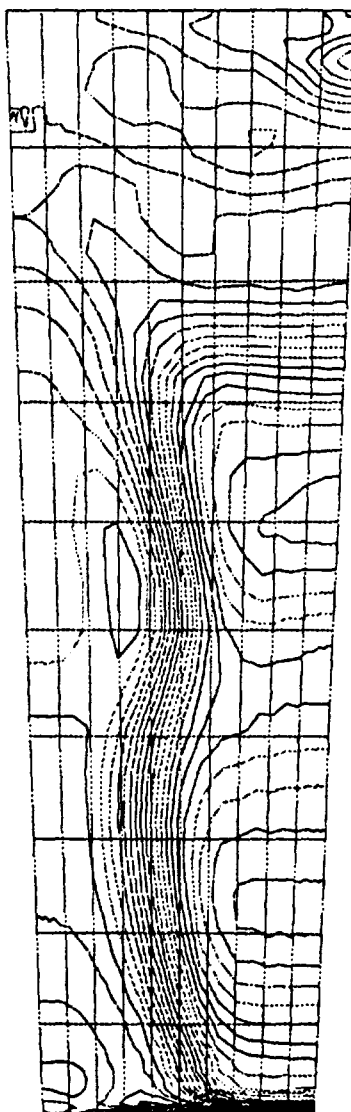


Figure 6.1.1.16: Pressure Contours at  $I = 54$ ,  $x'/Tx' = 0.96$  for  $CR = 3$ ,  
0% Cowl,  $Re = 2.15$  million/ft

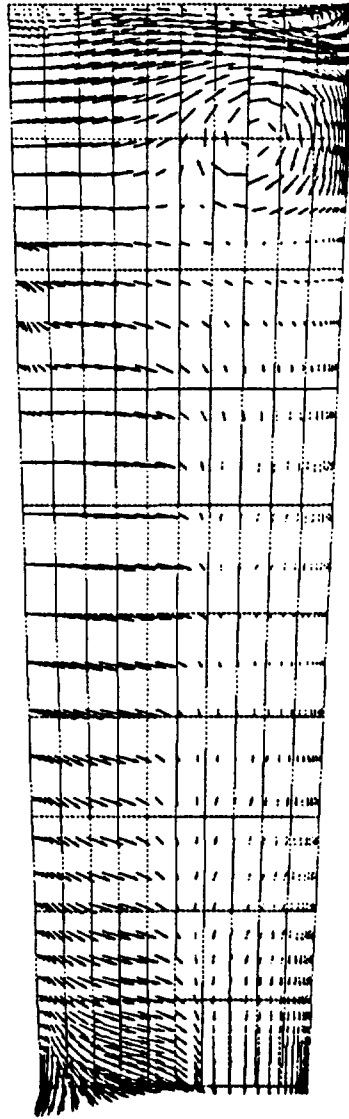


Figure 6.1.1.17: Crossflow Velocity Vectors at  $I = 54$ ,  $x'/Tx' = 0.96$  for  $CR = 3$ ,  
0% Cowl,  $Re = 2.15$  million/ft

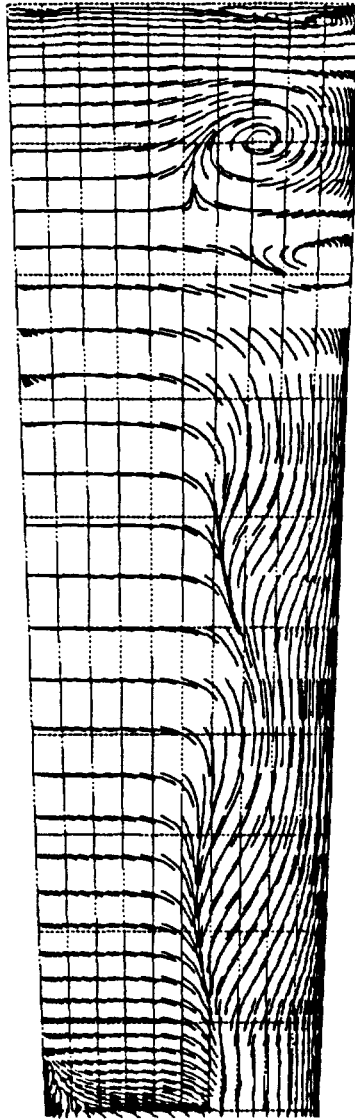


Figure 6.1.1.18: Particle Traces at  $I = 54$ ,  $x'/Tx' = 0.96$  for  $CR = 3$ ,  
0% Cowl,  $Re = 2.15$  million/ft

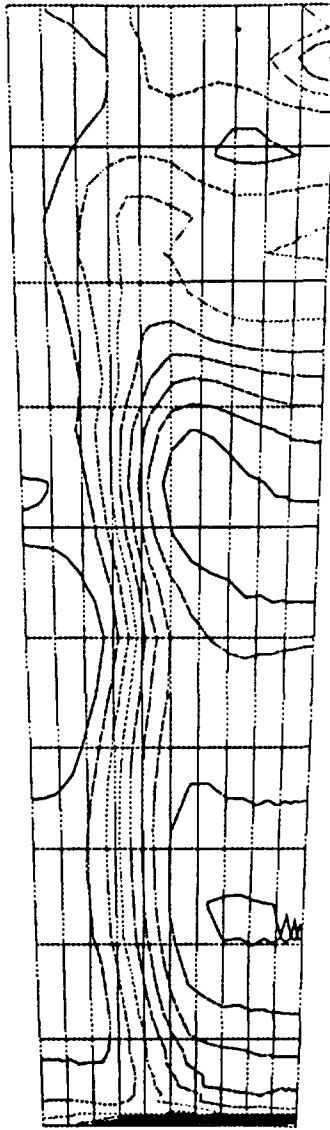


Figure 6.1.1.19: Pressure Contours at  $I = 55$ ,  $x'/Tx' = 1.00$  for  $CR = 3$ ,  
0% Cowl,  $Re = 2.15$  million/ft

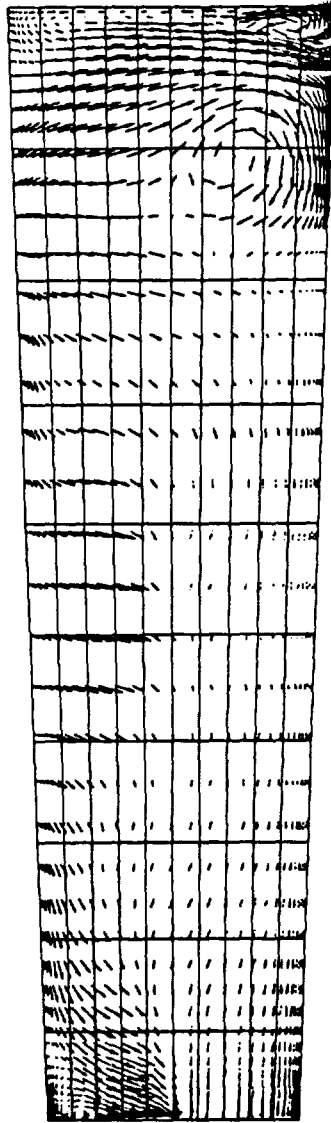


Figure 6.1.1.20: Crossflow Velocity Vectors at  $I = 55$ ,  $x'/Tx' = 1.00$  for  $CR = 3$ ,  
0% Cowl,  $Re = 2.15$  million/ft



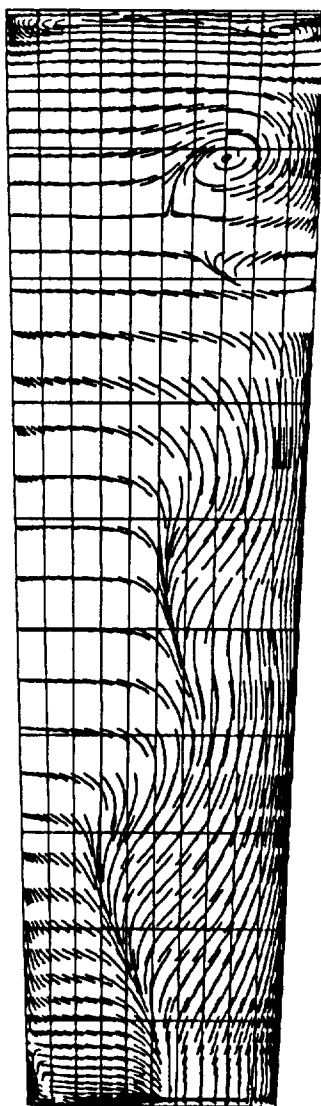


Figure 6.1.1.21: Particle Traces at  $I = 55$ ,  $x'/T_x' = 1.00$  for  $CR = 3$ ,  
0% Cowl,  $Re = 2.15$  million/ft

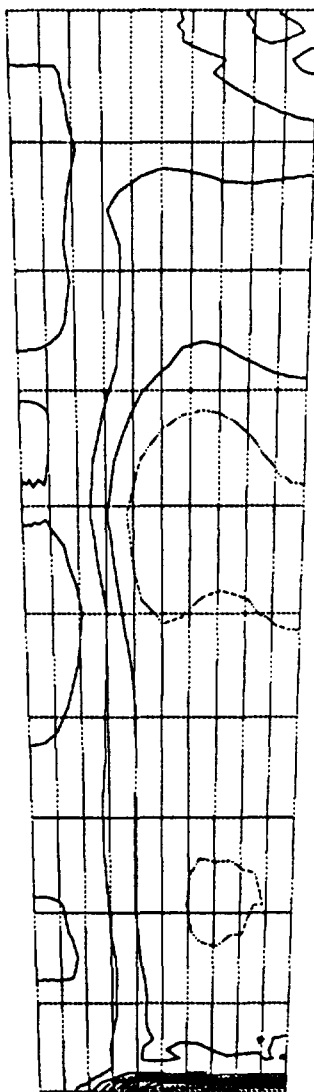


Figure 6.1.1.22: Pressure Contours at  $I = 56$ ,  $xs'/Te' = 0.06$  for  $CR = 3$ ,  
0% Cowl,  $Re = 2.15$  million/ft

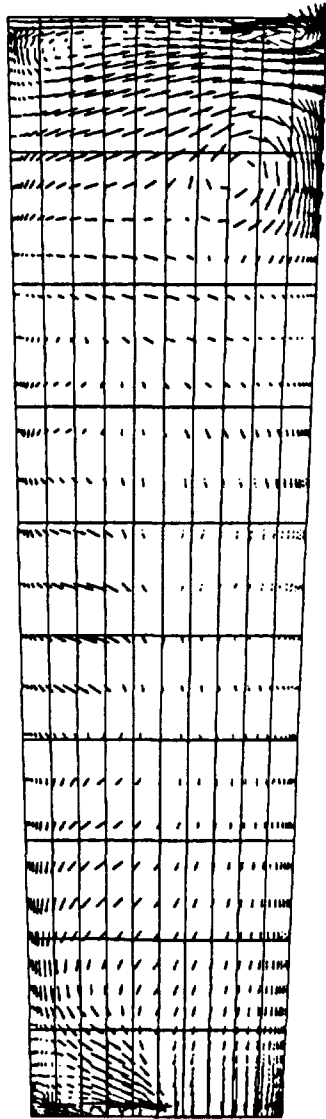


Figure 6.1.1.23: Crossflow Velocity Vectors at  $I = 56$ ,  $xs'/Te' = 0.06$  for  $CR = 3$ ,  
0% Cowl,  $Re = 2.15$  million/ft

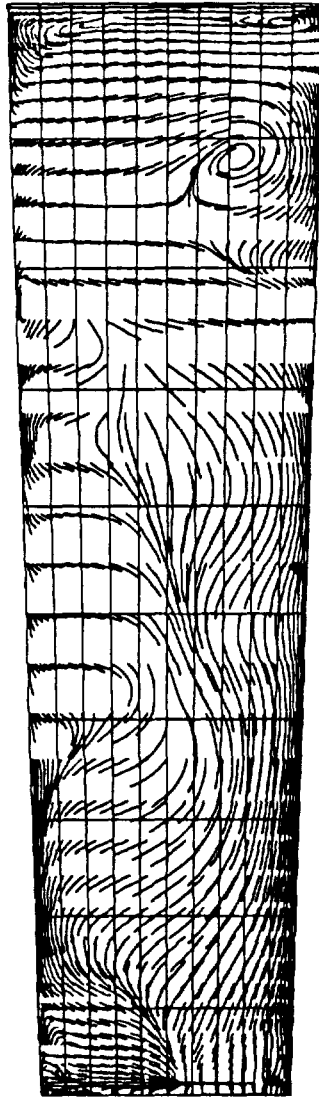


Figure 6.1.1.24: Particle Traces at  $I = 56$ ,  $xs'/Te' = 0.06$  for  $CR = 3$ ,  
0% Cowl,  $Re = 2.15$  million/ft

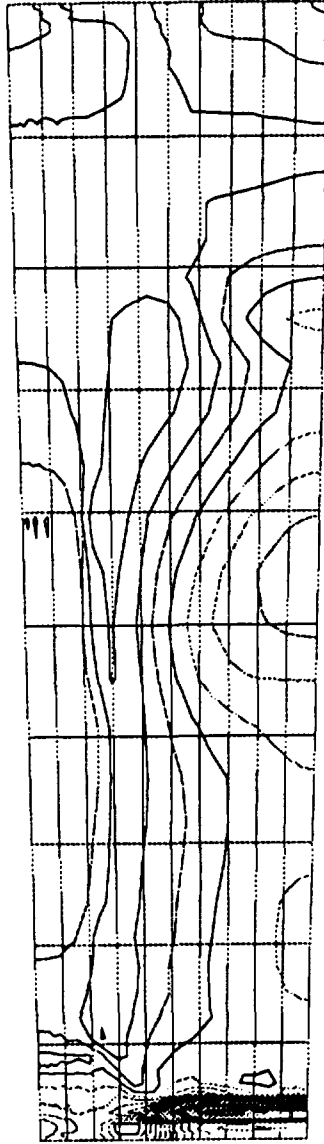


Figure 6.1.1.25: Pressure Contours at  $I = 60$ ,  $xs'/Te' = 0.29$  for  $CR = 3$ ,  
0% Cowl,  $Re = 2.15$  million/ft

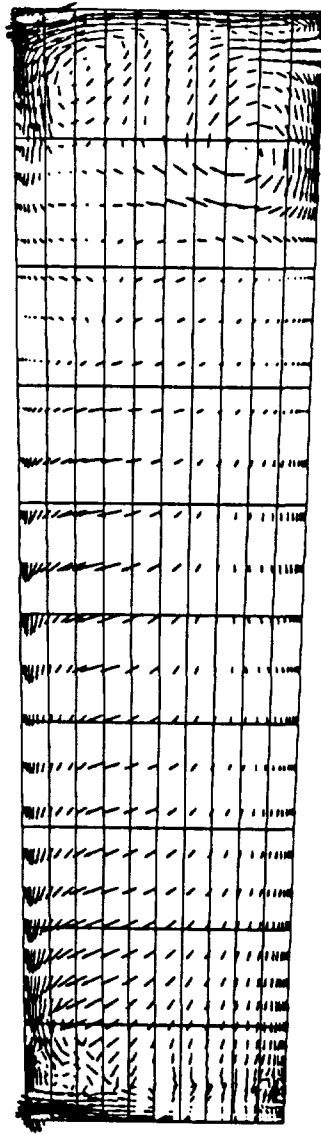


Figure 6.1.1.26: Crossflow Velocity Vectors at  $I = 60$ ,  $x_s'/Te' = 0.29$  for  $CR = 3$ ,  
0% Cowl,  $Re = 2.15$  million/ft

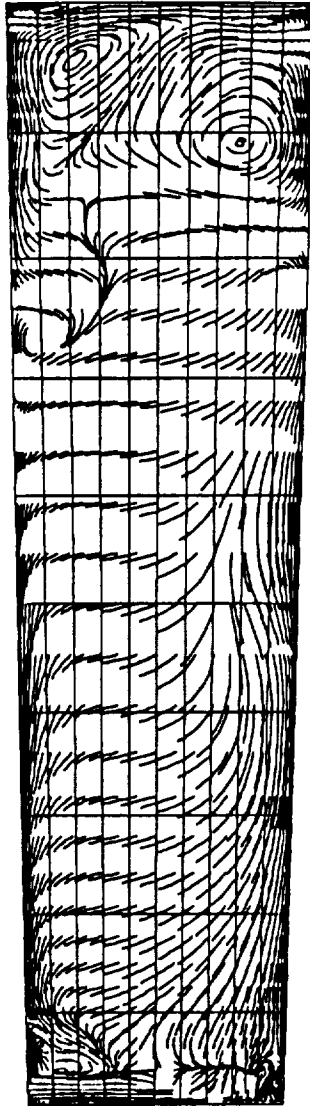


Figure 6.1.1.27: Particle Traces at  $I = 60$ ,  $x_s'/Te' = 0.29$  for  $CR = 3$ ,  
0% Cowl,  $Re = 2.15$  million/ft



Figure 6.1.1.28: Pressure Contours at  $I = 65$ ,  $xs'/Te' = 0.58$  for  $CR = 3$ ,  
0% Cowl,  $Re = 2.15$  million/ft



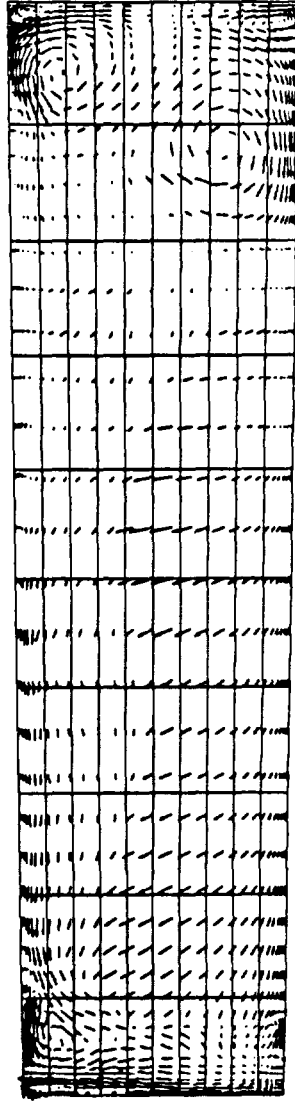


Figure 6.1.1.29: Crossflow Velocity Vectors at  $I = 65$ ,  $x_s'/Te' = 0.58$  for  $CR = 3$ ,  
0% Cowl,  $Re = 2.15$  million/ft

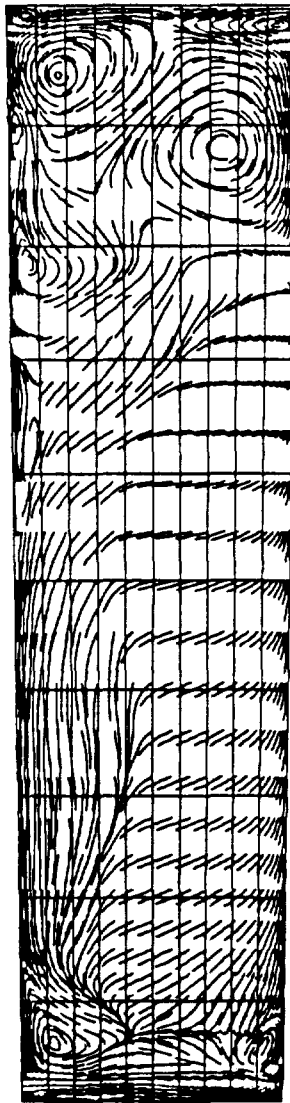


Figure 6.1.1.30: Particle Traces at  $I = 65$ ,  $xs'/Te' = 0.58$  for  $CR = 3$ ,  
0% Cowl,  $Re = 2.15$  million/ft

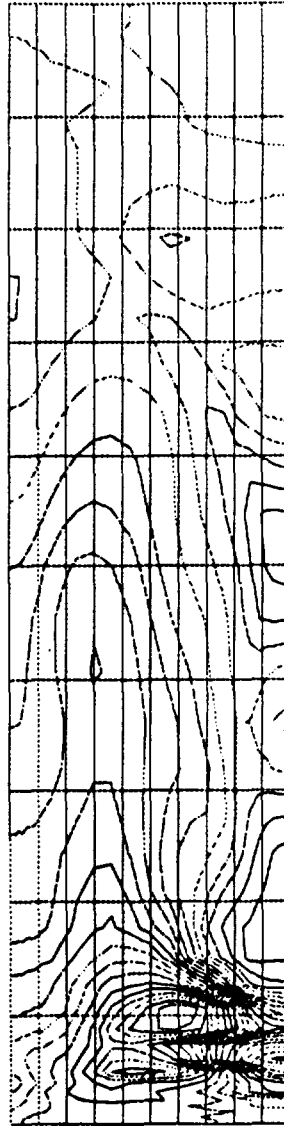


Figure 6.1.1.31: Pressure Contours at  $I = 72$ ,  $xs'/Te' = 1.00$  (Exit Plane) for  $CR = 3$ , 0% Cowl,  $Re = 2.15$  million/ft

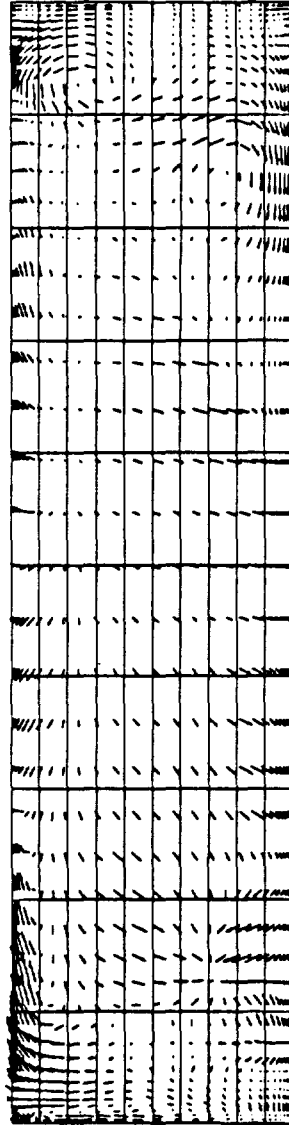


Figure 6.1.1.32: Crossflow Velocity Vectors at  $I = 72$ ,  $xs'/Te' = 1.00$  (Exit Plane) for  $CR = 3$ , 0% Cowl,  $Re = 2.15$  million/ft

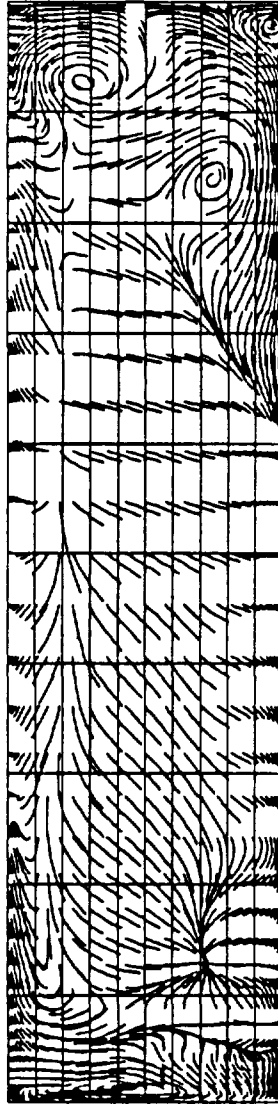


Figure 6.1.1.33: Particle Traces at  $I = 72$ ,  $xs'/Te' = 1.00$  (Exit Plane) for  $CR = 3$ ,  
0% Cowl,  $Re = 2.15$  million/ft

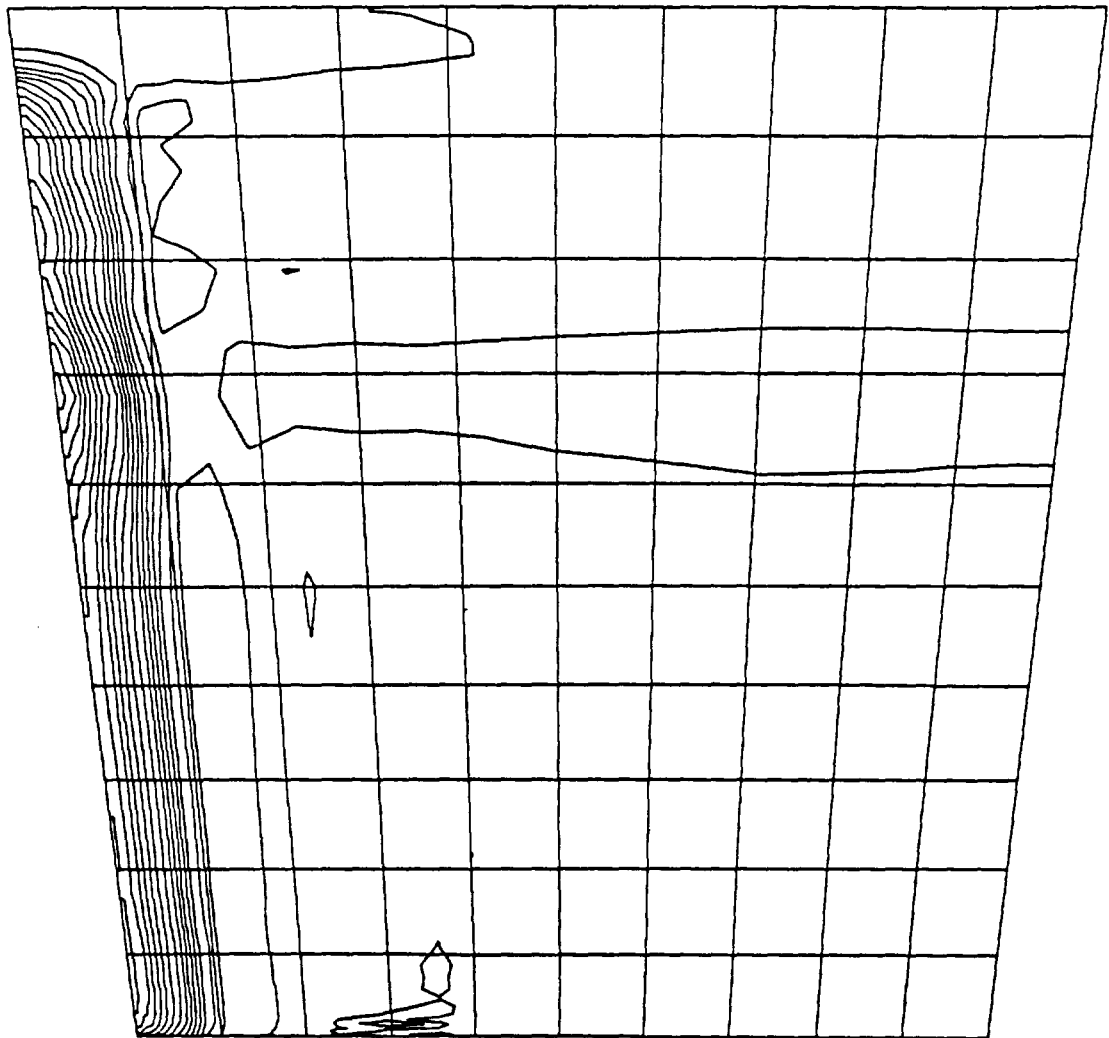


Figure 6.1.2.1: Pressure Contours at  $I = 31$ ,  $x'/Tx' = 0.04$  for  $CR = 5$ ,  
0% Cowl,  $Re = 2.15$  million/ft

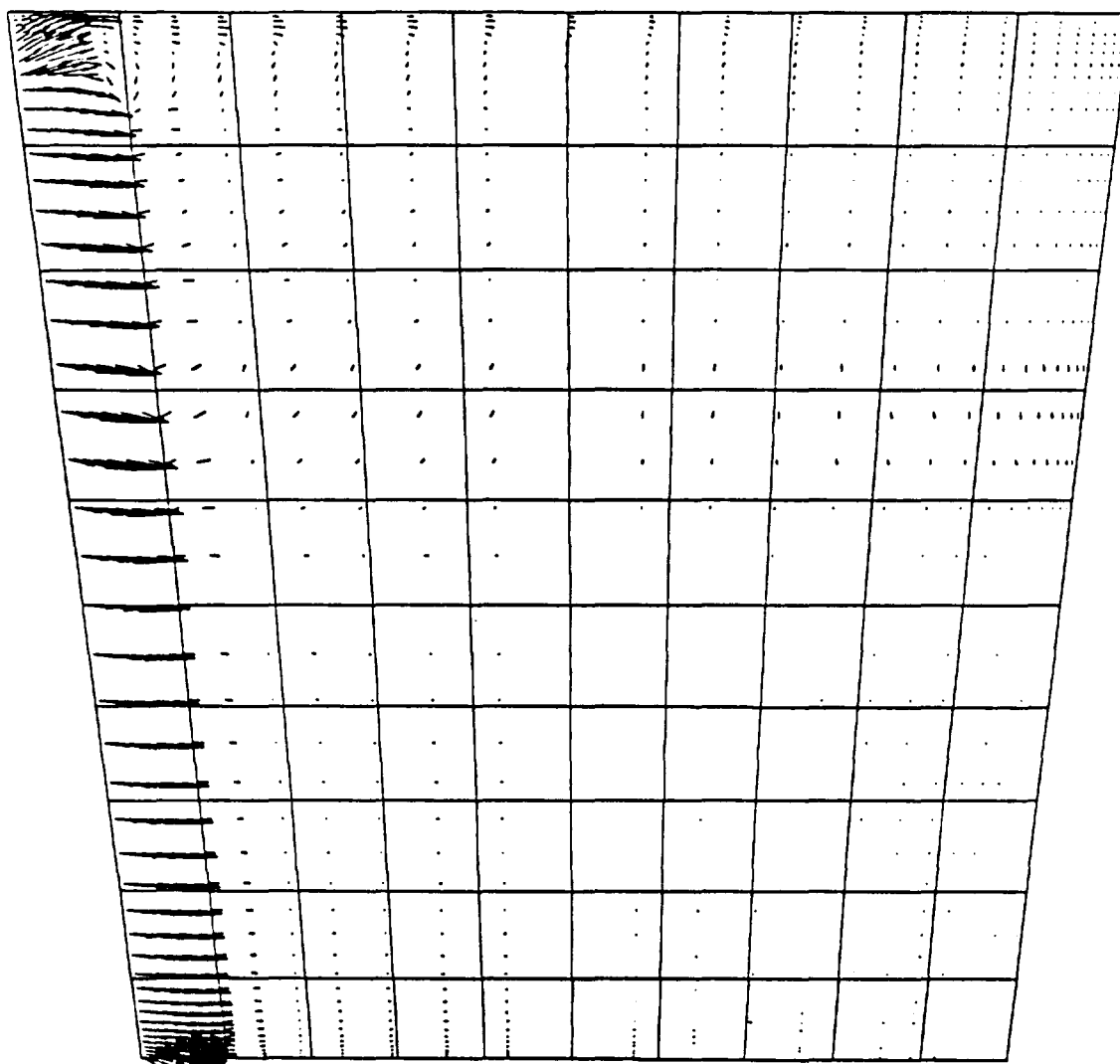


Figure 6.1.2.2: Crossflow Velocity Vectors at  $I = 31$ ,  $x'/Tx' = 0.04$  for  $CR = 5$ ,  
0% Cowl,  $Re = 2.15$  million/ft

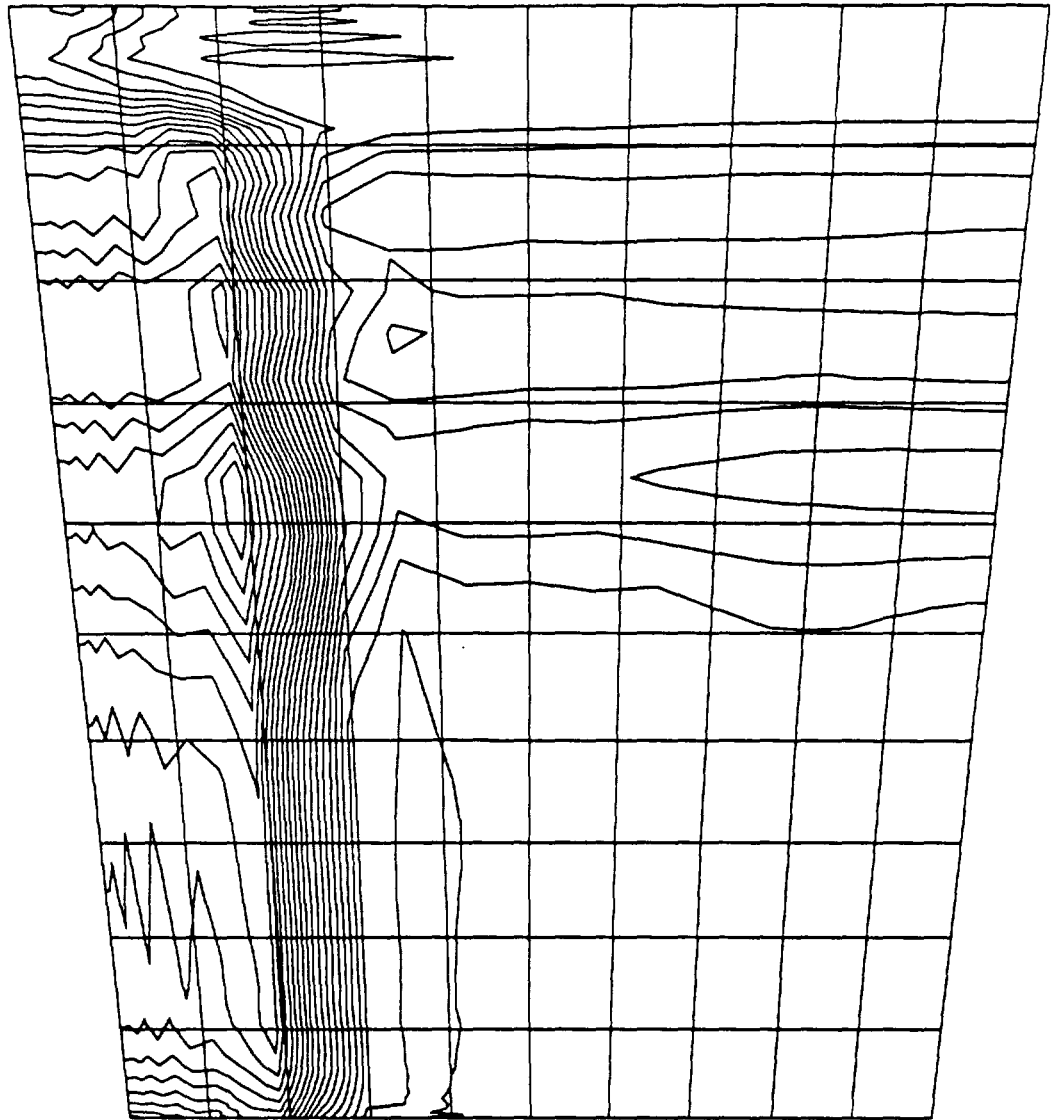


Figure 6.1.2.3: Pressure Contours at  $I = 35$ ,  $x'/Tx' = 0.20$  for  $CR = 5$ ,  
0% Cowl,  $Re = 2.15$  million/ft



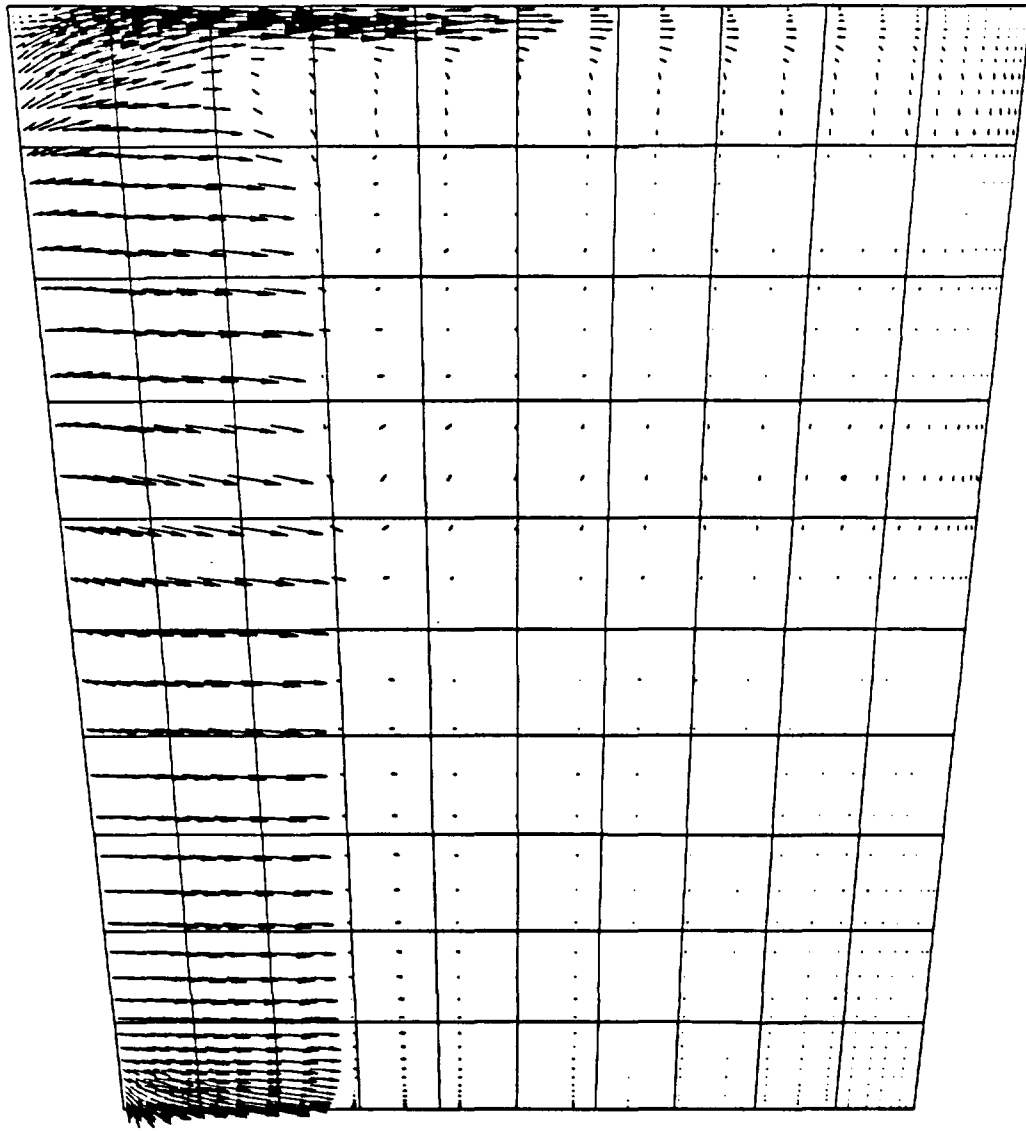


Figure 6.1.2.4: Crossflow Velocity Vectors at  $I = 35$ ,  $x'/Tx' = 0.20$  for  $CR = 5$ ,  
0% Cowl,  $Re = 2.15$  million/ft

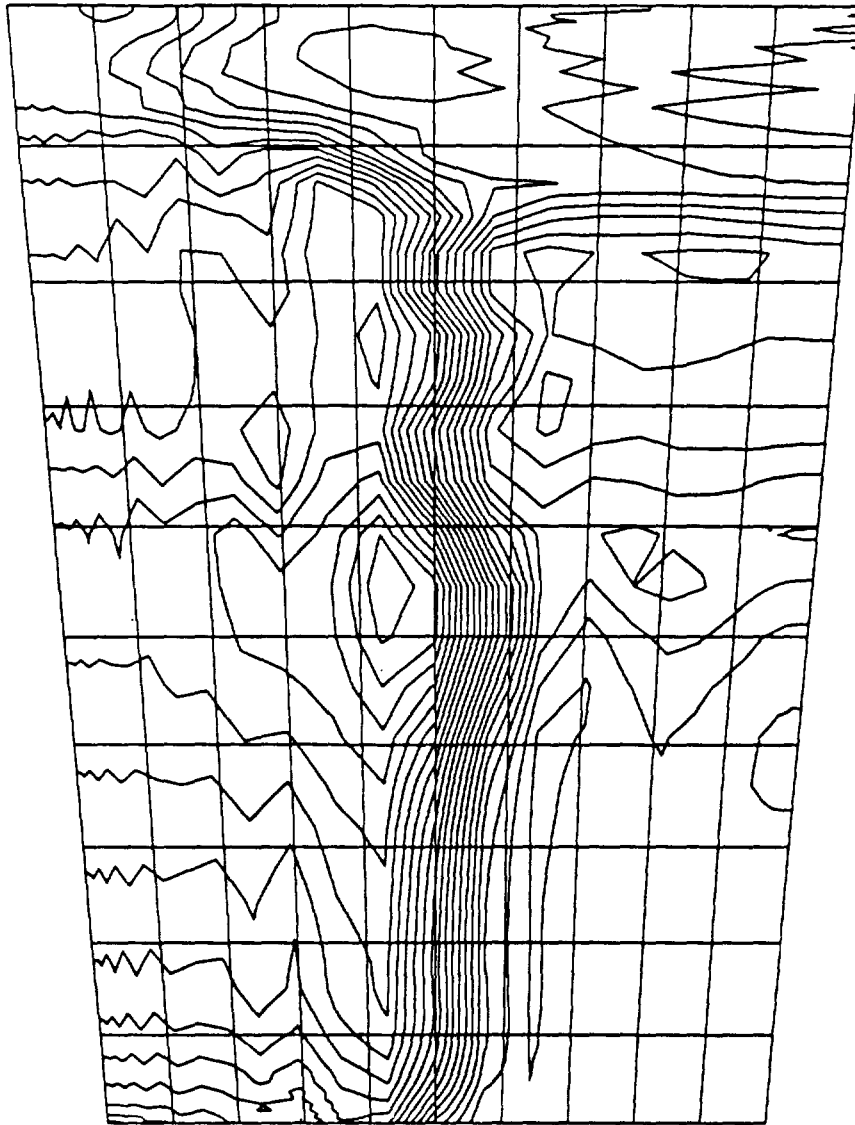


Figure 6.1.2.5: Pressure Contours at  $I = 40$ ,  $x'/Tx' = 0.40$  for  $CR = 5$ ,  
0% Cowl,  $Re = 2.15$  million/ft

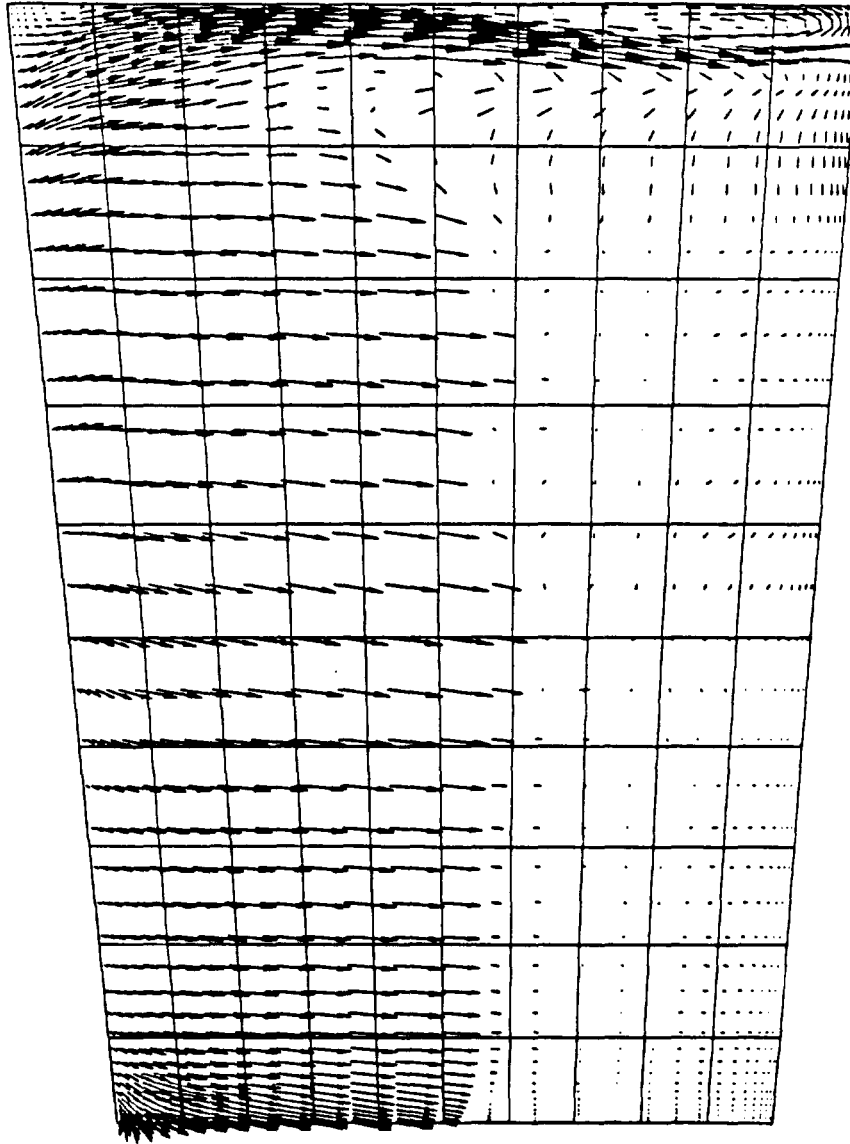


Figure 6.1.2.6: Crossflow Velocity Vectors at  $I = 40$ ,  $x'/Tx' = 0.40$  for  $CR = 5$ ,  
0% Cowl,  $Re = 2.15$  million/ft

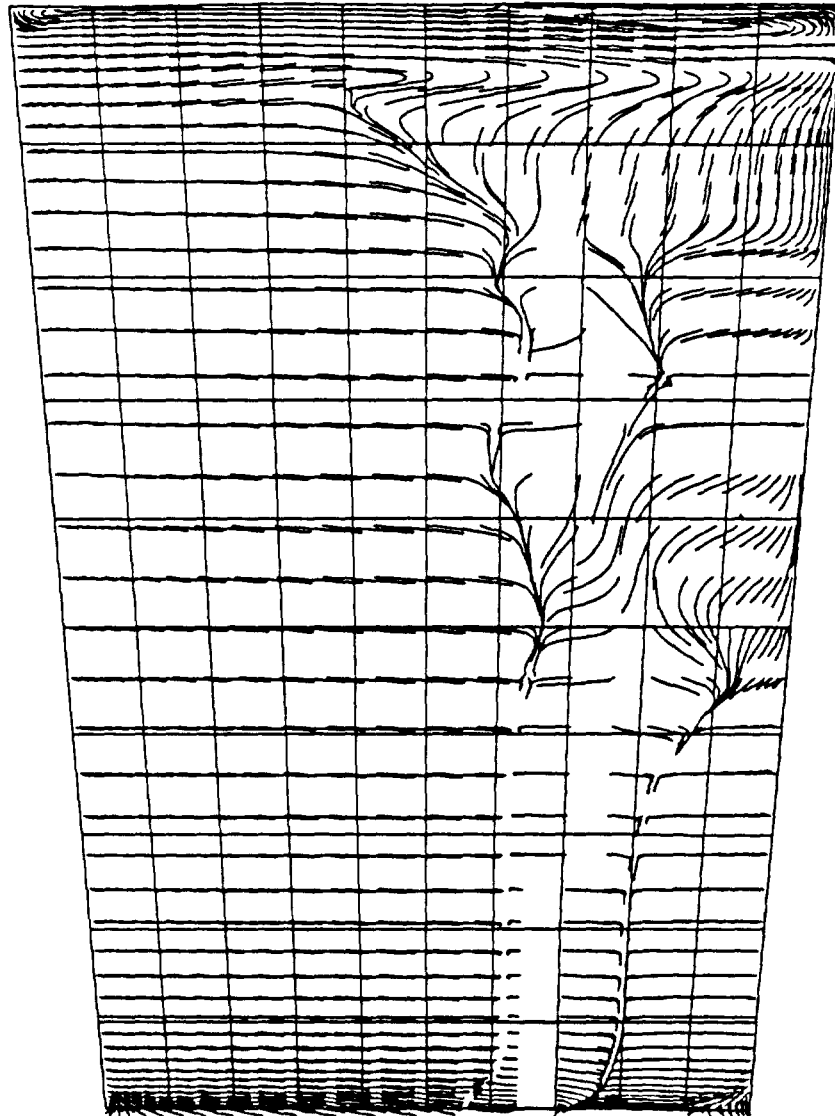


Figure 6.1.2.7: Particle Traces at  $I = 40$ ,  $x''Tx' = 0.40$  for  $CR = 5$ ,  
0% Cowl,  $Re = 2.15$  million/ft

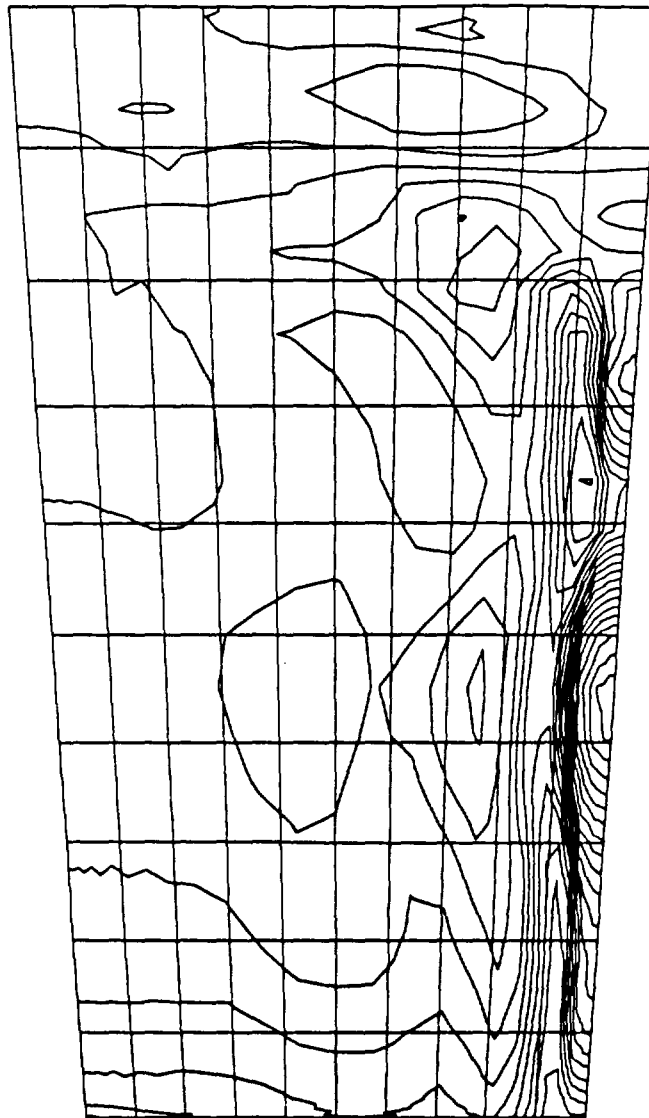


Figure 6.1.2.8: Pressure Contours at  $I = 45$ ,  $x'/Tx' = 0.60$  for  $CR = 5$ ,  
0% Cowl,  $Re = 2.15$  million/ft

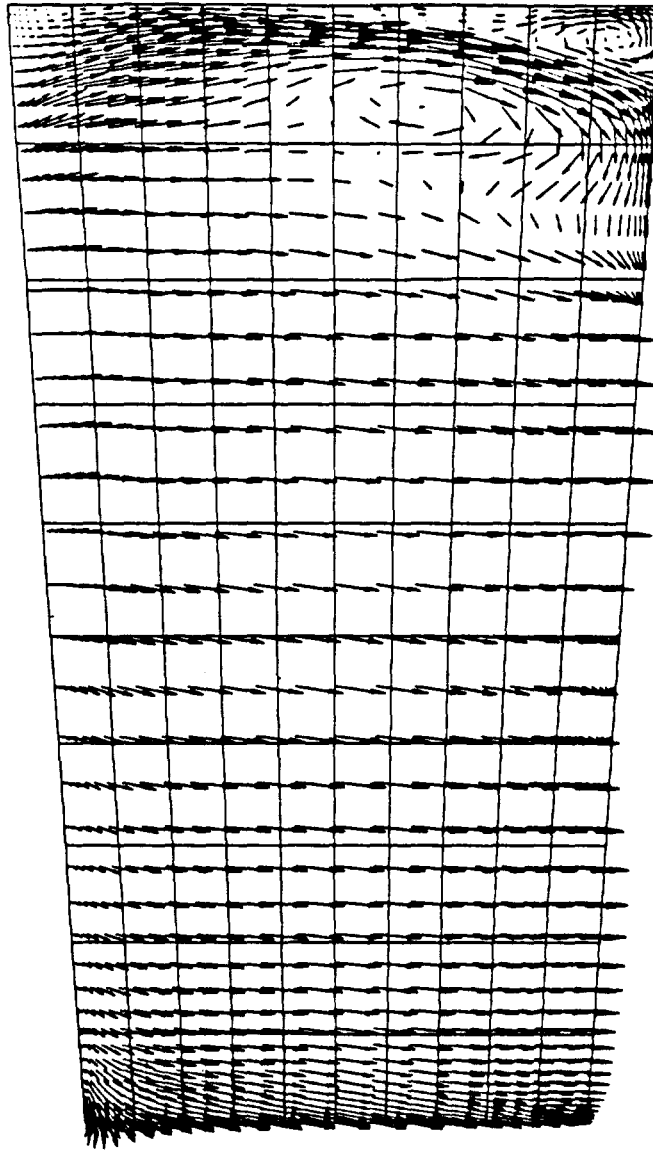


Figure 6.1.2.9: Crossflow Velocity Vectors at  $I = 45$ ,  $x'/Tx' = 0.60$  for  $CR = 5$ ,  
0% Cowl,  $Re = 2.15$  million/ft

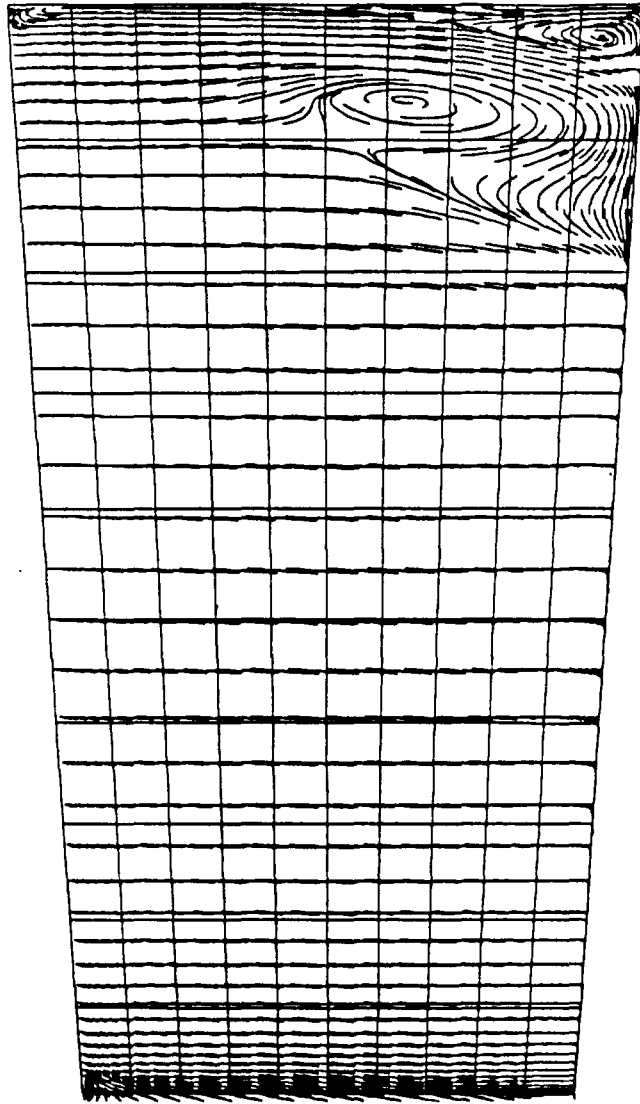


Figure 6.1.2.10: Particle Traces at  $I = 45$ ,  $x'/T_x' = 0.60$  for  $CR = 5$ ,  
0% Cowl,  $Re = 2.15$  million/ft

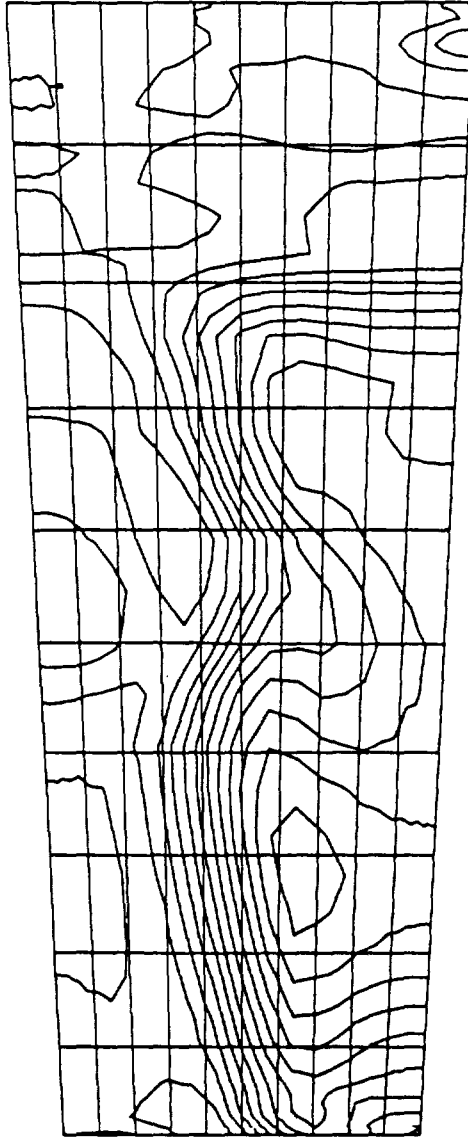


Figure 6.1.2.11: Pressure Contours at  $I = 50$ ,  $x'/Tx' = 0.79$  for  $CR = 5$ ,  
0% Cowl,  $Re = 2.15$  million/ft



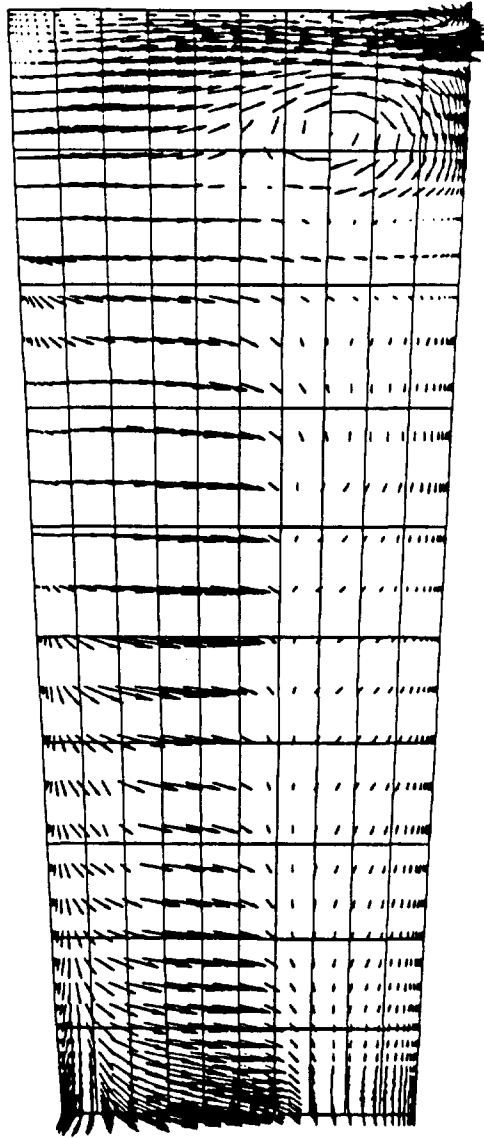


Figure 6.1.2.12: Crossflow Velocity Vectors at  $I = 50$ ,  $x'/Tx' = 0.79$  for  $CR = 5$ ,  
0% Cowl,  $Re = 2.15$  million/ft

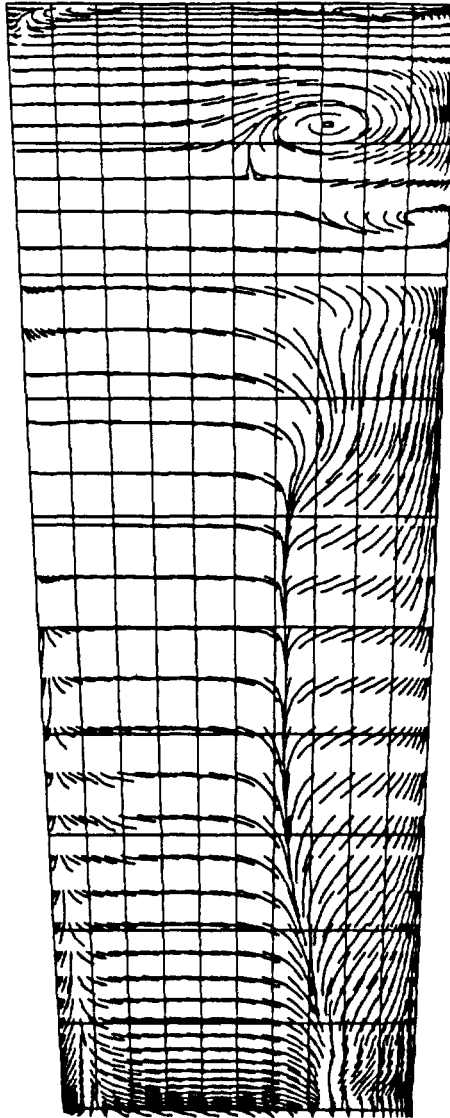


Figure 6.1.2.13: Particle Traces at  $I = 50$ ,  $x'/Tx' = 0.79$  for  $CR = 5$ ,  
0% Cowl,  $Re = 2.15$  million/ft

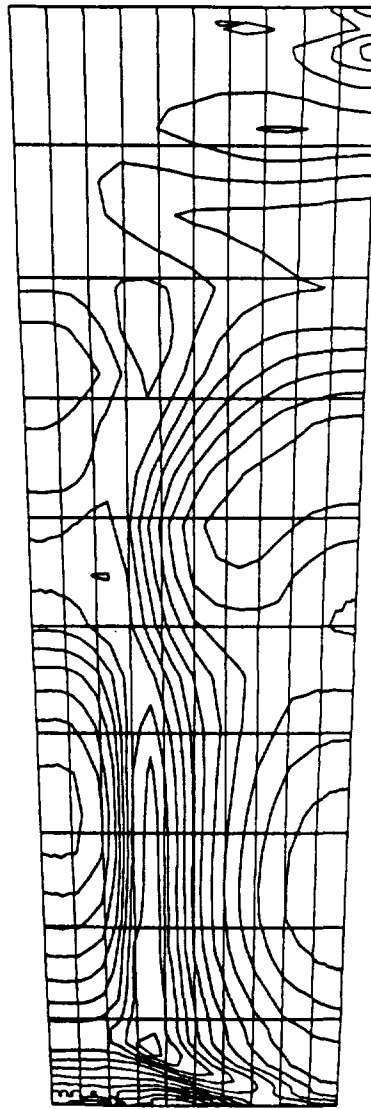


Figure 6.1.2.14: Pressure Contours at  $I = 52$ ,  $x'/Tx' = 0.87$  for  $CR = 5$ ,  
0% Cowl,  $Re = 2.15$  million/ft

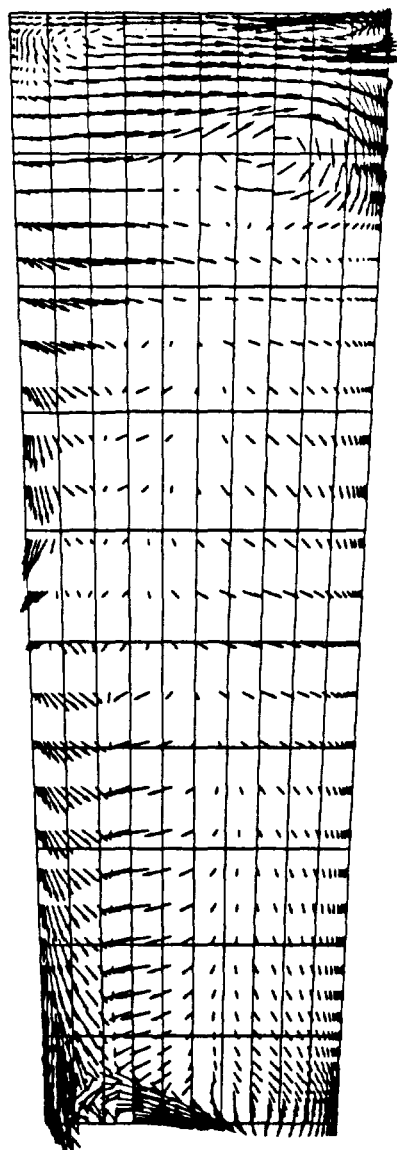


Figure 6.1.2.15: Crossflow Velocity Vectors at  $I = 52$ ,  $x'/Tx' = 0.87$  for  $CR = 5$ ,  
0% Cowl,  $Re = 2.15$  million/ft

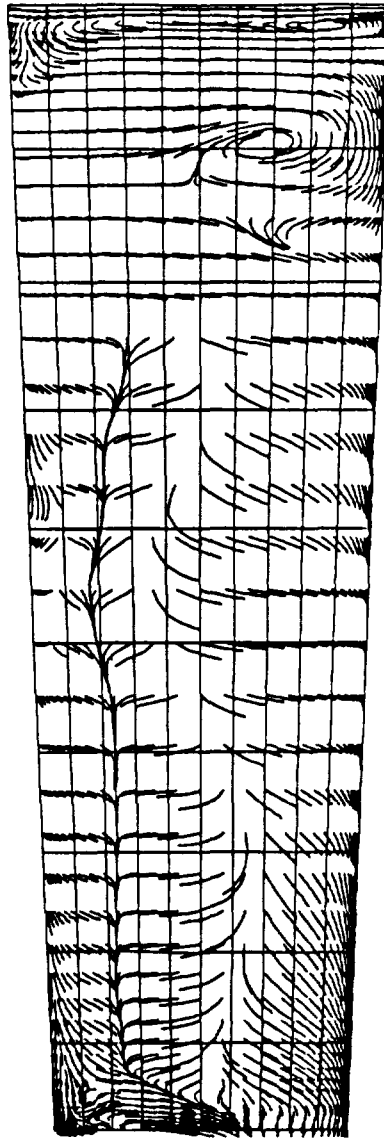


Figure 6.1.2.16: Particle Traces at  $I = 52$ ,  $x'/Tx' = 0.87$  for  $CR = 5$ ,  
0% Cowl,  $Re = 2.15$  million/ft

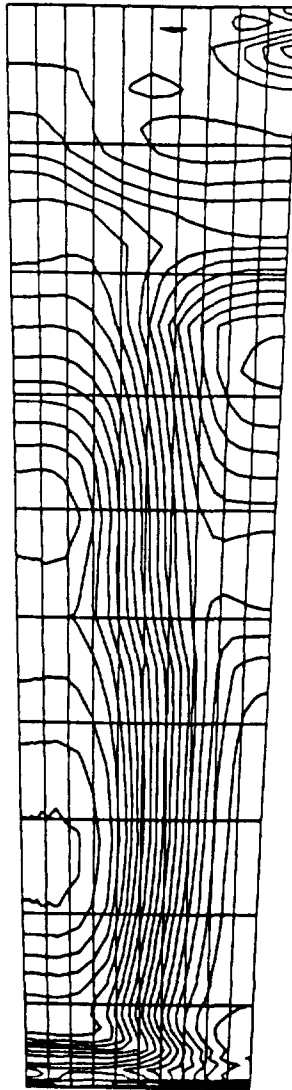


Figure 6.1.2.17: Pressure Contours at  $I = 54$ ,  $x'/Tx' = 0.96$  for  $CR = 5$ ,  
0% Cowl,  $Re = 2.15$  million/ft

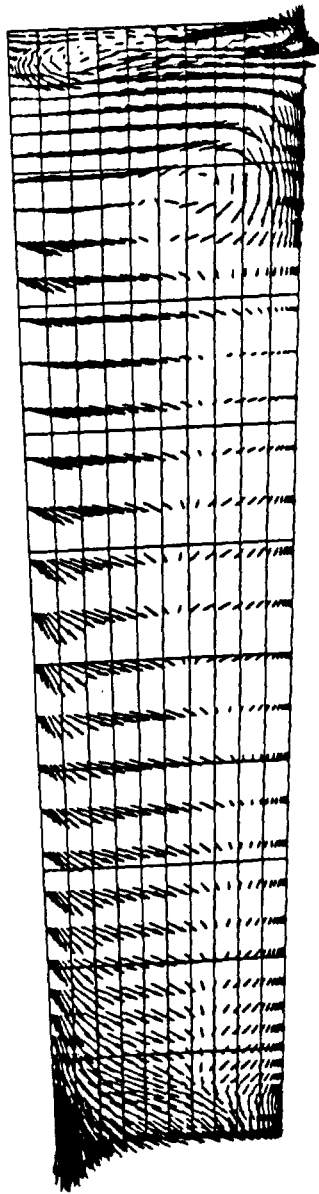


Figure 6.1.2.18: Crossflow Velocity Vectors at  $I = 54$ ,  $x'/Tx' = 0.96$  for  $CR = 5$ ,  
0% Cowl,  $Re = 2.15$  million/ft

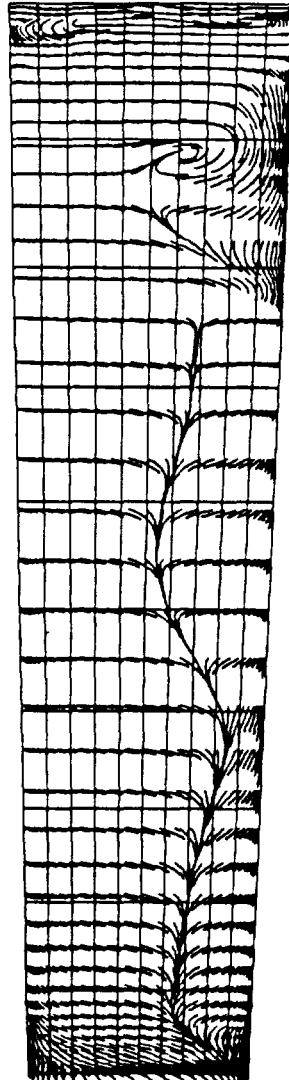


Figure 6.1.2.19: Particle Traces at  $I = 54$ ,  $x'/Tx' = 0.96$  for  $CR = 5$ ,  
0% Cowl,  $Re = 2.15$  million/ft



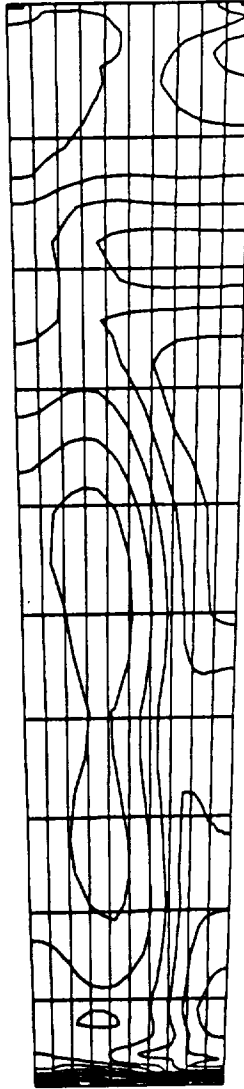


Figure 6.1.2.20: Pressure Contours at  $I = 55$ ,  $x'/Tx' = 1.00$  for  $CR = 5$ ,  
0% Cowl,  $Re = 2.15$  million/ft

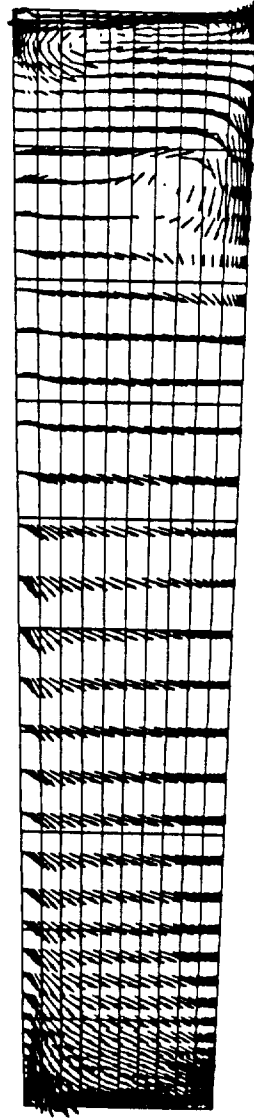


Figure 6.1.2.21: Crossflow Velocity Vectors at  $I = 55$ ,  $x'/Tx' = 1.00$  for  $CR = 5$ ,  
0% Cowl,  $Re = 2.15$  million/ft

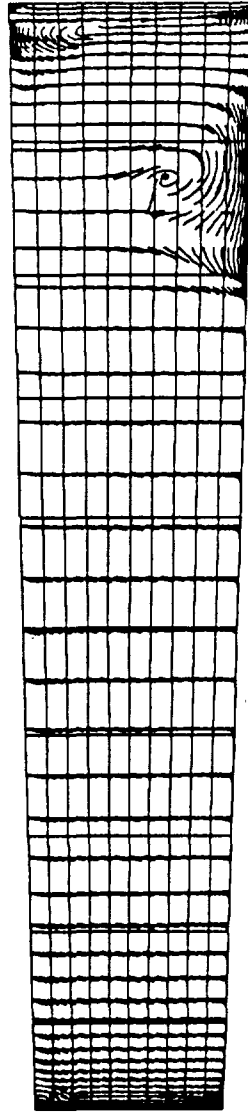


Figure 6.1.2.22: Particle Traces at  $I = 55$ ,  $x'/Tx' = 1.00$  for  $CR = 5$ ,  
0% Cowl,  $Re = 2.15$  million/ft

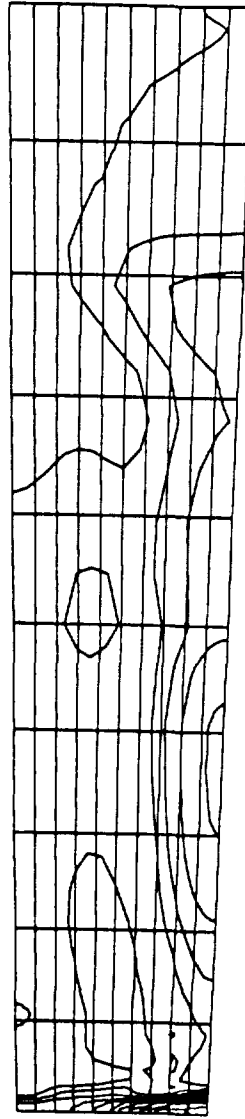


Figure 6.1.2.23: Pressure Contours at  $I = 56$ ,  $xs'/Te' = 0.06$  for  $CR = 5$ ,  
0% Cowl,  $Re = 2.15$  million/ft

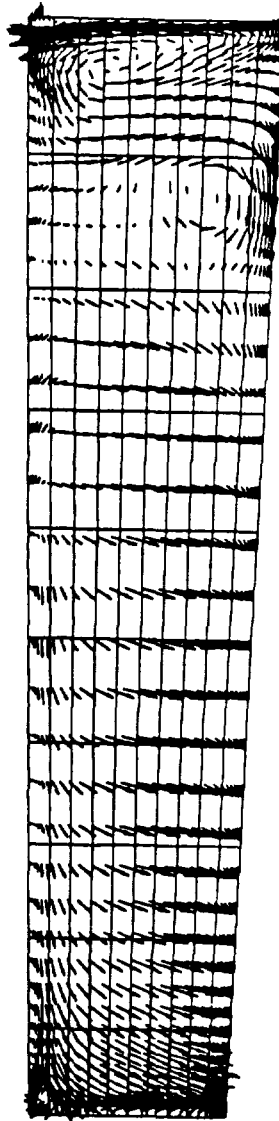


Figure 6.1.2.24: Crossflow Velocity Vectors at  $I = 56$ ,  $xs'/Te' = 0.06$  for  $CR = 5$ ,  
0% Cowl,  $Re = 2.15$  million/ft

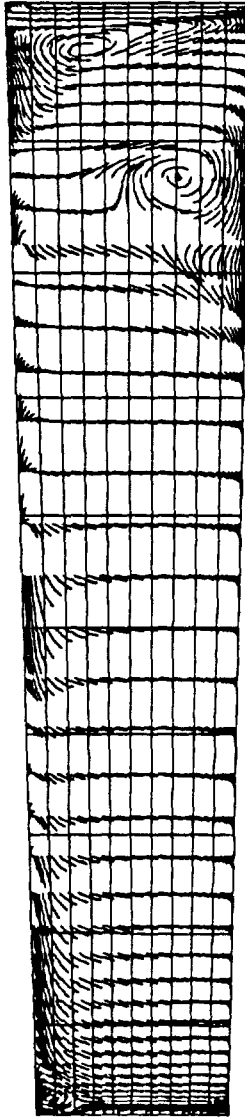


Figure 6.1.2.25: Particle Traces at  $I = 56$ ,  $xs'/Te' = 0.06$  for  $CR = 5$ ,  
0% Cowl,  $Re = 2.15$  million/ft

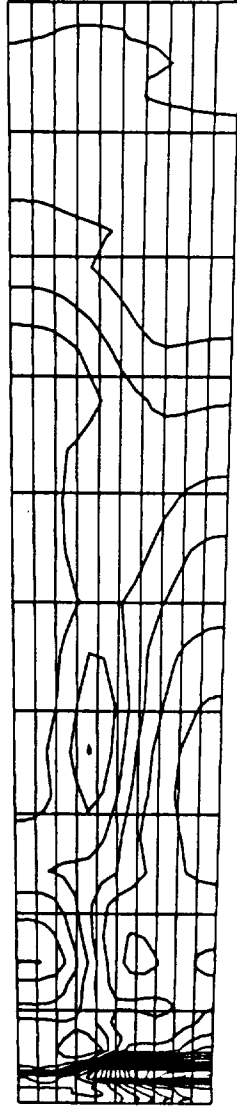


Figure 6.1.2.26: Pressure Contours at  $I = 60$ ,  $xs'/Te' = 0.29$  for  $CR = 5$ ,  
0% Cowl,  $Re = 2.15$  million/ft

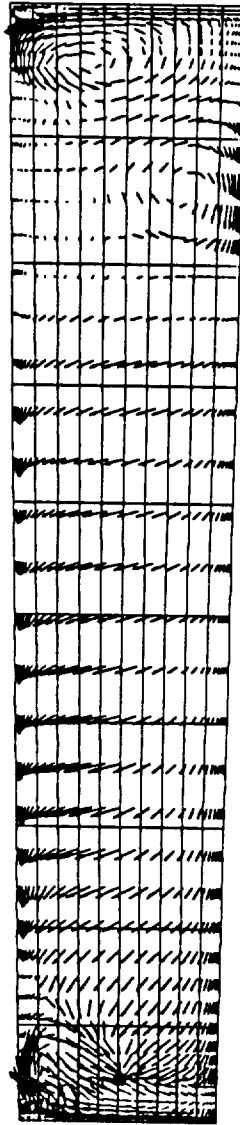


Figure 6.1.2.27: Crossflow Velocity Vectors at  $I = 60$ ,  $x_s'/Te' = 0.29$  for  $CR = 5$ ,  
0% Cowl,  $Re = 2.15$  million/ft



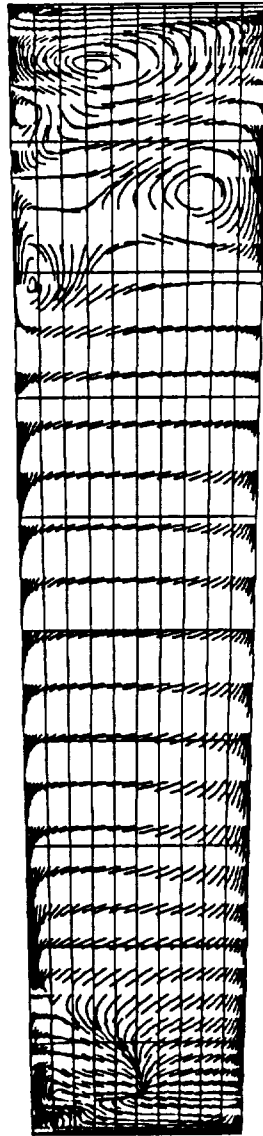


Figure 6.1.2.28: Particle Traces at  $I = 60$ ,  $xs'/Te' = 0.29$  for  $CR = 5$ ,  
0% Cowl,  $Re = 2.15$  million/ft

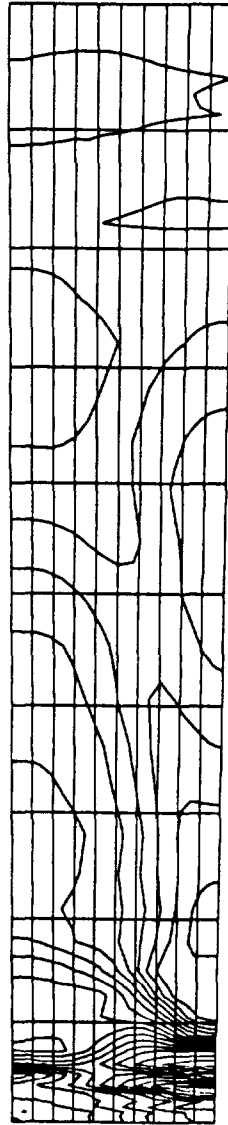


Figure 6.1.2.29: Pressure Contours at  $I = 65$ ,  $xs'/Te' = 0.58$  for  $CR = 5$ ,  
0% Cowl,  $Re = 2.15$  million/ft

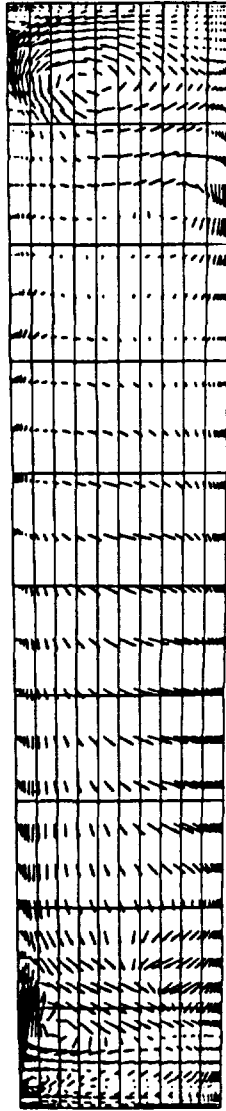


Figure 6.1.2.30: Crossflow Velocity Vectors at  $I = 65$ ,  $x_s'/Te' = 0.58$  for  $CR = 5$ ,  
0% Cowl,  $Re = 2.15$  million/ft

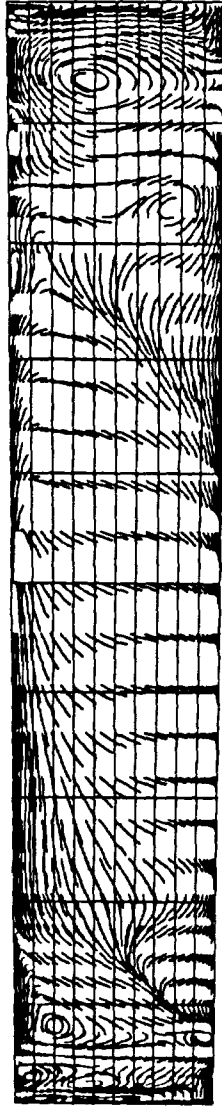


Figure 6.1.2.31: Particle Traces at  $I = 65$ ,  $xs'/Te' = 0.58$  for  $CR = 5$ ,  
0% Cowl,  $Re = 2.15$  million/ft

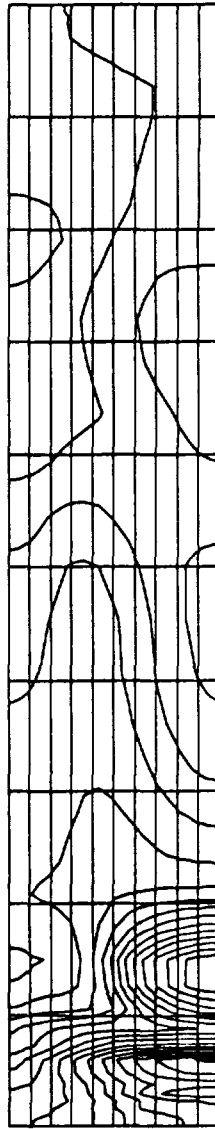


Figure 6.1.2.32: Pressure Contours at  $I = 72$ ,  $xs'/Te' = 1.00$  (Exit Plane) for  $CR = 5$ , 0% Cowl,  $Re = 2.15$  million/ft

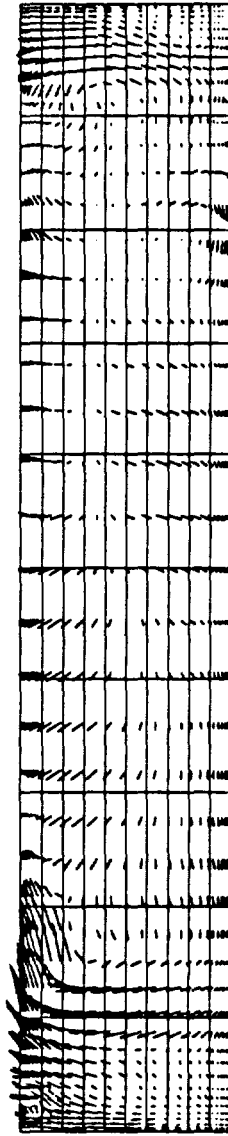


Figure 6.1.2.33: Crossflow Velocity Vectors at  $I = 72$ ,  $xs'/Te' = 1.00$  (Exit Plane)  
for  $CR = 5$ , 0% Cowl,  $Re = 2.15$  million/ft



Figure 6.1.2.34: Particle Traces at  $I = 72$ ,  $xs'/Te' = 1.00$  (Exit Plane)  
for  $CR = 5$ , 0% Cowl,  $Re = 2.15$  million/ft

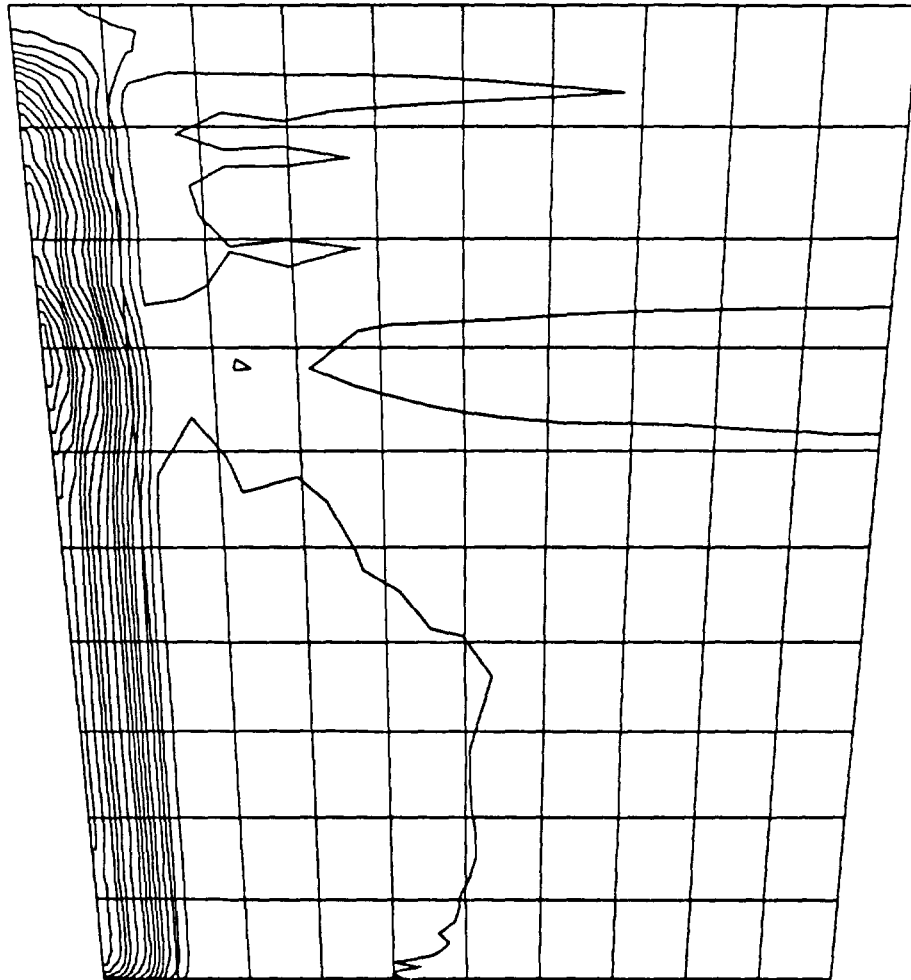


Figure 6.1.3.1: Pressure Contours at  $I = 31$ ,  $x'/T_x' = 0.04$  for  $CR = 9$ ,  
0% Cowl,  $Re = 2.15$  million/ft



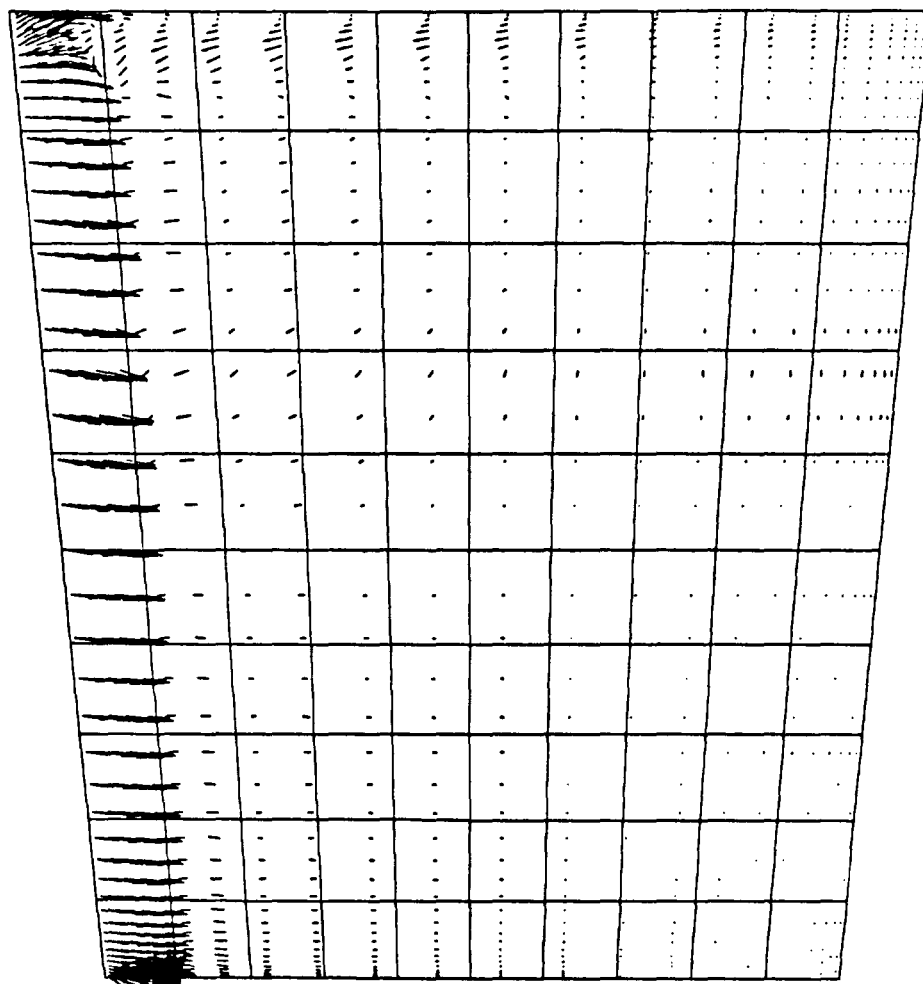


Figure 6.1.3.2: Crossflow Velocity Vectors at  $I = 31$ ,  $x'/Tx' = 0.04$  for  $CR = 9$ ,  
0% Cowl,  $Re = 2.15$  million/ft

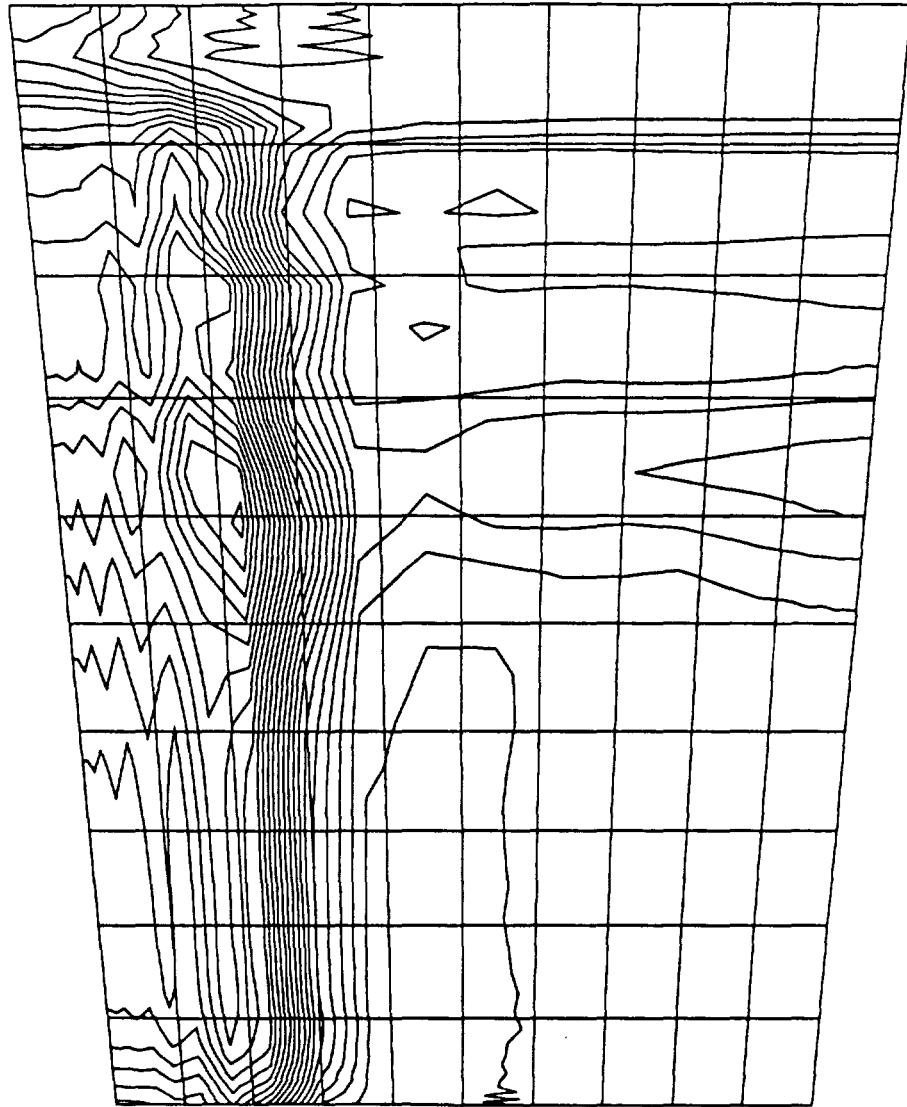


Figure 6.1.3.3: Pressure Contours at  $I=35$ ,  $x'/Tx' = 0.20$  for  $CR = 9$ ,  
0% Cowl,  $Re = 2.15$  million/ft

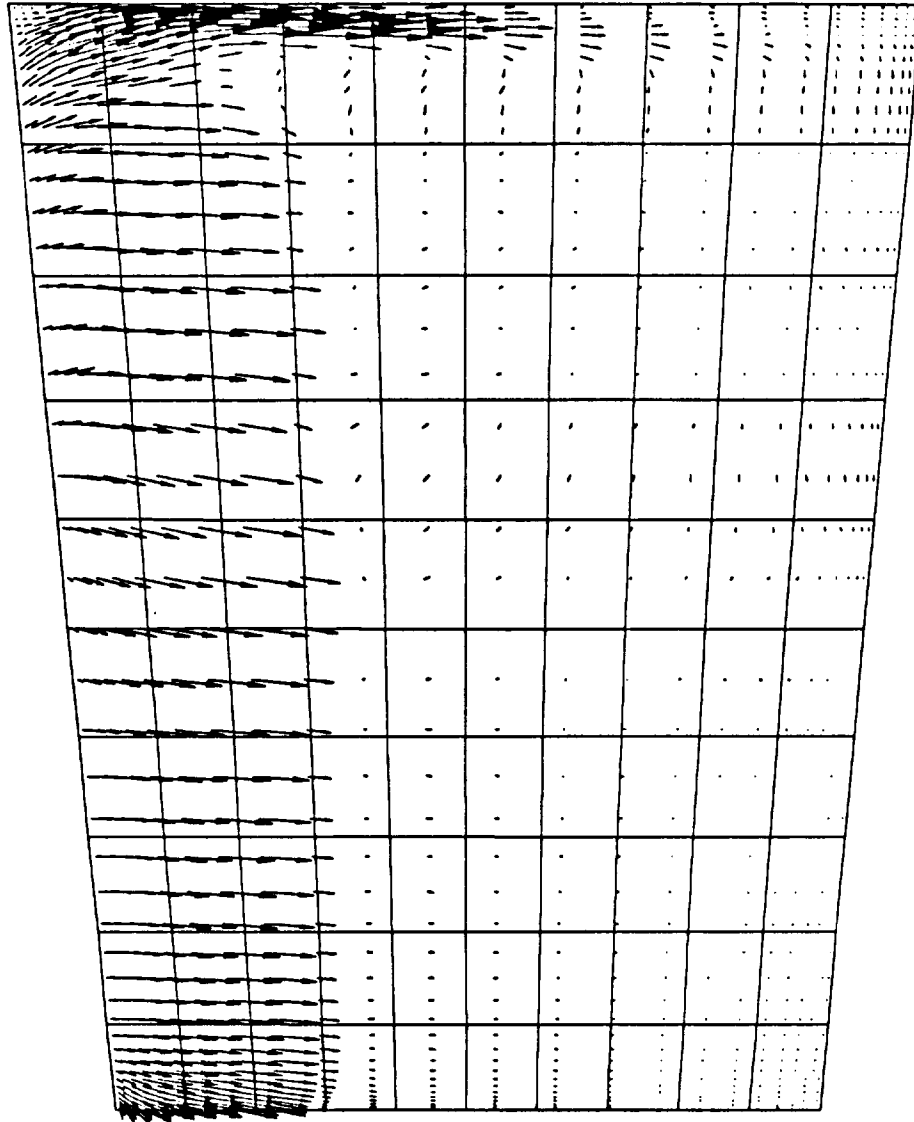


Figure 6.1.3.4: Crossflow Velocity Vectors at  $I = 35$ ,  $x'/T_x' = 0.20$  for  $CR = 9$ ,  
0% Cowl,  $Re = 2.15$  million/ft

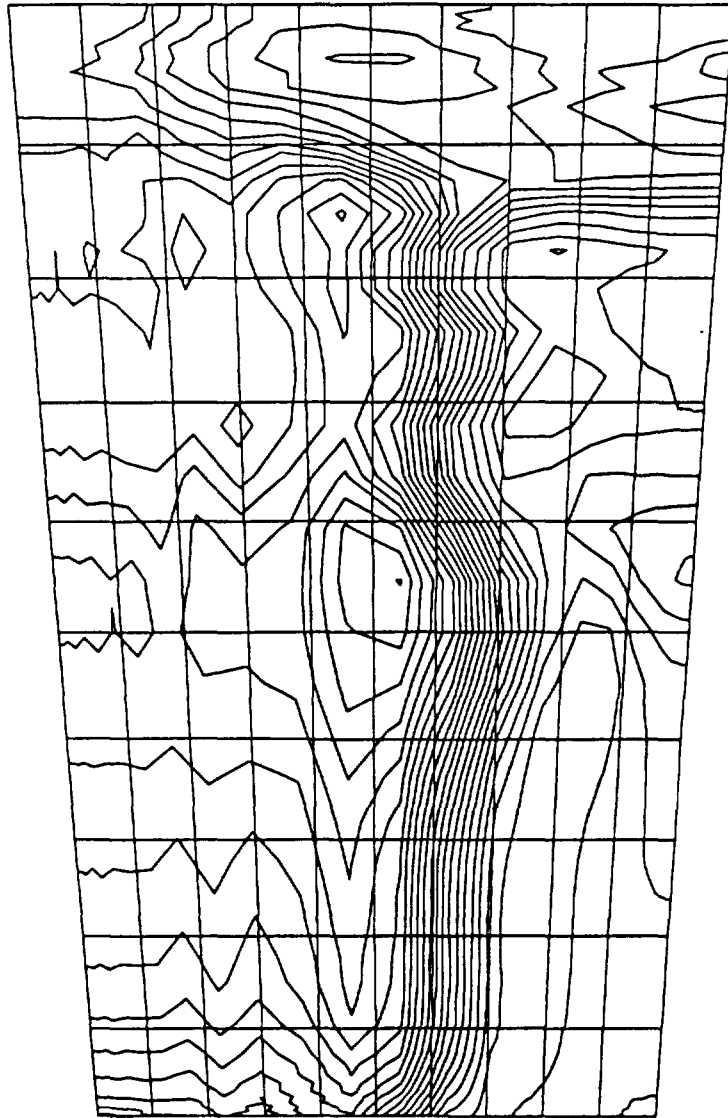


Figure 6.1.3.5: Pressure Contours at  $I = 40$ ,  $x'/T_{x'} = 0.40$  for  $CR = 9$ ,  
0% Cowl,  $Re = 2.15$  million/ft

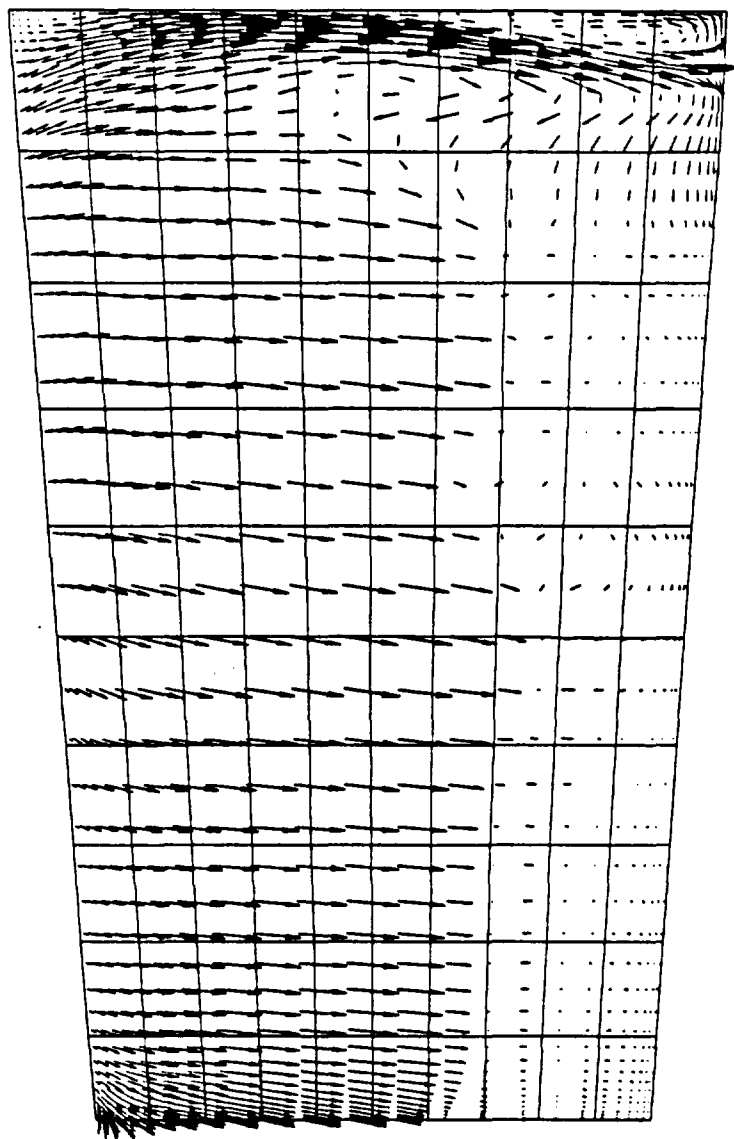


Figure 6.1.3.6: Crossflow Velocity Vectors at  $I = 40$ ,  $x'/Tx' = 0.40$  for  $CR = 9$ ,  
0% Cowl,  $Re = 2.15$  million/ft

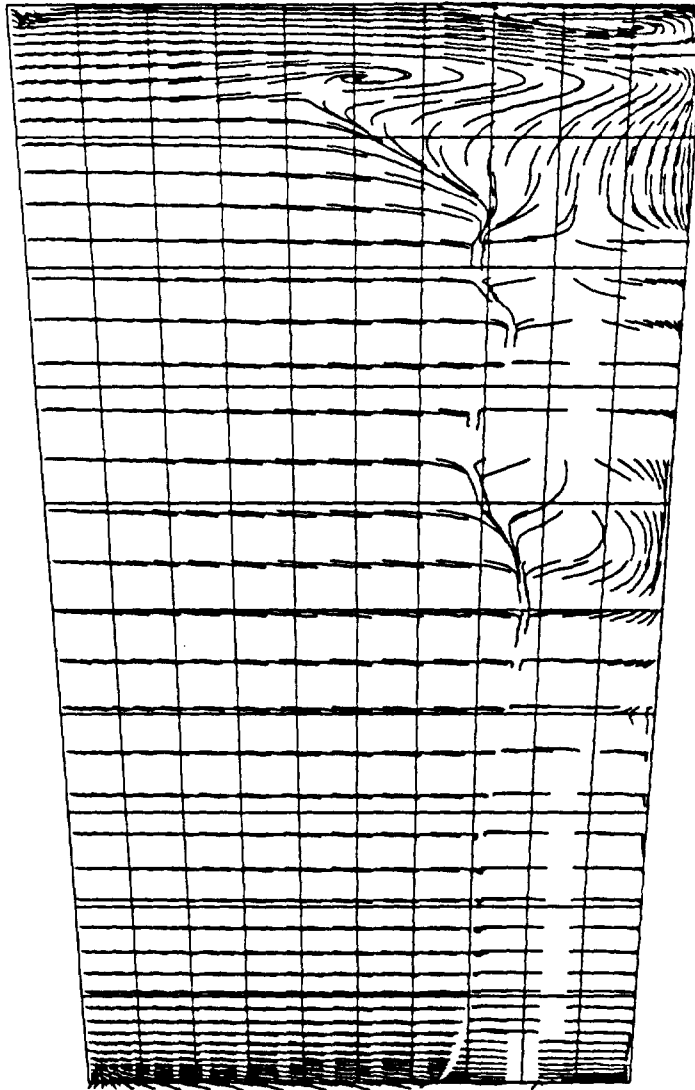


Figure 6.1.3.7: Particle Traces at  $I = 40$ ,  $x''/Tx' = 0.40$  for  $CR = 9$ ,  
0% Cowl,  $Re = 2.15$  million/ft

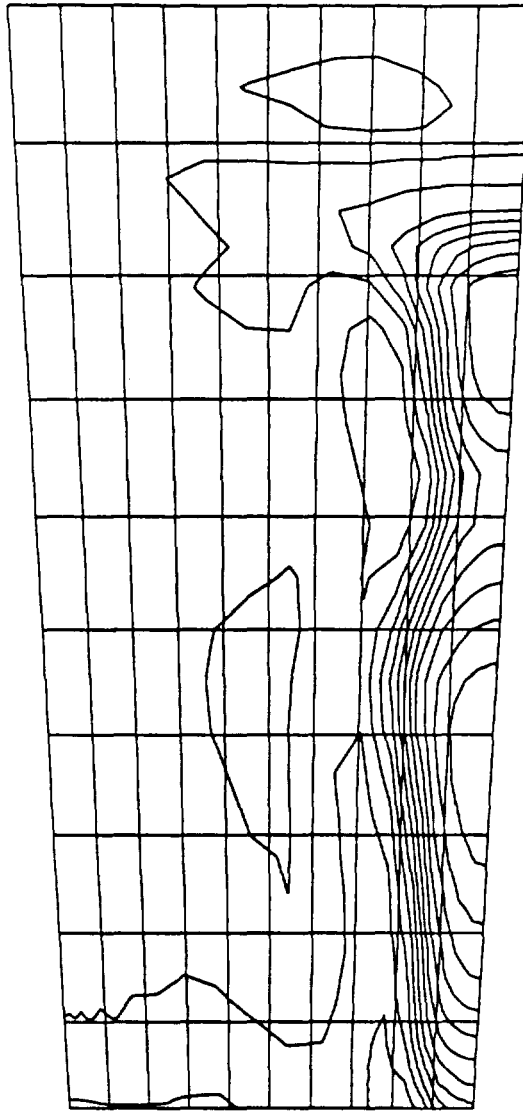


Figure 6.1.3.8: Pressure Contours at  $I = 45$ ,  $x'/Tx' = 0.60$  for  $CR = 9$ ,  
0% Cowl,  $Re = 2.15$  million/ft

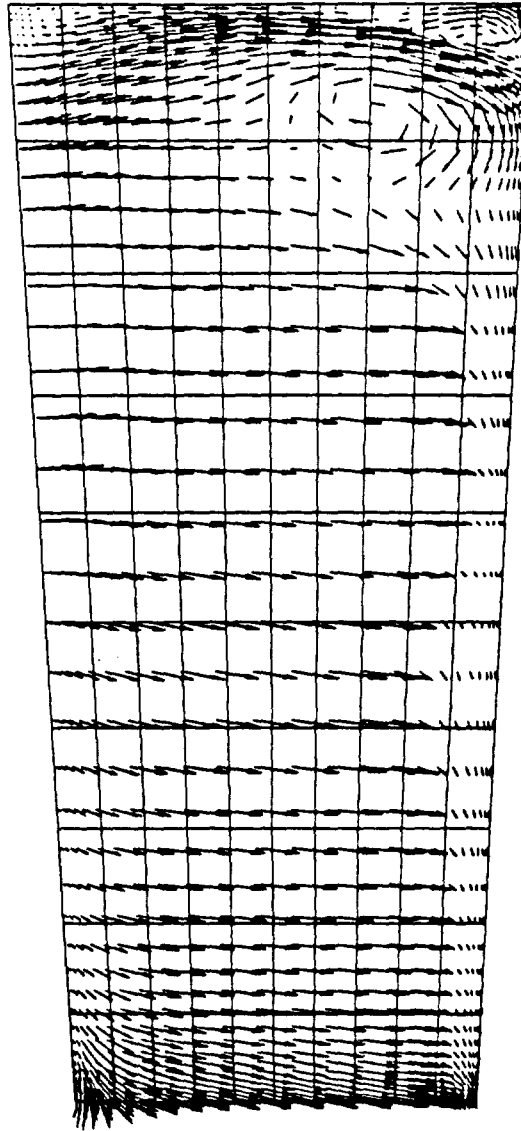


Figure 6.1.3.9: Crossflow Velocity Vectors at  $I=45$ ,  $x'/T_x' = 0.60$  for  $CR = 9$ ,  
0% Cowl,  $Re = 2.15$  million/ft



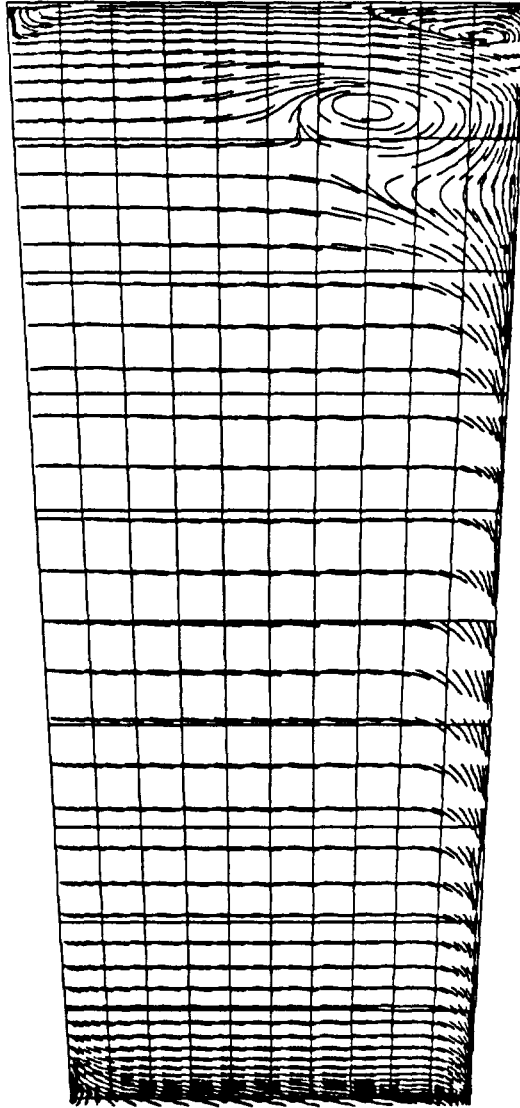


Figure 6.1.3.10: Particle Traces at  $I = 45$ ,  $x'/Tx' = 0.60$  for  $CR = 9$ ,  
0% Cowl,  $Re = 2.15$  million/ft

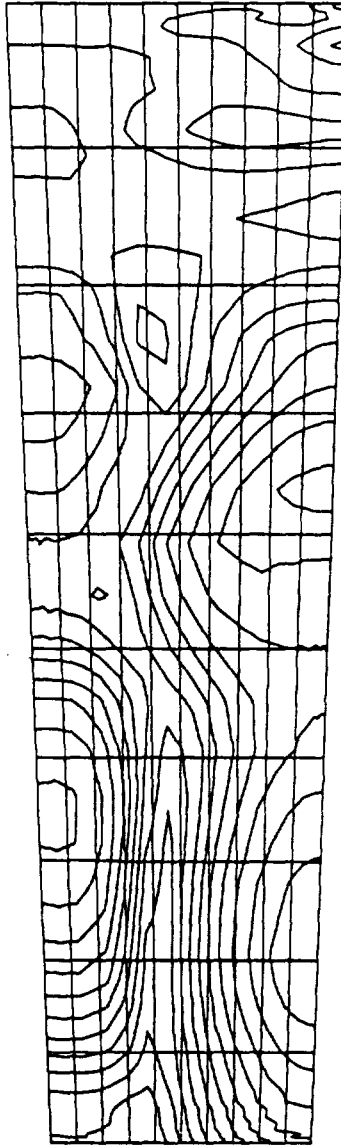


Figure 6.1.3.11: Pressure Contours at  $I = 50$ ,  $x'/Tx' = 0.79$  for  $CR = 9$ ,  
0% Cowl,  $Re = 2.15$  million/ft

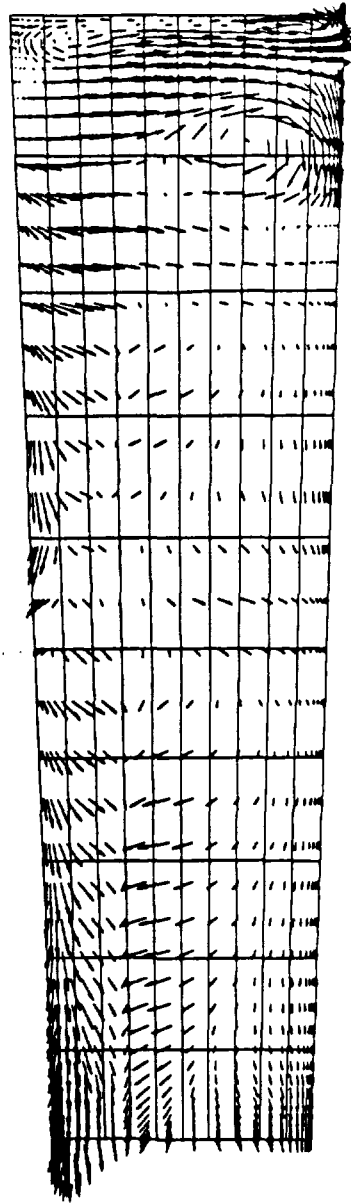


Figure 6.1.3.12: Crossflow Velocity Vectors at  $I = 50$ ,  $x'/Tx' = 0.79$  for  $CR = 9$ , 0% Cowl,  $Re = 2.15$  million/ft

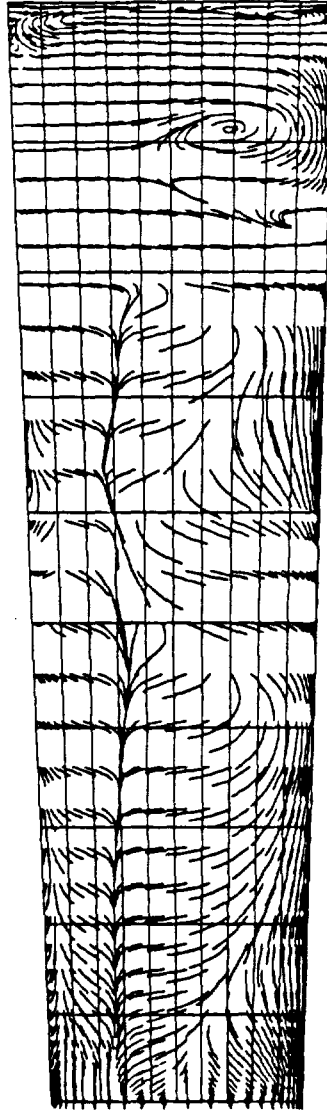


Figure 6.1.3.13: Particle Traces at  $I = 50$ ,  $x'/Tx' = 0.79$  for  $CR = 9$ ,  
0% Cowl,  $Re = 2.15$  million/ft

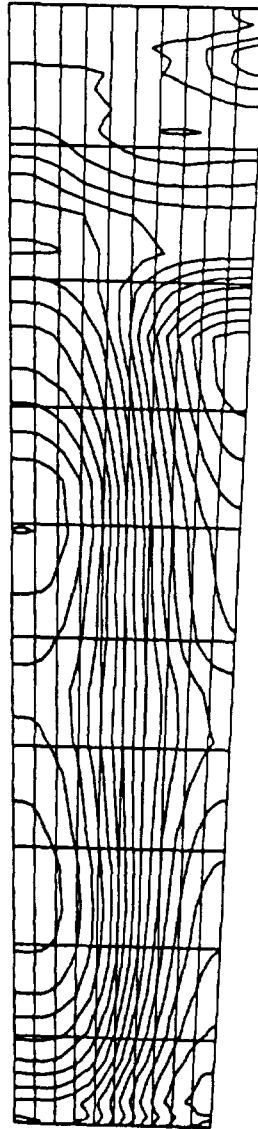


Figure 6.1.3.14: Pressure Contours at  $I = 52$ ,  $x'/Tx' = 0.87$  for  $CR = 9$ ,  
0% Cowl,  $Re = 2.15$  million/ft

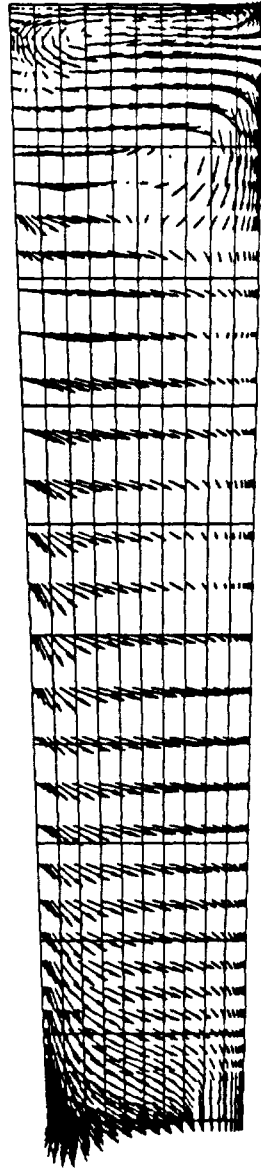


Figure 6.1.3.15: Crossflow Velocity Vectors at  $I = 52$ ,  $x'/Tx' = 0.87$  for  $CR = 9$ , 0% Cowl,  $Re = 2.15$  million/ft

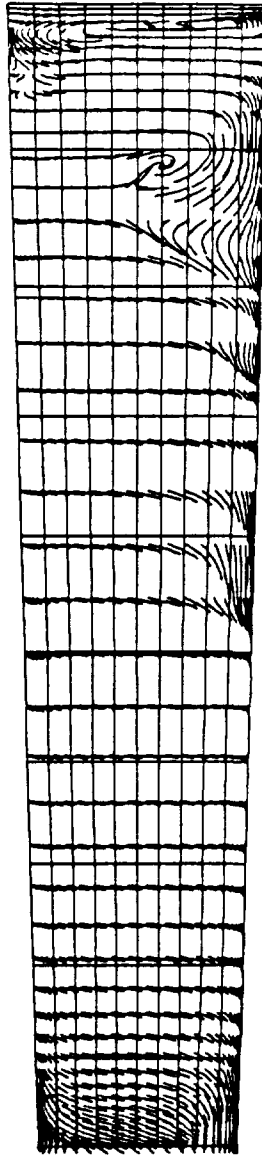


Figure 6.1.3.16: Particle Traces at  $I = 52$ ,  $x'/Tx' = 0.87$  for  $CR = 9$ ,  
0% Cowl,  $Re = 2.15$  million/ft

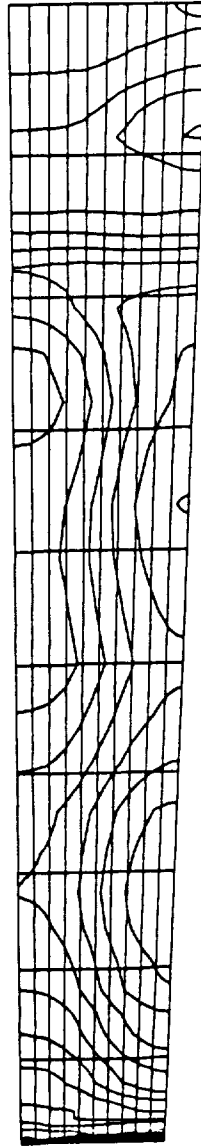


Figure 6.1.3.17: Pressure Contours at  $I = 54$ ,  $x'/Tx' = 0.96$  for  $CR = 9$ ,  
0% Cowl,  $Re = 2.15$  million/ft



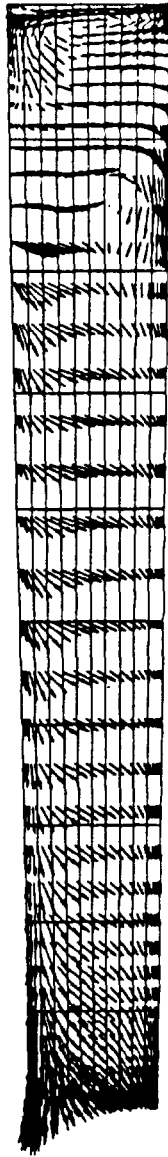


Figure 6.1.3.18: Crossflow Velocity Vectors at  $I = 54$ ,  $x'/Tx' = 0.96$  for  $CR = 9$ ,  
0% Cowl,  $Re = 2.15$  million/ft

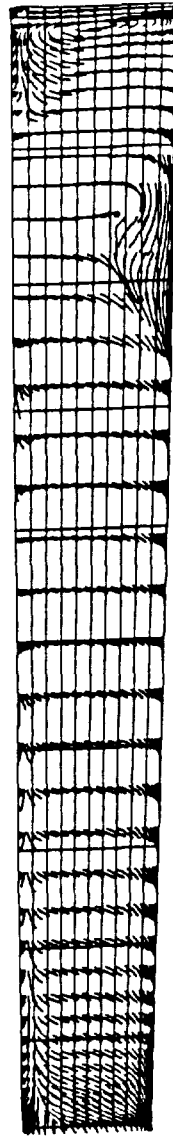


Figure 6.1.3.19: Particle Traces at  $I = 54$ ,  $x'/Tx' = 0.96$  for  $CR = 9$ ,  
0% Cowl,  $Re = 2.15$  million/ft

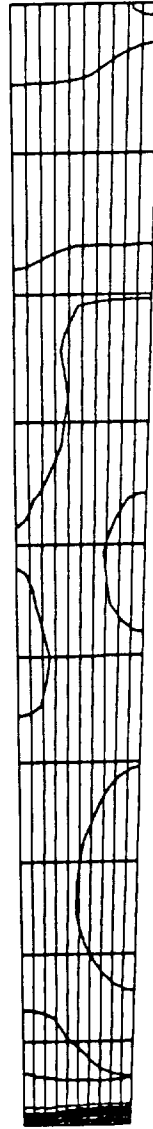


Figure 6.1.3.20: Pressure Contours at  $I = 55$ ,  $x'/Tx' = 1.00$  for  $CR = 9$ ,  
0% Cowl,  $Re = 2.15$  million/ft



Figure 6.1.3.21: Crossflow Velocity Vectors at  $I = 55$ ,  $x'/Tx' = 1.00$  for  $CR = 9$ ,  
0% Cowl,  $Re = 2.15$  million/ft

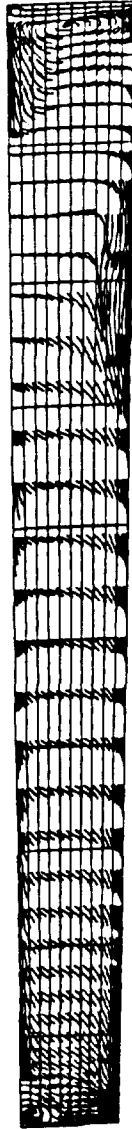


Figure 6.1.3.22: Particle Traces at  $I = 55$ ,  $x'/Tx' = 1.00$  for  $CR = 9$ ,  
0% Cowl,  $Re = 2.15$  million/ft



Figure 6.1.3.23: Pressure Contours at  $I = 56$ ,  $x_s'/Te' = 0.06$  for  $CR = 9$ ,  
0% Cowl,  $Re = 2.15$  million/ft

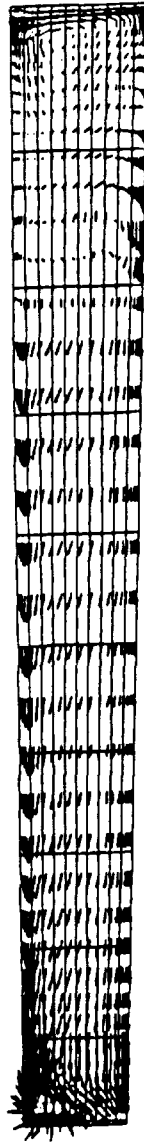


Figure 6.1.3.24: Crossflow Velocity Vectors at  $I = 56$ ,  $xs'/Te' = 0.06$  for  $CR = 9$ ,  
0% Cowl,  $Re = 2.15$  million/ft

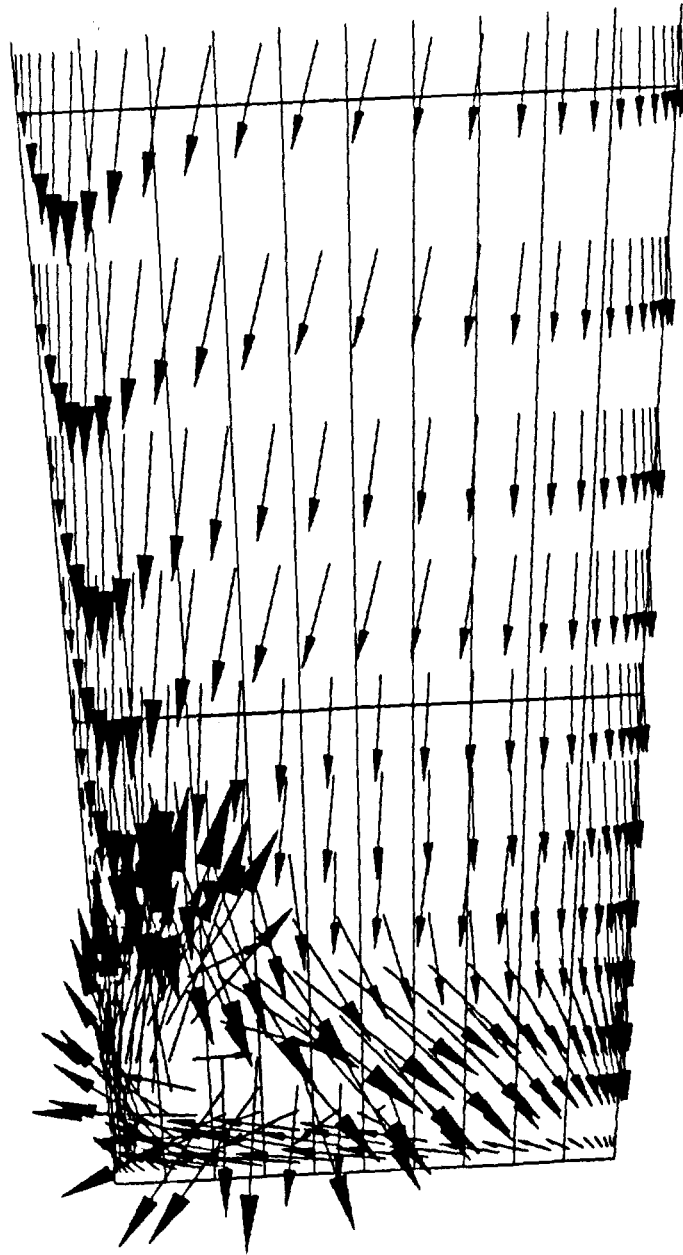


Figure 6.1.3.25: Crossflow Velocity Vectors Near Cowl at  $I = 56$ ,  $x_s'/Te' = 0.06$  for  $CR = 9$ , 0% Cowl,  $Re = 2.15$  million/ft



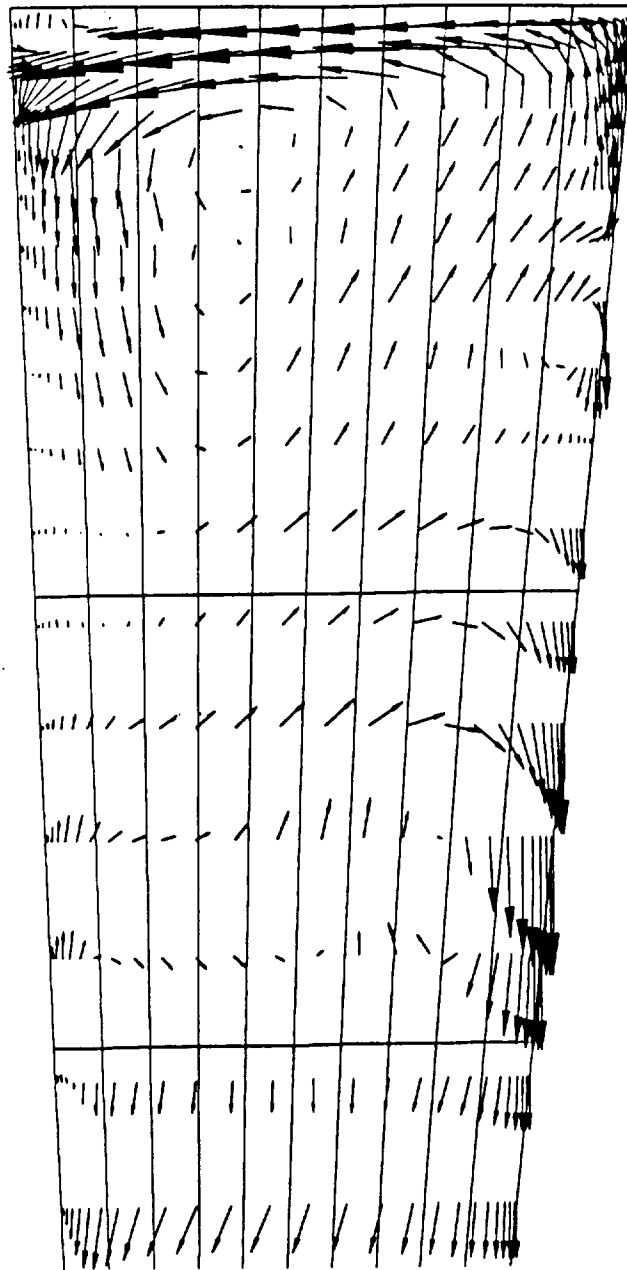


Figure 6.1.3.26: Crossflow Velocity Vectors Near Baseplate for  $I=56$ ,  $x_s'/Te'=0.06$   
for  $CR=9$ , 0% Cowl,  $Re=2.15$  million/ft

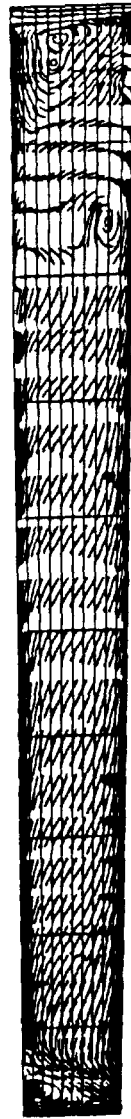


Figure 6.1.3.27: Particle Traces at  $I = 56$ ,  $xs'/Te' = 0.06$  for  $CR = 9$ ,  
0% Cowl,  $Re = 2.15$  million/ft



Figure 6.1.3.28: Pressure Contours at  $I = 60$ ,  $xs'/Te' = 0.29$  for  $CR = 9$ ,  
0% Cowl,  $Re = 2.15$  million/ft



Figure 6.1.3.29: Crossflow Velocity Vectors at  $I = 60$ ,  $xs'/Te' = 0.29$  for  $CR = 9$ ,  
0% Cowl,  $Re = 2.15$  million/ft

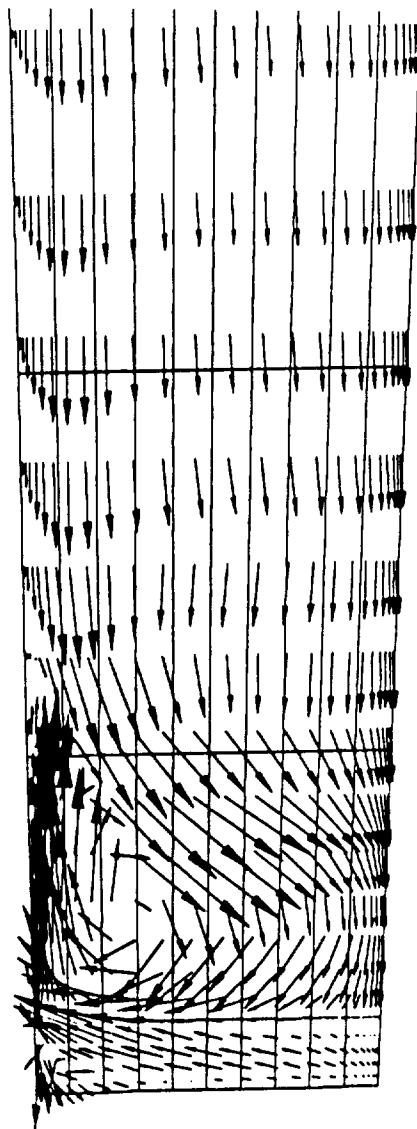


Figure 6.1.3.30: Crossflow Velocity Vectors Near Cowl at  $I = 60$ ,  $x_s'/Te' = 0.29$  for  $CR = 9$ , 0% Cowl,  $Re = 2.15$  million/ft

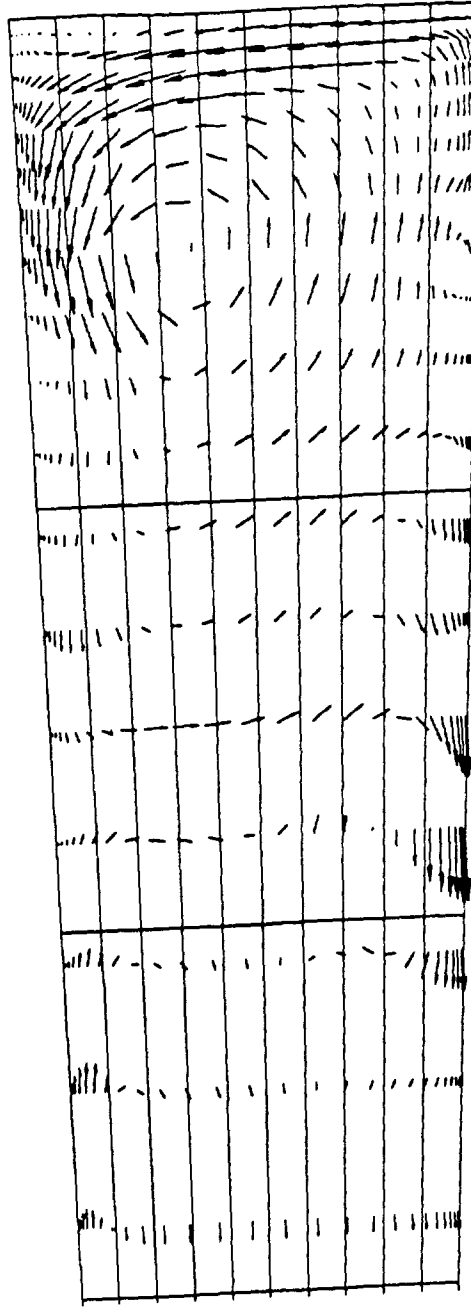


Figure 6.1.3.31: Crossflow Velocity Vectors Near Baseplate at  $I = 60$ ,  $xs'/Te' = 0.29$   
for  $CR = 9$ , 0% Cowl,  $Re = 2.15$  million/ft



Figure 6.1.3.32: Particle Traces at  $I = 60$ ,  $xs'/Te' = 0.29$  for  $CR = 9$ ,  
0% Cowl,  $Re = 2.15$  million/ft



Figure 6.1.3.33: Pressure Contours at  $I = 65$ ,  $xs'/Te' = 0.58$  for  $CR = 9$ ,  
0% Cowl,  $Re = 2.15$  million/ft





Figure 6.1.3.34: Crossflow Velocity Vectors at  $I = 65$ ,  $x_s'/Te' = 0.58$  for  $CR = 9$ ,  
0% Cowl,  $Re = 2.15$  million/ft



Figure 6.1.3.35: Particle Traces at  $I = 65$ ,  $xs'/Te' = 0.58$  for  $CR = 9$ ,  
0% Cowl,  $Re = 2.15$  million/ft

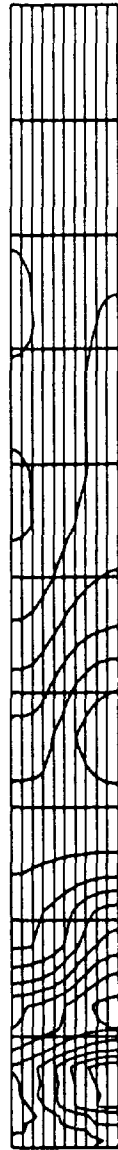


Figure 6.1.3.36: Pressure Contours at  $I = 72$ ,  $xs'/Te' = 1.00$  (Exit Plane) for  $CR = 9$ , 0% Cowl,  $Re = 2.15$  million/ft



Figure 6.1.3.37: Crossflow Velocity Vectors at  $I = 72$ ,  $xs'/Te' = 1.00$  (Exit Plane)  
for  $CR = 9$ , 0% Cowl,  $Re = 2.15$  million/ft



Figure 6.1.3.38: Particle Traces at  $I = 72$ ,  $xs'/Te' = 1.00$  (Exit Plane) for  $CR = 9$ ,  
0% Cowl,  $Re = 2.15$  million/ft



Figure 6.2.1(a): Pressure Contours at  $Z/H = 0.25$  for  $CR = 3$ ,  
 $Re = 2.15$  million/ft, 50% Cowl



Figure 6.2.1(b): Pressure Contours at  $Z/H = 0.50$  for  $CR = 3$ ,  
 $Re = 2.15$  million/ft, 50% Cowl



Figure 6.2.1(c): Pressure Contours at  $Z/H = 0.75$  for  $CR = 3$ ,  
 $Re = 2.15$  million/ft, 50% Cowl

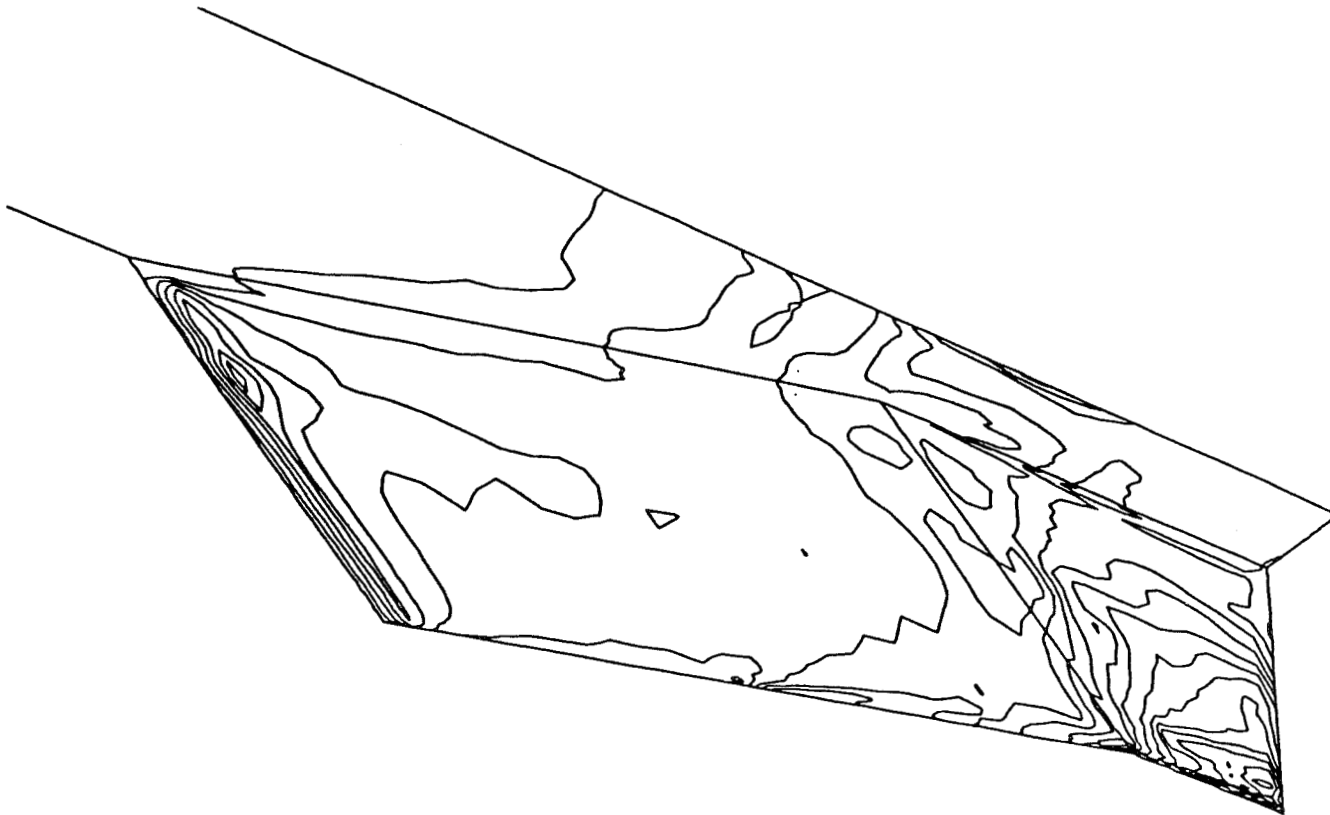


Figure 6.2.2: Sidewall and Baseplate Pressure Contours for  $CR = 3$ ,  
 $Re = 2.15$  million/ft, 50% Cowl

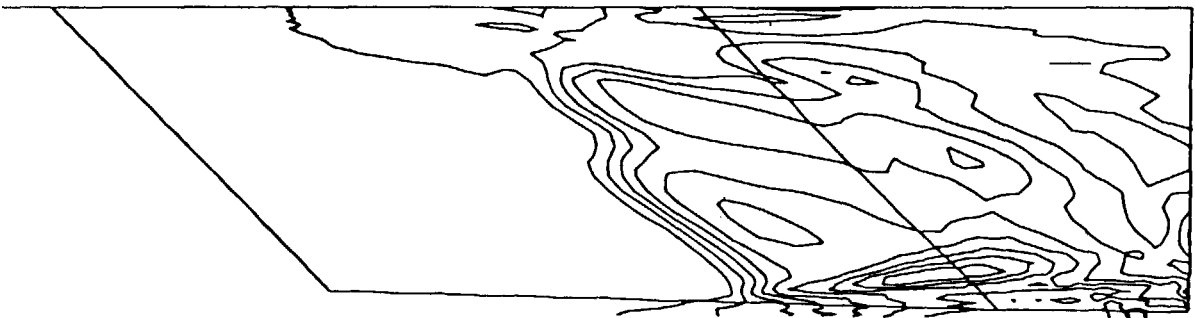


Figure 6.2.3: Centerline Pressure Contours for CR = 3,  
Re = 2.15 million/ft, 50% Cowl



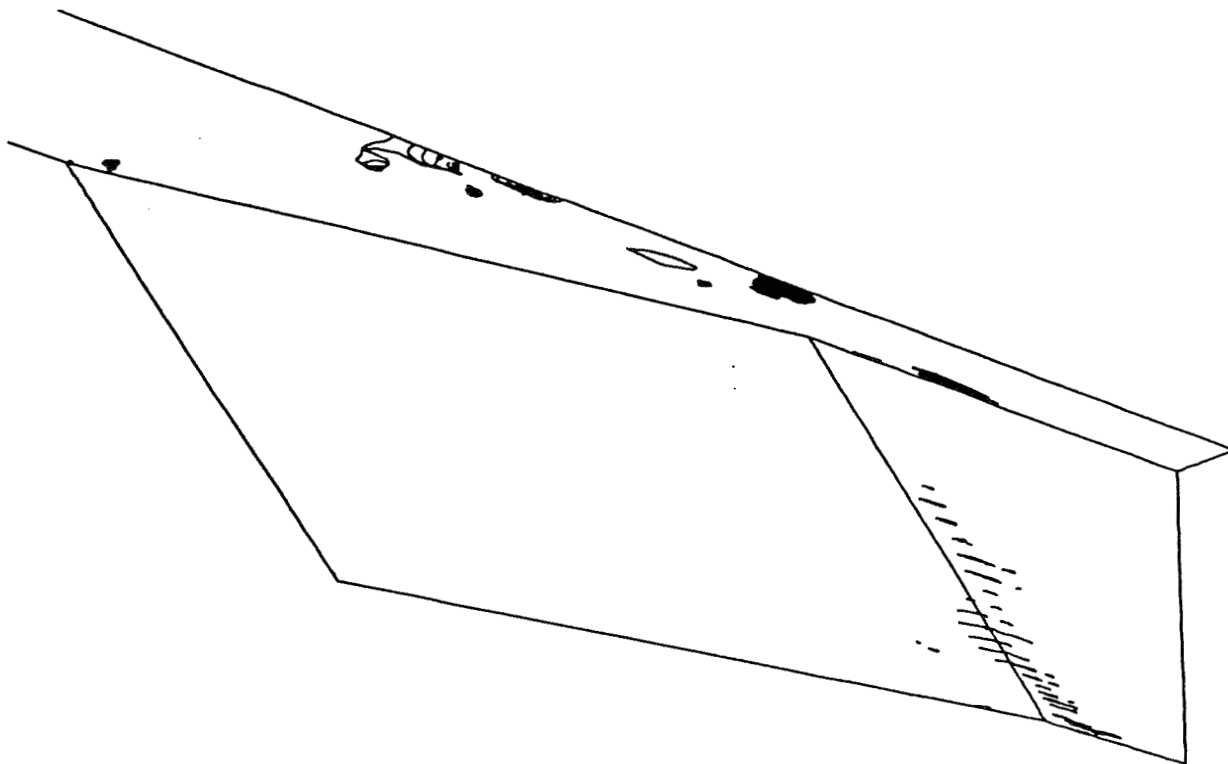


Figure 6.2.4: Streamwise Separation ( $U < 0$ ) for  $CR = 3$ ,  
 $Re = 2.15$  million/ft, 50% Cowl

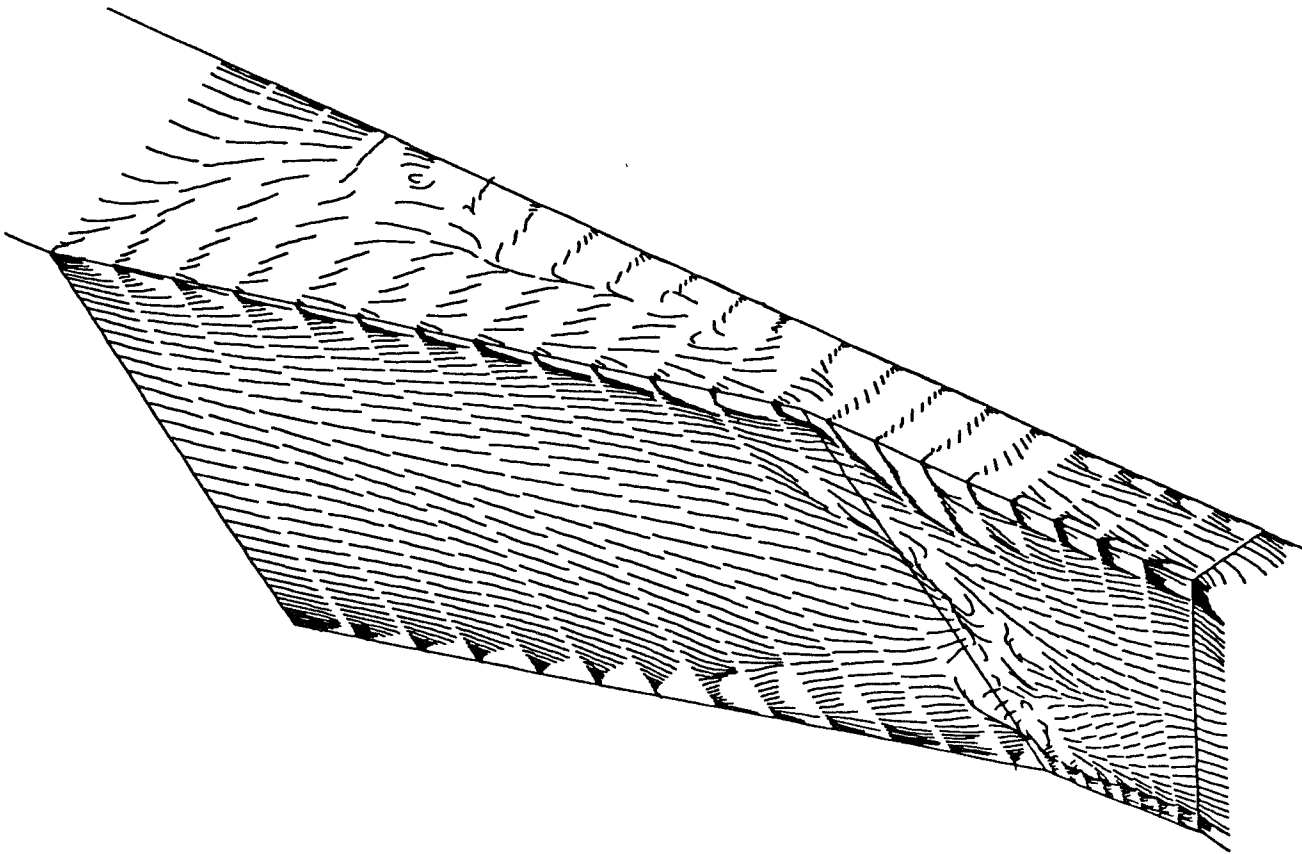


Figure 6.2.5: Simulated Oil Flow for  $CR = 3$ ,  $Re = 2.15$  million /ft, 50% Cowl

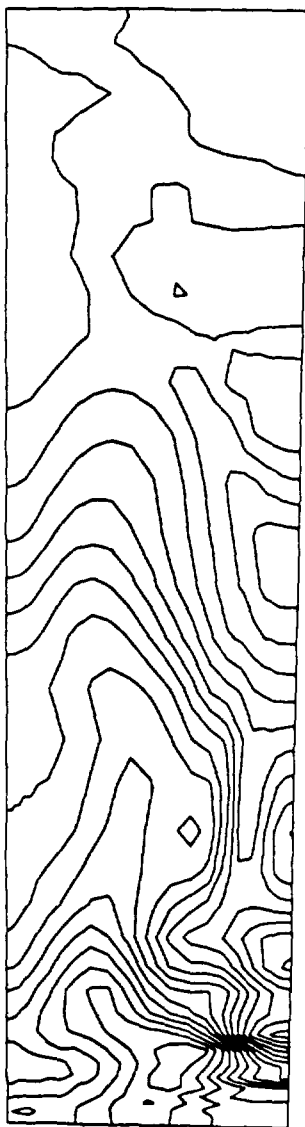


Figure 6.2.6: Exit Plane Pressure Contours for  $CR = 3$ ,  
 $Re = 2.15$  million/ft, 50% Cowl

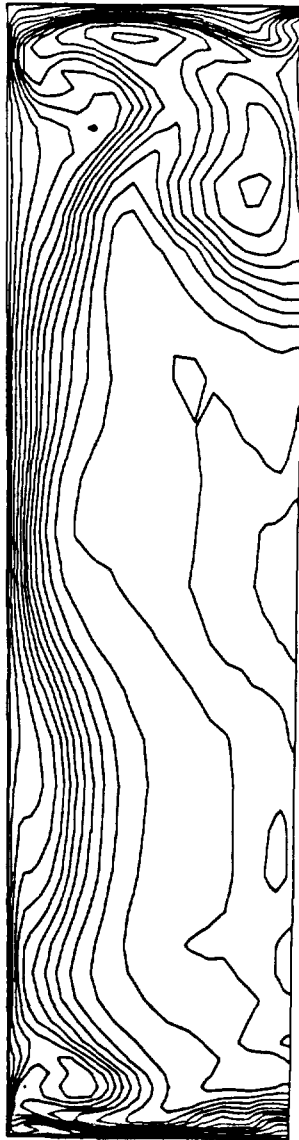


Figure 6.2.7: Exit Plane Mach Number Contours for  $CR = 3$ ,  
 $Re = 2.15$  million/ft, 50% Cowl

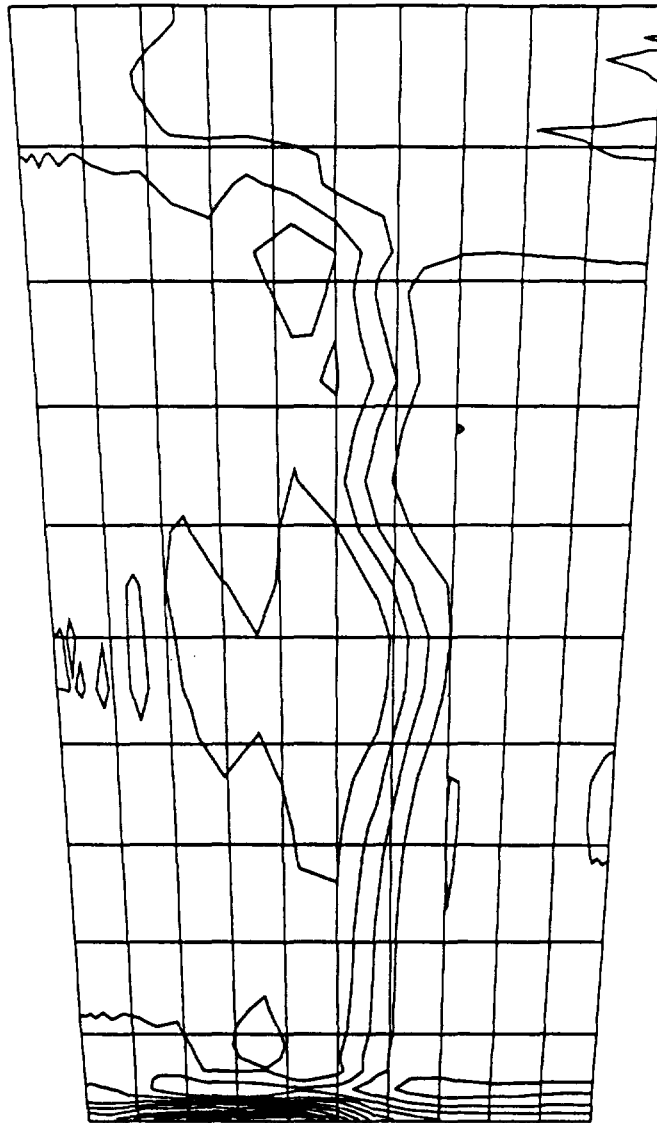


Figure 6.2.2.1: Pressure Contours at  $I=43$ ,  $x'/Tx' = 0.50$  for  $CR = 3$ ,  
50% Cowl,  $Re = 2.15$  million/ft

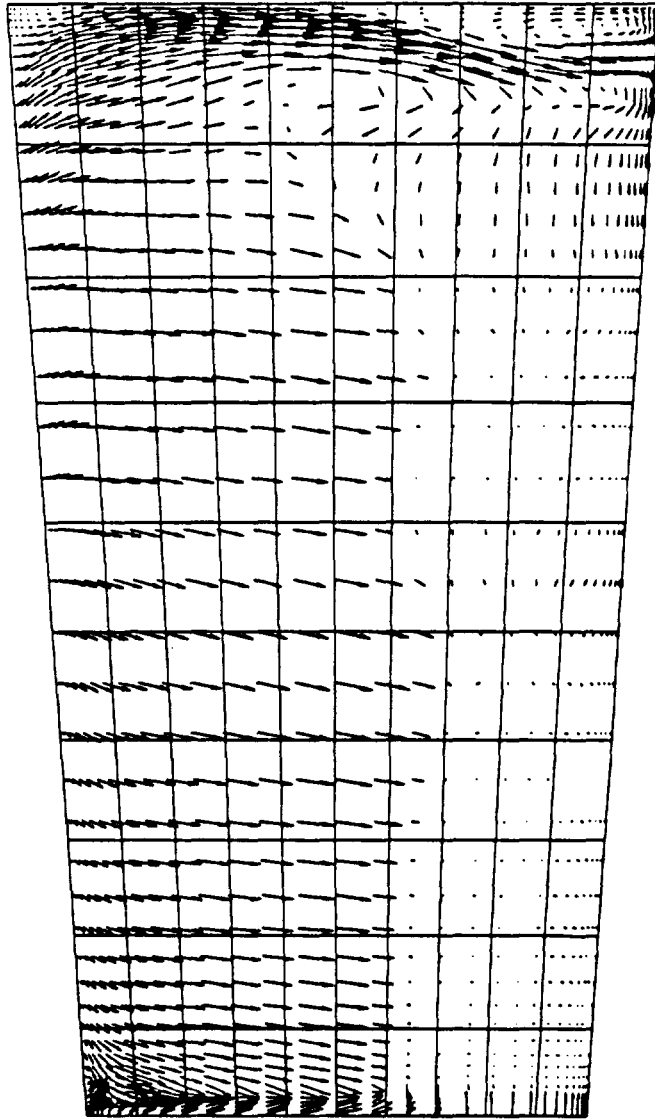


Figure 6.2.2.2: Crossflow Velocity Vectors at  $I = 43$ ,  $x'/Tx' = 0.50$  for  $CR = 3$ ,  
50% Cowl,  $Re = 2.15$  million/ft

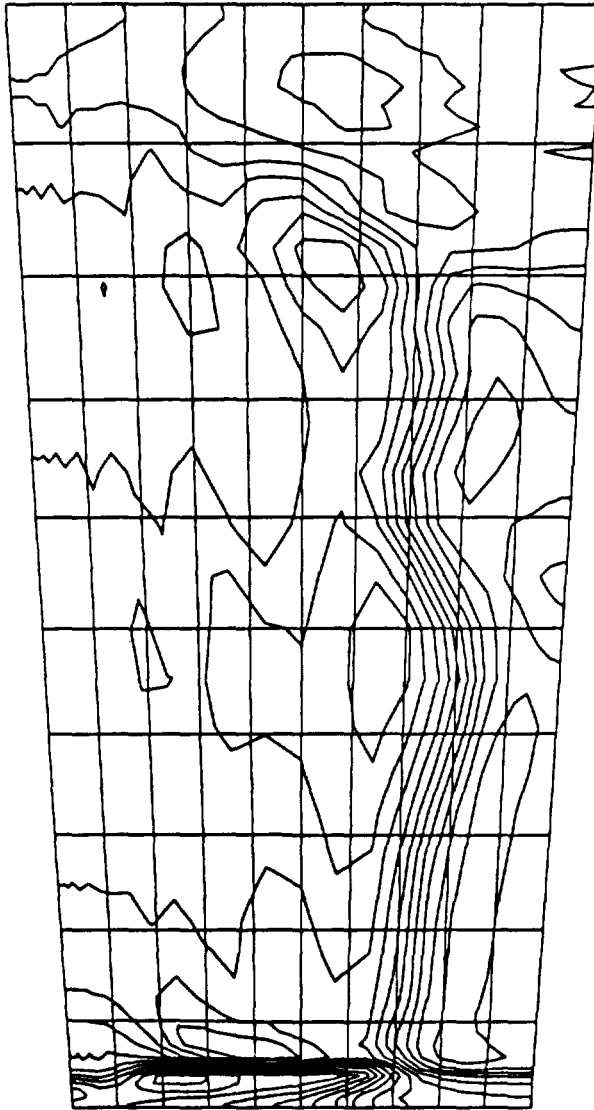


Figure 6.2.2.3: Pressure Contours at  $I = 45$ ,  $x'/Tx' = 0.60$  for  $CR = 3$ ,  
50% Cowl,  $Re = 2.15$  million/ft

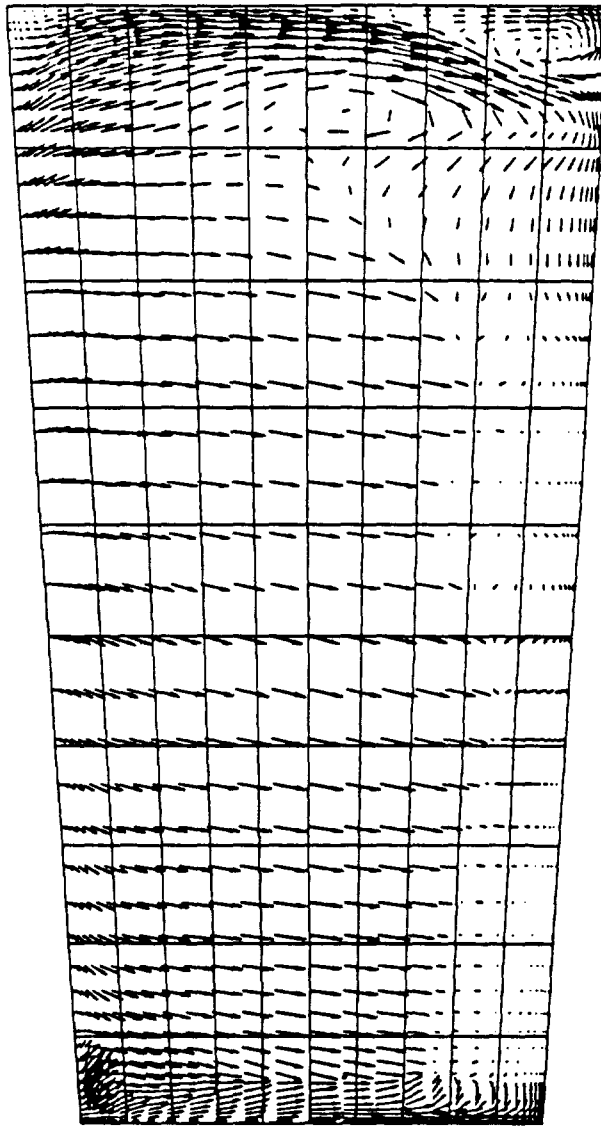


Figure 6.2.2.4: Crossflow Velocity Vectors at  $I = 45$ ,  $x'/Tx' = 0.60$  for  $CR = 3$ ,  
50% Cowl,  $Re = 2.15$  million/ft



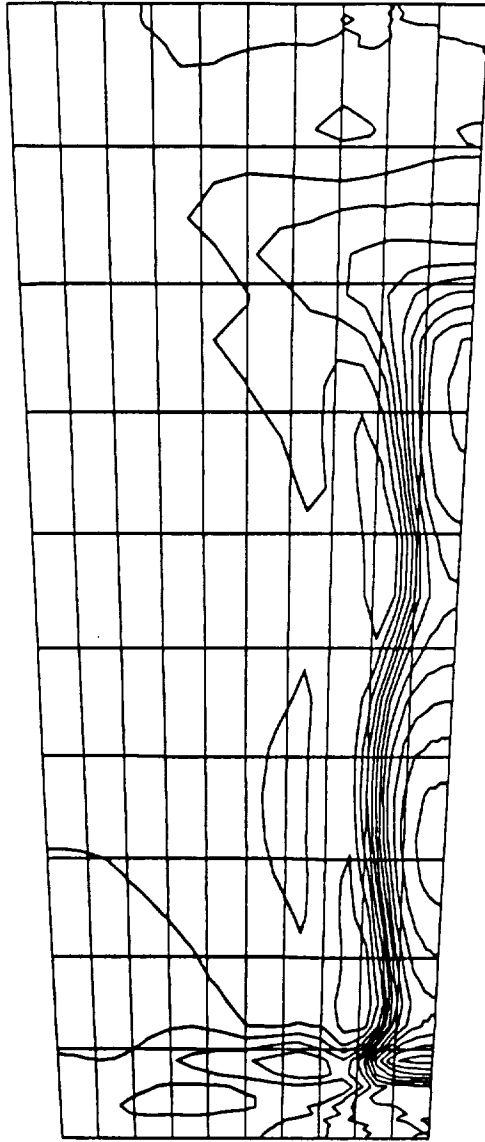


Figure 6.2.2.5: Pressure Contours at  $I = 50$ ,  $x'/Tx' = 0.79$  for  $CR = 3$ ,  
50% Cowl,  $Re = 2.15$  million/ft

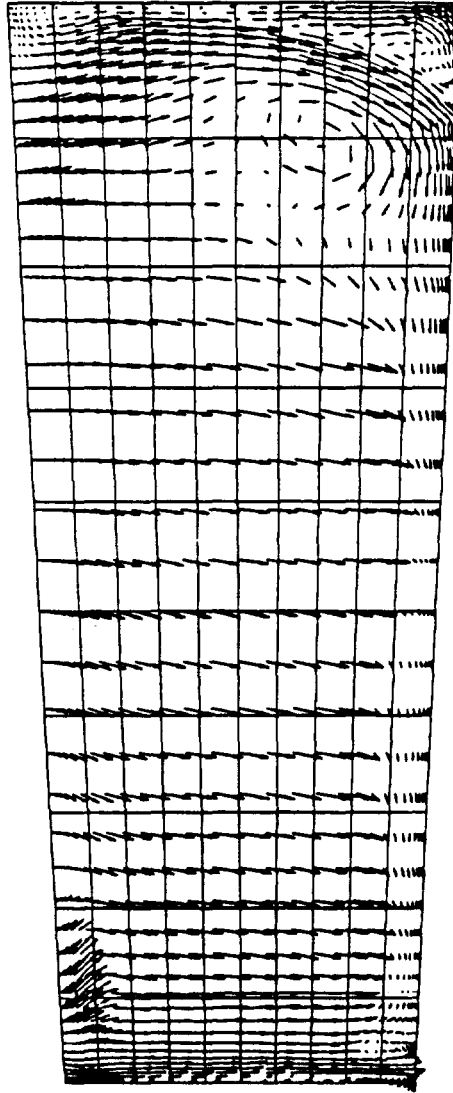


Figure 6.2.2.6: Crossflow Velocity Vectors at  $I = 50$ ,  $x'/T_x' = 0.79$  for  $CR = 3$ , 50% Cowl,  $Re = 2.15$  million/ft

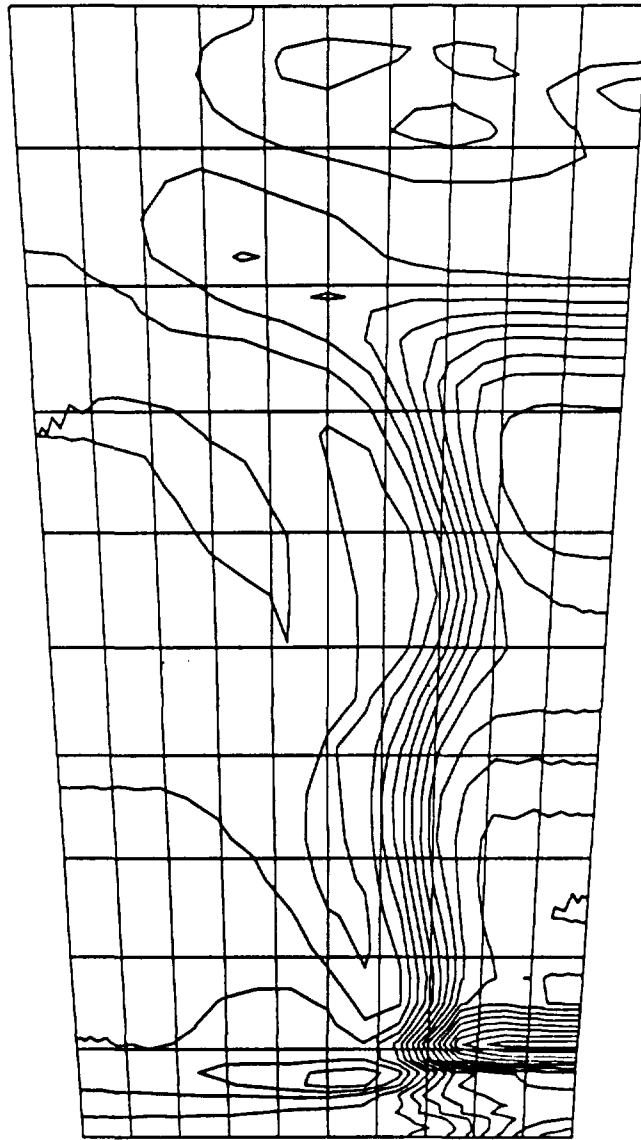


Figure 6.2.2.7: Pressure Contours at  $I = 52$ ,  $x'/Tx' = 0.87$  for  $CR = 3$ ,  
50% Cowl,  $Re = 2.15$  million/ft

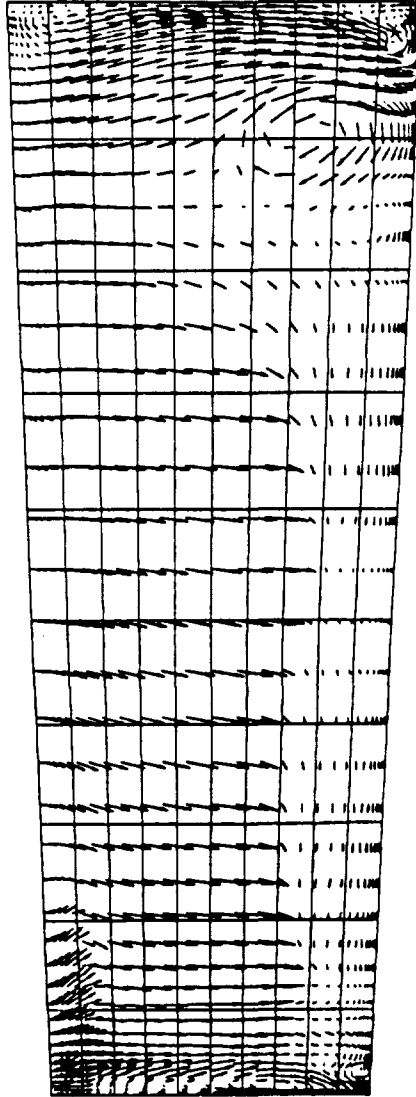


Figure 6.2.2.8: Crossflow Velocity Vectors at  $I = 52$ ,  $x'/Tx' = 0.87$  for  $CR = 3$ ,  
50% Cowl,  $Re = 2.15$  million/ft

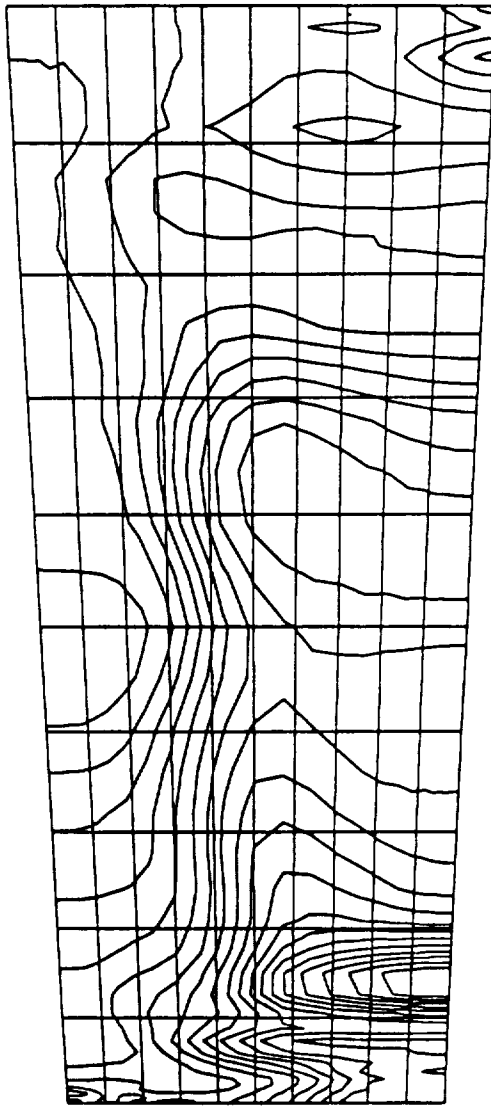


Figure 6.2.2.9: Pressure Contours at  $I = 55$ ,  $x'/Tx' = 1.00$  for  $CR = 3$ ,  
50% Cowl,  $Re = 2.15$  million/ft

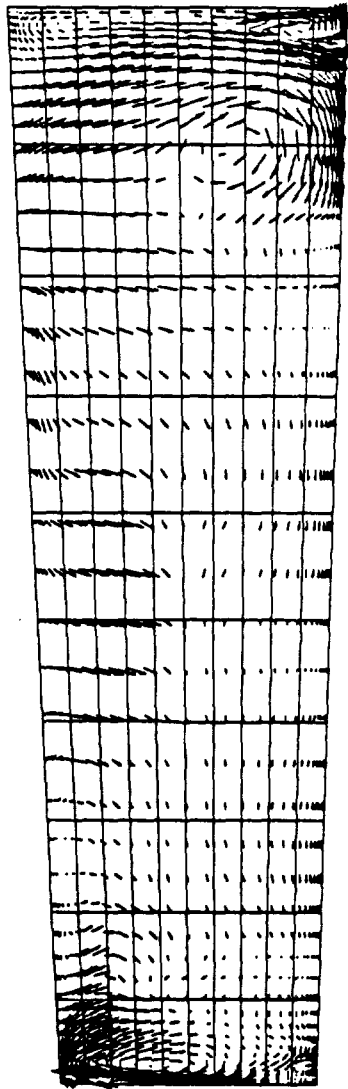


Figure 6.2.2.10 Crossflow Velocity Vectors at  $I = 55$ ,  $x'/T_x' = 1.00$  for  $CR = 3$ ,  
50% Cowl,  $Re = 2.15$  million/ft

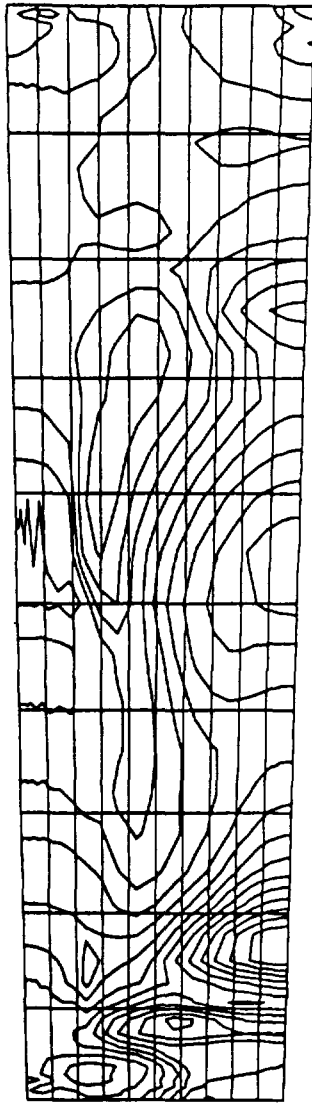


Figure 6.2.2.11: Pressure Contours at  $I = 60$ ,  $xs'/Te' = 0.29$  for  $CR = 3$ ,  
50% Cowl,  $Re = 2.15$  million/ft

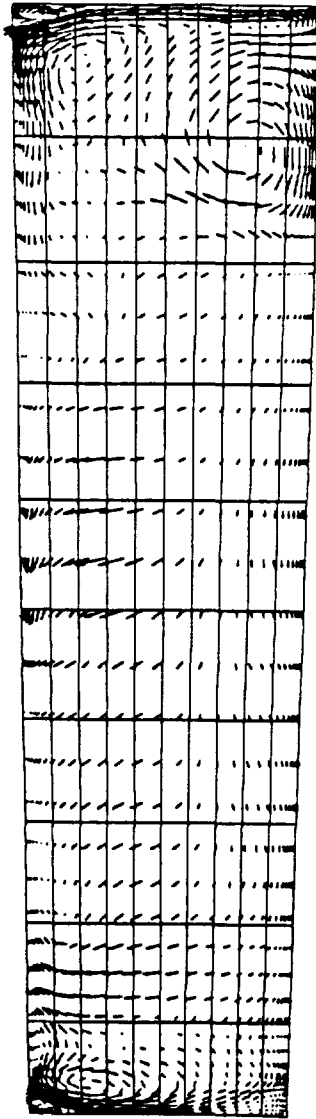


Figure 6.2.2.12: Crossflow Velocity Vectors at  $I = 60$ ,  $x_s'/Te' = 0.29$  for  $CR = 3$ ,  
50% Cowl,  $Re = 2.15$  million/ft



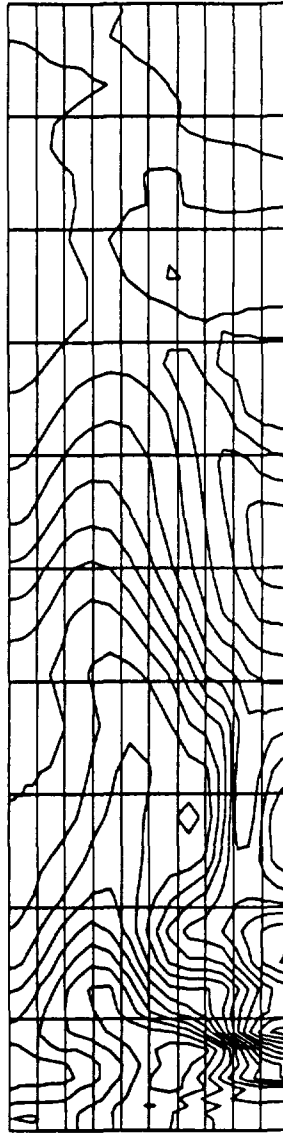


Figure 6.2.2.13: Pressure Contours at  $I = 72$ ,  $x_s'/Te' = 1.00$  (Exit Plane)  
for  $CR = 3$ , 50% Cowl,  $Re = 2.15$  million/ft

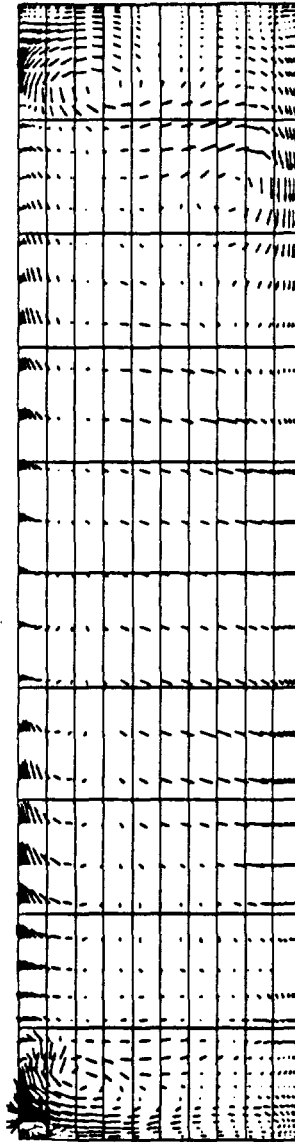


Figure 6.2.2.14: Crossflow Velocity Vectors at  $I = 72$ ,  $x_s'/Te' = 1.00$  (Exit Plane)  
for  $CR = 3$ , 50% Cowl,  $Re = 2.15$  million/ft



Figure 6.3.1(a): Pressure Contours at  $Z/H = 0.25$  for  $CR = 3$ ,  
 $Re = 0.55$  million/ft, 0% Cowl



Figure 6.3.1(b): Pressure Contours at  $Z/H = 0.50$  for  $CR = 3$ ,  
 $Re = 0.55$  million/ft, 0% Cowl

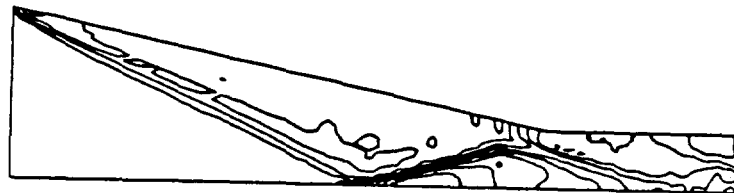


Figure 6.3.1(c): Pressure Contours at  $Z/H = 0.75$  for  $CR = 3$ ,  
 $Re = 0.55$  million/ft, 0% Cowl

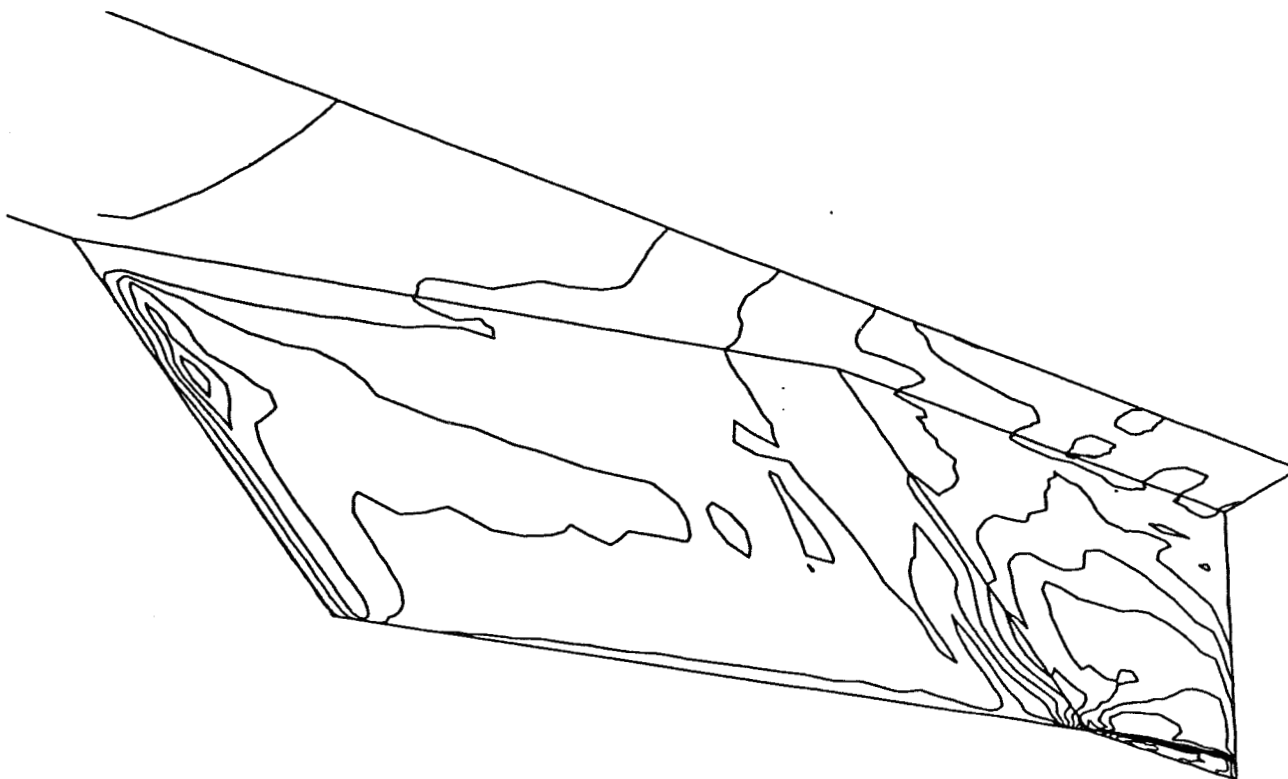


Figure 6.3.2: Sidewall and Baseplate Pressure Contours for CR = 3,  
Re = 0.55 million/ft, 0% Cowl

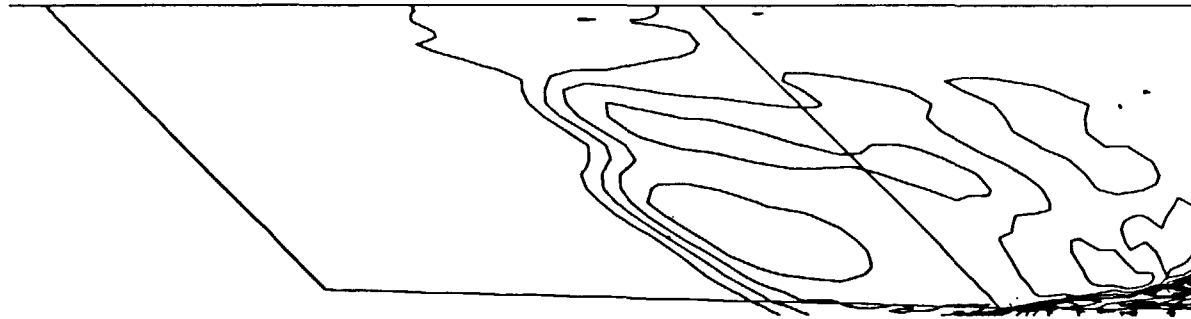


Figure 6.3.3: Centerline Pressure Contours for  $CR = 3$ ,  $Re = 0.55$  million/ft, 0% Cowl

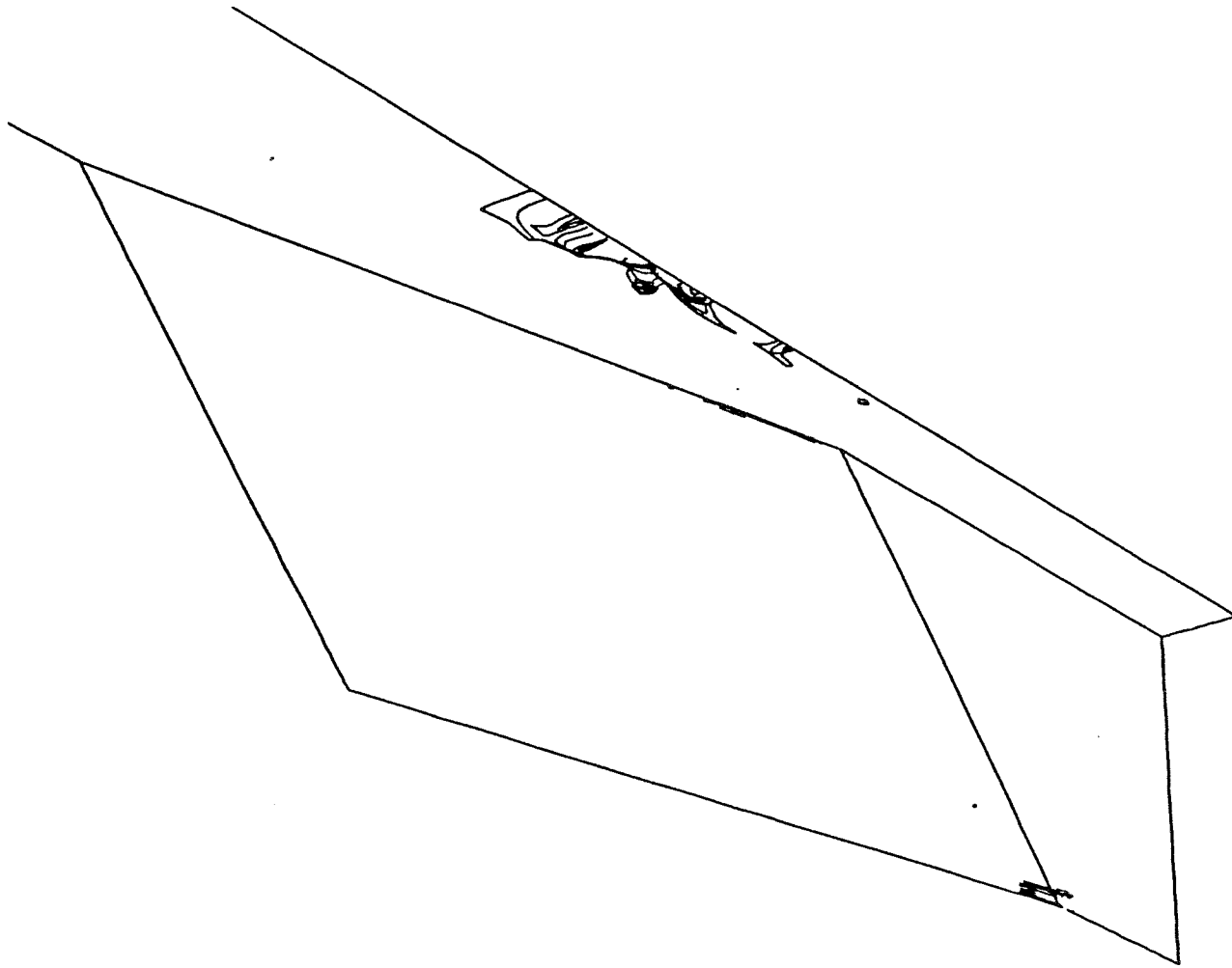


Figure 6.3.4: Streamwise Separation ( $U < 0$ ) for  $CR = 3$ ,  
 $Re = 0.55$  million/ft, 0% Cowl

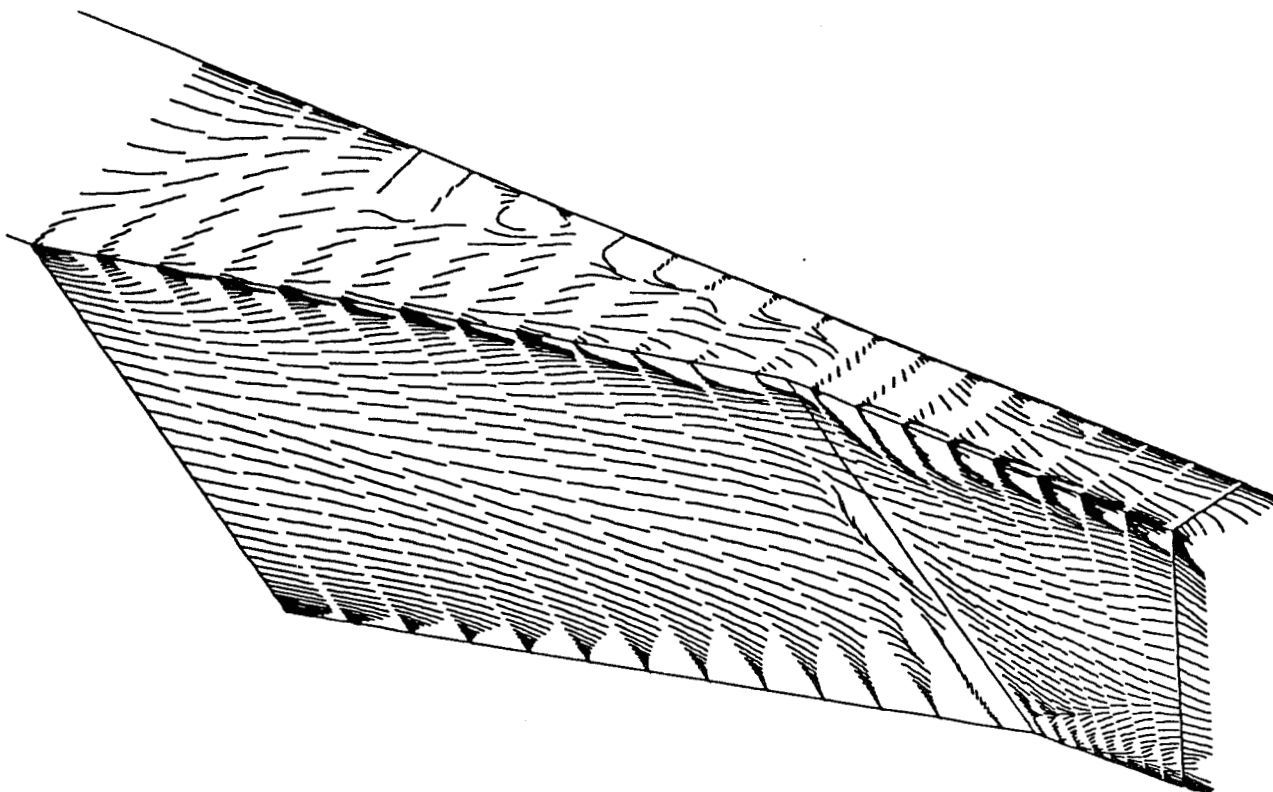


Figure 6.3.5: Simulated Oil Flow for  $CR = 3$ ,  $Re = 0.55$  million /ft, 0% Cowl

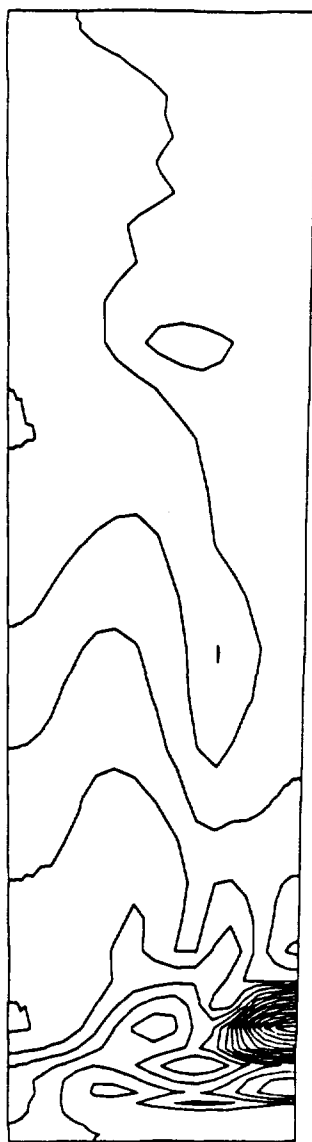


Figure 6.3.6: Exit Plane Pressure Contours for  $CR = 3$ ,  
 $Re = 0.55$  million/ft, 0% Cowl



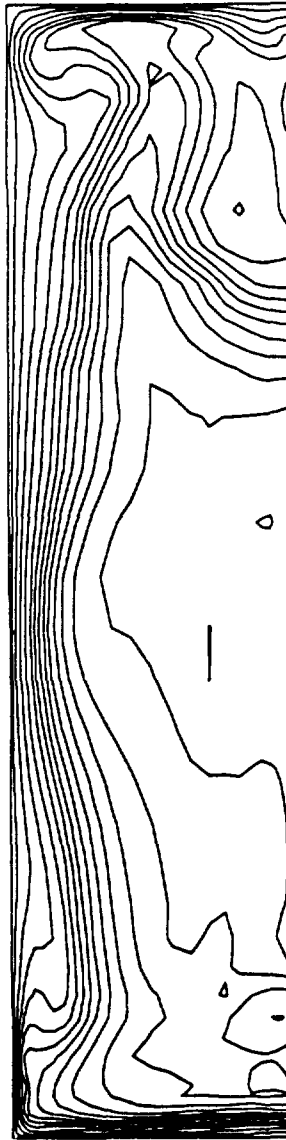


Figure 6.3.7: Exit Plane Mach Number Contours for  $CR = 3$ ,  
 $Re = 0.55$  million/ft, 0% Cowl

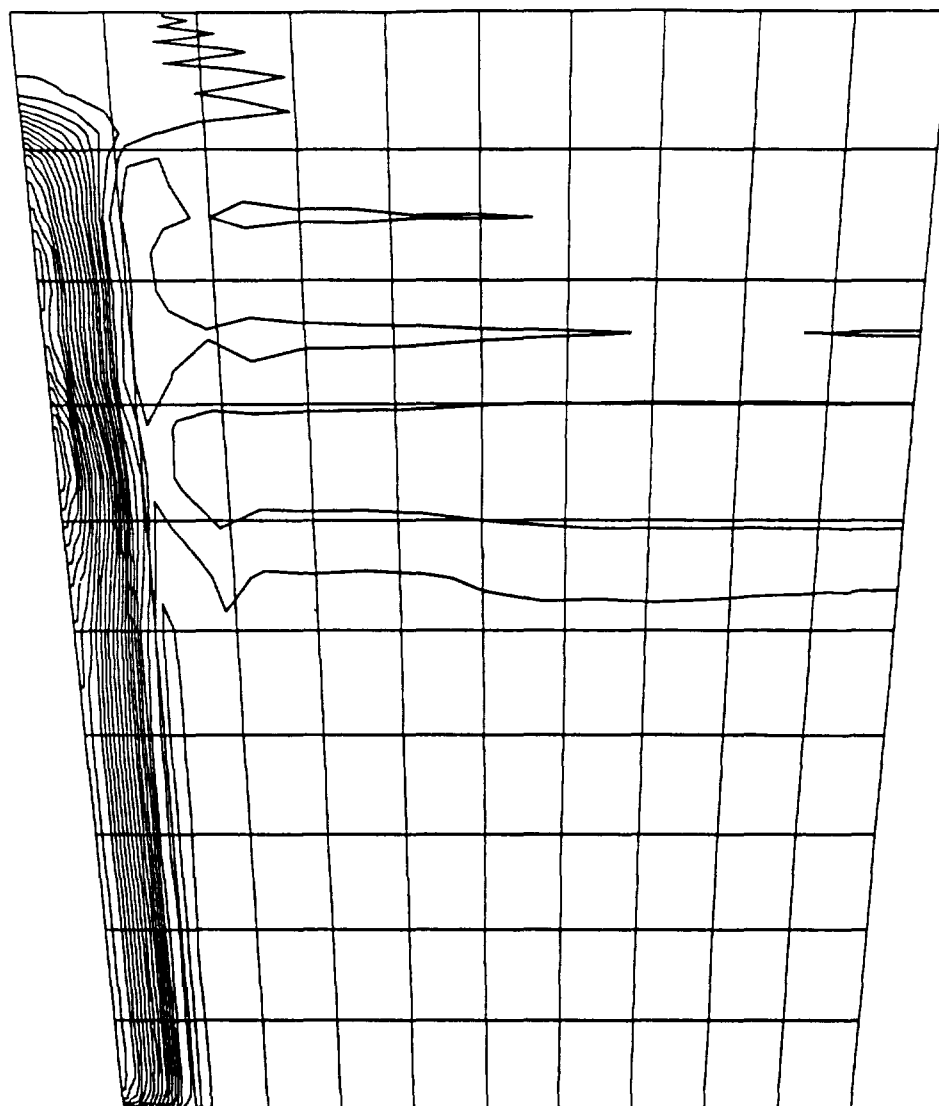


Figure 6.3.2.1: Pressure Contours at  $I = 31$ ,  $x'/Tx' = 0.04$  for  $CR = 3$ ,  
0% Cowl,  $Re = 0.55$  million/ft

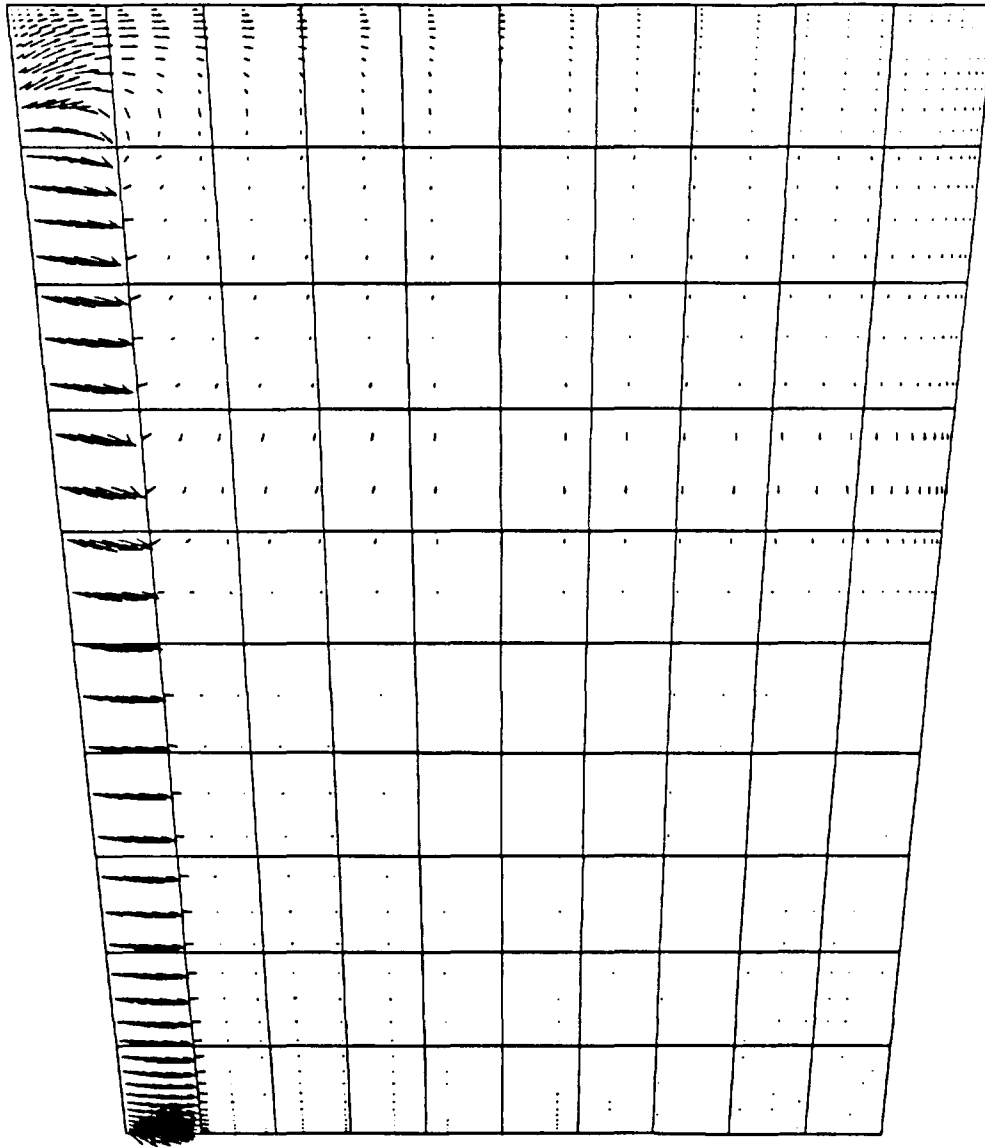


Figure 6.3.2.2: Crossflow Velocity Vectors at  $I = 31$ ,  $x'/Tx' = 0.04$  for  $CR = 3$ ,  
0% Cowl,  $Re = 0.55$  million/ft

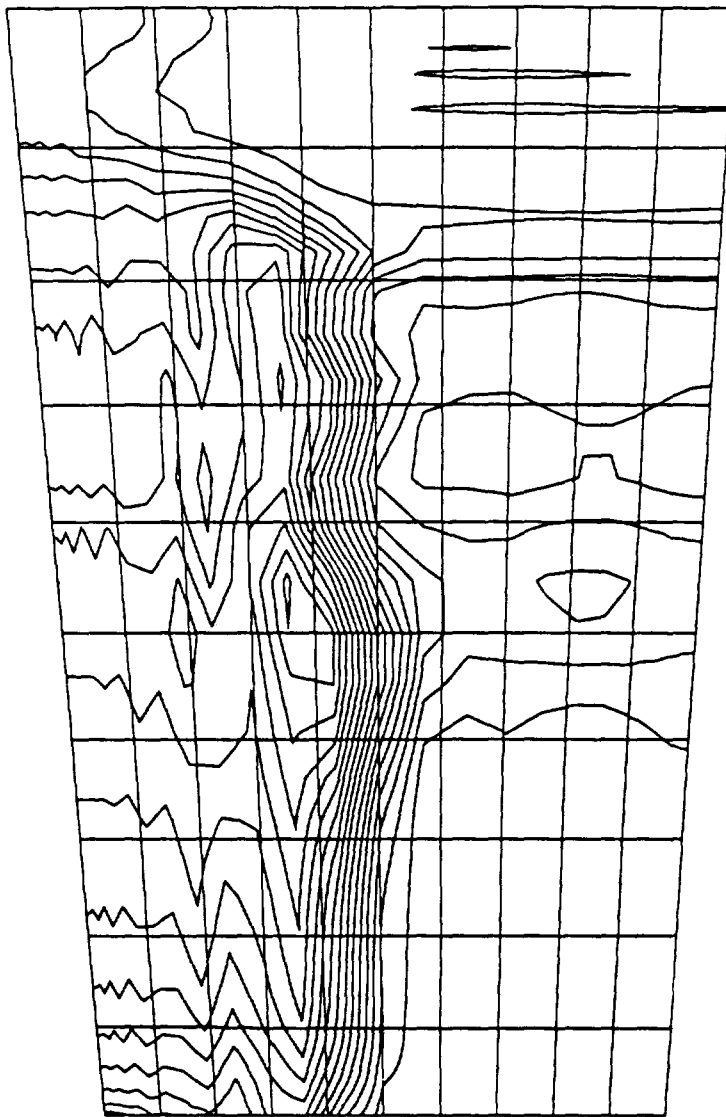


Figure 6.3.2.3: Pressure Contours at  $I = 40$ ,  $x'/Tx' = 0.40$  for  $CR = 3$ ,  
0% Cowl,  $Re = 0.55$  million/ft

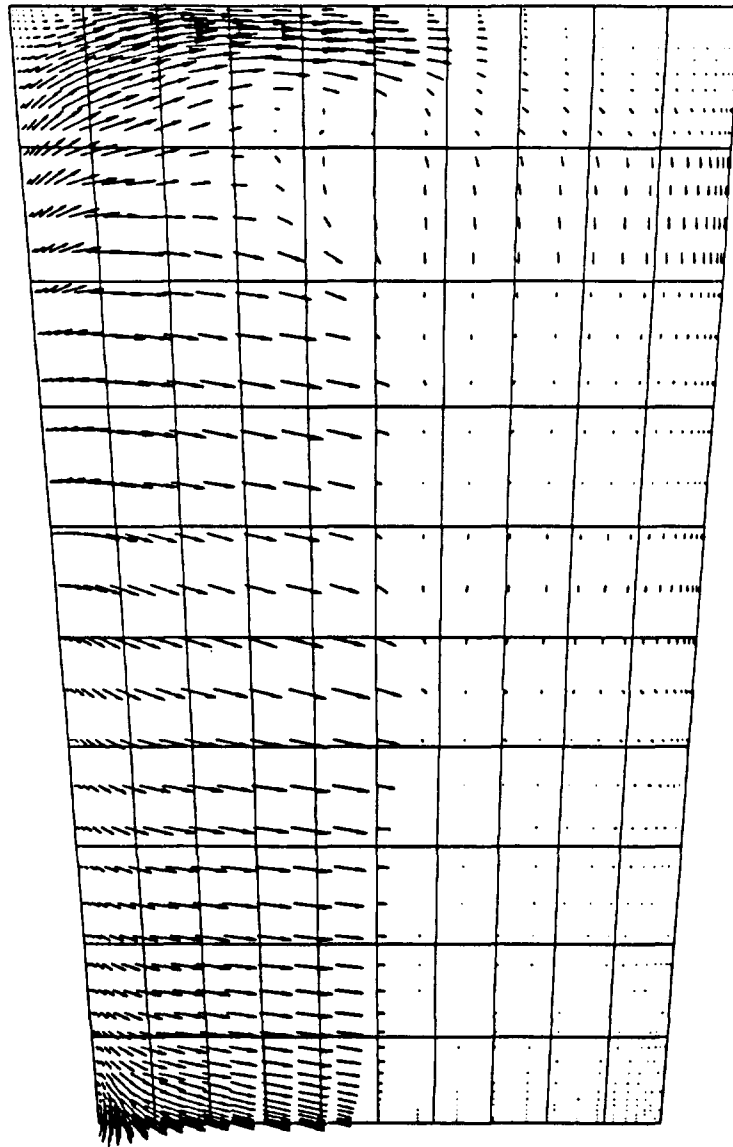


Figure 6.3.2.4: Crossflow Velocity Vectors at  $I = 40$ ,  $x'/Tx' = 0.40$  for  $CR = 3$ ,  
0% Cowl,  $Re = 0.55$  million/ft

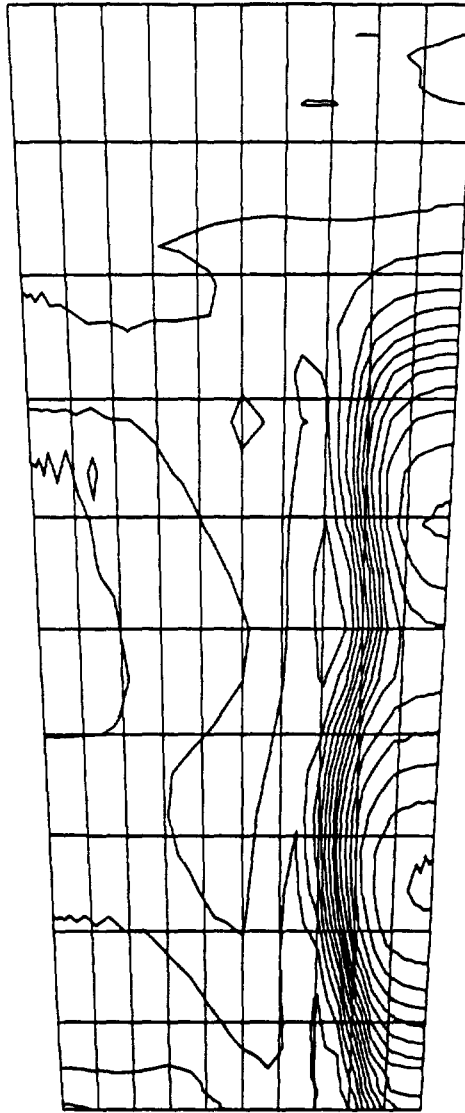


Figure 6.3.2.5: Pressure Contours at  $I = 50$ ,  $x'/Tx' = 0.79$  for  $CR = 3$ ,  
0% Cowl,  $Re = 0.55$  million/ft

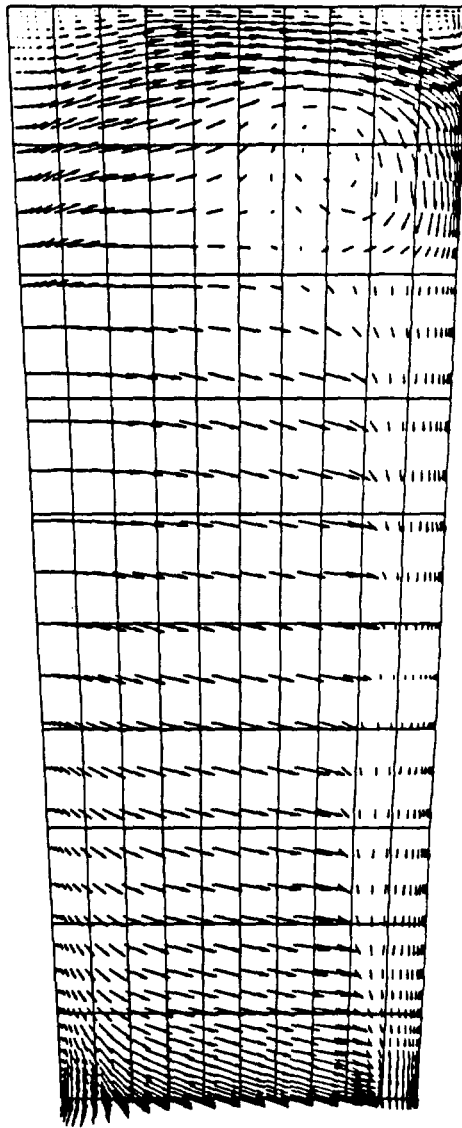


Figure 6.3.2.6: Crossflow Velocity Vectors at  $I = 50$ ,  $x'/Tx' = 0.79$  for  $CR = 3$ ,  
0% Cowl,  $Re = 0.55$  million/ft

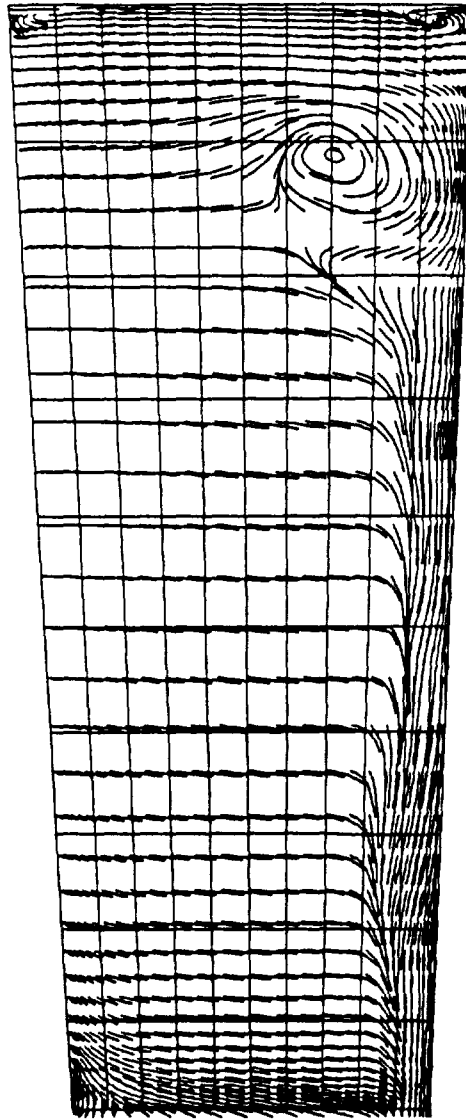


Figure 6.3.2.7: Particle Traces at  $I = 50$ ,  $x'/Tx' = 0.79$  for  $CR = 3$ ,  
0% Cowl,  $Re = 0.55$  million/ft



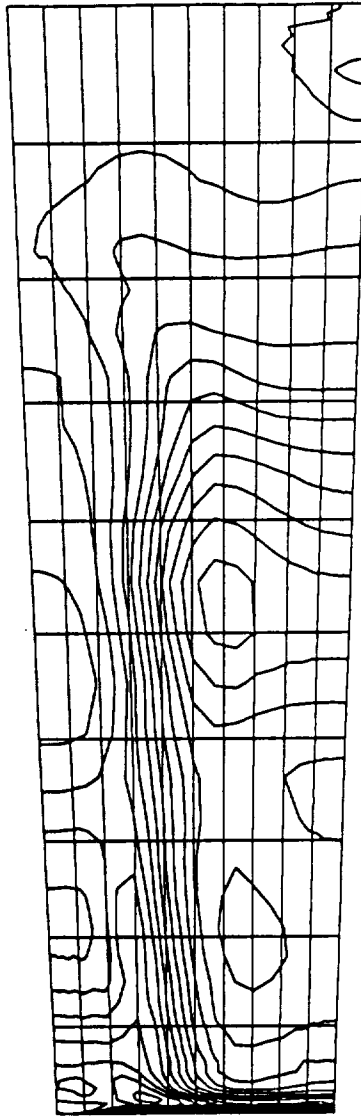


Figure 6.3.2.8: Pressure Contours at  $I = 54$ ,  $x'/Tx' = 0.96$  for  $CR = 3$ ,  
0% Cowl,  $Re = 0.55$  million/ft

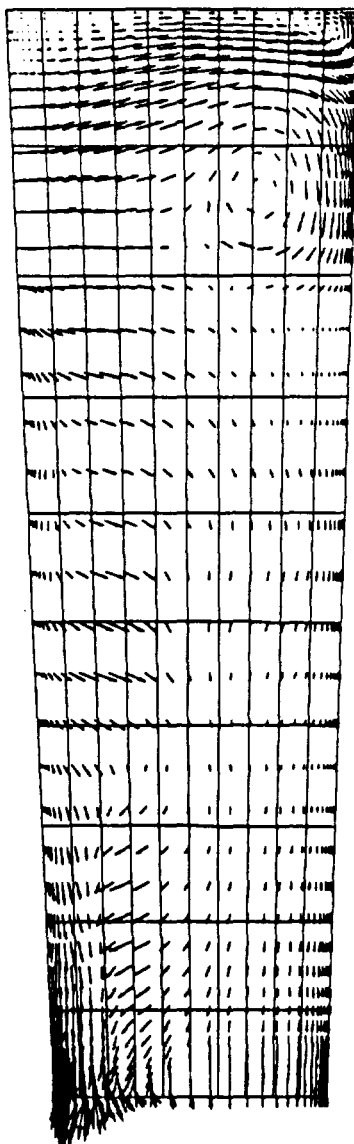


Figure 6.3.2.9: Crossflow Velocity Vectors at  $I = 54$ ,  $x'/Tx' = 0.96$  for  $CR = 3$ ,  
0% Cowl,  $Re = 0.55$  million/ft

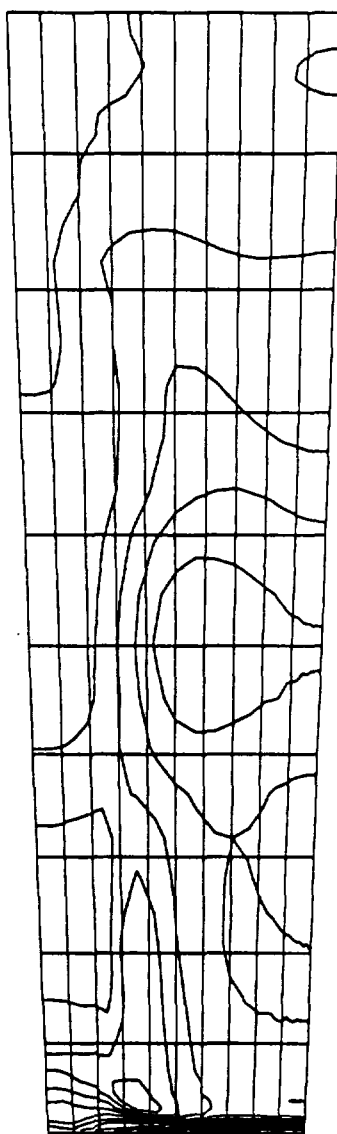


Figure 6.3.2.10: Pressure Contours at  $I = 55$ ,  $x'/Tx' = 1.00$  for  $CR = 3$ ,  
0% Cowl,  $Re = 0.55$  million/ft

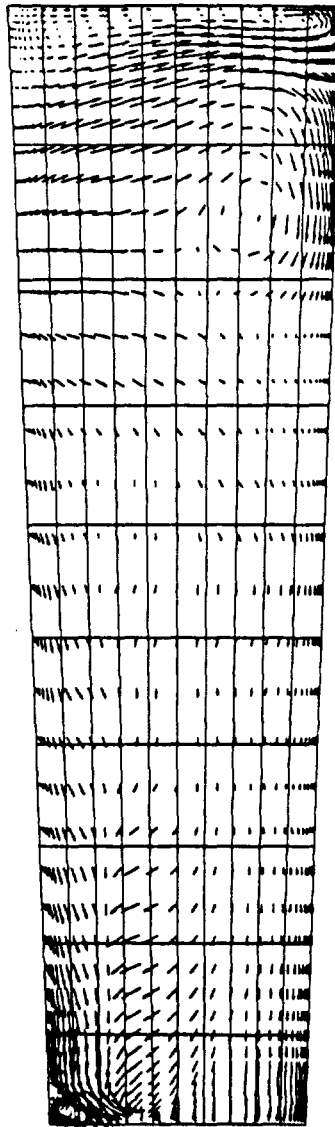


Figure 6.3.2.11 Crossflow Velocity Vectors at  $I = 55$ ,  $x'/Tx' = 1.00$  for  $CR = 3$ ,  
0% Cowl,  $Re = 0.55$  million/ft

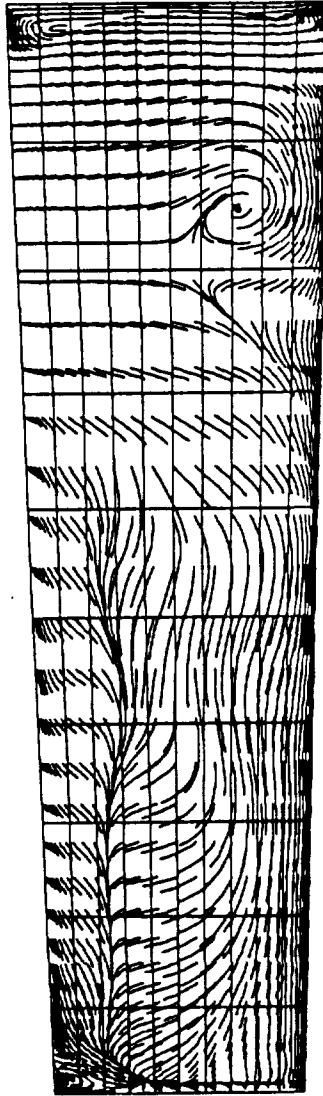


Figure 6.3.2.12: Particle Traces at  $I = 55$ ,  $x'/Tx' = 1.00$  for  $CR = 3$ ,  
0% Cowl,  $Re = 0.55$  million/ft

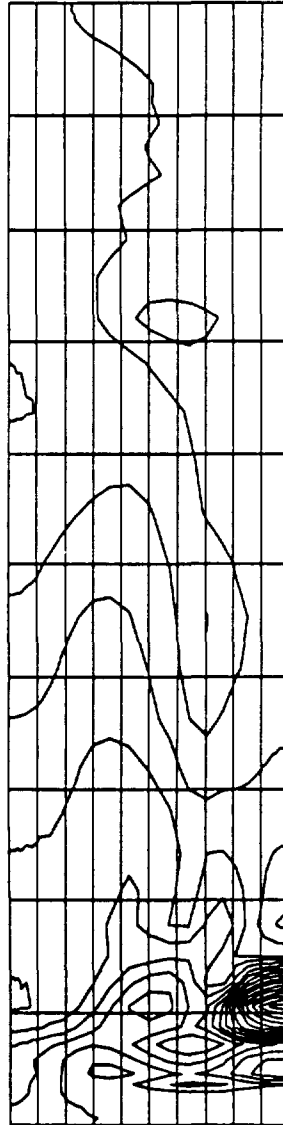


Figure 6.3.2.13: Pressure Contours at  $I = 72$ ,  $xs'/Te' = 1.00$  (Exit Plane) for  $CR = 3$ , 0% Cowl,  $Re = 0.55$  million/ft

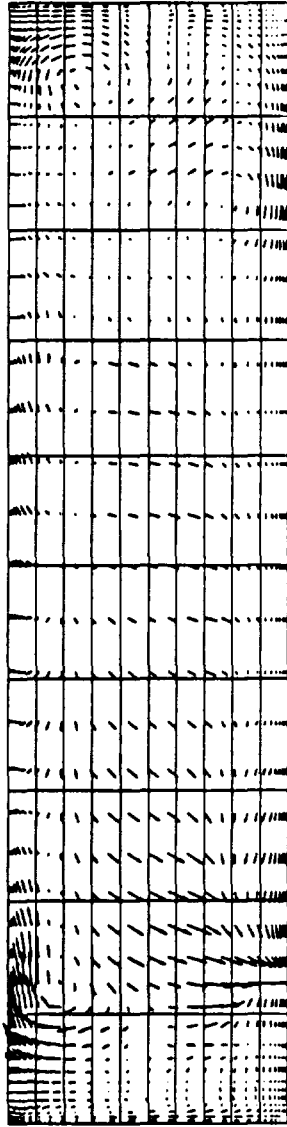


Figure 6.3.2.14: Crossflow Velocity Vectors at  $I = 72$ ,  $x_s'/Te' = 1.00$  (Exit Plane) for  $CR = 3$ , 0% Cowl,  $Re = 0.55$  million/ft



Figure 6.3.2.15: Particle Traces at  $I = 72$ ,  $xs'/Te' = 1.00$  (Exit Plane) for  $CR = 3$ ,  
0% Cowl,  $Re = 0.55$  million/ft



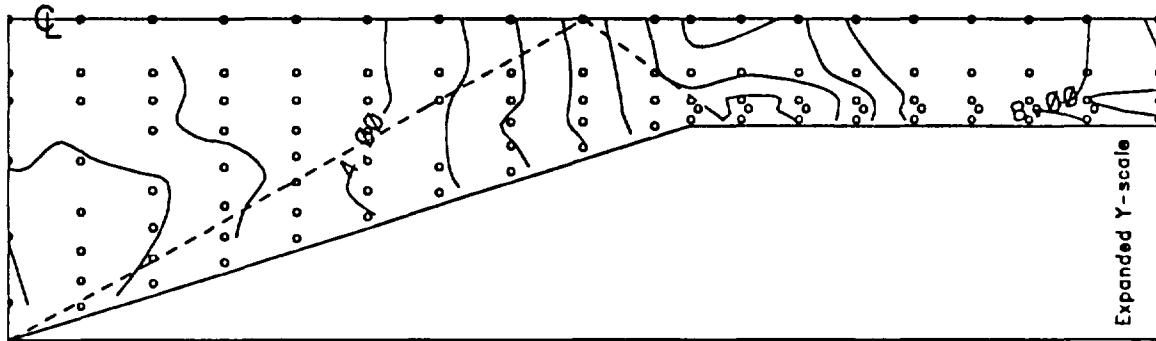


Figure 7.1.1.1(a): P/Plnf Baseplate Contours, CR=3, Re=0.55 million/ft, 0% Cowl, (RUN64)

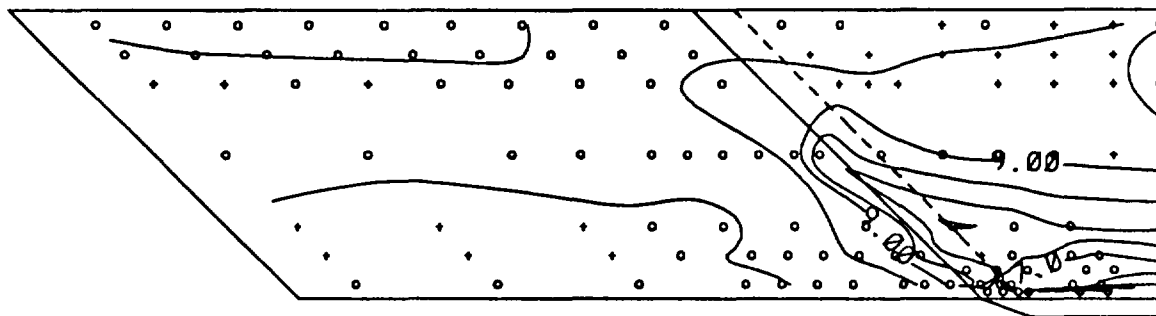


Figure 7.1.1.1(b): P/Plnf Sidewall Contours, CR=3, Re=0.55 million/ft, 0% Cowl, (RUN64)

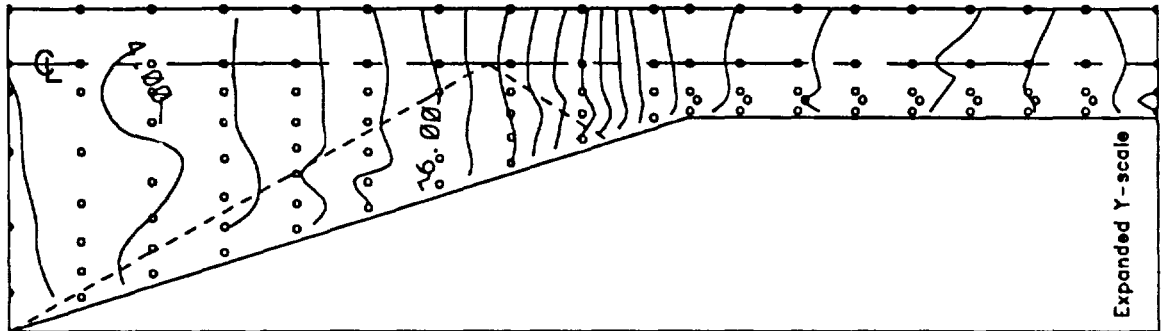


Figure 7.1.1.2(a): P/P<sub>inf</sub> Baseplate Contours, CR=5, Re=0.55 million/ft, 0% Cowl, (RUN44)

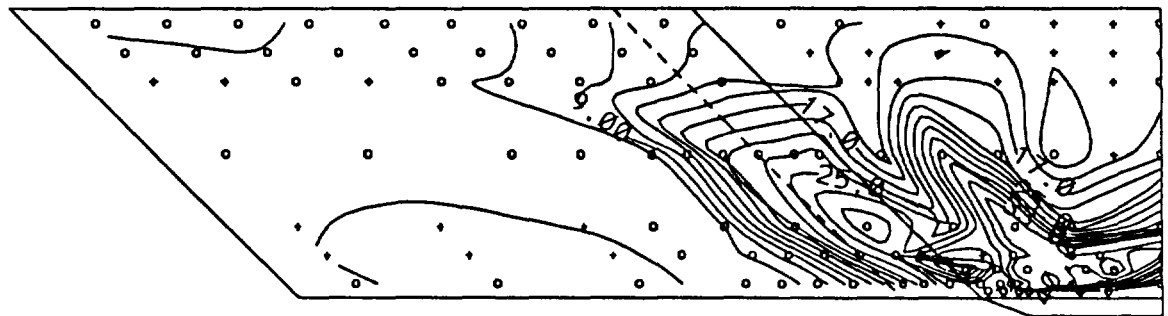


Figure 7.1.1.2(b): P/P<sub>inf</sub> Sidewall Contours, CR=5, Re=0.55 million/ft, 0% Cowl, (RUN44)

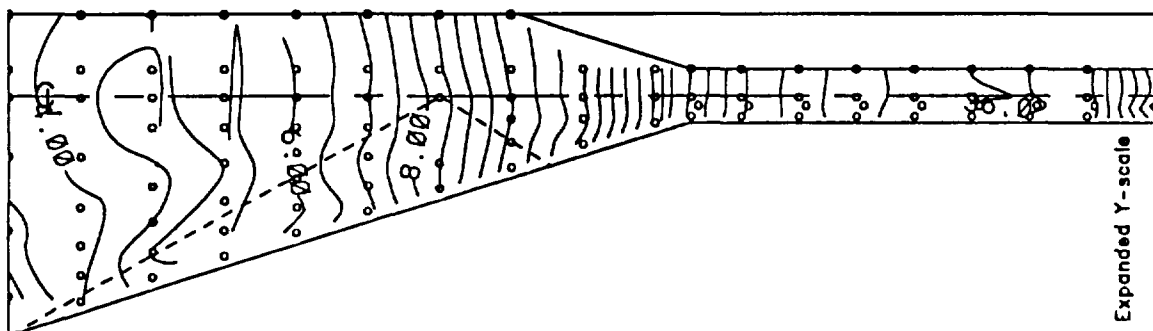


Figure 7.1.1.3(a): P/P<sub>inf</sub> Baseplate Contours, CR=9, Re=0.55 million/ft, 0% Cowl, (RUN47)

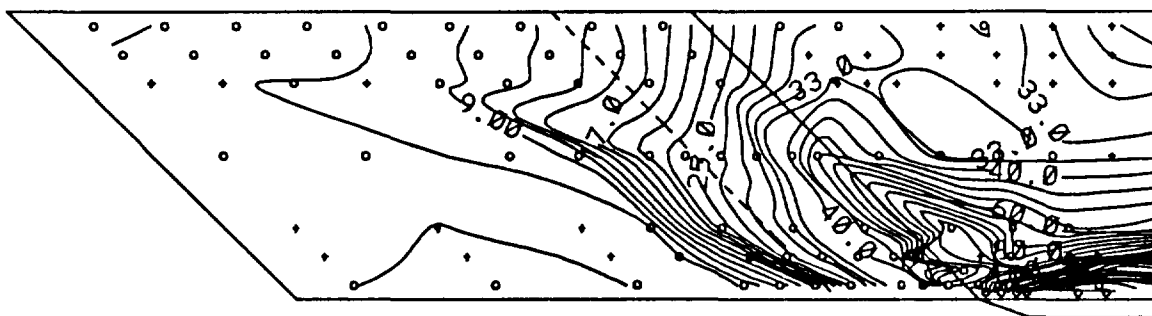
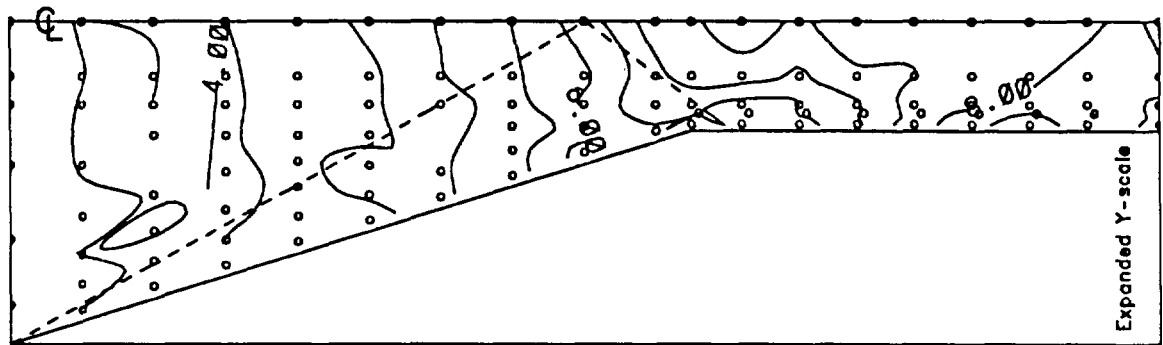


Figure 7.1.1.3(b): P/P<sub>inf</sub> Sidewall Contours, CR=9, Re=0.55 million/ft, 0% Cowl, (RUN47)



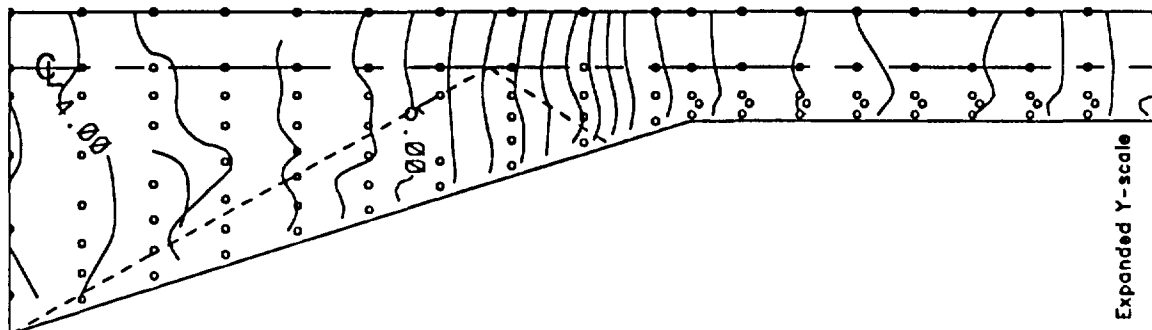


Figure 7.1.1.5(a): P/P<sub>inf</sub> Baseplate Contours, CR=5, Re=0.55 million/ft, 25% Cowl, (RUN41)

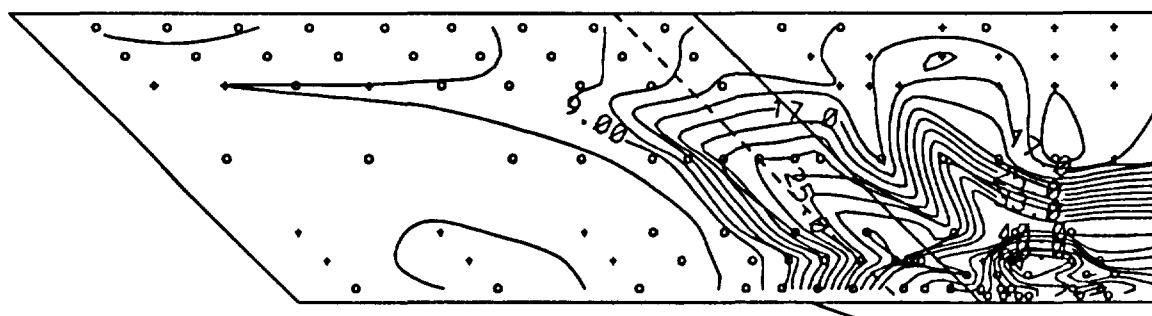


Figure 7.1.1.5(b): P/P<sub>inf</sub> Sidewall Contours, CR=5, Re=0.55 million/ft, 25% Cowl, (RUN41)

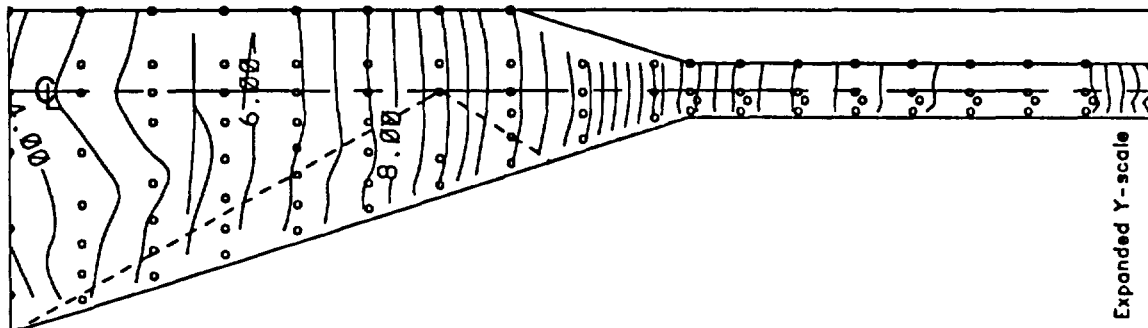


Figure 7.1.1.6(a): P/Plnf Baseplate Contours, CR=9, Re=0.55 million/ft, 25% Cowl, (RUN50)

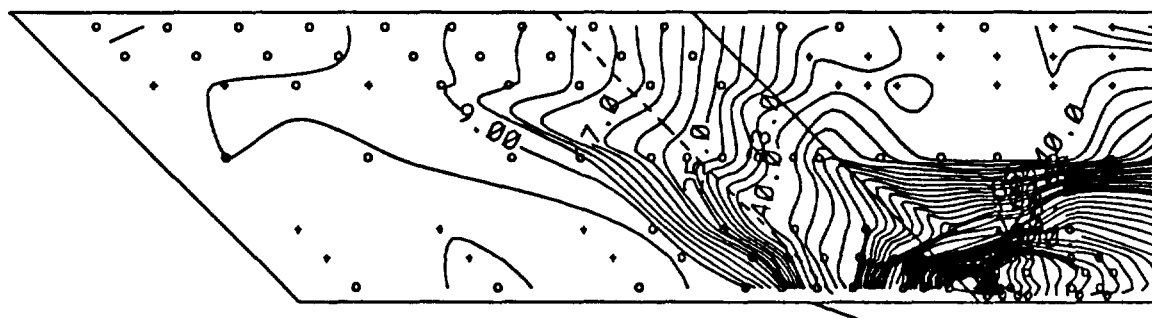


Figure 7.1.1.6(b): P/Plnf Sidewall Contours, CR=9, Re=0.55 million/ft, 25% Cowl, (RUN50)



Figure 7.1.1.7(a): P/P<sub>inf</sub> Baseplate Contours, CR=3, Re=0.55 million/ft, 50% Cowl, (RUN58)

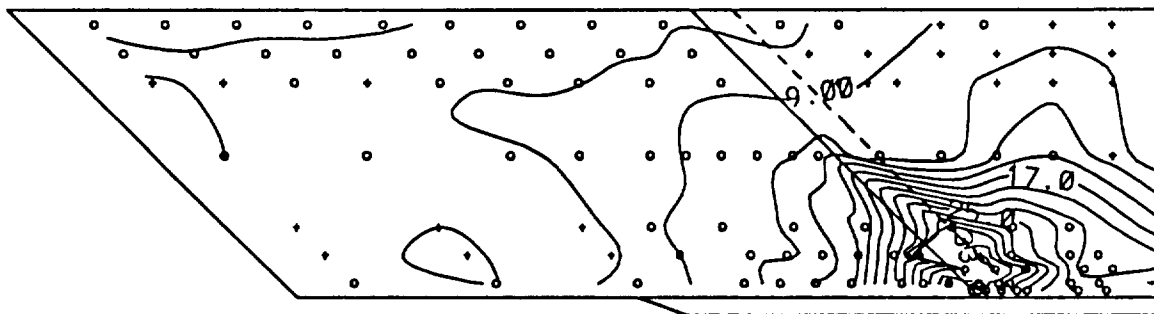


Figure 7.1.1.7(b): P/P<sub>inf</sub> Sidewall Contours, CR=3, Re=0.55 million/ft, 50% Cowl, (RUN58)

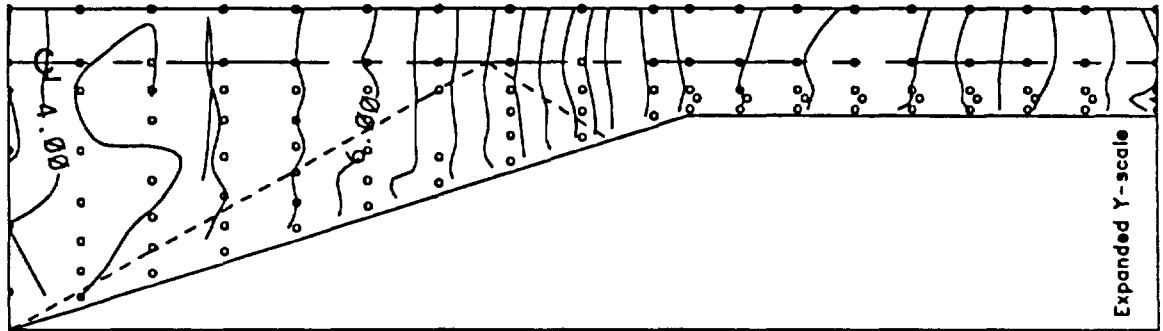


Figure 7.1.1.8(a): P/P<sub>inf</sub> Baseplate Contours, CR=5, Re=0.55 million/ft, 50% Cowl, (RUN37)

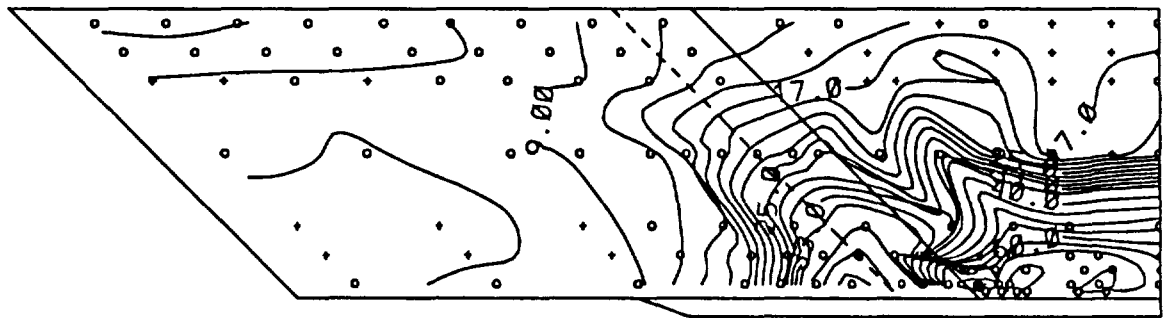


Figure 7.1.1.8(b): P/P<sub>inf</sub> Sidewall Contours, CR=5, Re=0.55 million/ft, 50% Cowl, (RUN37)



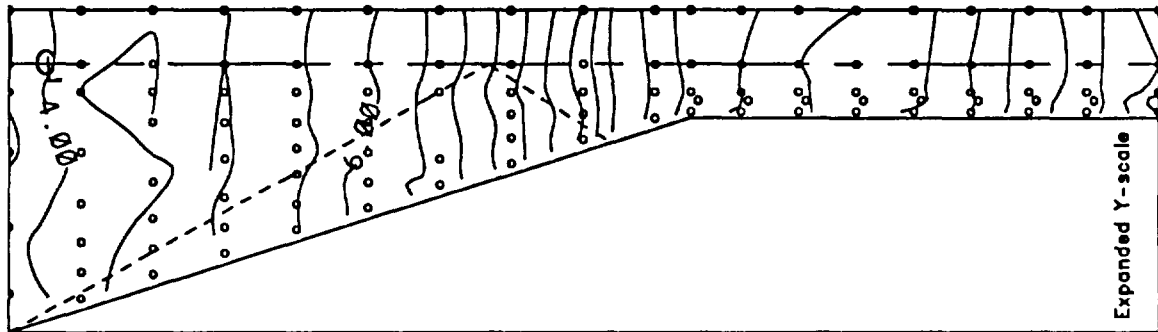


Figure 7.1.1.9(a): P/Pinf Baseplate Contours, CR=5, Re=0.55 million/ft, 50% Cowl, (RUN38)

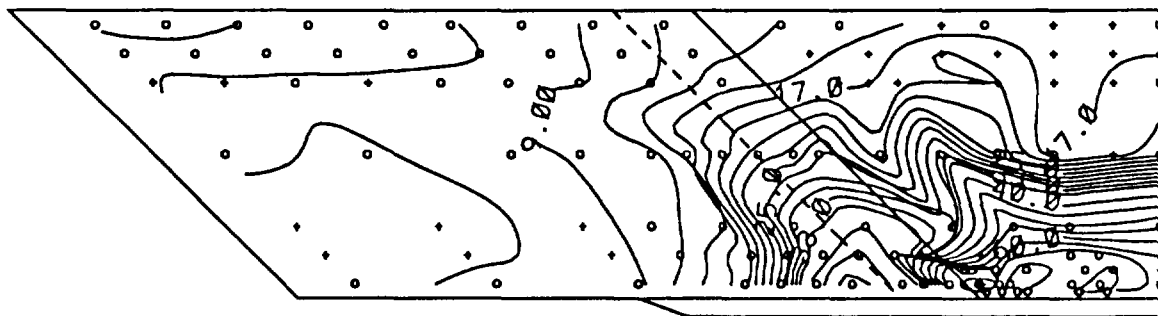


Figure 7.1.1.9(b): P/Pinf Sidewall Contours, CR=5, Re=0.55 million/ft, 50% Cowl, (RUN38)

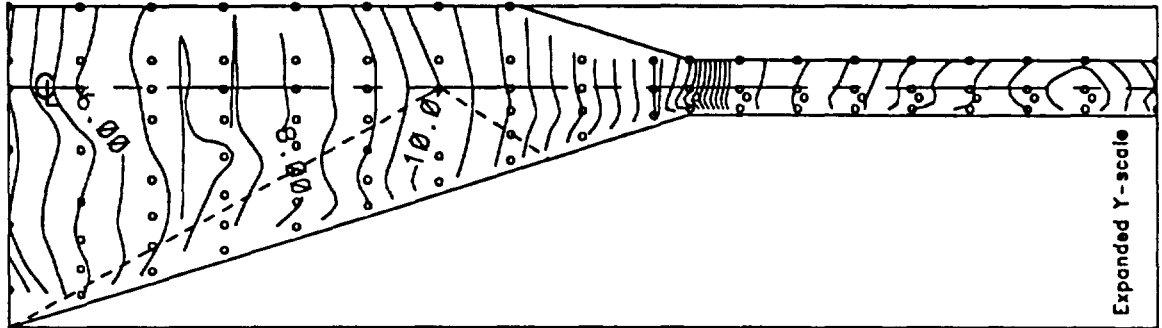


Figure 7.1.1.10(a): P/Plnf Baseplate Contours, CR=9, Re=0.55 million/ft, 50% Cowl, (RUN55)

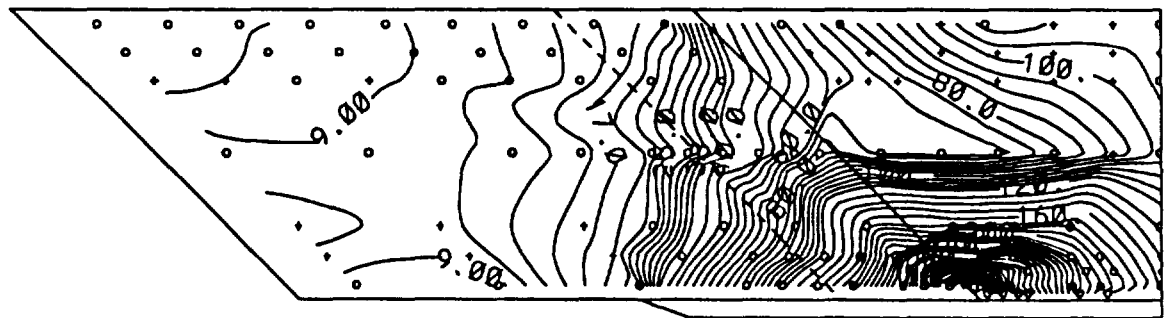


Figure 7.1.1.10(b): P/Plnf Sidewall Contours, CR=9, Re=0.55 million/ft, 50% Cowl, (RUN55)

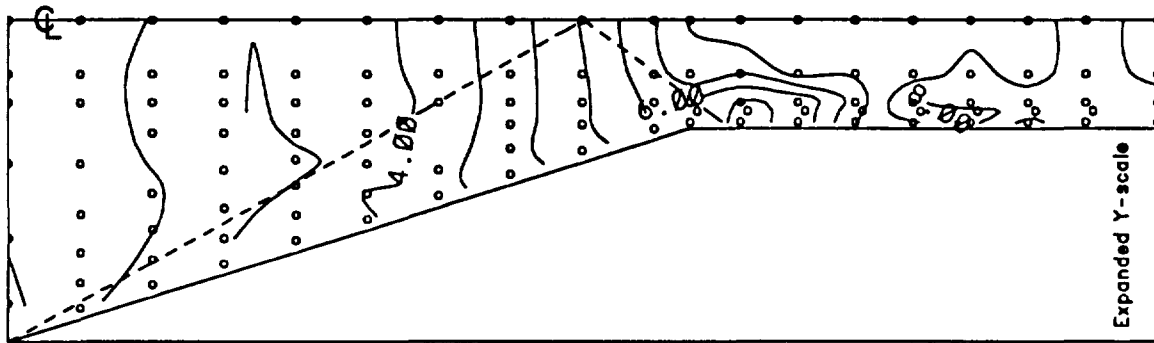


Figure 7.1.2.1(a): P/P<sub>inf</sub> Baseplate Contours, CR=3, Re=1.14 million/ft, 0% Cowl, (RUN65)

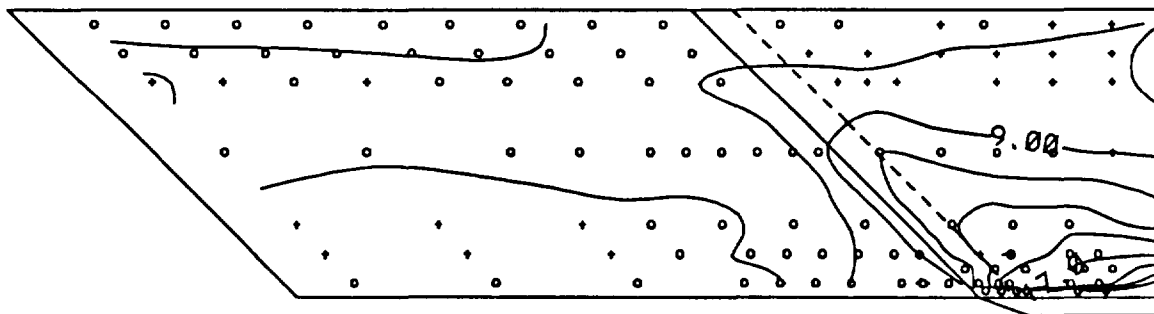


Figure 7.1.2.1(b): P/P<sub>inf</sub> Sidewall Contours, CR=3, Re=1.14 million/ft, 0% Cowl, (RUN65)

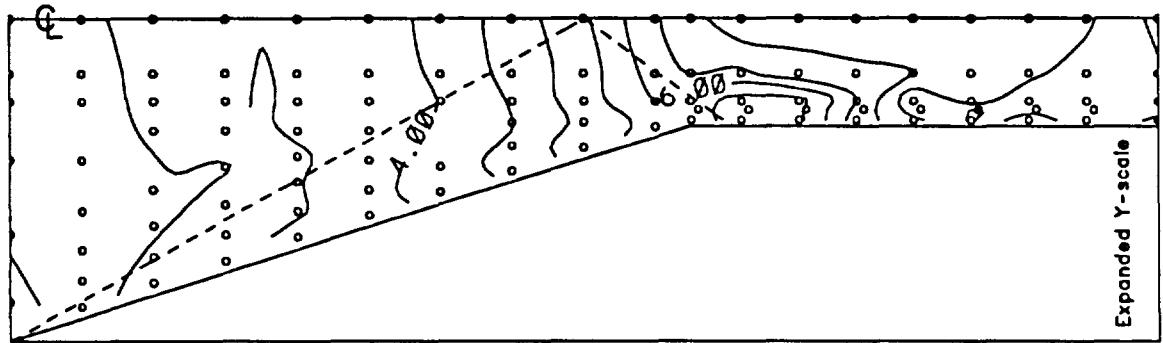


Figure 7.1.2.2(a): P/P<sub>inf</sub> Baseplate Contours, CR=3, Re=1.14 million/ft, 0% Cowl, (RUN67)

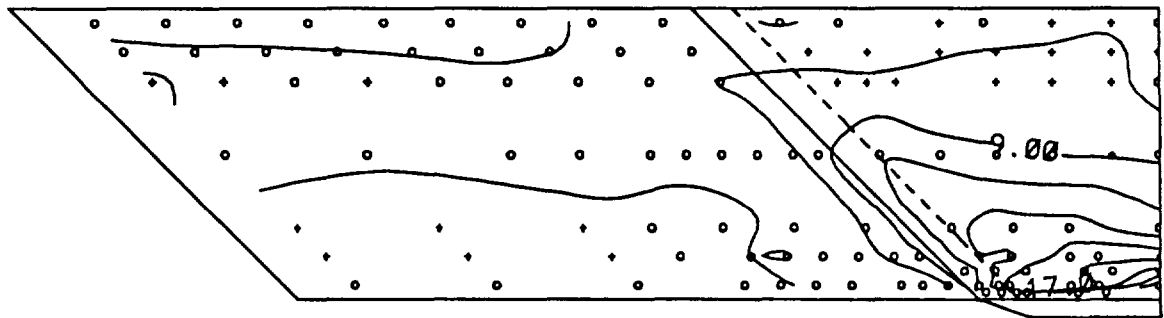


Figure 7.1.2.2(b): P/P<sub>inf</sub> Sidewall Contours, CR=3, Re=1.14 million/ft, 0% Cowl, (RUN67)

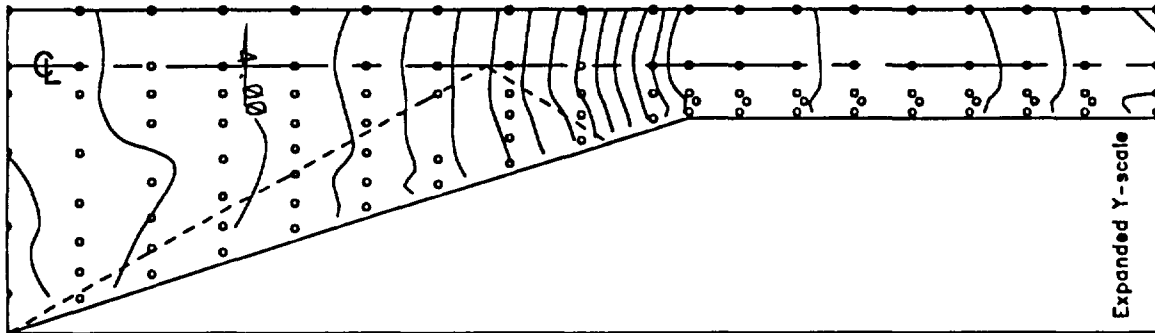


Figure 7.1.2.3(a): P/P<sub>inf</sub> Baseplate Contours, CR=5, Re=1.14 million/ft, 0% Cowl, (RUN45)

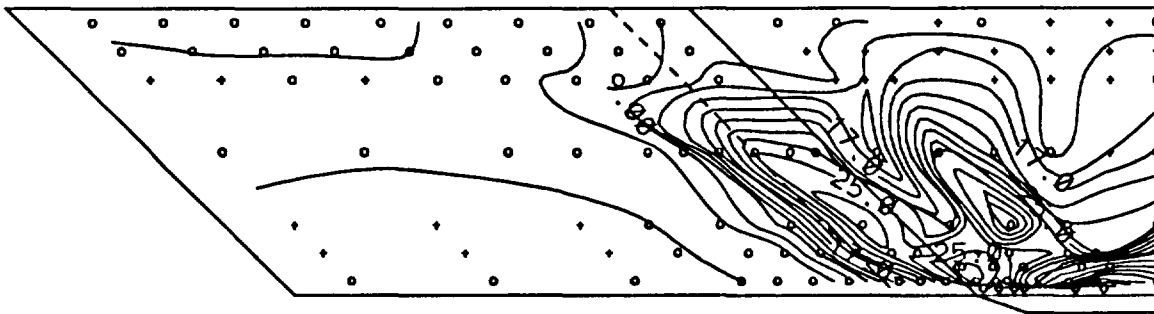


Figure 7.1.2.3(b): P/P<sub>inf</sub> Sidewall Contours, CR=5, Re=1.14 million/ft, 0% Cowl, (RUN45)

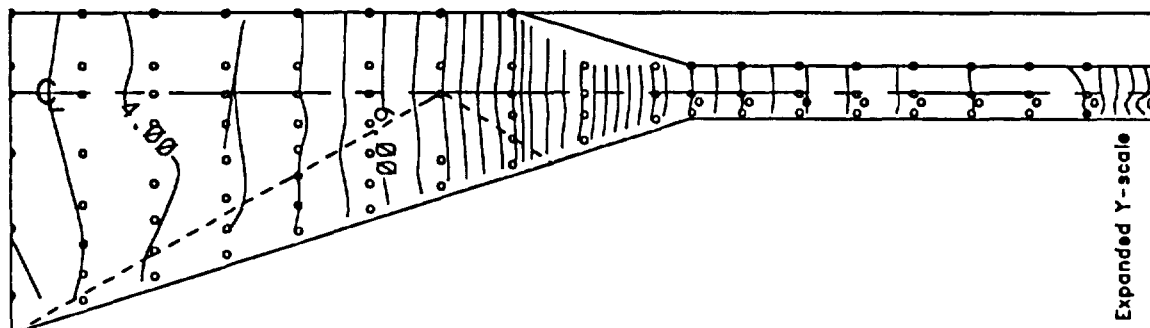


Figure 7.1.2.4(a): P/Pinf Baseplate Contours, CR=9, Re=1.14 million/ft, 0% Cowl, (RUN48)

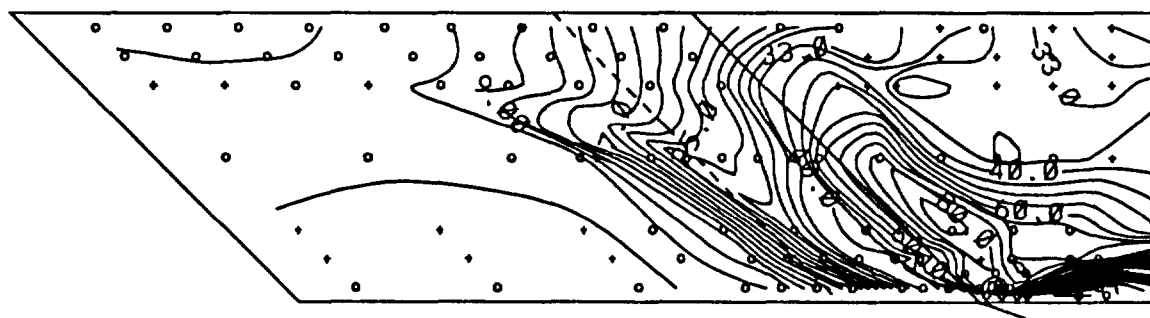


Figure 7.1.2.4(b): P/Pinf Sidewall Contours, CR=9, Re=1.14 million/ft, 0% Cowl, (RUN48)

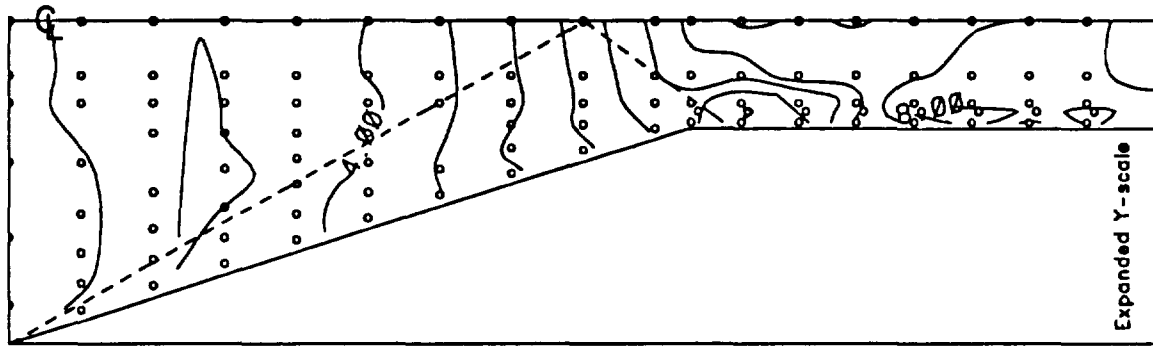


Figure 7.1.2.5(a): P/P<sub>inf</sub> Baseplate Contours, CR=3, Re=1.14 million/ft, 25% Cowl, (RUN63)

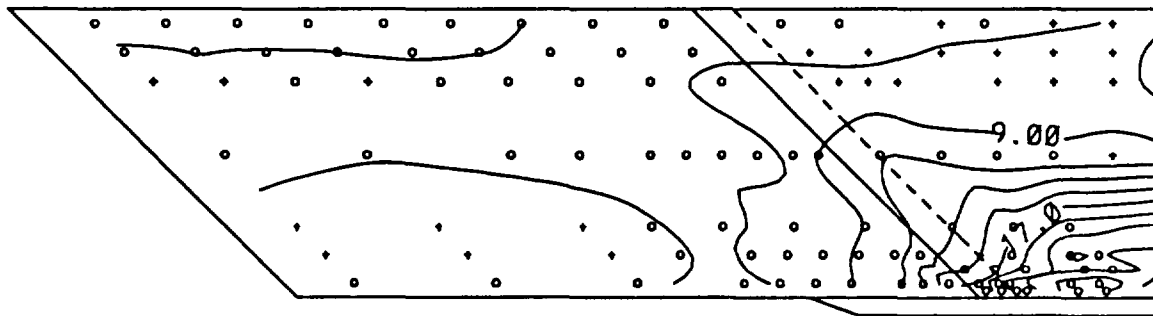


Figure 7.1.2.5(b): P/P<sub>inf</sub> Sidewall Contours, CR=3, Re=1.14 million/ft, 25% Cowl, (RUN63)

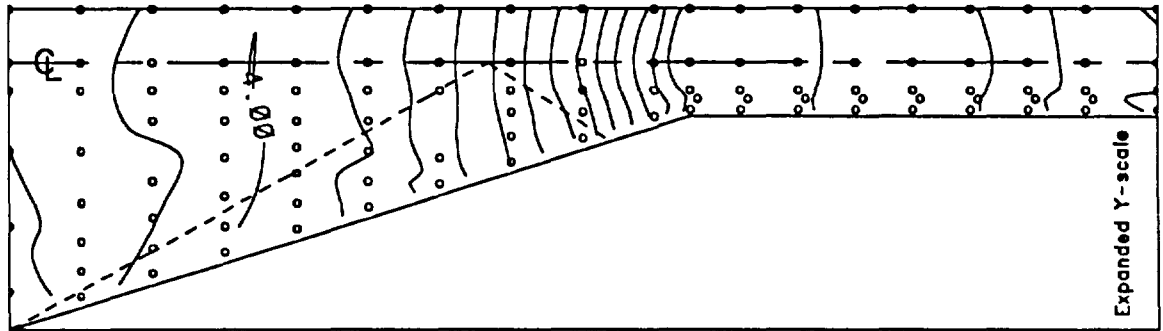


Figure 7.1.2.6(a): P/P<sub>inf</sub> Baseplate Contours, CR=5, Re=1.14 million/ft, 25% Cowl, (RUN42)

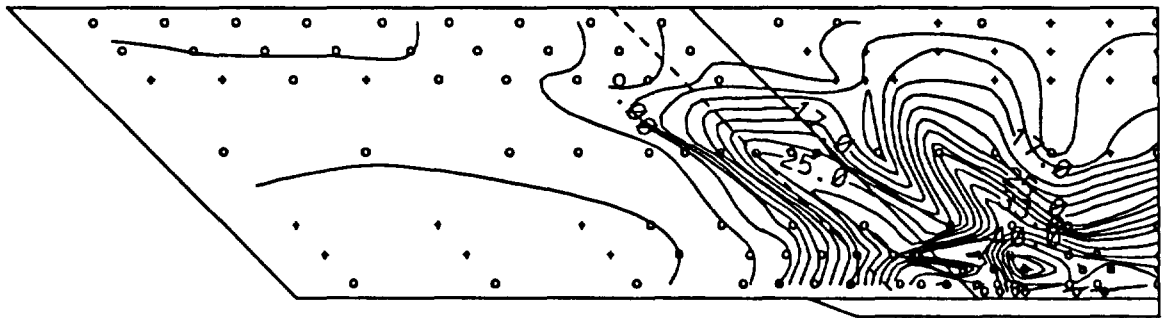


Figure 7.1.2.6(b): P/P<sub>inf</sub> Sidewall Contours, CR=5, Re=1.14 million/ft, 25% Cowl, (RUN42)



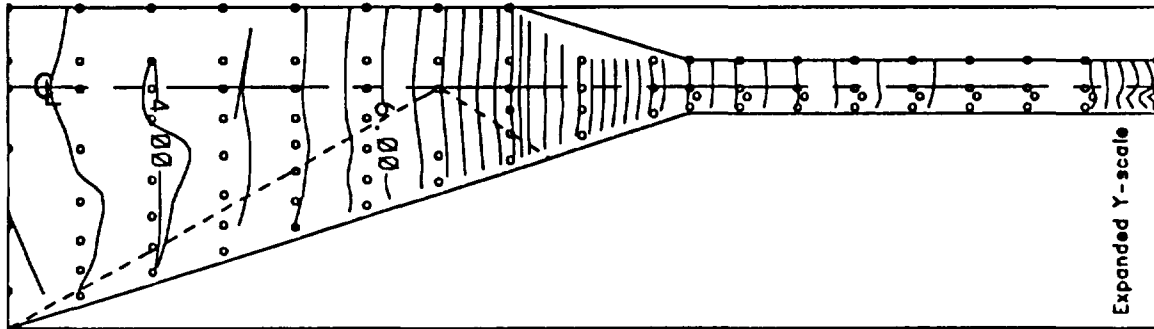


Figure 7.1.2.7(a): P/P<sub>inf</sub> Baseplate Contours, CR=9, Re=1.14 million/ft, 25% Cowl, (RUN52)

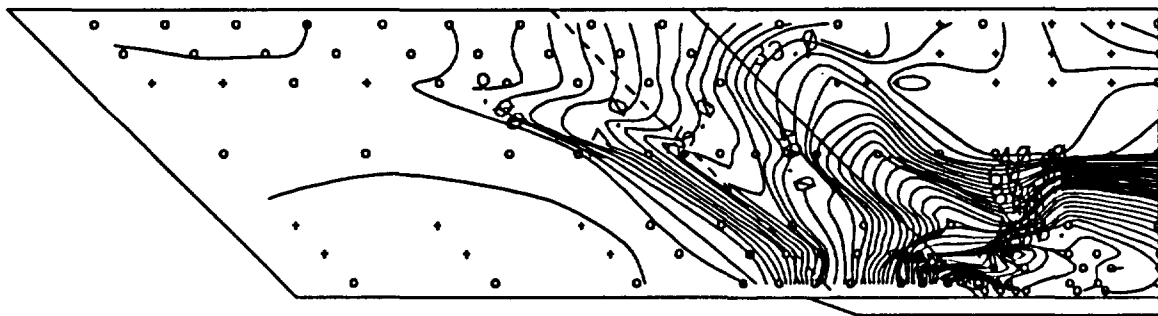


Figure 7.1.2.7(b): P/P<sub>inf</sub> Sidewall Contours, CR=9, Re=1.14 million/ft, 25% Cowl, (RUN52)

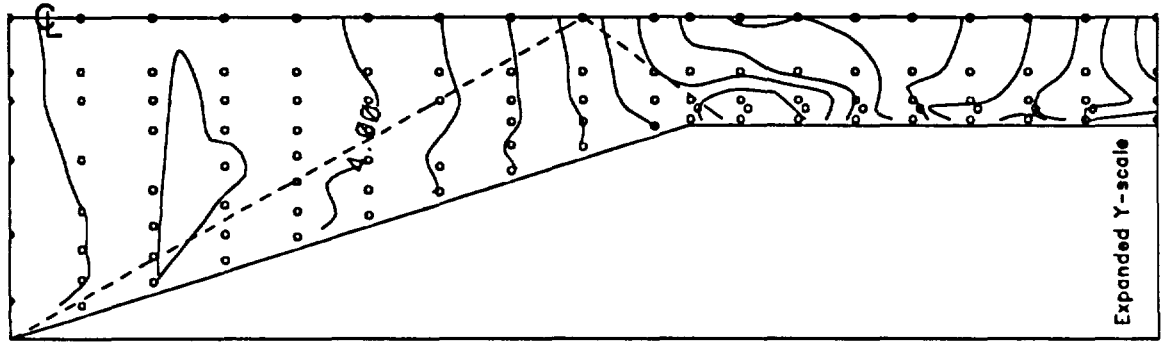


Figure 7.1.2.8(a): P/P<sub>inf</sub> Baseplate Contours, CR=3, Re=1.14 million/ft, 50% Cowl, (RUN59)

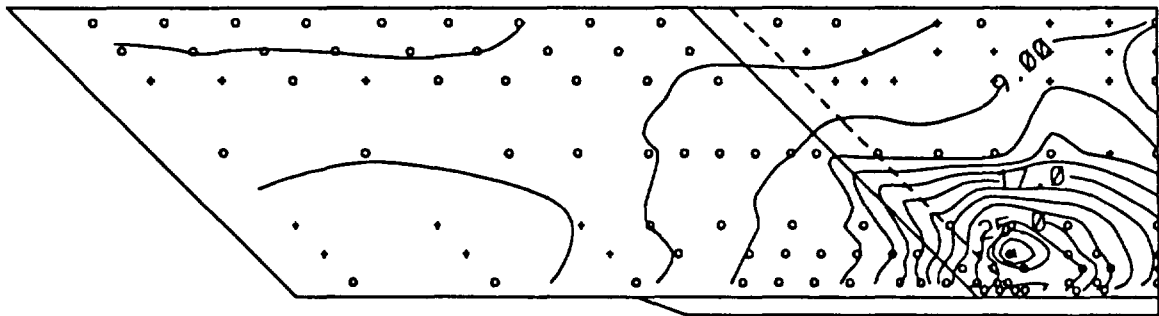


Figure 7.1.2.8(b): P/P<sub>inf</sub> Sidewall Contours, CR=3, Re=1.14 million/ft, 50% Cowl, (RUN59)

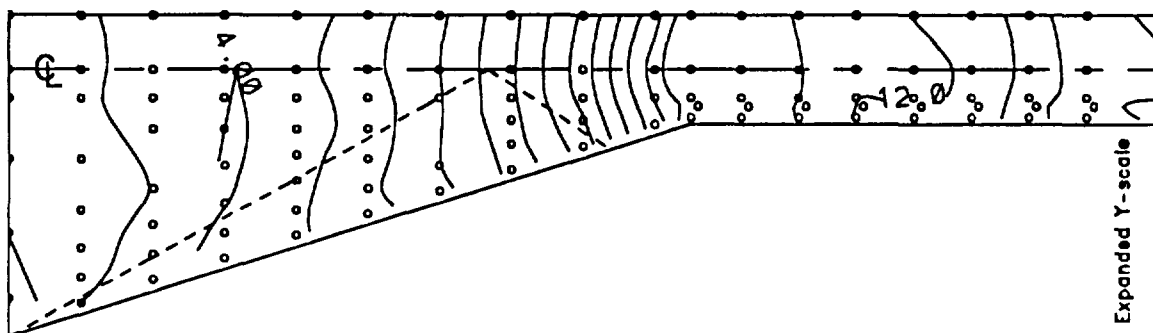


Figure 7.1.2.9(a): P/P<sub>inf</sub> Baseplate Contours, CR=5, Re=1.14 million/ft, 50% Cowl, (RUN39)

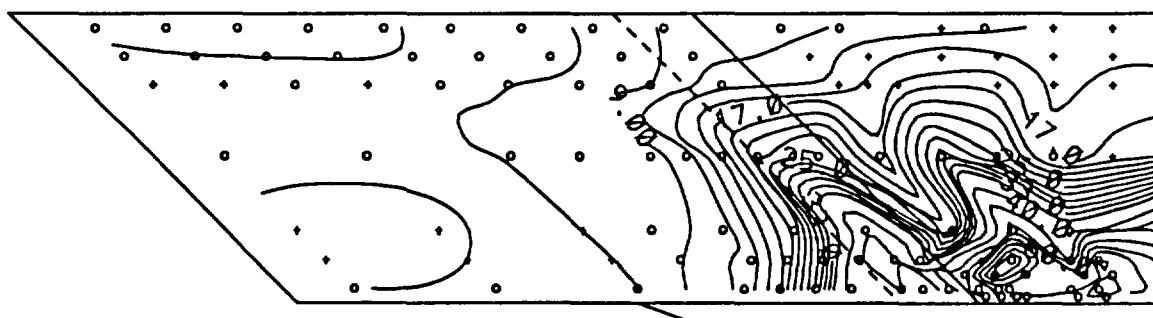


Figure 7.1.2.9(b): P/P<sub>inf</sub> Sidewall Contours, CR=5, Re=1.14 million/ft, 50% Cowl, (RUN39)

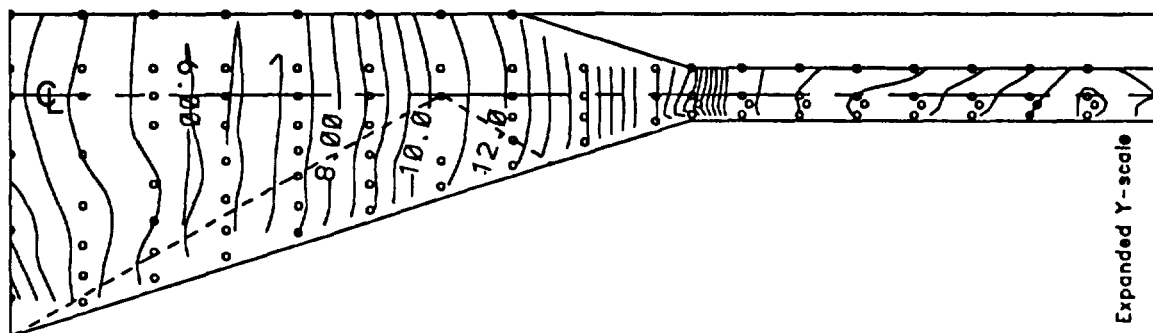


Figure 7.1.2.10(a): P/P<sub>inf</sub> Baseplate Contours, CR=9, Re=1.14 million/ft, 50% Cowl, (RUN56)

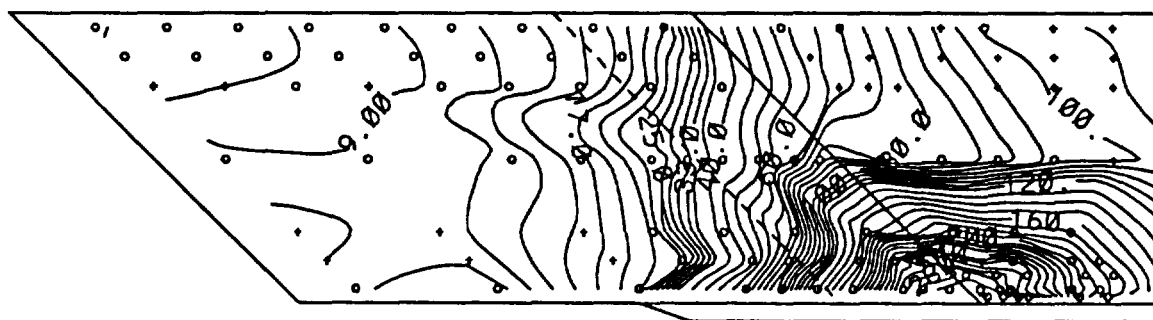


Figure 7.1.2.10(b): P/P<sub>inf</sub> Sidewall Contours, CR=9, Re=1.14 million/ft, 50% Cowl, (RUN56)

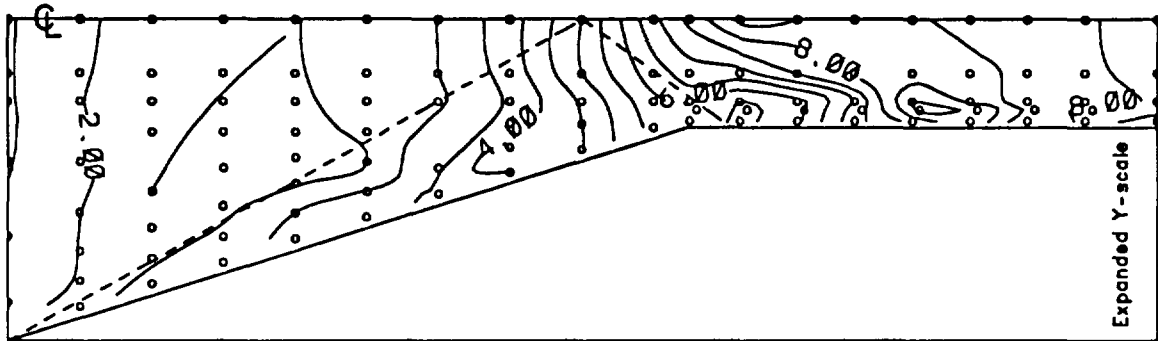


Figure 7.1.2.11(a): P/P<sub>inf</sub> Baseplate Contours, CR=3, Re=2.15 million/ft, 0% Cowl, (RUN66)

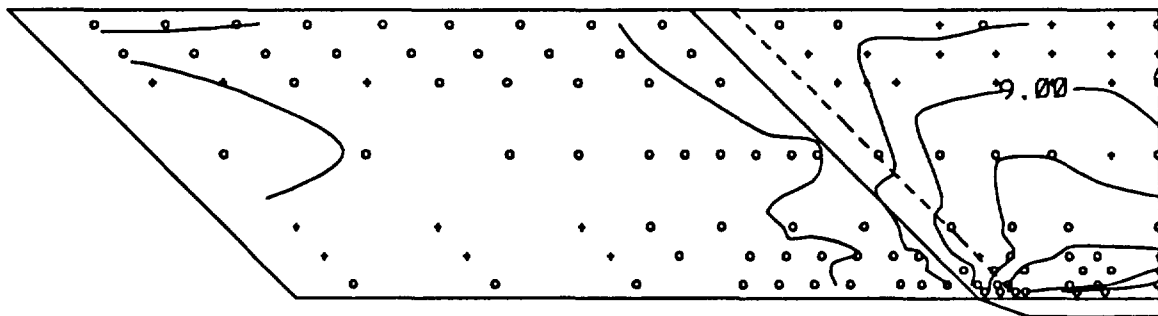


Figure 7.1.2.11(b): P/P<sub>inf</sub> Sidewall Contours, CR=3, Re=2.15 million/ft, 0% Cowl, (RUN66)

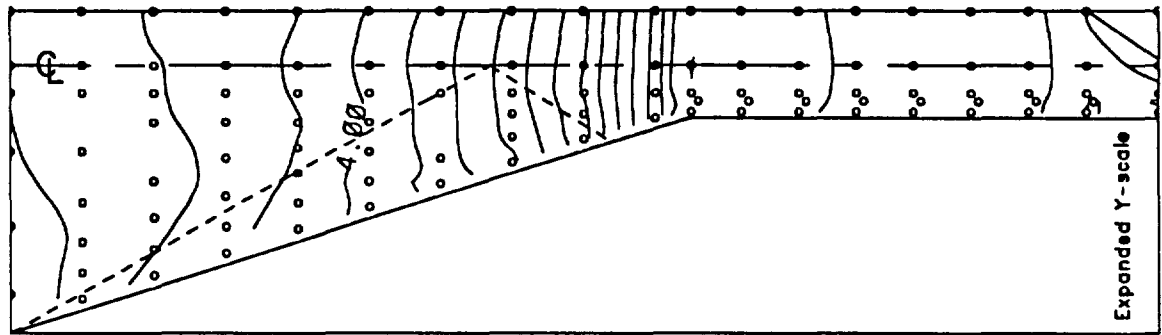


Figure 7.1.2.12(a): P/Plnf Baseplate Contours, CR=5, Re=2.15 million/ft, 0% Cowl, (RUN46)

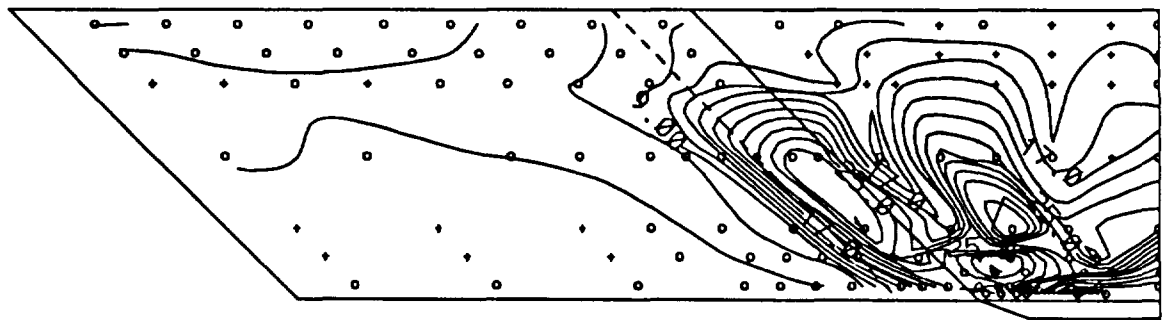


Figure 7.1.2.12(b): P/Plnf Sidewall Contours, CR=5, Re=2.15 million/ft, 0% Cowl, (RUN46)

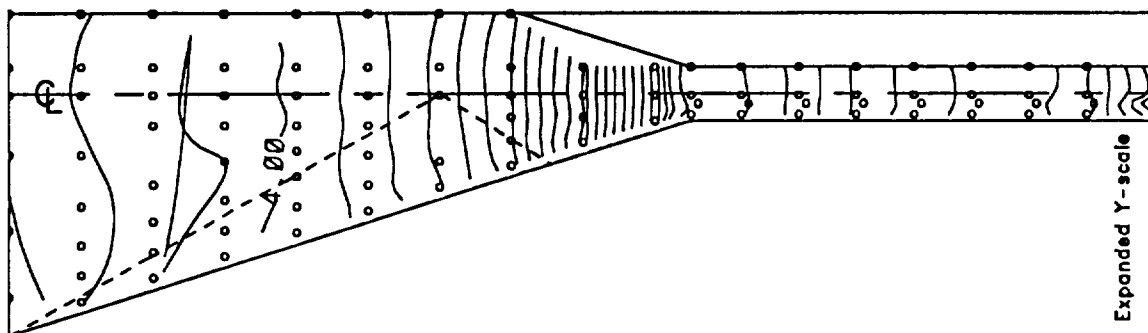


Figure 7.1.2.13(a): P/P<sub>inf</sub> Baseplate Contours, CR=9, Re=2.15 million/ft, 0% Cowl, (RUN49)

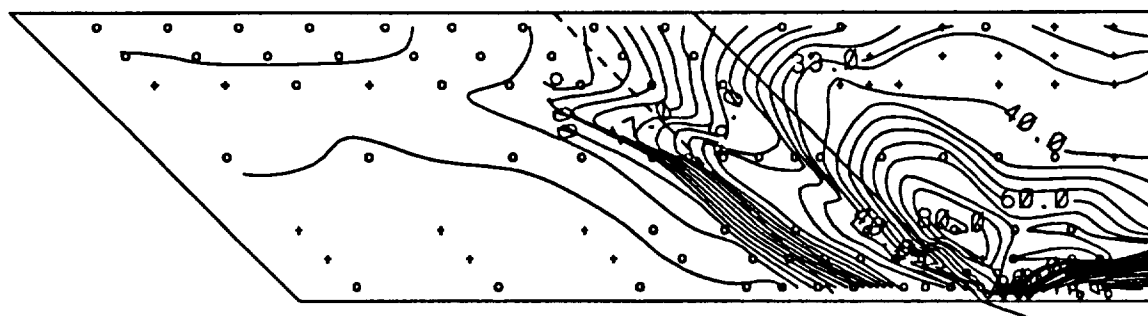


Figure 7.1.2.13(b): P/P<sub>inf</sub> Sidewall Contours, CR=9, Re=2.15 million/ft, 0% Cowl, (RUN49)



Figure 7.1.2.14(a): P/P<sub>inf</sub> Baseplate Contours, CR=3, Re=2.15 million/ft, 25% Cowl, (RUN62)

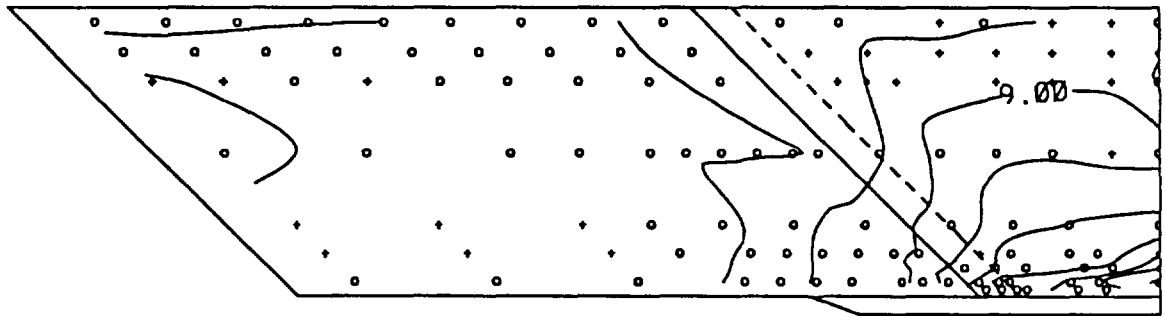


Figure 7.1.2.14(b): P/P<sub>inf</sub> Sidewall Contours, CR=3, Re=2.15 million/ft, 25% Cowl, (RUN62)



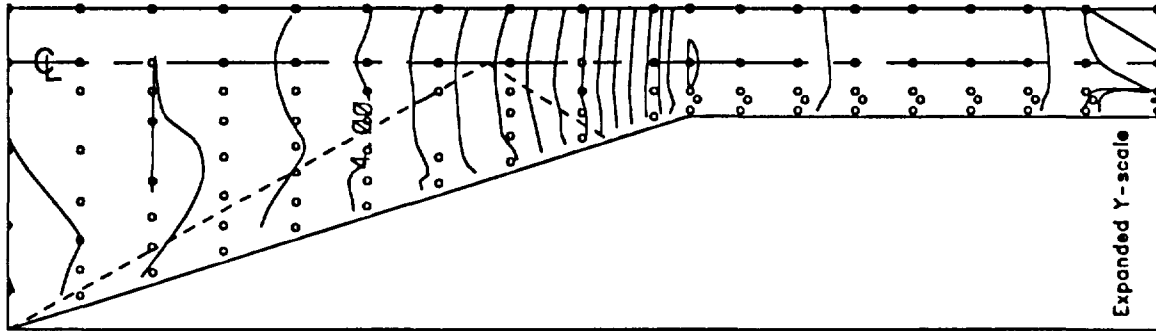


Figure 7.1.2.15(a): P/P<sub>inf</sub> Baseplate Contours, CR=5, Re=2.15 million/ft, 25% Cowl, (RUN43)

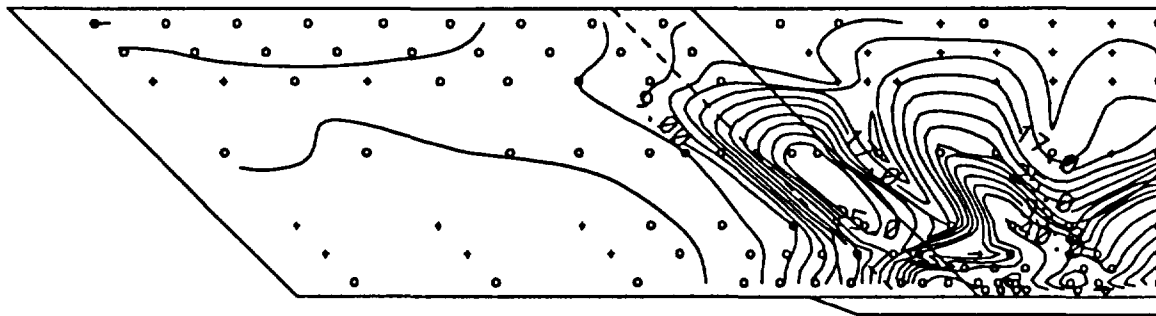


Figure 7.1.2.15(b): P/P<sub>inf</sub> Sidewall Contours, CR=5, Re=2.15 million/ft, 25% Cowl, (RUN43)

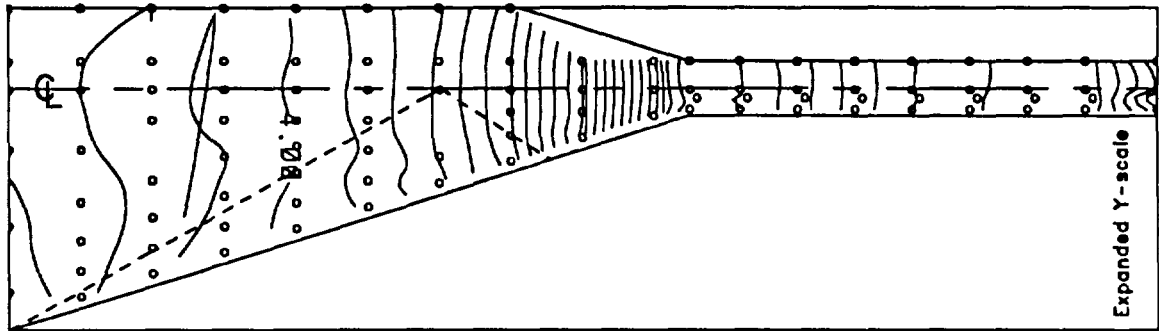


Figure 7.1.2.16(a): P/P<sub>inf</sub> Baseplate Contours, CR=9, Re=2.15 million/ft, 25% Cowl, (RUN53)

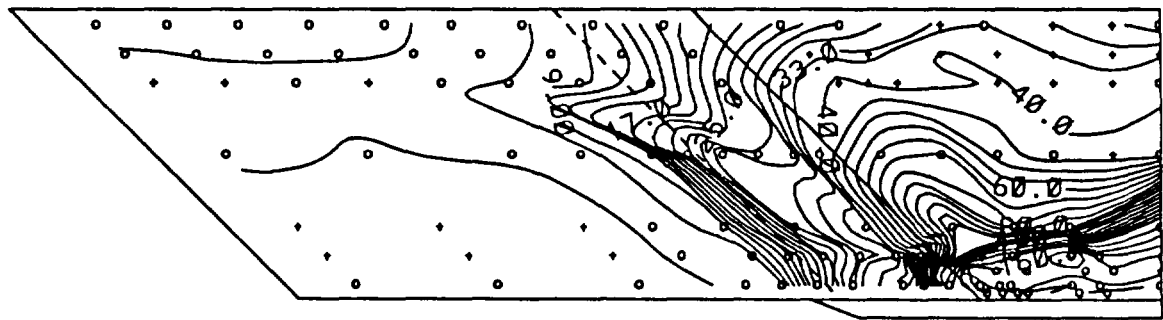


Figure 7.1.2.16(b): P/P<sub>inf</sub> Sidewall Contours, CR=9, Re=2.15 million/ft, 25% Cowl, (RUN53)

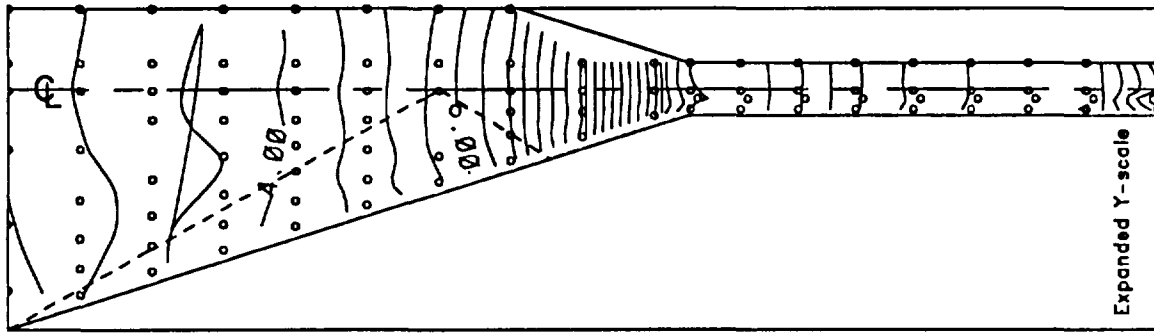


Figure 7.1.2.17(a): P/P<sub>inf</sub> Baseplate Contours, CR=9, Re=2.15 million/ft, 25% Cowl, (RUN54)

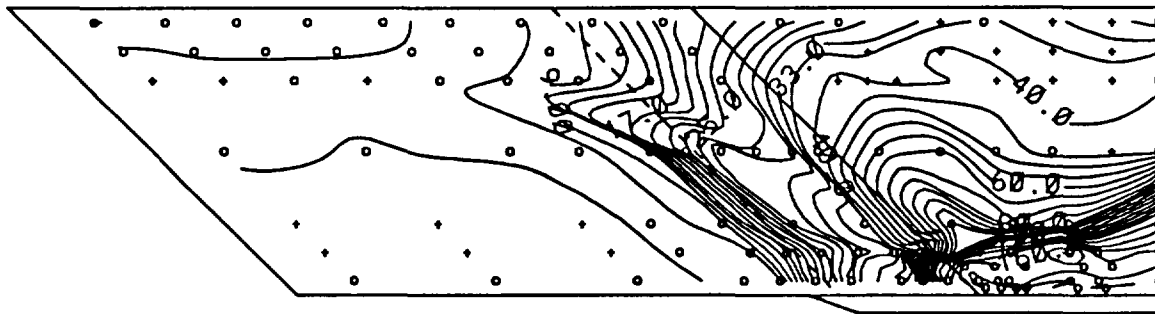


Figure 7.1.2.17(b): P/P<sub>inf</sub> Sidewall Contours, CR=9, Re=2.15 million/ft, 25% Cowl, (RUN54)

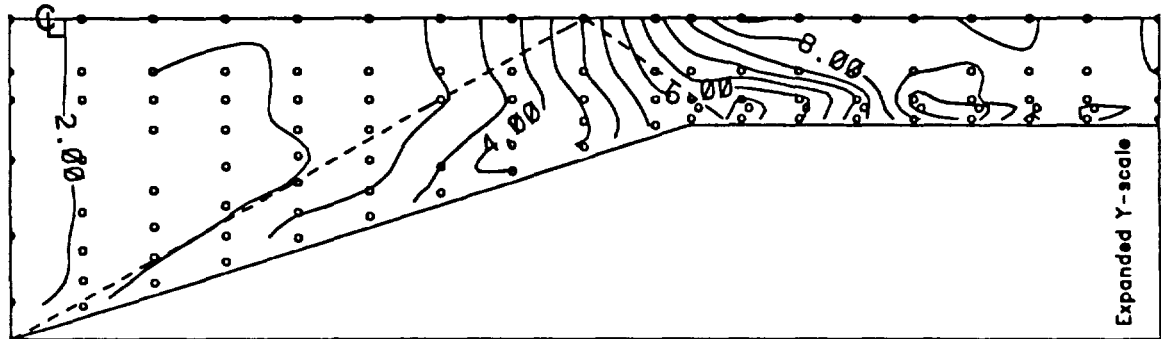


Figure 7.1.2.18(a): P/P<sub>inf</sub> Baseplate Contours, CR=3, Re=2.15 million/ft, 50% Cowl, (RUN60)

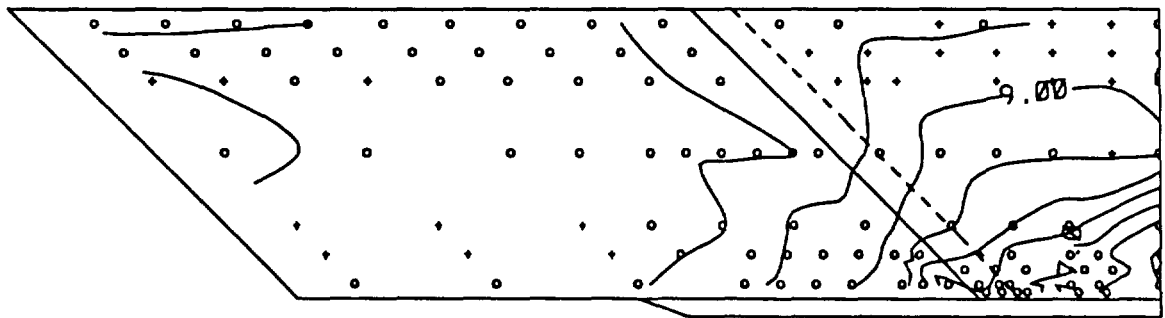


Figure 7.1.2.18(b): P/P<sub>inf</sub> Sidewall Contours, CR=3, Re=2.15 million/ft, 50% Cowl, (RUN60)

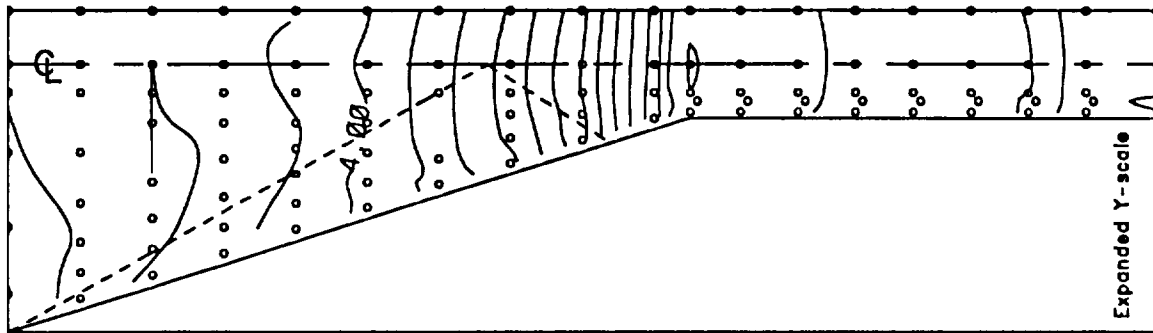


Figure 7.1.2.19(a): P/Pinf Baseplate Contours, CR=5, Re=2.15 million/ft, 50% Cowl, (RUN40)

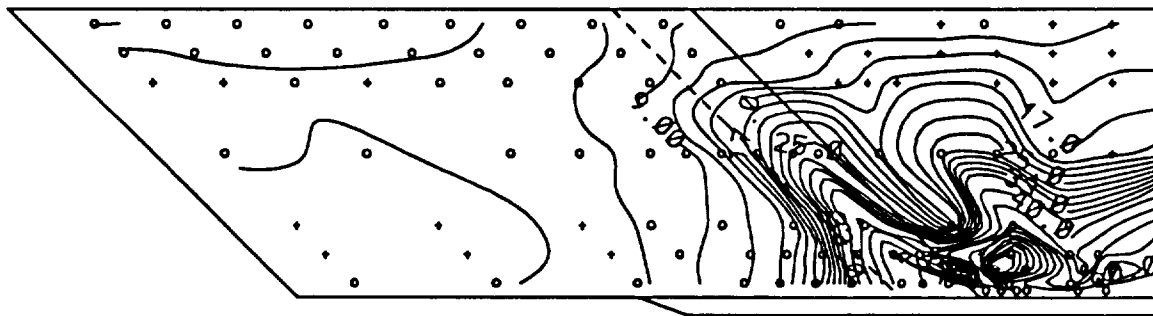


Figure 7.1.2.19(b): P/Pinf Sidewall Contours, CR=5, Re=2.15 million/ft, 50% Cowl, (RUN40)

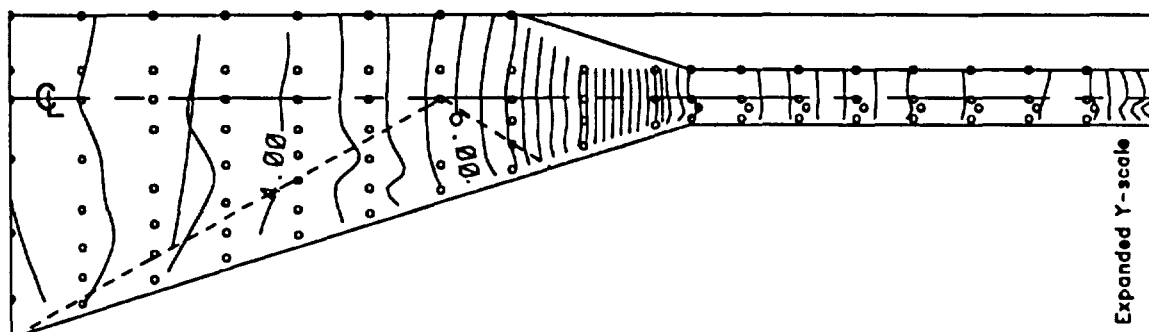


Figure 7.1.2.20(a): P/P<sub>inf</sub> Baseplate Contours, CR=9, Re=2.15 million/ft, 50% Cowl, (RUN57)

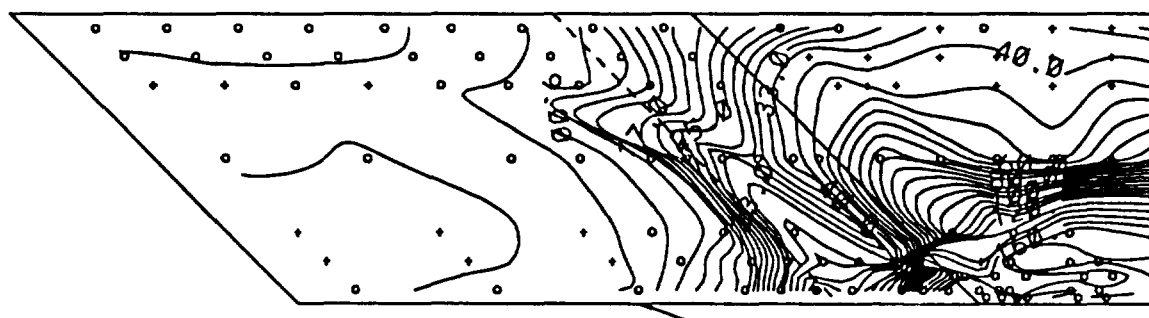
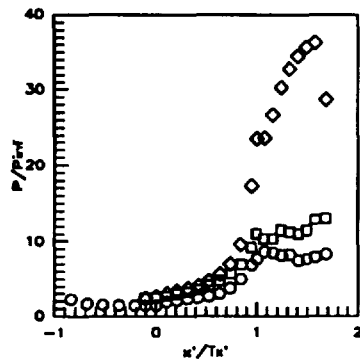
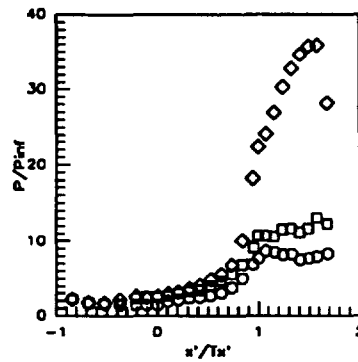


Figure 7.1.2.20(b): P/P<sub>inf</sub> Sidewall Contours, CR=9, Re=2.15 million/ft, 50% Cowl, (RUN57)



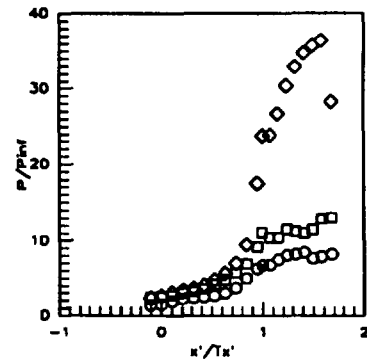
Sym	C.L. for	Run No.	CR/Re/CowI (millions)
○	CR=3	run66	3/2.15/ 0%
□	CR=5	run46	5/2.15/ 0%
◇	CR=9	run49	9/2.15/ 0%

Figure 7.2.1.1: CR Effects (Re=2.15million/ft, 0%CowI) Centerline Pressures



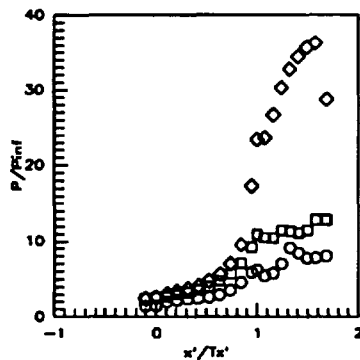
Sym	C.L. for	Run No.	CR/Re/CowI (millions)
○	CR=3	run66	3/2.15/ 0%
□	CR=3	run46	5/2.15/ 0%
◇	CR=3	run49	9/2.15/ 0%

Figure 7.2.1.2: CR Effects (Re=2.15million/ft, 0%CowI) CR=3 Centerline Pressures



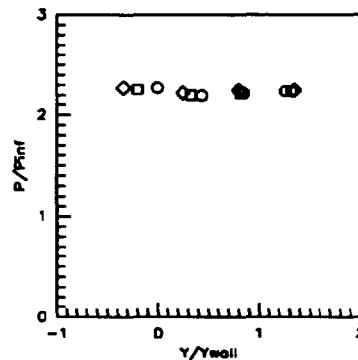
Sym	C.L. for	Run No.	CR/Re/CowI (millions)
○	CR=5	run66	3/2.15/ 0%
□	CR=5	run46	5/2.15/ 0%
◇	CR=5	run49	9/2.15/ 0%

Figure 7.2.1.3: CR Effects (Re=2.15million/ft, 0%CowI) CR=5 Centerline Pressures



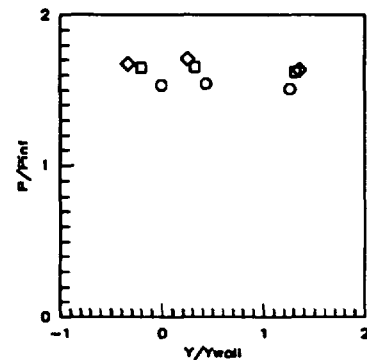
Sym	C.L. for	Run No.	CR/Re/CowI (millions)
○	CR=9	run66	3/2.15/ 0%
□	CR=9	run46	5/2.15/ 0%
◇	CR=9	run49	9/2.15/ 0%

Figure 7.2.1.4: CR Effects (Re=2.15million/ft, 0%CowI) CR=9 Centerline Pressures



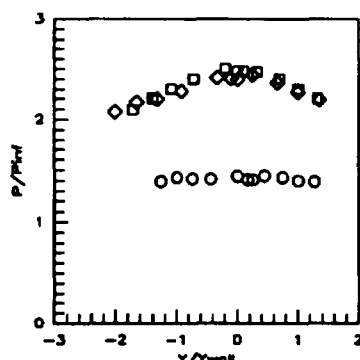
Sym	x'/Tx'	Run No.	CR/Re/CowI (millions)
○	-0.8412	run66	3/2.15/ 0%
□	-0.8412	run46	5/2.15/ 0%
◇	-0.8412	run49	9/2.15/ 0%

Figure 7.2.1.5: CR Effects (Re=2.15million/ft, 0%CowI) Baseplate Pressures



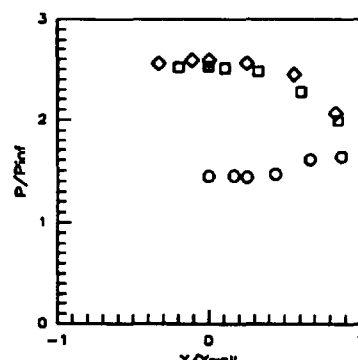
Sym	x'/Tx'	Run No.	CR/Re/CowI (millions)
○	-0.3258	run66	3/2.15/ 0%
□	-0.3258	run46	5/2.15/ 0%
◇	-0.3258	run49	9/2.15/ 0%

Figure 7.2.1.6: CR Effects (Re=2.15million/ft, 0%CowI) Baseplate Pressures



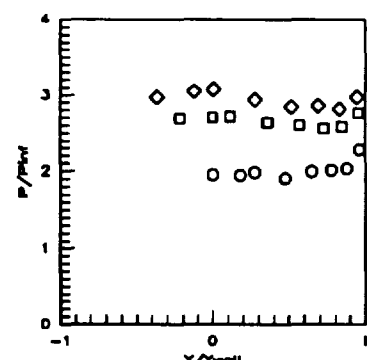
Sym	x'/Tx'	Run No.	CR/Re/CowI (millions)
○	-0.1052	run66	3/2.15/ 0%
□	-0.1052	run46	5/2.15/ 0%
◇	-0.1052	run49	9/2.15/ 0%

Figure 7.2.1.7: CR Effects (Re=2.15million/ft, 0%CowI) Baseplate Pressures



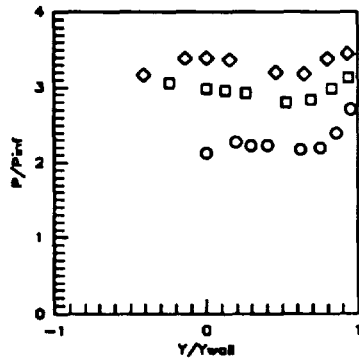
Sym	x'/Tx'	Run No.	CR/Re/CowI (millions)
○	0.0000	run66	3/2.15/ 0%
□	0.0000	run46	5/2.15/ 0%
◇	0.0000	run49	9/2.15/ 0%

Figure 7.2.1.8: CR Effects (Re=2.15million/ft, 0%CowI) Baseplate Pressures



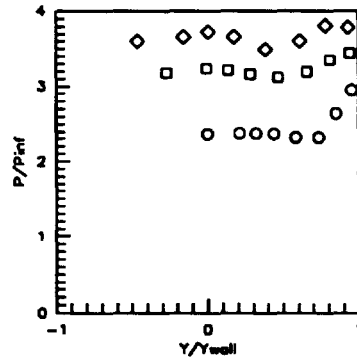
Sym	x'/Tx'	Run No.	CR/Re/CowI (millions)
○	0.1052	run66	3/2.15/ 0%
□	0.1052	run46	5/2.15/ 0%
◇	0.1052	run49	9/2.15/ 0%

Figure 7.2.1.9: CR Effects (Re=2.15million/ft, 0%CowI) Baseplate Pressures



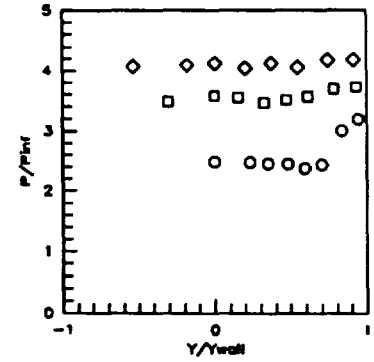
Sym	$x'/T_x'$	Run No.	CR/Re/Cowl (millions)
○	0.2103	run66	3/2.15/ 0%
□	0.2103	run46	5/2.15/ 0%
◇	0.2103	run49	9/2.15/ 0%

Figure 7.2.1.10: CR Effects  
( $Re=2.15$ million/ft, 0%CowI)  
Baseplate Pressures



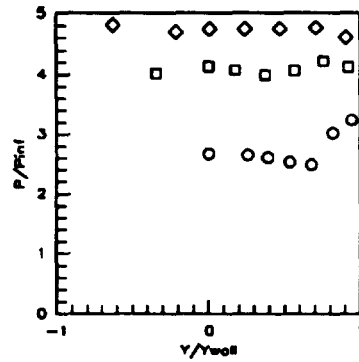
Sym	$x'/T_x'$	Run No.	CR/Re/Cowl (millions)
○	0.3154	run66	3/2.15/ 0%
□	0.3154	run46	5/2.15/ 0%
◇	0.3154	run49	9/2.15/ 0%

Figure 7.2.1.11: CR Effects  
( $Re=2.15$ million/ft, 0%CowI)  
Baseplate Pressures



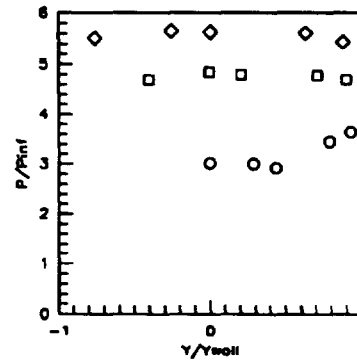
Sym	$x'/T_x'$	Run No.	CR/Re/Cowl (millions)
○	0.4206	run66	3/2.15/ 0%
□	0.4206	run46	5/2.15/ 0%
◇	0.4206	run49	9/2.15/ 0%

Figure 7.2.1.12: CR Effects  
( $Re=2.15$ million/ft, 0%CowI)  
Baseplate Pressures



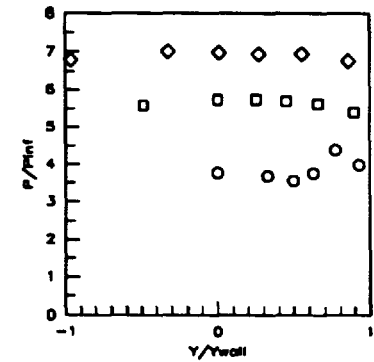
Sym	$x'/T_x'$	Run No.	CR/Re/Cowl (millions)
○	0.5258	run66	3/2.15/ 0%
□	0.5258	run46	5/2.15/ 0%
◇	0.5258	run49	9/2.15/ 0%

Figure 7.2.1.13: CR Effects  
( $Re=2.15$ million/ft, 0%CowI)  
Baseplate Pressures



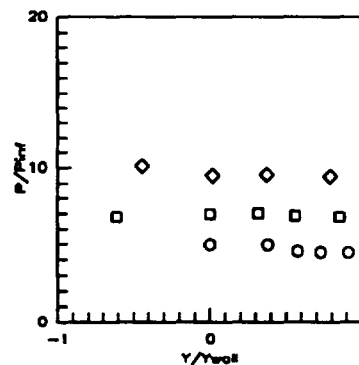
Sym	$x'/T_x'$	Run No.	CR/Re/Cowl (millions)
○	0.6309	run66	3/2.15/ 0%
□	0.6309	run46	5/2.15/ 0%
◇	0.6309	run49	9/2.15/ 0%

Figure 7.2.1.14: CR Effects  
( $Re=2.15$ million/ft, 0%CowI)  
Baseplate Pressures



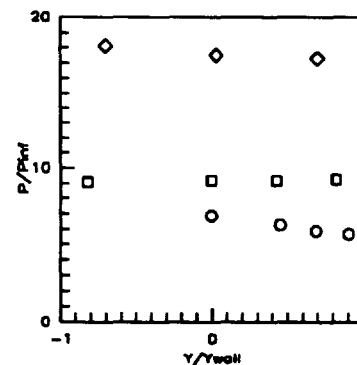
Sym	$x'/T_x'$	Run No.	CR/Re/Cowl (millions)
○	0.7361	run66	3/2.15/ 0%
□	0.7361	run46	5/2.15/ 0%
◇	0.7361	run49	9/2.15/ 0%

Figure 7.2.1.15: CR Effects  
( $Re=2.15$ million/ft, 0%CowI)  
Baseplate Pressures



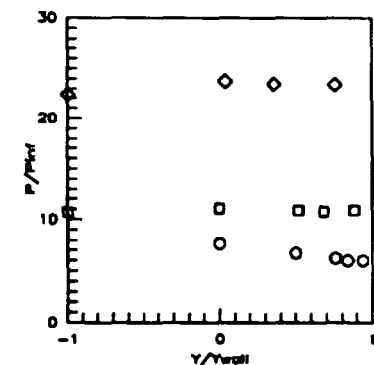
Sym	$x'/T_x'$	Run No.	CR/Re/Cowl (millions)
○	0.8412	run66	3/2.15/ 0%
□	0.8412	run46	5/2.15/ 0%
◇	0.8412	run49	9/2.15/ 0%

Figure 7.2.1.16: CR Effects  
( $Re=2.15$ million/ft, 0%CowI)  
Baseplate Pressures



Sym	$x'/T_x'$	Run No.	CR/Re/Cowl (millions)
○	0.9464	run66	3/2.15/ 0%
□	0.9464	run46	5/2.15/ 0%
◇	0.9464	run49	9/2.15/ 0%

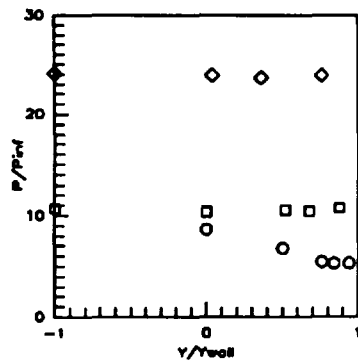
Figure 7.2.1.17: CR Effects  
( $Re=2.15$ million/ft, 0%CowI)  
Baseplate Pressures



Sym	$x'/T_x'$	Run No.	CR/Re/Cowl (millions)
○	1.0000	run66	3/2.15/ 0%
□	1.0000	run46	5/2.15/ 0%
◇	1.0000	run49	9/2.15/ 0%

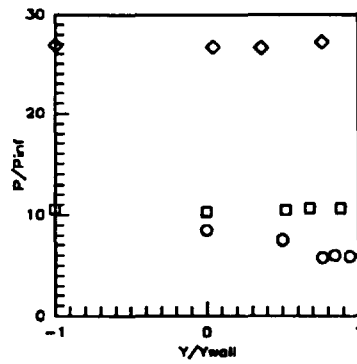
Figure 7.2.1.18: CR Effects  
( $Re=2.15$ million/ft, 0%CowI)  
Baseplate Pressures





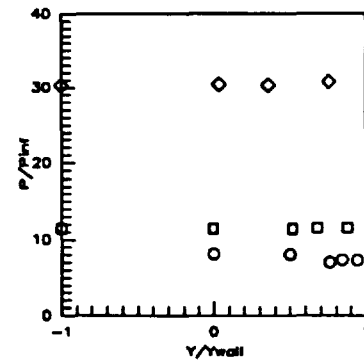
Sym	$x'/T_x'$	Run No.	CR/Re/CowI (millions)
o	1.0726	run86	3/2.15/ 0%
□	1.0726	run46	5/2.15/ 0%
○	1.0726	run49	9/2.15/ 0%

Figure 7.2.1.19: CR Effects (Re=2.15million/ft, 0%CowI) Baseplate Pressures



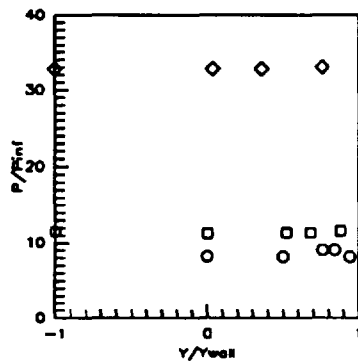
Sym	$x'/T_x'$	Run No.	CR/Re/CowI (millions)
o	1.1567	run86	3/2.15/ 0%
□	1.1567	run46	5/2.15/ 0%
○	1.1567	run49	9/2.15/ 0%

Figure 7.2.1.20: CR Effects (Re=2.15million/ft, 0%CowI) Baseplate Pressures



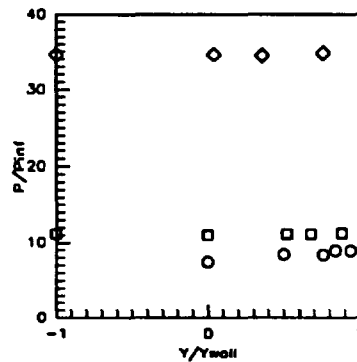
Sym	$x'/T_x'$	Run No.	CR/Re/CowI (millions)
o	1.2408	run86	3/2.15/ 0%
□	1.2408	run46	5/2.15/ 0%
○	1.2408	run49	9/2.15/ 0%

Figure 7.2.1.21: CR Effects (Re=2.15million/ft, 0%CowI) Baseplate Pressures



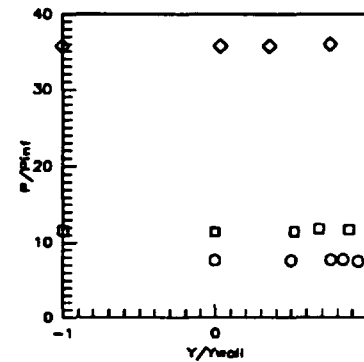
Sym	$x'/T_x'$	Run No.	CR/Re/CowI (millions)
o	1.3249	run86	3/2.15/ 0%
□	1.3249	run46	5/2.15/ 0%
○	1.3249	run49	9/2.15/ 0%

Figure 7.2.1.22: CR Effects (Re=2.15million/ft, 0%CowI) Baseplate Pressures



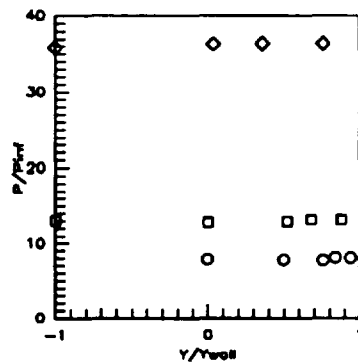
Sym	$x'/T_x'$	Run No.	CR/Re/CowI (millions)
o	1.4090	run86	3/2.15/ 0%
□	1.4090	run46	5/2.15/ 0%
○	1.4090	run49	9/2.15/ 0%

Figure 7.2.1.23: CR Effects (Re=2.15million/ft, 0%CowI) Baseplate Pressures



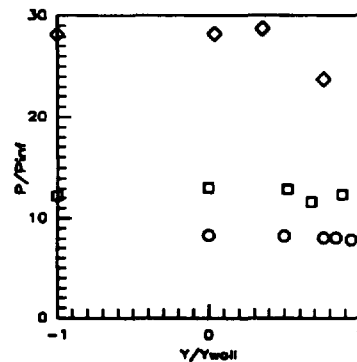
Sym	$x'/T_x'$	Run No.	CR/Re/CowI (millions)
o	1.4932	run86	3/2.15/ 0%
□	1.4932	run46	5/2.15/ 0%
○	1.4932	run49	9/2.15/ 0%

Figure 7.2.1.24: CR Effects (Re=2.15million/ft, 0%CowI) Baseplate Pressures



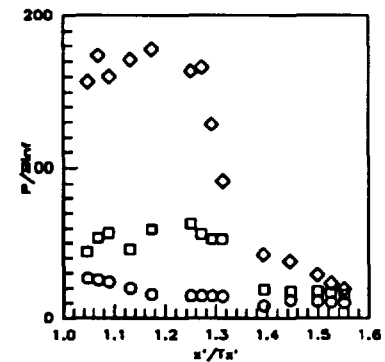
Sym	$x'/T_x'$	Run No.	CR/Re/CowI (millions)
o	1.5773	run86	3/2.15/ 0%
□	1.5773	run46	5/2.15/ 0%
○	1.5773	run49	9/2.15/ 0%

Figure 7.2.1.25: CR Effects (Re=2.15million/ft, 0%CowI) Baseplate Pressures



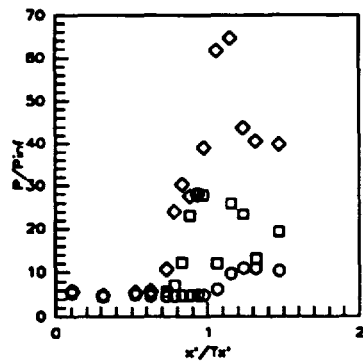
Sym	$x'/T_x'$	Run No.	CR/Re/CowI (millions)
o	1.6824	run86	3/2.15/ 0%
□	1.6824	run46	5/2.15/ 0%
○	1.6824	run49	9/2.15/ 0%

Figure 7.2.1.26: CR Effects (Re=2.15million/ft, 0%CowI) Baseplate Pressures



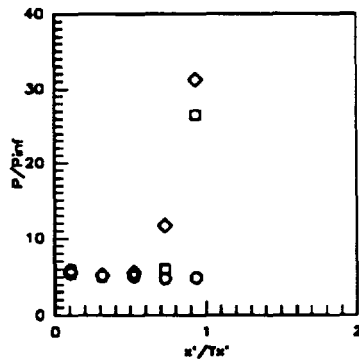
Sym	CowI Pos.	Run No.	CR/Re/CowI (millions)
o	0%	run86	3/2.15/ 0%
□	0%	run46	5/2.15/ 0%
○	0%	run49	9/2.15/ 0%

Figure 7.2.1.27: CR Effects (Re=2.15million/ft, 0%CowI) CowI Pressures



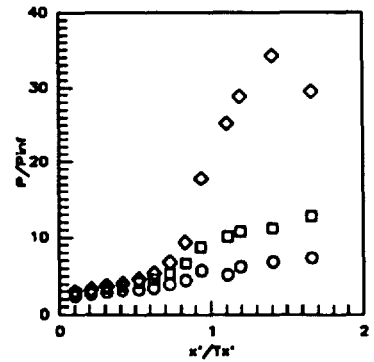
Sym	Z/H	Run No.	CR/Rs/Cowl (millions)
○	0.5RT	run66	3/2.15/ 0%
□	0.5RT	run46	5/2.15/ 0%
◇	0.5RT	run49	9/2.15/ 0%

Figure 7.2.1.28: CR Effects (Re=2.15million/ft, 0%Cowl) Sidewall Centerline Pressures



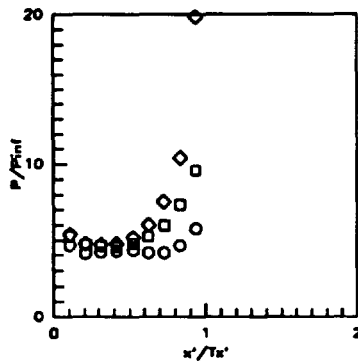
Sym	Z/H	Run No.	CR/Rs/Cowl (millions)
○	0.5LT	run66	3/2.15/ 0%
□	0.5LT	run46	5/2.15/ 0%
◇	0.5LT	run49	9/2.15/ 0%

Figure 7.2.1.29: CR Effects (Re=2.15million/ft, 0%Cowl) Sidewall Centerline Pressures



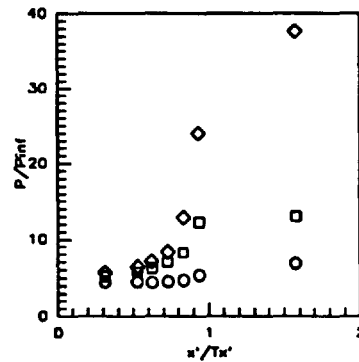
Sym	Z/H	Run No.	CR/Rs/Cowl (millions)
○	0.05	run66	3/2.15/ 0%
□	0.05	run46	5/2.15/ 0%
◇	0.05	run49	9/2.15/ 0%

Figure 7.2.1.30: CR Effects (Re=2.15million/ft, 0%Cowl) Sidewall Pressures



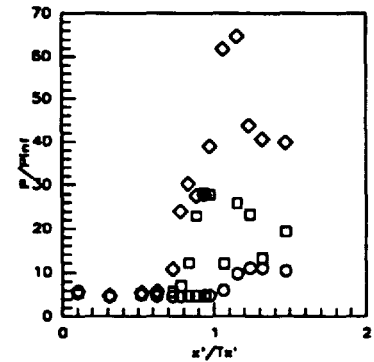
Sym	Z/H	Run No.	CR/Rs/Cowl (millions)
○	0.15	run66	3/2.15/ 0%
□	0.15	run46	5/2.15/ 0%
◇	0.15	run49	9/2.15/ 0%

Figure 7.2.1.31: CR Effects (Re=2.15million/ft, 0%Cowl) Sidewall Pressures



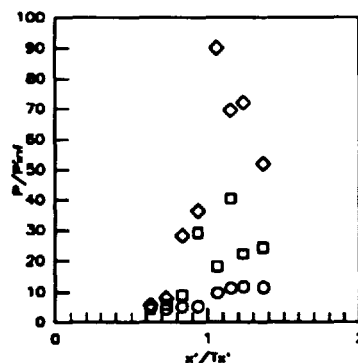
Sym	Z/H	Run No.	CR/Rs/Cowl (millions)
○	0.25	run66	3/2.15/ 0%
□	0.25	run46	5/2.15/ 0%
◇	0.25	run49	9/2.15/ 0%

Figure 7.2.1.32: CR Effects (Re=2.15million/ft, 0%Cowl) Sidewall Pressures



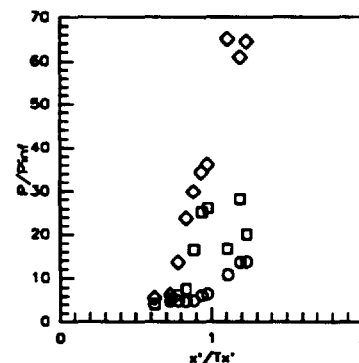
Sym	Z/H	Run No.	CR/Rs/Cowl (millions)
○	0.50	run66	3/2.15/ 0%
□	0.50	run46	5/2.15/ 0%
◇	0.50	run49	9/2.15/ 0%

Figure 7.2.1.33: CR Effects (Re=2.15million/ft, 0%Cowl) Sidewall Pressures



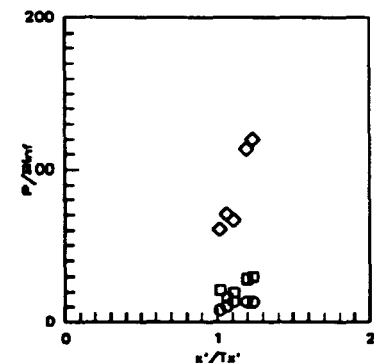
Sym	Z/H	Run No.	CR/Rs/Cowl (millions)
○	0.75	run66	3/2.15/ 0%
□	0.75	run46	5/2.15/ 0%
◇	0.75	run49	9/2.15/ 0%

Figure 7.2.1.34: CR Effects (Re=2.15million/ft, 0%Cowl) Sidewall Pressures



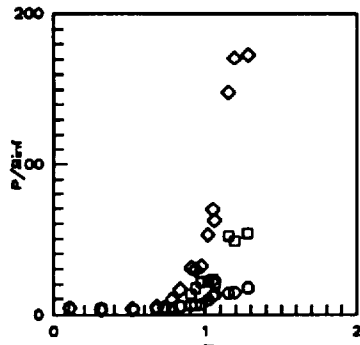
Sym	Z/H	Run No.	CR/Rs/Cowl (millions)
○	0.85	run66	3/2.15/ 0%
□	0.85	run46	5/2.15/ 0%
◇	0.85	run49	9/2.15/ 0%

Figure 7.2.1.35: CR Effects (Re=2.15million/ft, 0%Cowl) Sidewall Pressures



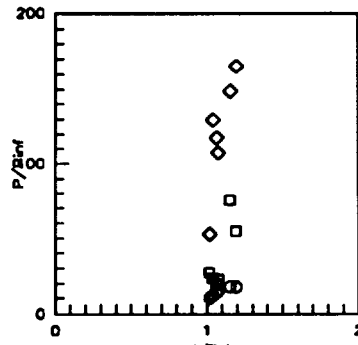
Sym	Z/H	Run No.	CR/Rs/Cowl (millions)
○	0.90	run66	3/2.15/ 0%
□	0.90	run46	5/2.15/ 0%
◇	0.90	run49	9/2.15/ 0%

Figure 7.2.1.36: CR Effects (Re=2.15million/ft, 0%Cowl) Sidewall Pressures



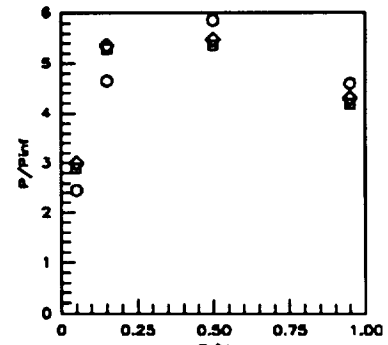
Sym	Z/H	Run No.	CR/Re/Cowl (millions)
o	0.95	run66	3/2.15/ 0%
o	0.95	run46	5/2.15/ 0%
o	0.95	run49	9/2.15/ 0%

Figure 7.2.1.37: CR Effects  
(Re=2.15million/ft, 0%Cowl)  
Sidewall Pressures



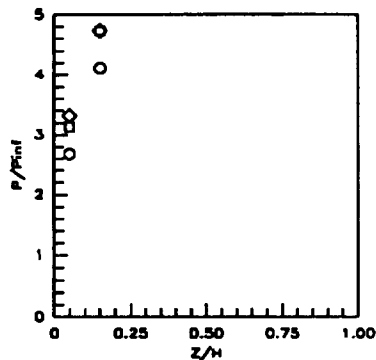
Sym	Z/H	Run No.	CR/Re/Cowl (millions)
o	0.975	run66	3/2.15/ 0%
o	0.975	run46	5/2.15/ 0%
o	0.975	run49	9/2.15/ 0%

Figure 7.2.1.38: CR Effects  
(Re=2.15million/ft, 0%Cowl)  
Sidewall Pressures



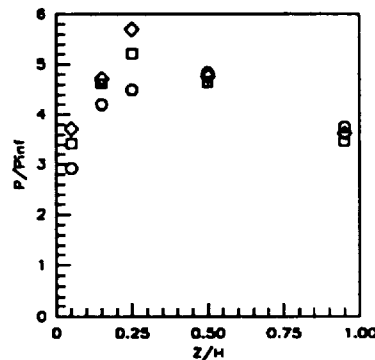
Sym	x'/Ts'	Run No.	CR/Re/Cowl (millions)
o	0.1042	run66	3/2.15/ 0%
o	0.1042	run46	5/2.15/ 0%
o	0.1042	run49	9/2.15/ 0%

Figure 7.2.1.39: CR Effects  
(Re=2.15million/ft, 0%Cowl)  
Sidewall Pressures



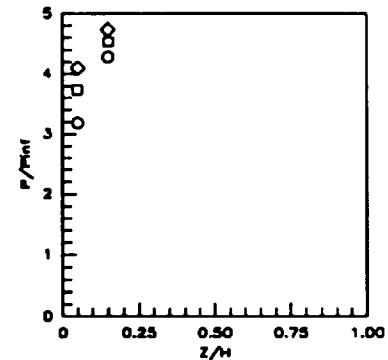
Sym	x'/Ts'	Run No.	CR/Re/Cowl (millions)
o	0.2083	run66	3/2.15/ 0%
o	0.2083	run46	5/2.15/ 0%
o	0.2083	run49	9/2.15/ 0%

Figure 7.2.1.40: CR Effects  
(Re=2.15million/ft, 0%Cowl)  
Sidewall Pressures



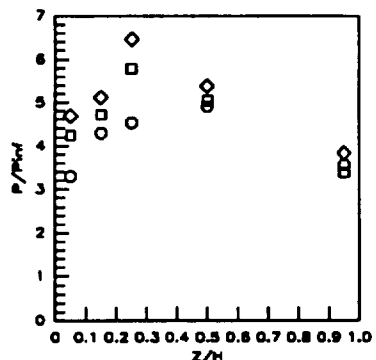
Sym	x'/Ts'	Run No.	CR/Re/Cowl (millions)
o	0.3125	run66	3/2.15/ 0%
o	0.3125	run46	5/2.15/ 0%
o	0.3125	run49	9/2.15/ 0%

Figure 7.2.1.41: CR Effects  
(Re=2.15million/ft, 0%Cowl)  
Sidewall Pressures



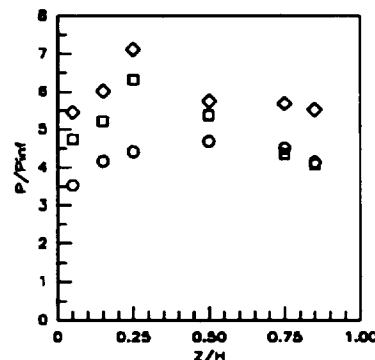
Sym	x'/Ts'	Run No.	CR/Re/Cowl (millions)
o	0.4167	run66	3/2.15/ 0%
o	0.4167	run46	5/2.15/ 0%
o	0.4167	run49	9/2.15/ 0%

Figure 7.2.1.42: CR Effects  
(Re=2.15million/ft, 0%Cowl)  
Sidewall Pressures



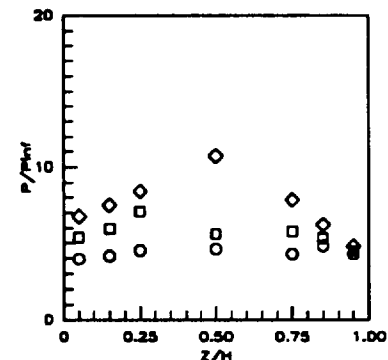
Sym	x'/Ts'	Run No.	CR/Re/Cowl (millions)
o	0.5259	run66	3/2.15/ 0%
o	0.5259	run46	5/2.15/ 0%
o	0.5259	run49	9/2.15/ 0%

Figure 7.2.1.43: CR Effects  
(Re=2.15million/ft, 0%Cowl)  
Sidewall Pressures



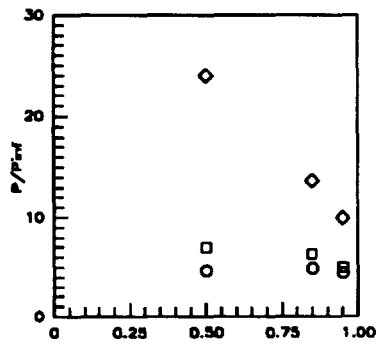
Sym	x'/Ts'	Run No.	CR/Re/Cowl (millions)
o	0.6252	run66	3/2.15/ 0%
o	0.6252	run46	5/2.15/ 0%
o	0.6252	run49	9/2.15/ 0%

Figure 7.2.1.44: CR Effects  
(Re=2.15million/ft, 0%Cowl)  
Sidewall Pressures



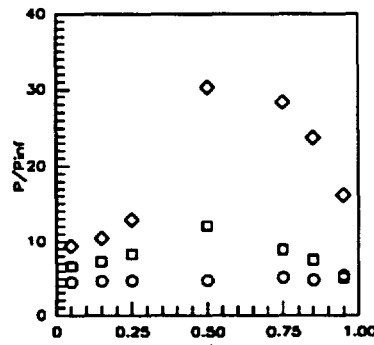
Sym	x'/Ts'	Run No.	CR/Re/Cowl (millions)
o	0.7294	run66	3/2.15/ 0%
o	0.7294	run46	5/2.15/ 0%
o	0.7294	run49	9/2.15/ 0%

Figure 7.2.1.45: CR Effects  
(Re=2.15million/ft, 0%Cowl)  
Sidewall Pressures



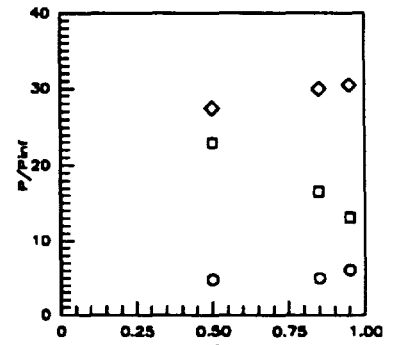
Sym	$x'/T_x'$	Run No.	CR/Re/Cowl (millions)
○	0.7815	run86	3/2.15/ 0%
□	0.7815	run46	5/2.15/ 0%
◇	0.7815	run49	9/2.15/ 0%

Figure 7.2.1.46: CR Effects (Re=2.15million/ft, 0%CowI) Sidewall Pressures



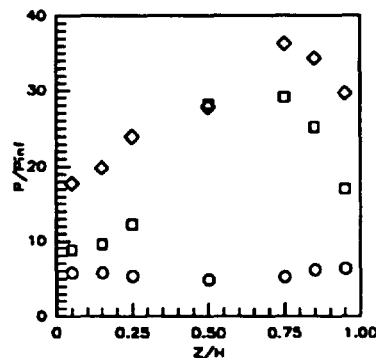
Sym	$x'/T_x'$	Run No.	CR/Re/Cowl (millions)
○	0.8336	run86	3/2.15/ 0%
□	0.8336	run48	5/2.15/ 0%
◇	0.8336	run49	9/2.15/ 0%

Figure 7.2.1.47: CR Effects (Re=2.15million/ft, 0%CowI) Sidewall Pressures



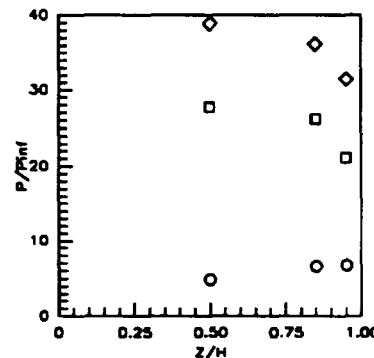
Sym	$x'/T_x'$	Run No.	CR/Re/Cowl (millions)
○	0.8857	run86	3/2.15/ 0%
□	0.8857	run46	5/2.15/ 0%
◇	0.8857	run49	9/2.15/ 0%

Figure 7.2.1.48: CR Effects (Re=2.15million/ft, 0%CowI) Sidewall Pressures



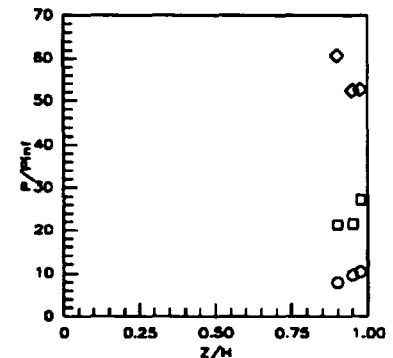
Sym	$x'/T_x'$	Run No.	CR/Re/Cowl (millions)
○	0.9378	run86	3/2.15/ 0%
□	0.9378	run46	5/2.15/ 0%
◇	0.9378	run49	9/2.15/ 0%

Figure 7.2.1.49: CR Effects (Re=2.15million/ft, 0%CowI) Sidewall Pressures



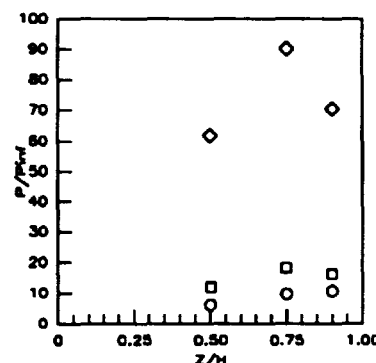
Sym	$x'/T_x'$	Run No.	CR/Re/Cowl (millions)
○	0.9751	run86	3/2.15/ 0%
□	0.9751	run48	5/2.15/ 0%
◇	0.9751	run49	9/2.15/ 0%

Figure 7.2.1.50: CR Effects (Re=2.15million/ft, 0%CowI) Sidewall Pressures



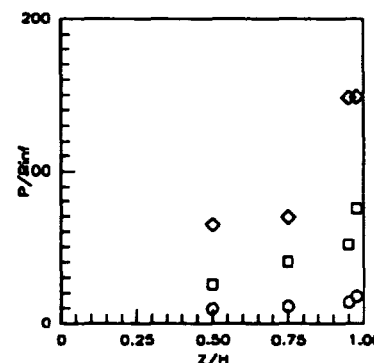
Sym	$x'/T_x'$	Run No.	CR/Re/Cowl (millions)
○	1.0187	run86	3/2.15/ 0%
□	1.0187	run46	5/2.15/ 0%
◇	1.0187	run49	9/2.15/ 0%

Figure 7.2.1.51: CR Effects (Re=2.15million/ft, 0%CowI) Sidewall Pressures



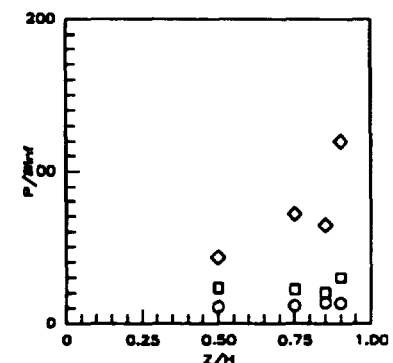
Sym	$x'/T_x'$	Run No.	CR/Re/Cowl (millions)
○	1.0843	run86	3/2.15/ 0%
□	1.0843	run46	5/2.15/ 0%
◇	1.0843	run49	9/2.15/ 0%

Figure 7.2.1.52: CR Effects (Re=2.15million/ft, 0%CowI) Sidewall Pressures



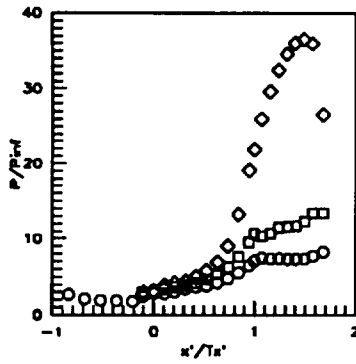
Sym	$x'/T_x'$	Run No.	CR/Re/Cowl (millions)
○	1.1537	run86	3/2.15/ 0%
□	1.1537	run48	5/2.15/ 0%
◇	1.1537	run49	9/2.15/ 0%

Figure 7.2.1.53: CR Effects (Re=2.15million/ft, 0%CowI) Sidewall Pressures



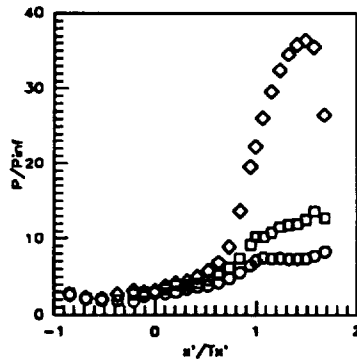
Sym	$x'/T_x'$	Run No.	CR/Re/Cowl (millions)
○	1.2356	run86	3/2.15/ 0%
□	1.2356	run46	5/2.15/ 0%
◇	1.2356	run49	9/2.15/ 0%

Figure 7.2.1.54: CR Effects (Re=2.15million/ft, 0%CowI) Sidewall Pressures



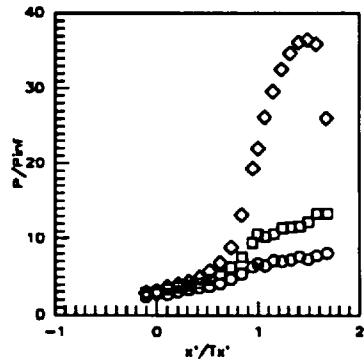
Sym	C.L. for	Run No.	CR/Re/CowI (milions)
○	CR=3	run65	3/1.14/ 0%
□	CR=5	run45	5/1.14/ 0%
◇	CR=9	run48	9/1.14/ 0%

Figure 7.2.1.55: CR Effects (Re=1.14million/ft, 0%CowI) Centerline Pressures



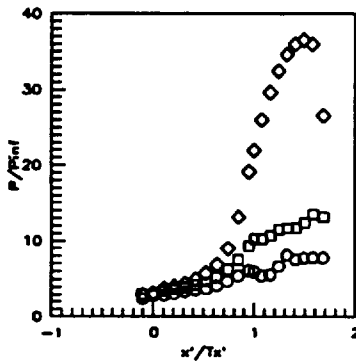
Sym	C.L. for	Run No.	CR/Re/CowI (milions)
○	CR=3	run65	3/1.14/ 0%
□	CR=3	run45	5/1.14/ 0%
◇	CR=3	run48	9/1.14/ 0%

Figure 7.2.1.56: CR Effects (Re=1.14million/ft, 0%CowI) CR=3 Centerline Pressures



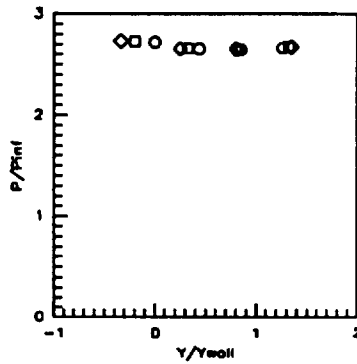
Sym	C.L. for	Run No.	CR/Re/CowI (milions)
○	CR=5	run65	3/1.14/ 0%
□	CR=5	run45	5/1.14/ 0%
◇	CR=5	run48	9/1.14/ 0%

Figure 7.2.1.57: CR Effects (Re=1.14million/ft, 0%CowI) CR=5 Centerline Pressures



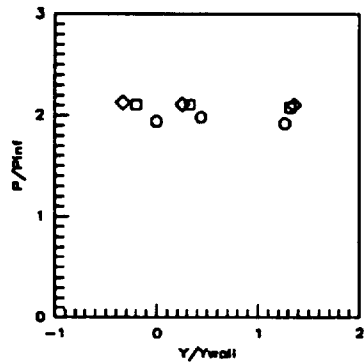
Sym	C.L. for	Run No.	CR/Re/CowI (milions)
○	CR=9	run65	3/1.14/ 0%
□	CR=9	run45	5/1.14/ 0%
◇	CR=9	run48	9/1.14/ 0%

Figure 7.2.1.58: CR Effects (Re=1.14million/ft, 0%CowI) CR=9 Centerline Pressures



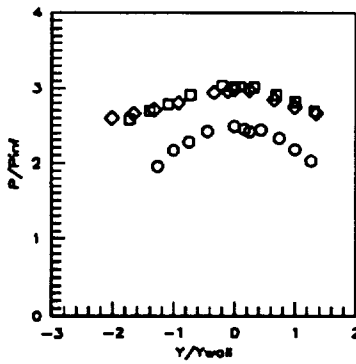
Sym	x'/Tx'	Run No.	CR/Re/CowI (milions)
○	-0.8412	run65	3/1.14/ 0%
□	-0.8412	run45	5/1.14/ 0%
◇	-0.8412	run48	9/1.14/ 0%

Figure 7.2.1.59: CR Effects (Re=1.14million/ft, 0%CowI) Baseplate Pressures



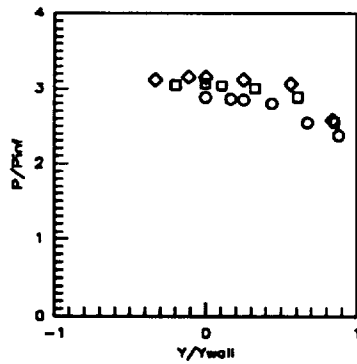
Sym	x'/Tx'	Run No.	CR/Re/CowI (milions)
○	-0.5258	run65	3/1.14/ 0%
□	-0.5258	run45	5/1.14/ 0%
◇	-0.5258	run48	9/1.14/ 0%

Figure 7.2.1.60: CR Effects (Re=1.14million/ft, 0%CowI) Baseplate Pressures



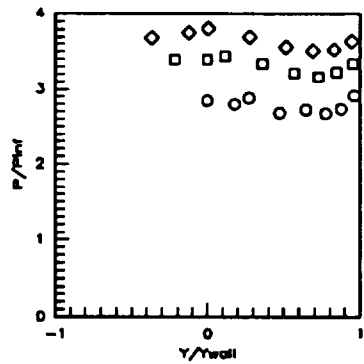
Sym	x'/Tx'	Run No.	CR/Re/CowI (milions)
○	-0.1052	run65	3/1.14/ 0%
□	-0.1052	run45	5/1.14/ 0%
◇	-0.1052	run48	9/1.14/ 0%

Figure 7.2.1.61: CR Effects (Re=1.14million/ft, 0%CowI) Baseplate Pressures



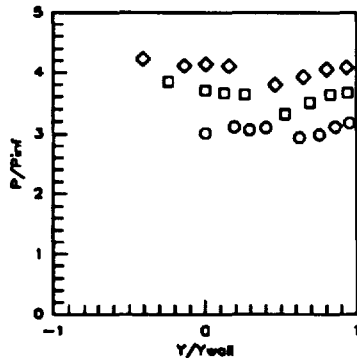
Sym	x'/Tx'	Run No.	CR/Re/CowI (milions)
○	0.0000	run65	3/1.14/ 0%
□	0.0000	run45	5/1.14/ 0%
◇	0.0000	run48	9/1.14/ 0%

Figure 7.2.1.62: CR Effects (Re=1.14million/ft, 0%CowI) Baseplate Pressures



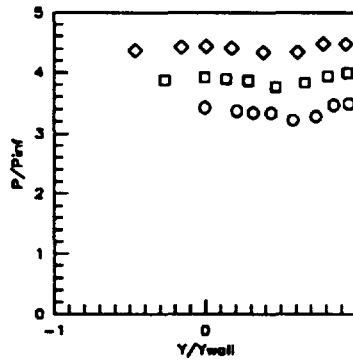
Sym	x'/Tx'	Run No.	CR/Re/CowI (milions)
○	0.1052	run65	3/1.14/ 0%
□	0.1052	run45	5/1.14/ 0%
◇	0.1052	run48	9/1.14/ 0%

Figure 7.2.1.63: CR Effects (Re=1.14million/ft, 0%CowI) Baseplate Pressures



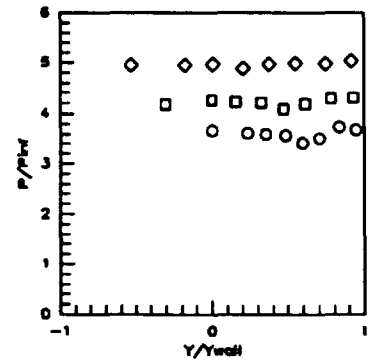
Sym	$x'/T_x'$	Run No.	CR/Re/CowI (millions)
○	0.2103	run65	3/1.14/ 0%
□	0.2103	run45	5/1.14/ 0%
◇	0.2103	run48	9/1.14/ 0%

Figure 7.2.1.64: CR Effects  
( $Re=1.14$ million/ft, 0%CowI)  
Baseplate Pressures



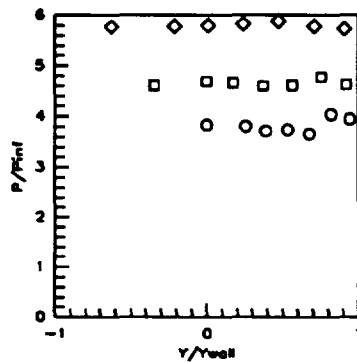
Sym	$x'/T_x'$	Run No.	CR/Re/CowI (millions)
○	0.3154	run65	3/1.14/ 0%
□	0.3154	run45	5/1.14/ 0%
◇	0.3154	run48	9/1.14/ 0%

Figure 7.2.1.65: CR Effects  
( $Re=1.14$ million/ft, 0%CowI)  
Baseplate Pressures



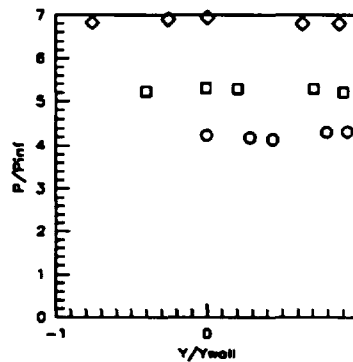
Sym	$x'/T_x'$	Run No.	CR/Re/CowI (millions)
○	0.4206	run65	3/1.14/ 0%
□	0.4206	run45	5/1.14/ 0%
◇	0.4206	run48	9/1.14/ 0%

Figure 7.2.1.66: CR Effects  
( $Re=1.14$ million/ft, 0%CowI)  
Baseplate Pressures



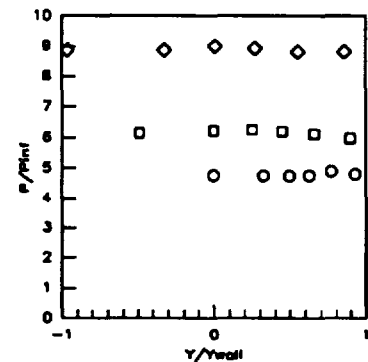
Sym	$x'/T_x'$	Run No.	CR/Re/CowI (millions)
○	0.5258	run65	3/1.14/ 0%
□	0.5258	run45	5/1.14/ 0%
◇	0.5258	run48	9/1.14/ 0%

Figure 7.2.1.67: CR Effects  
( $Re=1.14$ million/ft, 0%CowI)  
Baseplate Pressures



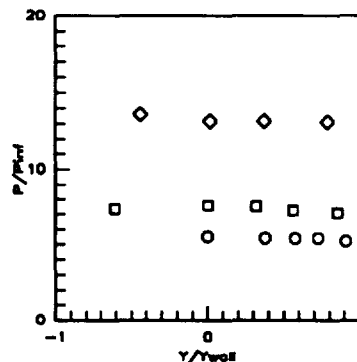
Sym	$x'/T_x'$	Run No.	CR/Re/CowI (millions)
○	0.6309	run65	3/1.14/ 0%
□	0.6309	run45	5/1.14/ 0%
◇	0.6309	run48	9/1.14/ 0%

Figure 7.2.1.68: CR Effects  
( $Re=1.14$ million/ft, 0%CowI)  
Baseplate Pressures



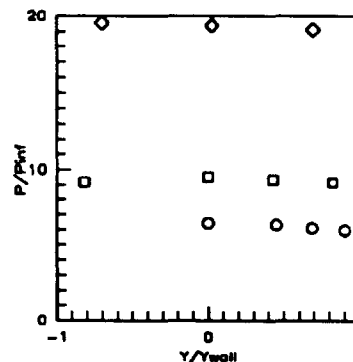
Sym	$x'/T_x'$	Run No.	CR/Re/CowI (millions)
○	0.7361	run65	3/1.14/ 0%
□	0.7361	run45	5/1.14/ 0%
◇	0.7361	run48	9/1.14/ 0%

Figure 7.2.1.69: CR Effects  
( $Re=1.14$ million/ft, 0%CowI)  
Baseplate Pressures



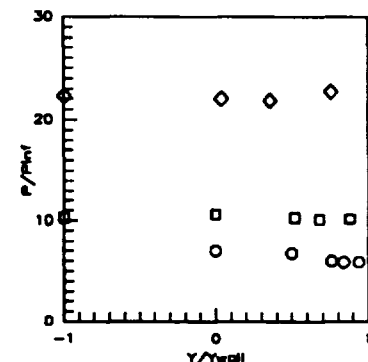
Sym	$x'/T_x'$	Run No.	CR/Re/CowI (millions)
○	0.8412	run65	3/1.14/ 0%
□	0.8412	run45	5/1.14/ 0%
◇	0.8412	run48	9/1.14/ 0%

Figure 7.2.1.70: CR Effects  
( $Re=1.14$ million/ft, 0%CowI)  
Baseplate Pressures



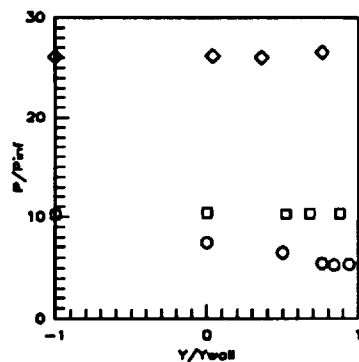
Sym	$x'/T_x'$	Run No.	CR/Re/CowI (millions)
○	0.9464	run65	3/1.14/ 0%
□	0.9464	run45	5/1.14/ 0%
◇	0.9464	run48	9/1.14/ 0%

Figure 7.2.1.71: CR Effects  
( $Re=1.14$ million/ft, 0%CowI)  
Baseplate Pressures



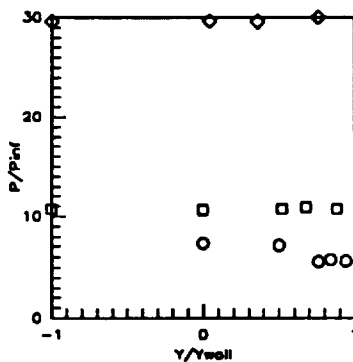
Sym	$x'/T_x'$	Run No.	CR/Re/CowI (millions)
○	1.0000	run65	3/1.14/ 0%
□	1.0000	run45	5/1.14/ 0%
◇	1.0000	run48	9/1.14/ 0%

Figure 7.2.1.72: CR Effects  
( $Re=1.14$ million/ft, 0%CowI)  
Baseplate Pressures



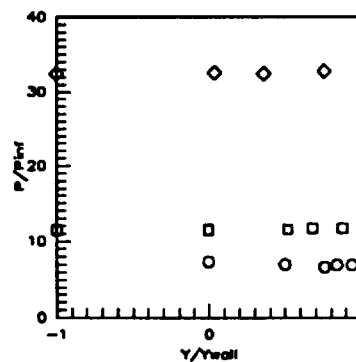
Sym	$x'/T_x'$	Run No.	CR/Re/CowI (millions)
○	1.0726	run65	3/1.14/ 0%
□	1.0726	run45	5/1.14/ 0%
◇	1.0726	run48	9/1.14/ 0%

Figure 7.2.1.73: CR Effects (Re=1.14million/ft, 0%CowI) Baseplate Pressures



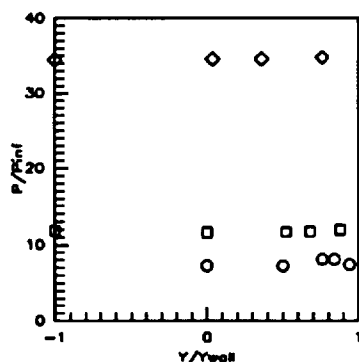
Sym	$x'/T_x'$	Run No.	CR/Re/CowI (millions)
○	1.1567	run65	3/1.14/ 0%
□	1.1567	run45	5/1.14/ 0%
◇	1.1567	run48	9/1.14/ 0%

Figure 7.2.1.74: CR Effects (Re=1.14million/ft, 0%CowI) Baseplate Pressures



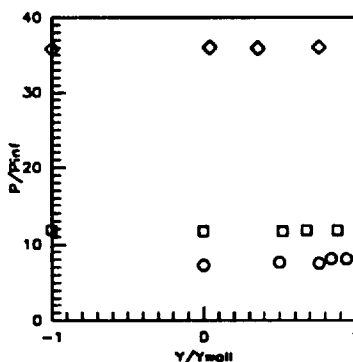
Sym	$x'/T_x'$	Run No.	CR/Re/CowI (millions)
○	1.2408	run65	3/1.14/ 0%
□	1.2408	run45	5/1.14/ 0%
◇	1.2408	run48	9/1.14/ 0%

Figure 7.2.1.75: CR Effects (Re=1.14million/ft, 0%CowI) Baseplate Pressures



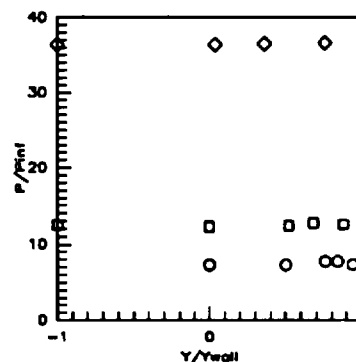
Sym	$x'/T_x'$	Run No.	CR/Re/CowI (millions)
○	1.3249	run65	3/1.14/ 0%
□	1.3249	run45	5/1.14/ 0%
◇	1.3249	run48	9/1.14/ 0%

Figure 7.2.1.76: CR Effects (Re=1.14million/ft, 0%CowI) Baseplate Pressures



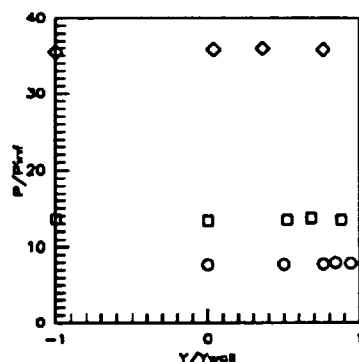
Sym	$x'/T_x'$	Run No.	CR/Re/CowI (millions)
○	1.4090	run65	3/1.14/ 0%
□	1.4090	run45	5/1.14/ 0%
◇	1.4090	run48	9/1.14/ 0%

Figure 7.2.1.77: CR Effects (Re=1.14million/ft, 0%CowI) Baseplate Pressures



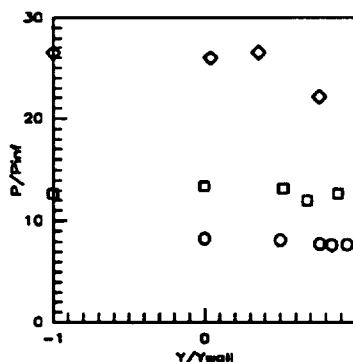
Sym	$x'/T_x'$	Run No.	CR/Re/CowI (millions)
○	1.4932	run65	3/1.14/ 0%
□	1.4932	run45	5/1.14/ 0%
◇	1.4932	run48	9/1.14/ 0%

Figure 7.2.1.78: CR Effects (Re=1.14million/ft, 0%CowI) Baseplate Pressures



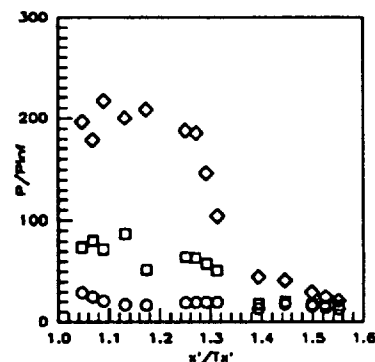
Sym	$x'/T_x'$	Run No.	CR/Re/CowI (millions)
○	1.5773	run65	3/1.14/ 0%
□	1.5773	run45	5/1.14/ 0%
◇	1.5773	run48	9/1.14/ 0%

Figure 7.2.1.79: CR Effects (Re=1.14million/ft, 0%CowI) Baseplate Pressures



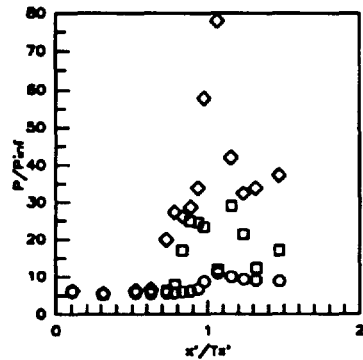
Sym	$x'/T_x'$	Run No.	CR/Re/CowI (millions)
○	1.6824	run65	3/1.14/ 0%
□	1.6824	run45	5/1.14/ 0%
◇	1.6824	run48	9/1.14/ 0%

Figure 7.2.1.80: CR Effects (Re=1.14million/ft, 0%CowI) Baseplate Pressures



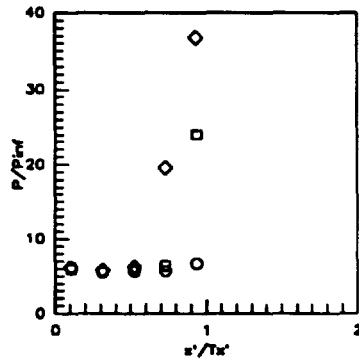
Sym	CowI Pos.	Run No.	CR/Re/CowI (millions)
○	0%	run65	3/1.14/ 0%
□	0%	run45	5/1.14/ 0%
◇	0%	run48	9/1.14/ 0%

Figure 7.2.1.81: CR Effects (Re=1.14million/ft, 0%CowI) CowI Pressures



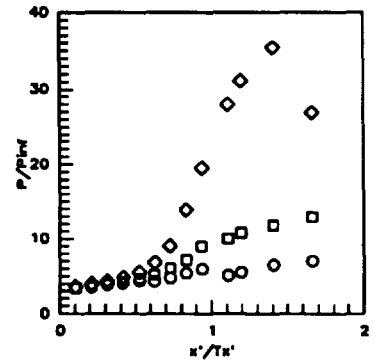
Sym	Z/H	Run No.	CR/Re/CowI (millions)
○	0.5RT	run65	3/1.14/ 0%
□	0.5RT	run45	5/1.14/ 0%
◇	0.5RT	run48	9/1.14/ 0%

Figure 7.2.1.82: CR Effects (Re=1.14million/ft, 0%CowI) Sidewall Centerline Pressures



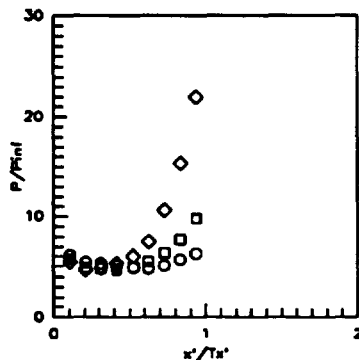
Sym	Z/H	Run No.	CR/Re/CowI (millions)
○	0.5LT	run65	3/1.14/ 0%
□	0.5LT	run45	5/1.14/ 0%
◇	0.5LT	run48	9/1.14/ 0%

Figure 7.2.1.83: CR Effects (Re=1.14million/ft, 0%CowI) Sidewall Centerline Pressures



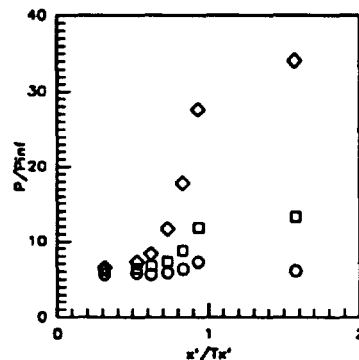
Sym	Z/H	Run No.	CR/Re/CowI (millions)
○	0.05	run65	3/1.14/ 0%
□	0.05	run45	5/1.14/ 0%
◇	0.05	run48	9/1.14/ 0%

Figure 7.2.1.84: CR Effects (Re=1.14million/ft, 0%CowI) Sidewall Pressures



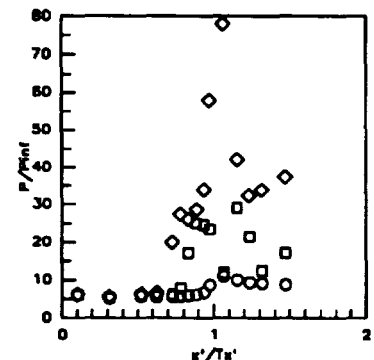
Sym	Z/H	Run No.	CR/Re/CowI (millions)
○	0.15	run65	3/1.14/ 0%
□	0.15	run45	5/1.14/ 0%
◇	0.15	run48	9/1.14/ 0%

Figure 7.2.1.85: CR Effects (Re=1.14million/ft, 0%CowI) Sidewall Pressures



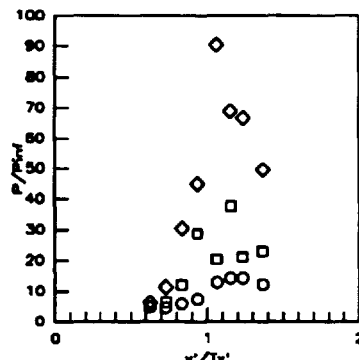
Sym	Z/H	Run No.	CR/Re/CowI (millions)
○	0.25	run65	3/1.14/ 0%
□	0.25	run45	5/1.14/ 0%
◇	0.25	run48	9/1.14/ 0%

Figure 7.2.1.86: CR Effects (Re=1.14million/ft, 0%CowI) Sidewall Pressures



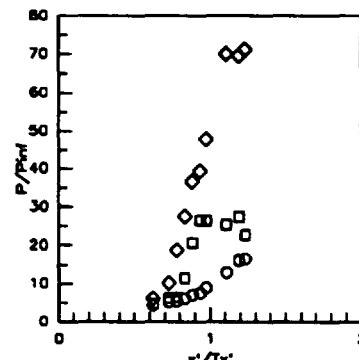
Sym	Z/H	Run No.	CR/Re/CowI (millions)
○	0.50	run65	3/1.14/ 0%
□	0.50	run45	5/1.14/ 0%
◇	0.50	run48	9/1.14/ 0%

Figure 7.2.1.87: CR Effects (Re=1.14million/ft, 0%CowI) Sidewall Pressures



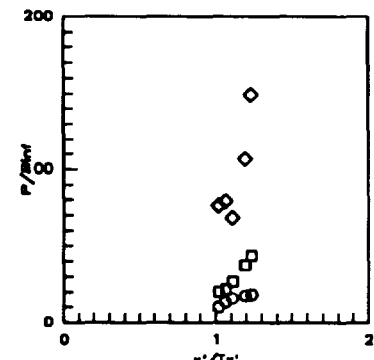
Sym	Z/H	Run No.	CR/Re/CowI (millions)
○	0.75	run65	3/1.14/ 0%
□	0.75	run45	5/1.14/ 0%
◇	0.75	run48	9/1.14/ 0%

Figure 7.2.1.88: CR Effects (Re=1.14million/ft, 0%CowI) Sidewall Pressures



Sym	Z/H	Run No.	CR/Re/CowI (millions)
○	0.85	run65	3/1.14/ 0%
□	0.85	run45	5/1.14/ 0%
◇	0.85	run48	9/1.14/ 0%

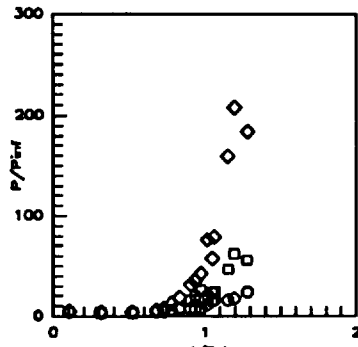
Figure 7.2.1.89: CR Effects (Re=1.14million/ft, 0%CowI) Sidewall Pressures



Sym	Z/H	Run No.	CR/Re/CowI (millions)
○	0.90	run65	3/1.14/ 0%
□	0.90	run45	5/1.14/ 0%
◇	0.90	run48	9/1.14/ 0%

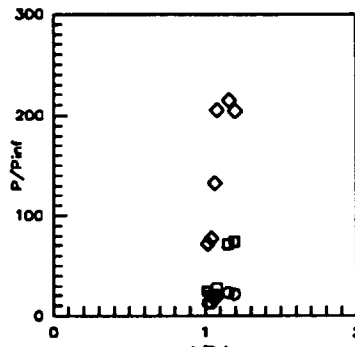
Figure 7.2.1.90: CR Effects (Re=1.14million/ft, 0%CowI) Sidewall Pressures





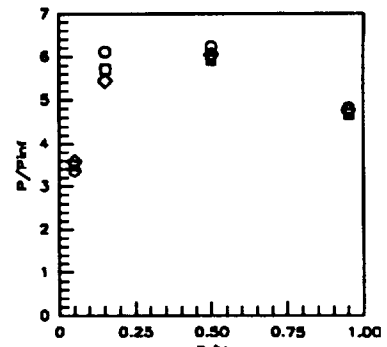
Sym	Z/H	Run No.	CR/Ra/Cowl (millions)
○	0.95	run65	3/1.14/ 0%
□	0.95	run45	5/1.14/ 0%
◇	0.95	run48	9/1.14/ 0%

Figure 7.2.1.91: CR Effects (Re=1.14million/ft, 0%CowI) Sidewall Pressures



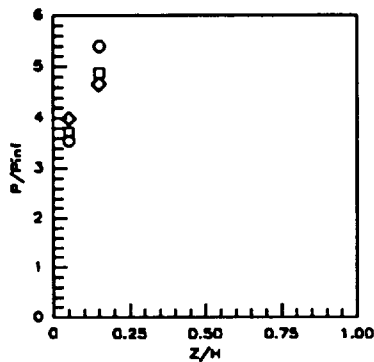
Sym	Z/H	Run No.	CR/Ra/Cowl (millions)
○	0.975	run65	3/1.14/ 0%
□	0.975	run45	5/1.14/ 0%
◇	0.975	run48	9/1.14/ 0%

Figure 7.2.1.92: CR Effects (Re=1.14million/ft, 0%CowI) Sidewall Pressures



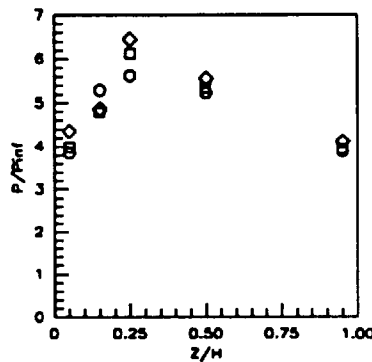
Sym	x'/Ts'	Run No.	CR/Ra/Cowl (millions)
○	0.1042	run65	3/1.14/ 0%
□	0.1042	run45	5/1.14/ 0%
◇	0.1042	run48	9/1.14/ 0%

Figure 7.2.1.93: CR Effects (Re=1.14million/ft, 0%CowI) Sidewall Pressures



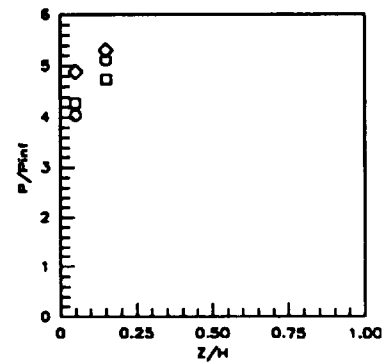
Sym	x'/Ts'	Run No.	CR/Ra/Cowl (millions)
○	0.2083	run65	3/1.14/ 0%
□	0.2083	run45	5/1.14/ 0%
◇	0.2083	run48	9/1.14/ 0%

Figure 7.2.1.94: CR Effects (Re=1.14million/ft, 0%CowI) Sidewall Pressures



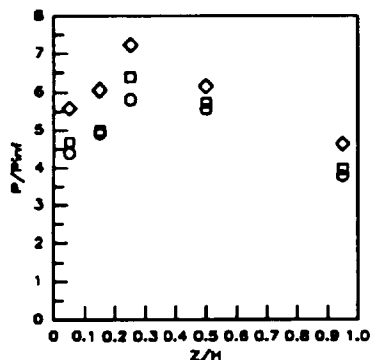
Sym	x'/Ts'	Run No.	CR/Ra/Cowl (millions)
○	0.3125	run65	3/1.14/ 0%
□	0.3125	run45	5/1.14/ 0%
◇	0.3125	run48	9/1.14/ 0%

Figure 7.2.1.95: CR Effects (Re=1.14million/ft, 0%CowI) Sidewall Pressures



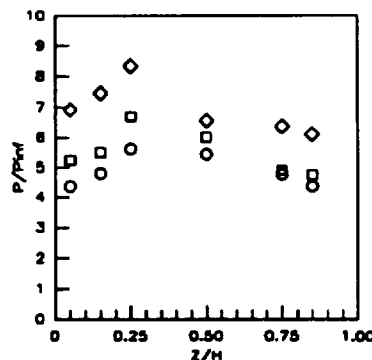
Sym	x'/Ts'	Run No.	CR/Ra/Cowl (millions)
○	0.4167	run65	3/1.14/ 0%
□	0.4167	run45	5/1.14/ 0%
◇	0.4167	run48	9/1.14/ 0%

Figure 7.2.1.96: CR Effects (Re=1.14million/ft, 0%CowI) Sidewall Pressures



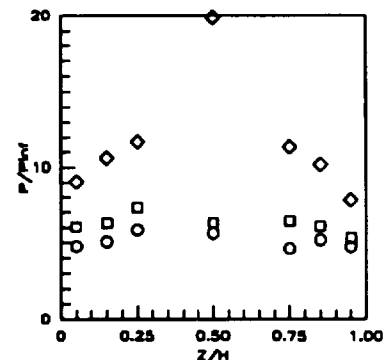
Sym	x'/Ts'	Run No.	CR/Ra/Cowl (millions)
○	0.5259	run65	3/1.14/ 0%
□	0.5259	run45	5/1.14/ 0%
◇	0.5259	run48	9/1.14/ 0%

Figure 7.2.1.97: CR Effects (Re=1.14million/ft, 0%CowI) Sidewall Pressures



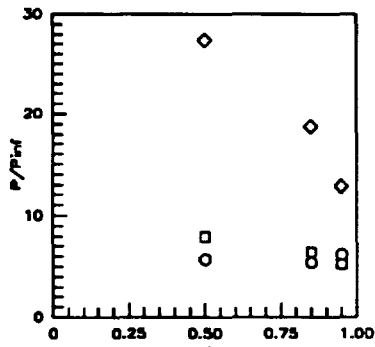
Sym	x'/Ts'	Run No.	CR/Ra/Cowl (millions)
○	0.6252	run65	3/1.14/ 0%
□	0.6252	run45	5/1.14/ 0%
◇	0.6252	run48	9/1.14/ 0%

Figure 7.2.1.98: CR Effects (Re=1.14million/ft, 0%CowI) Sidewall Pressures



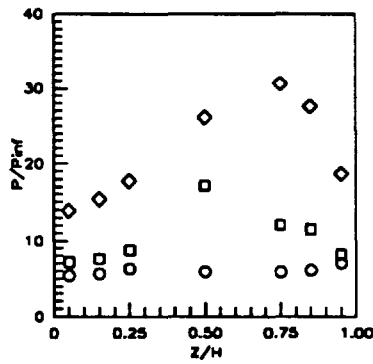
Sym	x'/Ts'	Run No.	CR/Ra/Cowl (millions)
○	0.7294	run65	3/1.14/ 0%
□	0.7294	run45	5/1.14/ 0%
◇	0.7294	run48	9/1.14/ 0%

Figure 7.2.1.99: CR Effects (Re=1.14million/ft, 0%CowI) Sidewall Pressures



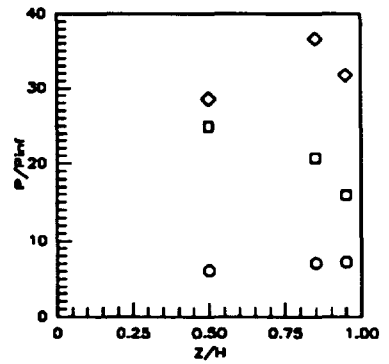
Sym	$x'/T_x'$	Run No.	CR/Re/CowI (millions)
◇	0.7815	run85	3/1.14/ 0%
□	0.7815	run45	5/1.14/ 0%
○	0.7815	run48	9/1.14/ 0%

Figure 7.2.1.100: CR Effects (Re=1.14million/ft, 0%CowI) Sidewall Pressures



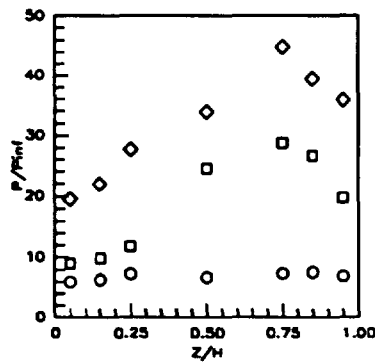
Sym	$x'/T_x'$	Run No.	CR/Re/CowI (millions)
◇	0.8336	run85	3/1.14/ 0%
□	0.8336	run45	5/1.14/ 0%
○	0.8336	run48	9/1.14/ 0%

Figure 7.2.1.101: CR Effects (Re=1.14million/ft, 0%CowI) Sidewall Pressures



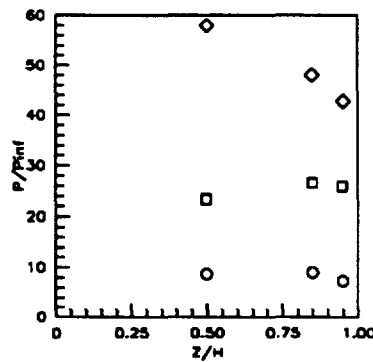
Sym	$x'/T_x'$	Run No.	CR/Re/CowI (millions)
◇	0.8857	run85	3/1.14/ 0%
□	0.8857	run45	5/1.14/ 0%
○	0.8857	run48	9/1.14/ 0%

Figure 7.2.1.102: CR Effects (Re=1.14million/ft, 0%CowI) Sidewall Pressures



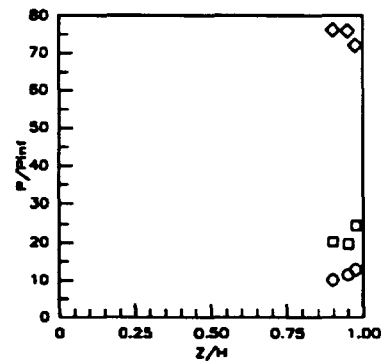
Sym	$x'/T_x'$	Run No.	CR/Re/CowI (millions)
◇	0.9378	run85	3/1.14/ 0%
□	0.9378	run45	5/1.14/ 0%
○	0.9378	run48	9/1.14/ 0%

Figure 7.2.1.103: CR Effects (Re=1.14million/ft, 0%CowI) Sidewall Pressures



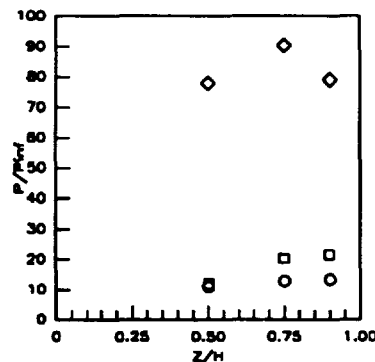
Sym	$x'/T_x'$	Run No.	CR/Re/CowI (millions)
◇	0.9751	run85	3/1.14/ 0%
□	0.9751	run45	5/1.14/ 0%
○	0.9751	run48	9/1.14/ 0%

Figure 7.2.1.104: CR Effects (Re=1.14million/ft, 0%CowI) Sidewall Pressures



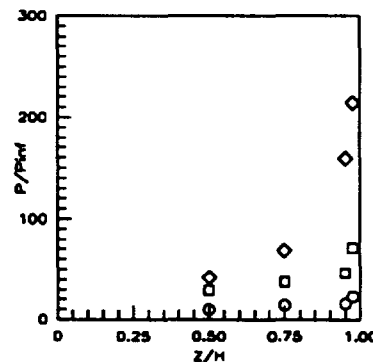
Sym	$x'/T_x'$	Run No.	CR/Re/CowI (millions)
◇	1.0197	run85	3/1.14/ 0%
□	1.0197	run45	5/1.14/ 0%
○	1.0197	run48	9/1.14/ 0%

Figure 7.2.1.105: CR Effects (Re=1.14million/ft, 0%CowI) Sidewall Pressures



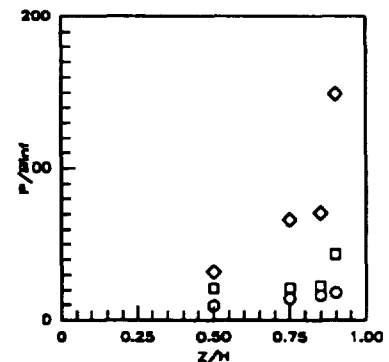
Sym	$x'/T_x'$	Run No.	CR/Re/CowI (millions)
◇	1.0843	run85	3/1.14/ 0%
□	1.0843	run45	5/1.14/ 0%
○	1.0843	run48	9/1.14/ 0%

Figure 7.2.1.106: CR Effects (Re=1.14million/ft, 0%CowI) Sidewall Pressures



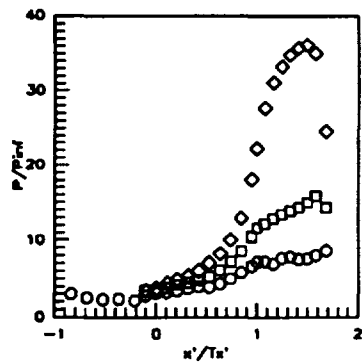
Sym	$x'/T_x'$	Run No.	CR/Re/CowI (millions)
◇	1.1537	run85	3/1.14/ 0%
□	1.1537	run45	5/1.14/ 0%
○	1.1537	run48	9/1.14/ 0%

Figure 7.2.1.107: CR Effects (Re=1.14million/ft, 0%CowI) Sidewall Pressures



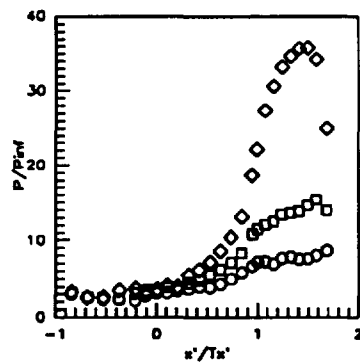
Sym	$x'/T_x'$	Run No.	CR/Re/CowI (millions)
◇	1.2356	run85	3/1.14/ 0%
□	1.2356	run45	5/1.14/ 0%
○	1.2356	run48	9/1.14/ 0%

Figure 7.2.1.108: CR Effects (Re=1.14million/ft, 0%CowI) Sidewall Pressures



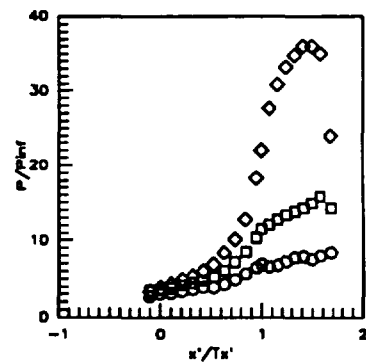
Sym	C.L. for	Run No.	CR/Re/CowI (millions)
○	CR=3	run64	3/0.55/ 0%
□	CR=5	run44	5/0.55/ 0%
◇	CR=9	run47	9/0.55/ 0%

Figure 7.2.1.109: CR Effects (Re=0.55million/ft, 0%CowI) Centerline Pressures



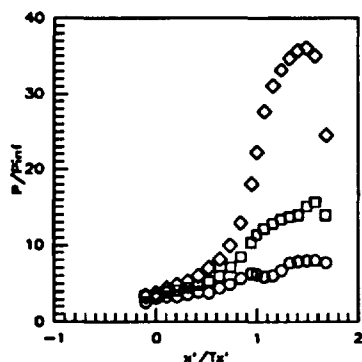
Sym	C.L. for	Run No.	CR/Re/CowI (millions)
○	CR=3	run64	3/0.55/ 0%
□	CR=3	run44	5/0.55/ 0%
◇	CR=3	run47	9/0.55/ 0%

Figure 7.2.1.110: CR Effects (Re=0.55million/ft, 0%CowI) CR=3 Centerline Pressures



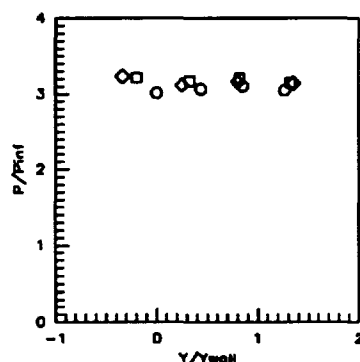
Sym	C.L. for	Run No.	CR/Re/CowI (millions)
○	CR=5	run64	3/0.55/ 0%
□	CR=5	run44	5/0.55/ 0%
◇	CR=5	run47	9/0.55/ 0%

Figure 7.2.1.111: CR Effects (Re=0.55million/ft, 0%CowI) CR=5 Centerline Pressures



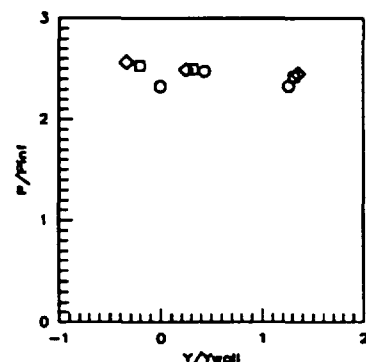
Sym	C.L. for	Run No.	CR/Re/CowI (millions)
○	CR=9	run64	3/0.55/ 0%
□	CR=9	run44	5/0.55/ 0%
◇	CR=9	run47	9/0.55/ 0%

Figure 7.2.1.112: CR Effects (Re=0.55million/ft, 0%CowI) CR=9 Centerline Pressures



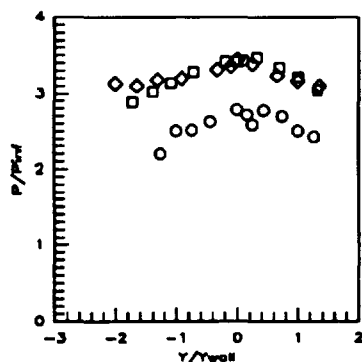
Sym	x'/Tx'	Run No.	CR/Re/CowI (millions)
○	-0.8412	run64	3/0.55/ 0%
□	-0.8412	run44	5/0.55/ 0%
◇	-0.8412	run47	9/0.55/ 0%

Figure 7.2.1.113: CR Effects (Re=0.55million/ft, 0%CowI) Baseplate Pressures



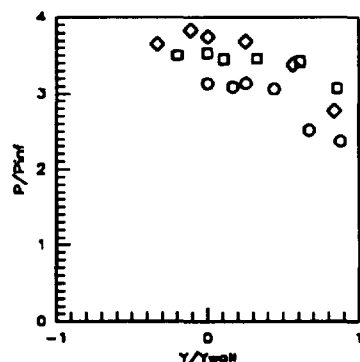
Sym	x'/Tx'	Run No.	CR/Re/CowI (millions)
○	-0.5258	run64	3/0.55/ 0%
□	-0.5258	run44	5/0.55/ 0%
◇	-0.5258	run47	9/0.55/ 0%

Figure 7.2.1.114: CR Effects (Re=0.55million/ft, 0%CowI) Baseplate Pressures



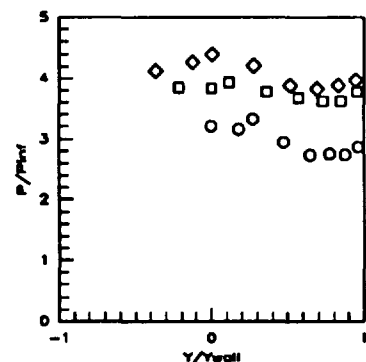
Sym	x'/Tx'	Run No.	CR/Re/CowI (millions)
○	-0.1052	run64	3/0.55/ 0%
□	-0.1052	run44	5/0.55/ 0%
◇	-0.1052	run47	9/0.55/ 0%

Figure 7.2.1.115: CR Effects (Re=0.55million/ft, 0%CowI) Baseplate Pressures



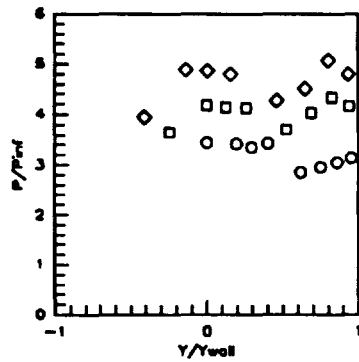
Sym	x'/Tx'	Run No.	CR/Re/CowI (millions)
○	0.0000	run64	3/0.55/ 0%
□	0.0000	run44	5/0.55/ 0%
◇	0.0000	run47	9/0.55/ 0%

Figure 7.2.1.116: CR Effects (Re=0.55million/ft, 0%CowI) Baseplate Pressures



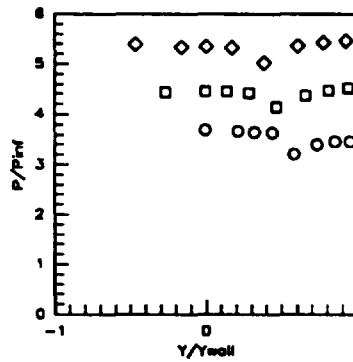
Sym	x'/Tx'	Run No.	CR/Re/CowI (millions)
○	0.1052	run64	3/0.55/ 0%
□	0.1052	run44	5/0.55/ 0%
◇	0.1052	run47	9/0.55/ 0%

Figure 7.2.1.117: CR Effects (Re=0.55million/ft, 0%CowI) Baseplate Pressures



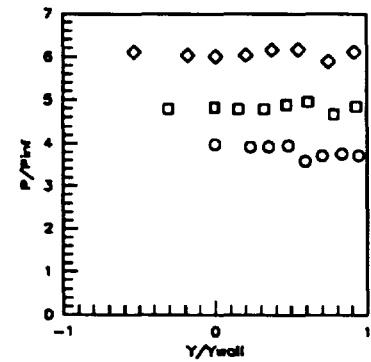
Sym	$x'/T_x'$	Run No.	CR/Re/Cowl (milions)
○	0.2103	run84	3/0.55/ 0%
□	0.2103	run44	5/0.55/ 0%
◇	0.2103	run47	9/0.55/ 0%

Figure 7.2.1.118: CR Effects (Re=0.55million/ft, 0%CowI) Baseplate Pressures



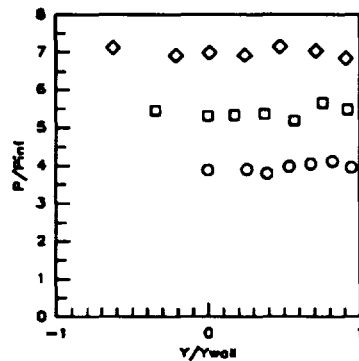
Sym	$x'/T_x'$	Run No.	CR/Re/Cowl (milions)
○	0.3154	run84	3/0.55/ 0%
□	0.3154	run44	5/0.55/ 0%
◇	0.3154	run47	9/0.55/ 0%

Figure 7.2.1.119: CR Effects (Re=0.55million/ft, 0%CowI) Baseplate Pressures



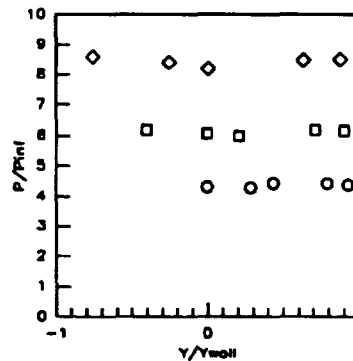
Sym	$x'/T_x'$	Run No.	CR/Re/Cowl (milions)
○	0.4208	run84	3/0.55/ 0%
□	0.4208	run44	5/0.55/ 0%
◇	0.4208	run47	9/0.55/ 0%

Figure 7.2.1.120: CR Effects (Re=0.55million/ft, 0%CowI) Baseplate Pressures



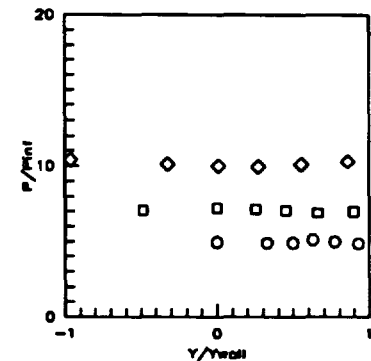
Sym	$x'/T_x'$	Run No.	CR/Re/Cowl (milions)
○	0.5258	run84	3/0.55/ 0%
□	0.5258	run44	5/0.55/ 0%
◇	0.5258	run47	9/0.55/ 0%

Figure 7.2.1.121: CR Effects (Re=0.55million/ft, 0%CowI) Baseplate Pressures



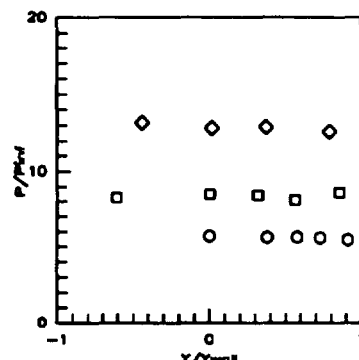
Sym	$x'/T_x'$	Run No.	CR/Re/Cowl (milions)
○	0.6309	run84	3/0.55/ 0%
□	0.6309	run44	5/0.55/ 0%
◇	0.6309	run47	9/0.55/ 0%

Figure 7.2.1.122: CR Effects (Re=0.55million/ft, 0%CowI) Baseplate Pressures



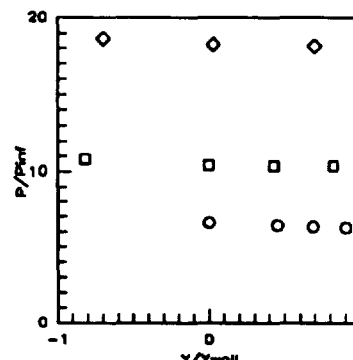
Sym	$x'/T_x'$	Run No.	CR/Re/Cowl (milions)
○	0.7361	run84	3/0.55/ 0%
□	0.7361	run44	5/0.55/ 0%
◇	0.7361	run47	9/0.55/ 0%

Figure 7.2.1.123: CR Effects (Re=0.55million/ft, 0%CowI) Baseplate Pressures



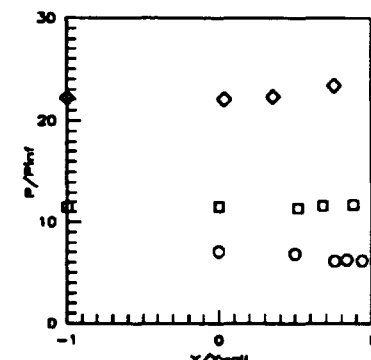
Sym	$x'/T_x'$	Run No.	CR/Re/Cowl (milions)
○	0.8412	run84	3/0.55/ 0%
□	0.8412	run44	5/0.55/ 0%
◇	0.8412	run47	9/0.55/ 0%

Figure 7.2.1.124: CR Effects (Re=0.55million/ft, 0%CowI) Baseplate Pressures



Sym	$x'/T_x'$	Run No.	CR/Re/Cowl (milions)
○	0.9484	run84	3/0.55/ 0%
□	0.9484	run44	5/0.55/ 0%
◇	0.9484	run47	9/0.55/ 0%

Figure 7.2.1.125: CR Effects (Re=0.55million/ft, 0%CowI) Baseplate Pressures



Sym	$x'/T_x'$	Run No.	CR/Re/Cowl (milions)
○	1.0000	run84	3/0.55/ 0%
□	1.0000	run44	5/0.55/ 0%
◇	1.0000	run47	9/0.55/ 0%

Figure 7.2.1.126: CR Effects (Re=0.55million/ft, 0%CowI) Baseplate Pressures

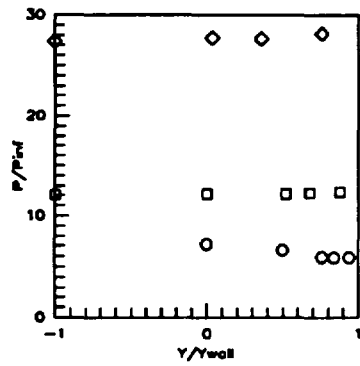


Figure 7.2.1.127: CR Effects  
( $Re=0.55$ million/ft, 0%CowI)  
Baseplate Pressures

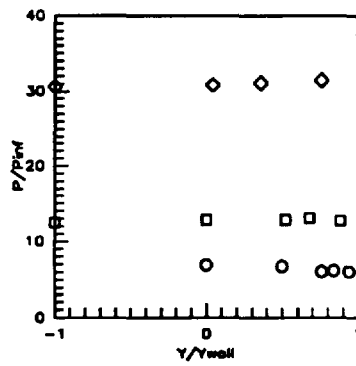


Figure 7.2.1.128: CR Effects  
( $Re=0.55$ million/ft, 0%CowI)  
Baseplate Pressures

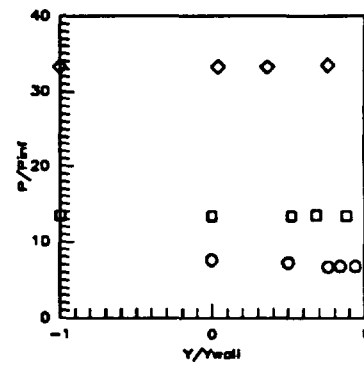


Figure 7.2.1.129: CR Effects  
( $Re=0.55$ million/ft, 0%CowI)  
Baseplate Pressures

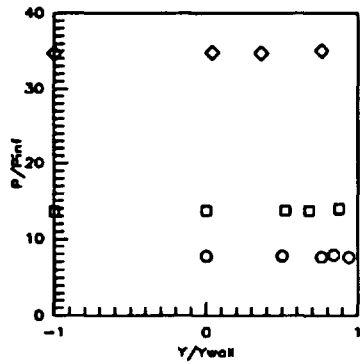


Figure 7.2.1.130: CR Effects  
( $Re=0.55$ million/ft, 0%CowI)  
Baseplate Pressures

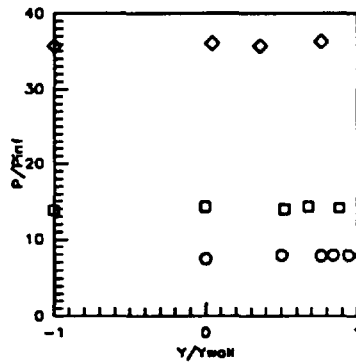


Figure 7.2.1.131: CR Effects  
( $Re=0.55$ million/ft, 0%CowI)  
Baseplate Pressures

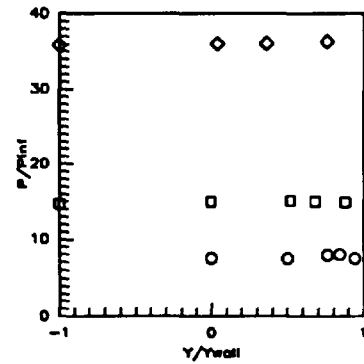


Figure 7.2.1.132: CR Effects  
( $Re=0.55$ million/ft, 0%CowI)  
Baseplate Pressures

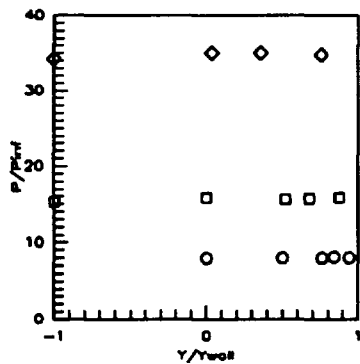


Figure 7.2.1.133: CR Effects  
( $Re=0.55$ million/ft, 0%CowI)  
Baseplate Pressures

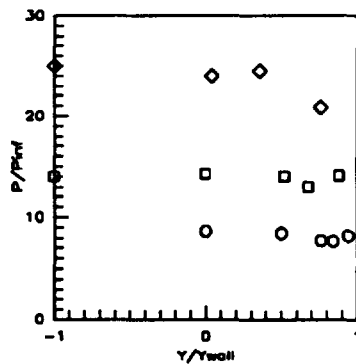


Figure 7.2.1.134: CR Effects  
( $Re=0.55$ million/ft, 0%CowI)  
Baseplate Pressures

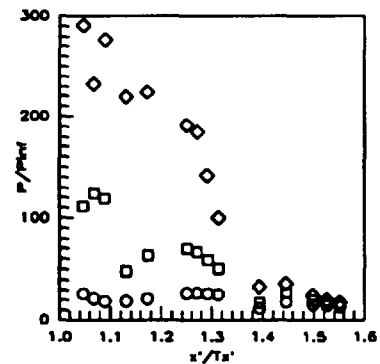
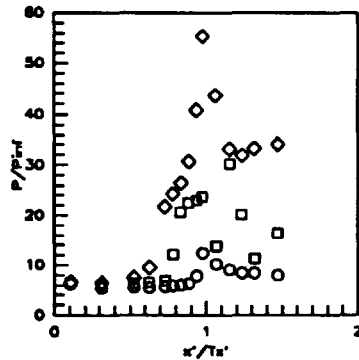
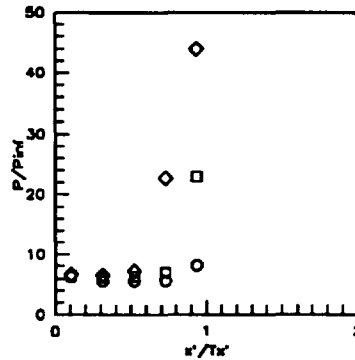


Figure 7.2.1.135: CR Effects  
( $Re=0.55$ million/ft, 0%CowI)  
Cowl Pressures



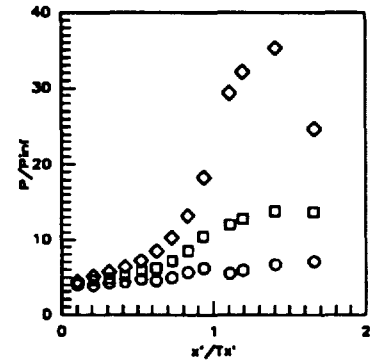
Sym	Z/H	Run No.	CR/Re/Cowl (millions)
○	0.5RT	run84	3/0.55/ 0%
□	0.5RT	run44	5/0.55/ 0%
◇	0.5RT	run47	9/0.55/ 0%

Figure 7.2.1.136: CR Effects (Re=0.55million/ft, 0%Cowl) Sidewall Centerline Pressures



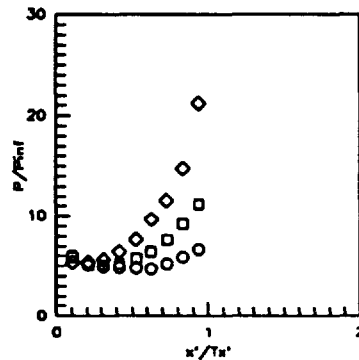
Sym	Z/H	Run No.	CR/Re/Cowl (millions)
○	0.5LT	run84	3/0.55/ 0%
□	0.5LT	run44	5/0.55/ 0%
◇	0.5LT	run47	9/0.55/ 0%

Figure 7.2.1.137: CR Effects (Re=0.55million/ft, 0%Cowl) Sidewall Centerline Pressures



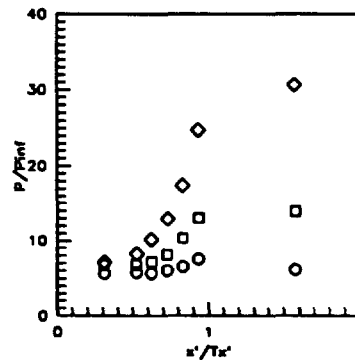
Sym	Z/H	Run No.	CR/Re/Cowl (millions)
○	0.05	run84	3/0.55/ 0%
□	0.05	run44	5/0.55/ 0%
◇	0.05	run47	9/0.55/ 0%

Figure 7.2.1.138: CR Effects (Re=0.55million/ft, 0%Cowl) Sidewall Pressures



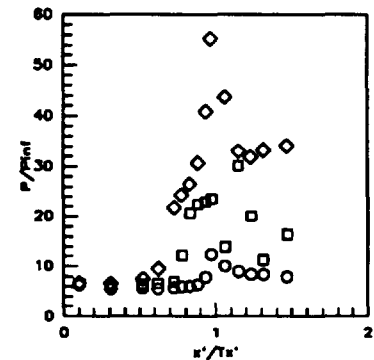
Sym	Z/H	Run No.	CR/Re/Cowl (millions)
○	0.15	run84	3/0.55/ 0%
□	0.15	run44	5/0.55/ 0%
◇	0.15	run47	9/0.55/ 0%

Figure 7.2.1.139: CR Effects (Re=0.55million/ft, 0%Cowl) Sidewall Pressures



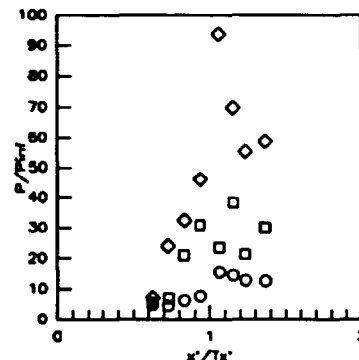
Sym	Z/H	Run No.	CR/Re/Cowl (millions)
○	0.25	run84	3/0.55/ 0%
□	0.25	run44	5/0.55/ 0%
◇	0.25	run47	9/0.55/ 0%

Figure 7.2.1.140: CR Effects (Re=0.55million/ft, 0%Cowl) Sidewall Pressures



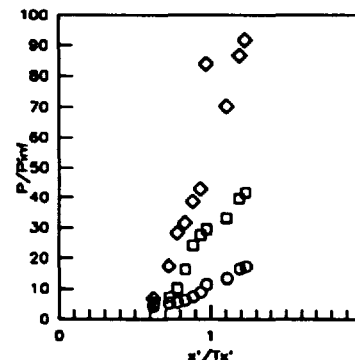
Sym	Z/H	Run No.	CR/Re/Cowl (millions)
○	0.50	run84	3/0.55/ 0%
□	0.50	run44	5/0.55/ 0%
◇	0.50	run47	9/0.55/ 0%

Figure 7.2.1.141: CR Effects (Re=0.55million/ft, 0%Cowl) Sidewall Pressures



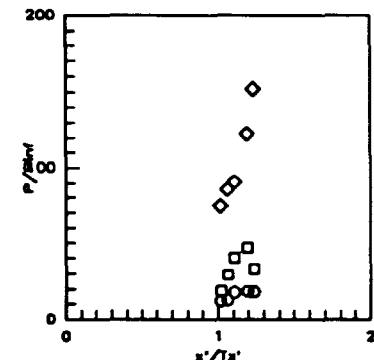
Sym	Z/H	Run No.	CR/Re/Cowl (millions)
○	0.75	run84	3/0.55/ 0%
□	0.75	run44	5/0.55/ 0%
◇	0.75	run47	9/0.55/ 0%

Figure 7.2.1.142: CR Effects (Re=0.55million/ft, 0%Cowl) Sidewall Pressures



Sym	Z/H	Run No.	CR/Re/Cowl (millions)
○	0.85	run84	3/0.55/ 0%
□	0.85	run44	5/0.55/ 0%
◇	0.85	run47	9/0.55/ 0%

Figure 7.2.1.143: CR Effects (Re=0.55million/ft, 0%Cowl) Sidewall Pressures



Sym	Z/H	Run No.	CR/Re/Cowl (millions)
○	0.90	run84	3/0.55/ 0%
□	0.90	run44	5/0.55/ 0%
◇	0.90	run47	9/0.55/ 0%

Figure 7.2.1.144: CR Effects (Re=0.55million/ft, 0%Cowl) Sidewall Pressures

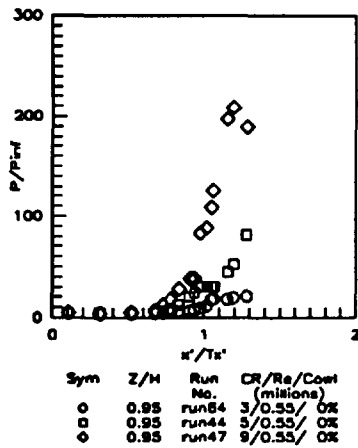


Figure 7.2.1.145: CR Effects (Re=0.55million/ft, 0%CowI) Sidewall Pressures

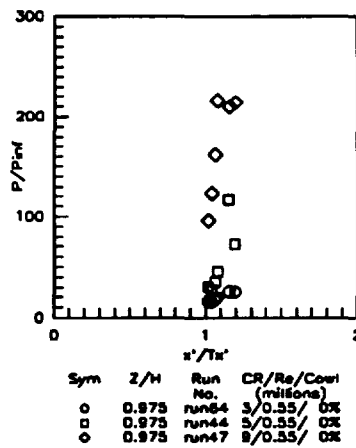


Figure 7.2.1.146: CR Effects (Re=0.55million/ft, 0%CowI) Sidewall Pressures

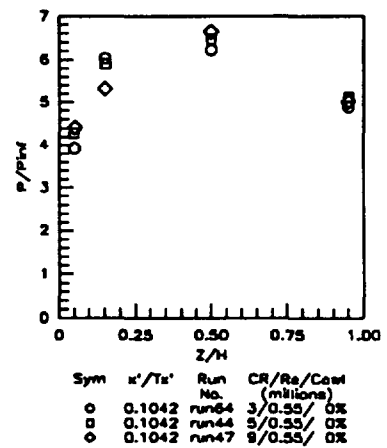


Figure 7.2.1.147: CR Effects (Re=0.55million/ft, 0%CowI) Sidewall Pressures

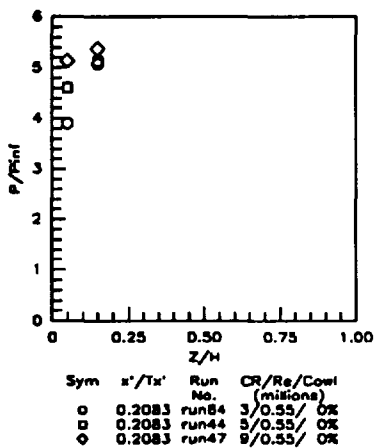


Figure 7.2.1.148: CR Effects (Re=0.55million/ft, 0%CowI) Sidewall Pressures

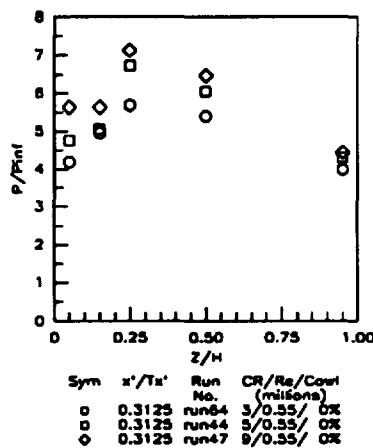


Figure 7.2.1.149: CR Effects (Re=0.55million/ft, 0%CowI) Sidewall Pressures

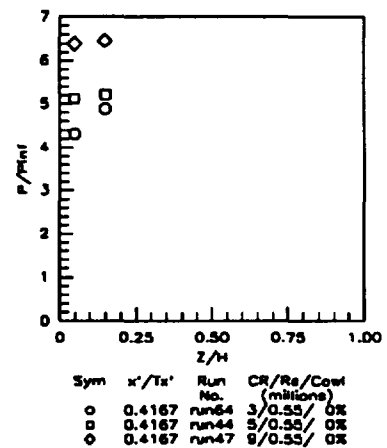


Figure 7.2.1.150: CR Effects (Re=0.55million/ft, 0%CowI) Sidewall Pressures

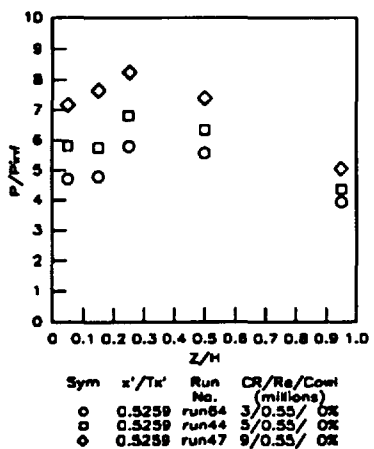


Figure 7.2.1.151: CR Effects (Re=0.55million/ft, 0%CowI) Sidewall Pressures

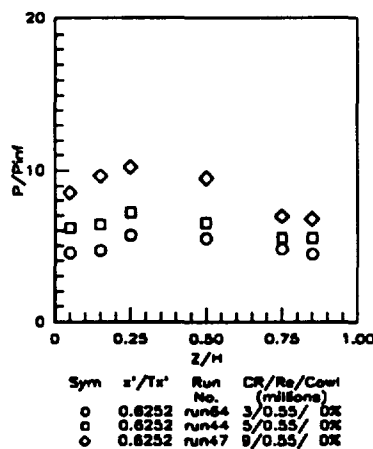


Figure 7.2.1.152: CR Effects (Re=0.55million/ft, 0%CowI) Sidewall Pressures

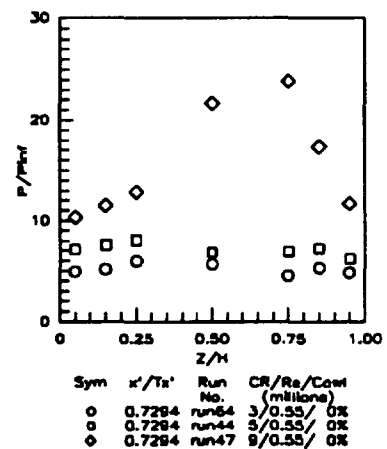
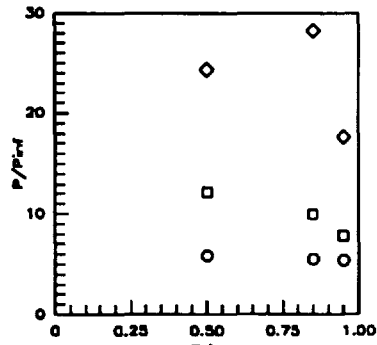
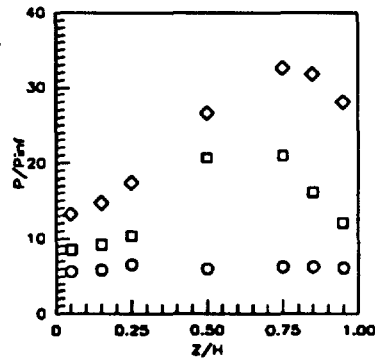


Figure 7.2.1.153: CR Effects (Re=0.55million/ft, 0%CowI) Sidewall Pressures



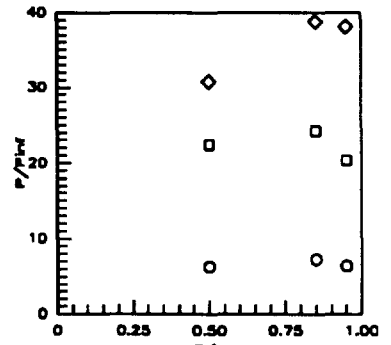
Sym	$x'/T_x'$	Run No.	CR/Re/Cowl (millions)
○	0.7815	run84	3/0.55/ 0%
□	0.7815	run44	5/0.55/ 0%
◇	0.7815	run47	9/0.55/ 0%

Figure 7.2.1.154: CR Effects (Re=0.55million/ft, 0%CowI) Sidewall Pressures



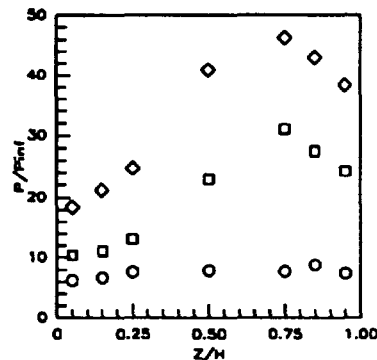
Sym	$x'/T_x'$	Run No.	CR/Re/Cowl (millions)
○	0.8336	run84	3/0.55/ 0%
□	0.8336	run44	5/0.55/ 0%
◇	0.8336	run47	9/0.55/ 0%

Figure 7.2.1.155: CR Effects (Re=0.55million/ft, 0%CowI) Sidewall Pressures



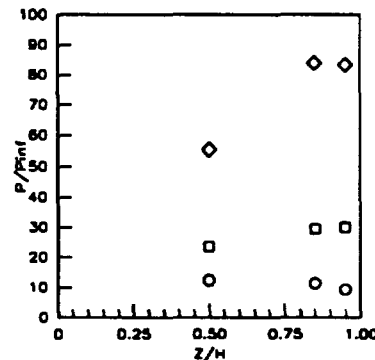
Sym	$x'/T_x'$	Run No.	CR/Re/Cowl (millions)
○	0.8857	run84	3/0.55/ 0%
□	0.8857	run44	5/0.55/ 0%
◇	0.8857	run47	9/0.55/ 0%

Figure 7.2.1.156: CR Effects (Re=0.55million/ft, 0%CowI) Sidewall Pressures



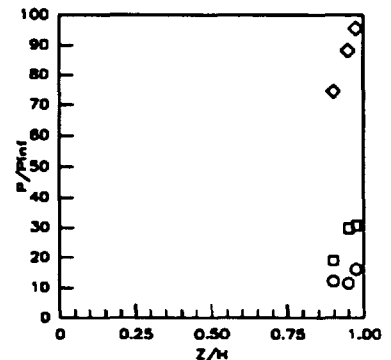
Sym	$x'/T_x'$	Run No.	CR/Re/Cowl (millions)
○	0.9378	run84	3/0.55/ 0%
□	0.9378	run44	5/0.55/ 0%
◇	0.9378	run47	9/0.55/ 0%

Figure 7.2.1.157: CR Effects (Re=0.55million/ft, 0%CowI) Sidewall Pressures



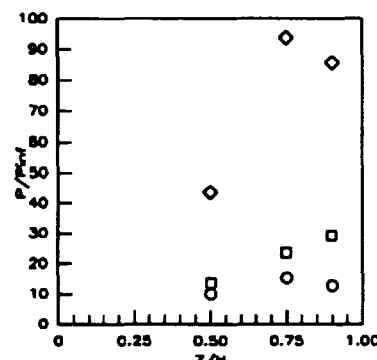
Sym	$x'/T_x'$	Run No.	CR/Re/Cowl (millions)
○	0.9751	run84	3/0.55/ 0%
□	0.9751	run44	5/0.55/ 0%
◇	0.9751	run47	9/0.55/ 0%

Figure 7.2.1.158: CR Effects (Re=0.55million/ft, 0%CowI) Sidewall Pressures



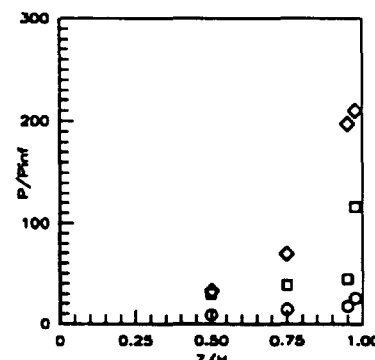
Sym	$x'/T_x'$	Run No.	CR/Re/Cowl (millions)
○	1.0187	run84	3/0.55/ 0%
□	1.0187	run44	5/0.55/ 0%
◇	1.0187	run47	9/0.55/ 0%

Figure 7.2.1.159: CR Effects (Re=0.55million/ft, 0%CowI) Sidewall Pressures



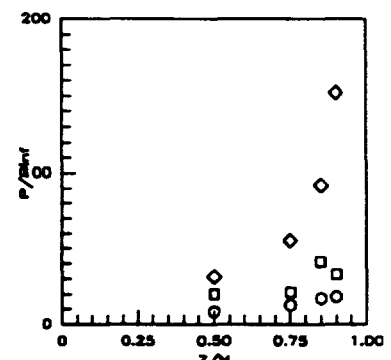
Sym	$x'/T_x'$	Run No.	CR/Re/Cowl (millions)
○	1.0843	run84	3/0.55/ 0%
□	1.0843	run44	5/0.55/ 0%
◇	1.0843	run47	9/0.55/ 0%

Figure 7.2.1.160: CR Effects (Re=0.55million/ft, 0%CowI) Sidewall Pressures



Sym	$x'/T_x'$	Run No.	CR/Re/Cowl (millions)
○	1.1537	run84	3/0.55/ 0%
□	1.1537	run44	5/0.55/ 0%
◇	1.1537	run47	9/0.55/ 0%

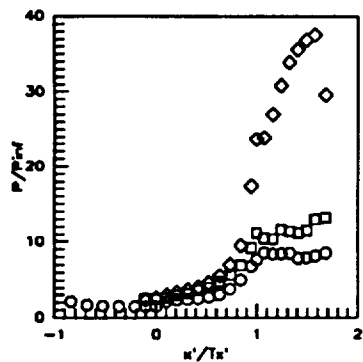
Figure 7.2.1.161: CR Effects (Re=0.55million/ft, 0%CowI) Sidewall Pressures



Sym	$x'/T_x'$	Run No.	CR/Re/Cowl (millions)
○	1.2356	run84	3/0.55/ 0%
□	1.2356	run44	5/0.55/ 0%
◇	1.2356	run47	9/0.55/ 0%

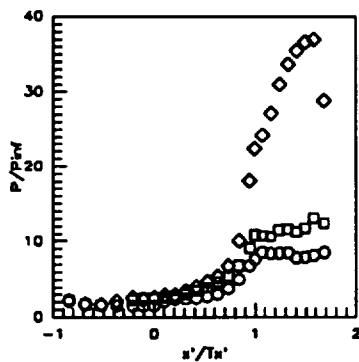
Figure 7.2.1.162: CR Effects (Re=0.55million/ft, 0%CowI) Sidewall Pressures





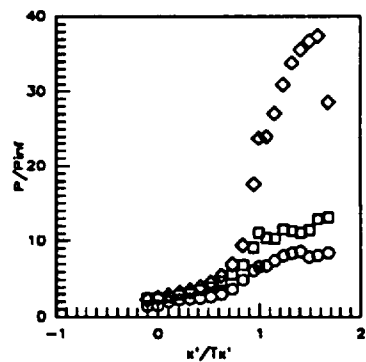
Sym	C.L. for	Run No.	CR/Re/CowI (millions)
○	CR=3	run62	3/2.15/25%
□	CR=5	run43	5/2.15/25%
◇	CR=9	run53	9/2.15/25%

Figure 7.2.1.163: CR Effects (Re=2.15million/ft, 25%CowI) Centerline Pressures



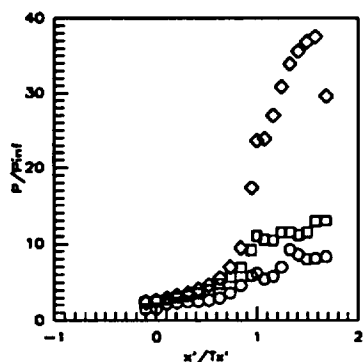
Sym	C.L. for	Run No.	CR/Re/CowI (millions)
○	CR=3	run62	3/2.15/25%
□	CR=3	run43	5/2.15/25%
◇	CR=3	run53	9/2.15/25%

Figure 7.2.1.164: CR Effects (Re=2.15million/ft, 25%CowI) CR=3 Centerline Pressures



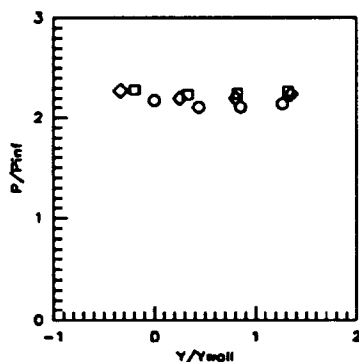
Sym	C.L. for	Run No.	CR/Re/CowI (millions)
○	CR=5	run62	3/2.15/25%
□	CR=5	run43	5/2.15/25%
◇	CR=5	run53	9/2.15/25%

Figure 7.2.1.165: CR Effects (Re=2.15million/ft, 25%CowI) CR=5 Centerline Pressures



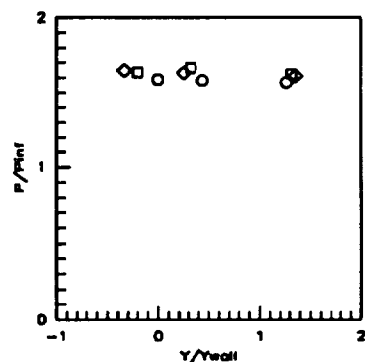
Sym	C.L. for	Run No.	CR/Re/CowI (millions)
○	CR=9	run62	3/2.15/25%
□	CR=9	run43	5/2.15/25%
◇	CR=9	run53	9/2.15/25%

Figure 7.2.1.166: CR Effects (Re=2.15million/ft, 25%CowI) CR=9 Centerline Pressures



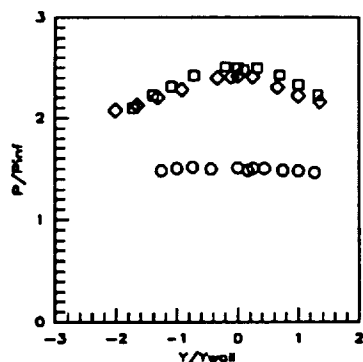
Sym	x'/Ts'	Run No.	CR/Re/CowI (millions)
○	-0.8412	run62	3/2.15/25%
□	-0.8412	run43	5/2.15/25%
◇	-0.8412	run53	9/2.15/25%

Figure 7.2.1.167: CR Effects (Re=2.15million/ft, 25%CowI) Baseplate Pressures



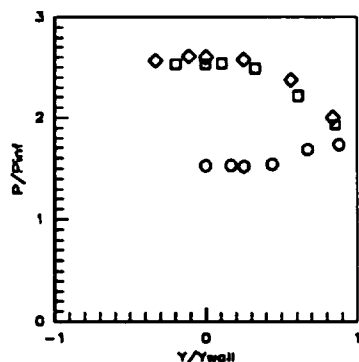
Sym	x'/Ts'	Run No.	CR/Re/CowI (millions)
○	-0.5258	run62	3/2.15/25%
□	-0.5258	run43	5/2.15/25%
◇	-0.5258	run53	9/2.15/25%

Figure 7.2.1.168: CR Effects (Re=2.15million/ft, 25%CowI) Baseplate Pressures



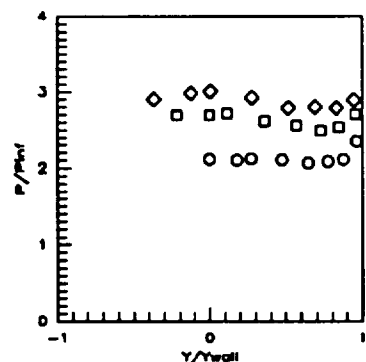
Sym	x'/Ts'	Run No.	CR/Re/CowI (millions)
○	-0.1052	run62	3/2.15/25%
□	-0.1052	run43	5/2.15/25%
◇	-0.1052	run53	9/2.15/25%

Figure 7.2.1.169: CR Effects (Re=2.15million/ft, 25%CowI) Baseplate Pressures



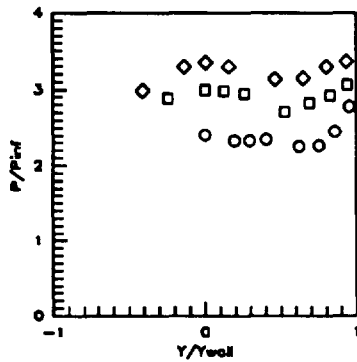
Sym	x'/Ts'	Run No.	CR/Re/CowI (millions)
○	0.0000	run62	3/2.15/25%
□	0.0000	run43	5/2.15/25%
◇	0.0000	run53	9/2.15/25%

Figure 7.2.1.170: CR Effects (Re=2.15million/ft, 25%CowI) Baseplate Pressures



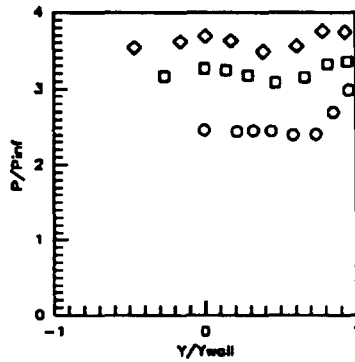
Sym	x'/Ts'	Run No.	CR/Re/CowI (millions)
○	0.1052	run62	3/2.15/25%
□	0.1052	run43	5/2.15/25%
◇	0.1052	run53	9/2.15/25%

Figure 7.2.1.171: CR Effects (Re=2.15million/ft, 25%CowI) Baseplate Pressures



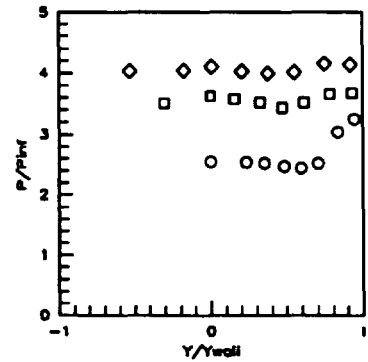
Sym	$x'/T_x'$	Run No.	CR/Re/CowI (millions)
○	0.2103	run62	3/2.15/25%
□	0.2103	run43	5/2.15/25%
◇	0.2103	run53	9/2.15/25%

Figure 7.2.1.172: CR Effects (Re=2.15million/ft, 25%CowI) Baseplate Pressures



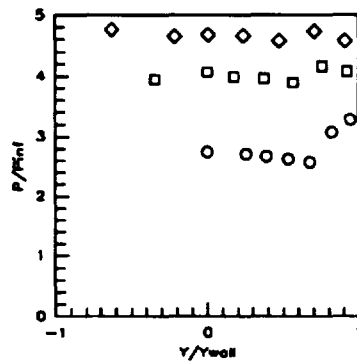
Sym	$x'/T_x'$	Run No.	CR/Re/CowI (millions)
○	0.3154	run62	3/2.15/25%
□	0.3154	run43	5/2.15/25%
◇	0.3154	run53	9/2.15/25%

Figure 7.2.1.173: CR Effects (Re=2.15million/ft, 25%CowI) Baseplate Pressures



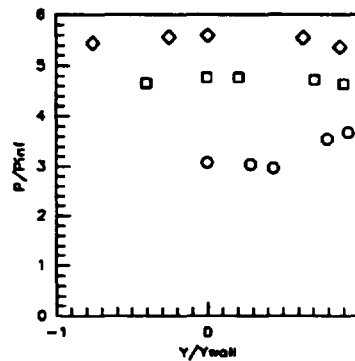
Sym	$x'/T_x'$	Run No.	CR/Re/CowI (millions)
○	0.4206	run62	3/2.15/25%
□	0.4206	run43	5/2.15/25%
◇	0.4206	run53	9/2.15/25%

Figure 7.2.1.174: CR Effects (Re=2.15million/ft, 25%CowI) Baseplate Pressures



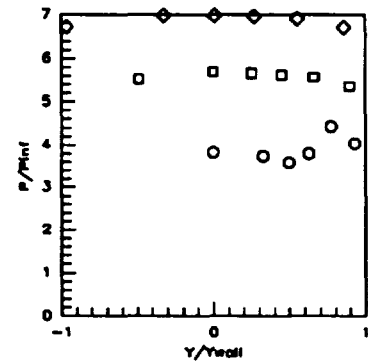
Sym	$x'/T_x'$	Run No.	CR/Re/CowI (millions)
○	0.5258	run62	3/2.15/25%
□	0.5258	run43	5/2.15/25%
◇	0.5258	run53	9/2.15/25%

Figure 7.2.1.175: CR Effects (Re=2.15million/ft, 25%CowI) Baseplate Pressures



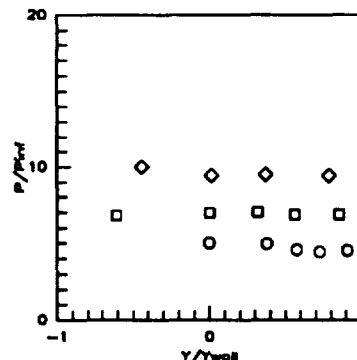
Sym	$x'/T_x'$	Run No.	CR/Re/CowI (millions)
○	0.6309	run62	3/2.15/25%
□	0.6309	run43	5/2.15/25%
◇	0.6309	run53	9/2.15/25%

Figure 7.2.1.176: CR Effects (Re=2.15million/ft, 25%CowI) Baseplate Pressures



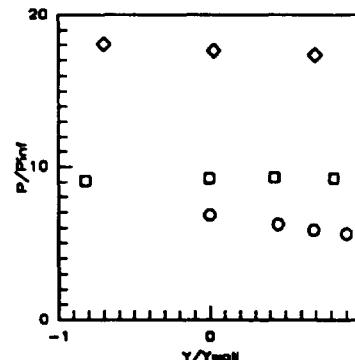
Sym	$x'/T_x'$	Run No.	CR/Re/CowI (millions)
○	0.7361	run62	3/2.15/25%
□	0.7361	run43	5/2.15/25%
◇	0.7361	run53	9/2.15/25%

Figure 7.2.1.177: CR Effects (Re=2.15million/ft, 25%CowI) Baseplate Pressures



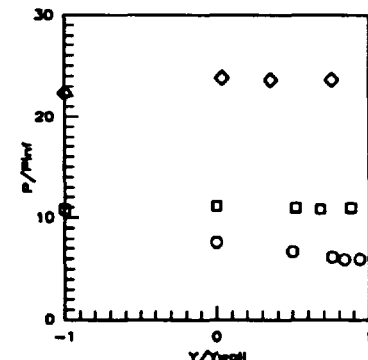
Sym	$x'/T_x'$	Run No.	CR/Re/CowI (millions)
○	0.8412	run62	3/2.15/25%
□	0.8412	run43	5/2.15/25%
◇	0.8412	run53	9/2.15/25%

Figure 7.2.1.178: CR Effects (Re=2.15million/ft, 25%CowI) Baseplate Pressures



Sym	$x'/T_x'$	Run No.	CR/Re/CowI (millions)
○	0.9464	run62	3/2.15/25%
□	0.9464	run43	5/2.15/25%
◇	0.9464	run53	9/2.15/25%

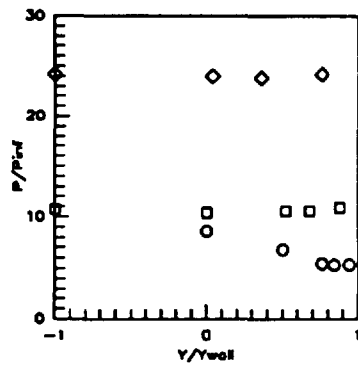
Figure 7.2.1.179: CR Effects (Re=2.15million/ft, 25%CowI) Baseplate Pressures



Sym	$x'/T_x'$	Run No.	CR/Re/CowI (millions)
○	1.0000	run62	3/2.15/25%
□	1.0000	run43	5/2.15/25%
◇	1.0000	run53	9/2.15/25%

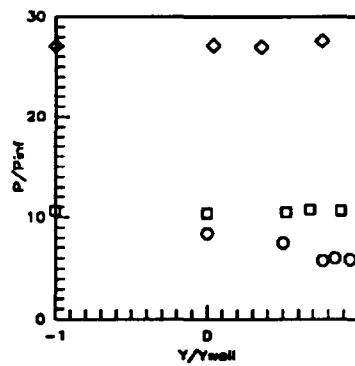
Figure 7.2.1.180: CR Effects (Re=2.15million/ft, 25%CowI) Baseplate Pressures

C<sub>v</sub>6



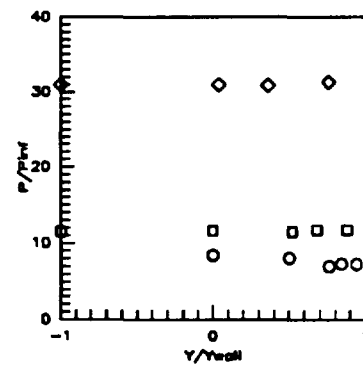
Sym	$x'/T_x'$	Run No.	CR/Re/Cowl (milions)
○	1.0726	run62	3/2.15/25%
□	1.0726	run43	5/2.15/25%
◇	1.0726	run53	9/2.15/25%

Figure 7.2.1.181: CR Effects (Re=2.15million/ft, 25%Cow) Baseplate Pressures



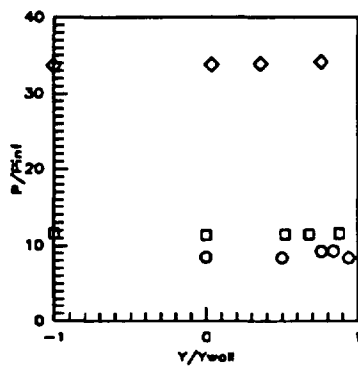
Sym	$x'/T_x'$	Run No.	CR/Re/Cowl (milions)
○	1.1567	run62	3/2.15/25%
□	1.1567	run43	5/2.15/25%
◇	1.1567	run53	9/2.15/25%

Figure 7.2.1.182: CR Effects (Re=2.15million/ft, 25%Cow) Baseplate Pressures



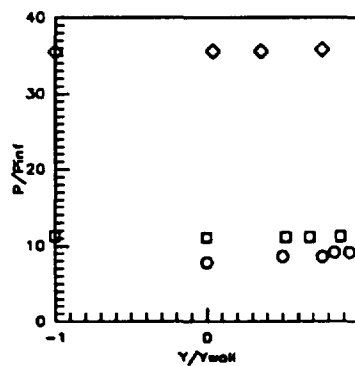
Sym	$x'/T_x'$	Run No.	CR/Re/Cowl (milions)
○	1.2408	run62	3/2.15/25%
□	1.2408	run43	5/2.15/25%
◇	1.2408	run53	9/2.15/25%

Figure 7.2.1.183: CR Effects (Re=2.15million/ft, 25%Cow) Baseplate Pressures



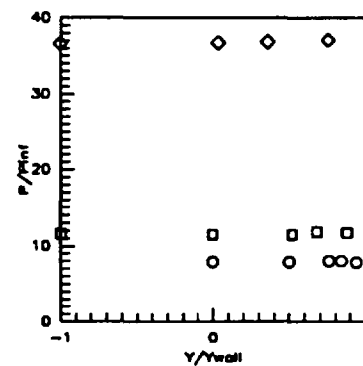
Sym	$x'/T_x'$	Run No.	CR/Re/Cowl (milions)
○	1.3249	run62	3/2.15/25%
□	1.3249	run43	5/2.15/25%
◇	1.3249	run53	9/2.15/25%

Figure 7.2.1.184: CR Effects (Re=2.15million/ft, 25%Cow) Baseplate Pressures



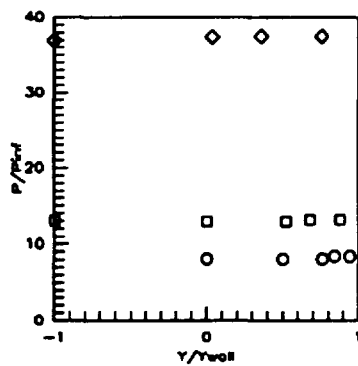
Sym	$x'/T_x'$	Run No.	CR/Re/Cowl (milions)
○	1.4090	run62	3/2.15/25%
□	1.4090	run43	5/2.15/25%
◇	1.4090	run53	9/2.15/25%

Figure 7.2.1.185: CR Effects (Re=2.15million/ft, 25%Cow) Baseplate Pressures



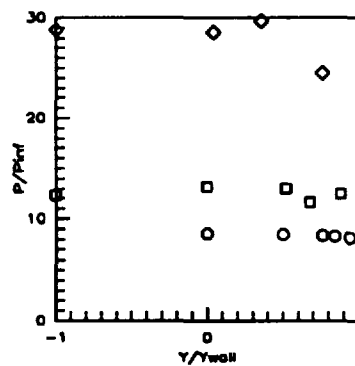
Sym	$x'/T_x'$	Run No.	CR/Re/Cowl (milions)
○	1.4932	run62	3/2.15/25%
□	1.4932	run43	5/2.15/25%
◇	1.4932	run53	9/2.15/25%

Figure 7.2.1.186: CR Effects (Re=2.15million/ft, 25%Cow) Baseplate Pressures



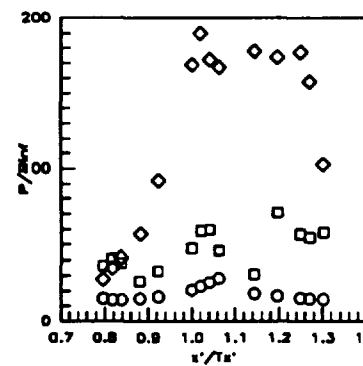
Sym	$x'/T_x'$	Run No.	CR/Re/Cowl (milions)
○	1.5773	run62	3/2.15/25%
□	1.5773	run43	5/2.15/25%
◇	1.5773	run53	9/2.15/25%

Figure 7.2.1.187: CR Effects (Re=2.15million/ft, 25%Cow) Baseplate Pressures



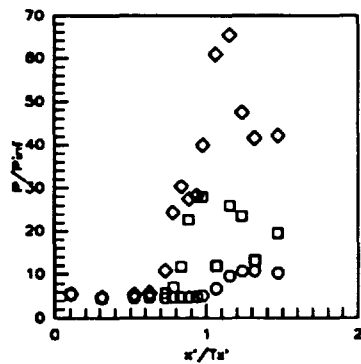
Sym	$x'/T_x'$	Run No.	CR/Re/Cowl (milions)
○	1.6824	run62	3/2.15/25%
□	1.6824	run43	5/2.15/25%
◇	1.6824	run53	9/2.15/25%

Figure 7.2.1.188: CR Effects (Re=2.15million/ft, 25%Cow) Baseplate Pressures



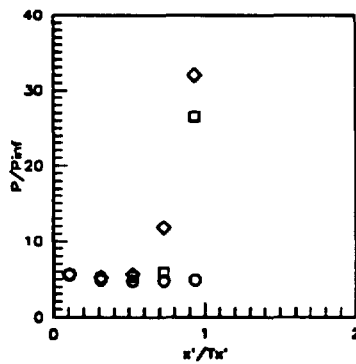
Sym	Cowl Pos.	Run No.	CR/Re/Cowl (milions)
○	25%	run62	3/2.15/25%
□	25%	run43	5/2.15/25%
◇	25%	run53	9/2.15/25%

Figure 7.2.1.189: CR Effects (Re=2.15million/ft, 25%Cow) Cowl Pressures



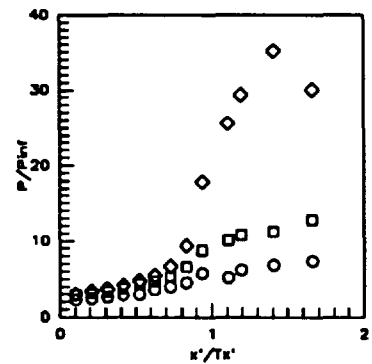
Sym	Z/H	Run No.	CR/Re/Cowl (millions)
○	0.5RT	run62	3/2.15/25%
□	0.5RT	run43	5/2.15/25%
◇	0.5RT	run53	9/2.15/25%

Figure 7.2.1.190: CR Effects (Re=2.15million/ft, 25%Cowl) Sidewall Centerline Pressures



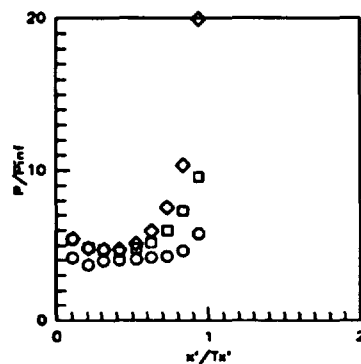
Sym	Z/H	Run No.	CR/Re/Cowl (millions)
○	0.5LT	run62	3/2.15/25%
□	0.5LT	run43	5/2.15/25%
◇	0.5LT	run53	9/2.15/25%

Figure 7.2.1.191: CR Effects (Re=2.15million/ft, 25%Cowl) Sidewall Centerline Pressures



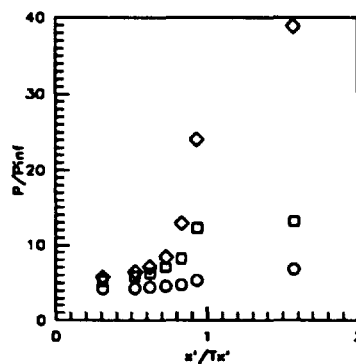
Sym	Z/H	Run No.	CR/Re/Cowl (millions)
○	0.05	run62	3/2.15/25%
□	0.05	run43	5/2.15/25%
◇	0.05	run53	9/2.15/25%

Figure 7.2.1.192: CR Effects (Re=2.15million/ft, 25%Cowl) Sidewall Pressures



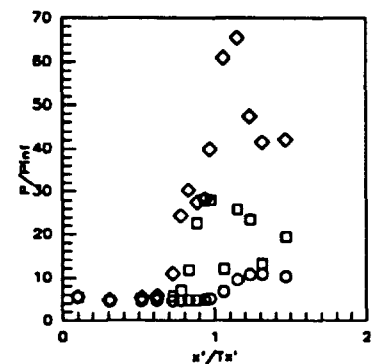
Sym	Z/H	Run No.	CR/Re/Cowl (millions)
○	0.15	run62	3/2.15/25%
□	0.15	run43	5/2.15/25%
◇	0.15	run53	9/2.15/25%

Figure 7.2.1.193: CR Effects (Re=2.15million/ft, 25%Cowl) Sidewall Pressures



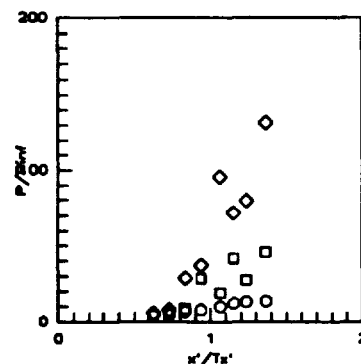
Sym	Z/H	Run No.	CR/Re/Cowl (millions)
○	0.25	run62	3/2.15/25%
□	0.25	run43	5/2.15/25%
◇	0.25	run53	9/2.15/25%

Figure 7.2.1.194: CR Effects (Re=2.15million/ft, 25%Cowl) Sidewall Pressures



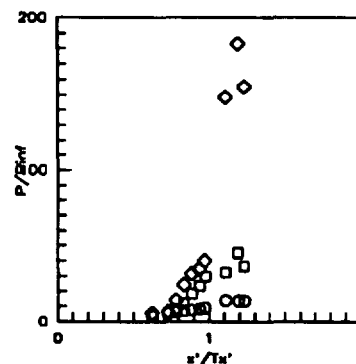
Sym	Z/H	Run No.	CR/Re/Cowl (millions)
○	0.50	run62	3/2.15/25%
□	0.50	run43	5/2.15/25%
◇	0.50	run53	9/2.15/25%

Figure 7.2.1.195: CR Effects (Re=2.15million/ft, 25%Cowl) Sidewall Pressures



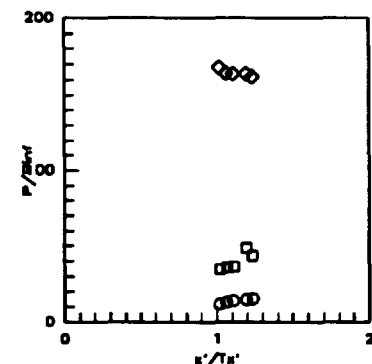
Sym	Z/H	Run No.	CR/Re/Cowl (millions)
○	0.75	run62	3/2.15/25%
□	0.75	run43	5/2.15/25%
◇	0.75	run53	9/2.15/25%

Figure 7.2.1.196: CR Effects (Re=2.15million/ft, 25%Cowl) Sidewall Pressures



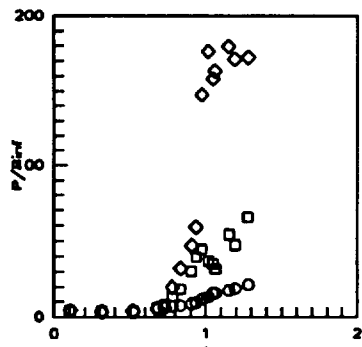
Sym	Z/H	Run No.	CR/Re/Cowl (millions)
○	0.85	run62	3/2.15/25%
□	0.85	run43	5/2.15/25%
◇	0.85	run53	9/2.15/25%

Figure 7.2.1.197: CR Effects (Re=2.15million/ft, 25%Cowl) Sidewall Pressures



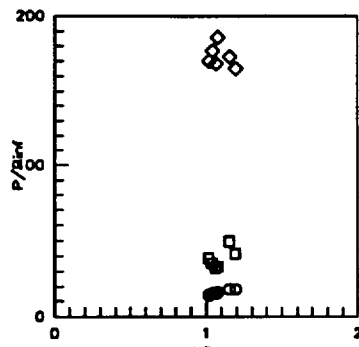
Sym	Z/H	Run No.	CR/Re/Cowl (millions)
○	0.90	run62	3/2.15/25%
□	0.90	run43	5/2.15/25%
◇	0.90	run53	9/2.15/25%

Figure 7.2.1.198: CR Effects (Re=2.15million/ft, 25%Cowl) Sidewall Pressures



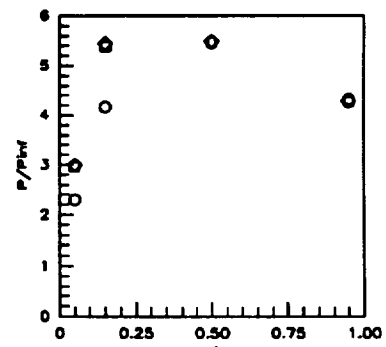
Sym	Z/H	Run No.	CR/Re/Cowl (milions)
○	0.95	run62	3/2.15/25%
□	0.95	run43	5/2.15/25%
◇	0.95	run53	9/2.15/25%

Figure 7.2.1.199: CR Effects (Re=2.15million/ft, 25%CowI) Sidewall Pressures



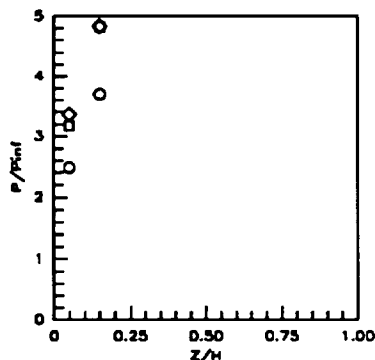
Sym	Z/H	Run No.	CR/Re/Cowl (milions)
○	0.975	run62	3/2.15/25%
□	0.975	run43	5/2.15/25%
◇	0.975	run53	9/2.15/25%

Figure 7.2.1.200: CR Effects (Re=2.15million/ft, 25%CowI) Sidewall Pressures



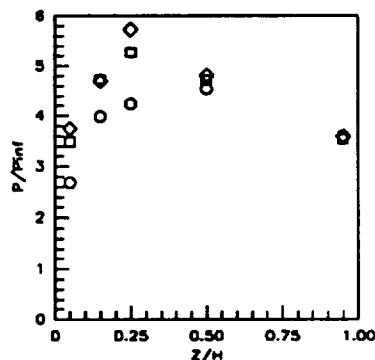
Sym	x'/Ts'	Run No.	CR/Re/Cowl (milions)
○	0.1042	run62	3/2.15/25%
□	0.1042	run43	5/2.15/25%
◇	0.1042	run53	9/2.15/25%

Figure 7.2.1.201: CR Effects (Re=2.15million/ft, 25%CowI) Sidewall Pressures



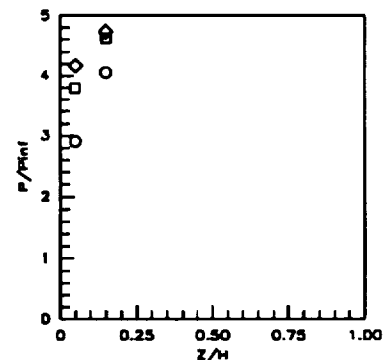
Sym	x'/Ts'	Run No.	CR/Re/Cowl (milions)
○	0.2083	run62	3/2.15/25%
□	0.2083	run43	5/2.15/25%
◇	0.2083	run53	9/2.15/25%

Figure 7.2.1.202: CR Effects (Re=2.15million/ft, 25%CowI) Sidewall Pressures



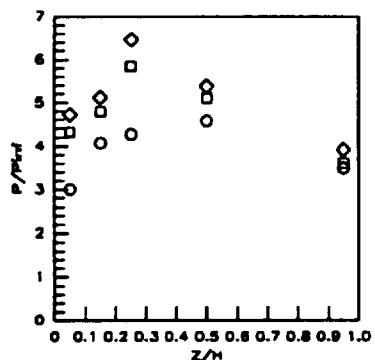
Sym	x'/Ts'	Run No.	CR/Re/Cowl (milions)
○	0.3125	run62	3/2.15/25%
□	0.3125	run43	5/2.15/25%
◇	0.3125	run53	9/2.15/25%

Figure 7.2.1.203: CR Effects (Re=2.15million/ft, 25%CowI) Sidewall Pressures



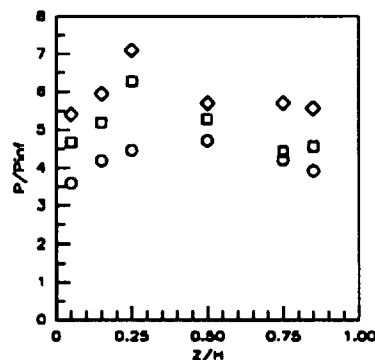
Sym	x'/Ts'	Run No.	CR/Re/Cowl (milions)
○	0.4167	run62	3/2.15/25%
□	0.4167	run43	5/2.15/25%
◇	0.4167	run53	9/2.15/25%

Figure 7.2.1.204: CR Effects (Re=2.15million/ft, 25%CowI) Sidewall Pressures



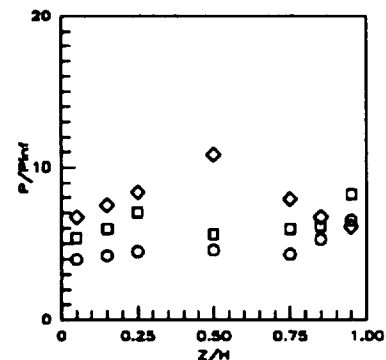
Sym	x'/Ts'	Run No.	CR/Re/Cowl (milions)
○	0.5258	run62	3/2.15/25%
□	0.5258	run43	5/2.15/25%
◇	0.5258	run53	9/2.15/25%

Figure 7.2.1.205: CR Effects (Re=2.15million/ft, 25%CowI) Sidewall Pressures



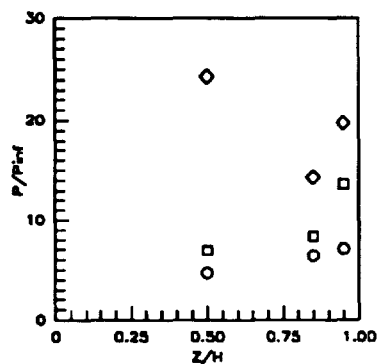
Sym	x'/Ts'	Run No.	CR/Re/Cowl (milions)
○	0.6252	run62	3/2.15/25%
□	0.6252	run43	5/2.15/25%
◇	0.6252	run53	9/2.15/25%

Figure 7.2.1.206: CR Effects (Re=2.15million/ft, 25%CowI) Sidewall Pressures



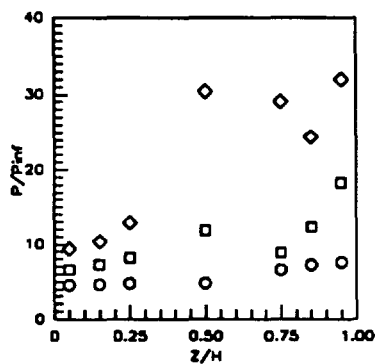
Sym	x'/Ts'	Run No.	CR/Re/Cowl (milions)
○	0.7294	run62	3/2.15/25%
□	0.7294	run43	5/2.15/25%
◇	0.7294	run53	9/2.15/25%

Figure 7.2.1.207: CR Effects (Re=2.15million/ft, 25%CowI) Sidewall Pressures



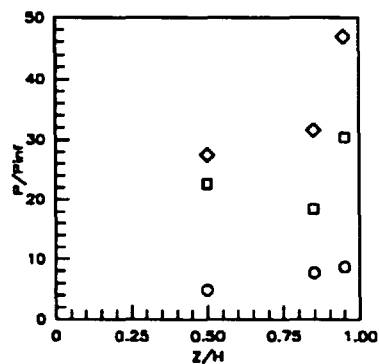
Sym	$x'/T_x'$	Run No.	CR/Re/Cowl (millions)
○	0.7815	run62	3/2.15/25%
□	0.7815	run43	5/2.15/25%
◇	0.7815	run53	9/2.15/25%

Figure 7.2.1.208: CR Effects  
( $Re=2.15$ million/ft, 25%CowI)  
Sidewall Pressures



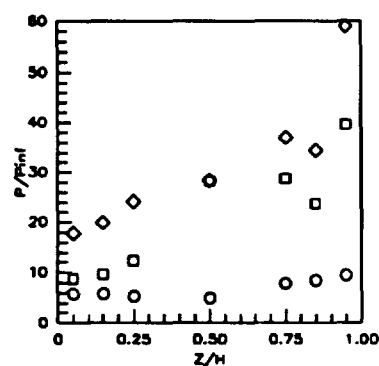
Sym	$x'/T_x'$	Run No.	CR/Re/Cowl (millions)
○	0.8336	run62	3/2.15/25%
□	0.8336	run43	5/2.15/25%
◇	0.8336	run53	9/2.15/25%

Figure 7.2.1.209: CR Effects  
( $Re=2.15$ million/ft, 25%CowI)  
Sidewall Pressures



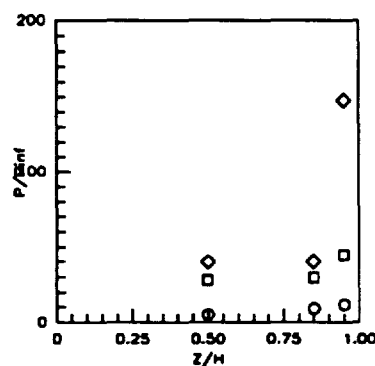
Sym	$x'/T_x'$	Run No.	CR/Re/Cowl (millions)
○	0.8857	run62	3/2.15/25%
□	0.8857	run43	5/2.15/25%
◇	0.8857	run53	9/2.15/25%

Figure 7.2.1.210: CR Effects  
( $Re=2.15$ million/ft, 25%CowI)  
Sidewall Pressures



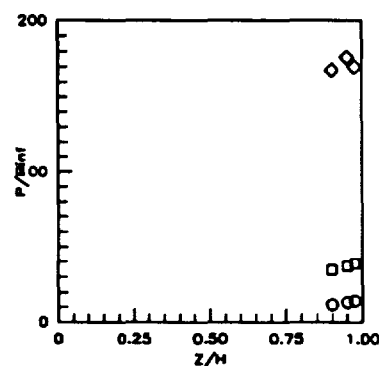
Sym	$x'/T_x'$	Run No.	CR/Re/Cowl (millions)
○	0.9378	run62	3/2.15/25%
□	0.9378	run43	5/2.15/25%
◇	0.9378	run53	9/2.15/25%

Figure 7.2.1.211: CR Effects  
( $Re=2.15$ million/ft, 25%CowI)  
Sidewall Pressures



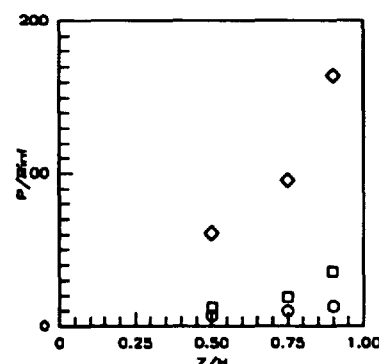
Sym	$x'/T_x'$	Run No.	CR/Re/Cowl (millions)
○	0.9751	run62	3/2.15/25%
□	0.9751	run43	5/2.15/25%
◇	0.9751	run53	9/2.15/25%

Figure 7.2.1.212: CR Effects  
( $Re=2.15$ million/ft, 25%CowI)  
Sidewall Pressures



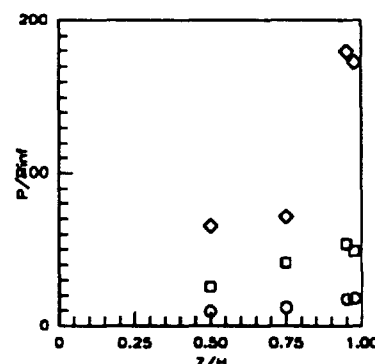
Sym	$x'/T_x'$	Run No.	CR/Re/Cowl (millions)
○	1.0187	run62	3/2.15/25%
□	1.0187	run43	5/2.15/25%
◇	1.0187	run53	9/2.15/25%

Figure 7.2.1.213: CR Effects  
( $Re=2.15$ million/ft, 25%CowI)  
Sidewall Pressures



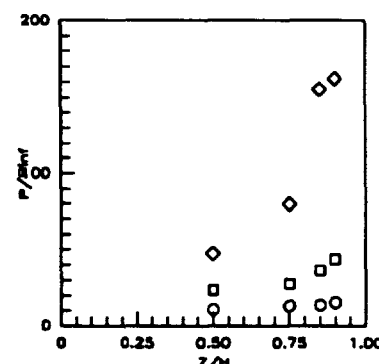
Sym	$x'/T_x'$	Run No.	CR/Re/Cowl (millions)
○	1.0843	run62	3/2.15/25%
□	1.0843	run43	5/2.15/25%
◇	1.0843	run53	9/2.15/25%

Figure 7.2.1.214: CR Effects  
( $Re=2.15$ million/ft, 25%CowI)  
Sidewall Pressures



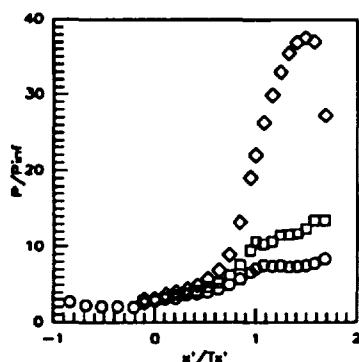
Sym	$x'/T_x'$	Run No.	CR/Re/Cowl (millions)
○	1.1537	run62	3/2.15/25%
□	1.1537	run43	5/2.15/25%
◇	1.1537	run53	9/2.15/25%

Figure 7.2.1.215: CR Effects  
( $Re=2.15$ million/ft, 25%CowI)  
Sidewall Pressures



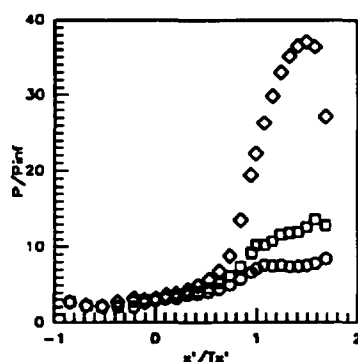
Sym	$x'/T_x'$	Run No.	CR/Re/Cowl (millions)
○	1.2358	run62	3/2.15/25%
□	1.2358	run43	5/2.15/25%
◇	1.2358	run53	9/2.15/25%

Figure 7.2.1.218: CR Effects  
( $Re=2.15$ million/ft, 25%CowI)  
Sidewall Pressures



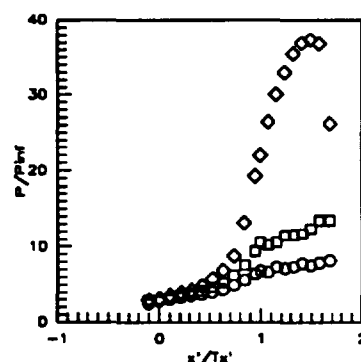
Sym	C.L.	Run	CR/Re/Cowl
	for	No.	(milsions)
o	CR=3	run83	3/1.14/25%
□	CR=5	run42	5/1.14/25%
◇	CR=9	run52	9/1.14/25%

Figure 7.2.1.217: CR Effects  
(Re=1.14million/ft, 25%CowI)  
Centerline Pressures



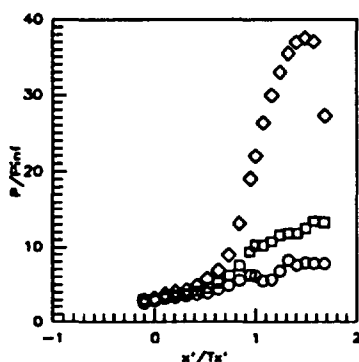
Sym	C.L.	Run	CR/Re/Cowl
	for	No.	(milsions)
o	CR=3	run83	3/1.14/25%
□	CR=3	run42	5/1.14/25%
◇	CR=3	run52	9/1.14/25%

Figure 7.2.1.218: CR Effects  
(Re=1.14million/ft, 25%CowI)  
CR=3 Centerline Pressures



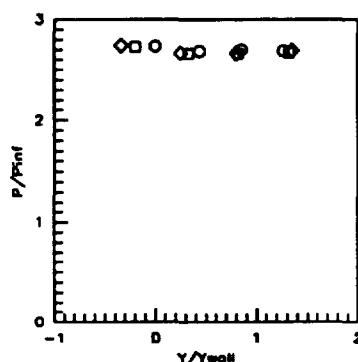
Sym	C.L.	Run	CR/Re/Cowl
	for	No.	(milsions)
o	CR=5	run83	3/1.14/25%
□	CR=5	run42	5/1.14/25%
◇	CR=5	run52	9/1.14/25%

Figure 7.2.1.219: CR Effects  
(Re=1.14million/ft, 25%CowI)  
CR=5 Centerline Pressures



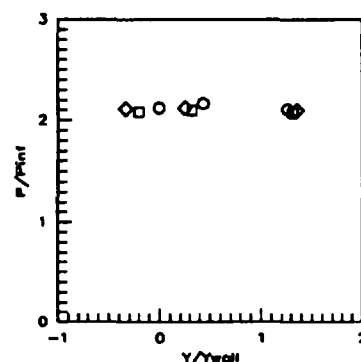
Sym	C.L.	Run	CR/Re/Cowl
	for	No.	(milsions)
o	CR=9	run83	3/1.14/25%
□	CR=9	run42	5/1.14/25%
◇	CR=9	run52	9/1.14/25%

Figure 7.2.1.220: CR Effects  
(Re=1.14million/ft, 25%CowI)  
CR=9 Centerline Pressures



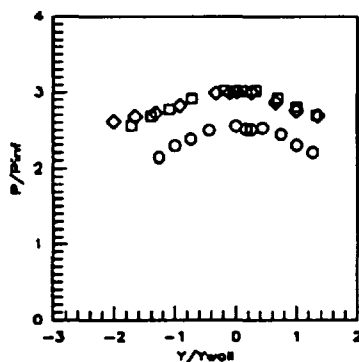
Sym	x'/Ts'	Run	CR/Re/Cowl
		No.	(milsions)
o	-0.8412	run83	3/1.14/25%
□	-0.8412	run42	5/1.14/25%
◇	-0.8412	run52	9/1.14/25%

Figure 7.2.1.221: CR Effects  
(Re=1.14million/ft, 25%CowI)  
Baseplate Pressures



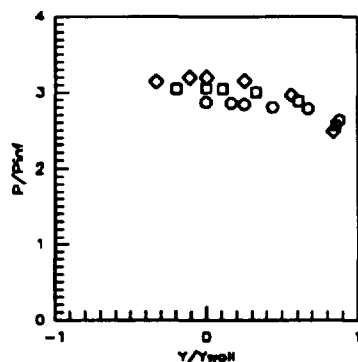
Sym	x'/Ts'	Run	CR/Re/Cowl
		No.	(milsions)
o	-0.5258	run83	3/1.14/25%
□	-0.5258	run42	5/1.14/25%
◇	-0.5258	run52	9/1.14/25%

Figure 7.2.1.222: CR Effects  
(Re=1.14million/ft, 25%CowI)  
Baseplate Pressures



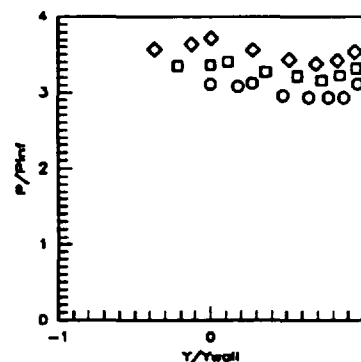
Sym	x'/Ts'	Run	CR/Re/Cowl
		No.	(milsions)
o	-0.1052	run83	3/1.14/25%
□	-0.1052	run42	5/1.14/25%
◇	-0.1052	run52	9/1.14/25%

Figure 7.2.1.223: CR Effects  
(Re=1.14million/ft, 25%CowI)  
Baseplate Pressures



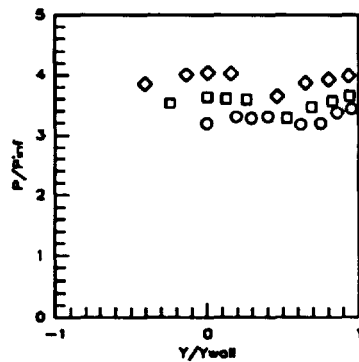
Sym	x'/Ts'	Run	CR/Re/Cowl
		No.	(milsions)
o	0.0000	run83	3/1.14/25%
□	0.0000	run42	5/1.14/25%
◇	0.0000	run52	9/1.14/25%

Figure 7.2.1.224: CR Effects  
(Re=1.14million/ft, 25%CowI)  
Baseplate Pressures



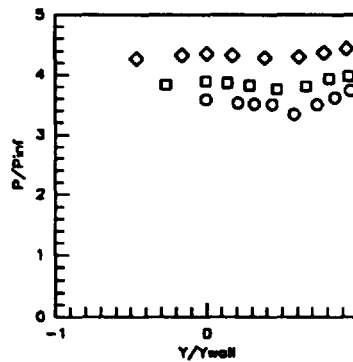
Sym	x'/Ts'	Run	CR/Re/Cowl
		No.	(milsions)
o	0.1052	run83	3/1.14/25%
□	0.1052	run42	5/1.14/25%
◇	0.1052	run52	9/1.14/25%

Figure 7.2.1.225: CR Effects  
(Re=1.14million/ft, 25%CowI)  
Baseplate Pressures



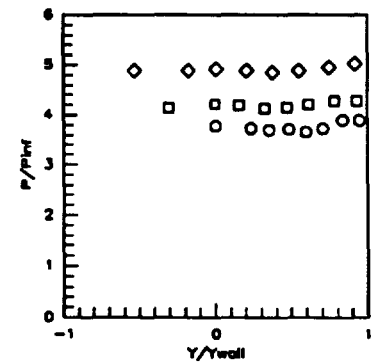
Sym	$x'/T_x'$	Run No.	CR/Re/Cowl (millions)
○	0.2103	run63	3/1.14/25%
□	0.2103	run42	5/1.14/25%
◇	0.2103	run52	9/1.14/25%

Figure 7.2.1.226: CR Effects (Re=1.14million/ft, 25%Cow) Baseplate Pressures



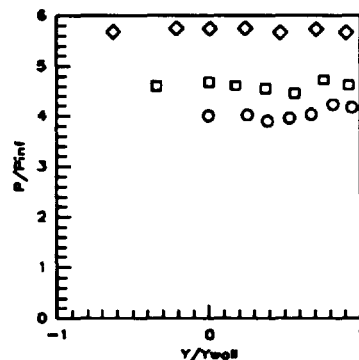
Sym	$x'/T_x'$	Run No.	CR/Re/Cowl (millions)
○	0.3154	run63	3/1.14/25%
□	0.3154	run42	5/1.14/25%
◇	0.3154	run52	9/1.14/25%

Figure 7.2.1.227: CR Effects (Re=1.14million/ft, 25%Cow) Baseplate Pressures



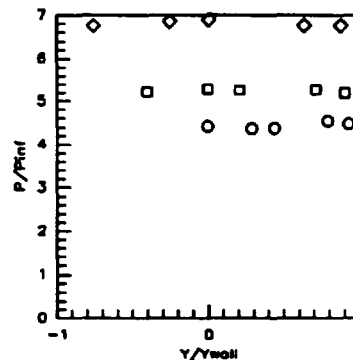
Sym	$x'/T_x'$	Run No.	CR/Re/Cowl (millions)
○	0.4208	run63	3/1.14/25%
□	0.4208	run42	5/1.14/25%
◇	0.4208	run52	9/1.14/25%

Figure 7.2.1.228: CR Effects (Re=1.14million/ft, 25%Cow) Baseplate Pressures



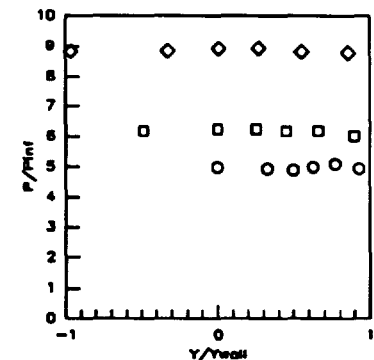
Sym	$x'/T_x'$	Run No.	CR/Re/Cowl (millions)
○	0.5238	run63	3/1.14/25%
□	0.5238	run42	5/1.14/25%
◇	0.5238	run52	9/1.14/25%

Figure 7.2.1.229: CR Effects (Re=1.14million/ft, 25%Cow) Baseplate Pressures



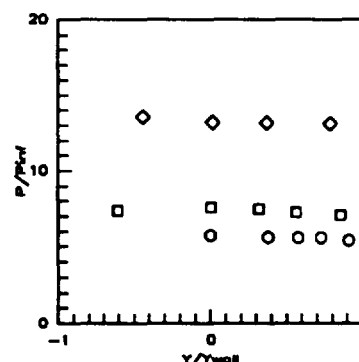
Sym	$x'/T_x'$	Run No.	CR/Re/Cowl (millions)
○	0.6309	run63	3/1.14/25%
□	0.6309	run42	5/1.14/25%
◇	0.6309	run52	9/1.14/25%

Figure 7.2.1.230: CR Effects (Re=1.14million/ft, 25%Cow) Baseplate Pressures



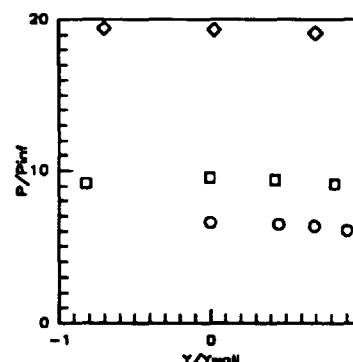
Sym	$x'/T_x'$	Run No.	CR/Re/Cowl (millions)
○	0.7361	run63	3/1.14/25%
□	0.7361	run42	5/1.14/25%
◇	0.7361	run52	9/1.14/25%

Figure 7.2.1.231: CR Effects (Re=1.14million/ft, 25%Cow) Baseplate Pressures



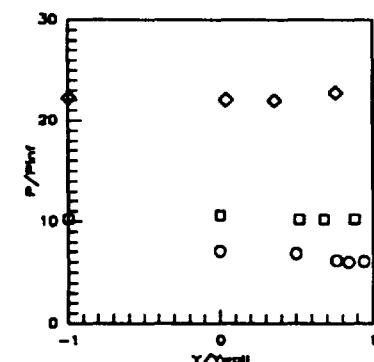
Sym	$x'/T_x'$	Run No.	CR/Re/Cowl (millions)
○	0.8412	run63	3/1.14/25%
□	0.8412	run42	5/1.14/25%
◇	0.8412	run52	9/1.14/25%

Figure 7.2.1.232: CR Effects (Re=1.14million/ft, 25%Cow) Baseplate Pressures



Sym	$x'/T_x'$	Run No.	CR/Re/Cowl (millions)
○	0.9464	run63	3/1.14/25%
□	0.9464	run42	5/1.14/25%
◇	0.9464	run52	9/1.14/25%

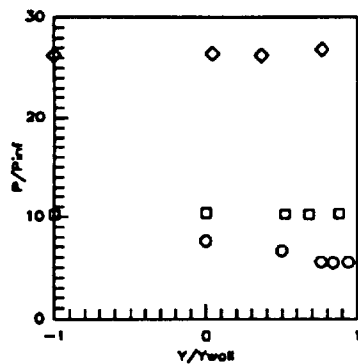
Figure 7.2.1.233: CR Effects (Re=1.14million/ft, 25%Cow) Baseplate Pressures



Sym	$x'/T_x'$	Run No.	CR/Re/Cowl (millions)
○	1.0000	run63	3/1.14/25%
□	1.0000	run42	5/1.14/25%
◇	1.0000	run52	9/1.14/25%

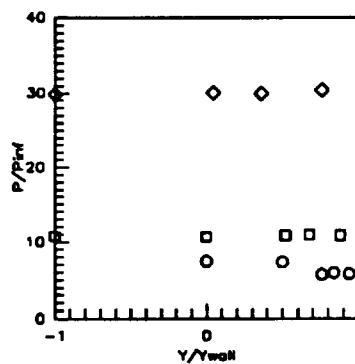
Figure 7.2.1.234: CR Effects (Re=1.14million/ft, 25%Cow) Baseplate Pressures





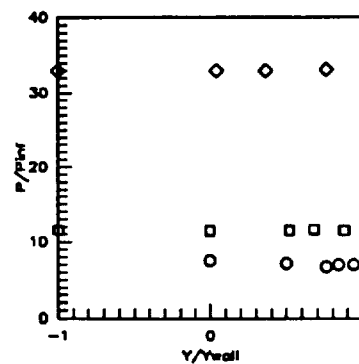
Sym	$x'/T_x'$	Run No.	CR/Re/Cowl (millions)
○	1.0726	run63	3/1.14/25%
□	1.0726	run42	5/1.14/25%
◇	1.0726	run52	9/1.14/25%

Figure 7.2.1.235: CR Effects (Re=1.14million/ft, 25%CowI) Baseplate Pressures



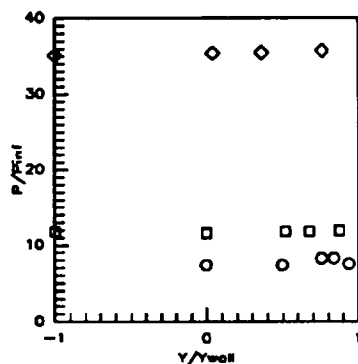
Sym	$x'/T_x'$	Run No.	CR/Re/Cowl (millions)
○	1.1567	run63	3/1.14/25%
□	1.1567	run42	5/1.14/25%
◇	1.1567	run52	9/1.14/25%

Figure 7.2.1.236: CR Effects (Re=1.14million/ft, 25%CowI) Baseplate Pressures



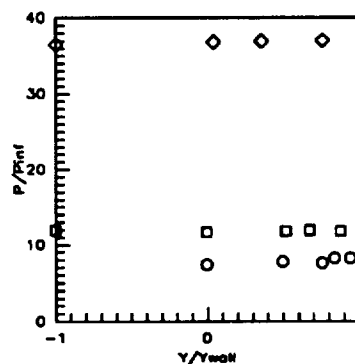
Sym	$x'/T_x'$	Run No.	CR/Re/Cowl (millions)
○	1.2408	run63	3/1.14/25%
□	1.2408	run42	5/1.14/25%
◇	1.2408	run52	9/1.14/25%

Figure 7.2.1.237: CR Effects (Re=1.14million/ft, 25%CowI) Baseplate Pressures



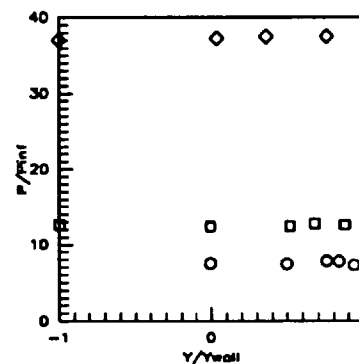
Sym	$x'/T_x'$	Run No.	CR/Re/Cowl (millions)
○	1.3249	run63	3/1.14/25%
□	1.3249	run42	5/1.14/25%
◇	1.3249	run52	9/1.14/25%

Figure 7.2.1.238: CR Effects (Re=1.14million/ft, 25%CowI) Baseplate Pressures



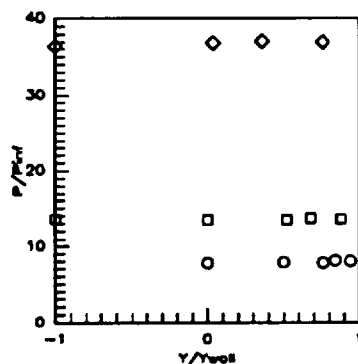
Sym	$x'/T_x'$	Run No.	CR/Re/Cowl (millions)
○	1.4090	run63	3/1.14/25%
□	1.4090	run42	5/1.14/25%
◇	1.4090	run52	9/1.14/25%

Figure 7.2.1.239: CR Effects (Re=1.14million/ft, 25%CowI) Baseplate Pressures



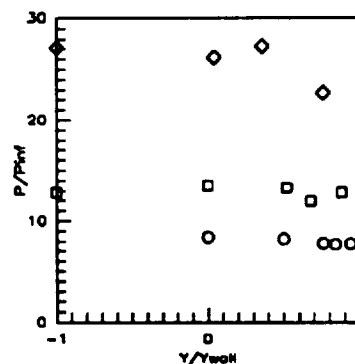
Sym	$x'/T_x'$	Run No.	CR/Re/Cowl (millions)
○	1.4932	run63	3/1.14/25%
□	1.4932	run42	5/1.14/25%
◇	1.4932	run52	9/1.14/25%

Figure 7.2.1.240: CR Effects (Re=1.14million/ft, 25%CowI) Baseplate Pressures



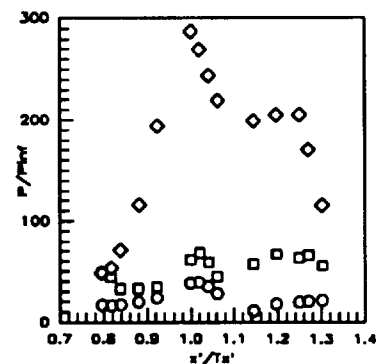
Sym	$x'/T_x'$	Run No.	CR/Re/Cowl (millions)
○	1.5773	run63	3/1.14/25%
□	1.5773	run42	5/1.14/25%
◇	1.5773	run52	9/1.14/25%

Figure 7.2.1.241: CR Effects (Re=1.14million/ft, 25%CowI) Baseplate Pressures



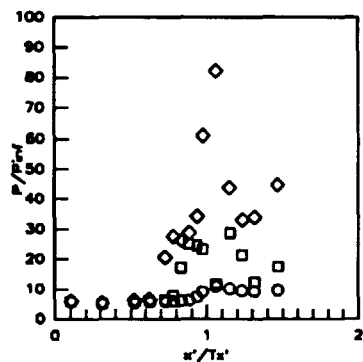
Sym	$x'/T_x'$	Run No.	CR/Re/Cowl (millions)
○	1.6824	run63	3/1.14/25%
□	1.6824	run42	5/1.14/25%
◇	1.6824	run52	9/1.14/25%

Figure 7.2.1.242: CR Effects (Re=1.14million/ft, 25%CowI) Baseplate Pressures



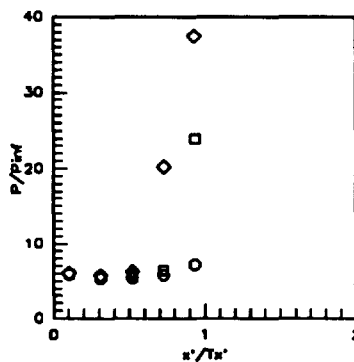
Sym	Cowl Pos.	Run No.	CR/Re/Cowl (millions)
○	25%	run63	3/1.14/25%
□	25%	run42	5/1.14/25%
◇	25%	run52	9/1.14/25%

Figure 7.2.1.243: CR Effects (Re=1.14million/ft, 25%CowI) Cowl Pressures



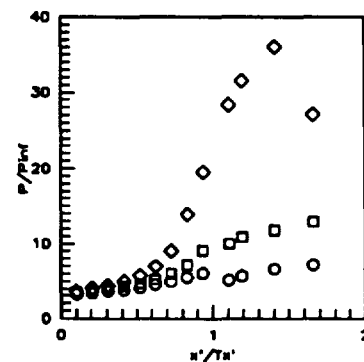
Sym	Z/H	Run No.	CR/Re/Cowl (millions)
○	0.5RT	run63	3/1.14/25%
□	0.5RT	run42	5/1.14/25%
◇	0.5RT	run52	9/1.14/25%

Figure 7.2.1.244: CR Effects (Re=1.14million/ft, 25%CowI) Sidewall Centerline Pressures



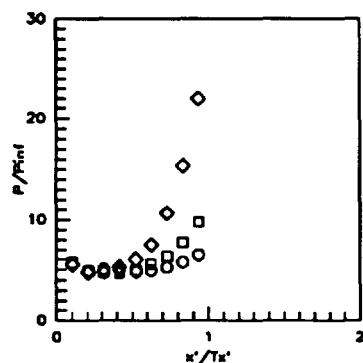
Sym	Z/H	Run No.	CR/Re/Cowl (millions)
○	0.5LT	run63	3/1.14/25%
□	0.5LT	run42	5/1.14/25%
◇	0.5LT	run52	9/1.14/25%

Figure 7.2.1.245: CR Effects (Re=1.14million/ft, 25%CowI) Sidewall Centerline Pressures



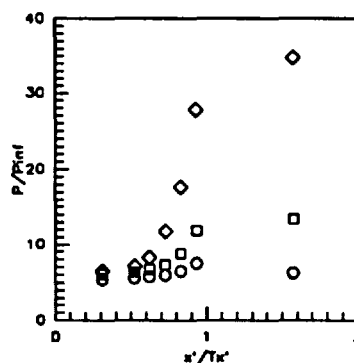
Sym	Z/H	Run No.	CR/Re/Cowl (millions)
○	0.05	run63	3/1.14/25%
□	0.05	run42	5/1.14/25%
◇	0.05	run52	9/1.14/25%

Figure 7.2.1.246: CR Effects (Re=1.14million/ft, 25%CowI) Sidewall Pressures



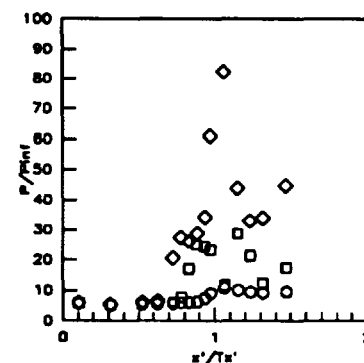
Sym	Z/H	Run No.	CR/Re/Cowl (millions)
○	0.15	run63	3/1.14/25%
□	0.15	run42	5/1.14/25%
◇	0.15	run52	9/1.14/25%

Figure 7.2.1.247: CR Effects (Re=1.14million/ft, 25%CowI) Sidewall Pressures



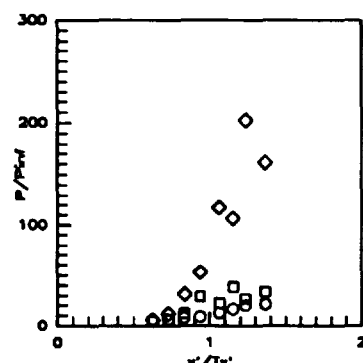
Sym	Z/H	Run No.	CR/Re/Cowl (millions)
○	0.25	run63	3/1.14/25%
□	0.25	run42	5/1.14/25%
◇	0.25	run52	9/1.14/25%

Figure 7.2.1.248: CR Effects (Re=1.14million/ft, 25%CowI) Sidewall Pressures



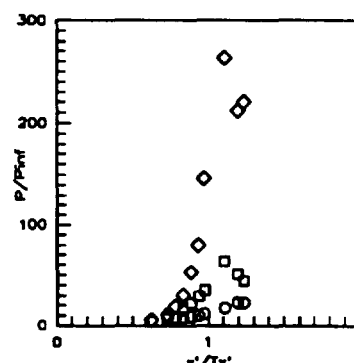
Sym	Z/H	Run No.	CR/Re/Cowl (millions)
○	0.50	run63	3/1.14/25%
□	0.50	run42	5/1.14/25%
◇	0.50	run52	9/1.14/25%

Figure 7.2.1.249: CR Effects (Re=1.14million/ft, 25%CowI) Sidewall Pressures



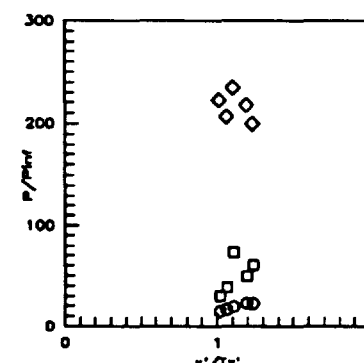
Sym	Z/H	Run No.	CR/Re/Cowl (millions)
○	0.75	run63	3/1.14/25%
□	0.75	run42	5/1.14/25%
◇	0.75	run52	9/1.14/25%

Figure 7.2.1.250: CR Effects (Re=1.14million/ft, 25%CowI) Sidewall Pressures



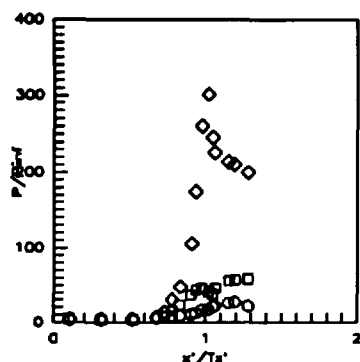
Sym	Z/H	Run No.	CR/Re/Cowl (millions)
○	0.85	run63	3/1.14/25%
□	0.85	run42	5/1.14/25%
◇	0.85	run52	9/1.14/25%

Figure 7.2.1.251: CR Effects (Re=1.14million/ft, 25%CowI) Sidewall Pressures



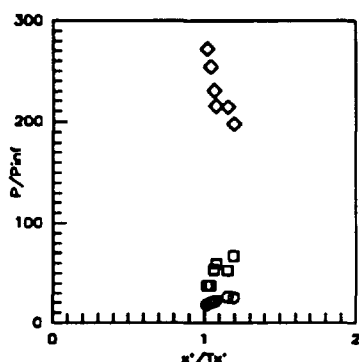
Sym	Z/H	Run No.	CR/Re/Cowl (millions)
○	0.90	run63	3/1.14/25%
□	0.90	run42	5/1.14/25%
◇	0.90	run52	9/1.14/25%

Figure 7.2.1.252: CR Effects (Re=1.14million/ft, 25%CowI) Sidewall Pressures



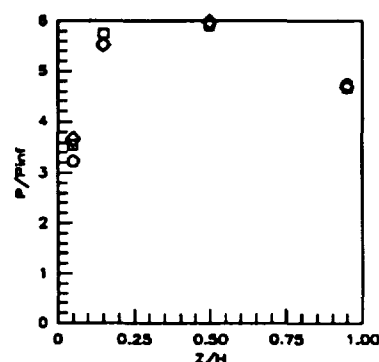
Sym	Z/H	Run No.	CR/Re/CowI (millions)
○	0.95	run63	3/1.14/25%
□	0.95	run42	5/1.14/25%
◇	0.95	run52	9/1.14/25%

Figure 7.2.1.253: CR Effects (Re=1.14million/ft, 25%CowI) Sidewall Pressures



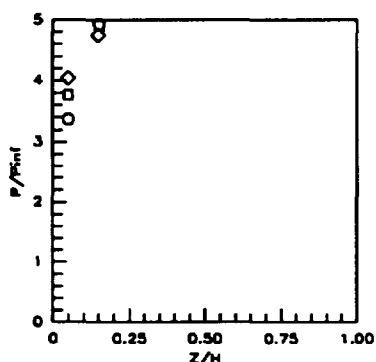
Sym	Z/H	Run No.	CR/Re/CowI (millions)
○	0.875	run63	3/1.14/25%
□	0.875	run42	5/1.14/25%
◇	0.875	run52	9/1.14/25%

Figure 7.2.1.254: CR Effects (Re=1.14million/ft, 25%CowI) Sidewall Pressures



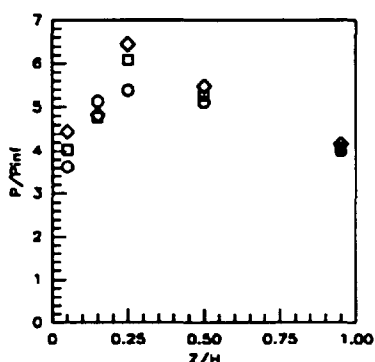
Sym	x'/Ts'	Run No.	CR/Re/CowI (millions)
○	0.1042	run63	3/1.14/25%
□	0.1042	run42	5/1.14/25%
◇	0.1042	run52	9/1.14/25%

Figure 7.2.1.255: CR Effects (Re=1.14million/ft, 25%CowI) Sidewall Pressures



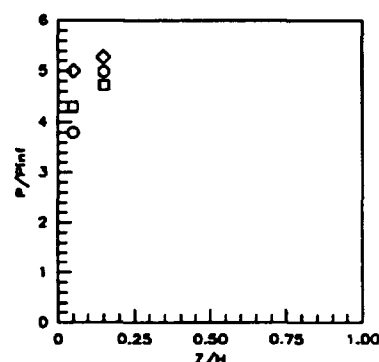
Sym	x'/Ts'	Run No.	CR/Re/CowI (millions)
○	0.2083	run63	3/1.14/25%
□	0.2083	run42	5/1.14/25%
◇	0.2083	run52	9/1.14/25%

Figure 7.2.1.256: CR Effects (Re=1.14million/ft, 25%CowI) Sidewall Pressures



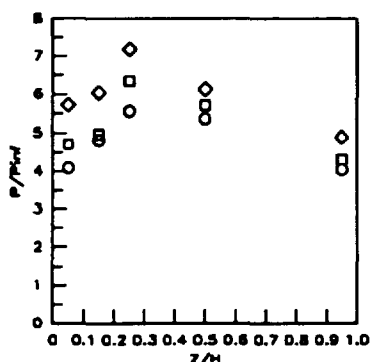
Sym	x'/Ts'	Run No.	CR/Re/CowI (millions)
○	0.3125	run63	3/1.14/25%
□	0.3125	run42	5/1.14/25%
◇	0.3125	run52	9/1.14/25%

Figure 7.2.1.257: CR Effects (Re=1.14million/ft, 25%CowI) Sidewall Pressures



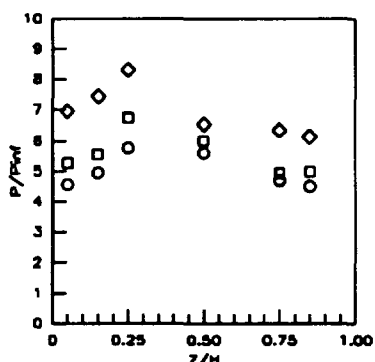
Sym	x'/Ts'	Run No.	CR/Re/CowI (millions)
○	0.4167	run63	3/1.14/25%
□	0.4167	run42	5/1.14/25%
◇	0.4167	run52	9/1.14/25%

Figure 7.2.1.258: CR Effects (Re=1.14million/ft, 25%CowI) Sidewall Pressures



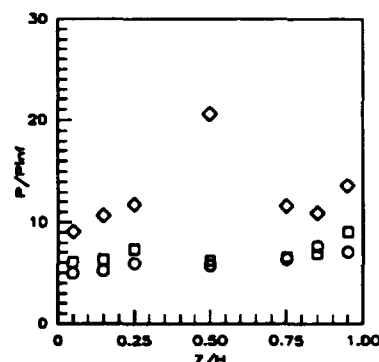
Sym	x'/Ts'	Run No.	CR/Re/CowI (millions)
○	0.5259	run63	3/1.14/25%
□	0.5259	run42	5/1.14/25%
◇	0.5259	run52	9/1.14/25%

Figure 7.2.1.259: CR Effects (Re=1.14million/ft, 25%CowI) Sidewall Pressures



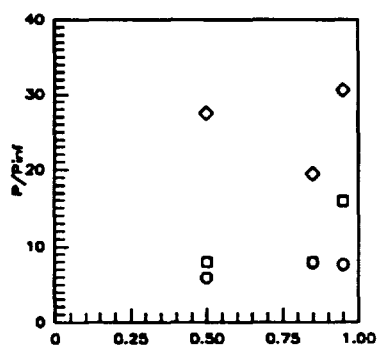
Sym	x'/Ts'	Run No.	CR/Re/CowI (millions)
○	0.6252	run63	3/1.14/25%
□	0.6252	run42	5/1.14/25%
◇	0.6252	run52	9/1.14/25%

Figure 7.2.1.260: CR Effects (Re=1.14million/ft, 25%CowI) Sidewall Pressures



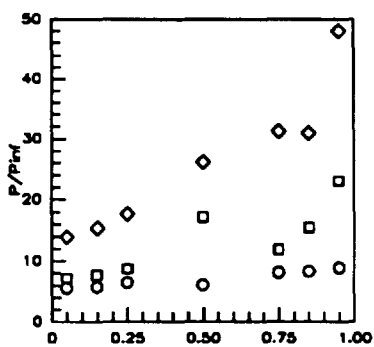
Sym	x'/Ts'	Run No.	CR/Re/CowI (millions)
○	0.7294	run63	3/1.14/25%
□	0.7294	run42	5/1.14/25%
◇	0.7294	run52	9/1.14/25%

Figure 7.2.1.261: CR Effects (Re=1.14million/ft, 25%CowI) Sidewall Pressures



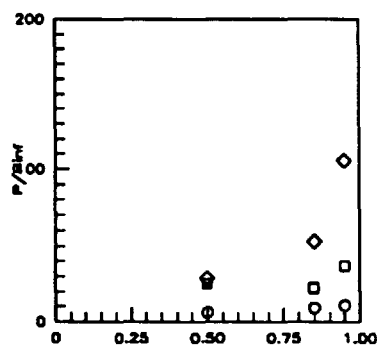
Sym	$x'/T_x'$	Run No.	CR/Re/Cowt (millions)
○	0.7815	run63	3/1.14/25%
□	0.7815	run42	5/1.14/25%
◇	0.7815	run52	9/1.14/25%

Figure 7.2.1.262: CR Effects (Re=1.14million/ft, 25%Cowt) Sidewall Pressures



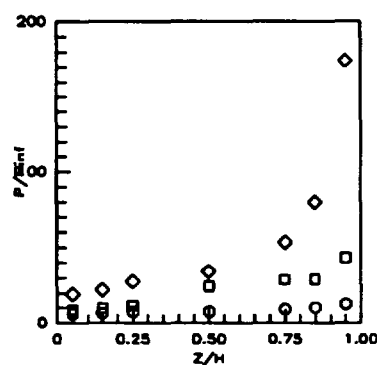
Sym	$x'/T_x'$	Run No.	CR/Re/Cowt (millions)
○	0.8336	run63	3/1.14/25%
□	0.8336	run42	5/1.14/25%
◇	0.8336	run52	9/1.14/25%

Figure 7.2.1.263: CR Effects (Re=1.14million/ft, 25%Cowt) Sidewall Pressures



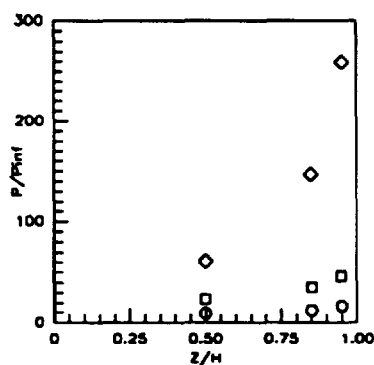
Sym	$x'/T_x'$	Run No.	CR/Re/Cowt (millions)
○	0.8857	run63	3/1.14/25%
□	0.8857	run42	5/1.14/25%
◇	0.8857	run52	9/1.14/25%

Figure 7.2.1.264: CR Effects (Re=1.14million/ft, 25%Cowt) Sidewall Pressures



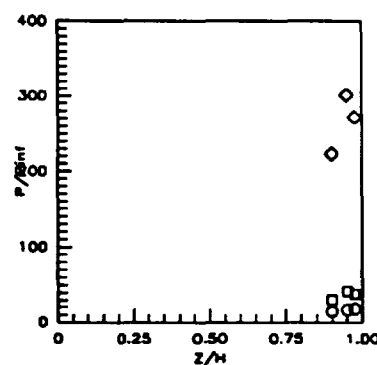
Sym	$x'/T_x'$	Run No.	CR/Re/Cowt (millions)
○	0.9378	run63	3/1.14/25%
□	0.9378	run42	5/1.14/25%
◇	0.9378	run52	9/1.14/25%

Figure 7.2.1.265: CR Effects (Re=1.14million/ft, 25%Cowt) Sidewall Pressures



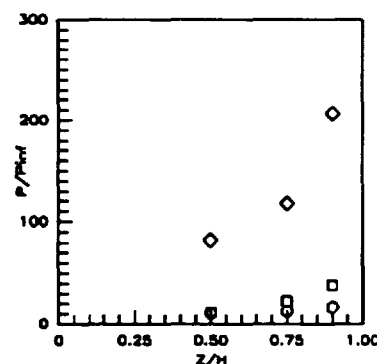
Sym	$x'/T_x'$	Run No.	CR/Re/Cowt (millions)
○	0.9751	run63	3/1.14/25%
□	0.9751	run42	5/1.14/25%
◇	0.9751	run52	9/1.14/25%

Figure 7.2.1.266: CR Effects (Re=1.14million/ft, 25%Cowt) Sidewall Pressures



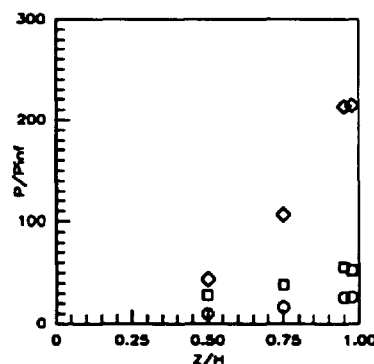
Sym	$x'/T_x'$	Run No.	CR/Re/Cowt (millions)
○	1.0187	run63	3/1.14/25%
□	1.0187	run42	5/1.14/25%
◇	1.0187	run52	9/1.14/25%

Figure 7.2.1.267: CR Effects (Re=1.14million/ft, 25%Cowt) Sidewall Pressures



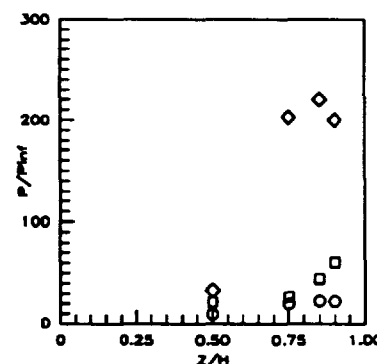
Sym	$x'/T_x'$	Run No.	CR/Re/Cowt (millions)
○	1.0643	run63	3/1.14/25%
□	1.0643	run42	5/1.14/25%
◇	1.0643	run52	9/1.14/25%

Figure 7.2.1.268: CR Effects (Re=1.14million/ft, 25%Cowt) Sidewall Pressures



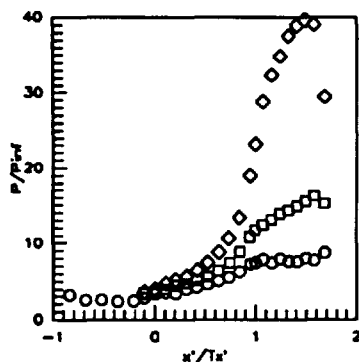
Sym	$x'/T_x'$	Run No.	CR/Re/Cowt (millions)
○	1.1537	run63	3/1.14/25%
□	1.1537	run42	5/1.14/25%
◇	1.1537	run52	9/1.14/25%

Figure 7.2.1.269: CR Effects (Re=1.14million/ft, 25%Cowt) Sidewall Pressures



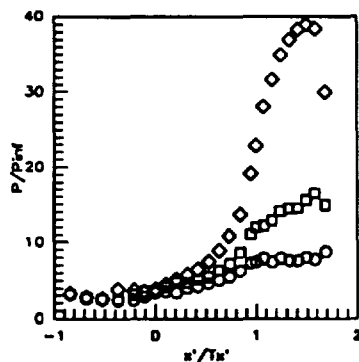
Sym	$x'/T_x'$	Run No.	CR/Re/Cowt (millions)
○	1.2356	run63	3/1.14/25%
□	1.2356	run42	5/1.14/25%
◇	1.2356	run52	9/1.14/25%

Figure 7.2.1.270: CR Effects (Re=1.14million/ft, 25%Cowt) Sidewall Pressures



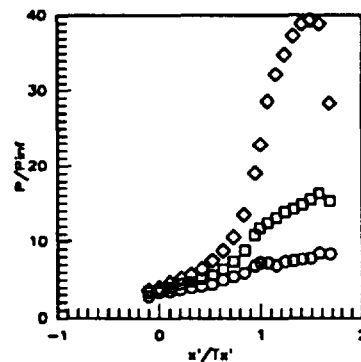
Sym	C.L. for	Run No.	CR/Re/Cowl (millions)
○	CR=3	run81	3/0.55/25%
□	CR=5	run41	5/0.55/25%
◇	CR=9	run50	9/0.55/25%

Figure 7.2.1.271: CR Effects (Re=0.55million/ft, 25%Cow) Centerline Pressures



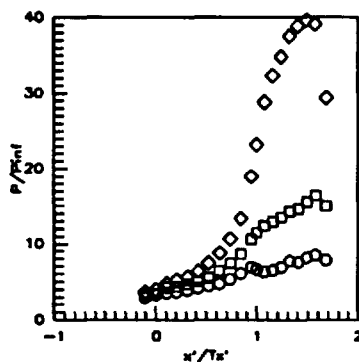
Sym	C.L. for	Run No.	CR/Re/Cowl (millions)
○	CR=3	run81	3/0.55/25%
□	CR=3	run41	5/0.55/25%
◇	CR=3	run50	9/0.55/25%

Figure 7.2.1.272: CR Effects (Re=0.55million/ft, 25%Cow) CR=3 Centerline Pressures



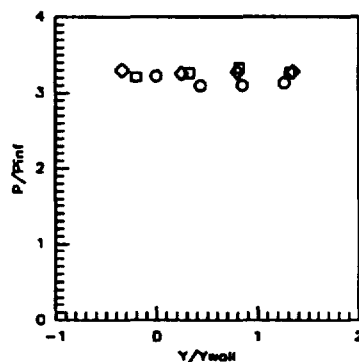
Sym	C.L. for	Run No.	CR/Re/Cowl (millions)
○	CR=5	run81	3/0.55/25%
□	CR=5	run41	5/0.55/25%
◇	CR=5	run50	9/0.55/25%

Figure 7.2.1.273: CR Effects (Re=0.55million/ft, 25%Cow) CR=5 Centerline Pressures



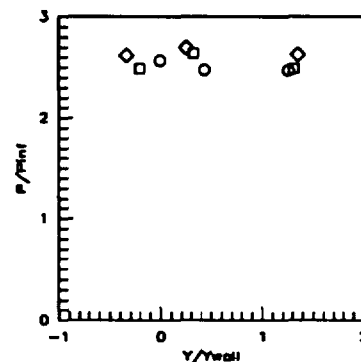
Sym	C.L. for	Run No.	CR/Re/Cowl (millions)
○	CR=9	run81	3/0.55/25%
□	CR=9	run41	5/0.55/25%
◇	CR=9	run50	9/0.55/25%

Figure 7.2.1.274: CR Effects (Re=0.55million/ft, 25%Cow) CR=9 Centerline Pressures



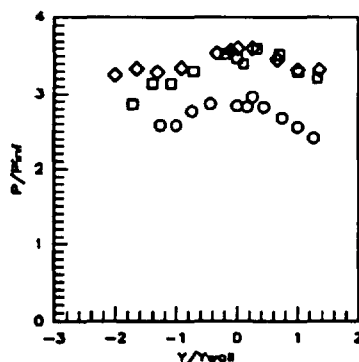
Sym	x'/Tx'	Run No.	CR/Re/Cowl (millions)
○	-0.8412	run81	3/0.55/25%
□	-0.8412	run41	5/0.55/25%
◇	-0.8412	run50	9/0.55/25%

Figure 7.2.1.275: CR Effects (Re=0.55million/ft, 25%Cow) Baseplate Pressures



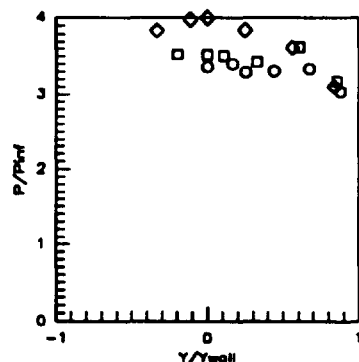
Sym	x'/Tx'	Run No.	CR/Re/Cowl (millions)
○	-0.5258	run81	3/0.55/25%
□	-0.5258	run41	5/0.55/25%
◇	-0.5258	run50	9/0.55/25%

Figure 7.2.1.276: CR Effects (Re=0.55million/ft, 25%Cow) Baseplate Pressures



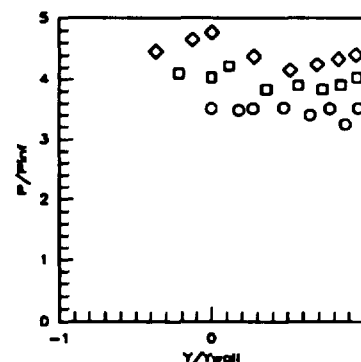
Sym	x'/Tx'	Run No.	CR/Re/Cowl (millions)
○	-0.1052	run81	3/0.55/25%
□	-0.1052	run41	5/0.55/25%
◇	-0.1052	run50	9/0.55/25%

Figure 7.2.1.277: CR Effects (Re=0.55million/ft, 25%Cow) Baseplate Pressures



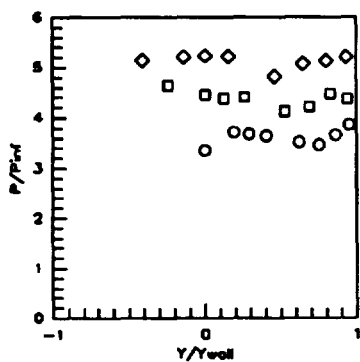
Sym	x'/Tx'	Run No.	CR/Re/Cowl (millions)
○	0.0000	run81	3/0.55/25%
□	0.0000	run41	5/0.55/25%
◇	0.0000	run50	9/0.55/25%

Figure 7.2.1.278: CR Effects (Re=0.55million/ft, 25%Cow) Baseplate Pressures



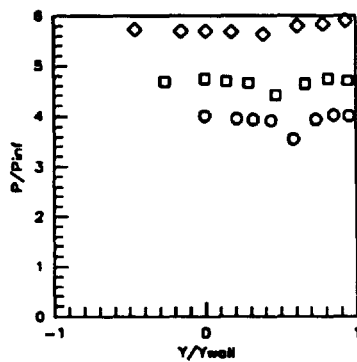
Sym	x'/Tx'	Run No.	CR/Re/Cowl (millions)
○	0.1052	run81	3/0.55/25%
□	0.1052	run41	5/0.55/25%
◇	0.1052	run50	9/0.55/25%

Figure 7.2.1.279: CR Effects (Re=0.55million/ft, 25%Cow) Baseplate Pressures



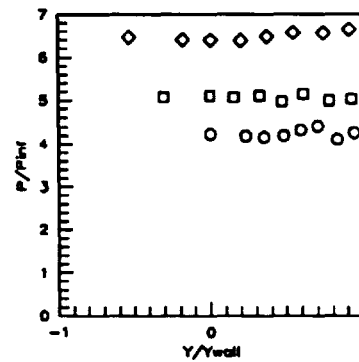
Sym	$x'/T_x'$	Run No.	CR/Re/Cowl (millions)
○	0.2103	run61	3/0.55/25%
□	0.2103	run41	5/0.55/25%
◇	0.2103	run50	9/0.55/25%

Figure 7.2.1.280: CR Effects (Re=0.55million/ft. 25%CowI) Baseplate Pressures



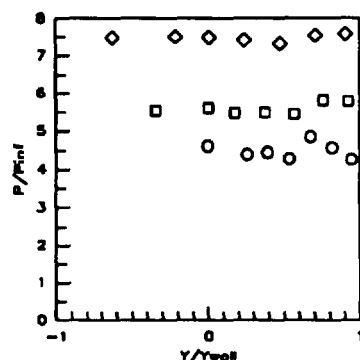
Sym	$x'/T_x'$	Run No.	CR/Re/Cowl (millions)
○	0.3154	run61	3/0.55/25%
□	0.3154	run41	5/0.55/25%
◇	0.3154	run50	9/0.55/25%

Figure 7.2.1.281: CR Effects (Re=0.55million/ft. 25%CowI) Baseplate Pressures



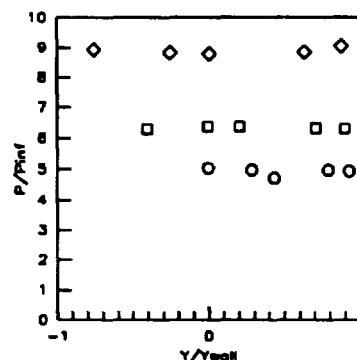
Sym	$x'/T_x'$	Run No.	CR/Re/Cowl (millions)
○	0.4206	run61	3/0.55/25%
□	0.4206	run41	5/0.55/25%
◇	0.4206	run50	9/0.55/25%

Figure 7.2.1.282: CR Effects (Re=0.55million/ft. 25%CowI) Baseplate Pressures



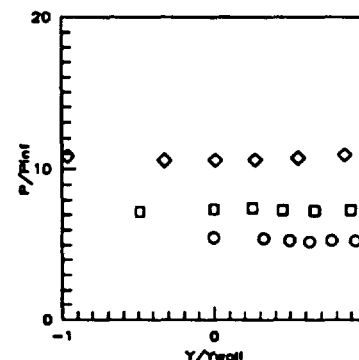
Sym	$x'/T_x'$	Run No.	CR/Re/Cowl (millions)
○	0.5258	run61	3/0.55/25%
□	0.5258	run41	5/0.55/25%
◇	0.5258	run50	9/0.55/25%

Figure 7.2.1.283: CR Effects (Re=0.55million/ft. 25%CowI) Baseplate Pressures



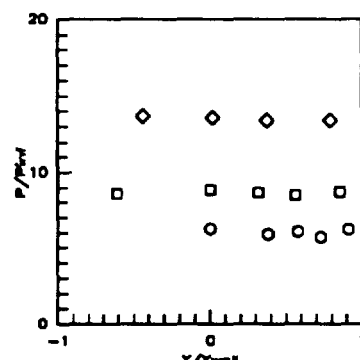
Sym	$x'/T_x'$	Run No.	CR/Re/Cowl (millions)
○	0.6309	run61	3/0.55/25%
□	0.6309	run41	5/0.55/25%
◇	0.6309	run50	9/0.55/25%

Figure 7.2.1.284: CR Effects (Re=0.55million/ft. 25%CowI) Baseplate Pressures



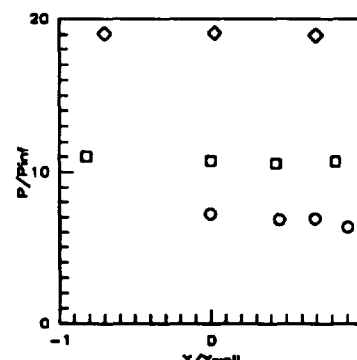
Sym	$x'/T_x'$	Run No.	CR/Re/Cowl (millions)
○	0.7361	run61	3/0.55/25%
□	0.7361	run41	5/0.55/25%
◇	0.7361	run50	9/0.55/25%

Figure 7.2.1.285: CR Effects (Re=0.55million/ft. 25%CowI) Baseplate Pressures



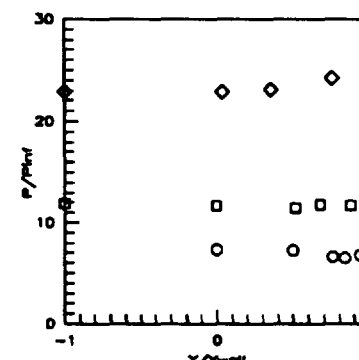
Sym	$x'/T_x'$	Run No.	CR/Re/Cowl (millions)
○	0.8412	run61	3/0.55/25%
□	0.8412	run41	5/0.55/25%
◇	0.8412	run50	9/0.55/25%

Figure 7.2.1.286: CR Effects (Re=0.55million/ft. 25%CowI) Baseplate Pressures



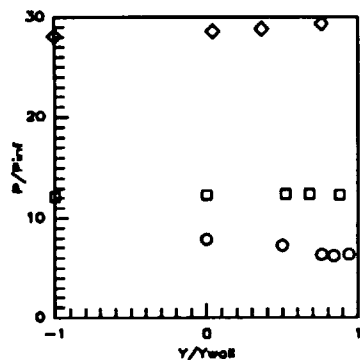
Sym	$x'/T_x'$	Run No.	CR/Re/Cowl (millions)
○	0.9484	run61	3/0.55/25%
□	0.9484	run41	5/0.55/25%
◇	0.9484	run50	9/0.55/25%

Figure 7.2.1.287: CR Effects (Re=0.55million/ft. 25%CowI) Baseplate Pressures



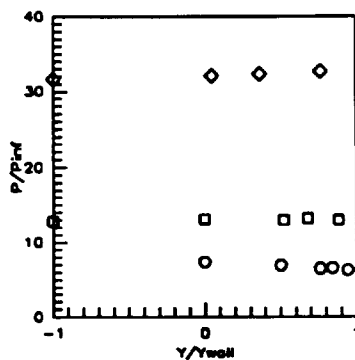
Sym	$x'/T_x'$	Run No.	CR/Re/Cowl (millions)
○	1.0000	run61	3/0.55/25%
□	1.0000	run41	5/0.55/25%
◇	1.0000	run50	9/0.55/25%

Figure 7.2.1.288: CR Effects (Re=0.55million/ft. 25%CowI) Baseplate Pressures



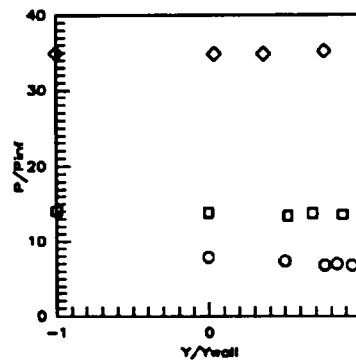
Sym	$x'/T_x'$	Run No.	CR/Ra/Cowl (milions)
○	1.0726	run81	3/0.55/25%
□	1.0726	run41	5/0.55/25%
◇	1.0726	run50	9/0.55/25%

Figure 7.2.1.288: CR Effects (Re=0.55million/ft, 25%CowI) Baseplate Pressures



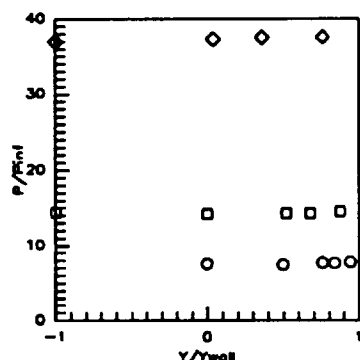
Sym	$x'/T_x'$	Run No.	CR/Ra/Cowl (milions)
○	1.1567	run81	3/0.55/25%
□	1.1567	run41	5/0.55/25%
◇	1.1567	run50	9/0.55/25%

Figure 7.2.1.290: CR Effects (Re=0.55million/ft, 25%CowI) Baseplate Pressures



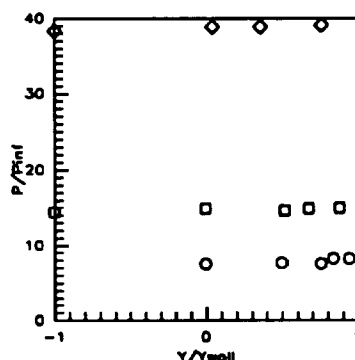
Sym	$x'/T_x'$	Run No.	CR/Ra/Cowl (milions)
○	1.2408	run81	3/0.55/25%
□	1.2408	run41	5/0.55/25%
◇	1.2408	run50	9/0.55/25%

Figure 7.2.1.291: CR Effects (Re=0.55million/ft, 25%CowI) Baseplate Pressures



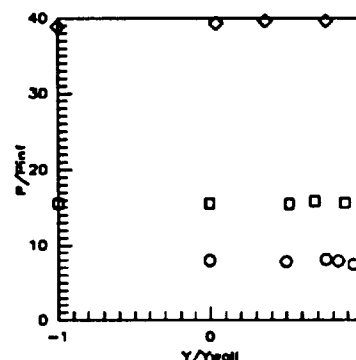
Sym	$x'/T_x'$	Run No.	CR/Ra/Cowl (milions)
○	1.3249	run81	3/0.55/25%
□	1.3249	run41	5/0.55/25%
◇	1.3249	run50	9/0.55/25%

Figure 7.2.1.292: CR Effects (Re=0.55million/ft, 25%CowI) Baseplate Pressures



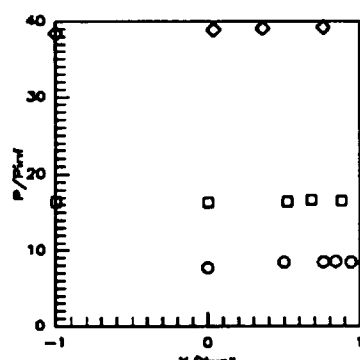
Sym	$x'/T_x'$	Run No.	CR/Ra/Cowl (milions)
○	1.4090	run81	3/0.55/25%
□	1.4090	run41	5/0.55/25%
◇	1.4090	run50	9/0.55/25%

Figure 7.2.1.293: CR Effects (Re=0.55million/ft, 25%CowI) Baseplate Pressures



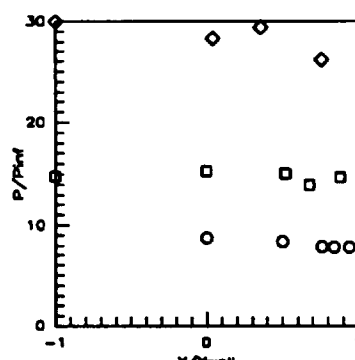
Sym	$x'/T_x'$	Run No.	CR/Ra/Cowl (milions)
○	1.4932	run81	3/0.55/25%
□	1.4932	run41	5/0.55/25%
◇	1.4932	run50	9/0.55/25%

Figure 7.2.1.294: CR Effects (Re=0.55million/ft, 25%CowI) Baseplate Pressures



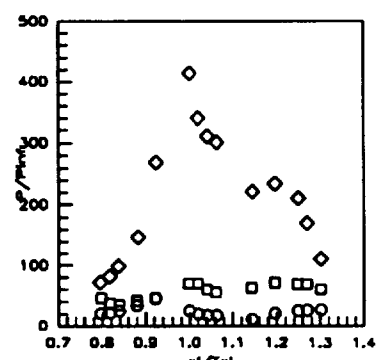
Sym	$x'/T_x'$	Run No.	CR/Ra/Cowl (milions)
○	1.5773	run81	3/0.55/25%
□	1.5773	run41	5/0.55/25%
◇	1.5773	run50	9/0.55/25%

Figure 7.2.1.295: CR Effects (Re=0.55million/ft, 25%CowI) Baseplate Pressures



Sym	$x'/T_x'$	Run No.	CR/Ra/Cowl (milions)
○	1.6824	run81	3/0.55/25%
□	1.6824	run41	5/0.55/25%
◇	1.6824	run50	9/0.55/25%

Figure 7.2.1.296: CR Effects (Re=0.55million/ft, 25%CowI) Baseplate Pressures



Sym	Cowl Pos.	Run No.	CR/Ra/Cowl (milions)
○	25%	run81	3/0.55/25%
□	25%	run41	5/0.55/25%
◇	25%	run50	9/0.55/25%

Figure 7.2.1.297: CR Effects (Re=0.55million/ft, 25%CowI) Cowl Pressures

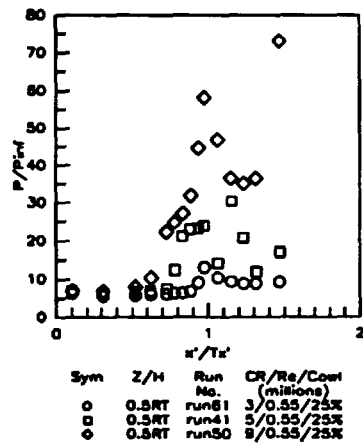


Figure 7.2.1.298: CR Effects  
( $Re=0.55$ million/ft, 25%Cowl)  
Sidewall Centerline Pressures

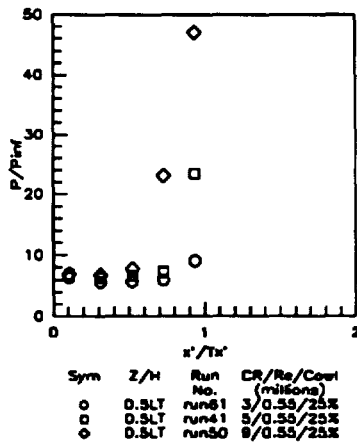


Figure 7.2.1.299: CR Effects  
( $Re=0.55$ million/ft, 25%Cowl)  
Sidewall Centerline Pressures

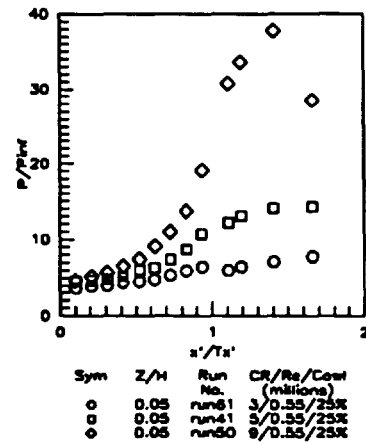


Figure 7.2.1.300: CR Effects  
( $Re=0.55$ million/ft, 25%Cowl)  
Sidewall Pressures

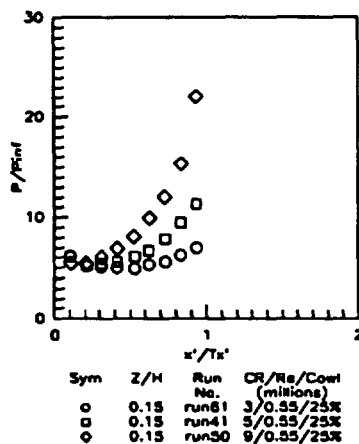


Figure 7.2.1.301: CR Effects  
( $Re=0.55$ million/ft, 25%Cowl)  
Sidewall Pressures

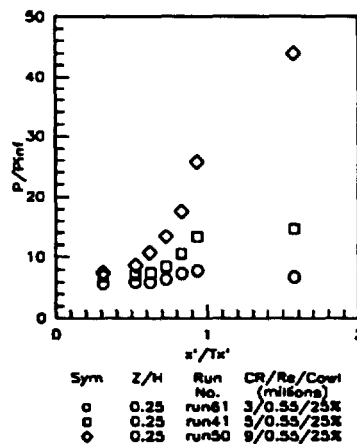


Figure 7.2.1.302: CR Effects  
( $Re=0.55$ million/ft, 25%Cowl)  
Sidewall Pressures

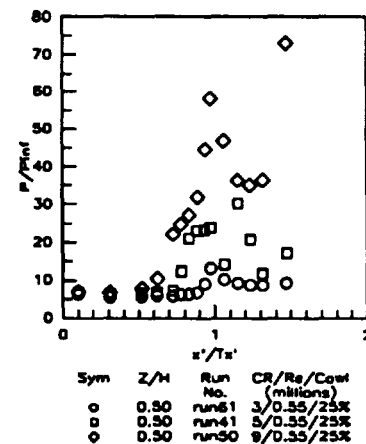


Figure 7.2.1.303: CR Effects  
( $Re=0.55$ million/ft, 25%Cowl)  
Sidewall Pressures

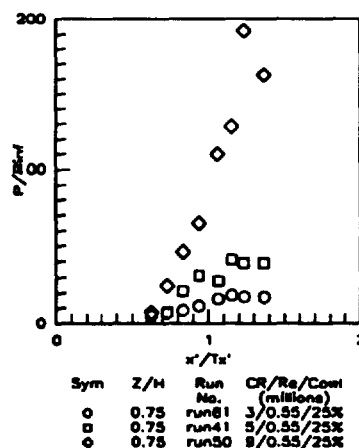


Figure 7.2.1.304: CR Effects  
( $Re=0.55$ million/ft, 25%Cowl)  
Sidewall Pressures

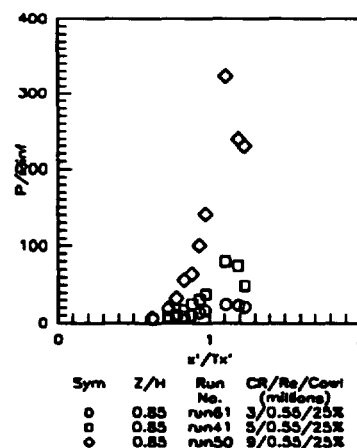


Figure 7.2.1.305: CR Effects  
( $Re=0.55$ million/ft, 25%Cowl)  
Sidewall Pressures

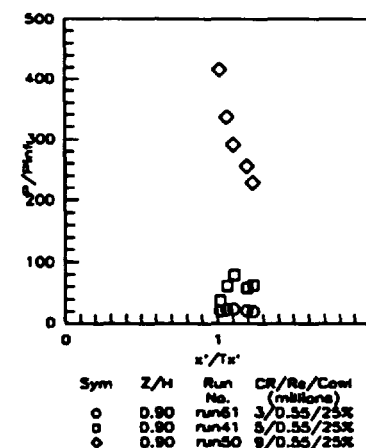
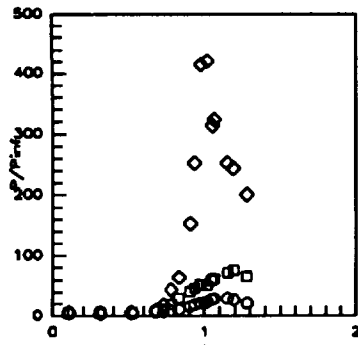


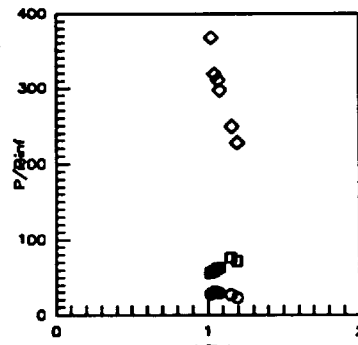
Figure 7.2.1.306: CR Effects  
( $Re=0.55$ million/ft, 25%Cowl)  
Sidewall Pressures





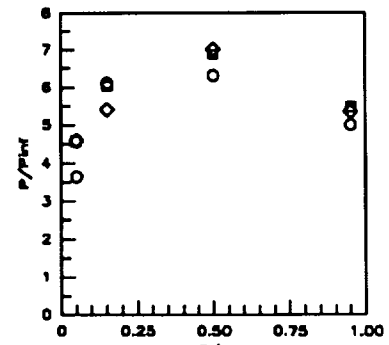
Sym	Z/H	Run No.	CR/Re/Cowl (milions)
○	0.95	run61	3/0.55/25%
□	0.95	run41	5/0.55/25%
◇	0.95	run50	9/0.55/25%

Figure 7.2.1.307: CR Effects (Re=0.55million/ft, 25%CowI) Sidewall Pressures



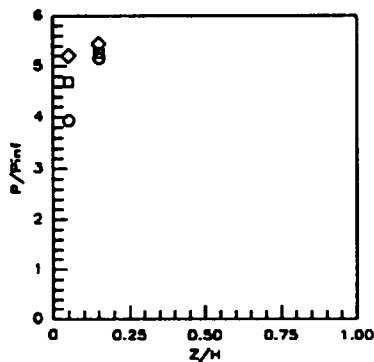
Sym	Z/H	Run No.	CR/Re/Cowl (milions)
○	0.975	run61	3/0.55/25%
□	0.975	run41	5/0.55/25%
◇	0.975	run50	9/0.55/25%

Figure 7.2.1.308: CR Effects (Re=0.55million/ft, 25%CowI) Sidewall Pressures



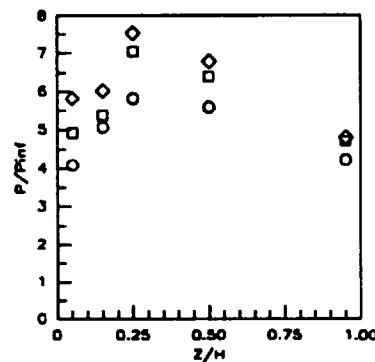
Sym	x'/Ts'	Run No.	CR/Re/Cowl (milions)
○	0.1042	run61	3/0.55/25%
□	0.1042	run41	5/0.55/25%
◇	0.1042	run50	9/0.55/25%

Figure 7.2.1.309: CR Effects (Re=0.55million/ft, 25%CowI) Sidewall Pressures



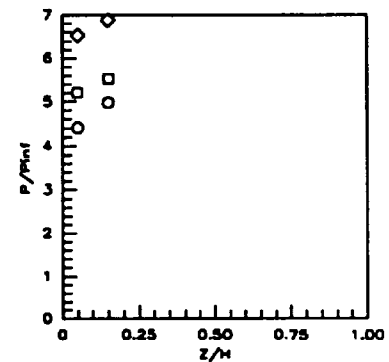
Sym	x'/Ts'	Run No.	CR/Re/Cowl (milions)
○	0.2083	run61	3/0.55/25%
□	0.2083	run41	5/0.55/25%
◇	0.2083	run50	9/0.55/25%

Figure 7.2.1.310: CR Effects (Re=0.55million/ft, 25%CowI) Sidewall Pressures



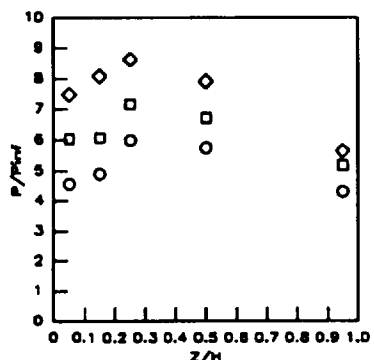
Sym	x'/Ts'	Run No.	CR/Re/Cowl (milions)
○	0.3125	run61	3/0.55/25%
□	0.3125	run41	5/0.55/25%
◇	0.3125	run50	9/0.55/25%

Figure 7.2.1.311: CR Effects (Re=0.55million/ft, 25%CowI) Sidewall Pressures



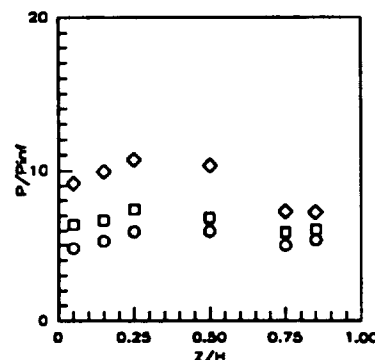
Sym	x'/Ts'	Run No.	CR/Re/Cowl (milions)
○	0.4167	run61	3/0.55/25%
□	0.4167	run41	5/0.55/25%
◇	0.4167	run50	9/0.55/25%

Figure 7.2.1.312: CR Effects (Re=0.55million/ft, 25%CowI) Sidewall Pressures



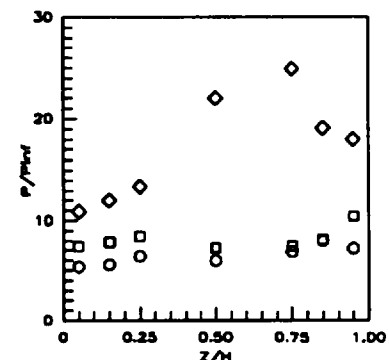
Sym	x'/Ts'	Run No.	CR/Re/Cowl (milions)
○	0.5259	run61	3/0.55/25%
□	0.5259	run41	5/0.55/25%
◇	0.5259	run50	9/0.55/25%

Figure 7.2.1.313: CR Effects (Re=0.55million/ft, 25%CowI) Sidewall Pressures



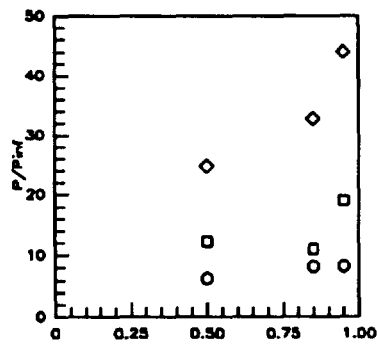
Sym	x'/Ts'	Run No.	CR/Re/Cowl (milions)
○	0.6252	run61	3/0.55/25%
□	0.6252	run41	5/0.55/25%
◇	0.6252	run50	9/0.55/25%

Figure 7.2.1.314: CR Effects (Re=0.55million/ft, 25%CowI) Sidewall Pressures



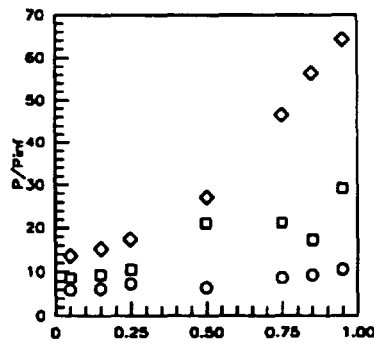
Sym	x'/Ts'	Run No.	CR/Re/Cowl (milions)
○	0.7294	run61	3/0.55/25%
□	0.7294	run41	5/0.55/25%
◇	0.7294	run50	9/0.55/25%

Figure 7.2.1.315: CR Effects (Re=0.55million/ft, 25%CowI) Sidewall Pressures



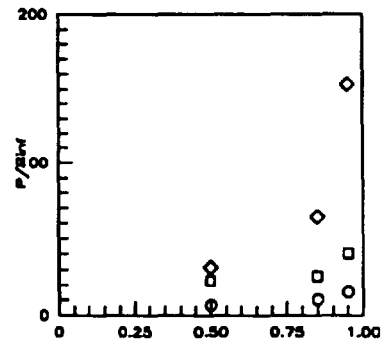
Sym	$x'/T_x'$	Run No.	CR/Re/Cowl (millions)
○	0.7815	run81	3/0.55/25%
□	0.7815	run41	5/0.55/25%
◇	0.7815	run50	9/0.55/25%

Figure 7.2.1.316: CR Effects (Re=0.55million/ft, 25%CowI) Sidewall Pressures



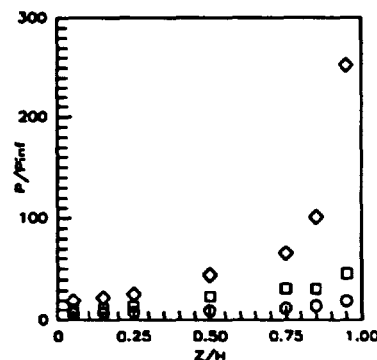
Sym	$x'/T_x'$	Run No.	CR/Re/Cowl (millions)
○	0.8336	run81	3/0.55/25%
□	0.8336	run41	5/0.55/25%
◇	0.8336	run50	9/0.55/25%

Figure 7.2.1.317: CR Effects (Re=0.55million/ft, 25%CowI) Sidewall Pressures



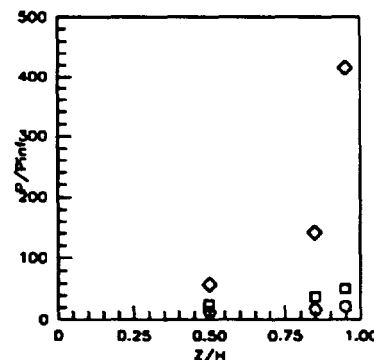
Sym	$x'/T_x'$	Run No.	CR/Re/Cowl (millions)
○	0.8857	run81	3/0.55/25%
□	0.8857	run41	5/0.55/25%
◇	0.8857	run50	9/0.55/25%

Figure 7.2.1.318: CR Effects (Re=0.55million/ft, 25%CowI) Sidewall Pressures



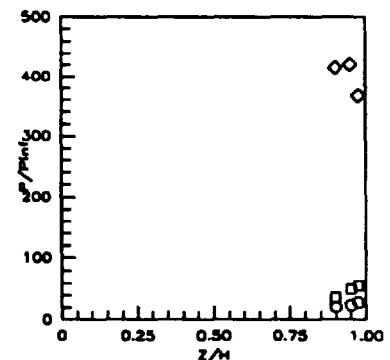
Sym	$x'/T_x'$	Run No.	CR/Re/Cowl (millions)
○	0.8378	run81	3/0.55/25%
□	0.8378	run41	5/0.55/25%
◇	0.8378	run50	9/0.55/25%

Figure 7.2.1.319: CR Effects (Re=0.55million/ft, 25%CowI) Sidewall Pressures



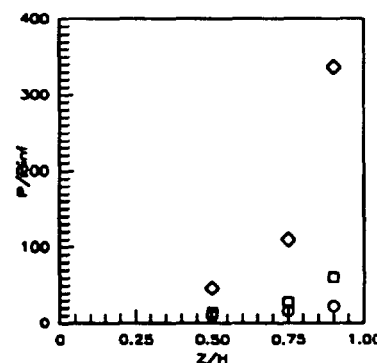
Sym	$x'/T_x'$	Run No.	CR/Re/Cowl (millions)
○	0.9751	run81	3/0.55/25%
□	0.9751	run41	5/0.55/25%
◇	0.9751	run50	9/0.55/25%

Figure 7.2.1.320: CR Effects (Re=0.55million/ft, 25%CowI) Sidewall Pressures



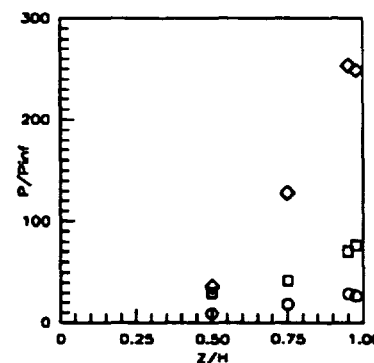
Sym	$x'/T_x'$	Run No.	CR/Re/Cowl (millions)
○	1.0187	run81	3/0.55/25%
□	1.0187	run41	5/0.55/25%
◇	1.0187	run50	9/0.55/25%

Figure 7.2.1.321: CR Effects (Re=0.55million/ft, 25%CowI) Sidewall Pressures



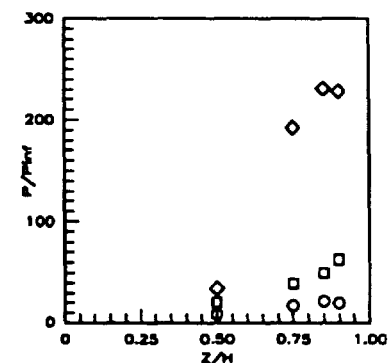
Sym	$x'/T_x'$	Run No.	CR/Re/Cowl (millions)
○	1.0843	run81	3/0.55/25%
□	1.0843	run41	5/0.55/25%
◇	1.0843	run50	9/0.55/25%

Figure 7.2.1.322: CR Effects (Re=0.55million/ft, 25%CowI) Sidewall Pressures



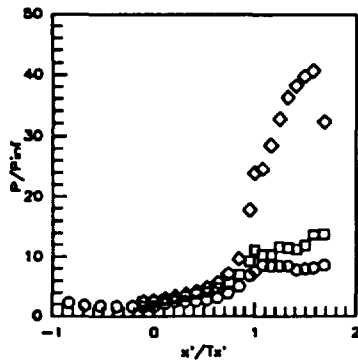
Sym	$x'/T_x'$	Run No.	CR/Re/Cowl (millions)
○	1.1537	run81	3/0.55/25%
□	1.1537	run41	5/0.55/25%
◇	1.1537	run50	9/0.55/25%

Figure 7.2.1.323: CR Effects (Re=0.55million/ft, 25%CowI) Sidewall Pressures



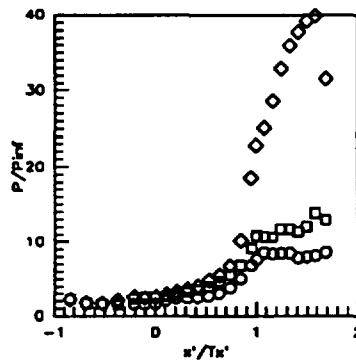
Sym	$x'/T_x'$	Run No.	CR/Re/Cowl (millions)
○	1.2356	run81	3/0.55/25%
□	1.2356	run41	5/0.55/25%
◇	1.2356	run50	9/0.55/25%

Figure 7.2.1.324: CR Effects (Re=0.55million/ft, 25%CowI) Sidewall Pressures



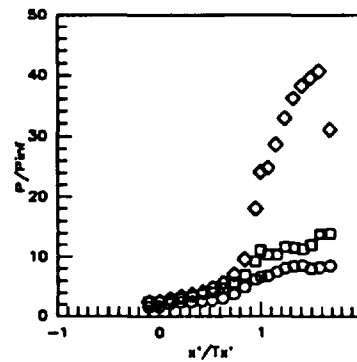
Sym	C.L. for	Run No.	CR/Re/Cowf (milions)
○	CR=3	run60	3/2.15/50%
□	CR=5	run40	5/2.15/50%
◇	CR=9	run57	9/2.15/50%

Figure 7.2.1.325: CR Effects (Re=2.15million/ft, 50%Cowf) Centerline Pressures



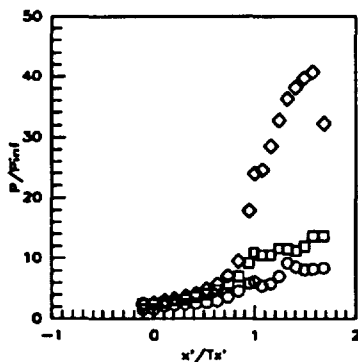
Sym	C.L. for	Run No.	CR/Re/Cowf (milions)
○	CR=3	run60	3/2.15/50%
□	CR=3	run40	5/2.15/50%
◇	CR=3	run57	9/2.15/50%

Figure 7.2.1.326: CR Effects (Re=2.15million/ft, 50%Cowf) CR=3 Centerline Pressures



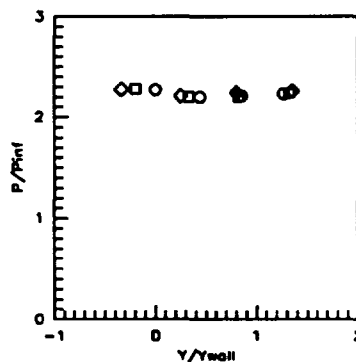
Sym	C.L. for	Run No.	CR/Re/Cowf (milions)
○	CR=5	run60	3/2.15/50%
□	CR=5	run40	5/2.15/50%
◇	CR=5	run57	9/2.15/50%

Figure 7.2.1.327: CR Effects (Re=2.15million/ft, 50%Cowf) CR=5 Centerline Pressures



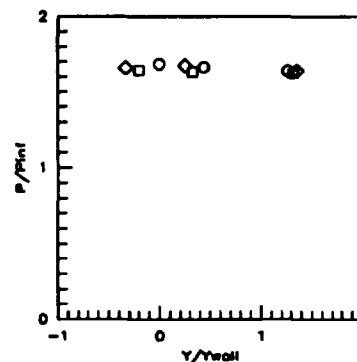
Sym	C.L. for	Run No.	CR/Re/Cowf (milions)
○	CR=9	run60	3/2.15/50%
□	CR=9	run40	5/2.15/50%
◇	CR=9	run57	9/2.15/50%

Figure 7.2.1.328: CR Effects (Re=2.15million/ft, 50%Cowf) CR=9 Centerline Pressures



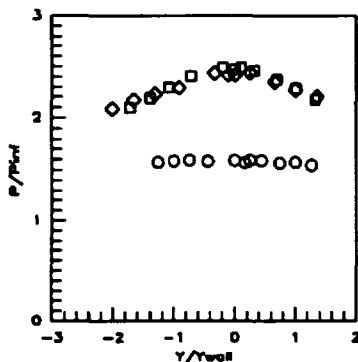
Sym	x'/Tx'	Run No.	CR/Re/Cowf (milions)
○	-0.8412	run60	3/2.15/50%
□	-0.8412	run40	5/2.15/50%
◇	-0.8412	run57	9/2.15/50%

Figure 7.2.1.329: CR Effects (Re=2.15million/ft, 50%Cowf) Baseplate Pressures



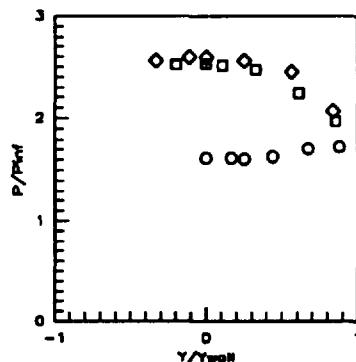
Sym	x'/Tx'	Run No.	CR/Re/Cowf (milions)
○	-0.5258	run60	3/2.15/50%
□	-0.5258	run40	5/2.15/50%
◇	-0.5258	run57	9/2.15/50%

Figure 7.2.1.330: CR Effects (Re=2.15million/ft, 50%Cowf) Baseplate Pressures



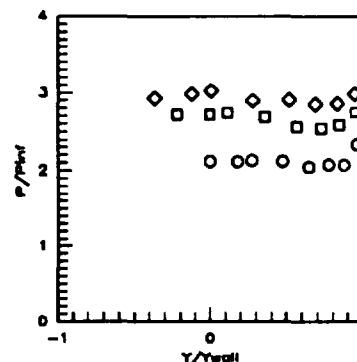
Sym	x'/Tx'	Run No.	CR/Re/Cowf (milions)
○	-0.1052	run60	3/2.15/50%
□	-0.1052	run40	5/2.15/50%
◇	-0.1052	run57	9/2.15/50%

Figure 7.2.1.331: CR Effects (Re=2.15million/ft, 50%Cowf) Baseplate Pressures



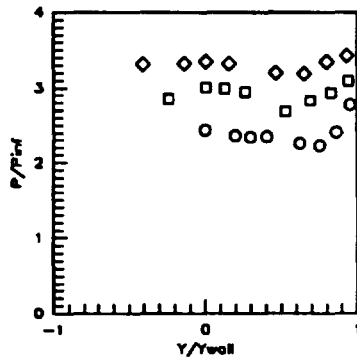
Sym	x'/Tx'	Run No.	CR/Re/Cowf (milions)
○	0.0000	run60	3/2.15/50%
□	0.0000	run40	5/2.15/50%
◇	0.0000	run57	9/2.15/50%

Figure 7.2.1.332: CR Effects (Re=2.15million/ft, 50%Cowf) Baseplate Pressures



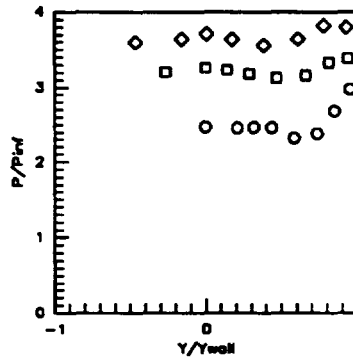
Sym	x'/Tx'	Run No.	CR/Re/Cowf (milions)
○	0.1052	run60	3/2.15/50%
□	0.1052	run40	5/2.15/50%
◇	0.1052	run57	9/2.15/50%

Figure 7.2.1.333: CR Effects (Re=2.15million/ft, 50%Cowf) Baseplate Pressures



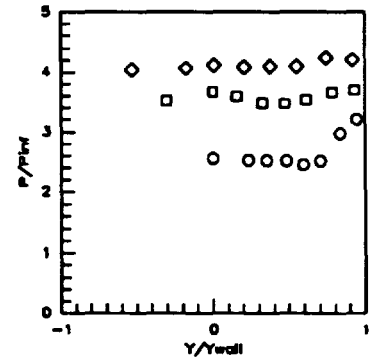
Sym	$x'/T_x'$	Run No.	CR/Re/Cowl (millions)
○	0.2103	run80	3/2.15/50%
□	0.2103	run40	5/2.15/50%
◇	0.2103	run57	9/2.15/50%

Figure 7.2.1.334: CR Effects (Re=2.15million/ft, 50%CowI) Baseplate Pressures



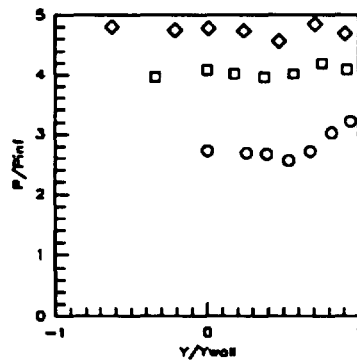
Sym	$x'/T_x'$	Run No.	CR/Re/Cowl (millions)
○	0.3154	run80	3/2.15/50%
□	0.3154	run40	5/2.15/50%
◇	0.3154	run57	9/2.15/50%

Figure 7.2.1.335: CR Effects (Re=2.15million/ft, 50%CowI) Baseplate Pressures



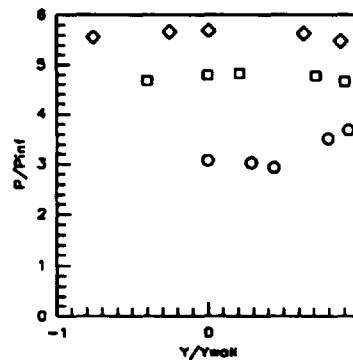
Sym	$x'/T_x'$	Run No.	CR/Re/Cowl (millions)
○	0.4206	run80	3/2.15/50%
□	0.4206	run40	5/2.15/50%
◇	0.4206	run57	9/2.15/50%

Figure 7.2.1.336: CR Effects (Re=2.15million/ft, 50%CowI) Baseplate Pressures



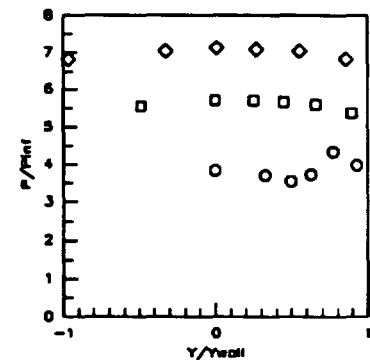
Sym	$x'/T_x'$	Run No.	CR/Re/Cowl (millions)
○	0.5258	run80	3/2.15/50%
□	0.5258	run40	5/2.15/50%
◇	0.5258	run57	9/2.15/50%

Figure 7.2.1.337: CR Effects (Re=2.15million/ft, 50%CowI) Baseplate Pressures



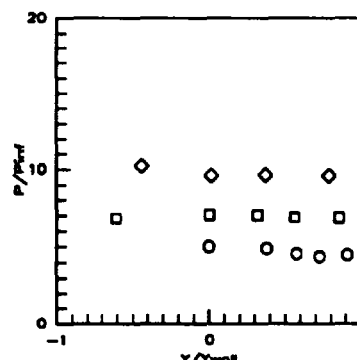
Sym	$x'/T_x'$	Run No.	CR/Re/Cowl (millions)
○	0.6308	run80	3/2.15/50%
□	0.6308	run40	5/2.15/50%
◇	0.6308	run57	9/2.15/50%

Figure 7.2.1.338: CR Effects (Re=2.15million/ft, 50%CowI) Baseplate Pressures



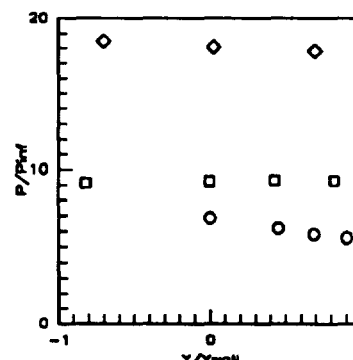
Sym	$x'/T_x'$	Run No.	CR/Re/Cowl (millions)
○	0.7361	run80	3/2.15/50%
□	0.7361	run40	5/2.15/50%
◇	0.7361	run57	9/2.15/50%

Figure 7.2.1.339: CR Effects (Re=2.15million/ft, 50%CowI) Baseplate Pressures



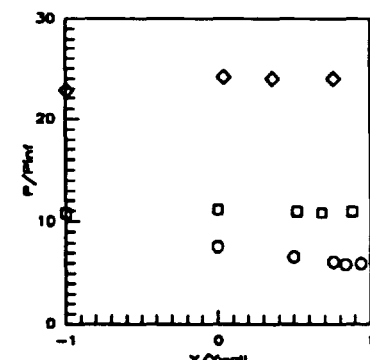
Sym	$x'/T_x'$	Run No.	CR/Re/Cowl (millions)
○	0.8412	run80	3/2.15/50%
□	0.8412	run40	5/2.15/50%
◇	0.8412	run57	9/2.15/50%

Figure 7.2.1.340: CR Effects (Re=2.15million/ft, 50%CowI) Baseplate Pressures



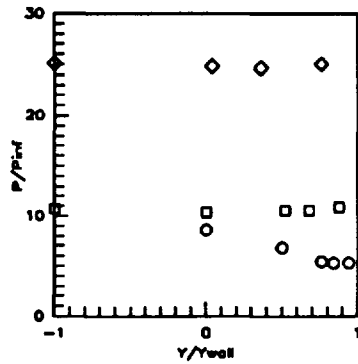
Sym	$x'/T_x'$	Run No.	CR/Re/Cowl (millions)
○	0.9484	run80	3/2.15/50%
□	0.9484	run40	5/2.15/50%
◇	0.9484	run57	9/2.15/50%

Figure 7.2.1.341: CR Effects (Re=2.15million/ft, 50%CowI) Baseplate Pressures



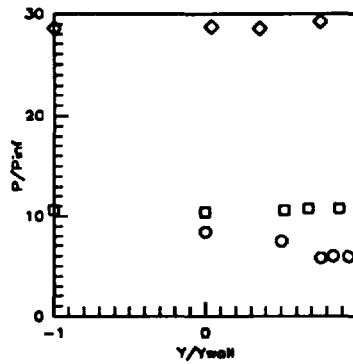
Sym	$x'/T_x'$	Run No.	CR/Re/Cowl (millions)
○	1.0000	run80	3/2.15/50%
□	1.0000	run40	5/2.15/50%
◇	1.0000	run57	9/2.15/50%

Figure 7.2.1.342: CR Effects (Re=2.15million/ft, 50%CowI) Baseplate Pressures



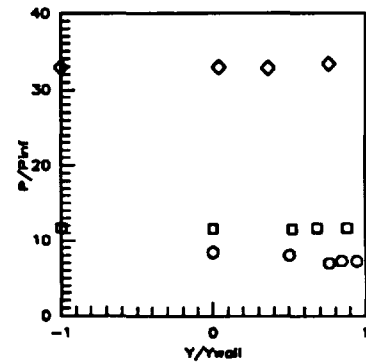
Sym	$x'/Ts'$	Run No.	CR/Re/Cowl (millions)
○	1.0726	run80	3/2.15/50%
□	1.0726	run40	5/2.15/50%
◇	1.0726	run57	9/2.15/50%

Figure 7.2.1.343: CR Effects (Re=2.15million/ft, 50%CowI) Baseplate Pressures



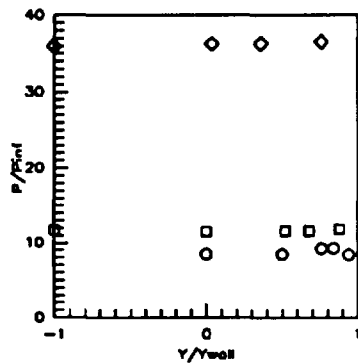
Sym	$x'/Ts'$	Run No.	CR/Re/Cowl (millions)
○	1.1567	run80	3/2.15/50%
□	1.1567	run40	5/2.15/50%
◇	1.1567	run57	9/2.15/50%

Figure 7.2.1.344: CR Effects (Re=2.15million/ft, 50%CowI) Baseplate Pressures



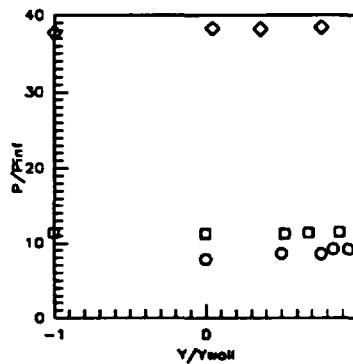
Sym	$x'/Ts'$	Run No.	CR/Re/Cowl (millions)
○	1.2408	run80	3/2.15/50%
□	1.2408	run40	5/2.15/50%
◇	1.2408	run57	9/2.15/50%

Figure 7.2.1.345: CR Effects (Re=2.15million/ft, 50%CowI) Baseplate Pressures



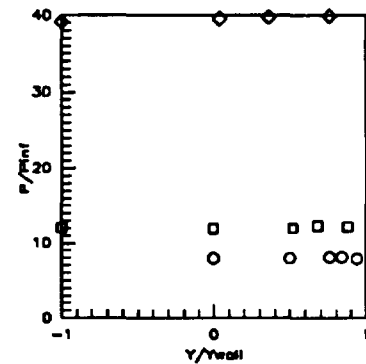
Sym	$x'/Ts'$	Run No.	CR/Re/Cowl (millions)
○	1.3248	run80	3/2.15/50%
□	1.3248	run40	5/2.15/50%
◇	1.3248	run57	9/2.15/50%

Figure 7.2.1.346: CR Effects (Re=2.15million/ft, 50%CowI) Baseplate Pressures



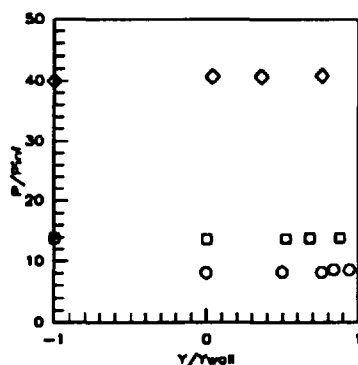
Sym	$x'/Ts'$	Run No.	CR/Re/Cowl (millions)
○	1.4090	run80	3/2.15/50%
□	1.4090	run40	5/2.15/50%
◇	1.4090	run57	9/2.15/50%

Figure 7.2.1.347: CR Effects (Re=2.15million/ft, 50%CowI) Baseplate Pressures



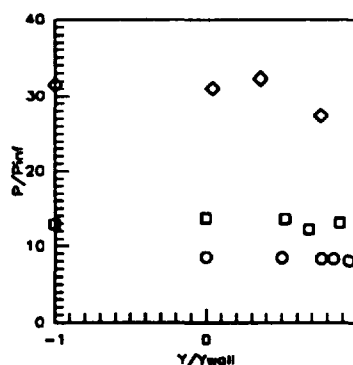
Sym	$x'/Ts'$	Run No.	CR/Re/Cowl (millions)
○	1.4932	run80	3/2.15/50%
□	1.4932	run40	5/2.15/50%
◇	1.4932	run57	9/2.15/50%

Figure 7.2.1.348: CR Effects (Re=2.15million/ft, 50%CowI) Baseplate Pressures



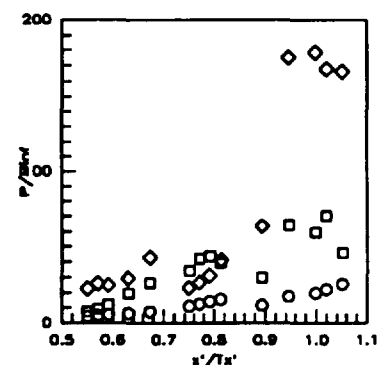
Sym	$x'/Ts'$	Run No.	CR/Re/Cowl (millions)
○	1.5773	run80	3/2.15/50%
□	1.5773	run40	5/2.15/50%
◇	1.5773	run57	9/2.15/50%

Figure 7.2.1.349: CR Effects (Re=2.15million/ft, 50%CowI) Baseplate Pressures



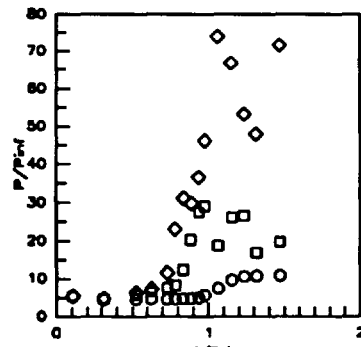
Sym	$x'/Ts'$	Run No.	CR/Re/Cowl (millions)
○	1.6824	run80	3/2.15/50%
□	1.6824	run40	5/2.15/50%
◇	1.6824	run57	9/2.15/50%

Figure 7.2.1.350: CR Effects (Re=2.15million/ft, 50%CowI) Baseplate Pressures



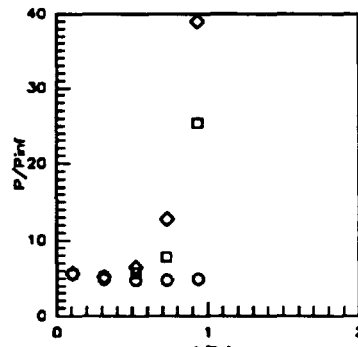
Sym	Cowl Pos.	Run No.	CR/Re/Cowl (millions)
○	50%	run80	3/2.15/50%
□	50%	run40	5/2.15/50%
◇	50%	run57	9/2.15/50%

Figure 7.2.1.351: CR Effects (Re=2.15million/ft, 50%CowI) Cowl Pressures



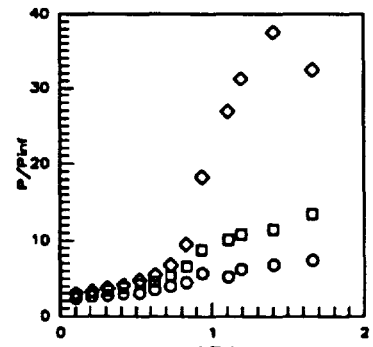
Sym	Z/H	Run No.	CR/Re/Cowl (millions)
○	0.5RT	run80	3/2.15/50%
□	0.5RT	run40	5/2.15/50%
○	0.5RT	run57	9/2.15/50%

Figure 7.2.1.352: CR Effects (Re=2.15million/ft, 50%Cowl) Sidewall Centerline Pressures



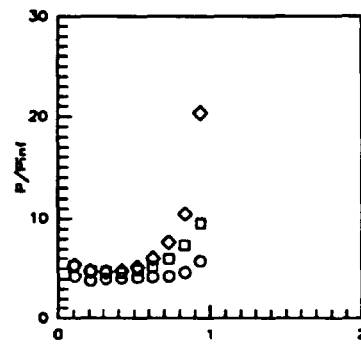
Sym	Z/H	Run No.	CR/Re/Cowl (millions)
○	0.5LT	run80	3/2.15/50%
□	0.5LT	run40	5/2.15/50%
○	0.5LT	run57	9/2.15/50%

Figure 7.2.1.353: CR Effects (Re=2.15million/ft, 50%Cowl) Sidewall Centerline Pressures



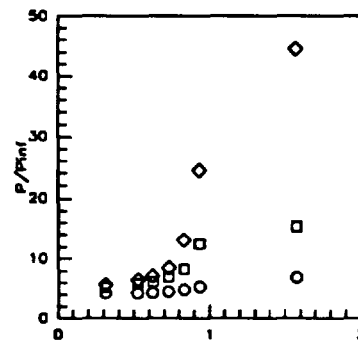
Sym	Z/H	Run No.	CR/Re/Cowl (millions)
○	0.05	run80	3/2.15/50%
□	0.05	run40	5/2.15/50%
○	0.05	run57	9/2.15/50%

Figure 7.2.1.354: CR Effects (Re=2.15million/ft, 50%Cowl) Sidewall Pressures



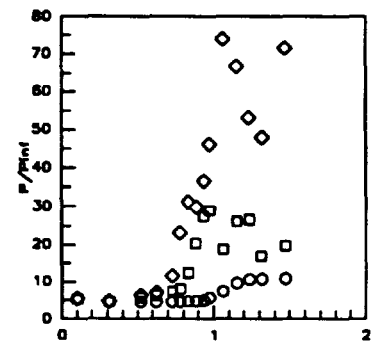
Sym	Z/H	Run No.	CR/Re/Cowl (millions)
○	0.15	run80	3/2.15/50%
□	0.15	run40	5/2.15/50%
○	0.15	run57	9/2.15/50%

Figure 7.2.1.355: CR Effects (Re=2.15million/ft, 50%Cowl) Sidewall Pressures



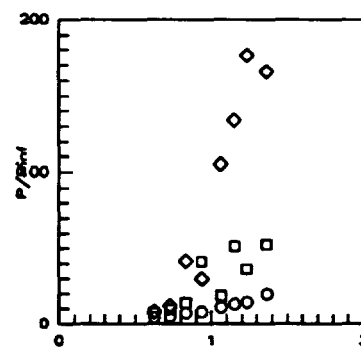
Sym	Z/H	Run No.	CR/Re/Cowl (millions)
○	0.25	run80	3/2.15/50%
□	0.25	run40	5/2.15/50%
○	0.25	run57	9/2.15/50%

Figure 7.2.1.356: CR Effects (Re=2.15million/ft, 50%Cowl) Sidewall Pressures



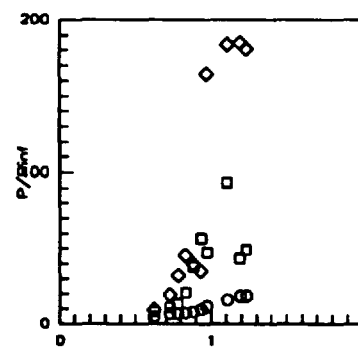
Sym	Z/H	Run No.	CR/Re/Cowl (millions)
○	0.50	run80	3/2.15/50%
□	0.50	run40	5/2.15/50%
○	0.50	run57	9/2.15/50%

Figure 7.2.1.357: CR Effects (Re=2.15million/ft, 50%Cowl) Sidewall Pressures



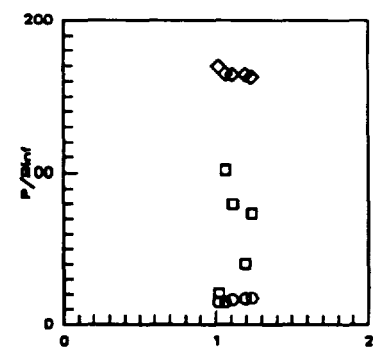
Sym	Z/H	Run No.	CR/Re/Cowl (millions)
○	0.75	run80	3/2.15/50%
□	0.75	run40	5/2.15/50%
○	0.75	run57	9/2.15/50%

Figure 7.2.1.358: CR Effects (Re=2.15million/ft, 50%Cowl) Sidewall Pressures



Sym	Z/H	Run No.	CR/Re/Cowl (millions)
○	0.85	run80	3/2.15/50%
□	0.85	run40	5/2.15/50%
○	0.85	run57	9/2.15/50%

Figure 7.2.1.359: CR Effects (Re=2.15million/ft, 50%Cowl) Sidewall Pressures



Sym	Z/H	Run No.	CR/Re/Cowl (millions)
○	0.90	run80	3/2.15/50%
□	0.90	run40	5/2.15/50%
○	0.90	run57	9/2.15/50%

Figure 7.2.1.360: CR Effects (Re=2.15million/ft, 50%Cowl) Sidewall Pressures

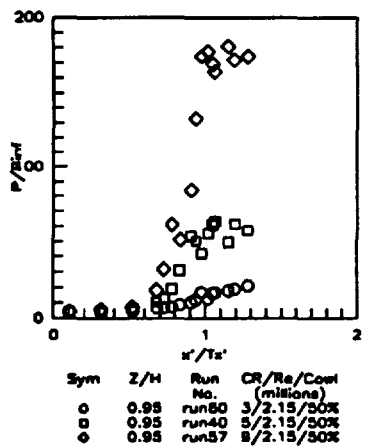


Figure 7.2.1.361: CR Effects (Re=2.15million/ft, 50%CowI) Sidewall Pressures

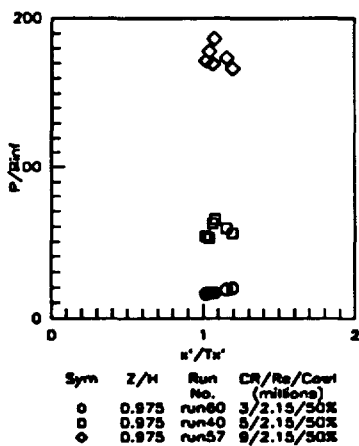


Figure 7.2.1.362: CR Effects (Re=2.15million/ft, 50%CowI) Sidewall Pressures

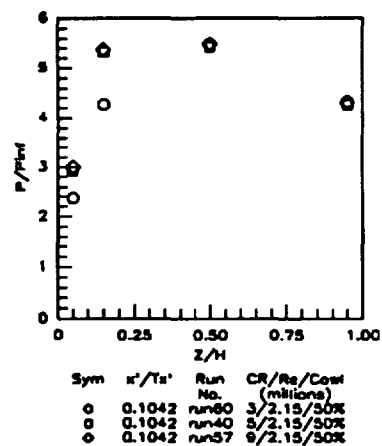


Figure 7.2.1.363: CR Effects (Re=2.15million/ft, 50%CowI) Sidewall Pressures

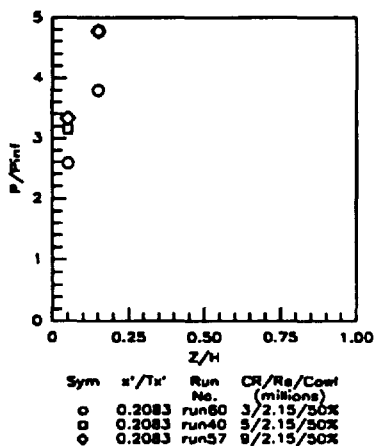


Figure 7.2.1.364: CR Effects (Re=2.15million/ft, 50%CowI) Sidewall Pressures

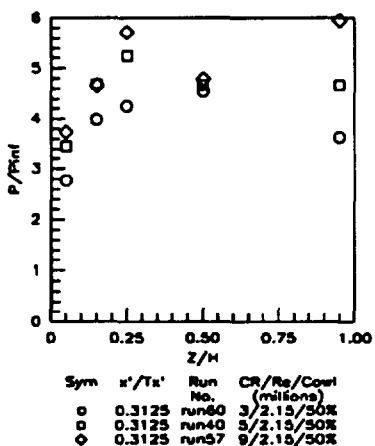


Figure 7.2.1.365: CR Effects (Re=2.15million/ft, 50%CowI) Sidewall Pressures

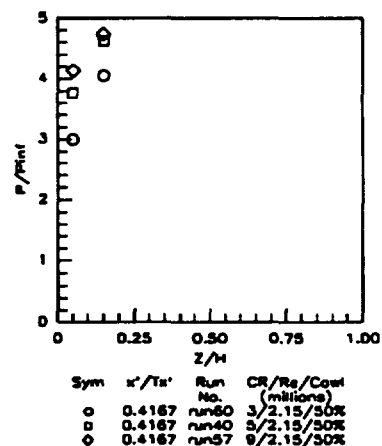


Figure 7.2.1.366: CR Effects (Re=2.15million/ft, 50%CowI) Sidewall Pressures

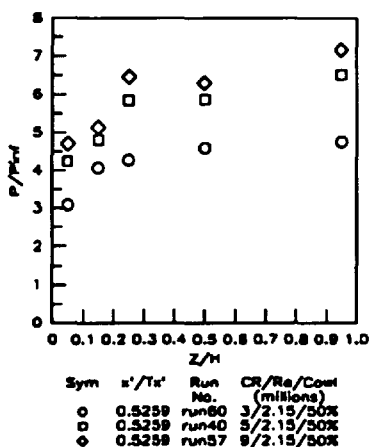


Figure 7.2.1.367: CR Effects (Re=2.15million/ft, 50%CowI) Sidewall Pressures

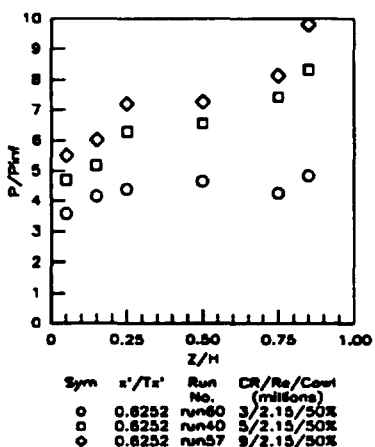


Figure 7.2.1.368: CR Effects (Re=2.15million/ft, 50%CowI) Sidewall Pressures

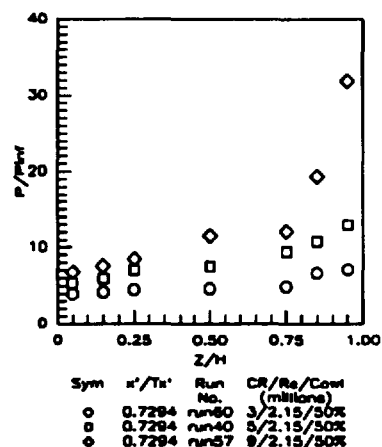
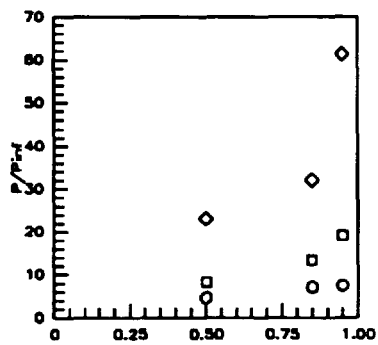
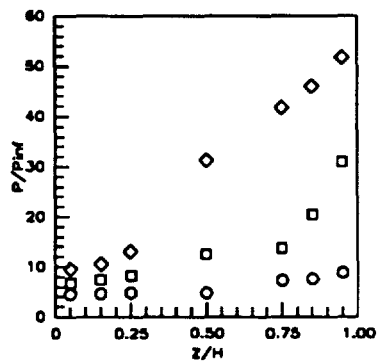


Figure 7.2.1.369: CR Effects (Re=2.15million/ft, 50%CowI) Sidewall Pressures



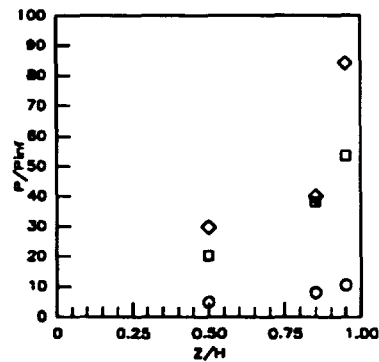
Sym	$x'/T_x'$	Run No.	CR/Re/Cowl (milions)
○	0.7815	run60	3/2.15/50%
□	0.7815	run40	5/2.15/50%
◇	0.7815	run57	9/2.15/50%

Figure 7.2.1.370: CR Effects (Re=2.15million/ft, 50%CowI) Sidewall Pressures



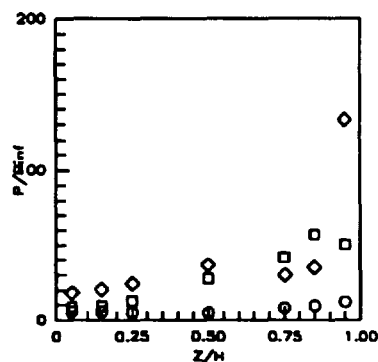
Sym	$x'/T_x'$	Run No.	CR/Re/Cowl (milions)
○	0.8336	run60	3/2.15/50%
□	0.8336	run40	5/2.15/50%
◇	0.8336	run57	9/2.15/50%

Figure 7.2.1.371: CR Effects (Re=2.15million/ft, 50%CowI) Sidewall Pressures



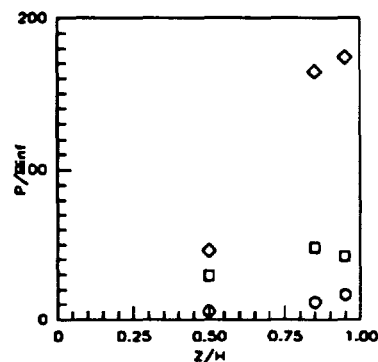
Sym	$x'/T_x'$	Run No.	CR/Re/Cowl (milions)
○	0.8857	run60	3/2.15/50%
□	0.8857	run40	5/2.15/50%
◇	0.8857	run57	9/2.15/50%

Figure 7.2.1.372: CR Effects (Re=2.15million/ft, 50%CowI) Sidewall Pressures



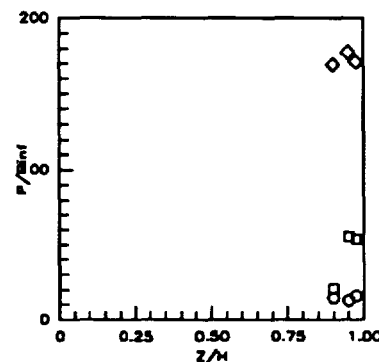
Sym	$x'/T_x'$	Run No.	CR/Re/Cowl (milions)
○	0.9378	run60	3/2.15/50%
□	0.9378	run40	5/2.15/50%
◇	0.9378	run57	9/2.15/50%

Figure 7.2.1.373: CR Effects (Re=2.15million/ft, 50%CowI) Sidewall Pressures



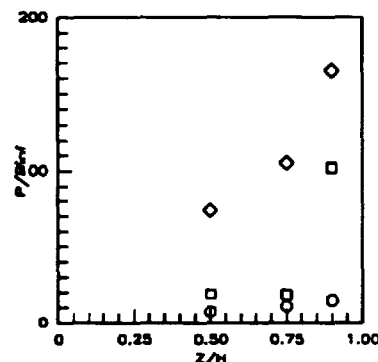
Sym	$x'/T_x'$	Run No.	CR/Re/Cowl (milions)
○	0.9751	run60	3/2.15/50%
□	0.9751	run40	5/2.15/50%
◇	0.9751	run57	9/2.15/50%

Figure 7.2.1.374: CR Effects (Re=2.15million/ft, 50%CowI) Sidewall Pressures



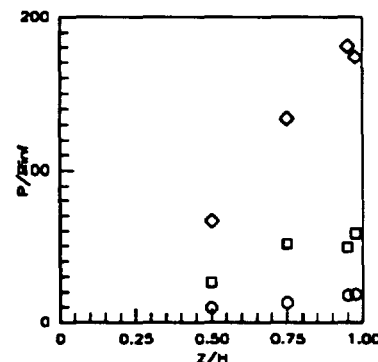
Sym	$x'/T_x'$	Run No.	CR/Re/Cowl (milions)
○	1.0197	run60	3/2.15/50%
□	1.0197	run40	5/2.15/50%
◇	1.0197	run57	9/2.15/50%

Figure 7.2.1.375: CR Effects (Re=2.15million/ft, 50%CowI) Sidewall Pressures



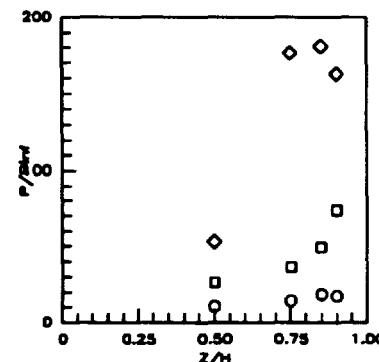
Sym	$x'/T_x'$	Run No.	CR/Re/Cowl (milions)
○	1.0643	run60	3/2.15/50%
□	1.0643	run40	5/2.15/50%
◇	1.0643	run57	9/2.15/50%

Figure 7.2.1.376: CR Effects (Re=2.15million/ft, 50%CowI) Sidewall Pressures



Sym	$x'/T_x'$	Run No.	CR/Re/Cowl (milions)
○	1.1537	run60	3/2.15/50%
□	1.1537	run40	5/2.15/50%
◇	1.1537	run57	9/2.15/50%

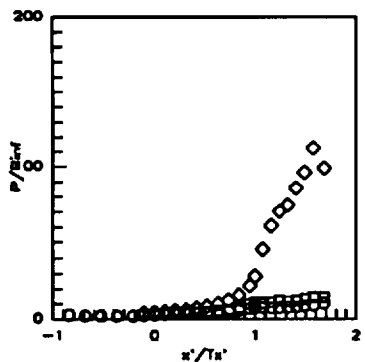
Figure 7.2.1.377: CR Effects (Re=2.15million/ft, 50%CowI) Sidewall Pressures



Sym	$x'/T_x'$	Run No.	CR/Re/Cowl (milions)
○	1.2356	run60	3/2.15/50%
□	1.2356	run40	5/2.15/50%
◇	1.2356	run57	9/2.15/50%

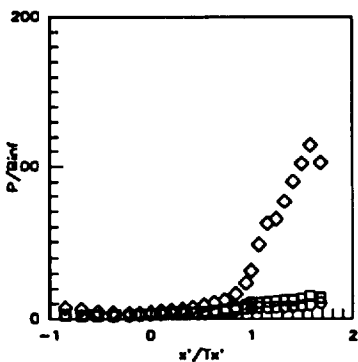
Figure 7.2.1.378: CR Effects (Re=2.15million/ft, 50%CowI) Sidewall Pressures





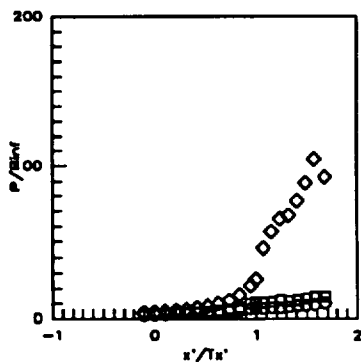
Sym	C.L. for	Run No.	CR/Re/Cowf (millions)
○	CR=3	run59	3/1.14/50%
□	CR=5	run39	5/1.14/50%
◇	CR=9	run56	9/1.14/50%

Figure 7.2.1.379: CR Effects (Re=1.14million/ft, 50%Cowf) Centerline Pressures



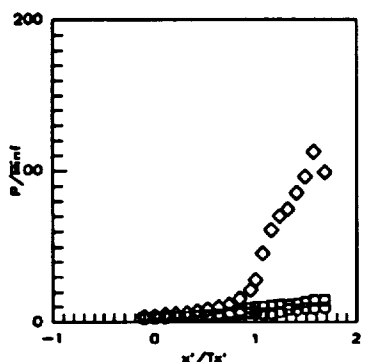
Sym	C.L. for	Run No.	CR/Re/Cowf (millions)
○	CR=3	run59	3/1.14/50%
□	CR=3	run39	5/1.14/50%
◇	CR=3	run56	9/1.14/50%

Figure 7.2.1.380: CR Effects (Re=1.14million/ft, 50%Cowf) CR=3 Centerline Pressures



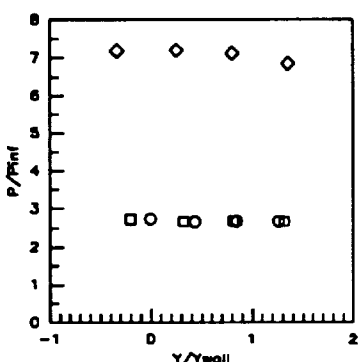
Sym	C.L. for	Run No.	CR/Re/Cowf (millions)
○	CR=5	run59	3/1.14/50%
□	CR=5	run39	5/1.14/50%
◇	CR=5	run56	9/1.14/50%

Figure 7.2.1.381: CR Effects (Re=1.14million/ft, 50%Cowf) CR=5 Centerline Pressures



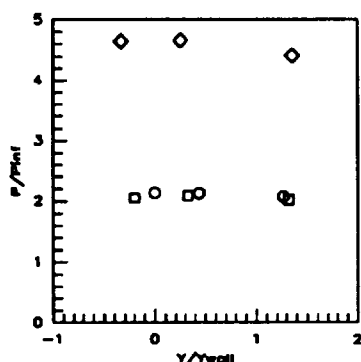
Sym	C.L. for	Run No.	CR/Re/Cowf (millions)
○	CR=9	run59	3/1.14/50%
□	CR=9	run39	5/1.14/50%
◇	CR=9	run56	9/1.14/50%

Figure 7.2.1.382: CR Effects (Re=1.14million/ft, 50%Cowf) CR=9 Centerline Pressures



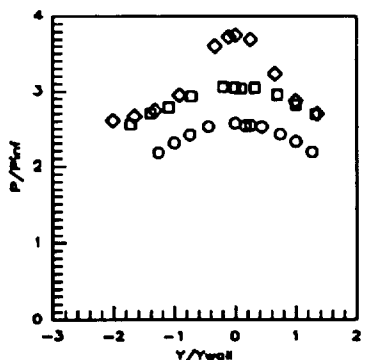
Sym	x'/Ts'	Run No.	CR/Re/Cowf (millions)
○	-0.8412	run59	3/1.14/50%
□	-0.8412	run39	5/1.14/50%
◇	-0.8412	run56	9/1.14/50%

Figure 7.2.1.383: CR Effects (Re=1.14million/ft, 50%Cowf) Baseplate Pressures



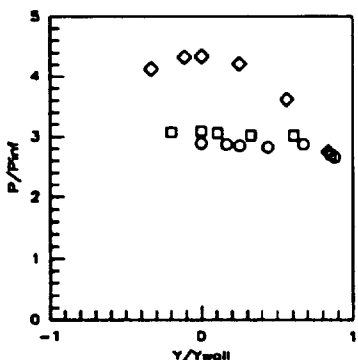
Sym	x'/Ts'	Run No.	CR/Re/Cowf (millions)
○	-0.5258	run59	3/1.14/50%
□	-0.5258	run39	5/1.14/50%
◇	-0.5258	run56	9/1.14/50%

Figure 7.2.1.384: CR Effects (Re=1.14million/ft, 50%Cowf) Baseplate Pressures



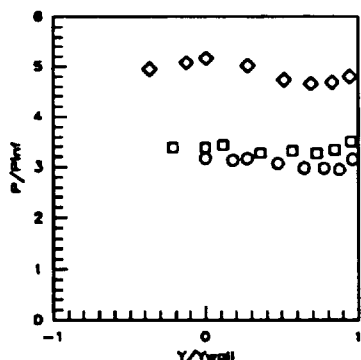
Sym	x'/Ts'	Run No.	CR/Re/Cowf (millions)
○	-0.1052	run59	3/1.14/50%
□	-0.1052	run39	5/1.14/50%
◇	-0.1052	run56	9/1.14/50%

Figure 7.2.1.385: CR Effects (Re=1.14million/ft, 50%Cowf) Baseplate Pressures



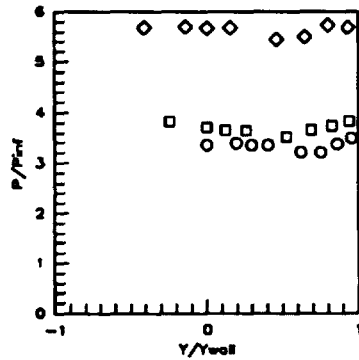
Sym	x'/Ts'	Run No.	CR/Re/Cowf (millions)
○	0.0000	run59	3/1.14/50%
□	0.0000	run39	5/1.14/50%
◇	0.0000	run56	9/1.14/50%

Figure 7.2.1.386: CR Effects (Re=1.14million/ft, 50%Cowf) Baseplate Pressures



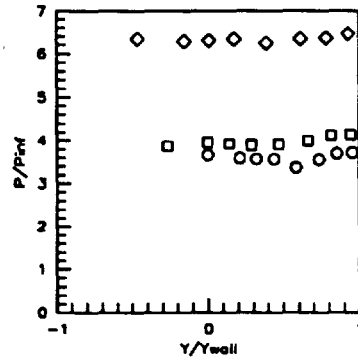
Sym	x'/Ts'	Run No.	CR/Re/Cowf (millions)
○	0.1052	run59	3/1.14/50%
□	0.1052	run39	5/1.14/50%
◇	0.1052	run56	9/1.14/50%

Figure 7.2.1.387: CR Effects (Re=1.14million/ft, 50%Cowf) Baseplate Pressures



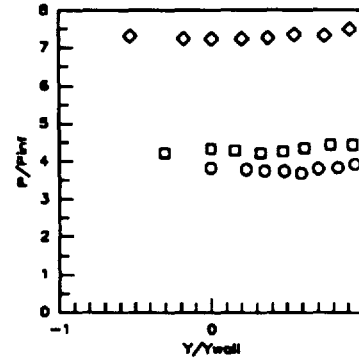
Sym	$x'/Tx'$	Run No.	CR/Re/CowI (milions)
◇	0.2103	run59	3/1.14/50%
□	0.2103	run39	5/1.14/50%
○	0.2103	run56	9/1.14/50%

Figure 7.2.1.388: CR Effects (Re=1.14million/ft, 50%CowI) Baseplate Pressures



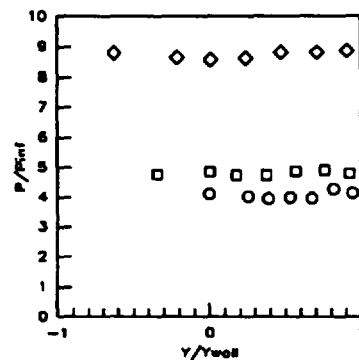
Sym	$x'/Tx'$	Run No.	CR/Re/CowI (milions)
◇	0.3154	run59	3/1.14/50%
□	0.3154	run39	5/1.14/50%
○	0.3154	run56	9/1.14/50%

Figure 7.2.1.389: CR Effects (Re=1.14million/ft, 50%CowI) Baseplate Pressures



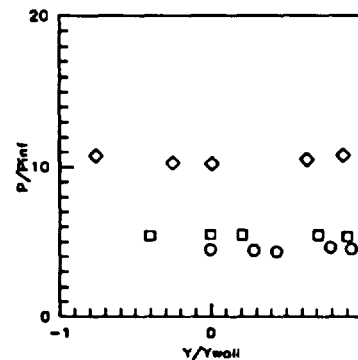
Sym	$x'/Tx'$	Run No.	CR/Re/CowI (milions)
◇	0.4206	run59	3/1.14/50%
□	0.4206	run39	5/1.14/50%
○	0.4206	run56	9/1.14/50%

Figure 7.2.1.390: CR Effects (Re=1.14million/ft, 50%CowI) Baseplate Pressures



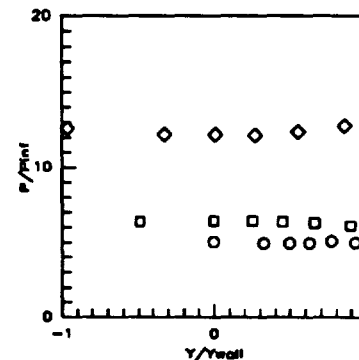
Sym	$x'/Tx'$	Run No.	CR/Re/CowI (milions)
◇	0.5258	run59	3/1.14/50%
□	0.5258	run39	5/1.14/50%
○	0.5258	run56	9/1.14/50%

Figure 7.2.1.391: CR Effects (Re=1.14million/ft, 50%CowI) Baseplate Pressures



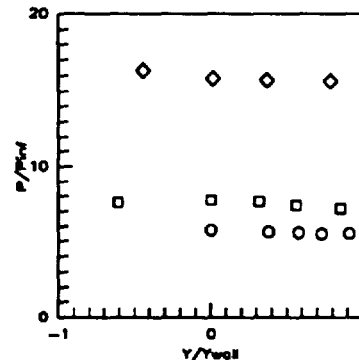
Sym	$x'/Tx'$	Run No.	CR/Re/CowI (milions)
◇	0.6309	run59	3/1.14/50%
□	0.6309	run39	5/1.14/50%
○	0.6309	run56	9/1.14/50%

Figure 7.2.1.392: CR Effects (Re=1.14million/ft, 50%CowI) Baseplate Pressures



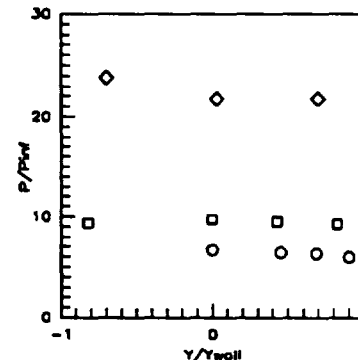
Sym	$x'/Tx'$	Run No.	CR/Re/CowI (milions)
◇	0.7361	run59	3/1.14/50%
□	0.7361	run39	5/1.14/50%
○	0.7361	run56	9/1.14/50%

Figure 7.2.1.393: CR Effects (Re=1.14million/ft, 50%CowI) Baseplate Pressures



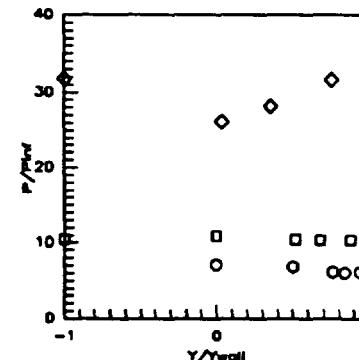
Sym	$x'/Tx'$	Run No.	CR/Re/CowI (milions)
◇	0.8412	run59	3/1.14/50%
□	0.8412	run39	5/1.14/50%
○	0.8412	run56	9/1.14/50%

Figure 7.2.1.394: CR Effects (Re=1.14million/ft, 50%CowI) Baseplate Pressures



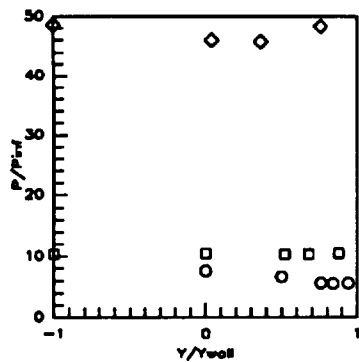
Sym	$x'/Tx'$	Run No.	CR/Re/CowI (milions)
◇	0.9464	run59	3/1.14/50%
□	0.9464	run39	5/1.14/50%
○	0.9464	run56	9/1.14/50%

Figure 7.2.1.395: CR Effects (Re=1.14million/ft, 50%CowI) Baseplate Pressures



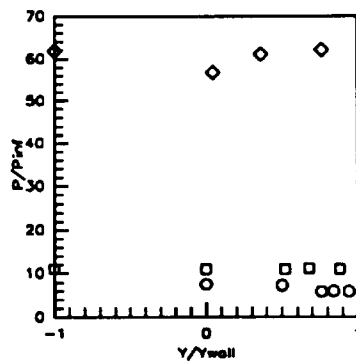
Sym	$x'/Tx'$	Run No.	CR/Re/CowI (milions)
◇	1.0000	run59	3/1.14/50%
□	1.0000	run39	5/1.14/50%
○	1.0000	run56	9/1.14/50%

Figure 7.2.1.396: CR Effects (Re=1.14million/ft, 50%CowI) Baseplate Pressures



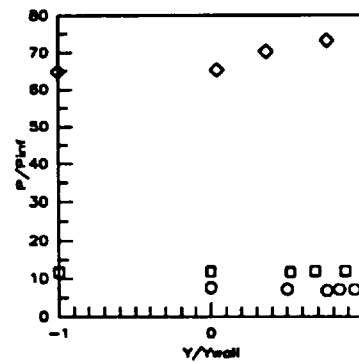
Sym	$x'/T_x'$	Run No.	CR/Re/Cowl (millions)
○	1.0726	run59	3/1.14/50%
□	1.0726	run39	5/1.14/50%
◇	1.0726	run56	9/1.14/50%

Figure 7.2.1.397: CR Effects (Re=1.14million/ft, 50%CowI) Baseplate Pressures



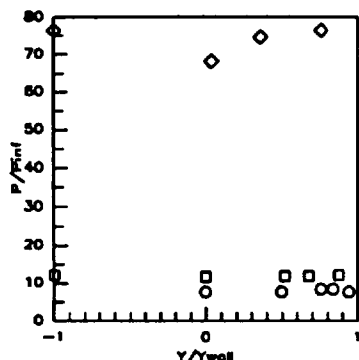
Sym	$x'/T_x'$	Run No.	CR/Re/Cowl (millions)
○	1.1587	run59	3/1.14/50%
□	1.1587	run39	5/1.14/50%
◇	1.1587	run56	9/1.14/50%

Figure 7.2.1.398: CR Effects (Re=1.14million/ft, 50%CowI) Baseplate Pressures



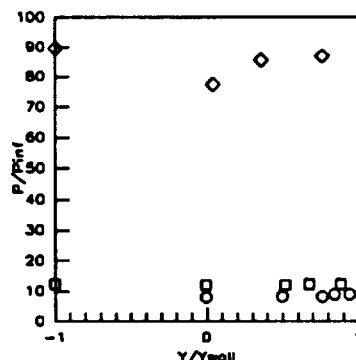
Sym	$x'/T_x'$	Run No.	CR/Re/Cowl (millions)
○	1.2408	run59	3/1.14/50%
□	1.2408	run39	5/1.14/50%
◇	1.2408	run56	9/1.14/50%

Figure 7.2.1.399: CR Effects (Re=1.14million/ft, 50%CowI) Baseplate Pressures



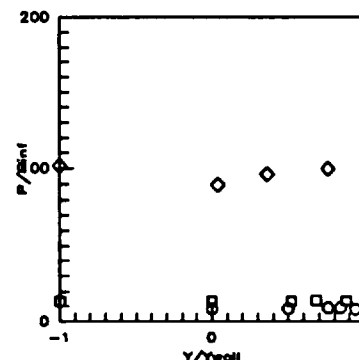
Sym	$x'/T_x'$	Run No.	CR/Re/Cowl (millions)
○	1.3248	run59	3/1.14/50%
□	1.3248	run39	5/1.14/50%
◇	1.3248	run56	9/1.14/50%

Figure 7.2.1.400: CR Effects (Re=1.14million/ft, 50%CowI) Baseplate Pressures



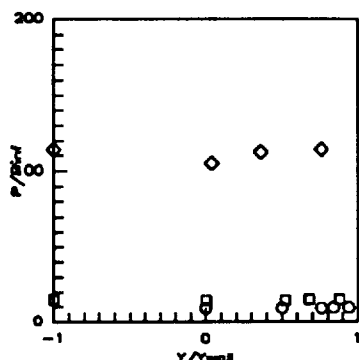
Sym	$x'/T_x'$	Run No.	CR/Re/Cowl (millions)
○	1.4090	run59	3/1.14/50%
□	1.4090	run39	5/1.14/50%
◇	1.4090	run56	9/1.14/50%

Figure 7.2.1.401: CR Effects (Re=1.14million/ft, 50%CowI) Baseplate Pressures



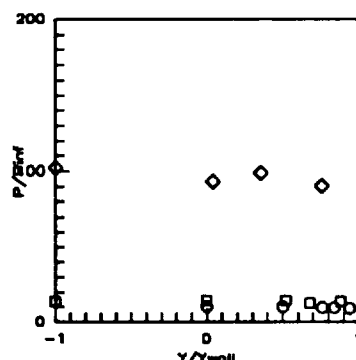
Sym	$x'/T_x'$	Run No.	CR/Re/Cowl (millions)
○	1.4932	run59	3/1.14/50%
□	1.4932	run39	5/1.14/50%
◇	1.4932	run56	9/1.14/50%

Figure 7.2.1.402: CR Effects (Re=1.14million/ft, 50%CowI) Baseplate Pressures



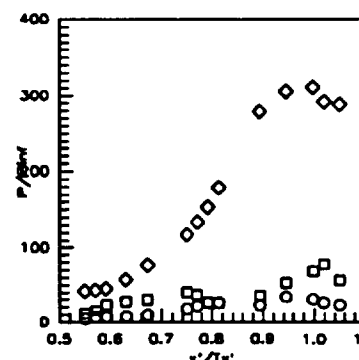
Sym	$x'/T_x'$	Run No.	CR/Re/Cowl (millions)
○	1.5773	run59	3/1.14/50%
□	1.5773	run39	5/1.14/50%
◇	1.5773	run56	9/1.14/50%

Figure 7.2.1.403: CR Effects (Re=1.14million/ft, 50%CowI) Baseplate Pressures



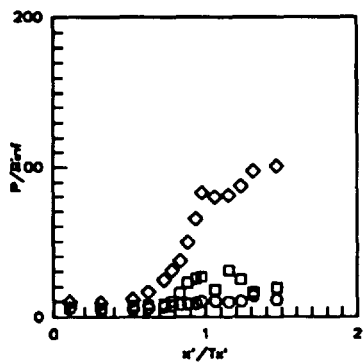
Sym	$x'/T_x'$	Run No.	CR/Re/Cowl (millions)
○	1.6824	run59	3/1.14/50%
□	1.6824	run39	5/1.14/50%
◇	1.6824	run56	9/1.14/50%

Figure 7.2.1.404: CR Effects (Re=1.14million/ft, 50%CowI) Baseplate Pressures



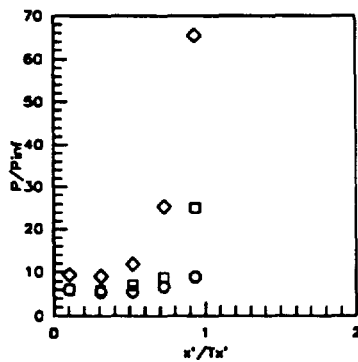
Sym	Cowl Pos.	Run No.	CR/Re/Cowl (millions)
○	50%	run59	3/1.14/50%
□	50%	run39	5/1.14/50%
◇	50%	run56	9/1.14/50%

Figure 7.2.1.405: CR Effects (Re=1.14million/ft, 50%CowI) Cowl Pressures



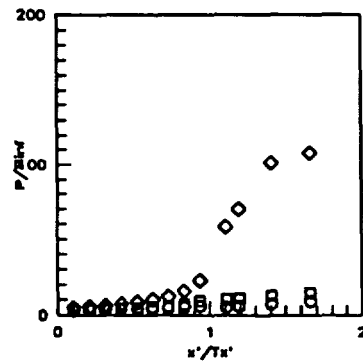
Sym	Z/H	Run No.	CR/Re/Cowl (millions)
○	0.5RT	run59	3/1.14/50%
□	0.5RT	run39	5/1.14/50%
◇	0.5RT	run56	9/1.14/50%

Figure 7.2.1.406: CR Effects (Re=1.14million/ft, 50%Cow) Sidewall Centerline Pressures



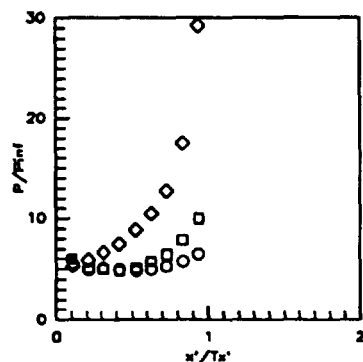
Sym	Z/H	Run No.	CR/Re/Cowl (millions)
○	0.5LT	run59	3/1.14/50%
□	0.5LT	run39	5/1.14/50%
◇	0.5LT	run56	9/1.14/50%

Figure 7.2.1.407: CR Effects (Re=1.14million/ft, 50%Cow) Sidewall Centerline Pressures



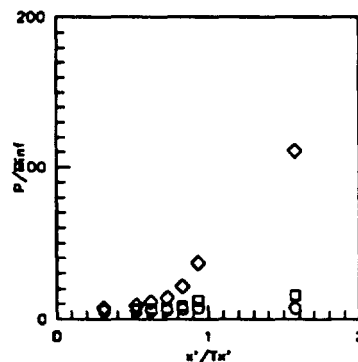
Sym	Z/H	Run No.	CR/Re/Cowl (millions)
○	0.05	run59	3/1.14/50%
□	0.05	run39	5/1.14/50%
◇	0.05	run56	9/1.14/50%

Figure 7.2.1.408: CR Effects (Re=1.14million/ft, 50%Cow) Sidewall Pressures



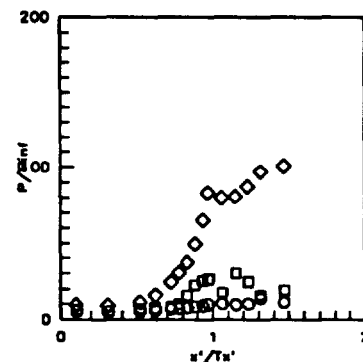
Sym	Z/H	Run No.	CR/Re/Cowl (millions)
○	0.15	run59	3/1.14/50%
□	0.15	run39	5/1.14/50%
◇	0.15	run56	9/1.14/50%

Figure 7.2.1.409: CR Effects (Re=1.14million/ft, 50%Cow) Sidewall Pressures



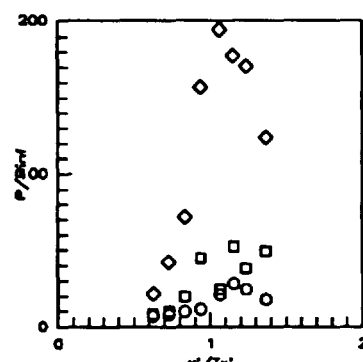
Sym	Z/H	Run No.	CR/Re/Cowl (millions)
○	0.25	run59	3/1.14/50%
□	0.25	run39	5/1.14/50%
◇	0.25	run56	9/1.14/50%

Figure 7.2.1.410: CR Effects (Re=1.14million/ft, 50%Cow) Sidewall Pressures



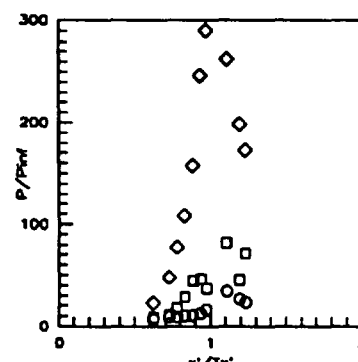
Sym	Z/H	Run No.	CR/Re/Cowl (millions)
○	0.50	run59	3/1.14/50%
□	0.50	run39	5/1.14/50%
◇	0.50	run56	9/1.14/50%

Figure 7.2.1.411: CR Effects (Re=1.14million/ft, 50%Cow) Sidewall Pressures



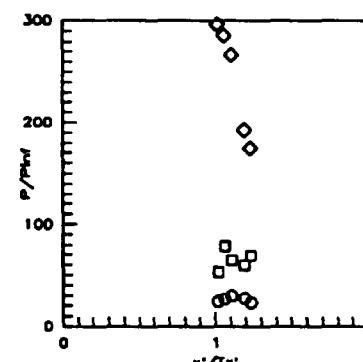
Sym	Z/H	Run No.	CR/Re/Cowl (millions)
○	0.75	run59	3/1.14/50%
□	0.75	run39	5/1.14/50%
◇	0.75	run56	9/1.14/50%

Figure 7.2.1.412: CR Effects (Re=1.14million/ft, 50%Cow) Sidewall Pressures



Sym	Z/H	Run No.	CR/Re/Cowl (millions)
○	0.85	run59	3/1.14/50%
□	0.85	run39	5/1.14/50%
◇	0.85	run56	9/1.14/50%

Figure 7.2.1.413: CR Effects (Re=1.14million/ft, 50%Cow) Sidewall Pressures



Sym	Z/H	Run No.	CR/Re/Cowl (millions)
○	0.90	run59	3/1.14/50%
□	0.90	run39	5/1.14/50%
◇	0.90	run56	9/1.14/50%

Figure 7.2.1.414: CR Effects (Re=1.14million/ft, 50%Cow) Sidewall Pressures

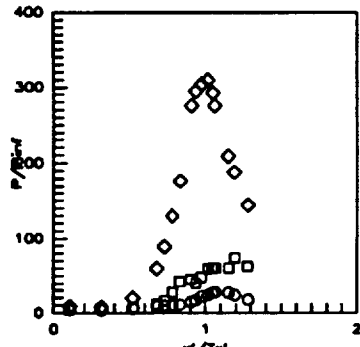


Figure 7.2.1.415: CR Effects  
(Re=1.14million/ft, 50%CowI)  
Sidewall Pressures

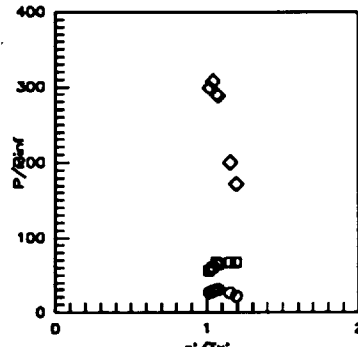


Figure 7.2.1.416: CR Effects  
(Re=1.14million/ft, 50%CowI)  
Sidewall Pressures

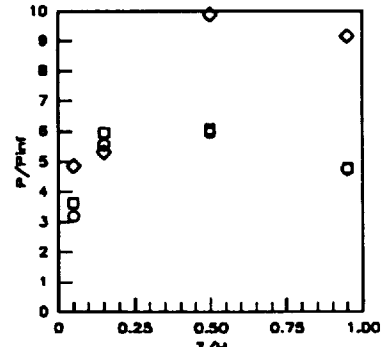


Figure 7.2.1.417: CR Effects  
(Re=1.14million/ft, 50%CowI)  
Sidewall Pressures

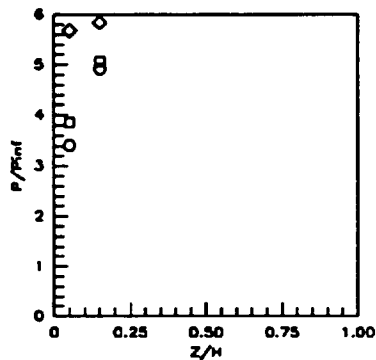


Figure 7.2.1.418: CR Effects  
(Re=1.14million/ft, 50%CowI)  
Sidewall Pressures

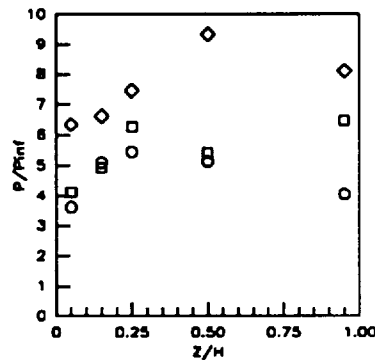


Figure 7.2.1.419: CR Effects  
(Re=1.14million/ft, 50%CowI)  
Sidewall Pressures

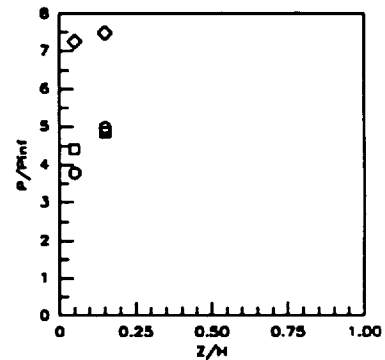


Figure 7.2.1.420: CR Effects  
(Re=1.14million/ft, 50%CowI)  
Sidewall Pressures

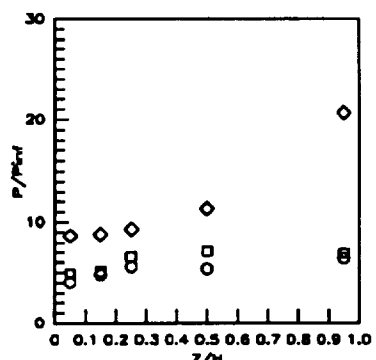


Figure 7.2.1.421: CR Effects  
(Re=1.14million/ft, 50%CowI)  
Sidewall Pressures

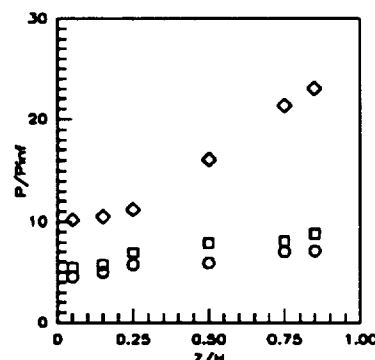


Figure 7.2.1.422: CR Effects  
(Re=1.14million/ft, 50%CowI)  
Sidewall Pressures

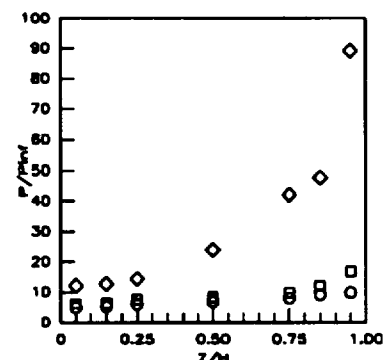
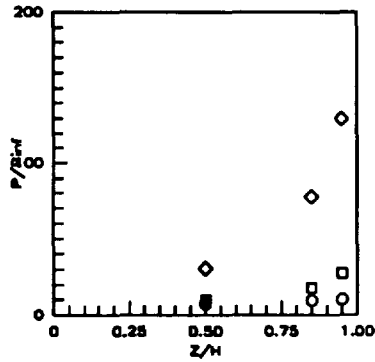
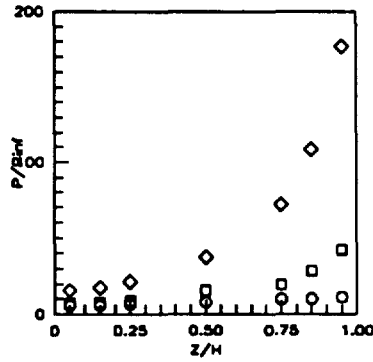


Figure 7.2.1.423: CR Effects  
(Re=1.14million/ft, 50%CowI)  
Sidewall Pressures



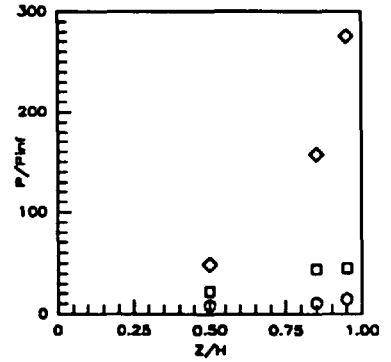
Sym	$x'/T_x'$	Run No.	CR/Re/Cowl (millions)
○	0.7815	run59	3/1.14/50%
□	0.7815	run39	5/1.14/50%
◇	0.7815	run56	9/1.14/50%

Figure 7.2.1.424: CR Effects (Re=1.14million/ft, 50%CowI) Sidewall Pressures



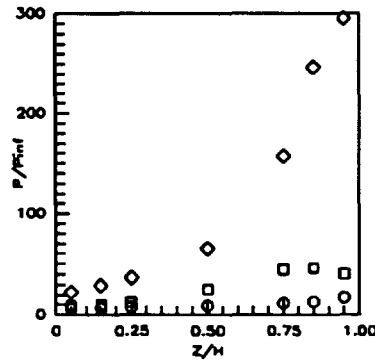
Sym	$x'/T_x'$	Run No.	CR/Re/Cowl (millions)
○	0.8336	run59	3/1.14/50%
□	0.8336	run39	5/1.14/50%
◇	0.8336	run56	9/1.14/50%

Figure 7.2.1.425: CR Effects (Re=1.14million/ft, 50%CowI) Sidewall Pressures



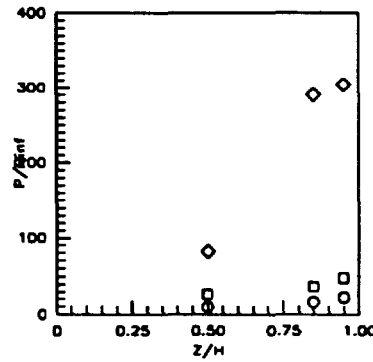
Sym	$x'/T_x'$	Run No.	CR/Re/Cowl (millions)
○	0.8857	run59	3/1.14/50%
□	0.8857	run39	5/1.14/50%
◇	0.8857	run56	9/1.14/50%

Figure 7.2.1.426: CR Effects (Re=1.14million/ft, 50%CowI) Sidewall Pressures



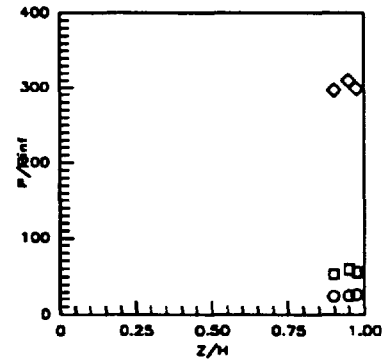
Sym	$x'/T_x'$	Run No.	CR/Re/Cowl (millions)
○	0.9378	run59	3/1.14/50%
□	0.9378	run39	5/1.14/50%
◇	0.9378	run56	9/1.14/50%

Figure 7.2.1.427: CR Effects (Re=1.14million/ft, 50%CowI) Sidewall Pressures



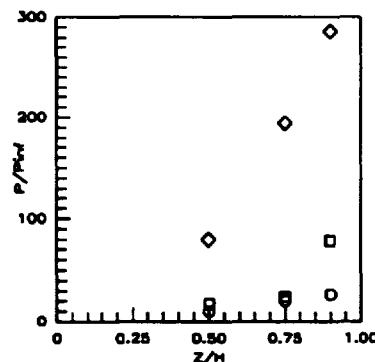
Sym	$x'/T_x'$	Run No.	CR/Re/Cowl (millions)
○	0.9751	run59	3/1.14/50%
□	0.9751	run39	5/1.14/50%
◇	0.9751	run56	9/1.14/50%

Figure 7.2.1.428: CR Effects (Re=1.14million/ft, 50%CowI) Sidewall Pressures



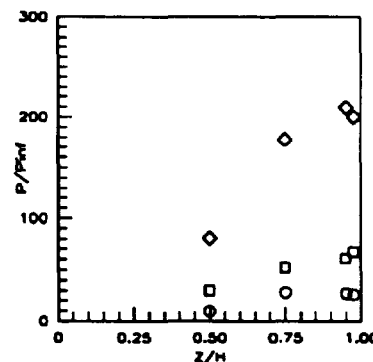
Sym	$x'/T_x'$	Run No.	CR/Re/Cowl (millions)
○	1.0187	run59	3/1.14/50%
□	1.0187	run39	5/1.14/50%
◇	1.0187	run56	9/1.14/50%

Figure 7.2.1.429: CR Effects (Re=1.14million/ft, 50%CowI) Sidewall Pressures



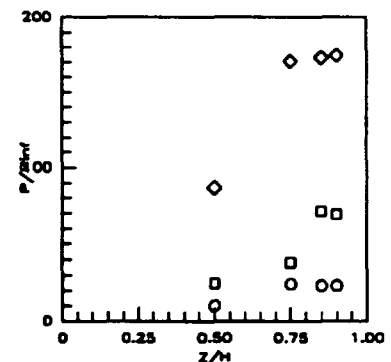
Sym	$x'/T_x'$	Run No.	CR/Re/Cowl (millions)
○	1.0643	run59	3/1.14/50%
□	1.0643	run39	5/1.14/50%
◇	1.0643	run56	9/1.14/50%

Figure 7.2.1.430: CR Effects (Re=1.14million/ft, 50%CowI) Sidewall Pressures



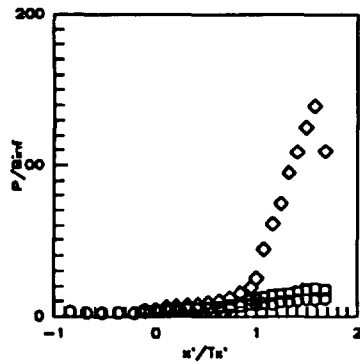
Sym	$x'/T_x'$	Run No.	CR/Re/Cowl (millions)
○	1.1537	run59	3/1.14/50%
□	1.1537	run39	5/1.14/50%
◇	1.1537	run56	9/1.14/50%

Figure 7.2.1.431: CR Effects (Re=1.14million/ft, 50%CowI) Sidewall Pressures



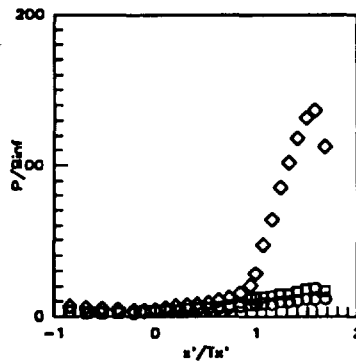
Sym	$x'/T_x'$	Run No.	CR/Re/Cowl (millions)
○	1.2356	run59	3/1.14/50%
□	1.2356	run39	5/1.14/50%
◇	1.2356	run56	9/1.14/50%

Figure 7.2.1.432: CR Effects (Re=1.14million/ft, 50%CowI) Sidewall Pressures



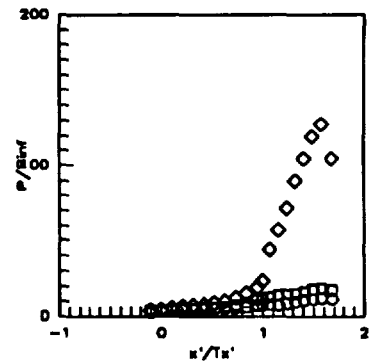
Sym	C.L. for	Run No.	CR/Re/Cowl (millions)
○	CR=3	run58	3/0.55/50%
□	CR=5	run37	5/0.55/50%
◇	CR=9	run55	9/0.55/50%

Figure 7.2.1.433: CR Effects (Re=0.55million/ft. 50%Cow) Centerline Pressures



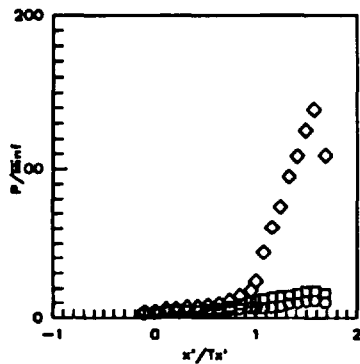
Sym	C.L. for	Run No.	CR/Re/Cowl (millions)
○	CR=3	run58	3/0.55/50%
□	CR=3	run37	5/0.55/50%
◇	CR=3	run55	9/0.55/50%

Figure 7.2.1.434: CR Effects (Re=0.55million/ft. 50%Cow) CR=3 Centerline Pressures



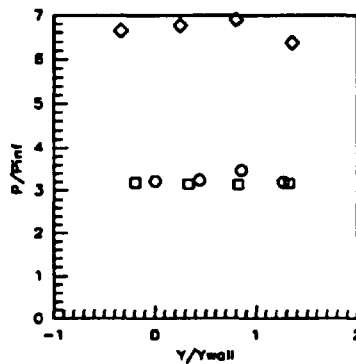
Sym	C.L. for	Run No.	CR/Re/Cowl (millions)
○	CR=5	run58	3/0.55/50%
□	CR=5	run37	5/0.55/50%
◇	CR=5	run55	9/0.55/50%

Figure 7.2.1.435: CR Effects (Re=0.55million/ft. 50%Cow) CR=5 Centerline Pressures



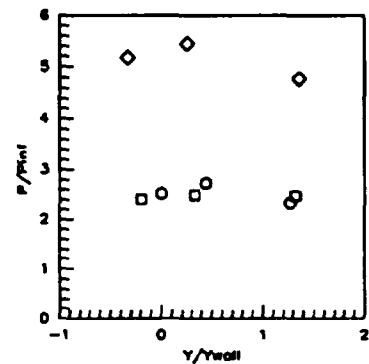
Sym	C.L. for	Run No.	CR/Re/Cowl (millions)
○	CR=9	run58	3/0.55/50%
□	CR=9	run37	5/0.55/50%
◇	CR=9	run55	9/0.55/50%

Figure 7.2.1.436: CR Effects (Re=0.55million/ft. 50%Cow) CR=9 Centerline Pressures



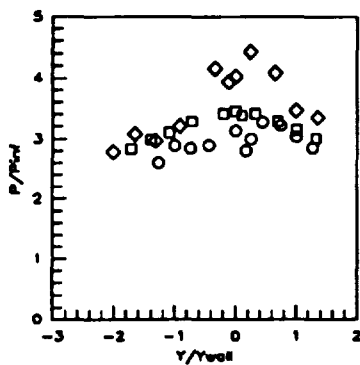
Sym	x'/Ts'	Run No.	CR/Re/Cowl (millions)
○	-0.8412	run58	3/0.55/50%
□	-0.8412	run37	5/0.55/50%
◇	-0.8412	run55	9/0.55/50%

Figure 7.2.1.437: CR Effects (Re=0.55million/ft. 50%Cow) Baseplate Pressures



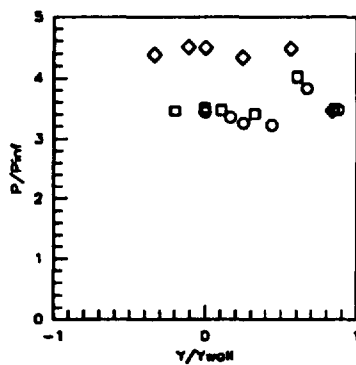
Sym	x'/Ts'	Run No.	CR/Re/Cowl (millions)
○	-0.5258	run58	3/0.55/50%
□	-0.5258	run37	5/0.55/50%
◇	-0.5258	run55	9/0.55/50%

Figure 7.2.1.438: CR Effects (Re=0.55million/ft. 50%Cow) Baseplate Pressures



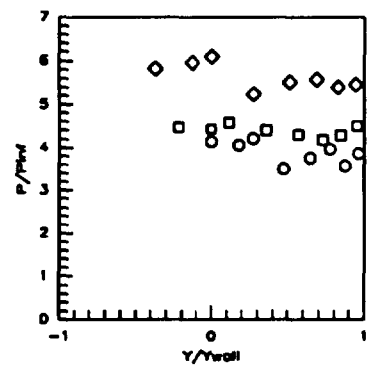
Sym	x'/Ts'	Run No.	CR/Re/Cowl (millions)
○	-0.1052	run58	3/0.55/50%
□	-0.1052	run37	5/0.55/50%
◇	-0.1052	run55	9/0.55/50%

Figure 7.2.1.439: CR Effects (Re=0.55million/ft. 50%Cow) Baseplate Pressures



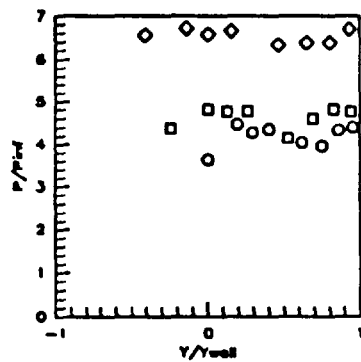
Sym	x'/Ts'	Run No.	CR/Re/Cowl (millions)
○	0.0000	run58	3/0.55/50%
□	0.0000	run37	5/0.55/50%
◇	0.0000	run55	9/0.55/50%

Figure 7.2.1.440: CR Effects (Re=0.55million/ft. 50%Cow) Baseplate Pressures



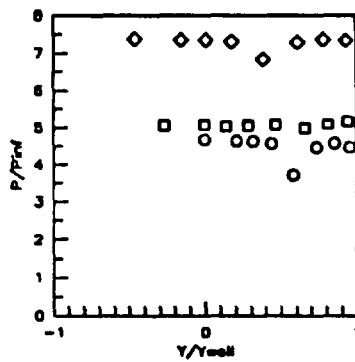
Sym	x'/Ts'	Run No.	CR/Re/Cowl (millions)
○	0.1052	run58	3/0.55/50%
□	0.1052	run37	5/0.55/50%
◇	0.1052	run55	9/0.55/50%

Figure 7.2.1.441: CR Effects (Re=0.55million/ft. 50%Cow) Baseplate Pressures



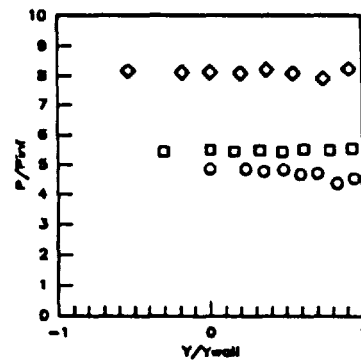
Sym	$x'/T_x'$	Run No.	CR/Re/Cowl (milions)
○	0.2103	run58	3/0.55/50%
□	0.2103	run37	5/0.55/50%
◇	0.2103	run55	8/0.55/50%

Figure 7.2.1.442: CR Effects (Re=0.55million/ft, 50%CowI) Baseplate Pressures



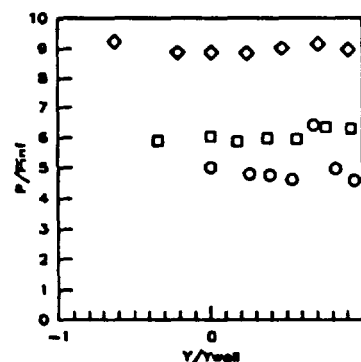
Sym	$x'/T_x'$	Run No.	CR/Re/Cowl (milions)
○	0.3154	run58	3/0.55/50%
□	0.3154	run37	5/0.55/50%
◇	0.3154	run55	8/0.55/50%

Figure 7.2.1.443: CR Effects (Re=0.55million/ft, 50%CowI) Baseplate Pressures



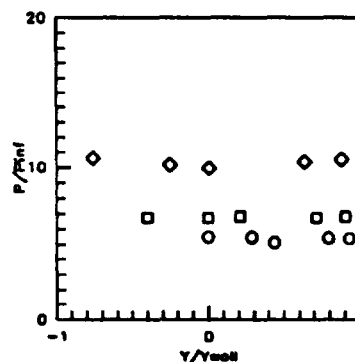
Sym	$x'/T_x'$	Run No.	CR/Re/Cowl (milions)
○	0.4206	run58	3/0.55/50%
□	0.4206	run37	5/0.55/50%
◇	0.4206	run55	8/0.55/50%

Figure 7.2.1.444: CR Effects (Re=0.55million/ft, 50%CowI) Baseplate Pressures



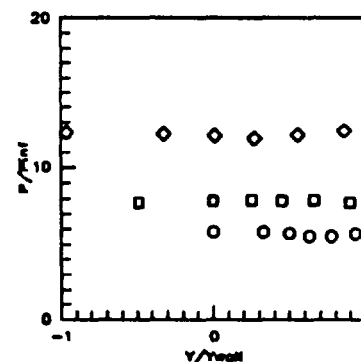
Sym	$x'/T_x'$	Run No.	CR/Re/Cowl (milions)
○	0.5258	run58	3/0.55/50%
□	0.5258	run37	5/0.55/50%
◇	0.5258	run55	8/0.55/50%

Figure 7.2.1.445: CR Effects (Re=0.55million/ft, 50%CowI) Baseplate Pressures



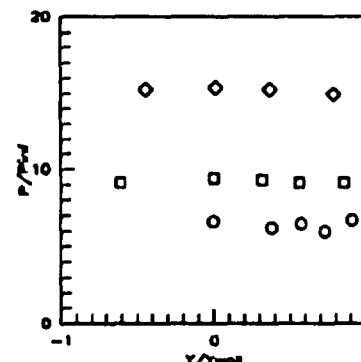
Sym	$x'/T_x'$	Run No.	CR/Re/Cowl (milions)
○	0.6308	run58	3/0.55/50%
□	0.6308	run37	5/0.55/50%
◇	0.6308	run55	8/0.55/50%

Figure 7.2.1.446: CR Effects (Re=0.55million/ft, 50%CowI) Baseplate Pressures



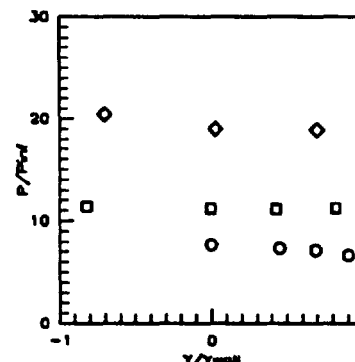
Sym	$x'/T_x'$	Run No.	CR/Re/Cowl (milions)
○	0.7361	run58	3/0.55/50%
□	0.7361	run37	5/0.55/50%
◇	0.7361	run55	8/0.55/50%

Figure 7.2.1.447: CR Effects (Re=0.55million/ft, 50%CowI) Baseplate Pressures



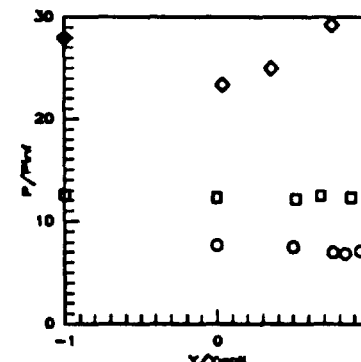
Sym	$x'/T_x'$	Run No.	CR/Re/Cowl (milions)
○	0.8412	run58	3/0.55/50%
□	0.8412	run37	5/0.55/50%
◇	0.8412	run55	8/0.55/50%

Figure 7.2.1.448: CR Effects (Re=0.55million/ft, 50%CowI) Baseplate Pressures



Sym	$x'/T_x'$	Run No.	CR/Re/Cowl (milions)
○	0.9464	run58	3/0.55/50%
□	0.9464	run37	5/0.55/50%
◇	0.9464	run55	8/0.55/50%

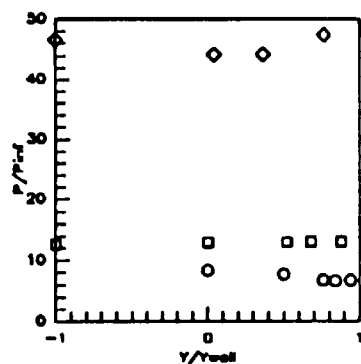
Figure 7.2.1.449: CR Effects (Re=0.55million/ft, 50%CowI) Baseplate Pressures



Sym	$x'/T_x'$	Run No.	CR/Re/Cowl (milions)
○	1.0000	run58	3/0.55/50%
□	1.0000	run37	5/0.55/50%
◇	1.0000	run55	8/0.55/50%

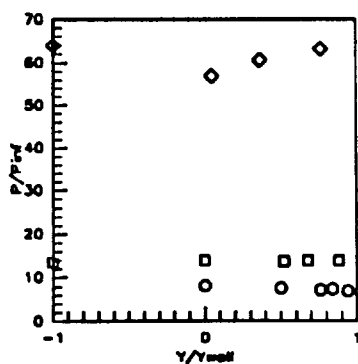
Figure 7.2.1.450: CR Effects (Re=0.55million/ft, 50%CowI) Baseplate Pressures





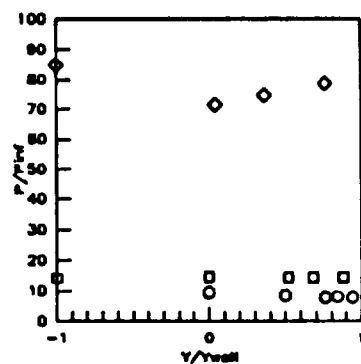
Sym	$x'/T_x'$	Run No.	CR/Re/Cowl (millions)
○	1.0728	run58	3/0.55/50%
□	1.0728	run37	5/0.55/50%
○	1.0728	run55	9/0.55/50%

Figure 7.2.1.451: CR Effects (Re=0.55million/ft, 50%Cow) Baseplate Pressures



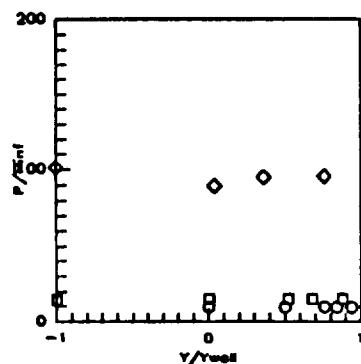
Sym	$x'/T_x'$	Run No.	CR/Re/Cowl (millions)
○	1.1587	run58	3/0.55/50%
□	1.1587	run37	5/0.55/50%
○	1.1587	run55	9/0.55/50%

Figure 7.2.1.452: CR Effects (Re=0.55million/ft, 50%Cow) Baseplate Pressures



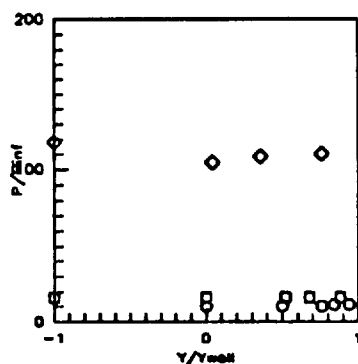
Sym	$x'/T_x'$	Run No.	CR/Re/Cowl (millions)
○	1.2408	run58	3/0.55/50%
□	1.2408	run37	5/0.55/50%
○	1.2408	run55	9/0.55/50%

Figure 7.2.1.453: CR Effects (Re=0.55million/ft, 50%Cow) Baseplate Pressures



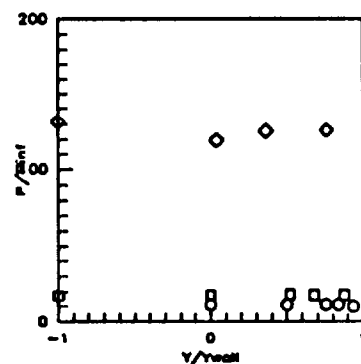
Sym	$x'/T_x'$	Run No.	CR/Re/Cowl (millions)
○	1.3248	run58	3/0.55/50%
□	1.3248	run37	5/0.55/50%
○	1.3248	run55	9/0.55/50%

Figure 7.2.1.454: CR Effects (Re=0.55million/ft, 50%Cow) Baseplate Pressures



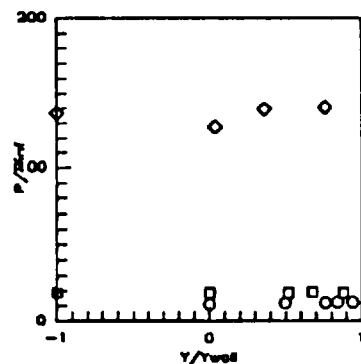
Sym	$x'/T_x'$	Run No.	CR/Re/Cowl (millions)
○	1.4090	run58	3/0.55/50%
□	1.4090	run37	5/0.55/50%
○	1.4090	run55	9/0.55/50%

Figure 7.2.1.455: CR Effects (Re=0.55million/ft, 50%Cow) Baseplate Pressures



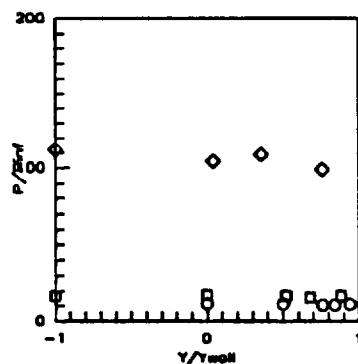
Sym	$x'/T_x'$	Run No.	CR/Re/Cowl (millions)
○	1.4932	run58	3/0.55/50%
□	1.4932	run37	5/0.55/50%
○	1.4932	run55	9/0.55/50%

Figure 7.2.1.456: CR Effects (Re=0.55million/ft, 50%Cow) Baseplate Pressures



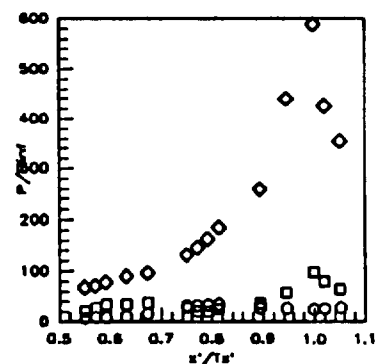
Sym	$x'/T_x'$	Run No.	CR/Re/Cowl (millions)
○	1.5773	run58	3/0.55/50%
□	1.5773	run37	5/0.55/50%
○	1.5773	run55	9/0.55/50%

Figure 7.2.1.457: CR Effects (Re=0.55million/ft, 50%Cow) Baseplate Pressures



Sym	$x'/T_x'$	Run No.	CR/Re/Cowl (millions)
○	1.8824	run58	3/0.55/50%
□	1.8824	run37	5/0.55/50%
○	1.8824	run55	9/0.55/50%

Figure 7.2.1.458: CR Effects (Re=0.55million/ft, 50%Cow) Baseplate Pressures



Sym	Cowl Pos.	Run No.	CR/Re/Cowl (millions)
○	50%	run58	3/0.55/50%
□	50%	run37	5/0.55/50%
○	50%	run55	9/0.55/50%

Figure 7.2.1.459: CR Effects (Re=0.55million/ft, 50%Cow) Cowl Pressures

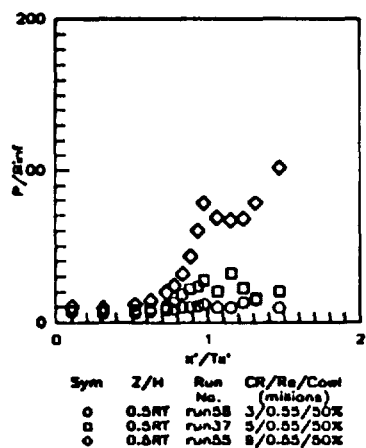


Figure 7.2.1.480: CR Effects  
(Re=0.55million/ft, 50%CowI)  
Sidewall Centerline Pressures

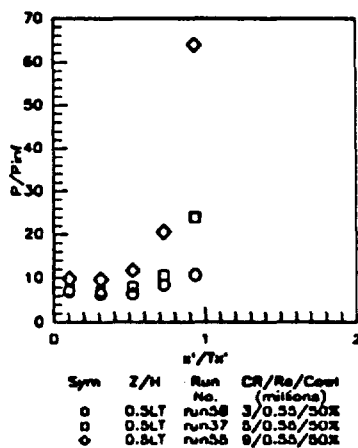


Figure 7.2.1.481: CR Effects  
(Re=0.55million/ft, 50%CowI)  
Sidewall Centerline Pressures

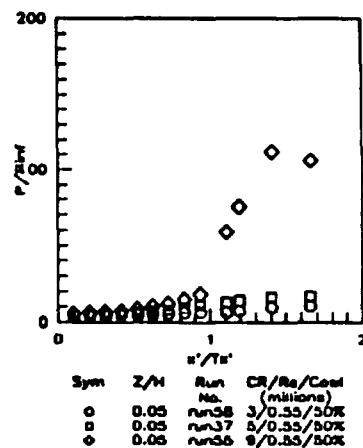


Figure 7.2.1.482: CR Effects  
(Re=0.55million/ft, 50%CowI)  
Sidewall Pressures

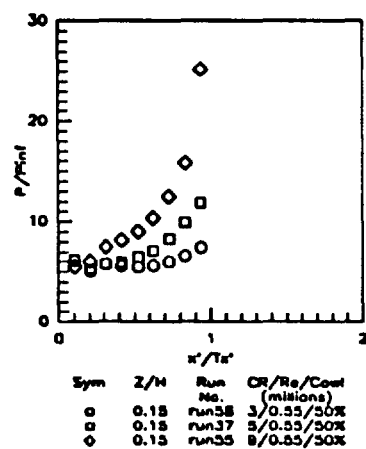


Figure 7.2.1.483: CR Effects  
(Re=0.55million/ft, 50%CowI)  
Sidewall Pressures

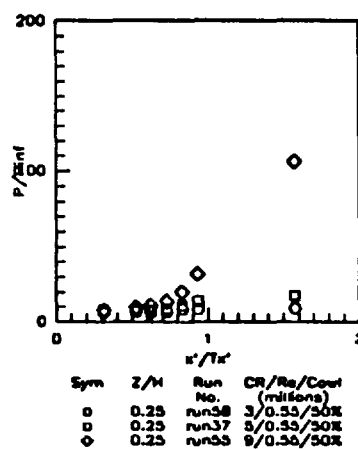


Figure 7.2.1.484: CR Effects  
(Re=0.55million/ft, 50%CowI)  
Sidewall Pressures

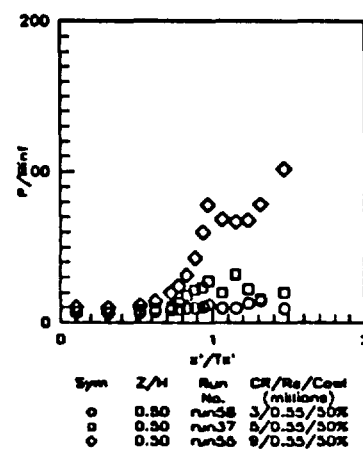


Figure 7.2.1.485: CR Effects  
(Re=0.55million/ft, 50%CowI)  
Sidewall Pressures

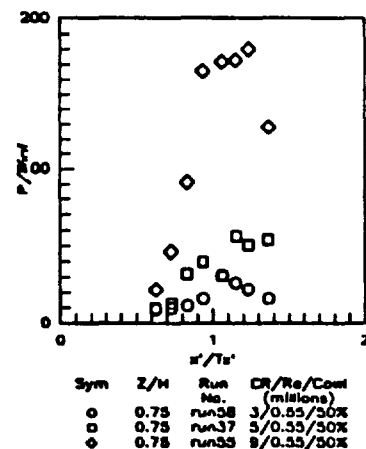


Figure 7.2.1.486: CR Effects  
(Re=0.55million/ft, 50%CowI)  
Sidewall Pressures

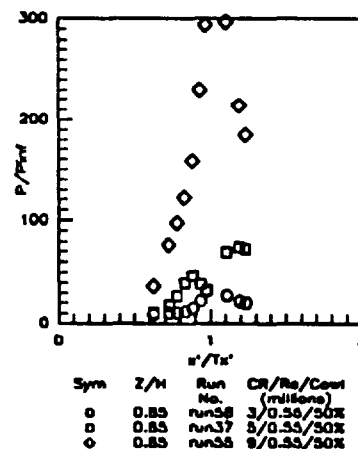


Figure 7.2.1.487: CR Effects  
(Re=0.55million/ft, 50%CowI)  
Sidewall Pressures

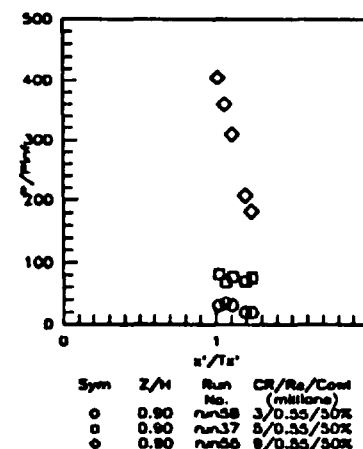
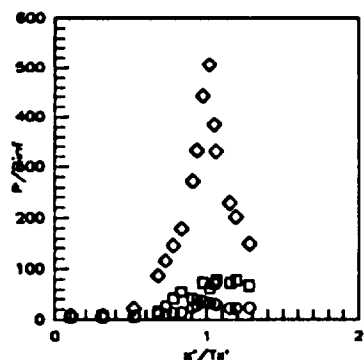


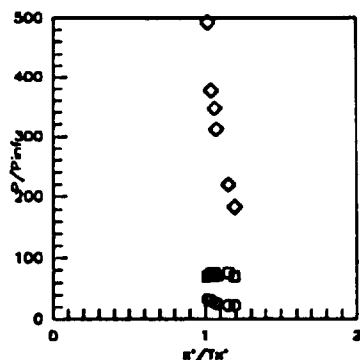
Figure 7.2.1.488: CR Effects  
(Re=0.55million/ft, 50%CowI)  
Sidewall Pressures



Sym	$z/h$	Run No.	CR/Re/Coal (milions)
-----	-------	---------	----------------------

○	0.95	run58	3/0.55/50%
□	0.98	run37	5/0.55/50%
◇	0.99	run55	9/0.55/50%

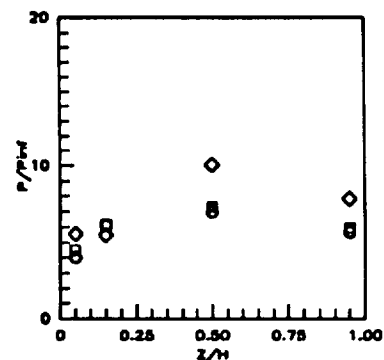
Figure 7.2.1.469: CR Effects (Re=0.55million/ft, 50%Coal) Sidewall Pressures



Sym	$z/h$	Run No.	CR/Re/Coal (milions)
-----	-------	---------	----------------------

○	0.975	run58	3/0.55/50%
□	0.978	run37	5/0.55/50%
◇	0.979	run55	9/0.55/50%

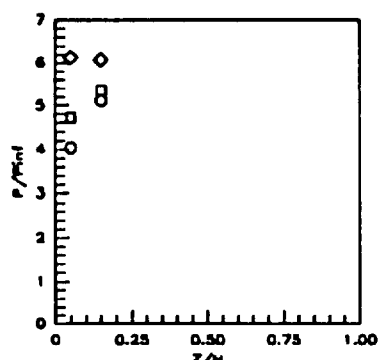
Figure 7.2.1.470: CR Effects (Re=0.55million/ft, 50%Coal) Sidewall Pressures



Sym	$x'/Ts'$	Run No.	CR/Re/Coal (milions)
-----	----------	---------	----------------------

○	0.1042	run58	3/0.55/50%
□	0.1042	run37	5/0.55/50%
◇	0.1042	run55	9/0.55/50%

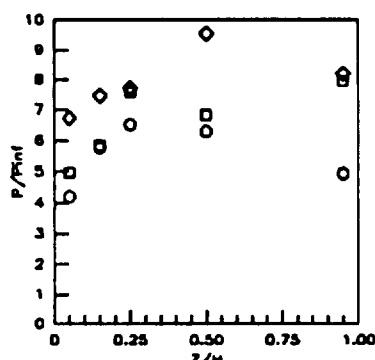
Figure 7.2.1.471: CR Effects (Re=0.55million/ft, 50%Coal) Sidewall Pressures



Sym	$x'/Ts'$	Run No.	CR/Re/Coal (milions)
-----	----------	---------	----------------------

○	0.2083	run58	3/0.55/50%
□	0.2083	run37	5/0.55/50%
◇	0.2083	run55	9/0.55/50%

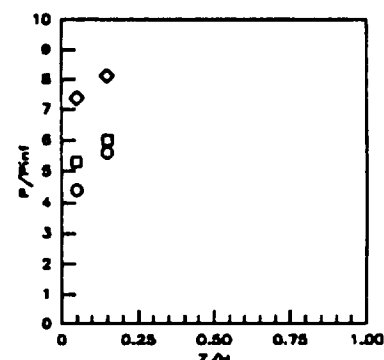
Figure 7.2.1.472: CR Effects (Re=0.55million/ft, 50%Coal) Sidewall Pressures



Sym	$x'/Ts'$	Run No.	CR/Re/Coal (milions)
-----	----------	---------	----------------------

○	0.3125	run58	3/0.55/50%
□	0.3125	run37	5/0.55/50%
◇	0.3125	run55	9/0.55/50%

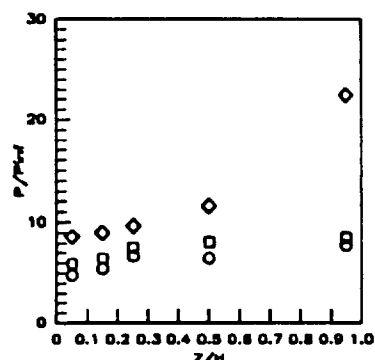
Figure 7.2.1.473: CR Effects (Re=0.55million/ft, 50%Coal) Sidewall Pressures



Sym	$x'/Ts'$	Run No.	CR/Re/Coal (milions)
-----	----------	---------	----------------------

○	0.4167	run58	3/0.55/50%
□	0.4167	run37	5/0.55/50%
◇	0.4167	run55	9/0.55/50%

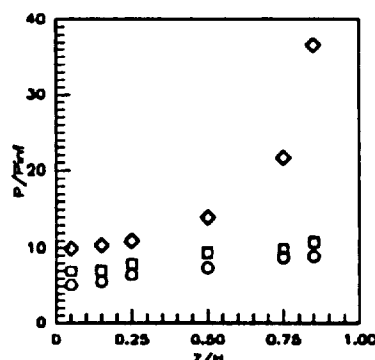
Figure 7.2.1.474: CR Effects (Re=0.55million/ft, 50%Coal) Sidewall Pressures



Sym	$x'/Ts'$	Run No.	CR/Re/Coal (milions)
-----	----------	---------	----------------------

○	0.5259	run58	3/0.55/50%
□	0.5259	run37	5/0.55/50%
◇	0.5259	run55	9/0.55/50%

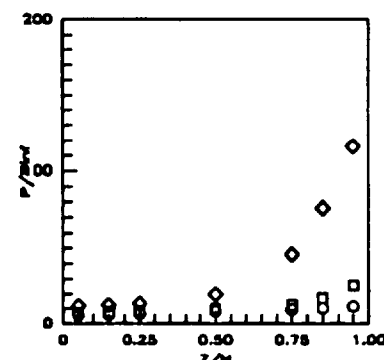
Figure 7.2.1.475: CR Effects (Re=0.55million/ft, 50%Coal) Sidewall Pressures



Sym	$x'/Ts'$	Run No.	CR/Re/Coal (milions)
-----	----------	---------	----------------------

○	0.8252	run58	3/0.55/50%
□	0.8252	run37	5/0.55/50%
◇	0.8252	run55	9/0.55/50%

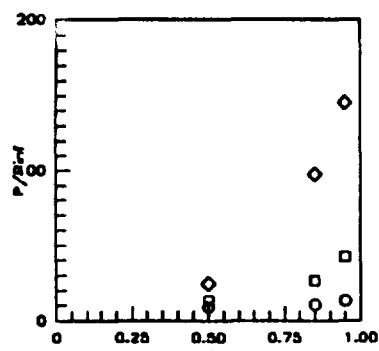
Figure 7.2.1.476: CR Effects (Re=0.55million/ft, 50%Coal) Sidewall Pressures



Sym	$x'/Ts'$	Run No.	CR/Re/Coal (milions)
-----	----------	---------	----------------------

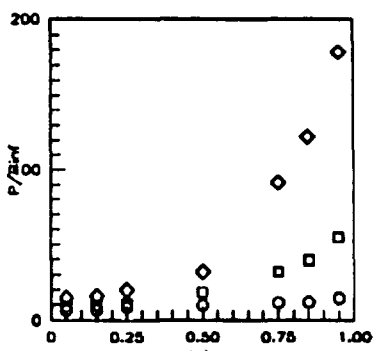
○	0.7284	run58	3/0.55/50%
□	0.7284	run37	5/0.55/50%
◇	0.7284	run55	9/0.55/50%

Figure 7.2.1.477: CR Effects (Re=0.55million/ft, 50%Coal) Sidewall Pressures



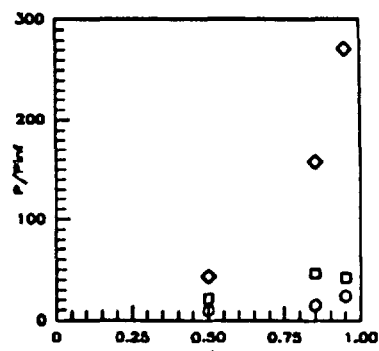
Sym	$\alpha'/T\alpha'$	Run No.	CR/Re/Cowl (milions)
○	0.7815	run58	3/0.55/50%
□	0.7815	run37	5/0.55/50%
◇	0.7815	run55	9/0.55/50%

Figure 7.2.1.478: CR Effects  
(Re=0.55million/ft, 50%CowI)  
Sidewall Pressures



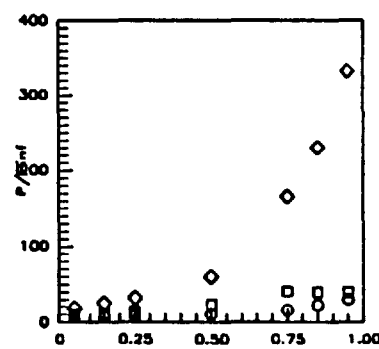
Sym	$\alpha'/T\alpha'$	Run No.	CR/Re/Cowl (milions)
○	0.8336	run58	3/0.55/50%
□	0.8336	run37	5/0.55/50%
◇	0.8336	run55	9/0.55/50%

Figure 7.2.1.479: CR Effects  
(Re=0.55million/ft, 50%CowI)  
Sidewall Pressures



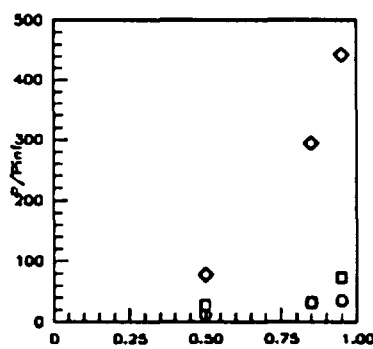
Sym	$\alpha'/T\alpha'$	Run No.	CR/Re/Cowl (milions)
○	0.8857	run58	3/0.55/50%
□	0.8857	run37	5/0.55/50%
◇	0.8857	run55	9/0.55/50%

Figure 7.2.1.480: CR Effects  
(Re=0.55million/ft, 50%CowI)  
Sidewall Pressures



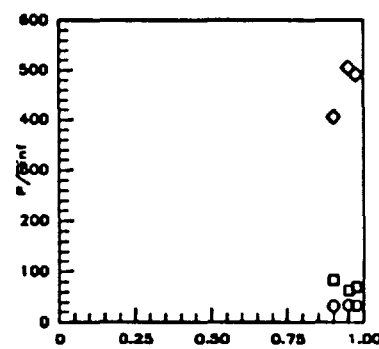
Sym	$\alpha'/T\alpha'$	Run No.	CR/Re/Cowl (milions)
○	0.9378	run58	3/0.55/50%
□	0.9378	run37	5/0.55/50%
◇	0.9378	run55	9/0.55/50%

Figure 7.2.1.481: CR Effects  
(Re=0.55million/ft, 50%CowI)  
Sidewall Pressures



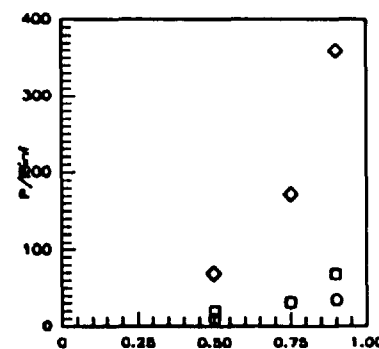
Sym	$\alpha'/T\alpha'$	Run No.	CR/Re/Cowl (milions)
○	0.9751	run58	3/0.55/50%
□	0.9751	run37	5/0.55/50%
◇	0.9751	run55	9/0.55/50%

Figure 7.2.1.482: CR Effects  
(Re=0.55million/ft, 50%CowI)  
Sidewall Pressures



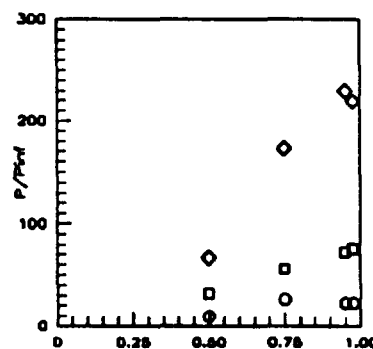
Sym	$\alpha'/T\alpha'$	Run No.	CR/Re/Cowl (milions)
○	1.0197	run58	3/0.55/50%
□	1.0197	run37	5/0.55/50%
◇	1.0197	run55	9/0.55/50%

Figure 7.2.1.483: CR Effects  
(Re=0.55million/ft, 50%CowI)  
Sidewall Pressures



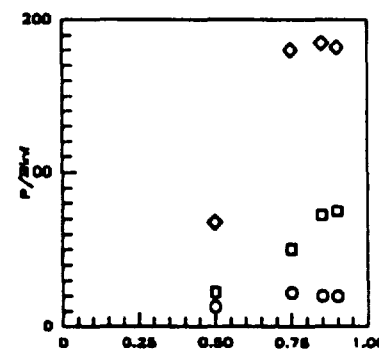
Sym	$\alpha'/T\alpha'$	Run No.	CR/Re/Cowl (milions)
○	1.0843	run58	3/0.55/50%
□	1.0843	run37	5/0.55/50%
◇	1.0843	run55	9/0.55/50%

Figure 7.2.1.484: CR Effects  
(Re=0.55million/ft, 50%CowI)  
Sidewall Pressures



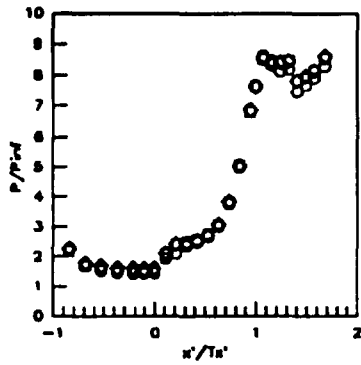
Sym	$\alpha'/T\alpha'$	Run No.	CR/Re/Cowl (milions)
○	1.1537	run58	3/0.55/50%
□	1.1537	run37	5/0.55/50%
◇	1.1537	run55	9/0.55/50%

Figure 7.2.1.485: CR Effects  
(Re=0.55million/ft, 50%CowI)  
Sidewall Pressures



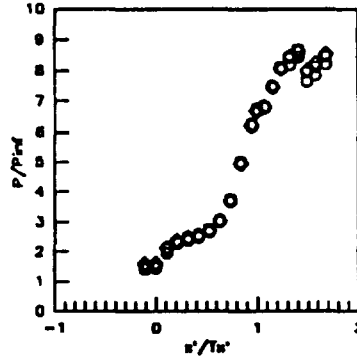
Sym	$\alpha'/T\alpha'$	Run No.	CR/Re/Cowl (milions)
○	1.2356	run58	3/0.55/50%
□	1.2356	run37	5/0.55/50%
◇	1.2356	run55	9/0.55/50%

Figure 7.2.1.486: CR Effects  
(Re=0.55million/ft, 50%CowI)  
Sidewall Pressures



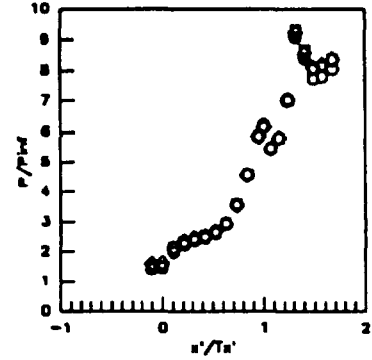
Sym	C.L.	Run	CR/Re/Cowl
		No.	(millions)
○	CR=3	run66	3/2.15/ 0%
□	CR=3	run62	3/2.15/25%
◇	CR=3	run60	3/2.15/50%

Figure 7.2.2.1: Cowl Effects  
(CR=3, Re=2.15million/ft)  
CR=3 Centerline Pressures



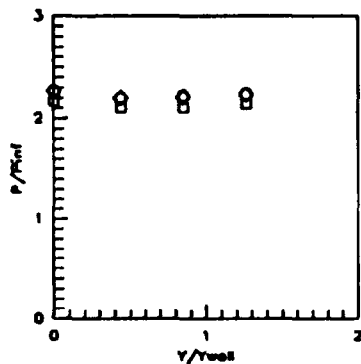
Sym	C.L.	Run	CR/Re/Cowl
		No.	(millions)
○	CR=5	run66	3/2.15/ 0%
□	CR=5	run62	3/2.15/25%
◇	CR=5	run60	3/2.15/50%

Figure 7.2.2.2: Cowl Effects  
(CR=5, Re=2.15million/ft)  
CR=5 Centerline Pressures



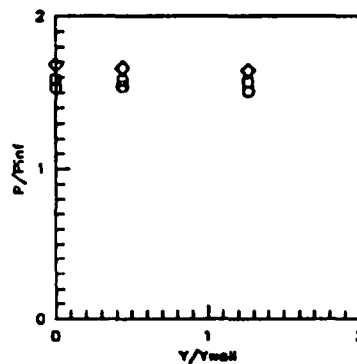
Sym	C.L.	Run	CR/Re/Cowl
		No.	(millions)
○	CR=8	run66	3/2.15/ 0%
□	CR=8	run62	3/2.15/25%
◇	CR=8	run60	3/2.15/50%

Figure 7.2.2.3: Cowl Effects  
(CR=3, Re=2.15million/ft)  
CR=8 Centerline Pressures



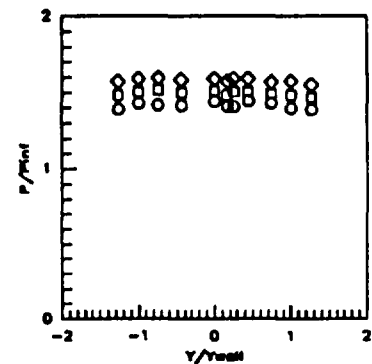
Sym	x'/Ts'	Run	CR/Re/Cowl
		No.	(millions)
○	-0.8412	run66	3/2.15/ 0%
□	-0.8412	run62	3/2.15/25%
◇	-0.8412	run60	3/2.15/50%

Figure 7.2.2.4: Cowl Effects  
(CR=3, Re=2.15million/ft)  
Baseplate Pressures



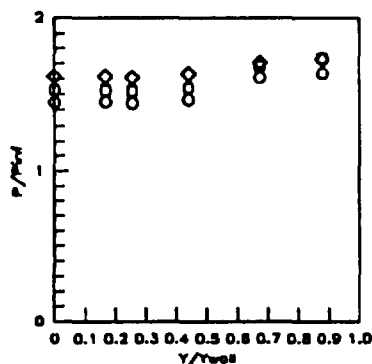
Sym	x'/Ts'	Run	CR/Re/Cowl
		No.	(millions)
○	-0.5258	run66	3/2.15/ 0%
□	-0.5258	run62	3/2.15/25%
◇	-0.5258	run60	3/2.15/50%

Figure 7.2.2.5: Cowl Effects  
(CR=3, Re=2.15million/ft)  
Baseplate Pressures



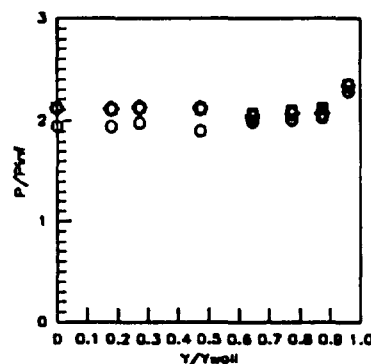
Sym	x'/Ts'	Run	CR/Re/Cowl
		No.	(millions)
○	-0.1052	run66	3/2.15/ 0%
□	-0.1052	run62	3/2.15/25%
◇	-0.1052	run60	3/2.15/50%

Figure 7.2.2.6: Cowl Effects  
(CR=3, Re=2.15million/ft)  
Baseplate Pressures



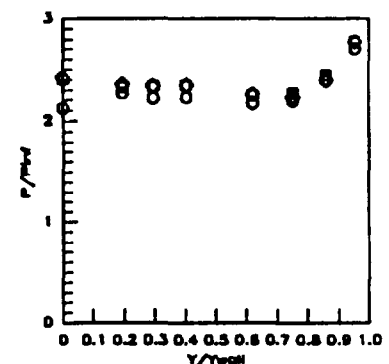
Sym	x'/Ts'	Run	CR/Re/Cowl
		No.	(millions)
○	0.0000	run66	3/2.15/ 0%
□	0.0000	run62	3/2.15/25%
◇	0.0000	run60	3/2.15/50%

Figure 7.2.2.7: Cowl Effects  
(CR=3, Re=2.15million/ft)  
Baseplate Pressures



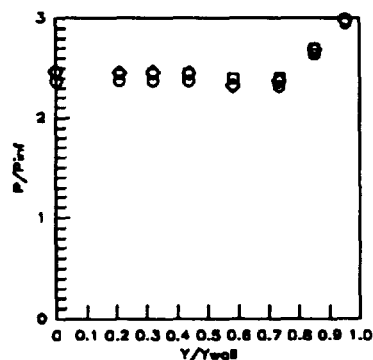
Sym	x'/Ts'	Run	CR/Re/Cowl
		No.	(millions)
○	0.1052	run66	3/2.15/ 0%
□	0.1052	run62	3/2.15/25%
◇	0.1052	run60	3/2.15/50%

Figure 7.2.2.8: Cowl Effects  
(CR=3, Re=2.15million/ft)  
Baseplate Pressures



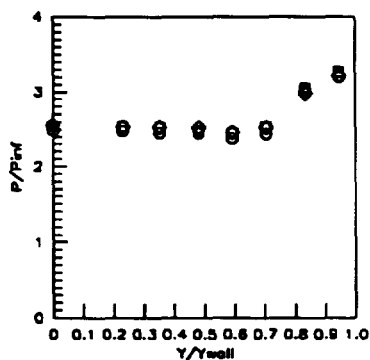
Sym	x'/Ts'	Run	CR/Re/Cowl
		No.	(millions)
○	0.2103	run66	3/2.15/ 0%
□	0.2103	run62	3/2.15/25%
◇	0.2103	run60	3/2.15/50%

Figure 7.2.2.9: Cowl Effects  
(CR=3, Re=2.15million/ft)  
Baseplate Pressures



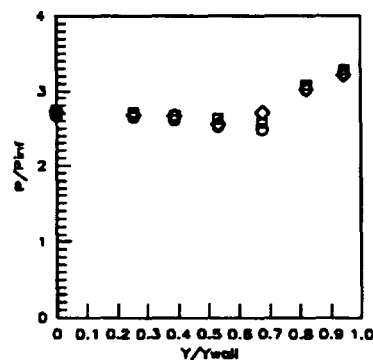
Sym	x'/Ts'	Run No.	CR/Re/Cowl (millions)
○	0.3154	run66	3/2.15/ 0%
□	0.3154	run62	3/2.15/25%
◇	0.3154	run60	3/2.15/50%

Figure 7.2.2.10: Cowl Effects (CR=3, Re=2.15million/ft) Baseplate Pressures



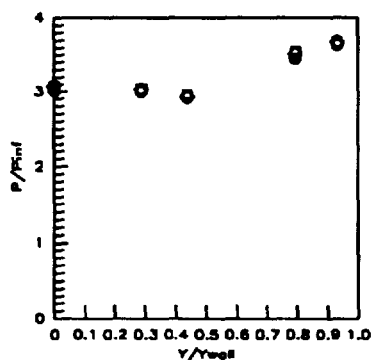
Sym	x'/Ts'	Run No.	CR/Re/Cowl (millions)
○	0.4206	run66	3/2.15/ 0%
□	0.4206	run62	3/2.15/25%
◇	0.4206	run60	3/2.15/50%

Figure 7.2.2.11: Cowl Effects (CR=3, Re=2.15million/ft) Baseplate Pressures



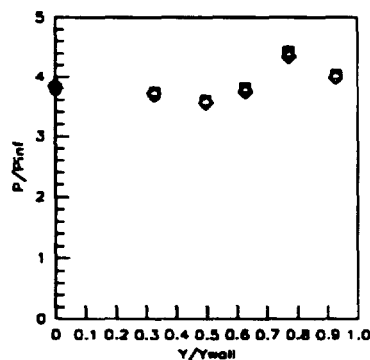
Sym	x'/Ts'	Run No.	CR/Re/Cowl (millions)
○	0.5258	run66	3/2.15/ 0%
□	0.5258	run62	3/2.15/25%
◇	0.5258	run60	3/2.15/50%

Figure 7.2.2.12: Cowl Effects (CR=3, Re=2.15million/ft) Baseplate Pressures



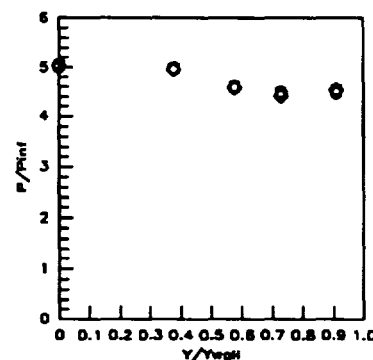
Sym	x'/Ts'	Run No.	CR/Re/Cowl (millions)
○	0.6309	run66	3/2.15/ 0%
□	0.6309	run62	3/2.15/25%
◇	0.6309	run60	3/2.15/50%

Figure 7.2.2.13: Cowl Effects (CR=3, Re=2.15million/ft) Baseplate Pressures



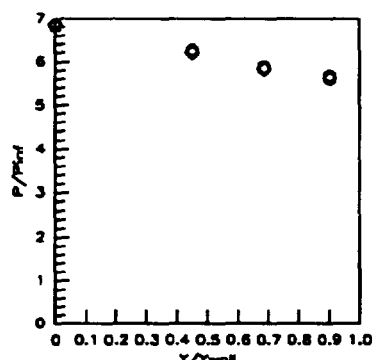
Sym	x'/Ts'	Run No.	CR/Re/Cowl (millions)
○	0.7361	run66	3/2.15/ 0%
□	0.7361	run62	3/2.15/25%
◇	0.7361	run60	3/2.15/50%

Figure 7.2.2.14: Cowl Effects (CR=3, Re=2.15million/ft) Baseplate Pressures



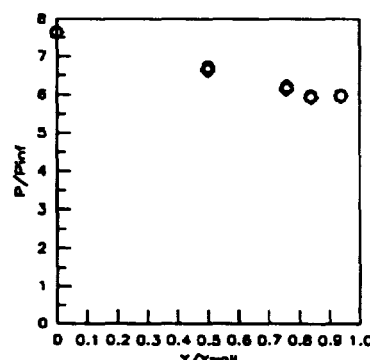
Sym	x'/Ts'	Run No.	CR/Re/Cowl (millions)
○	0.8412	run66	3/2.15/ 0%
□	0.8412	run62	3/2.15/25%
◇	0.8412	run60	3/2.15/50%

Figure 7.2.2.15: Cowl Effects (CR=3, Re=2.15million/ft) Baseplate Pressures



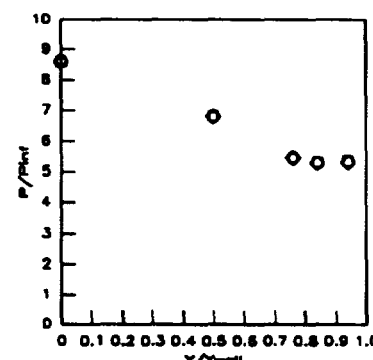
Sym	x'/Ts'	Run No.	CR/Re/Cowl (millions)
○	0.9464	run66	3/2.15/ 0%
□	0.9464	run62	3/2.15/25%
◇	0.9464	run60	3/2.15/50%

Figure 7.2.2.16: Cowl Effects (CR=3, Re=2.15million/ft) Baseplate Pressures



Sym	x'/Ts'	Run No.	CR/Re/Cowl (millions)
○	1.0000	run66	3/2.15/ 0%
□	1.0000	run62	3/2.15/25%
◇	1.0000	run60	3/2.15/50%

Figure 7.2.2.17: Cowl Effects (CR=3, Re=2.15million/ft) Baseplate Pressures



Sym	x'/Ts'	Run No.	CR/Re/Cowl (millions)
○	1.0726	run66	3/2.15/ 0%
□	1.0726	run62	3/2.15/25%
◇	1.0726	run60	3/2.15/50%

Figure 7.2.2.18: Cowl Effects (CR=3, Re=2.15million/ft) Baseplate Pressures

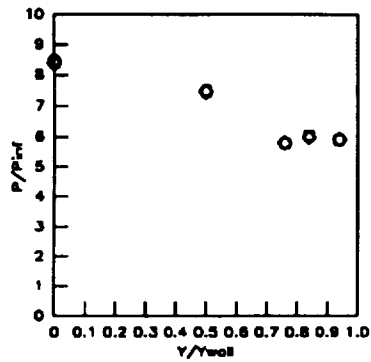


Figure 7.2.2.19: Cowl Effects  
(CR=3, Re=2.15million/ft)  
Baseplate Pressures

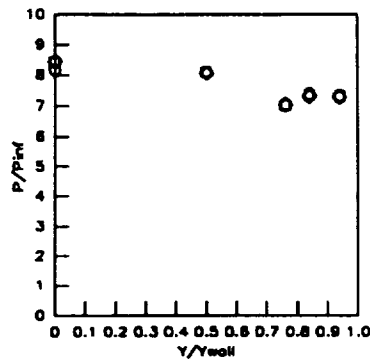


Figure 7.2.2.20: Cowl Effects  
(CR=3, Re=2.15million/ft)  
Baseplate Pressures

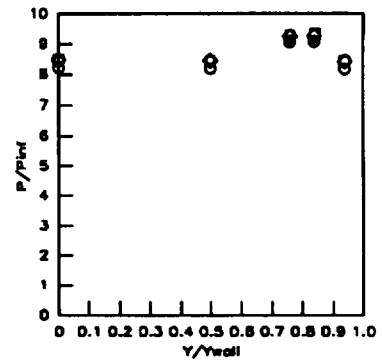


Figure 7.2.2.21: Cowl Effects  
(CR=3, Re=2.15million/ft)  
Baseplate Pressures

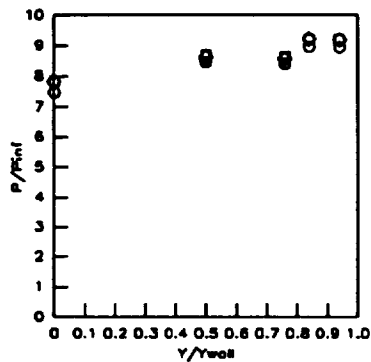


Figure 7.2.2.22: Cowl Effects  
(CR=3, Re=2.15million/ft)  
Baseplate Pressures

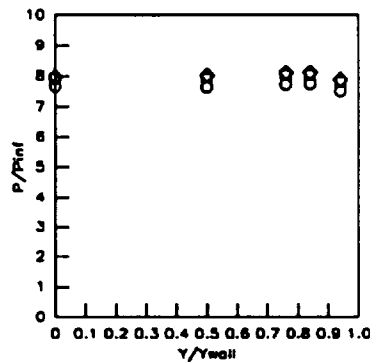


Figure 7.2.2.23: Cowl Effects  
(CR=3, Re=2.15million/ft)  
Baseplate Pressures

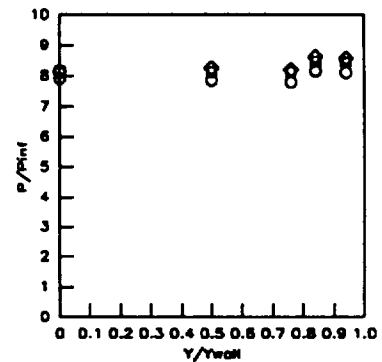


Figure 7.2.2.24: Cowl Effects  
(CR=3, Re=2.15million/ft)  
Baseplate Pressures

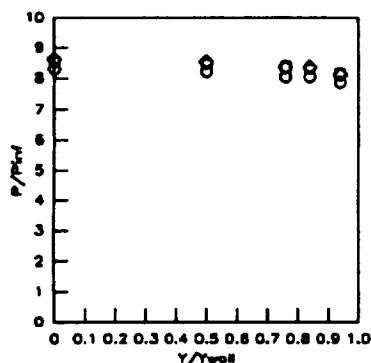


Figure 7.2.2.25: Cowl Effects  
(CR=3, Re=2.15million/ft)  
Baseplate Pressures

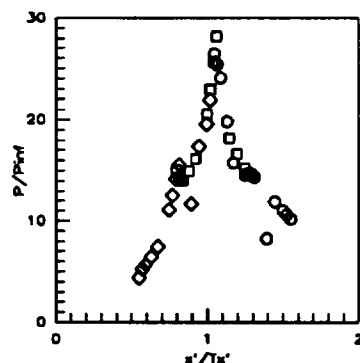


Figure 7.2.2.26: Cowl Effects  
(CR=3, Re=2.15million/ft)  
Cowl Pressures

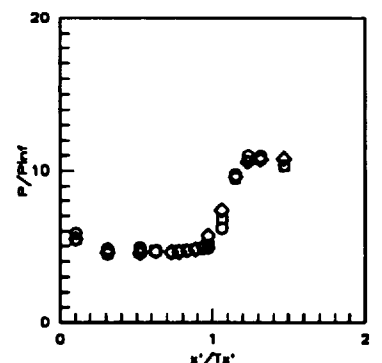
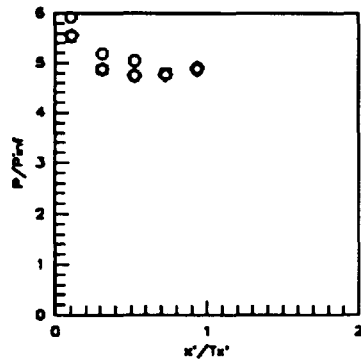
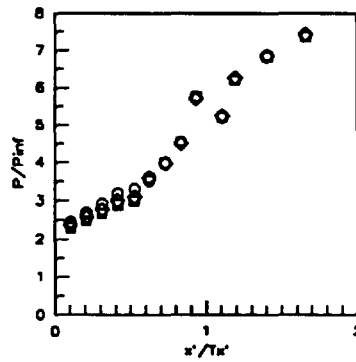


Figure 7.2.2.27: Cowl Effects  
(CR=3, Re=2.15million/ft)  
Sidewall Centerline Pressures



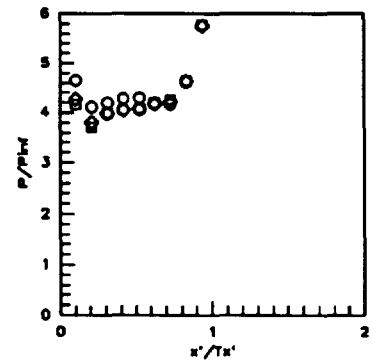
Sym	Z/H	Run No.	CR/Re/Cowl (millions)
○	0.5LT	run86	3/2.15/0%
○	0.5LT	run82	3/2.15/25%
○	0.5LT	run80	3/2.15/50%

Figure 7.2.2.28: Cowl Effects (CR=3, Re=2.15million/ft) Sidewall Centerline Pressures



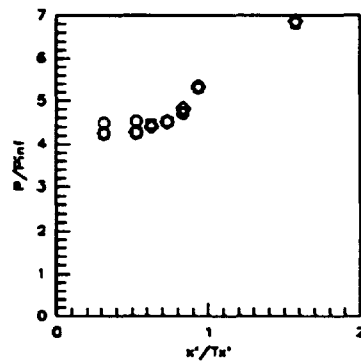
Sym	Z/H	Run No.	CR/Re/Cowl (millions)
○	0.05	run86	3/2.15/0%
○	0.05	run82	3/2.15/25%
○	0.05	run80	3/2.15/50%

Figure 7.2.2.29: Cowl Effects (CR=3, Re=2.15million/ft) Sidewall Pressures



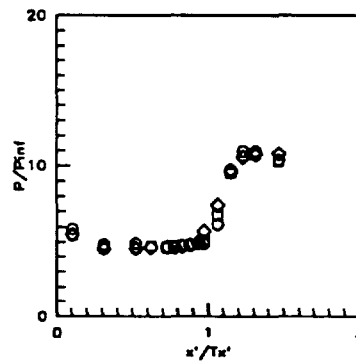
Sym	Z/H	Run No.	CR/Re/Cowl (millions)
○	0.15	run86	3/2.15/0%
○	0.15	run82	3/2.15/25%
○	0.15	run80	3/2.15/50%

Figure 7.2.2.30: Cowl Effects (CR=3, Re=2.15million/ft) Sidewall Pressures



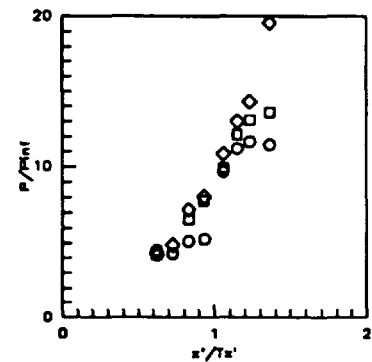
Sym	Z/H	Run No.	CR/Re/Cowl (millions)
○	0.25	run86	3/2.15/0%
○	0.25	run82	3/2.15/25%
○	0.25	run80	3/2.15/50%

Figure 7.2.2.31: Cowl Effects (CR=3, Re=2.15million/ft) Sidewall Pressures



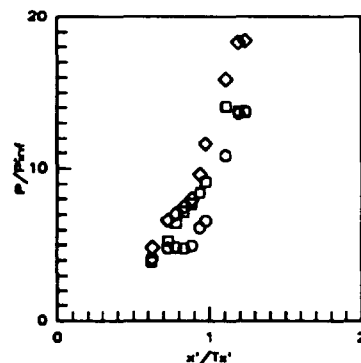
Sym	Z/H	Run No.	CR/Re/Cowl (millions)
○	0.50	run86	3/2.15/0%
○	0.50	run82	3/2.15/25%
○	0.50	run80	3/2.15/50%

Figure 7.2.2.32: Cowl Effects (CR=3, Re=2.15million/ft) Sidewall Pressures



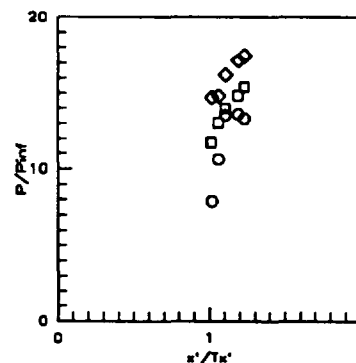
Sym	Z/H	Run No.	CR/Re/Cowl (millions)
○	0.75	run86	3/2.15/0%
○	0.75	run82	3/2.15/25%
○	0.75	run80	3/2.15/50%

Figure 7.2.2.33: Cowl Effects (CR=3, Re=2.15million/ft) Sidewall Pressures



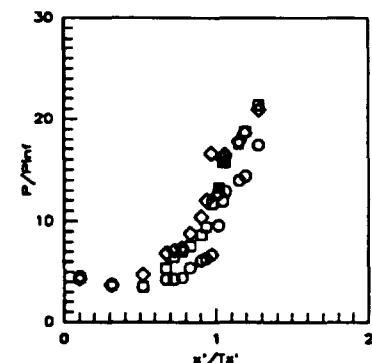
Sym	Z/H	Run No.	CR/Re/Cowl (millions)
○	0.85	run86	3/2.15/0%
○	0.85	run82	3/2.15/25%
○	0.85	run80	3/2.15/50%

Figure 7.2.2.34: Cowl Effects (CR=3, Re=2.15million/ft) Sidewall Pressures



Sym	Z/H	Run No.	CR/Re/Cowl (millions)
○	0.90	run86	3/2.15/0%
○	0.90	run82	3/2.15/25%
○	0.90	run80	3/2.15/50%

Figure 7.2.2.35: Cowl Effects (CR=3, Re=2.15million/ft) Sidewall Pressures



Sym	Z/H	Run No.	CR/Re/Cowl (millions)
○	0.95	run86	3/2.15/0%
○	0.95	run82	3/2.15/25%
○	0.95	run80	3/2.15/50%

Figure 7.2.2.36: Cowl Effects (CR=3, Re=2.15million/ft) Sidewall Pressures



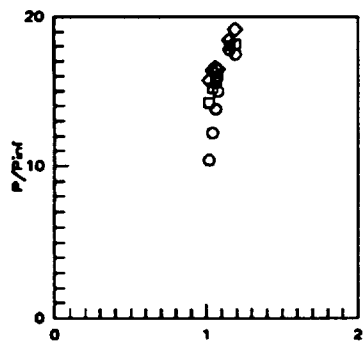


Figure 7.2.2.37: Cowl Effects  
(CR=3, Re=2.15million/ft)  
Sidewall Pressures

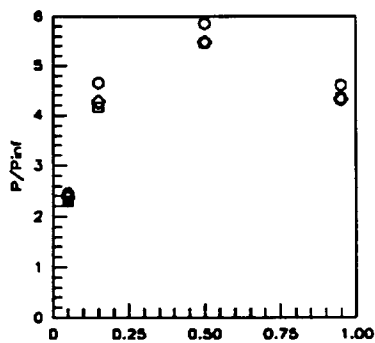


Figure 7.2.2.38: Cowl Effects  
(CR=3, Re=2.15million/ft)  
Sidewall Pressures

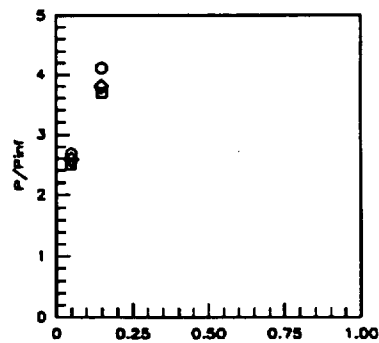


Figure 7.2.2.39: Cowl Effects  
(CR=3, Re=2.15million/ft)  
Sidewall Pressures

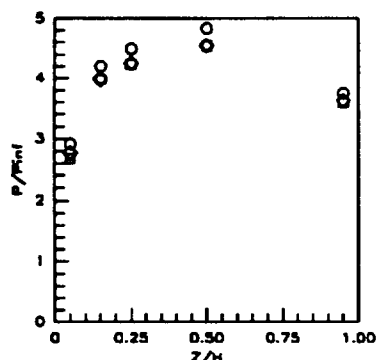


Figure 7.2.2.40: Cowl Effects  
(CR=3, Re=2.15million/ft)  
Sidewall Pressures

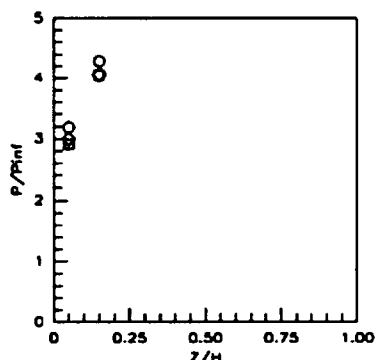


Figure 7.2.2.41: Cowl Effects  
(CR=3, Re=2.15million/ft)  
Sidewall Pressures

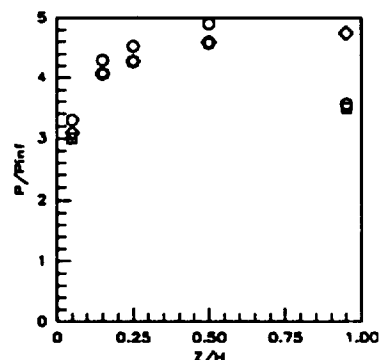


Figure 7.2.2.42: Cowl Effects  
(CR=3, Re=2.15million/ft)  
Sidewall Pressures

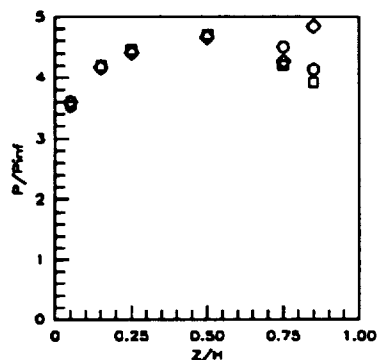


Figure 7.2.2.43: Cowl Effects  
(CR=3, Re=2.15million/ft)  
Sidewall Pressures

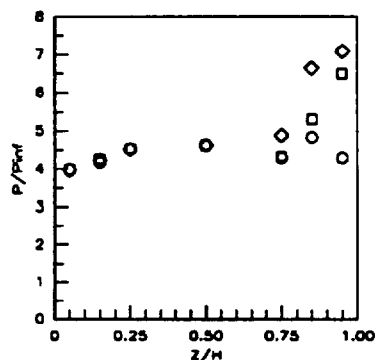


Figure 7.2.2.44: Cowl Effects  
(CR=3, Re=2.15million/ft)  
Sidewall Pressures

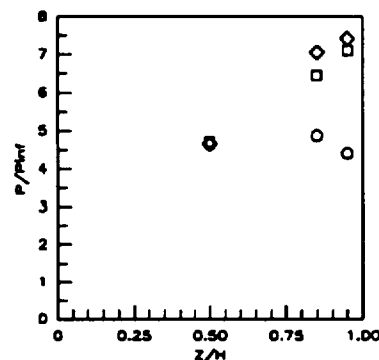
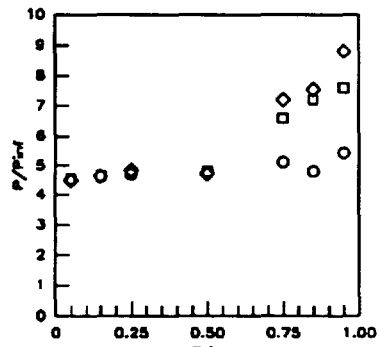
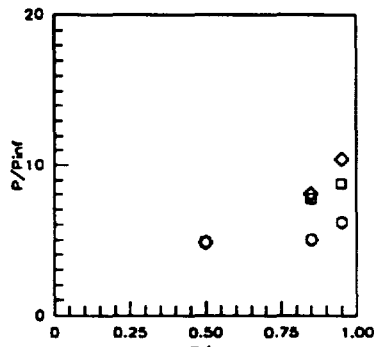


Figure 7.2.2.45: Cowl Effects  
(CR=3, Re=2.15million/ft)  
Sidewall Pressures



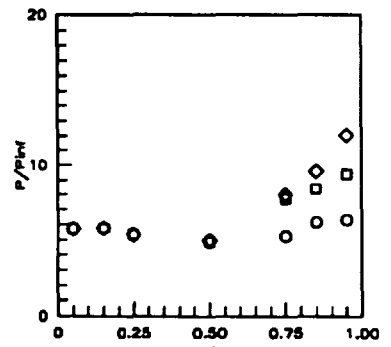
Sym	$x'/T_x'$	Run No.	CR/Re/Cowl (millions)
○	0.8336	run66	3/2.15/0%
□	0.8336	run62	3/2.15/25%
◇	0.8336	run60	3/2.15/50%

Figure 7.2.2.46: Cowl Effects (CR=3, Re=2.15million/ft) Sidewall Pressures



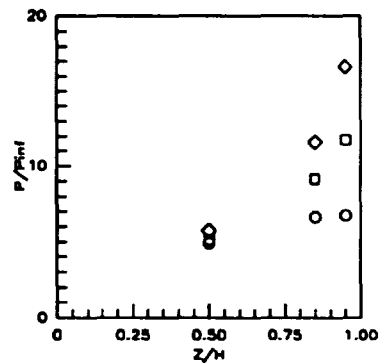
Sym	$x'/T_x'$	Run No.	CR/Re/Cowl (millions)
○	0.8857	run66	3/2.15/0%
□	0.8857	run62	3/2.15/25%
◇	0.8857	run60	3/2.15/50%

Figure 7.2.2.47: Cowl Effects (CR=3, Re=2.15million/ft) Sidewall Pressures



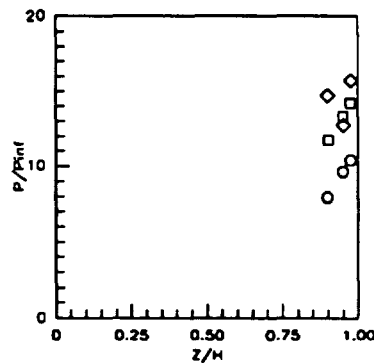
Sym	$x'/T_x'$	Run No.	CR/Re/Cowl (millions)
○	0.9378	run66	3/2.15/0%
□	0.9378	run62	3/2.15/25%
◇	0.9378	run60	3/2.15/50%

Figure 7.2.2.48: Cowl Effects (CR=3, Re=2.15million/ft) Sidewall Pressures



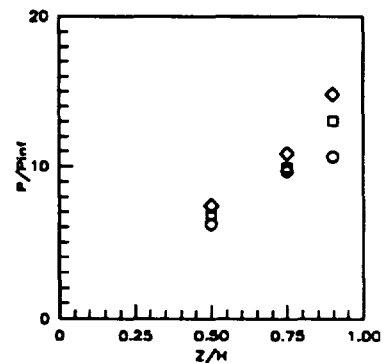
Sym	$x'/T_x'$	Run No.	CR/Re/Cowl (millions)
○	0.9751	run66	3/2.15/0%
□	0.9751	run62	3/2.15/25%
◇	0.9751	run60	3/2.15/50%

Figure 7.2.2.49: Cowl Effects (CR=3, Re=2.15million/ft) Sidewall Pressures



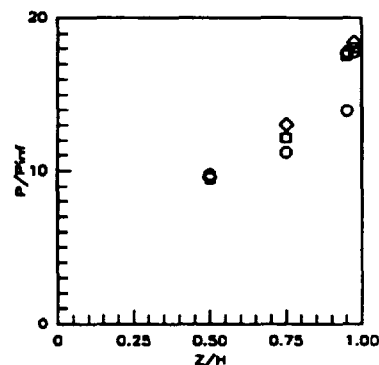
Sym	$x'/T_x'$	Run No.	CR/Re/Cowl (millions)
○	1.0197	run66	3/2.15/0%
□	1.0197	run62	3/2.15/25%
◇	1.0197	run60	3/2.15/50%

Figure 7.2.2.50: Cowl Effects (CR=3, Re=2.15million/ft) Sidewall Pressures



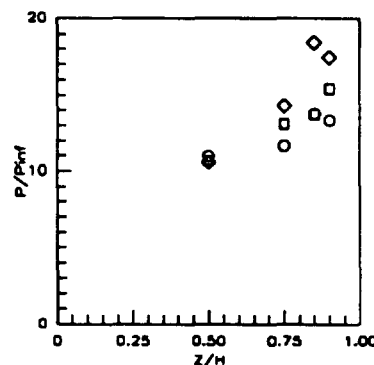
Sym	$x'/T_x'$	Run No.	CR/Re/Cowl (millions)
○	1.0643	run66	3/2.15/0%
□	1.0643	run62	3/2.15/25%
◇	1.0643	run60	3/2.15/50%

Figure 7.2.2.51: Cowl Effects (CR=3, Re=2.15million/ft) Sidewall Pressures



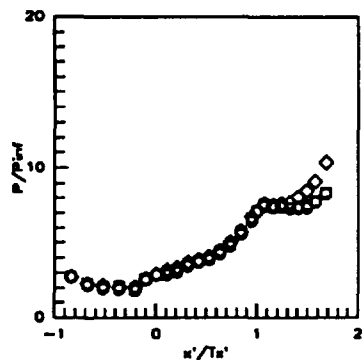
Sym	$x'/T_x'$	Run No.	CR/Re/Cowl (millions)
○	1.1537	run66	3/2.15/0%
□	1.1537	run62	3/2.15/25%
◇	1.1537	run60	3/2.15/50%

Figure 7.2.2.52: Cowl Effects (CR=3, Re=2.15million/ft) Sidewall Pressures



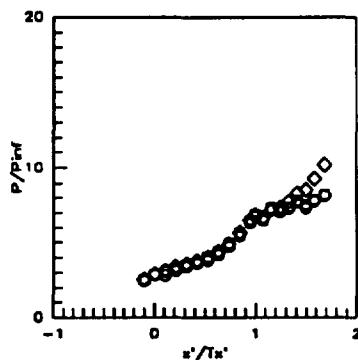
Sym	$x'/T_x'$	Run No.	CR/Re/Cowl (millions)
○	1.2356	run66	3/2.15/0%
□	1.2356	run62	3/2.15/25%
◇	1.2356	run60	3/2.15/50%

Figure 7.2.2.53: Cowl Effects (CR=3, Re=2.15million/ft) Sidewall Pressures



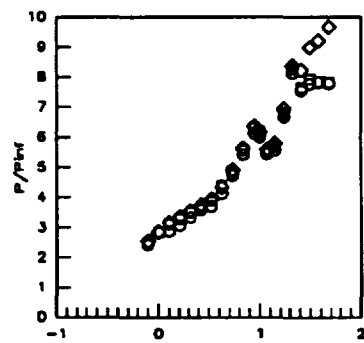
Sym	C.L. for	Run No.	CR/Re/Cowl (millions)
○	CR=3	run85	3/1.14/0%
◻	CR=3	run83	3/1.14/25%
◇	CR=3	run59	3/1.14/50%

Figure 7.2.2.54: Cowl Effects  
(CR=3, Re=1.14million/ft)  
CR=3 Centerline Pressures



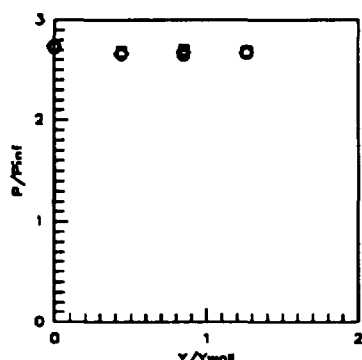
Sym	C.L. for	Run No.	CR/Re/Cowl (millions)
○	CR=5	run85	3/1.14/0%
◻	CR=5	run83	3/1.14/25%
◇	CR=5	run59	3/1.14/50%

Figure 7.2.2.55: Cowl Effects  
(CR=3, Re=1.14million/ft)  
CR=5 Centerline Pressures



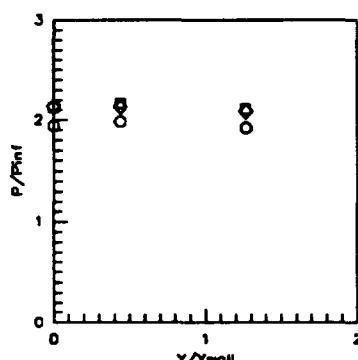
Sym	C.L. for	Run No.	CR/Re/Cowl (millions)
○	CR=9	run85	3/1.14/0%
◻	CR=9	run83	3/1.14/25%
◇	CR=9	run59	3/1.14/50%

Figure 7.2.2.56: Cowl Effects  
(CR=3, Re=1.14million/ft)  
CR=9 Centerline Pressures



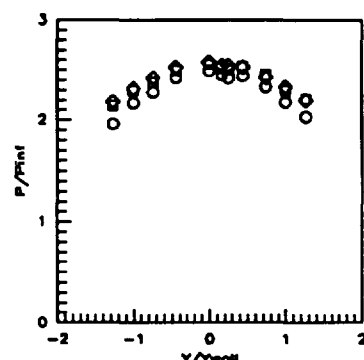
Sym	x'/Tx'	Run No.	CR/Re/Cowl (millions)
○	-0.8412	run85	3/1.14/0%
◻	-0.8412	run83	3/1.14/25%
◇	-0.8142	run59	3/1.14/50%

Figure 7.2.2.57: Cowl Effects  
(CR=3, Re=1.14million/ft)  
Baseplate Pressures



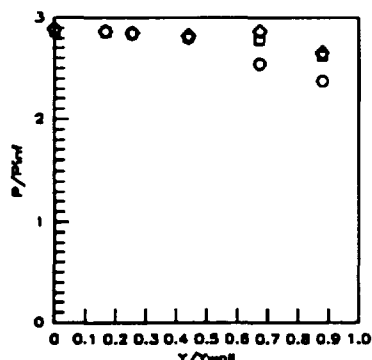
Sym	x'/Tx'	Run No.	CR/Re/Cowl (millions)
○	-0.5258	run85	3/1.14/0%
◻	-0.5258	run83	3/1.14/25%
◇	-0.5258	run59	3/1.14/50%

Figure 7.2.2.58: Cowl Effects  
(CR=3, Re=1.14million/ft)  
Baseplate Pressures



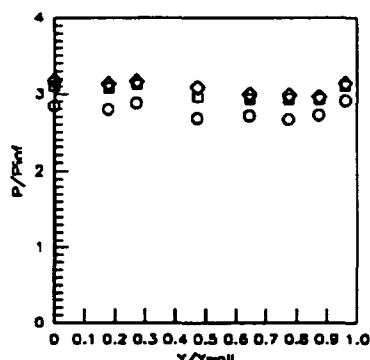
Sym	x'/Tx'	Run No.	CR/Re/Cowl (millions)
○	-0.1052	run85	3/1.14/0%
◻	-0.1052	run83	3/1.14/25%
◇	-0.1052	run59	3/1.14/50%

Figure 7.2.2.59: Cowl Effects  
(CR=3, Re=1.14million/ft)  
Baseplate Pressures



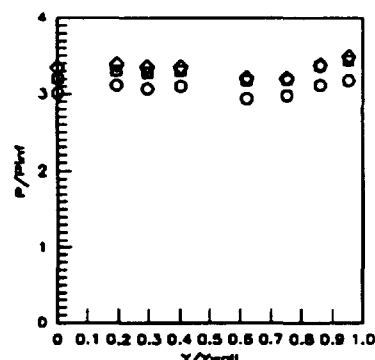
Sym	x'/Tx'	Run No.	CR/Re/Cowl (millions)
○	0.0000	run85	3/1.14/0%
◻	0.0000	run83	3/1.14/25%
◇	0.0000	run59	3/1.14/50%

Figure 7.2.2.60: Cowl Effects  
(CR=3, Re=1.14million/ft)  
Baseplate Pressures



Sym	x'/Tx'	Run No.	CR/Re/Cowl (millions)
○	0.1052	run85	3/1.14/0%
◻	0.1052	run83	3/1.14/25%
◇	0.1052	run59	3/1.14/50%

Figure 7.2.2.61: Cowl Effects  
(CR=3, Re=1.14million/ft)  
Baseplate Pressures



Sym	x'/Tx'	Run No.	CR/Re/Cowl (millions)
○	0.2103	run85	3/1.14/0%
◻	0.2103	run83	3/1.14/25%
◇	0.2103	run59	3/1.14/50%

Figure 7.2.2.62: Cowl Effects  
(CR=3, Re=1.14million/ft)  
Baseplate Pressures

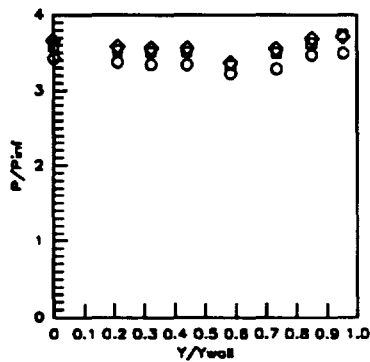


Figure 7.2.2.63: Cowl Effects  
(CR=3, Re=1.14million/ft)  
Baseplate Pressures

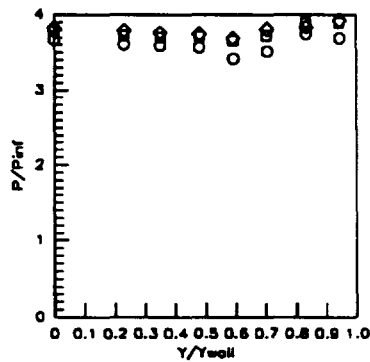


Figure 7.2.2.64: Cowl Effects  
(CR=3, Re=1.14million/ft)  
Baseplate Pressures

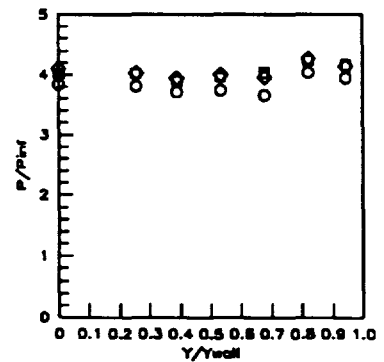


Figure 7.2.2.65: Cowl Effects  
(CR=3, Re=1.14million/ft)  
Baseplate Pressures

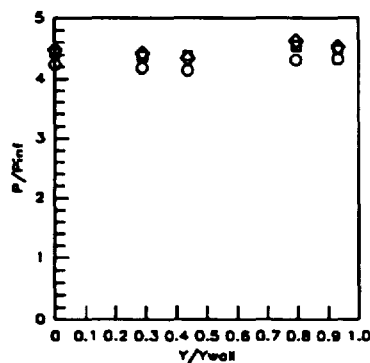


Figure 7.2.2.66: Cowl Effects  
(CR=3, Re=1.14million/ft)  
Baseplate Pressures

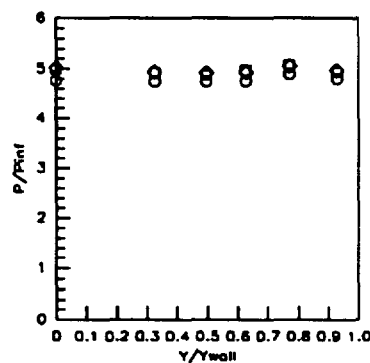


Figure 7.2.2.67: Cowl Effects  
(CR=3, Re=1.14million/ft)  
Baseplate Pressures

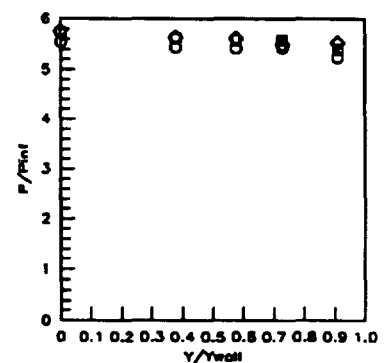


Figure 7.2.2.68: Cowl Effects  
(CR=3, Re=1.14million/ft)  
Baseplate Pressures

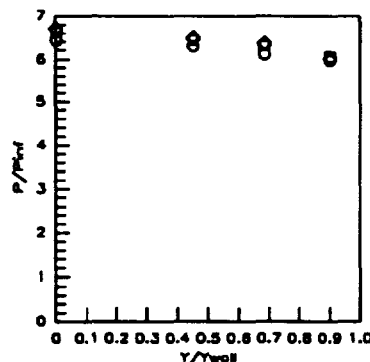


Figure 7.2.2.69: Cowl Effects  
(CR=3, Re=1.14million/ft)  
Baseplate Pressures

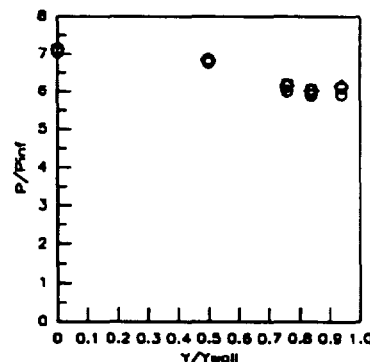


Figure 7.2.2.70: Cowl Effects  
(CR=3, Re=1.14million/ft)  
Baseplate Pressures

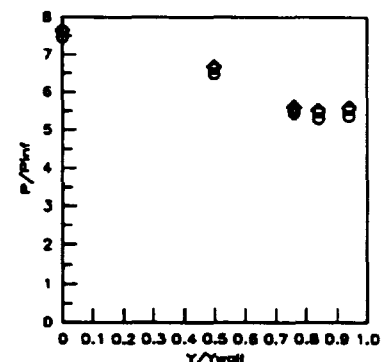
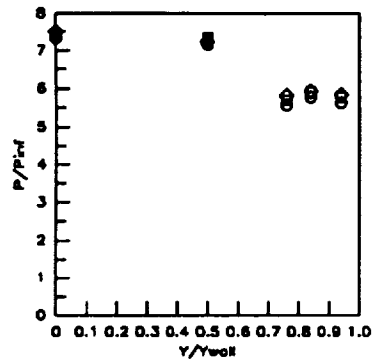
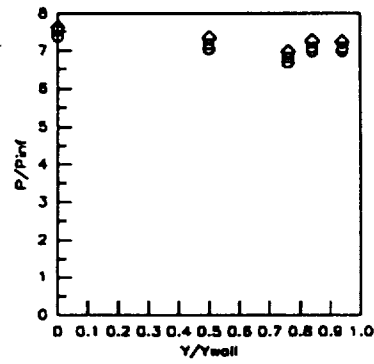


Figure 7.2.2.71: Cowl Effects  
(CR=3, Re=1.14million/ft)  
Baseplate Pressures



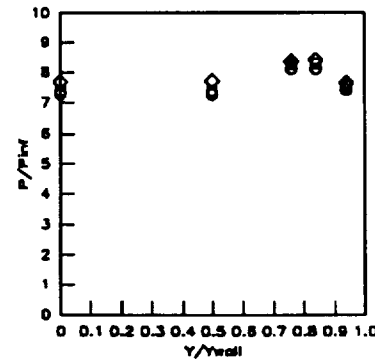
Sym	$x'/T_x'$	Run No.	CR/Re/Cowl (millions)
o	1.1567	run85	3/1.14/0%
□	1.1567	run83	3/1.14/25%
◇	1.1567	run59	3/1.14/50%

Figure 7.2.2.72: Cowl Effects (CR=3, Re=1.14million/ft) Baseplate Pressures



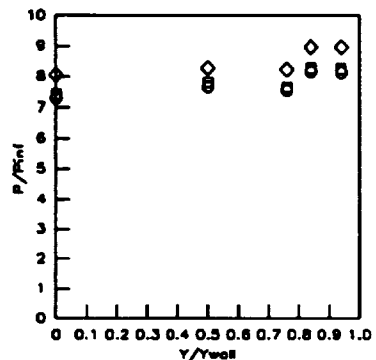
Sym	$x'/T_x'$	Run No.	CR/Re/Cowl (millions)
o	1.2408	run85	3/1.14/0%
□	1.2408	run83	3/1.14/25%
◇	1.2408	run59	3/1.14/50%

Figure 7.2.2.73: Cowl Effects (CR=3, Re=1.14million/ft) Baseplate Pressures



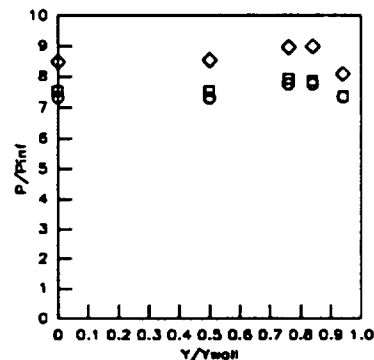
Sym	$x'/T_x'$	Run No.	CR/Re/Cowl (millions)
o	1.3249	run85	3/1.14/0%
□	1.3249	run83	3/1.14/25%
◇	1.3249	run59	3/1.14/50%

Figure 7.2.2.74: Cowl Effects (CR=3, Re=1.14million/ft) Baseplate Pressures



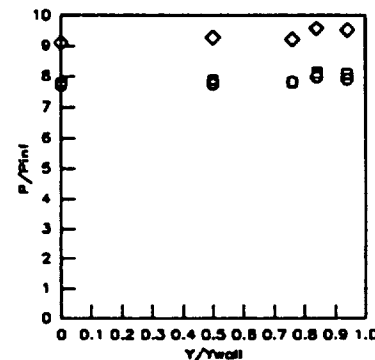
Sym	$x'/T_x'$	Run No.	CR/Re/Cowl (millions)
o	1.4090	run85	3/1.14/0%
□	1.4090	run83	3/1.14/25%
◇	1.4090	run59	3/1.14/50%

Figure 7.2.2.75: Cowl Effects (CR=3, Re=1.14million/ft) Baseplate Pressures



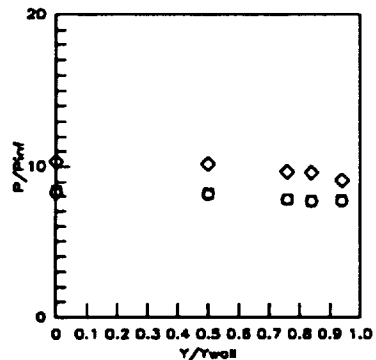
Sym	$x'/T_x'$	Run No.	CR/Re/Cowl (millions)
o	1.4932	run85	3/1.14/0%
□	1.4932	run83	3/1.14/25%
◇	1.4932	run59	3/1.14/50%

Figure 7.2.2.76: Cowl Effects (CR=3, Re=1.14million/ft) Baseplate Pressures



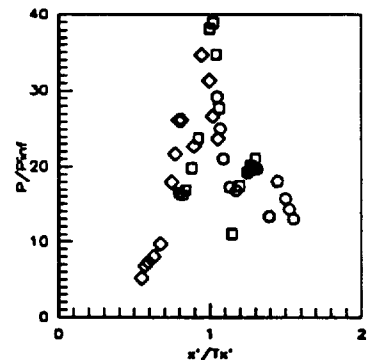
Sym	$x'/T_x'$	Run No.	CR/Re/Cowl (millions)
o	1.5773	run85	3/1.14/0%
□	1.5773	run83	3/1.14/25%
◇	1.5773	run59	3/1.14/50%

Figure 7.2.2.77: Cowl Effects (CR=3, Re=1.14million/ft) Baseplate Pressures



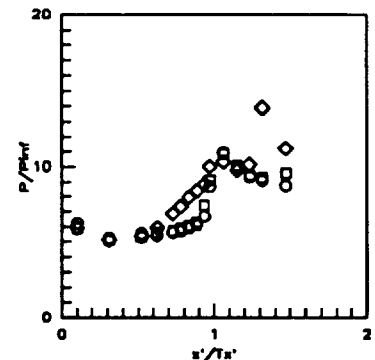
Sym	$x'/T_x'$	Run No.	CR/Re/Cowl (millions)
o	1.6824	run85	3/1.14/0%
□	1.6824	run83	3/1.14/25%
◇	1.6824	run59	3/1.14/50%

Figure 7.2.2.78: Cowl Effects (CR=3, Re=1.14million/ft) Baseplate Pressures



Sym	Cowl Pos.	Run No.	CR/Re/Cowl (millions)
o	0%	run85	3/1.14/0%
□	25%	run83	3/1.14/25%
◇	50%	run59	3/1.14/50%

Figure 7.2.2.79: Cowl Effects (CR=3, Re=1.14million/ft) Cowl Pressures



Sym	Z/H	Run No.	CR/Re/Cowl (millions)
o	0.5RT	run85	3/1.14/0%
□	0.5RT	run83	3/1.14/25%
◇	0.5RT	run59	3/1.14/50%

Figure 7.2.2.80: Cowl Effects (CR=3, Re=1.14million/ft) Sidewall Centerline Pressures

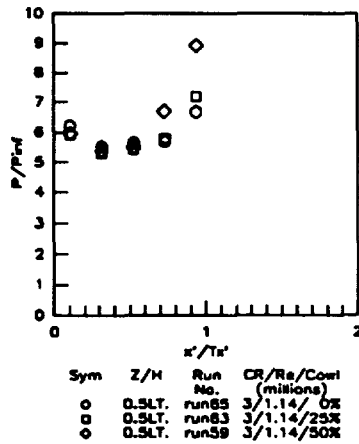


Figure 7.2.2.81: Cowl Effects (CR=3, Re=1.14million/ft) Sidewall Centerline Pressures

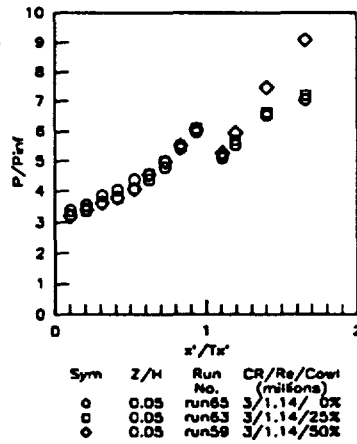


Figure 7.2.2.82: Cowl Effects (CR=3, Re=1.14million/ft) Sidewall Pressures

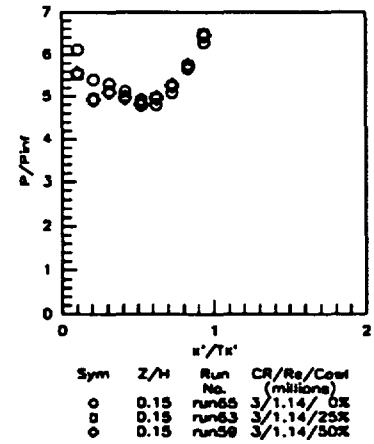


Figure 7.2.2.83: Cowl Effects (CR=3, Re=1.14million/ft) Sidewall Pressures

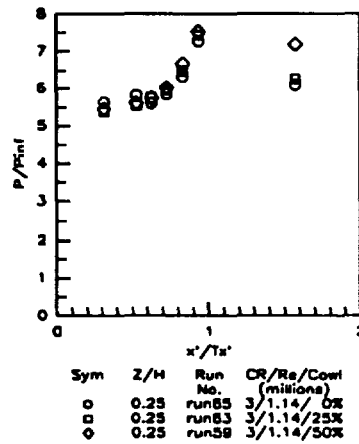


Figure 7.2.2.84: Cowl Effects (CR=3, Re=1.14million/ft) Sidewall Pressures

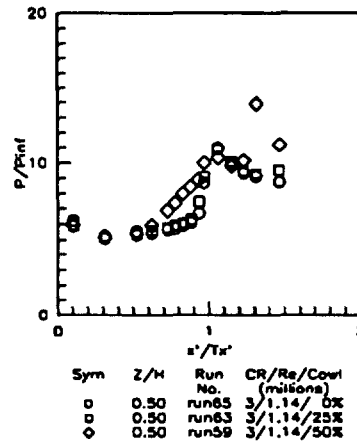


Figure 7.2.2.85: Cowl Effects (CR=3, Re=1.14million/ft) Sidewall Pressures

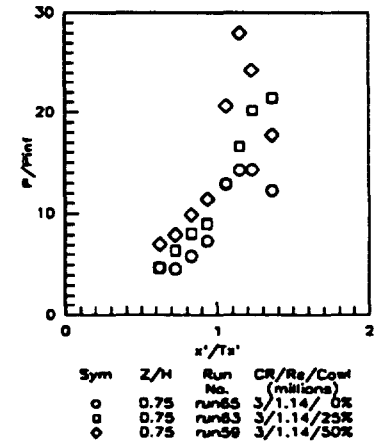


Figure 7.2.2.86: Cowl Effects (CR=3, Re=1.14million/ft) Sidewall Pressures

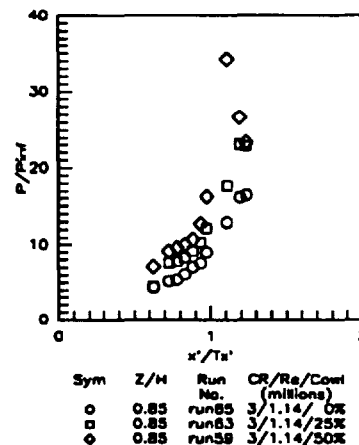


Figure 7.2.2.87: Cowl Effects (CR=3, Re=1.14million/ft) Sidewall Pressures

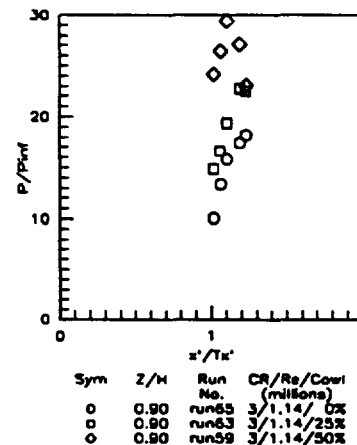


Figure 7.2.2.88: Cowl Effects (CR=3, Re=1.14million/ft) Sidewall Pressures

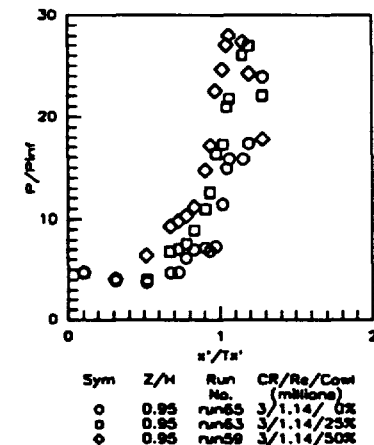
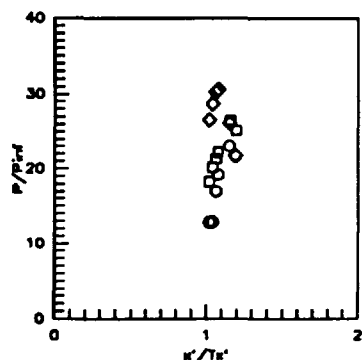
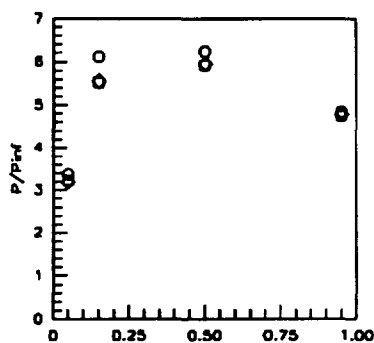


Figure 7.2.2.89: Cowl Effects (CR=3, Re=1.14million/ft) Sidewall Pressures



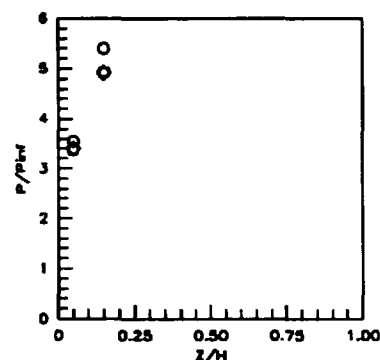
Sym	Z/H	Run No.	CR/Re/Cowl (millions)
○	0.975	run65	3/1.14/0%
□	0.975	run63	3/1.14/25%
◇	0.975	run58	3/1.14/50%

Figure 7.2.2.90: Cowl Effects (CR=3, Re=1.14million/ft) Sidewall Pressures



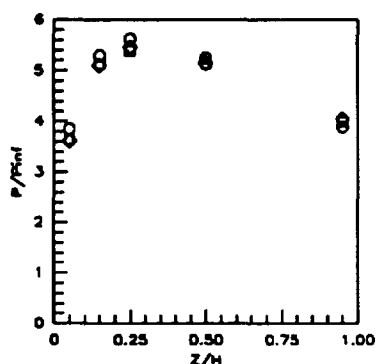
Sym	x'/Ts'	Run No.	CR/Re/Cowl (millions)
○	0.1042	run65	3/1.14/0%
□	0.1042	run63	3/1.14/25%
◇	0.1042	run58	3/1.14/50%

Figure 7.2.2.91: Cowl Effects (CR=3, Re=1.14million/ft) Sidewall Pressures



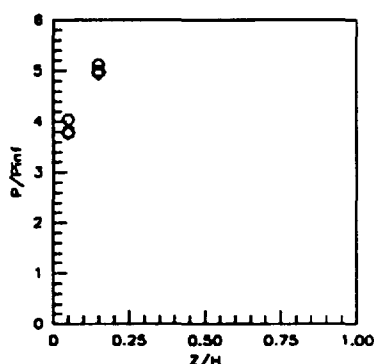
Sym	x'/Ts'	Run No.	CR/Re/Cowl (millions)
○	0.2063	run65	3/1.14/0%
□	0.2063	run63	3/1.14/25%
◇	0.2063	run58	3/1.14/50%

Figure 7.2.2.92: Cowl Effects (CR=3, Re=1.14million/ft) Sidewall Pressures



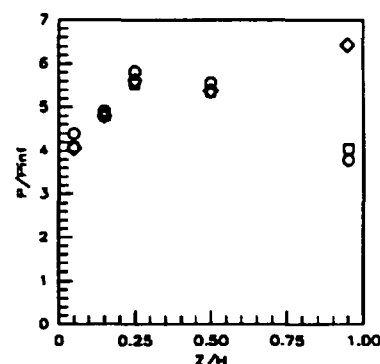
Sym	x'/Ts'	Run No.	CR/Re/Cowl (millions)
○	0.3125	run65	3/1.14/0%
□	0.3125	run63	3/1.14/25%
◇	0.3125	run58	3/1.14/50%

Figure 7.2.2.93: Cowl Effects (CR=3, Re=1.14million/ft) Sidewall Pressures



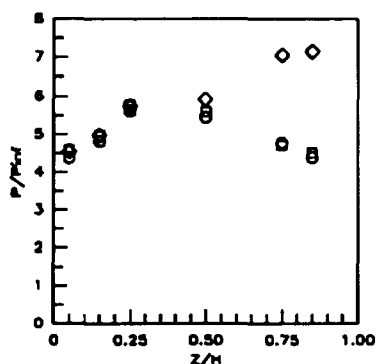
Sym	x'/Ts'	Run No.	CR/Re/Cowl (millions)
○	0.4167	run65	3/1.14/0%
□	0.4167	run63	3/1.14/25%
◇	0.4167	run58	3/1.14/50%

Figure 7.2.2.94: Cowl Effects (CR=3, Re=1.14million/ft) Sidewall Pressures



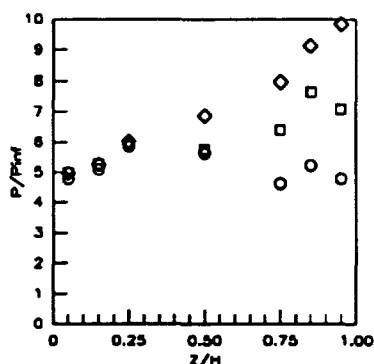
Sym	x'/Ts'	Run No.	CR/Re/Cowl (millions)
○	0.5250	run65	3/1.14/0%
□	0.5250	run63	3/1.14/25%
◇	0.5250	run58	3/1.14/50%

Figure 7.2.2.95: Cowl Effects (CR=3, Re=1.14million/ft) Sidewall Pressures



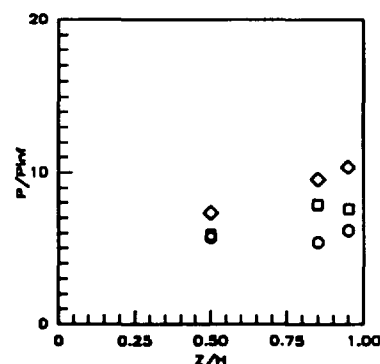
Sym	x'/Ts'	Run No.	CR/Re/Cowl (millions)
○	0.6252	run65	3/1.14/0%
□	0.6252	run63	3/1.14/25%
◇	0.6252	run58	3/1.14/50%

Figure 7.2.2.96: Cowl Effects (CR=3, Re=1.14million/ft) Sidewall Pressures



Sym	x'/Ts'	Run No.	CR/Re/Cowl (millions)
○	0.7294	run65	3/1.14/0%
□	0.7294	run63	3/1.14/25%
◇	0.7294	run58	3/1.14/50%

Figure 7.2.2.97: Cowl Effects (CR=3, Re=1.14million/ft) Sidewall Pressures



Sym	x'/Ts'	Run No.	CR/Re/Cowl (millions)
○	0.7815	run65	3/1.14/0%
□	0.7815	run63	3/1.14/25%
◇	0.7815	run58	3/1.14/50%

Figure 7.2.2.98: Cowl Effects (CR=3, Re=1.14million/ft) Sidewall Pressures

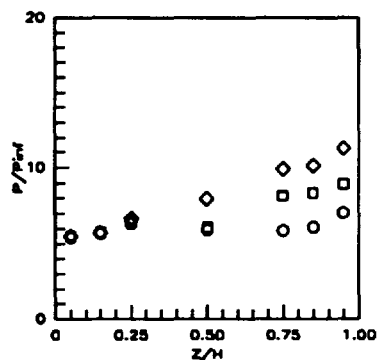


Figure 7.2.2.99: Cowl Effects  
(CR=3, Re=1.14million/ft)  
Sidewall Pressures

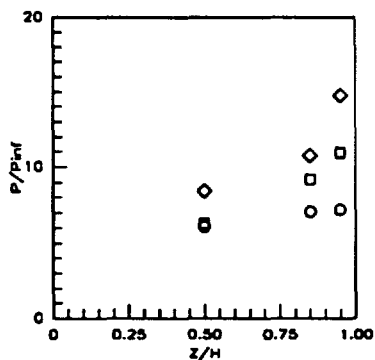


Figure 7.2.2.100: Cowl Effects  
(CR=3, Re=1.14million/ft)  
Sidewall Pressures

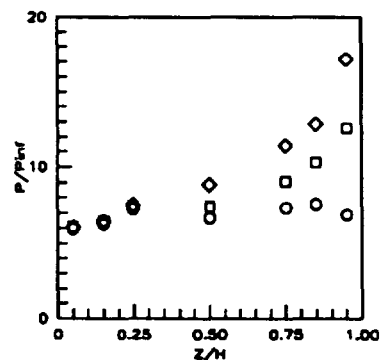


Figure 7.2.2.101: Cowl Effects  
(CR=3, Re=1.14million/ft)  
Sidewall Pressures

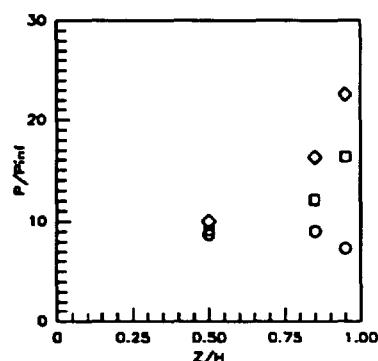


Figure 7.2.2.102: Cowl Effects  
(CR=3, Re=1.14million/ft)  
Sidewall Pressures

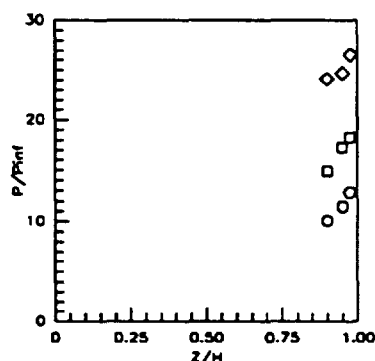


Figure 7.2.2.103: Cowl Effects  
(CR=3, Re=1.14million/ft)  
Sidewall Pressures

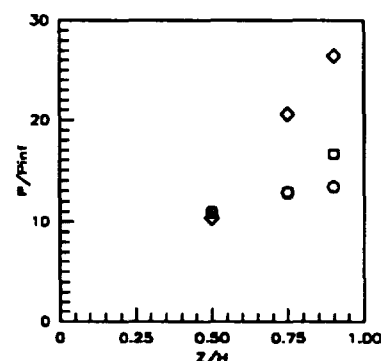


Figure 7.2.2.104: Cowl Effects  
(CR=3, Re=1.14million/ft)  
Sidewall Pressures

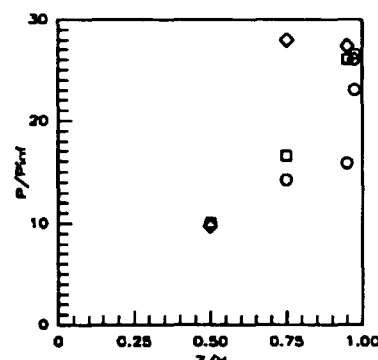


Figure 7.2.2.105: Cowl Effects  
(CR=3, Re=1.14million/ft)  
Sidewall Pressures

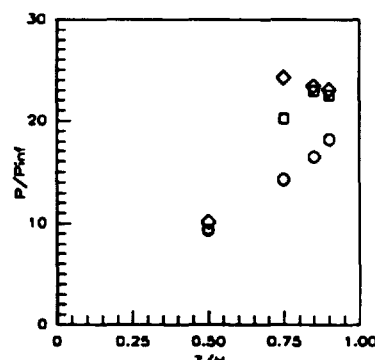
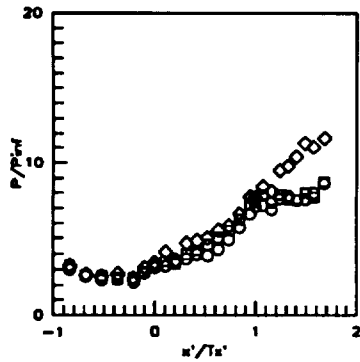


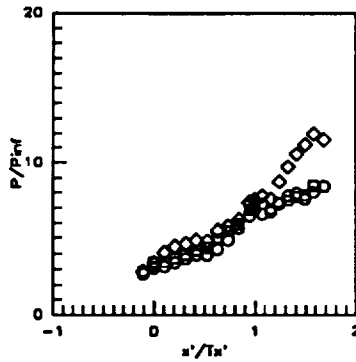
Figure 7.2.2.106: Cowl Effects  
(CR=3, Re=1.14million/ft)  
Sidewall Pressures





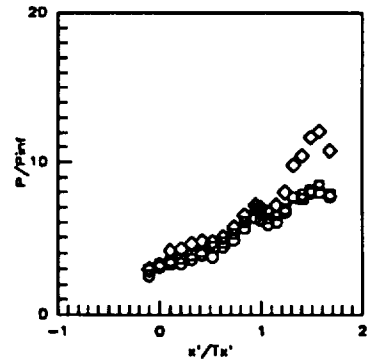
Sym	C.L. for	Run No.	CR/Re/Cowl (millions)
○	CR=3	run64	3/0.55/ 0%
□	CR=3	run61	3/0.55/25%
◇	CR=3	run58	3/0.55/50%

Figure 7.2.2.107: Cowl Effects (CR=3, Re=0.55million/ft)  
CR=3 Centerline Pressures



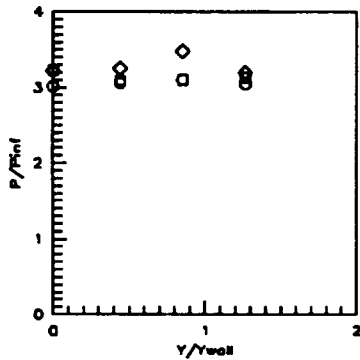
Sym	C.L. for	Run No.	CR/Re/Cowl (millions)
○	CR=5	run64	3/0.55/ 0%
□	CR=5	run61	3/0.55/25%
◇	CR=5	run58	3/0.55/50%

Figure 7.2.2.108: Cowl Effects (CR=3, Re=0.55million/ft)  
CR=5 Centerline Pressures



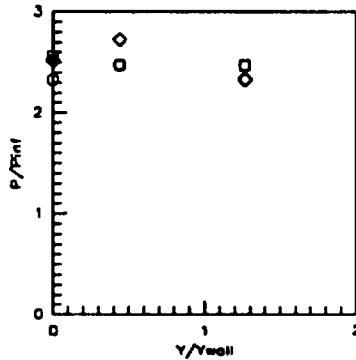
Sym	C.L. for	Run No.	CR/Re/Cowl (millions)
○	CR=9	run64	3/0.55/ 0%
□	CR=9	run61	3/0.55/25%
◇	CR=9	run58	3/0.55/50%

Figure 7.2.2.109: Cowl Effects (CR=3, Re=0.55million/ft)  
CR=9 Centerline Pressures



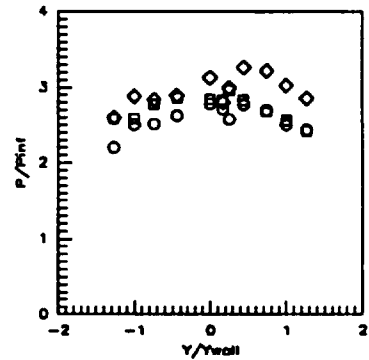
Sym	x'/Ts'	Run No.	CR/Re/Cowl (millions)
○	-0.8412	run64	3/0.55/ 0%
□	-0.8412	run61	3/0.55/25%
◇	-0.8142	run58	3/0.55/50%

Figure 7.2.2.110: Cowl Effects (CR=3, Re=0.55million/ft)  
Baseplate Pressures



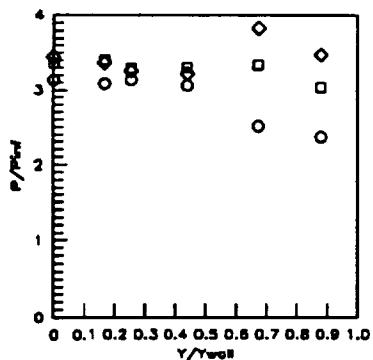
Sym	x'/Ts'	Run No.	CR/Re/Cowl (millions)
○	-0.5258	run64	3/0.55/ 0%
□	-0.5258	run61	3/0.55/25%
◇	-0.5258	run58	3/0.55/50%

Figure 7.2.2.111: Cowl Effects (CR=3, Re=0.55million/ft)  
Baseplate Pressures



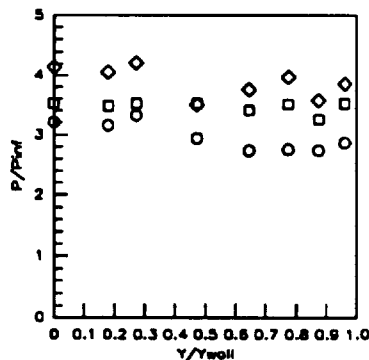
Sym	x'/Ts'	Run No.	CR/Re/Cowl (millions)
○	-0.1052	run64	3/0.55/ 0%
□	-0.1052	run61	3/0.55/25%
◇	-0.1052	run58	3/0.55/50%

Figure 7.2.2.112: Cowl Effects (CR=3, Re=0.55million/ft)  
Baseplate Pressures



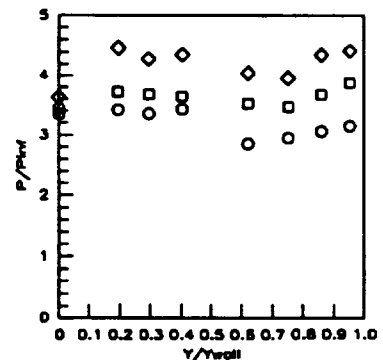
Sym	x'/Ts'	Run No.	CR/Re/Cowl (millions)
○	0.0000	run64	3/0.55/ 0%
□	0.0000	run61	3/0.55/25%
◇	0.0000	run58	3/0.55/50%

Figure 7.2.2.113: Cowl Effects (CR=3, Re=0.55million/ft)  
Baseplate Pressures



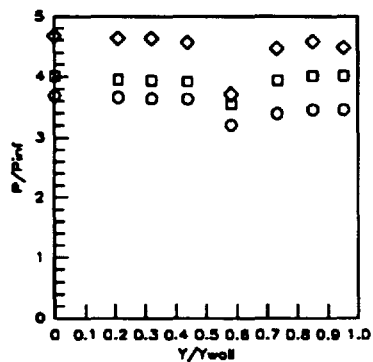
Sym	x'/Ts'	Run No.	CR/Re/Cowl (millions)
○	0.1052	run64	3/0.55/ 0%
□	0.1052	run61	3/0.55/25%
◇	0.1052	run58	3/0.55/50%

Figure 7.2.2.114: Cowl Effects (CR=3, Re=0.55million/ft)  
Baseplate Pressures



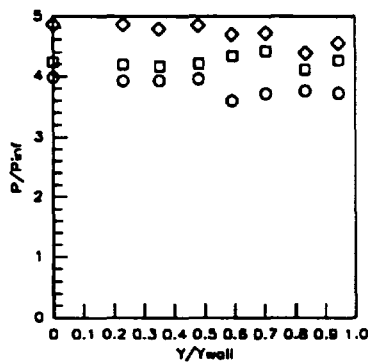
Sym	x'/Ts'	Run No.	CR/Re/Cowl (millions)
○	0.2103	run64	3/0.55/ 0%
□	0.2103	run61	3/0.55/25%
◇	0.2103	run58	3/0.55/50%

Figure 7.2.2.115: Cowl Effects (CR=3, Re=0.55million/ft)  
Baseplate Pressures



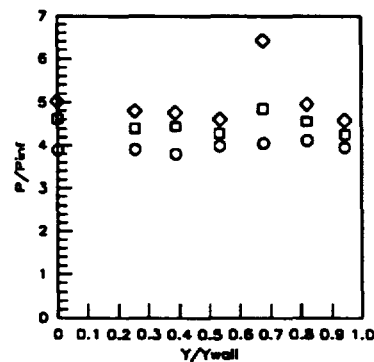
Sym	x'/Ts'	Run No.	CR/Re/Cowl (millions)
o	0.3154	run64	3/0.55/0%
o	0.3154	run61	3/0.55/25%
o	0.3154	run58	3/0.55/50%

Figure 7.2.2.116: Cowl Effects (CR=3, Re=0.55million/ft) Baseplate Pressures



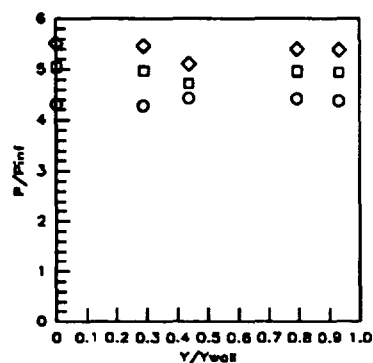
Sym	x'/Ts'	Run No.	CR/Re/Cowl (millions)
o	0.4206	run64	3/0.55/0%
o	0.4206	run61	3/0.55/25%
o	0.4206	run58	3/0.55/50%

Figure 7.2.2.117: Cowl Effects (CR=3, Re=0.55million/ft) Baseplate Pressures



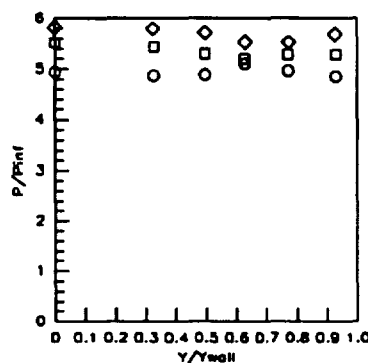
Sym	x'/Ts'	Run No.	CR/Re/Cowl (millions)
o	0.53258	run64	3/0.55/0%
o	0.53258	run61	3/0.55/25%
o	0.53258	run58	3/0.55/50%

Figure 7.2.2.118: Cowl Effects (CR=3, Re=0.55million/ft) Baseplate Pressures



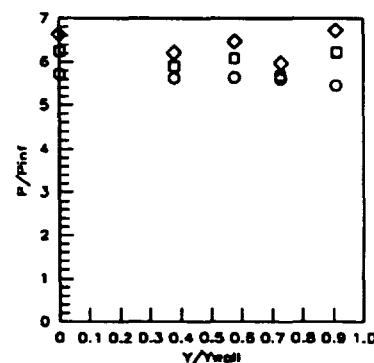
Sym	x'/Ts'	Run No.	CR/Re/Cowl (millions)
o	0.6309	run64	3/0.55/0%
o	0.6309	run61	3/0.55/25%
o	0.6309	run58	3/0.55/50%

Figure 7.2.2.119: Cowl Effects (CR=3, Re=0.55million/ft) Baseplate Pressures



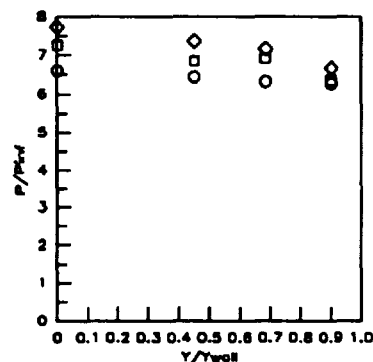
Sym	x'/Ts'	Run No.	CR/Re/Cowl (millions)
o	0.7361	run64	3/0.55/0%
o	0.7361	run61	3/0.55/25%
o	0.7361	run58	3/0.55/50%

Figure 7.2.2.120: Cowl Effects (CR=3, Re=0.55million/ft) Baseplate Pressures



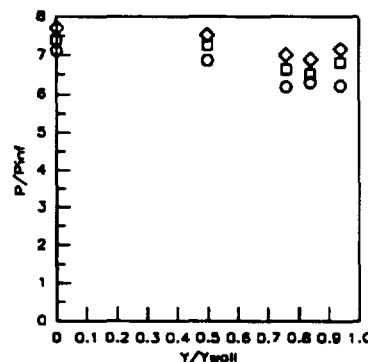
Sym	x'/Ts'	Run No.	CR/Re/Cowl (millions)
o	0.8412	run64	3/0.55/0%
o	0.8412	run61	3/0.55/25%
o	0.8412	run58	3/0.55/50%

Figure 7.2.2.121: Cowl Effects (CR=3, Re=0.55million/ft) Baseplate Pressures



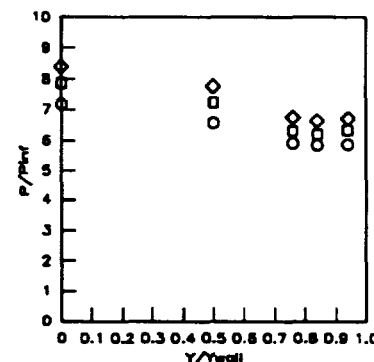
Sym	x'/Ts'	Run No.	CR/Re/Cowl (millions)
o	0.9464	run64	3/0.55/0%
o	0.9464	run61	3/0.55/25%
o	0.9464	run58	3/0.55/50%

Figure 7.2.2.122: Cowl Effects (CR=3, Re=0.55million/ft) Baseplate Pressures



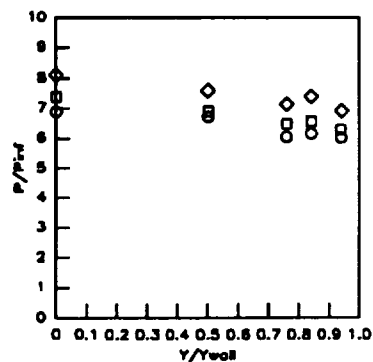
Sym	x'/Ts'	Run No.	CR/Re/Cowl (millions)
o	1.0000	run64	3/0.55/0%
o	1.0000	run61	3/0.55/25%
o	1.0000	run58	3/0.55/50%

Figure 7.2.2.123: Cowl Effects (CR=3, Re=0.55million/ft) Baseplate Pressures



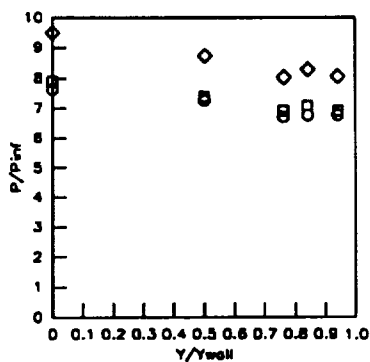
Sym	x'/Ts'	Run No.	CR/Re/Cowl (millions)
o	1.0726	run64	3/0.55/0%
o	1.0726	run61	3/0.55/25%
o	1.0726	run58	3/0.55/50%

Figure 7.2.2.124: Cowl Effects (CR=3, Re=0.55million/ft) Baseplate Pressures



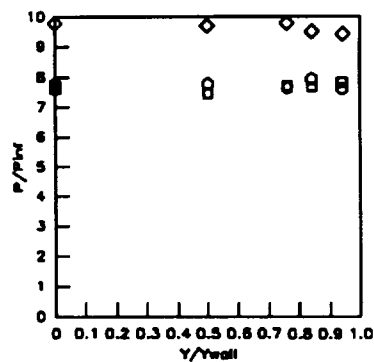
Sym	$x'/T_x'$	Run No.	CR/Re/Cowl (millions)
○	1.1567	run64	3/0.55/0%
□	1.1567	run61	3/0.55/25%
◇	1.1567	run58	3/0.55/50%

Figure 7.2.2.125: Cowl Effects (CR=3, Re=0.55million/ft) Baseplate Pressures



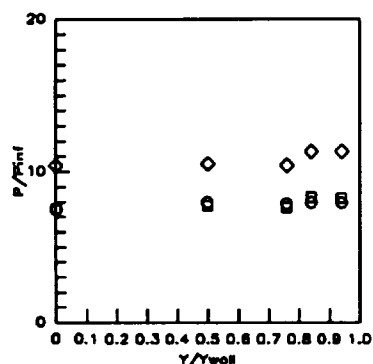
Sym	$x'/T_x'$	Run No.	CR/Re/Cowl (millions)
○	1.2408	run64	3/0.55/0%
□	1.2408	run61	3/0.55/25%
◇	1.2408	run58	3/0.55/50%

Figure 7.2.2.126: Cowl Effects (CR=3, Re=0.55million/ft) Baseplate Pressures



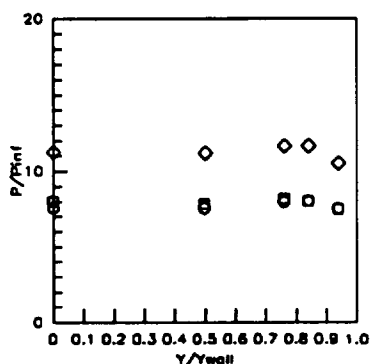
Sym	$x'/T_x'$	Run No.	CR/Re/Cowl (millions)
○	1.3249	run64	3/0.55/0%
□	1.3249	run61	3/0.55/25%
◇	1.3249	run58	3/0.55/50%

Figure 7.2.2.127: Cowl Effects (CR=3, Re=0.55million/ft) Baseplate Pressures



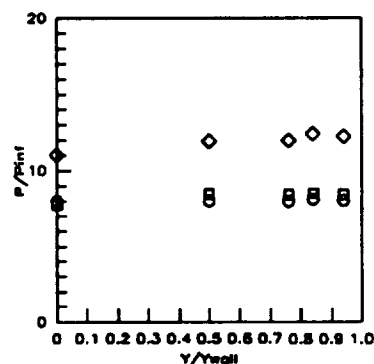
Sym	$x'/T_x'$	Run No.	CR/Re/Cowl (millions)
○	1.4090	run64	3/0.55/0%
□	1.4090	run61	3/0.55/25%
◇	1.4090	run58	3/0.55/50%

Figure 7.2.2.128: Cowl Effects (CR=3, Re=0.55million/ft) Baseplate Pressures



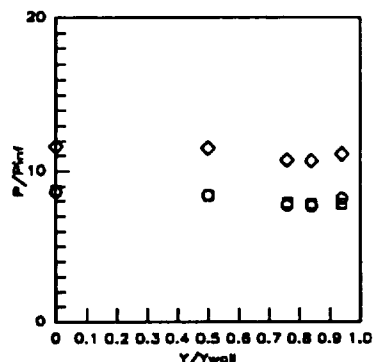
Sym	$x'/T_x'$	Run No.	CR/Re/Cowl (millions)
○	1.4932	run64	3/0.55/0%
□	1.4932	run61	3/0.55/25%
◇	1.4932	run58	3/0.55/50%

Figure 7.2.2.129: Cowl Effects (CR=3, Re=0.55million/ft) Baseplate Pressures



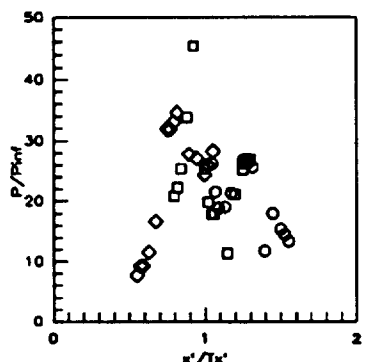
Sym	$x'/T_x'$	Run No.	CR/Re/Cowl (millions)
○	1.5773	run64	3/0.55/0%
□	1.5773	run61	3/0.55/25%
◇	1.5773	run58	3/0.55/50%

Figure 7.2.2.130: Cowl Effects (CR=3, Re=0.55million/ft) Baseplate Pressures



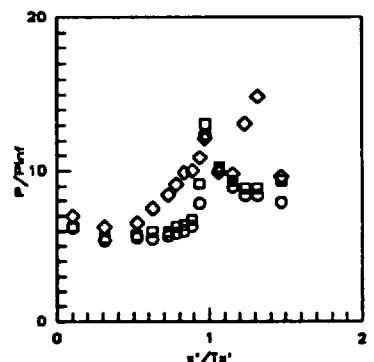
Sym	$x'/T_x'$	Run No.	CR/Re/Cowl (millions)
○	1.6824	run64	3/0.55/0%
□	1.6824	run61	3/0.55/25%
◇	1.6824	run58	3/0.55/50%

Figure 7.2.2.131: Cowl Effects (CR=3, Re=0.55million/ft) Baseplate Pressures



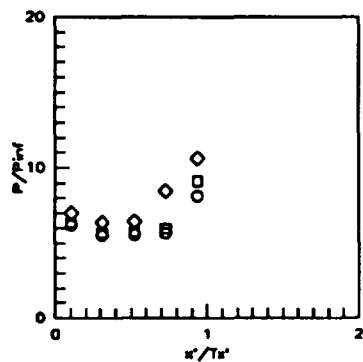
Sym	Cowl Pos.	Run No.	CR/Re/Cowl (millions)
○	0%	run64	3/0.55/0%
□	25%	run61	3/0.55/25%
◇	50%	run58	3/0.55/50%

Figure 7.2.2.132: Cowl Effects (CR=3, Re=0.55million/ft) Cowl Pressures



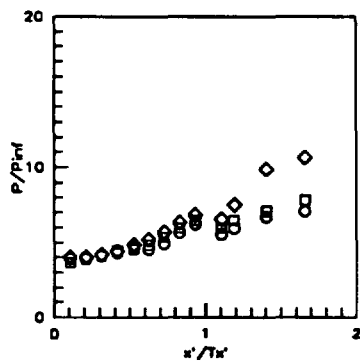
Sym	Z/H	Run No.	CR/Re/Cowl (millions)
○	0.5RT	run64	3/0.55/0%
□	0.5RT	run61	3/0.55/25%
◇	0.5RT	run58	3/0.55/50%

Figure 7.2.2.133: Cowl Effects (CR=3, Re=0.55million/ft) Sidewall Centerline Pressures



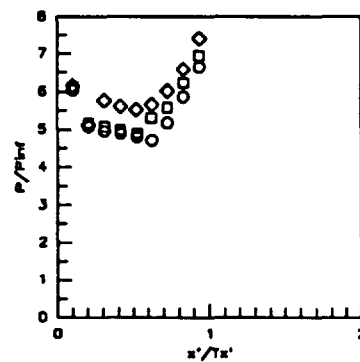
Sym	Z/H	Run No.	CR/Re/Cowl (millions)
○	0.5LT	run64	3/0.55/0%
□	0.5LT	run61	3/0.55/25%
◇	0.5LT	run58	3/0.55/50%

Figure 7.2.2.134: Cowl Effects (CR=3, Re=0.55million/ft) Sidewall Centerline Pressures



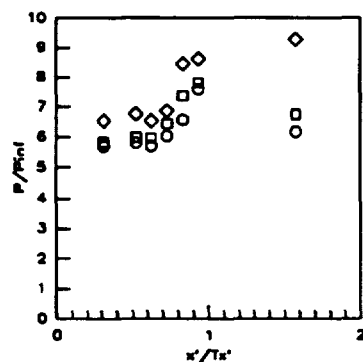
Sym	Z/H	Run No.	CR/Re/Cowl (millions)
○	0.05	run64	3/0.55/0%
□	0.05	run61	3/0.55/25%
◇	0.05	run58	3/0.55/50%

Figure 7.2.2.135: Cowl Effects (CR=3, Re=0.55million/ft) Sidewall Pressures



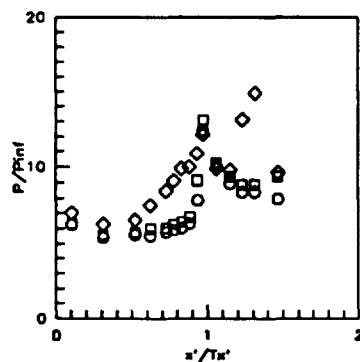
Sym	Z/H	Run No.	CR/Re/Cowl (millions)
○	0.15	run64	3/0.55/0%
□	0.15	run61	3/0.55/25%
◇	0.15	run58	3/0.55/50%

Figure 7.2.2.136: Cowl Effects (CR=3, Re=0.55million/ft) Sidewall Pressures



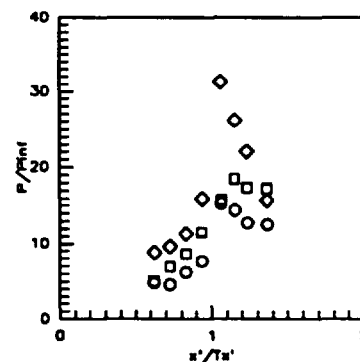
Sym	Z/H	Run No.	CR/Re/Cowl (millions)
○	0.25	run64	3/0.55/0%
□	0.25	run61	3/0.55/25%
◇	0.25	run58	3/0.55/50%

Figure 7.2.2.137: Cowl Effects (CR=3, Re=0.55million/ft) Sidewall Pressures



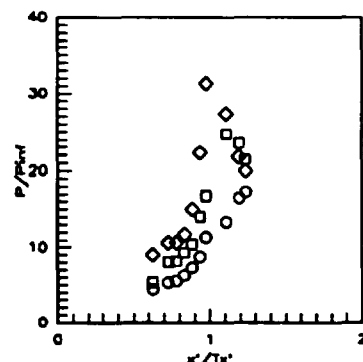
Sym	Z/H	Run No.	CR/Re/Cowl (millions)
○	0.50	run64	3/0.55/0%
□	0.50	run61	3/0.55/25%
◇	0.50	run58	3/0.55/50%

Figure 7.2.2.138: Cowl Effects (CR=3, Re=0.55million/ft) Sidewall Pressures



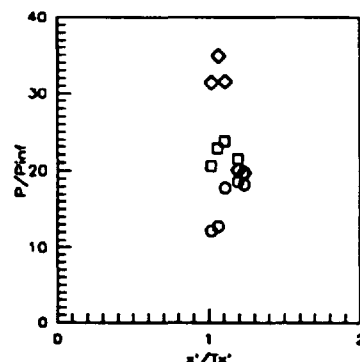
Sym	Z/H	Run No.	CR/Re/Cowl (millions)
○	0.75	run64	3/0.55/0%
□	0.75	run61	3/0.55/25%
◇	0.75	run58	3/0.55/50%

Figure 7.2.2.139: Cowl Effects (CR=3, Re=0.55million/ft) Sidewall Pressures



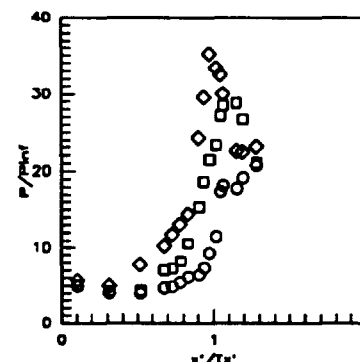
Sym	Z/H	Run No.	CR/Re/Cowl (millions)
○	0.85	run64	3/0.55/0%
□	0.85	run61	3/0.55/25%
◇	0.85	run58	3/0.55/50%

Figure 7.2.2.140: Cowl Effects (CR=3, Re=0.55million/ft) Sidewall Pressures



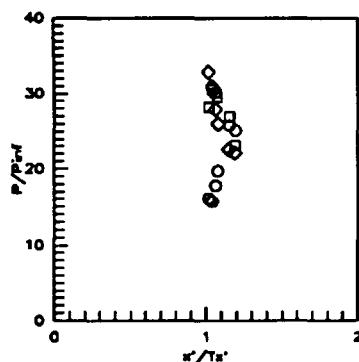
Sym	Z/H	Run No.	CR/Re/Cowl (millions)
○	0.90	run64	3/0.55/0%
□	0.90	run61	3/0.55/25%
◇	0.90	run58	3/0.55/50%

Figure 7.2.2.141: Cowl Effects (CR=3, Re=0.55million/ft) Sidewall Pressures



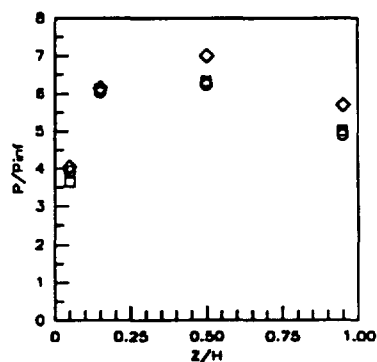
Sym	Z/H	Run No.	CR/Re/Cowl (millions)
○	0.95	run64	3/0.55/0%
□	0.95	run61	3/0.55/25%
◇	0.95	run58	3/0.55/50%

Figure 7.2.2.142: Cowl Effects (CR=3, Re=0.55million/ft) Sidewall Pressures



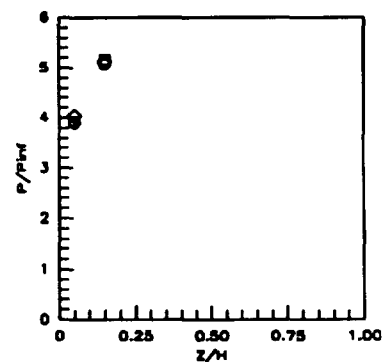
Sym	Z/H	Run No.	CR/Re/Cowl (millions)
○	0.975	run64	3/0.55/0%
□	0.975	run61	3/0.55/25%
◇	0.975	run58	3/0.55/50%

Figure 7.2.2.143: Cowl Effects (CR=3, Re=0.55million/ft) Sidewall Pressures



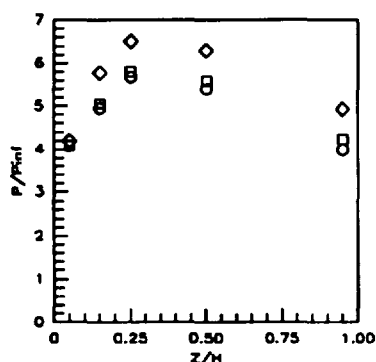
Sym	x'/Ts'	Run No.	CR/Re/Cowl (millions)
○	0.1042	run64	3/0.55/0%
□	0.1042	run61	3/0.55/25%
◇	0.1042	run58	3/0.55/50%

Figure 7.2.2.144: Cowl Effects (CR=3, Re=0.55million/ft) Sidewall Pressures



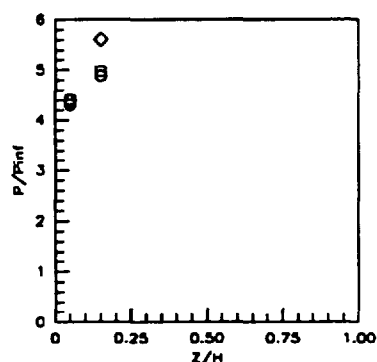
Sym	x'/Ts'	Run No.	CR/Re/Cowl (millions)
○	0.2083	run64	3/0.55/0%
□	0.2083	run61	3/0.55/25%
◇	0.2083	run58	3/0.55/50%

Figure 7.2.2.145: Cowl Effects (CR=3, Re=0.55million/ft) Sidewall Pressures



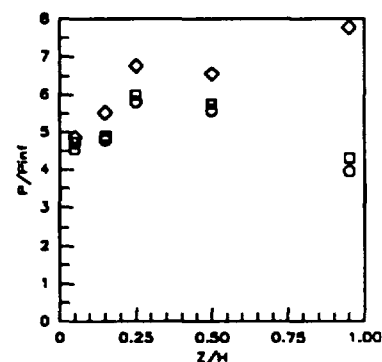
Sym	x'/Ts'	Run No.	CR/Re/Cowl (millions)
○	0.3125	run64	3/0.55/0%
□	0.3125	run61	3/0.55/25%
◇	0.3125	run58	3/0.55/50%

Figure 7.2.2.146: Cowl Effects (CR=3, Re=0.55million/ft) Sidewall Pressures



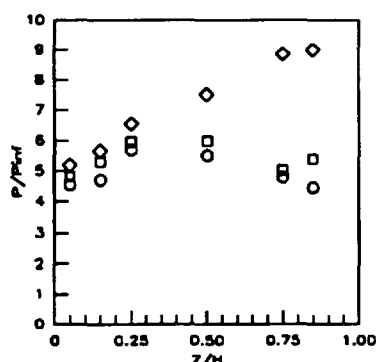
Sym	x'/Ts'	Run No.	CR/Re/Cowl (millions)
○	0.4167	run64	3/0.55/0%
□	0.4167	run61	3/0.55/25%
◇	0.4167	run58	3/0.55/50%

Figure 7.2.2.147: Cowl Effects (CR=3, Re=0.55million/ft) Sidewall Pressures



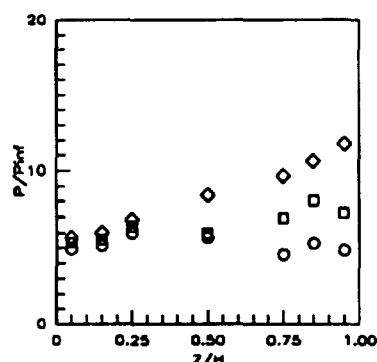
Sym	x'/Ts'	Run No.	CR/Re/Cowl (millions)
○	0.5250	run64	3/0.55/0%
□	0.5250	run61	3/0.55/25%
◇	0.5250	run58	3/0.55/50%

Figure 7.2.2.148: Cowl Effects (CR=3, Re=0.55million/ft) Sidewall Pressures



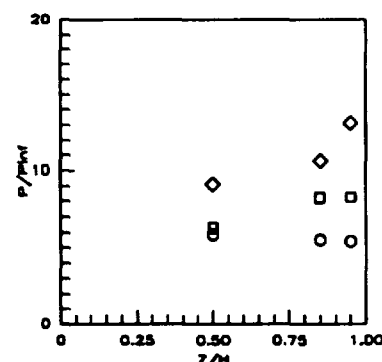
Sym	x'/Ts'	Run No.	CR/Re/Cowl (millions)
○	0.6252	run64	3/0.55/0%
□	0.6252	run61	3/0.55/25%
◇	0.6252	run58	3/0.55/50%

Figure 7.2.2.149: Cowl Effects (CR=3, Re=0.55million/ft) Sidewall Pressures



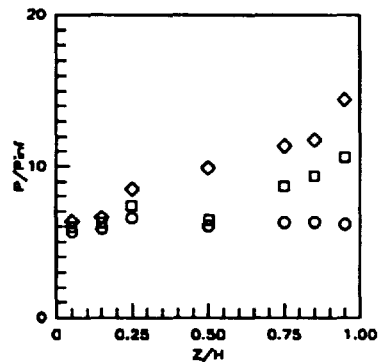
Sym	x'/Ts'	Run No.	CR/Re/Cowl (millions)
○	0.7294	run64	3/0.55/0%
□	0.7294	run61	3/0.55/25%
◇	0.7294	run58	3/0.55/50%

Figure 7.2.2.150: Cowl Effects (CR=3, Re=0.55million/ft) Sidewall Pressures



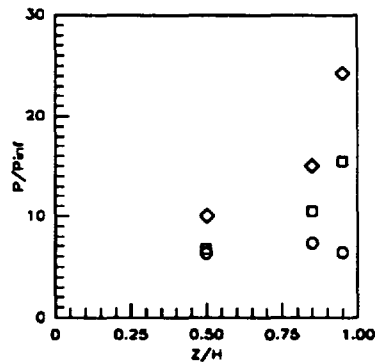
Sym	x'/Ts'	Run No.	CR/Re/Cowl (millions)
○	0.7815	run64	3/0.55/0%
□	0.7815	run61	3/0.55/25%
◇	0.7815	run58	3/0.55/50%

Figure 7.2.2.151: Cowl Effects (CR=3, Re=0.55million/ft) Sidewall Pressures



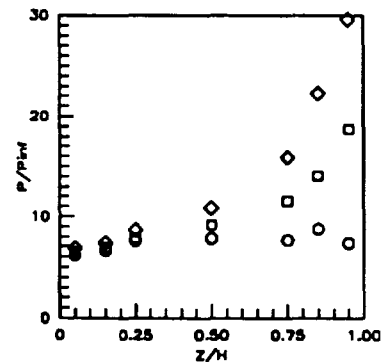
Sym	$x'/T_x'$	Run No.	CR/Re/Cowl (millions)
○	0.8336	run84	3/0.55/0%
□	0.8336	run81	3/0.55/25%
◇	0.8336	run58	3/0.55/50%

Figure 7.2.2.152: Cowl Effects (CR=3, Re=0.55million/ft) Sidewall Pressures



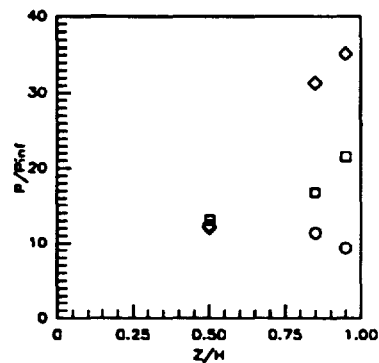
Sym	$x'/T_x'$	Run No.	CR/Re/Cowl (millions)
○	0.8857	run84	3/0.55/0%
□	0.8857	run81	3/0.55/25%
◇	0.8857	run58	3/0.55/50%

Figure 7.2.2.153: Cowl Effects (CR=3, Re=0.55million/ft) Sidewall Pressures



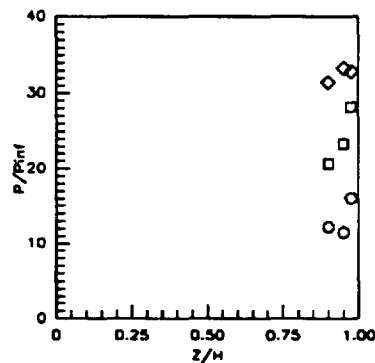
Sym	$x'/T_x'$	Run No.	CR/Re/Cowl (millions)
○	0.9378	run84	3/0.55/0%
□	0.9378	run81	3/0.55/25%
◇	0.9378	run58	3/0.55/50%

Figure 7.2.2.154: Cowl Effects (CR=3, Re=0.55million/ft) Sidewall Pressures



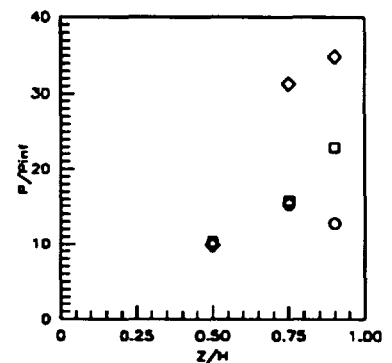
Sym	$x'/T_x'$	Run No.	CR/Re/Cowl (millions)
○	0.9751	run84	3/0.55/0%
□	0.9751	run81	3/0.55/25%
◇	0.9751	run58	3/0.55/50%

Figure 7.2.2.155: Cowl Effects (CR=3, Re=0.55million/ft) Sidewall Pressures



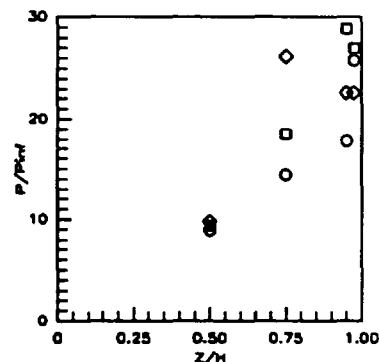
Sym	$x'/T_x'$	Run No.	CR/Re/Cowl (millions)
○	1.0197	run84	3/0.55/0%
□	1.0197	run81	3/0.55/25%
◇	1.0197	run58	3/0.55/50%

Figure 7.2.2.156: Cowl Effects (CR=3, Re=0.55million/ft) Sidewall Pressures



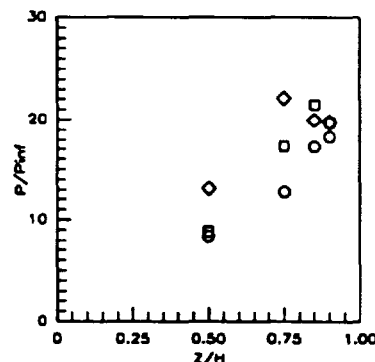
Sym	$x'/T_x'$	Run No.	CR/Re/Cowl (millions)
○	1.0643	run84	3/0.55/0%
□	1.0643	run81	3/0.55/25%
◇	1.0643	run58	3/0.55/50%

Figure 7.2.2.157: Cowl Effects (CR=3, Re=0.55million/ft) Sidewall Pressures



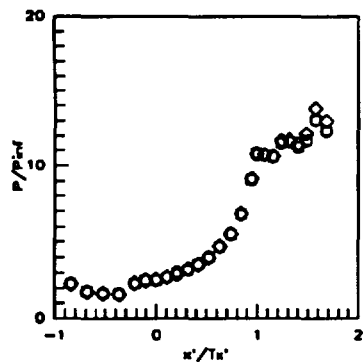
Sym	$x'/T_x'$	Run No.	CR/Re/Cowl (millions)
○	1.1537	run84	3/0.55/0%
□	1.1537	run81	3/0.55/25%
◇	1.1537	run58	3/0.55/50%

Figure 7.2.2.158: Cowl Effects (CR=3, Re=0.55million/ft) Sidewall Pressures



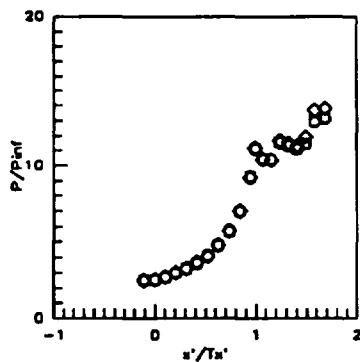
Sym	$x'/T_x'$	Run No.	CR/Re/Cowl (millions)
○	1.2356	run84	3/0.55/0%
□	1.2356	run81	3/0.55/25%
◇	1.2356	run58	3/0.55/50%

Figure 7.2.2.159: Cowl Effects (CR=3, Re=0.55million/ft) Sidewall Pressures



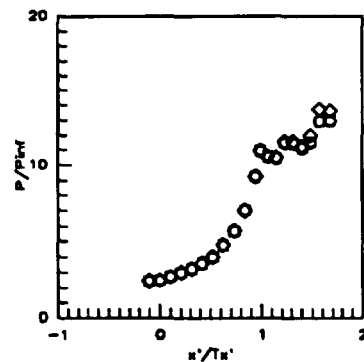
Sym	C.L.	Run	CR/Re/Cowl
	for	No.	(millions)
○	CR=3	run46	5/2.15/ 0%
□	CR=3	run43	5/2.15/25%
◇	CR=3	run40	5/2.15/50%

Figure 7.2.2.160: Cowl Effects  
(CR=5, Re=2.15million/ft)  
CR=3 Centerline Pressures



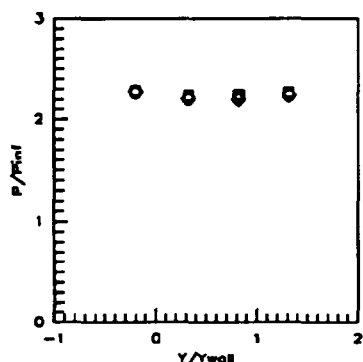
Sym	C.L.	Run	CR/Re/Cowl
	for	No.	(millions)
○	CR=5	run46	5/2.15/ 0%
□	CR=5	run43	5/2.15/25%
◇	CR=5	run40	5/2.15/50%

Figure 7.2.2.161: Cowl Effects  
(CR=5, Re=2.15million/ft)  
CR=5 Centerline Pressures



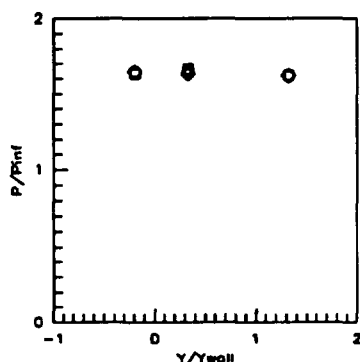
Sym	C.L.	Run	CR/Re/Cowl
	for	No.	(millions)
○	CR=9	run46	5/2.15/ 0%
□	CR=9	run43	5/2.15/25%
◇	CR=9	run40	5/2.15/50%

Figure 7.2.2.162: Cowl Effects  
(CR=5, Re=2.15million/ft)  
CR=9 Centerline Pressures



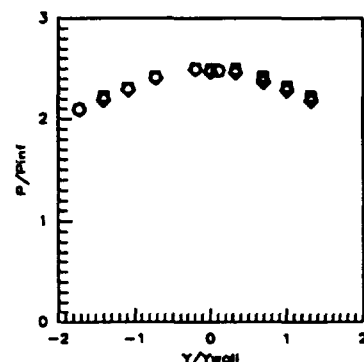
Sym	x'/Tx'	Run	CR/Re/Cowl
		No.	(millions)
○	-0.8412	run46	5/2.15/ 0%
□	-0.8412	run43	5/2.15/25%
◇	-0.8412	run40	5/2.15/50%

Figure 7.2.2.163: Cowl Effects  
(CR=5, Re=2.15million/ft)  
Baseplate Pressures



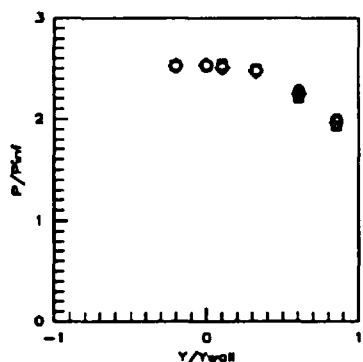
Sym	x'/Tx'	Run	CR/Re/Cowl
		No.	(millions)
○	-0.5258	run46	5/2.15/ 0%
□	-0.5258	run43	5/2.15/25%
◇	-0.5258	run40	5/2.15/50%

Figure 7.2.2.164: Cowl Effects  
(CR=5, Re=2.15million/ft)  
Baseplate Pressures



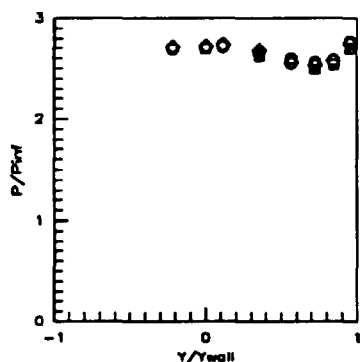
Sym	x'/Tx'	Run	CR/Re/Cowl
		No.	(millions)
○	-0.1052	run46	5/2.15/ 0%
□	-0.1052	run43	5/2.15/25%
◇	-0.1052	run40	5/2.15/50%

Figure 7.2.2.165: Cowl Effects  
(CR=5, Re=2.15million/ft)  
Baseplate Pressures



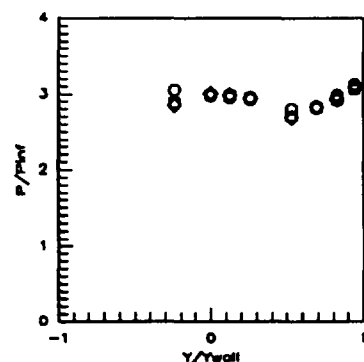
Sym	x'/Tx'	Run	CR/Re/Cowl
		No.	(millions)
○	0.0000	run46	5/2.15/ 0%
□	0.0000	run43	5/2.15/25%
◇	0.0000	run40	5/2.15/50%

Figure 7.2.2.166: Cowl Effects  
(CR=5, Re=2.15million/ft)  
Baseplate Pressures



Sym	x'/Tx'	Run	CR/Re/Cowl
		No.	(millions)
○	0.1052	run46	5/2.15/ 0%
□	0.1052	run43	5/2.15/25%
◇	0.1052	run40	5/2.15/50%

Figure 7.2.2.167: Cowl Effects  
(CR=5, Re=2.15million/ft)  
Baseplate Pressures



Sym	x'/Tx'	Run	CR/Re/Cowl
		No.	(millions)
○	0.2103	run46	5/2.15/ 0%
□	0.2103	run43	5/2.15/25%
◇	0.2103	run40	5/2.15/50%

Figure 7.2.2.168: Cowl Effects  
(CR=5, Re=2.15million/ft)  
Baseplate Pressures

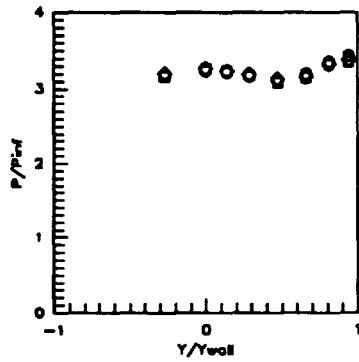


Figure 7.2.2.169: Cowl Effects  
(CR=5, Re=2.15million/ft)  
Baseplate Pressures

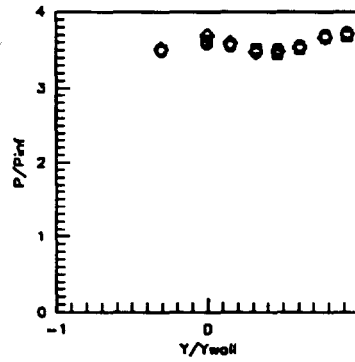


Figure 7.2.2.170: Cowl Effects  
(CR=5, Re=2.15million/ft)  
Baseplate Pressures

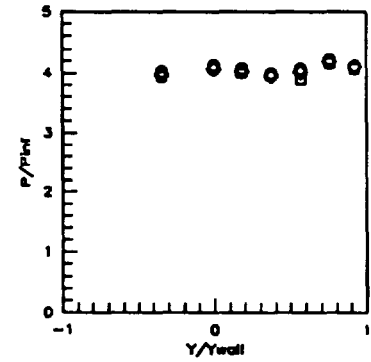


Figure 7.2.2.171: Cowl Effects  
(CR=5, Re=2.15million/ft)  
Baseplate Pressures

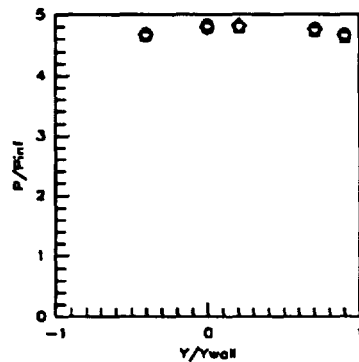


Figure 7.2.2.172: Cowl Effects  
(CR=5, Re=2.15million/ft)  
Baseplate Pressures

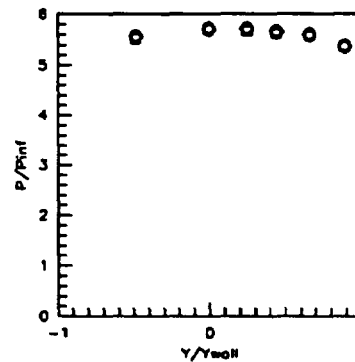


Figure 7.2.2.173: Cowl Effects  
(CR=5, Re=2.15million/ft)  
Baseplate Pressures

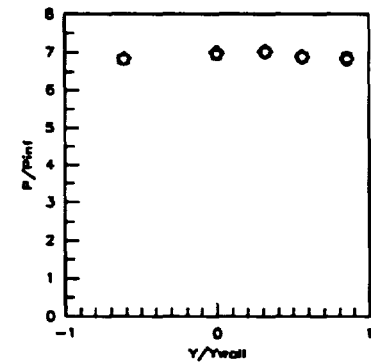


Figure 7.2.2.174: Cowl Effects  
(CR=5, Re=2.15million/ft)  
Baseplate Pressures

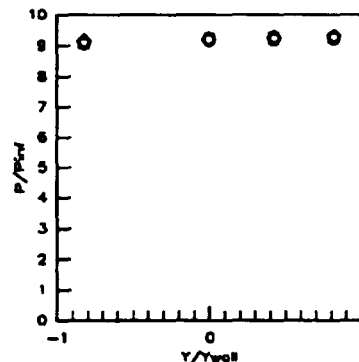


Figure 7.2.2.175: Cowl Effects  
(CR=5, Re=2.15million/ft)  
Baseplate Pressures

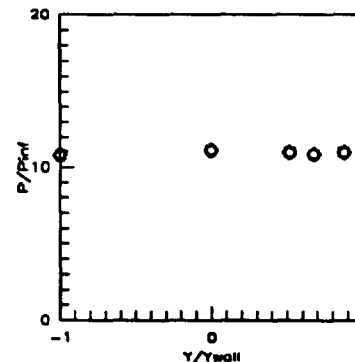


Figure 7.2.2.176: Cowl Effects  
(CR=5, Re=2.15million/ft)  
Baseplate Pressures

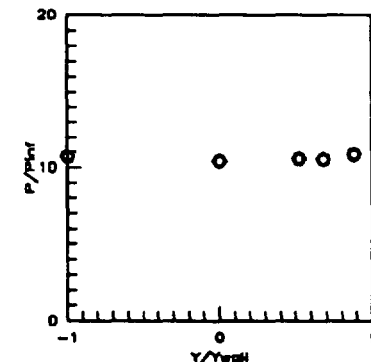
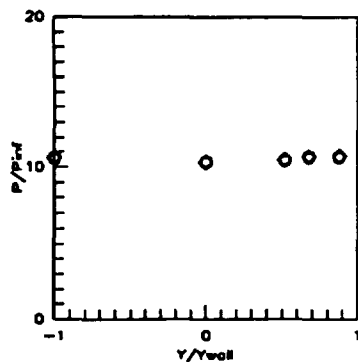


Figure 7.2.2.177: Cowl Effects  
(CR=5, Re=2.15million/ft)  
Baseplate Pressures

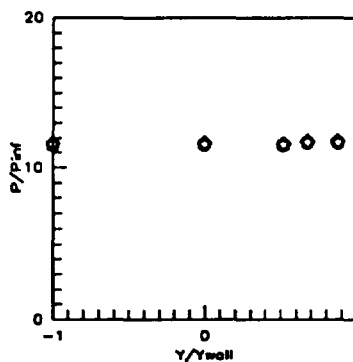




Sym	$x'/T_x'$	Run No.	CR/Re/Cowl (millions)
-----	-----------	---------	-----------------------

○	1.1567	run46	5/2.15/0%
□	1.1567	run43	5/2.15/25%
◇	1.1567	run40	5/2.15/50%

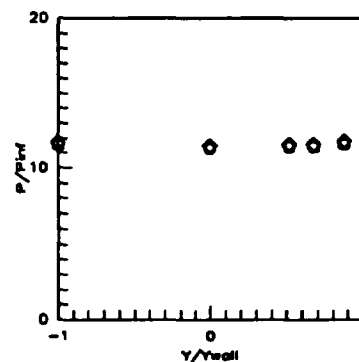
Figure 7.2.2.178: Cowl Effects (CR=5, Re=2.15million/ft) Baseplate Pressures



Sym	$x'/T_x'$	Run No.	CR/Re/Cowl (millions)
-----	-----------	---------	-----------------------

○	1.2408	run46	5/2.15/0%
□	1.2408	run43	5/2.15/25%
◇	1.2408	run40	5/2.15/50%

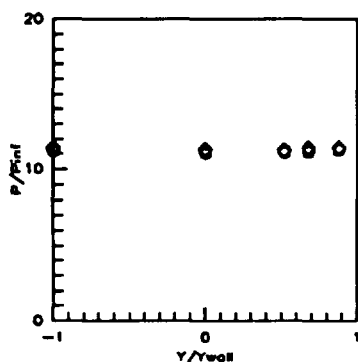
Figure 7.2.2.179: Cowl Effects (CR=5, Re=2.15million/ft) Baseplate Pressures



Sym	$x'/T_x'$	Run No.	CR/Re/Cowl (millions)
-----	-----------	---------	-----------------------

○	1.3249	run46	5/2.15/0%
□	1.3249	run43	5/2.15/25%
◇	1.3249	run40	5/2.15/50%

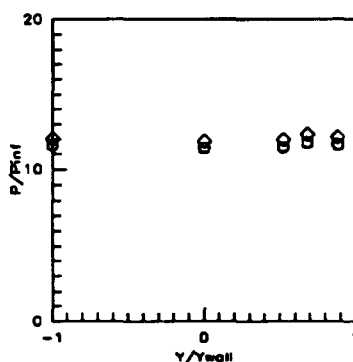
Figure 7.2.2.180: Cowl Effects (CR=5, Re=2.15million/ft) Baseplate Pressures



Sym	$x'/T_x'$	Run No.	CR/Re/Cowl (millions)
-----	-----------	---------	-----------------------

○	1.4080	run46	5/2.15/0%
□	1.4080	run43	5/2.15/25%
◇	1.4080	run40	5/2.15/50%

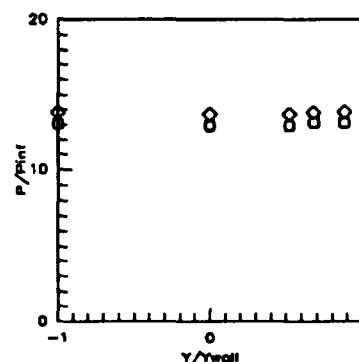
Figure 7.2.2.181: Cowl Effects (CR=5, Re=2.15million/ft) Baseplate Pressures



Sym	$x'/T_x'$	Run No.	CR/Re/Cowl (millions)
-----	-----------	---------	-----------------------

○	1.4932	run46	5/2.15/0%
□	1.4932	run43	5/2.15/25%
◇	1.4932	run40	5/2.15/50%

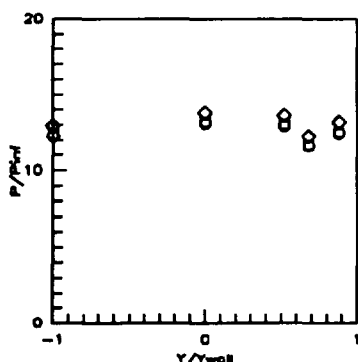
Figure 7.2.2.182: Cowl Effects (CR=5, Re=2.15million/ft) Baseplate Pressures



Sym	$x'/T_x'$	Run No.	CR/Re/Cowl (millions)
-----	-----------	---------	-----------------------

○	1.5773	run46	5/2.15/0%
□	1.5773	run43	5/2.15/25%
◇	1.5773	run40	5/2.15/50%

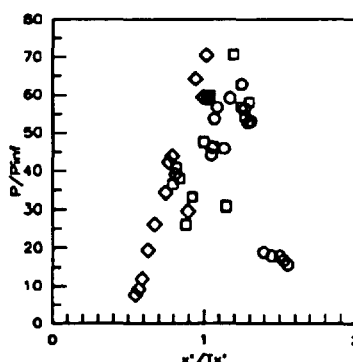
Figure 7.2.2.183: Cowl Effects (CR=5, Re=2.15million/ft) Baseplate Pressures



Sym	$x'/T_x'$	Run No.	CR/Re/Cowl (millions)
-----	-----------	---------	-----------------------

○	1.6824	run46	5/2.15/0%
□	1.6824	run43	5/2.15/25%
◇	1.6824	run40	5/2.15/50%

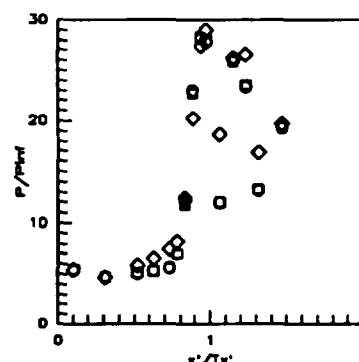
Figure 7.2.2.184: Cowl Effects (CR=5, Re=2.15million/ft) Baseplate Pressures



Sym	Cowl Pos.	Run No.	CR/Re/Cowl (millions)
-----	-----------	---------	-----------------------

○	0%	run46	5/2.15/0%
□	25%	run43	5/2.15/25%
◇	50%	run40	5/2.15/50%

Figure 7.2.2.185: Cowl Effects (CR=5, Re=2.15million/ft) Cowl Pressures



Sym	Z/H	Run No.	CR/Re/Cowl (millions)
-----	-----	---------	-----------------------

○	0.5RT	run46	5/2.15/0%
□	0.5RT	run43	5/2.15/25%
◇	0.5RT	run40	5/2.15/50%

Figure 7.2.2.186: Cowl Effects (CR=5, Re=2.15million/ft) Sidewall Centerline Pressures

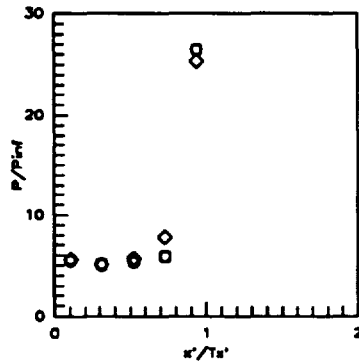


Figure 7.2.2.187: Cowl Effects  
(CR=5, Re=2.15million/ft)  
Sidewall Centerline Pressures

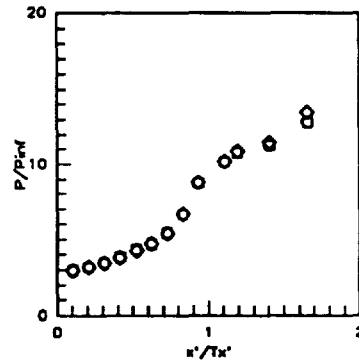


Figure 7.2.2.188: Cowl Effects  
(CR=5, Re=2.15million/ft)  
Sidewall Pressures

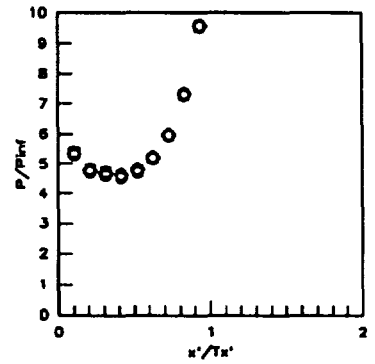


Figure 7.2.2.189: Cowl Effects  
(CR=5, Re=2.15million/ft)  
Sidewall Pressures

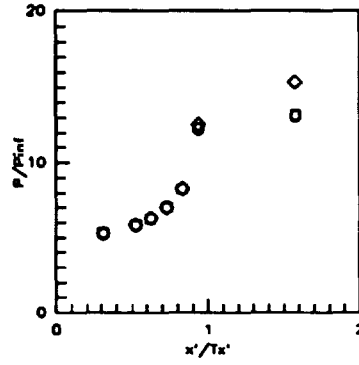


Figure 7.2.2.190: Cowl Effects  
(CR=5, Re=2.15million/ft)  
Sidewall Pressures

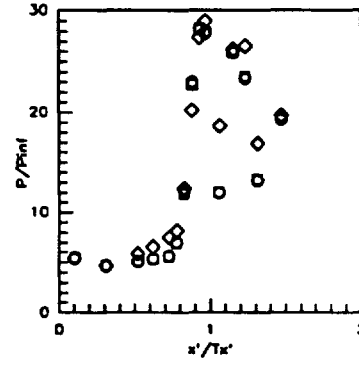


Figure 7.2.2.191: Cowl Effects  
(CR=5, Re=2.15million/ft)  
Sidewall Pressures

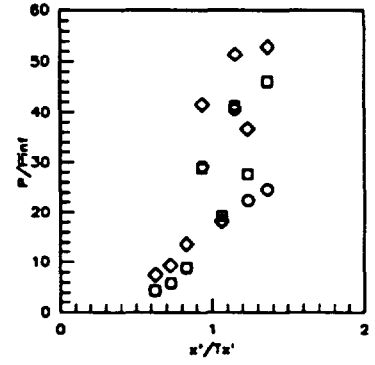


Figure 7.2.2.192: Cowl Effects  
(CR=5, Re=2.15million/ft)  
Sidewall Pressures

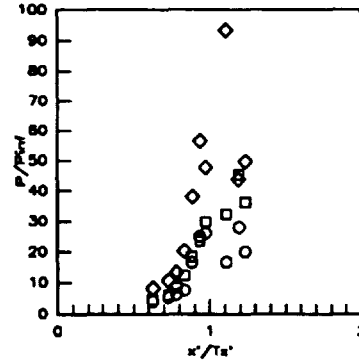


Figure 7.2.2.193: Cowl Effects  
(CR=5, Re=2.15million/ft)  
Sidewall Pressures

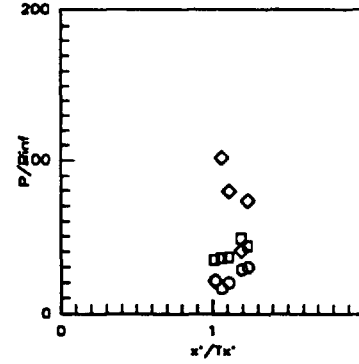


Figure 7.2.2.194: Cowl Effects  
(CR=5, Re=2.15million/ft)  
Sidewall Pressures

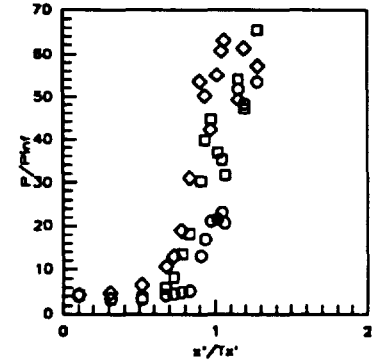
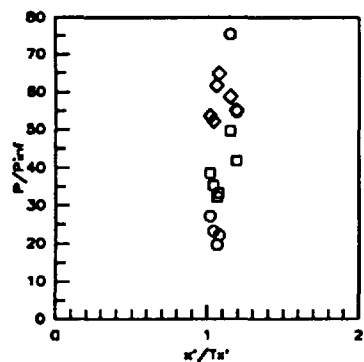
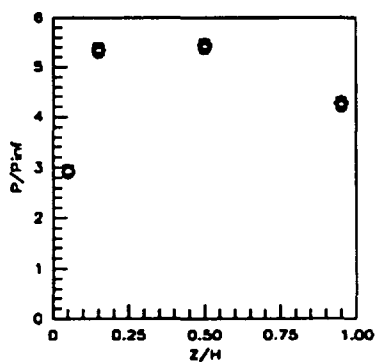


Figure 7.2.2.195: Cowl Effects  
(CR=5, Re=2.15million/ft)  
Sidewall Pressures



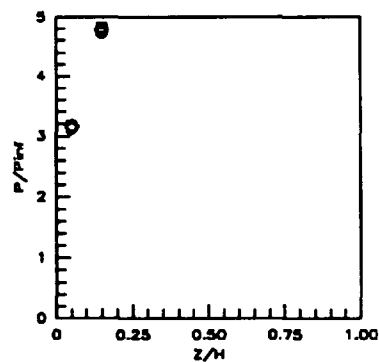
Sym	$x'/Ts'$	Run No.	CR/Re/Cowl (millions)
○	0.975	run46	5/2.15/ 0%
□	0.975	run43	5/2.15/25%
◇	0.975	run40	5/2.15/50%

Figure 7.2.2.196: Cowl Effects (CR=5, Re=2.15million/ft) Sidewall Pressures



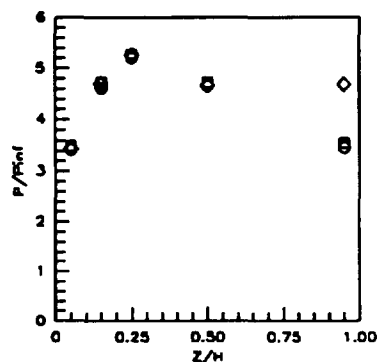
Sym	$x'/Ts'$	Run No.	CR/Re/Cowl (millions)
○	0.1042	run46	5/2.15/ 0%
□	0.1042	run43	5/2.15/25%
◇	0.1042	run40	5/2.15/50%

Figure 7.2.2.197: Cowl Effects (CR=5, Re=2.15million/ft) Sidewall Pressures



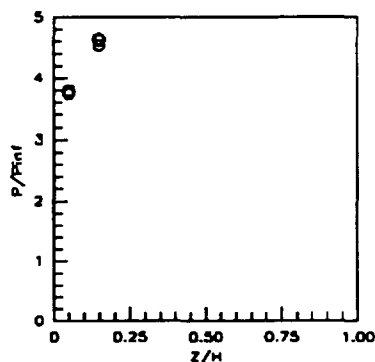
Sym	$x'/Ts'$	Run No.	CR/Re/Cowl (millions)
○	0.2063	run46	5/2.15/ 0%
□	0.2063	run43	5/2.15/25%
◇	0.2063	run40	5/2.15/50%

Figure 7.2.2.198: Cowl Effects (CR=5, Re=2.15million/ft) Sidewall Pressures



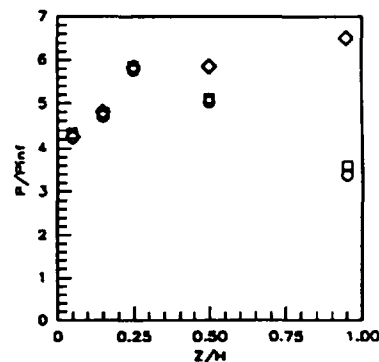
Sym	$x'/Ts'$	Run No.	CR/Re/Cowl (millions)
○	0.3125	run46	5/2.15/ 0%
□	0.3125	run43	5/2.15/25%
◇	0.3125	run40	5/2.15/50%

Figure 7.2.2.199: Cowl Effects (CR=5, Re=2.15million/ft) Sidewall Pressures



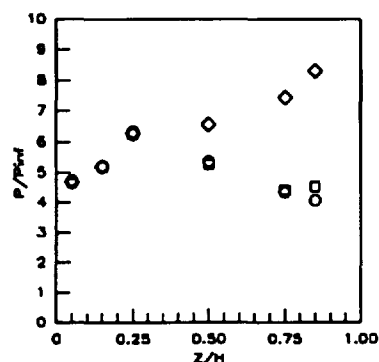
Sym	$x'/Ts'$	Run No.	CR/Re/Cowl (millions)
○	0.4167	run46	5/2.15/ 0%
□	0.4167	run43	5/2.15/25%
◇	0.4167	run40	5/2.15/50%

Figure 7.2.2.200: Cowl Effects (CR=5, Re=2.15million/ft) Sidewall Pressures



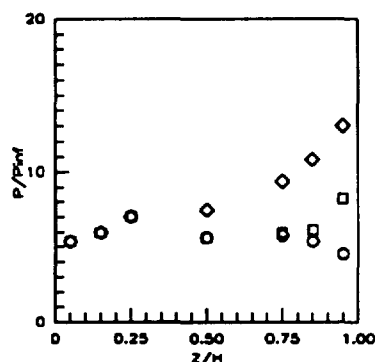
Sym	$x'/Ts'$	Run No.	CR/Re/Cowl (millions)
○	0.5250	run46	5/2.15/ 0%
□	0.5250	run43	5/2.15/25%
◇	0.5250	run40	5/2.15/50%

Figure 7.2.2.201: Cowl Effects (CR=5, Re=2.15million/ft) Sidewall Pressures



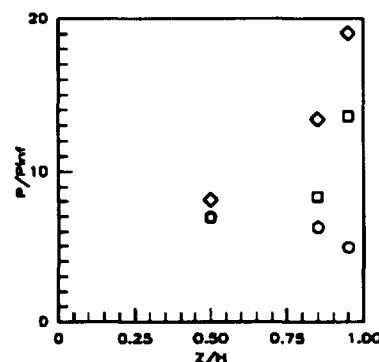
Sym	$x'/Ts'$	Run No.	CR/Re/Cowl (millions)
○	0.6252	run46	5/2.15/ 0%
□	0.6252	run43	5/2.15/25%
◇	0.6252	run40	5/2.15/50%

Figure 7.2.2.202: Cowl Effects (CR=5, Re=2.15million/ft) Sidewall Pressures



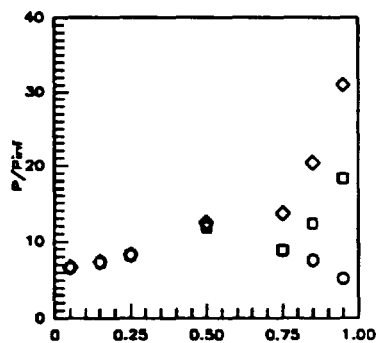
Sym	$x'/Ts'$	Run No.	CR/Re/Cowl (millions)
○	0.7294	run46	5/2.15/ 0%
□	0.7294	run43	5/2.15/25%
◇	0.7294	run40	5/2.15/50%

Figure 7.2.2.203: Cowl Effects (CR=5, Re=2.15million/ft) Sidewall Pressures



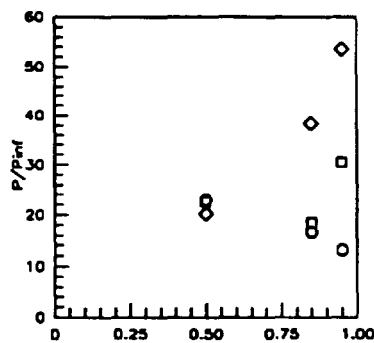
Sym	$x'/Ts'$	Run No.	CR/Re/Cowl (millions)
○	0.7815	run46	5/2.15/ 0%
□	0.7815	run43	5/2.15/25%
◇	0.7815	run40	5/2.15/50%

Figure 7.2.2.204: Cowl Effects (CR=5, Re=2.15million/ft) Sidewall Pressures



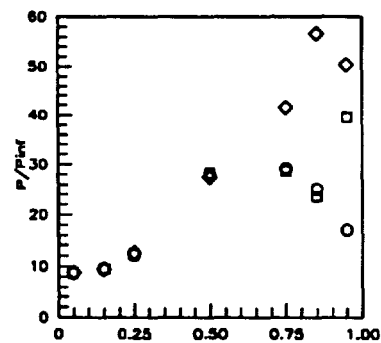
Sym	$x'/T_x'$	Run No.	CR/Re/Cowl (millions)
○	0.8336	run46	5/2.15/0%
□	0.8336	run43	5/2.15/25%
◇	0.8336	run40	5/2.15/50%

Figure 7.2.2.205: Cowl Effects (CR=5, Re=2.15million/ft) Sidewall Pressures



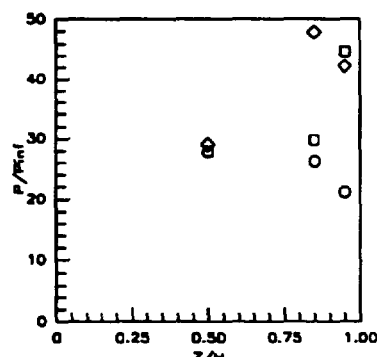
Sym	$x'/T_x'$	Run No.	CR/Re/Cowl (millions)
○	0.8857	run46	5/2.15/0%
□	0.8857	run43	5/2.15/25%
◇	0.8857	run40	5/2.15/50%

Figure 7.2.2.206: Cowl Effects (CR=5, Re=2.15million/ft) Sidewall Pressures



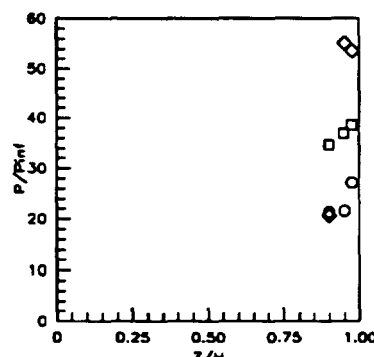
Sym	$x'/T_x'$	Run No.	CR/Re/Cowl (millions)
○	0.9378	run46	5/2.15/0%
□	0.9378	run43	5/2.15/25%
◇	0.9378	run40	5/2.15/50%

Figure 7.2.2.207: Cowl Effects (CR=5, Re=2.15million/ft) Sidewall Pressures



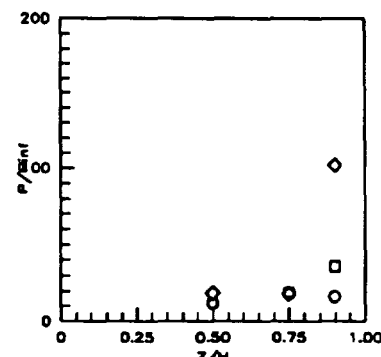
Sym	$x'/T_x'$	Run No.	CR/Re/Cowl (millions)
○	0.9751	run46	5/2.15/0%
□	0.9751	run43	5/2.15/25%
◇	0.9751	run40	5/2.15/50%

Figure 7.2.2.208: Cowl Effects (CR=5, Re=2.15million/ft) Sidewall Pressures



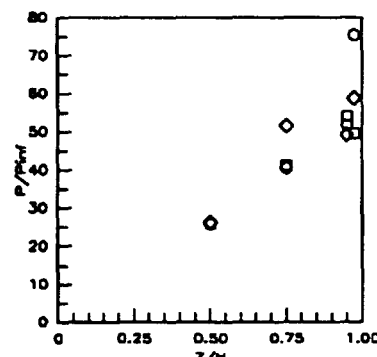
Sym	$x'/T_x'$	Run No.	CR/Re/Cowl (millions)
○	1.0197	run46	5/2.15/0%
□	1.0197	run43	5/2.15/25%
◇	1.0197	run40	5/2.15/50%

Figure 7.2.2.209: Cowl Effects (CR=5, Re=2.15million/ft) Sidewall Pressures



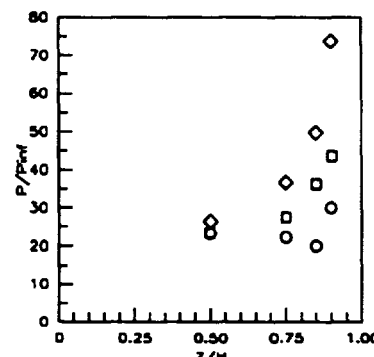
Sym	$x'/T_x'$	Run No.	CR/Re/Cowl (millions)
○	1.0843	run46	5/2.15/0%
□	1.0843	run43	5/2.15/25%
◇	1.0843	run40	5/2.15/50%

Figure 7.2.2.210: Cowl Effects (CR=5, Re=2.15million/ft) Sidewall Pressures



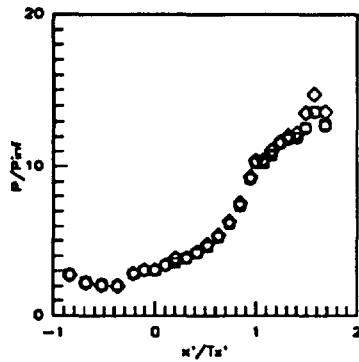
Sym	$x'/T_x'$	Run No.	CR/Re/Cowl (millions)
○	1.1537	run46	5/2.15/0%
□	1.1537	run43	5/2.15/25%
◇	1.1537	run40	5/2.15/50%

Figure 7.2.2.211: Cowl Effects (CR=5, Re=2.15million/ft) Sidewall Pressures



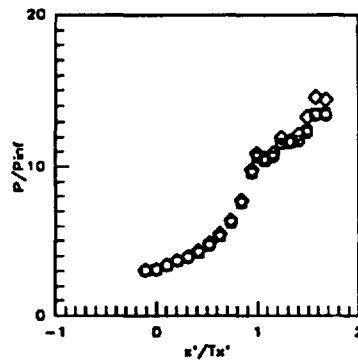
Sym	$x'/T_x'$	Run No.	CR/Re/Cowl (millions)
○	1.2356	run46	5/2.15/0%
□	1.2356	run43	5/2.15/25%
◇	1.2356	run40	5/2.15/50%

Figure 7.2.2.212: Cowl Effects (CR=5, Re=2.15million/ft) Sidewall Pressures



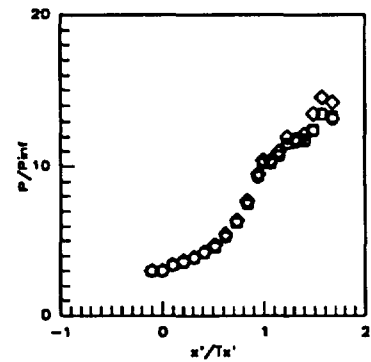
Sym	C.L. for	Run No.	CR/Re/Cowl (millions)
○	CR=3	run45	5/1.14/0%
□	CR=3	run42	5/1.14/25%
◇	CR=3	run39	5/1.14/50%

Figure 7.2.2.213: Cowl Effects (CR=5, Re=1.14million/ft) CR=3 Centerline Pressures



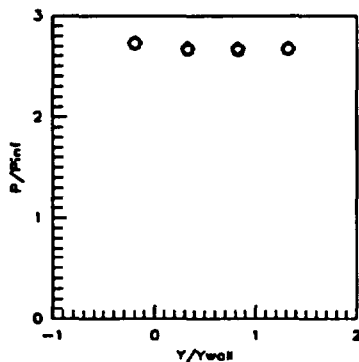
Sym	C.L. for	Run No.	CR/Re/Cowl (millions)
○	CR=5	run45	5/1.14/0%
□	CR=5	run42	5/1.14/25%
◇	CR=5	run39	5/1.14/50%

Figure 7.2.2.214: Cowl Effects (CR=5, Re=1.14million/ft) CR=5 Centerline Pressures



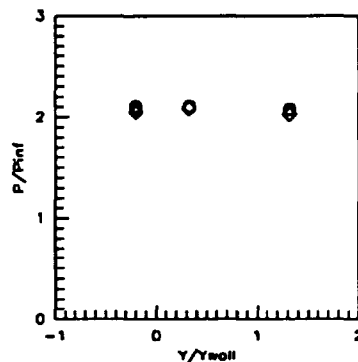
Sym	C.L. for	Run No.	CR/Re/Cowl (millions)
○	CR=9	run45	5/1.14/0%
□	CR=9	run42	5/1.14/25%
◇	CR=9	run39	5/1.14/50%

Figure 7.2.2.215: Cowl Effects (CR=5, Re=1.14million/ft) CR=9 Centerline Pressures



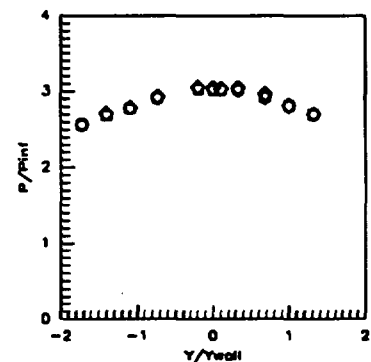
Sym	x'/Tx'	Run No.	CR/Re/Cowl (millions)
○	-0.8412	run45	5/1.14/0%
□	-0.8412	run42	5/1.14/25%
◇	-0.8412	run39	5/1.14/50%

Figure 7.2.2.216: Cowl Effects (CR=5, Re=1.14million/ft) Baseplate Pressures



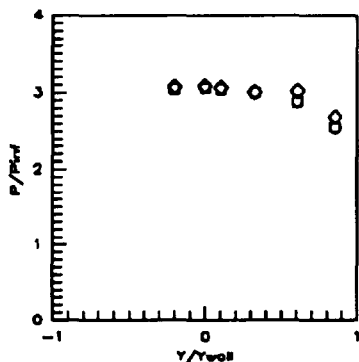
Sym	x'/Tx'	Run No.	CR/Re/Cowl (millions)
○	-0.5258	run45	5/1.14/0%
□	-0.5258	run42	5/1.14/25%
◇	-0.5258	run39	5/1.14/50%

Figure 7.2.2.217: Cowl Effects (CR=5, Re=1.14million/ft) Baseplate Pressures



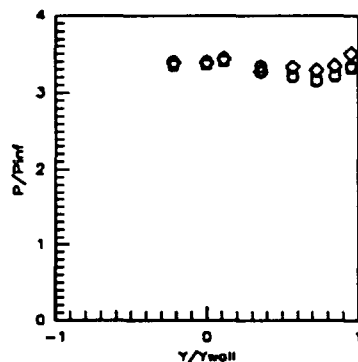
Sym	x'/Tx'	Run No.	CR/Re/Cowl (millions)
○	-0.1052	run45	5/1.14/0%
□	-0.1052	run42	5/1.14/25%
◇	-0.1052	run39	5/1.14/50%

Figure 7.2.2.218: Cowl Effects (CR=5, Re=1.14million/ft) Baseplate Pressures



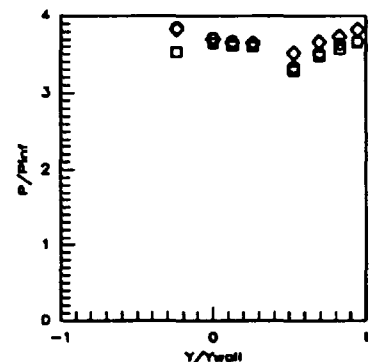
Sym	x'/Tx'	Run No.	CR/Re/Cowl (millions)
○	0.0000	run45	5/1.14/0%
□	0.0000	run42	5/1.14/25%
◇	0.0000	run39	5/1.14/50%

Figure 7.2.2.219: Cowl Effects (CR=5, Re=1.14million/ft) Baseplate Pressures



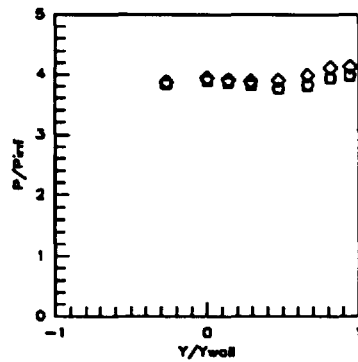
Sym	x'/Tx'	Run No.	CR/Re/Cowl (millions)
○	0.1052	run45	5/1.14/0%
□	0.1052	run42	5/1.14/25%
◇	0.1052	run39	5/1.14/50%

Figure 7.2.2.220: Cowl Effects (CR=5, Re=1.14million/ft) Baseplate Pressures



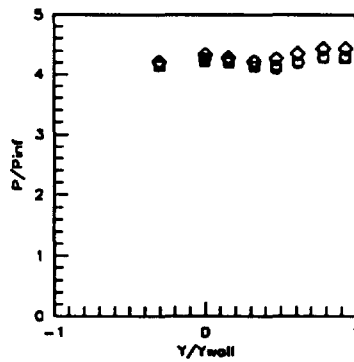
Sym	x'/Tx'	Run No.	CR/Re/Cowl (millions)
○	0.2103	run45	5/1.14/0%
□	0.2103	run42	5/1.14/25%
◇	0.2103	run39	5/1.14/50%

Figure 7.2.2.221: Cowl Effects (CR=5, Re=1.14million/ft) Baseplate Pressures



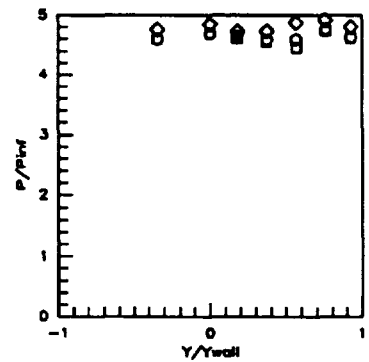
Sym	x'/Ts'	Run No.	CR/Re/Cowl (millions)
o	0.3154	run45	5/1.14/0%
o	0.3154	run42	5/1.14/25%
o	0.3154	run39	5/1.14/50%

Figure 7.2.2.222: Cowl Effects (CR=5, Re=1.14million/ft) Baseplate Pressures



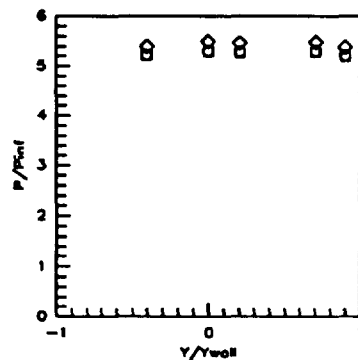
Sym	x'/Ts'	Run No.	CR/Re/Cowl (millions)
o	0.4206	run45	5/1.14/0%
o	0.4206	run42	5/1.14/25%
o	0.4206	run39	5/1.14/50%

Figure 7.2.2.223: Cowl Effects (CR=5, Re=1.14million/ft) Baseplate Pressures



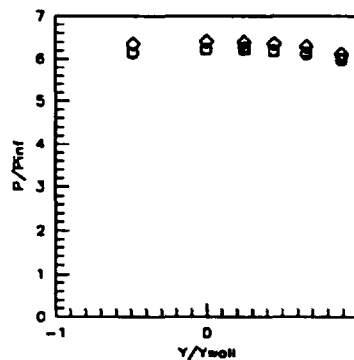
Sym	x'/Ts'	Run No.	CR/Re/Cowl (millions)
o	0.5258	run45	5/1.14/0%
o	0.5258	run42	5/1.14/25%
o	0.5258	run39	5/1.14/50%

Figure 7.2.2.224: Cowl Effects (CR=5, Re=1.14million/ft) Baseplate Pressures



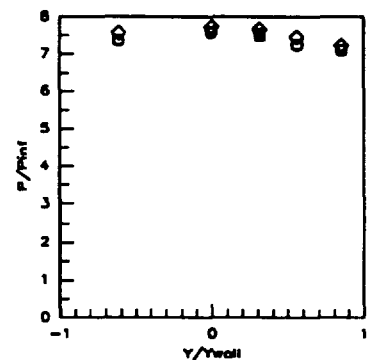
Sym	x'/Ts'	Run No.	CR/Re/Cowl (millions)
o	0.6309	run45	5/1.14/0%
o	0.6309	run42	5/1.14/25%
o	0.6309	run39	5/1.14/50%

Figure 7.2.2.225: Cowl Effects (CR=5, Re=1.14million/ft) Baseplate Pressures



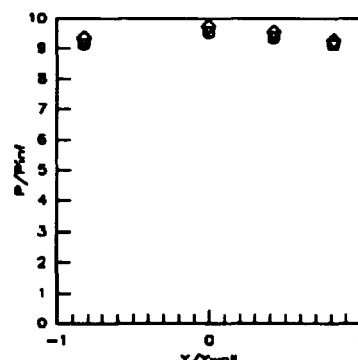
Sym	x'/Ts'	Run No.	CR/Re/Cowl (millions)
o	0.7381	run45	5/1.14/0%
o	0.7381	run42	5/1.14/25%
o	0.7381	run39	5/1.14/50%

Figure 7.2.2.226: Cowl Effects (CR=5, Re=1.14million/ft) Baseplate Pressures



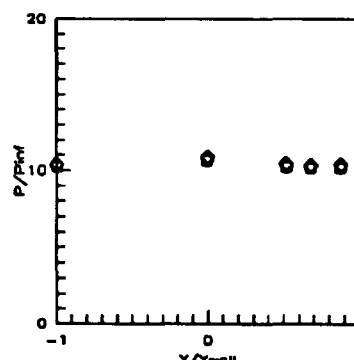
Sym	x'/Ts'	Run No.	CR/Re/Cowl (millions)
o	0.8412	run45	5/1.14/0%
o	0.8412	run42	5/1.14/25%
o	0.8412	run39	5/1.14/50%

Figure 7.2.2.227: Cowl Effects (CR=5, Re=1.14million/ft) Baseplate Pressures



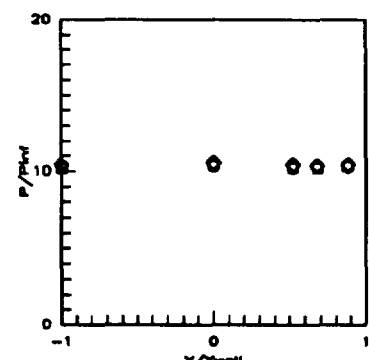
Sym	x'/Ts'	Run No.	CR/Re/Cowl (millions)
o	0.9484	run45	5/1.14/0%
o	0.9484	run42	5/1.14/25%
o	0.9484	run39	5/1.14/50%

Figure 7.2.2.228: Cowl Effects (CR=5, Re=1.14million/ft) Baseplate Pressures



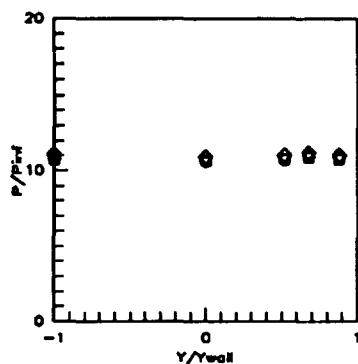
Sym	x'/Ts'	Run No.	CR/Re/Cowl (millions)
o	1.0000	run45	5/1.14/0%
o	1.0000	run42	5/1.14/25%
o	1.0000	run39	5/1.14/50%

Figure 7.2.2.229: Cowl Effects (CR=5, Re=1.14million/ft) Baseplate Pressures



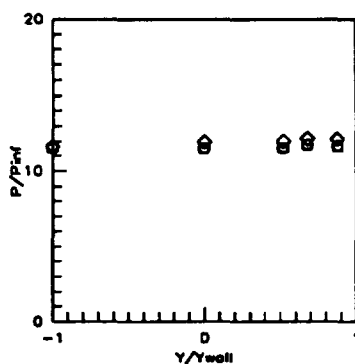
Sym	x'/Ts'	Run No.	CR/Re/Cowl (millions)
o	1.0726	run45	5/1.14/0%
o	1.0726	run42	5/1.14/25%
o	1.0726	run39	5/1.14/50%

Figure 7.2.2.230: Cowl Effects (CR=5, Re=1.14million/ft) Baseplate Pressures



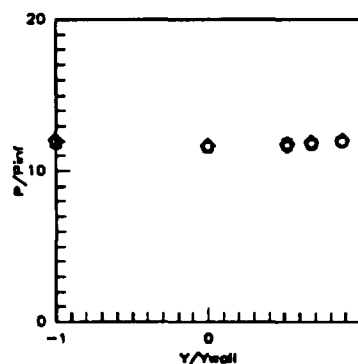
Sym	x'/Tx'	Run No.	CR/Re/Cowl (millions)
-----	--------	---------	-----------------------

Figure 7.2.2.231: Cowl Effects (CR=5, Re=1.14million/ft) Baseplate Pressures



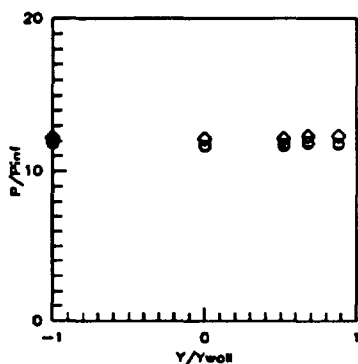
Sym	x'/Tx'	Run No.	CR/Re/Cowl (millions)
-----	--------	---------	-----------------------

Figure 7.2.2.232: Cowl Effects (CR=5, Re=1.14million/ft) Baseplate Pressures



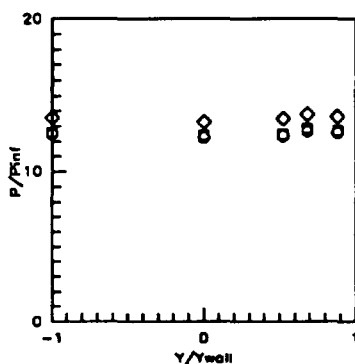
Sym	x'/Tx'	Run No.	CR/Re/Cowl (millions)
-----	--------	---------	-----------------------

Figure 7.2.2.233: Cowl Effects (CR=5, Re=1.14million/ft) Baseplate Pressures



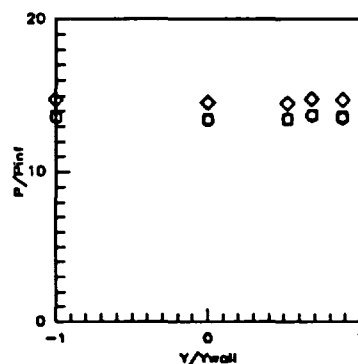
Sym	x'/Tx'	Run No.	CR/Re/Cowl (millions)
-----	--------	---------	-----------------------

Figure 7.2.2.234: Cowl Effects (CR=5, Re=1.14million/ft) Baseplate Pressures



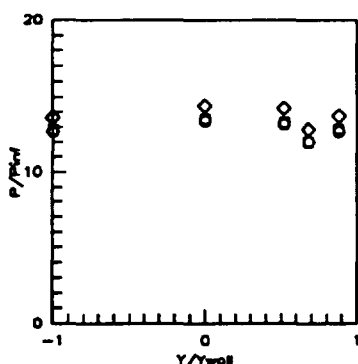
Sym	x'/Tx'	Run No.	CR/Re/Cowl (millions)
-----	--------	---------	-----------------------

Figure 7.2.2.235: Cowl Effects (CR=5, Re=1.14million/ft) Baseplate Pressures



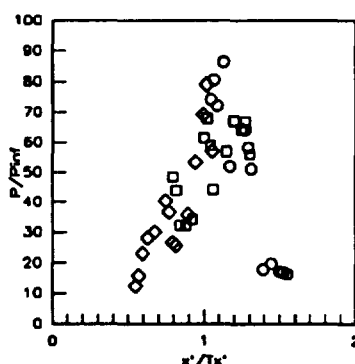
Sym	x'/Tx'	Run No.	CR/Re/Cowl (millions)
-----	--------	---------	-----------------------

Figure 7.2.2.236: Cowl Effects (CR=5, Re=1.14million/ft) Baseplate Pressures



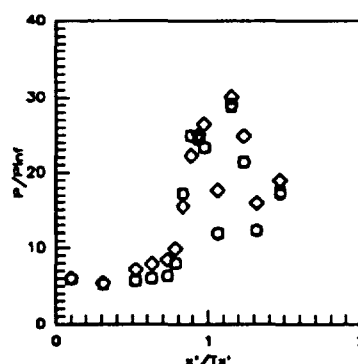
Sym	x'/Tx'	Run No.	CR/Re/Cowl (millions)
-----	--------	---------	-----------------------

Figure 7.2.2.237: Cowl Effects (CR=5, Re=1.14million/ft) Baseplate Pressures



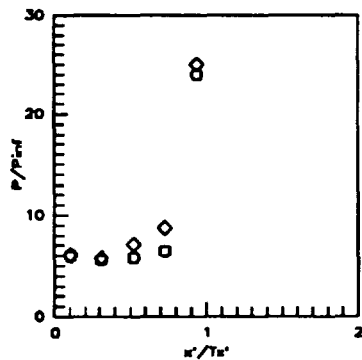
Sym	Cowl Pos.	Run No.	CR/Re/Cowl (millions)
-----	-----------	---------	-----------------------

Figure 7.2.2.238: Cowl Effects (CR=5, Re=1.14million/ft) Cowl Pressures



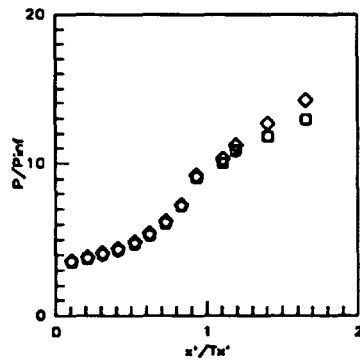
Sym	Z/H	Run No.	CR/Re/Cowl (millions)
-----	-----	---------	-----------------------

Figure 7.2.2.239: Cowl Effects (CR=5, Re=1.14million/ft) Sidewall Centerline Pressures



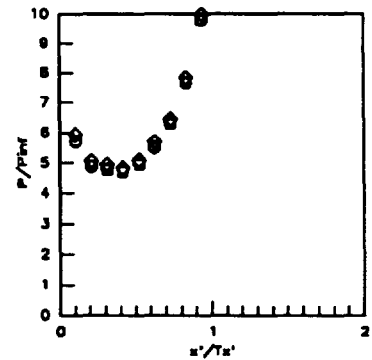
Sym	Z/H	Run No.	CR/Re/Cowl (millions)
○	0.5LT	run45	5/1.14/0%
□	0.5LT	run42	5/1.14/25%
◇	0.5LT	run39	5/1.14/50%

Figure 7.2.2.240: Cowl Effects (CR=5, Re=1.14million/ft) Sidewall Centerline Pressures



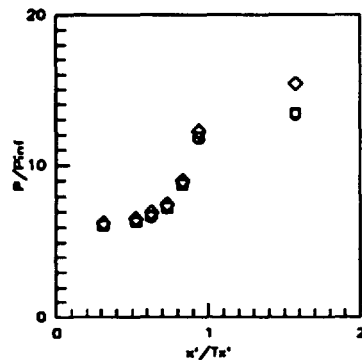
Sym	Z/H	Run No.	CR/Re/Cowl (millions)
○	0.05	run45	5/1.14/0%
□	0.05	run42	5/1.14/25%
◇	0.05	run39	5/1.14/50%

Figure 7.2.2.241: Cowl Effects (CR=5, Re=1.14million/ft) Sidewall Pressures



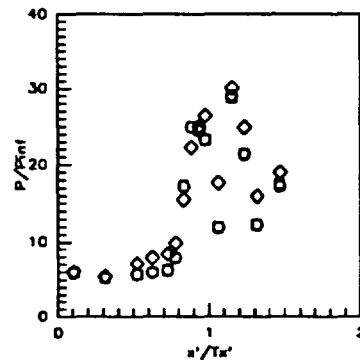
Sym	Z/H	Run No.	CR/Re/Cowl (millions)
○	0.15	run45	5/1.14/0%
□	0.15	run42	5/1.14/25%
◇	0.15	run39	5/1.14/50%

Figure 7.2.2.242: Cowl Effects (CR=5, Re=1.14million/ft) Sidewall Pressures



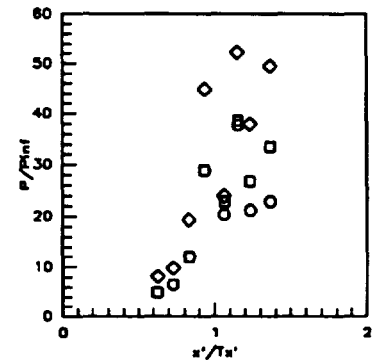
Sym	Z/H	Run No.	CR/Re/Cowl (millions)
○	0.25	run45	5/1.14/0%
□	0.25	run42	5/1.14/25%
◇	0.25	run39	5/1.14/50%

Figure 7.2.2.243: Cowl Effects (CR=5, Re=1.14million/ft) Sidewall Pressures



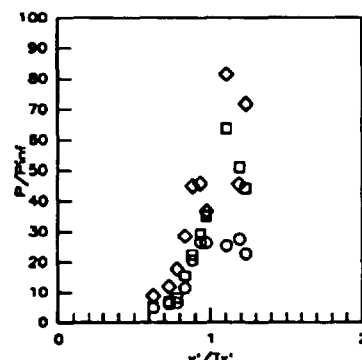
Sym	Z/H	Run No.	CR/Re/Cowl (millions)
○	0.50	run45	5/1.14/0%
□	0.50	run42	5/1.14/25%
◇	0.50	run39	5/1.14/50%

Figure 7.2.2.244: Cowl Effects (CR=5, Re=1.14million/ft) Sidewall Pressures



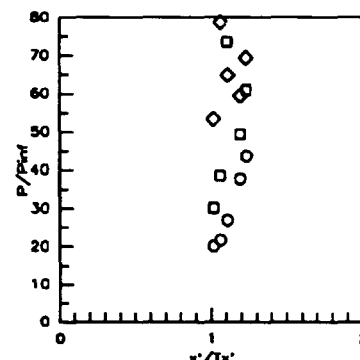
Sym	Z/H	Run No.	CR/Re/Cowl (millions)
○	0.75	run45	5/1.14/0%
□	0.75	run42	5/1.14/25%
◇	0.75	run39	5/1.14/50%

Figure 7.2.2.245: Cowl Effects (CR=5, Re=1.14million/ft) Sidewall Pressures



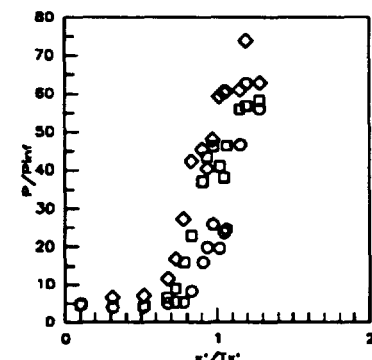
Sym	Z/H	Run No.	CR/Re/Cowl (millions)
○	0.85	run45	5/1.14/0%
□	0.85	run42	5/1.14/25%
◇	0.85	run39	5/1.14/50%

Figure 7.2.2.246: Cowl Effects (CR=5, Re=1.14million/ft) Sidewall Pressures



Sym	Z/H	Run No.	CR/Re/Cowl (millions)
○	0.90	run45	5/1.14/0%
□	0.90	run42	5/1.14/25%
◇	0.90	run39	5/1.14/50%

Figure 7.2.2.247: Cowl Effects (CR=5, Re=1.14million/ft) Sidewall Pressures



Sym	Z/H	Run No.	CR/Re/Cowl (millions)
○	0.95	run45	5/1.14/0%
□	0.95	run42	5/1.14/25%
◇	0.95	run39	5/1.14/50%

Figure 7.2.2.248: Cowl Effects (CR=5, Re=1.14million/ft) Sidewall Pressures



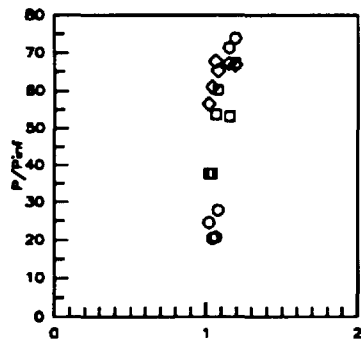


Figure 7.2.2.249: Cowl Effects  
(CR=5, Re=1.14million/ft)  
Sidewall Pressures

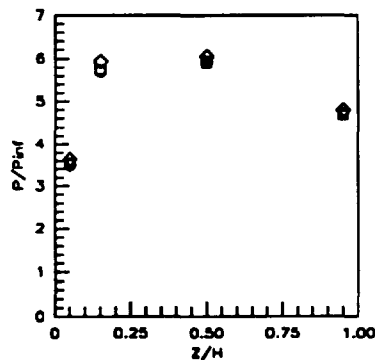


Figure 7.2.2.250: Cowl Effects  
(CR=5, Re=1.14million/ft)  
Sidewall Pressures

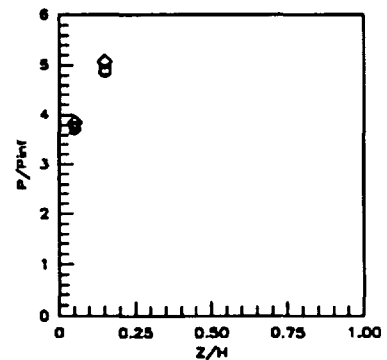


Figure 7.2.2.251: Cowl Effects  
(CR=5, Re=1.14million/ft)  
Sidewall Pressures

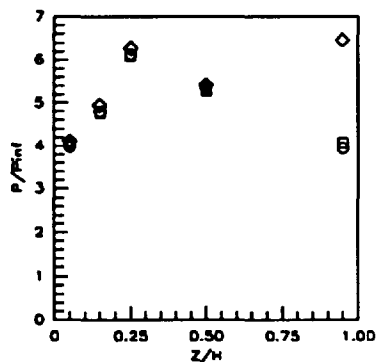


Figure 7.2.2.252: Cowl Effects  
(CR=5, Re=1.14million/ft)  
Sidewall Pressures

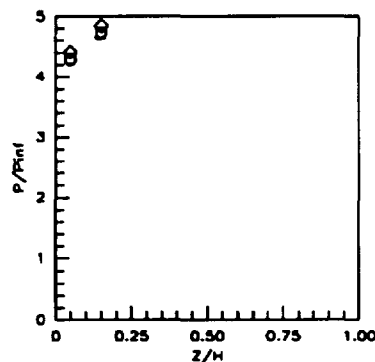


Figure 7.2.2.253: Cowl Effects  
(CR=5, Re=1.14million/ft)  
Sidewall Pressures

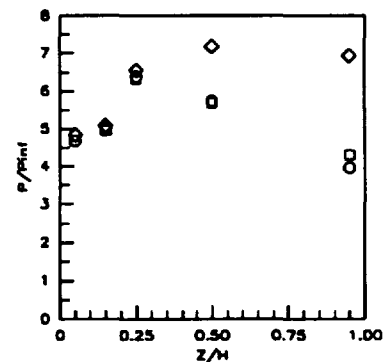


Figure 7.2.2.254: Cowl Effects  
(CR=5, Re=1.14million/ft)  
Sidewall Pressures

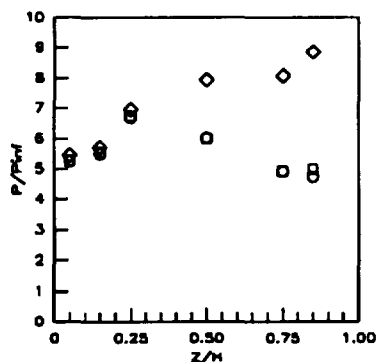


Figure 7.2.2.255: Cowl Effects  
(CR=5, Re=1.14million/ft)  
Sidewall Pressures

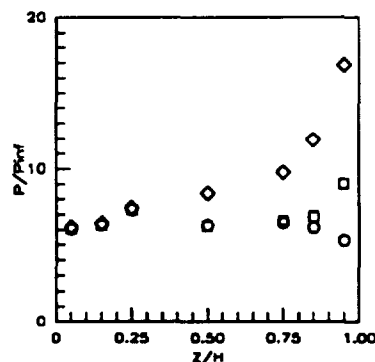


Figure 7.2.2.256: Cowl Effects  
(CR=5, Re=1.14million/ft)  
Sidewall Pressures

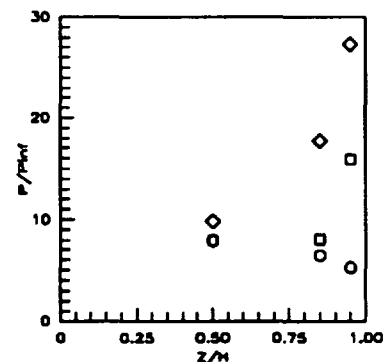
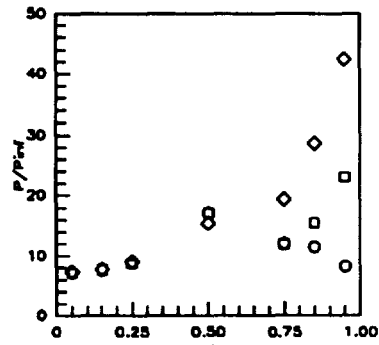
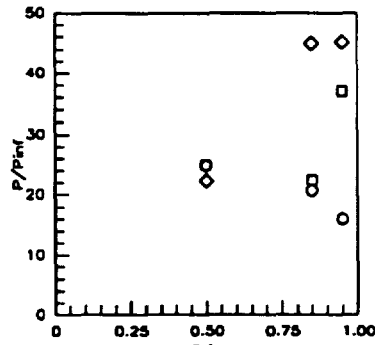


Figure 7.2.2.257: Cowl Effects  
(CR=5, Re=1.14million/ft)  
Sidewall Pressures



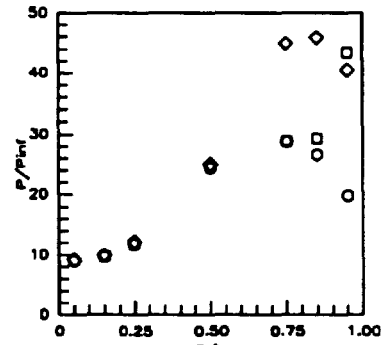
Sym	$x'/T_x'$	Run No.	CR/Re/Cowl (millions)
○	0.8336	run45	5/1.14/0%
□	0.8336	run42	5/1.14/25%
◇	0.8336	run38	5/1.14/50%

Figure 7.2.2.258: Cowl Effects (CR=5, Re=1.14million/ft) Sidewall Pressures



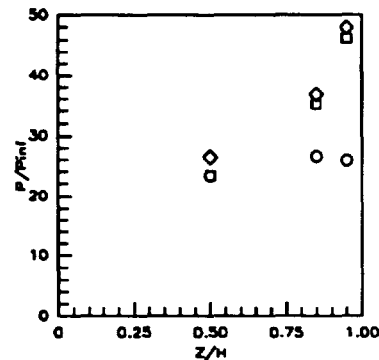
Sym	$x'/T_x'$	Run No.	CR/Re/Cowl (millions)
○	0.8857	run45	5/1.14/0%
□	0.8857	run42	5/1.14/25%
◇	0.8857	run38	5/1.14/50%

Figure 7.2.2.259: Cowl Effects (CR=5, Re=1.14million/ft) Sidewall Pressures



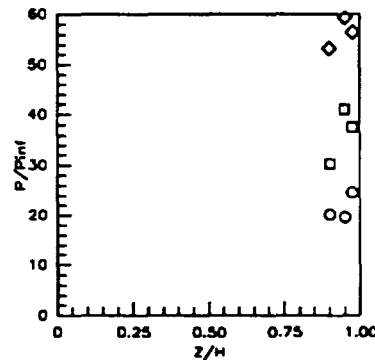
Sym	$x'/T_x'$	Run No.	CR/Re/Cowl (millions)
○	0.9378	run45	5/1.14/0%
□	0.9378	run42	5/1.14/25%
◇	0.9378	run38	5/1.14/50%

Figure 7.2.2.260: Cowl Effects (CR=5, Re=1.14million/ft) Sidewall Pressures



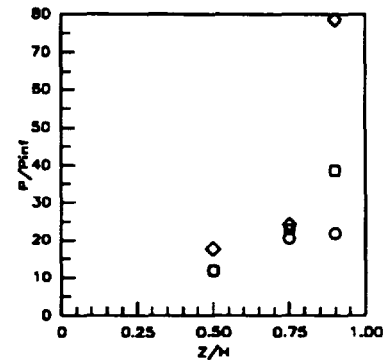
Sym	$x'/T_x'$	Run No.	CR/Re/Cowl (millions)
○	0.9751	run45	5/1.14/0%
□	0.9751	run42	5/1.14/25%
◇	0.9751	run38	5/1.14/50%

Figure 7.2.2.261: Cowl Effects (CR=5, Re=1.14million/ft) Sidewall Pressures



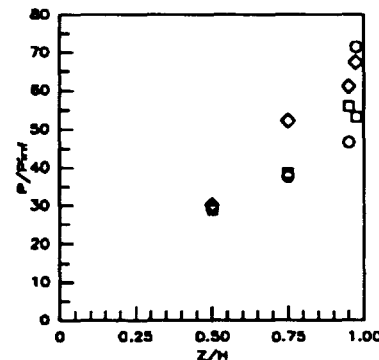
Sym	$x'/T_x'$	Run No.	CR/Re/Cowl (millions)
○	1.0197	run45	5/1.14/0%
□	1.0197	run42	5/1.14/25%
◇	1.0197	run38	5/1.14/50%

Figure 7.2.2.262: Cowl Effects (CR=5, Re=1.14million/ft) Sidewall Pressures



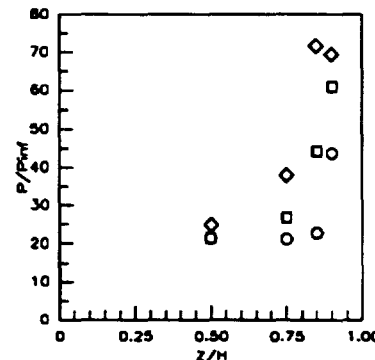
Sym	$x'/T_x'$	Run No.	CR/Re/Cowl (millions)
○	1.0843	run45	5/1.14/0%
□	1.0843	run42	5/1.14/25%
◇	1.0843	run38	5/1.14/50%

Figure 7.2.2.263: Cowl Effects (CR=5, Re=1.14million/ft) Sidewall Pressures



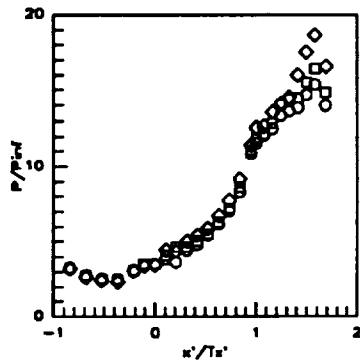
Sym	$x'/T_x'$	Run No.	CR/Re/Cowl (millions)
○	1.1537	run45	5/1.14/0%
□	1.1537	run42	5/1.14/25%
◇	1.1537	run38	5/1.14/50%

Figure 7.2.2.264: Cowl Effects (CR=5, Re=1.14million/ft) Sidewall Pressures



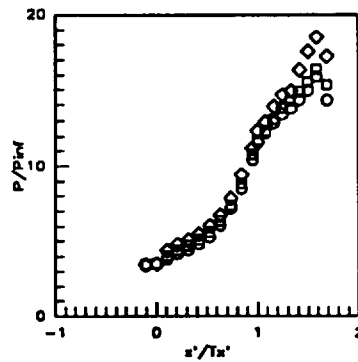
Sym	$x'/T_x'$	Run No.	CR/Re/Cowl (millions)
○	1.2356	run45	5/1.14/0%
□	1.2356	run42	5/1.14/25%
◇	1.2356	run38	5/1.14/50%

Figure 7.2.2.265: Cowl Effects (CR=5, Re=1.14million/ft) Sidewall Pressures



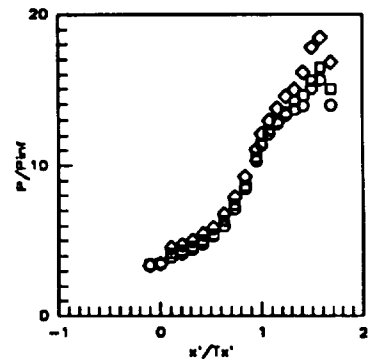
Sym	C.L. for	Run No.	CR/Re/Cowl (millions)
○	CR=3	run44	5/0.55/0%
□	CR=3	run41	5/0.55/25%
◇	CR=3	run37	5/0.55/50%

Figure 7.2.2.266: Cowl Effects (CR=5, Re=0.55million/ft) CR=3 Centerline Pressures



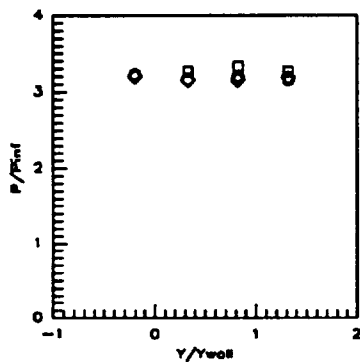
Sym	C.L. for	Run No.	CR/Re/Cowl (millions)
○	CR=5	run44	5/0.55/0%
□	CR=5	run41	5/0.55/25%
◇	CR=5	run37	5/0.55/50%

Figure 7.2.2.267: Cowl Effects (CR=5, Re=0.55million/ft) CR=5 Centerline Pressures



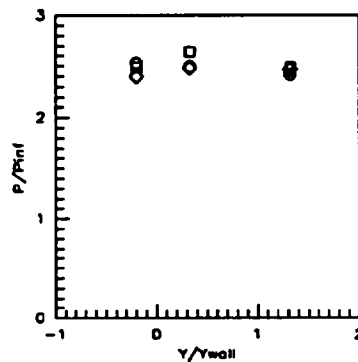
Sym	C.L. for	Run No.	CR/Re/Cowl (millions)
○	CR=9	run44	5/0.55/0%
□	CR=9	run41	5/0.55/25%
◇	CR=9	run37	5/0.55/50%

Figure 7.2.2.268: Cowl Effects (CR=5, Re=0.55million/ft) CR=9 Centerline Pressures



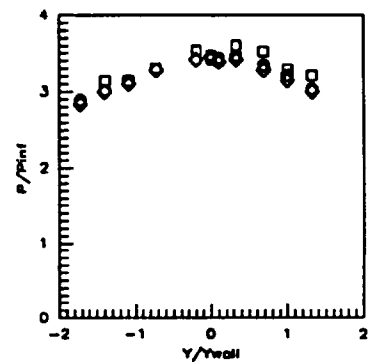
Sym	x'/Ts'	Run No.	CR/Re/Cowl (millions)
○	-0.8412	run44	5/0.55/0%
□	-0.8412	run41	5/0.55/25%
◇	-0.8142	run37	5/0.55/50%

Figure 7.2.2.269: Cowl Effects (CR=5, Re=0.55million/ft) Baseplate Pressures



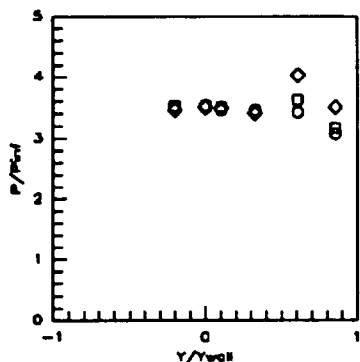
Sym	x'/Ts'	Run No.	CR/Re/Cowl (millions)
○	-0.5258	run44	5/0.55/0%
□	-0.5258	run41	5/0.55/25%
◇	-0.5258	run37	5/0.55/50%

Figure 7.2.2.270: Cowl Effects (CR=5, Re=0.55million/ft) Baseplate Pressures



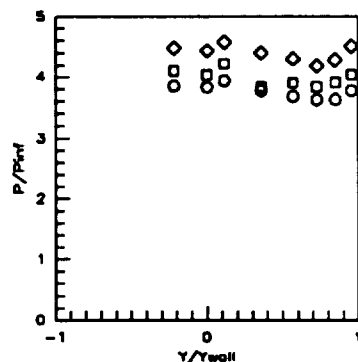
Sym	x'/Ts'	Run No.	CR/Re/Cowl (millions)
○	-0.1052	run44	5/0.55/0%
□	-0.1052	run41	5/0.55/25%
◇	-0.1052	run37	5/0.55/50%

Figure 7.2.2.271: Cowl Effects (CR=5, Re=0.55million/ft) Baseplate Pressures



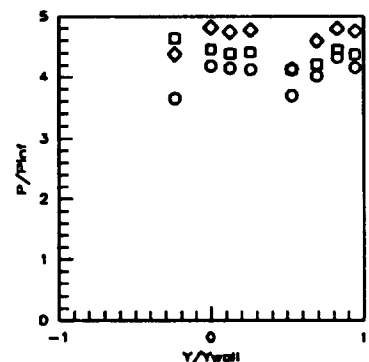
Sym	x'/Ts'	Run No.	CR/Re/Cowl (millions)
○	0.0000	run44	5/0.55/0%
□	0.0000	run41	5/0.55/25%
◇	0.0000	run37	5/0.55/50%

Figure 7.2.2.272: Cowl Effects (CR=5, Re=0.55million/ft) Baseplate Pressures



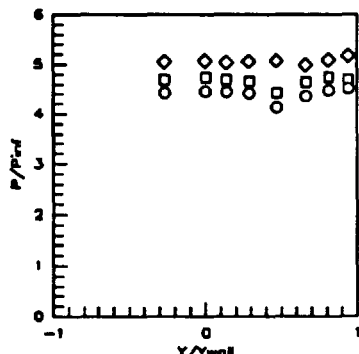
Sym	x'/Ts'	Run No.	CR/Re/Cowl (millions)
○	0.1052	run44	5/0.55/0%
□	0.1052	run41	5/0.55/25%
◇	0.1052	run37	5/0.55/50%

Figure 7.2.2.273: Cowl Effects (CR=5, Re=0.55million/ft) Baseplate Pressures



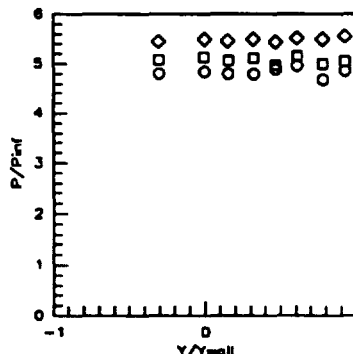
Sym	x'/Ts'	Run No.	CR/Re/Cowl (millions)
○	0.2103	run44	5/0.55/0%
□	0.2103	run41	5/0.55/25%
◇	0.2103	run37	5/0.55/50%

Figure 7.2.2.274: Cowl Effects (CR=5, Re=0.55million/ft) Baseplate Pressures



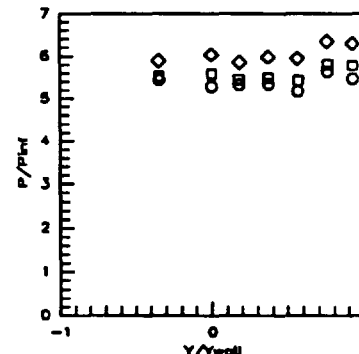
Sym	$x'/T_x'$	Run No.	CR/Re/Cowl (millions)
○	0.3184	run44	5/0.55/0%
□	0.3184	run41	5/0.55/25%
◇	0.3184	run37	5/0.55/50%

Figure 7.2.2.275: Cowl Effects (CR=5, Re=0.55million/ft) Baseplate Pressures



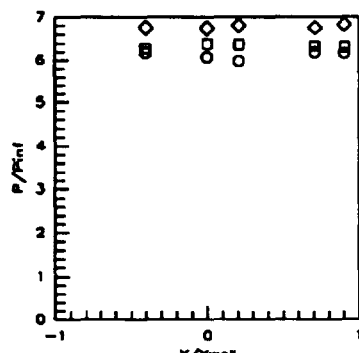
Sym	$x'/T_x'$	Run No.	CR/Re/Cowl (millions)
○	0.4206	run44	5/0.55/0%
□	0.4206	run41	5/0.55/25%
◇	0.4206	run37	5/0.55/50%

Figure 7.2.2.276: Cowl Effects (CR=5, Re=0.55million/ft) Baseplate Pressures



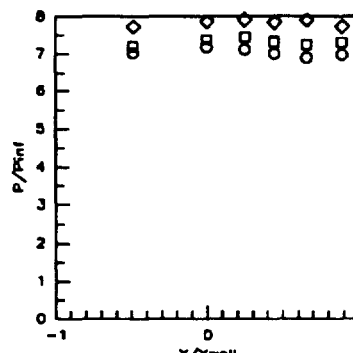
Sym	$x'/T_x'$	Run No.	CR/Re/Cowl (millions)
○	0.5258	run44	5/0.55/0%
□	0.5258	run41	5/0.55/25%
◇	0.5258	run37	5/0.55/50%

Figure 7.2.2.277: Cowl Effects (CR=5, Re=0.55million/ft) Baseplate Pressures



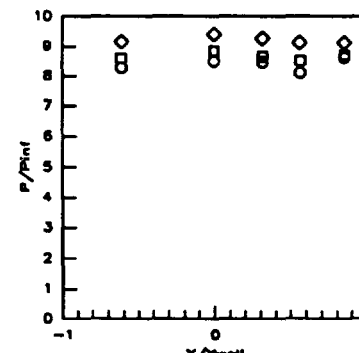
Sym	$x'/T_x'$	Run No.	CR/Re/Cowl (millions)
○	0.6309	run44	5/0.55/0%
□	0.6309	run41	5/0.55/25%
◇	0.6309	run37	5/0.55/50%

Figure 7.2.2.278: Cowl Effects (CR=5, Re=0.55million/ft) Baseplate Pressures



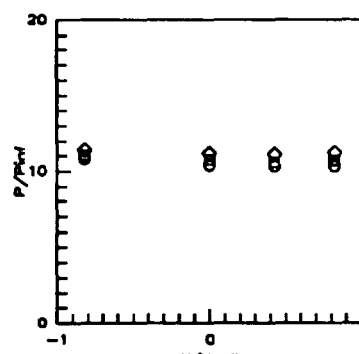
Sym	$x'/T_x'$	Run No.	CR/Re/Cowl (millions)
○	0.7361	run44	5/0.55/0%
□	0.7361	run41	5/0.55/25%
◇	0.7361	run37	5/0.55/50%

Figure 7.2.2.279: Cowl Effects (CR=5, Re=0.55million/ft) Baseplate Pressures



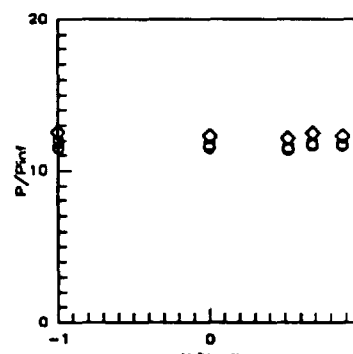
Sym	$x'/T_x'$	Run No.	CR/Re/Cowl (millions)
○	0.8412	run44	5/0.55/0%
□	0.8412	run41	5/0.55/25%
◇	0.8412	run37	5/0.55/50%

Figure 7.2.2.280: Cowl Effects (CR=5, Re=0.55million/ft) Baseplate Pressures



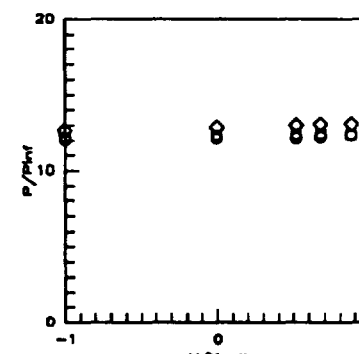
Sym	$x'/T_x'$	Run No.	CR/Re/Cowl (millions)
○	0.9484	run44	5/0.55/0%
□	0.9484	run41	5/0.55/25%
◇	0.9484	run37	5/0.55/50%

Figure 7.2.2.281: Cowl Effects (CR=5, Re=0.55million/ft) Baseplate Pressures



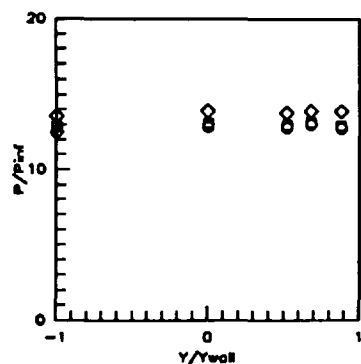
Sym	$x'/T_x'$	Run No.	CR/Re/Cowl (millions)
○	1.0000	run44	5/0.55/0%
□	1.0000	run41	5/0.55/25%
◇	1.0000	run37	5/0.55/50%

Figure 7.2.2.282: Cowl Effects (CR=5, Re=0.55million/ft) Baseplate Pressures



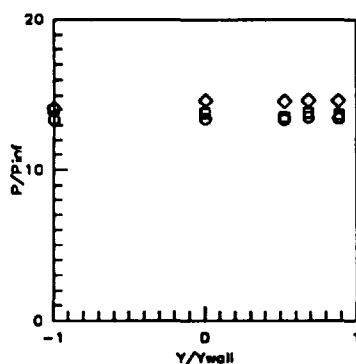
Sym	$x'/T_x'$	Run No.	CR/Re/Cowl (millions)
○	1.0728	run44	5/0.55/0%
□	1.0728	run41	5/0.55/25%
◇	1.0728	run37	5/0.55/50%

Figure 7.2.2.283: Cowl Effects (CR=5, Re=0.55million/ft) Baseplate Pressures



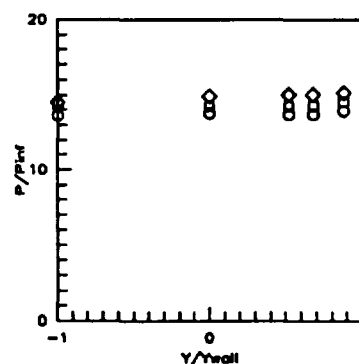
Sym	$x'/T_x'$	Run No.	CR/Re/Cowl (millions)
○	1.1867	run44	5/0.55/0%
□	1.1867	run41	5/0.55/25%
◇	1.1867	run37	5/0.55/50%

Figure 7.2.2.284: Cowl Effects (CR=5, Re=0.55million/ft) Baseplate Pressures



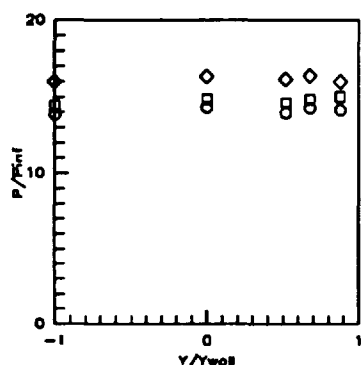
Sym	$x'/T_x'$	Run No.	CR/Re/Cowl (millions)
○	1.2408	run44	5/0.55/0%
□	1.2408	run41	5/0.55/25%
◇	1.2408	run37	5/0.55/50%

Figure 7.2.2.285: Cowl Effects (CR=5, Re=0.55million/ft) Baseplate Pressures



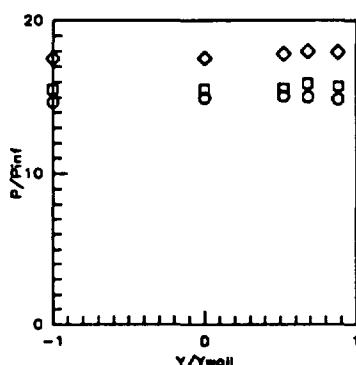
Sym	$x'/T_x'$	Run No.	CR/Re/Cowl (millions)
○	1.3249	run44	5/0.55/0%
□	1.3249	run41	5/0.55/25%
◇	1.3249	run37	5/0.55/50%

Figure 7.2.2.286: Cowl Effects (CR=5, Re=0.55million/ft) Baseplate Pressures



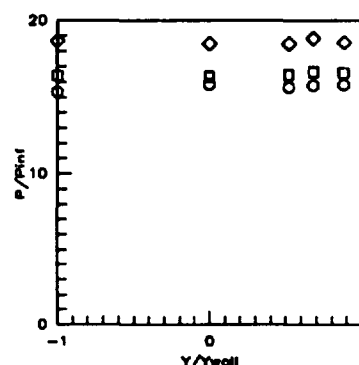
Sym	$x'/T_x'$	Run No.	CR/Re/Cowl (millions)
○	1.4080	run44	5/0.55/0%
□	1.4080	run41	5/0.55/25%
◇	1.4080	run37	5/0.55/50%

Figure 7.2.2.287: Cowl Effects (CR=5, Re=0.55million/ft) Baseplate Pressures



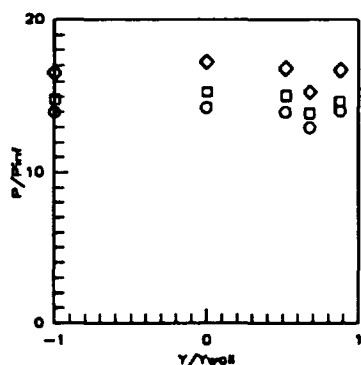
Sym	$x'/T_x'$	Run No.	CR/Re/Cowl (millions)
○	1.4932	run44	5/0.55/0%
□	1.4932	run41	5/0.55/25%
◇	1.4932	run37	5/0.55/50%

Figure 7.2.2.288: Cowl Effects (CR=5, Re=0.55million/ft) Baseplate Pressures



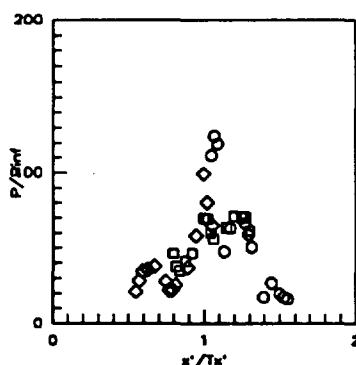
Sym	$x'/T_x'$	Run No.	CR/Re/Cowl (millions)
○	1.5773	run44	5/0.55/0%
□	1.5773	run41	5/0.55/25%
◇	1.5773	run37	5/0.55/50%

Figure 7.2.2.289: Cowl Effects (CR=5, Re=0.55million/ft) Baseplate Pressures



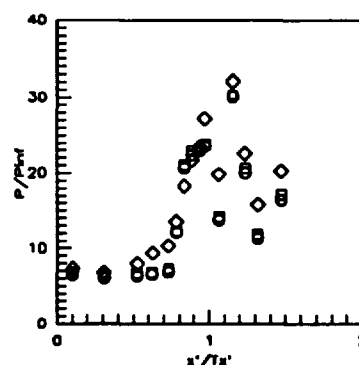
Sym	$x'/T_x'$	Run No.	CR/Re/Cowl (millions)
○	1.6824	run44	5/0.55/0%
□	1.6824	run41	5/0.55/25%
◇	1.6824	run37	5/0.55/50%

Figure 7.2.2.290: Cowl Effects (CR=5, Re=0.55million/ft) Baseplate Pressures



Sym	Cowl Pos.	Run No.	CR/Re/Cowl (millions)
○	0%	run44	5/0.55/0%
□	25%	run41	5/0.55/25%
◇	50%	run37	5/0.55/50%

Figure 7.2.2.291: Cowl Effects (CR=5, Re=0.55million/ft) Cowl Pressures



Sym	Z/H	Run No.	CR/Re/Cowl (millions)
○	0.5RT	run44	5/0.55/0%
□	0.5RT	run41	5/0.55/25%
◇	0.5RT	run37	5/0.55/50%

Figure 7.2.2.292: Cowl Effects (CR=5, Re=0.55million/ft) Sidewall Centerline Pressures

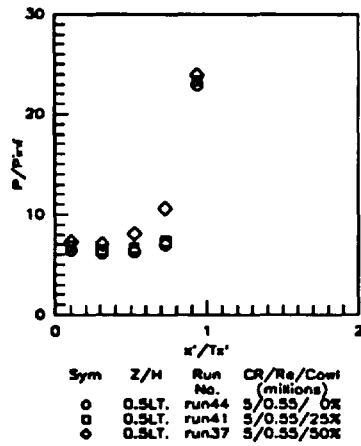


Figure 7.2.2.293: Cowl Effects  
(CR=5, Re=0.55million/ft)  
Sidewall Centerline Pressures

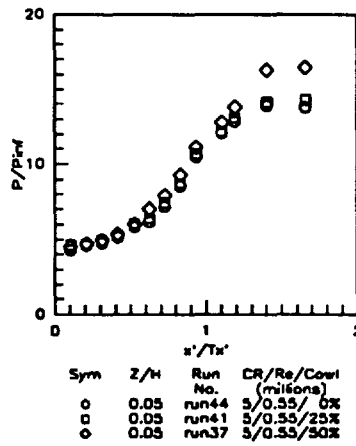


Figure 7.2.2.294: Cowl Effects  
(CR=5, Re=0.55million/ft)  
Sidewall Pressures

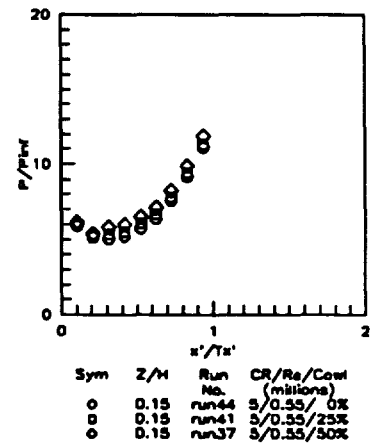


Figure 7.2.2.295: Cowl Effects  
(CR=5, Re=0.55million/ft)  
Sidewall Pressures

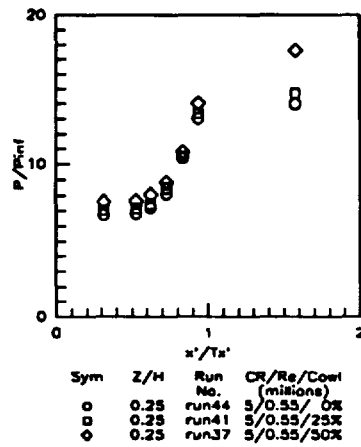


Figure 7.2.2.296: Cowl Effects  
(CR=5, Re=0.55million/ft)  
Sidewall Pressures

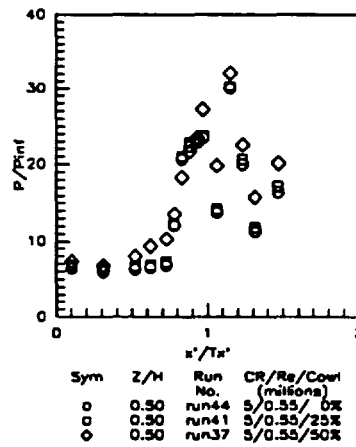


Figure 7.2.2.297: Cowl Effects  
(CR=5, Re=0.55million/ft)  
Sidewall Pressures

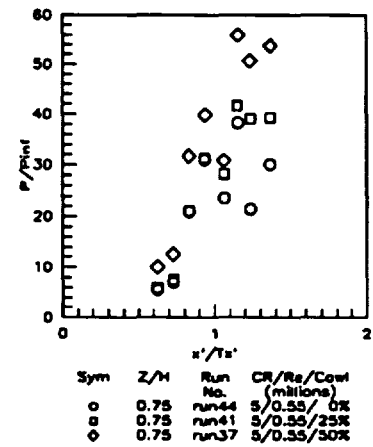


Figure 7.2.2.298: Cowl Effects  
(CR=5, Re=0.55million/ft)  
Sidewall Pressures

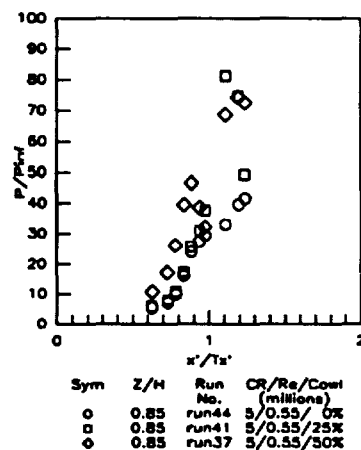


Figure 7.2.2.299: Cowl Effects  
(CR=5, Re=0.55million/ft)  
Sidewall Pressures

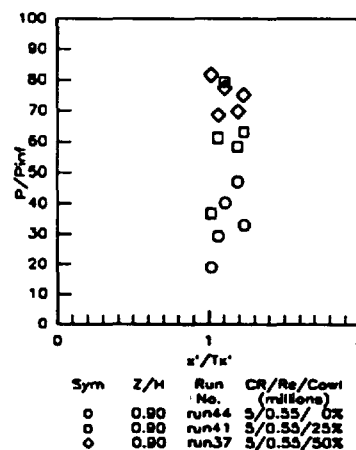


Figure 7.2.2.300: Cowl Effects  
(CR=5, Re=0.55million/ft)  
Sidewall Pressures

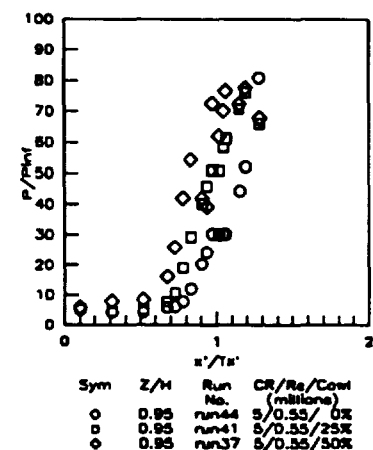
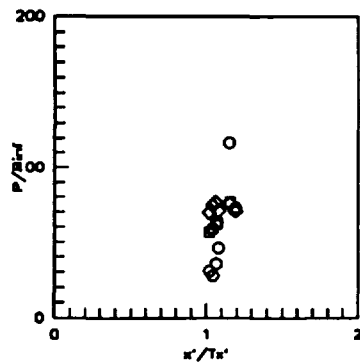
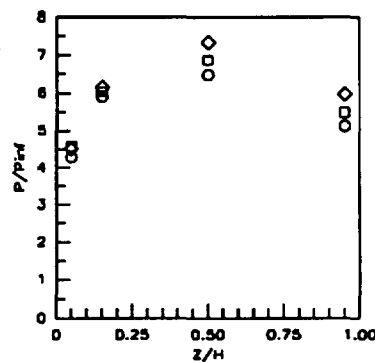


Figure 7.2.2.301: Cowl Effects  
(CR=5, Re=0.55million/ft)  
Sidewall Pressures



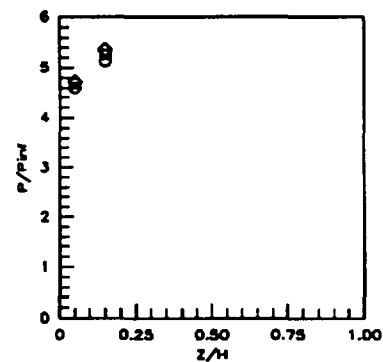
Sym	$x'/Ts'$	Run No.	CR/Re/Cowl (millions)
-----	----------	---------	-----------------------

Figure 7.2.2.302: Cowl Effects (CR=5, Re=0.55million/ft) Sidewall Pressures



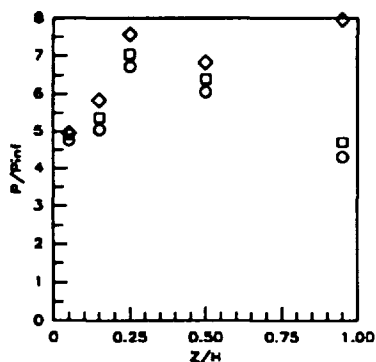
Sym	$x'/Ts'$	Run No.	CR/Re/Cowl (millions)
-----	----------	---------	-----------------------

Figure 7.2.2.303: Cowl Effects (CR=5, Re=0.55million/ft) Sidewall Pressures



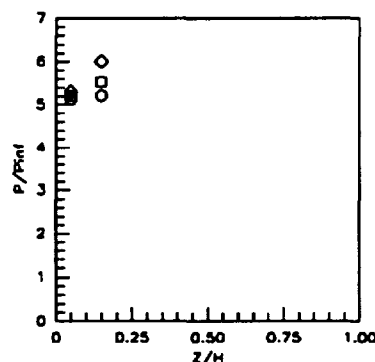
Sym	$x'/Ts'$	Run No.	CR/Re/Cowl (millions)
-----	----------	---------	-----------------------

Figure 7.2.2.304: Cowl Effects (CR=5, Re=0.55million/ft) Sidewall Pressures



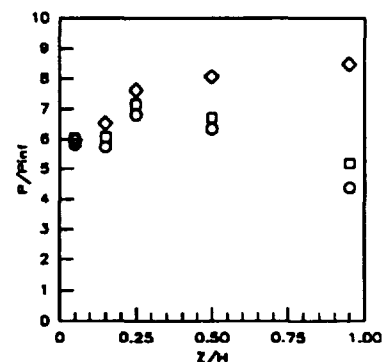
Sym	$x'/Ts'$	Run No.	CR/Re/Cowl (millions)
-----	----------	---------	-----------------------

Figure 7.2.2.305: Cowl Effects (CR=5, Re=0.55million/ft) Sidewall Pressures



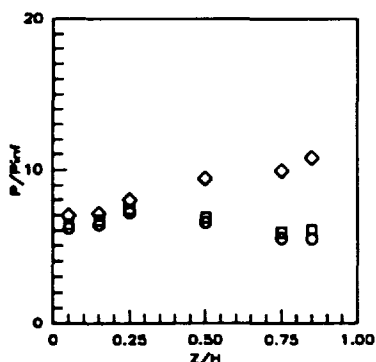
Sym	$x'/Ts'$	Run No.	CR/Re/Cowl (millions)
-----	----------	---------	-----------------------

Figure 7.2.2.306: Cowl Effects (CR=5, Re=0.55million/ft) Sidewall Pressures



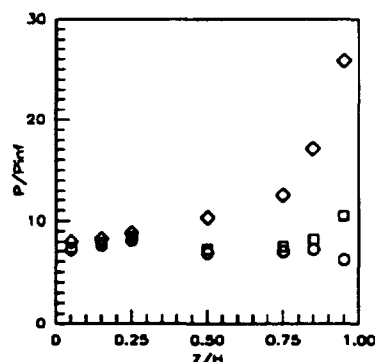
Sym	$x'/Ts'$	Run No.	CR/Re/Cowl (millions)
-----	----------	---------	-----------------------

Figure 7.2.2.307: Cowl Effects (CR=5, Re=0.55million/ft) Sidewall Pressures



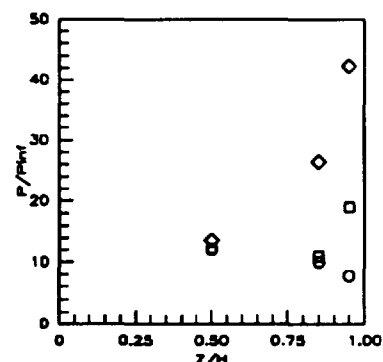
Sym	$x'/Ts'$	Run No.	CR/Re/Cowl (millions)
-----	----------	---------	-----------------------

Figure 7.2.2.308: Cowl Effects (CR=5, Re=0.55million/ft) Sidewall Pressures



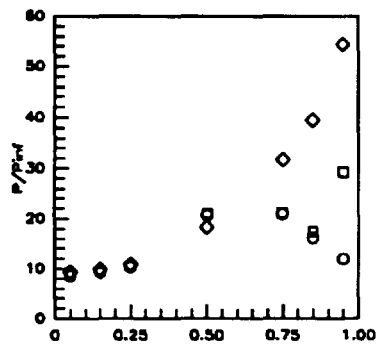
Sym	$x'/Ts'$	Run No.	CR/Re/Cowl (millions)
-----	----------	---------	-----------------------

Figure 7.2.2.309: Cowl Effects (CR=5, Re=0.55million/ft) Sidewall Pressures



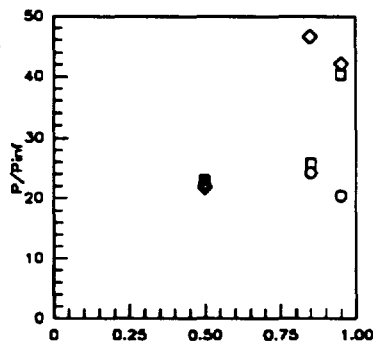
Sym	$x'/Ts'$	Run No.	CR/Re/Cowl (millions)
-----	----------	---------	-----------------------

Figure 7.2.2.310: Cowl Effects (CR=5, Re=0.55million/ft) Sidewall Pressures



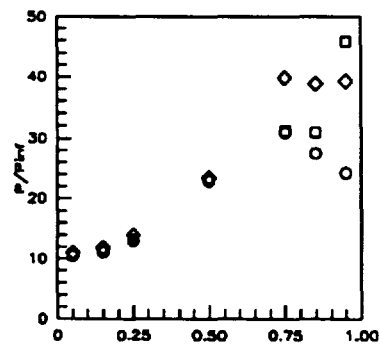
Sym	$x'/T_x'$	Run No.	CR/Re/Cowl (millions)
○	0.8336	run44	5/0.55/0%
□	0.8336	run41	5/0.55/25%
◇	0.8336	run37	5/0.55/50%

Figure 7.2.2.311: Cowl Effects (CR=5, Re=0.55million/ft) Sidewall Pressures



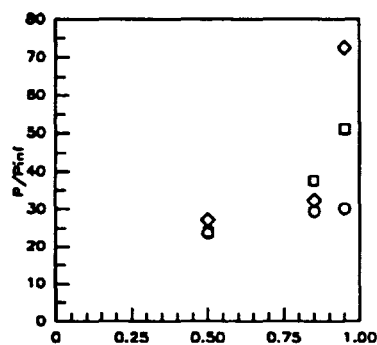
Sym	$x'/T_x'$	Run No.	CR/Re/Cowl (millions)
○	0.8857	run44	5/0.55/0%
□	0.8857	run41	5/0.55/25%
◇	0.8857	run37	5/0.55/50%

Figure 7.2.2.312: Cowl Effects (CR=5, Re=0.55million/ft) Sidewall Pressures



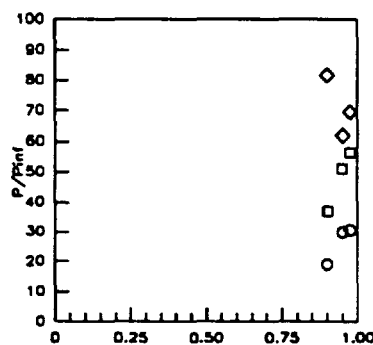
Sym	$x'/T_x'$	Run No.	CR/Re/Cowl (millions)
○	0.9378	run44	5/0.55/0%
□	0.9378	run41	5/0.55/25%
◇	0.9378	run37	5/0.55/50%

Figure 7.2.2.313: Cowl Effects (CR=5, Re=0.55million/ft) Sidewall Pressures



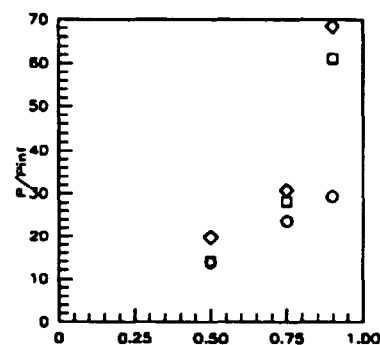
Sym	$x'/T_x'$	Run No.	CR/Re/Cowl (millions)
○	0.9751	run44	5/0.55/0%
□	0.9751	run41	5/0.55/25%
◇	0.9751	run37	5/0.55/50%

Figure 7.2.2.314: Cowl Effects (CR=5, Re=0.55million/ft) Sidewall Pressures



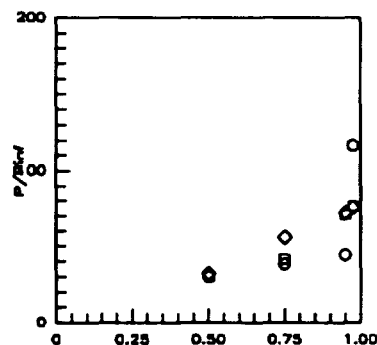
Sym	$x'/T_x'$	Run No.	CR/Re/Cowl (millions)
○	1.0197	run44	5/0.55/0%
□	1.0197	run41	5/0.55/25%
◇	1.0197	run37	5/0.55/50%

Figure 7.2.2.315: Cowl Effects (CR=5, Re=0.55million/ft) Sidewall Pressures



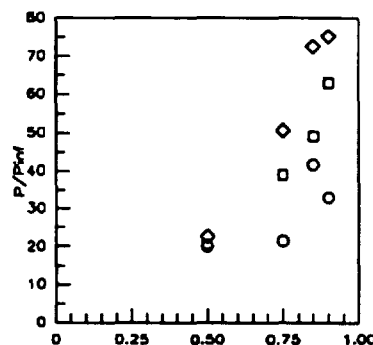
Sym	$x'/T_x'$	Run No.	CR/Re/Cowl (millions)
○	1.0843	run44	5/0.55/0%
□	1.0843	run41	5/0.55/25%
◇	1.0843	run37	5/0.55/50%

Figure 7.2.2.316: Cowl Effects (CR=5, Re=0.55million/ft) Sidewall Pressures



Sym	$x'/T_x'$	Run No.	CR/Re/Cowl (millions)
○	1.1537	run44	5/0.55/0%
□	1.1537	run41	5/0.55/25%
◇	1.1537	run37	5/0.55/50%

Figure 7.2.2.317: Cowl Effects (CR=5, Re=0.55million/ft) Sidewall Pressures



Sym	$x'/T_x'$	Run No.	CR/Re/Cowl (millions)
○	1.2356	run44	5/0.55/0%
□	1.2356	run41	5/0.55/25%
◇	1.2356	run37	5/0.55/50%

Figure 7.2.2.318: Cowl Effects (CR=5, Re=0.55million/ft) Sidewall Pressures



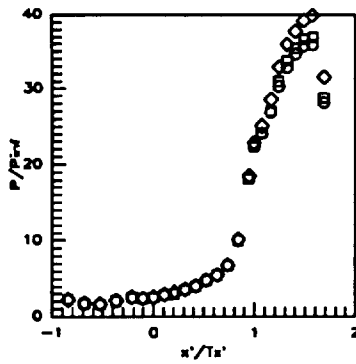


Figure 7.2.2.319: Cowl Effects  
(CR=9, Re=2.15million/ft)  
CR=3 Centerline Pressures

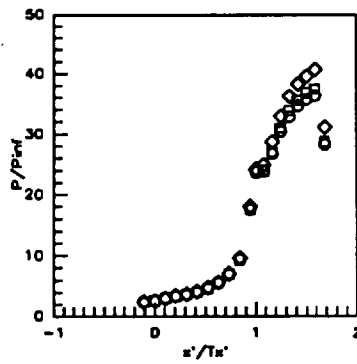


Figure 7.2.2.320: Cowl Effects  
(CR=9, Re=2.15million/ft)  
CR=5 Centerline Pressures

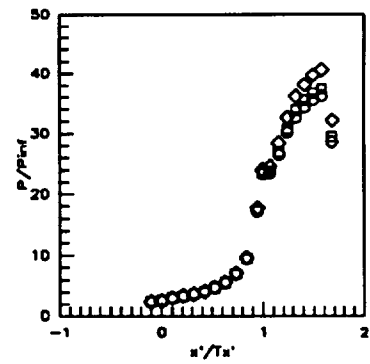


Figure 7.2.2.321: Cowl Effects  
(CR=9, Re=2.15million/ft)  
CR=9 Centerline Pressures

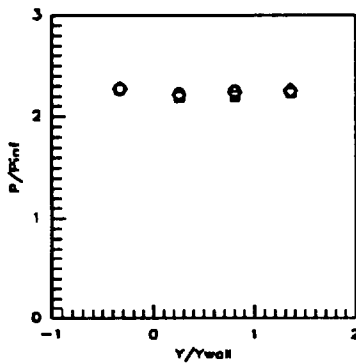


Figure 7.2.2.322: Cowl Effects  
(CR=9, Re=2.15million/ft)  
Baseplate Pressures

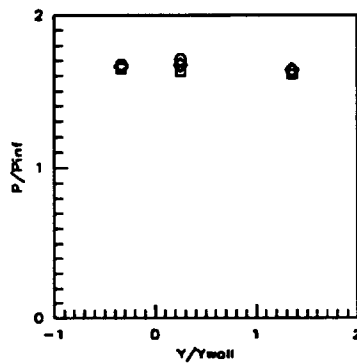


Figure 7.2.2.323: Cowl Effects  
(CR=9, Re=2.15million/ft)  
Baseplate Pressures

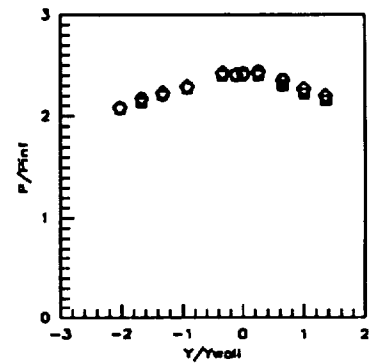


Figure 7.2.2.324: Cowl Effects  
(CR=9, Re=2.15million/ft)  
Baseplate Pressures

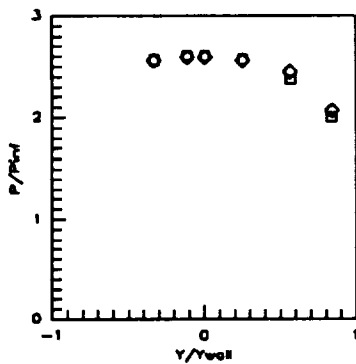


Figure 7.2.2.325: Cowl Effects  
(CR=9, Re=2.15million/ft)  
Baseplate Pressures

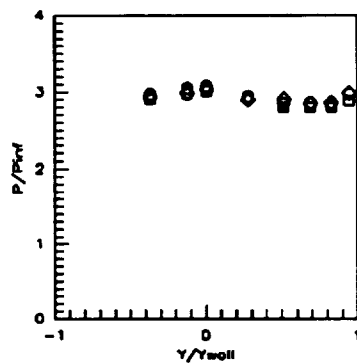


Figure 7.2.2.326: Cowl Effects  
(CR=9, Re=2.15million/ft)  
Baseplate Pressures

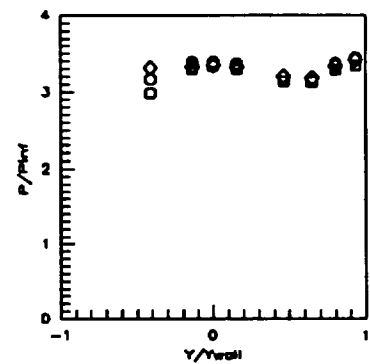


Figure 7.2.2.327: Cowl Effects  
(CR=9, Re=2.15million/ft)  
Baseplate Pressures

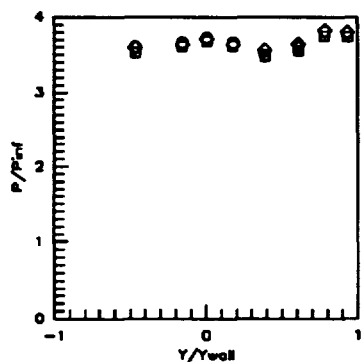


Figure 7.2.2.328: Cowl Effects (CR=9, Re=2.15million/ft) Baseplate Pressures

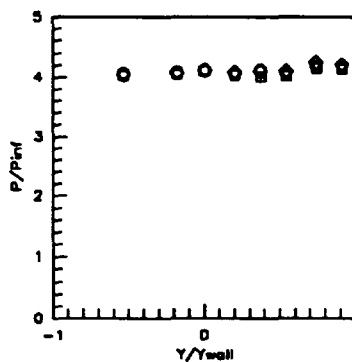


Figure 7.2.2.329: Cowl Effects (CR=9, Re=2.15million/ft) Baseplate Pressures

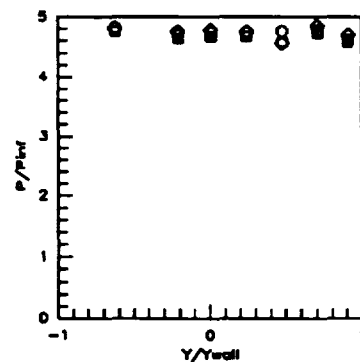


Figure 7.2.2.330: Cowl Effects (CR=9, Re=2.15million/ft) Baseplate Pressures

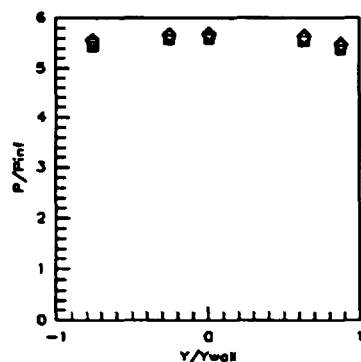


Figure 7.2.2.331: Cowl Effects (CR=9, Re=2.15million/ft) Baseplate Pressures

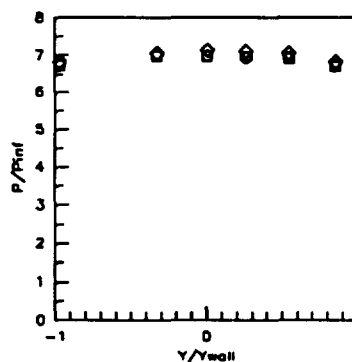


Figure 7.2.2.332: Cowl Effects (CR=9, Re=2.15million/ft) Baseplate Pressures

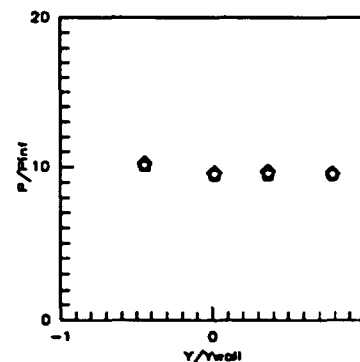


Figure 7.2.2.333: Cowl Effects (CR=9, Re=2.15million/ft) Baseplate Pressures

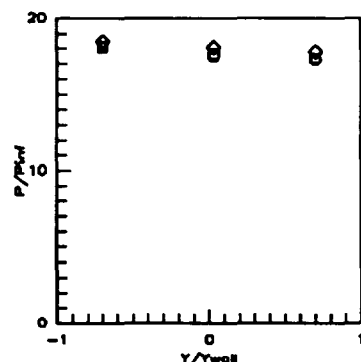


Figure 7.2.2.334: Cowl Effects (CR=9, Re=2.15million/ft) Baseplate Pressures

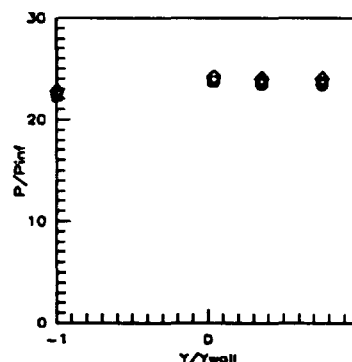


Figure 7.2.2.335: Cowl Effects (CR=9, Re=2.15million/ft) Baseplate Pressures

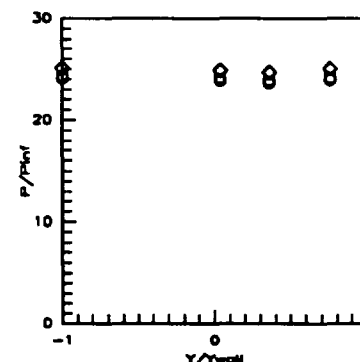
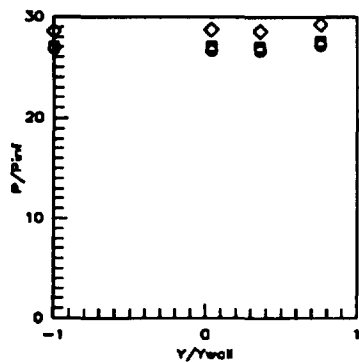
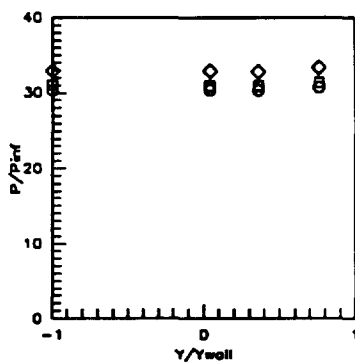


Figure 7.2.2.336: Cowl Effects (CR=9, Re=2.15million/ft) Baseplate Pressures



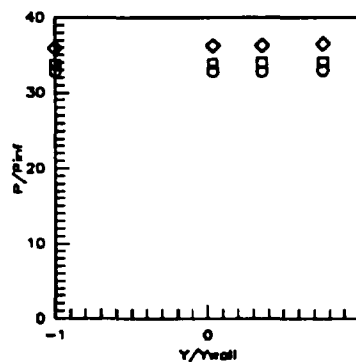
Sym	$x'/T_x'$	Run No.	CR/Re/Cowl (millions)
○	1.1567	run48	9/2.15/0%
□	1.1567	run53	9/2.15/25%
◇	1.1567	run57	9/2.15/50%

Figure 7.2.2.337: Cowl Effects (CR=9, Re=2.15million/ft) Baseplate Pressures



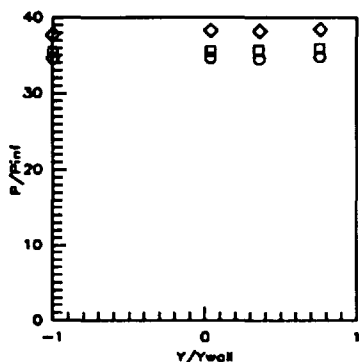
Sym	$x'/T_x'$	Run No.	CR/Re/Cowl (millions)
○	1.2408	run49	9/2.15/0%
□	1.2408	run53	9/2.15/25%
◇	1.2408	run57	9/2.15/50%

Figure 7.2.2.338: Cowl Effects (CR=9, Re=2.15million/ft) Baseplate Pressures



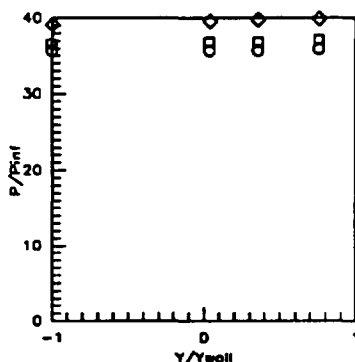
Sym	$x'/T_x'$	Run No.	CR/Re/Cowl (millions)
○	1.3249	run49	9/2.15/0%
□	1.3249	run53	9/2.15/25%
◇	1.3249	run57	9/2.15/50%

Figure 7.2.2.339: Cowl Effects (CR=9, Re=2.15million/ft) Baseplate Pressures



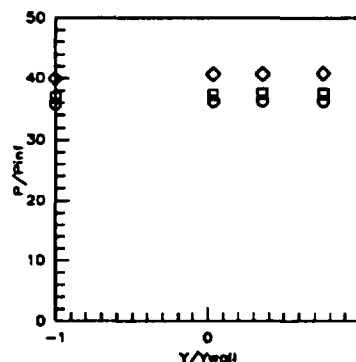
Sym	$x'/T_x'$	Run No.	CR/Re/Cowl (millions)
○	1.4090	run49	9/2.15/0%
□	1.4090	run53	9/2.15/25%
◇	1.4090	run57	9/2.15/50%

Figure 7.2.2.340: Cowl Effects (CR=9, Re=2.15million/ft) Baseplate Pressures



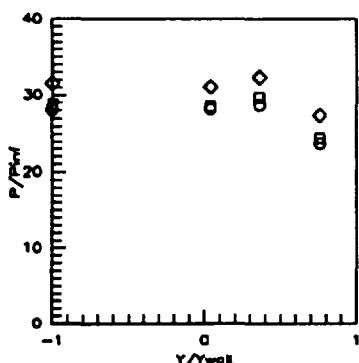
Sym	$x'/T_x'$	Run No.	CR/Re/Cowl (millions)
○	1.4832	run49	9/2.15/0%
□	1.4832	run53	9/2.15/25%
◇	1.4832	run57	9/2.15/50%

Figure 7.2.2.341: Cowl Effects (CR=9, Re=2.15million/ft) Baseplate Pressures



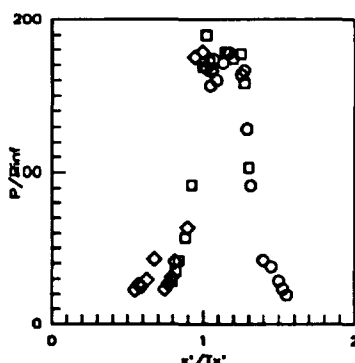
Sym	$x'/T_x'$	Run No.	CR/Re/Cowl (millions)
○	1.5773	run49	9/2.15/0%
□	1.5773	run53	9/2.15/25%
◇	1.5773	run57	9/2.15/50%

Figure 7.2.2.342: Cowl Effects (CR=9, Re=2.15million/ft) Baseplate Pressures



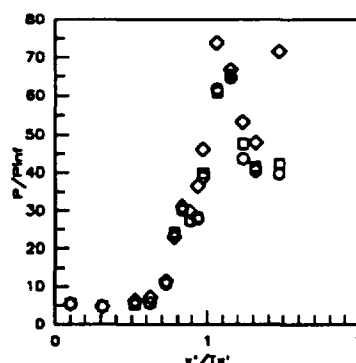
Sym	$x'/T_x'$	Run No.	CR/Re/Cowl (millions)
○	1.6824	run49	9/2.15/0%
□	1.6824	run53	9/2.15/25%
◇	1.6824	run57	9/2.15/50%

Figure 7.2.2.343: Cowl Effects (CR=9, Re=2.15million/ft) Baseplate Pressures



Sym	Cowl Pos.	Run No.	CR/Re/Cowl (millions)
○	0%	run49	9/2.15/0%
□	25%	run53	9/2.15/25%
◇	50%	run57	9/2.15/50%

Figure 7.2.2.344: Cowl Effects (CR=9, Re=2.15million/ft) Cowl Pressures



Sym	Z/H	Run No.	CR/Re/Cowl (millions)
○	0.5RT	run49	9/2.15/0%
□	0.5RT	run53	9/2.15/25%
◇	0.5RT	run57	9/2.15/50%

Figure 7.2.2.345: Cowl Effects (CR=9, Re=2.15million/ft) Sidewall Centerline Pressures

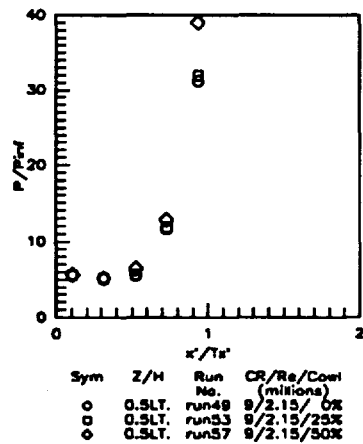


Figure 7.2.2.346: Cowl Effects  
(CR=9, Re=2.15million/ft)  
Sidewall Centerline Pressures

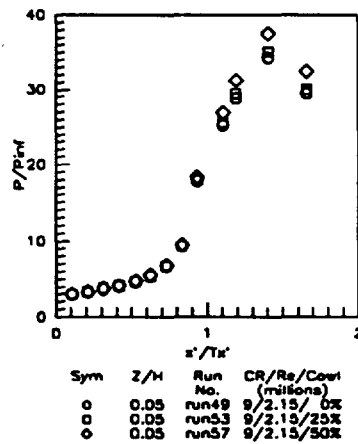


Figure 7.2.2.347: Cowl Effects  
(CR=9, Re=2.15million/ft)  
Sidewall Pressures

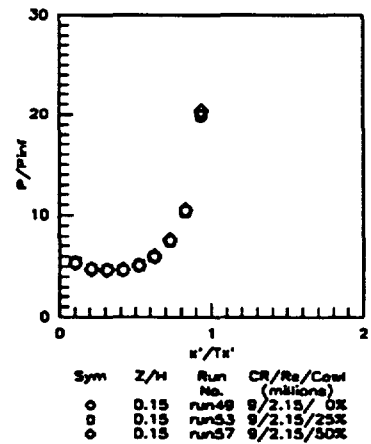


Figure 7.2.2.348: Cowl Effects  
(CR=9, Re=2.15million/ft)  
Sidewall Pressures

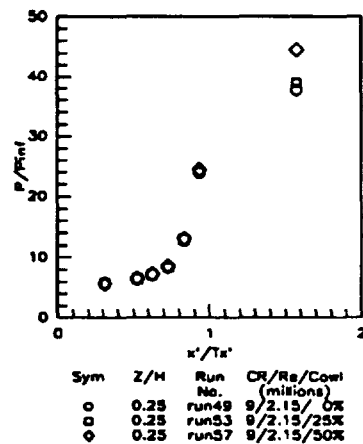


Figure 7.2.2.349: Cowl Effects  
(CR=9, Re=2.15million/ft)  
Sidewall Pressures

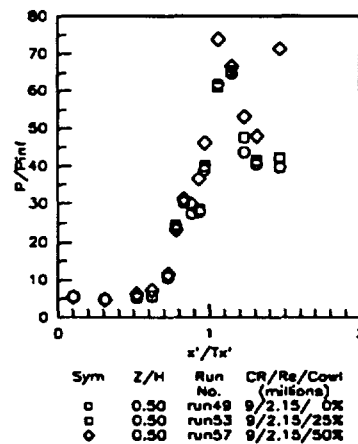


Figure 7.2.2.350: Cowl Effects  
(CR=9, Re=2.15million/ft)  
Sidewall Pressures

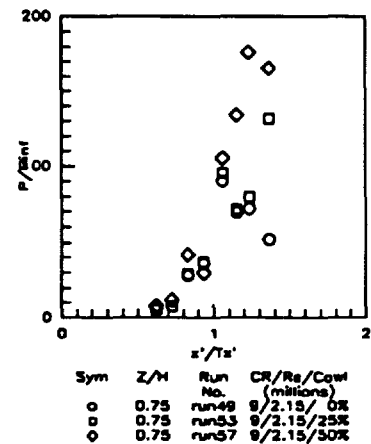


Figure 7.2.2.351: Cowl Effects  
(CR=9, Re=2.15million/ft)  
Sidewall Pressures

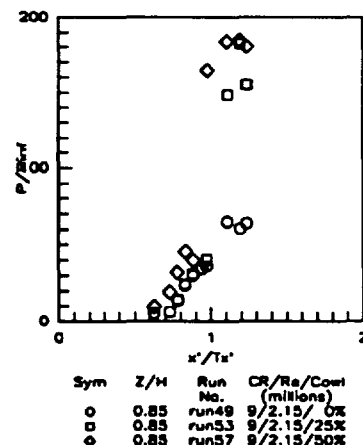


Figure 7.2.2.352: Cowl Effects  
(CR=9, Re=2.15million/ft)  
Sidewall Pressures

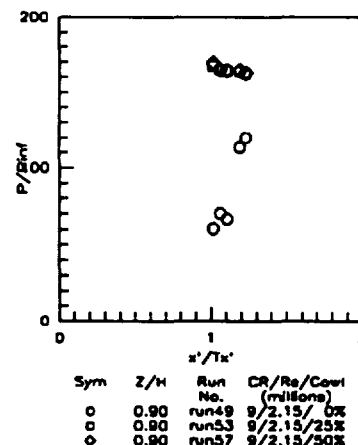


Figure 7.2.2.353: Cowl Effects  
(CR=9, Re=2.15million/ft)  
Sidewall Pressures

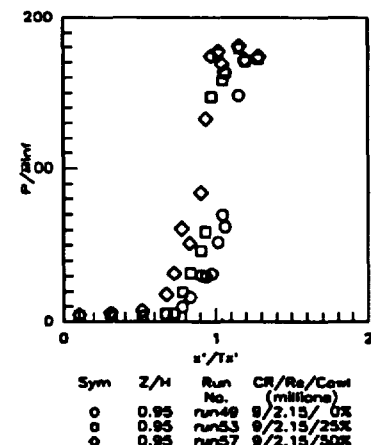


Figure 7.2.2.354: Cowl Effects  
(CR=9, Re=2.15million/ft)  
Sidewall Pressures

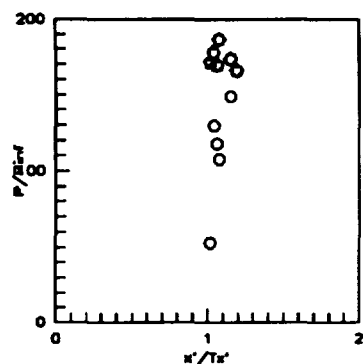


Figure 7.2.2.355: Cowl Effects (CR=9, Re=2.15million/ft) Sidewall Pressures

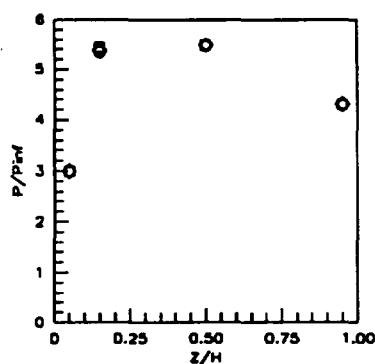


Figure 7.2.2.356: Cowl Effects (CR=9, Re=2.15million/ft) Sidewall Pressures

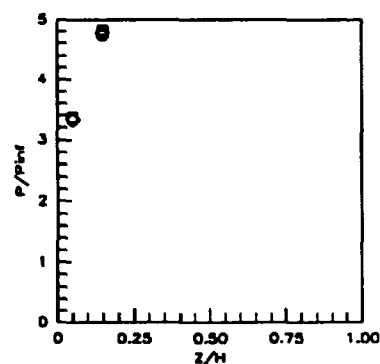


Figure 7.2.2.357: Cowl Effects (CR=9, Re=2.15million/ft) Sidewall Pressures

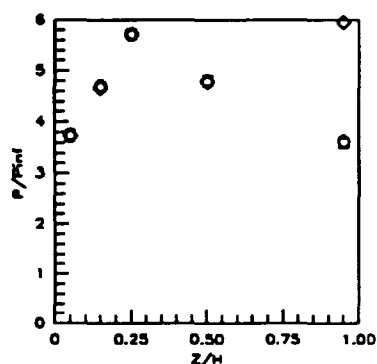


Figure 7.2.2.358: Cowl Effects (CR=9, Re=2.15million/ft) Sidewall Pressures

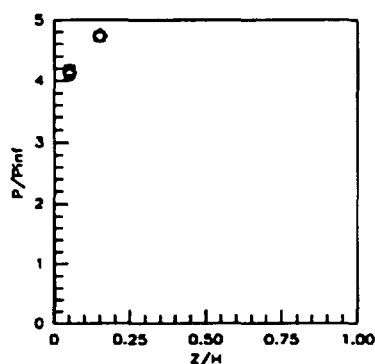


Figure 7.2.2.359: Cowl Effects (CR=9, Re=2.15million/ft) Sidewall Pressures

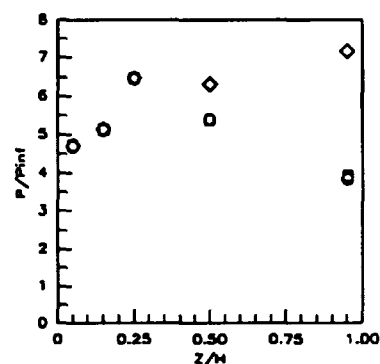


Figure 7.2.2.360: Cowl Effects (CR=9, Re=2.15million/ft) Sidewall Pressures

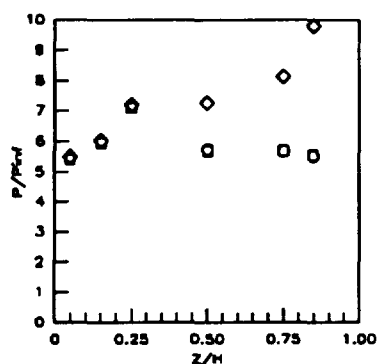


Figure 7.2.2.361: Cowl Effects (CR=9, Re=2.15million/ft) Sidewall Pressures

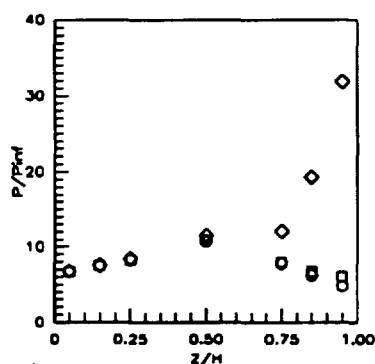


Figure 7.2.2.362: Cowl Effects (CR=9, Re=2.15million/ft) Sidewall Pressures

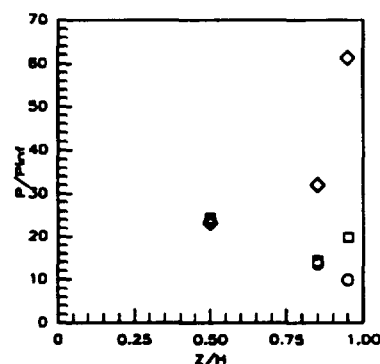


Figure 7.2.2.363: Cowl Effects (CR=9, Re=2.15million/ft) Sidewall Pressures

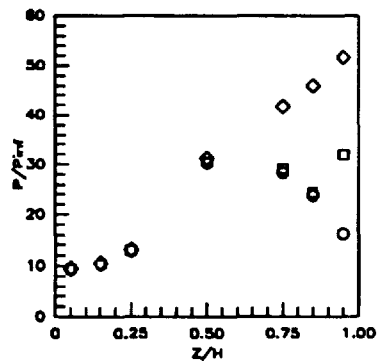


Figure 7.2.2.364: Cowl Effects (CR=9, Re=2.15million/ft) Sidewall Pressures

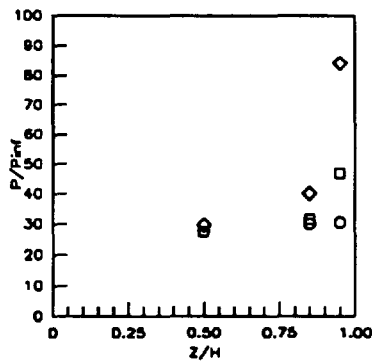


Figure 7.2.2.365: Cowl Effects (CR=9, Re=2.15million/ft) Sidewall Pressures

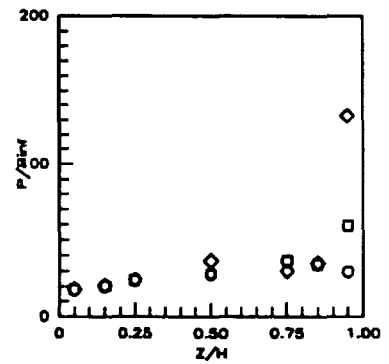


Figure 7.2.2.366: Cowl Effects (CR=9, Re=2.15million/ft) Sidewall Pressures

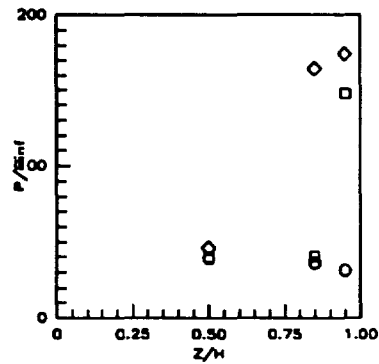


Figure 7.2.2.367: Cowl Effects (CR=9, Re=2.15million/ft) Sidewall Pressures

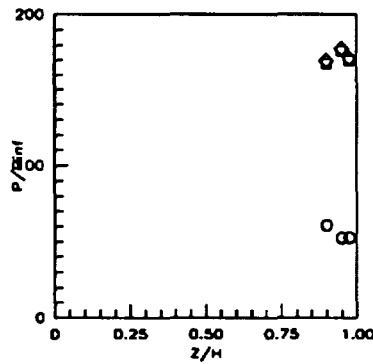


Figure 7.2.2.368: Cowl Effects (CR=9, Re=2.15million/ft) Sidewall Pressures

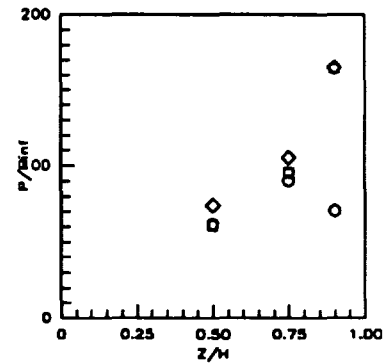


Figure 7.2.2.369: Cowl Effects (CR=9, Re=2.15million/ft) Sidewall Pressures

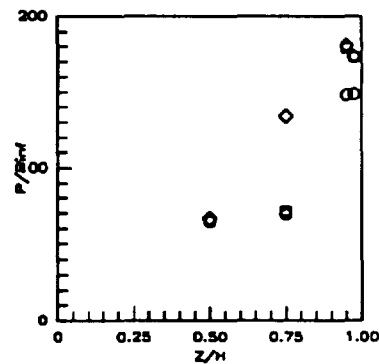


Figure 7.2.2.370: Cowl Effects (CR=9, Re=2.15million/ft) Sidewall Pressures

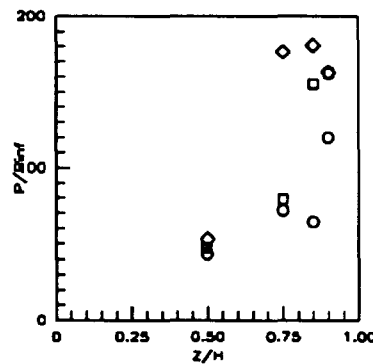
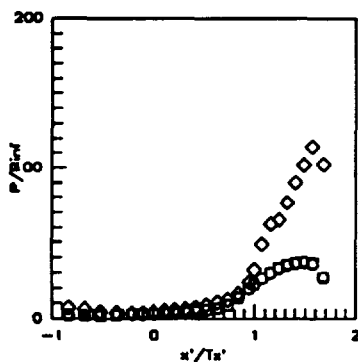
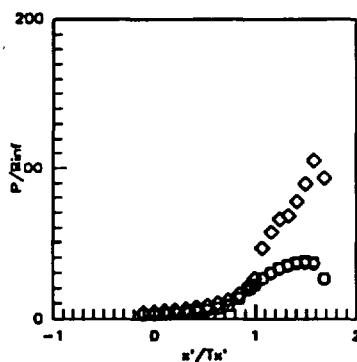


Figure 7.2.2.371: Cowl Effects (CR=9, Re=2.15million/ft) Sidewall Pressures



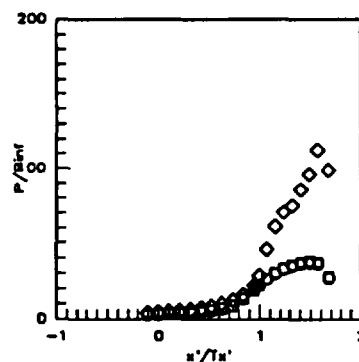
Sym	C.L.	Run	CR/Re/Cowl
	for	No.	(milions)
○	CR=3	run48	9/1.14/ 0%
□	CR=3	run52	9/1.14/25%
◇	CR=3	run56	9/1.14/50%

Figure 7.2.2.372: Cowl Effects  
(CR=9, Re=1.14million/ft)  
CR=3 Centerline Pressures



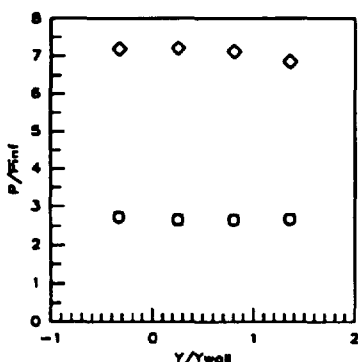
Sym	C.L.	Run	CR/Re/Cowl
	for	No.	(milions)
○	CR=5	run48	9/1.14/ 0%
□	CR=5	run52	9/1.14/25%
◇	CR=5	run56	9/1.14/50%

Figure 7.2.2.373: Cowl Effects  
(CR=9, Re=1.14million/ft)  
CR=5 Centerline Pressures



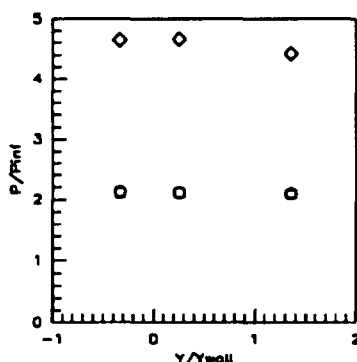
Sym	C.L.	Run	CR/Re/Cowl
	for	No.	(milions)
○	CR=9	run48	9/1.14/ 0%
□	CR=9	run52	9/1.14/25%
◇	CR=9	run56	9/1.14/50%

Figure 7.2.2.374: Cowl Effects  
(CR=9, Re=1.14million/ft)  
CR=9 Centerline Pressures



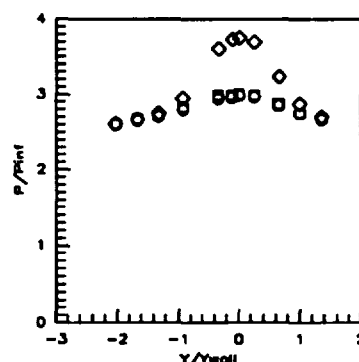
Sym	x'/Ts'	Run	CR/Re/Cowl
		No.	(milions)
○	-0.8412	run48	9/1.14/ 0%
□	-0.8412	run52	9/1.14/25%
◇	-0.8412	run56	9/1.14/50%

Figure 7.2.2.375: Cowl Effects  
(CR=9, Re=1.14million/ft)  
Baseplate Pressures



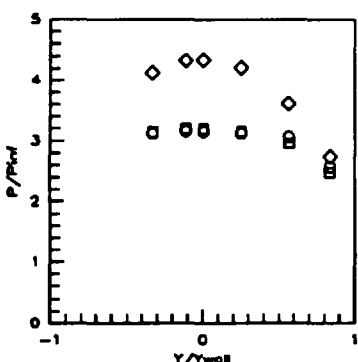
Sym	x'/Ts'	Run	CR/Re/Cowl
		No.	(milions)
○	-0.5258	run48	9/1.14/ 0%
□	-0.5258	run52	9/1.14/25%
◇	-0.5258	run56	9/1.14/50%

Figure 7.2.2.376: Cowl Effects  
(CR=9, Re=1.14million/ft)  
Baseplate Pressures



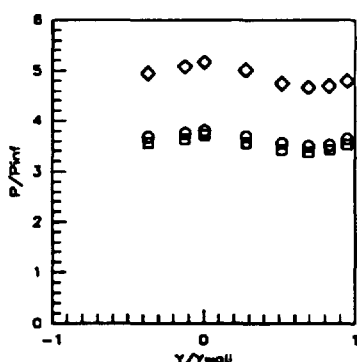
Sym	x'/Ts'	Run	CR/Re/Cowl
		No.	(milions)
○	-0.1052	run48	9/1.14/ 0%
□	-0.1052	run52	9/1.14/25%
◇	-0.1052	run56	9/1.14/50%

Figure 7.2.2.377: Cowl Effects  
(CR=9, Re=1.14million/ft)  
Baseplate Pressures



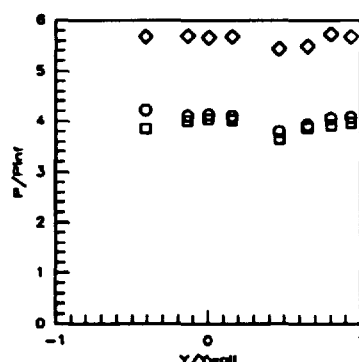
Sym	x'/Ts'	Run	CR/Re/Cowl
		No.	(milions)
○	0.0000	run48	9/1.14/ 0%
□	0.0000	run52	9/1.14/25%
◇	0.0000	run56	9/1.14/50%

Figure 7.2.2.378: Cowl Effects  
(CR=9, Re=1.14million/ft)  
Baseplate Pressures



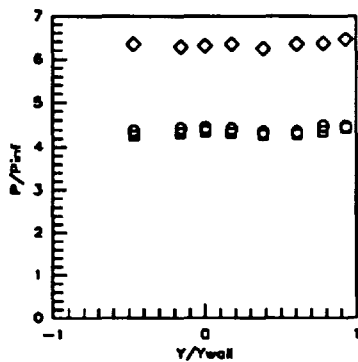
Sym	x'/Ts'	Run	CR/Re/Cowl
		No.	(milions)
○	0.1052	run48	9/1.14/ 0%
□	0.1052	run52	9/1.14/25%
◇	0.1052	run56	9/1.14/50%

Figure 7.2.2.379: Cowl Effects  
(CR=9, Re=1.14million/ft)  
Baseplate Pressures



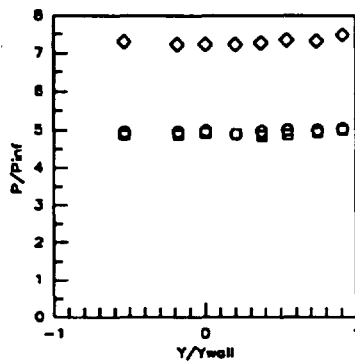
Sym	x'/Ts'	Run	CR/Re/Cowl
		No.	(milions)
○	0.2103	run48	9/1.14/ 0%
□	0.2103	run52	9/1.14/25%
◇	0.2103	run56	9/1.14/50%

Figure 7.2.2.380: Cowl Effects  
(CR=9, Re=1.14million/ft)  
Baseplate Pressures



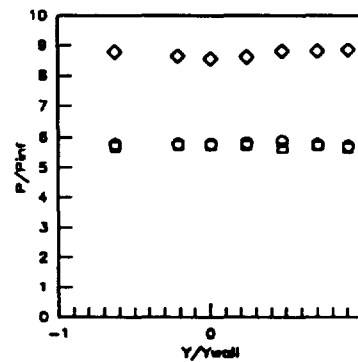
Sym	x'/Tx'	Run No.	CR/Re/Cowl (millions)
○	0.3154	run48	9/1.14/0%
□	0.3154	run52	9/1.14/25%
◇	0.3154	run56	9/1.14/50%

Figure 7.2.2.381: Cowl Effects (CR=9, Re=1.14million/ft) Baseplate Pressures



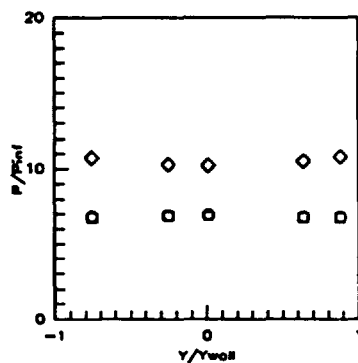
Sym	x'/Tx'	Run No.	CR/Re/Cowl (millions)
○	0.4206	run48	9/1.14/0%
□	0.4206	run52	9/1.14/25%
◇	0.4206	run56	9/1.14/50%

Figure 7.2.2.382: Cowl Effects (CR=9, Re=1.14million/ft) Baseplate Pressures



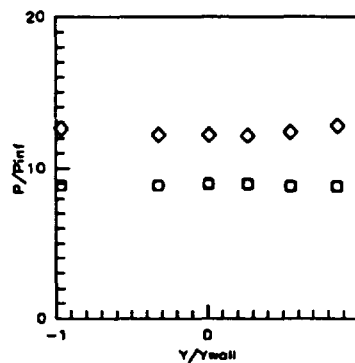
Sym	x'/Tx'	Run No.	CR/Re/Cowl (millions)
○	0.5258	run48	9/1.14/0%
□	0.5258	run52	9/1.14/25%
◇	0.5258	run56	9/1.14/50%

Figure 7.2.2.383: Cowl Effects (CR=9, Re=1.14million/ft) Baseplate Pressures



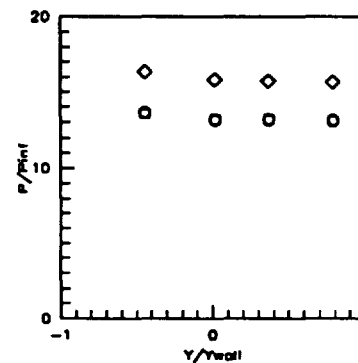
Sym	x'/Tx'	Run No.	CR/Re/Cowl (millions)
○	0.6309	run48	9/1.14/0%
□	0.6309	run52	9/1.14/25%
◇	0.6309	run56	9/1.14/50%

Figure 7.2.2.384: Cowl Effects (CR=9, Re=1.14million/ft) Baseplate Pressures



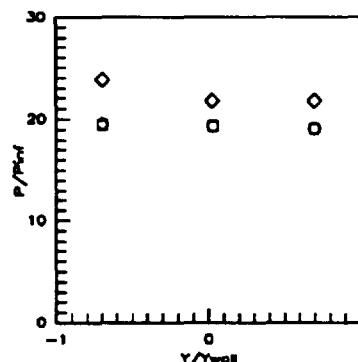
Sym	x'/Tx'	Run No.	CR/Re/Cowl (millions)
○	0.7361	run48	9/1.14/0%
□	0.7361	run52	9/1.14/25%
◇	0.7361	run56	9/1.14/50%

Figure 7.2.2.385: Cowl Effects (CR=9, Re=1.14million/ft) Baseplate Pressures



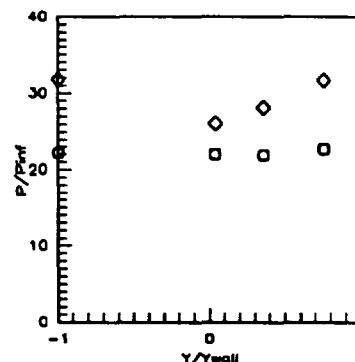
Sym	x'/Tx'	Run No.	CR/Re/Cowl (millions)
○	0.8412	run48	9/1.14/0%
□	0.8412	run52	9/1.14/25%
◇	0.8412	run56	9/1.14/50%

Figure 7.2.2.386: Cowl Effects (CR=9, Re=1.14million/ft) Baseplate Pressures



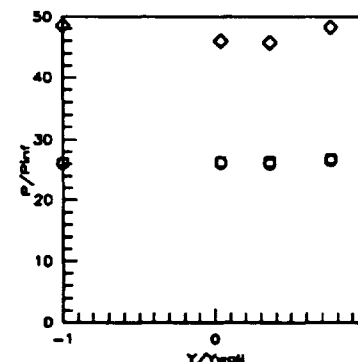
Sym	x'/Tx'	Run No.	CR/Re/Cowl (millions)
○	0.9464	run48	9/1.14/0%
□	0.9464	run52	9/1.14/25%
◇	0.9464	run56	9/1.14/50%

Figure 7.2.2.387: Cowl Effects (CR=9, Re=1.14million/ft) Baseplate Pressures



Sym	x'/Tx'	Run No.	CR/Re/Cowl (millions)
○	1.0000	run48	9/1.14/0%
□	1.0000	run52	9/1.14/25%
◇	1.0000	run56	9/1.14/50%

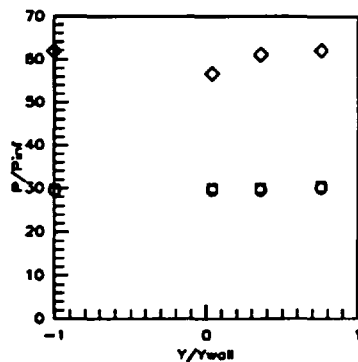
Figure 7.2.2.388: Cowl Effects (CR=9, Re=1.14million/ft) Baseplate Pressures



Sym	x'/Tx'	Run No.	CR/Re/Cowl (millions)
○	1.0726	run48	9/1.14/0%
□	1.0726	run52	9/1.14/25%
◇	1.0726	run56	9/1.14/50%

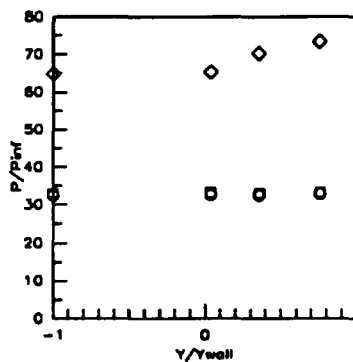
Figure 7.2.2.389: Cowl Effects (CR=9, Re=1.14million/ft) Baseplate Pressures





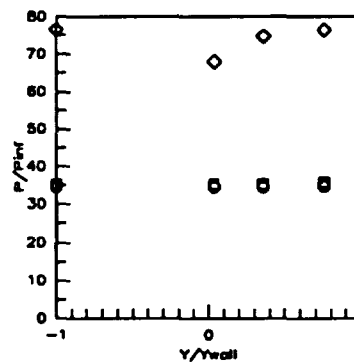
Sym	x'/Ts'	Run No.	CR/Re/Cowl (millions)
○	1.1567	run48	9/1.14/0%
□	1.1567	run52	9/1.14/25%
◇	1.1567	run56	9/1.14/50%

Figure 7.2.2.390: Cowl Effects (CR=9, Re=1.14million/ft) Baseplate Pressures



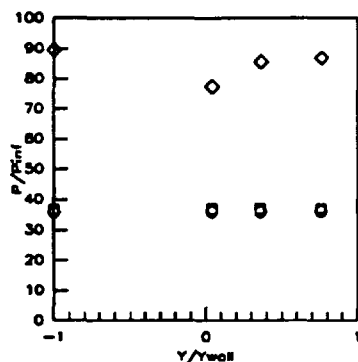
Sym	x'/Ts'	Run No.	CR/Re/Cowl (millions)
○	1.2408	run48	9/1.14/0%
□	1.2408	run52	9/1.14/25%
◇	1.2408	run56	9/1.14/50%

Figure 7.2.2.391: Cowl Effects (CR=9, Re=1.14million/ft) Baseplate Pressures



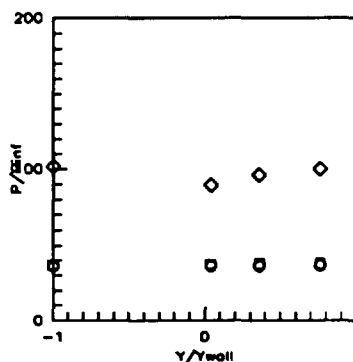
Sym	x'/Ts'	Run No.	CR/Re/Cowl (millions)
○	1.3249	run48	9/1.14/0%
□	1.3249	run52	9/1.14/25%
◇	1.3249	run56	9/1.14/50%

Figure 7.2.2.392: Cowl Effects (CR=9, Re=1.14million/ft) Baseplate Pressures



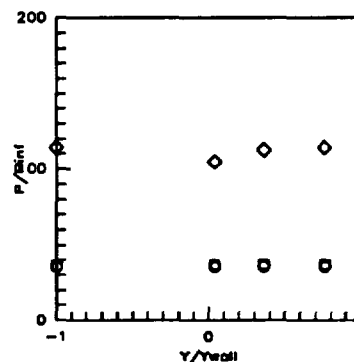
Sym	x'/Ts'	Run No.	CR/Re/Cowl (millions)
○	1.4090	run48	9/1.14/0%
□	1.4090	run52	9/1.14/25%
◇	1.4090	run56	9/1.14/50%

Figure 7.2.2.393: Cowl Effects (CR=9, Re=1.14million/ft) Baseplate Pressures



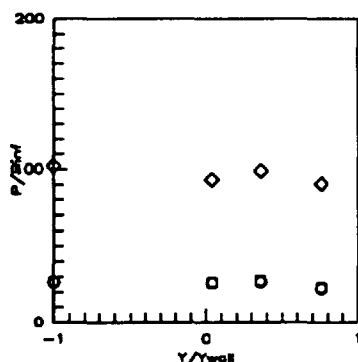
Sym	x'/Ts'	Run No.	CR/Re/Cowl (millions)
○	1.4932	run48	9/1.14/0%
□	1.4932	run52	9/1.14/25%
◇	1.4932	run56	9/1.14/50%

Figure 7.2.2.394: Cowl Effects (CR=9, Re=1.14million/ft) Baseplate Pressures



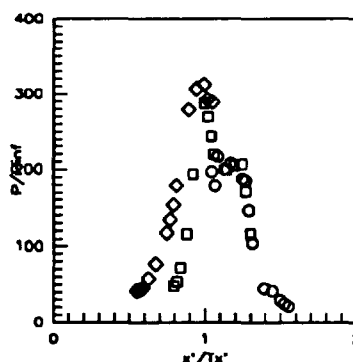
Sym	x'/Ts'	Run No.	CR/Re/Cowl (millions)
○	1.5773	run48	9/1.14/0%
□	1.5773	run52	9/1.14/25%
◇	1.5773	run56	9/1.14/50%

Figure 7.2.2.395: Cowl Effects (CR=9, Re=1.14million/ft) Baseplate Pressures



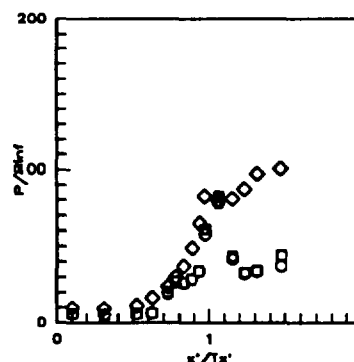
Sym	x'/Ts'	Run No.	CR/Re/Cowl (millions)
○	1.6824	run48	9/1.14/0%
□	1.6824	run52	9/1.14/25%
◇	1.6824	run56	9/1.14/50%

Figure 7.2.2.396: Cowl Effects (CR=9, Re=1.14million/ft) Baseplate Pressures



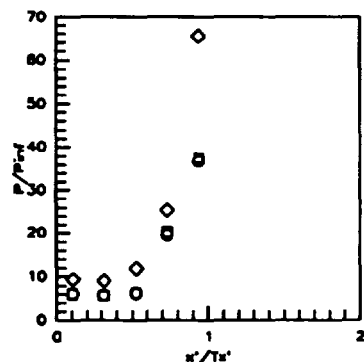
Sym	Cowl Pos.	Run No.	CR/Re/Cowl (millions)
○	0%	run48	9/1.14/0%
□	25%	run52	9/1.14/25%
◇	50%	run56	9/1.14/50%

Figure 7.2.2.397: Cowl Effects (CR=9, Re=1.14million/ft) Cowl Pressures



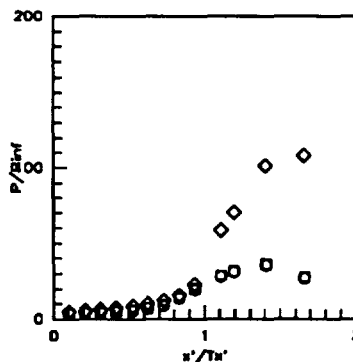
Sym	Z/H	Run No.	CR/Re/Cowl (millions)
○	0.5RT	run48	9/1.14/0%
□	0.5RT	run52	9/1.14/25%
◇	0.5RT	run56	9/1.14/50%

Figure 7.2.2.398: Cowl Effects (CR=9, Re=1.14million/ft) Sidewall Centerline Pressures



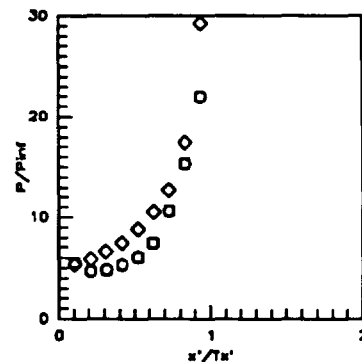
Sym	Z/H	Run	CR/Re/Cowl
○	0.5LT	run48	9/1.14/0%
□	0.5LT	run52	9/1.14/25%
◇	0.5LT	run56	9/1.14/50%

Figure 7.2.2.399: Cowl Effects  
(CR=9, Re=1.14million/ft)  
Sidewall Centerline Pressures



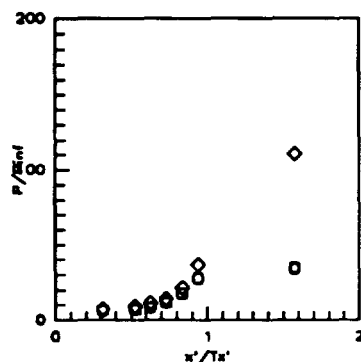
Sym	Z/H	Run	CR/Re/Cowl
○	0.05	run48	9/1.14/0%
□	0.05	run52	9/1.14/25%
◇	0.05	run56	9/1.14/50%

Figure 7.2.2.400: Cowl Effects  
(CR=9, Re=1.14million/ft)  
Sidewall Pressures



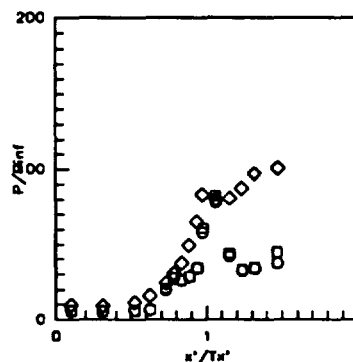
Sym	Z/H	Run	CR/Re/Cowl
○	0.15	run48	9/1.14/0%
□	0.15	run52	9/1.14/25%
◇	0.15	run56	9/1.14/50%

Figure 7.2.2.401: Cowl Effects  
(CR=9, Re=1.14million/ft)  
Sidewall Pressures



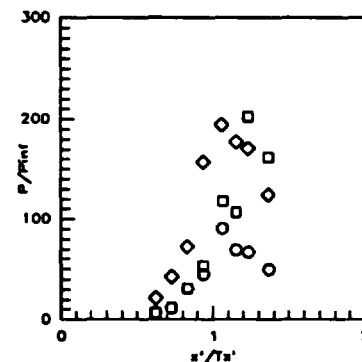
Sym	Z/H	Run	CR/Re/Cowl
○	0.25	run48	9/1.14/0%
□	0.25	run52	9/1.14/25%
◇	0.25	run56	9/1.14/50%

Figure 7.2.2.402: Cowl Effects  
(CR=9, Re=1.14million/ft)  
Sidewall Pressures



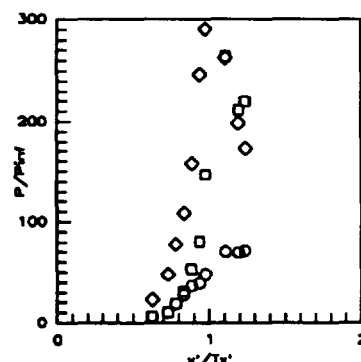
Sym	Z/H	Run	CR/Re/Cowl
○	0.50	run48	9/1.14/0%
□	0.50	run52	9/1.14/25%
◇	0.50	run56	9/1.14/50%

Figure 7.2.2.403: Cowl Effects  
(CR=9, Re=1.14million/ft)  
Sidewall Pressures



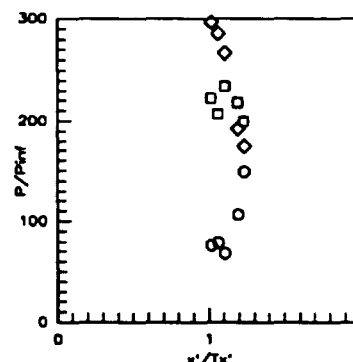
Sym	Z/H	Run	CR/Re/Cowl
○	0.75	run48	9/1.14/0%
□	0.75	run52	9/1.14/25%
◇	0.75	run56	9/1.14/50%

Figure 7.2.2.404: Cowl Effects  
(CR=9, Re=1.14million/ft)  
Sidewall Pressures



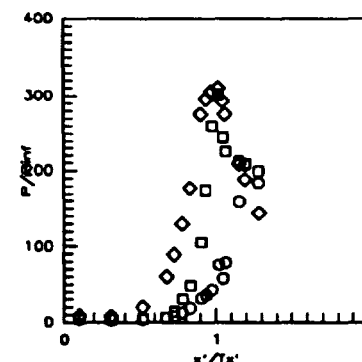
Sym	Z/H	Run	CR/Re/Cowl
○	0.85	run48	9/1.14/0%
□	0.85	run52	9/1.14/25%
◇	0.85	run56	9/1.14/50%

Figure 7.2.2.405: Cowl Effects  
(CR=9, Re=1.14million/ft)  
Sidewall Pressures



Sym	Z/H	Run	CR/Re/Cowl
○	0.90	run48	9/1.14/0%
□	0.90	run52	9/1.14/25%
◇	0.90	run56	9/1.14/50%

Figure 7.2.2.406: Cowl Effects  
(CR=9, Re=1.14million/ft)  
Sidewall Pressures



Sym	Z/H	Run	CR/Re/Cowl
○	0.95	run48	9/1.14/0%
□	0.95	run52	9/1.14/25%
◇	0.95	run56	9/1.14/50%

Figure 7.2.2.407: Cowl Effects  
(CR=9, Re=1.14million/ft)  
Sidewall Pressures

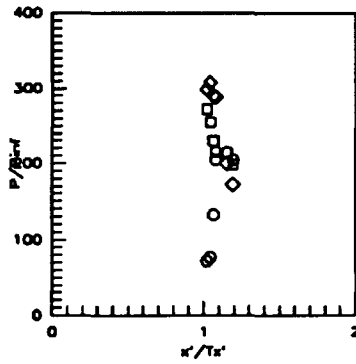


Figure 7.2.2.408: Cowl Effects (CR=9, Re=1.14million/ft) Sidewall Pressures

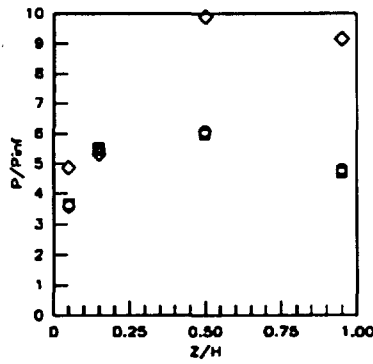


Figure 7.2.2.409: Cowl Effects (CR=9, Re=1.14million/ft) Sidewall Pressures

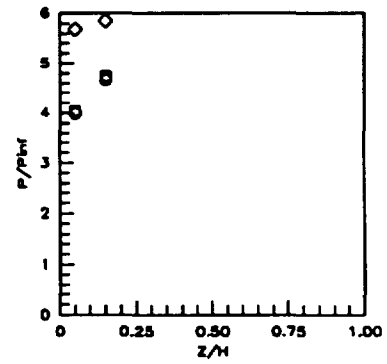


Figure 7.2.2.410: Cowl Effects (CR=9, Re=1.14million/ft) Sidewall Pressures

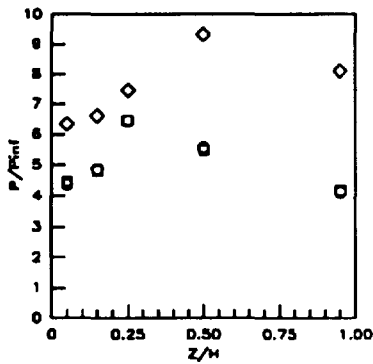


Figure 7.2.2.411: Cowl Effects (CR=9, Re=1.14million/ft) Sidewall Pressures

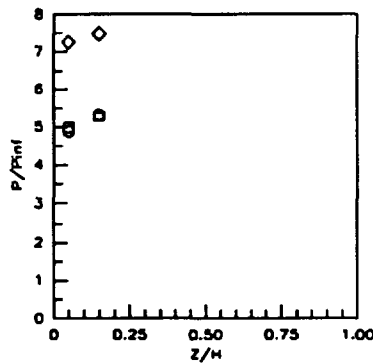


Figure 7.2.2.412: Cowl Effects (CR=9, Re=1.14million/ft) Sidewall Pressures

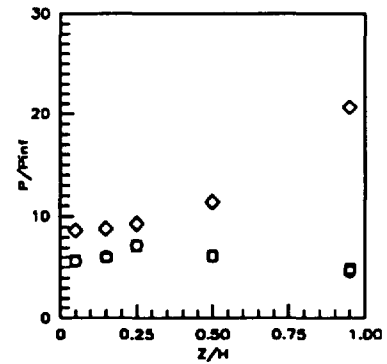


Figure 7.2.2.413: Cowl Effects (CR=9, Re=1.14million/ft) Sidewall Pressures

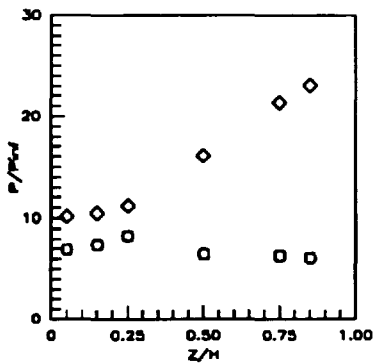


Figure 7.2.2.414: Cowl Effects (CR=9, Re=1.14million/ft) Sidewall Pressures

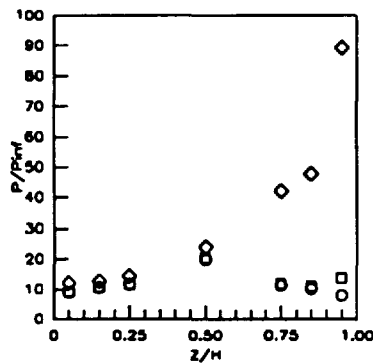


Figure 7.2.2.415: Cowl Effects (CR=9, Re=1.14million/ft) Sidewall Pressures

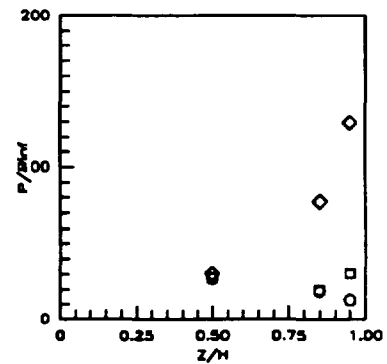
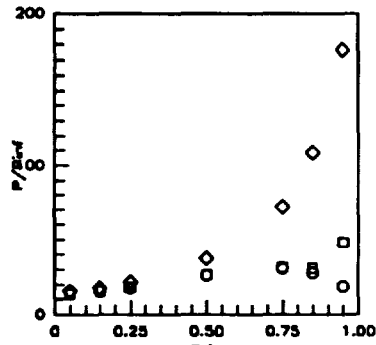
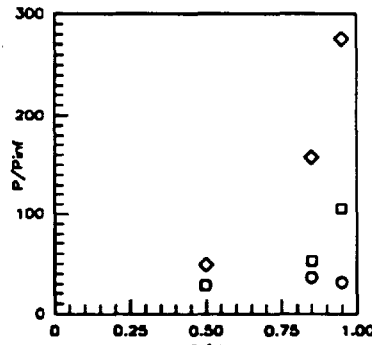


Figure 7.2.2.416: Cowl Effects (CR=9, Re=1.14million/ft) Sidewall Pressures



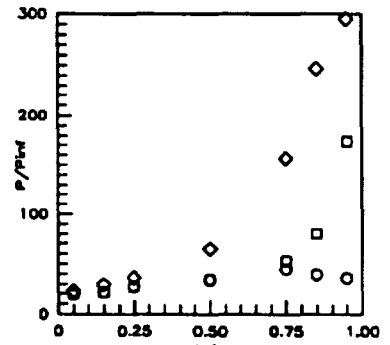
Sym	$x'/T_x'$	Run No.	CR/Re/Cowl (millions)
○	0.8336	run48	9/1.14/0%
□	0.8336	run52	9/1.14/25%
◇	0.8336	run56	9/1.14/50%

Figure 7.2.2.417: Cowl Effects (CR=9, Re=1.14million/ft) Sidewall Pressures



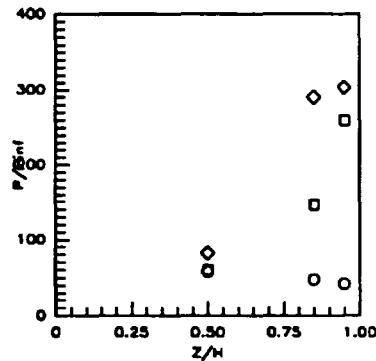
Sym	$x'/T_x'$	Run No.	CR/Re/Cowl (millions)
○	0.8857	run48	9/1.14/0%
□	0.8857	run52	9/1.14/25%
◇	0.8857	run56	9/1.14/50%

Figure 7.2.2.418: Cowl Effects (CR=9, Re=1.14million/ft) Sidewall Pressures



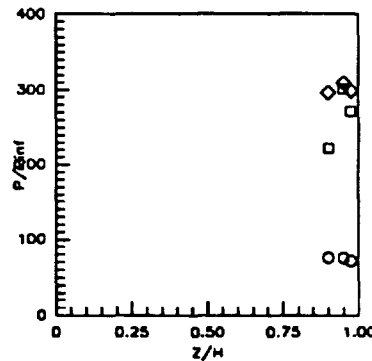
Sym	$x'/T_x'$	Run No.	CR/Re/Cowl (millions)
○	0.9378	run48	9/1.14/0%
□	0.9378	run52	9/1.14/25%
◇	0.9378	run56	9/1.14/50%

Figure 7.2.2.419: Cowl Effects (CR=9, Re=1.14million/ft) Sidewall Pressures



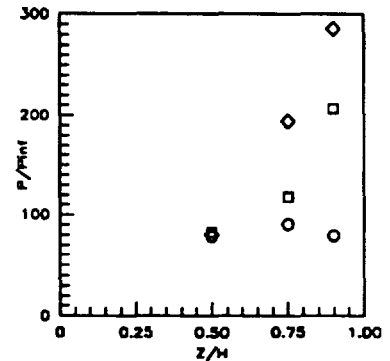
Sym	$x'/T_x'$	Run No.	CR/Re/Cowl (millions)
○	0.9751	run48	9/1.14/0%
□	0.9751	run52	9/1.14/25%
◇	0.9751	run56	9/1.14/50%

Figure 7.2.2.420: Cowl Effects (CR=9, Re=1.14million/ft) Sidewall Pressures



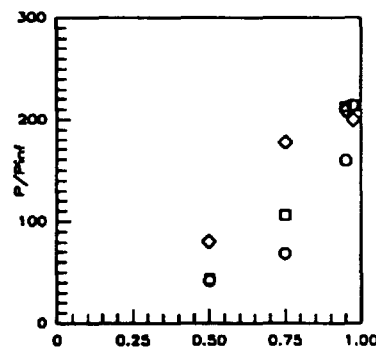
Sym	$x'/T_x'$	Run No.	CR/Re/Cowl (millions)
○	1.0197	run48	9/1.14/0%
□	1.0197	run52	9/1.14/25%
◇	1.0197	run56	9/1.14/50%

Figure 7.2.2.421: Cowl Effects (CR=9, Re=1.14million/ft) Sidewall Pressures



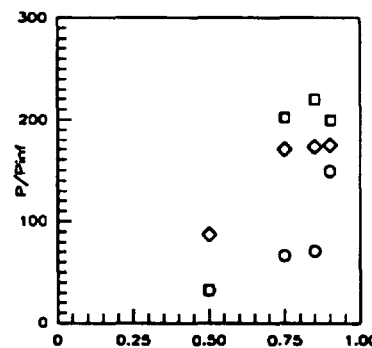
Sym	$x'/T_x'$	Run No.	CR/Re/Cowl (millions)
○	1.0843	run48	9/1.14/0%
□	1.0843	run52	9/1.14/25%
◇	1.0843	run56	9/1.14/50%

Figure 7.2.2.422: Cowl Effects (CR=9, Re=1.14million/ft) Sidewall Pressures



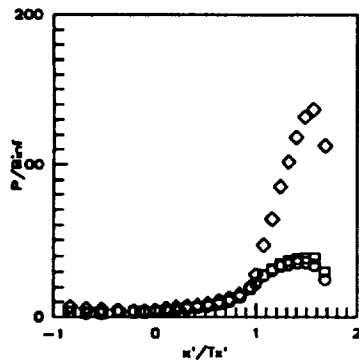
Sym	$x'/T_x'$	Run No.	CR/Re/Cowl (millions)
○	1.1537	run48	9/1.14/0%
□	1.1537	run52	9/1.14/25%
◇	1.1537	run56	9/1.14/50%

Figure 7.2.2.423: Cowl Effects (CR=9, Re=1.14million/ft) Sidewall Pressures



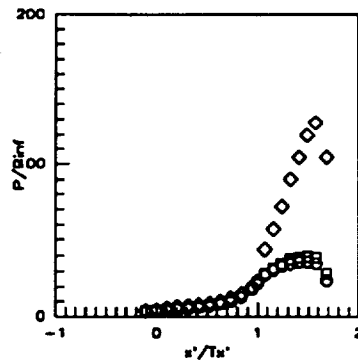
Sym	$x'/T_x'$	Run No.	CR/Re/Cowl (millions)
○	1.2356	run48	9/1.14/0%
□	1.2356	run52	9/1.14/25%
◇	1.2356	run56	9/1.14/50%

Figure 7.2.2.424: Cowl Effects (CR=9, Re=1.14million/ft) Sidewall Pressures



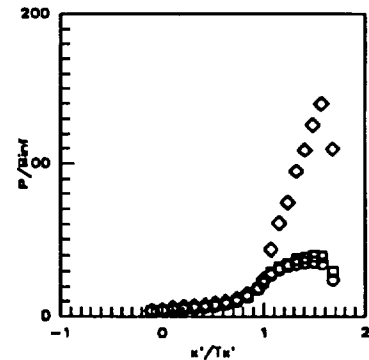
Sym	C.L. for	Run No.	CR/Re/Cowl (millions)
○	CR=3	run47	9/0.55/0%
□	CR=3	run50	9/0.55/25%
◇	CR=3	run55	9/0.55/50%

Figure 7.2.2.425: Cowl Effects (CR=9, Re=0.55million/ft) CR=3 Centerline Pressures



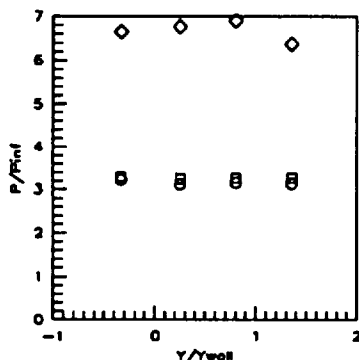
Sym	C.L. for	Run No.	CR/Re/Cowl (millions)
○	CR=5	run47	9/0.55/0%
□	CR=5	run50	9/0.55/25%
◇	CR=5	run55	9/0.55/50%

Figure 7.2.2.426: Cowl Effects (CR=9, Re=0.55million/ft) CR=5 Centerline Pressures



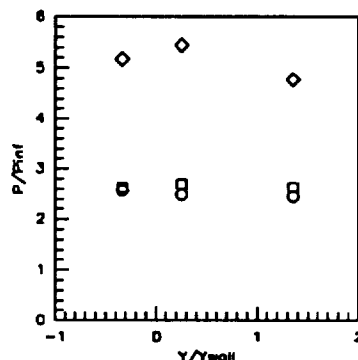
Sym	C.L. for	Run No.	CR/Re/Cowl (millions)
○	CR=9	run47	9/0.55/0%
□	CR=9	run50	9/0.55/25%
◇	CR=9	run55	9/0.55/50%

Figure 7.2.2.427: Cowl Effects (CR=9, Re=0.55million/ft) CR=9 Centerline Pressures



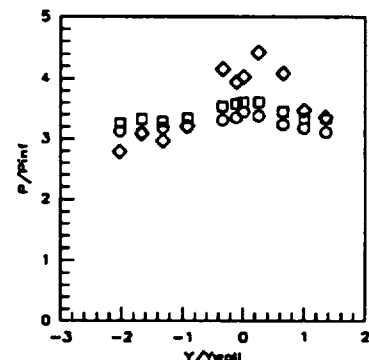
Sym	x'/Ts'	Run No.	CR/Re/Cowl (millions)
○	-0.8412	run47	9/0.55/0%
□	-0.8412	run50	9/0.55/25%
◇	-0.8412	run55	9/0.55/50%

Figure 7.2.2.428: Cowl Effects (CR=9, Re=0.55million/ft) Baseplate Pressures



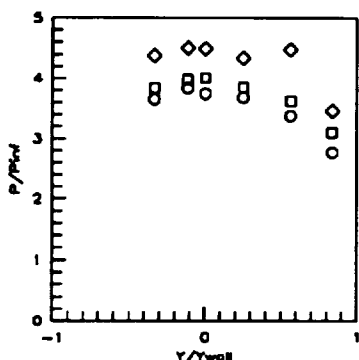
Sym	x'/Ts'	Run No.	CR/Re/Cowl (millions)
○	-0.5258	run47	9/0.55/0%
□	-0.5258	run50	9/0.55/25%
◇	-0.5258	run55	9/0.55/50%

Figure 7.2.2.429: Cowl Effects (CR=9, Re=0.55million/ft) Baseplate Pressures



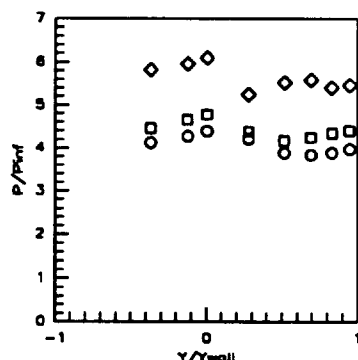
Sym	x'/Ts'	Run No.	CR/Re/Cowl (millions)
○	-0.1052	run47	9/0.55/0%
□	-0.1052	run50	9/0.55/25%
◇	-0.1052	run55	9/0.55/50%

Figure 7.2.2.430: Cowl Effects (CR=9, Re=0.55million/ft) Baseplate Pressures



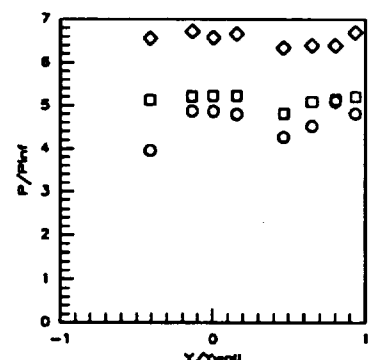
Sym	x'/Ts'	Run No.	CR/Re/Cowl (millions)
○	0.0000	run47	9/0.55/0%
□	0.0000	run50	9/0.55/25%
◇	0.0000	run55	9/0.55/50%

Figure 7.2.2.431: Cowl Effects (CR=9, Re=0.55million/ft) Baseplate Pressures



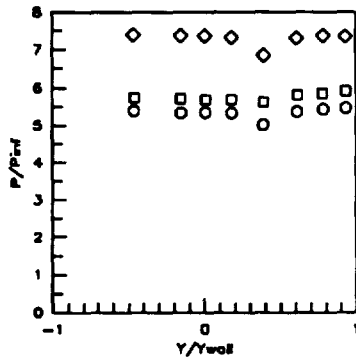
Sym	x'/Ts'	Run No.	CR/Re/Cowl (millions)
○	0.1052	run47	9/0.55/0%
□	0.1052	run50	9/0.55/25%
◇	0.1052	run55	9/0.55/50%

Figure 7.2.2.432: Cowl Effects (CR=9, Re=0.55million/ft) Baseplate Pressures



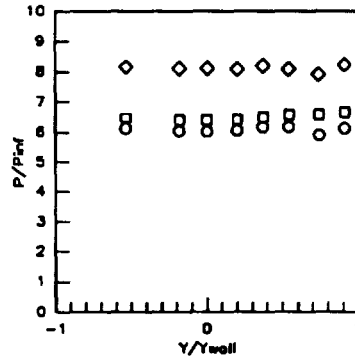
Sym	x'/Ts'	Run No.	CR/Re/Cowl (millions)
○	0.2103	run47	9/0.55/0%
□	0.2103	run50	9/0.55/25%
◇	0.2103	run55	9/0.55/50%

Figure 7.2.2.433: Cowl Effects (CR=9, Re=0.55million/ft) Baseplate Pressures



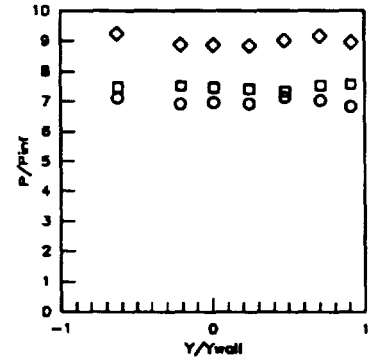
Sym	x'/Ts'	Run No.	CR/Re/Cowl (millions)
○	0.3154	run47	9/0.55/ 0%
□	0.3154	run50	9/0.55/25%
◇	0.3154	run55	9/0.55/50%

Figure 7.2.2.434: Cowl Effects (CR=9, Re=0.55million/ft) Baseplate Pressures



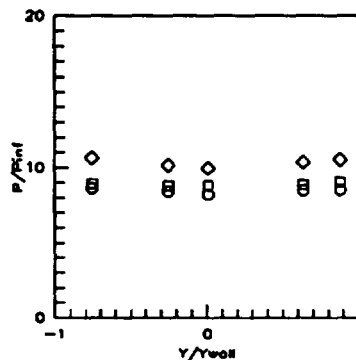
Sym	x'/Ts'	Run No.	CR/Re/Cowl (millions)
○	0.4206	run47	9/0.55/ 0%
□	0.4206	run50	9/0.55/25%
◇	0.4206	run55	9/0.55/50%

Figure 7.2.2.435: Cowl Effects (CR=9, Re=0.55million/ft) Baseplate Pressures



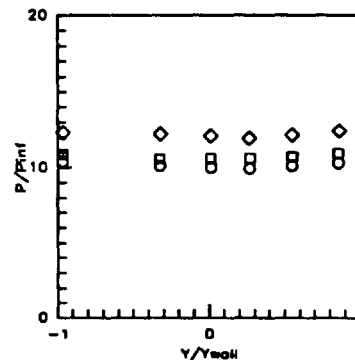
Sym	x'/Ts'	Run No.	CR/Re/Cowl (millions)
○	0.5258	run47	9/0.55/ 0%
□	0.5258	run50	9/0.55/25%
◇	0.5258	run55	9/0.55/50%

Figure 7.2.2.436: Cowl Effects (CR=9, Re=0.55million/ft) Baseplate Pressures



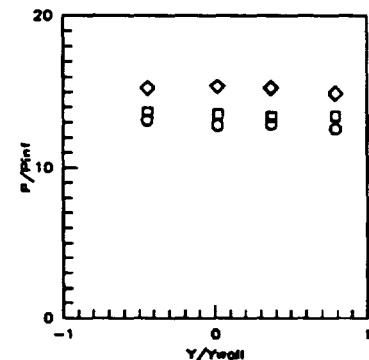
Sym	x'/Ts'	Run No.	CR/Re/Cowl (millions)
○	0.6309	run47	9/0.55/ 0%
□	0.6309	run50	9/0.55/25%
◇	0.6309	run55	9/0.55/50%

Figure 7.2.2.437: Cowl Effects (CR=9, Re=0.55million/ft) Baseplate Pressures



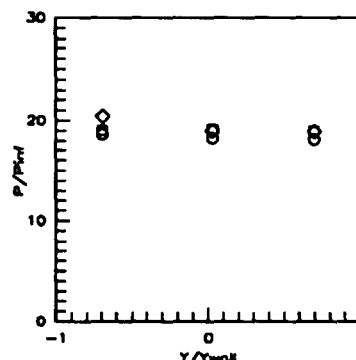
Sym	x'/Ts'	Run No.	CR/Re/Cowl (millions)
○	0.7361	run47	9/0.55/ 0%
□	0.7361	run50	9/0.55/25%
◇	0.7361	run55	9/0.55/50%

Figure 7.2.2.438: Cowl Effects (CR=9, Re=0.55million/ft) Baseplate Pressures



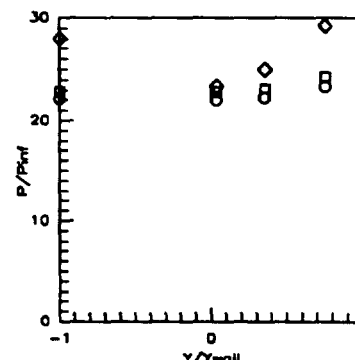
Sym	x'/Ts'	Run No.	CR/Re/Cowl (millions)
○	0.8412	run47	9/0.55/ 0%
□	0.8412	run50	9/0.55/25%
◇	0.8412	run55	9/0.55/50%

Figure 7.2.2.439: Cowl Effects (CR=9, Re=0.55million/ft) Baseplate Pressures



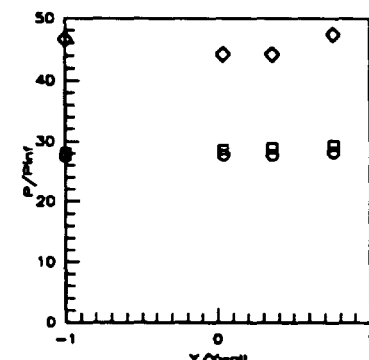
Sym	x'/Ts'	Run No.	CR/Re/Cowl (millions)
○	0.9464	run47	9/0.55/ 0%
□	0.9464	run50	9/0.55/25%
◇	0.9464	run55	9/0.55/50%

Figure 7.2.2.440: Cowl Effects (CR=9, Re=0.55million/ft) Baseplate Pressures



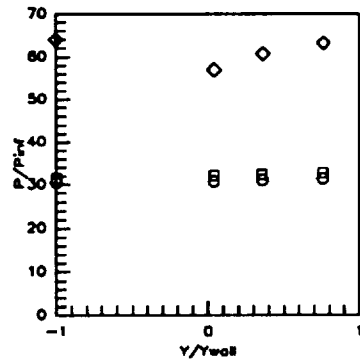
Sym	x'/Ts'	Run No.	CR/Re/Cowl (millions)
○	1.0000	run47	9/0.55/ 0%
□	1.0000	run50	9/0.55/25%
◇	1.0000	run55	9/0.55/50%

Figure 7.2.2.441: Cowl Effects (CR=9, Re=0.55million/ft) Baseplate Pressures



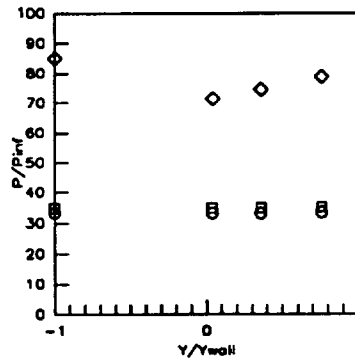
Sym	x'/Ts'	Run No.	CR/Re/Cowl (millions)
○	1.0726	run47	9/0.55/ 0%
□	1.0726	run50	9/0.55/25%
◇	1.0726	run55	9/0.55/50%

Figure 7.2.2.442: Cowl Effects (CR=9, Re=0.55million/ft) Baseplate Pressures



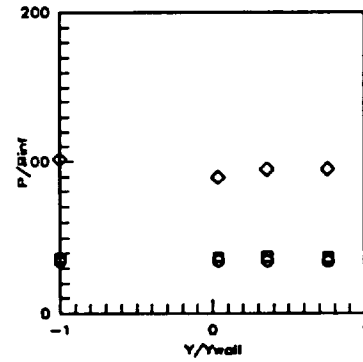
Sym	x'/Tx'	Run No.	CR/Re/Cowl (millions)
○	1.1567	run47	9/0.55/ 0%
□	1.1567	run50	9/0.55/25%
◇	1.1567	run55	9/0.55/50%

Figure 7.2.2.443: Cowl Effects (CR=9, Re=0.55million/ft) Baseplate Pressures



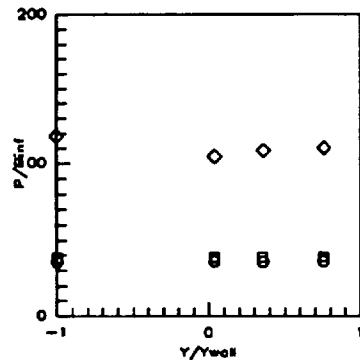
Sym	x'/Tx'	Run No.	CR/Re/Cowl (millions)
○	1.2408	run47	9/0.55/ 0%
□	1.2408	run50	9/0.55/25%
◇	1.2408	run55	9/0.55/50%

Figure 7.2.2.444: Cowl Effects (CR=9, Re=0.55million/ft) Baseplate Pressures



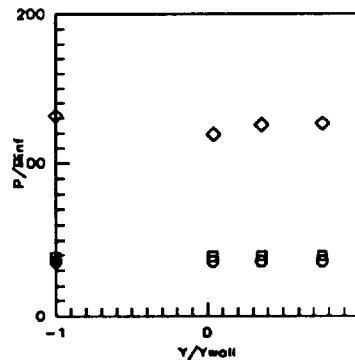
Sym	x'/Tx'	Run No.	CR/Re/Cowl (millions)
○	1.3249	run47	9/0.55/ 0%
□	1.3249	run50	9/0.55/25%
◇	1.3249	run55	9/0.55/50%

Figure 7.2.2.445: Cowl Effects (CR=9, Re=0.55million/ft) Baseplate Pressures



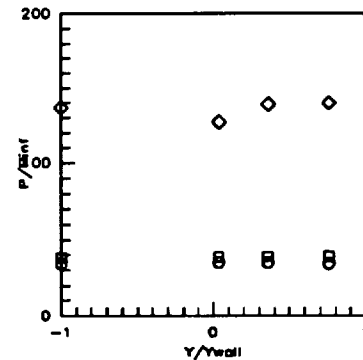
Sym	x'/Tx'	Run No.	CR/Re/Cowl (millions)
○	1.4090	run47	9/0.55/ 0%
□	1.4090	run50	9/0.55/25%
◇	1.4090	run55	9/0.55/50%

Figure 7.2.2.446: Cowl Effects (CR=9, Re=0.55million/ft) Baseplate Pressures



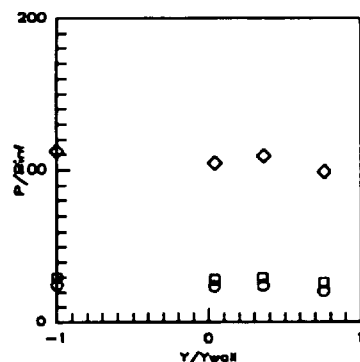
Sym	x'/Tx'	Run No.	CR/Re/Cowl (millions)
○	1.4832	run47	9/0.55/ 0%
□	1.4832	run50	9/0.55/25%
◇	1.4832	run55	9/0.55/50%

Figure 7.2.2.447: Cowl Effects (CR=9, Re=0.55million/ft) Baseplate Pressures



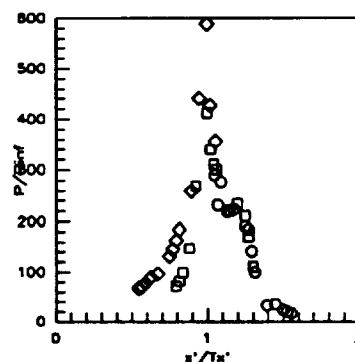
Sym	x'/Tx'	Run No.	CR/Re/Cowl (millions)
○	1.5773	run47	9/0.55/ 0%
□	1.5773	run50	9/0.55/25%
◇	1.5773	run55	9/0.55/50%

Figure 7.2.2.448: Cowl Effects (CR=9, Re=0.55million/ft) Baseplate Pressures



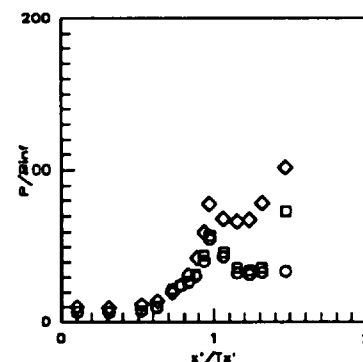
Sym	x'/Tx'	Run No.	CR/Re/Cowl (millions)
○	1.6824	run47	9/0.55/ 0%
□	1.6824	run50	9/0.55/25%
◇	1.6824	run55	9/0.55/50%

Figure 7.2.2.449: Cowl Effects (CR=9, Re=0.55million/ft) Baseplate Pressures



Sym	Cowl Pos.	Run No.	CR/Re/Cowl (millions)
○	0%	run47	9/0.55/ 0%
□	25%	run50	9/0.55/25%
◇	50%	run55	9/0.55/50%

Figure 7.2.2.450: Cowl Effects (CR=9, Re=0.55million/ft) Cowl Pressures



Sym	Z/H	Run No.	CR/Re/Cowl (millions)
○	0.5RT.	run47	9/0.55/ 0%
□	0.5RT.	run50	9/0.55/25%
◇	0.5RT.	run55	9/0.55/50%

Figure 7.2.2.451: Cowl Effects (CR=9, Re=0.55million/ft) Sidewall Centerline Pressures

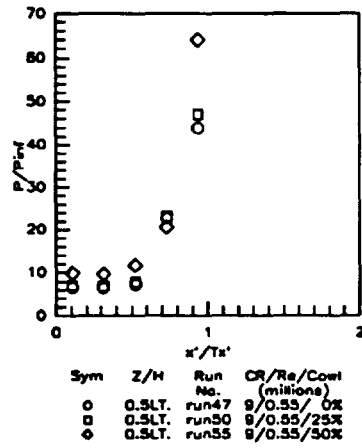


Figure 7.2.2.452: Cowl Effects (CR=9, Re=0.55million/ft) Sidewall Centerline Pressures

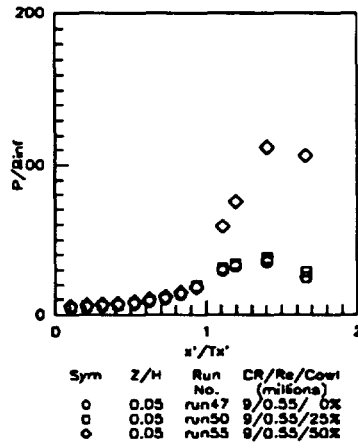


Figure 7.2.2.453: Cowl Effects (CR=9, Re=0.55million/ft) Sidewall Pressures

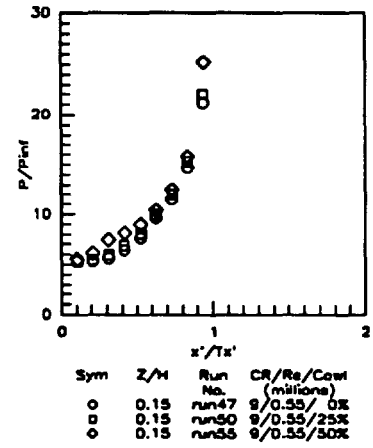


Figure 7.2.2.454: Cowl Effects (CR=9, Re=0.55million/ft) Sidewall Pressures

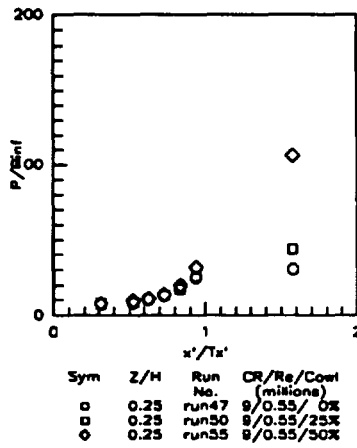


Figure 7.2.2.455: Cowl Effects (CR=9, Re=0.55million/ft) Sidewall Pressures

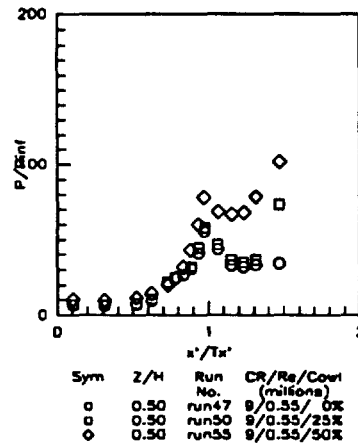


Figure 7.2.2.456: Cowl Effects (CR=9, Re=0.55million/ft) Sidewall Pressures

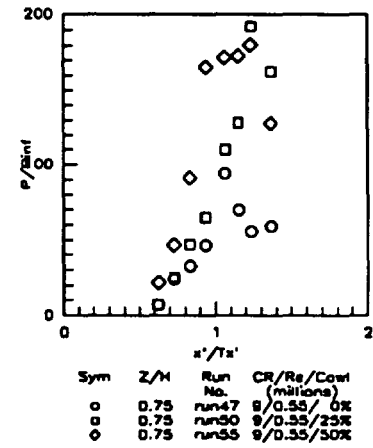


Figure 7.2.2.457: Cowl Effects (CR=9, Re=0.55million/ft) Sidewall Pressures

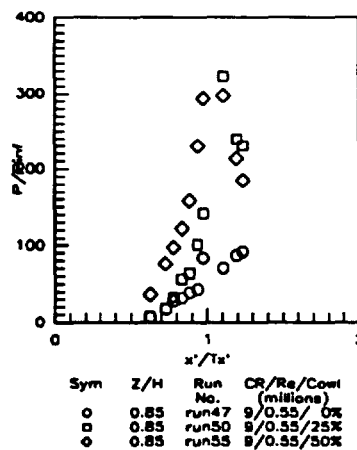


Figure 7.2.2.458: Cowl Effects (CR=9, Re=0.55million/ft) Sidewall Pressures

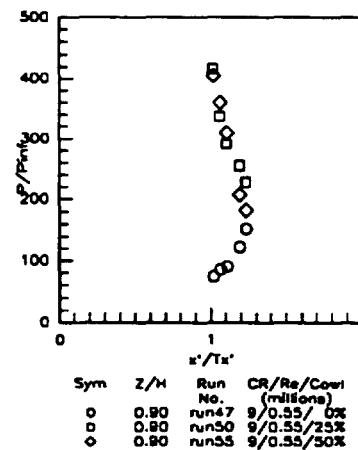


Figure 7.2.2.459: Cowl Effects (CR=9, Re=0.55million/ft) Sidewall Pressures

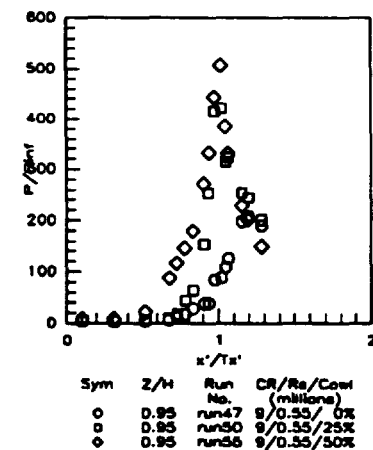
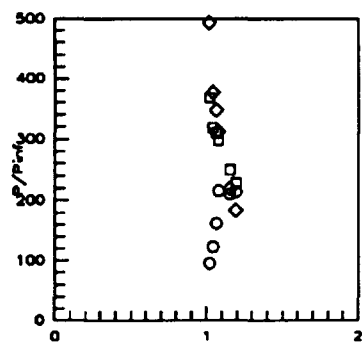


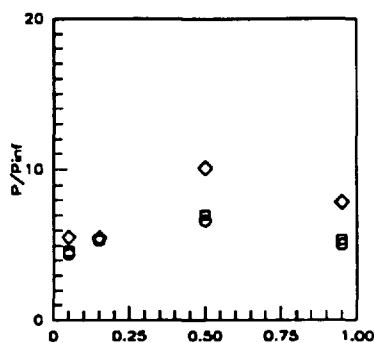
Figure 7.2.2.460: Cowl Effects (CR=9, Re=0.55million/ft) Sidewall Pressures





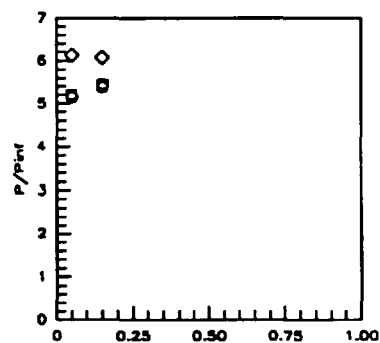
Sym	$x'/T_x'$	Run No.	CR/Re/Cowl (millions)
○	0.975	run47	9/0.55/0%
□	0.975	run50	9/0.55/25%
◇	0.975	run55	9/0.55/50%

Figure 7.2.2.461: Cowl Effects (CR=9, Re=0.55million/ft) Sidewall Pressures



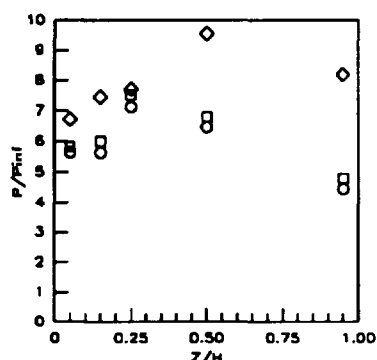
Sym	$x'/T_x'$	Run No.	CR/Re/Cowl (millions)
○	0.1042	run47	9/0.55/0%
□	0.1042	run50	9/0.55/25%
◇	0.1042	run55	9/0.55/50%

Figure 7.2.2.462: Cowl Effects (CR=9, Re=0.55million/ft) Sidewall Pressures



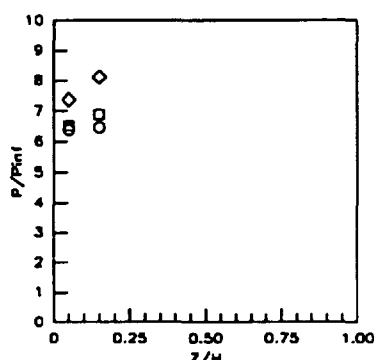
Sym	$x'/T_x'$	Run No.	CR/Re/Cowl (millions)
○	0.2083	run47	9/0.55/0%
□	0.2083	run50	9/0.55/25%
◇	0.2083	run55	9/0.55/50%

Figure 7.2.2.463: Cowl Effects (CR=9, Re=0.55million/ft) Sidewall Pressures



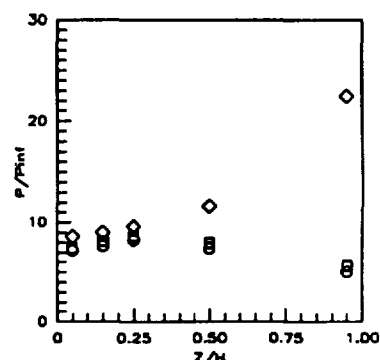
Sym	$x'/T_x'$	Run No.	CR/Re/Cowl (millions)
○	0.3125	run47	9/0.55/0%
□	0.3125	run50	9/0.55/25%
◇	0.3125	run55	9/0.55/50%

Figure 7.2.2.464: Cowl Effects (CR=9, Re=0.55million/ft) Sidewall Pressures



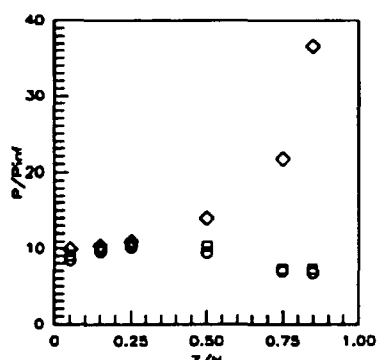
Sym	$x'/T_x'$	Run No.	CR/Re/Cowl (millions)
○	0.4167	run47	9/0.55/0%
□	0.4167	run50	9/0.55/25%
◇	0.4167	run55	9/0.55/50%

Figure 7.2.2.465: Cowl Effects (CR=9, Re=0.55million/ft) Sidewall Pressures



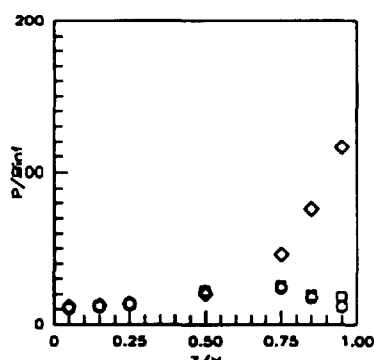
Sym	$x'/T_x'$	Run No.	CR/Re/Cowl (millions)
○	0.5259	run47	9/0.55/0%
□	0.5259	run50	9/0.55/25%
◇	0.5259	run55	9/0.55/50%

Figure 7.2.2.466: Cowl Effects (CR=9, Re=0.55million/ft) Sidewall Pressures



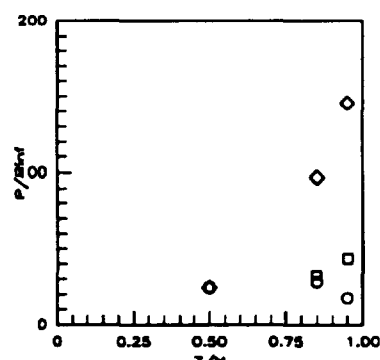
Sym	$x'/T_x'$	Run No.	CR/Re/Cowl (millions)
○	0.6252	run47	9/0.55/0%
□	0.6252	run50	9/0.55/25%
◇	0.6252	run55	9/0.55/50%

Figure 7.2.2.467: Cowl Effects (CR=9, Re=0.55million/ft) Sidewall Pressures



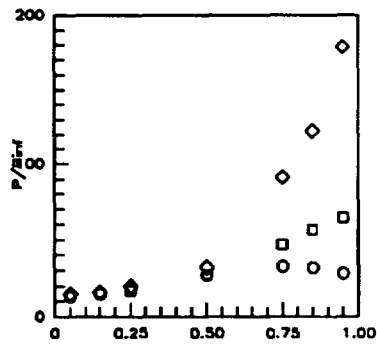
Sym	$x'/T_x'$	Run No.	CR/Re/Cowl (millions)
○	0.7294	run47	9/0.55/0%
□	0.7294	run50	9/0.55/25%
◇	0.7294	run55	9/0.55/50%

Figure 7.2.2.468: Cowl Effects (CR=9, Re=0.55million/ft) Sidewall Pressures



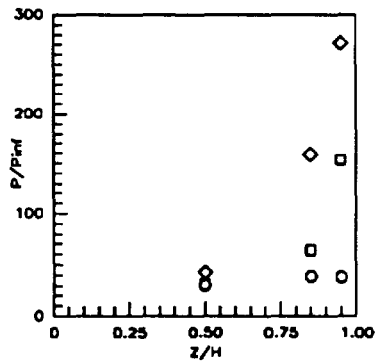
Sym	$x'/T_x'$	Run No.	CR/Re/Cowl (millions)
○	0.7815	run47	9/0.55/0%
□	0.7815	run50	9/0.55/25%
◇	0.7815	run55	9/0.55/50%

Figure 7.2.2.469: Cowl Effects (CR=9, Re=0.55million/ft) Sidewall Pressures



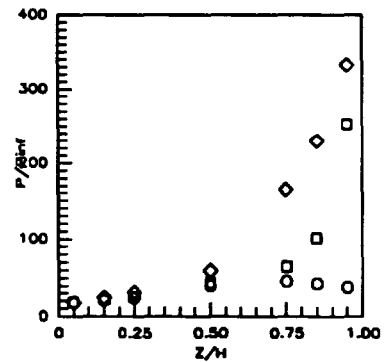
Sym	$x'/T_x'$	Run No.	CR/Re/Cowl (millions)
○	0.8336	run47	9/0.55/0%
□	0.8336	run50	9/0.55/25%
◇	0.8336	run55	9/0.55/50%

Figure 7.2.2.470: Cowl Effects (CR=9, Re=0.55million/ft) Sidewall Pressures



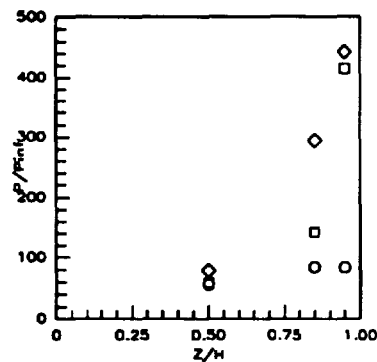
Sym	$x'/T_x'$	Run No.	CR/Re/Cowl (millions)
○	0.8857	run47	9/0.55/0%
□	0.8857	run50	9/0.55/25%
◇	0.8857	run55	9/0.55/50%

Figure 7.2.2.471: Cowl Effects (CR=9, Re=0.55million/ft) Sidewall Pressures



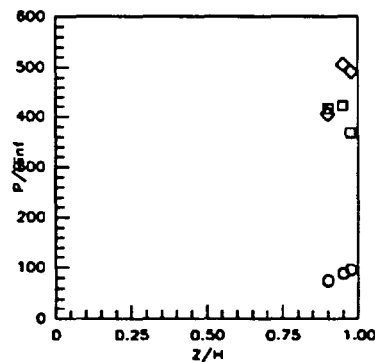
Sym	$x'/T_x'$	Run No.	CR/Re/Cowl (millions)
○	0.9378	run47	9/0.55/0%
□	0.9378	run50	9/0.55/25%
◇	0.9378	run55	9/0.55/50%

Figure 7.2.2.472: Cowl Effects (CR=9, Re=0.55million/ft) Sidewall Pressures



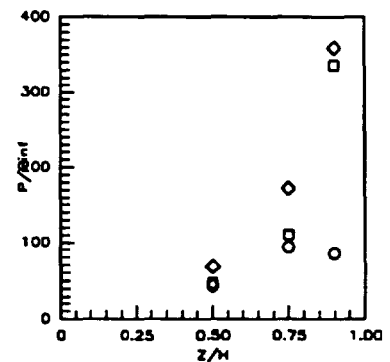
Sym	$x'/T_x'$	Run No.	CR/Re/Cowl (millions)
○	0.9751	run47	9/0.55/0%
□	0.9751	run50	9/0.55/25%
◇	0.9751	run55	9/0.55/50%

Figure 7.2.2.473: Cowl Effects (CR=9, Re=0.55million/ft) Sidewall Pressures



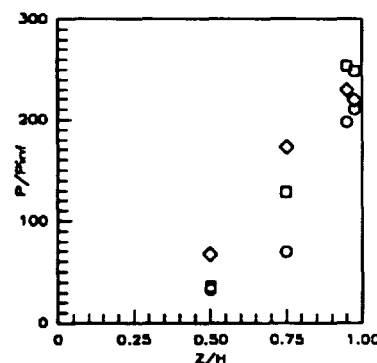
Sym	$x'/T_x'$	Run No.	CR/Re/Cowl (millions)
○	1.0197	run47	9/0.55/0%
□	1.0197	run50	9/0.55/25%
◇	1.0197	run55	9/0.55/50%

Figure 7.2.2.474: Cowl Effects (CR=9, Re=0.55million/ft) Sidewall Pressures



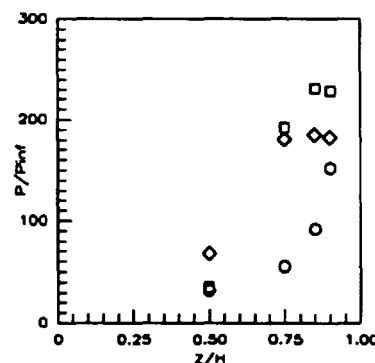
Sym	$x'/T_x'$	Run No.	CR/Re/Cowl (millions)
○	1.0643	run47	9/0.55/0%
□	1.0643	run50	9/0.55/25%
◇	1.0643	run55	9/0.55/50%

Figure 7.2.2.475: Cowl Effects (CR=9, Re=0.55million/ft) Sidewall Pressures



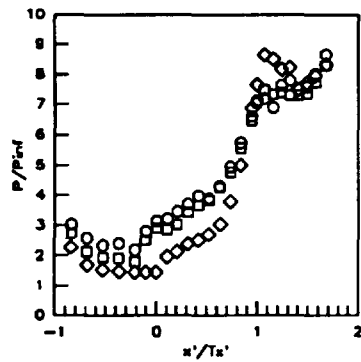
Sym	$x'/T_x'$	Run No.	CR/Re/Cowl (millions)
○	1.1537	run47	9/0.55/0%
□	1.1537	run50	9/0.55/25%
◇	1.1537	run55	9/0.55/50%

Figure 7.2.2.476: Cowl Effects (CR=9, Re=0.55million/ft) Sidewall Pressures



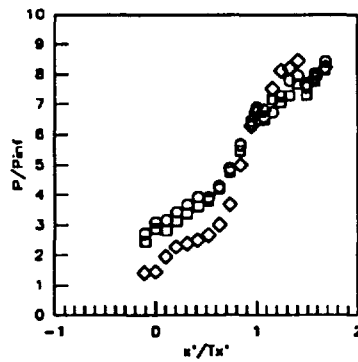
Sym	$x'/T_x'$	Run No.	CR/Re/Cowl (millions)
○	1.2356	run47	9/0.55/0%
□	1.2356	run50	9/0.55/25%
◇	1.2356	run55	9/0.55/50%

Figure 7.2.2.477: Cowl Effects (CR=9, Re=0.55million/ft) Sidewall Pressures



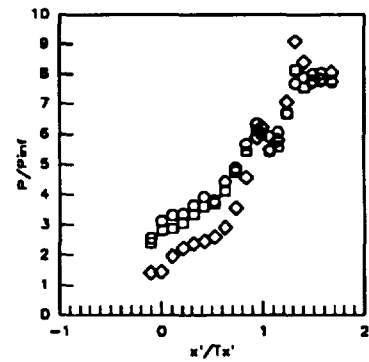
Sym	C.L. for	Run No.	CR/Re/Cowl (millions)
○	CR=3	run84	3/0.55/ 0%
□	CR=3	run85	3/1.14/ 0%
◇	CR=3	run86	3/2.15/ 0%

Figure 7.2.3.1: Re Effects  
(CR=3, 0% CowI)  
CR=3 Centerline Pressures



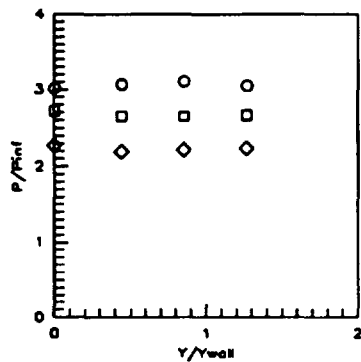
Sym	C.L. for	Run No.	CR/Re/Cowl (millions)
○	CR=5	run84	3/0.55/ 0%
□	CR=5	run85	3/1.14/ 0%
◇	CR=5	run86	3/2.15/ 0%

Figure 7.2.3.2: Re Effects  
(CR=5, 0% CowI)  
CR=5 Centerline Pressures



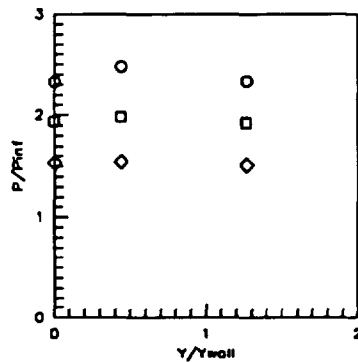
Sym	C.L. for	Run No.	CR/Re/Cowl (millions)
○	CR=9	run84	3/0.55/ 0%
□	CR=9	run85	3/1.14/ 0%
◇	CR=9	run86	3/2.15/ 0%

Figure 7.2.3.3: Re Effects  
(CR=9, 0% CowI)  
CR=9 Centerline Pressures



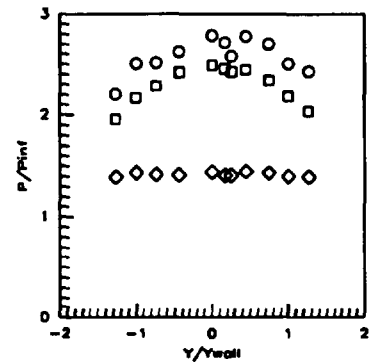
Sym	x'/Ts'	Run No.	CR/Re/Cowl (millions)
○	-0.8412	run84	3/0.55/ 0%
□	-0.8412	run85	3/1.14/ 0%
◇	-0.8412	run86	3/2.15/ 0%

Figure 7.2.3.4: Re Effects  
(CR=3, 0% CowI)  
Baseplate Pressures



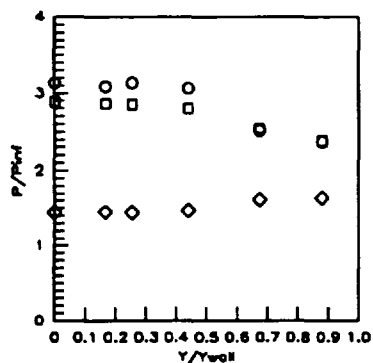
Sym	x'/Ts'	Run No.	CR/Re/Cowl (millions)
○	-0.5258	run84	3/0.55/ 0%
□	-0.5258	run85	3/1.14/ 0%
◇	-0.5258	run86	3/2.15/ 0%

Figure 7.2.3.5: Re Effects  
(CR=5, 0% CowI)  
Baseplate Pressures



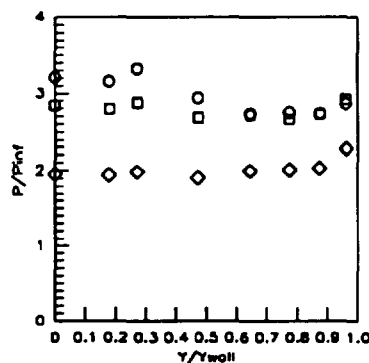
Sym	x'/Ts'	Run No.	CR/Re/Cowl (millions)
○	-0.1052	run84	3/0.55/ 0%
□	-0.1052	run85	3/1.14/ 0%
◇	-0.1052	run86	3/2.15/ 0%

Figure 7.2.3.6: Re Effects  
(CR=9, 0% CowI)  
Baseplate Pressures



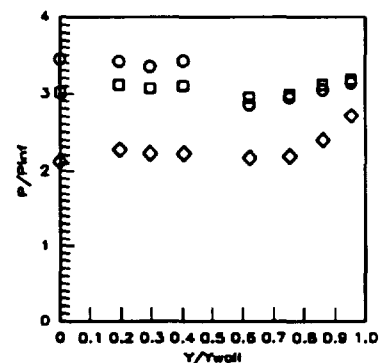
Sym	x'/Ts'	Run No.	CR/Re/Cowl (millions)
○	0.0000	run84	3/0.55/ 0%
□	0.0000	run85	3/1.14/ 0%
◇	0.0000	run86	3/2.15/ 0%

Figure 7.2.3.7: Re Effects  
(CR=3, 0% CowI)  
Baseplate Pressures



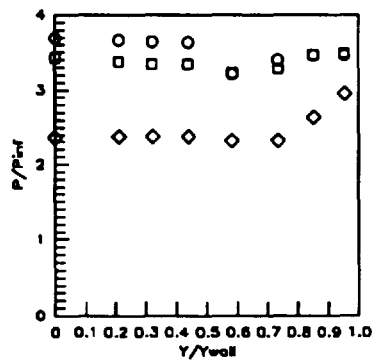
Sym	x'/Ts'	Run No.	CR/Re/Cowl (millions)
○	0.1052	run84	3/0.55/ 0%
□	0.1052	run85	3/1.14/ 0%
◇	0.1052	run86	3/2.15/ 0%

Figure 7.2.3.8: Re Effects  
(CR=5, 0% CowI)  
Baseplate Pressures



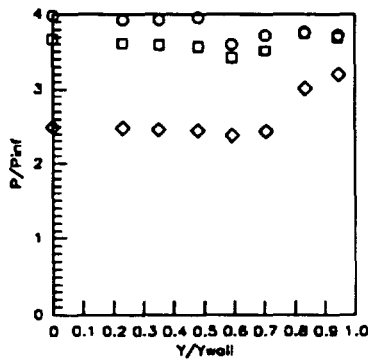
Sym	x'/Ts'	Run No.	CR/Re/Cowl (millions)
○	0.2103	run84	3/0.55/ 0%
□	0.2103	run85	3/1.14/ 0%
◇	0.2103	run86	3/2.15/ 0%

Figure 7.2.3.9: Re Effects  
(CR=9, 0% CowI)  
Baseplate Pressures



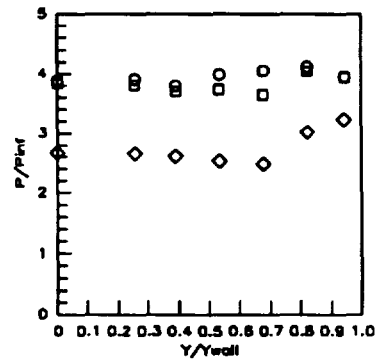
Sym	$x'/T_x'$	Run No.	CR/Re/Cowi (millions)
○	0.3154	run84	3/0.55/ 0%
□	0.3154	run85	3/1.14/ 0%
◇	0.3154	run86	3/2.15/ 0%

Figure 7.2.3.10: Re Effects (CR=3, 0% Cowi) Baseplate Pressures



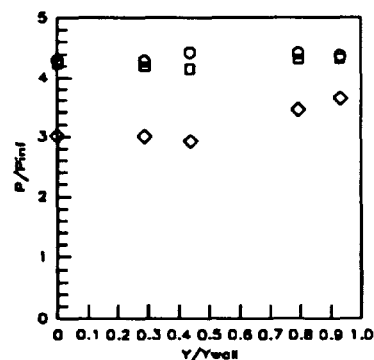
Sym	$x'/T_x'$	Run No.	CR/Re/Cowi (millions)
○	0.4206	run84	3/0.55/ 0%
□	0.4206	run85	3/1.14/ 0%
◇	0.4206	run86	3/2.15/ 0%

Figure 7.2.3.11: Re Effects (CR=3, 0% Cowi) Baseplate Pressures



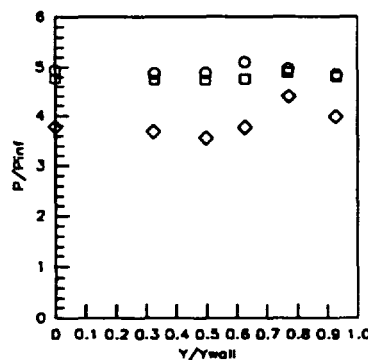
Sym	$x'/T_x'$	Run No.	CR/Re/Cowi (millions)
○	0.5258	run84	3/0.55/ 0%
□	0.5258	run85	3/1.14/ 0%
◇	0.5258	run86	3/2.15/ 0%

Figure 7.2.3.12: Re Effects (CR=3, 0% Cowi) Baseplate Pressures



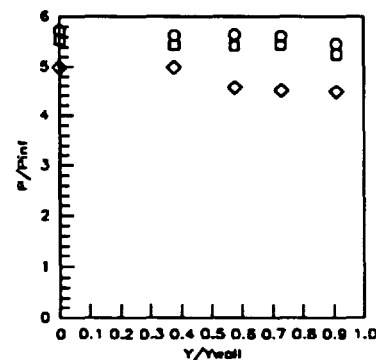
Sym	$x'/T_x'$	Run No.	CR/Re/Cowi (millions)
○	0.6309	run84	3/0.55/ 0%
□	0.6309	run85	3/1.14/ 0%
◇	0.6309	run86	3/2.15/ 0%

Figure 7.2.3.13: Re Effects (CR=3, 0% Cowi) Baseplate Pressures



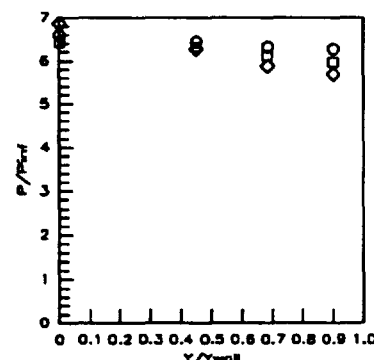
Sym	$x'/T_x'$	Run No.	CR/Re/Cowi (millions)
○	0.7361	run84	3/0.55/ 0%
□	0.7361	run85	3/1.14/ 0%
◇	0.7361	run86	3/2.15/ 0%

Figure 7.2.3.14: Re Effects (CR=3, 0% Cowi) Baseplate Pressures



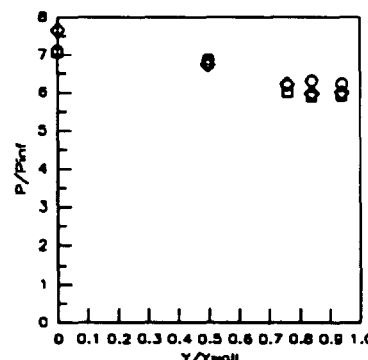
Sym	$x'/T_x'$	Run No.	CR/Re/Cowi (millions)
○	0.8412	run84	3/0.55/ 0%
□	0.8412	run85	3/1.14/ 0%
◇	0.8412	run86	3/2.15/ 0%

Figure 7.2.3.15: Re Effects (CR=3, 0% Cowi) Baseplate Pressures



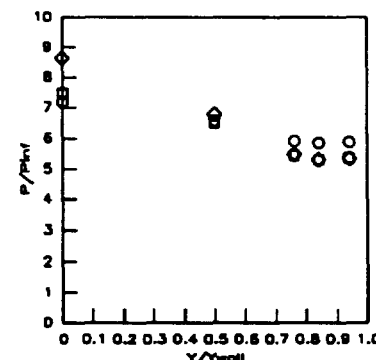
Sym	$x'/T_x'$	Run No.	CR/Re/Cowi (millions)
○	0.9464	run84	3/0.55/ 0%
□	0.9464	run85	3/1.14/ 0%
◇	0.9464	run86	3/2.15/ 0%

Figure 7.2.3.16: Re Effects (CR=3, 0% Cowi) Baseplate Pressures



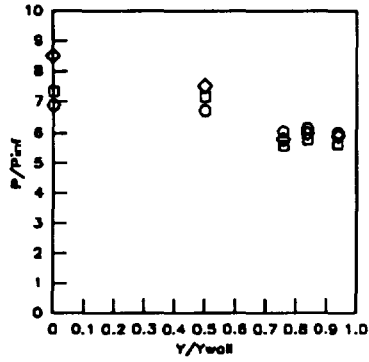
Sym	$x'/T_x'$	Run No.	CR/Re/Cowi (millions)
○	1.0000	run84	3/0.55/ 0%
□	1.0000	run85	3/1.14/ 0%
◇	1.0000	run86	3/2.15/ 0%

Figure 7.2.3.17: Re Effects (CR=3, 0% Cowi) Baseplate Pressures



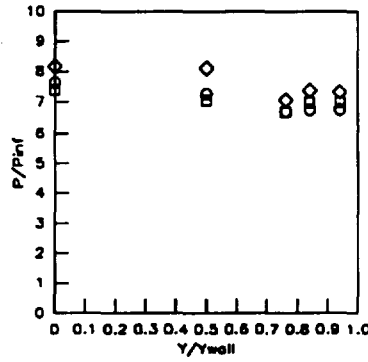
Sym	$x'/T_x'$	Run No.	CR/Re/Cowi (millions)
○	1.0728	run84	3/0.55/ 0%
□	1.0728	run85	3/1.14/ 0%
◇	1.0728	run86	3/2.15/ 0%

Figure 7.2.3.18: Re Effects (CR=3, 0% Cowi) Baseplate Pressures



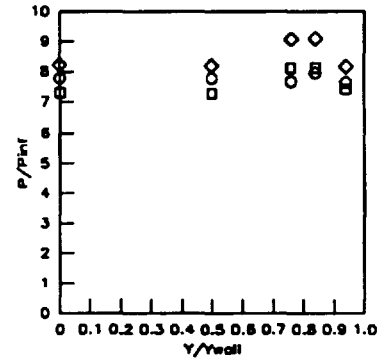
Sym	$x'/T_x'$	Run No.	CR/Re/Cowi (millions)
○	1.1587	run84	3/0.55/ 0%
□	1.1567	run85	3/1.14/ 0%
◇	1.1567	run86	3/2.15/ 0%

Figure 7.2.3.19: Re Effects (CR=3, 0% Cowi) Baseplate Pressures



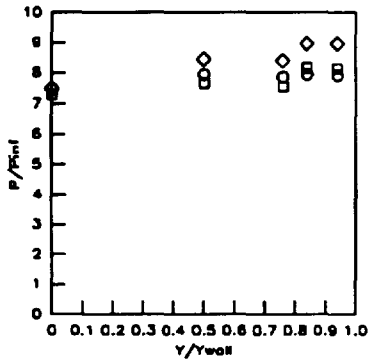
Sym	$x'/T_x'$	Run No.	CR/Re/Cowi (millions)
○	1.2408	run84	3/0.55/ 0%
□	1.2408	run85	3/1.14/ 0%
◇	1.2408	run86	3/2.15/ 0%

Figure 7.2.3.20: Re Effects (CR=3, 0% Cowi) Baseplate Pressures



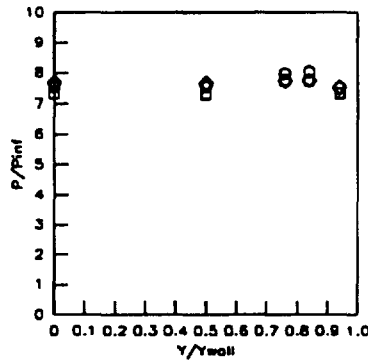
Sym	$x'/T_x'$	Run No.	CR/Re/Cowi (millions)
○	1.3249	run84	3/0.55/ 0%
□	1.3249	run85	3/1.14/ 0%
◇	1.3249	run86	3/2.15/ 0%

Figure 7.2.3.21: Re Effects (CR=3, 0% Cowi) Baseplate Pressures



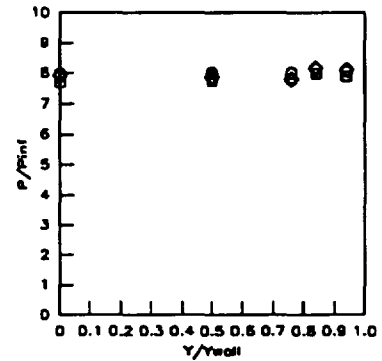
Sym	$x'/T_x'$	Run No.	CR/Re/Cowi (millions)
○	1.4090	run84	3/0.55/ 0%
□	1.4090	run85	3/1.14/ 0%
◇	1.4090	run86	3/2.15/ 0%

Figure 7.2.3.22: Re Effects (CR=3, 0% Cowi) Baseplate Pressures



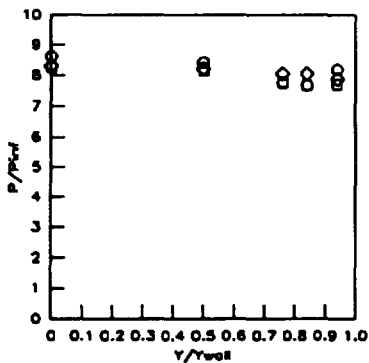
Sym	$x'/T_x'$	Run No.	CR/Re/Cowi (millions)
○	1.4932	run84	3/0.55/ 0%
□	1.4932	run85	3/1.14/ 0%
◇	1.4932	run86	3/2.15/ 0%

Figure 7.2.3.23: Re Effects (CR=3, 0% Cowi) Baseplate Pressures



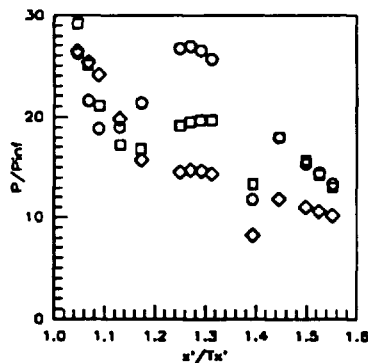
Sym	$x'/T_x'$	Run No.	CR/Re/Cowi (millions)
○	1.5773	run84	3/0.55/ 0%
□	1.5773	run85	3/1.14/ 0%
◇	1.5773	run86	3/2.15/ 0%

Figure 7.2.3.24: Re Effects (CR=3, 0% Cowi) Baseplate Pressures



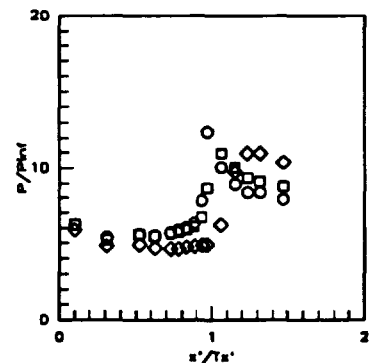
Sym	$x'/T_x'$	Run No.	CR/Re/Cowi (millions)
○	1.6824	run84	3/0.55/ 0%
□	1.6824	run85	3/1.14/ 0%
◇	1.6824	run86	3/2.15/ 0%

Figure 7.2.3.25: Re Effects (CR=3, 0% Cowi) Baseplate Pressures



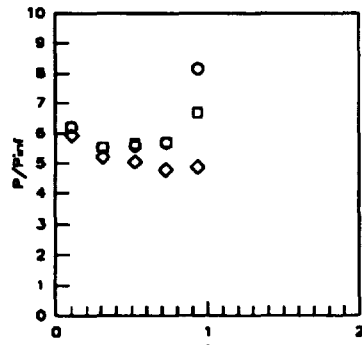
Sym	Cowi Pos.	Run No.	CR/Re/Cowi (millions)
○	0%	run84	3/0.55/ 0%
□	0%	run85	3/1.14/ 0%
◇	0%	run86	3/2.15/ 0%

Figure 7.2.3.26: Re Effects (CR=3, 0% Cowi) Cowi Pressures



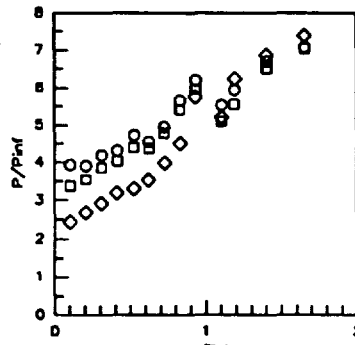
Sym	Z/H	Run No.	CR/Re/Cowi (millions)
○	0.5RT	run84	3/0.55/ 0%
□	0.5RT	run85	3/1.14/ 0%
◇	0.5RT	run86	3/2.15/ 0%

Figure 7.2.3.27: Re Effects (CR=3, 0% Cowi) Sidewall Centerline Pressures



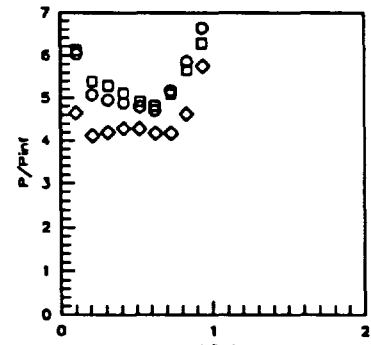
Sym	Z/H	Run No.	CR/Re/Cowl (millions)
○	0.5LT	run84	3/0.55/ 0%
□	0.5LT	run85	3/1.14/ 0%
◇	0.5LT	run86	3/2.15/ 0%

Figure 7.2.3.28: Re Effects  
(CR=3, 0%Cowl)  
Sidewall Centerline Pressures



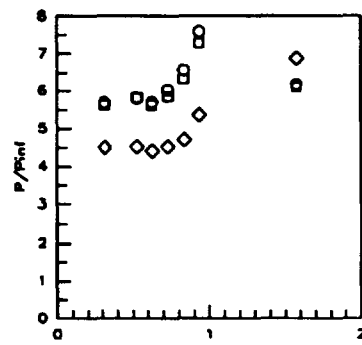
Sym	Z/H	Run No.	CR/Re/Cowl (millions)
○	0.050	run84	3/0.55/ 0%
□	0.050	run85	3/1.14/ 0%
◇	0.050	run86	3/2.15/ 0%

Figure 7.2.3.29: Re Effects  
(CR=3, 0%Cowl)  
Sidewall Pressures



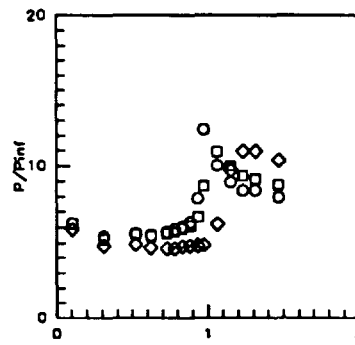
Sym	Z/H	Run No.	CR/Re/Cowl (millions)
○	0.15	run84	3/0.55/ 0%
□	0.15	run85	3/1.14/ 0%
◇	0.15	run86	3/2.15/ 0%

Figure 7.2.3.30: Re Effects  
(CR=3, 0%Cowl)  
Sidewall Pressures



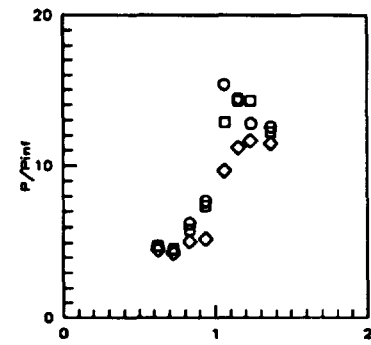
Sym	Z/H	Run No.	CR/Re/Cowl (millions)
○	0.25	run84	3/0.55/ 0%
□	0.25	run85	3/1.14/ 0%
◇	0.25	run86	3/2.15/ 0%

Figure 7.2.3.31: Re Effects  
(CR=3, 0%Cowl)  
Sidewall Pressures



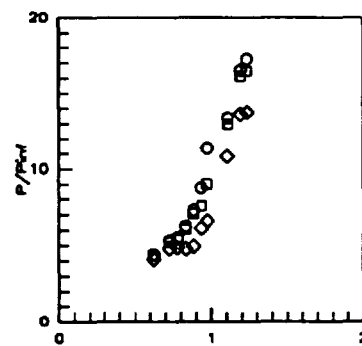
Sym	Z/H	Run No.	CR/Re/Cowl (millions)
○	0.50	run84	3/0.55/ 0%
□	0.50	run85	3/1.14/ 0%
◇	0.50	run86	3/2.15/ 0%

Figure 7.2.3.32: Re Effects  
(CR=3, 0%Cowl)  
Sidewall Pressures



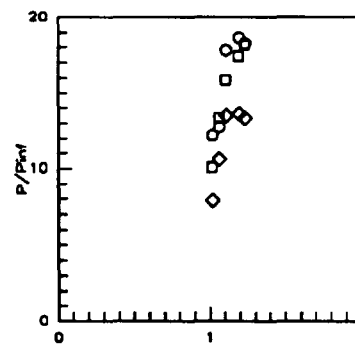
Sym	Z/H	Run No.	CR/Re/Cowl (millions)
○	0.75	run84	3/0.55/ 0%
□	0.75	run85	3/1.14/ 0%
◇	0.75	run86	3/2.15/ 0%

Figure 7.2.3.33: Re Effects  
(CR=3, 0%Cowl)  
Sidewall Pressures



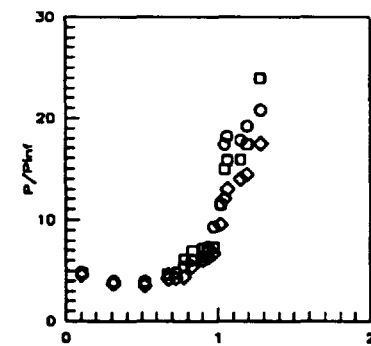
Sym	Z/H	Run No.	CR/Re/Cowl (millions)
○	0.85	run84	3/0.55/ 0%
□	0.85	run85	3/1.14/ 0%
◇	0.85	run86	3/2.15/ 0%

Figure 7.2.3.34: Re Effects  
(CR=3, 0%Cowl)  
Sidewall Pressures



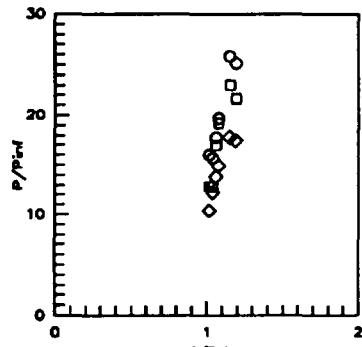
Sym	Z/H	Run No.	CR/Re/Cowl (millions)
○	0.90	run84	3/0.55/ 0%
□	0.90	run85	3/1.14/ 0%
◇	0.90	run86	3/2.15/ 0%

Figure 7.2.3.35: Re Effects  
(CR=3, 0%Cowl)  
Sidewall Pressures



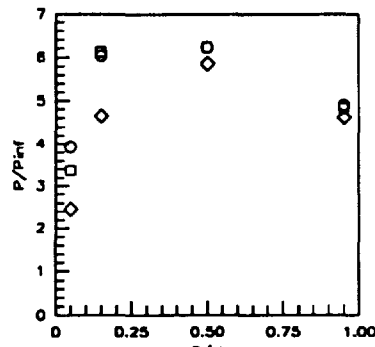
Sym	Z/H	Run No.	CR/Re/Cowl (millions)
○	0.95	run84	3/0.55/ 0%
□	0.95	run85	3/1.14/ 0%
◇	0.95	run86	3/2.15/ 0%

Figure 7.2.3.36: Re Effects  
(CR=3, 0%Cowl)  
Sidewall Pressures



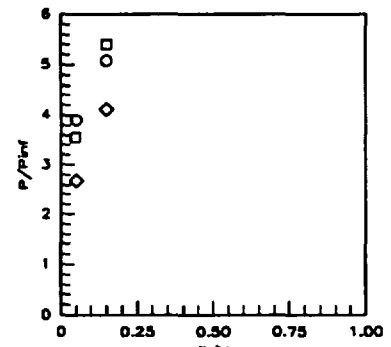
Sym	Z/H	Run No.	CR/Re/Cowi (millions)
○	0.975	run64	3/0.55/ 0%
○	0.975	run65	3/1.14/ 0%
○	0.975	run66	3/2.15/ 0%

Figure 7.2.3.37: Re Effects (CR=3, 0% Cowi) Sidewall Pressures



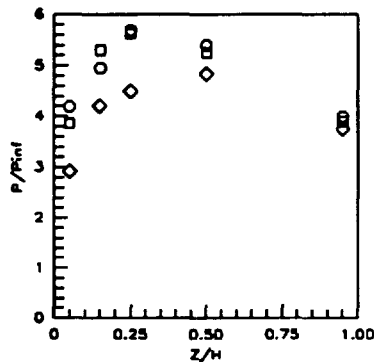
Sym	x'/Tx'	Run No.	CR/Re/Cowi (millions)
○	0.1042	run64	3/0.55/ 0%
○	0.1042	run65	3/1.14/ 0%
○	0.1042	run66	3/2.15/ 0%

Figure 7.2.3.38: Re Effects (CR=3, 0% Cowi) Sidewall Pressures



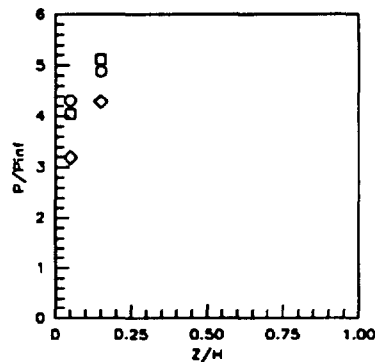
Sym	x'/Tx'	Run No.	CR/Re/Cowi (millions)
○	0.2083	run64	3/0.55/ 0%
○	0.2083	run65	3/1.14/ 0%
○	0.2083	run66	3/2.15/ 0%

Figure 7.2.3.39: Re Effects (CR=3, 0% Cowi) Sidewall Pressures



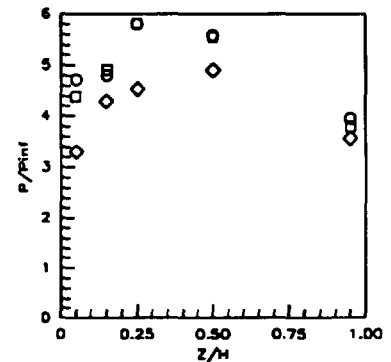
Sym	x'/Tx'	Run No.	CR/Re/Cowi (millions)
○	0.3125	run64	3/0.55/ 0%
○	0.3125	run65	3/1.14/ 0%
○	0.3125	run66	3/2.15/ 0%

Figure 7.2.3.40: Re Effects (CR=3, 0% Cowi) Sidewall Pressures



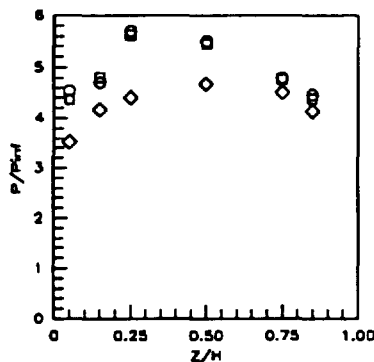
Sym	x'/Tx'	Run No.	CR/Re/Cowi (millions)
○	0.4167	run64	3/0.55/ 0%
○	0.4167	run65	3/1.14/ 0%
○	0.4167	run66	3/2.15/ 0%

Figure 7.2.3.41: Re Effects (CR=3, 0% Cowi) Sidewall Pressures



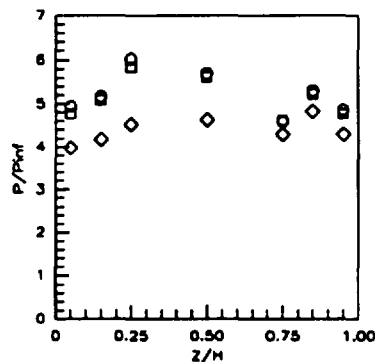
Sym	x'/Tx'	Run No.	CR/Re/Cowi (millions)
○	0.5259	run64	3/0.55/ 0%
○	0.5259	run65	3/1.14/ 0%
○	0.5259	run66	3/2.15/ 0%

Figure 7.2.3.42: Re Effects (CR=3, 0% Cowi) Sidewall Pressures



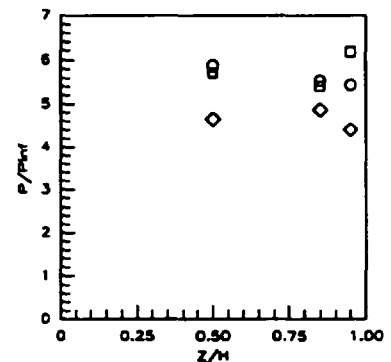
Sym	x'/Tx'	Run No.	CR/Re/Cowi (millions)
○	0.6252	run64	3/0.55/ 0%
○	0.6252	run65	3/1.14/ 0%
○	0.6252	run66	3/2.15/ 0%

Figure 7.2.3.43: Re Effects (CR=3, 0% Cowi) Sidewall Pressures



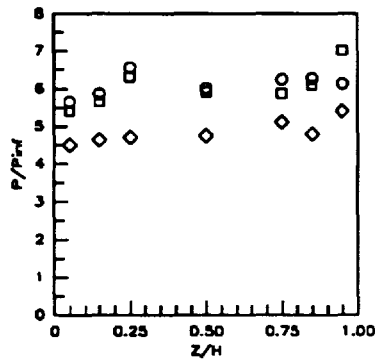
Sym	x'/Tx'	Run No.	CR/Re/Cowi (millions)
○	0.7294	run64	3/0.55/ 0%
○	0.7294	run65	3/1.14/ 0%
○	0.7294	run66	3/2.15/ 0%

Figure 7.2.3.44: Re Effects (CR=3, 0% Cowi) Sidewall Pressures



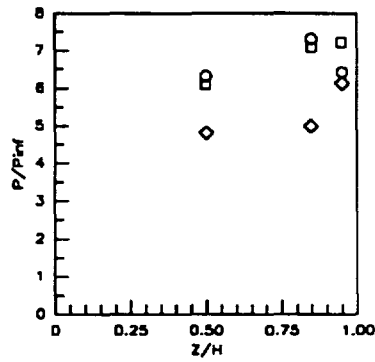
Sym	x'/Tx'	Run No.	CR/Re/Cowi (millions)
○	0.7815	run64	3/0.55/ 0%
○	0.7815	run65	3/1.14/ 0%
○	0.7815	run66	3/2.15/ 0%

Figure 7.2.3.45: Re Effects (CR=3, 0% Cowi) Sidewall Pressures



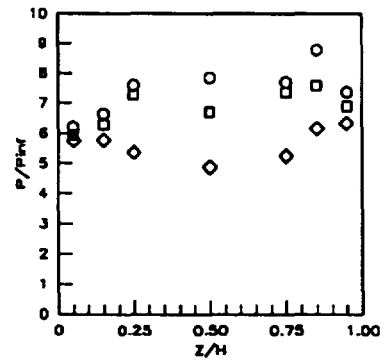
Sym	$x'/T_x'$	Run No.	CR/Re/CowI (millions)
○	0.8336	run84	3/0.55/ 0%
□	0.8336	run85	3/1.14/ 0%
◇	0.8336	run86	3/2.15/ 0%

Figure 7.2.3.46: Re Effects (CR=3, 0%CowI) Sidewall Pressures



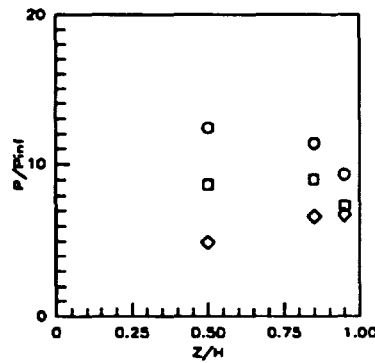
Sym	$x'/T_x'$	Run No.	CR/Re/CowI (millions)
○	0.8857	run84	3/0.55/ 0%
□	0.8857	run85	3/1.14/ 0%
◇	0.8857	run86	3/2.15/ 0%

Figure 7.2.3.47: Re Effects (CR=3, 0%CowI) Sidewall Pressures



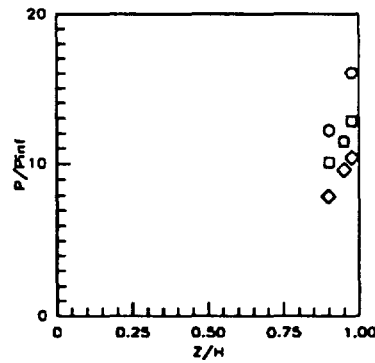
Sym	$x'/T_x'$	Run No.	CR/Re/CowI (millions)
○	0.9378	run84	3/0.55/ 0%
□	0.9378	run85	3/1.14/ 0%
◇	0.9378	run86	3/2.15/ 0%

Figure 7.2.3.48: Re Effects (CR=3, 0%CowI) Sidewall Pressures



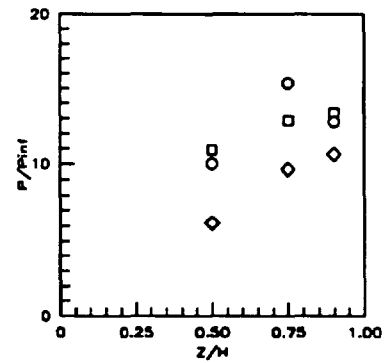
Sym	$x'/T_x'$	Run No.	CR/Re/CowI (millions)
○	0.9751	run84	3/0.55/ 0%
□	0.9751	run85	3/1.14/ 0%
◇	0.9751	run86	3/2.15/ 0%

Figure 7.2.3.49: Re Effects (CR=3, 0%CowI) Sidewall Pressures



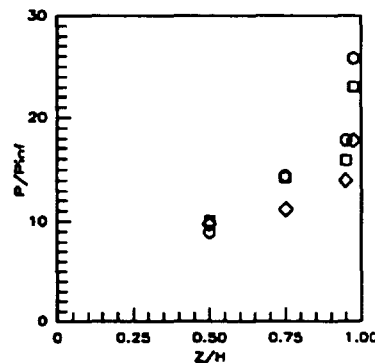
Sym	$x'/T_x'$	Run No.	CR/Re/CowI (millions)
○	1.0197	run84	3/0.55/ 0%
□	1.0197	run85	3/1.14/ 0%
◇	1.0197	run86	3/2.15/ 0%

Figure 7.2.3.50: Re Effects (CR=3, 0%CowI) Sidewall Pressures



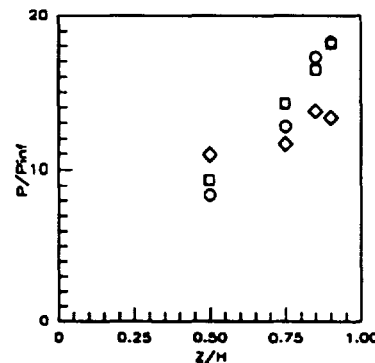
Sym	$x'/T_x'$	Run No.	CR/Re/CowI (millions)
○	1.0643	run84	3/0.55/ 0%
□	1.0643	run85	3/1.14/ 0%
◇	1.0643	run86	3/2.15/ 0%

Figure 7.2.3.51: Re Effects (CR=3, 0%CowI) Sidewall Pressures



Sym	$x'/T_x'$	Run No.	CR/Re/CowI (millions)
○	1.1537	run84	3/0.55/ 0%
□	1.1537	run85	3/1.14/ 0%
◇	1.1537	run86	3/2.15/ 0%

Figure 7.2.3.52: Re Effects (CR=3, 0%CowI) Sidewall Pressures



Sym	$x'/T_x'$	Run No.	CR/Re/CowI (millions)
○	1.2356	run84	3/0.55/ 0%
□	1.2356	run85	3/1.14/ 0%
◇	1.2356	run86	3/2.15/ 0%

Figure 7.2.3.53: Re Effects (CR=3, 0%CowI) Sidewall Pressures



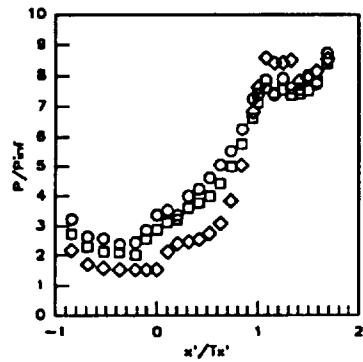


Figure 7.2.3.54: Re Effects  
(CR=3, 25% CowI)  
CR=3 Centerline Pressures

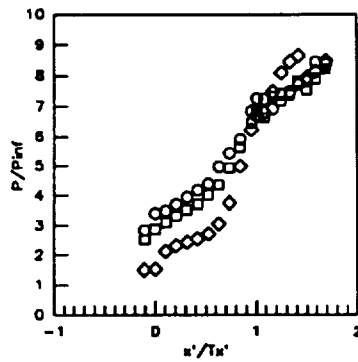


Figure 7.2.3.55: Re Effects  
(CR=3, 25% CowI)  
CR=5 Centerline Pressures

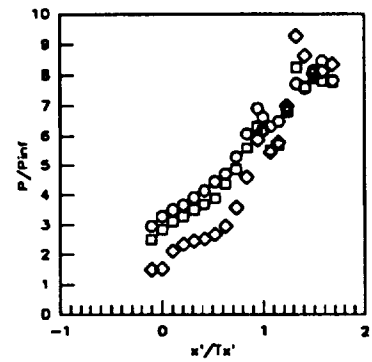


Figure 7.2.3.56: Re Effects  
(CR=3, 25% CowI)  
CR=8 Centerline Pressures

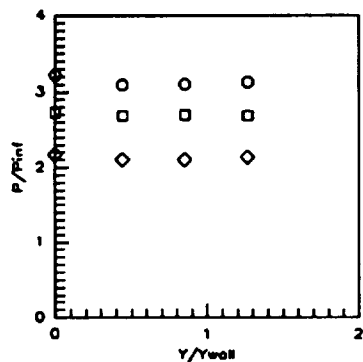


Figure 7.2.3.57: Re Effects  
(CR=3, 25% CowI)  
Baseplate Pressures

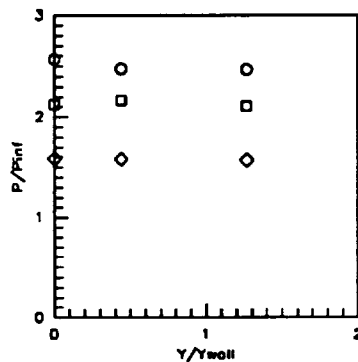


Figure 7.2.3.58: Re Effects  
(CR=3, 25% CowI)  
Baseplate Pressures

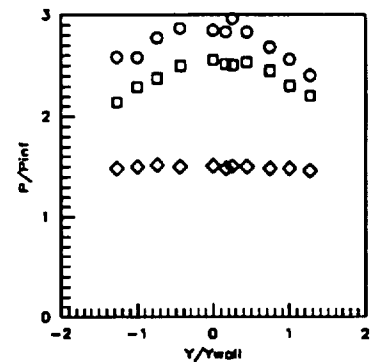


Figure 7.2.3.59: Re Effects  
(CR=3, 25% CowI)  
Baseplate Pressures

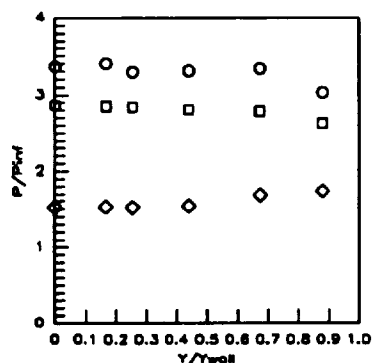


Figure 7.2.3.60: Re Effects  
(CR=3, 25% CowI)  
Baseplate Pressures

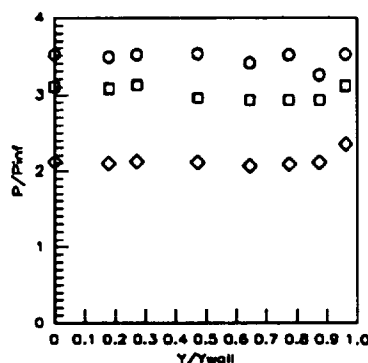


Figure 7.2.3.61: Re Effects  
(CR=3, 25% CowI)  
Baseplate Pressures

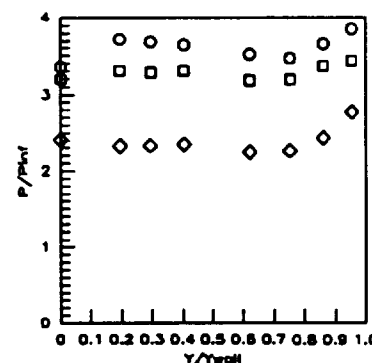
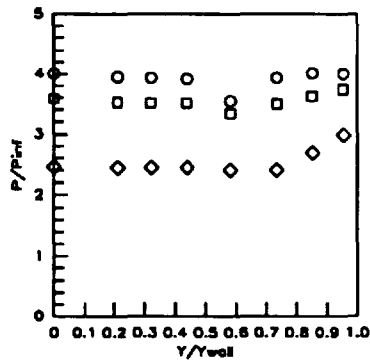
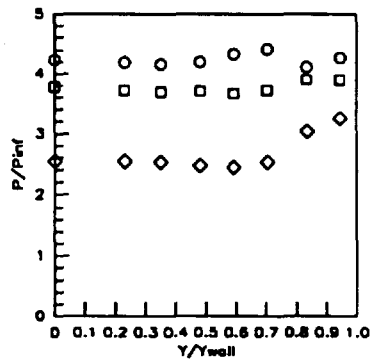


Figure 7.2.3.62: Re Effects  
(CR=3, 25% CowI)  
Baseplate Pressures



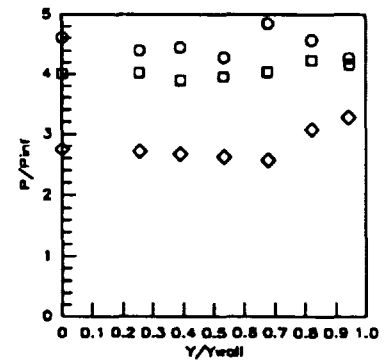
Sym	$x'/T_x'$	Run No.	CR/Re/Cowl (millions)
○	0.3154	run61	3/0.55/25%
□	0.3154	run63	3/1.14/25%
◇	0.3154	run62	3/2.15/25%

Figure 7.2.3.63: Re Effects (CR=3, 25% Cowl) Baseplate Pressures



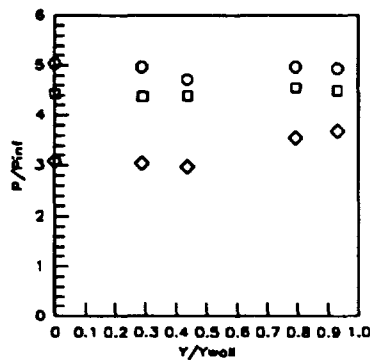
Sym	$x'/T_x'$	Run No.	CR/Re/Cowl (millions)
○	0.4206	run61	3/0.55/25%
□	0.4206	run63	3/1.14/25%
◇	0.4206	run62	3/2.15/25%

Figure 7.2.3.64: Re Effects (CR=3, 25% Cowl) Baseplate Pressures



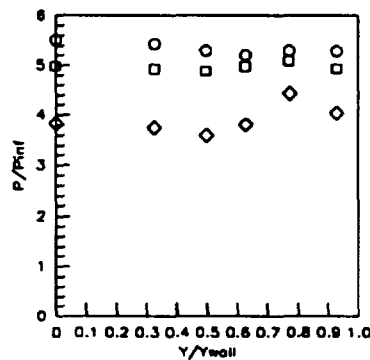
Sym	$x'/T_x'$	Run No.	CR/Re/Cowl (millions)
○	0.5258	run61	3/0.55/25%
□	0.5258	run63	3/1.14/25%
◇	0.5258	run62	3/2.15/25%

Figure 7.2.3.65: Re Effects (CR=3, 25% Cowl) Baseplate Pressures



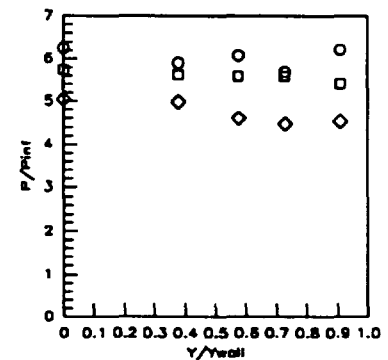
Sym	$x'/T_x'$	Run No.	CR/Re/Cowl (millions)
○	0.6309	run61	3/0.55/25%
□	0.6309	run63	3/1.14/25%
◇	0.6309	run62	3/2.15/25%

Figure 7.2.3.66: Re Effects (CR=3, 25% Cowl) Baseplate Pressures



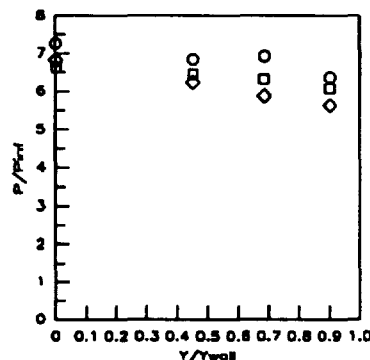
Sym	$x'/T_x'$	Run No.	CR/Re/Cowl (millions)
○	0.7361	run61	3/0.55/25%
□	0.7361	run63	3/1.14/25%
◇	0.7361	run62	3/2.15/25%

Figure 7.2.3.67: Re Effects (CR=3, 25% Cowl) Baseplate Pressures



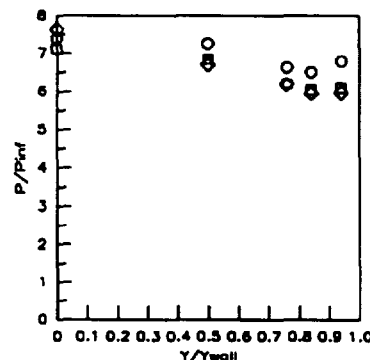
Sym	$x'/T_x'$	Run No.	CR/Re/Cowl (millions)
○	0.8412	run61	3/0.55/25%
□	0.8412	run63	3/1.14/25%
◇	0.8412	run62	3/2.15/25%

Figure 7.2.3.68: Re Effects (CR=3, 25% Cowl) Baseplate Pressures



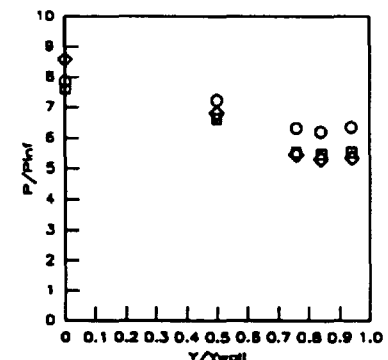
Sym	$x'/T_x'$	Run No.	CR/Re/Cowl (millions)
○	0.9454	run61	3/0.55/25%
□	0.9454	run63	3/1.14/25%
◇	0.9454	run62	3/2.15/25%

Figure 7.2.3.69: Re Effects (CR=3, 25% Cowl) Baseplate Pressures



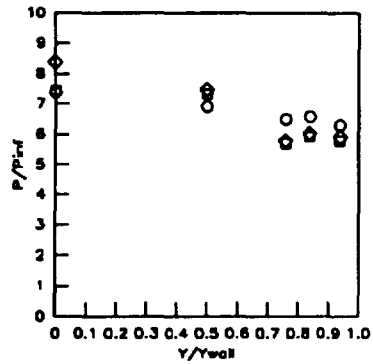
Sym	$x'/T_x'$	Run No.	CR/Re/Cowl (millions)
○	1.0000	run61	3/0.55/25%
□	1.0000	run63	3/1.14/25%
◇	1.0000	run62	3/2.15/25%

Figure 7.2.3.70: Re Effects (CR=3, 25% Cowl) Baseplate Pressures



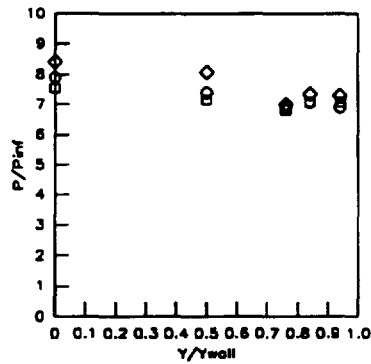
Sym	$x'/T_x'$	Run No.	CR/Re/Cowl (millions)
○	1.0726	run61	3/0.55/25%
□	1.0726	run63	3/1.14/25%
◇	1.0726	run62	3/2.15/25%

Figure 7.2.3.71: Re Effects (CR=3, 25% Cowl) Baseplate Pressures



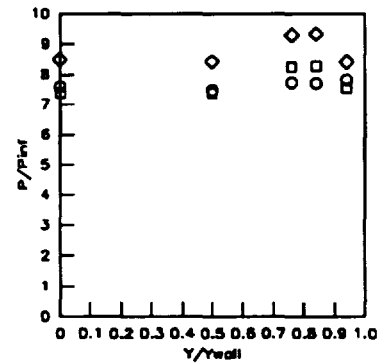
Sym	$x'/Ts'$	Run No.	CR/Re/Cowl (millions)
○	1.1567	run81	3/0.55/25%
□	1.1567	run83	3/1.14/25%
◇	1.1567	run82	3/2.15/25%

Figure 7.2.3.72: Re Effects (CR=3, 25% Cowl) Baseplate Pressures



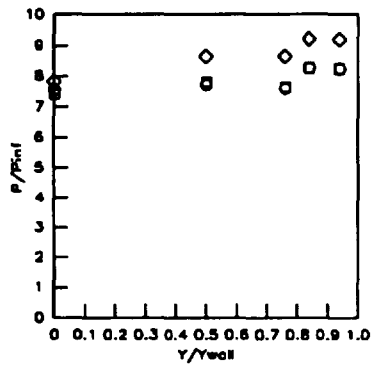
Sym	$x'/Ts'$	Run No.	CR/Re/Cowl (millions)
○	1.2408	run81	3/0.55/25%
□	1.2408	run83	3/1.14/25%
◇	1.2408	run82	3/2.15/25%

Figure 7.2.3.73: Re Effects (CR=3, 25% Cowl) Baseplate Pressures



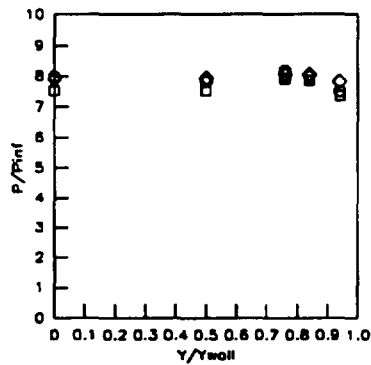
Sym	$x'/Ts'$	Run No.	CR/Re/Cowl (millions)
○	1.3249	run81	3/0.55/25%
□	1.3249	run83	3/1.14/25%
◇	1.3249	run82	3/2.15/25%

Figure 7.2.3.74: Re Effects (CR=3, 25% Cowl) Baseplate Pressures



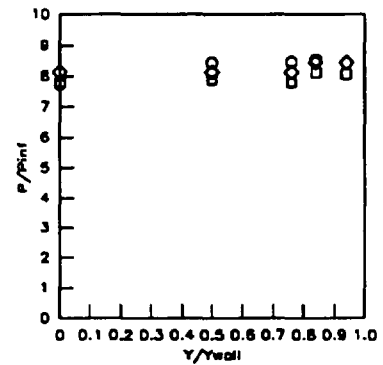
Sym	$x'/Ts'$	Run No.	CR/Re/Cowl (millions)
○	1.4090	run81	3/0.55/25%
□	1.4090	run83	3/1.14/25%
◇	1.4090	run82	3/2.15/25%

Figure 7.2.3.75: Re Effects (CR=3, 25% Cowl) Baseplate Pressures



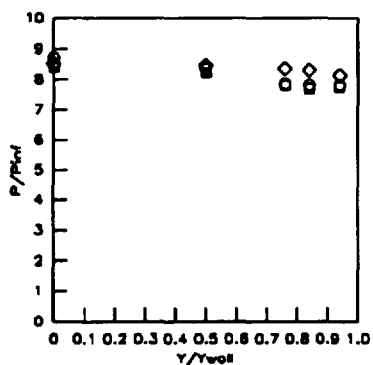
Sym	$x'/Ts'$	Run No.	CR/Re/Cowl (millions)
○	1.4932	run81	3/0.55/25%
□	1.4932	run83	3/1.14/25%
◇	1.4932	run82	3/2.15/25%

Figure 7.2.3.76: Re Effects (CR=3, 25% Cowl) Baseplate Pressures



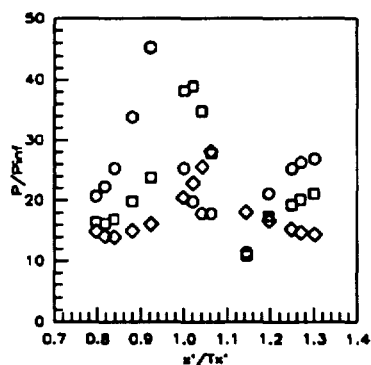
Sym	$x'/Ts'$	Run No.	CR/Re/Cowl (millions)
○	1.5773	run81	3/0.55/25%
□	1.5773	run83	3/1.14/25%
◇	1.5773	run82	3/2.15/25%

Figure 7.2.3.77: Re Effects (CR=3, 25% Cowl) Baseplate Pressures



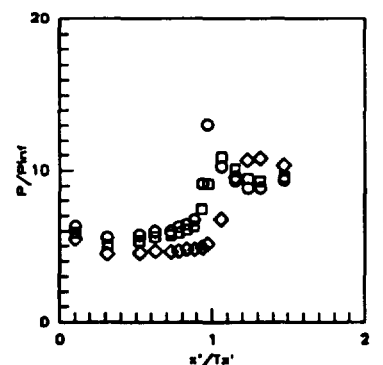
Sym	$x'/Ts'$	Run No.	CR/Re/Cowl (millions)
○	1.6824	run81	3/0.55/25%
□	1.6824	run83	3/1.14/25%
◇	1.6824	run82	3/2.15/25%

Figure 7.2.3.78: Re Effects (CR=3, 25% Cowl) Baseplate Pressures



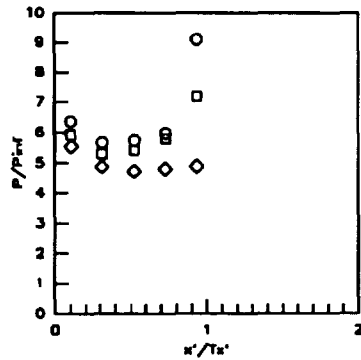
Sym	Cowl Pos.	Run No.	CR/Re/Cowl (millions)
○	25%	run81	3/0.55/25%
□	25%	run83	3/1.14/25%
◇	25%	run82	3/2.15/25%

Figure 7.2.3.79: Re Effects (CR=3, 25% Cowl) Cowl Pressures



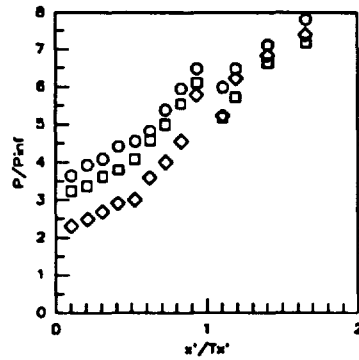
Sym	$x'/Ts'$	Run No.	CR/Re/Cowl (millions)
○	0.5RT	run81	3/0.55/25%
□	0.5RT	run83	3/1.14/25%
◇	0.5RT	run82	3/2.15/25%

Figure 7.2.3.80: Re Effects (CR=3, 25% Cowl) Sidewall Centerline Pressures



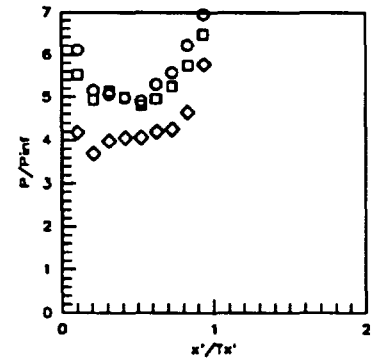
Sym	Z/H	Run No.	CR/Re/Cowl (millions)
○	0.5LT	run81	3/0.55/25%
□	0.5LT	run83	3/1.14/25%
◇	0.5LT	run82	3/2.15/25%

Figure 7.2.3.81: Re Effects  
(CR=3, 25%Cowl)  
Sidewall Centerline Pressures



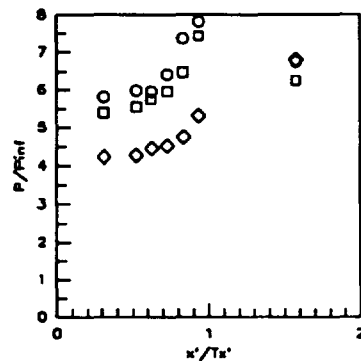
Sym	Z/H	Run No.	CR/Re/Cowl (millions)
○	0.050	run81	3/0.55/25%
□	0.050	run83	3/1.14/25%
◇	0.050	run82	3/2.15/25%

Figure 7.2.3.82: Re Effects  
(CR=3, 25%Cowl)  
Sidewall Pressures



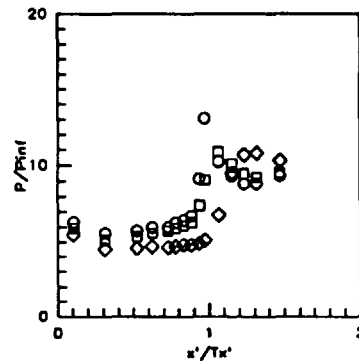
Sym	Z/H	Run No.	CR/Re/Cowl (millions)
○	0.15	run81	3/0.55/25%
□	0.15	run83	3/1.14/25%
◇	0.15	run82	3/2.15/25%

Figure 7.2.3.83: Re Effects  
(CR=3, 25%Cowl)  
Sidewall Pressures



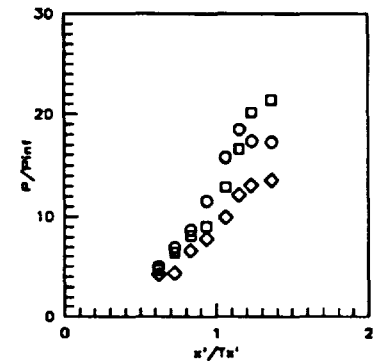
Sym	Z/H	Run No.	CR/Re/Cowl (millions)
○	0.25	run81	3/0.55/25%
□	0.25	run83	3/1.14/25%
◇	0.25	run82	3/2.15/25%

Figure 7.2.3.84: Re Effects  
(CR=3, 25%Cowl)  
Sidewall Pressures



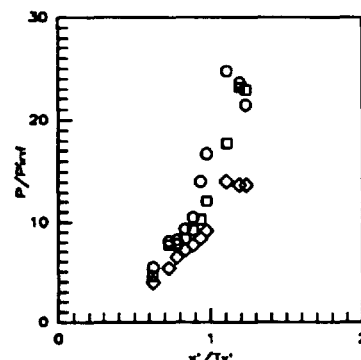
Sym	Z/H	Run No.	CR/Re/Cowl (millions)
○	0.50	run81	3/0.55/25%
□	0.50	run83	3/1.14/25%
◇	0.50	run82	3/2.15/25%

Figure 7.2.3.85: Re Effects  
(CR=3, 25%Cowl)  
Sidewall Pressures



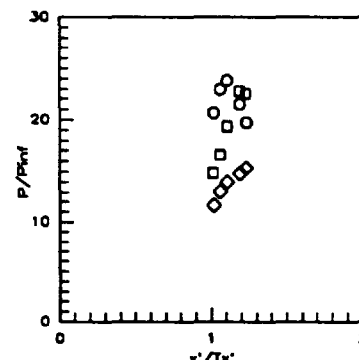
Sym	Z/H	Run No.	CR/Re/Cowl (millions)
○	0.75	run81	3/0.55/25%
□	0.75	run83	3/1.14/25%
◇	0.75	run82	3/2.15/25%

Figure 7.2.3.86: Re Effects  
(CR=3, 25%Cowl)  
Sidewall Pressures



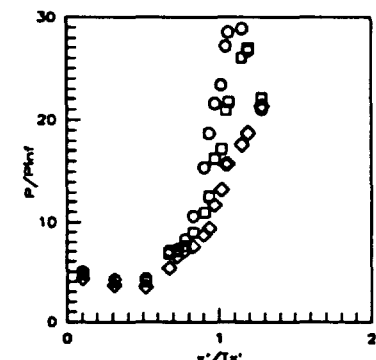
Sym	Z/H	Run No.	CR/Re/Cowl (millions)
○	0.85	run81	3/0.55/25%
□	0.85	run83	3/1.14/25%
◇	0.85	run82	3/2.15/25%

Figure 7.2.3.87: Re Effects  
(CR=3, 25%Cowl)  
Sidewall Pressures



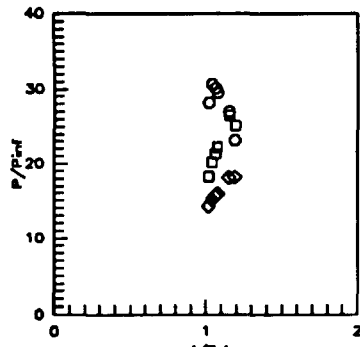
Sym	Z/H	Run No.	CR/Re/Cowl (millions)
○	0.90	run81	3/0.55/25%
□	0.90	run83	3/1.14/25%
◇	0.90	run82	3/2.15/25%

Figure 7.2.3.88: Re Effects  
(CR=3, 25%Cowl)  
Sidewall Pressures



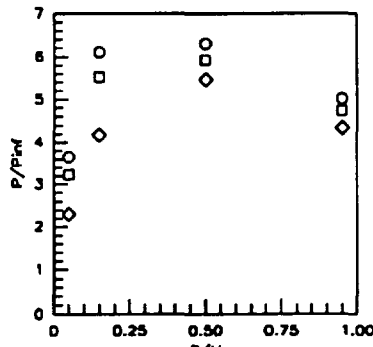
Sym	Z/H	Run No.	CR/Re/Cowl (millions)
○	0.95	run81	3/0.55/25%
□	0.95	run83	3/1.14/25%
◇	0.95	run82	3/2.15/25%

Figure 7.2.3.89: Re Effects  
(CR=3, 25%Cowl)  
Sidewall Pressures



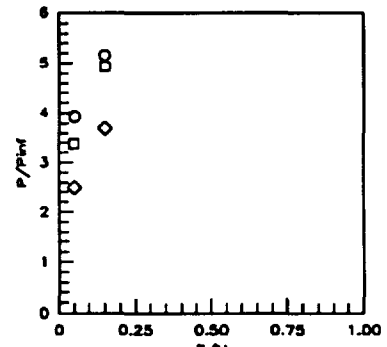
Sym	Z/H	Run No.	CR/Re/Cowl (millions)
○	0.975	run61	3/0.55/25%
□	0.975	run63	3/1.14/25%
◇	0.975	run62	3/2.15/25%

Figure 7.2.3.90: Re Effects  
(CR=3, 25%Cowl)  
Sidewall Pressures



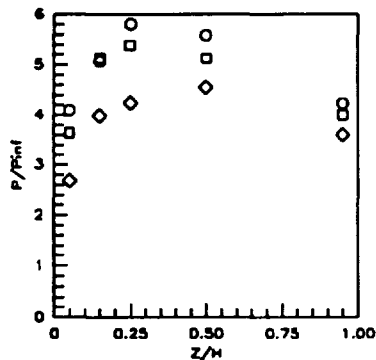
Sym	x'/Ts'	Run No.	CR/Re/Cowl (millions)
○	0.1042	run61	3/0.55/25%
□	0.1042	run63	3/1.14/25%
◇	0.1042	run62	3/2.15/25%

Figure 7.2.3.91: Re Effects  
(CR=3, 25%Cowl)  
Sidewall Pressures



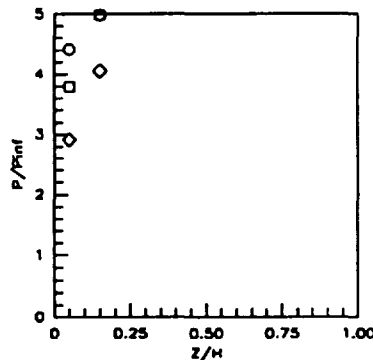
Sym	x'/Ts'	Run No.	CR/Re/Cowl (millions)
○	0.2063	run61	3/0.55/25%
□	0.2063	run63	3/1.14/25%
◇	0.2063	run62	3/2.15/25%

Figure 7.2.3.92: Re Effects  
(CR=3, 25%Cowl)  
Sidewall Pressures



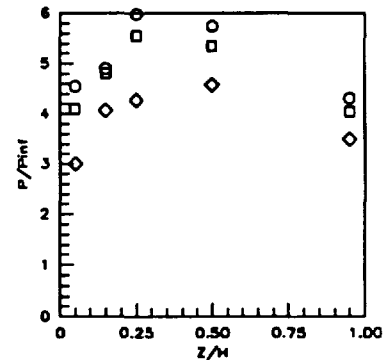
Sym	x'/Ts'	Run No.	CR/Re/Cowl (millions)
○	0.3125	run61	3/0.55/25%
□	0.3125	run63	3/1.14/25%
◇	0.3125	run62	3/2.15/25%

Figure 7.2.3.93: Re Effects  
(CR=3, 25%Cowl)  
Sidewall Pressures



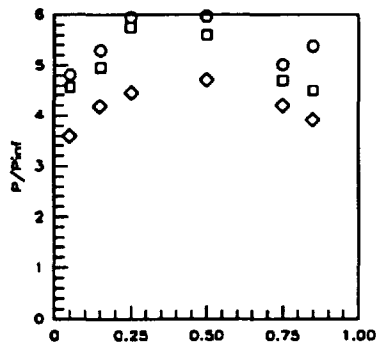
Sym	x'/Ts'	Run No.	CR/Re/Cowl (millions)
○	0.4167	run61	3/0.55/25%
□	0.4167	run63	3/1.14/25%
◇	0.4167	run62	3/2.15/25%

Figure 7.2.3.94: Re Effects  
(CR=3, 25%Cowl)  
Sidewall Pressures



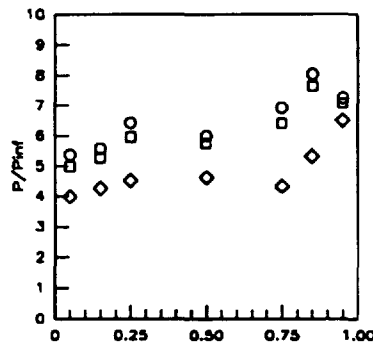
Sym	x'/Ts'	Run No.	CR/Re/Cowl (millions)
○	0.5259	run61	3/0.55/25%
□	0.5259	run63	3/1.14/25%
◇	0.5259	run62	3/2.15/25%

Figure 7.2.3.95: Re Effects  
(CR=3, 25%Cowl)  
Sidewall Pressures



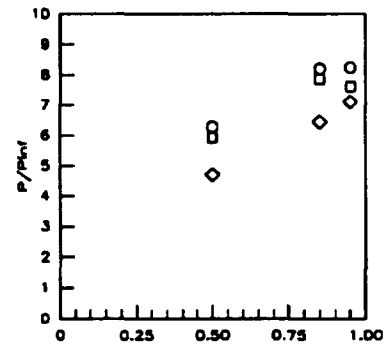
Sym	x'/Ts'	Run No.	CR/Re/Cowl (millions)
○	0.6252	run61	3/0.55/25%
□	0.6252	run63	3/1.14/25%
◇	0.6252	run62	3/2.15/25%

Figure 7.2.3.96: Re Effects  
(CR=3, 25%Cowl)  
Sidewall Pressures



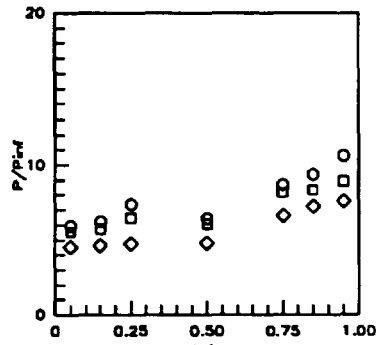
Sym	x'/Ts'	Run No.	CR/Re/Cowl (millions)
○	0.7294	run61	3/0.55/25%
□	0.7294	run63	3/1.14/25%
◇	0.7294	run62	3/2.15/25%

Figure 7.2.3.97: Re Effects  
(CR=3, 25%Cowl)  
Sidewall Pressures



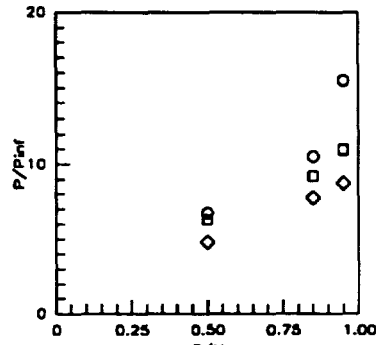
Sym	x'/Ts'	Run No.	CR/Re/Cowl (millions)
○	0.7815	run61	3/0.55/25%
□	0.7815	run63	3/1.14/25%
◇	0.7815	run62	3/2.15/25%

Figure 7.2.3.98: Re Effects  
(CR=3, 25%Cowl)  
Sidewall Pressures



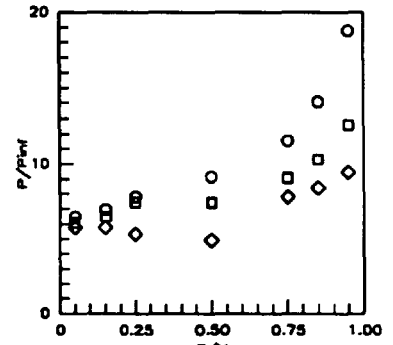
Sym	$x'/T_x'$	Run No.	CR/Re/Cowl (millions)
○	0.8336	run61	3/0.55/25%
□	0.8336	run63	3/1.14/25%
◇	0.8336	run62	3/2.15/25%

Figure 7.2.3.99: Re Effects  
(CR=3, 25% CowI)  
Sidewall Pressures



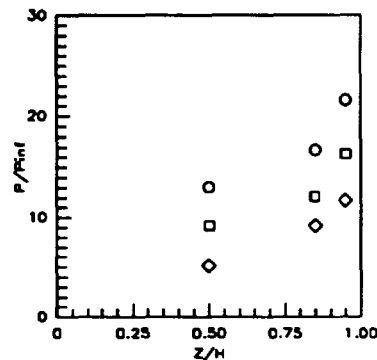
Sym	$x'/T_x'$	Run No.	CR/Re/Cowl (millions)
○	0.8857	run61	3/0.55/25%
□	0.8857	run63	3/1.14/25%
◇	0.8857	run62	3/2.15/25%

Figure 7.2.3.100: Re Effects  
(CR=3, 25% CowI)  
Sidewall Pressures



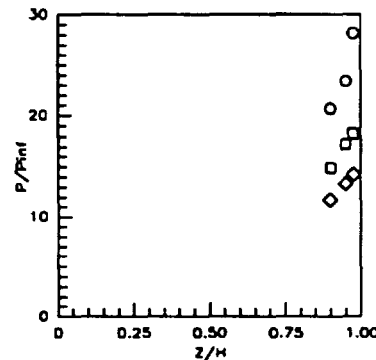
Sym	$x'/T_x'$	Run No.	CR/Re/Cowl (millions)
○	0.9378	run61	3/0.55/25%
□	0.9378	run63	3/1.14/25%
◇	0.9378	run62	3/2.15/25%

Figure 7.2.3.101: Re Effects  
(CR=3, 25% CowI)  
Sidewall Pressures



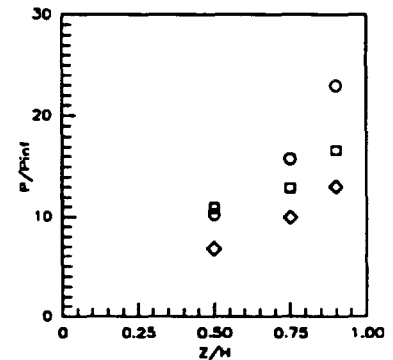
Sym	$x'/T_x'$	Run No.	CR/Re/Cowl (millions)
○	0.9751	run61	3/0.55/25%
□	0.9751	run63	3/1.14/25%
◇	0.9751	run62	3/2.15/25%

Figure 7.2.3.102: Re Effects  
(CR=3, 25% CowI)  
Sidewall Pressures



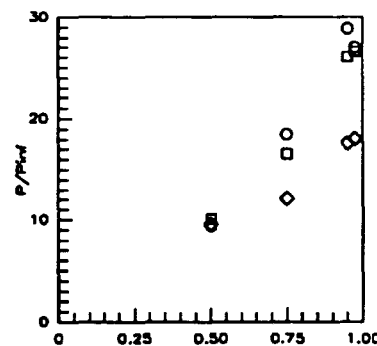
Sym	$x'/T_x'$	Run No.	CR/Re/Cowl (millions)
○	1.0197	run61	3/0.55/25%
□	1.0197	run63	3/1.14/25%
◇	1.0197	run62	3/2.15/25%

Figure 7.2.3.103: Re Effects  
(CR=3, 25% CowI)  
Sidewall Pressures



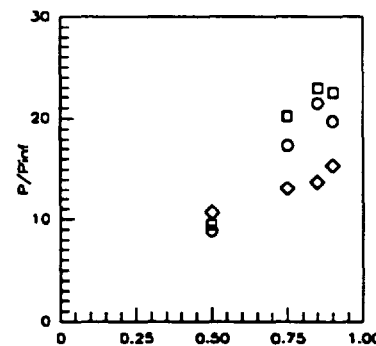
Sym	$x'/T_x'$	Run No.	CR/Re/Cowl (millions)
○	1.0843	run61	3/0.55/25%
□	1.0843	run63	3/1.14/25%
◇	1.0843	run62	3/2.15/25%

Figure 7.2.3.104: Re Effects  
(CR=3, 25% CowI)  
Sidewall Pressures



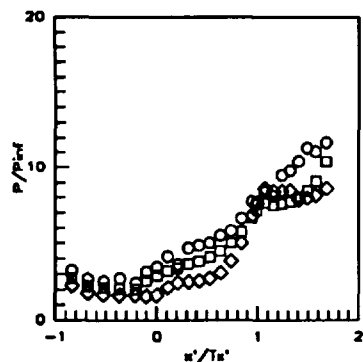
Sym	$x'/T_x'$	Run No.	CR/Re/Cowl (millions)
○	1.1537	run61	3/0.55/25%
□	1.1537	run63	3/1.14/25%
◇	1.1537	run62	3/2.15/25%

Figure 7.2.3.105: Re Effects  
(CR=3, 25% CowI)  
Sidewall Pressures



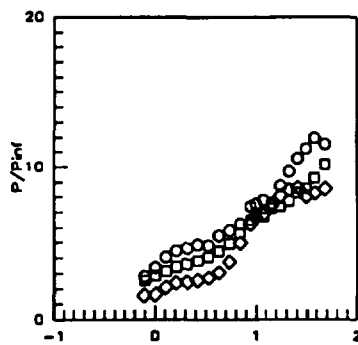
Sym	$x'/T_x'$	Run No.	CR/Re/Cowl (millions)
○	1.2356	run61	3/0.55/25%
□	1.2356	run63	3/1.14/25%
◇	1.2356	run62	3/2.15/25%

Figure 7.2.3.106: Re Effects  
(CR=3, 25% CowI)  
Sidewall Pressures



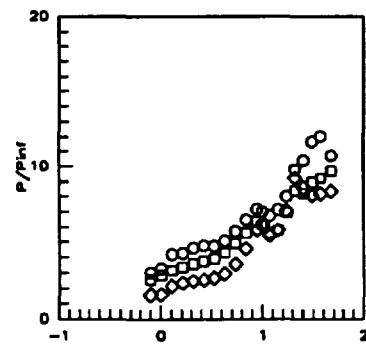
Sym	C.L. for	Run No.	CR/Re/Cowi (millions)
○	CR=3	run58	3/0.55/50%
□	CR=3	run59	3/1.14/50%
◇	CR=3	run80	3/2.15/50%

Figure 7.2.3.107: Re Effects (CR=3, 50% Cowi) Centerline Pressures



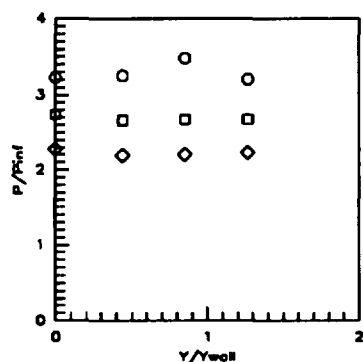
Sym	C.L. for	Run No.	CR/Re/Cowi (millions)
○	CR=5	run58	3/0.55/50%
□	CR=5	run59	3/1.14/50%
◇	CR=5	run80	3/2.15/50%

Figure 7.2.3.108: Re Effects (CR=5, 50% Cowi) Centerline Pressures



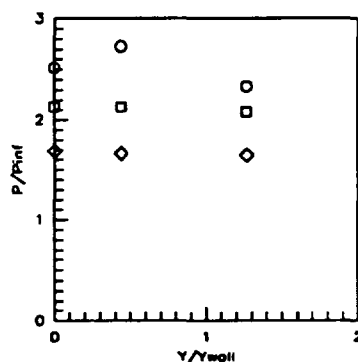
Sym	C.L. for	Run No.	CR/Re/Cowi (millions)
○	CR=9	run58	3/0.55/50%
□	CR=9	run59	3/1.14/50%
◇	CR=9	run80	3/2.15/50%

Figure 7.2.3.109: Re Effects (CR=9, 50% Cowi) Centerline Pressures



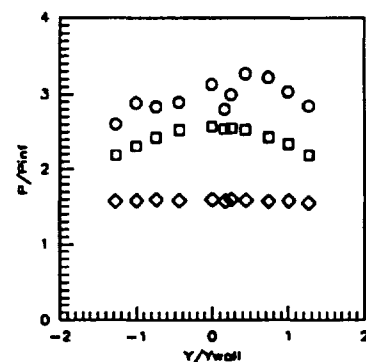
Sym	x'/Tx'	Run No.	CR/Re/Cowi (millions)
○	-0.8412	run58	3/0.55/50%
□	-0.8412	run59	3/1.14/50%
◇	-0.8412	run80	3/2.15/50%

Figure 7.2.3.110: Re Effects (CR=3, 50% Cowi) Baseplate Pressures



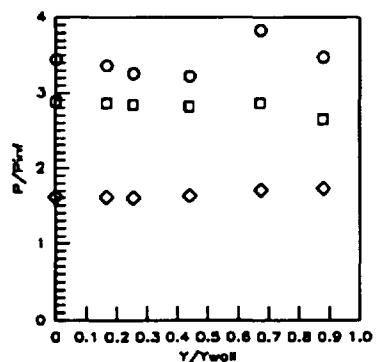
Sym	x'/Tx'	Run No.	CR/Re/Cowi (millions)
○	-0.5258	run58	3/0.55/50%
□	-0.5258	run59	3/1.14/50%
◇	-0.5258	run80	3/2.15/50%

Figure 7.2.3.111: Re Effects (CR=5, 50% Cowi) Baseplate Pressures



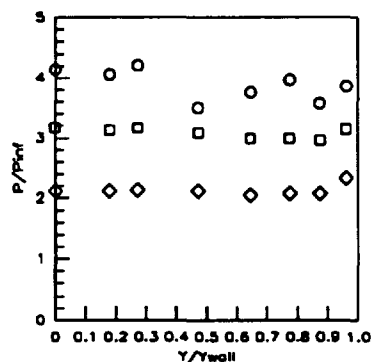
Sym	x'/Tx'	Run No.	CR/Re/Cowi (millions)
○	-0.1052	run58	3/0.55/50%
□	-0.1052	run59	3/1.14/50%
◇	-0.1052	run80	3/2.15/50%

Figure 7.2.3.112: Re Effects (CR=9, 50% Cowi) Baseplate Pressures



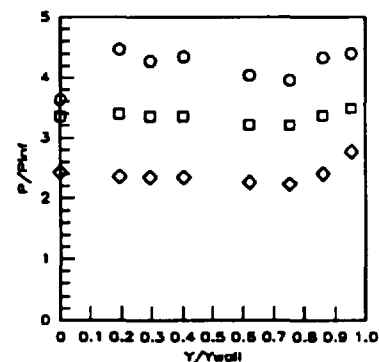
Sym	x'/Tx'	Run No.	CR/Re/Cowi (millions)
○	0.0000	run58	3/0.55/50%
□	0.0000	run59	3/1.14/50%
◇	0.0000	run80	3/2.15/50%

Figure 7.2.3.113: Re Effects (CR=3, 50% Cowi) Baseplate Pressures



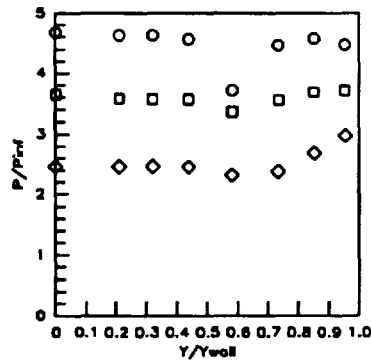
Sym	x'/Tx'	Run No.	CR/Re/Cowi (millions)
○	0.1052	run58	3/0.55/50%
□	0.1052	run59	3/1.14/50%
◇	0.1052	run80	3/2.15/50%

Figure 7.2.3.114: Re Effects (CR=5, 50% Cowi) Baseplate Pressures



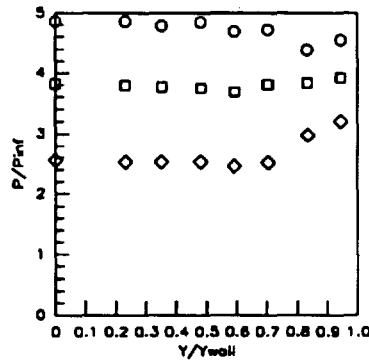
Sym	x'/Tx'	Run No.	CR/Re/Cowi (millions)
○	0.2103	run58	3/0.55/50%
□	0.2103	run59	3/1.14/50%
◇	0.2103	run80	3/2.15/50%

Figure 7.2.3.115: Re Effects (CR=9, 50% Cowi) Baseplate Pressures



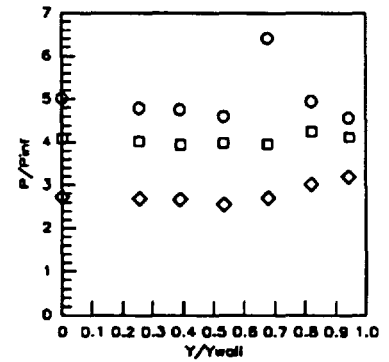
Sym	$x'/T_x'$	Run No.	CR/Re/Cowi (millions)
○	0.3154	run58	3/0.55/50%
□	0.3154	run59	3/1.14/50%
◇	0.3154	run60	3/2.15/50%

Figure 7.2.3.116: Re Effects (CR=3, 50% Cowi) Baseplate Pressures



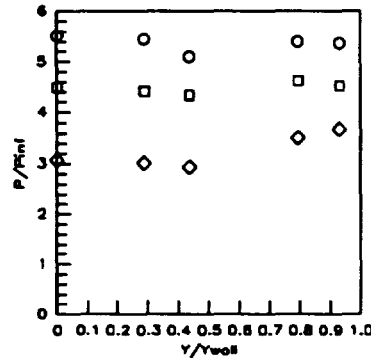
Sym	$x'/T_x'$	Run No.	CR/Re/Cowi (millions)
○	0.4206	run58	3/0.55/50%
□	0.4206	run59	3/1.14/50%
◇	0.4206	run60	3/2.15/50%

Figure 7.2.3.117: Re Effects (CR=3, 50% Cowi) Baseplate Pressures



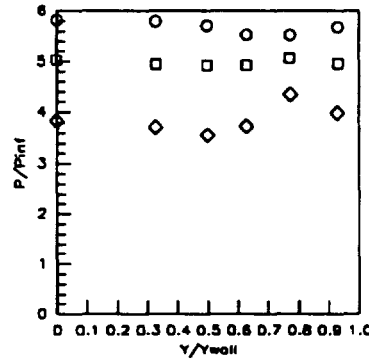
Sym	$x'/T_x'$	Run No.	CR/Re/Cowi (millions)
○	0.5258	run58	3/0.55/50%
□	0.5258	run59	3/1.14/50%
◇	0.5258	run60	3/2.15/50%

Figure 7.2.3.118: Re Effects (CR=3, 50% Cowi) Baseplate Pressures



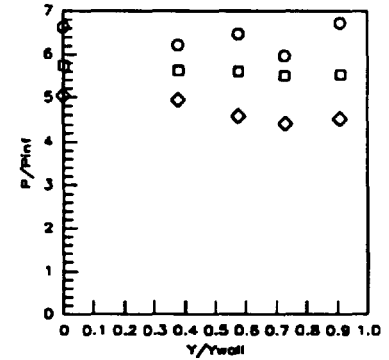
Sym	$x'/T_x'$	Run No.	CR/Re/Cowi (millions)
○	0.6309	run58	3/0.55/50%
□	0.6309	run59	3/1.14/50%
◇	0.6309	run60	3/2.15/50%

Figure 7.2.3.119: Re Effects (CR=3, 50% Cowi) Baseplate Pressures



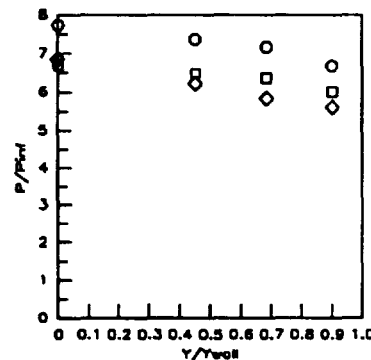
Sym	$x'/T_x'$	Run No.	CR/Re/Cowi (millions)
○	0.7361	run58	3/0.55/50%
□	0.7361	run59	3/1.14/50%
◇	0.7361	run60	3/2.15/50%

Figure 7.2.3.120: Re Effects (CR=3, 50% Cowi) Baseplate Pressures



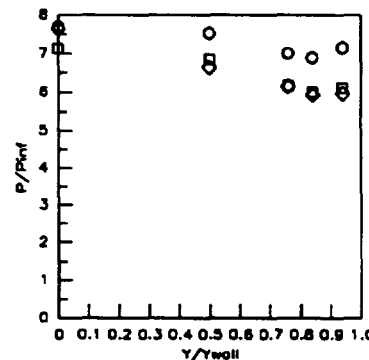
Sym	$x'/T_x'$	Run No.	CR/Re/Cowi (millions)
○	0.8412	run58	3/0.55/50%
□	0.8412	run59	3/1.14/50%
◇	0.8412	run60	3/2.15/50%

Figure 7.2.3.121: Re Effects (CR=3, 50% Cowi) Baseplate Pressures



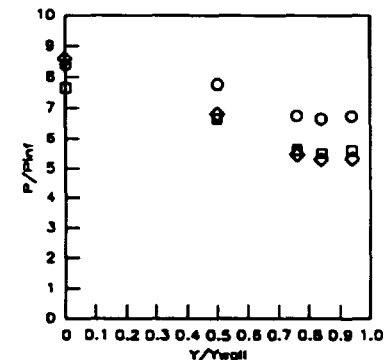
Sym	$x'/T_x'$	Run No.	CR/Re/Cowi (millions)
○	0.9464	run58	3/0.55/50%
□	0.9464	run59	3/1.14/50%
◇	0.9464	run60	3/2.15/50%

Figure 7.2.3.122: Re Effects (CR=3, 50% Cowi) Baseplate Pressures



Sym	$x'/T_x'$	Run No.	CR/Re/Cowi (millions)
○	1.0000	run58	3/0.55/50%
□	1.0000	run59	3/1.14/50%
◇	1.0000	run60	3/2.15/50%

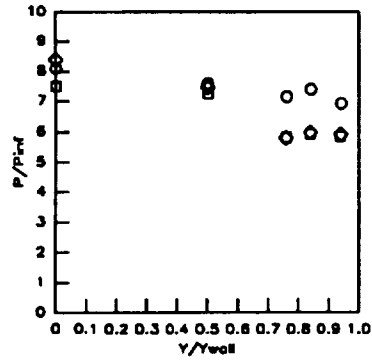
Figure 7.2.3.123: Re Effects (CR=3, 50% Cowi) Baseplate Pressures



Sym	$x'/T_x'$	Run No.	CR/Re/Cowi (millions)
○	1.0726	run58	3/0.55/50%
□	1.0726	run59	3/1.14/50%
◇	1.0726	run60	3/2.15/50%

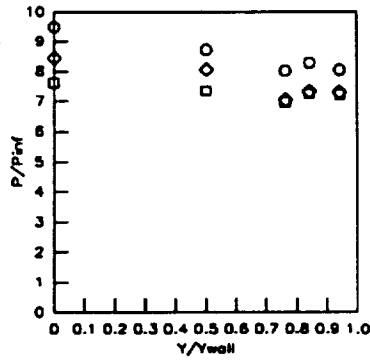
Figure 7.2.3.124: Re Effects (CR=3, 50% Cowi) Baseplate Pressures





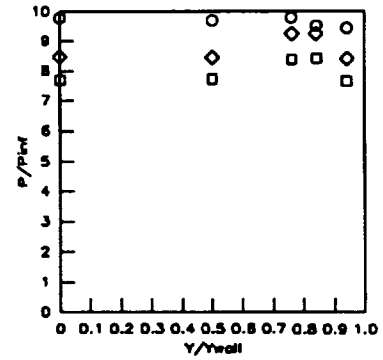
Sym	$x'/T_s'$	Run No.	CR/Re/Cowl (millions)
○	1.1567	run58	3/0.55/50%
□	1.1567	run59	3/1.14/50%
◇	1.1567	run60	3/2.15/50%

Figure 7.2.3.125: Re Effects Baseplate Pressures



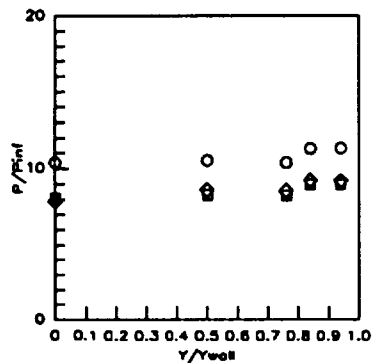
Sym	$x'/T_s'$	Run No.	CR/Re/Cowl (millions)
○	1.2408	run58	3/0.55/50%
□	1.2408	run59	3/1.14/50%
◇	1.2408	run60	3/2.15/50%

Figure 7.2.3.126: Re Effects Baseplate Pressures



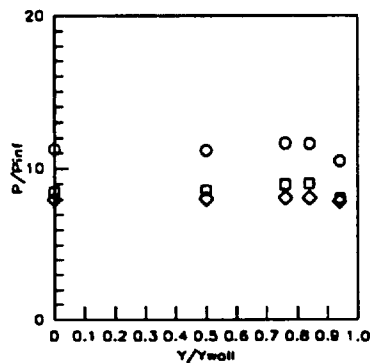
Sym	$x'/T_s'$	Run No.	CR/Re/Cowl (millions)
○	1.3249	run58	3/0.55/50%
□	1.3249	run59	3/1.14/50%
◇	1.3249	run60	3/2.15/50%

Figure 7.2.3.127: Re Effects Baseplate Pressures



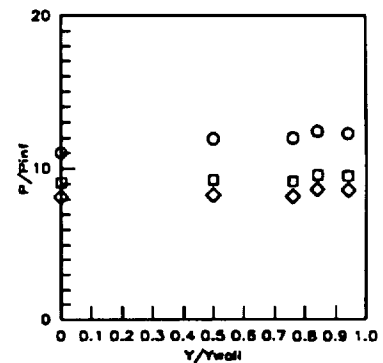
Sym	$x'/T_s'$	Run No.	CR/Re/Cowl (millions)
○	1.4090	run58	3/0.55/50%
□	1.4090	run59	3/1.14/50%
◇	1.4090	run60	3/2.15/50%

Figure 7.2.3.128: Re Effects Baseplate Pressures



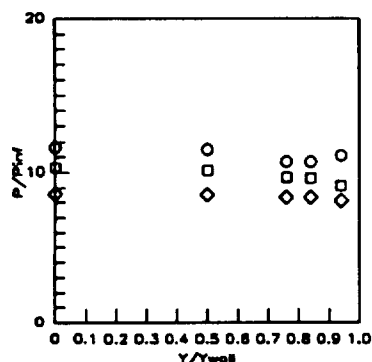
Sym	$x'/T_s'$	Run No.	CR/Re/Cowl (millions)
○	1.4832	run58	3/0.55/50%
□	1.4832	run59	3/1.14/50%
◇	1.4832	run60	3/2.15/50%

Figure 7.2.3.129: Re Effects Baseplate Pressures



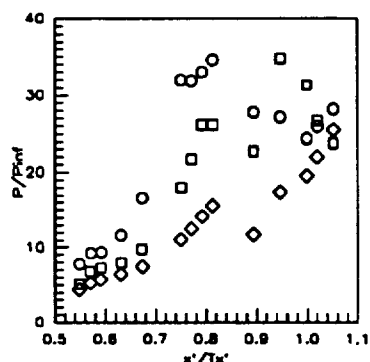
Sym	$x'/T_s'$	Run No.	CR/Re/Cowl (millions)
○	1.5773	run58	3/0.55/50%
□	1.5773	run59	3/1.14/50%
◇	1.5773	run60	3/2.15/50%

Figure 7.2.3.130: Re Effects Baseplate Pressures



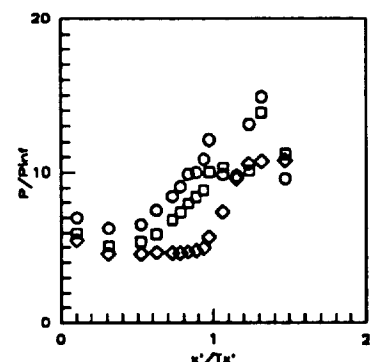
Sym	$x'/T_s'$	Run No.	CR/Re/Cowl (millions)
○	1.6824	run58	3/0.55/50%
□	1.6824	run59	3/1.14/50%
◇	1.6824	run60	3/2.15/50%

Figure 7.2.3.131: Re Effects Baseplate Pressures



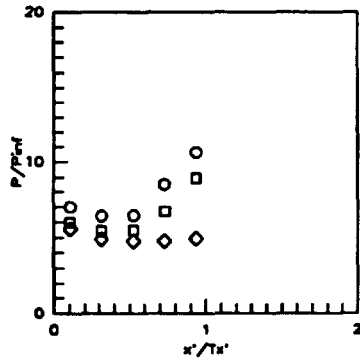
Sym	Cowl Pos.	Run No.	CR/Re/Cowl (millions)
○	50%	run58	3/0.55/50%
□	50%	run59	3/1.14/50%
◇	50%	run60	3/2.15/50%

Figure 7.2.3.132: Re Effects Cowl Pressures



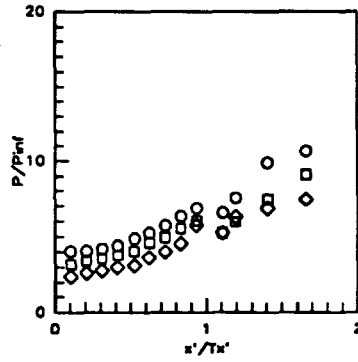
Sym	Z/H	Run No.	CR/Re/Cowl (millions)
○	0.5RT	run58	3/0.55/50%
□	0.5RT	run59	3/1.14/50%
◇	0.5RT	run60	3/2.15/50%

Figure 7.2.3.133: Re Effects Sidewall Centerline Pressures



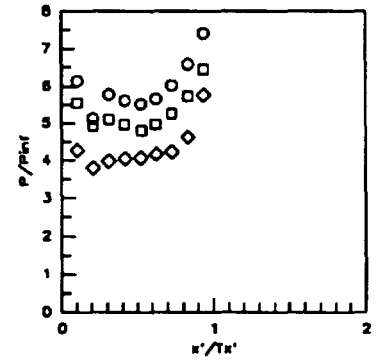
Sym	Z/H	Run No.	CR/Re/Cowi (millions)
o	0.5LT	run58	3/0.55/50%
o	0.5LT	run59	3/1.14/50%
o	0.5LT	run60	3/2.15/50%

Figure 7.2.3.134: Re Effects (CR=3, 50% Cowi) Sidewall Centerline Pressures



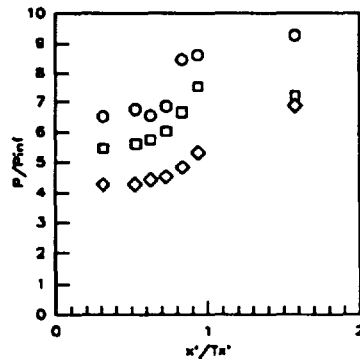
Sym	Z/H	Run No.	CR/Re/Cowi (millions)
o	0.050	run58	3/0.55/50%
o	0.050	run59	3/1.14/50%
o	0.050	run60	3/2.15/50%

Figure 7.2.3.135: Re Effects (CR=3, 50% Cowi) Sidewall Pressures



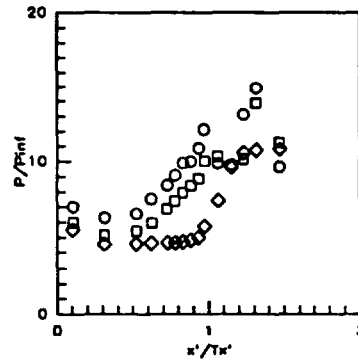
Sym	Z/H	Run No.	CR/Re/Cowi (millions)
o	0.15	run58	3/0.55/50%
o	0.15	run59	3/1.14/50%
o	0.15	run60	3/2.15/50%

Figure 7.2.3.136: Re Effects (CR=3, 50% Cowi) Sidewall Pressures



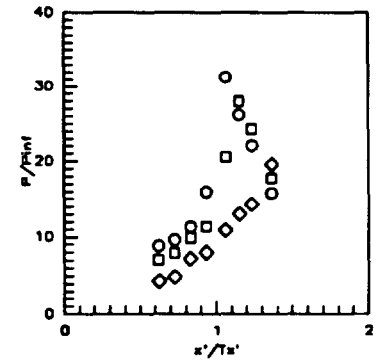
Sym	Z/H	Run No.	CR/Re/Cowi (millions)
o	0.25	run58	3/0.55/50%
o	0.25	run59	3/1.14/50%
o	0.25	run60	3/2.15/50%

Figure 7.2.3.137: Re Effects (CR=3, 50% Cowi) Sidewall Pressures



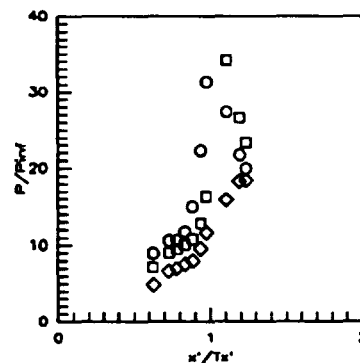
Sym	Z/H	Run No.	CR/Re/Cowi (millions)
o	0.50	run58	3/0.55/50%
o	0.50	run59	3/1.14/50%
o	0.50	run60	3/2.15/50%

Figure 7.2.3.138: Re Effects (CR=3, 50% Cowi) Sidewall Pressures



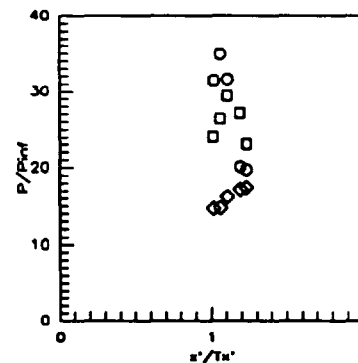
Sym	Z/H	Run No.	CR/Re/Cowi (millions)
o	0.75	run58	3/0.55/50%
o	0.75	run59	3/1.14/50%
o	0.75	run60	3/2.15/50%

Figure 7.2.3.139: Re Effects (CR=3, 50% Cowi) Sidewall Pressures



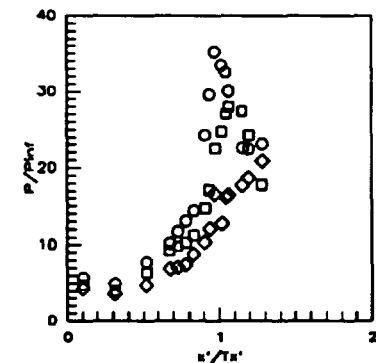
Sym	Z/H	Run No.	CR/Re/Cowi (millions)
o	0.85	run58	3/0.55/50%
o	0.85	run59	3/1.14/50%
o	0.85	run60	3/2.15/50%

Figure 7.2.3.140: Re Effects (CR=3, 50% Cowi) Sidewall Pressures



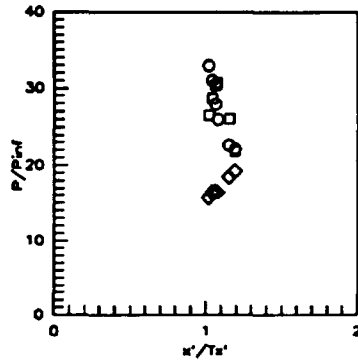
Sym	Z/H	Run No.	CR/Re/Cowi (millions)
o	0.90	run58	3/0.55/50%
o	0.90	run59	3/1.14/50%
o	0.90	run60	3/2.15/50%

Figure 7.2.3.141: Re Effects (CR=3, 50% Cowi) Sidewall Pressures



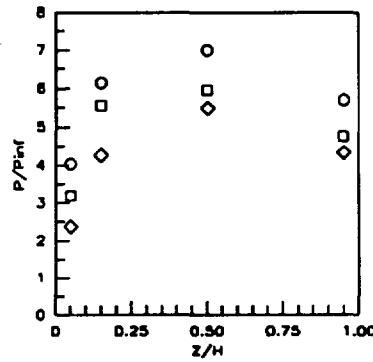
Sym	Z/H	Run No.	CR/Re/Cowi (millions)
o	0.95	run58	3/0.55/50%
o	0.95	run59	3/1.14/50%
o	0.95	run60	3/2.15/50%

Figure 7.2.3.142: Re Effects (CR=3, 50% Cowi) Sidewall Pressures



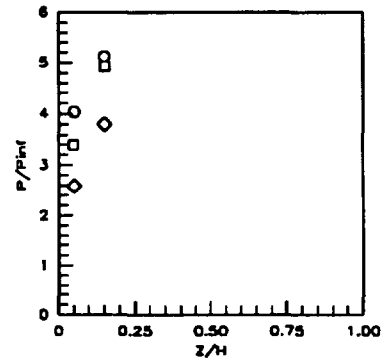
Sym	$x'/Ts'$	Run No.	CR/Re/Cowl (millions)
-----	----------	---------	-----------------------

Figure 7.2.3.143: Re Effects  
(CR=3, 50%Cowl)  
Sidewall Pressures



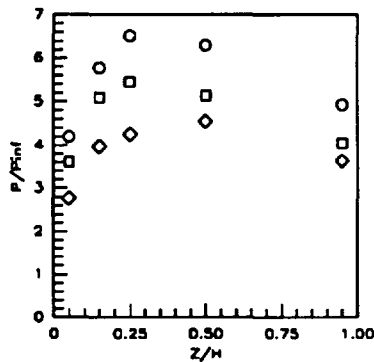
Sym	$x'/Ts'$	Run No.	CR/Re/Cowl (millions)
-----	----------	---------	-----------------------

Figure 7.2.3.144: Re Effects  
(CR=3, 50%Cowl)  
Sidewall Pressures



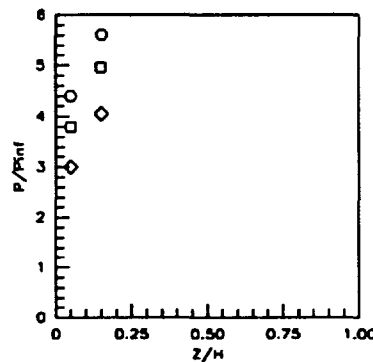
Sym	$x'/Ts'$	Run No.	CR/Re/Cowl (millions)
-----	----------	---------	-----------------------

Figure 7.2.3.145: Re Effects  
(CR=3, 50%Cowl)  
Sidewall Pressures



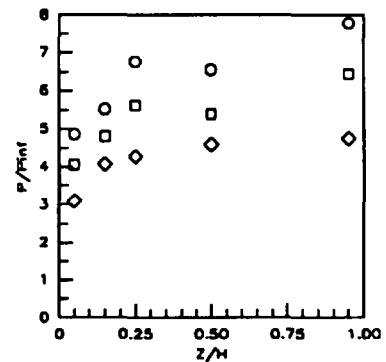
Sym	$x'/Ts'$	Run No.	CR/Re/Cowl (millions)
-----	----------	---------	-----------------------

Figure 7.2.3.146: Re Effects  
(CR=3, 50%Cowl)  
Sidewall Pressures



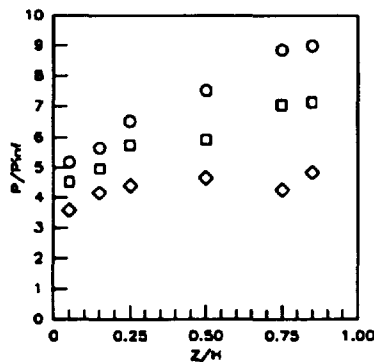
Sym	$x'/Ts'$	Run No.	CR/Re/Cowl (millions)
-----	----------	---------	-----------------------

Figure 7.2.3.147: Re Effects  
(CR=3, 50%Cowl)  
Sidewall Pressures



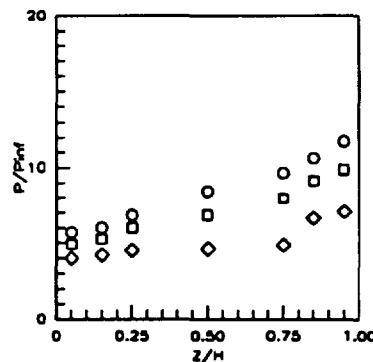
Sym	$x'/Ts'$	Run No.	CR/Re/Cowl (millions)
-----	----------	---------	-----------------------

Figure 7.2.3.148: Re Effects  
(CR=3, 50%Cowl)  
Sidewall Pressures



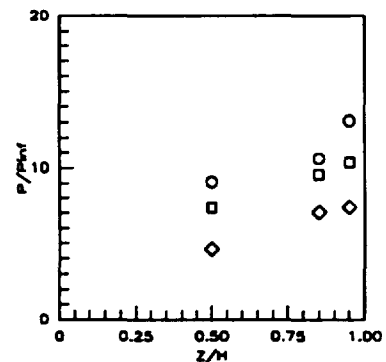
Sym	$x'/Ts'$	Run No.	CR/Re/Cowl (millions)
-----	----------	---------	-----------------------

Figure 7.2.3.149: Re Effects  
(CR=3, 50%Cowl)  
Sidewall Pressures



Sym	$x'/Ts'$	Run No.	CR/Re/Cowl (millions)
-----	----------	---------	-----------------------

Figure 7.2.3.150: Re Effects  
(CR=3, 50%Cowl)  
Sidewall Pressures



Sym	$x'/Ts'$	Run No.	CR/Re/Cowl (millions)
-----	----------	---------	-----------------------

Figure 7.2.3.151: Re Effects  
(CR=3, 50%Cowl)  
Sidewall Pressures

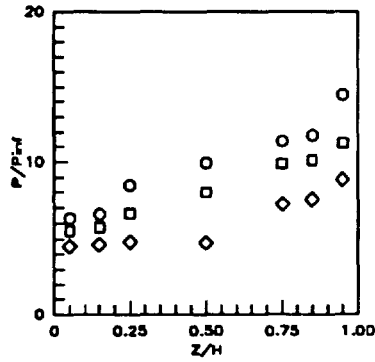


Figure 7.2.3.152: Re Effects  
(CR=3, 50%Cowl)  
Sidewall Pressures

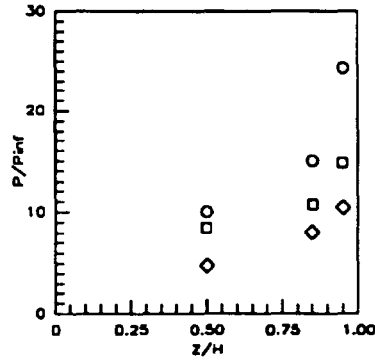


Figure 7.2.3.153: Re Effects  
(CR=3, 50%Cowl)  
Sidewall Pressures

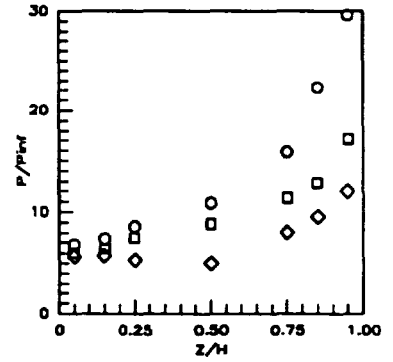


Figure 7.2.3.154: Re Effects  
(CR=3, 50%Cowl)  
Sidewall Pressures

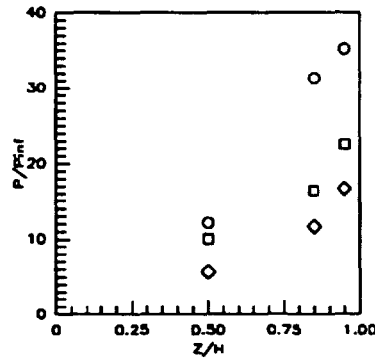


Figure 7.2.3.155: Re Effects  
(CR=3, 50%Cowl)  
Sidewall Pressures

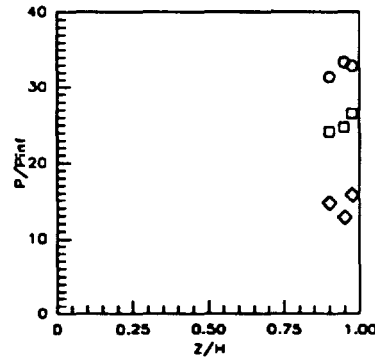


Figure 7.2.3.156: Re Effects  
(CR=3, 50%Cowl)  
Sidewall Pressures

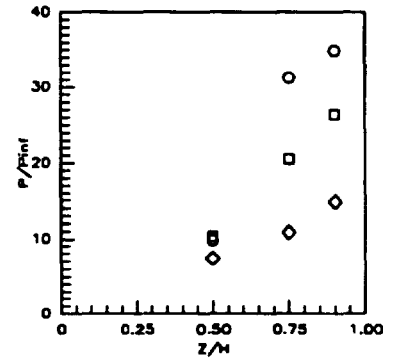


Figure 7.2.3.157: Re Effects  
(CR=3, 50%Cowl)  
Sidewall Pressures

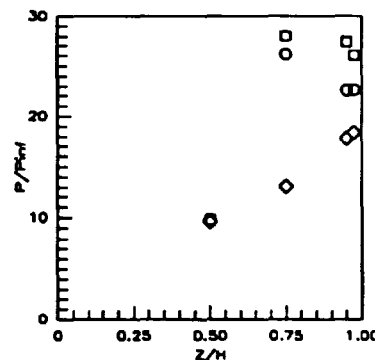


Figure 7.2.3.158: Re Effects  
(CR=3, 50%Cowl)  
Sidewall Pressures

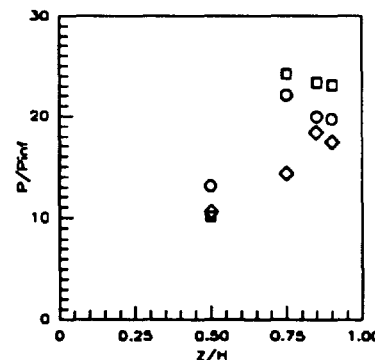
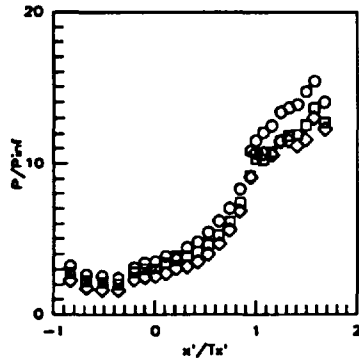
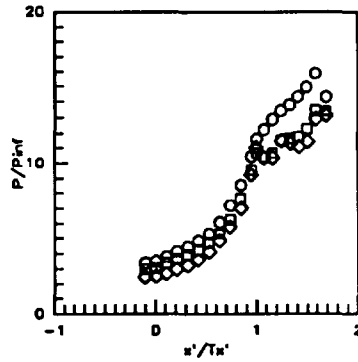


Figure 7.2.3.159: Re Effects  
(CR=3, 50%Cowl)  
Sidewall Pressures



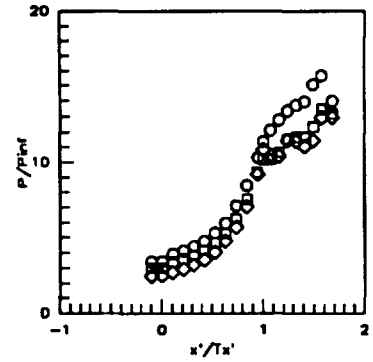
Sym	C.L. for	Run No.	CR/Re/Cowl (millions)
○	CR=3	run44	5/0.55/ 0%
□	CR=3	run45	5/1.14/ 0%
◇	CR=3	run46	5/2.15/ 0%

Figure 7.2.3.180: Re Effects (CR=5, 0% Cowl)  
CR=3 Centerline Pressures



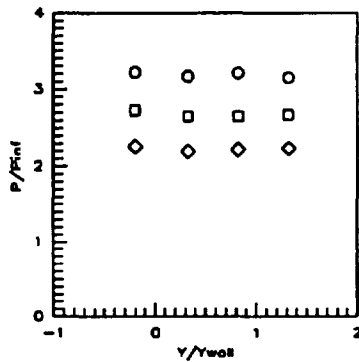
Sym	C.L. for	Run No.	CR/Re/Cowl (millions)
○	CR=5	run44	5/0.55/ 0%
□	CR=5	run45	5/1.14/ 0%
◇	CR=5	run46	5/2.15/ 0%

Figure 7.2.3.181: Re Effects (CR=5, 0% Cowl)  
CR=5 Centerline Pressures



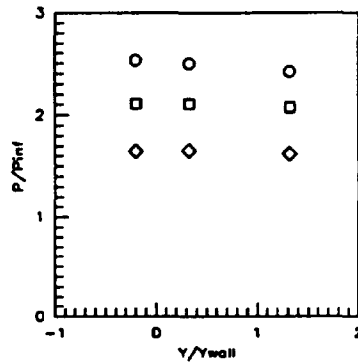
Sym	C.L. for	Run No.	CR/Re/Cowl (millions)
○	CR=9	run44	5/0.55/ 0%
□	CR=9	run45	5/1.14/ 0%
◇	CR=9	run46	5/2.15/ 0%

Figure 7.2.3.182: Re Effects (CR=9, 0% Cowl)  
CR=9 Centerline Pressures



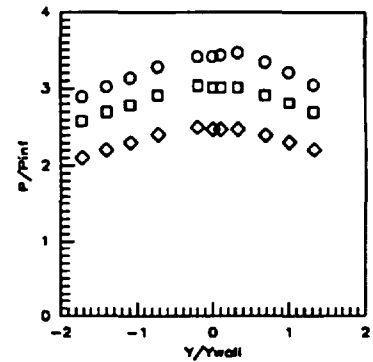
Sym	x'/Tx'	Run No.	CR/Re/Cowl (millions)
○	-0.8412	run44	5/0.55/ 0%
□	-0.8412	run45	5/1.14/ 0%
◇	-0.8412	run46	5/2.15/ 0%

Figure 7.2.3.163: Re Effects (CR=5, 0% Cowl)  
Baseplate Pressures



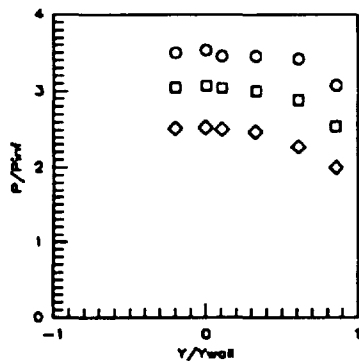
Sym	x'/Tx'	Run No.	CR/Re/Cowl (millions)
○	-0.5258	run44	5/0.55/ 0%
□	-0.5258	run45	5/1.14/ 0%
◇	-0.5258	run46	5/2.15/ 0%

Figure 7.2.3.164: Re Effects (CR=5, 0% Cowl)  
Baseplate Pressures



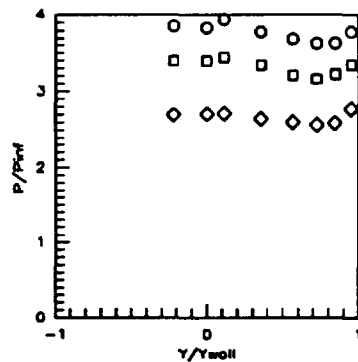
Sym	x'/Tx'	Run No.	CR/Re/Cowl (millions)
○	-0.1052	run44	5/0.55/ 0%
□	-0.1052	run45	5/1.14/ 0%
◇	-0.1052	run46	5/2.15/ 0%

Figure 7.2.3.165: Re Effects (CR=5, 0% Cowl)  
Baseplate Pressures



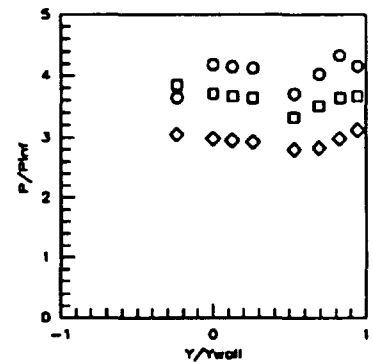
Sym	x'/Tx'	Run No.	CR/Re/Cowl (millions)
○	0.0000	run44	5/0.55/ 0%
□	0.0000	run45	5/1.14/ 0%
◇	0.0000	run46	5/2.15/ 0%

Figure 7.2.3.166: Re Effects (CR=5, 0% Cowl)  
Baseplate Pressures



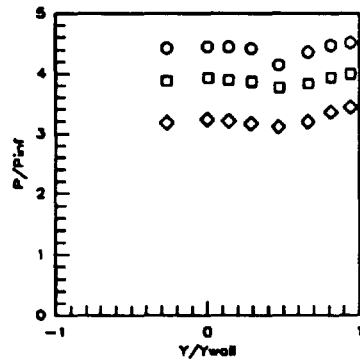
Sym	x'/Tx'	Run No.	CR/Re/Cowl (millions)
○	0.1052	run44	5/0.55/ 0%
□	0.1052	run45	5/1.14/ 0%
◇	0.1052	run46	5/2.15/ 0%

Figure 7.2.3.167: Re Effects (CR=5, 0% Cowl)  
Baseplate Pressures



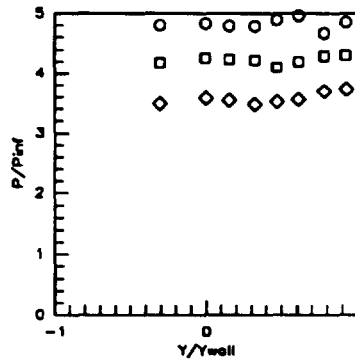
Sym	x'/Tx'	Run No.	CR/Re/Cowl (millions)
○	0.2103	run44	5/0.55/ 0%
□	0.2103	run45	5/1.14/ 0%
◇	0.2103	run46	5/2.15/ 0%

Figure 7.2.3.168: Re Effects (CR=5, 0% Cowl)  
Baseplate Pressures



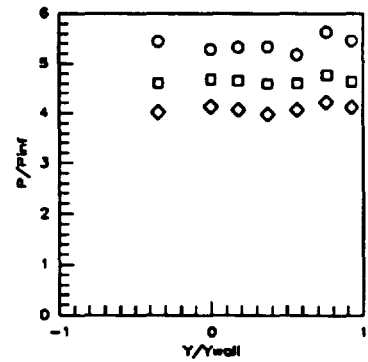
Sym	$x'/T_x'$	Run No.	CR/Re/Cowl (millions)
○	0.3154	run44	5/0.55/ 0%
□	0.3154	run45	5/1.14/ 0%
◇	0.3154	run46	5/2.15/ 0%

Figure 7.2.3.169: Re Effects (CR=5, 0%Cowl) Baseplate Pressures



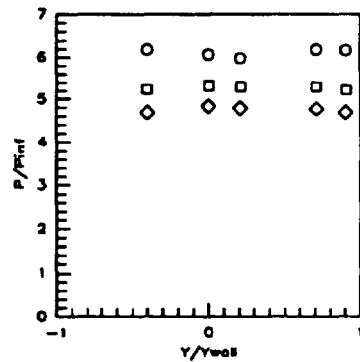
Sym	$x'/T_x'$	Run No.	CR/Re/Cowl (millions)
○	0.4206	run44	5/0.55/ 0%
□	0.4206	run45	5/1.14/ 0%
◇	0.4206	run46	5/2.15/ 0%

Figure 7.2.3.170: Re Effects (CR=5, 0%Cowl) Baseplate Pressures



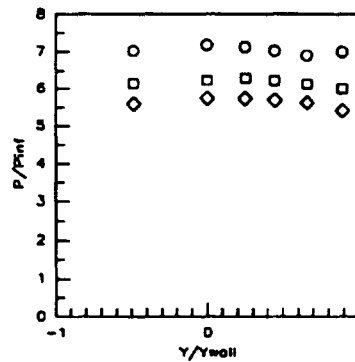
Sym	$x'/T_x'$	Run No.	CR/Re/Cowl (millions)
○	0.5258	run44	5/0.55/ 0%
□	0.5258	run45	5/1.14/ 0%
◇	0.5258	run46	5/2.15/ 0%

Figure 7.2.3.171: Re Effects (CR=5, 0%Cowl) Baseplate Pressures



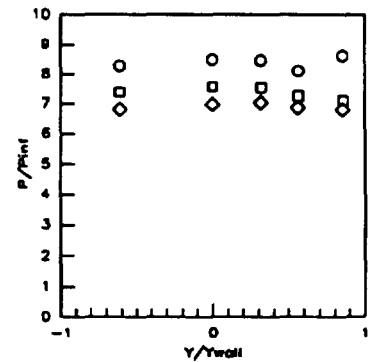
Sym	$x'/T_x'$	Run No.	CR/Re/Cowl (millions)
○	0.6309	run44	5/0.55/ 0%
□	0.6309	run45	5/1.14/ 0%
◇	0.6309	run46	5/2.15/ 0%

Figure 7.2.3.172: Re Effects (CR=5, 0%Cowl) Baseplate Pressures



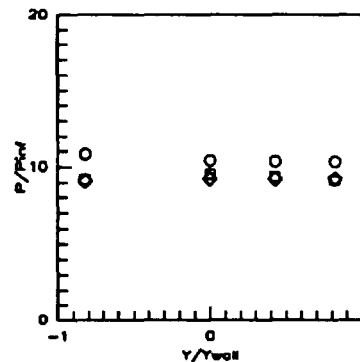
Sym	$x'/T_x'$	Run No.	CR/Re/Cowl (millions)
○	0.7361	run44	5/0.55/ 0%
□	0.7361	run45	5/1.14/ 0%
◇	0.7361	run46	5/2.15/ 0%

Figure 7.2.3.173: Re Effects (CR=5, 0%Cowl) Baseplate Pressures



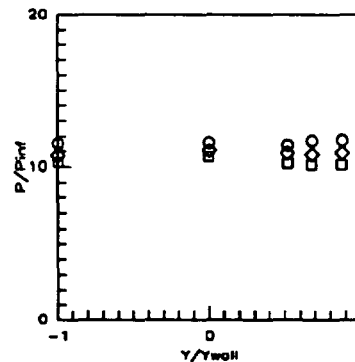
Sym	$x'/T_x'$	Run No.	CR/Re/Cowl (millions)
○	0.8412	run44	5/0.55/ 0%
□	0.8412	run45	5/1.14/ 0%
◇	0.8412	run46	5/2.15/ 0%

Figure 7.2.3.174: Re Effects (CR=5, 0%Cowl) Baseplate Pressures



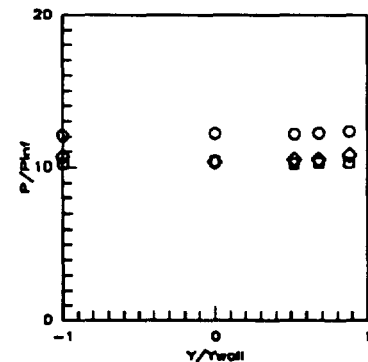
Sym	$x'/T_x'$	Run No.	CR/Re/Cowl (millions)
○	0.9464	run44	5/0.55/ 0%
□	0.9464	run45	5/1.14/ 0%
◇	0.9464	run46	5/2.15/ 0%

Figure 7.2.3.175: Re Effects (CR=5, 0%Cowl) Baseplate Pressures



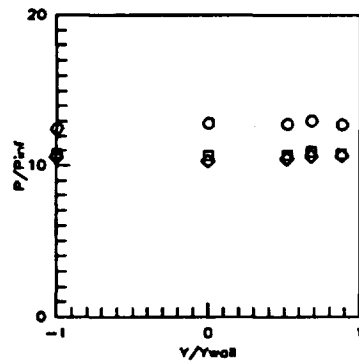
Sym	$x'/T_x'$	Run No.	CR/Re/Cowl (millions)
○	1.0000	run44	5/0.55/ 0%
□	1.0000	run45	5/1.14/ 0%
◇	1.0000	run46	5/2.15/ 0%

Figure 7.2.3.176: Re Effects (CR=5, 0%Cowl) Baseplate Pressures



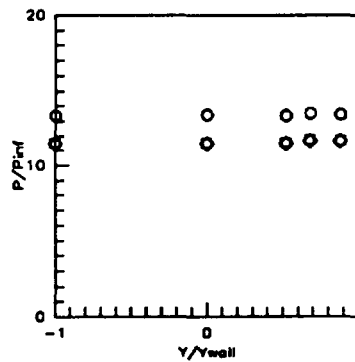
Sym	$x'/T_x'$	Run No.	CR/Re/Cowl (millions)
○	1.0728	run44	5/0.55/ 0%
□	1.0728	run45	5/1.14/ 0%
◇	1.0728	run46	5/2.15/ 0%

Figure 7.2.3.177: Re Effects (CR=5, 0%Cowl) Baseplate Pressures



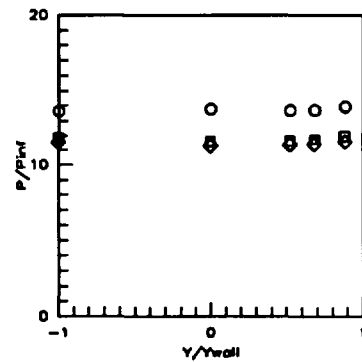
Sym	x'/Ts'	Run No.	CR/Re/Cowi (millions)
○	1.1567	run44	5/0.55/ 0%
□	1.1567	run45	5/1.14/ 0%
◇	1.1567	run46	5/2.15/ 0%

Figure 7.2.3.178: Re Effects (CR=5, 0% Cowi) Baseplate Pressures



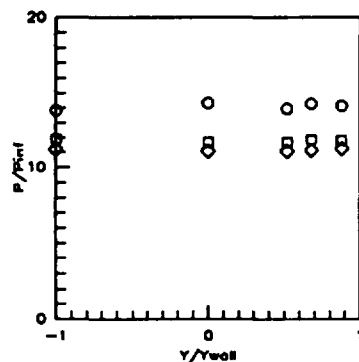
Sym	x'/Ts'	Run No.	CR/Re/Cowi (millions)
○	1.2408	run44	5/0.55/ 0%
□	1.2408	run45	5/1.14/ 0%
◇	1.2408	run46	5/2.15/ 0%

Figure 7.2.3.179: Re Effects (CR=5, 0% Cowi) Baseplate Pressures



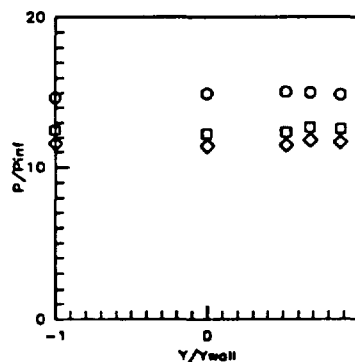
Sym	x'/Ts'	Run No.	CR/Re/Cowi (millions)
○	1.3249	run44	5/0.55/ 0%
□	1.3249	run45	5/1.14/ 0%
◇	1.3249	run46	5/2.15/ 0%

Figure 7.2.3.180: Re Effects (CR=5, 0% Cowi) Baseplate Pressures



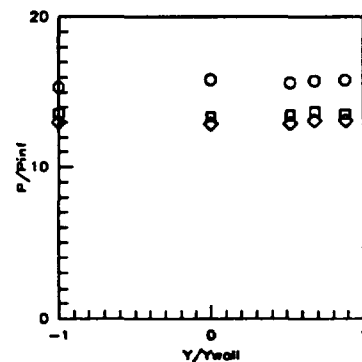
Sym	x'/Ts'	Run No.	CR/Re/Cowi (millions)
○	1.4090	run44	5/0.55/ 0%
□	1.4090	run45	5/1.14/ 0%
◇	1.4090	run46	5/2.15/ 0%

Figure 7.2.3.181: Re Effects (CR=5, 0% Cowi) Baseplate Pressures



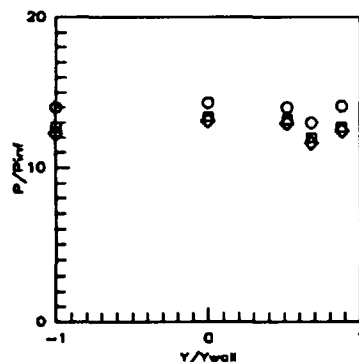
Sym	x'/Ts'	Run No.	CR/Re/Cowi (millions)
○	1.4932	run44	5/0.55/ 0%
□	1.4932	run45	5/1.14/ 0%
◇	1.4932	run46	5/2.15/ 0%

Figure 7.2.3.182: Re Effects (CR=5, 0% Cowi) Baseplate Pressures



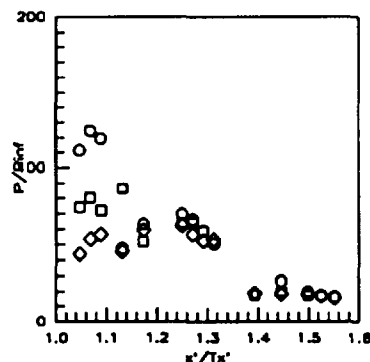
Sym	x'/Ts'	Run No.	CR/Re/Cowi (millions)
○	1.5773	run44	5/0.55/ 0%
□	1.5773	run45	5/1.14/ 0%
◇	1.5773	run46	5/2.15/ 0%

Figure 7.2.3.183: Re Effects (CR=5, 0% Cowi) Baseplate Pressures



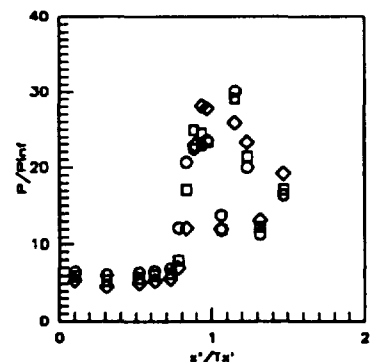
Sym	x'/Ts'	Run No.	CR/Re/Cowi (millions)
○	1.6824	run44	5/0.55/ 0%
□	1.6824	run45	5/1.14/ 0%
◇	1.6824	run46	5/2.15/ 0%

Figure 7.2.3.184: Re Effects (CR=5, 0% Cowi) Baseplate Pressures



Sym	Cowi Pos.	Run No.	CR/Re/Cowi (millions)
○	0%	run44	5/0.55/ 0%
□	0%	run45	5/1.14/ 0%
◇	0%	run46	5/2.15/ 0%

Figure 7.2.3.185: Re Effects (CR=5, 0% Cowi) Cowi Pressures



Sym	Z/H	Run No.	CR/Re/Cowi (millions)
○	0.5RT	run44	5/0.55/ 0%
□	0.5RT	run45	5/1.14/ 0%
◇	0.5RT	run46	5/2.15/ 0%

Figure 7.2.3.186: Re Effects (CR=5, 0% Cowi) Sidewall Centerline Pressures

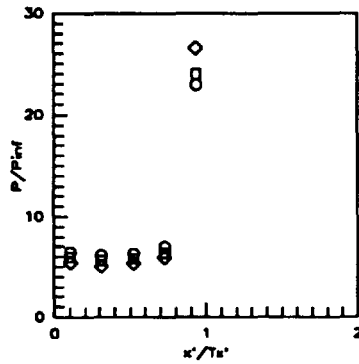


Figure 7.2.3.187: Re Effects  
(CR=5, 0% Cowi)  
Sidewall Centerline Pressures

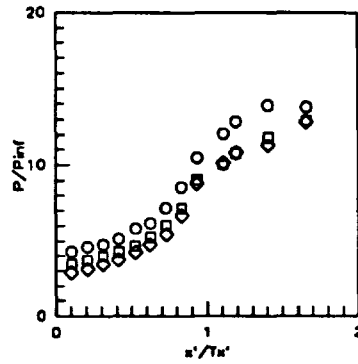


Figure 7.2.3.188: Re Effects  
(CR=5, 0% Cowi)  
Sidewall Pressures

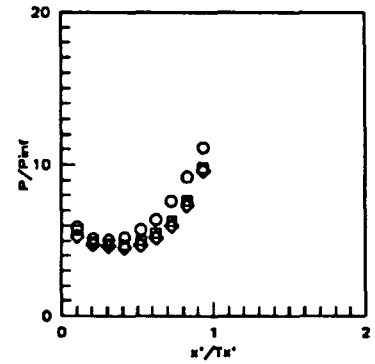


Figure 7.2.3.189: Re Effects  
(CR=5, 0% Cowi)  
Sidewall Pressures

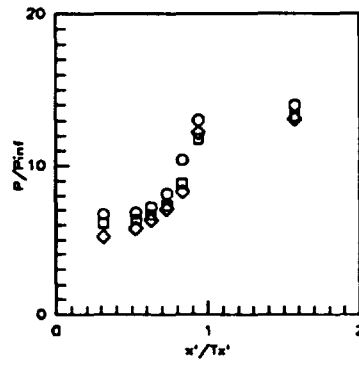


Figure 7.2.3.190: Re Effects  
(CR=5, 0% Cowi)  
Sidewall Pressures

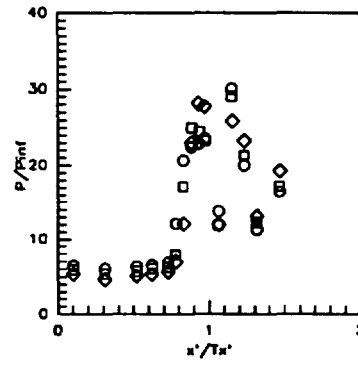


Figure 7.2.3.191: Re Effects  
(CR=5, 0% Cowi)  
Sidewall Pressures

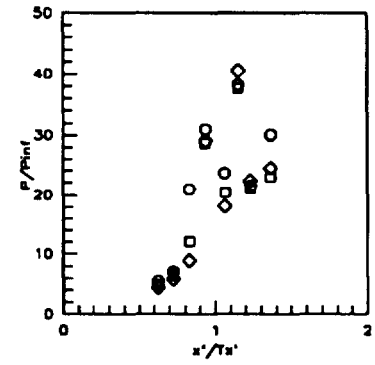


Figure 7.2.3.192: Re Effects  
(CR=5, 0% Cowi)  
Sidewall Pressures

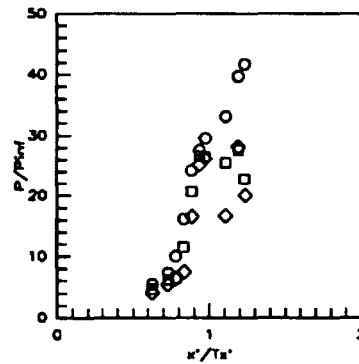


Figure 7.2.3.193: Re Effects  
(CR=5, 0% Cowi)  
Sidewall Pressures

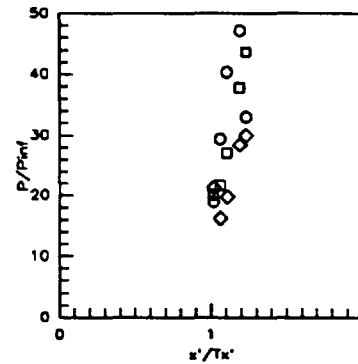


Figure 7.2.3.194: Re Effects  
(CR=5, 0% Cowi)  
Sidewall Pressures

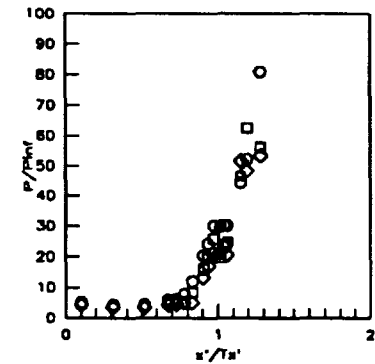
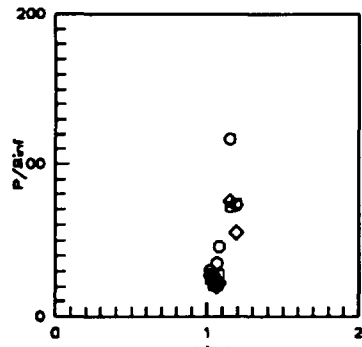


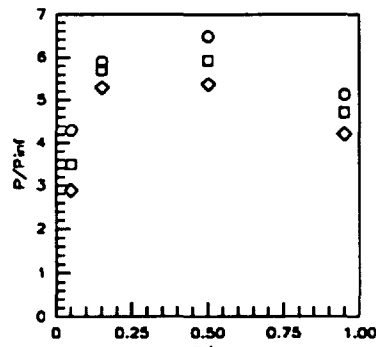
Figure 7.2.3.195: Re Effects  
(CR=5, 0% Cowi)  
Sidewall Pressures





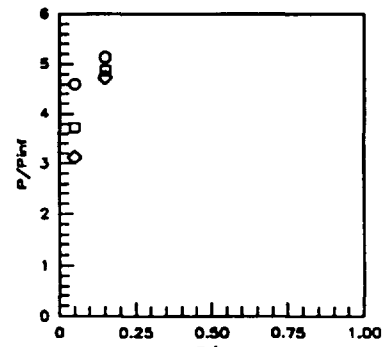
Sym	Z/H	Run No.	CR/Re/Cowl (millions)
○	0.975	run44	5/0.55/ 0%
○	0.975	run45	5/1.14/ 0%
○	0.975	run46	5/2.15/ 0%

Figure 7.2.3.196: Re Effects  
(CR=5, 0%Cowl)  
Sidewall Pressures



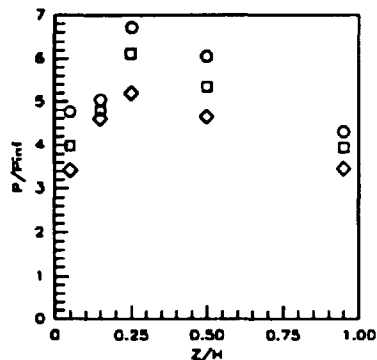
Sym	x'/Ts'	Run No.	CR/Re/Cowl (millions)
○	0.1042	run44	5/0.55/ 0%
○	0.1042	run45	5/1.14/ 0%
○	0.1042	run46	5/2.15/ 0%

Figure 7.2.3.197: Re Effects  
(CR=5, 0%Cowl)  
Sidewall Pressures



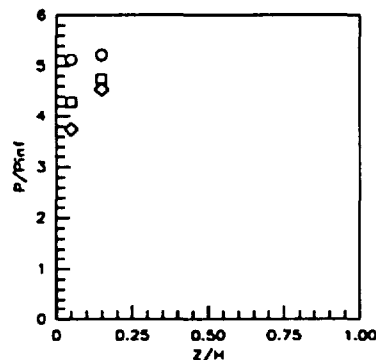
Sym	x'/Ts'	Run No.	CR/Re/Cowl (millions)
○	0.2083	run44	5/0.55/ 0%
○	0.2083	run45	5/1.14/ 0%
○	0.2083	run46	5/2.15/ 0%

Figure 7.2.3.198: Re Effects  
(CR=5, 0%Cowl)  
Sidewall Pressures



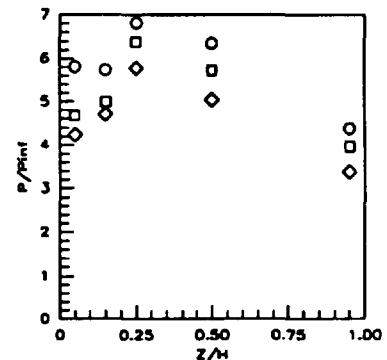
Sym	x'/Ts'	Run No.	CR/Re/Cowl (millions)
○	0.3125	run44	5/0.55/ 0%
○	0.3125	run45	5/1.14/ 0%
○	0.3125	run46	5/2.15/ 0%

Figure 7.2.3.199: Re Effects  
(CR=5, 0%Cowl)  
Sidewall Pressures



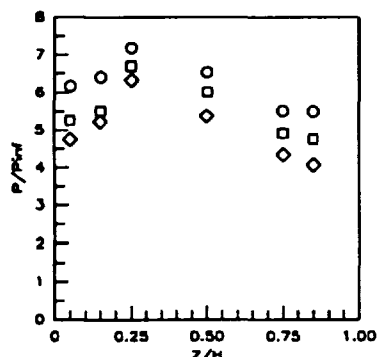
Sym	x'/Ts'	Run No.	CR/Re/Cowl (millions)
○	0.4187	run44	5/0.55/ 0%
○	0.4187	run45	5/1.14/ 0%
○	0.4187	run46	5/2.15/ 0%

Figure 7.2.3.200: Re Effects  
(CR=5, 0%Cowl)  
Sidewall Pressures



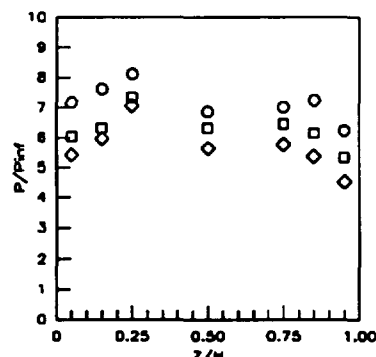
Sym	x'/Ts'	Run No.	CR/Re/Cowl (millions)
○	0.5259	run44	5/0.55/ 0%
○	0.5259	run45	5/1.14/ 0%
○	0.5259	run46	5/2.15/ 0%

Figure 7.2.3.201: Re Effects  
(CR=5, 0%Cowl)  
Sidewall Pressures



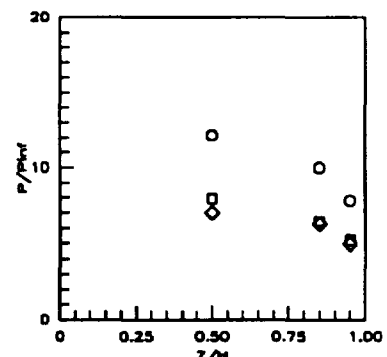
Sym	x'/Ts'	Run No.	CR/Re/Cowl (millions)
○	0.6252	run44	5/0.55/ 0%
○	0.6252	run45	5/1.14/ 0%
○	0.6252	run46	5/2.15/ 0%

Figure 7.2.3.202: Re Effects  
(CR=5, 0%Cowl)  
Sidewall Pressures



Sym	x'/Ts'	Run No.	CR/Re/Cowl (millions)
○	0.7294	run44	5/0.55/ 0%
○	0.7294	run45	5/1.14/ 0%
○	0.7294	run46	5/2.15/ 0%

Figure 7.2.3.203: Re Effects  
(CR=5, 0%Cowl)  
Sidewall Pressures



Sym	x'/Ts'	Run No.	CR/Re/Cowl (millions)
○	0.7815	run44	5/0.55/ 0%
○	0.7815	run45	5/1.14/ 0%
○	0.7815	run46	5/2.15/ 0%

Figure 7.2.3.204: Re Effects  
(CR=5, 0%Cowl)  
Sidewall Pressures

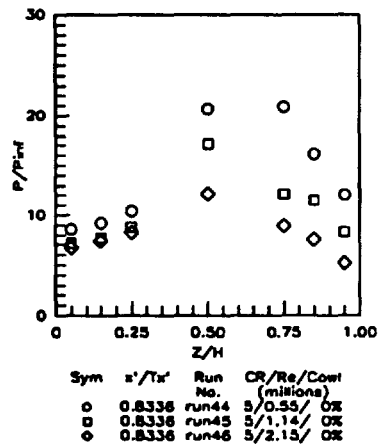


Figure 7.2.3.205: Re Effects (CR=5, 0%CowI) Sidewall Pressures

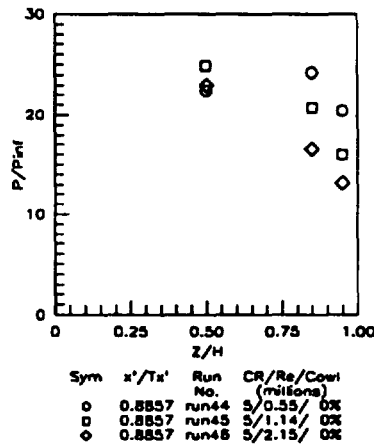


Figure 7.2.3.208: Re Effects (CR=5, 0%CowI) Sidewall Pressures

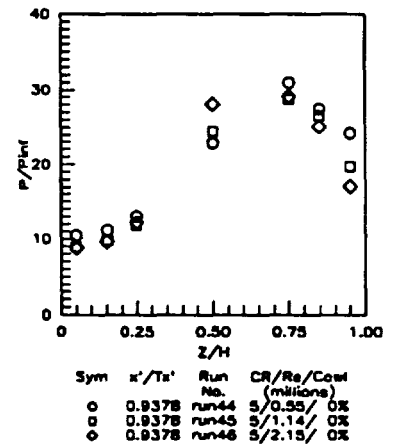


Figure 7.2.3.207: Re Effects (CR=5, 0%CowI) Sidewall Pressures

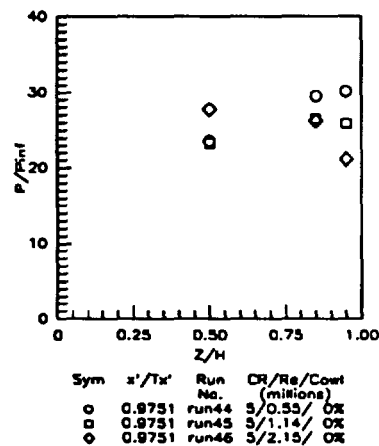


Figure 7.2.3.206: Re Effects (CR=5, 0%CowI) Sidewall Pressures

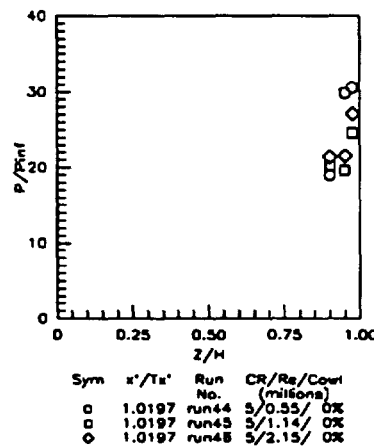


Figure 7.2.3.209: Re Effects (CR=5, 0%CowI) Sidewall Pressures

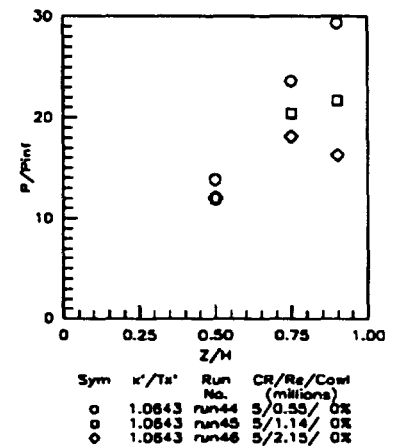


Figure 7.2.3.210: Re Effects (CR=5, 0%CowI) Sidewall Pressures

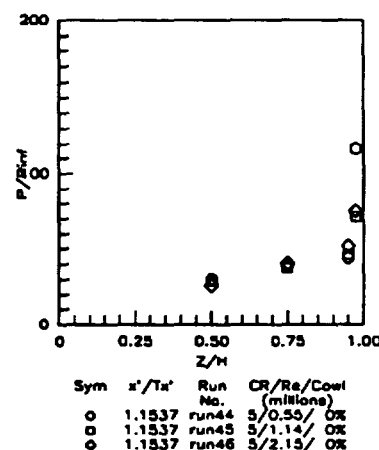


Figure 7.2.3.211: Re Effects (CR=5, 0%CowI) Sidewall Pressures

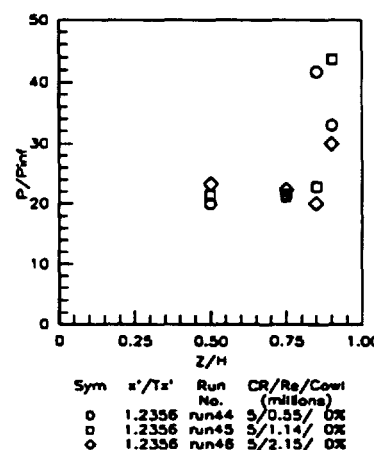
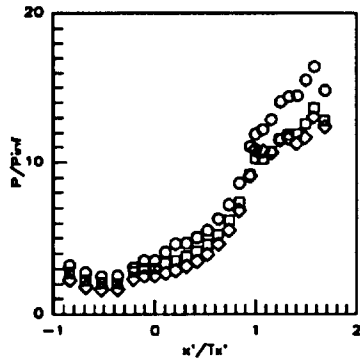
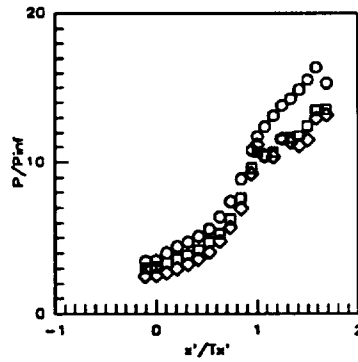


Figure 7.2.3.212: Re Effects (CR=5, 0%CowI) Sidewall Pressures



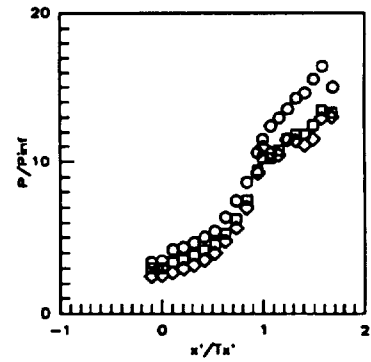
Sym	C.L. for	Run No.	CR/Re/CowI (millions)
○	CR=3	run41	5/0.55/25%
□	CR=3	run42	5/1.14/25%
◇	CR=3	run43	5/2.15/25%

Figure 7.2.3.213: Re Effects (CR=5, 25% CowI)  
CR=5 Centerline Pressures



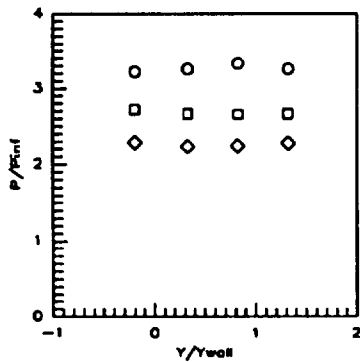
Sym	C.L. for	Run No.	CR/Re/CowI (millions)
○	CR=5	run41	5/0.55/25%
□	CR=5	run42	5/1.14/25%
◇	CR=5	run43	5/2.15/25%

Figure 7.2.3.214: Re Effects (CR=5, 25% CowI)  
CR=5 Centerline Pressures



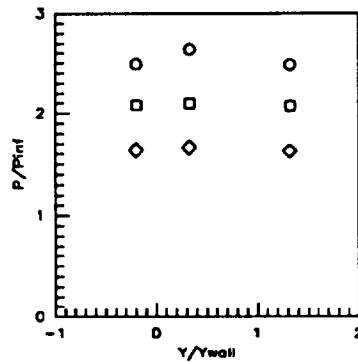
Sym	C.L. for	Run No.	CR/Re/CowI (millions)
○	CR=9	run41	5/0.55/25%
□	CR=9	run42	5/1.14/25%
◇	CR=9	run43	5/2.15/25%

Figure 7.2.3.215: Re Effects (CR=5, 25% CowI)  
CR=9 Centerline Pressures



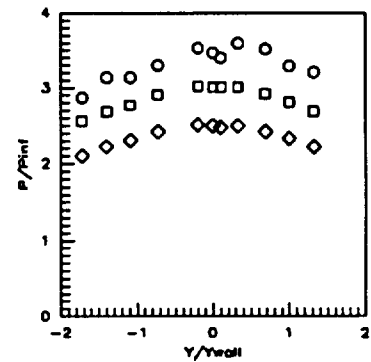
Sym	x'/Tx'	Run No.	CR/Re/CowI (millions)
○	-0.8412	run41	5/0.55/25%
□	-0.8412	run42	5/1.14/25%
◇	-0.8412	run43	5/2.15/25%

Figure 7.2.3.216: Re Effects (CR=5, 25% CowI)  
Baseplate Pressures



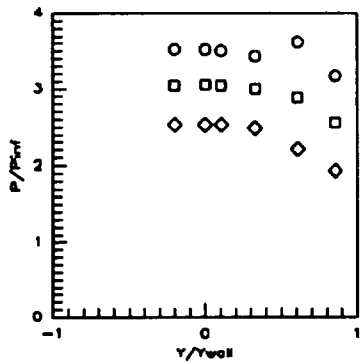
Sym	x'/Tx'	Run No.	CR/Re/CowI (millions)
○	-0.5258	run41	5/0.55/25%
□	-0.5258	run42	5/1.14/25%
◇	-0.5258	run43	5/2.15/25%

Figure 7.2.3.217: Re Effects (CR=5, 25% CowI)  
Baseplate Pressures



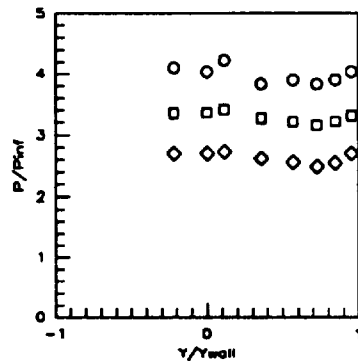
Sym	x'/Tx'	Run No.	CR/Re/CowI (millions)
○	-0.1052	run41	5/0.55/25%
□	-0.1052	run42	5/1.14/25%
◇	-0.1052	run43	5/2.15/25%

Figure 7.2.3.218: Re Effects (CR=5, 25% CowI)  
Baseplate Pressures



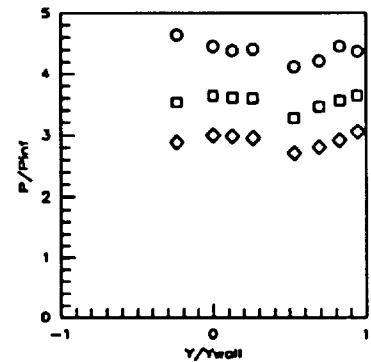
Sym	x'/Tx'	Run No.	CR/Re/CowI (millions)
○	0.0000	run41	5/0.55/25%
□	0.0000	run42	5/1.14/25%
◇	0.0000	run43	5/2.15/25%

Figure 7.2.3.219: Re Effects (CR=5, 25% CowI)  
Baseplate Pressures



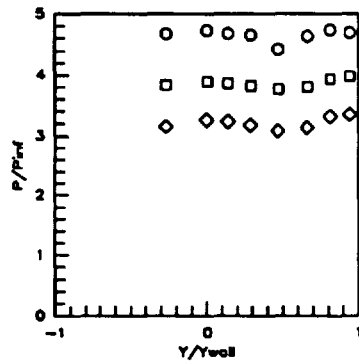
Sym	x'/Tx'	Run No.	CR/Re/CowI (millions)
○	0.1052	run41	5/0.55/25%
□	0.1052	run42	5/1.14/25%
◇	0.1052	run43	5/2.15/25%

Figure 7.2.3.220: Re Effects (CR=5, 25% CowI)  
Baseplate Pressures



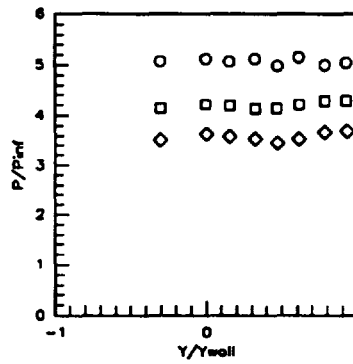
Sym	x'/Tx'	Run No.	CR/Re/CowI (millions)
○	0.2103	run41	5/0.55/25%
□	0.2103	run42	5/1.14/25%
◇	0.2103	run43	5/2.15/25%

Figure 7.2.3.221: Re Effects (CR=5, 25% CowI)  
Baseplate Pressures



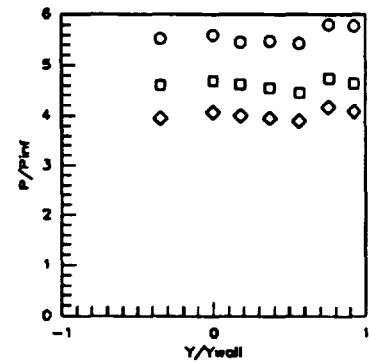
Sym	$x'/Tx'$	Run No.	CR/Re/Cowl (millions)
○	0.3154	run41	5/0.55/25%
□	0.3154	run42	5/1.14/25%
◇	0.3154	run43	5/2.15/25%

Figure 7.2.3.222: Re Effects (CR=5, 25% Cow) Baseplate Pressures



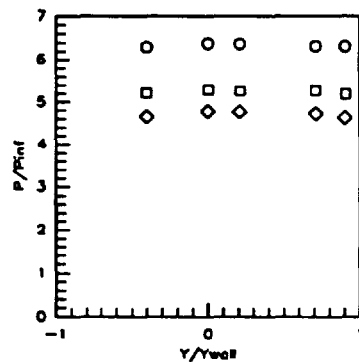
Sym	$x'/Tx'$	Run No.	CR/Re/Cowl (millions)
○	0.4206	run41	5/0.55/25%
□	0.4206	run42	5/1.14/25%
◇	0.4206	run43	5/2.15/25%

Figure 7.2.3.223: Re Effects (CR=5, 25% Cow) Baseplate Pressures



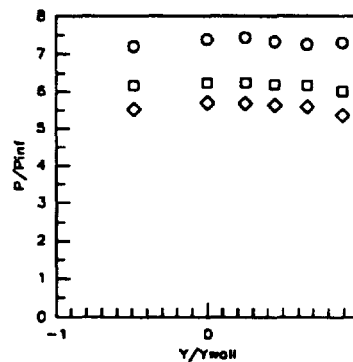
Sym	$x'/Tx'$	Run No.	CR/Re/Cowl (millions)
○	0.5258	run41	5/0.55/25%
□	0.5258	run42	5/1.14/25%
◇	0.5258	run43	5/2.15/25%

Figure 7.2.3.224: Re Effects (CR=5, 25% Cow) Baseplate Pressures



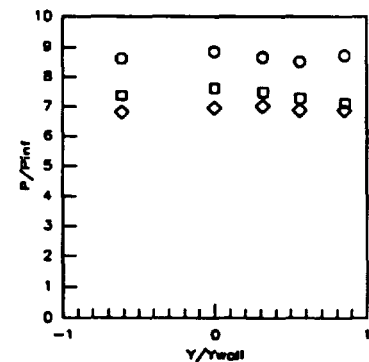
Sym	$x'/Tx'$	Run No.	CR/Re/Cowl (millions)
○	0.6309	run41	5/0.55/25%
□	0.6309	run42	5/1.14/25%
◇	0.6309	run43	5/2.15/25%

Figure 7.2.3.225: Re Effects (CR=5, 25% Cow) Baseplate Pressures



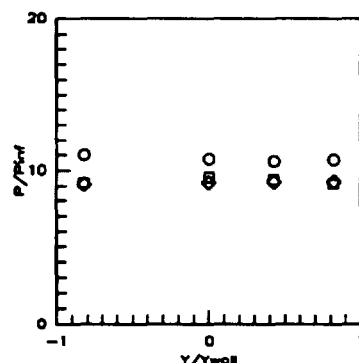
Sym	$x'/Tx'$	Run No.	CR/Re/Cowl (millions)
○	0.7361	run41	5/0.55/25%
□	0.7361	run42	5/1.14/25%
◇	0.7361	run43	5/2.15/25%

Figure 7.2.3.226: Re Effects (CR=5, 25% Cow) Baseplate Pressures



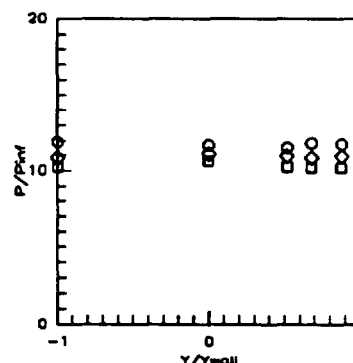
Sym	$x'/Tx'$	Run No.	CR/Re/Cowl (millions)
○	0.8412	run41	5/0.55/25%
□	0.8412	run42	5/1.14/25%
◇	0.8412	run43	5/2.15/25%

Figure 7.2.3.227: Re Effects (CR=5, 25% Cow) Baseplate Pressures



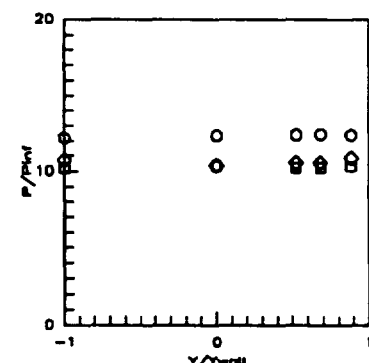
Sym	$x'/Tx'$	Run No.	CR/Re/Cowl (millions)
○	0.9464	run41	5/0.55/25%
□	0.9464	run42	5/1.14/25%
◇	0.9464	run43	5/2.15/25%

Figure 7.2.3.228: Re Effects (CR=5, 25% Cow) Baseplate Pressures



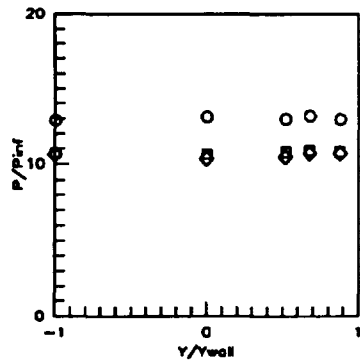
Sym	$x'/Tx'$	Run No.	CR/Re/Cowl (millions)
○	1.0000	run41	5/0.55/25%
□	1.0000	run42	5/1.14/25%
◇	1.0000	run43	5/2.15/25%

Figure 7.2.3.229: Re Effects (CR=5, 25% Cow) Baseplate Pressures



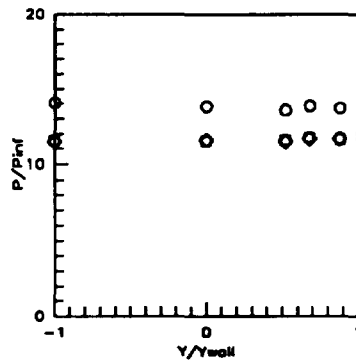
Sym	$x'/Tx'$	Run No.	CR/Re/Cowl (millions)
○	1.0726	run41	5/0.55/25%
□	1.0726	run42	5/1.14/25%
◇	1.0726	run43	5/2.15/25%

Figure 7.2.3.230: Re Effects (CR=5, 25% Cow) Baseplate Pressures



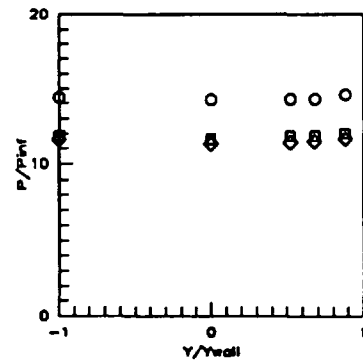
Sym	$x'/Ts'$	Run No.	CR/Re/Cowl (millions)
○	1.1567	run41	5/0.55/25%
□	1.1567	run42	5/1.14/25%
◇	1.1567	run43	5/2.15/25%

Figure 7.2.3.231: Re Effects (CR=5, 25% Cowl) Baseplate Pressures



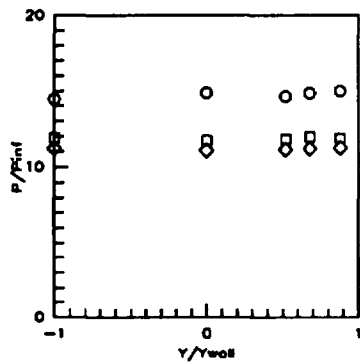
Sym	$x'/Ts'$	Run No.	CR/Re/Cowl (millions)
○	1.2408	run41	5/0.55/25%
□	1.2408	run42	5/1.14/25%
◇	1.2408	run43	5/2.15/25%

Figure 7.2.3.232: Re Effects (CR=5, 25% Cowl) Baseplate Pressures



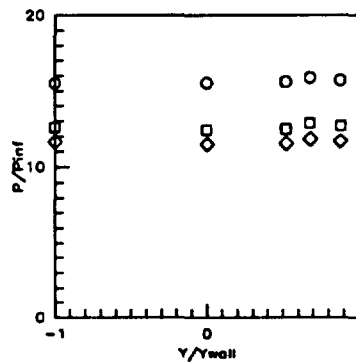
Sym	$x'/Ts'$	Run No.	CR/Re/Cowl (millions)
○	1.3249	run41	5/0.55/25%
□	1.3249	run42	5/1.14/25%
◇	1.3249	run43	5/2.15/25%

Figure 7.2.3.233: Re Effects (CR=5, 25% Cowl) Baseplate Pressures



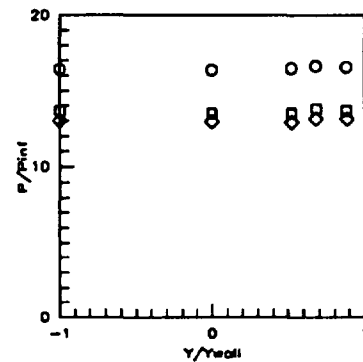
Sym	$x'/Ts'$	Run No.	CR/Re/Cowl (millions)
○	1.4090	run41	5/0.55/25%
□	1.4090	run42	5/1.14/25%
◇	1.4090	run43	5/2.15/25%

Figure 7.2.3.234: Re Effects (CR=5, 25% Cowl) Baseplate Pressures



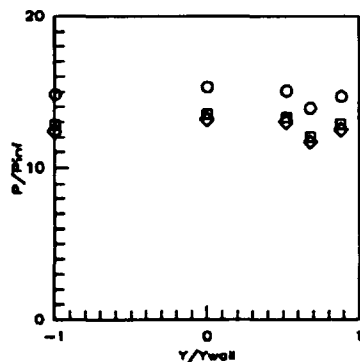
Sym	$x'/Ts'$	Run No.	CR/Re/Cowl (millions)
○	1.4932	run41	5/0.55/25%
□	1.4932	run42	5/1.14/25%
◇	1.4932	run43	5/2.15/25%

Figure 7.2.3.235: Re Effects (CR=5, 25% Cowl) Baseplate Pressures



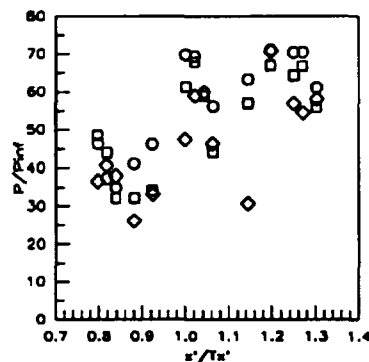
Sym	$x'/Ts'$	Run No.	CR/Re/Cowl (millions)
○	1.5773	run41	5/0.55/25%
□	1.5773	run42	5/1.14/25%
◇	1.5773	run43	5/2.15/25%

Figure 7.2.3.236: Re Effects (CR=5, 25% Cowl) Baseplate Pressures



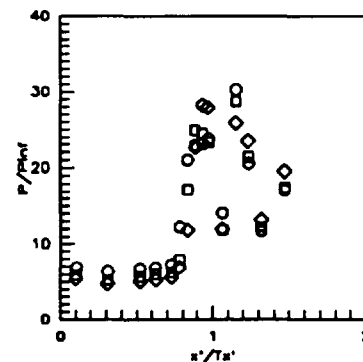
Sym	$x'/Ts'$	Run No.	CR/Re/Cowl (millions)
○	1.6824	run41	5/0.55/25%
□	1.6824	run42	5/1.14/25%
◇	1.6824	run43	5/2.15/25%

Figure 7.2.3.237: Re Effects (CR=5, 25% Cowl) Baseplate Pressures



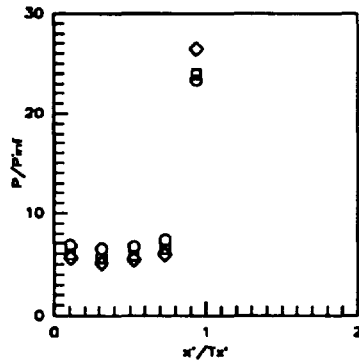
Sym	Cowl Pos.	Run No.	CR/Re/Cowl (millions)
○	25%	run41	5/0.55/25%
□	25%	run42	5/1.14/25%
◇	25%	run43	5/2.15/25%

Figure 7.2.3.238: Re Effects (CR=5, 25% Cowl) Cowl Pressures



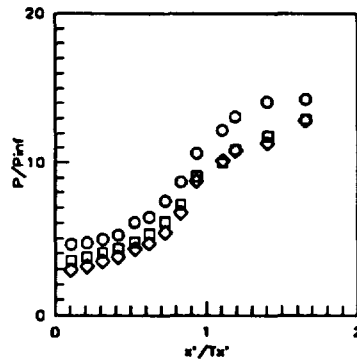
Sym	Z/H	Run No.	CR/Re/Cowl (millions)
○	0.5RT.	run41	5/0.55/25%
□	0.5RT.	run42	5/1.14/25%
◇	0.5RT.	run43	5/2.15/25%

Figure 7.2.3.239: Re Effects (CR=5, 25% Cowl) Sidewall Centerline Pressures



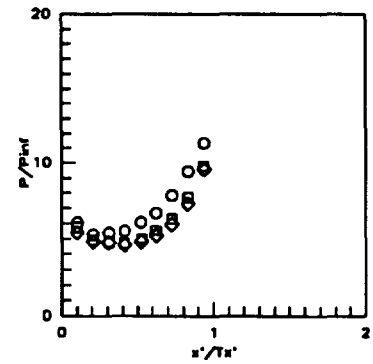
Sym	Z/H	Run No.	CR/Re/Cowl (millions)
○	0.5LT.	run41	5/0.55/25%
□	0.5LT.	run42	5/1.14/25%
◇	0.5LT.	run43	5/2.15/25%

Figure 7.2.3.240: Re Effects (CR=5, 25%Cowl) Sidewall Centerline Pressures



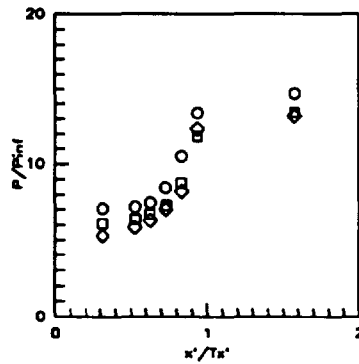
Sym	Z/H	Run No.	CR/Re/Cowl (millions)
○	0.050	run41	5/0.55/25%
□	0.050	run42	5/1.14/25%
◇	0.050	run43	5/2.15/25%

Figure 7.2.3.241: Re Effects (CR=5, 25%Cowl) Sidewall Pressures



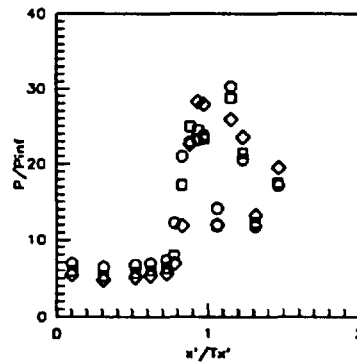
Sym	Z/H	Run No.	CR/Re/Cowl (millions)
○	0.15	run41	5/0.55/25%
□	0.15	run42	5/1.14/25%
◇	0.15	run43	5/2.15/25%

Figure 7.2.3.242: Re Effects (CR=5, 25%Cowl) Sidewall Pressures



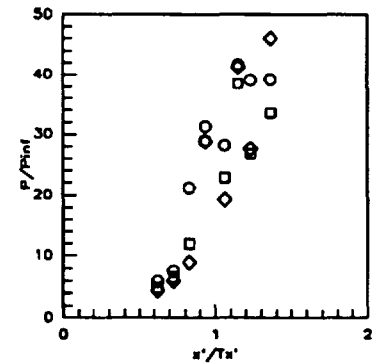
Sym	Z/H	Run No.	CR/Re/Cowl (millions)
○	0.25	run41	5/0.55/25%
□	0.25	run42	5/1.14/25%
◇	0.25	run43	5/2.15/25%

Figure 7.2.3.243: Re Effects (CR=5, 25%Cowl) Sidewall Pressures



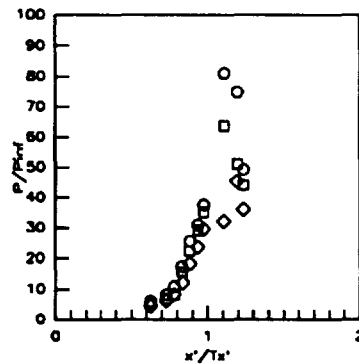
Sym	Z/H	Run No.	CR/Re/Cowl (millions)
○	0.50	run41	5/0.55/25%
□	0.50	run42	5/1.14/25%
◇	0.50	run43	5/2.15/25%

Figure 7.2.3.244: Re Effects (CR=5, 25%Cowl) Sidewall Pressures



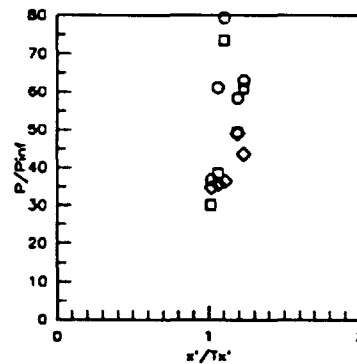
Sym	Z/H	Run No.	CR/Re/Cowl (millions)
○	0.75	run41	5/0.55/25%
□	0.75	run42	5/1.14/25%
◇	0.75	run43	5/2.15/25%

Figure 7.2.3.245: Re Effects (CR=5, 25%Cowl) Sidewall Pressures



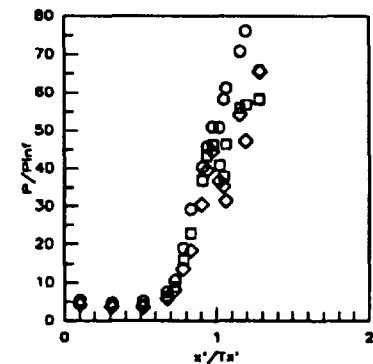
Sym	Z/H	Run No.	CR/Re/Cowl (millions)
○	0.85	run41	5/0.55/25%
□	0.85	run42	5/1.14/25%
◇	0.85	run43	5/2.15/25%

Figure 7.2.3.246: Re Effects (CR=5, 25%Cowl) Sidewall Pressures



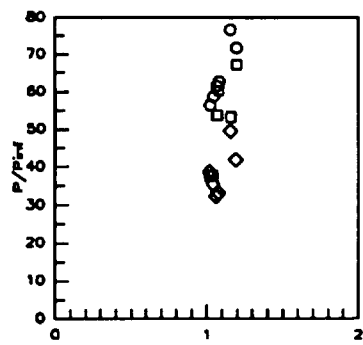
Sym	Z/H	Run No.	CR/Re/Cowl (millions)
○	0.90	run41	5/0.55/25%
□	0.90	run42	5/1.14/25%
◇	0.90	run43	5/2.15/25%

Figure 7.2.3.247: Re Effects (CR=5, 25%Cowl) Sidewall Pressures



Sym	Z/H	Run No.	CR/Re/Cowl (millions)
○	0.95	run41	5/0.55/25%
□	0.95	run42	5/1.14/25%
◇	0.95	run43	5/2.15/25%

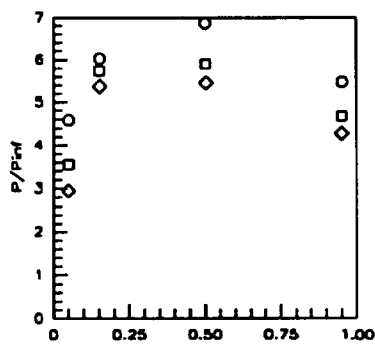
Figure 7.2.3.248: Re Effects (CR=5, 25%Cowl) Sidewall Pressures



Sym	$x'/Ts'$	Run No.	CR/Re/Cowi (millions)
-----	----------	---------	-----------------------

○	0.975	run41	5/0.55/25%
□	0.975	run42	5/1.14/25%
◇	0.975	run43	5/2.15/25%

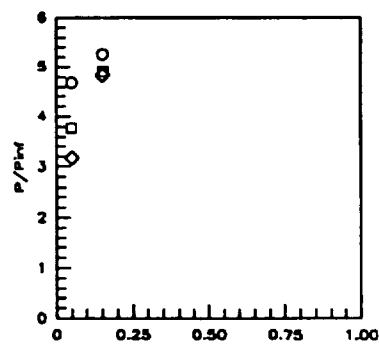
Figure 7.2.3.249: Re Effects (CR=5, 25% Cowi) Sidewall Pressures



Sym	$x'/Ts'$	Run No.	CR/Re/Cowi (millions)
-----	----------	---------	-----------------------

○	0.1042	run41	5/0.55/25%
□	0.1042	run42	5/1.14/25%
◇	0.1042	run43	5/2.15/25%

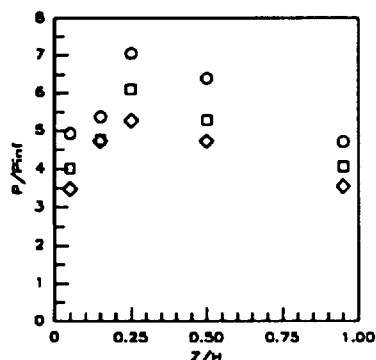
Figure 7.2.3.250: Re Effects (CR=5, 25% Cowi) Sidewall Pressures



Sym	$x'/Ts'$	Run No.	CR/Re/Cowi (millions)
-----	----------	---------	-----------------------

○	0.2083	run41	5/0.55/25%
□	0.2083	run42	5/1.14/25%
◇	0.2083	run43	5/2.15/25%

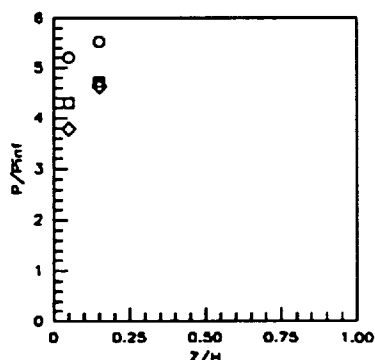
Figure 7.2.3.251: Re Effects (CR=5, 25% Cowi) Sidewall Pressures



Sym	$x'/Ts'$	Run No.	CR/Re/Cowi (millions)
-----	----------	---------	-----------------------

○	0.3125	run41	5/0.55/25%
□	0.3125	run42	5/1.14/25%
◇	0.3125	run43	5/2.15/25%

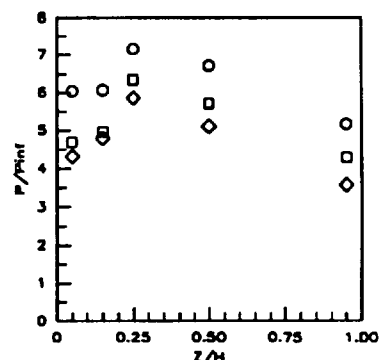
Figure 7.2.3.252: Re Effects (CR=5, 25% Cowi) Sidewall Pressures



Sym	$x'/Ts'$	Run No.	CR/Re/Cowi (millions)
-----	----------	---------	-----------------------

○	0.4167	run41	5/0.55/25%
□	0.4167	run42	5/1.14/25%
◇	0.4167	run43	5/2.15/25%

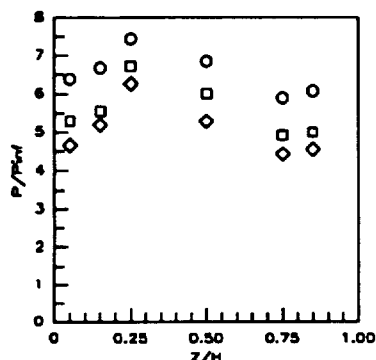
Figure 7.2.3.253: Re Effects (CR=5, 25% Cowi) Sidewall Pressures



Sym	$x'/Ts'$	Run No.	CR/Re/Cowi (millions)
-----	----------	---------	-----------------------

○	0.5259	run41	5/0.55/25%
□	0.5259	run42	5/1.14/25%
◇	0.5259	run43	5/2.15/25%

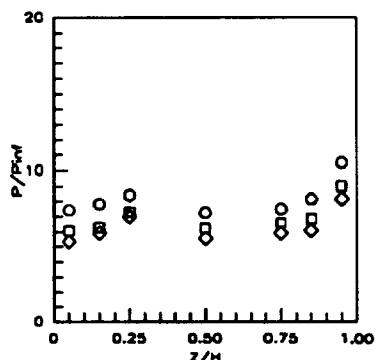
Figure 7.2.3.254: Re Effects (CR=5, 25% Cowi) Sidewall Pressures



Sym	$x'/Ts'$	Run No.	CR/Re/Cowi (millions)
-----	----------	---------	-----------------------

○	0.6252	run41	5/0.55/25%
□	0.6252	run42	5/1.14/25%
◇	0.6252	run43	5/2.15/25%

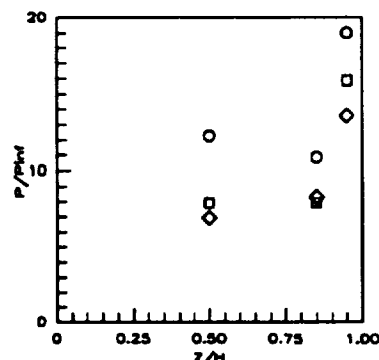
Figure 7.2.3.255: Re Effects (CR=5, 25% Cowi) Sidewall Pressures



Sym	$x'/Ts'$	Run No.	CR/Re/Cowi (millions)
-----	----------	---------	-----------------------

○	0.7294	run41	5/0.55/25%
□	0.7294	run42	5/1.14/25%
◇	0.7294	run43	5/2.15/25%

Figure 7.2.3.256: Re Effects (CR=5, 25% Cowi) Sidewall Pressures



Sym	$x'/Ts'$	Run No.	CR/Re/Cowi (millions)
-----	----------	---------	-----------------------

○	0.7815	run41	5/0.55/25%
□	0.7815	run42	5/1.14/25%
◇	0.7815	run43	5/2.15/25%

Figure 7.2.3.257: Re Effects (CR=5, 25% Cowi) Sidewall Pressures

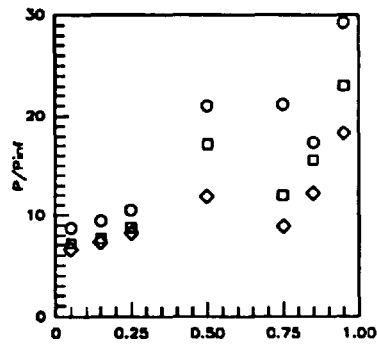


Figure 7.2.3.258: Re Effects (CR=5, 25% Cowl) Sidewall Pressures

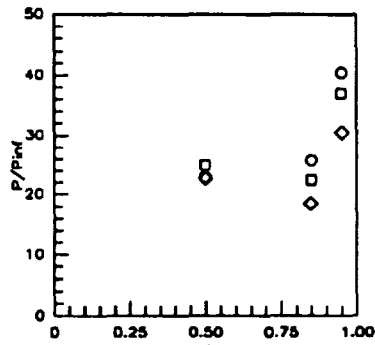


Figure 7.2.3.259: Re Effects (CR=5, 25% Cowl) Sidewall Pressures

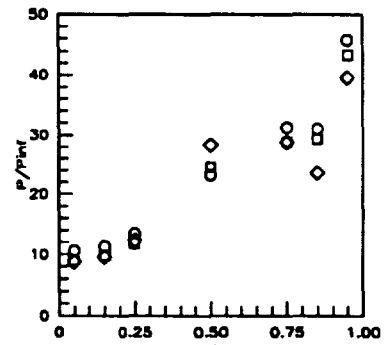


Figure 7.2.3.260: Re Effects (CR=5, 25% Cowl) Sidewall Pressures

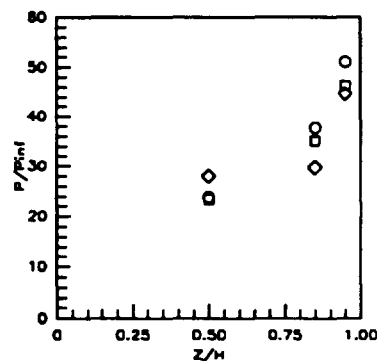


Figure 7.2.3.261: Re Effects (CR=5, 25% Cowl) Sidewall Pressures

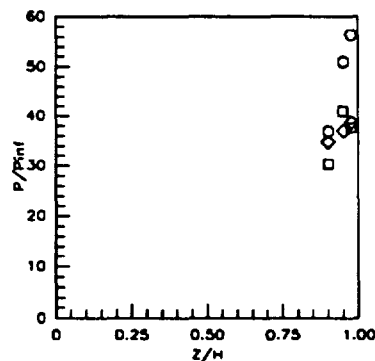


Figure 7.2.3.262: Re Effects (CR=5, 25% Cowl) Sidewall Pressures

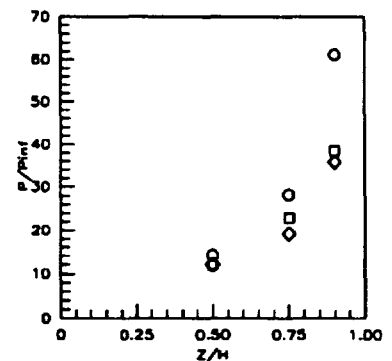


Figure 7.2.3.263: Re Effects (CR=5, 25% Cowl) Sidewall Pressures

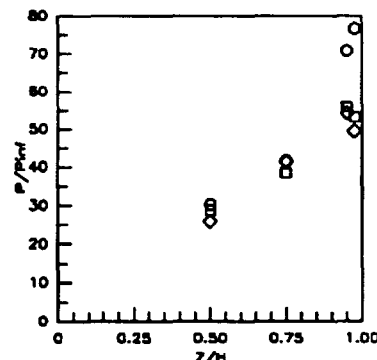


Figure 7.2.3.264: Re Effects (CR=5, 25% Cowl) Sidewall Pressures

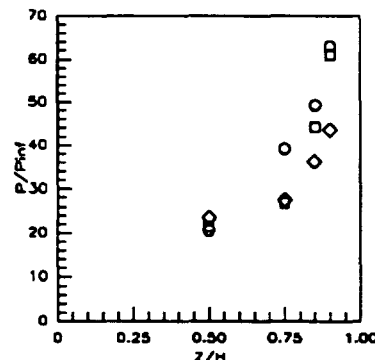
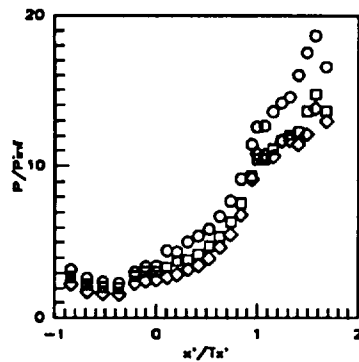


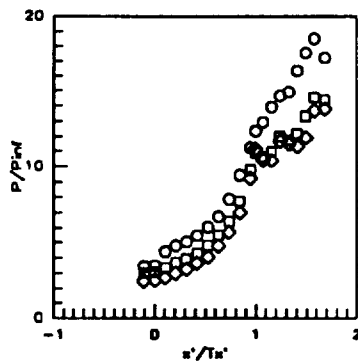
Figure 7.2.3.265: Re Effects (CR=5, 25% Cowl) Sidewall Pressures





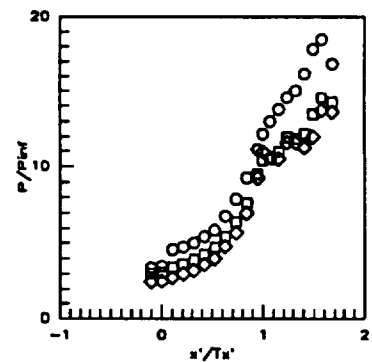
Sym	C.L. for	Run No.	CR/Re/Cowl (millions)
○	CR=3	run37	5/0.55/50%
□	CR=3	run39	5/1.14/50%
◇	CR=3	run40	5/2.15/50%

Figure 7.2.3.266: Re Effects (CR=5, 50% CowI) Centerline Pressures



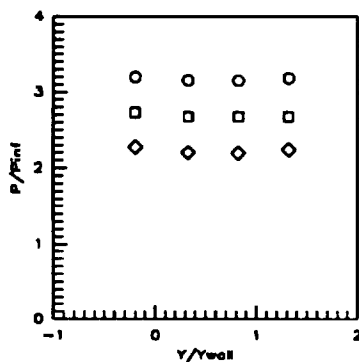
Sym	C.L. for	Run No.	CR/Re/Cowl (millions)
○	CR=5	run37	5/0.55/50%
□	CR=5	run39	5/1.14/50%
◇	CR=5	run40	5/2.15/50%

Figure 7.2.3.267: Re Effects (CR=5, 50% CowI) Centerline Pressures



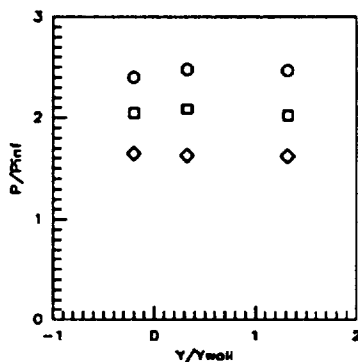
Sym	C.L. for	Run No.	CR/Re/Cowl (millions)
○	CR=8	run37	5/0.55/50%
□	CR=8	run39	5/1.14/50%
◇	CR=8	run40	5/2.15/50%

Figure 7.2.3.268: Re Effects (CR=5, 50% CowI) Centerline Pressures



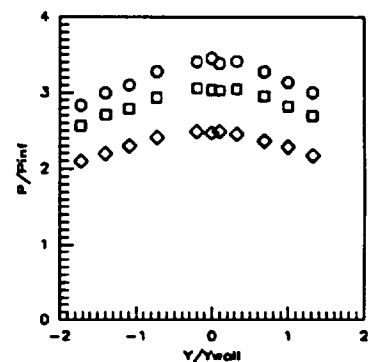
Sym	x'/Tx'	Run No.	CR/Re/Cowl (millions)
○	-0.8412	run37	5/0.55/50%
□	-0.8412	run39	5/1.14/50%
◇	-0.8412	run40	5/2.15/50%

Figure 7.2.3.269: Re Effects (CR=5, 50% CowI) Baseplate Pressures



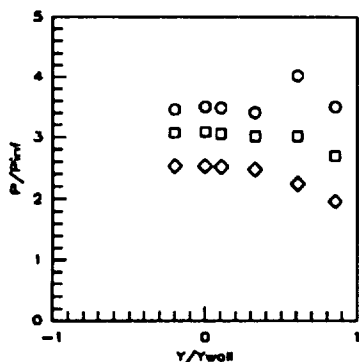
Sym	x'/Tx'	Run No.	CR/Re/Cowl (millions)
○	-0.5258	run37	5/0.55/50%
□	-0.5258	run39	5/1.14/50%
◇	-0.5258	run40	5/2.15/50%

Figure 7.2.3.270: Re Effects (CR=5, 50% CowI) Baseplate Pressures



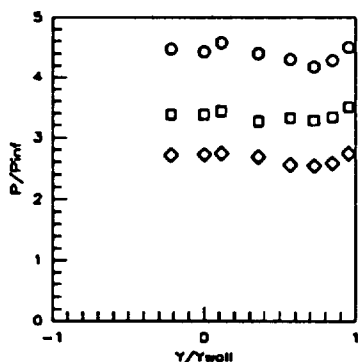
Sym	x'/Tx'	Run No.	CR/Re/Cowl (millions)
○	-0.1052	run37	5/0.55/50%
□	-0.1052	run39	5/1.14/50%
◇	-0.1052	run40	5/2.15/50%

Figure 7.2.3.271: Re Effects (CR=5, 50% CowI) Baseplate Pressures



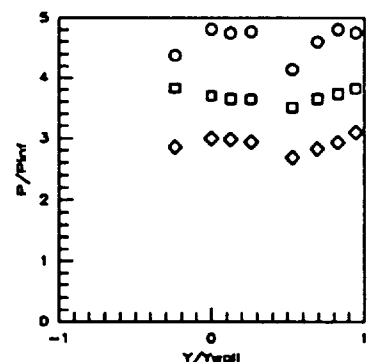
Sym	x'/Tx'	Run No.	CR/Re/Cowl (millions)
○	0.0000	run37	5/0.55/50%
□	0.0000	run39	5/1.14/50%
◇	0.0000	run40	5/2.15/50%

Figure 7.2.3.272: Re Effects (CR=5, 50% CowI) Baseplate Pressures



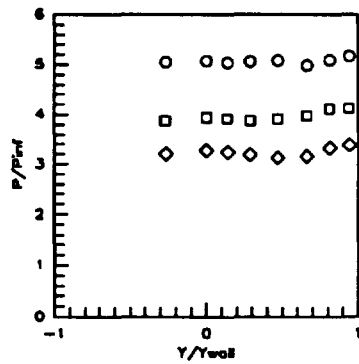
Sym	x'/Tx'	Run No.	CR/Re/Cowl (millions)
○	0.1052	run37	5/0.55/50%
□	0.1052	run39	5/1.14/50%
◇	0.1052	run40	5/2.15/50%

Figure 7.2.3.273: Re Effects (CR=5, 50% CowI) Baseplate Pressures



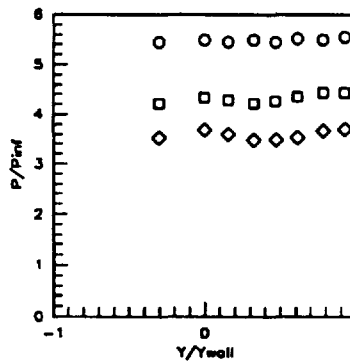
Sym	x'/Tx'	Run No.	CR/Re/Cowl (millions)
○	0.2103	run37	5/0.55/50%
□	0.2103	run39	5/1.14/50%
◇	0.2103	run40	5/2.15/50%

Figure 7.2.3.274: Re Effects (CR=5, 50% CowI) Baseplate Pressures



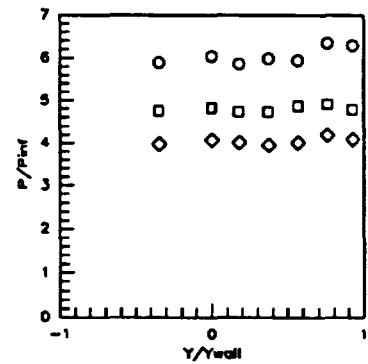
Sym	$x'/T_x'$	Run No.	CR/Re/Cowl (millions)
○	0.3154	run37	5/0.55/50%
□	0.3154	run39	5/1.14/50%
◇	0.3154	run40	5/2.15/50%

Figure 7.2.3.275: Re Effects (CR=5, 50% CowI) Baseplate Pressures



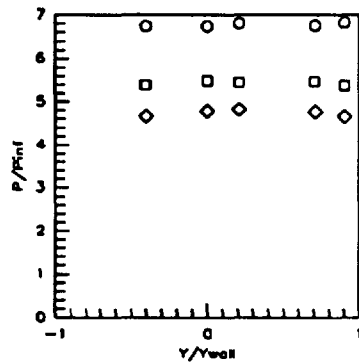
Sym	$x'/T_x'$	Run No.	CR/Re/Cowl (millions)
○	0.4206	run37	5/0.55/50%
□	0.4206	run39	5/1.14/50%
◇	0.4206	run40	5/2.15/50%

Figure 7.2.3.276: Re Effects (CR=5, 50% CowI) Baseplate Pressures



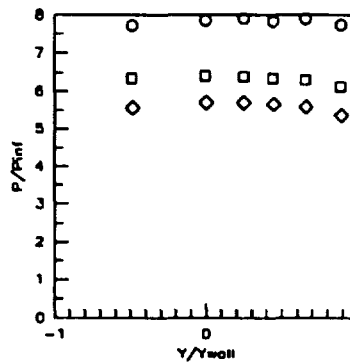
Sym	$x'/T_x'$	Run No.	CR/Re/Cowl (millions)
○	0.5258	run37	5/0.55/50%
□	0.5258	run39	5/1.14/50%
◇	0.5258	run40	5/2.15/50%

Figure 7.2.3.277: Re Effects (CR=5, 50% CowI) Baseplate Pressures



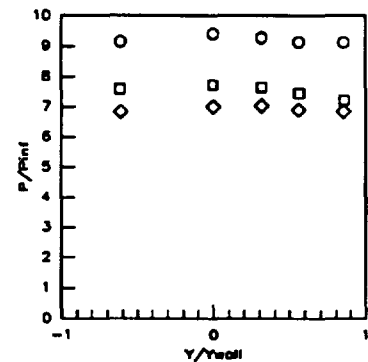
Sym	$x'/T_x'$	Run No.	CR/Re/Cowl (millions)
○	0.6309	run37	5/0.55/50%
□	0.6309	run39	5/1.14/50%
◇	0.6309	run40	5/2.15/50%

Figure 7.2.3.278: Re Effects (CR=5, 50% CowI) Baseplate Pressures



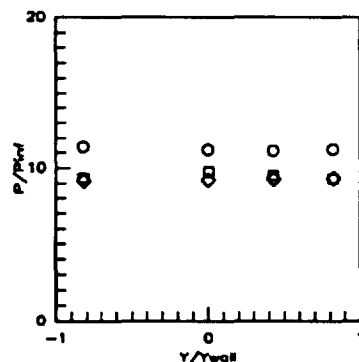
Sym	$x'/T_x'$	Run No.	CR/Re/Cowl (millions)
○	0.7381	run37	5/0.55/50%
□	0.7381	run39	5/1.14/50%
◇	0.7381	run40	5/2.15/50%

Figure 7.2.3.279: Re Effects (CR=5, 50% CowI) Baseplate Pressures



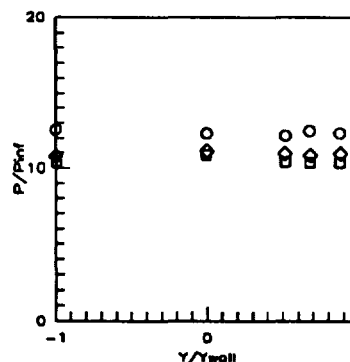
Sym	$x'/T_x'$	Run No.	CR/Re/Cowl (millions)
○	0.8412	run37	5/0.55/50%
□	0.8412	run39	5/1.14/50%
◇	0.8412	run40	5/2.15/50%

Figure 7.2.3.280: Re Effects (CR=5, 50% CowI) Baseplate Pressures



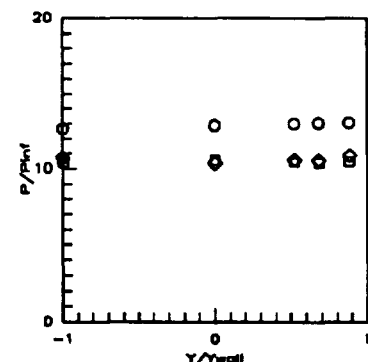
Sym	$x'/T_x'$	Run No.	CR/Re/Cowl (millions)
○	0.9464	run37	5/0.55/50%
□	0.9464	run39	5/1.14/50%
◇	0.9464	run40	5/2.15/50%

Figure 7.2.3.281: Re Effects (CR=5, 50% CowI) Baseplate Pressures



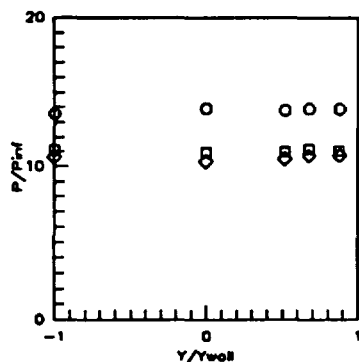
Sym	$x'/T_x'$	Run No.	CR/Re/Cowl (millions)
○	1.0000	run37	5/0.55/50%
□	1.0000	run39	5/1.14/50%
◇	1.0000	run40	5/2.15/50%

Figure 7.2.3.282: Re Effects (CR=5, 50% CowI) Baseplate Pressures



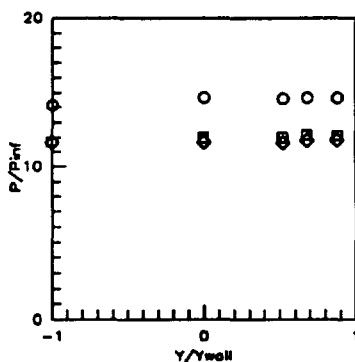
Sym	$x'/T_x'$	Run No.	CR/Re/Cowl (millions)
○	1.0728	run37	5/0.55/50%
□	1.0728	run39	5/1.14/50%
◇	1.0728	run40	5/2.15/50%

Figure 7.2.3.283: Re Effects (CR=5, 50% CowI) Baseplate Pressures



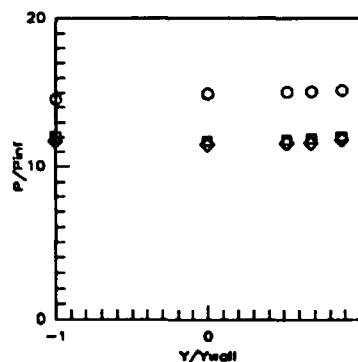
Sym	x'/Ts'	Run No.	CR/Re/Cowi (millions)
○	1.1567	run37	5/0.55/50%
□	1.1567	run39	5/1.14/50%
◇	1.1567	run40	5/2.15/50%

Figure 7.2.3.284: Re Effects (CR=5, 50% Cowi) Baseplate Pressures



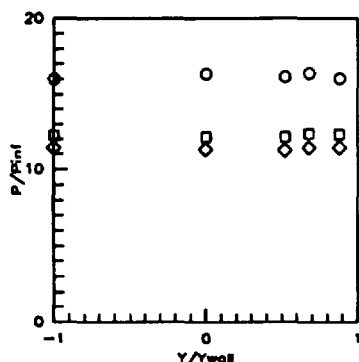
Sym	x'/Ts'	Run No.	CR/Re/Cowi (millions)
○	1.2408	run37	5/0.55/50%
□	1.2408	run39	5/1.14/50%
◇	1.2408	run40	5/2.15/50%

Figure 7.2.3.285: Re Effects (CR=5, 50% Cowi) Baseplate Pressures



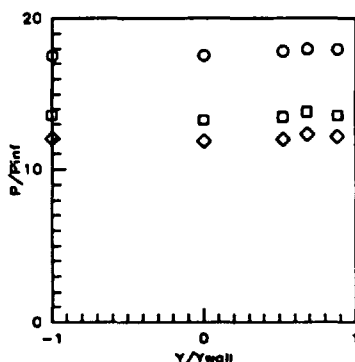
Sym	x'/Ts'	Run No.	CR/Re/Cowi (millions)
○	1.3249	run37	5/0.55/50%
□	1.3249	run39	5/1.14/50%
◇	1.3249	run40	5/2.15/50%

Figure 7.2.3.286: Re Effects (CR=5, 50% Cowi) Baseplate Pressures



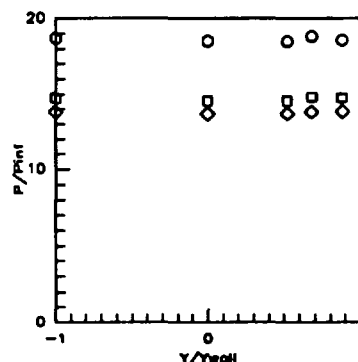
Sym	x'/Ts'	Run No.	CR/Re/Cowi (millions)
○	1.4090	run37	5/0.55/50%
□	1.4090	run39	5/1.14/50%
◇	1.4090	run40	5/2.15/50%

Figure 7.2.3.287: Re Effects (CR=5, 50% Cowi) Baseplate Pressures



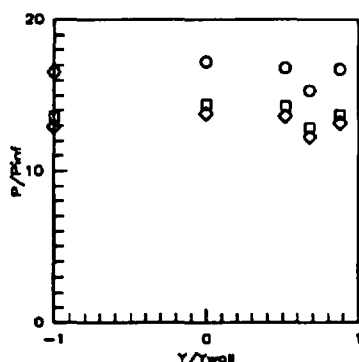
Sym	x'/Ts'	Run No.	CR/Re/Cowi (millions)
○	1.4932	run37	5/0.55/50%
□	1.4932	run39	5/1.14/50%
◇	1.4932	run40	5/2.15/50%

Figure 7.2.3.288: Re Effects (CR=5, 50% Cowi) Baseplate Pressures



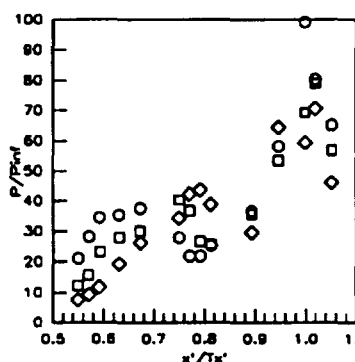
Sym	x'/Ts'	Run No.	CR/Re/Cowi (millions)
○	1.5773	run37	5/0.55/50%
□	1.5773	run39	5/1.14/50%
◇	1.5773	run40	5/2.15/50%

Figure 7.2.3.289: Re Effects (CR=5, 50% Cowi) Baseplate Pressures



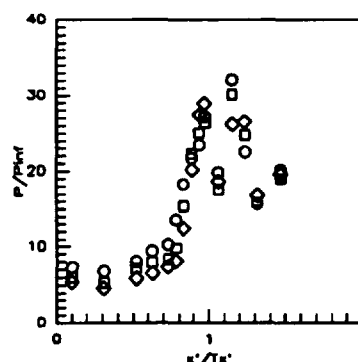
Sym	x'/Ts'	Run No.	CR/Re/Cowi (millions)
○	1.6824	run37	5/0.55/50%
□	1.6824	run39	5/1.14/50%
◇	1.6824	run40	5/2.15/50%

Figure 7.2.3.290: Re Effects (CR=5, 50% Cowi) Baseplate Pressures



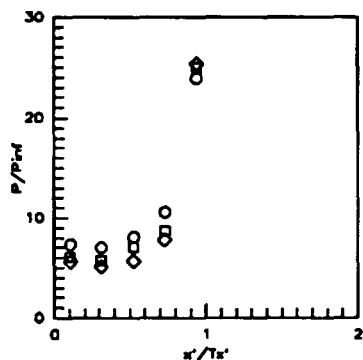
Sym	Cowi Pos.	Run No.	CR/Re/Cowi (millions)
○	50%	run37	5/0.55/50%
□	50%	run39	5/1.14/50%
◇	50%	run40	5/2.15/50%

Figure 7.2.3.291: Re Effects (CR=5, 50% Cowi) Cowi Pressures



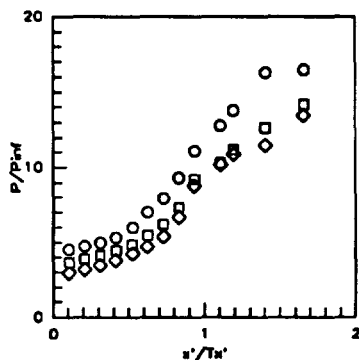
Sym	Z/H	Run No.	CR/Re/Cowi (millions)
○	0.5RT	run37	5/0.55/50%
□	0.5RT	run39	5/1.14/50%
◇	0.5RT	run40	5/2.15/50%

Figure 7.2.3.292: Re Effects (CR=5, 50% Cowi) Sidewall Centerline Pressures



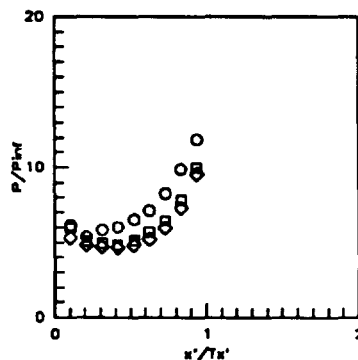
Sym	Z/H	Run No.	CR/Re/Cowl (millions)
○	0.5LT	run37	5/0.55/50%
□	0.5LT	run39	5/1.14/50%
◇	0.5LT	run40	5/2.15/50%

Figure 7.2.3.293: Re Effects (CR=5, 50% CowI) Sidewall Centerline Pressures



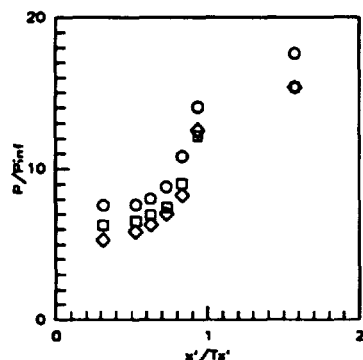
Sym	Z/H	Run No.	CR/Re/Cowl (millions)
○	0.050	run37	5/0.55/50%
□	0.050	run39	5/1.14/50%
◇	0.050	run40	5/2.15/50%

Figure 7.2.3.294: Re Effects (CR=5, 50% CowI) Sidewall Pressures



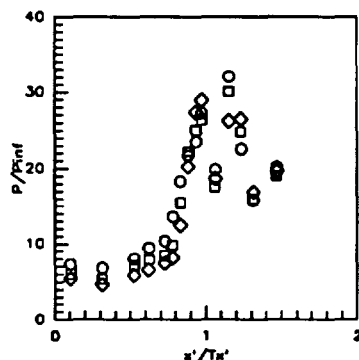
Sym	Z/H	Run No.	CR/Re/Cowl (millions)
○	0.15	run37	5/0.55/50%
□	0.15	run39	5/1.14/50%
◇	0.15	run40	5/2.15/50%

Figure 7.2.3.295: Re Effects (CR=5, 50% CowI) Sidewall Pressures



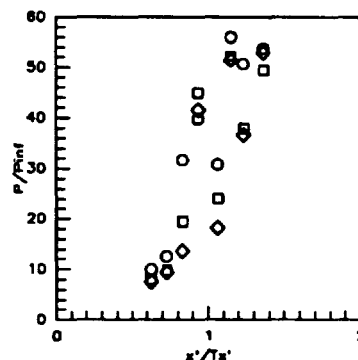
Sym	Z/H	Run No.	CR/Re/Cowl (millions)
○	0.25	run37	5/0.55/50%
□	0.25	run39	5/1.14/50%
◇	0.25	run40	5/2.15/50%

Figure 7.2.3.296: Re Effects (CR=5, 50% CowI) Sidewall Pressures



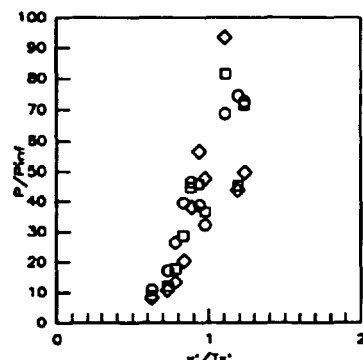
Sym	Z/H	Run No.	CR/Re/Cowl (millions)
○	0.50	run37	5/0.55/50%
□	0.50	run39	5/1.14/50%
◇	0.50	run40	5/2.15/50%

Figure 7.2.3.297: Re Effects (CR=5, 50% CowI) Sidewall Pressures



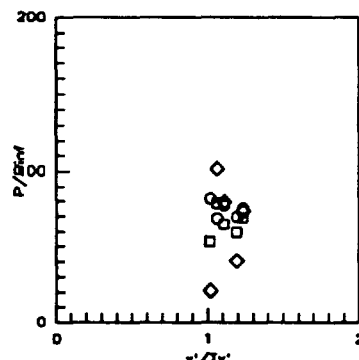
Sym	Z/H	Run No.	CR/Re/Cowl (millions)
○	0.75	run37	5/0.55/50%
□	0.75	run39	5/1.14/50%
◇	0.75	run40	5/2.15/50%

Figure 7.2.3.298: Re Effects (CR=5, 50% CowI) Sidewall Pressures



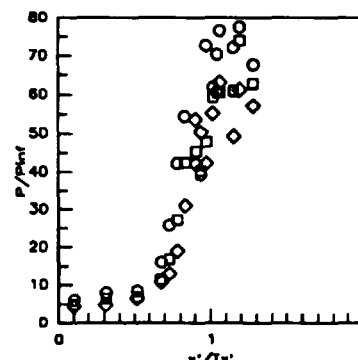
Sym	Z/H	Run No.	CR/Re/Cowl (millions)
○	0.85	run37	5/0.55/50%
□	0.85	run39	5/1.14/50%
◇	0.85	run40	5/2.15/50%

Figure 7.2.3.299: Re Effects (CR=5, 50% CowI) Sidewall Pressures



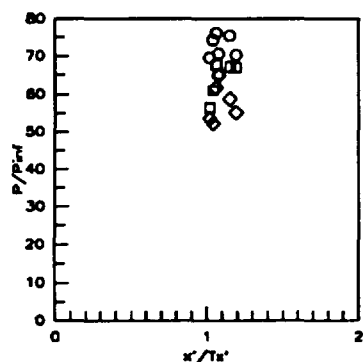
Sym	Z/H	Run No.	CR/Re/Cowl (millions)
○	0.90	run37	5/0.55/50%
□	0.90	run39	5/1.14/50%
◇	0.90	run40	5/2.15/50%

Figure 7.2.3.300: Re Effects (CR=5, 50% CowI) Sidewall Pressures



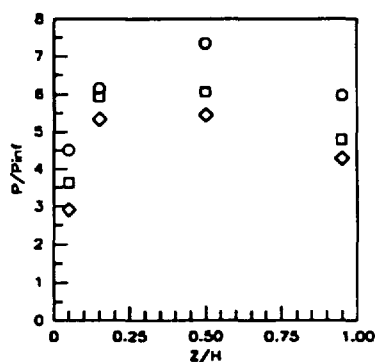
Sym	Z/H	Run No.	CR/Re/Cowl (millions)
○	0.95	run37	5/0.55/50%
□	0.95	run39	5/1.14/50%
◇	0.95	run40	5/2.15/50%

Figure 7.2.3.301: Re Effects (CR=5, 50% CowI) Sidewall Pressures



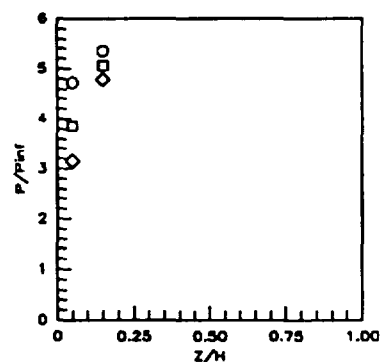
Sym	$x'/Ts'$	Run No.	CR/Re/Cowi (millions)
○	0.875	run37	5/0.55/50%
□	0.875	run39	5/1.14/50%
◇	0.875	run40	5/2.15/50%

Figure 7.2.3.302: Re Effects (CR=5, 50% Cowi) Sidewall Pressures



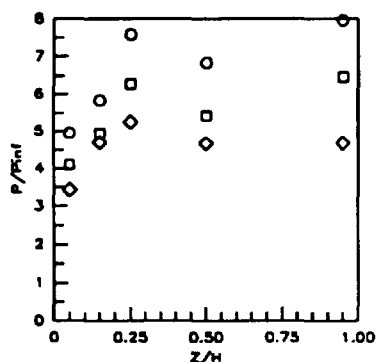
Sym	$x'/Ts'$	Run No.	CR/Re/Cowi (millions)
○	0.1042	run37	5/0.55/50%
□	0.1042	run39	5/1.14/50%
◇	0.1042	run40	5/2.15/50%

Figure 7.2.3.303: Re Effects (CR=5, 50% Cowi) Sidewall Pressures



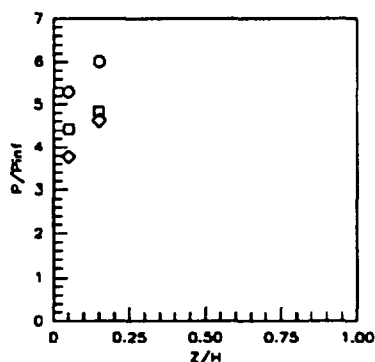
Sym	$x'/Ts'$	Run No.	CR/Re/Cowi (millions)
○	0.2083	run37	5/0.55/50%
□	0.2083	run39	5/1.14/50%
◇	0.2083	run40	5/2.15/50%

Figure 7.2.3.304: Re Effects (CR=5, 50% Cowi) Sidewall Pressures



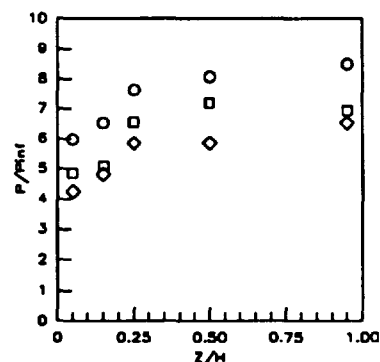
Sym	$x'/Ts'$	Run No.	CR/Re/Cowi (millions)
○	0.3125	run37	5/0.55/50%
□	0.3125	run39	5/1.14/50%
◇	0.3125	run40	5/2.15/50%

Figure 7.2.3.305: Re Effects (CR=5, 50% Cowi) Sidewall Pressures



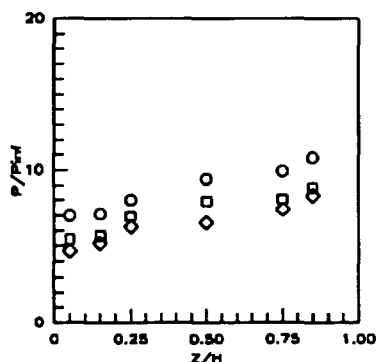
Sym	$x'/Ts'$	Run No.	CR/Re/Cowi (millions)
○	0.4187	run37	5/0.55/50%
□	0.4187	run39	5/1.14/50%
◇	0.4187	run40	5/2.15/50%

Figure 7.2.3.306: Re Effects (CR=5, 50% Cowi) Sidewall Pressures



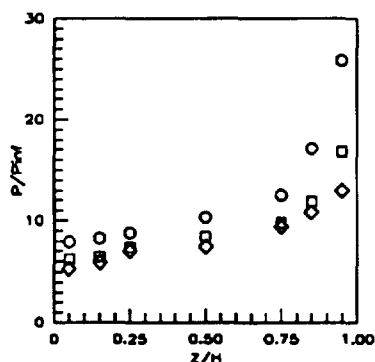
Sym	$x'/Ts'$	Run No.	CR/Re/Cowi (millions)
○	0.5259	run37	5/0.55/50%
□	0.5259	run39	5/1.14/50%
◇	0.5259	run40	5/2.15/50%

Figure 7.2.3.307: Re Effects (CR=5, 50% Cowi) Sidewall Pressures



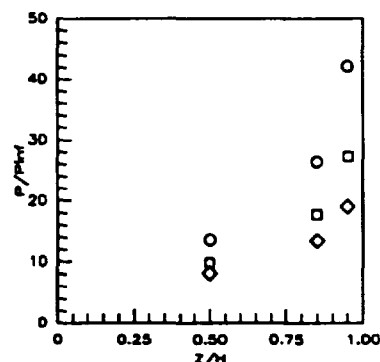
Sym	$x'/Ts'$	Run No.	CR/Re/Cowi (millions)
○	0.6252	run37	5/0.55/50%
□	0.6252	run39	5/1.14/50%
◇	0.6252	run40	5/2.15/50%

Figure 7.2.3.308: Re Effects (CR=5, 50% Cowi) Sidewall Pressures



Sym	$x'/Ts'$	Run No.	CR/Re/Cowi (millions)
○	0.7294	run37	5/0.55/50%
□	0.7294	run39	5/1.14/50%
◇	0.7294	run40	5/2.15/50%

Figure 7.2.3.309: Re Effects (CR=5, 50% Cowi) Sidewall Pressures



Sym	$x'/Ts'$	Run No.	CR/Re/Cowi (millions)
○	0.7815	run37	5/0.55/50%
□	0.7815	run39	5/1.14/50%
◇	0.7815	run40	5/2.15/50%

Figure 7.2.3.310: Re Effects (CR=5, 50% Cowi) Sidewall Pressures

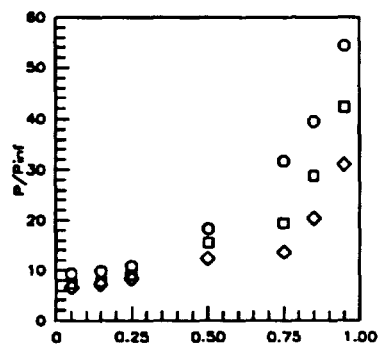


Figure 7.2.3.311: Re Effects (CR=5, 50% Cowl) Sidewall Pressures

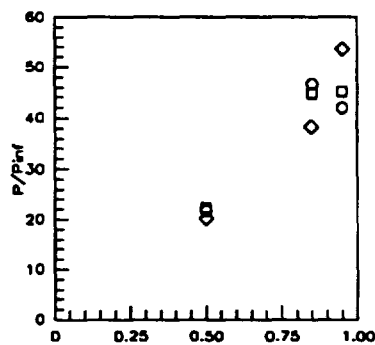


Figure 7.2.3.312: Re Effects (CR=5, 50% Cowl) Sidewall Pressures

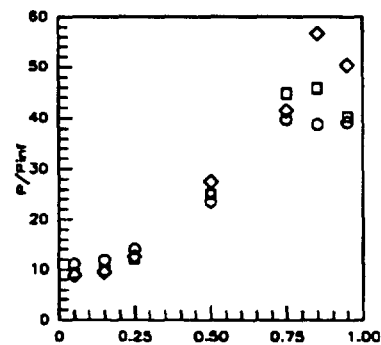


Figure 7.2.3.313: Re Effects (CR=5, 50% Cowl) Sidewall Pressures

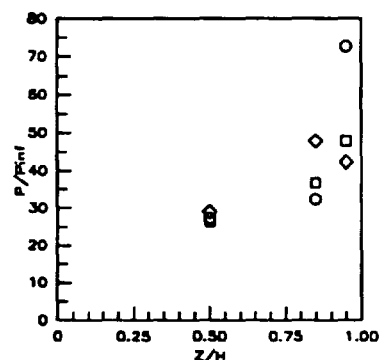


Figure 7.2.3.314: Re Effects (CR=5, 50% Cowl) Sidewall Pressures

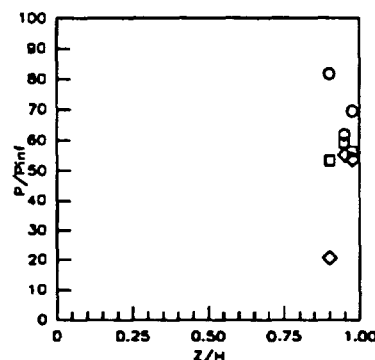


Figure 7.2.3.315: Re Effects (CR=5, 50% Cowl) Sidewall Pressures

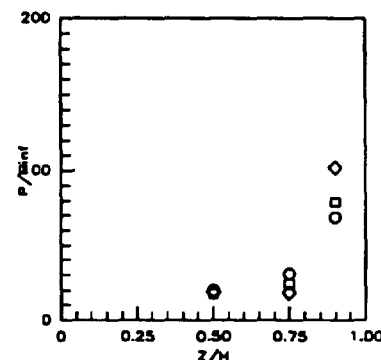


Figure 7.2.3.318: Re Effects (CR=5, 50% Cowl) Sidewall Pressures

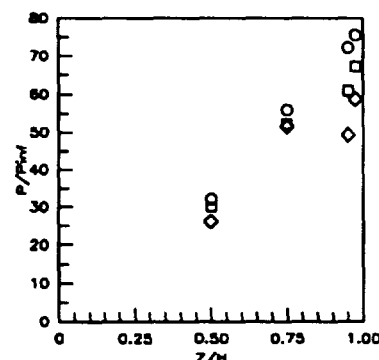


Figure 7.2.3.317: Re Effects (CR=5, 50% Cowl) Sidewall Pressures

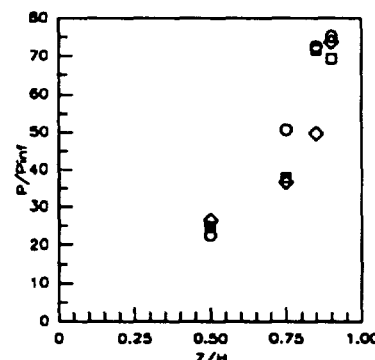
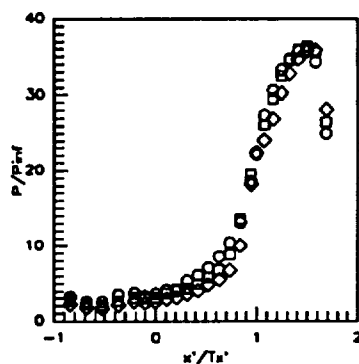
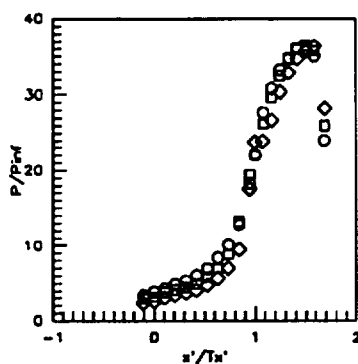


Figure 7.2.3.318: Re Effects (CR=5, 50% Cowl) Sidewall Pressures



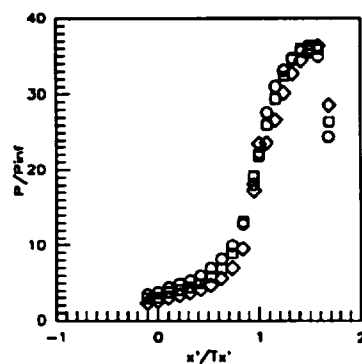
Sym	C.L. for	Run No.	CR/Re/Cowi (millions)
○	CR=3	run47	9/0.55/ 0%
□	CR=3	run48	9/1.14/ 0%
◇	CR=3	run49	9/2.15/ 0%

Figure 7.2.3.319: Re Effects (CR=9, 0% Cowi)  
CR=3 Centerline Pressures



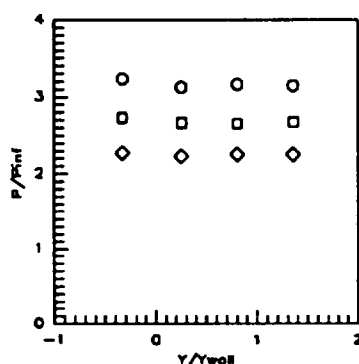
Sym	C.L. for	Run No.	CR/Re/Cowi (millions)
○	CR=5	run47	9/0.55/ 0%
□	CR=5	run48	9/1.14/ 0%
◇	CR=5	run49	9/2.15/ 0%

Figure 7.2.3.320: Re Effects (CR=9, 0% Cowi)  
CR=5 Centerline Pressures



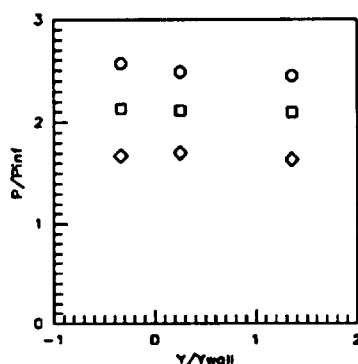
Sym	C.L. for	Run No.	CR/Re/Cowi (millions)
○	CR=9	run47	9/0.55/ 0%
□	CR=9	run48	9/1.14/ 0%
◇	CR=9	run49	9/2.15/ 0%

Figure 7.2.3.321: Re Effects (CR=9, 0% Cowi)  
CR=9 Centerline Pressures



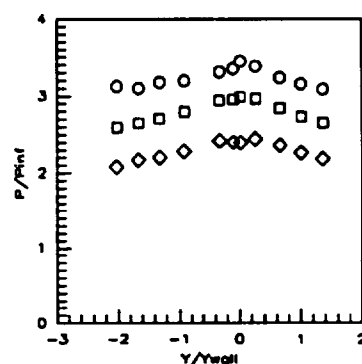
Sym	x'/Ts'	Run No.	CR/Re/Cowi (millions)
○	-0.8412	run47	9/0.55/ 0%
□	-0.8412	run48	9/1.14/ 0%
◇	-0.8412	run49	9/2.15/ 0%

Figure 7.2.3.322: Re Effects (CR=9, 0% Cowi)  
Baseplate Pressures



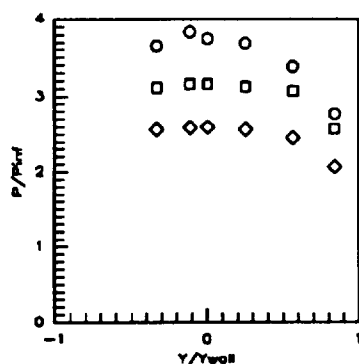
Sym	x'/Ts'	Run No.	CR/Re/Cowi (millions)
○	-0.5258	run47	9/0.55/ 0%
□	-0.5258	run48	9/1.14/ 0%
◇	-0.5258	run49	9/2.15/ 0%

Figure 7.2.3.323: Re Effects (CR=9, 0% Cowi)  
Baseplate Pressures



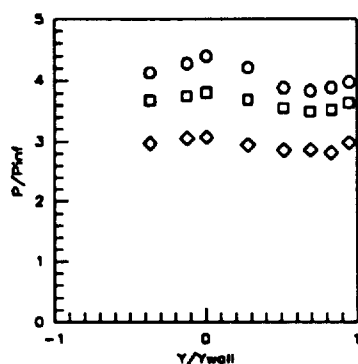
Sym	x'/Ts'	Run No.	CR/Re/Cowi (millions)
○	-0.1052	run47	9/0.55/ 0%
□	-0.1052	run48	9/1.14/ 0%
◇	-0.1052	run49	9/2.15/ 0%

Figure 7.2.3.324: Re Effects (CR=9, 0% Cowi)  
Baseplate Pressures



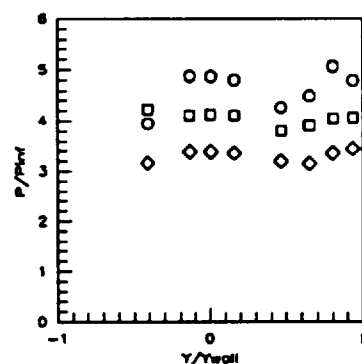
Sym	x'/Ts'	Run No.	CR/Re/Cowi (millions)
○	0.0000	run47	9/0.55/ 0%
□	0.0000	run48	9/1.14/ 0%
◇	0.0000	run49	9/2.15/ 0%

Figure 7.2.3.325: Re Effects (CR=9, 0% Cowi)  
Baseplate Pressures



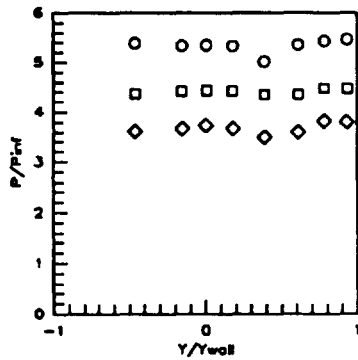
Sym	x'/Ts'	Run No.	CR/Re/Cowi (millions)
○	0.1052	run47	9/0.55/ 0%
□	0.1052	run48	9/1.14/ 0%
◇	0.1052	run49	9/2.15/ 0%

Figure 7.2.3.326: Re Effects (CR=9, 0% Cowi)  
Baseplate Pressures



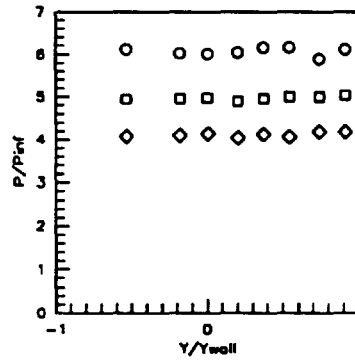
Sym	x'/Ts'	Run No.	CR/Re/Cowi (millions)
○	0.2103	run47	9/0.55/ 0%
□	0.2103	run48	9/1.14/ 0%
◇	0.2103	run49	9/2.15/ 0%

Figure 7.2.3.327: Re Effects (CR=9, 0% Cowi)  
Baseplate Pressures



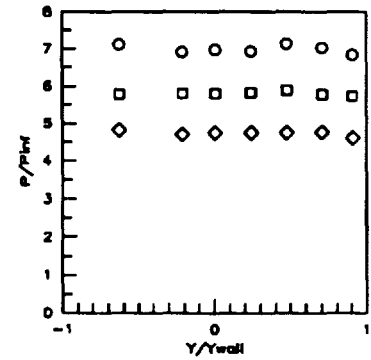
Sym	$x'/T_x'$	Run No.	CR/Re/Cowl (millions)
○	0.3154	run47	9/0.55/ 0%
□	0.3154	run48	9/1.14/ 0%
◇	0.3154	run49	9/2.15/ 0%

Figure 7.2.3.328: Re Effects  
(CR=9, 0%Cowl)  
Baseplate Pressures



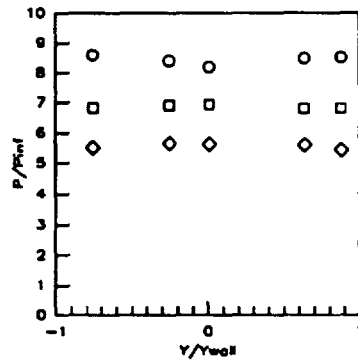
Sym	$x'/T_x'$	Run No.	CR/Re/Cowl (millions)
○	0.4206	run47	9/0.55/ 0%
□	0.4206	run48	9/1.14/ 0%
◇	0.4206	run49	9/2.15/ 0%

Figure 7.2.3.329: Re Effects  
(CR=9, 0%Cowl)  
Baseplate Pressures



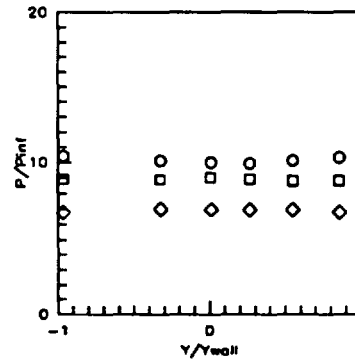
Sym	$x'/T_x'$	Run No.	CR/Re/Cowl (millions)
○	0.5258	run47	9/0.55/ 0%
□	0.5258	run48	9/1.14/ 0%
◇	0.5258	run49	9/2.15/ 0%

Figure 7.2.3.330: Re Effects  
(CR=9, 0%Cowl)  
Baseplate Pressures



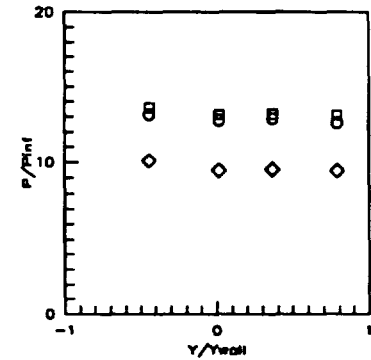
Sym	$x'/T_x'$	Run No.	CR/Re/Cowl (millions)
○	0.6309	run47	9/0.55/ 0%
□	0.6309	run48	9/1.14/ 0%
◇	0.6309	run49	9/2.15/ 0%

Figure 7.2.3.331: Re Effects  
(CR=9, 0%Cowl)  
Baseplate Pressures



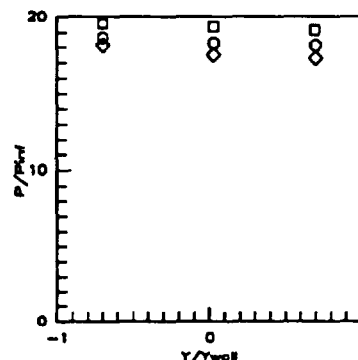
Sym	$x'/T_x'$	Run No.	CR/Re/Cowl (millions)
○	0.7361	run47	9/0.55/ 0%
□	0.7361	run48	9/1.14/ 0%
◇	0.7361	run49	9/2.15/ 0%

Figure 7.2.3.332: Re Effects  
(CR=9, 0%Cowl)  
Baseplate Pressures



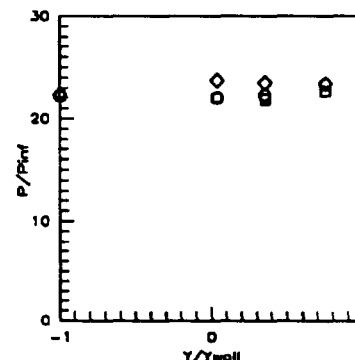
Sym	$x'/T_x'$	Run No.	CR/Re/Cowl (millions)
○	0.8412	run47	9/0.55/ 0%
□	0.8412	run48	9/1.14/ 0%
◇	0.8412	run49	9/2.15/ 0%

Figure 7.2.3.333: Re Effects  
(CR=9, 0%Cowl)  
Baseplate Pressures



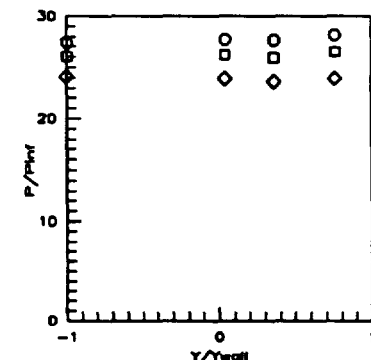
Sym	$x'/T_x'$	Run No.	CR/Re/Cowl (millions)
○	0.9464	run47	9/0.55/ 0%
□	0.9464	run48	9/1.14/ 0%
◇	0.9464	run49	9/2.15/ 0%

Figure 7.2.3.334: Re Effects  
(CR=9, 0%Cowl)  
Baseplate Pressures



Sym	$x'/T_x'$	Run No.	CR/Re/Cowl (millions)
○	1.0000	run47	9/0.55/ 0%
□	1.0000	run48	9/1.14/ 0%
◇	1.0000	run49	9/2.15/ 0%

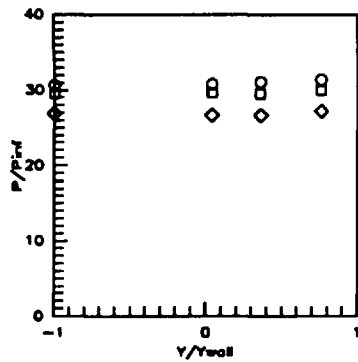
Figure 7.2.3.335: Re Effects  
(CR=9, 0%Cowl)  
Baseplate Pressures



Sym	$x'/T_x'$	Run No.	CR/Re/Cowl (millions)
○	1.0726	run47	9/0.55/ 0%
□	1.0726	run48	9/1.14/ 0%
◇	1.0726	run49	9/2.15/ 0%

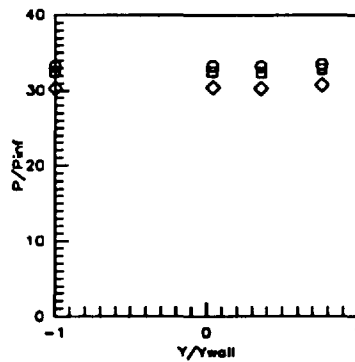
Figure 7.2.3.336: Re Effects  
(CR=9, 0%Cowl)  
Baseplate Pressures





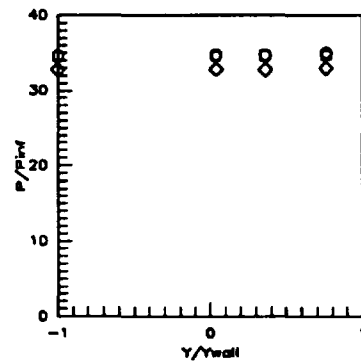
Sym	$x'/Ts'$	Run No.	CR/Re/Cowl (millions)
○	1.1567	run47	9/0.55/ 0%
□	1.1567	run48	9/1.14/ 0%
◇	1.1567	run49	9/2.15/ 0%

Figure 7.2.3.337: Re Effects (CR=9, 0%Cowl) Baseplate Pressures



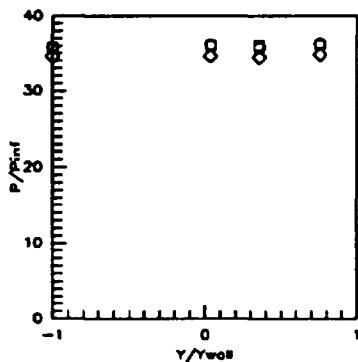
Sym	$x'/Ts'$	Run No.	CR/Re/Cowl (millions)
○	1.2408	run47	9/0.55/ 0%
□	1.2408	run48	9/1.14/ 0%
◇	1.2408	run49	9/2.15/ 0%

Figure 7.2.3.338: Re Effects (CR=9, 0%Cowl) Baseplate Pressures



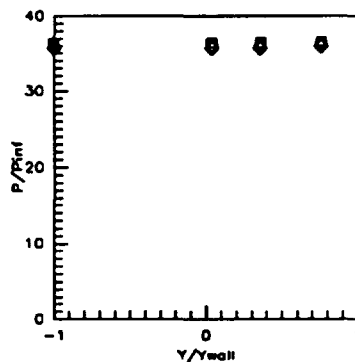
Sym	$x'/Ts'$	Run No.	CR/Re/Cowl (millions)
○	1.3249	run47	9/0.55/ 0%
□	1.3249	run48	9/1.14/ 0%
◇	1.3249	run49	9/2.15/ 0%

Figure 7.2.3.339: Re Effects (CR=9, 0%Cowl) Baseplate Pressures



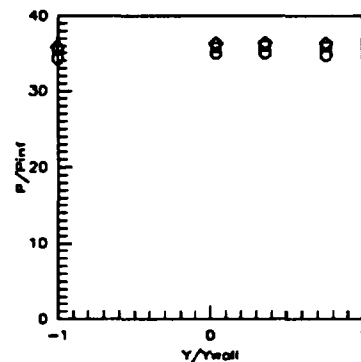
Sym	$x'/Ts'$	Run No.	CR/Re/Cowl (millions)
○	1.4090	run47	9/0.55/ 0%
□	1.4090	run48	9/1.14/ 0%
◇	1.4090	run49	9/2.15/ 0%

Figure 7.2.3.340: Re Effects (CR=9, 0%Cowl) Baseplate Pressures



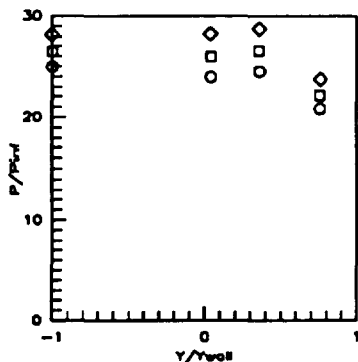
Sym	$x'/Ts'$	Run No.	CR/Re/Cowl (millions)
○	1.4932	run47	9/0.55/ 0%
□	1.4932	run48	9/1.14/ 0%
◇	1.4932	run49	9/2.15/ 0%

Figure 7.2.3.341: Re Effects (CR=9, 0%Cowl) Baseplate Pressures



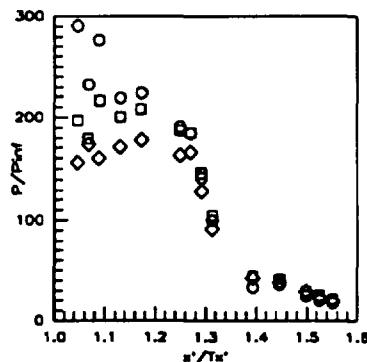
Sym	$x'/Ts'$	Run No.	CR/Re/Cowl (millions)
○	1.5773	run47	9/0.55/ 0%
□	1.5773	run48	9/1.14/ 0%
◇	1.5773	run49	9/2.15/ 0%

Figure 7.2.3.342: Re Effects (CR=9, 0%Cowl) Baseplate Pressures



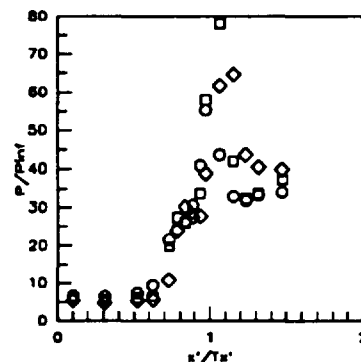
Sym	$x'/Ts'$	Run No.	CR/Re/Cowl (millions)
○	1.6824	run47	9/0.55/ 0%
□	1.6824	run48	9/1.14/ 0%
◇	1.6824	run49	9/2.15/ 0%

Figure 7.2.3.343: Re Effects (CR=9, 0%Cowl) Baseplate Pressures



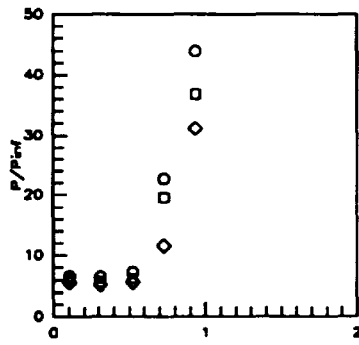
Sym	Cowl Pos.	Run No.	CR/Re/Cowl (millions)
○	0%	run47	9/0.55/ 0%
□	0%	run48	9/1.14/ 0%
◇	0%	run49	9/2.15/ 0%

Figure 7.2.3.344: Re Effects (CR=9, 0%Cowl) Cowl Pressures



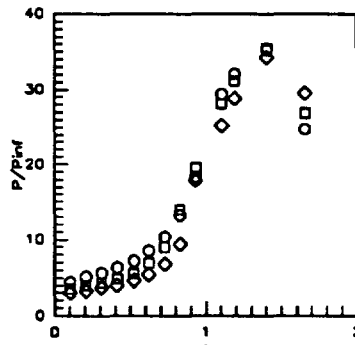
Sym	Z/H	Run No.	CR/Re/Cowl (millions)
○	0.5RT	run47	9/0.55/ 0%
□	0.5RT	run48	9/1.14/ 0%
◇	0.5RT	run49	9/2.15/ 0%

Figure 7.2.3.345: Re Effects (CR=9, 0%Cowl) Sidewall Centerline Pressures



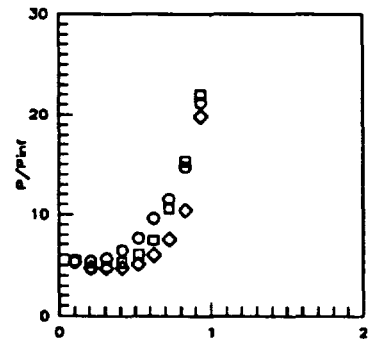
Sym	Z/H	Run No.	CR/Re/Cowl (millions)
○	0.5LT.	run47	9/0.55/ 0%
□	0.5LT.	run48	9/1.14/ 0%
◇	0.5LT.	run49	9/2.15/ 0%

Figure 7.2.3.346: Re Effects  
(CR=9, 0%Cowl)  
Sidewall Centerline Pressures



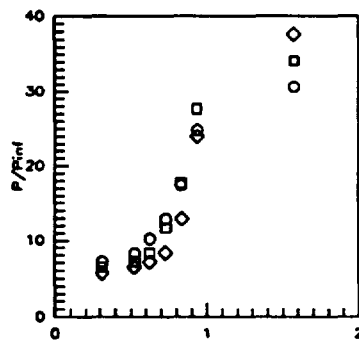
Sym	Z/H	Run No.	CR/Re/Cowl (millions)
○	0.050	run47	9/0.55/ 0%
□	0.050	run48	9/1.14/ 0%
◇	0.050	run49	9/2.15/ 0%

Figure 7.2.3.347: Re Effects  
(CR=9, 0%Cowl)  
Sidewall Pressures



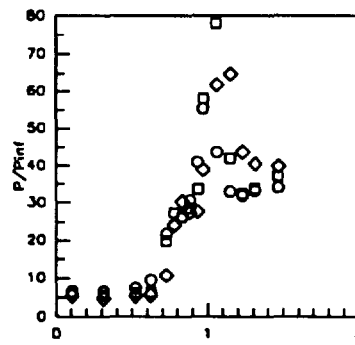
Sym	Z/H	Run No.	CR/Re/Cowl (millions)
○	0.15	run47	9/0.55/ 0%
□	0.15	run48	9/1.14/ 0%
◇	0.15	run49	9/2.15/ 0%

Figure 7.2.3.348: Re Effects  
(CR=9, 0%Cowl)  
Sidewall Pressures



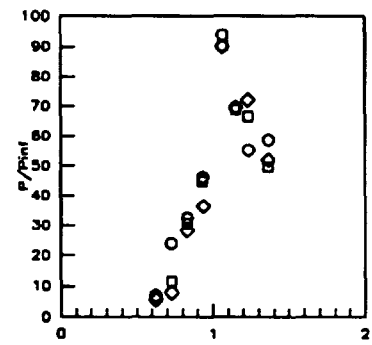
Sym	Z/H	Run No.	CR/Re/Cowl (millions)
○	0.25	run47	9/0.55/ 0%
□	0.25	run48	9/1.14/ 0%
◇	0.25	run49	9/2.15/ 0%

Figure 7.2.3.349: Re Effects  
(CR=9, 0%Cowl)  
Sidewall Pressures



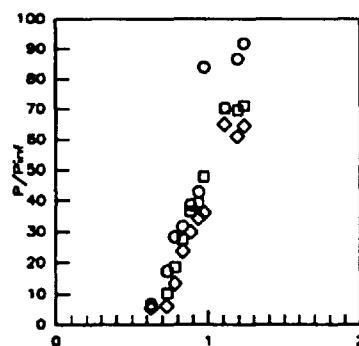
Sym	Z/H	Run No.	CR/Re/Cowl (millions)
○	0.50	run47	9/0.55/ 0%
□	0.50	run48	9/1.14/ 0%
◇	0.50	run49	9/2.15/ 0%

Figure 7.2.3.350: Re Effects  
(CR=9, 0%Cowl)  
Sidewall Pressures



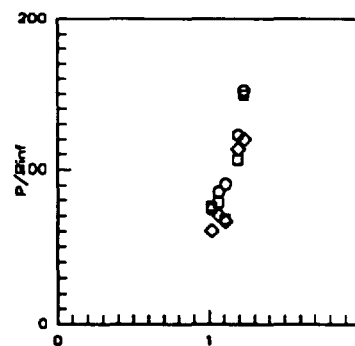
Sym	Z/H	Run No.	CR/Re/Cowl (millions)
○	0.75	run47	9/0.55/ 0%
□	0.75	run48	9/1.14/ 0%
◇	0.75	run49	9/2.15/ 0%

Figure 7.2.3.351: Re Effects  
(CR=9, 0%Cowl)  
Sidewall Pressures



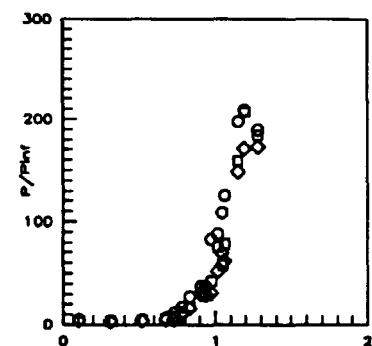
Sym	Z/H	Run No.	CR/Re/Cowl (millions)
○	0.85	run47	9/0.55/ 0%
□	0.85	run48	9/1.14/ 0%
◇	0.85	run49	9/2.15/ 0%

Figure 7.2.3.352: Re Effects  
(CR=9, 0%Cowl)  
Sidewall Pressures



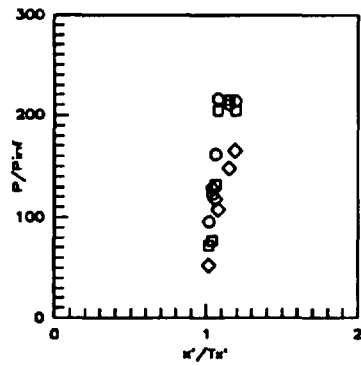
Sym	Z/H	Run No.	CR/Re/Cowl (millions)
○	0.90	run47	9/0.55/ 0%
□	0.90	run48	9/1.14/ 0%
◇	0.90	run49	9/2.15/ 0%

Figure 7.2.3.353: Re Effects  
(CR=9, 0%Cowl)  
Sidewall Pressures



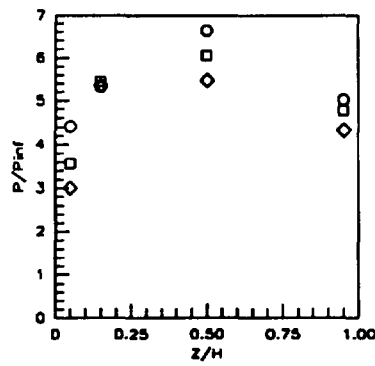
Sym	Z/H	Run No.	CR/Re/Cowl (millions)
○	0.95	run47	9/0.55/ 0%
□	0.95	run48	9/1.14/ 0%
◇	0.95	run49	9/2.15/ 0%

Figure 7.2.3.354: Re Effects  
(CR=9, 0%Cowl)  
Sidewall Pressures



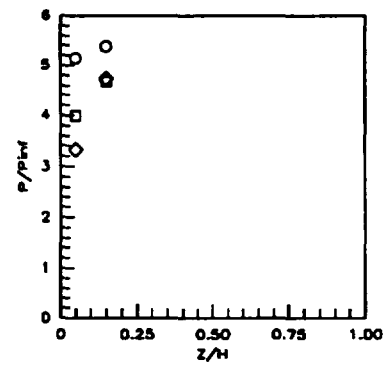
Sym	Z/H	Run No.	CR/Re/Cowl (millions)
○	0.975	run47	9/0.55/ 0%
□	0.975	run48	9/1.14/ 0%
◇	0.975	run49	9/2.15/ 0%

Figure 7.2.3.355: Re Effects  
(CR=9, 0%Cowl)  
Sidewall Pressures



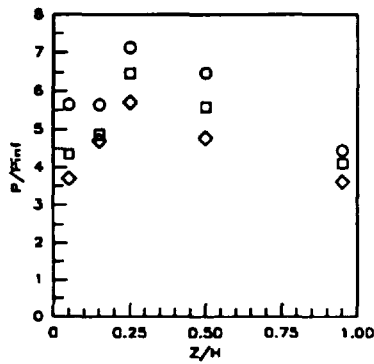
Sym	x'/Ts'	Run No.	CR/Re/Cowl (millions)
○	0.1042	run47	9/0.55/ 0%
□	0.1042	run48	9/1.14/ 0%
◇	0.1042	run49	9/2.15/ 0%

Figure 7.2.3.356: Re Effects  
(CR=9, 0%Cowl)  
Sidewall Pressures



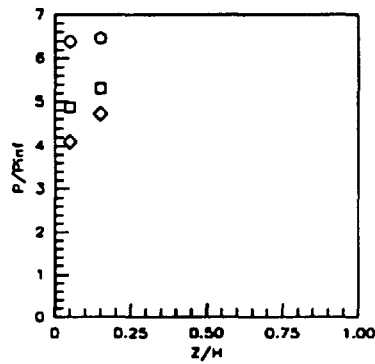
Sym	x'/Ts'	Run No.	CR/Re/Cowl (millions)
○	0.2063	run47	9/0.55/ 0%
□	0.2063	run48	9/1.14/ 0%
◇	0.2063	run49	9/2.15/ 0%

Figure 7.2.3.357: Re Effects  
(CR=9, 0%Cowl)  
Sidewall Pressures



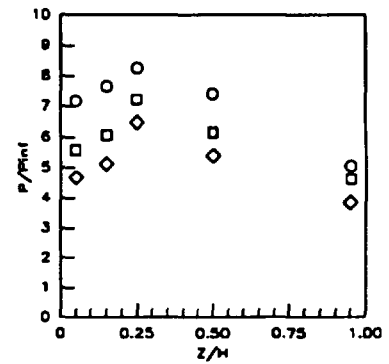
Sym	x'/Ts'	Run No.	CR/Re/Cowl (millions)
○	0.3125	run47	9/0.55/ 0%
□	0.3125	run48	9/1.14/ 0%
◇	0.3125	run49	9/2.15/ 0%

Figure 7.2.3.358: Re Effects  
(CR=9, 0%Cowl)  
Sidewall Pressures



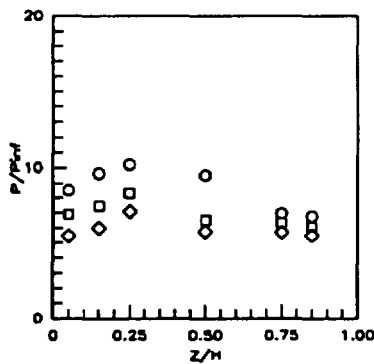
Sym	x'/Ts'	Run No.	CR/Re/Cowl (millions)
○	0.4167	run47	9/0.55/ 0%
□	0.4167	run48	9/1.14/ 0%
◇	0.4167	run49	9/2.15/ 0%

Figure 7.2.3.359: Re Effects  
(CR=9, 0%Cowl)  
Sidewall Pressures



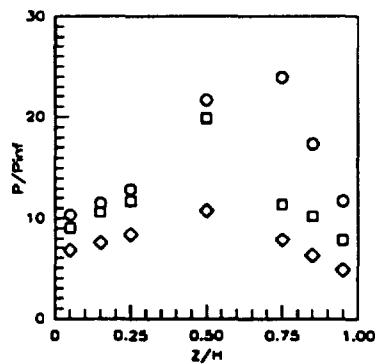
Sym	x'/Ts'	Run No.	CR/Re/Cowl (millions)
○	0.5259	run47	9/0.55/ 0%
□	0.5259	run48	9/1.14/ 0%
◇	0.5259	run49	9/2.15/ 0%

Figure 7.2.3.360: Re Effects  
(CR=9, 0%Cowl)  
Sidewall Pressures



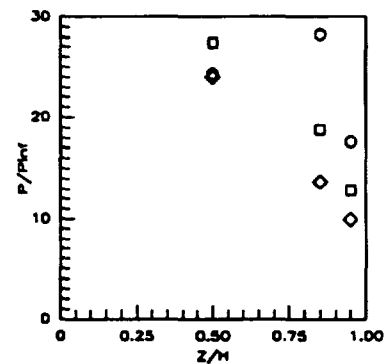
Sym	x'/Ts'	Run No.	CR/Re/Cowl (millions)
○	0.6252	run47	9/0.55/ 0%
□	0.6252	run48	9/1.14/ 0%
◇	0.6252	run49	9/2.15/ 0%

Figure 7.2.3.361: Re Effects  
(CR=9, 0%Cowl)  
Sidewall Pressures



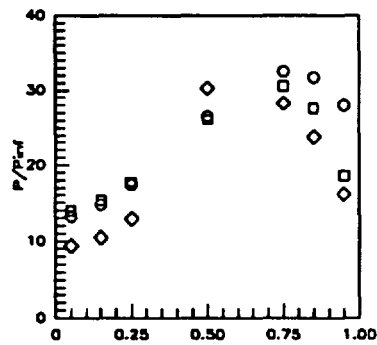
Sym	x'/Ts'	Run No.	CR/Re/Cowl (millions)
○	0.7294	run47	9/0.55/ 0%
□	0.7294	run48	9/1.14/ 0%
◇	0.7294	run49	9/2.15/ 0%

Figure 7.2.3.362: Re Effects  
(CR=9, 0%Cowl)  
Sidewall Pressures



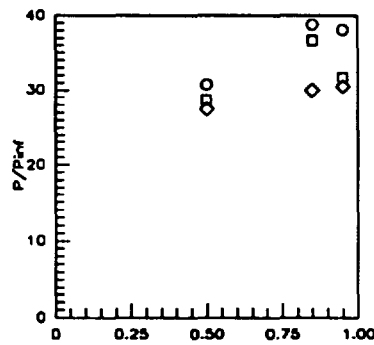
Sym	x'/Ts'	Run No.	CR/Re/Cowl (millions)
○	0.7815	run47	9/0.55/ 0%
□	0.7815	run48	9/1.14/ 0%
◇	0.7815	run49	9/2.15/ 0%

Figure 7.2.3.363: Re Effects  
(CR=9, 0%Cowl)  
Sidewall Pressures



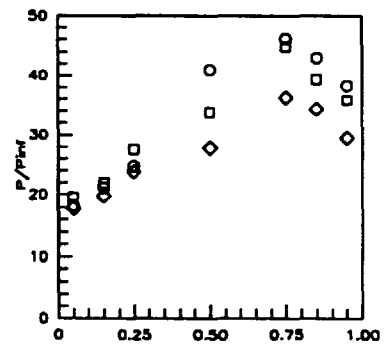
Sym	$x'/T_x'$	Run No.	CR/Re/Cowl (millions)
○	0.8336	run47	9/0.55/ 0%
□	0.8336	run48	9/1.14/ 0%
◇	0.8336	run49	9/2.15/ 0%

Figure 7.2.3.364: Re Effects (CR=9, 0%Cow) Sidewall Pressures



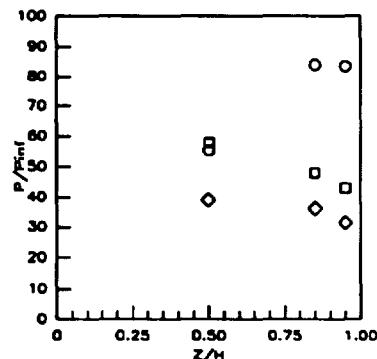
Sym	$x'/T_x'$	Run No.	CR/Re/Cowl (millions)
○	0.8857	run47	9/0.55/ 0%
□	0.8857	run48	9/1.14/ 0%
◇	0.8857	run49	9/2.15/ 0%

Figure 7.2.3.365: Re Effects (CR=9, 0%Cow) Sidewall Pressures



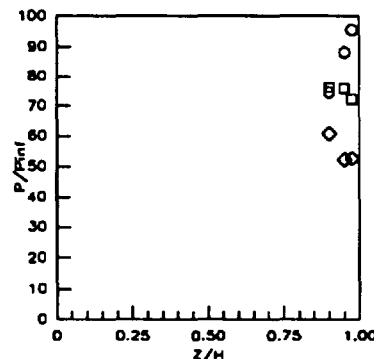
Sym	$x'/T_x'$	Run No.	CR/Re/Cowl (millions)
○	0.9378	run47	9/0.55/ 0%
□	0.9378	run48	9/1.14/ 0%
◇	0.9378	run49	9/2.15/ 0%

Figure 7.2.3.366: Re Effects (CR=9, 0%Cow) Sidewall Pressures



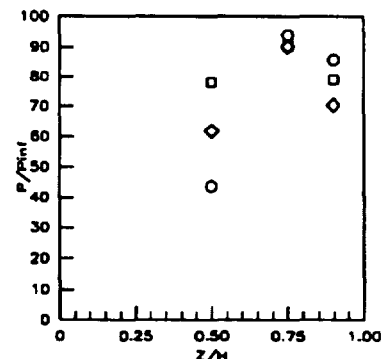
Sym	$x'/T_x'$	Run No.	CR/Re/Cowl (millions)
○	0.9751	run47	9/0.55/ 0%
□	0.9751	run48	9/1.14/ 0%
◇	0.9751	run49	9/2.15/ 0%

Figure 7.2.3.367: Re Effects (CR=9, 0%Cow) Sidewall Pressures



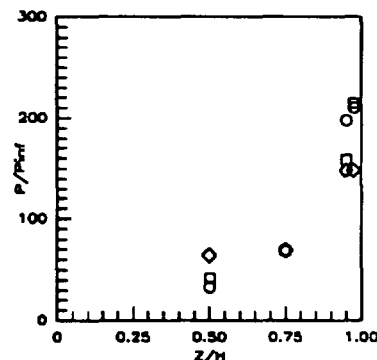
Sym	$x'/T_x'$	Run No.	CR/Re/Cowl (millions)
○	1.0197	run47	9/0.55/ 0%
□	1.0197	run48	9/1.14/ 0%
◇	1.0197	run49	9/2.15/ 0%

Figure 7.2.3.368: Re Effects (CR=9, 0%Cow) Sidewall Pressures



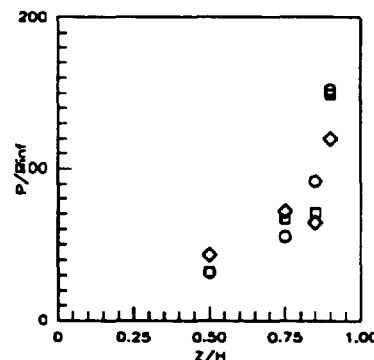
Sym	$x'/T_x'$	Run No.	CR/Re/Cowl (millions)
○	1.0843	run47	9/0.55/ 0%
□	1.0843	run48	9/1.14/ 0%
◇	1.0843	run49	9/2.15/ 0%

Figure 7.2.3.369: Re Effects (CR=9, 0%Cow) Sidewall Pressures



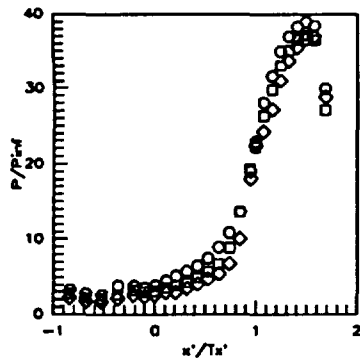
Sym	$x'/T_x'$	Run No.	CR/Re/Cowl (millions)
○	1.1537	run47	9/0.55/ 0%
□	1.1537	run48	9/1.14/ 0%
◇	1.1537	run49	9/2.15/ 0%

Figure 7.2.3.370: Re Effects (CR=9, 0%Cow) Sidewall Pressures



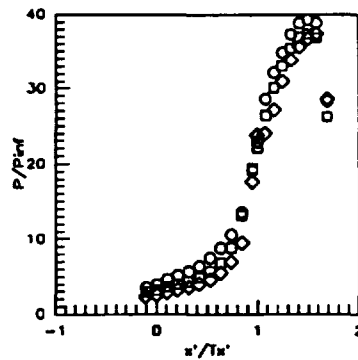
Sym	$x'/T_x'$	Run No.	CR/Re/Cowl (millions)
○	1.2356	run47	9/0.55/ 0%
□	1.2356	run48	9/1.14/ 0%
◇	1.2356	run49	9/2.15/ 0%

Figure 7.2.3.371: Re Effects (CR=9, 0%Cow) Sidewall Pressures



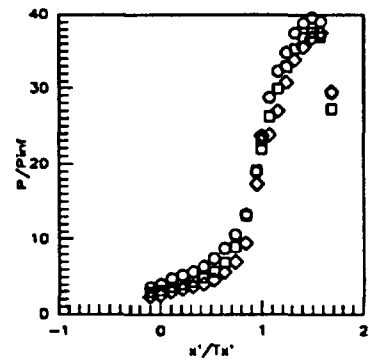
Sym	C.L. for	Run No.	CR/Re/Cowi (millions)
○	CR=3	run50	9/0.55/25%
□	CR=3	run52	9/1.14/25%
◇	CR=3	run53	9/2.15/25%

Figure 7.2.3.372: Re Effects (CR=9, 25% Cowi)  
CR=3 Centerline Pressures



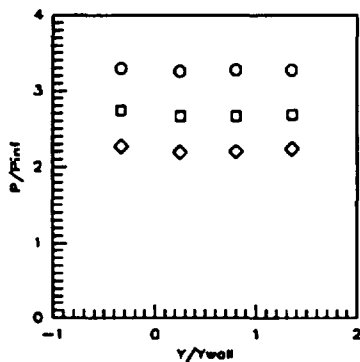
Sym	C.L. for	Run No.	CR/Re/Cowi (millions)
○	CR=5	run50	9/0.55/25%
□	CR=5	run52	9/1.14/25%
◇	CR=5	run53	9/2.15/25%

Figure 7.2.3.373: Re Effects (CR=9, 25% Cowi)  
CR=5 Centerline Pressures



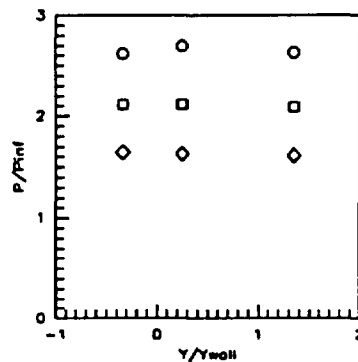
Sym	C.L. for	Run No.	CR/Re/Cowi (millions)
○	CR=9	run50	9/0.55/25%
□	CR=9	run52	9/1.14/25%
◇	CR=9	run53	9/2.15/25%

Figure 7.2.3.374: Re Effects (CR=9, 25% Cowi)  
CR=9 Centerline Pressures



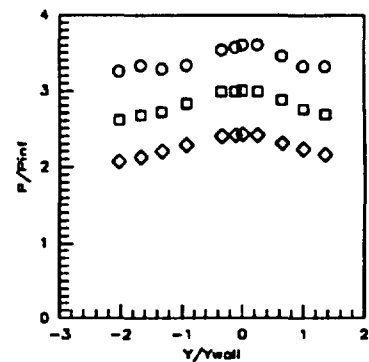
Sym	x'/Tx'	Run No.	CR/Re/Cowi (millions)
○	-0.8412	run50	9/0.55/25%
□	-0.8412	run52	9/1.14/25%
◇	-0.8412	run53	9/2.15/25%

Figure 7.2.3.375: Re Effects (CR=9, 25% Cowi)  
Baseplate Pressures



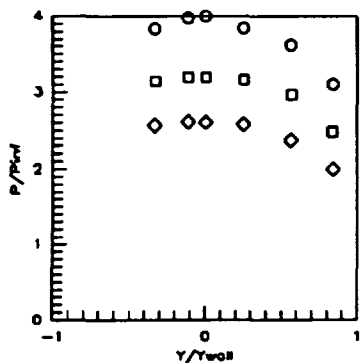
Sym	x'/Tx'	Run No.	CR/Re/Cowi (millions)
○	-0.5258	run50	9/0.55/25%
□	-0.5258	run52	9/1.14/25%
◇	-0.5258	run53	9/2.15/25%

Figure 7.2.3.376: Re Effects (CR=9, 25% Cowi)  
Baseplate Pressures



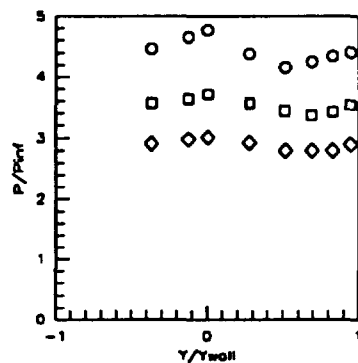
Sym	x'/Tx'	Run No.	CR/Re/Cowi (millions)
○	-0.1052	run50	9/0.55/25%
□	-0.1052	run52	9/1.14/25%
◇	-0.1052	run53	9/2.15/25%

Figure 7.2.3.377: Re Effects (CR=9, 25% Cowi)  
Baseplate Pressures



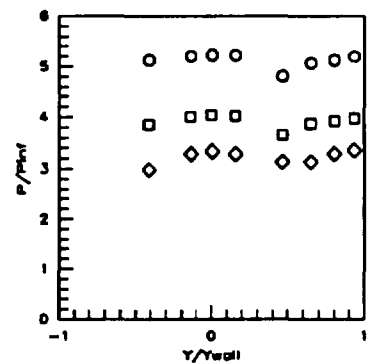
Sym	x'/Tx'	Run No.	CR/Re/Cowi (millions)
○	0.0000	run50	9/0.55/25%
□	0.0000	run52	9/1.14/25%
◇	0.0000	run53	9/2.15/25%

Figure 7.2.3.378: Re Effects (CR=9, 25% Cowi)  
Baseplate Pressures



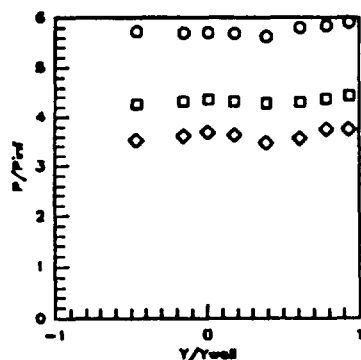
Sym	x'/Tx'	Run No.	CR/Re/Cowi (millions)
○	0.1052	run50	9/0.55/25%
□	0.1052	run52	9/1.14/25%
◇	0.1052	run53	9/2.15/25%

Figure 7.2.3.379: Re Effects (CR=9, 25% Cowi)  
Baseplate Pressures



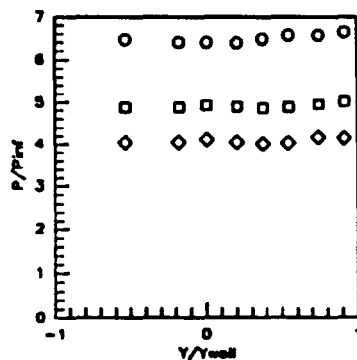
Sym	x'/Tx'	Run No.	CR/Re/Cowi (millions)
○	0.2103	run50	9/0.55/25%
□	0.2103	run52	9/1.14/25%
◇	0.2103	run53	9/2.15/25%

Figure 7.2.3.380: Re Effects (CR=9, 25% Cowi)  
Baseplate Pressures



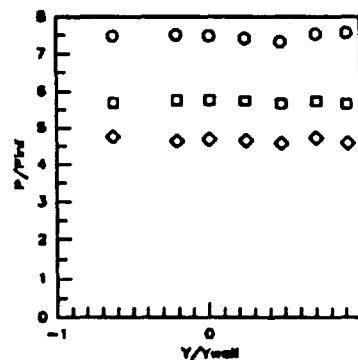
Sym	$x'/T_x'$	Run No.	CR/Re/Cool (millions)
○	0.3184	run50	9/0.55/25%
□	0.3184	run52	9/1.14/25%
◇	0.3184	run53	9/2.15/25%

Figure 7.2.3.381: Re Effects (CR=9, 25%Cool) Baseplate Pressures



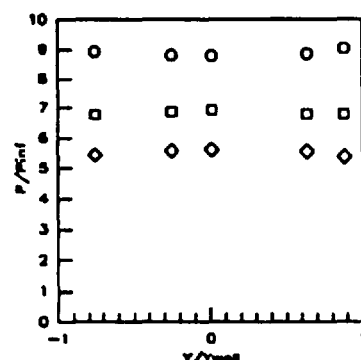
Sym	$x'/T_x'$	Run No.	CR/Re/Cool (millions)
○	0.4206	run50	9/0.55/25%
□	0.4206	run52	9/1.14/25%
◇	0.4206	run53	9/2.15/25%

Figure 7.2.3.382: Re Effects (CR=9, 25%Cool) Baseplate Pressures



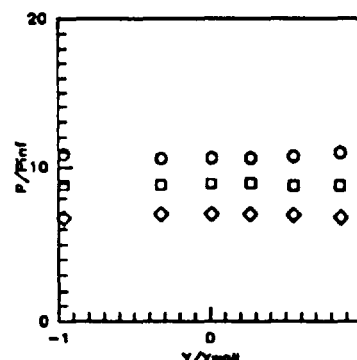
Sym	$x'/T_x'$	Run No.	CR/Re/Cool (millions)
○	0.5258	run50	9/0.55/25%
□	0.5258	run52	9/1.14/25%
◇	0.5258	run53	9/2.15/25%

Figure 7.2.3.383: Re Effects (CR=9, 25%Cool) Baseplate Pressures



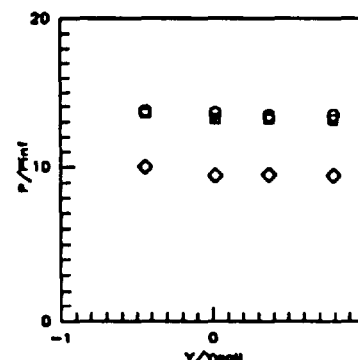
Sym	$x'/T_x'$	Run No.	CR/Re/Cool (millions)
○	0.6309	run50	9/0.55/25%
□	0.6309	run52	9/1.14/25%
◇	0.6309	run53	9/2.15/25%

Figure 7.2.3.384: Re Effects (CR=9, 25%Cool) Baseplate Pressures



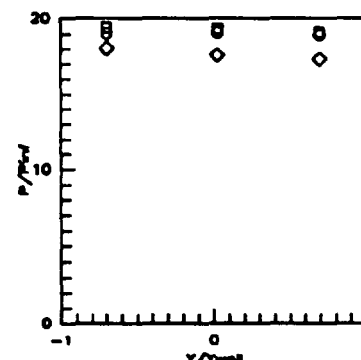
Sym	$x'/T_x'$	Run No.	CR/Re/Cool (millions)
○	0.7361	run50	9/0.55/25%
□	0.7361	run52	9/1.14/25%
◇	0.7361	run53	9/2.15/25%

Figure 7.2.3.385: Re Effects (CR=9, 25%Cool) Baseplate Pressures



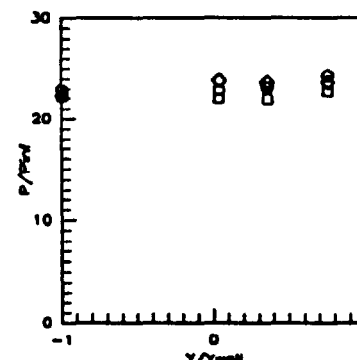
Sym	$x'/T_x'$	Run No.	CR/Re/Cool (millions)
○	0.8412	run50	9/0.55/25%
□	0.8412	run52	9/1.14/25%
◇	0.8412	run53	9/2.15/25%

Figure 7.2.3.386: Re Effects (CR=9, 25%Cool) Baseplate Pressures



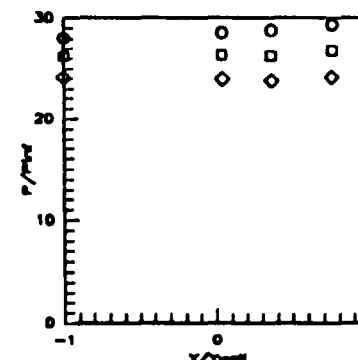
Sym	$x'/T_x'$	Run No.	CR/Re/Cool (millions)
○	0.9464	run50	9/0.55/25%
□	0.9464	run52	9/1.14/25%
◇	0.9464	run53	9/2.15/25%

Figure 7.2.3.387: Re Effects (CR=9, 25%Cool) Baseplate Pressures



Sym	$x'/T_x'$	Run No.	CR/Re/Cool (millions)
○	1.0000	run50	9/0.55/25%
□	1.0000	run52	9/1.14/25%
◇	1.0000	run53	9/2.15/25%

Figure 7.2.3.388: Re Effects (CR=9, 25%Cool) Baseplate Pressures



Sym	$x'/T_x'$	Run No.	CR/Re/Cool (millions)
○	1.0728	run50	9/0.55/25%
□	1.0728	run52	9/1.14/25%
◇	1.0728	run53	9/2.15/25%

Figure 7.2.3.389: Re Effects (CR=9, 25%Cool) Baseplate Pressures

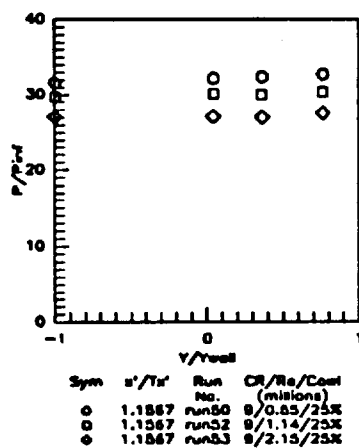


Figure 7.2.3.390: Re Effects (CR=9, 25% Cowi) Baseplate Pressures

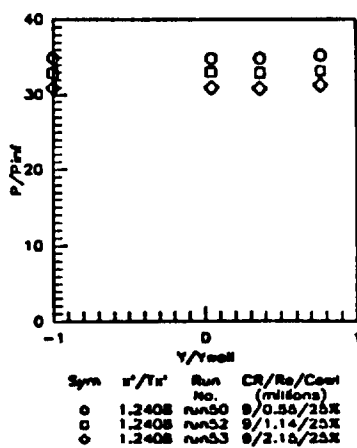


Figure 7.2.3.391: Re Effects (CR=9, 25% Cowi) Baseplate Pressures

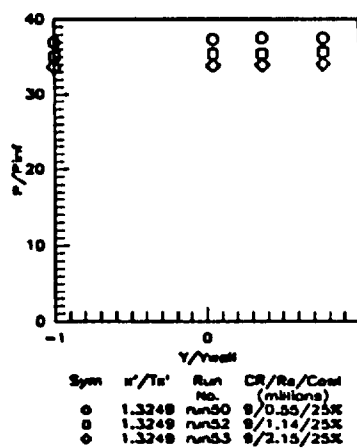


Figure 7.2.3.392: Re Effects (CR=9, 25% Cowi) Baseplate Pressures

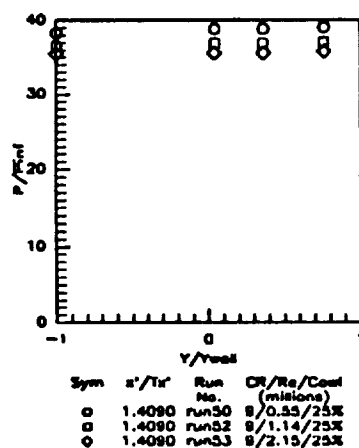


Figure 7.2.3.393: Re Effects (CR=9, 25% Cowi) Baseplate Pressures

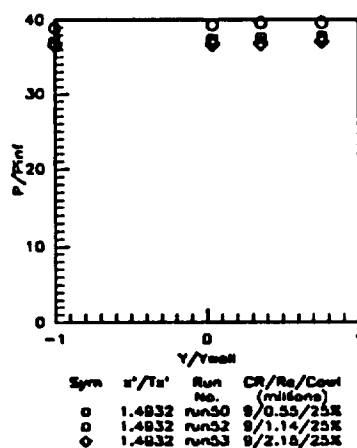


Figure 7.2.3.394: Re Effects (CR=9, 25% Cowi) Baseplate Pressures

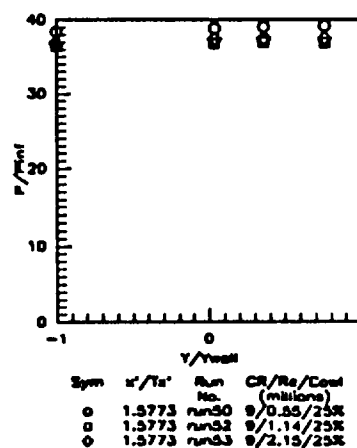


Figure 7.2.3.395: Re Effects (CR=9, 25% Cowi) Baseplate Pressures

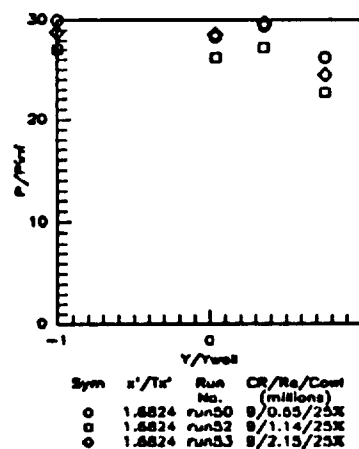


Figure 7.2.3.396: Re Effects (CR=9, 25% Cowi) Baseplate Pressures

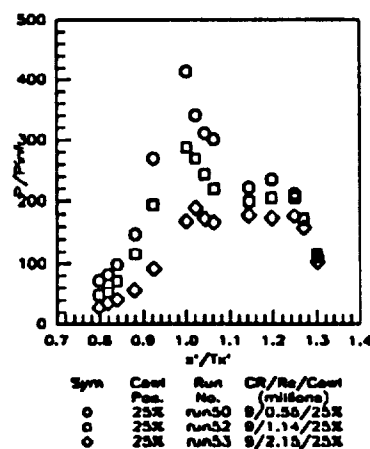


Figure 7.2.3.397: Re Effects (CR=9, 25% Cowi) CowI Pressures

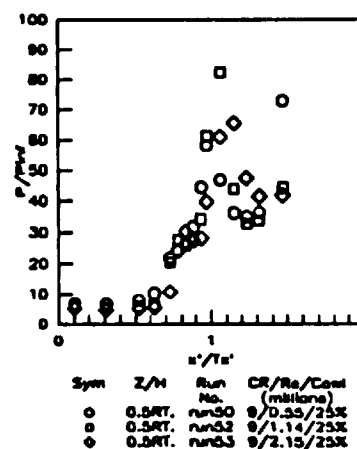
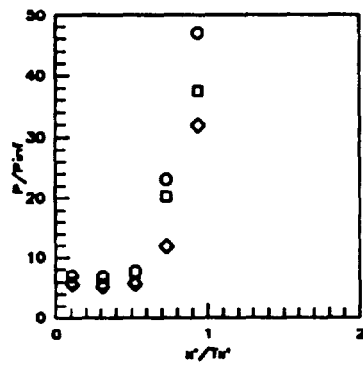
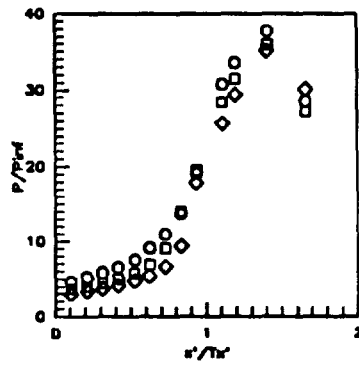


Figure 7.2.3.398: Re Effects (CR=9, 25% Cowi) Sidewall Centerline Pressures



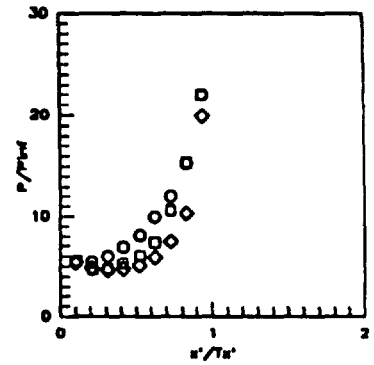
Sym	Z/H	Run No.	CR/Re/Cowi (millions)
○	0.34T	run50	9/0.55/25%
□	0.34T	run52	9/1.14/25%
◇	0.34T	run53	9/2.15/25%

Figure 7.2.3.399: Re Effects (CR=9, 25% Cowi) Sidewall Centerline Pressures



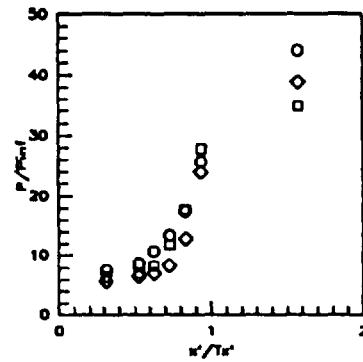
Sym	Z/H	Run No.	CR/Re/Cowi (millions)
○	0.050	run50	9/0.55/25%
□	0.050	run52	9/1.14/25%
◇	0.050	run53	9/2.15/25%

Figure 7.2.3.400: Re Effects (CR=9, 25% Cowi) Sidewall Pressures



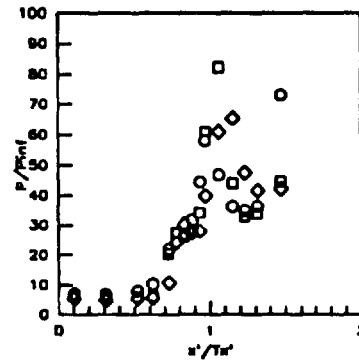
Sym	Z/H	Run No.	CR/Re/Cowi (millions)
○	0.15	run50	9/0.55/25%
□	0.15	run52	9/1.14/25%
◇	0.15	run53	9/2.15/25%

Figure 7.2.3.401: Re Effects (CR=9, 25% Cowi) Sidewall Pressures



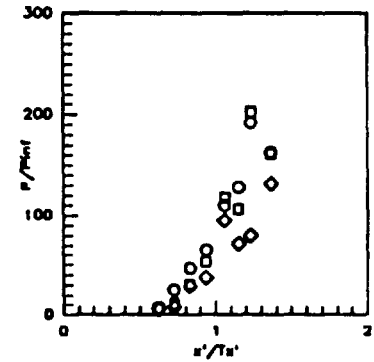
Sym	Z/H	Run No.	CR/Re/Cowi (millions)
○	0.25	run50	9/0.55/25%
□	0.25	run52	9/1.14/25%
◇	0.25	run53	9/2.15/25%

Figure 7.2.3.402: Re Effects (CR=9, 25% Cowi) Sidewall Pressures



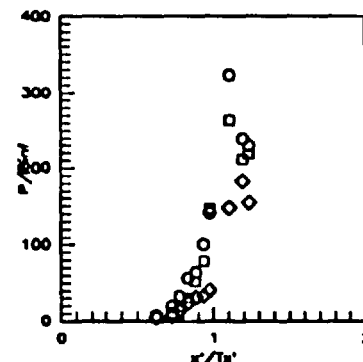
Sym	Z/H	Run No.	CR/Re/Cowi (millions)
○	0.50	run50	9/0.55/25%
□	0.50	run52	9/1.14/25%
◇	0.50	run53	9/2.15/25%

Figure 7.2.3.403: Re Effects (CR=9, 25% Cowi) Sidewall Pressures



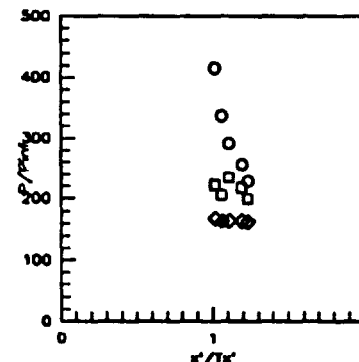
Sym	Z/H	Run No.	CR/Re/Cowi (millions)
○	0.75	run50	9/0.55/25%
□	0.75	run52	9/1.14/25%
◇	0.75	run53	9/2.15/25%

Figure 7.2.3.404: Re Effects (CR=9, 25% Cowi) Sidewall Pressures



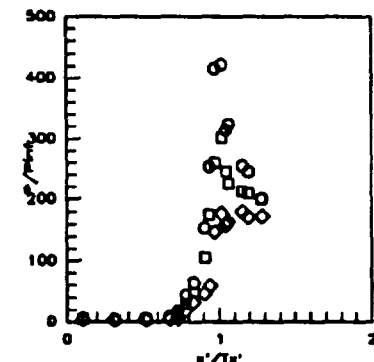
Sym	Z/H	Run No.	CR/Re/Cowi (millions)
○	0.85	run50	9/0.55/25%
□	0.85	run52	9/1.14/25%
◇	0.85	run53	9/2.15/25%

Figure 7.2.3.405: Re Effects (CR=9, 25% Cowi) Sidewall Pressures



Sym	Z/H	Run No.	CR/Re/Cowi (millions)
○	0.90	run50	9/0.55/25%
□	0.90	run52	9/1.14/25%
◇	0.90	run53	9/2.15/25%

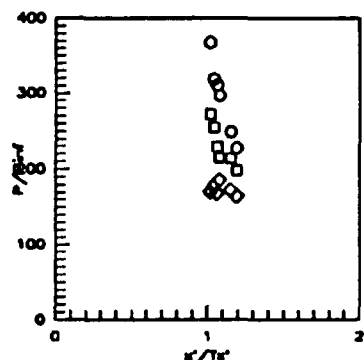
Figure 7.2.3.406: Re Effects (CR=9, 25% Cowi) Sidewall Pressures



Sym	Z/H	Run No.	CR/Re/Cowi (millions)
○	0.95	run50	9/0.55/25%
□	0.95	run52	9/1.14/25%
◇	0.95	run53	9/2.15/25%

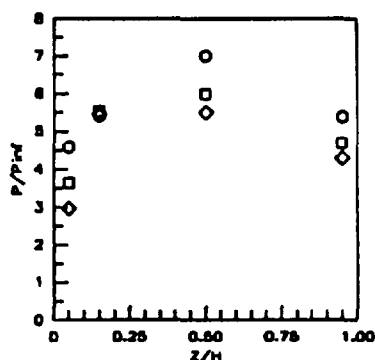
Figure 7.2.3.407: Re Effects (CR=9, 25% Cowi) Sidewall Pressures





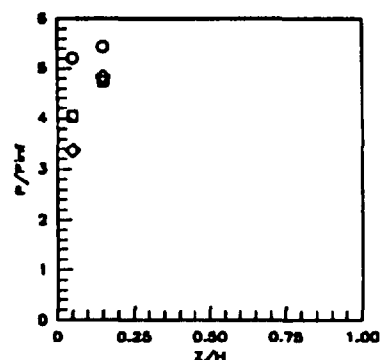
Sym	$z'/T_s'$	Run No.	CR/Rs/Cowl (milions)
-----	-----------	---------	----------------------

Figure 7.2.3.408: Re Effects (CR=9, 25% Cowl) Sidewall Pressures



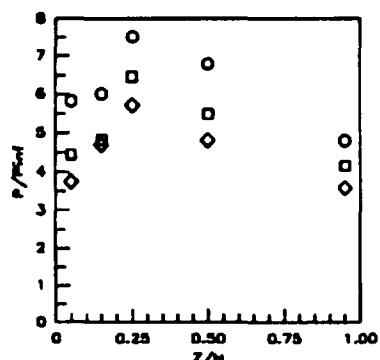
Sym	$z'/T_s'$	Run No.	CR/Rs/Cowl (milions)
-----	-----------	---------	----------------------

Figure 7.2.3.409: Re Effects (CR=9, 25% Cowl) Sidewall Pressures



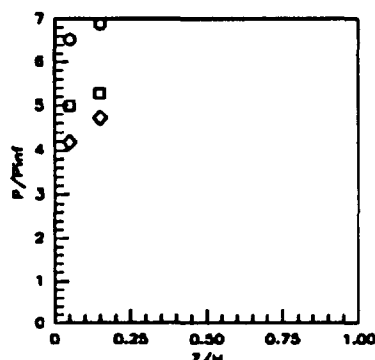
Sym	$z'/T_s'$	Run No.	CR/Rs/Cowl (milions)
-----	-----------	---------	----------------------

Figure 7.2.3.410: Re Effects (CR=9, 25% Cowl) Sidewall Pressures



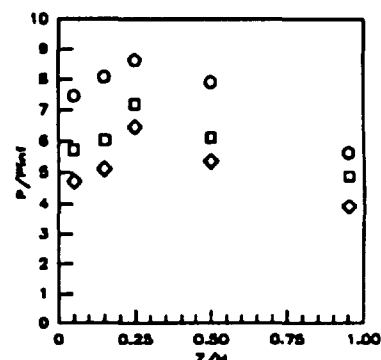
Sym	$z'/T_s'$	Run No.	CR/Rs/Cowl (milions)
-----	-----------	---------	----------------------

Figure 7.2.3.411: Re Effects (CR=9, 25% Cowl) Sidewall Pressures



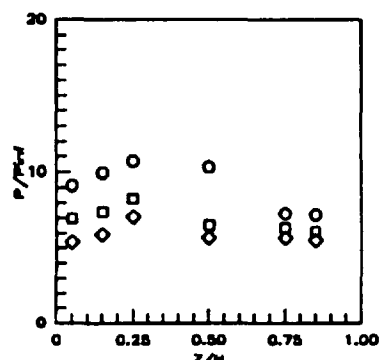
Sym	$z'/T_s'$	Run No.	CR/Rs/Cowl (milions)
-----	-----------	---------	----------------------

Figure 7.2.3.412: Re Effects (CR=9, 25% Cowl) Sidewall Pressures



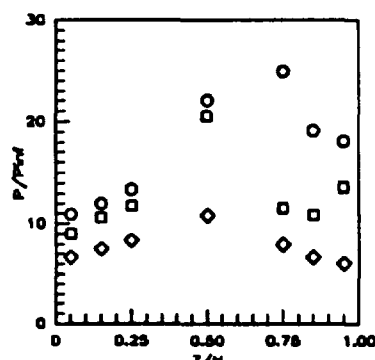
Sym	$z'/T_s'$	Run No.	CR/Rs/Cowl (milions)
-----	-----------	---------	----------------------

Figure 7.2.3.413: Re Effects (CR=9, 25% Cowl) Sidewall Pressures



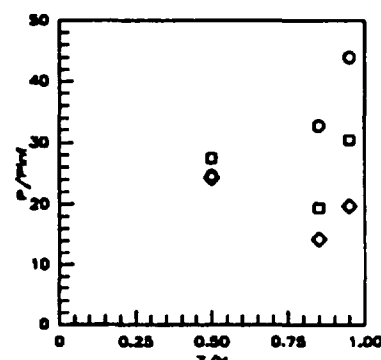
Sym	$z'/T_s'$	Run No.	CR/Rs/Cowl (milions)
-----	-----------	---------	----------------------

Figure 7.2.3.414: Re Effects (CR=9, 25% Cowl) Sidewall Pressures



Sym	$z'/T_s'$	Run No.	CR/Rs/Cowl (milions)
-----	-----------	---------	----------------------

Figure 7.2.3.415: Re Effects (CR=9, 25% Cowl) Sidewall Pressures



Sym	$z'/T_s'$	Run No.	CR/Rs/Cowl (milions)
-----	-----------	---------	----------------------

Figure 7.2.3.416: Re Effects (CR=9, 25% Cowl) Sidewall Pressures

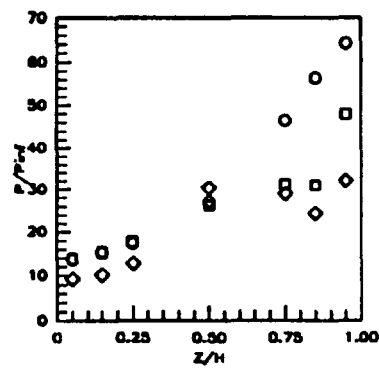


Figure 7.2.3.417: Re Effects  
(CR=9, 25%Cowl)  
Sidewall Pressures

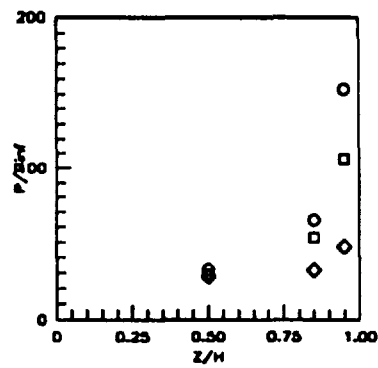


Figure 7.2.3.418: Re Effects  
(CR=9, 25%Cowl)  
Sidewall Pressures

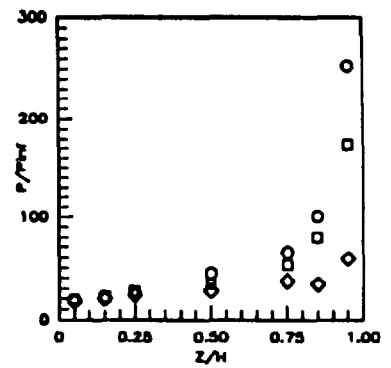


Figure 7.2.3.419: Re Effects  
(CR=9, 25%Cowl)  
Sidewall Pressures

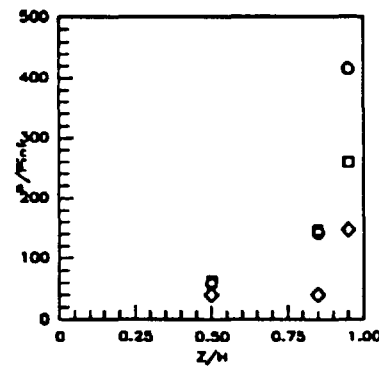


Figure 7.2.3.420: Re Effects  
(CR=9, 25%Cowl)  
Sidewall Pressures

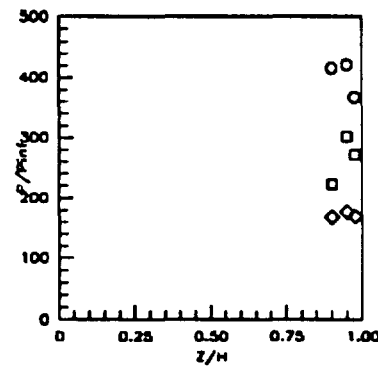


Figure 7.2.3.421: Re Effects  
(CR=9, 25%Cowl)  
Sidewall Pressures

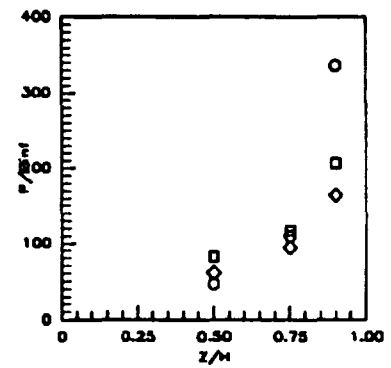


Figure 7.2.3.422: Re Effects  
(CR=9, 25%Cowl)  
Sidewall Pressures

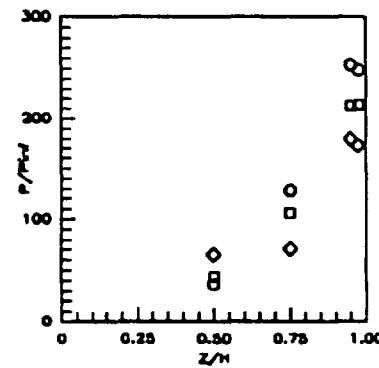


Figure 7.2.3.423: Re Effects  
(CR=9, 25%Cowl)  
Sidewall Pressures

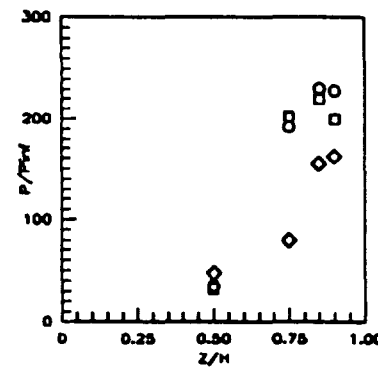


Figure 7.2.3.424: Re Effects  
(CR=9, 25%Cowl)  
Sidewall Pressures

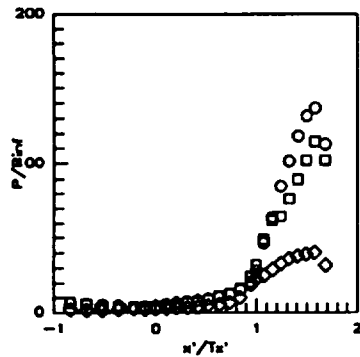


Figure 7.2.3.425: Re Effects  
(CR=9, 50% Cowi)  
CR=3 Centerline Pressures

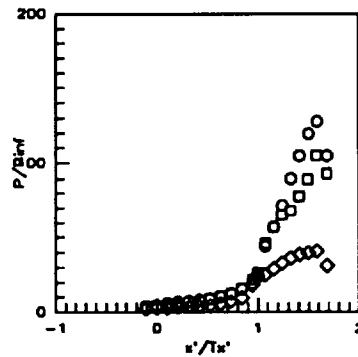


Figure 7.2.3.426: Re Effects  
(CR=9, 50% Cowi)  
CR=5 Centerline Pressures

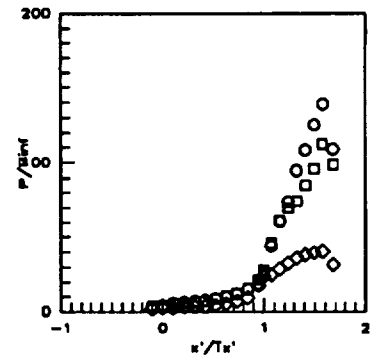


Figure 7.2.3.427: Re Effects  
(CR=9, 50% Cowi)  
CR=9 Centerline Pressures

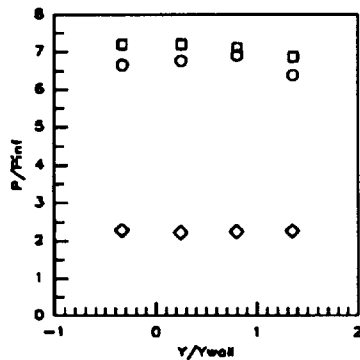


Figure 7.2.3.428: Re Effects  
(CR=9, 50% Cowi)  
Baseplate Pressures

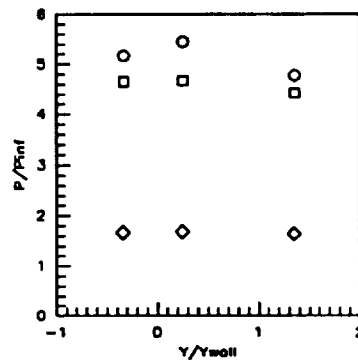


Figure 7.2.3.429: Re Effects  
(CR=9, 50% Cowi)  
Baseplate Pressures

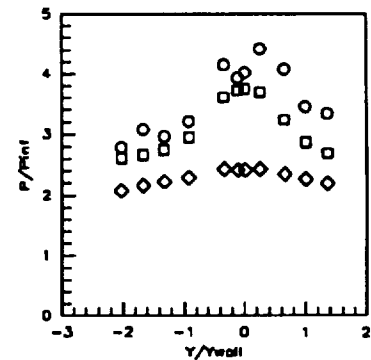


Figure 7.2.3.430: Re Effects  
(CR=9, 50% Cowi)  
Baseplate Pressures

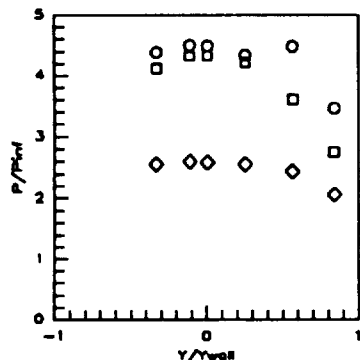


Figure 7.2.3.431: Re Effects  
(CR=9, 50% Cowi)  
Baseplate Pressures

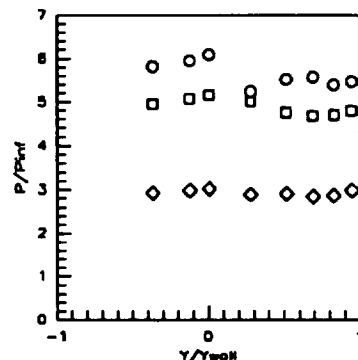


Figure 7.2.3.432: Re Effects  
(CR=9, 50% Cowi)  
Baseplate Pressures

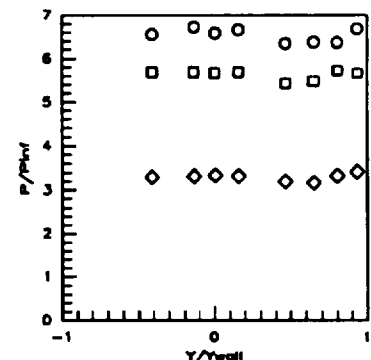
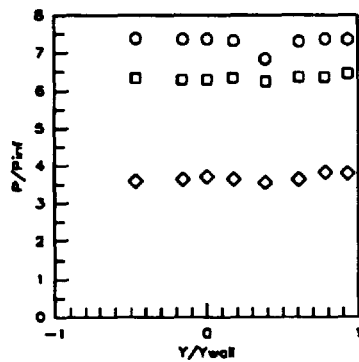
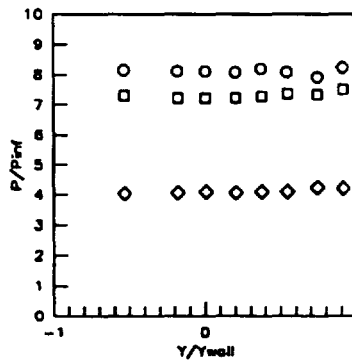


Figure 7.2.3.433: Re Effects  
(CR=9, 50% Cowi)  
Baseplate Pressures



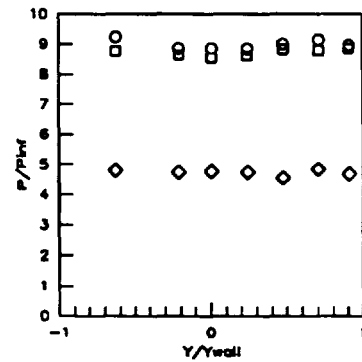
Sym	x'/Ts'	Run No.	CR/Re/Cowl (millions)
○	0.3154	run55	9/0.55/50%
□	0.3154	run56	9/1.14/50%
◇	0.3154	run57	9/2.15/50%

Figure 7.2.3.434: Re Effects (CR=9, 50%Cowl) Baseplate Pressures



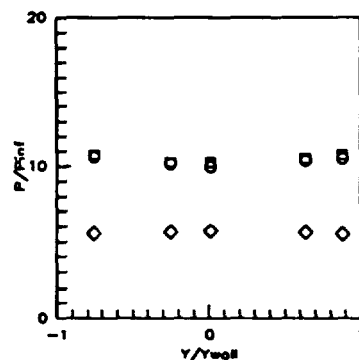
Sym	x'/Ts'	Run No.	CR/Re/Cowl (millions)
○	0.4206	run55	9/0.55/50%
□	0.4206	run56	9/1.14/50%
◇	0.4206	run57	9/2.15/50%

Figure 7.2.3.435: Re Effects (CR=9, 50%Cowl) Baseplate Pressures



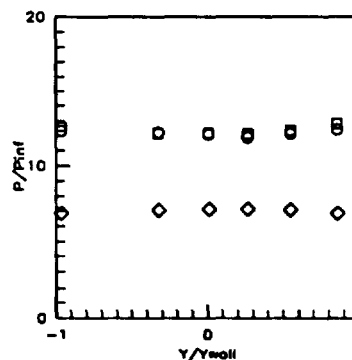
Sym	x'/Ts'	Run No.	CR/Re/Cowl (millions)
○	0.5258	run55	9/0.55/50%
□	0.5258	run56	9/1.14/50%
◇	0.5258	run57	9/2.15/50%

Figure 7.2.3.436: Re Effects (CR=9, 50%Cowl) Baseplate Pressures



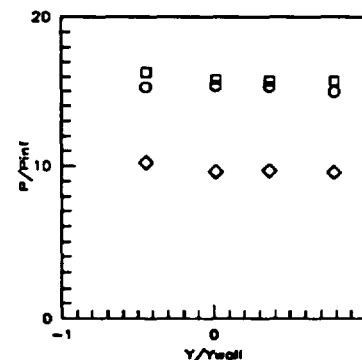
Sym	x'/Ts'	Run No.	CR/Re/Cowl (millions)
○	0.6309	run55	9/0.55/50%
□	0.6309	run56	9/1.14/50%
◇	0.6309	run57	9/2.15/50%

Figure 7.2.3.437: Re Effects (CR=9, 50%Cowl) Baseplate Pressures



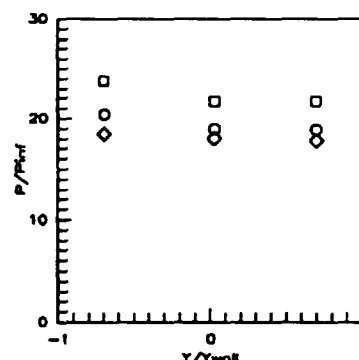
Sym	x'/Ts'	Run No.	CR/Re/Cowl (millions)
○	0.7361	run55	9/0.55/50%
□	0.7361	run56	9/1.14/50%
◇	0.7361	run57	9/2.15/50%

Figure 7.2.3.438: Re Effects (CR=9, 50%Cowl) Baseplate Pressures



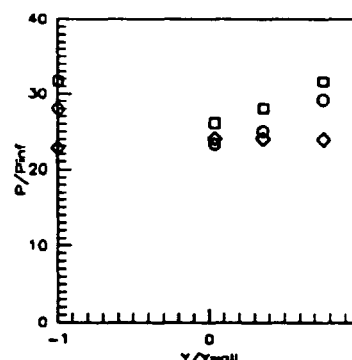
Sym	x'/Ts'	Run No.	CR/Re/Cowl (millions)
○	0.8412	run55	9/0.55/50%
□	0.8412	run56	9/1.14/50%
◇	0.8412	run57	9/2.15/50%

Figure 7.2.3.439: Re Effects (CR=9, 50%Cowl) Baseplate Pressures



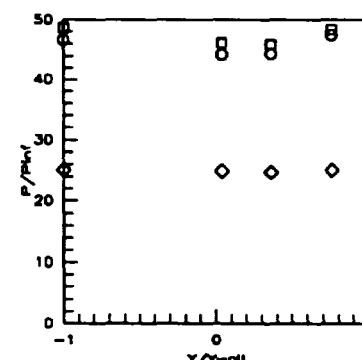
Sym	x'/Ts'	Run No.	CR/Re/Cowl (millions)
○	0.9464	run55	9/0.55/50%
□	0.9464	run56	9/1.14/50%
◇	0.9464	run57	9/2.15/50%

Figure 7.2.3.440: Re Effects (CR=9, 50%Cowl) Baseplate Pressures



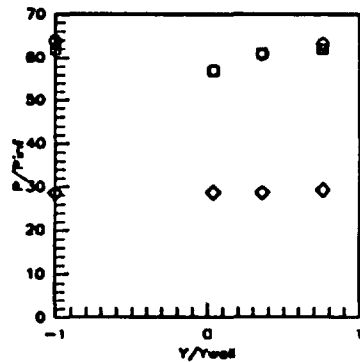
Sym	x'/Ts'	Run No.	CR/Re/Cowl (millions)
○	1.0000	run55	9/0.55/50%
□	1.0000	run56	9/1.14/50%
◇	1.0000	run57	9/2.15/50%

Figure 7.2.3.441: Re Effects (CR=9, 50%Cowl) Baseplate Pressures



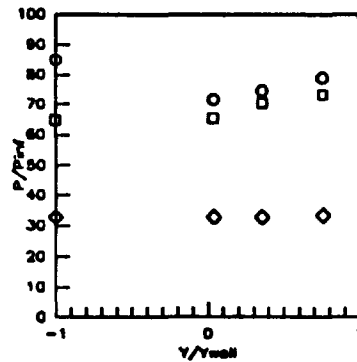
Sym	x'/Ts'	Run No.	CR/Re/Cowl (millions)
○	1.0726	run55	9/0.55/50%
□	1.0726	run56	9/1.14/50%
◇	1.0726	run57	9/2.15/50%

Figure 7.2.3.442: Re Effects (CR=9, 50%Cowl) Baseplate Pressures



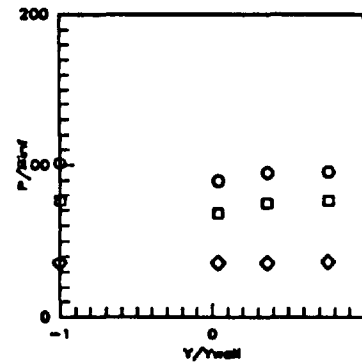
Sym	$x'/T_x'$	Run No.	CR/Re/Cowl (millions)
○	1.1887	run55	9/0.55/50%
□	1.1887	run56	9/1.14/50%
◇	1.1887	run57	9/2.15/50%

Figure 7.2.3.443: Re Effects (CR=9, 50%Cowl) Baseplate Pressures



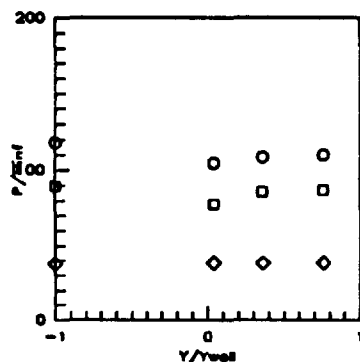
Sym	$x'/T_x'$	Run No.	CR/Re/Cowl (millions)
○	1.2408	run58	9/0.55/50%
□	1.2408	run59	9/1.14/50%
◇	1.2408	run67	9/2.15/50%

Figure 7.2.3.444: Re Effects (CR=9, 50%Cowl) Baseplate Pressures



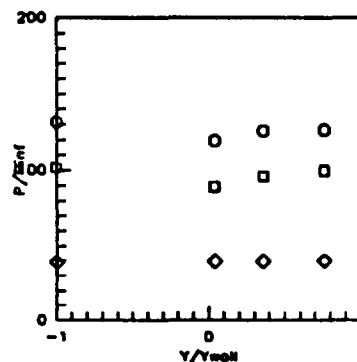
Sym	$x'/T_x'$	Run No.	CR/Re/Cowl (millions)
○	1.3249	run56	9/0.55/50%
□	1.3249	run58	9/1.14/50%
◇	1.3249	run67	9/2.15/50%

Figure 7.2.3.445: Re Effects (CR=9, 50%Cowl) Baseplate Pressures



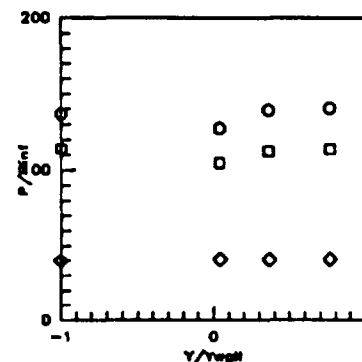
Sym	$x'/T_x'$	Run No.	CR/Re/Cowl (millions)
○	1.4090	run55	9/0.55/50%
□	1.4090	run56	9/1.14/50%
◇	1.4090	run57	9/2.15/50%

Figure 7.2.3.446: Re Effects (CR=9, 50%Cowl) Baseplate Pressures



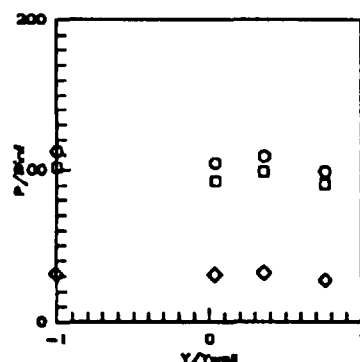
Sym	$x'/T_x'$	Run No.	CR/Re/Cowl (millions)
○	1.4832	run55	9/0.55/50%
□	1.4832	run56	9/1.14/50%
◇	1.4832	run57	9/2.15/50%

Figure 7.2.3.447: Re Effects (CR=9, 50%Cowl) Baseplate Pressures



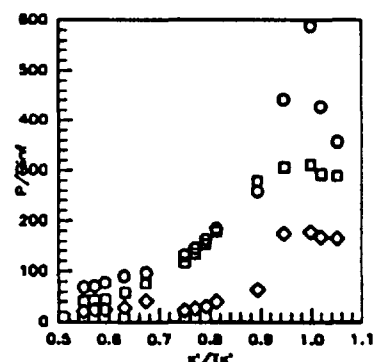
Sym	$x'/T_x'$	Run No.	CR/Re/Cowl (millions)
○	1.5773	run55	9/0.55/50%
□	1.5773	run56	9/1.14/50%
◇	1.5773	run57	9/2.15/50%

Figure 7.2.3.448: Re Effects (CR=9, 50%Cowl) Baseplate Pressures



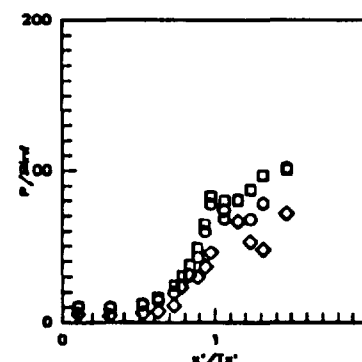
Sym	$x'/T_x'$	Run No.	CR/Re/Cowl (millions)
○	1.6824	run55	9/0.55/50%
□	1.6824	run56	9/1.14/50%
◇	1.6824	run57	9/2.15/50%

Figure 7.2.3.449: Re Effects (CR=9, 50%Cowl) Baseplate Pressures



Sym	Cowl Pos.	Run No.	CR/Re/Cowl (millions)
○	50%	run58	9/0.55/50%
□	50%	run59	9/1.14/50%
◇	50%	run67	9/2.15/50%

Figure 7.2.3.450: Re Effects (CR=9, 50%Cowl) Cowl Pressures



Sym	Z/H	Run No.	CR/Re/Cowl (millions)
○	0.5RT	run56	9/0.55/50%
□	0.5RT	run58	9/1.14/50%
◇	0.5RT	run57	9/2.15/50%

Figure 7.2.3.451: Re Effects (CR=9, 50%Cowl) Sidewall Centerline Pressures

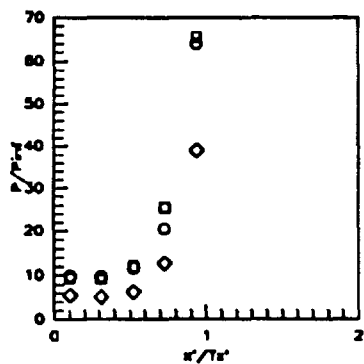


Figure 7.2.3.452: Re Effects (CR=9, 50% Cowi) Sidewall Centerline Pressures

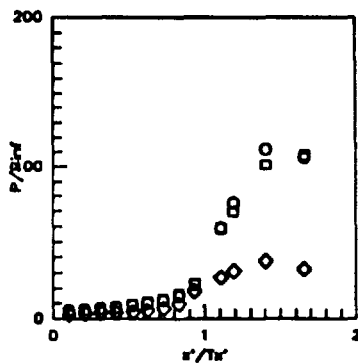


Figure 7.2.3.453: Re Effects (CR=9, 50% Cowi) Sidewall Pressures

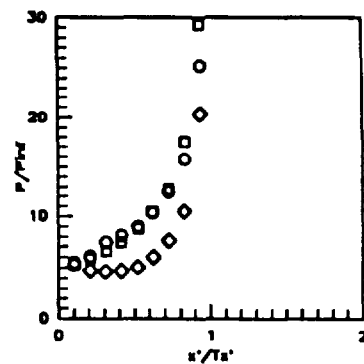


Figure 7.2.3.454: Re Effects (CR=9, 50% Cowi) Sidewall Pressures

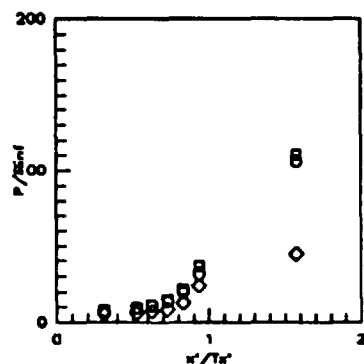


Figure 7.2.3.455: Re Effects (CR=9, 50% Cowi) Sidewall Pressures

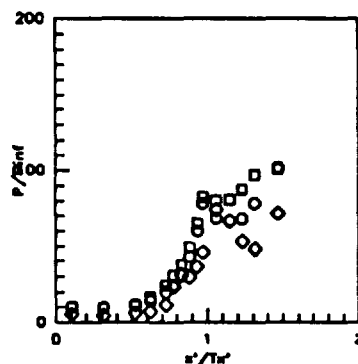


Figure 7.2.3.456: Re Effects (CR=9, 50% Cowi) Sidewall Pressures

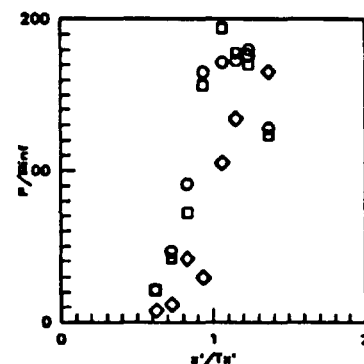


Figure 7.2.3.457: Re Effects (CR=9, 50% Cowi) Sidewall Pressures

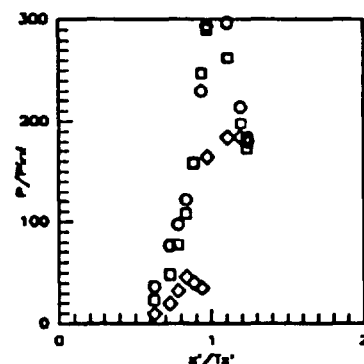


Figure 7.2.3.458: Re Effects (CR=9, 50% Cowi) Sidewall Pressures

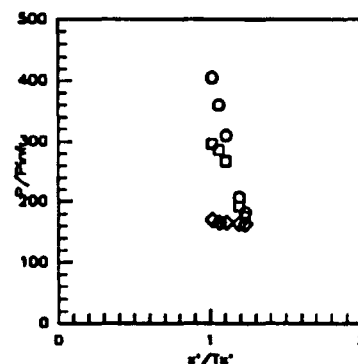


Figure 7.2.3.459: Re Effects (CR=9, 50% Cowi) Sidewall Pressures

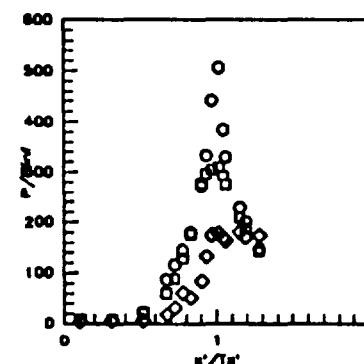
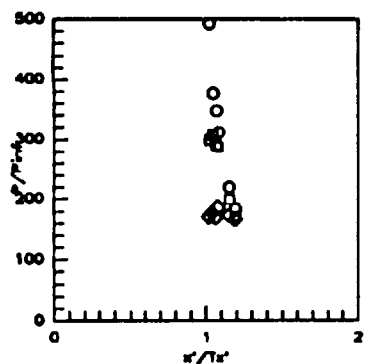


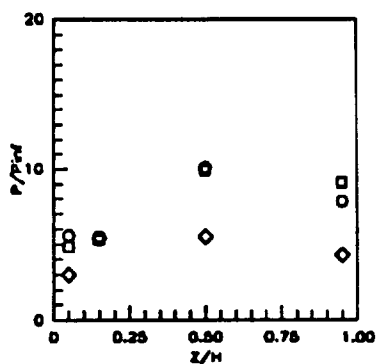
Figure 7.2.3.460: Re Effects (CR=9, 50% Cowi) Sidewall Pressures



Sym	Z/H	Run No.	CR/Re/Coal (milions)
-----	-----	---------	----------------------

○ 0.975 run55 9/0.55/50%  
 ○ 0.975 run56 9/1.14/50%  
 ○ 0.975 run57 9/2.15/50%

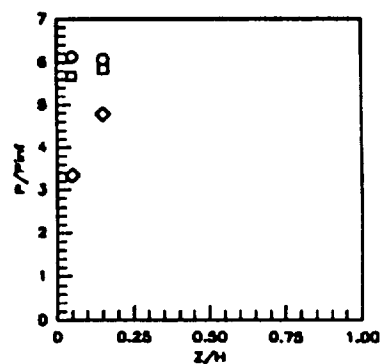
Figure 7.2.3.461: Re Effects (CR=9, 50%Coal) Sidewall Pressures



Sym	$x'/T_s'$	Run No.	CR/Re/Coal (milions)
-----	-----------	---------	----------------------

○ 0.1042 run55 9/0.55/50%  
 ○ 0.1042 run56 9/1.14/50%  
 ○ 0.1042 run57 9/2.15/50%

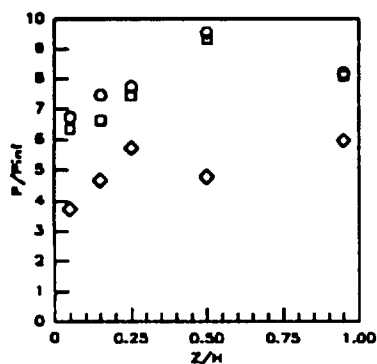
Figure 7.2.3.462: Re Effects (CR=9, 50%Coal) Sidewall Pressures



Sym	$x'/T_s'$	Run No.	CR/Re/Coal (milions)
-----	-----------	---------	----------------------

○ 0.2083 run55 9/0.55/50%  
 ○ 0.2083 run56 9/1.14/50%  
 ○ 0.2083 run57 9/2.15/50%

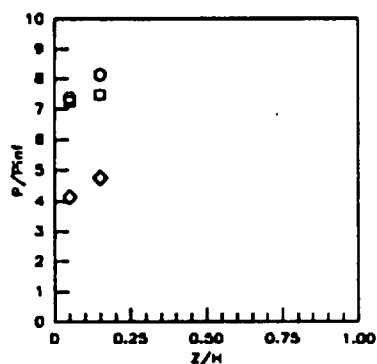
Figure 7.2.3.463: Re Effects (CR=9, 50%Coal) Sidewall Pressures



Sym	$x'/T_s'$	Run No.	CR/Re/Coal (milions)
-----	-----------	---------	----------------------

○ 0.3125 run55 9/0.55/50%  
 ○ 0.3125 run56 9/1.14/50%  
 ○ 0.3125 run57 9/2.15/50%

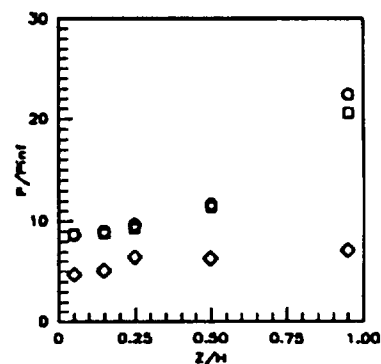
Figure 7.2.3.464: Re Effects (CR=9, 50%Coal) Sidewall Pressures



Sym	$x'/T_s'$	Run No.	CR/Re/Coal (milions)
-----	-----------	---------	----------------------

○ 0.4167 run55 9/0.55/50%  
 ○ 0.4167 run56 9/1.14/50%  
 ○ 0.4167 run57 9/2.15/50%

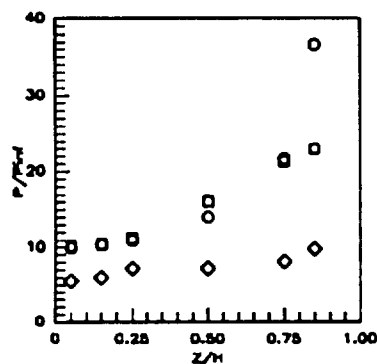
Figure 7.2.3.465: Re Effects (CR=9, 50%Coal) Sidewall Pressures



Sym	$x'/T_s'$	Run No.	CR/Re/Coal (milions)
-----	-----------	---------	----------------------

○ 0.5259 run55 9/0.55/50%  
 ○ 0.5259 run56 9/1.14/50%  
 ○ 0.5259 run57 9/2.15/50%

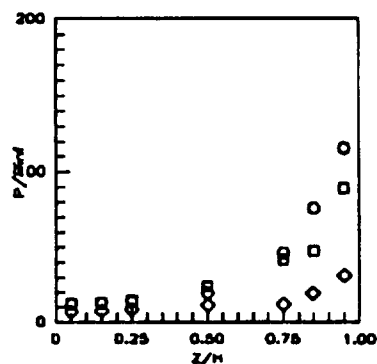
Figure 7.2.3.466: Re Effects (CR=9, 50%Coal) Sidewall Pressures



Sym	$x'/T_s'$	Run No.	CR/Re/Coal (milions)
-----	-----------	---------	----------------------

○ 0.6252 run55 9/0.55/50%  
 ○ 0.6252 run56 9/1.14/50%  
 ○ 0.6252 run57 9/2.15/50%

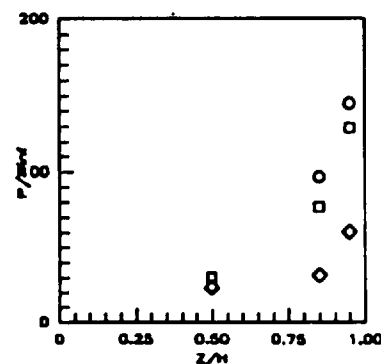
Figure 7.2.3.467: Re Effects (CR=9, 50%Coal) Sidewall Pressures



Sym	$x'/T_s'$	Run No.	CR/Re/Coal (milions)
-----	-----------	---------	----------------------

○ 0.7294 run55 9/0.55/50%  
 ○ 0.7294 run56 9/1.14/50%  
 ○ 0.7294 run57 9/2.15/50%

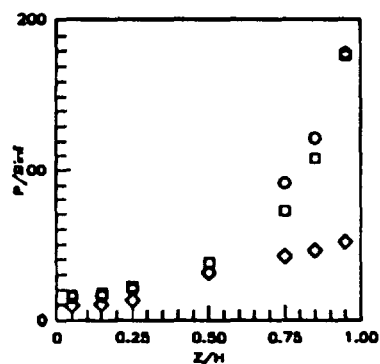
Figure 7.2.3.468: Re Effects (CR=9, 50%Coal) Sidewall Pressures



Sym	$x'/T_s'$	Run No.	CR/Re/Coal (milions)
-----	-----------	---------	----------------------

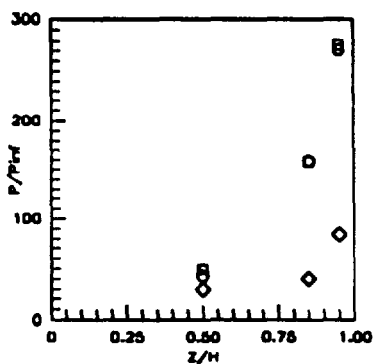
○ 0.7815 run55 9/0.55/50%  
 ○ 0.7815 run56 9/1.14/50%  
 ○ 0.7815 run57 9/2.15/50%

Figure 7.2.3.469: Re Effects (CR=9, 50%Coal) Sidewall Pressures



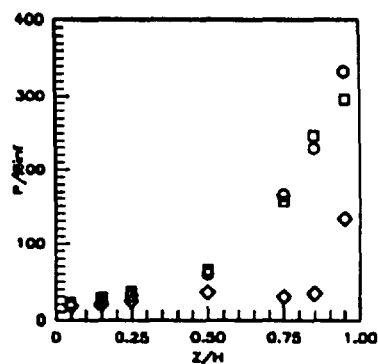
Sym	$x'/T_s'$	Run No.	CR/Re/Cowl (milions)
○	0.8336	run55	9/0.55/50%
□	0.8336	run56	9/1.14/50%
◇	0.8336	run57	9/2.15/50%

Figure 7.2.3.470: Re Effects  
(CR=9, 50%Cowl)  
Sidewall Pressures



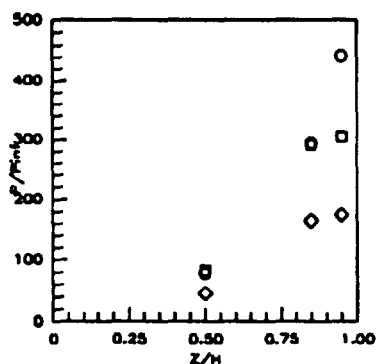
Sym	$x'/T_s'$	Run No.	CR/Re/Cowl (milions)
○	0.8857	run55	9/0.55/50%
□	0.8857	run56	9/1.14/50%
◇	0.8857	run57	9/2.15/50%

Figure 7.2.3.471: Re Effects  
(CR=9, 50%Cowl)  
Sidewall Pressures



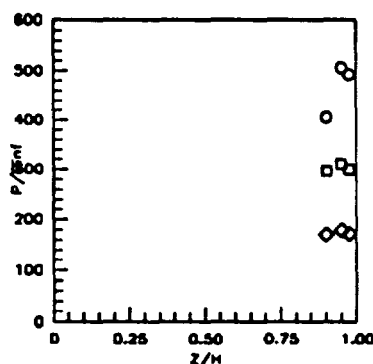
Sym	$x'/T_s'$	Run No.	CR/Re/Cowl (milions)
○	0.9378	run55	9/0.55/50%
□	0.9378	run56	9/1.14/50%
◇	0.9378	run57	9/2.15/50%

Figure 7.2.3.472: Re Effects  
(CR=9, 50%Cowl)  
Sidewall Pressures



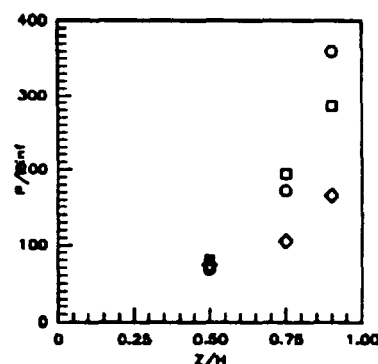
Sym	$x'/T_s'$	Run No.	CR/Re/Cowl (milions)
○	0.9751	run55	9/0.55/50%
□	0.9751	run56	9/1.14/50%
◇	0.9751	run57	9/2.15/50%

Figure 7.2.3.473: Re Effects  
(CR=9, 50%Cowl)  
Sidewall Pressures



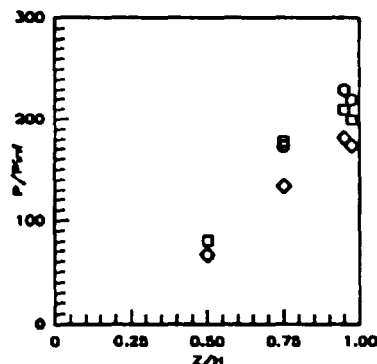
Sym	$x'/T_s'$	Run No.	CR/Re/Cowl (milions)
○	1.0197	run55	9/0.55/50%
□	1.0197	run56	9/1.14/50%
◇	1.0197	run57	9/2.15/50%

Figure 7.2.3.474: Re Effects  
(CR=9, 50%Cowl)  
Sidewall Pressures



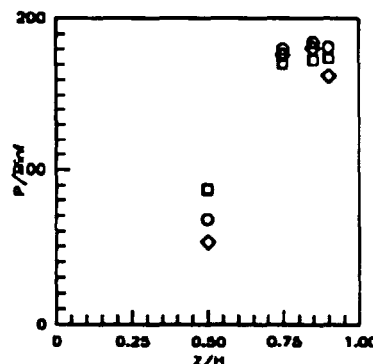
Sym	$x'/T_s'$	Run No.	CR/Re/Cowl (milions)
○	1.0643	run55	9/0.55/50%
□	1.0643	run56	9/1.14/50%
◇	1.0643	run57	9/2.15/50%

Figure 7.2.3.475: Re Effects  
(CR=9, 50%Cowl)  
Sidewall Pressures



Sym	$x'/T_s'$	Run No.	CR/Re/Cowl (milions)
○	1.1537	run55	9/0.55/50%
□	1.1537	run56	9/1.14/50%
◇	1.1537	run57	9/2.15/50%

Figure 7.2.3.476: Re Effects  
(CR=9, 50%Cowl)  
Sidewall Pressures

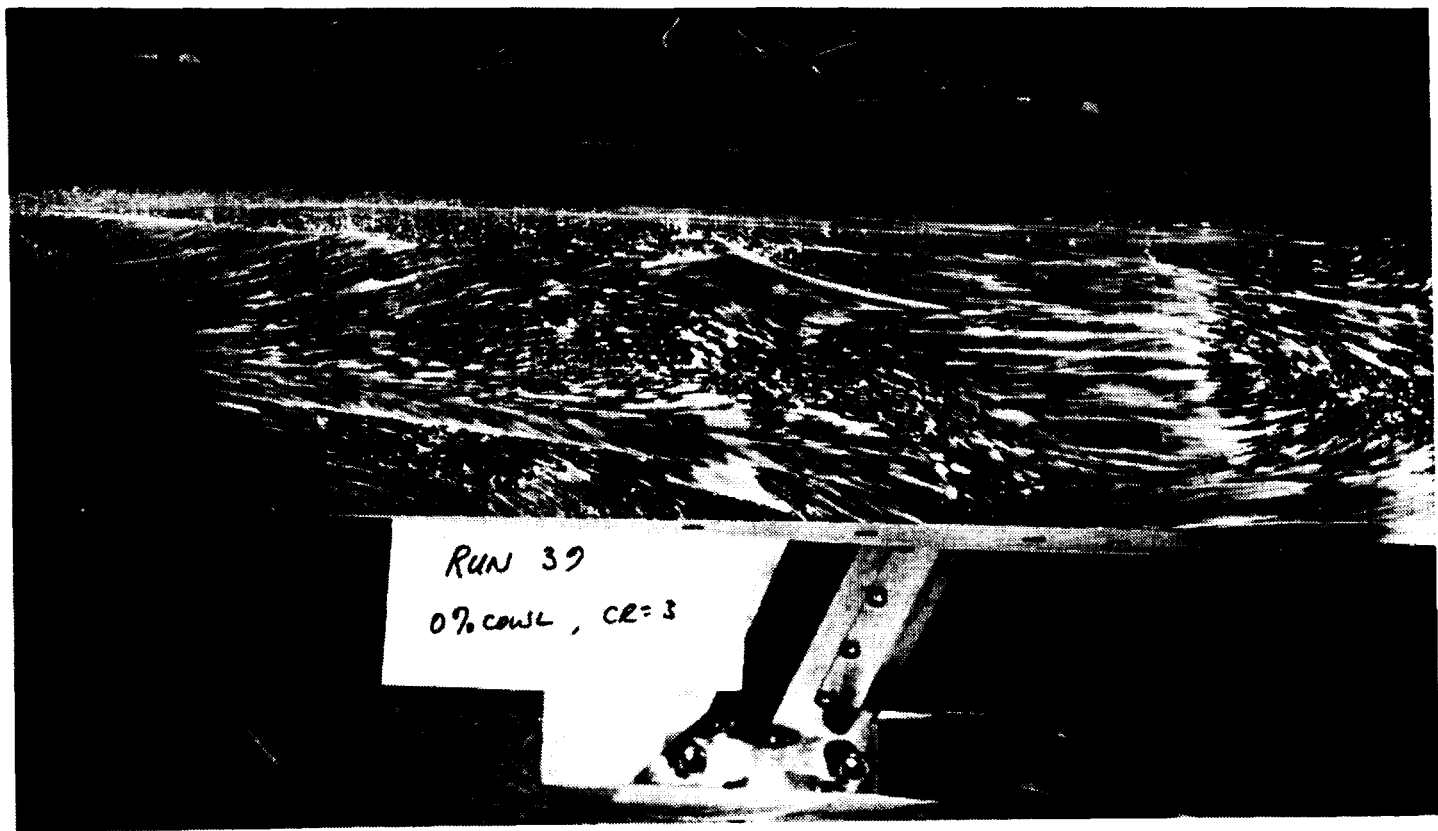


Sym	$x'/T_s'$	Run No.	CR/Re/Cowl (milions)
○	1.2356	run55	9/0.55/50%
□	1.2356	run56	9/1.14/50%
◇	1.2356	run57	9/2.15/50%

Figure 7.2.3.477: Re Effects  
(CR=9, 50%Cowl)  
Sidewall Pressures



TOP PAGE  
FROM THE PHOTOGRAPH



RUN 39  
0% cowl, CR=3

Figure 7.3.1: Oil Flow on Inlet Sidewall for  $CR = 3$ ,  $Re = 2.15$  million/ft, 0% Cowl



Figure 7.3.2: Oil Flow on Inlet Sidewall for  $CR = 5$ ,  $Re = 2.15$  million/ft, 0% Cowl

ORIGINAL PAGE  
BLACK AND WHITE PHOTOGRAPH



Figure 7.3.3: Oil Flow on Baseplate for  $CR = 9$ ,  $Re = 2.15$  million/ft,  
0% Cowl Showing Forward Extent of Separation

ORIGINAL PAGE  
BLACK AND WHITE PHOTOGRAPH

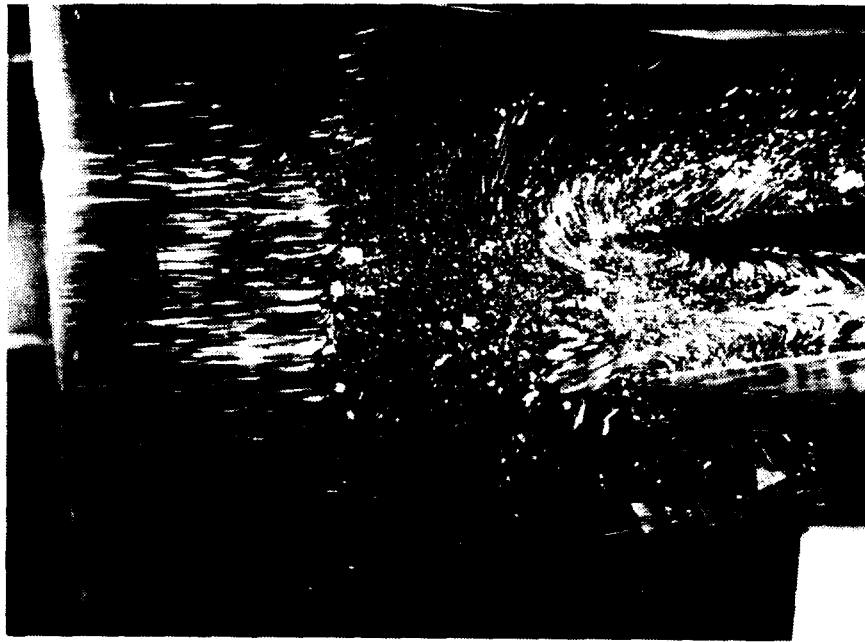


Figure 7.3.4: Oil Flow on Baseplate for  $CR = 9$ ,  $Re = 2.15$  million/ft, 0% Cowl  
Showing Oil Streaks Exiting Front of Inlet and Spilling around Sidewalls

ORIGINAL PAGE  
BLACK AND WHITE PHOTOGRAPH

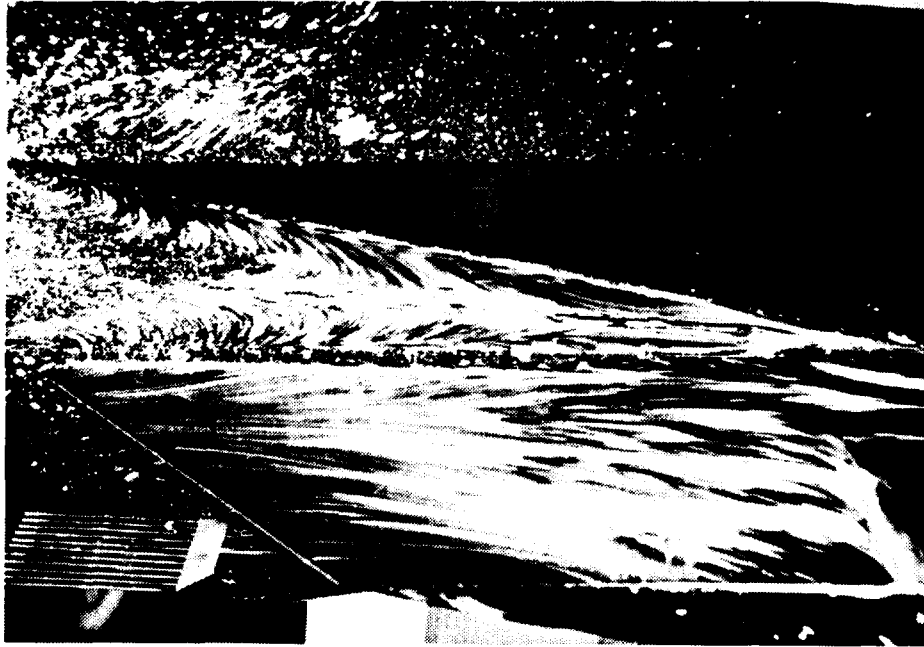


Figure 7.3.5: Close up of Oil Flow on Baseplate and Sidewall for  $CR = 9$ ,  
 $Re = 2.15$  million/ft, 0% Cowl

ORIGINAL PAGE  
BLACK AND WHITE PHOTOGRAPH



Figure 7.3.6: Close up of Oil Flow on Baseplate for  $CR = 9$ ,  $Re = 2.15$  million/ft, 0% Cowl Showing Oil Streaks Exiting Front of Inlet and Spilling around Sidewalls

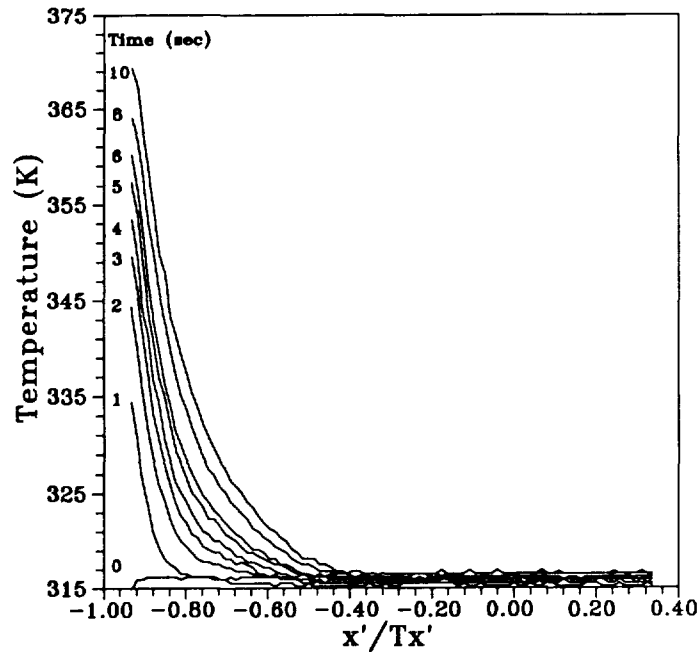


Figure 7.4.1: Surface Temperature Distribution  
Down Inlet Baseplate Centerline  
CR=3, Re=2.15 million/ft, 0% Cowl

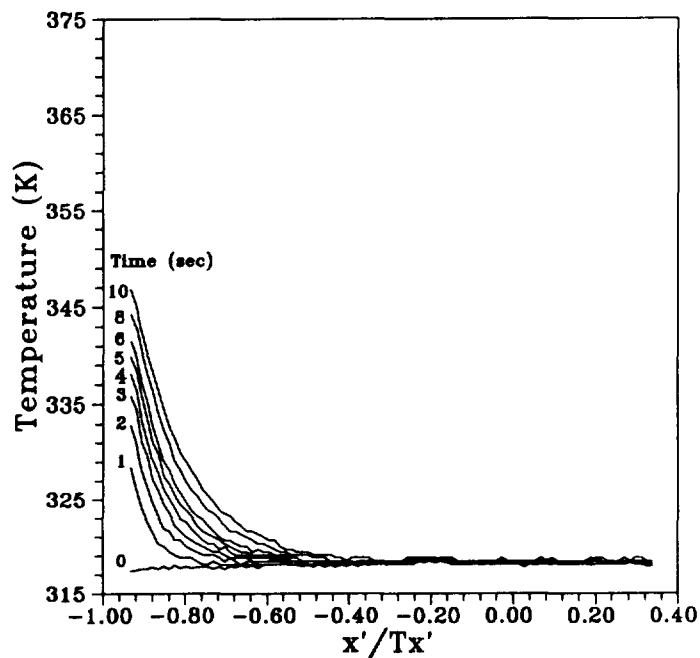


Figure 7.4.2: Surface Temperature Distribution  
Down Inlet Baseplate Centerline  
CR=3, Re=0.55 million/ft, 0% Cowl

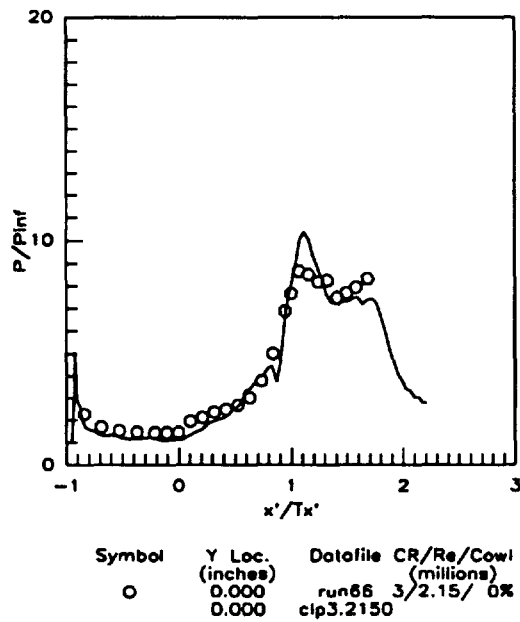


Figure 8.1(a): Comparison of CFD and Exp.  
(CR=3, Re=2.15 million/ft, 0% Cowl)  
CR=3 Centerline Pressures

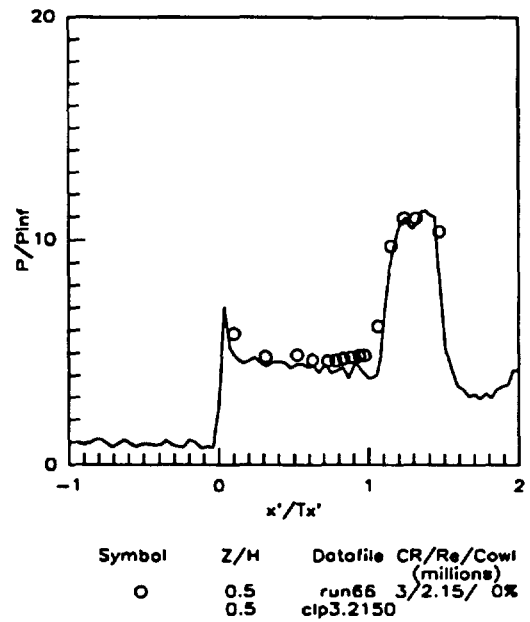


Figure 8.1(b): Comparison of CFD and Exp.  
(CR=3, Re=2.15 million/ft, 0% Cowl)  
Sidewall Centerline Pressures

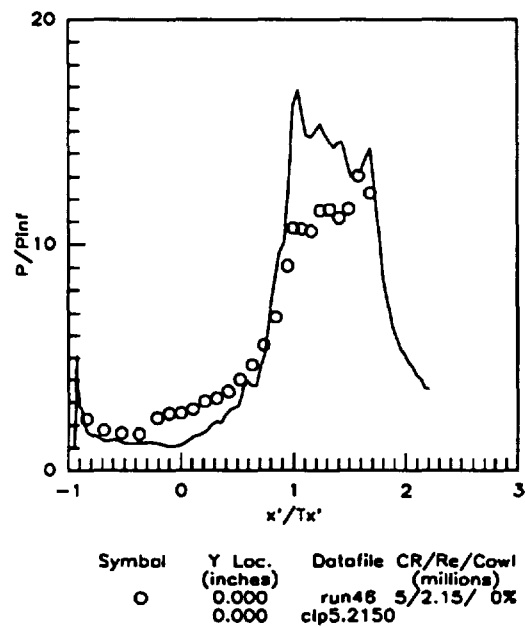


Figure 8.2(a): Comparison of CFD and Exp.  
(CR=5, Re=2.15 million/ft, 0% Cowl)  
CR=5 Centerline Pressures

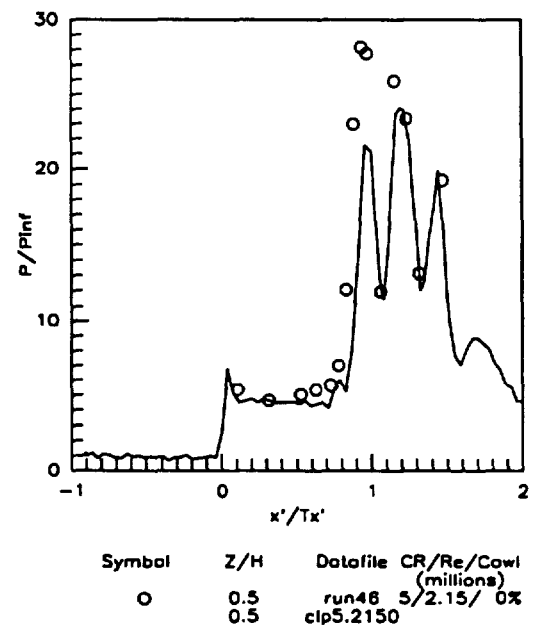
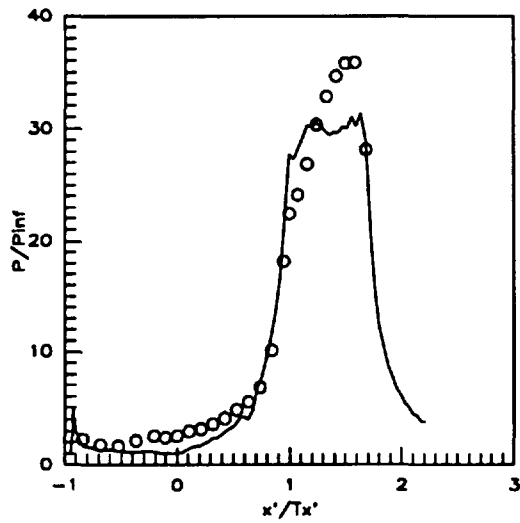


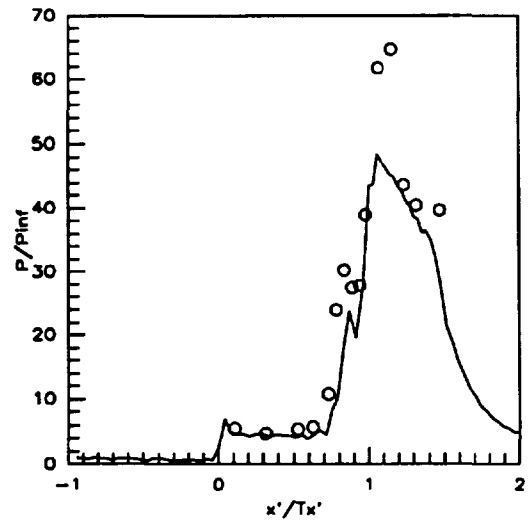
Figure 8.2(b): Comparison of CFD and Exp.  
(CR=5, Re=2.15 million/ft, 0% Cowl)  
Sidewall Centerline Pressures





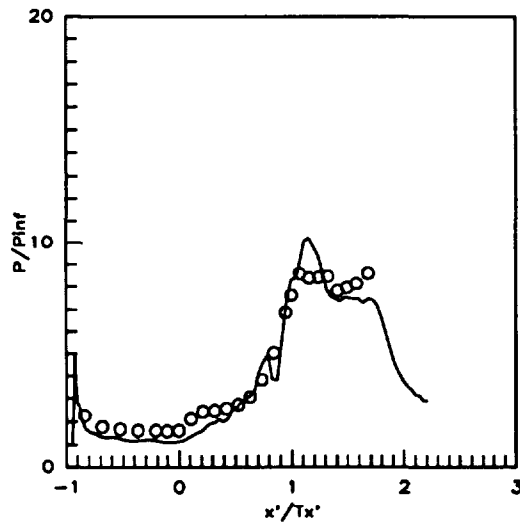
Symbol	Y Loc. (inches)	Datfile	CR/Re/Cowl (millions)
O	0.000	run49	9/2.15/ 0%
	0.000	clp9.2150	

Figure 8.3(a): Comparison of CFD and Exp.  
(CR=9, Re=2.15 million/ft, 0% Cowl)  
CR=9 Centerline Pressures



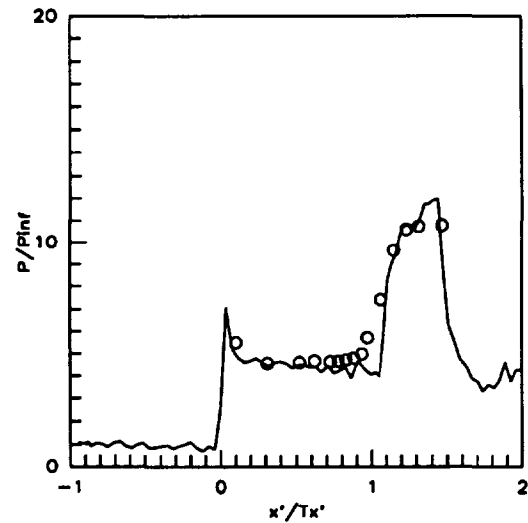
Symbol	Z/H	Datfile	CR/Re/Cowl (millions)
O	0.5	run49	9/2.15/ 0%
	0.5	clp9.2150	

Figure 8.3(b): Comparison of CFD and Exp.  
(CR=9, Re=2.15 million/ft, 0% Cowl)  
Sidewall Centerline Pressures



Symbol	Y Loc. (inches)	Datfile	CR/Re/Cowl (millions)
O	0.000	run60	3/2.15/50%
	0.000	clp3.2155	

Figure 8.4(a): Comparison of CFD and Exp.  
(CR=3, Re=2.15 million/ft, 50% Cowl)  
CR=3 Centerline Pressures



Symbol	Z/H	Datfile	CR/Re/Cowl (millions)
O	0.5	run60	3/2.15/50%
	0.5	clp3.2155	

Figure 8.4(b): Comparison of CFD and Exp.  
(CR=3, Re=2.15 million/ft, 50% Cowl)  
Sidewall Centerline Pressures

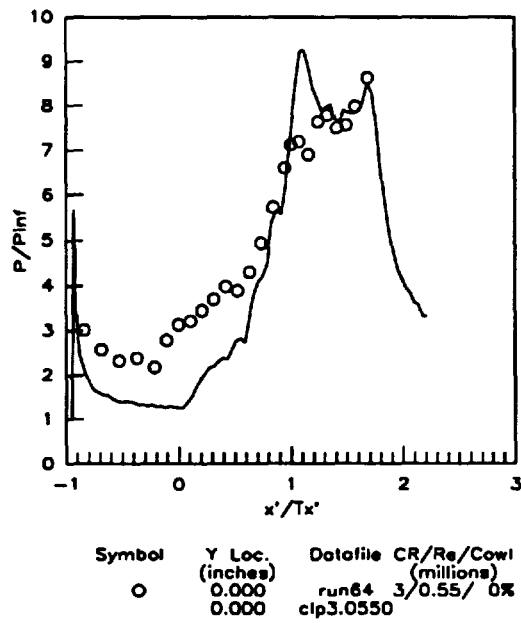


Figure 8.5(a): Comparison of CFD and Exp.  
(CR=3, Re=0.55 million/ft, 0% Cowl)  
CR=3 Centerline Pressures

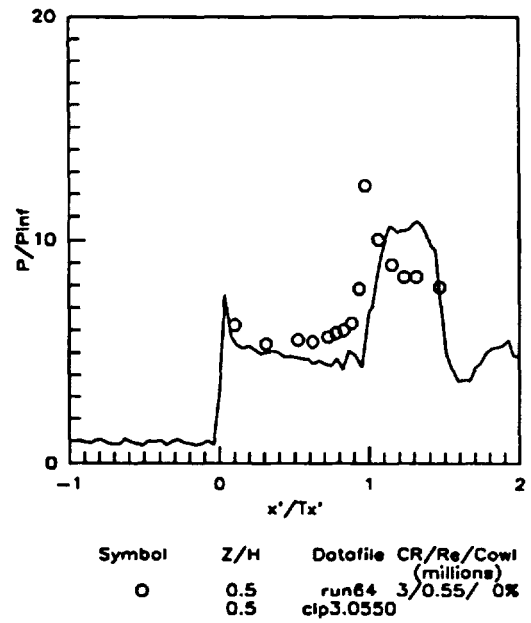


Figure 8.5(b): Comparison of CFD and Exp.  
(CR=3, Re=0.55 million/ft, 0% Cowl)  
Sidewall Centerline Pressures

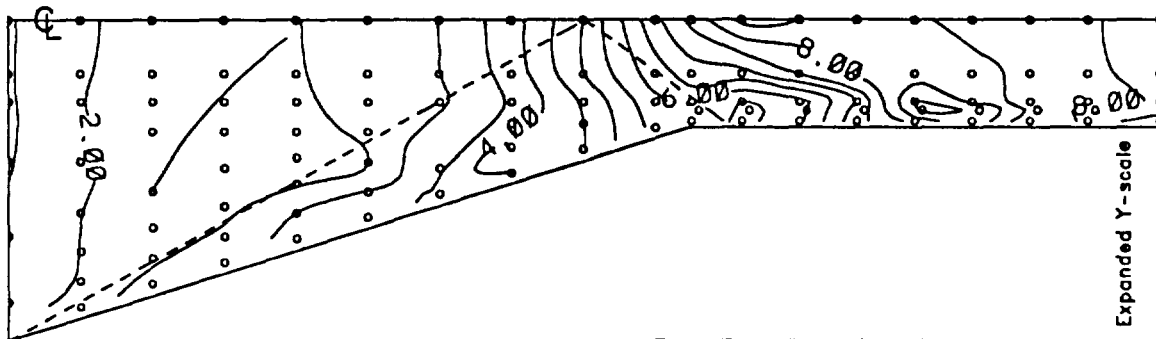


Figure 8.1.1(a): P/P<sub>inf</sub> Measured Baseplate Contours,  
CR=3, Re=2.15 million/ft, 0% Cowl, (RUN66)

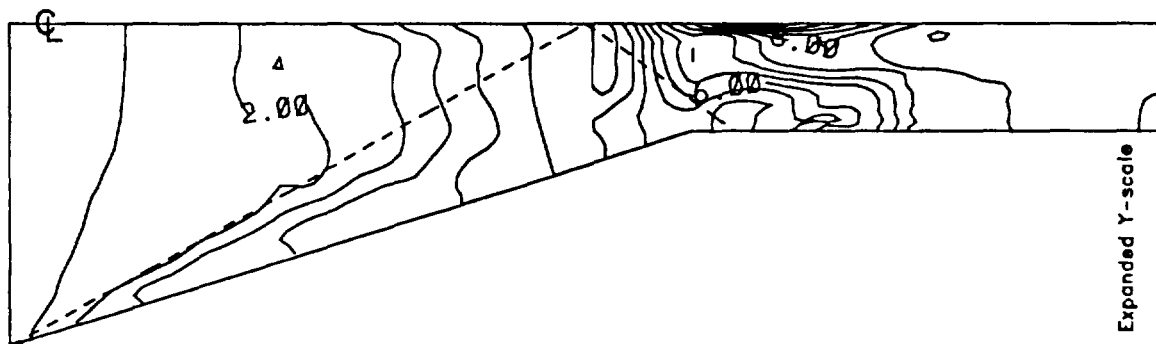


Figure 8.1.1(b): P/P<sub>inf</sub> Computed Baseplate Contours,  
CR=3, Re=2.15 million/ft, 0% Cowl

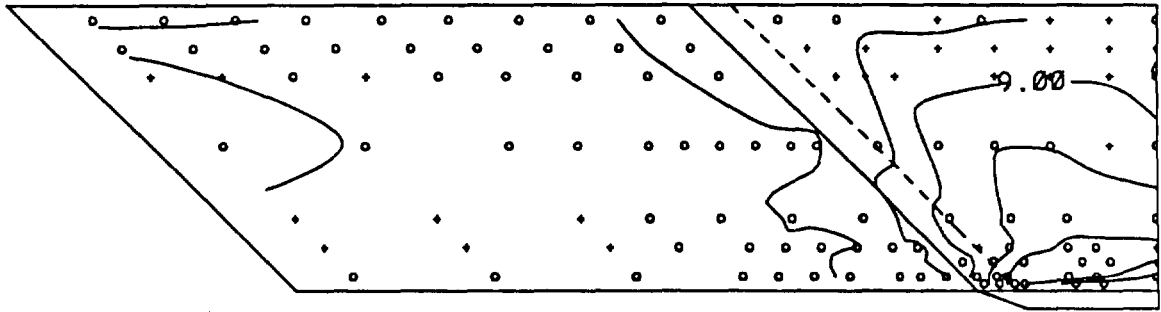


Figure 8.1.2(a): P/P<sub>inf</sub> Measured Sidewall Contours,  
CR=3, Re=2.15 million/ft, 0% Cowl, (RUN66)

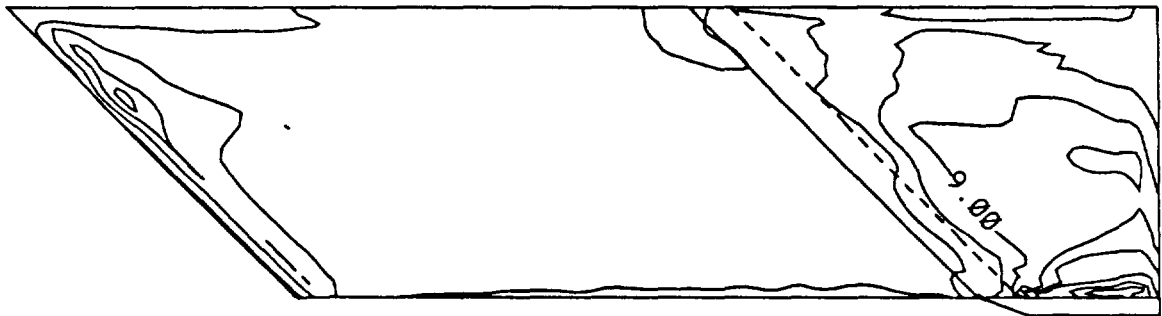


Figure 8.1.2(b): P/P<sub>inf</sub> Computed Sidewall Contours,  
CR=3, Re=2.15 million/ft, 0% Cowl

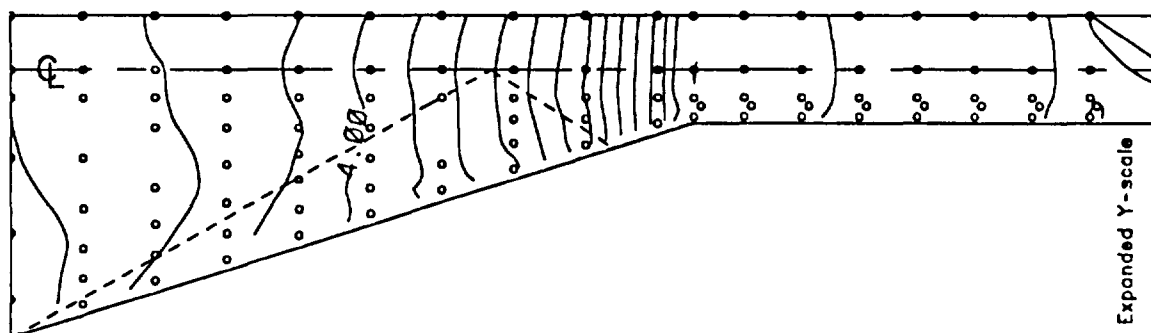


Figure 8.1.3(a): P/P<sub>inf</sub> Measured Baseplate Contours,  
CR=5, Re=2.15 million/ft, 0% Cowl, (RUN46)

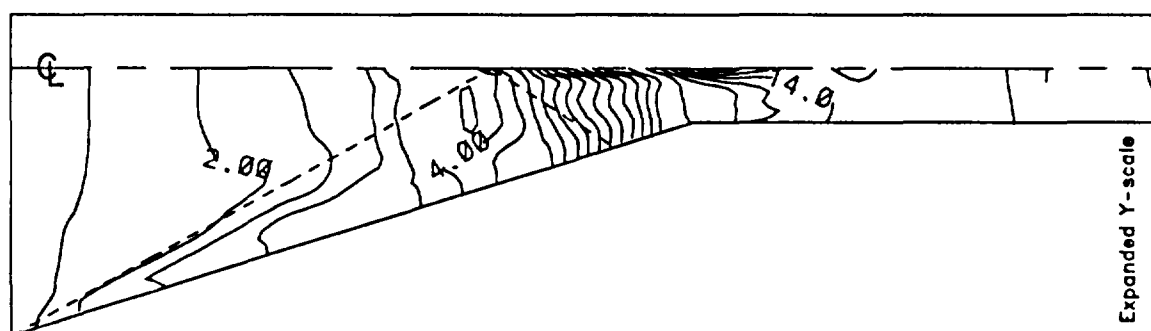


Figure 8.1.3(b): P/P<sub>inf</sub> Computed Baseplate Contours,  
CR=5, Re=2.15 million/ft, 0% Cowl

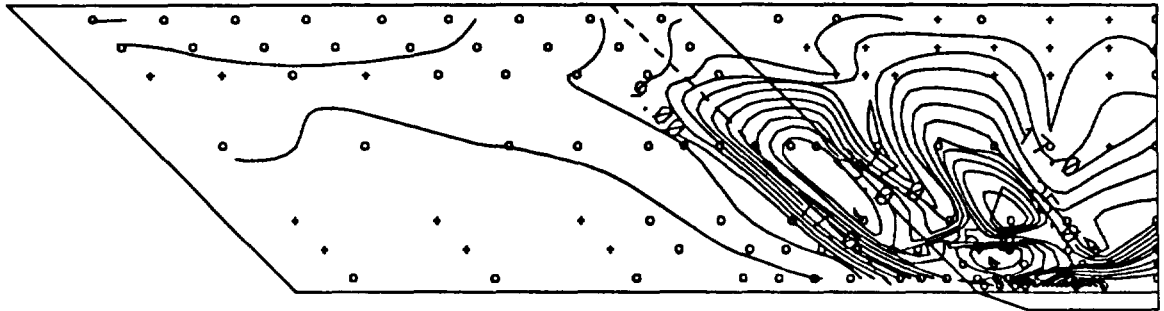


Figure 8.1.4(a): P/P<sub>inf</sub> Measured Sidewall Contours,  
CR=5, Re=2.15 million/ft, 0% Cowl, (RUN46)

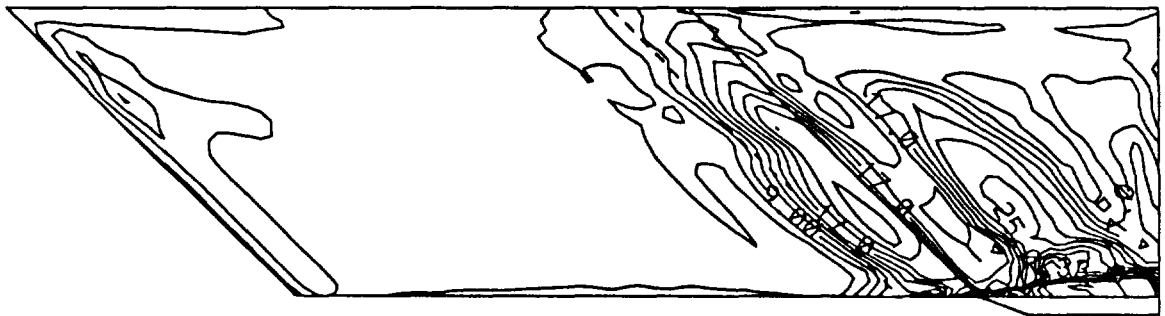


Figure 8.1.4(b): P/P<sub>inf</sub> Computed Sidewall Contours,  
CR=5, Re=2.15 million/ft, 0% Cowl

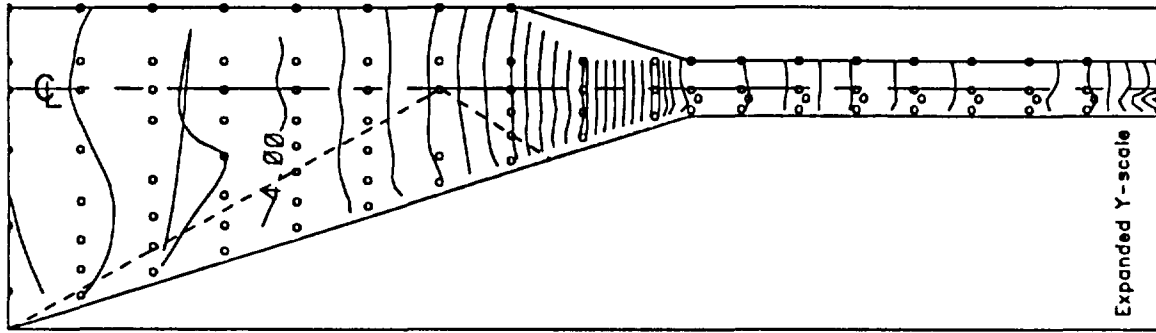


Figure 8.1.5(a): P/P<sub>inf</sub> Measured Baseplate Contours,  
CR=9, Re=2.15 million/ft, 0% Cowl, (RUN49)

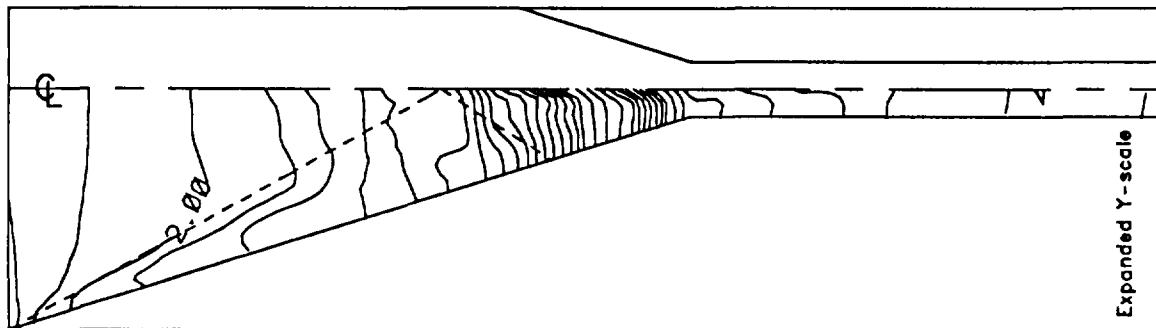


Figure 8.1.5(b): P/P<sub>inf</sub> Computed Baseplate Contours,  
CR=9, Re=2.15 million/ft, 0% Cowl

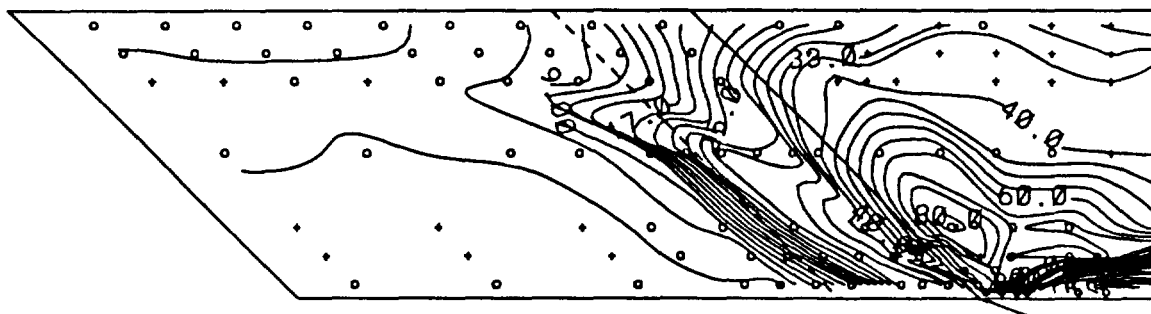


Figure 8.1.6(a): P/P<sub>inf</sub> Measured Sidewall Contours,  
CR=9, Re=2.15 million/ft, 0% Cowl, (RUN49)



Figure 8.1.6(b): P/P<sub>inf</sub> Computed Sidewall Contours,  
CR=9, Re=2.15 million/ft, 0% Cowl



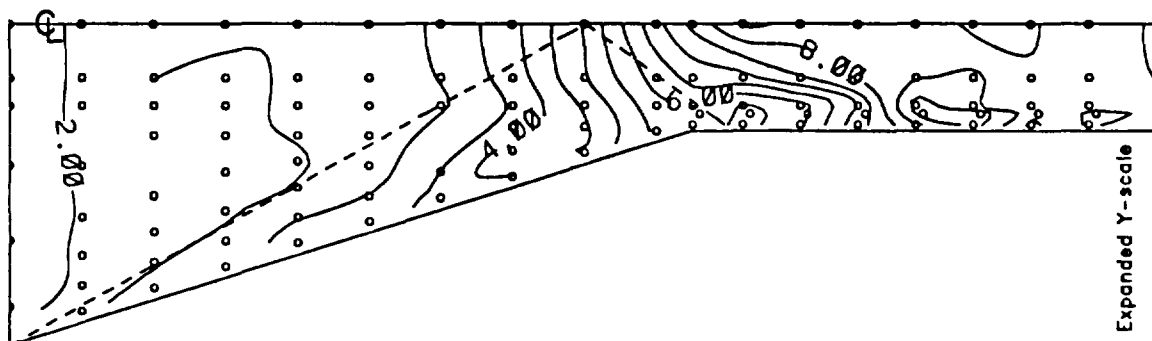


Figure 8.1.7(a): P/P<sub>inf</sub> Measured Baseplate Contours,  
CR=3, Re=2.15 million/ft, 50% Cowl, (RUN60)

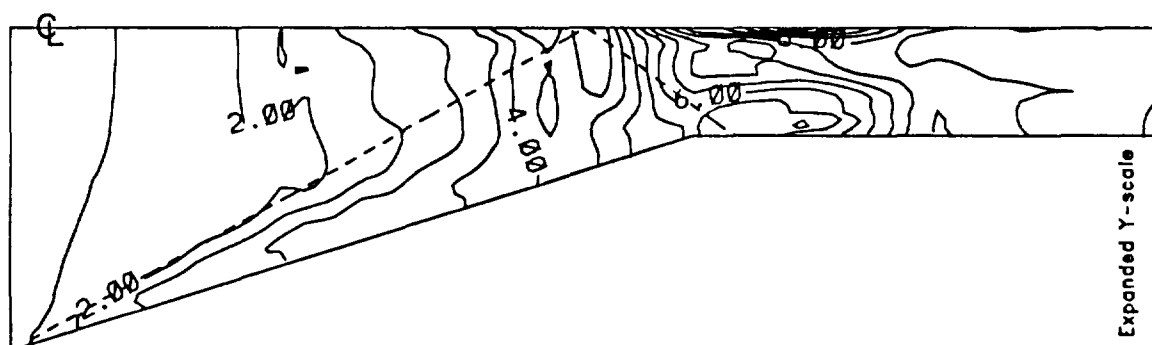


Figure 8.1.7(b): P/P<sub>inf</sub> Computed Baseplate Contours,  
CR=3, Re=2.15 million/ft, 50% Cowl

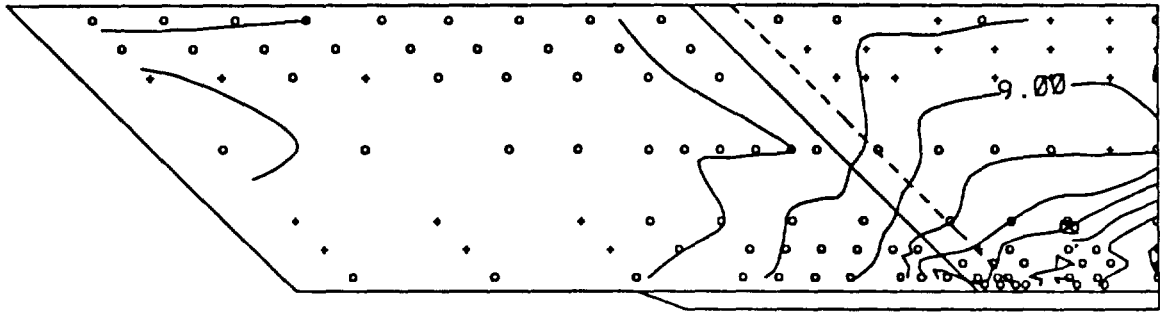


Figure 8.1.8(a): P/P<sub>inf</sub> Measured Sidewall Contours,  
CR=3, Re=2.15 million/ft, 50% Cowl, (RUN60)

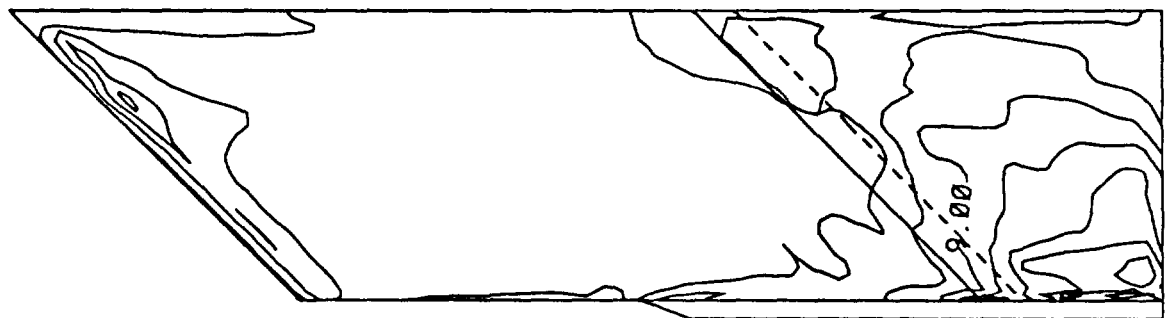


Figure 8.1.8(b): P/P<sub>inf</sub> Computed Sidewall Contours,  
CR=3, Re=2.15 million/ft, 50% Cowl

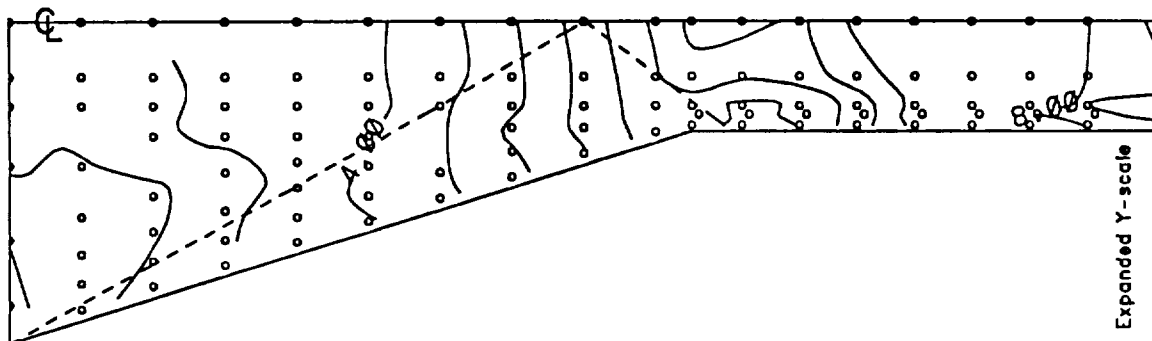


Figure 8.1.9(a): P/P<sub>inf</sub> Measured Baseplate Contours,  
CR=3, Re=0.55 million/ft, 0% Cowl, (RUN64)

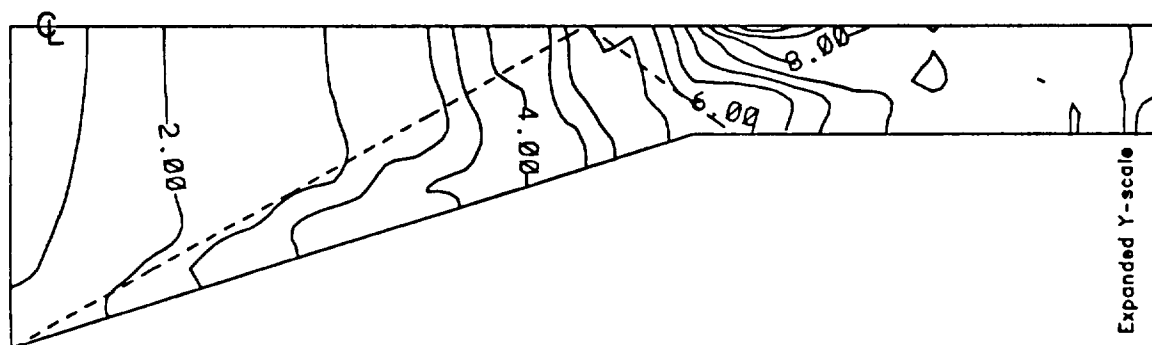


Figure 8.1.9(b): P/P<sub>inf</sub> Computed Baseplate Contours,  
CR=3, Re=0.55 million/ft, 0% Cowl

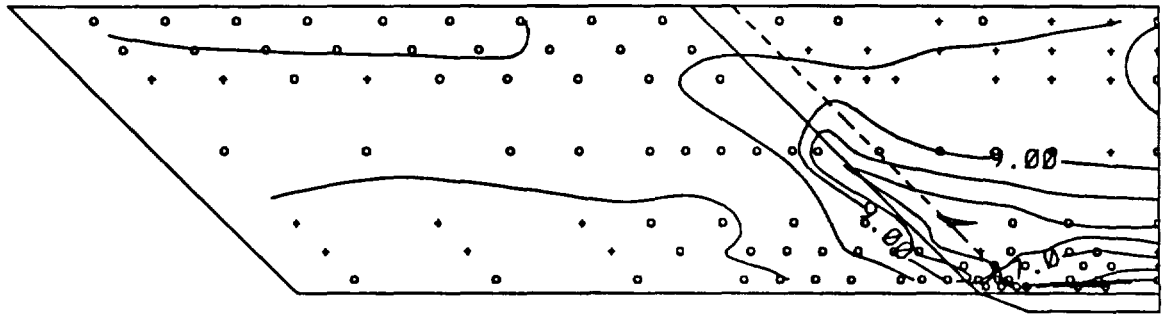


Figure 8.1.10(a): P/P<sub>inf</sub> Measured Sidewall Contours,  
CR=3, Re=0.55 million/ft, 0% Cowl, (RUN64)

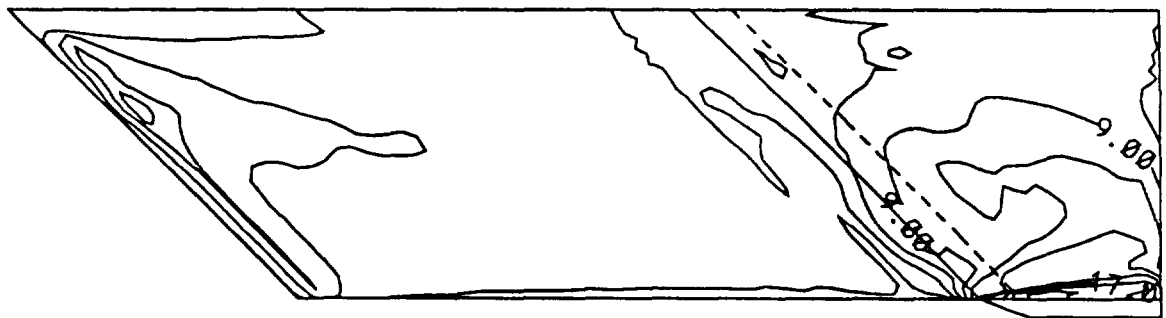
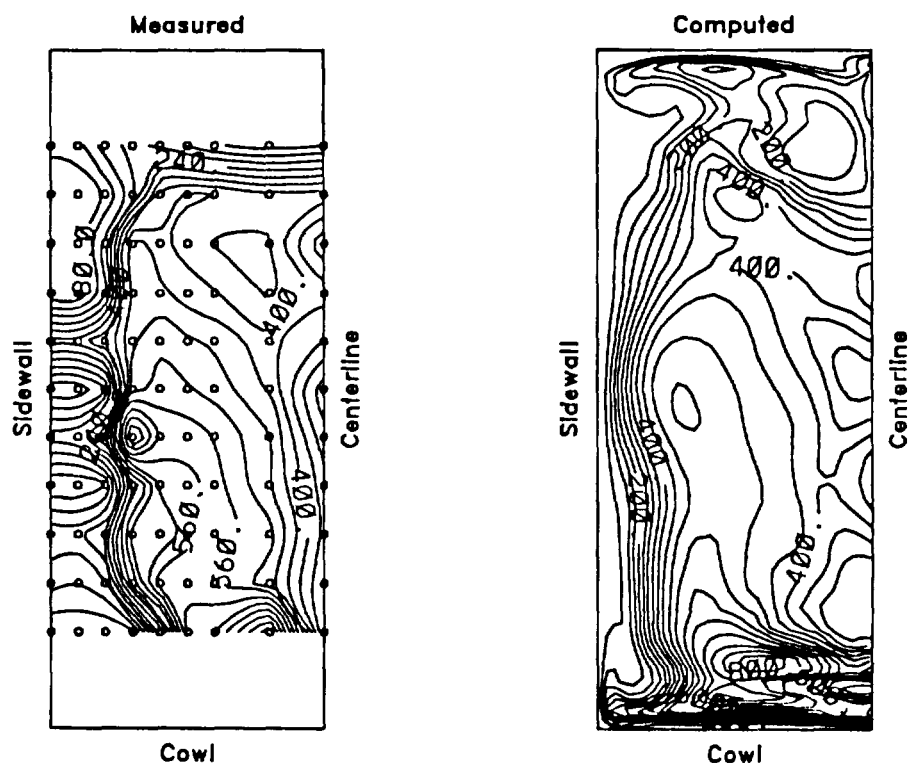


Figure 8.1.10(b): P/P<sub>inf</sub> Computed Sidewall Contours,  
CR=3, Re=0.55 million/ft, 0% Cowl



**Figure 8.2.1: Comparison of Measured and Computed  
PITOT/Pinf Exit Plane Contours,  
CR=3, Re=2.15 million/ft, 0% Cowl, (RUN73)**

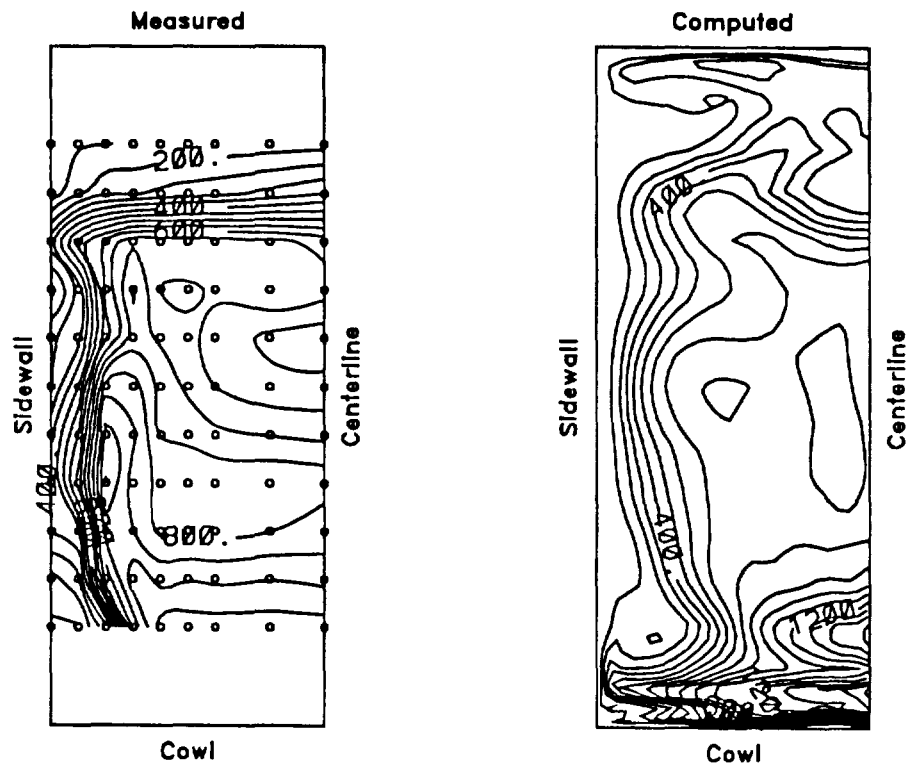


Figure 8.2.2: Comparison of Measured and Computed  
PITOT/Pinf Exit Plane Contours,  
CR=5, Re=2.15 million/ft, 0% Cowl, (RUN91)

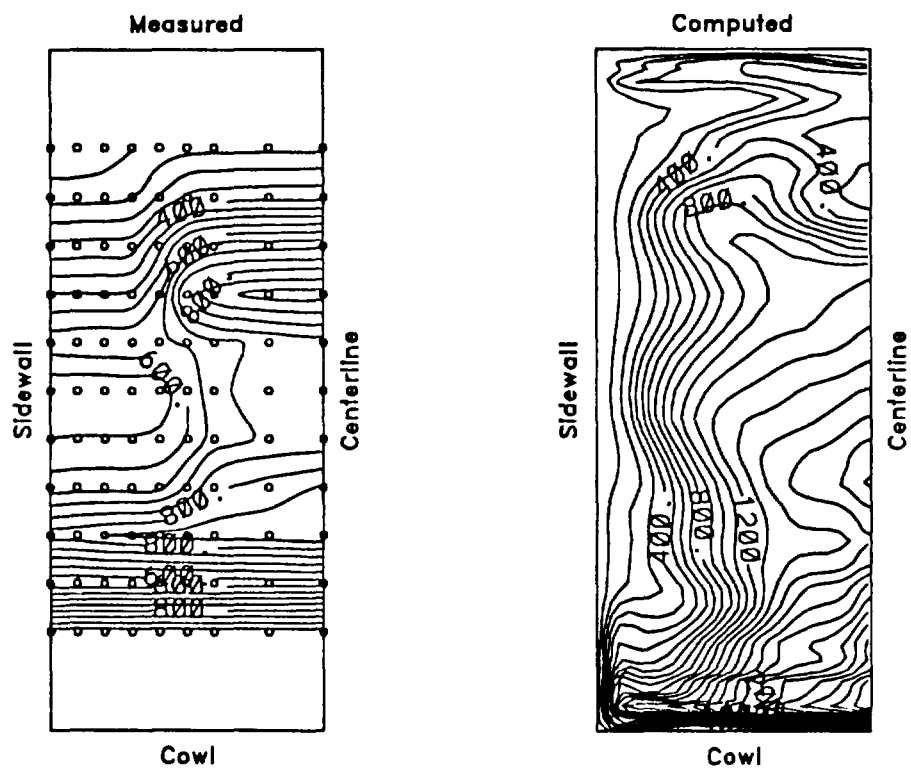


Figure 8.2.3: Comparison of Measured and Computed  
PITOT/Plnt Exit Plane Contours,  
CR=9, Re=2.15 million/ft, 0% Cowl, (RUN94)

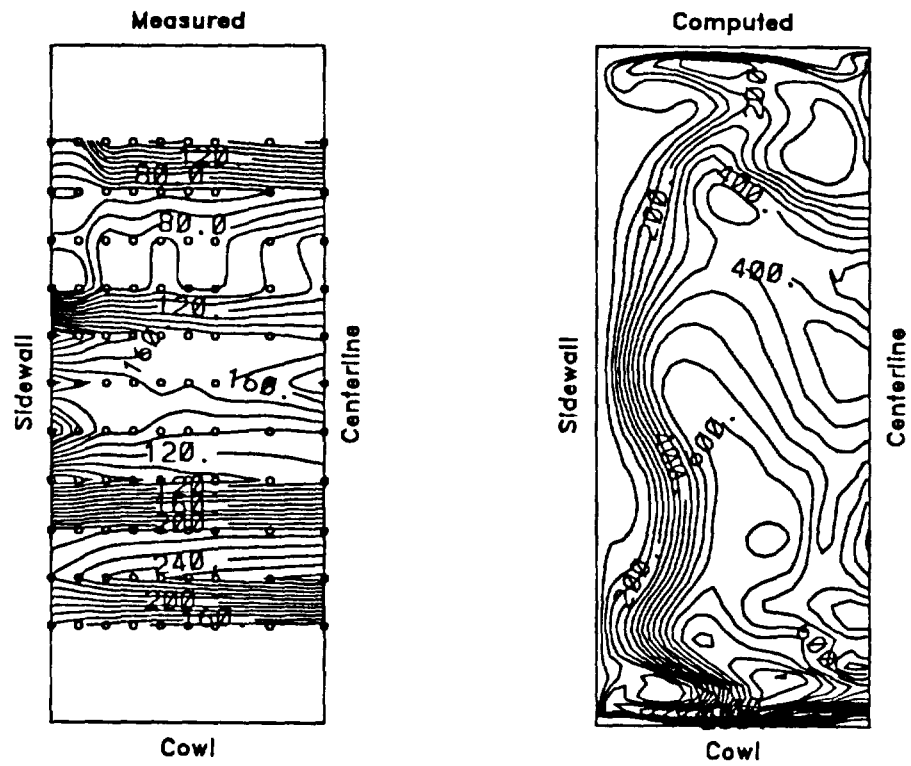


Figure 8.2.4: Comparison of Measured and Computed  
PITOT/Pinf Exit Plane Contours,  
CR=3, Re=2.15 million/ft, 50% Cowl, (RUN81)



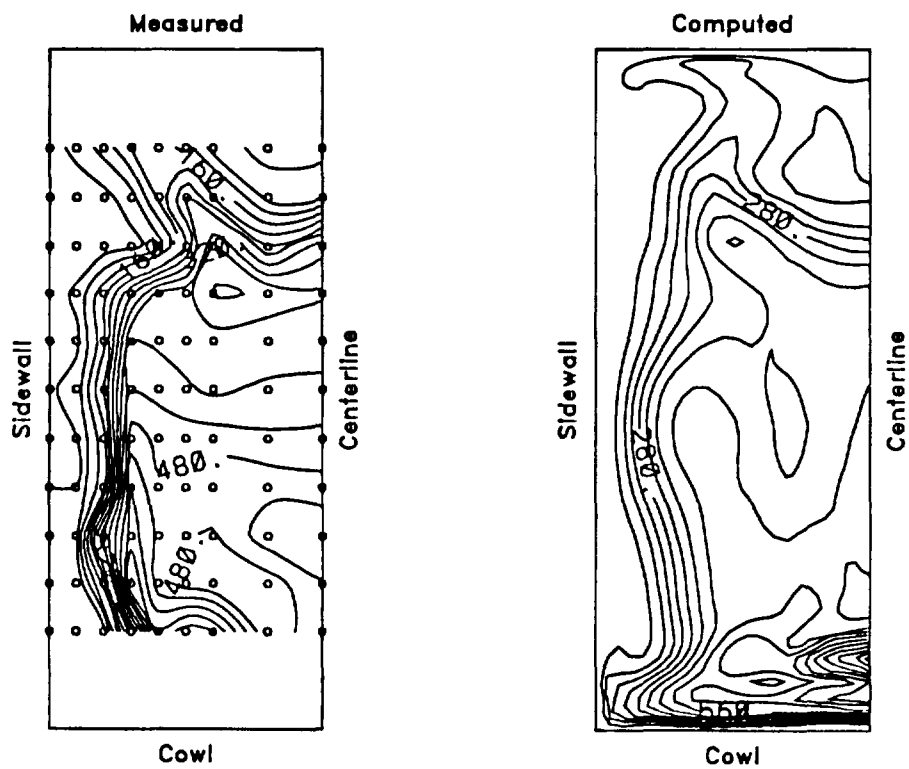


Figure 8.2.5: Comparison of Measured and Computed  
PITOT/Plnf Exit Plane Contours,  
CR=3, Re=0.55 million/ft, 0% Cowl, (RUN71)

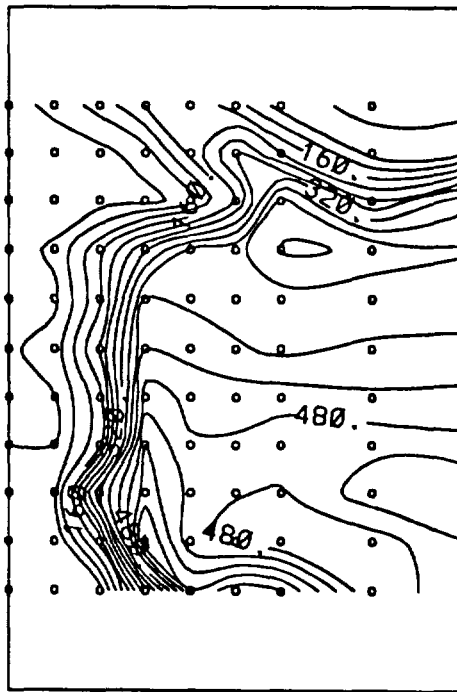


Figure 8.2.6: PITOT/Pinf Exit plane Contours,  
CR=3, Re=0.55 million/ft, 0% Cowl, (RUN71)

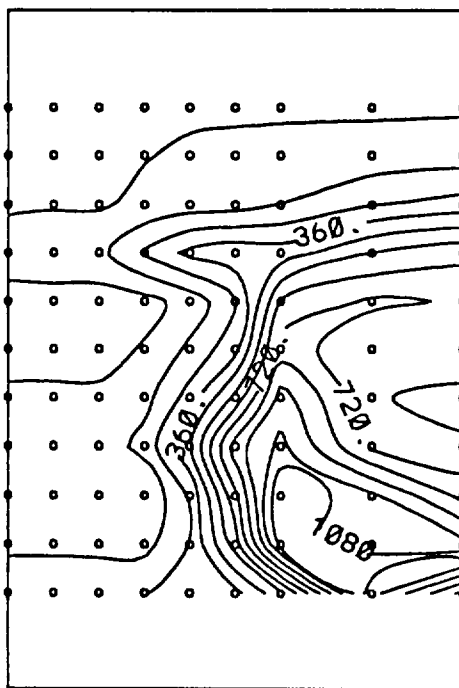


Figure 8.2.7: PITOT/Pinf Exit plane Contours,  
CR=5, Re=0.55 million/ft, 0% Cowl, (RUN89)

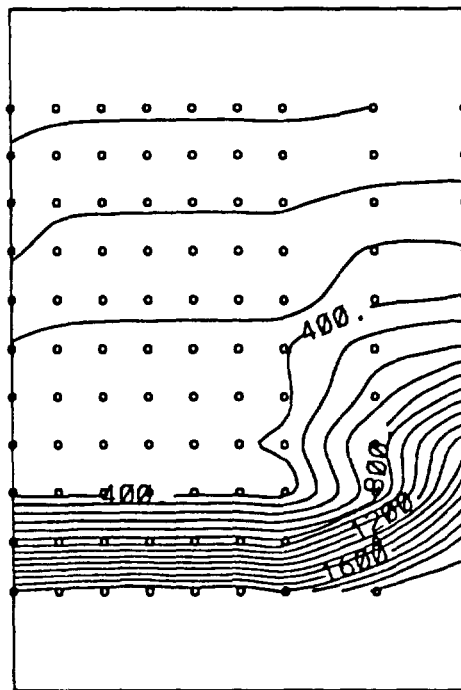


Figure 8.2.8: PITOT/Plnf Exit plane Contours,  
CR=9, Re=0.55 million/ft, 0% Cowl, (RUN92)

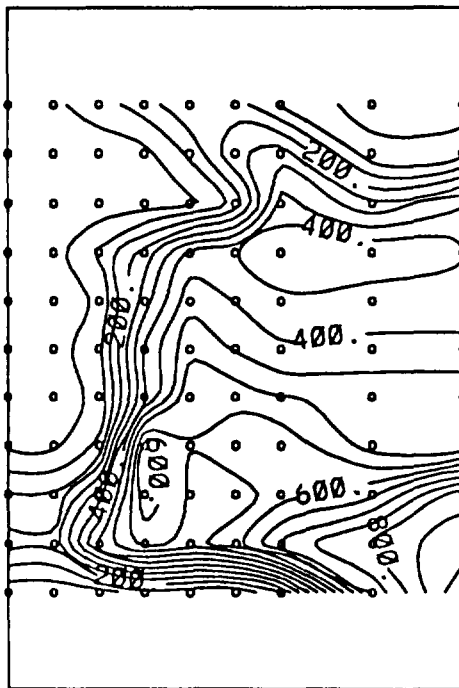


Figure 8.2.9: PITOT/Pinf Exit plane Contours,  
CR=3, Re=0.55 million/ft, 25% Cowl, (RUN76)

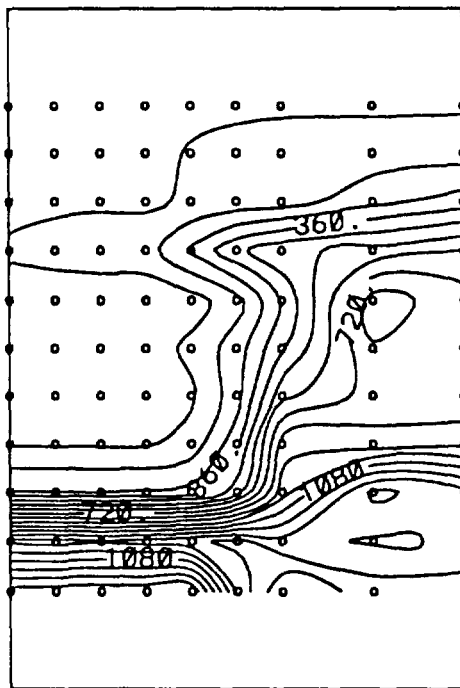


Figure 8.2.10: PITOT/Pinf Exit plane Contours,  
CR=5, Re=0.55 million/ft, 25% Cowl, (RUN86)

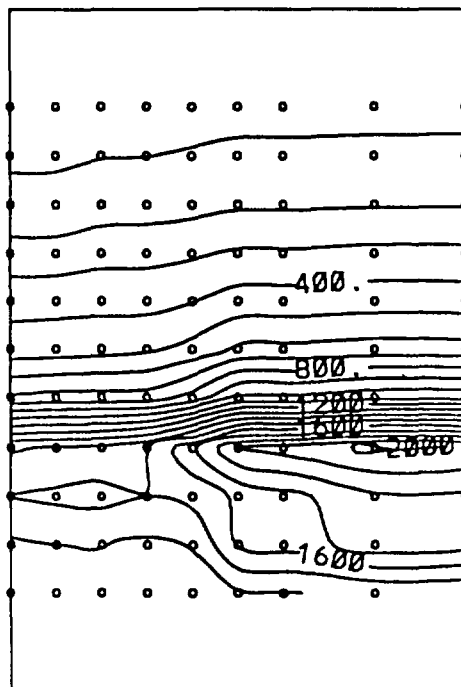


Figure 8.2.11: PITOT/Plnf Exit plane Contours,  
CR=9, Re=0.55 million/ft, 25% Cowl, (RUN95)

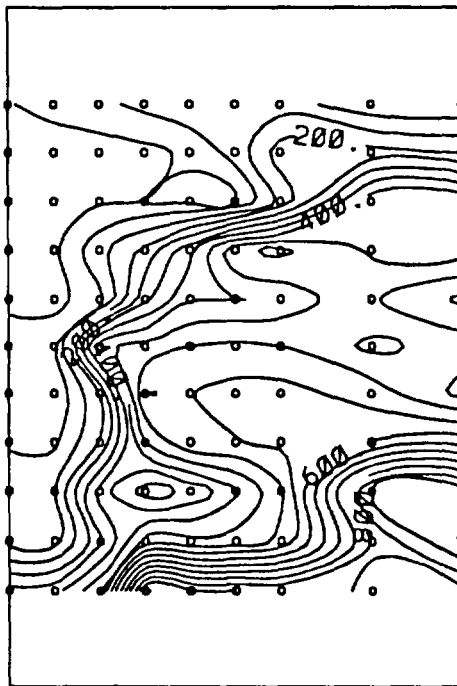


Figure 8.2.12: PITOT/Pinf Exit plane Contours,  
CR=3, Re=0.55 million/ft, 50% Cowl, (RUN78)



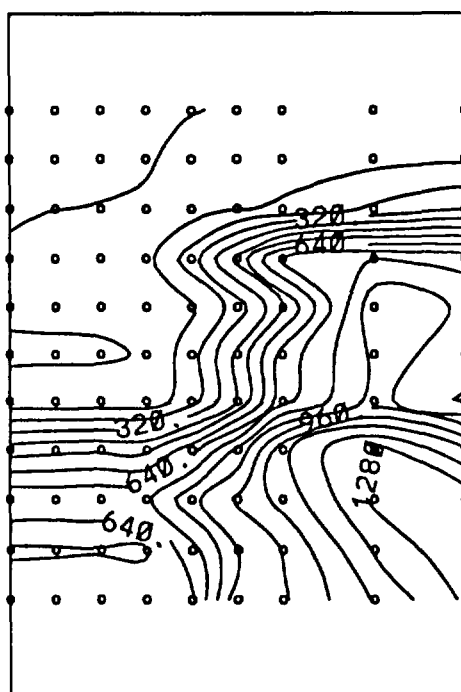


Figure 8.2.13: PITOT/Pinf Exit plane Contours,  
CR=5, Re=0.55 million/ft, 50% Cowl, (RUN83)

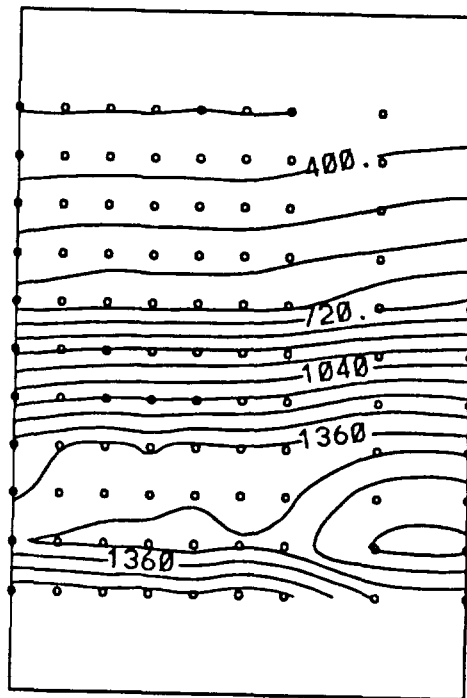


Figure 8.2.14: PITOT/Plnf Exit plane Contours,  
CR=9, Re=0.55 million/ft, 50% Cowl, (RUN97)

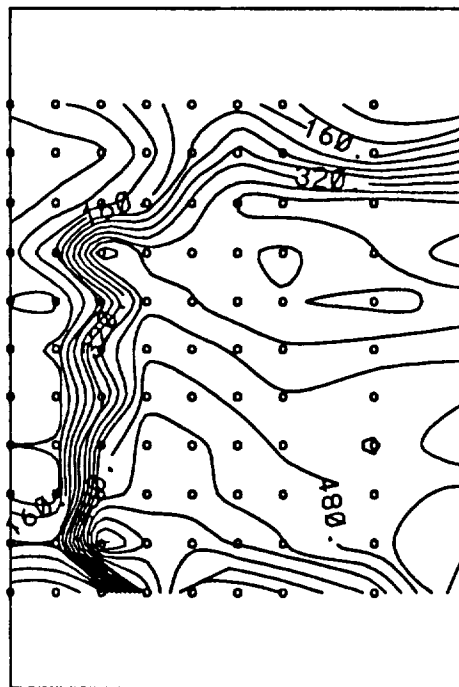
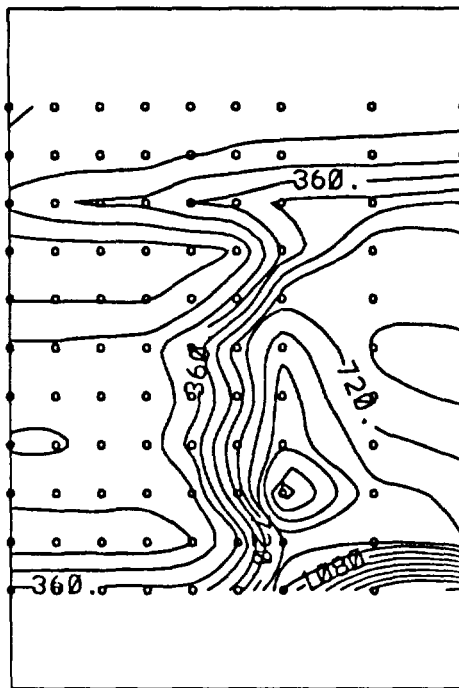


Figure 8.2.15: PITOT/Plnf Exit plane Contours,  
CR=3, Re=1.14 million/ft, 0% Cowl, (RUN72)



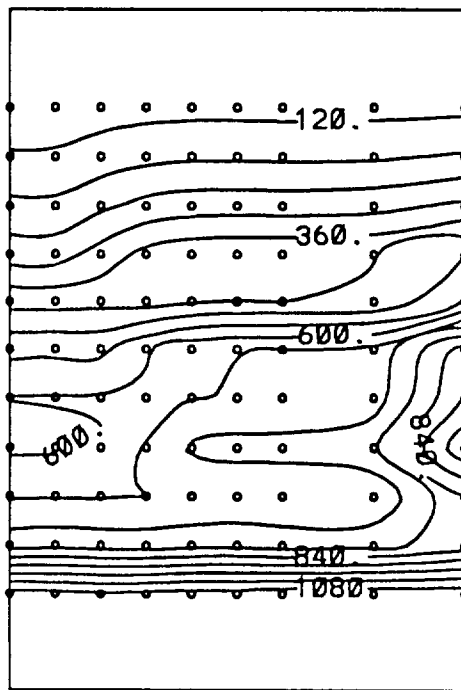


Figure 8.2.17: PITOT/Plnf Exit plane Contours,  
CR=9, Re=1.14 million/ft, 0% Cowl, (RUN93)

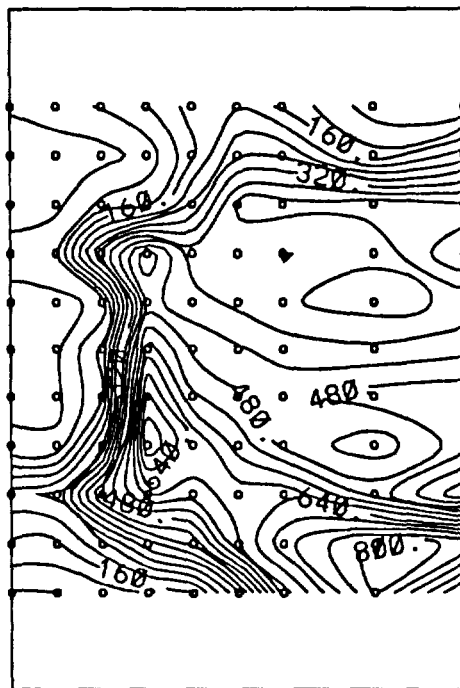


Figure 8.2.18: PITOT/Pinf Exit plane Contours,  
CR=3, Re=1.14 million/ft, 25% Cowl, (RUN77)

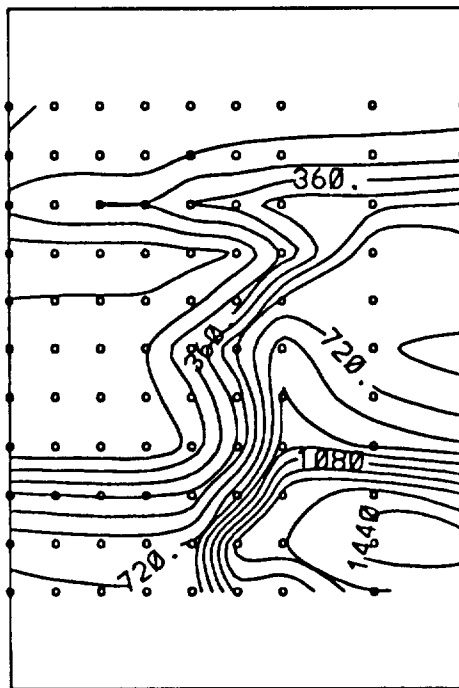


Figure 8.2.19: PITOT/Pinf Exit plane Contours,  
CR=5, Re=1.14 million/ft, 25% Cowl, (RUN87)

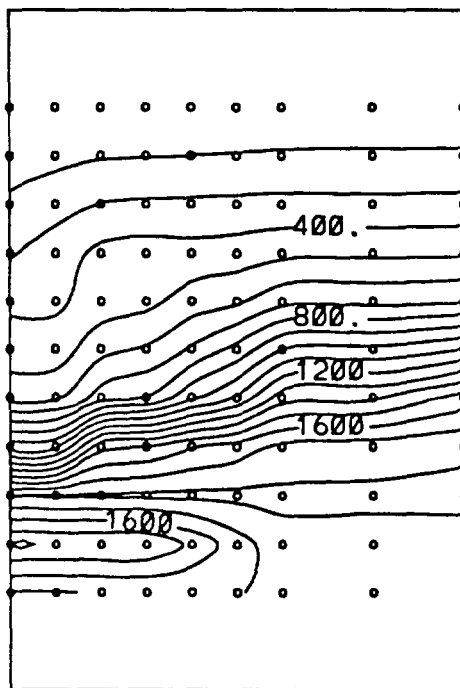


Figure 8.2.20: PITOT/Plnf Exit plane Contours,  
CR=9, Re=1.14 million/ft, 25% Cowl, (RUN96)



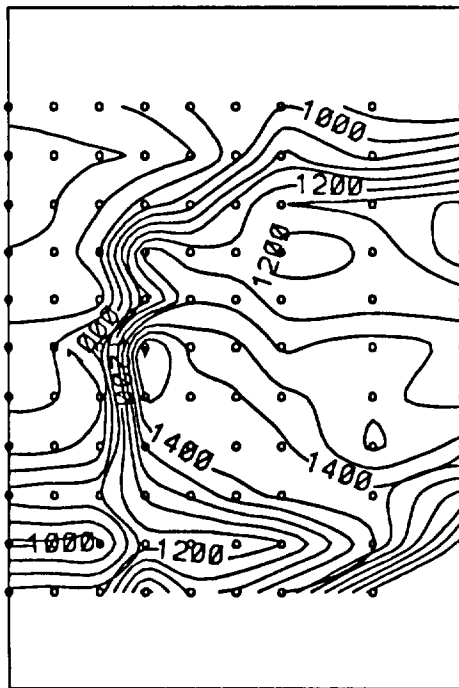


Figure 8.2.21: PITOT/ $P_{inf}$  Exit plane Contours,  
 $CR=3$ ,  $Re=1.14$  million/ft, 50% Cowl, (RUN79)

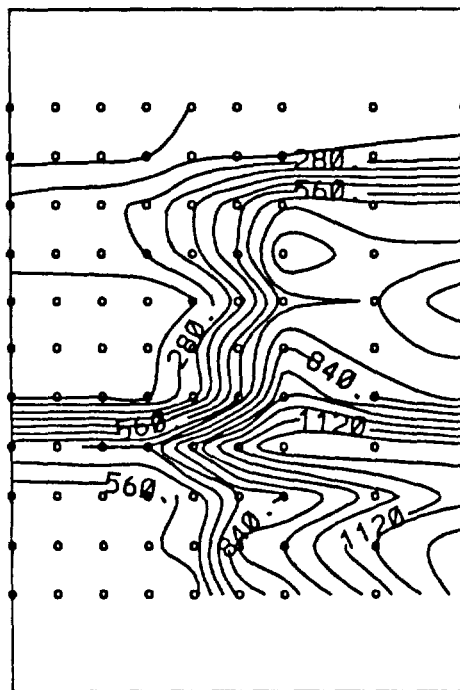


Figure 8.2.22: PITOT/Plnf Exit plane Contours,  
CR=5, Re=1.14 million/ft, 50% Cowl, (RUN84)

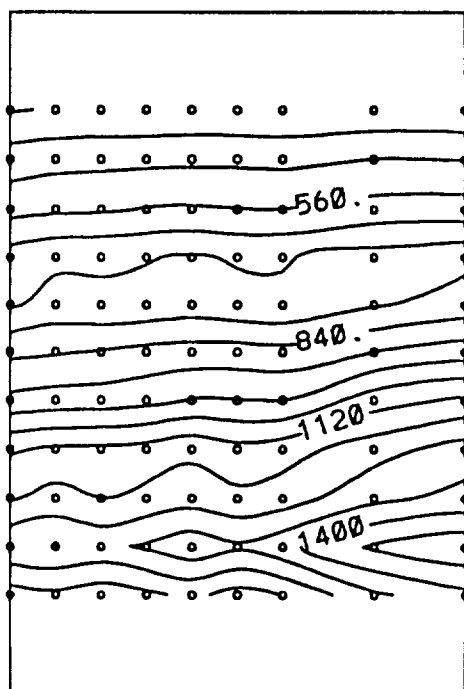


Figure 8.2.23: PITOT/Pinf Exit plane Contours,  
CR=9, Re=1.14 million/ft, 50% Cowl, (RUN98)

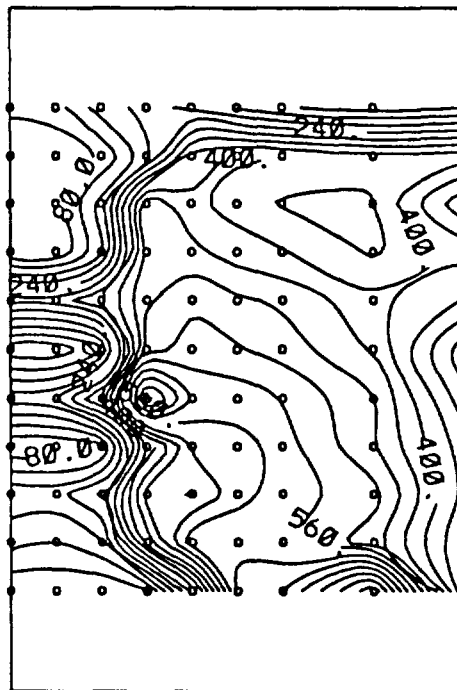


Figure 8.2.24: PITOT/Pinf Exit plane Contours,  
CR=3, Re=2.15 million/ft, 0% Cowl, (RUN73)

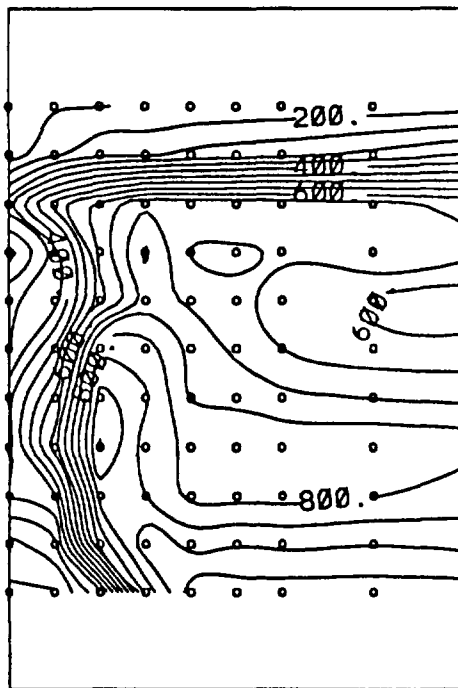


Figure 8.2.25: PITOT/Pinf Exit plane Contours,  
CR=5, Re=2.15 million/ft, 0% Cowl, (RUN91)

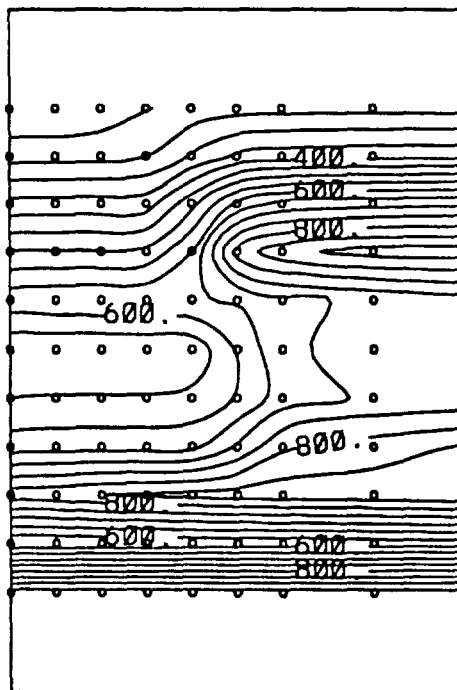


Figure 8.2.26: PITOT/Pinf Exit plane Contours,  
CR=9, Re=2.15 million/ft, 0% Cowl, (RUN94)

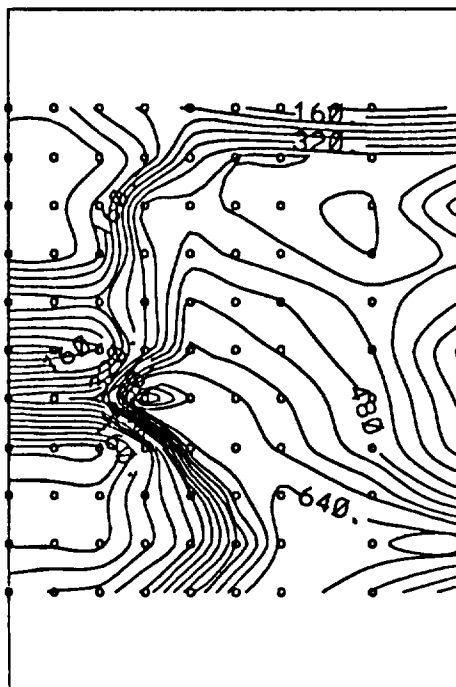


Figure 8.2.27: PITOT/ $P_{inf}$  Exit plane Contours,  
CR=3, Re=2.15 million/ft, 25% Cowl, (RUN75)

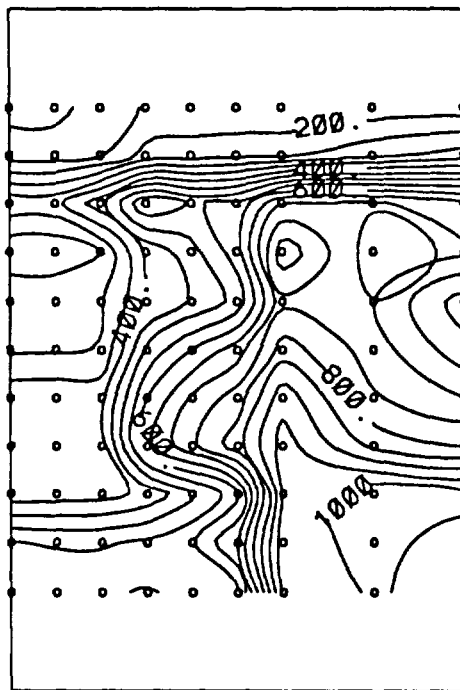


Figure 8.2.28: PITOT/Pinf Exit plane Contours,  
CR=5, Re=2.15 million/ft, 25% Cowl, (RUN88)



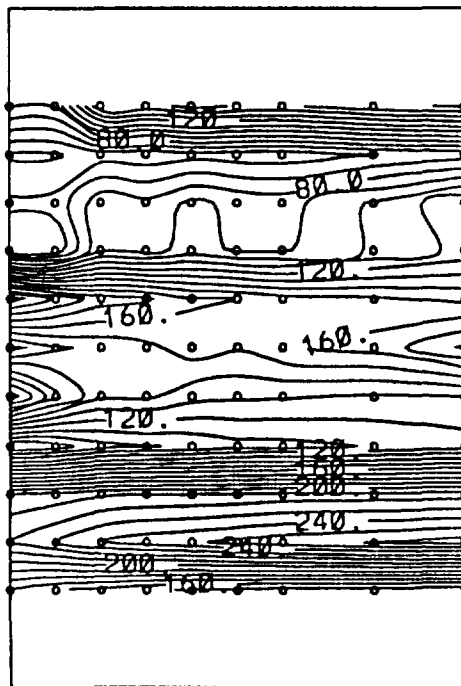


Figure 8.2.29: PITOT/Pinf Exit plane Contours,  
CR=3, Re=2.15 million/ft, 50% Cowl, (RUN81)

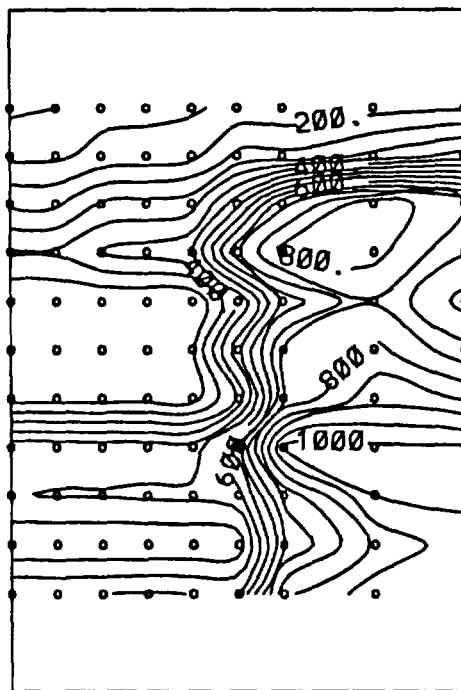


Figure 8.2.30: PITOT/Pinf Exit plane Contours,  
CR=5, Re=2.15 million/ft, 50% Cowl, (RUN85)

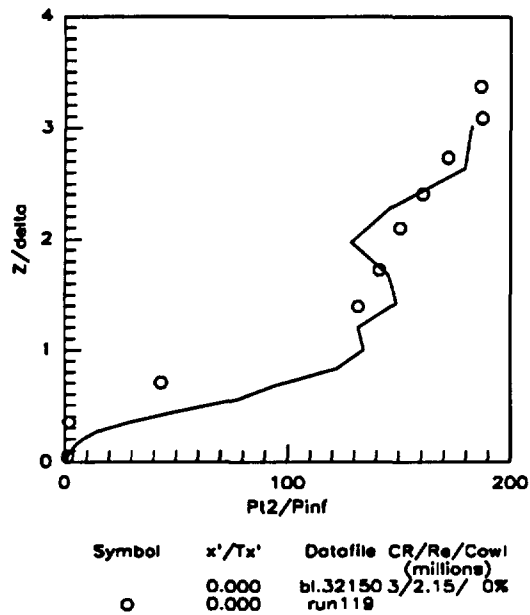


Figure 8.3.1: Entrance Boundary Layer Profile  
(CR=3, Re=2.15 million/ft, 0% Cowl)  
B.L. Pitot Pressure Profile

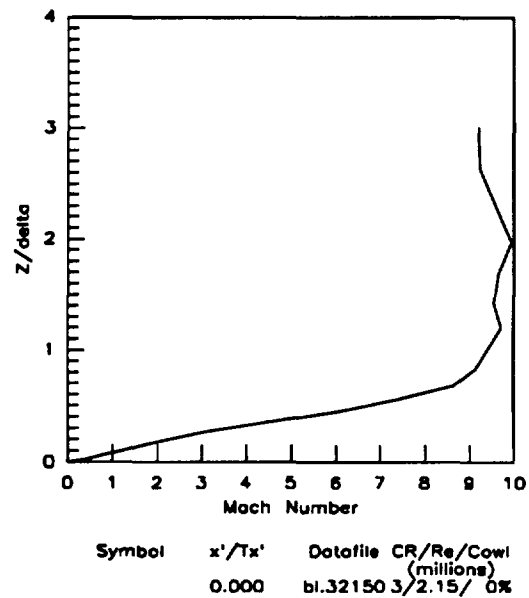


Figure 8.3.2: Entrance Boundary Layer Profile  
(CR=3, Re=2.15 million/ft, 0% Cowl)  
B.L. Mach Profile

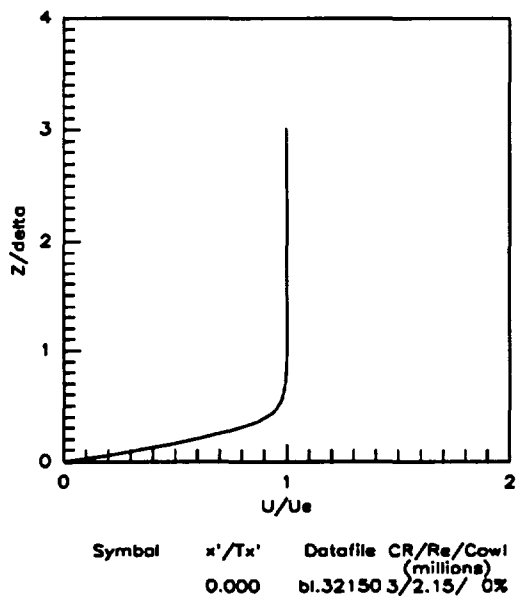


Figure 8.3.3: Entrance Boundary Layer Profile  
(CR=3, Re=2.15 million/ft, 0% Cowl)  
B.L. Velocity Profile

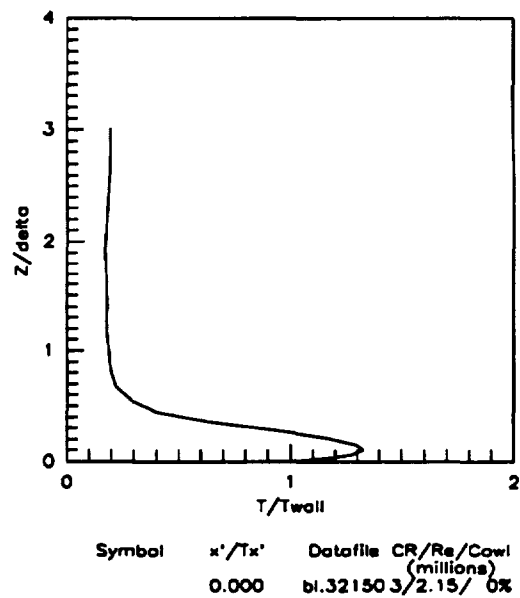


Figure 8.3.4: Entrance Boundary Layer Profile  
(CR=3, Re=2.15 million/ft, 0% Cowl)  
B.L. Temperature Profile

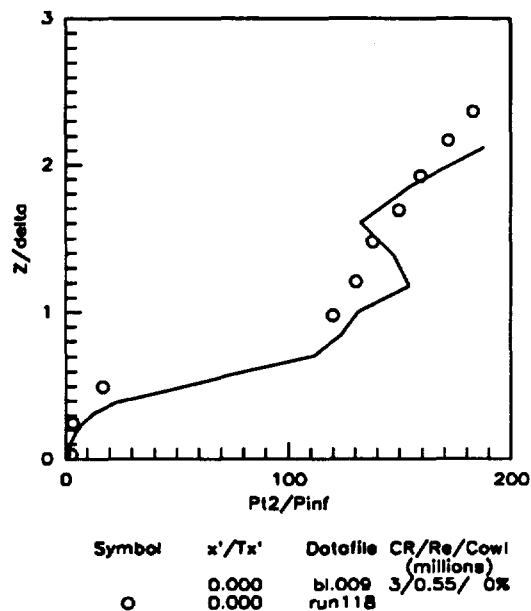


Figure 8.3.5: Entrance Boundary Layer Profile  
(CR=3, Re=0.55 million/ft, 0% Cowl)  
B.L. Pitot Pressure Profile

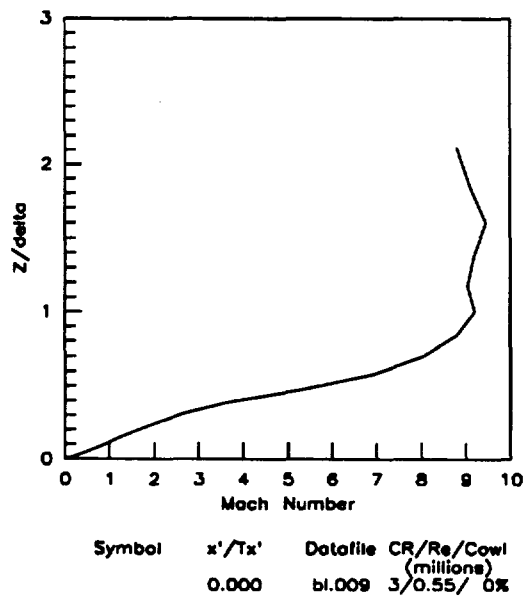


Figure 8.3.6: Entrance Boundary Layer Profile  
(CR=3, Re=0.55 million/ft, 0% Cowl)  
B.L. Mach Profile

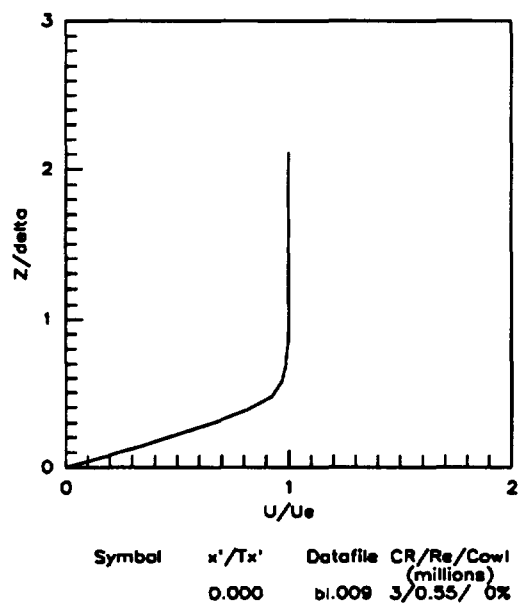


Figure 8.3.7: Entrance Boundary Layer Profile  
(CR=3, Re=0.55 million/ft, 0% Cowl)  
B.L. Velocity Profile

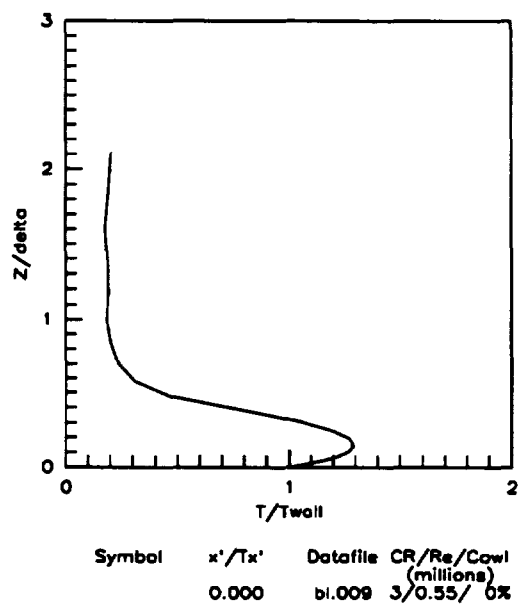


Figure 8.3.8: Entrance Boundary Layer Profile  
(CR=3, Re=0.55 million/ft, 0% Cowl)  
B.L. Temperature Profile